

DISS. ETH NO. 30337

Terpene Patterns Across Analytical Techniques for Advanced Authenticity Control of Natural Products

A thesis submitted to attain the degree of

DOCTOR OF SCIENCES
(Dr. sc. ETH Zurich)

presented by

JUSTINE NICOLE RAEBER

MSc ETH in Pharmacy, ETH Zurich

born on 03.10.1994

accepted on the recommendation of

Prof. Dr. Gisbert Schneider, examiner

Prof. Dr. Robin Teufel, co-examiner

Dr. Christian Steuer, co-examiner

2024

In loving memory of Yoshi and my grandfather Paul.

Summary

Natural products are secondary metabolites produced by plants to protect against environmental stressors, attract pollinators, and enhance survival. Terpenes, the largest class of these metabolites, are synthesised through the linkage of isoprene units and diversified by specific enzymes. While some terpenes are species-specific, others appear ubiquitous in the plant kingdom. Terpene patterns in plants are not random but are shaped by evolutionary pressures, making them a rich source for drug discovery and development, as they are inherently optimised drug-like molecules. Terpenes exhibit structures with chiral centres, and their composition in natural products is influenced by genetic and environmental factors, such as growth conditions, but also ageing and processing. Detailed analysis of terpene patterns can serve as a fingerprint to verify the identity and authenticity of natural products, as deliberate adulteration can lead to altered compositions. However, due to their structural similarities, terpenes pose analytical challenges requiring high resolution separation and reliable detection methods, which can be time-consuming and difficult to interpret.

This thesis focuses on the holistic characterisation of natural products, with a particular emphasis on terpenes, achieved through optimising separation and detection methods, alongside computational analysis. The methods developed further prioritise speed and ease of use.

Firstly, this thesis investigates optimised separation methods for terpenes in *Cannabis sativa* L. and *Rosa damascena*. Gas chromatography (GC) and liquid chromatography (LC) were evaluated using different column polarities, resulting in five validated methods for both qualitative and quantitative profiling of natural products. These methods enable the authenticity control of *R. damascena* essential oil (EO) beyond current international standardisation guidelines and an in-depth cultivar determination for *C. sativa* L., inclusive of minor cannabinoids and terpenes. An enantiomeric excess was found in *R. damascena* for (-)-cis rose oxide, (-)-linalool, and (-)-citronellol, which differs from adulterations with pelargonium oil. In *C. sativa* L. an excess of

(+)- α -pinene, (+)- β -pinene, (S)-limonene, (+)-linalool, (-)-citronellol, (-)-camphene, (+)-trans-nerolidol, and (-)-cis-menthone were identified. However, indoor-grown *C. sativa* L. plants lacking citronellol exhibited an excess of (-)- α - and (-)- β -pinene, indicating that cultivation conditions (indoor vs. outdoor) and plant protective agents alter enantiomer production. The entourage effect, a synergistic interplay between secondary metabolites, is also discussed, as contradictory study outcomes may stem from varying enantiomer ratios. Additionally, the validated methods were applied to investigate the effect of storage and ageing on terpene patterns. Stability studies revealed isomerisation, polymerisation, oxidation, and cyclisation reactions, with p-cymene identified as an ageing marker. No enantiomeric conversions were observed.

Secondly, different detection methods for terpenes were explored. These ranged from flame ionisation detection (FID) to mass spectrometry (MS) with different ionisation methods. Atmospheric pressure chemical ionisation (APCI) proved suitable for ionising terpenes and is compatible with LC. Dielectric barrier discharge ionisation (DBDI), a low-temperature plasma method, was investigated for GC. The ionisation process in DBDI is not straightforward and remains a subject of ongoing research. In contrast to APCI, which predominantly produces $[M+H]^+$ adducts, DBDI generates a diverse range of adduct species, primarily influenced by functional groups within the analytes. Oxygenated terpenes primarily formed adducts such as $[M]^+$, $[M+H]^+$, $[M+2H]^+$, and $[M+NH_4]^+$, while non-oxygenated terpenes formed adducts like $[M-H+2O]^+$, $[M+H+3O]^+$, $[M+H+2O]^+$, and $[M+H_2O_2]^+$. Furthermore, DBDI-MS spectra enable the distinction of constitutional isomers and diastereomers.

Lastly, predictive machine learning models were evaluated, which integrate data from multiple analytical techniques to assess the originality of *R. damascena* EO. Single-block models using data from one technique were compared to multi-block models, which make use of data fusion across analytical platforms. The highest classification accuracy was achieved with a model based on the quantitative profile with partial least-squares discriminant analysis (PLS-DA). However, a comparable model based on DBDI-MS data achieved similar classification accuracy in a fraction of the amount of time. While multi-block analysis did not exceed the classification accuracy of single-

block models, combining FT-IR data with DBDI-MS data improved accuracy compared to using FT-IR data alone in the single-block approach.

This thesis introduces a versatile toolbox for the analytical chemist that is suitable for the analysis of terpenes. The methodologies outlined here are neither limited to terpene analysis nor the two model plants studied: they can be extended to a broad range of other secondary plant metabolites. This approach contributes to the safe use of natural products in human applications.

Zusammenfassung

Naturstoffe sind sekundäre Stoffwechselprodukte, die von Pflanzen gebildet werden, um sich vor Umwelteinflüssen zu schützen, Bestäuber anzulocken und ihr Überleben zu sichern. Terpene, die grösste Klasse dieser Metaboliten, werden durch die Verknüpfung von Isopreneinheiten synthetisiert und durch spezifische Enzyme diversifiziert. Während einige Terpene für eine Art spezifisch sind, sind andere im Pflanzenreich allgegenwärtig. Die Terpenmuster in Pflanzen sind nicht zufällig, sondern durch evolutionären Druck entstanden, was sie zu einer ergiebigen Quelle für die Entdeckung und Entwicklung von Arzneimitteln macht, da sie von Natur aus optimierte arzneimittelähnliche Moleküle sind. Terpene weisen Strukturen mit chiralen Zentren auf, und ihre Zusammensetzung in Naturprodukten wird durch genetische und Umweltfaktoren wie Wachstumsbedingungen, sowie Alterung und Verarbeitung beeinflusst. Eine detaillierte Analyse der Terpenmuster kann als Fingerabdruck dienen, um die Identität und Authentizität von Naturprodukten zu überprüfen, da absichtliche Verfälschungen zu veränderten Zusammensetzungen führen können. Aufgrund ihrer strukturellen Ähnlichkeit stellen Terpene jedoch eine analytische Herausforderung dar, die eine hochauflösende Trennung und zuverlässige Nachweismethoden erfordert, die zeitaufwändig und schwierig zu interpretieren sein können.

Diese Arbeit widmet sich der ganzheitlichen Charakterisierung von Naturstoffen, mit besonderem Schwerpunkt auf Terpenen, was durch die Optimierung von Trenn- und Nachweisverfahren sowie durch computergestützte Analysen erreicht wird. Bei den entwickelten Methoden wird ausserdem Wert auf Schnelligkeit und Benutzerfreundlichkeit gelegt.

In dieser Arbeit wurden zunächst optimierte Trennmethoden für Terpene in *Cannabis sativa* L. und *Rosa damascena* untersucht. Gaschromatographie (GC) und Flüssigchromatographie (LC) wurden unter Verwendung verschiedener Säulenpolaritäten evaluiert, was zu fünf validierten Methoden für die qualitative und quantitative Profilerstellung von Naturprodukten führte. Diese Methoden ermöglichen

eine Echtheitskontrolle des ätherischen Öls (EO) von *R. damascena*, die über die aktuellen internationalen Standardisierungsrichtlinien hinausgeht, und eine detaillierte Kultursortenbestimmung für *C. sativa* L., einschliesslich der geringfügigen Cannabinoide und Terpene. In *R. damascena* wurde ein Enantiomerenüberschuss für (-)-cis-Rosenoxid, (-)-Linalool und (-)-Citronellol festgestellt, der sich von Verfälschungen mit Pelargoniumöl unterscheidet. In *C. sativa* L. wurde ein Überschuss an (+)- α -Pinen, (+)- β -Pinen, (S)-Limonen, (+)-Linalool, (-)-Citronellol, (-)-Camphen, (+)-trans-Nerolidol und (-)-cis-Menton festgestellt. Allerdings wiesen *C. sativa* L. Pflanzen, welche in Innenräumen gezüchtet worden sind und kein Citronellol enthielten, einen Überschuss an (-)- α - und (-)- β -Pinen auf, was darauf hindeutet, dass die Anbaubedingungen (drinnen vs. draussen) und der Einsatz von Pflanzenschutzmitteln die Enantiomerenproduktion beeinflussen können. Der Entourage-Effekt, ein synergistisches Zusammenspiel zwischen Sekundärmetaboliten, wird ebenfalls diskutiert, da widersprüchliche Studienergebnisse auf unterschiedliche Enantiomerenverhältnisse zurückzuführen sein könnten. Darüber hinaus wurden die validierten Methoden eingesetzt, um den Einfluss von Lagerung und Alterung auf die Terpenmuster zu untersuchen. Die Stabilitätsstudien ergaben Isomerisierungs-, Polymerisierungs-, Oxidations- und Zyklisierungsreaktionen, wobei p-Cymol als Alterungsmarker identifiziert wurde. Enantiomerenumwandlungen wurden nicht beobachtet.

Zweitens wurden verschiedene Nachweismethoden für Terpene untersucht. Diese reichten von der Flammenionisationsdetektion (FID) bis zur Massenspektrometrie (MS) mit verschiedenen Ionisationsmethoden. Die chemische Ionisierung bei Atmosphärendruck (APCI) erwies sich als geeignet für die Ionisierung von Terpenen und ist mit der LC kompatibel. Für die GC wurde die dielektrische Barriereentladung Ionisation (DBDI), eine Niedertemperatur-Plasmamethode, untersucht. Der Ionisationsprozess bei DBDI ist nicht gradlinig und bleibt Gegenstand laufender Forschung. Im Gegensatz zur APCI, bei der überwiegend $[M+H]^+$ -Addukte gebildet werden, erzeugt DBDI eine Vielzahl von Adduktspezies, die vor allem durch die funktionellen Gruppen der Analyten beeinflusst werden. Sauerstoffhaltige Terpene bildeten hauptsächlich Addukte wie $[M]^+$, $[M+H]^+$, $[M+2H]^+$ und $[M+NH_4]^+$, während nicht-sauerstoffhaltige Terpene Addukte wie $[M-H+2O]^+$, $[M+H+3O]^+$, $[M+H+2O]^+$ und

$[M+H_2O_2]^+$ bildeten. Darüber hinaus erlauben die DBDI-MS-Spektren die Unterscheidung von konstitutionellen Isomeren und Diastereomeren.

Schliesslich wurden Modelle für prädiktives maschinelles Lernen bewertet, die Daten von mehreren Analyseplattformen integrieren, um die Herkunft von *R. damascena* EO zu bestimmen. Einzelblockmodelle, die Daten aus einer einzigen Technik verwenden, wurden mit Multiblockmodellen verglichen, die die Datenfusion zwischen verschiedenen analytischen Plattformen nutzen. Die höchste Klassifizierungsgenauigkeit wurde mit einem Modell der partiellen kleinsten Quadrate-Diskriminanzanalyse (PLS-DA) auf der Basis des quantitativen Profils erzielt. Ein ähnliches Modell, das auf DBDI-MS-Daten basierte, erreichte jedoch eine ähnliche Klassifizierungsgenauigkeit in einem Bruchteil der Zeit. Während die Multiblock-Analyse die Klassifizierungsgenauigkeit von Einzelblock-Modellen nicht übertraf, verbesserte die Kombination von FT-IR-Daten mit DBDI-MS-Daten die Genauigkeit im Vergleich zur Verwendung von FT-IR-Daten allein im Einzelblock-Ansatz.

In dieser Arbeit wird ein vielseitiger Werkzeugkasten für den analytischen Chemiker vorgestellt, der für die Analyse von Terpenen geeignet ist. Die hier beschriebenen Methoden sind weder auf die hier analysierten Terpene noch auf die beiden untersuchten Modellpflanzen beschränkt: Sie können auf eine breite Palette anderer sekundärer Pflanzenmetabolite ausgedehnt werden. Damit wird ein Beitrag zur sicheren Anwendung von Naturstoffen in der Humanmedizin geleistet.

Publications

The following publications form part of this thesis:

Raeber J, Bajor B, Poetzsch M, Steuer C. Comprehensive analysis of chemical and enantiomeric stability of terpenes in *Cannabis sativa* L. flowers. *Phytochemical Analysis* 2024; 1-13. DOI:10.1002/pca.3432.

Raeber J, Poetzsch M, Schmidli A, Favrod S, Steuer C. Simultaneous quantification of terpenes and cannabinoids by reversed-phase LC-APCI-MS/MS in *Cannabis sativa* L. samples combined with a subsequent chemometric analysis. *Analytical and Bioanalytical Chemistry* 2024. DOI: 10.1007/s00216-024-05349-y.

Raeber J, Steuer C. Exploring new dimensions: Single and multi-block analysis of essential oils using DBDI-MS and FT-IR for enhanced authenticity control. *Analytica Chimica Acta* 2023; 1277: 341657. DOI: <https://doi.org/10.1016/j.aca.2023.341657>.

Raeber J, Favrod S, Steuer C. Determination of Major, Minor and Chiral Components as Quality and Authenticity Markers of *Rosa damascena* Oil by GC-FID. *Plants* 2023; 12. DOI: 10.3390/plants12030506.

Abbreviations

APCI	Atmospheric Pressure Chemical Ionisation
Cal	Calibration Standard
CE	Collision Energy
CAD	Collision Gas
CV	Cross-Validation
cps	Counts per Second
CUR	Curtain Gas
CXP	Cell Exit Potential
DBDI	Dielectric Barrier Discharge Ionisation
DE	Diastereomeric Excess
DMAPP	Dimethylallyl Pyrophosphate
DP	Declustering Potential
EE	Enantiomeric Excess
EP	Entrance Potential
EO	Essential Oil
ESI	Electrospray Ionisation
FID	Flame Ionisation Detection
FT-IR	Fourier Transform Infrared Spectroscopy
GC	Gas Chromatography
GS1	Ion Source Gas 1
HPLC	High Performance Liquid Chromatography
HRMS	High Resolution Mass Spectrometry
ICH	International Council for Harmonisation of Technical Requirements for Registration of Pharmaceuticals for Human Use
IPP	Isopentenyl Pyrophosphate
IS	Internal Standard
ISO	The International Organisation for Standardisation
LC	Liquid Chromatography
LOOCV	Leave-One-Out Cross-Validation
LoD	Limit of Detection
LoQ	Limit of Quantification
LTP	Low Temperature Plasma

LV	Latent Variable
MB-PCA	Multi-Block Principal Component Analysis
MB-PLS	Multi-Block Partial Least-Squares Regression
MCR-ALS	Multivariate Curve Resolution-Alternating Least Squares
MEP	2-C-methyl-D-erythritol-4-phosphate
MIC	Minimum Inhibitory Concentration
MRM	Multiple Reaction Monitoring
MS	Mass Spectrometry
MVA	Mevalonate
NC	Nebulizer Current
PA	Peak Area
PARAFAC2	Parallel Factor Analysis 2
PCA	Principal Component Analysis
PEG	Polyethylene Glycol
Ph. Eur.	Pharmacopeia Europea
PLS-DA	Partial Least-Squares Discriminant Analysis
QC	Quality Control
RE	Recovery Effect
RI	Retention Index
RMSE	Root Mean Square Error
RMSECV	Root Mean Square Error of Cross Validation
RMSEP	Root Mean Square Error of Prediction
RNV	Robust Normal Variate
R_s	Resolution
RSD_R	Interday Imprecision
RSD_T	Intraday Imprecision
RT	Retention Time
SNV	Standard Normal Variate
SO-PLS-LDA	Sequential and Orthogonalised Partial Least-Squares Linear Discriminant Analysis
TEM	Temperature

Table of contents

Summary	i
Zusammenfassung	iv
Publications	vii
Abbreviations	viii
Table of contents	x
1. Introduction	1
1.1. Biosynthesis pathway of terpenes from common precursors	1
1.2. Structural diversification of terpenes	2
1.3. Terpene patterns	5
1.3.1. Terpene patterns and their biological context	5
1.3.2. Terpene patterns for authenticity control	5
1.3.3. Terpene patterns for understanding cultivar and chemovar	6
1.3.4. Terpene patterns for understanding synergism	7
1.3.5. Ageing and storage markers of EOs	9
1.4. Separation science of terpenes	9
1.5. Detection methods for terpenes and other secondary metabolites	11
1.6. Chemometrics and computational analysis	15
Aim of the thesis	18
Chapter 1: Separation Techniques for Terpenes Covering Minor, Major, and Chiral components	19
2.1. Determination of Major, Minor and Chiral Components as Quality and Authenticity Markers of <i>Rosa damascena</i> Oil by GC-FID	21
2.1.1. Results and discussion	21
2.1.2. Materials and methods	35
2.1.2.1. Instrumental setup	35
2.1.2.2. Data processing and analysis	35
2.1.2.3. Method validation	36
2.1.2.4. Authentic sample preparation	37

2.2. Simultaneous Quantification of Terpenes and Cannabinoids by Reversed-Phase LC-APCI-MS/MS in <i>Cannabis sativa</i> L. Samples Combined with a Subsequent Chemometric Analysis	38
2.2.1. Results and discussion	38
2.2.2. Materials and methods	54
2.2.2.1. Instrumental setup	54
2.2.2.2. Method validation	55
2.2.2.3. Preparation of standards	56
2.2.2.4. Preparation and analysis of authentic <i>C. sativa</i> L. samples	57
2.2.2.5. Method comparison to GC-FID	58
2.2.2.6. Data visualisation and analysis	58
2.3. Comprehensive Analysis of Chemical and Enantiomeric Stability of Terpenes in <i>Cannabis sativa</i> L. flowers	60
2.3.1. Results and discussion	60
2.3.1.1. Method validation	61
2.3.1.2. Stress testing of single analytes and multi-mix	75
2.3.1.3. Stress testing of authentic <i>C. sativa</i> L. samples	82
2.3.2. Materials and methods	87
2.3.2.1. Instrumental setup: Chiral analysis	87
2.3.2.2. Instrumental setup: Polar analysis	87
2.3.2.3. Instrumental setup: Apolar analysis	88
2.3.2.4. Method validation and data analysis	88
2.3.2.5. Authentic sample preparation	89
2.3.2.6. Heat and UV treatment of control samples	89
2.3.2.7. Data analysis and visualisation	90
Chapter 2: Ionisation Techniques for Terpenes	91
3.1. Dielectric Barrier Discharge Ionisation Coupled to GC for Structure Elucidation of Terpenes	92
3.1.1. Optimising settings for the DBDI source	93
3.1.2. Terpene patterns generated by modifying the ionisation environment	94
3.1.3. DBDI-MS spectra for structure elucidation of related terpenes	101
3.2.1. Materials and methods	133
3.2.2. Instrumental setup	133
3.2.3. Determining optimal settings for the DBDI source	133

3.2.4. Identifying adducts generated by DBDI.....	134
3.2.5. High resolution analysis of selected terpenes	134
3.2.6. GC-EI-MS spectra acquisition	135
Chapter 3: Computational Methods and Data Fusion for Enhanced Classification of Natural Products	136
4.1. Exploring New Dimensions: Single and Multi-Block Analysis of Essential Oils using DBDI-MS and FT-IR for Enhanced Authenticity Control	137
4.1.1. Results and discussion	137
4.2.1. Materials and methods	156
4.2.1.1. Authentic samples	156
4.2.1.2. FT-IR analysis and data acquisition	156
4.2.1.3. DBDI-MS analysis and data acquisition	157
4.2.1.4. GC-FID analysis and data acquisition	158
4.2.1.5. Data pre-processing and computational analysis.....	158
5. Conclusion and Outlook	160
6. Acknowledgments	164
7. References	165
Curriculum Vitae	183
Appendix	186

1. Introduction

1.1. Biosynthesis pathway of terpenes from common precursors

Natural products are a broad class of chemicals produced by living organisms such as plants, fungi, and bacteria. They are secondary metabolites and, as the name suggests, while not primarily essential to life, they perform vital functions such as protecting against predators, attracting pollinators or defending against abiotic and biotic stresses, thereby enhancing survival fitness.¹⁻⁴ Plants synthesise terpenes, polyketides, alkaloids, phenylpropanoids, and phenolic compounds as secondary metabolites, which have their distinct biosynthetic pathways and may be unique to a particular plant species. Combinations of these phytochemicals are possible, allowing the synthesis of complex molecules.⁴ Terpenes and their oxygenated derivatives, the terpenoids (generally referred to as oxygenated terpenes for convenience), are widespread throughout the plant kingdom and form the largest class of secondary metabolites. With over 55,000-80,000 described members, they represent a diverse group and are the primary constituents of essential oils (EOs).⁵⁻⁷ EOs are widely used in the flavour and fragrance industry, find application in medicine and aromatherapy, and in the food industry. EOs are extracted by water, steam, and dry distillation or extraction, and consist of volatile components. Depending on the plant, an EO can contain anywhere from a few to several hundred different compounds, predominantly comprising of monoterpenes, sesquiterpenes, and aromatic compounds like phenylpropanoids.^{5, 8} Two biosynthetic pathways are recognised for terpene synthesis: the 2-C-methyl-D-erythritol-4-phosphate (MEP) pathway, which takes place in the plastids and the mevalonate (MVA) pathway operating in the cytoplasm, endoplasmic reticulum, and peroxisomes.⁷ Terpenes are synthesised phytochemically by linking isopentenyl pyrophosphate (IPP) and its isomer dimethylallyl pyrophosphate (DMAPP), both of which are isoprene units containing five carbon atoms (Figure 1). Terpenes are classified according to the number of these units, ranging from monoterpenes (C₁₀), sesquiterpenes (C₁₅) to larger non-volatile substances such as di-, tri-, tetra- and polyterpenes.⁴ Terpene enzymes catalyse the diversification of these carbon skeletons through processes like oxidation, rearrangement, and

cyclisation, resulting in a structurally diverse array of compounds.^{1, 6} Although the terpene synthesis pathway appears to be conserved among plants, each species only produces a handful of selected terpenes that are relevant to its ecological niche. Terpene synthesis does not occur random, but directed and stereoselective and is the result of evolutionary pressure and selection.^{1, 7, 9, 10} As a result of this evolutionary pressure, natural products are inherently optimised drug-like molecules and serve as a rich source of chemical leads for drug discovery.^{11, 12}

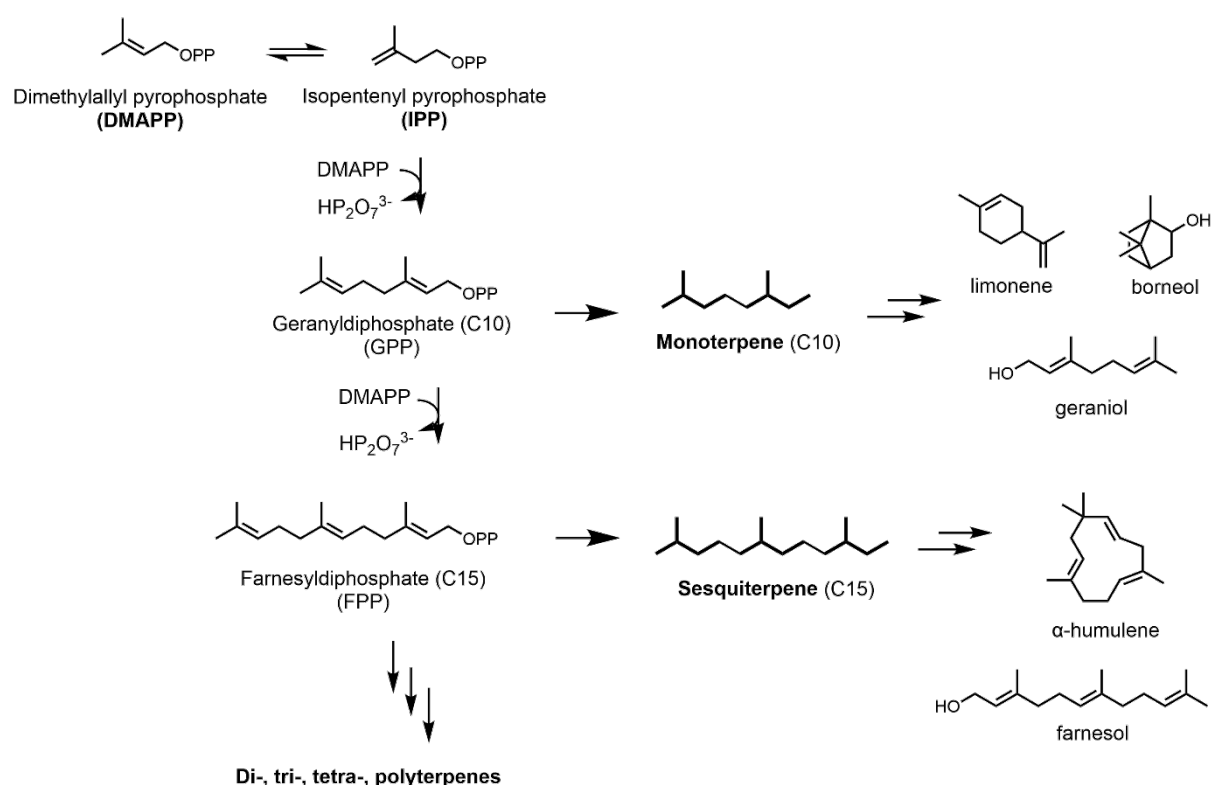


Figure 1: Synthesis pathway of terpenes from the common precursors DMAPP and IPP. Synthesis pathway based on the description by Dubey et al.¹³

1.2. Structural diversification of terpenes

The common biosynthetic pathway, following the isoprene rule established by Leopold Ruzicka, gives rise to diverse structures with carbon backbones of C10, C15, C20 and beyond.¹⁴ Currently, there are about 25 different subclasses of terpenes.⁵ While terpenes are initially classified on the basis of their isoprene units, a more detailed categorisation can be made by considering their structural intricacies. Terpenes have different structural forms, including acyclic, cyclic, and oxygenated or non-oxygenated

types. Cyclic terpenes can be further subdivided according to their number of ring structures. For example, monoterpenes can form monocyclic, bicyclic, and tricyclic structures. Alcohol, carboxyl, aldehyde, ester, and ketone functional groups can be found in oxygenated terpenes.^{5, 15} Figure 2 provides an overview of a few commonly found terpenes.

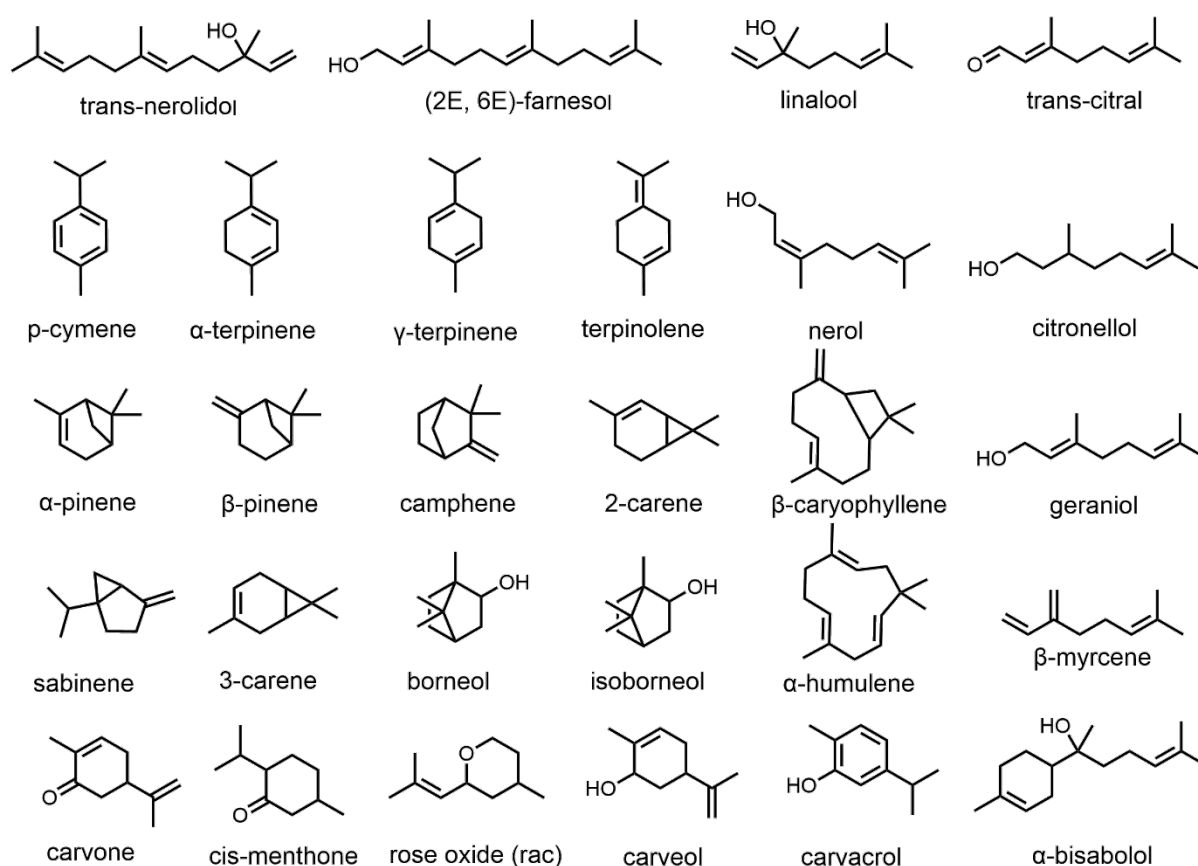


Figure 2: Overview of mono- and sesquiterpene structures from linear, monocyclic to bicyclic subclasses. For some compounds, alcohol, ketone or aldehyde groups can be observed.

So far in this thesis, only the planar structures of terpenes have been categorised. However, terpene synthesis in plants is stereoselective, yielding complex structures with multiple chiral centres. Chirality is of biological importance due to the stereospecificity of enzymes. In addition, depending on their origin or species, plants produce specific non-racemic mixtures with enantiomeric (EE) or diastereomeric (DE) excesses.¹⁶⁻¹⁸ Figure 3 gives an overview of the different isomers found for terpenes. In general, stereoisomers and constitutional isomers can be distinguished by having either different or the same connectivity between atoms. Enantiomers are mirror images that cannot be superimposed. In terms of nomenclature, enantiomers are

named based on their direction in which they rotate polarised light. Left-hand rotations are denoted by the (-) symbol, while right-hand rotations by the (+) symbol. The absolute configuration is described by the S- and R-descriptors, which define the order of the bonds around the chiral centres. They can be either clockwise (R) or anti-clockwise (S).¹⁹

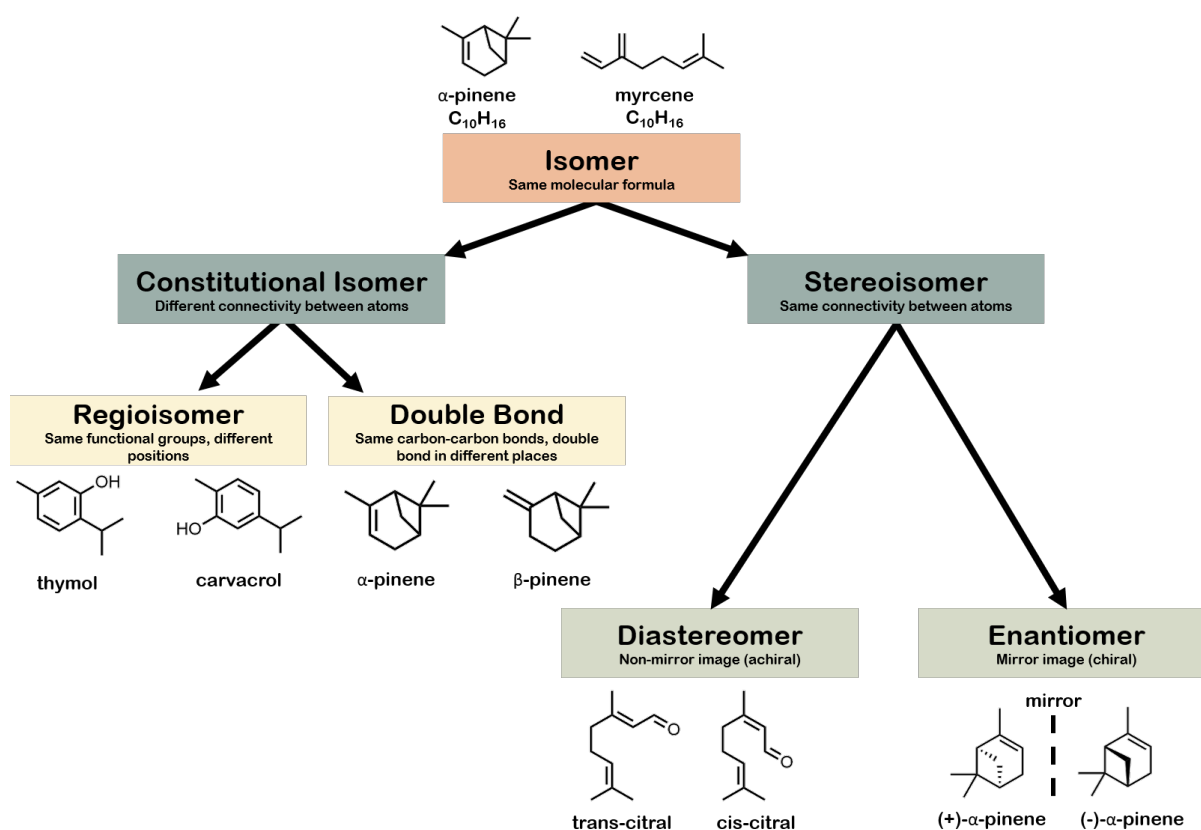


Figure 3: Overview of nomenclature for different isomers found for terpenes.

Due to their common origin and the isoprene rule, many terpenes share the same molecular formula. Although different arrangements of carbon atoms are possible, terpenes differ in subtleties such as chirality or the position of double bonds and/or functional groups. This results in a wide range of isomers, many of which can occur in the same plant.²⁰

1.3. Terpene patterns

1.3.1. Terpene patterns and their biological context

The terpene patterns in plants are not a rigid structure; instead, the composition of secondary metabolites is subject to dynamic change. While certain ratios or excesses of enantiomers and diastereomers may be specific to a particular species, they may also depend on factors such as origin, climate, soil conditions or the growth cycle.²¹⁻²³ For instance, in *Cannabis sativa* L., a plant known for its medicinal, recreational and food uses, terpene ratios shift from primarily sesquiterpenes at the onset of flowering to mostly monoterpenes at the end of flowering.²⁴ The composition of terpenes in natural products such as EOs can be crucial to ensure product authenticity and quality.²³ Enantiomers, for instance, can have different organoleptic properties or can even exhibit different pharmacological effects. For example, (+)- and (-)- α -pinene exhibit either strong antibacterial or insecticidal activities.^{25, 26} Another example is carvone. For (R)-(-)-carvone, a spearmint-like odour is perceived, whereas for (S)-(+)-carvone, a caraway-like odour is perceived, underlining the stereoselectivity of e.g. human receptors.²⁷ The lack of understanding of isomers and enantiomeric ratios in natural products may have contributed to conflicting results in the literature on the biological activity of terpenes, emphasising the need to determine the EE and DE.²⁸

1.3.2. Terpene patterns for authenticity control

As EOs are natural products, production is limited and may be rare for certain plants. This scarcity, combined with time-consuming production and high demand, can lead to fluctuations in market prices. Consequently, EOs are susceptible to adulteration in order to reduce costs and/or increase profits. For example, *Rosa damascena* EO, a highly valued oil in the perfume industry, requires up to 4 tonnes of rose petals to yield just 1 kg of EO. It is therefore traded as one of the most expensive EOs in the world, making it a lucrative target for falsification. Common adulteration techniques include adding natural or synthetic compounds, deliberate blending with other cheaper EOs such as palmarosa or pelargonium EO, or diluting with mineral and/or vegetable oils.²⁹⁻³³ The Pharmacopoeia Europea (Ph. Eur.) and The International Organisation for Standardisation (ISO) serve as regulatory frameworks and quality standards for

EOs, depending on the area of application. However, these standards are limited by the number of EOs and/or constituents they cover. Notably, chiral analysis is not part of the standard analysis.^{10, 32, 34} Adulteration of EOs and other natural products is not only a financial fraud, but can also pose health risks. When synthetic or natural constituents are added, the enantiomeric ratio is often altered and in most cases it would be too costly for the adulterator to use enantiomer pure constituents.³⁰ In the case of α -pinene, however, this can have an impact on the pharmacological effect, as the two enantiomers have varying antibacterial activities.²⁶ Similar observations have been made for numerous terpenes, such as (+/-)-carvone, (+/-)-rose oxide, and (+/-)-linalool, where the enantiomers exhibit different therapeutic properties or toxicities.³⁵ Consequently, adulteration can be harmful to health or reduce the efficacy of a natural product. Understanding the terpene pattern in its diversity, chirality and abundance does not only provide information about a natural products authenticity and growth cycle, it further offers clues about ageing and storage processes as well as the chemical variant (chemovar).

1.3.3. Terpene patterns for understanding cultivar and chemovar

Since the beginning of cultivation, people have selectively bred plants to improve desirable traits by crossing varieties that perform well. Morphological characteristics are not the only determining factor for a plant variety, as morphology can be strongly influenced by the environment. Understanding different markers and characteristics of a cultivar is crucial to improve the selection of varieties. While the cultivar can be determined by genetic testing such as identifying DNA markers or single-nucleotide-polymorphisms, they are not necessarily representative of the final phenotype.^{36, 37} *C. sativa* L. is gaining traction as a multi-component medicinal plant, for which around 100 cannabinoids and 200 terpenes have been described.^{38, 39} Kannapedia, a library dedicated to cannabis genetics, currently lists 1280 different registered strains based on genetic testing for *C. sativa* L.⁴⁰ The large number of varieties raises the question of which are best suited for medical purposes. However, it is not only the variety that is of interest, but also the chemical composition, i.e. the chemovar of the plant, as effects such as synergism or the entourage effect are suspected.⁴¹ Cannabis cultivation was originally based on organoleptic properties, such as the odour produced by terpenes, in addition to its psychoactive properties, which shaped the

varieties known today.⁴² Current classification methods are mostly based on the determination of the ratio between the main cannabinoids THC and CBD and have been included, for example, in the Ph. Eur.⁴³ This classification method is useful in terms of legal limits and the psychoactive effects of THC, but does not take into account minor components such as terpenes, although they are present at pharmacological relevant concentrations.⁴² The classification of *C. sativa* L. is still a widely debated topic with various approaches.^{44, 45} However, a metabolomics study by Hazekamp and Fishedick found that the chemical profile of the same variety was reproducible, although influences such as drying, storage and processing can lead to variations in the chemical profile.⁴¹ Understanding the chemical composition and the terpene patterns of plants such as *C. sativa* L. can provide valuable insights into their growing environment, including soil and climate, as well as the processing and storage conditions of the finished herbal drug. This knowledge can enhance the classification of cultivars with an outlook on their chemovar.

1.3.4. Terpene patterns for understanding synergism

Terpenes have a variety of different pharmacological properties, due to their function as secondary metabolites to increase plant fitness. They potentially serve as antibacterial, anticancer, antiviral, antifungal, anti-insect, antiplasmodial, antimicrobial, antidiabetic and antidepressant agents.² In particular, their use as alternatives to existing antibiotics is currently under intense investigation, spurred by the growing threat of bacterial resistance and treatment-resistant infections that threaten human health. Terpenes are proposed to act as efflux pump inhibitors, counteracting bacterial resistance mechanisms commonly used to evade antibiotics.^{46, 47} Research suggests that terpenes such as (S)-limonene can synergistically enhance the efficacy of antibiotics, for example in the treatment of tuberculosis, by lowering the minimum inhibitory concentration (MIC). In addition, combinations of terpenes and other EO components have shown similar effects on pathogens, exhibiting synergistic, additive or inhibitory activities.^{47, 48} The synergistic interaction of natural products through modulation of pharmacological activities has also given rise to phenomena such as the “entourage effect”, first observed by Ben-Shabat and co-workers in 1998.⁴⁹ It is proposed that the pharmacological effect of isolated compounds differ from that of a mixture, such as crude plant extracts. This synergism can occur within the same

compound class, such as CBD reducing the side effects of THC, or between different compound classes, such as terpenes and cannabinoids. While agonistic binding to the CB₂ cannabinoid receptor has been observed for β -caryophyllene, it has been refuted for other major terpenes found in *C. sativa* L. Furthermore, in epilepsy and pain management - two indications for which *C. sativa* L. is used and approved - improved clinical outcomes have been reported when extracts were used instead of the isolated cannabinoids.⁵⁰⁻⁵⁵ The entourage effect is still a subject of debate, remains controversial and has been most prevalent in the area of *C. sativa* L. research. While the prevailing theory for the entourage effect suggests that terpenes bind to cannabinoid receptors, synergism may also be initiated by other mechanisms of action. Four distinct types of synergism have been described by Wagner et al.:

- (i) A multi-target effect is possible, which occurs when different compounds target different enzymes.
- (ii) Pharmacokinetic effects, such as improved bioavailability and solubility, may enhance the efficacy of another compound.
- (iii) Interactions with proteins can enhance compound activity, as seen in bacterial resistance mechanisms where terpenes act as efflux pump inhibitors, thereby potentially improving antibiotic efficacy.
- (iv) Adverse effects can be modulated, as demonstrated by the combination of THC and CBD, which potentially reduces intoxicating effects of THC.^{54, 56}

The contradictory results for the entourage effect could be explained by the inadequate characterisation of the plant extracts. In addition, studies investigating cannabinoid receptor modulation have focused on direct binding of these receptors. However, synergism may result from multi-target effects or altered pharmacokinetics. Access to well-characterised plant extracts could allow these investigations to be carried out in a controlled manner. In addition, the studies did not address the stereoselectivity of the targets, nor did they include chiral analysis of the extracts.

1.3.5. Ageing and storage markers of EOs

Terpenes and other components of EOs are sensitive to stressors such as oxygen, light and heat. However, EOs also have antioxidant properties and could be used as preservatives.^{57, 58} Bueno et al. discovered that having a mixture of terpenes and cannabinoids reduced the degradation of THC by 50%. Depending on the composition and concentration of terpenes, they can prolong the shelf life of herbal medicines.^{58, 59} In addition to their antioxidant properties, terpenes can also be used as ageing and storage markers. As terpenes have a variety of isomeric forms, rearrangements can be easily induced by light and heat, but can also occur spontaneously over time. Reactions such as isomerisation, dehydrogenation and oxidation have been described.⁶⁰⁻⁶⁴ Consequently, storage and stressors can significantly influence the terpene composition and pattern. Isomerisation may result in the conversion of one enantiomer to the other, which can further alter the pharmacological activity.

1.4. Separation science of terpenes

Detailed analysis of EOs, especially terpenes, requires high separation performance. Gas chromatography (GC) has become the state-of-the-art method because of its high resolution, which produces narrow, well-separated chromatographic peaks that facilitate the separation and quantification of structurally similar compounds (Figure 4). It also has the ability to separate a few hundred compounds in a single chromatographic run. A wide range of column coatings and polarities are available for the separation with GC, ranging from polar polyethylene glycol (PEG) columns, to apolar ones and chiral phases for the separation of enantiomers. The requirements for an analyte to be analysed by GC are thermal stability, gas phase transition and molecular weights below 1500 Da for analytes.^{10, 65-67} Terpenes and other volatile components of EOs are ideal analytes for this purpose. However, GC may not be optimal for the analysis of other phytochemicals. In the case of cannabinoids, for example, the acid forms such as THCA and CBDA occur predominantly in the plant and are only converted to the neutral form by heating or processing. Yet during GC analysis, these acids decarboxylate in an uncontrolled manner during injection. To avoid this reaction, complex protocols have been developed to derivatise the acid forms. However, these reactions can be incomplete and non-specific, which is why

analysis by liquid chromatography (LC) has been preferred for the analysis of cannabinoids.⁶⁸⁻⁷⁰ As a consequence, if both terpenes and cannabinoids are to be determined, the analysis requires either complex and time-consuming sample preparation or two separate analyses, making full quantification a cumbersome process.⁷¹⁻⁷⁴ LC is widely used for the analysis of other natural products, but is not considered ideal for the analysis of terpenes, despite some reports in the literature.^{75, 76} Several reports have demonstrated the use of LC for the analysis of oxidation products of terpenes, such as hydroperoxides of linalool and limonene, as well as oxygenated terpenes. In addition, LC is often used for the analysis of terpene lactones, for example in *Ginkgo biloba*.⁷⁷⁻⁸⁰ Although the use of LC for terpene analysis is uncommon and unusual, it offers certain advantages: separation occurs at low temperatures, reducing decomposition and isomerisation reactions. In addition, LC is non-destructive, making it widely used for preparative purposes.⁸¹⁻⁸³

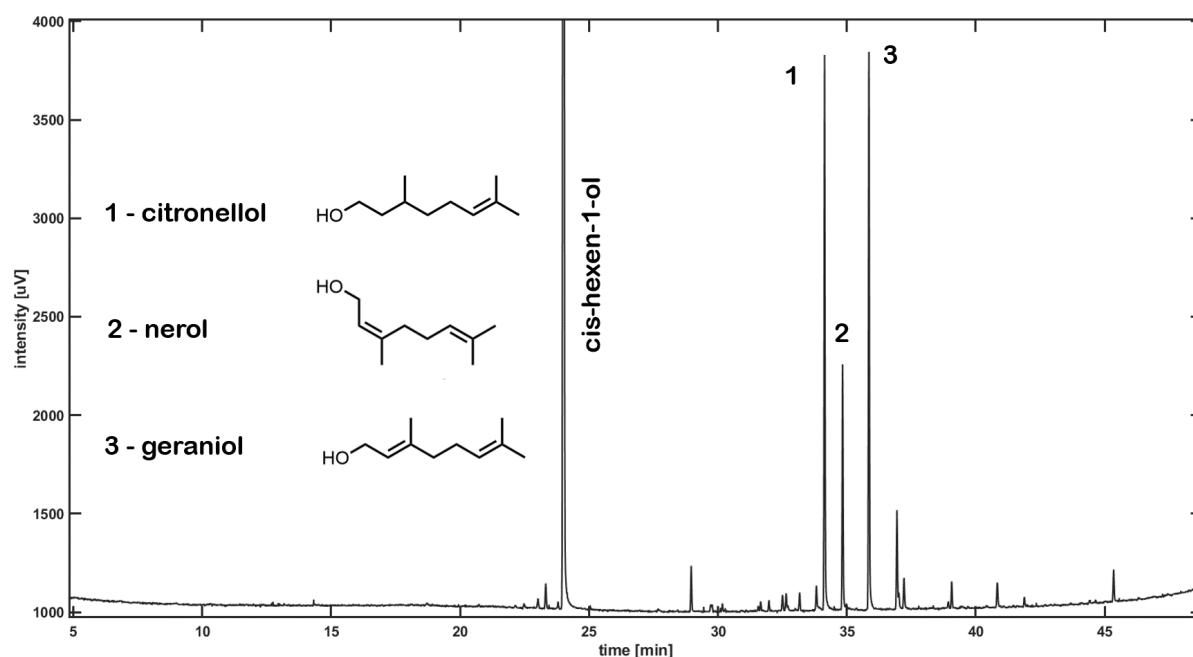


Figure 4: Chromatographic profile of *R. damascena* EO originating from Bulgaria. Analysis was conducted on a DB-wax column using GC-FID. Cis-hexen-1-ol was added as an internal standard (IS). Chromatogram was acquired by the author.

1.5. Detection methods for terpenes and other secondary metabolites

While chromatography is responsible for separating a mixture of substances, it must be coupled with a detection method to register the individual analytes. For EOs separated by GC, flame ionisation detection (FID) and mass spectrometry (MS) have proven to be the gold standard.^{10,84} FID provides a broad linear range for quantification and high sensitivity, often outperforming MS. Additionally, FID is insensitive towards the carrier gas and offers low baseline noise levels. However, FID is only effective for the detection of carbon-containing structures.⁸⁵ In combination with GC, FID only provides the retention time of the analyte and no further characterisation is possible. The retention index (RI) is a unitless parameter used to standardise retention times across different devices and laboratories. In GC experiments, the RI helps identify analytes by comparing experimental values with literature values, thereby improving compound identification. To determine the RI, a homologous series of an n-alkane mixture is measured using the same GC temperature method as for the analyte. The RI can be calculated using the van den Dool and Kratz equation (Formula 1). The abbreviations used are as follows: RT stands for retention time, n represents the number of carbon atoms in the n-alkanes, n (as a subscript) refers to the pre-eluting n-alkane, and $n+1$ refers to the post-eluting n-alkane.^{86, 87}

$$RI = 100 \times \left(n + \frac{RT_{unknown} - RT_n}{RT_{n+1} - RT_n} \right) \quad 1$$

FID provides information solely about retention times, whereas MS offers an additional advantage. In MS, the analyte is ionised, undergoes reproducible fragmentation, and the fragments are separated based on their mass-to-charge ratio in a vacuum. Electron impact (EI) ionisation is commonly employed with GC. A fixed voltage of 70 eV is applied, which can lead to complete fragmentation of the analyte. As a result, the molecular ion is occasionally not preserved. The resulting fragment spectra are specific and reproducible, as they are not strongly dependent on the instrument type, and can be compared using databases such as NIST or the Adams library.⁸⁸⁻⁹¹ EI is considered a “hard” ionisation method due to the frequent loss of the molecular ion, which can be an important compound identification marker. As terpenes are composed of the same building blocks and are structural isomers, EI can result in similar if not

identical MS spectra, making analyte identification challenging. Figure 5 shows the EI-MS spectra of limonene and linalool, which have different molecular weights. While the molecular ion of limonene is preserved, linalool undergoes complete fragmentation. Although the spectra are distinguishable, the loss of the molecular ion may lead to incorrect analyte identity assignments.

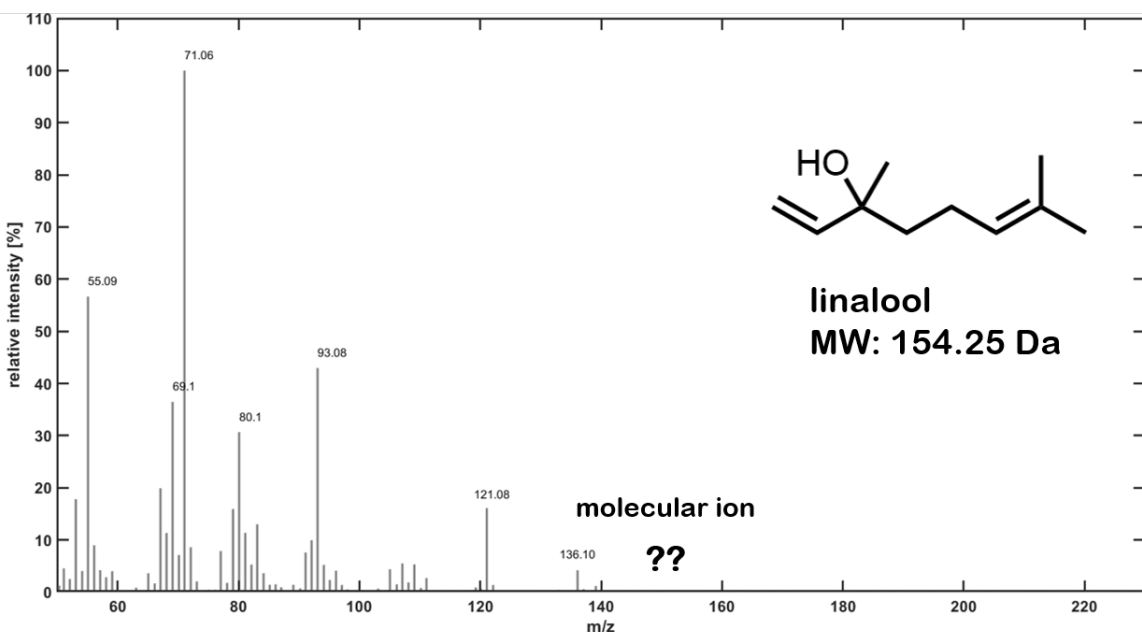
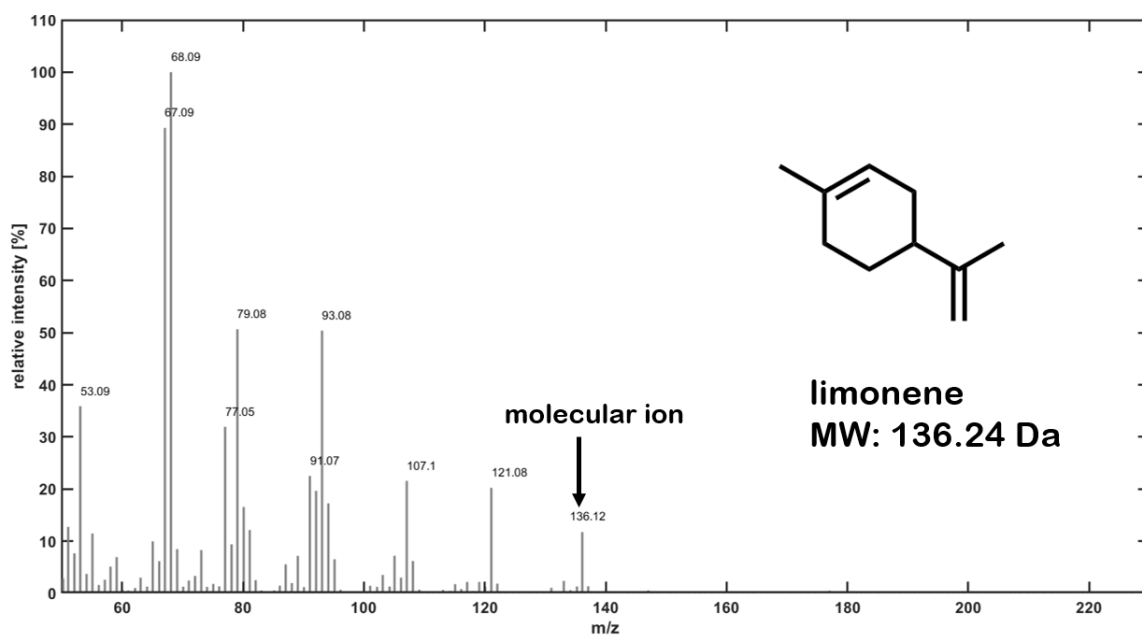


Figure 5: Comparison of two GC-EI-MS spectra. The molecular ion $[M]^+$ for limonene is detectable, but not for linalool, hindering precise identification of the spectra. The spectra were recorded by the author at an energy of 70 eV.

This drawback has led to the use of “soft” ionisation methods that operate at atmospheric pressure, such as chemical ionisation (CI) or low-temperature plasma (LTP) for GC.⁹² Ambient ionisation methods offer several advantages: they can be decoupled from chromatography, allowing real-time data acquisition and *in-situ* analysis. They can also reduce or even eliminate sample preparation by reducing analysis to a single step. Furthermore, they are less susceptible to contamination or carryover, as samples have little contact with the instrumentation.⁹³⁻⁹⁶ Sample analysis can be as simple as holding an EO in front of the ion source (Figure 6).



Figure 6: Direct sampling of an EO using a LTP-source. Operating at atmospheric pressure, the open architecture allows direct sampling. Photo was taken by the author.

Dielectric barrier discharge ionisation (DBDI) is an LTP-based ionisation method first commercialised by Plasmion in 2018 under the name SICRIT.⁹⁷ The ion source consists of two electrodes separated by a dielectric barrier, typically glass, to generate a highly ionised gas known as a LTP.^{98, 99} DBDI can be coupled to both GC and LC, allowing the direct use of the same MS instrument. Unlike other state-of-the-art ionisation methods for LC such as electrospray ionisation (ESI) and atmospheric pressure chemical ionisation (APCI), DBDI is considered to be less susceptible to matrix effects such as ion suppression.^{100, 101} Furthermore, unlike spray or other

plasma ionisation techniques, DBDI profits from an in-line set up compared to the open architecture of for example ESI and APCI. In DBDI, the ionisation process occurs simultaneous with the analyte introduction into the MS, allowing a greater proportion of ionised analytes to enter the MS, resulting in a higher sensitivity.¹⁰²⁻¹⁰⁴ DBDI is thought to ionise a wider range of analytes, spanning from polar to apolar compounds, compared to ESI and APCI. In particular, the increase in voltage results in improved ionisation from polar to apolar analytes, due to an increase in electrons in the plasma. The resulting ionisation products are expected to be similar to those observed with APCI. DBDI also provides a wide linear quantification range for various analytes, as demonstrated with pesticides, explosives, chemical warfare agents, and alkanes.^{101, 102, 105-109} The exact ionisation mechanism of DBDI is not yet fully understood, but appears to be mainly based on charge transfer reactions. Possible charge transfer reactions include transfer from radical dopant species to the analyte via Penning ionisation and electron ionisation.^{99, 110} DBDI is a small reaction chamber, containing a variety of excited species such as NO_3 , O_2^+ , H_3O^+ , N_2^+ , N_2H^+ , NO^+ , N_3^+ , and N_4^+ , which can change depending on the discharge gas.^{99, 111} They further depend on the applied voltage and dopants. The main species observed for DBDI are $[\text{M}+\text{H}]^+$ and $[\text{M}]^+$ ions. In the example of polycyclic hydrocarbons, the formation of the $[\text{M}+\text{H}]^+$ adduct was favoured over the $[\text{M}]^+$ ions as the humidity increased. It was also found, that the formation of radical cations increased from CO_2 , to N_2 , to air.^{99, 102, 110} At low voltage, mainly $[\text{M}]^+$ ions are formed, by increasing the voltage however, incorporation of nitrogen can occur, forming $[\text{M}+\text{N}]^+$ ions. This reaction seems to be stereoselective. In the example of alkylbenzene isomers, the position of the alkyl substituent was critical for the nitrogen-incorporation, producing additional product ions and thus improving compound identification by MS.¹¹² In another study by Begley et al., the unusual exchange of a carbon atom for a nitrogen atom was observed for aromatic ring structures in DBDI, which could be derived from the excited nitrogen species such as N^+ , N_2^+ , and N_4^+ .¹¹³ Similar to APCI, hydronium cluster formation has been observed in DBDI. However, DBDI does not appear to rely solely on these clusters for ionisation and $[\text{M}+\text{H}]^+$ adduct formation.^{111, 114} Depending on the ionisation atmosphere, reactions such as in-source fragmentation, as well as the formation of various adducts such as $[\text{M}+\text{OH}]^+$, $[\text{M}-\text{H}]^+$, $[\text{M}+\text{H}]^+$, and $[\text{M}-\text{OH}]^+$ species have been observed.^{111, 114} The effect of DBDI on terpenes has been little studied. A study conducted by Liu et al. found the formation of $[\text{M}+\text{H}+\text{H}_2\text{O}]^+$ and $[\text{M}+\text{H}-\text{H}_2\text{O}]^+$ adducts

for limonene and linalool, respectively. Their total study was however limited to four terpenes.¹¹⁵ A larger study conducted by Weber et al. analysed the effect of different dopants on the adduct formation of 21 terpenes. For non-oxygenated terpenes, the $[M+H]^+$ adduct was predominantly observed under all conditions, in contrast to oxygenated terpenes, which predominantly formed $[M-OH]^+$ adducts. Room air provided the highest ionisation efficiency.¹¹⁶ Direct and rapid analysis using DBDI offers a novel method that does not necessarily require upstream coupling to chromatography.^{21, 117} For example, in a study by Massaro et al., the authenticity of monofloral honeys was determined by DBDI-HRMS. However, their analysis required subsequent chemometric analysis.¹¹⁷ DBDI coupled to MS provides a high-throughput approach, generating large data sets that in turn require sophisticated computational methods for further evaluation.

1.6. Chemometrics and computational analysis

High-throughput techniques have become commonplace in the analytical laboratory. A variety of modern techniques such as ambient ionisation coupled to MS, ultra-high performance LC, fast GC and the development of portable spectral and hyperspectral imaging devices have led to the acquisition of large chemical data sets in seconds to minutes. High-throughput methods are used in a variety of areas including biomarker and drug discovery, real-time analysis during quality control and forced degradation studies.^{21, 94, 118, 119} The bottleneck is no longer necessarily the analytical methods or the data acquisition, but the processing, handling and interpretation of the data, which can be time-consuming.¹²⁰ Recent advances in computer science and software engineering have provided an extensive toolbox to address these challenges, but require a deep understanding of the underlying algorithms and data structures in order to use them successfully.¹²¹ Chemometrics, in particular, deals with the extraction of relevant information from chemical datasets and today lies at the intersection of (multivariate) statistics, numerical analysis, machine learning, and deep learning.¹²²⁻¹²⁴ Pre-processing is a crucial first step in chemometric data analysis after data acquisition. Correct pre-processing can be essential for further analysis and has the primary goal of removing unwanted variation such as instrumental and experimental artefacts.¹²⁰ It also deals with scaling discrepancies in variables, normalisation, missing values, outlier detection, and chromatographic variations such

as baseline drifts and retention time shifts. Pre-processing steps are highly dependent on the nature of the instrumental data and require individual workflows. For example, Fourier Transform Infrared (FT-IR) spectroscopy measures the absorption of a chemical substance and can suffer from light scattering artefacts. To overcome this, standard normal variate (SNV) or robust normal variate (RNV) can be applied. In LC or GC-MS experiments, analyte co-elution and overlapping of isotopic patterns can occur, requiring both improved peak resolution and deconvolution. Various algorithms have been developed to address these challenges, including Multivariate Curve Resolution-Alternating Least Squares (MCR-ALS), Parallel Factor Analysis 2 (PARAFAC2), and deep learning models. The Savitzky-Golay algorithm, for example, is used for noise correction by applying polynomials to smooth data. The order, in which pre-processing methods should be applied, is not predetermined. Instead, it has become common practise to test a selection of pre-processing methods by trial and error and to evaluate prediction models through metrics such as root mean square error of prediction (RMSEP) and root mean square error of cross validation (RMSECV).^{120, 125-129} Not only should different pre-processing methods be tested, but it is also advisable to include raw data alone in the prediction model. There is a risk that pre-processing methods can eliminate essential variance, rather than simply improving data quality.^{130, 131} After pre-processing the raw data, chemometric analysis can be performed. Chemometrics can be used to answer a wide range of analytical questions. It includes regression analysis for prediction, classification, and discrimination methods. Additionally, chemometrics is used for clustering, pattern recognition, and quantitative measurements such as calibration. The overall goal of chemometrics is to uncover hidden information, e.g. by extracting variables for biomarker discovery and dimension reduction.¹³²⁻¹³⁴ Rapid data collection has enabled the measurement of the same sample using multiple analytical techniques in a short amount of time. Since these techniques such as FT-IR and DBDI-MS capture different properties of the molecular composition of an analyte, they can provide complementary information. This development has led to the rise of data fusion and multi-block analysis, a recent advancement in chemometrics.¹³⁵ These novel techniques have been primarily driven by the food sector, as food fraud is a major economic and public health challenge.¹³⁶ Current chemometric tools do not exploit the full range of information captured by using multiple data acquisition methods. Efforts have been made to overcome this challenge by developing novel algorithms.

Sequential and Orthogonalised Partial Least-Squares Linear Discriminant Analysis (SO-PLS-LDA) is a prediction model designed to extract complementary data from multi-modal datasets. The algorithm uses Fisher's linear classifier to separate two or more classes (e.g. true and false or dogs, cats and birds). However, LDA requires a well-conditioned covariance matrix, which can be generated by using PLS for dimensionality reduction. PLS transforms the original multivariate data into a smaller number of latent orthogonal variables by maximising the covariance. Because data fusion combines two or more blocks of data (e.g. MS and FT-IR data), parts of the information contained in the data blocks may be redundant. By sequentially orthogonalising one data block to the other, unique information can be extracted. The SO-PLS-LDA model is just one of many strategies for extracting complementary information from high-dimensional data derived from different sources.¹³⁷⁻¹⁴⁴ Data fusion not only requires specialised algorithms to extract unique information, but also presents new challenges for pre-processing. Different data fusion levels are possible ranging from low, mid to high. Mid-level strategies include preceding feature/variable extraction steps (e.g., SO-PLS), while high-level strategies incorporate results obtained from separate models calculated for each block. As data from different sources are combined, the datasets will not have the same scale. Some multi-block methods, such as Multi-Block Principal Component Analysis (MB-PCA) and Multi-Block Partial Least-Squares regression (MB-PLS), cannot be applied unless the scale is adjusted. However, other methods such as SO-PLS have been developed to be scale invariant.^{145, 146} Multi-block and data fusion strategies have the advantage of providing improved classification efficiency compared to their single-block counterparts, as demonstrated in numerous publications.¹⁴⁷⁻¹⁵⁴

Aim of the thesis

This thesis aims to address three main aspects: separation, detection and computational analysis of secondary metabolites found in plants, with emphasis on terpenes. The overall aim is to provide a *detailed* and *holistic* characterisation of natural products that can be used to assess authenticity, origin, ageing, cultivar, and chemovar classification and/or standardisation as herbal medicines.

Hypothesis 1:

The chromatographic analysis of minor and major components, along with the enantiomeric and diastereomeric distribution provides valuable information on the authenticity, origin, ageing, and/or chemovar of a natural product.

Hypothesis 2:

MS is a suitable detection method for the holistic characterisation of natural products and stands out for its speed. Coupling MS with different ionisation techniques such as EI, APCI, and DBDI allows for a broad coverage of different secondary metabolites in plants.

Hypothesis 3:

Chemometrics, along with data fusion from different analytical sources, enhances the classification performance of predictive models. The combination of MS and chemometrics eliminates the need for time-consuming chromatography.

Elucidating the chemical structure of natural products such as terpenes is challenging due to their related structures and complex stereochemistry. As their composition is not the result of random synthesis but rather a consequence of evolutionary pressures, understanding the precise composition can serve as a molecular fingerprint. Furthermore, given the continuing importance of natural products as a valuable source of pharmacophores in drug discovery, novel, reliable, rapid, and robust analytical methods are required to bring them to light.

Chapter 1: Separation Techniques for Terpenes Covering Minor, Major, and Chiral components

This chapter forms part of the following publications:

1. **Raeber J**, Favrod S, Steuer C. Determination of Major, Minor and Chiral Components as Quality and Authenticity Markers of *Rosa damascena* Oil by GC-FID. *Plants* 2023; 12. DOI: 10.3390/plants12030506.

Contributions:

JR: conceptualisation, method development and validation, experimental design, data acquisition, analysis and data interpretation, investigation, software development. **SF**: software development. **CS**: supervision, data analysis, reviewing, resources, conceptualisation.

Licencing:

This article has been published under the terms of the Creative Commons CC-BY 4.0 DEED licence (<https://creativecommons.org/licenses/by/4.0/>), which allows its unrestricted use, provided it is properly cited.

2. **Raeber J**, Poetzsch M, Schmidli A, Favrod S, Steuer C. Simultaneous quantification of terpenes and cannabinoids by reversed-phase LC-APCI-MS/MS in *Cannabis sativa* L. samples combined with a subsequent chemometric analysis. *Analytical and Bioanalytical Chemistry* 2024. DOI: 10.1007/s00216-024-05349-y.

Contributions:

JR: conceptualisation, method development and validation, investigation, experimental design, data acquisition, analysis and data interpretation. **MP**: sample preparation, data interpretation and analysis. **AS**: chromatographic method development. **SF**: sample preparation and method development. **CS**: supervision, data analysis, reviewing, resources, conceptualisation.

Licencing:

This article has been published under the terms of the Creative Commons CC-BY 4.0 DEED licence (<https://creativecommons.org/licenses/by/4.0/>), which allows its unrestricted use, provided it is properly cited.

3. **Raeber J**, Bajor B, Poetzsch M, Steuer C. Comprehensive analysis of chemical and enantiomeric stability of terpenes in *Cannabis sativa* L. flowers. *Phytochemical Analysis* 2024; 1-13. DOI:10.1002/pca.3432.

Contributions: **JR**: experimental design, method development, method validation, data acquisition, data analysis, conceptualisation, writing, editing. **BB**: authentic sample data acquisition, authentic sample preparation, data analysis of authentic samples, reviewing. **MP**: resources, editing, reviewing. **CS**: conceptualisation, writing, editing, resources, reviewing.

Licencing:

This article has been published under the terms of the Creative Commons CC-BY 4.0 DEED licence (<https://creativecommons.org/licenses/by/4.0/>), which allows its unrestricted use, provided it is properly cited.

2.1. Determination of Major, Minor and Chiral Components as Quality and Authenticity Markers of *Rosa damascena* Oil by GC-FID

2.1.1. Results and discussion

R. damascena EO is obtained through steam distillation of fresh flowers, which contain relatively low amounts of EOs.¹⁰ There is a significant demand for reliable and robust methods to quantify *R. damascena* EO due to its high economic value, which makes it susceptible to adulteration. ISO 9842:2003, a standardisation norm for *R. damascena* EO, describes the acquisition of a chromatographic profile using GC-FID that includes the analytes ethanol, citronellol, nerol, geraniol, β -phenylethanol, heptadecane, nonadecane, and heneicosane. It further distinguishes different relative terpene concentrations in flowers sourced from Bulgaria, Turkey, and Morocco.¹⁵⁵ In particular, citronellol, geraniol, nerol, and linalool are known to be abundant and common compounds in *R. damascena* EO, accounting for up to 60% of the EO. Although they make up the majority of the oil's volume, minor compounds such as β -damascenone and rose oxide are considered important contributors to the characteristic smell of rose oil and are not covered by the ISO norm.¹⁵⁶ GC-FID was selected as the method of choice based on the ISO standard. Two methods based on a polar DB-wax column and a BGB 178 30% CD chiral column with a run time below 60 minutes were developed. 22 analytes were successfully separated including the enantiomers of camphene, cis-rose oxide, linalool, citronellol, and citronellyl acetate as well as the two diastereomers of citral and β -damascenone. The identity of the analytes in authentic *R. damascena* EO samples was further confirmed by GC-EI-MS experiments to exclude co-elution. The full chromatographic profile of a standard analysed on the DB-wax column and the BGB 178 30% CD chiral column is shown in Figures 7 and 8, respectively.

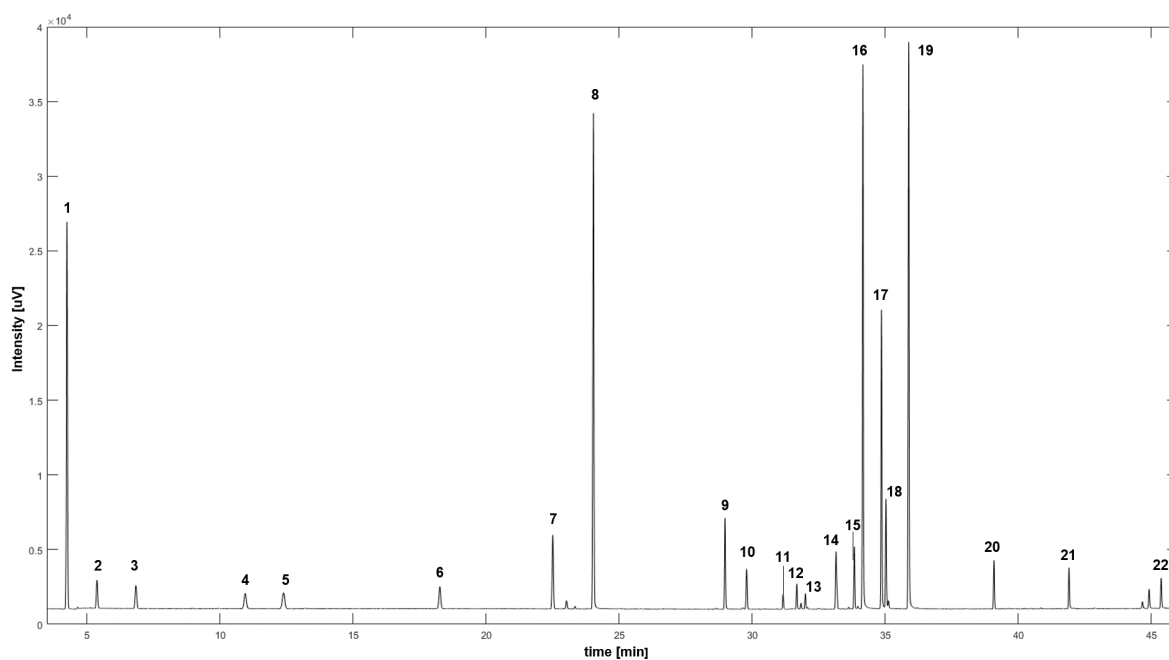


Figure 7: Chromatographic profile of 22 analytes including the IS separated on a DB-wax column with GC-FID. Figure adapted from Raeber et al.¹⁰

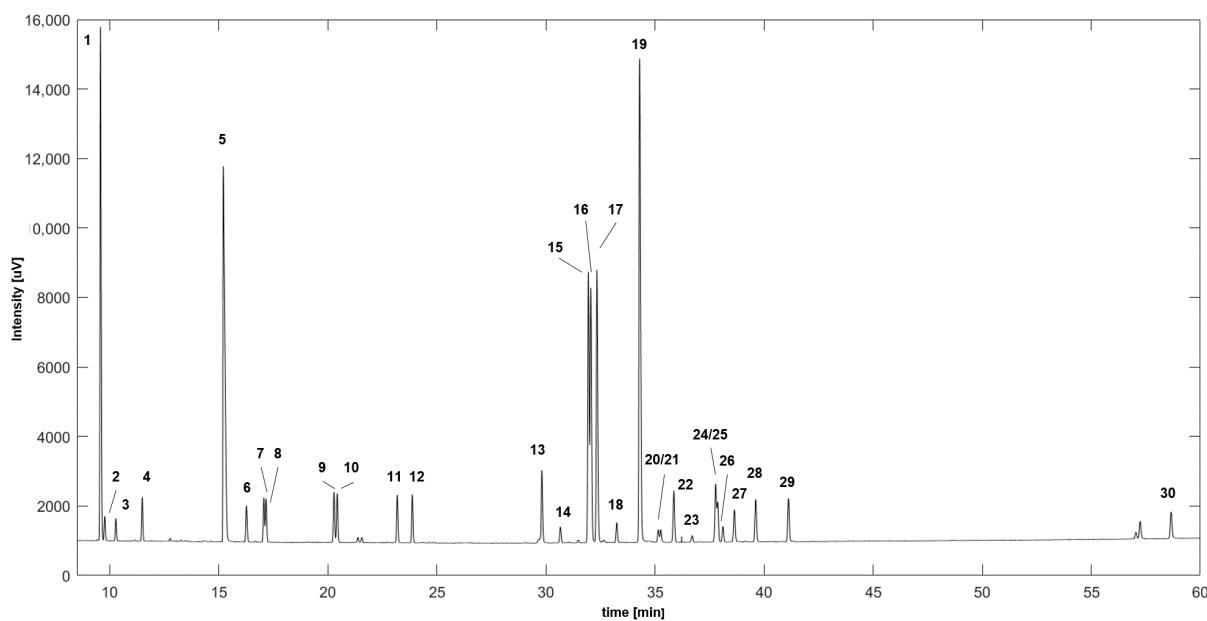


Figure 8: Chromatographic profile of 30 analytes including the IS separated on a BGB 178 30% CD column with GC-FID. Figure adapted from Raeber et al.¹⁰

The method development on the DB-Wax column achieved a baseline separation with a resolution (R_s) > 2.4 for all analytes. The Limit of Detection (LoD) ranged from 0.96 to 4.55 ng, while the Limit of Quantification (LoQ) ranged from 2.90 to 13.78 ng, reflecting the high sensitivity of FID as a detection method. Method validation was conducted over five individual days. Accuracy was assessed in terms of bias and

found to be in the range of $\pm 15\%$. Precision was evaluated in terms of intra- (RSD_T) and interday (RSD_R) imprecision and found to be below the cut-off of $\pm 20\%$. The results of the method validation of the DB-wax column are shown in Table 1. The stability of the calibration was evaluated by calculating the concentration of the quality control (QC) samples over these five validation days, using the calibration from the first validation day. Results are shown in Figure A3 in the Appendix. Calibration functions and plots can be viewed in Figure A5 in the Appendix.

The method development on the BGB 178 30% chiral column achieved a separation of 30 analytes with a $R_s > 0.7$. Complete peak separation is expected at a $R_s > 1.5$, however following the Gaussian distribution, a R_s value of 0.7 corresponds to a peak overlap of 8%. Although complete separation was not achieved, results from validation and spiking experiments confirmed reliable quantification (Table 2). The LoD ranged from 0.03 to 1.28 ng, while the LoQ ranged from 0.10 to 3.75 ng. The bias, RSD_T and RSD_R were found to be in the range of $\pm 15\%$. The stability of the calibration can be studied in Figure A4 in the Appendix. In contrast to the analysis using the DB-wax column, no literature RI values were available for comparison with the BGB 178 30% column. Calibration functions and plots can be viewed in Figure A6 in the Appendix.

Table 1: Results of the method validation of the DB-Wax column. Resolution (R_s), Retention Time (RT), Retention Index (RI) and Quality Control (QC) are abbreviated. Accuracy is presented as the bias [%], intra- (RSD_T) and interday (RSD_R) imprecision. Numbering is corresponding to Figure 7. Table adapted from Raeber et al.¹⁰

#	Analyte	R_s	RT [min]	Range [$\mu\text{g/mL}$]	LoD/LoQ [ng]	$RI_{\text{Cal}}/RI_{\text{Lit}}^{157-168}$	QC _{high}			QC _{med}			QC _{low}		
							Bias [%]	RSD_R [%]	RSD_T [%]	Bias [%]	RSD_R [%]	RSD_T [%]	Bias [%]	RSD_R [%]	RSD_T [%]
1	α -pinene	16.1	4.2 \pm 0.0	6 - 620	0.96/2.90	1013/1013	5.2	9.4	9.5	4.4	7.4	8.2	13.2	4.0	5.1
2	camphene	12.3	5.4 \pm 0.0	1 - 60	1.30/3.94	1048/1053	-6.2	8.6	8.4	2.3	9.9	9.4	3.9	9.9	10.8
3	β -pinene	22.7	6.8 \pm 0.0	1 - 60	1.27/3.85	1096/1096	2.4	7.8	8.8	1.8	9.6	8.5	11.2	8.8	8.4
4	α -terpinene	6.0	11.0 \pm 0.0	1 - 70	1.48/4.49	1159/1159	-2.9	7.0	10.0	-0.8	10.4	14.1	4.0	10.8	10.1
5	limonene	28.3	12.4 \pm 0.0	1 - 70	1.53/4.46	1166/1176	2.4	11.8	13.1	-0.2	10.1	15.3	6.8	9.5	9.2
6	p-cymene	34.1	18.3 \pm 0.0	1 - 60	1.42/4.31	1264/1268	2.1	12.1	12.6	-2.6	12.9	12.0	7.2	6.4	7.1
7	cis-rose oxide	17.6	22.5 \pm 0.0	2 - 200	1.65/4.99	1344/1339	1.1	11.4	12.5	3.5	11.5	13.1	9.9	7.0	8.8
8	cis-hexen-1-ol	85.8	24.0 \pm 0.0	NA	NA	NA	NA	NA	NA	NA	NA	NA	NA	NA	NA
9	linalool	11.3	29.0 \pm 0.0	3 - 160	1.89/5.71	1383/1380	-13.1	12.2	9.9	-14.0	9.2	10.2	-7.1	13.6	11.9
10	β -caryophyllene	16.8	29.8 \pm 0.0	1 - 60	2.59/7.84	1550/1548	2.1	14.6	11.0	2.1	16.3	13.2	1.2	9.4	12.5
11	β -damascenone	6.3	31.2 \pm 0.0	10 - 1000	1.80/5.44	1582/1586	3.7	14.2	10.9	0.4	10.9	10.0	-0.9	8.3	12.3
12	citronellyl acetate	4.0	31.7 \pm 0.0	1 - 60	2.71/8.21	1636/1803	3.1	14.0	11.0	1.0	14.3	11.0	-3.6	4.7	13.1
13	citral	14.2	32.0 \pm 0.0	1 - 55	2.40/7.27	1659/1658	-0.9	9.2	8.8	1.7	14.0	11.6	-7.8	14.3	16.0
14	neryl acetate	8.5	33.2 \pm 0.0	1 - 100	1.94/5.87	1671/1678	2.6	10.4	11.2	3.8	11.8	13.1	2.7	8.3	9.7
15	geranyl acetate	4.8	33.8 \pm 0.0	1 - 100	1.94/5.93	1722/1719	3.4	13.2	10.1	3.3	17.3	13.3	0.5	10.7	8.1
16	citronellol	10.6	34.6 \pm 0.0	10 - 1000	1.73/5.24	1754/1746	4.1	10.9	8.9	2.9	15.3	13.6	5.9	10.0	10.3
17	nerol	2.4	34.9 \pm 0.0	5 - 500	2.18/6.61	1768/1755	3.0	9.4	10.1	3.4	15.1	13.5	4.9	10.1	8.5
18	phenylethanol	13.0	35.0 \pm 0.0	1 - 120	1.84/5.58	1800/1798	4.4	7.4	8.9	7.9	11.1	9.6	9.2	6.1	5.7
19	geraniol	44.0	35.9 \pm 0.0	10 - 1000	1.99/6.02	1806/1875	4.0	10.5	9.7	3.3	15.2	13.5	6.4	10.2	10.9
20	methyleugenol	38.6	39.1 \pm 0.0	3 - 120	3.06/9.28	1848/1841	3.5	13.0	10.5	0.5	12.0	14.2	-1.0	7.5	9.6
21	eugenol	47.6	41.9 \pm 0.0	1 - 120	3.19/9.68	2008/2001	3.6	10.8	11.7	4.3	11.4	12.4	2.4	8.6	10.8
22	farnesol	NA	45.4 \pm 0.0	1 - 100	4.55/13.78	2161/2167	1.4	9.7	9.9	-2.0	5.2	9.7	2.5	18.0	13.8

Table 2: Results of the method validation of the chiral column. Resolution (Rs), Retention Time (RT), Retention Index (RI) and Quality Control (QC) are abbreviated. Accuracy is presented as the bias [%], intra- (RSD_T) and interday (RSD_R) imprecision. Numbering is corresponding to Figure 8. Table adapted from Raeber et al.¹⁰

#	Analyte	R _s	RT [min]	Range [µg/mL]	LoD/LoQ [ng]	RI _{Cal}	QC _{high}			QC _{med}			QC _{low}		
							Bias [%]	RSD _R [%]	RSD _T [%]	Bias [%]	RSD _R [%]	RSD _T [%]	Bias [%]	RSD _R [%]	RSD _T [%]
1	(+)-α-pinene	2.4	9.58 ± 0.00	6 - 620	0.35/1.07	927	-1.3	2.5	4.9	-1.5	2.1	3.8	10.4	2.4	5.3
2	(+/-)-camphene 1	5.9	9.77 ± 0.00	3 - 57	0.63/1.90	931	7.0	4.5	4.5	0.6	5.1	4.5	5.6	5.5	6.0
3	(+/-)-camphene 2	12.0	10.27 ± 0.00	3 - 57	0.59/1.79	942	-3.6	4.2	4.7	-6.8	2.3	6.2	0.5	4.3	8.6
4	(-)-β-pinene	28.6	11.49 ± 0.00	3 - 56	0.60/1.81	967	4.1	2.6	6.8	2.3	1.9	4.4	11.5	3.7	3.9
5	cis-3-hexen-1-ol	8.3	15.21 ± 0.00	NA	NA	NA	NA	NA	NA	NA	NA	NA	NA	NA	NA
6	α-terpinene	7.9	16.26 ± 0.00	3 - 62	0.54/1.63	1057	1.8	2.8	2.8	-2.7	2.6	4.0	3.9	3.8	8.9
7	limonene	1.2	17.06 ± 0.00	3 - 62	0.73/2.22	1071	4.3	3.2	7.5	4.0	1.8	3.7	12.8	6.6	6.8
8	p-cymene	30.6	17.16 ± 0.00	3 - 56	0.73/2.22	1073	6.4	2.4	3.0	1.7	1.5	2.9	5.8	5.0	5.4
9	(+)-cis-rose oxide 1	1.5	20.28 ± 0.00	10 - 199	0.75/2.27	1126	0.3	2.7	3.5	1.2	1.8	2.6	11.5	5.1	4.1
10	(-)-cis-rose oxide 2	27.1	20.43 ± 0.00	10 - 199	0.79/2.39	1129	0.8	2.8	3.6	1.3	1.0	2.5	10.9	5.2	4.7
11	(-)-linalool	6.7	23.18 ± 0.00	3 - 166	0.63/1.90	1175	-0.3	3.0	3.5	0.4	1.9	2.5	11.4	4.8	3.9
12	(+)-linalool	58.4	23.87 ± 0.00	3 - 166	0.52/1.57	1186	-0.6	3.2	4.0	-0.2	1.5	2.6	11.4	4.6	3.6
13	phenylethanol	6.7	29.82 ± 0.00	2 - 122	0.44/1.32	1286	-4.4	4.1	5.4	-4.8	2.6	3.7	9.9	6.5	6.7
14	cis-citral	9.0	30.66 ± 0.00	3 - 64	0.74/2.25	1300	-3.3	4.4	3.6	-4.7	3.8	3.5	8.9	5.3	5.7
15	(+/-)-citronellol 1	0.9	31.95 ± 0.00	10 - 994	0.63/1.90	1321	-6.9	6.0	4.6	-7.2	3.9	3.3	7.1	6.2	8.6
16	(+/-)-citronellol 2	2.2	32.06 ± 0.00	10 - 994	0.85/2.57	1323	-4.7	5.5	5.7	-5.8	3.8	4.1	9.8	6.7	5.6
17	nerol	7.7	32.35 ± 0.00	5 - 507	0.42/1.29	1328	2.9	3.1	2.9	2.3	1.8	2.3	9.6	9.6	8.5
18	trans-citral	7.3	33.26 ± 0.00	3 - 64	0.72/2.18	1344	-1.8	4.9	4.9	-3.5	3.7	3.9	9.4	8.3	7.6
19	geraniol	5.9	34.30 ± 0.00	10 - 1006	0.43/1.29	1361	-3.3	5.8	5.7	-5.7	4.0	4.1	7.2	7.6	6.1
20	(+/-)-citronellyl acetate 1	0.8	35.16 ± 0.00	8 - 54	1.18/3.58	1376	-4.6	4.5	5.5	-10.3	5.8	5.8	1.6	5.7	8.6
21	(+/-)-citronellyl acetate 2	4.1	35.27 ± 0.00	8 - 54	1.24/3.75	1378	0.3	3.6	5.2	-4.6	6.0	4.5	5.6	3.4	6.0
22	neryl acetate	6.5	35.87 ± 0.00	2 - 110	0.57/1.73	1388	0.7	4.3	4.4	-0.3	2.1	2.3	9.3	6.3	4.6

23	(cis/trans)- β -damascenone 1	8.4	36.70 \pm 0.00	51 - 1014	1.28/3.89	1402	-1.0	6.5	5.1	3.6	4.8	4.6	9.2	4.1	5.5
24	geranyl acetate	0.7	37.78 \pm 0.00	6 - 127	0.85/2.57	1421	1.5	4.9	5.6	0.6	4.2	6.4	4.4	7.3	9.9
25	β -caryophyllene	1.9	37.87 \pm 0.00	3 - 67	0.82/2.49	1423	-4.9	4.5	5.4	-2.2	2.3	3.0	9.9	7.3	5.7
26	(cis/trans)- β -damascenone 2	4.0	38.11 \pm 0.00	51 - 1014	0.75/2.27	1427	6.8	3.6	3.1	5.7	2.8	5.1	13.3	2.9	4.2
27	β -damascone	7.6	38.64 \pm 0.00	1 - 66	0.77/2.34	1436	-1.1	5.2	4.6	-2.5	2.1	3.5	7.5	7.5	6.5
28	eugenol	11.6	39.61 \pm 0.00	3 - 123	0.64/1.95	1453	-0.2	4.7	4.5	-1.9	2.5	2.9	7.9	5.2	4.1
29	methyleugenol	76.1	41.11 \pm 0.00	2 - 115	0.03/0.10	1479	0.3	4.4	4.1	0.5	2.4	2.9	7.6	4.1	4.6
30	farnesol	NA	58.67 \pm 0.00	6 - 123	0.79/2.39	1802	2.7	8.5	10.1	-0.3	2.7	4.3	2.8	5.1	6.2

Spiking experiments showed satisfactory results for both the DB-wax and the BGB 178 30% columns. The recovery excess (RE) did not exceed 20% (Table 3 and 4) for authentic rose oils. Spiking experiments for EOs derived from other species showed mixed results. For example, the RE for linalool showed satisfactory results for one enantiomer but was overestimated for the other in lavender oil. This can be traced back to the inherent concentration of linalool in lavender oil, as it is the major component and is outside the calibration range used in this study. Furthermore, and this can be observed for the majority of plants, one enantiomer of linalool was predominant, underlining the significance of stereoselective synthesis in plants. In lavender oil in particular, Krupčík and colleagues found an EE of 88% in favour of (-)-linalool.^{169, 170} A satisfactory recovery of the spiked QC_{med} concentration was therefore not possible for linalool. The same phenomenon was observed for limonene in lemon oil. The limonene peak in lemon oil was so broad, that it co-eluted with the spiked p-cymene. In addition, caraway oil contained high concentrations of limonene, which led to an overestimation of the RE value for both limonene and p-cymene. Overall, however, the method was successfully transferred to the analysis of other EOs and by adjusting the dilution factors, the split factor and/or the calibration range, successful analysis of other oils is possible. Chromatograms from these spiking experiments are available in Figure A1-A2 in the Appendix. To determine the recovery rates of particularly high and particularly low concentrations, authentic *R. damascena* oil samples were spiked with concentrations in the QC_{high} and QC_{low} ranges. The RE was determined to be below 20%. This confirmed the suitability of the chosen concentration range and the reliability of recovering both high and low concentrations in the oil of interest. Finally, the robustness of the method was confirmed by adjusting the split ratio, FID and inlet temperature parameters, flow rate and temperature ramp. Changes in the chromatogram were as expected: adjustment of these parameters resulted in changes in peak intensities for the adjusted split ratios, FID and inlet temperatures. Changing the temperature ramp and flow led to changes in retention time. An extensive list can be found in the Appendix in Tables A2-A3.

Table 3: Results for spiking experiments using the DB-wax column. Abbreviations are as follows: recovery excess (RE), authentic rose oil (RO), Bulgaria (BG), Morocco (MA) and Turkey (TR). Values, which were out of range, are marked in grey. Table taken from Raeber et al.¹⁰

Analyte	RE Authentic RO		RE RO _{BG} [%] (n=3)	RE RO _{MA} [%] (n=3)	RE RO _{TR} [%] (n=3)	RE RO _{real} [%] (n=3)	RE Lavender [%] (n=3)	RE Rosemary [%] (n=3)	RE Lemon [%] (n=3)	RE Caraway [%] (n=3)
	[%] (n=5)									
	QC _{high}	QC _{low}								
α-pinene	104.5 ± 9.8	110.0 ± 3.2	94.6 ± 2.0	99.5 ± 7.3	87.8 ± 2.2	92.5 ± 1.2	99.0 ± 2.7	111.3 ± 4.7	98.6 ± 1.5	101.7 ± 3.1
camphene	107.1 ± 8.4	107.3 ± 12.9	104.4 ± 4.4	111.2 ± 3.3	101.3 ± 3.5	109.3 ± 4.5	104.3 ± 2.3	133.3 ± 9.4	119.2 ± 4.8	110.9 ± 0.0
β-pinene	107.2 ± 11.7	119.9 ± 3.9	95.3 ± 3.0	99.1 ± 9.5	86.5 ± 3.5	91.2 ± 3.0	90.6 ± 7.5	142.0 ± 14.6	133.3 ± 11.5	103.0 ± 3.5
α-terpinene	106.5 ± 15.7	88.3 ± 10.3	91.9 ± 1.7	98.3 ± 9.2	86.6 ± 3.1	89.9 ± 2.6	95.7 ± 1.6	105.6 ± 4.5	101.6 ± 1.7	105.0 ± 5.7
limonene	104.7 ± 13.6	84.2 ± 5.9	89.6 ± 1.7	99.5 ± 10.7	82.6 ± 4.0	90.2 ± 1.5	91.6 ± 2.3	126.6 ± 13.0	259.3 ± 10.8	568.4 ± 131.2
p-cymene	104.6 ± 12.9	114.0 ± 6.1	94.3 ± 2.8	98.1 ± 9.9	90.2 ± 1.5	88.1 ± 1.6	104.4 ± 4.0	116.2 ± 8.1	97.6 ± 0.5	107.9 ± 5.3
rose oxide	103.7 ± 16.7	114.6 ± 5.6	90.7 ± 1.9	85.7 ± 2.7	80.0 ± 1.8	84.2 ± 3.0	96.0 ± 2.4	101.9 ± 4.4	92.7 ± 0.4	103.4 ± 5.5
cis-hexen-1-ol	NA	NA	NA	NA	NA	NA	NA	NA	NA	NA
linalool	104.1 ± 16.8	99.4 ± 8.6	85.9 ± 3.0	94.1 ± 6.7	83.2 ± 2.2	84.8 ± 3.4	93.8 ± 6.8	104.5 ± 6.0	93.0 ± 1.2	103.9 ± 5.5
β-caryophyllene	95.5 ± 16.2	97.2 ± 15.9	80.5 ± 1.2	85.3 ± 7.5	100.2 ± 2.0	82.5 ± 6.9	73.3 ± 2.1	123.0 ± 26.2	85.5 ± 1.7	104.2 ± 5.1
β-damascenone	94.6 ± 16.6	103.5 ± 3.7	87.5 ± 7.8	85.1 ± 5.7	87.5 ± 1.7	85.7 ± 4.6	92.8 ± 0.8	105.5 ± 14.2	99.2 ± 8.4	111.9 ± 6.6
citronellyl acetate	96.7 ± 13.6	116.5 ± 14.5	81.9 ± 0.9	92.2 ± 5.6	82.8 ± 1.2	83.6 ± 3.7	95.9 ± 0.3	110.2 ± 10.9	101.8 ± 8.9	111.8 ± 8.5
citral	102.6 ± 16.5	119.2 ± 9.3	86.1 ± 7.4	85.1 ± 8.3	87.7 ± 1.5	83.1 ± 9.0	91.2 ± 2.3	108.6 ± 9.3	112.7 ± 4.7	107.6 ± 7.4
neryl acetate	93.2 ± 14.5	115.5 ± 13.5	85.0 ± 1.8	92.8 ± 8.0	81.4 ± 0.5	84.3 ± 6.7	92.6 ± 0.1	105.2 ± 7.7	105.1 ± 0.6	750.9 ± 161.1
geranyl acetate	106.9 ± 12.1	103.2 ± 11.8	81.7 ± 2.7	81.1 ± 4.5	93.5 ± 1.8	84.8 ± 8.6	115.6 ± 0.8	92.9 ± 3.4	82.4 ± 8.8	90.6 ± 5.0
citronellol	110.2 ± 9.5	82.6 ± 18.8	109.6 ± 3.6	88.8 ± 5.5	87.0 ± 2.6	113.3 ± 10.2	92.9 ± 0.8	98.5 ± 6.4	87.9 ± 0.0	101.9 ± 6.4
nerol	93.9 ± 17.7	104.3 ± 10.0	104.1 ± 3.2	92.7 ± 4.9	92.8 ± 1.6	88.1 ± 6.5	95.3 ± 0.4	96.8 ± 6.3	93.1 ± 6.7	100.2 ± 6.2
phenylethanol	103.6 ± 17.4	119.1 ± 9.3	101.4 ± 4.2	98.6 ± 5.1	85.0 ± 1.0	95.5 ± 4.4	105.5 ± 0.4	109.7 ± 6.1	101.2 ± 2.4	109.0 ± 5.2
geraniol	93.9 ± 16.3	110.7 ± 11.0	103.2 ± 3.2	83.9 ± 4.8	87.3 ± 1.4	82.3 ± 7.1	89.5 ± 1.2	94.6 ± 6.7	84.1 ± 0.1	98.5 ± 6.4
methyleugenol	91.8 ± 18.0	90.8 ± 10.1	81.9 ± 1.8	83.0 ± 5.5	82.0 ± 2.9	85.3 ± 11.4	90.5 ± 0.4	97.6 ± 7.3	83.7 ± 1.0	104.5 ± 5.9
eugenol	110.5 ± 11.1	100.8 ± 14.7	104.7 ± 1.3	92.4 ± 3.2	96.7 ± 1.1	99.9 ± 4.5	95.4 ± 0.6	107.9 ± 14.2	93.9 ± 0.7	115.1 ± 8.8
farnesol	87.5 ± 30.1	96.0 ± 17.8	97.6 ± 4.7	89.5 ± 15.7	116.3 ± 15.7	88.1 ± 9.8	99.1 ± 2.8	110.9 ± 12.2	101.6 ± 7.1	125.3 ± 10.9

Table 4: Results for spiking experiments using the BGB 178 30% column. Abbreviations are as follows: recovery excess (RE), authentic rose oil (RO), Bulgaria (BG), Morocco (MA) and Turkey (TR). Values, which were out of range, are marked in grey. Table taken from Raeber et al.¹⁰

Analyte	RE Authentic RO		RE RO _{BG}	RE RO _{MA}	RE RO _{TR}	RE RO _{real}	RE Lavender	RE Rosemary	RE Lemon	RE Caraway							
	[%] (n=5)										[%] (n=3)	[%] (n=3)	[%] (n=3)	[%] (n=3)	[%] (n=3)	[%] (n=3)	[%] (n=3)
	QC _{high}	QC _{low}															
(+)- α -pinene	91.2 \pm 0.9	88.0 \pm 0.8	87.7 \pm 0.2	92.2 \pm 0.8	89.3 \pm 0.5	92.4 \pm 4.1	94.4 \pm 8.4	96.5 \pm 3.3	90.7 \pm 0.9	87.8 \pm 2.9							
(+/-)-camphene 1	100.2 \pm 1.6	118.3 \pm 3.2	104.7 \pm 1.4	109.2 \pm 1.5	104.3 \pm 2.2	111.6 \pm 1.3	116.0 \pm 6.5	116.3 \pm 5.8	117.3 \pm 4.8	100.4 \pm 1.9							
(+/-)-camphene 2	91.7 \pm 6.3	107.3 \pm 3.5	92.0 \pm 4.3	98.0 \pm 1.0	91.9 \pm 1.5	95.3 \pm 4.3	104.6 \pm 12.4	98.7 \pm 12.4	94.3 \pm 4.5	87.1 \pm 5.5							
(-)- β -pinene	91.1 \pm 1.8	105.3 \pm 10.5	91.6 \pm 1.1	96.6 \pm 0.8	93.4 \pm 0.4	95.6 \pm 4.7	100.3 \pm 9.6	105.4 \pm 11.4	83.5 \pm 18.0	89.0 \pm 3.3							
cis-3-hexen-1-ol	NA	NA	NA	NA	NA	NA	NA	NA	NA	NA							
α -terpinene	91.9 \pm 1.5	100.8 \pm 2.6	91.9 \pm 4.2	92.5 \pm 4.6	89.6 \pm 1.5	94.8 \pm 3.0	93.9 \pm 6.2	99.2 \pm 12.8	95.6 \pm 7.7	90.8 \pm 3.4							
limonene	99.7 \pm 4.8	119.8 \pm 2.9	88.5 \pm 1.9	101.5 \pm 7.5	91.1 \pm 2.4	97.2 \pm 4.9	98.1 \pm 4.6	108.2 \pm 24.3	54.6 \pm 101.9	229.5 \pm 102.2							
p-cymene	97.2 \pm 3.9	116.1 \pm 1.9	89.8 \pm 1.3	89.7 \pm 3.0	90.6 \pm 0.9	88.8 \pm 1.8	86.1 \pm 18.8	87.7 \pm 13.3	36.7 \pm 7.4	252.1 \pm 420.3							
(+)-cis-rose oxide	96.4 \pm 2.0	106.5 \pm 5.9	88.7 \pm 0.7	96.7 \pm 1.4	91.5 \pm 0.1	96.6 \pm 4.7	93.6 \pm 6.2	103.0 \pm 3.1	92.0 \pm 4.0	107.7 \pm 6.0							
(-)-cis-rose oxide	98.7 \pm 1.6	112.6 \pm 5.1	91.4 \pm 1.2	96.5 \pm 2.1	93.6 \pm 0.3	97.4 \pm 3.7	93.6 \pm 1.8	96.9 \pm 1.8	94.1 \pm 4.3	95.5 \pm 3.6							
(-)-linalool	95.1 \pm 1.5	87.5 \pm 3.9	86.5 \pm 1.5	91.3 \pm 1.2	88.4 \pm 1.7	93.7 \pm 7.5	128.5 \pm 88.5	97.4 \pm 2.6	94.4 \pm 3.1	89.9 \pm 3.7							
(+)-linalool	95.3 \pm 1.3	110.4 \pm 3.1	86.6 \pm 1.4	92.3 \pm 0.8	89.1 \pm 1.4	94.8 \pm 6.7	90.4 \pm 3.8	94.7 \pm 1.7	89.0 \pm 1.7	94.7 \pm 4.2							
phenylethanol	91.7 \pm 1.8	92.0 \pm 1.5	88.8 \pm 0.8	89.9 \pm 3.1	87.9 \pm 3.1	92.2 \pm 4.0	82.8 \pm 3.4	90.5 \pm 0.6	91.1 \pm 2.6	85.5 \pm 3.6							
cis -citral	107.8 \pm 2.3	117.7 \pm 7.1	93.0 \pm 2.8	98.4 \pm 6.1	86.2 \pm 5.8	96.3 \pm 8.7	81.0 \pm 2.2	91.3 \pm 5.0	89.5 \pm 7.2	104.0 \pm 13.7							
(+/-)-citronellol 1	103.7 \pm 3.7	107.4 \pm 2.6	106.1 \pm 5.3	117.6 \pm 10.7	106.5 \pm 7.4	95.9 \pm 10.6	103.8 \pm 3.6	97.6 \pm 3.4	100.2 \pm 3.2	99.5 \pm 5.8							
(+/-)-citronellol 2	103.0 \pm 2.7	118.6 \pm 13.0	90.5 \pm 4.9	104.6 \pm 9.4	99.1 \pm 9.1	84.8 \pm 9.1	101.1 \pm 4.3	103.5 \pm 2.9	99.5 \pm 2.4	95.3 \pm 3.2							
nerol	94.5 \pm 1.5	103.0 \pm 5.3	89.9 \pm 2.2	94.2 \pm 4.4	101.0 \pm 2.5	98.7 \pm 12.8	92.5 \pm 3.2	96.9 \pm 2.2	94.3 \pm 2.8	111.3 \pm 35.4							
trans-citral	103.2 \pm 3.2	117.0 \pm 2.2	99.7 \pm 3.7	104.8 \pm 7.9	97.7 \pm 3.7	104.2 \pm 8.2	98.5 \pm 8.1	96.8 \pm 3.8	95.4 \pm 8.5	96.1 \pm 8.0							
geraniol	94.5 \pm 1.5	112.2 \pm 4.7	87.5 \pm 3.4	93.9 \pm 1.6	98.3 \pm 1.4	99.1 \pm 9.6	92.4 \pm 4.1	92.6 \pm 2.1	90.2 \pm 2.7	88.4 \pm 4.3							
(+/-)-citronellyl acetate 1	107.0 \pm 5.7	110.8 \pm 4.7	89.0 \pm 3.7	110.7 \pm 11.0	85.4 \pm 4.4	88.6 \pm 17.8	103.7 \pm 8.9	103.2 \pm 3.9	98.8 \pm 4.6	116.4 \pm 19.8							
(+/-)-citronellyl acetate 2	109.0 \pm 2.5	117.6 \pm 3.0	91.6 \pm 2.3	101.9 \pm 8.9	94.5 \pm 4.2	100.7 \pm 8.5	89.6 \pm 9.3	107.4 \pm 3.5	97.9 \pm 13.6	89.8 \pm 11.5							
neryl acetate	95.3 \pm 2.0	108.2 \pm 1.5	92.4 \pm 3.1	97.4 \pm 1.7	89.7 \pm 2.6	90.8 \pm 11.1	92.8 \pm 9.6	94.0 \pm 1.7	92.9 \pm 3.7	88.5 \pm 6.5							
(cis/trans)- β -damascenone 1	97.6 \pm 2.2	86.3 \pm 0.0	99.4 \pm 3.2	105.7 \pm 11.5	85.0 \pm 6.9	94.8 \pm 11.7	86.7 \pm 6.0	100.4 \pm 9.0	89.2 \pm 12.2	85.6 \pm 0.6							
geranyl acetate	93.3 \pm 8.7	109.6 \pm 4.7	81.7 \pm 3.9	80.2 \pm 1.4	81.2 \pm 3.2	87.6 \pm 10.6	91.2 \pm 4.0	84.8 \pm 3.1	103.1 \pm 18.4	103.7 \pm 2.3							
β -caryophyllene	101.0 \pm 11.8	110.3 \pm 3.3	93.5 \pm 0.6	92.4 \pm 3.6	88.4 \pm 2.7	93.6 \pm 3.3	95.0 \pm 9.1	109.5 \pm 9.9	113.9 \pm 15.2	99.1 \pm 1.8							
(cis/trans)- β -damascenone 2	96.9 \pm 3.0	119.4 \pm 3.5	91.7 \pm 4.4	92.1 \pm 5.2	89.8 \pm 5.1	86.7 \pm 6.7	90.7 \pm 5.8	90.4 \pm 2.3	93.2 \pm 10.2	88.6 \pm 10.2							

β -damascone	95.9 \pm 2.3	96.9 \pm 3.0	93.5 \pm 3.3	97.9 \pm 1.4	92.6 \pm 2.8	93.1 \pm 4.7	92.7 \pm 4.0	94.1 \pm 2.3	94.4 \pm 4.2	90.5 \pm 3.4
eugenol	97.3 \pm 2.3	85.5 \pm 13.2	91.5 \pm 4.8	95.9 \pm 1.7	102.8 \pm 2.7	108.9 \pm 9.6	91.9 \pm 3.6	96.9 \pm 2.7	94.5 \pm 4.2	91.2 \pm 3.3
methyleugenol	95.2 \pm 1.8	83.8 \pm 12.6	91.0 \pm 4.1	98.4 \pm 1.1	101.6 \pm 3.7	102.7 \pm 9.9	94.7 \pm 3.3	99.3 \pm 2.5	96.1 \pm 4.4	93.4 \pm 4.0
farnesol	95.8 \pm 1.6	108.1 \pm 10.1	97.4 \pm 20.8	120.0 \pm 4.9	113.9 \pm 8.5	118.3 \pm 19.8	102.8 \pm 17.8	117.6 \pm 7.1	114.5 \pm 6.2	114.7 \pm 4.9

The herein validated methods were applied to the analysis of ten authentic rose oil samples and quantitation results for the DB-wax and BGB 178 30% CD capillary columns were compared using Bland-Altman plots of six major compounds, which did not exhibit a separable stereoisomer (Figure 9). Full quantitation results on both columns can be studied in Tables A4-A5 in the Appendix.

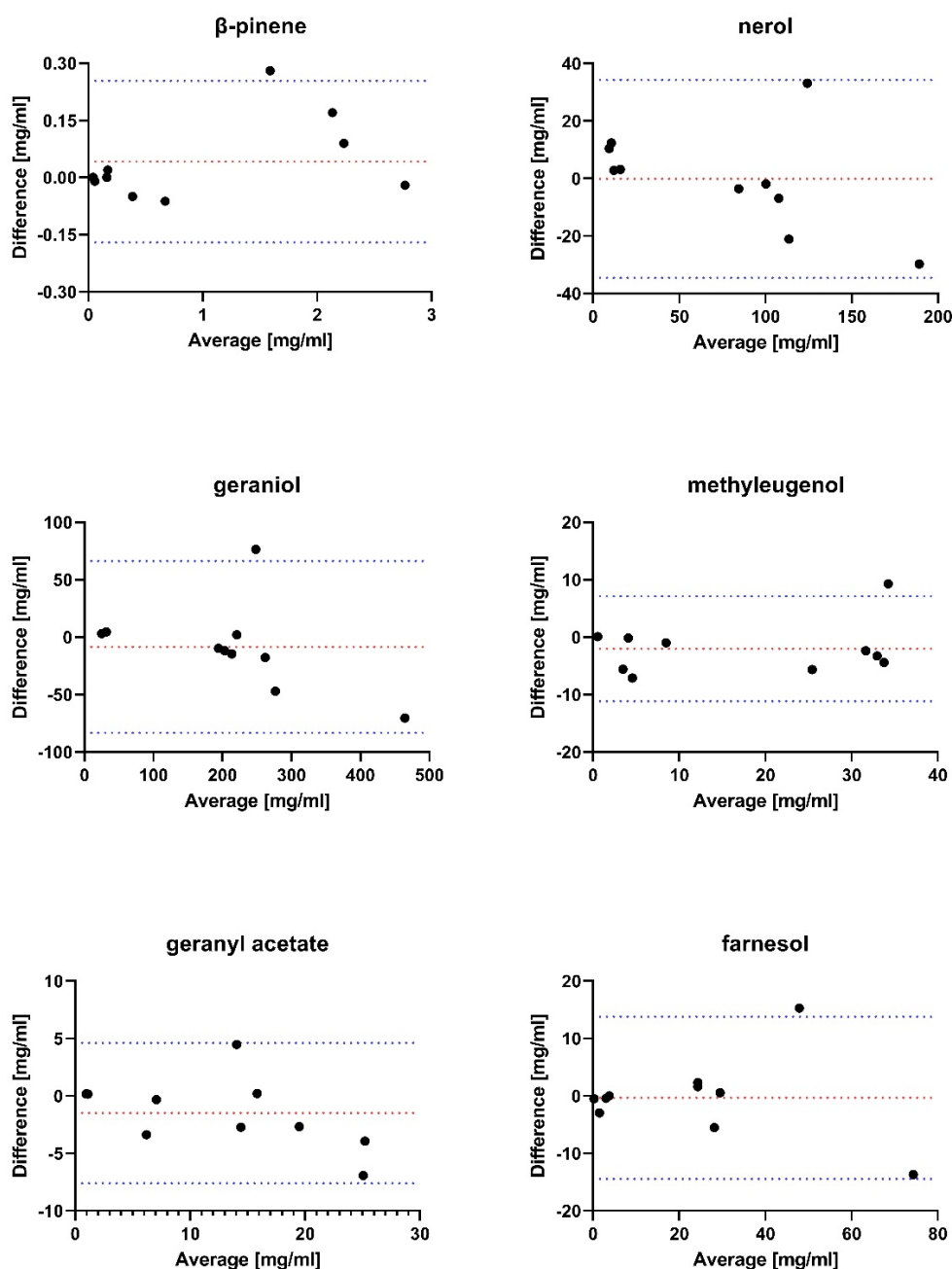


Figure 9: Bland-Altman plots for rose oil components quantified in authentic samples (n=10) on both the DB-wax and BGB 178 30% CD column with GC-FID. The average concentration in [mg/ml] between both methods was compared to the concentration difference between both methods in [%]. Red dotted lines present the bias and blue dotted lines the 95% limits of agreement. Figure taken from Raeber et al.¹⁰

From the Bland-Altman comparison, it can be concluded that the majority of the analysed EOs were within the 95% limits of agreement. Quantitation results between both columns and methods are comparable. According to the classification standards of the International Metabolomics Society, a metabolite is considered to be identified when two or more orthogonal properties are available for both the experimental analyte and a chemical standard.¹⁷¹ Therefore, the correct annotation of an isomer depends on the commercial availability of a pure enantiomeric standard, which was not the case for most of the analytes studied here. Another approach to overcome this limitation would be to compare RI literature values. As these were not available, a semi-qualitative approach was chosen to determine the EE and DE. Definite compound identification was neglected and the peak areas of two enantiomers/diastereomers were compared according to the Formula 3. The results for the EE and DE are presented in Table A5 in the Appendix. From the EE and DE values it was concluded, that either only one isomer was produced or one of them was present in slight excess. Specific isomeric patterns occur for both *R. damascena* and *P. graveolens* (geranium oil), a common adulterant of *R. damascena* oil.¹⁷² (-)-cis rose oxide was the predominant enantiomer identified in *R. damascena* oil. It was recognised as the only enantiomer present, with the exception of two samples, which contained an excess of 81% and 78%, respectively. This might be an indication of adulteration, but it has been reported that processes such as ageing, storage and heat can cause isomerisation and shifts in enantiomeric ratios.¹⁷³ (-)-cis rose oxide is present in a slight excess in *Pelargonium graveolens*, but (+)-cis rose oxide is also found to be present in non-negligible concentrations. The same observation was made for (+/-)-citronellol. *R. damascena* seems to produce exclusively one enantiomer, whereas for *P. graveolens* a slight excess of one enantiomer over the other was observed. One of the *R. damascena* samples was identified as a potential outlier using the Grubbs test ($\alpha = 0.05$) and was excluded from further analysis. As the literature describes the presence of (-)-citronellol and not (+)-citronellol in *R. damascena*, this analyte was putatively annotated as (-)-citronellol.¹⁷⁴⁻¹⁷⁶ An excess of approximately 13% (-)-linalool was identified. This finding was consistent with the results of a study by Krupčík et al. They found an excess of 10% in *R. damascena* oil samples from Bulgaria and 20% in samples from Turkey.¹⁷⁷ However, we did not observe any differences between *R. damascena* oils derived from different countries. This could however also be due to the small number of samples (Bulgaria n=4, Turkey n=3,

Morocco n=1). Inconsistent results were observed for the EE of (-)-linalool in *P. graveolens*. One sample had a balanced ratio, while the other had an excess of (+)-linalool. Both *R. damascena* and *P. graveolens* exhibited a DE for trans-citral. The DE for β -damascenone showed mixed results. While no β -damascenone was detected in half of the *R. damascena* samples, one diastereomer was present in a slight excess in both *P. graveolens* samples. Finally, the enantiomers for (+/-)-citronellyl acetate showed a stereoselective synthesis for (+/-)-citronellyl acetate 1. As it was not possible to annotate the enantiomer, the elution order was used to differentiate between the two enantiomers. The same sample as for citronellol was identified as an outlier using the Grubbs test ($\alpha=0.05$) and excluded from analysis presented in Figure 10.

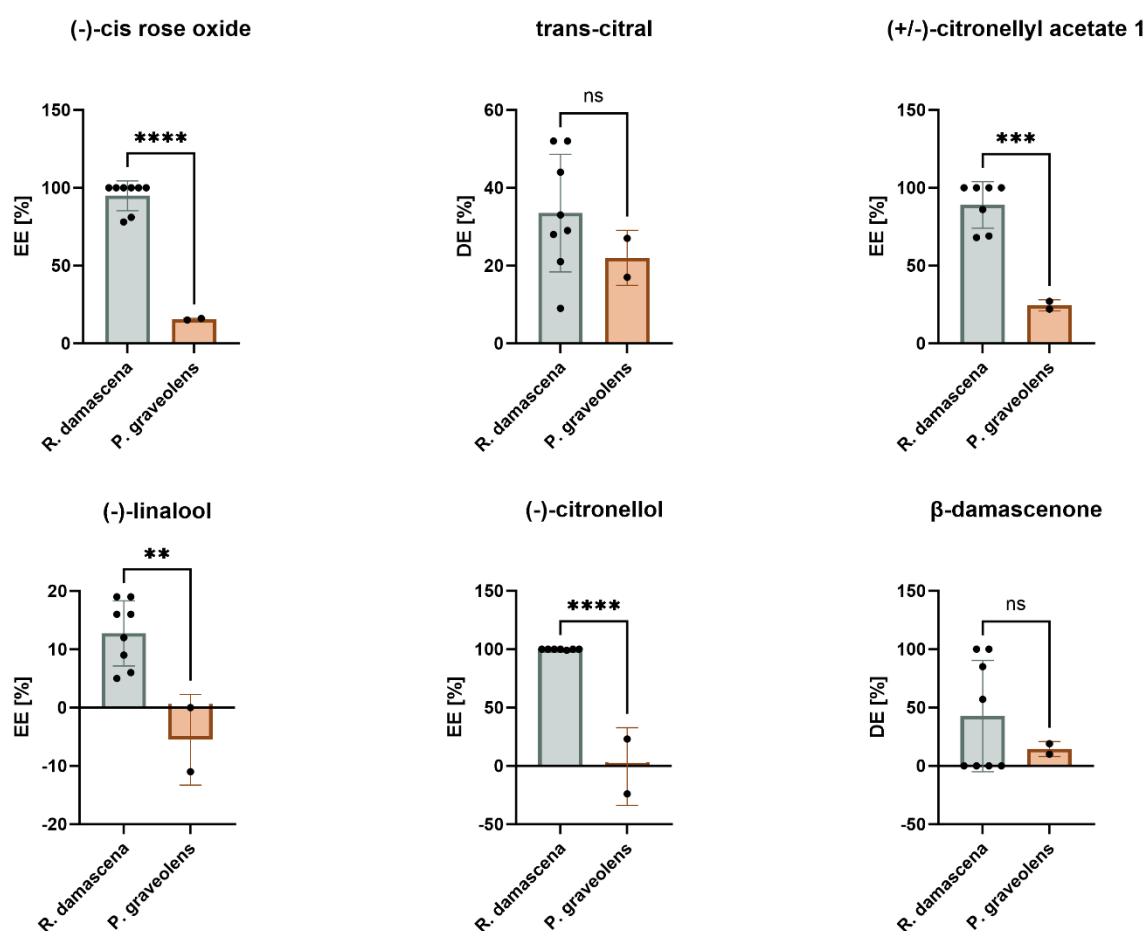


Figure 10: EE and DE [%] for six analytes found present in both *R. damascena* (n=8) and *P. graveolens* (n=2). An unpaired t-test was performed between both species. Significance levels were set at ns for $P > 0.05$, * for $P \leq 0.05$, ** for $P \leq 0.01$, *** for $P \leq 0.001$ and **** for $P \leq 0.0001$. One outlier was removed for (-)-citronellol and (+/-)-citronellyl acetate 1 after the Grubbs test ($\alpha=0.05$).

Considering the concentration profile of terpenes in Table A4 in the Appendix, nerol, citronellol, and geraniol were identified as major components. All other analytes were identified as minor compounds or in trace amounts. These observations for authentic sample analysis are in agreement with previous studies on *R. damascena* terpene profiles.^{29, 31, 156} To verify (+/-)-citronellyl acetate 1 as a potential biomarker for genuine *R. damascena* oil, a larger study population would be required. However, comparing the EE and DE of EOs can provide valuable information about the authenticity of a product. However, the effects of ageing and stressors such as heat and storage need to be further investigated to exclude isomerisation as a potential influence.

To confirm the selectivity of the GC-FID method with the DB-wax column, the method was transferred to GC-MS for further comparison. MS spectra were acquired from chemical reference substances, which served as a reference spectra for MS spectra acquired from authentic rose oil samples. The method transfer can be simply performed by adjusting the transfer line temperature and MS settings. However, a lack of sensitivity was observed for GC-MS compared to GC-FID. The analyte β -damascenone detected by GC-FID in authentic samples was not assigned in the GC-MS chromatograms. Sensitivity issues were observed for methyleugenol, eugenol, and farnesol in *P. graveolens* samples, which were detected during GC-FID analysis but not in GC-MS. Overall, however, GC-FID is on a par with GC-MS for discriminating between analytes, with the added advantage of higher sensitivity. MS could add another orthogonal feature for unambiguous identification by generating a fragment spectrum. However, the reduced sensitivity could lead to a loss in the detection of minor components, which could be crucial biomarkers in discriminating between authentic and adulterated EO samples. The use of RI and data acquisition on a polar and chiral column allows additional variables to be generated for identification. In addition, MS is expensive to maintain and purchase and requires well-trained staff. GC-FID on the other hand is robust, easy to maintain and generates low noise chromatograms. The methods presented here for the qualification and quantification of *R. damascena* EO are in no way inferior to MS and appear to be sufficient for the discrimination of authentic oils with or without fragment spectra. Generated spectra for authentic and reference samples can be studied in Figure A7 in the Appendix.

2.1.2. Materials and methods

2.1.2.1. Instrumental setup

A table of all materials and chemicals used can be found in Appendix Table A1. Both GC-FID analyses were carried out on a Thermo Fisher Scientific Focus GC (Thermo Fisher Scientific, Waltham, Massachusetts, USA) equipped with either a DB-wax capillary column (30 m x 0.25 mm x 0.25 μ m, Agilent J&W, Santa Clara, USA) or a BGB 178 30% CD capillary column, consisting of 2,6-diethyl-6-tert-butyl-dimethylsilyl-beta-cyclodextrin dissolved in a combination of 15% phenyl- and 85% methylpolysiloxane (25 m x 0.25 mm x 0.25 μ m BGB, Analytik AG, Boeckten, Switzerland). For the polar analysis on the DB-wax column, the following GC-settings were used: inlet and detector temperature were set to 220 °C and 250 °C, respectively. A constant flow rate at 2.0 ml/min was selected with a split flow of 100 ml/min and a split ratio of 1:50. The oven temperature was initially set to 45 °C and held constant for 15 min and then gradually increased by 5 °C/min up to a temperature of 220 °C, which was held constant for another 9 minutes. The injection volume was set to 1 μ l and helium was selected as a carrier gas. For the chiral analysis on the BGB 178 30% CD column the following GC-settings were used: inlet and detector temperature were set to 250 and 260 °C, respectively. A constant pressure at 100 kPa was applied with a split flow of 140 ml/min and a split ratio of 1:60. The oven temperature was initially set to 60 °C and held constant for 2 min and then gradually increased by 2 °C/min up to a temperature of 180 °C, which was held constant for 3 min. The injection volume was set to 1 μ l and helium was selected as a carrier gas.

2.1.2.2. Data processing and analysis

Data acquisition was performed using ChromCard (Thermo Fisher Scientific, Version 2.9) and peak processing using MATLAB (Version R2021b 9.11.0.176998). The MATLAB code used for the peak integration can be studied in the Appendix in Script A1. Statistical evaluation and visualisation were performed using GraphPad Prism (Version 9.2.0).

2.1.2.3. Method validation

Method validation followed the guidelines of the International Council for Harmonisation of Technical Requirements for Registration of Pharmaceuticals for Human Use (ICH) Q2 (R2).¹⁷⁸ The calibration regression was constructed using six calibration standards (Cal) and three quality control standards (QC) covering the high, medium and low calibration ranges (QC_{high} , QC_{med} , QC_{low}). A stock solution was prepared consisting of 7.3 mM (-)- β -pinene, 88.1 mM (+)- α -pinene, 7.3 mM α -terpinene, 4.9 mM β -caryophyllene, 5.2 mM β -damascone, 7.3 mM camphene, 6.6 mM citral, 128.0 mM citronellol, 5.0 mM citronellyl acetate, 105.1 mM β -damascenone, 7.3 mM limonene, 12.2 mM eugenol, 11.2 mM methyleugenol, 9.0 mM farnesol, 129.7 mM geraniol, 10.2 mM geranyl acetate, 19.4 mM linalool, 64.8 mM nerol, 10.2 mM neryl acetate, 7.5 mM p-cymene, 7.5 mM phenylethanol and 25.9 mM rose oxide diluted in n-heptane. Cal and QCs were derived from this stock solution by serial dilution and cis-3-hexen-1-ol was added at a final concentration of 10 mM as an IS. Method validation was performed on five separate days, with all Cal samples measured in singlet and all QC samples measured in duplicate. Accuracy was assessed as the bias in % and precision as both the intraday (RSD_R) and interday (RSD_T) imprecision as a standard deviation according to Peters et al.¹⁷⁹ Specificity was assessed by spiking authentic rose oil samples and four different EO samples with concentrations at the QC_{med} level. An additional spiking experiment was performed by spiking authentic rose oil samples with QC_{high} and QC_{low} concentration levels. The RE was used as a metric to determine method specificity and was calculated using the Formula 2.⁶⁹

$$RE [\%] = \frac{CONC_{spiked\ sample} - CONC_{sample}}{CONC_{spiking}} \times 100 \quad 2$$

Specificity was further verified by comparing the acquired RI with literature values. The RI was calculated using the equation of van den Dool and Kratz (Formula 1).⁸⁶ As co-elution is an inherent risk of chromatography, a GC-MS analysis was carried out using the DB-wax capillary column in a Trace GC Ultra connected to a TriPlus autosampler and DSQ II MS (Thermo Fisher Scientific, Waltham, MA, USA). The temperature profile followed that described in *Section 2.1.2.1*. Ten authentic rose oil samples were

additionally analysed by GC-MS and the acquired MS spectra were compared with reference spectra derived from reference compounds. An extensive list of the analysed authentic samples can be found in Table A6 in the Appendix. Data acquisition and analysis were performed using XCalibur (Thermo Fisher Scientific, Version 2.2 SP1.48). The instrument setup was as follows: ion source and MS transfer line were heated to 220 °C and 250 °C, respectively. The mass range scanned was from 50 - 650 Da at a scan rate of 500 amu/s. Ionisation was performed in positive mode using electron impact (EI) at a voltage of 70 eV. Other metrics such as the peak resolution (R_s) were determined according to the Pharmacopeia Europea 10.6.¹⁸⁰ LoD and LoQ were determined according to the ICH Q2 (R2) guidelines based on the standard deviation of the response and the slope of the calibration curve.¹⁷⁸ Finally, robustness was confirmed by adjusting the split ratio, flow rate, detector temperature, inlet temperature and temperature ramp for each method.

2.1.2.4. Authentic sample preparation

Authentic samples were prepared at both 1:10 and 1:500 dilutions with a final concentration of 10 mM cis-hexen-1-ol as an IS to cover both minor and major components. GC-FID analysis was performed on both the polar and chiral columns. For samples analysed on the chiral column, the EE and DE was calculated using Formula 3.²³ The EE/DE is the ratio of the peak areas (PA) of the major and minor isomers.

$$EE/DE [\%] = \frac{PA_{major\ isomer} - PA_{minor\ isomer}}{PA_{major\ isomer} + PA_{minor\ isomer}} \times 100 \quad 3$$

2.2. Simultaneous Quantification of Terpenes and Cannabinoids by Reversed-Phase LC-APCI-MS/MS in *Cannabis sativa* L. Samples Combined with a Subsequent Chemometric Analysis

2.2.1. Results and discussion

Cannabis sativa L. has undergone a dramatic paradigm shift from a prohibited drug to a promoted medicinal plant. This has led to a change in the current legal framework, which is translated into simplified pharmacy dispensing and medical use.⁷⁰ These changes have also fostered the need for well-characterised cannabis products, as reflected in the inclusion of *C. sativa* L. flower monographs in, for example, the Pharmacopeia Europea 11.5.^{43, 70} Current chemotype classifications are based on the ratio of THC and CBD for legal purposes, but with an increasing focus on synergism, attention has also shifted to minor constituents such as other cannabinoids and terpenes. This shift has led to further controversy in classification efforts. As discussed in *Section 1.4*, the gold standard for separation and analysis of terpenes is GC coupled to either FID or MS. This analysis however requires derivatisation of naturally occurring acid forms of THC and other cannabinoids in order to prevent premature degradation. Therefore, LC has become the method of choice for cannabinoid analysis. Currently, *C. sativa* L. flowers are characterised by LC and GC, or derivatisation reactions are performed if both terpenes and cannabinoids are to be covered. This makes holistic *C. sativa* L. characterisation time-consuming, expensive in reagents, requires the validation of two analytical methods, and may necessitate environmentally harmful chemicals. There are limited reports of LC analysis of terpenes in the literature, but to date there appears to be no single validated LC-MS method that combines both cannabinoids and terpenes in a single chromatographic step, which further eliminates the need for acid-derivatisations.^{75, 76} In an effort to find a suitable solution to this challenge, a LC-APCI-MS/MS method was developed and validated that separates 16 terpenes and 7 cannabinoids, as well as some of their acid forms. The MS method is based on multiple reaction monitoring (MRM), which allows co-eluting substances to be distinguished because of their mass. Two transitions were selected for MRM to act as a qualifier and quantifier. The energies for the transitions

were optimised using compound tuning and are presented in Table 5. To compensate for any device-specific deviations, two substances, namely propylparaben (for menthone and citronellol) and THC-D3 (all other analytes), were selected as the IS.

Table 5: Parameters for the analysis of terpenes and cannabinoids in a single LC-APCI-MS/MS run. Declustering Potential (DP), Collision Energy (CE) and Cell Exit Potential (CXP) are abbreviated. The quantifier and qualifier transitions are each below each other. Table was taken from Raeber et al.⁷⁰

#	Analyte	Retention time [min]	Q1 [Da]	Q3 [Da]	DP [V]	CE [V]	CXP [V]
1	cis-citral	4.18	153.1	41.2	41	35	10
			153.1	69.1	41	17	12
2	carvacrol	4.46	151.1	91.1	51	33	8
			151.1	77.1	51	39	8
3	trans-citral	4.51	153.1	41.2	41	35	10
			153.1	69.1	41	17	12
4	trans-menthone	4.88	155.1	81.1	51	17	8
			155.1	79.1	51	35	6
5	linalool	5.17	137.0	81.1	61	19	8
			137.0	77.1	61	31	6
6	cis-menthone	5.74	155.1	81.1	51	17	8
			155.1	79.1	51	35	6
7	citronellol	6.17	157.0	83.1	36	15	8
			157.0	55.1	36	29	6
8	CBDV	7.77	287.1	165.2	61	31	12
			287.1	123.1	61	51	12
9	isobornyl acetate	8.58	137.0	81.0	61	17	8
			137.0	77.0	61	31	8
10	geranyl acetate	9.06	137.0	81.0	61	17	8
			137.0	77.0	61	31	8
11	CBG	11.18	317.2	193.3	41	31	16
			317.2	123.2	41	41	4
12	CBD	11.20	315.2	193.2	41	33	14
			315.2	123.1	41	45	12
13	CBDA	11.87	315.2	193.2	41	33	14
			315.2	123.1	41	45	12
14	sabinene	13.11	137.1	81.1	26	17	8
			137.1	77.0	26	33	8
15	myrcene	13.45	137.0	81.1	56	19	8
			137.0	77.0	56	31	8

16	CBN	14.09	311.1	178.3	41	83	14
			311.1	152.1	41	103	12
17	β -pinene	14.42	137.1	81.1	26	19	8
			137.1	77.1	26	33	6
18	limonene	15.12	137.1	81.1	26	17	8
			137.1	77.0	26	33	8
19	THC	15.30	315.1	193.0	41	27	4
			315.1	76.9	41	79	12
20	α -pinene	15.46	137.1	81.1	26	19	8
			137.1	77.1	26	33	6
21	THCA	19.22	315.1	193.0	41	27	4
			315.1	76.9	41	79	12
22	α -humulene	21.13	205.1	93.2	21	31	6
			205.1	109.2	21	23	4
23	β -caryophyllene	21.44	205.1	93.2	21	31	6
			205.1	109.2	21	23	4
IS	propylparaben	2.93	181.0	139.1	31	17	10
			181.0	95.1	31	27	10
IS	THC-D3	15.30	318.1	196.0	41	27	4
			318.1	76.9	41	79	12

Trans-citral (**2**) and carvacrol (**3**) as well as CBG (**11**) and CBD (**12**) were not separated chromatographically but by mass. The total ion chromatogram (TIC) is shown in Figure 11. Separation was further achieved for two diastereomers, namely the cis/trans isomers of both menthone (**4,6**) and citral (**1,3**).

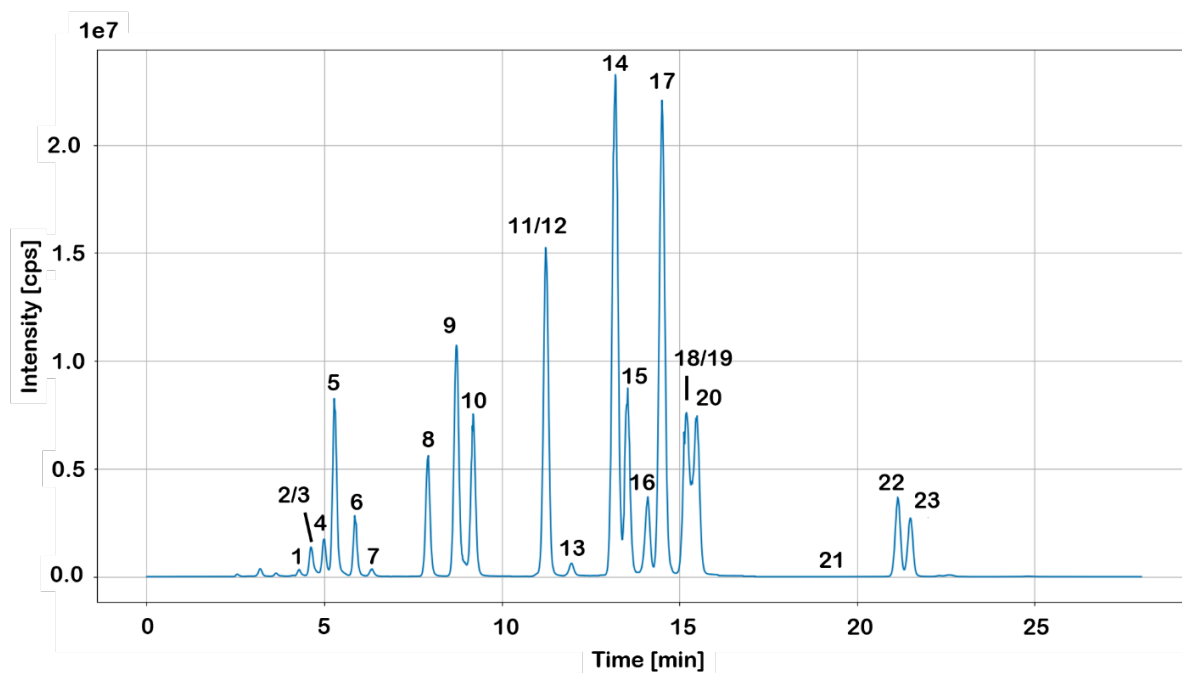


Figure 11: TIC of 23 analytes separated on a reversed phased C18 column. The intensity was measured as counts per seconds (cps). Figure adapted from Raeber et al.⁷⁰

Figure 11 shows different intensities for the individual peaks for the analytes, although they were all present at the same concentration during acquisition. Cannabinoids are much more efficiently ionised by APCI than terpenes. When comparing the terpenes within their own class, it is again noticeable that they show varying intensities. For the determination of terpenes, normalisation methods are often used instead of full quantification. As normalisation methods do not require complex calibration, they are faster, but carry the risk of over- and underestimating the presence of an analyte. A clear chromatographic overview is obtained with an extracted ion chromatogram (XIC) as shown in Figure 12.

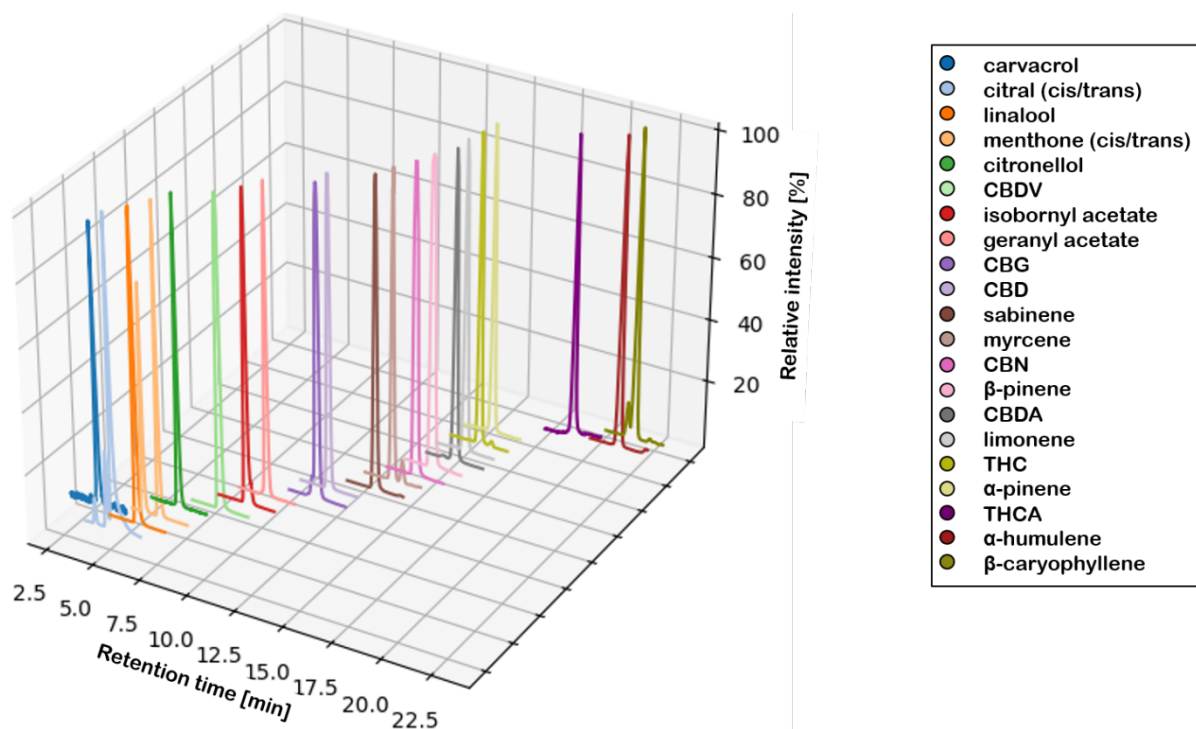


Figure 12: XIC of transition ions for terpenes and cannabinoids. Intensity is presented as the relative intensity in [%]. Figure adapted from Raeber et al.⁷⁰

The analysis of both THCA and CBDA uses the same mass transitions as their respective neutral forms, as they decarboxylate to THC and CBD in a reproducible manner during the ionisation process. Potential interferences with other cannabinoids were excluded by recording a mixture of 10 µg/ml THCV, THCVA, CBG, CBGA, CBDV, CBDVA, CBC, CBCA, CBNA, and Δ^8 -THC in acetonitrile. The same mass transitions were used as for the cannabinoids that were part of the method validation. All cannabinoids were chromatographically separable, underlining the specificity of the method. An overlay of the chromatograms for the interference mixture and the validated method is shown in Figure 13.

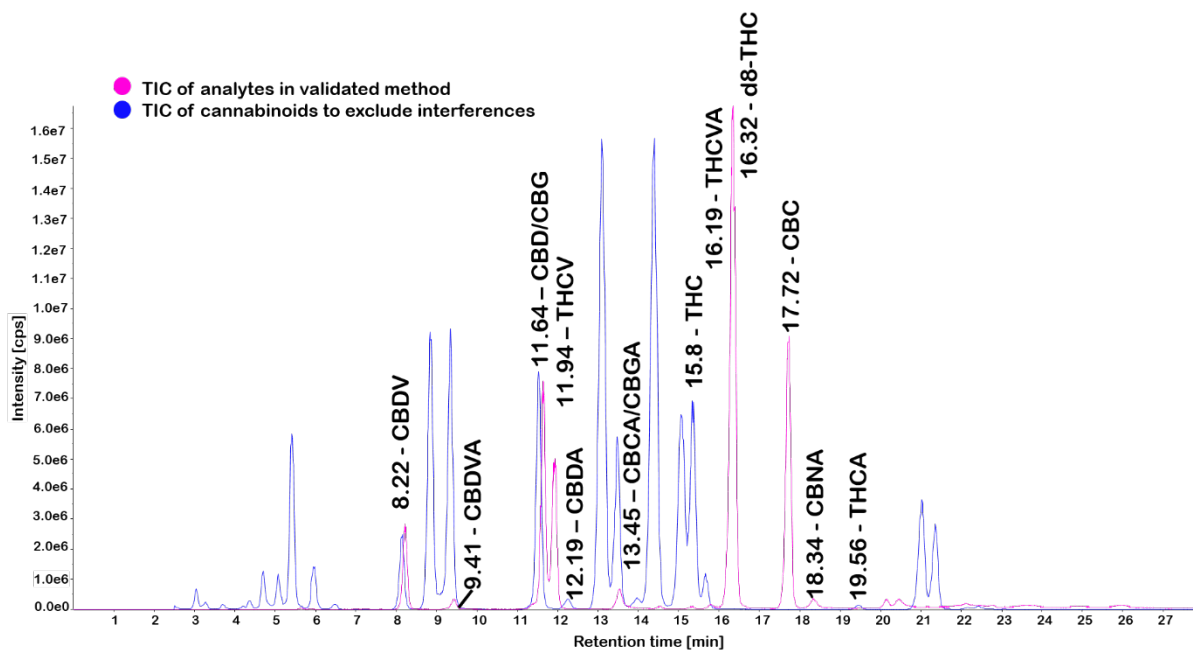


Figure 13: Overlay of the interference mixture with the TIC of analytes as part of method validation. Intensity is expressed as cps. Figure modified from Raeber et al.⁷⁰

Due to the isomeric structures of terpenes and cannabinoids, selectivity was of paramount importance. Identity was only guaranteed, if the relative retention time between the analyte and its respective IS did not differ more than ± 0.02 , both qualifier and quantifier ions were present and the ion ratio between the two did not exceed 40%. These parameters were meticulously chosen during method validation and established as cut-off criteria for authentic samples, ensuring the accurate identification of analytes. Due to the considerable variability in cannabis chemotypes, particularly in the concentration of the main cannabinoids THC and CBD, it was unavoidable to perform method validation over two concentration ranges. This decision was based on the observation that THCA and CBDA required two regression models at high and low concentrations and that CBG showed detector saturation at higher concentrations. Furthermore, the use of two different weighting factors improved the accuracy for CBD in both the low and high concentration ranges. Due to the lower ionisation efficiency of terpenes, they showed suitable intensities only in undiluted samples, whereas highly concentrated cannabinoids oversaturated the detector. As a result, two dilution steps were implemented: minor constituents were analysed in undiluted samples, while major constituents were diluted 100-fold. Table 6 and 7 list the calibration models for the minor and major concentrations, respectively.

Terpenes were excluded from the higher calibration range, as they are always present in low concentrations in *C. sativa* L.

Table 6: Calibration models for the low calibration range. Table taken from Raeber et al.⁷⁰

Analyte	Calibration model	Weight	Function	R ²
cis-citral	quadratic	1/x	$Y = -0.04 + 0.08 * X + 0.00005 * X^2$	0.9957
carvacrol	quadratic	1/x	$Y = -0.04 + 0.02 * X + 0.00001 * X^2$	0.9965
trans-citral	quadratic	1/x	$Y = -0.22 + 0.26 * X + 0.00009 * X^2$	0.9973
trans-menthone	quadratic	1/x	$Y = -0.01 + 0.01 * X + 0.00001 * X^2$	0.9980
linalool	quadratic	1/x	$Y = -3.71 + 2.90 * X - 0.002 * X^2$	0.9984
cis-menthone	quadratic	1/x	$Y = -0.02 + 0.02 * X + 0.00004 * X^2$	0.9971
citronellol	quadratic	1/x	$Y = -0.0006 + 0.0006 * X + 0.0000007 * X^2$	0.9992
CBDV	quadratic	1/x	$Y = -0.23 + 11.86 * X - 0.05 * X^2$	0.9999
isobornyl acetate	quadratic	1/x	$Y = -6.14 + 2.52 * X - 0.0010 * X^2$	0.9947
geranyl acetate	quadratic	1/x	$Y = -5.72 + 2.14 * X - 0.002 * X^2$	0.9951
CBG	quadratic	1/x	$Y = -0.59 + 23.22 * X - 0.21 * X^2$	0.9997
CBD	quadratic	1/x	$Y = -0.18 + 9.28 * X - 0.04 * X^2$	0.9999
CBDA	quadratic	1/x	$Y = 0.32 + 0.66 * X - 0.004 * X^2$	0.9989
sabinene	quadratic	1/x	$Y = -7.74 + 3.59 * X - 0.002 * X^2$	0.9960
myrcene	quadratic	1/x	$Y = 0.82 + 0.60 * X + 0.0004 * X^2$	0.9947
CBN	quadratic	1/x	$Y = -0.08 + 4.14 * X - 0.005 * X^2$	0.9998
β-pinene	quadratic	1/x	$Y = -3.94 + 1.78 * X + 0.0002 * X^2$	0.9934
limonene	quadratic	1/x	$Y = -0.51 + 0.80 * X + 0.0004 * X^2$	0.9986
THC	quadratic	1/x	$Y = -0.09 + 4.86 * X - 0.01 * X^2$	0.9997
α-pinene	quadratic	1/x	$Y = -0.80 + 1.01 * X + 0.0002 * X^2$	0.9990
THCA	quadratic	1/x	$Y = 0.26 + 0.64 * X - 0.005 * X^2$	0.9995
α-humulene	quadratic	1/x	$Y = -0.72 + 0.56 * X + 0.0003 * X^2$	0.9964
β-caryophyllene	quadratic	1/x	$Y = -0.53 + 0.33 * X + 0.00008 * X^2$	0.9964

Table 7: Calibration models for the high calibration range. Table taken from Raeber et al.⁷⁰

Analyte	Calibration model	Weight	Function	R ²
CBD	quadratic	1/y	$Y = -0.03 + 9.65 * X - 0.04 * X^2$	0.9988
CBDA	quadratic	1/x	$Y = 0.40 + 0.40 * X - 0.0004 * X^2$	0.9989
CBDV	quadratic	1/x	$Y = -0.14 + 13.77 * X - 0.08 * X^2$	0.9988
CBG	quadratic	1/x	$Y = 0.38 + 25.62 * X - 0.22 * X^2$	0.9952
CBN	quadratic	1/x	$Y = -0.10 + 4.91 * X - 0.02 * X^2$	0.9934
THC	quadratic	1/x	$Y = 0.04 + 5.53 * X - 0.02 * X^2$	0.9984
THCA	quadratic	1/x	$Y = 0.11 + 0.41 * X - 0.001 * X^2$	0.9873

Method validation was conducted according to the ICH Q2 (R2) guidelines on three individual days.¹⁷⁸ Accuracy was determined as the bias and found to be below 15% for all analytes in both calibration ranges. Imprecision was determined in terms of RSD_R and RSD_T and was found to be below the cut-off value of 20%. Individual validation results can be studied in Tables 8 and 9. A spiking experiment was also performed by adding the analytes at low, medium and high concentrations to extracts of *Humulus lupulus*. *H. lupulus* is closely related to *C. sativa* L., but does not produce cannabinoids and represents a cannabinoid-free matrix. *H. lupulus* samples were measured in both blank and spiked conditions and the RE was determined using the Formula 4. This experiment was only carried out for the minor calibration range, as the matrix is diluted 100-fold for the major calibration range, which further reduces matrix effects. The RE was in an acceptable range for all analytes (Table 8), supporting APCI as an ionisation source, which is known to be less susceptible to matrix effects such as ion enhancement and suppression compared to ESI.¹⁸¹

Table 8: Results for accuracy (expressed as bias), imprecision (expressed as RSD_R and RSD_T) and recovery effect, abbreviated as RE, for the low concentration range. Table was taken from Raeber et al.⁷⁰

#	Analyte	RT [min]	Range [µg/mL]	Expected Ion Ratio	Bias [%]	QC ^{high}		Bias [%]	QC ^{med}		Bias [%]	QC ^{low}		RE [%] High	RE [%] Med	RE [%] Low
						RSD _R [%]	RSD _T [%]		RSD _R [%]	RSD _T [%]		RSD _R [%]	RSD _T [%]			
1	cis-citral	4.18	2.5 - 125	0.31	-8.0	4.47	5.83	-7.3	1.68	3.73	6.4	3.48	2.81	87.0 ± 2.9	86.2 ± 1.5	88.3 ± 4.5
2	carvacrol	4.46	5 - 250	0.71	-5.4	6.65	5.87	-3.1	9.34	8.78	8.9	4.95	8.68	99.1 ± 1.1	89.7 ± 5.3	92.1 ± 3.8
3	trans-citral	4.51	2.5 - 125	1.11	-7.6	4.65	3.38	-8.0	4.17	4.93	-0.7	6.67	5.33	113.5 ± 4.9	113.8 ± 3.1	95.6 ± 4.0
4	trans-menthone	4.88	2.5 - 100	0.15	-5.0	4.24	5.95	3.2	7.76	6.63	10.0	5.31	4.13	103.7 ± 1.1	106.7 ± 1.7	109.5 ± 5.4
5	linalool	5.17	5 - 250	0.03	-5.8	3.87	4.23	0.7	4.64	7.03	10.6	6.06	4.71	86.2 ± 1.3	87.3 ± 4.3	100.2 ± 4.5
6	cis-menthone	5.74	5.5 - 225	0.15	-6.4	3.44	3.79	1.6	4.83	5.25	12.3	4.73	3.96	105.4 ± 2.3	105.4 ± 2.2	104.0 ± 6.3
7	citronellol	6.17	5 - 250	0.67	-7.4	2.65	3.13	-2.7	6.32	8.56	8.3	6.64	7.89	115.9 ± 3.1	122.1 ± 2.8	106.1 ± 5.9
8	CBDV	7.77	0.1 - 20	0.48	1.4	2.48	4.30	2.5	2.86	4.52	2.0	8.29	6.99	85.6 ± 0.4	77.9 ± 2.4	93.5 ± 5.4
9	isobornyl acetate	8.58	5 - 250	0.03	-3.4	3.83	3.77	-3.6	4.08	4.82	4.4	7.62	7.63	95.0 ± 0.5	90.8 ± 5.0	97.9 ± 6.6
10	geranyl acetate	9.06	5 - 250	0.03	-4.9	4.17	4.54	0.5	6.09	5.70	11.0	4.75	4.37	93.4 ± 1.5	91.0 ± 0.9	95.8 ± 6.1
11	CBG	11.18	0.1 - 20	0.40	2.8	3.03	6.01	0.5	4.27	6.07	1.0	11.80	8.87	88.5 ± 1.5	81.1 ± 2.7	89.0 ± 5.5
12	CBD	11.20	0.1 - 20	0.75	0.4	1.37	2.95	0.7	2.98	4.49	2.8	10.34	8.11	90.8 ± 0.4	84.8 ± 2.0	91.3 ± 5.4
13	CBDA	11.87	2 - 20	0.73	-1.1	2.95	4.26	0.1	4.45	12.56	1.0	2.61	15.41	91.8 ± 1.0	81.8 ± 1.5	94.0 ± 7.3
14	sabinene	13.11	5 - 250	0.03	-2.8	4.18	6.38	-4.6	4.06	7.28	7.0	8.06	6.60	102.0 ± 3.0	98.2 ± 3.4	94.4 ± 9.4
15	myrcene	13.45	5 - 250	0.03	-0.1	2.55	3.29	-4.8	10.01	8.46	6.7	10.90	7.87	95.2 ± 3.6	91.2 ± 2.8	82.4 ± 4.6
16	CBN	14.09	0.1 - 20	0.72	2.5	1.70	1.79	-1.3	2.88	2.80	0.2	9.20	6.66	97.7 ± 1.4	92.8 ± 4.9	93.8 ± 5.3
17	β-pinene	14.42	5 - 250	0.03	-3.7	3.96	5.16	-5.0	5.81	5.40	6.5	9.38	6.65	102.0 ± 4.7	96.5 ± 0.5	89.8 ± 8.4
18	limonene	15.12	5 - 250	0.03	-4.8	2.08	5.33	-0.5	4.59	10.30	4.6	4.69	4.28	108.7 ± 1.5	93.9 ± 9.8	96.3 ± 2.6
19	THC	15.30	0.1 - 20	0.42	2.4	0.50	2.61	1.8	3.63	4.79	3.3	9.09	7.51	98.0 ± 0.7	91.2 ± 4.2	93.6 ± 5.7
20	α-pinene	15.46	5 - 250	0.06	-3.8	5.32	7.67	-1.7	3.82	6.93	7.4	4.36	4.25	90.1 ± 2.0	85.9 ± 1.7	83.1 ± 6.1
21	THCA	19.22	2 - 20	0.43	-9.9	5.36	12.00	-9.1	8.82	12.23	-3.6	11.23	13.57	83.1 ± 4.6	70.4 ± 8.7	84.1 ± 4.6
22	α-humulene	21.13	5 - 250	0.72	-3.2	1.74	5.98	-1.3	3.30	7.44	6.6	7.19	10.33	88.7 ± 2.1	83.7 ± 3.3	100.1 ± 3.2
23	β-caryophyllene	21.44	5 - 250	1.03	-4.2	1.25	3.67	-2.5	3.39	4.99	9.7	4.21	3.58	86.2 ± 1.2	80.4 ± 2.6	95.4 ± 4.3

Table 9: Results for accuracy (expressed as bias), imprecision (expressed as RSD_R and RSD_T) for the high concentration range. Table was taken from Raeber et al.⁷⁰

#	Analyte	RT [min]	Range [µg/mL]	Expected Ion Ratio	Bias [%]	QC ^{high}		Bias [%]	QC ^{med}		Bias [%]	QC ^{low}	
						RSD _R [%]	RSD _T [%]		RSD _R [%]	RSD _T [%]		RSD _R [%]	RSD _T [%]
8	CBDV	7.77	0.1 - 60	0.49	-6.5	2.77	4.43	2.9	4.74	5.14	-11.4	5.63	6.89
11	CBG	11.18	0.1 - 60	0.43	-13.3	7.46	7.86	4.8	5.57	8.05	-17.2	3.00	6.18
12	CBD	11.20	0.1 - 60	0.75	-0.1	2.24	3.18	9.7	3.54	4.59	-7.8	4.83	7.04
13	CBDA	11.87	1.0 - 60	0.72	-5.7	5.79	7.26	-1.6	8.00	13.03	6.1	1.92	15.73
16	CBN	14.09	0.1 - 60	0.71	0.0	4.42	4.82	9.0	4.34	4.04	-10.2	4.24	6.76
19	THC	15.30	0.1 - 60	0.42	-4.6	1.41	2.72	3.2	5.13	5.14	-12.2	3.09	5.00
22	THCA	19.22	0.1 - 60	0.43	-6.7	4.16	4.57	-0.3	8.28	7.76	2.8	5.38	12.99

As LC is an unconventional technique for the analysis of terpenes, a comparison was made with the state-of-the-art method GC-FID. Fifteen randomly selected samples, previously analysed by LC-APCI-MS/MS, were additionally analysed by GC-FID, and the results were compared. While LC is a well-established method for cannabinoid analysis, this experiment focused exclusively on terpenes. Comparison was made using Bland-Altman plots, which compared the mean concentration determined by both methods with the percentage difference between them. This analysis included only analytes present above the LoQ in at least ten samples, which was met for α -pinene, β -pinene, linalool, limonene, myrcene, α -humulene, and β -caryophyllene. These terpenes are commonly reported as constituents of *C. sativa* L. Figure 14 shows the Bland-Altman plots for six of the seven terpenes as they compare favourably.

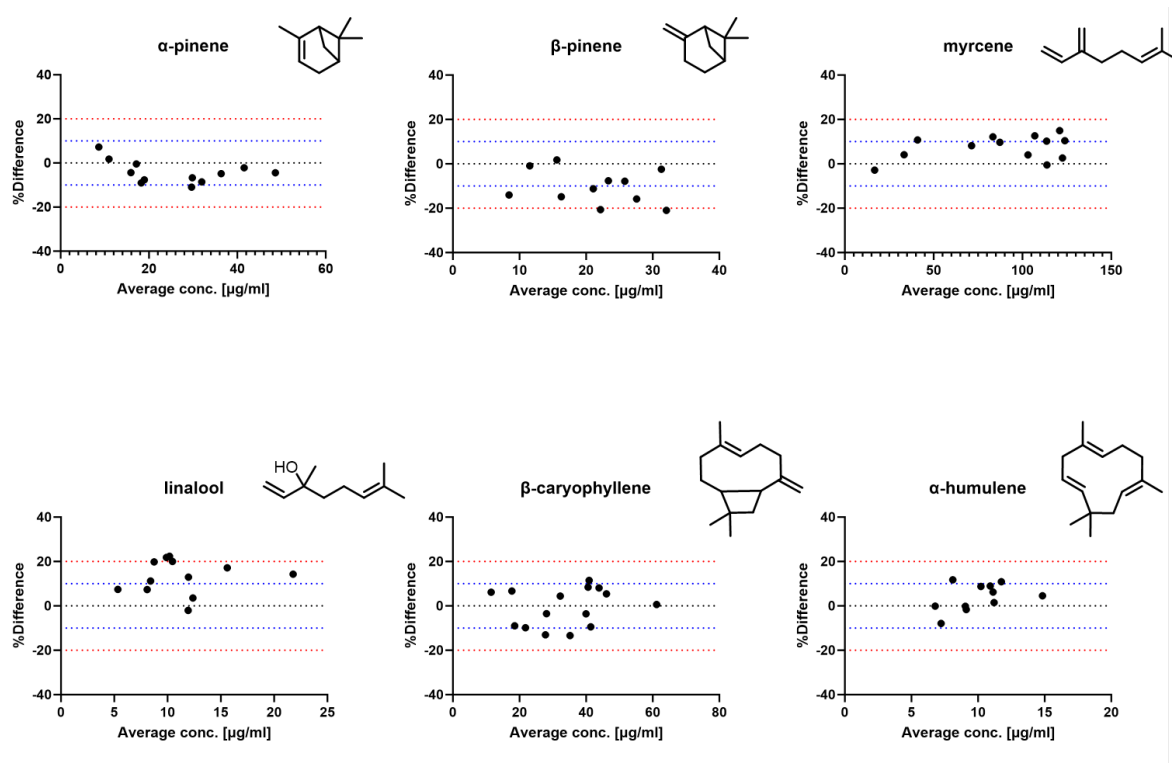


Figure 14: Bland-Altman plots for method comparison between LC-APCI-MS/MS and GC-FID. Terpenes were quantified and the average concentration is plotted against the %-difference. Blue and red dotted lines indicate 10% and 20% thresholds, respectively. Figure adapted from Raeber et al.⁷⁰

Limonene showed significantly higher concentrations by LC-APCI-MS/MS than GC-FID and is shown in Figure 15. However, when comparing the peak area ratios of limonene across samples for both analytical techniques, a consistent ratio pattern emerges.

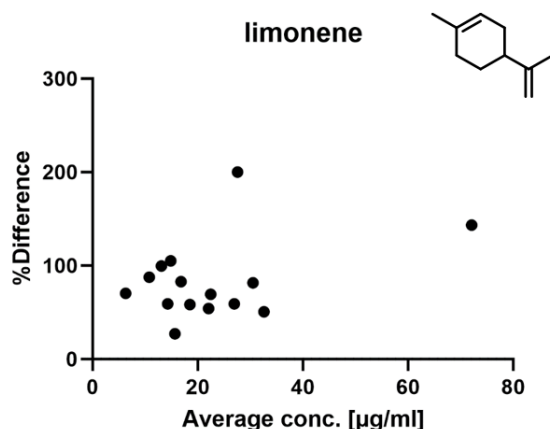


Figure 15: Bland-Altman plots for method comparison between LC-APCI-MS/MS and GC-FID. Limonene was quantified and the average concentration is plotted against the %-difference. Figure adapted from Raeber et al.⁷⁰

LC-APCI-MS/MS quantification shows a trend towards higher terpene concentrations, as seen for limonene, linalool, myrcene, and α -humulene, suggesting a relationship with the detection method. Several key differences might influence this trend: The LC method uses a cooled sample rack and column oven, in addition, the sample is sprayed and the solvent evaporated during detection, providing a gentler process compared to GC-FID. In contrast, GC-FID lacks a cooled sample rack and exposes samples directly to high temperatures during injection to transfer them to the gas phase. As terpenes are structurally related and temperature induced isomerisation reactions are possible, the influence of such factors may play a role in the different results.

Co-elution is a frequent concern in chromatography and is expected to be significantly higher for LC than for GC, especially in the case of terpenes. Specifically, α - and γ -terpinene are double bond isomers of limonene and cannot be distinguished by MRM. Furthermore, these compounds are recognised as typical secondary metabolites of *C. sativa* L. As co-elution was initially suspected for the almost double concentration of limonene obtained by LC-APCI-MS/MS, the presence of α - and γ -terpinene was excluded by GC-FID. Chromatograms for the fifteen authentic *C. sativa* L. extracts as well as the calibration models and ranges used for GC-FID quantification can be found in Figure A11 and A13 and Table A8 in the Appendix.

Therefore, the different achieved concentration values for limonene appear to be mainly due to the detection method.

The applicability of the LC-APCI-MS/MS method was further tested on 55 authentic *C. sativa* L. extracts. Chromatograms for all 55 samples can be found in Figure A12 in the Appendix. Following the classification method in the Ph. Eur. 11.5., all samples belonged to the CBD-dominant chemotype with CBD values ranging from 7.5 to 30%.⁴³ Acquired concentrations for all cannabinoids and terpenes determined for the 55 samples can be found in Table A9 in the Appendix. Sample 16 was an exception with a CBD concentration above the detection range and a relatively high CBN concentration compared to the other samples. External cannabinoid analysis by an ISO-certified laboratory confirmed that this sample was spiked by the producer. Therefore, it can be concluded that the method is also suitable for the detection of fraudulent samples. Total THC levels were below 1% and within legal limits. Minor cannabinoids such as CBDV, CBN, and CBG were detected in the majority of samples, with CBG reaching concentrations of up to 1%. The total concentration of CBD and THC is mostly derived from their acid forms, as these are the forms synthesised by the plant. Processing and heating induce decarboxylation, leading to the formation of THC and CBD. High levels of the acid forms may indicate gentle processing.¹⁸² The detected terpenes are consistent with observations in the literature. Myrcene is dominant in CBD-rich chemotypes, while other terpenes such as β -caryophyllene, α -humulene, α - and β -pinene are found in lower amounts.¹⁸³ The terpene profiles, as well as the profiles for THC and CBD, can be viewed in Figure 16 as violin plots and in the Appendix in Figure A8 with the individual data points. Terpenes make up only 3-5% w/w of the flowers, which aligns with the concentrations shown in Figure 16.¹⁸³ However, only a concentration of 0.05% w/w is required for a terpene to reach pharmacologically relevant concentrations.⁵⁴ This concentration was achieved for the common major terpenes.

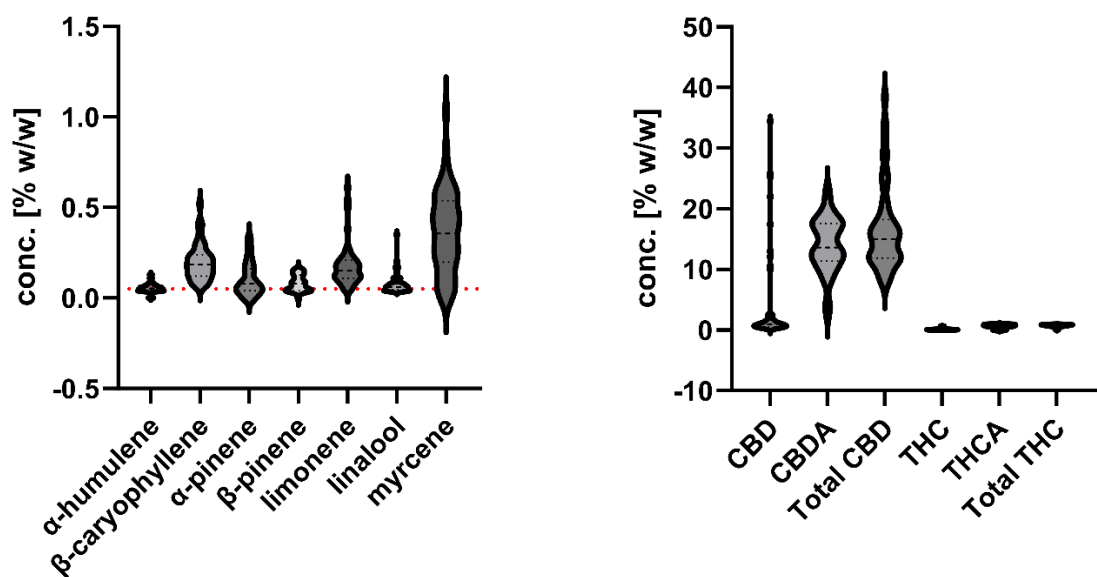


Figure 16: Violin plot for the terpene profile on the left and the major cannabinoids on the right. Red dotted line indicates the cut-off of 0.05% w/w, which is considered necessary for pharmacological activity. Figure taken from Raeber et al.⁷⁰

Terpenes and cannabinoids share a common precursor, namely GPP.¹⁸⁴ As a correlation between terpene and cannabinoid concentrations can be hypothetically assumed, as they share common resources, a Pearson correlation was performed, as shown in detail in Figure 17. The colour gradient ranging from blue to red represents either a positive or negative correlation for the studied constituents of *C. sativa* L. There is an inverse correlation between cannabinoid acids and neutral cannabinoids, which can be attributed to the biosynthetic pathway of cannabinoids (Figure 18).

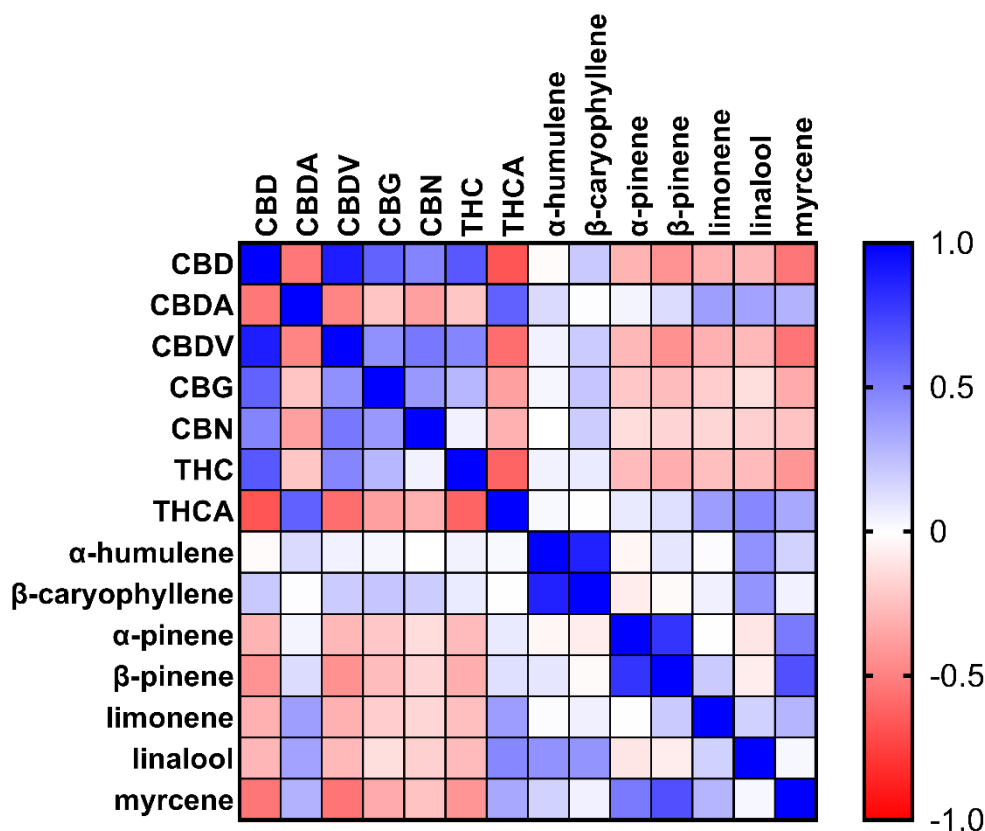


Figure 17: Pearson correlation for analytes detected in 55 *C. sativa* L. samples. Figure taken from Raeber et al.⁷⁰

The plant exclusively produces the acidic forms, which can undergo decarboxylation through flower processing and heat exposure. Notably, CBN concentrations do not correlate with Δ^9 -THC, although it is thought that Δ^9 -THC is readily oxidised to CBN under stressors such as oxygen, light, and heat.¹⁸⁵ It is possible that most CBN is derived from Δ^9 -THCA, as a negative correlation was observed. It should also be noted that the overall THC concentrations were significantly lower than THCA concentrations. In addition, α -humulene and β -caryophyllene, two sesquiterpenes, show a slight positive correlation with cannabinoids, while monoterpenes exhibit an inverse relationship with the neutral cannabinoids. As the neutral cannabinoids are a result of flower handling, this can also trigger the evaporation of terpenes, which is another indicator of ageing and storage. Another hypothesis is that due to the common use of GPP, once secondary metabolite biosynthesis is engineered towards the production of cannabinoids, there are fewer precursors available for monoterpene synthesis.

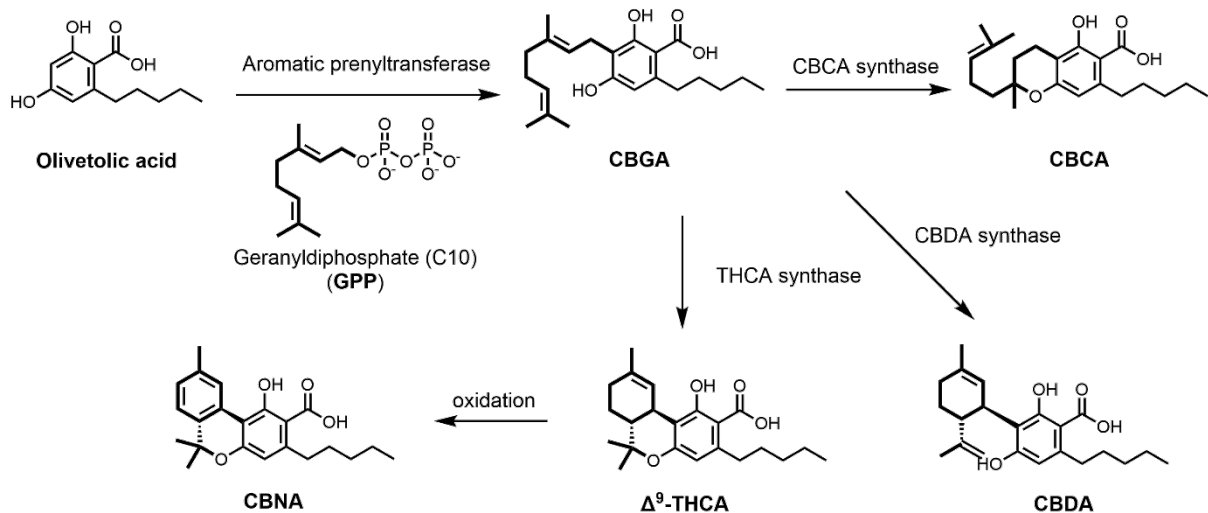


Figure 18: Biosynthesis of cannabinoids with further diversification towards CBDA, Δ^9 -THCA, CBNA, and CBDA. Bold lines indicate the common precursor GPP, which is also used in terpene biosynthesis. Synthesis pathway was based on Tahir et al.¹⁸⁵

One question that remains unanswered is whether the positive correlation of α -humulene and β -caryophyllene with the cannabinoids is due to human cultivation, or whether it has a special function in the plant that allocates resources to it. β -caryophyllene is the only terpene known to interact with the endocannabinoid receptor CB₂. Strong antiviral properties have been attributed to β -caryophyllene, making it potentially indispensable to the plant.^{50, 60}

Principal component analysis (PCA) is a common chemometric technique used to explore the chemical space and potentially identify outliers. All samples and their analytes were subjected to PCA, and the results are presented as a biplot in Figure 19. The contribution of each variable to spatial segregation is represented as a blue vector, and the first two PCs account for a total of 50.4% of the variability. The formation of two or possibly three groups is noticeable. The right side of the plot gives rise to mostly highly processed samples, some of which were hashish samples (*C. sativa* L. sample **8**, **16**, **45**, **47**) and contained above 25% total CBD. The group in the lower left quadrant is characterised by high levels of myrcene, α - and β -pinene, and citronellol. While a third group is characterised by the two cannabinoid acids THCA and CBDA, and the vectors of α -humulene, β -caryophyllene, linalool and limonene extend in the same direction. The observations from the biplot are partially congruent with the Pearson correlation, but also show the distinction of three groups in the 55 samples. Whether Pearson correlation or PCA analysis: both indicate that the chemical composition of *C. sativa* L. is not random and distinct cannabinoid and terpene patterns arise. Whether these patterns are the result of cultivation or have biological significance remains to be clarified. A limitation of this analysis is certainly that only one of the three official chemotypes of *C. sativa* L. was analysed. The behaviour of the terpene pattern for balanced THC:CBD and THC-dominant chemotypes could further be investigated using the method described here. The two calibration ranges have been deliberately chosen to be broad enough to allow these further analyses to be performed. The study presented here suggests that terpenes may play a role in storage and ageing, potentially serving as markers for these processes. The analysis focused exclusively on *C. sativa* L. plants cultivated in Switzerland. However, the pattern of secondary metabolites is heavily shaped by the plant's environment and growth conditions. Therefore, comparing *C. sativa* L. samples from various regions could provide characteristic fingerprints for their origin.

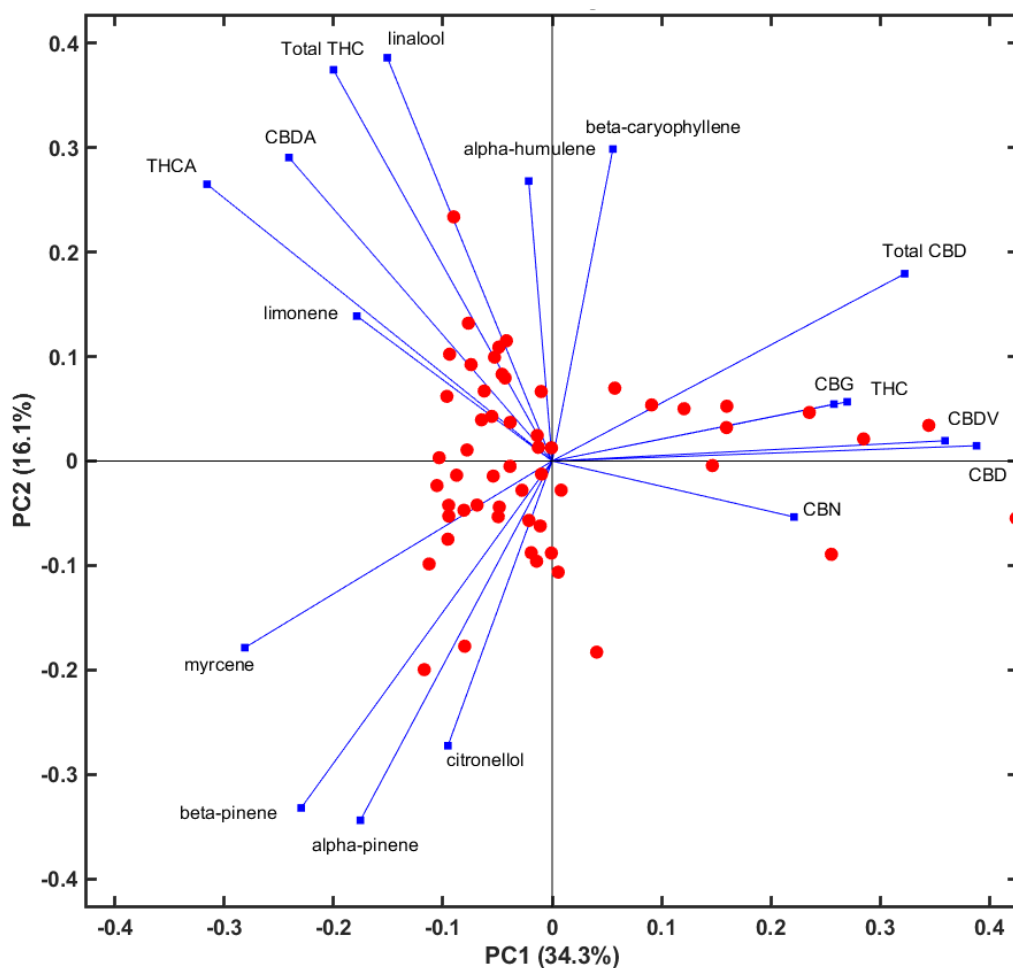


Figure 19: PCA represented as a biplot for 55 authentic *C. sativa* L. samples analysed and quantified using LC-APCI-MS/MS. The red dots represent the individual samples, while the blue vectors represent the direction and contribution of the individual variables. The plot may reveal three potential groups. Figure taken from Raeber et al.⁷⁰

2.2.2. Materials and methods

2.2.2.1. Instrumental setup

Used chemicals and reagents are listed in Table A7 in the Appendix. For the chromatographic setup a LC-MS/MS system was used, consisting of a Sciex ExionLC HPLC linked to a TripleQuad 3500 MS with an APCI source (AB Sciex, Redwood City, CA, USA). Separation of compounds was accomplished using a Symmetry® C18 column (4.6 x 100 mm, particle size 3.5 µm) from Waters (Milford, Massachusetts, USA), maintained at 45 °C. To safeguard against premature column degradation, a pre-column (UHPLC polar C18, 2.1 mm ID, SecurityGuard™, ULTRA Cartridges from

Phenomenex) was installed. The mobile phases, A and B, consisted of 2 mM ammonium acetate with 0.1% (v/v) formic acid in water and 2 mM ammonium acetate with 0.1% (v/v) formic acid and 5% (v/v) water in methanol, respectively. Injection volume was fixed at 5 μ l. The solvent gradient was initiated with 70% B from 0 to 1 min at a flow rate of 0.7 ml/min, followed by a gradual increase to 98% B by minute 20 at a flow rate of 0.6 ml/min. Conditions were maintained until minute 26.5, and swiftly returned to 70% B, which was held until minute 28. The autosampler temperature was maintained at 15 °C. MS data acquisition was performed in positive mode, with the following source conditions: curtain gas (CUR) 20.0 psi, collision gas (CAD) 9 psi, nebulizer current (NC) 5.0 μ A, temperature (TEM) 500.0 °C and ion source gas 1 (GS1) 45.0 psi. Entrance potential (EP) was set to 10.0 V. Parameters such as the DP, CE and collision CXP were optimised individually for each analyte, as detailed in Table 5. MRM was conducted as a scheduled experiment with a detection window of 200 sec, and a target cycle time of 1 sec per single MRM experiment, resulting in a total of 1680 cycles. Data acquisition utilised Analyst® software (AB Sciex, Version 1.7.2.), while data processing was performed using Sciex OS (AB Sciex, Version 2.0.0.45330).

2.2.2.2. Method validation

Method validation followed the guidelines of the International Council for Harmonisation of Technical Requirements for Registration of Pharmaceuticals for Human Use (ICH) Q2(R2), including accuracy, precision, specificity, linearity, range and robustness.¹⁷⁸ Six Cal and three QC samples were prepared over the low, medium and high concentration ranges to assess accuracy and precision. Two calibration ranges were selected to cover different chemotypes of *C. sativa* L. and their respective products (e.g. oils, resins, and hashish). The LoQ was fixed at the lowest calibrator. Over the course of a week, both Cals and QCs were measured on three separate days. Accuracy, expressed as the bias, was evaluated by back-calculating the concentrations of the duplicate QC samples using the calibration and the corresponding fitted regression function, and then determining the relative difference between experimental and theoretical concentrations. Precision was assessed as the relative standard deviation and reported as imprecision for both intra- and interday performance, following the methods outlined by Peters et al.¹⁷⁹ Method specificity was

guaranteed by detecting both quantifier and qualifier ions, and by comparing the ion ratios of the MRM transitions for each analyte. Furthermore, the relative retention time of each analyte was constrained to be within +/- 0.02 of the IS. To assess matrix effects, three *Humulus lupulus* samples were spiked with varying concentrations within the high, medium and low calibration ranges to provide a cannabinoid-free matrix. *H. lupulus*, in addition to lacking cannabinoids, exhibits a terpene profile similar to that of *C. sativa*. These spiked samples were analysed in triplicate, and the RE was calculated using Formula (4).¹⁰

$$RE [\%] = \left(\frac{conc_{spiked\ sample} - conc_{authentic\ sample}}{conc_{spiking}} \right) \times 100 \quad (4)$$

2.2.2.3. Preparation of standards

Two calibration ranges were selected and validated. For the minor calibration range, two stock solutions were prepared, containing concentrations of 1000 µg/ml for terpenes and 40 µg/ml for cannabinoids, respectively. Direct dilutions were prepared by mixing these stock solutions in various ratios. Each validation day involved combining 100 µl of the respective Cal or QC with 20 µl of an IS stock solution, resulting in a final IS concentration of 20 µg/ml for propylparaben and 0.18 µg/ml for Δ⁹-THC-D3. The concentration scheme for the minor calibration range is listed in Table 10. The concentration scheme for the major calibration range is listed in Table 11 and was derived by direct dilution of commercially available cannabinoid solutions with a concentration of 1000 µg/ml. On each validation day, the Cal and QC stock solutions were diluted 1:1 with an IS stock solution, resulting in a final IS concentration of 0.18 µg/ml for Δ⁹-THC-D3.

Table 10: Concentration scheme of Cals and QCs for the lower calibration range. Taken from Raeber et al.⁷⁰

	Cal 1	Cal 2	Cal 3	Cal 4	Cal 5	Cal 6	QC _{High}	QC _{med}	QC _{low}
Terpene conc. [µg/ml]	250	200	100	50	10	5	225	75	30
Cannabinoids conc. [µg/ml]	20	15	8	5	1	0,1	18	6	0,3
Cannabinoid acids conc. [µg/ml]	20	15	8	5	1	0,5	18	6	2

Table 11: Concentration scheme of Cals and QCs for the high calibration range. Taken from Raeber et al.⁷⁰

	Cal 1	Cal 2	Cal 3	Cal 4	Cal 5	Cal 6	QC ^{High}	QC ^{med}	QC ^{low}
Cannabinoids conc. [µg/ml]	60	40	20	5	1	0.1	55	30	0.25
CBDA conc. [µg/ml]	60	40	20	8	5	1	55	30	3

2.2.2.4. Preparation and analysis of authentic *C. sativa* L. samples

The extraction of *C. sativa* L. flowers and *H. lupulus* was performed according to the scheme shown in Figure 20. Authentic sample preparation was carried out by the Swiss Drug Testing Lab (Winterthur, Switzerland) and generously provided to this study. On the day of the analysis, the crude ethanolic extract was combined with an IS stock solution, resulting in a final concentration of 20 µg/ml for propylparaben and 0.18 µg/ml for Δ^9 -THC-D3. These samples were subjected to LC-APCI-MS/MS analysis for minor compound quantification. For major compound quantification, the crude extract was first diluted 50-fold with ethanol and then mixed in a 1:1 ratio with an IS stock solution, resulting in a final concentration of 0.18 µg/ml Δ^9 -THC-D3. The instrument was tested with a system suitability test consisting of 200 µg/ml α -pinene, β -pinene, α -humulene, β -caryophyllene and cis- and trans-citral after every 10 measurements. Carryover was controlled by injecting a blank ethanol sample after every five samples. In addition, low, medium and high QC samples were acquired after every 20 injections.

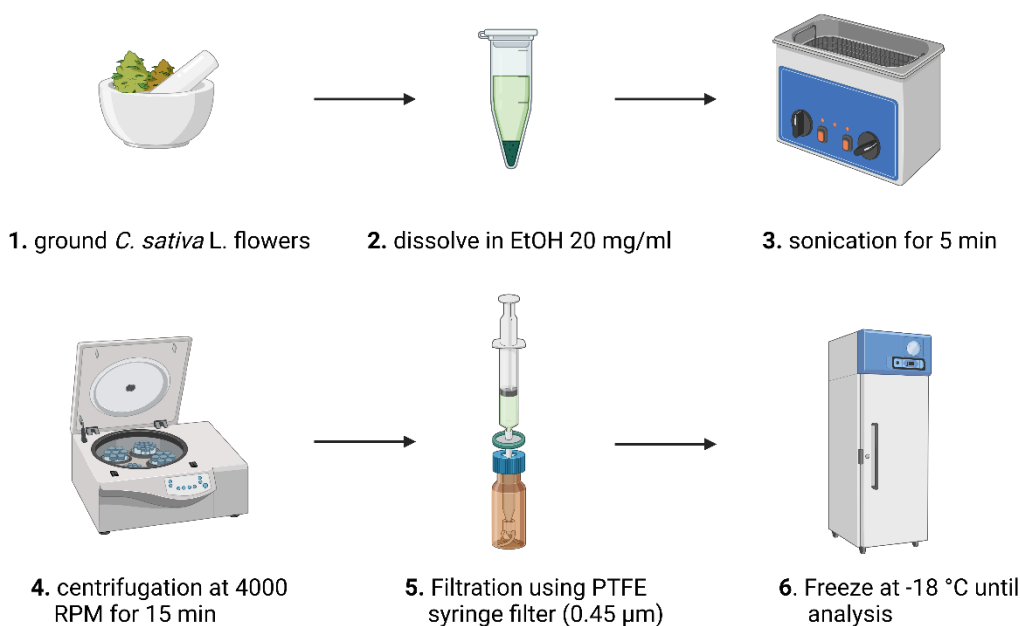


Figure 20: Sample preparation scheme for authentic *C. sativa* L. samples. Created with BioRender.com.

2.2.2.5. Method comparison to GC-FID

15 randomly selected authentic *C. sativa* L. extracts were subjected to additional GC-FID analysis following the method previously published.¹⁰ The instrument setup consisted of a GC Trace 1600 equipped with an AI 3000 autosampler (Thermo Fisher Scientific, Waltham, MA, USA). Separation was achieved with a BGB-wax column (30 m x 0.25 mm x 0.25 μ m, BGB Analytik, Boeckten, Switzerland). Adjustments to the method were made by lowering the split ratio to 1:10. Helium 6.0 (PanGas, Dagmersellen, Switzerland) served as a carrier gas. Data acquisition was carried out using Chromeleon software (Thermo Fisher Scientific, Version 7.3.1.). Calibration solutions according to the scheme in Table 10 were used to construct regression functions for the quantification of *C. sativa* L. samples.

2.2.2.6. Data visualisation and analysis

Data visualisation and analysis were performed using different software tools. Chromatograms were generated using Python (Version 3.11.6), including the matplotlib and seaborn libraries. Pearson correlation and violin plots were generated

using GraphPad Prism (Version: 10.1.2). PCA was performed using MATLAB (Version: Release R2022b, version: 9.13.0; The Mathworks Inc.). Before analysis, the data was pre-processed, which involved excluding variables with zero entries and applying auto-scaling. The programming code used for both Python and MATLAB is available in the Appendix in the Scripts A2-A4.

2.3. Comprehensive Analysis of Chemical and Enantiomeric Stability of Terpenes in *Cannabis sativa* L. flowers

2.3.1. Results and discussion

So far, the development of a GC-based method for the separation of major, minor, and chiral components of *R. damascena* and an LC-based method for the simultaneous analysis and quantification of terpenes and cannabinoids in *C. sativa* L. have been discussed. While these methods can help determine the authenticity, chemotype, and/or origin of a natural product, the role of ageing and stressors such as light and heat on terpene patterns remains to be elucidated. Altered terpene patterns may be due not only to adulteration and species confusion, but also to processing, storage, and ageing parameters. Terpenes are highly susceptible to atmospheric oxygen, temperature, and UV exposure. These stressors can in return lead to reactions such as isomerisation, (photo)oxidation, dehydrogenation, polymerisation, and thermal rearrangement.⁶⁰⁻⁶⁴ This section presents the development of four analytical methods for determining selected terpenes in *C. sativa* L., utilising apolar, polar, and chiral GC separation with either MS or FID detection. The ageing and stability of cannabinoids in *C. sativa* L. is well understood and has been studied in detail, but it is not yet known how the stability of the terpenes is affected and whether or what type of rearrangement reactions occur.^{59, 186, 187} The identification of these ageing products is not without relevance: These chemical transformations can lead to the formation of allergenic substances. They can also be converted into other terpenes, which can lead to a loss of quality and/or pharmacological activity in a natural product.^{58, 60} In particular, terpenes found in *C. sativa* L. appear to play a crucial role in the overall stability of cannabis-based pharmaceuticals. A study by Bueno et al. found that the addition of terpenes reduced the degradation of THC by almost 50% over time.⁵⁹ Terpenes therefore also play a crucial role as natural stability enhancers.

2.3.1.1. Method validation

A total of 29 analytes were included in the method development and validation, comprising of 13 enantiomers and five diastereomers. With the exception of sabinene, all enantiomers were satisfactorily separated. However, none of the chiral columns used in this study could separate all analytes simultaneously, as evidenced by the co-elution of (S)-limonene with p-cymene and α -terpinene on the respective chiral columns. The separation on both chiral columns is partially complementary. During the chromatographic separation of farnesol, three peaks were observed on both the BGB-wax and the chiral BGB 178 30% CD column, corresponding to the E/Z, E/E, and Z/E configurations of farnesol. As the exact assignment of these configurations was not possible, they were labelled based on their elution order (e.g., Farnesol 1, 2, 3). The same approach was taken for enantiomers lacking literature RI values for the respective chiral column. Co-eluting analytes were excluded from method validation. Following the specifications in the Ph. Eur. 11.5, complete peak separation is achieved when the R_s value is greater than 1.5.¹⁸⁸ Co-elution was observed for neryl acetate (**22**) and trans-citral (**23**) on the BGB-wax column, showcased in Figure 21. However, all other analytes exhibited R_s values greater than 1.5.

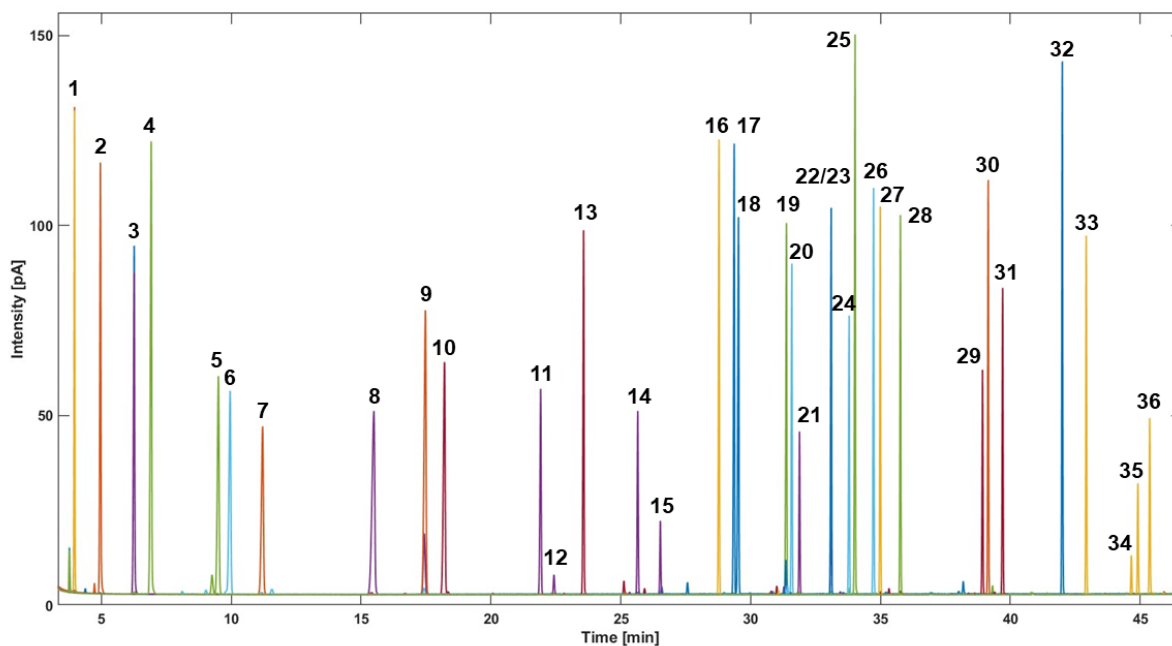


Figure 21: Chromatographic profile of 29 analytes separated on a BGB-wax column. Figure taken from Raeber et al.¹⁸⁹

Results for method validation of the BGB-wax column resulted in a bias, RSD_R , and RSD_T within $\pm 15\%$ (Table 12). Plots displaying the fitted regression curves can be found in Figure A14 in the Appendix. Table A11 in the Appendix contains the results for the respective regression functions. Co-elution was observed for α -terpinene (**9**), (S)-limonene (**10**), (+/-)-cis-menthone (**21**) and (+)-linalool (**22**) on the BGB 178 30% CD column, presented in Figure 22. The R_s value was below 1.5 for numerous analytes (Table 13). However, method validation showed acceptable results within the range of $\pm 20\%$, ensuring reliable quantification of lower-resolved peaks. Validation failed for some analytes in the QC_{low} range, namely (+)- β -pinene, (+/-)-trans-rose oxide 2, (+/-)-trans-menthone 1 and 2, (+/-)-cis-nerolidol 1, farnesol 1 as well as trans- and cis-citral. Enantiomeric separation added an additional dilution step, rendering the lower calibration range only semi-quantitative. Plots displaying the fitted regression curves can be seen in Figure A15 in the Appendix. Table A12 in the Appendix contains the results for the respective regression functions.

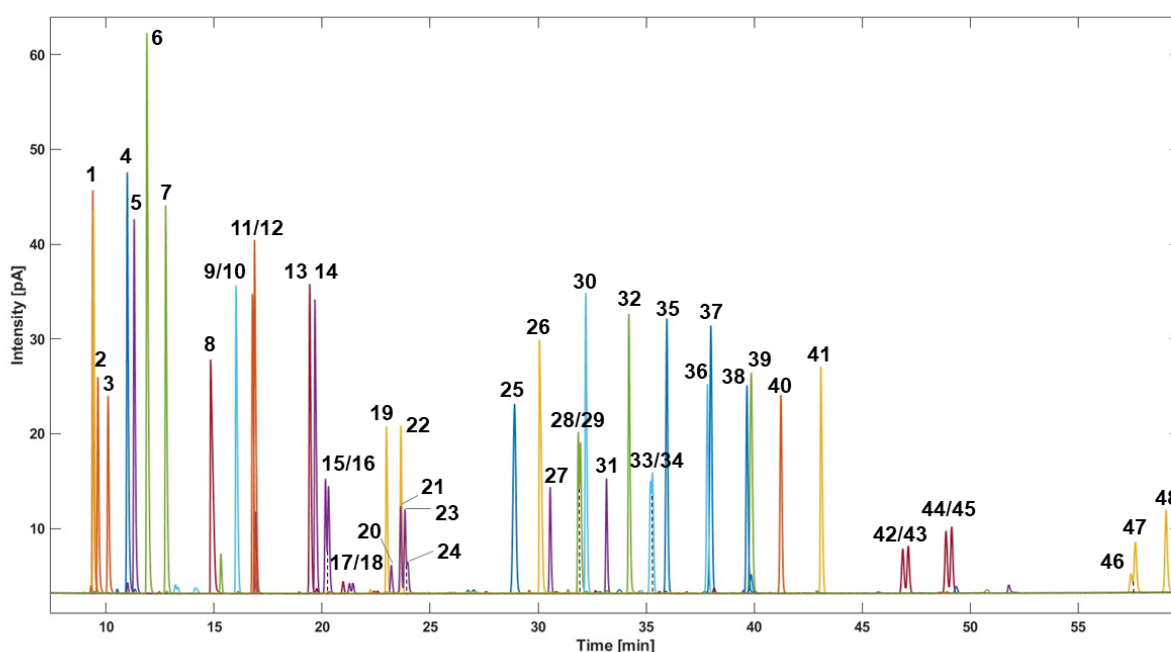


Figure 22: Chromatographic profile of 29 analytes separated on a BGB 178 30% CD column. Figure taken from Raeber et al.¹⁸⁹

Co-elution was observed for (+)- β -pinene (**7**), cis-hexen-1-ol (**8**), p-cymene (**11**), (S)-limonene (**12**), nerol (**30**) and (+/-)-citronellol (**31**) on the BGB 176 SE column as displayed in Figure 23. R_s values below 1.5 did also not appear to affect quantitation.

However, validation failed in the QC_{low} range for cis-citral, (+/-)-trans-rose oxide and (+/-)-trans menthone 2. Validation data for the respective column is available in Table 14. Plots displaying the fitted regression curves are shown in Figure A16 in the Appendix. Table A13 in the Appendix contains the results for the respective regression functions.

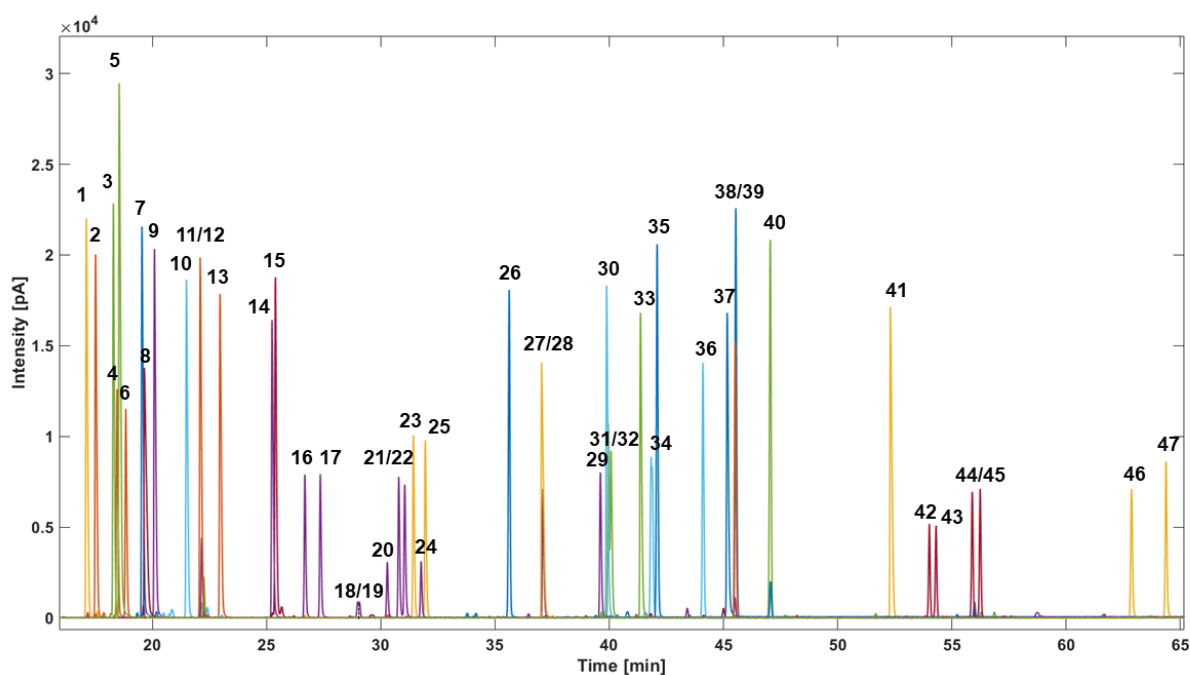


Figure 23: Chromatographic profile of 29 analytes separated on a BGB 176 SE column. Figure taken from Raeber et al.¹⁸⁹

Lastly, a method based on GC-MS was developed. Satisfactory separation was achieved for most analytes, with the exception of nerol (**18**), citronellol (**19**), citronellyl acetate (**25**), and eugenol (**26**), as displayed in Figure 24. Validation results were all within the $\pm 20\%$ cut-off. Detailed results of the validation can be studied in Table 15. Plots displaying the fitted regression curves can be seen in Figure A17 in the Appendix. Table A14 in the Appendix contains the results for the respective regression functions. The difference in sensitivity between the GC-MS DB-5 MS and GC-FID DB-wax based methods is striking. The LoD and LoQ values were two to ten times higher in GC-MS than for GC-FID. The results of the method validations confirm that one method rarely fits all analytes.

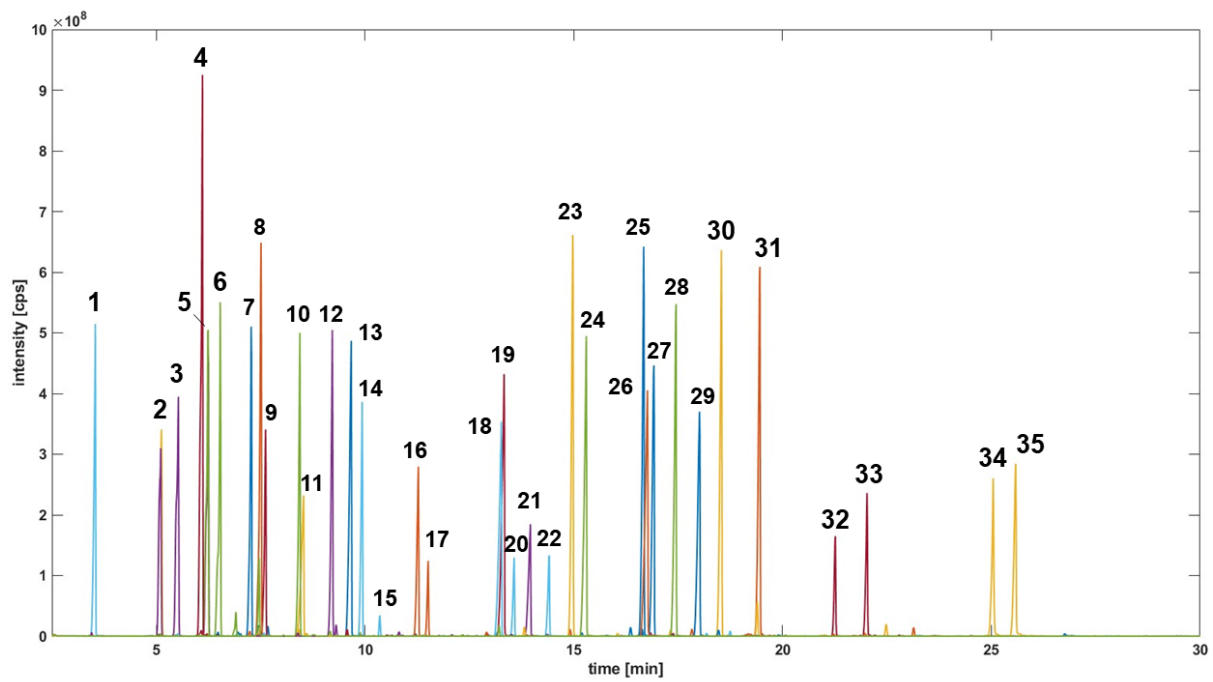


Figure 24: Chromatographic profile of 29 analytes separated on a DB-5 MS column. Figure taken from Raeber et al.¹⁸⁹

Table 12: Results from a five-day method validation for GC-FID using a BGB-wax column. Abbreviations correspond as follows: retention time (RT), resolution (R_s), retention index (RI), quality control (QC), intraday and interday imprecision (RSD_R and RSD_T). Table taken from Raeber et al.¹⁸⁹

#	Analyte	RT [min]	R_s	RI	Range [$\mu\text{g/ml}$]	LoD/LoQ [ng]	QC _{high}			QC _{med}			QC _{low}		
							Bias [%]	RSD_R [%]	RSD_T [%]	Bias [%]	RSD_R [%]	RSD_T [%]	Bias [%]	RSD_R [%]	RSD_T [%]
1	α -pinene	3.98 \pm 0.01	13.84	1013	30-875	0.87/2.64	-2.3	1.67	1.54	-2.0	1.74	1.80	7.2	1.50	4.60
2	camphene	4.96 \pm 0.01	15.73	1048	25-760	0.90/2.72	-2.1	1.29	1.26	-1.9	1.67	1.72	7.9	1.58	3.52
3	β -pinene	6.27 \pm 0.00	7.10	1095	40-1260	0.91/2.76	-1.7	1.50	1.21	-1.5	1.71	1.71	7.4	1.32	3.71
4	sabinene	6.91 \pm 0.01	25.68	1108	10-300	0.97/2.93	-2.1	1.43	1.35	-1.8	2.26	2.18	9.0	1.39	2.83
5	myrcene	9.51 \pm 0.02	3.39	1150	25-780	1.09/3.29	-1.7	1.30	1.38	-1.4	2.28	2.08	10.5	1.94	4.74
6	α -terpinene	9.96 \pm 0.02	8.75	1157	30-990	0.99/3.01	-2.0	1.74	1.30	-2.1	2.01	2.29	9.0	1.85	4.41
7	limonene	11.23 \pm 0.03	23.77	1177	30-860	1.08/3.27	-1.7	0.89	0.91	-1.4	1.81	1.54	9.3	1.03	3.59
8	γ -terpinene	15.48 \pm 0.05	13.10	1237	30-840	1.06/3.20	-0.5	0.53	0.87	-1.3	2.31	2.14	10.1	1.07	3.41
9	p-cymene	17.48 \pm 0.03	5.60	1263	30-830	1.06/3.21	-1.4	0.44	1.08	-1.5	1.30	1.53	7.2	1.02	4.67
10	α -terpinolene	18.23 \pm 0.02	33.77	1272	30-1000	1.06/3.23	-0.9	0.22	0.68	-1.4	1.72	1.52	9.4	0.84	2.50
11	cis-rose oxide	21.93 \pm 0.03	5.56	1338	30-830	0.04/0.11	0.7	0.21	0.65	2.7	0.92	1.14	-7.0	2.40	3.69
12	trans-rose-oxide	22.45 \pm 0.03	12.71	1350	3-85	0.25/0.74	1.7	1.97	1.62	3.5	1.85	1.36	-7.1	4.58	5.09
13	cis-3-hexen-1-ol	23.56 \pm 0.01	23.71	1377	NA	NA	NA	NA	NA	NA	NA	NA	NA	NA	NA
14	trans-menthone	25.66 \pm 0.02	9.98	1437	20-630	0.15/0.45	1.0	0.40	0.89	2.4	0.96	1.04	-6.3	2.73	3.65
15	cis-menthone	26.53 \pm 0.02	25.53	1464	10-260	0.15/0.45	1.9	1.10	1.81	2.1	1.23	1.31	-3.1	3.12	6.91
16	linalool	28.78 \pm 0.01	6.58	1542	25-770	0.43/1.30	0.9	0.69	0.73	2.0	1.11	1.10	-8.1	0.91	2.50
17	isobornyl acetate	29.37 \pm 0.01	1.70	1564	30-930	1.34/4.07	0.2	1.53	1.81	-1.5	1.66	1.71	8.2	0.84	3.29
18	β -caryophyllene	29.54 \pm 0.02	20.99	1571	30-940	0.37/1.12	0.4	1.97	2.61	1.5	1.59	1.39	-8.2	0.29	2.15
19	α -humulene	31.38 \pm 0.02	2.50	1643	25-800	0.28/0.84	0.6	1.70	2.38	2.2	2.33	2.56	-10.0	0.83	5.20
20	citronellyl acetate	31.59 \pm 0.01	3.52	1652	30-980	0.19/0.58	1.1	1.35	2.21	1.5	1.58	1.23	-6.7	1.71	3.25

21	cis-citral	31.89 ± 0.02	13.73	1664	10-370	0.45/1.36	-0.1	3.85	5.36	0.4	3.38	6.10	0.6	1.03	6.05
22	neryl acetate	33.10 ± 0.01	6.63	1716	NA	NA	NA	NA	NA	NA	NA	NA	NA	NA	NA
23	trans-citral	33.10 ± 0.01	6.63	1716	NA	NA	NA	NA	NA	NA	NA	NA	NA	NA	NA
24	geranyl acetate	33.80 ± 0.01	3.33	1747	30-950	0.42/1.28	0.9	1.59	2.44	1.3	2.01	1.68	-7.6	0.66	2.34
25	citronellol	34.01 ± 0.01	16.34	1756	30-920	0.23/0.69	1.6	1.17	1.83	1.7	1.55	1.40	-6.0	1.73	3.02
26	nerol	34.73 ± 0.01	5.67	1788	35-1000	0.43/1.31	0.9	1.32	1.88	1.5	1.68	1.39	-7.6	0.67	2.37
27	phenylethanol	34.97 ± 0.01	17.93	1799	20-580	0.51/1.54	0.5	1.24	1.34	1.8	1.20	1.14	-8.7	0.39	2.22
28	geraniol	35.76 ± 0.01	40.98	1837	35-990	0.24/0.73	1.1	1.42	2.12	1.3	1.87	1.53	-7.0	1.38	2.07
29	cis-nerolidol	38.93 ± 0.01	2.50	1992	10-310	0.58/1.75	1.5	2.76	4.10	0.8	2.58	2.33	-4.6	1.62	3.25
30	methyleugenol	39.15 ± 0.01	7.13	2003	2-1065	0.54/1.64	1.0	1.72	2.69	1.4	2.20	1.89	-7.3	1.37	2.15
31	trans-nerolidol	39.70 ± 0.01	29.82	2031	15-450	0.76/2.30	1.4	3.04	4.09	-0.6	2.93	4.41	-5.1	1.98	4.42
32	eugenol	41.99 ± 0.01	14.44	2152	35-1000	1.24/3.75	1.4	1.53	2.65	1.3	2.25	2.24	-3.2	1.99	3.45
33	carvacrol	42.91 ± 0.01	21.61	2202	30-970	1.09/3.29	1.3	2.05	3.20	1.5	2.27	2.22	-2.8	2.04	2.74
34	farnesol 1	44.66 ± 0.01	3.11	2301	4-120	0.73/2.22	1.0	6.53	7.07	-1.1	4.11	7.17	-0.3	8.95	7.81
35	farnesol 2	44.91 ± 0.01	6.99	2316	11-330	1.84/5.58	0.6	5.86	6.34	0.0	4.29	4.66	1.0	10.57	8.75
36	farnesol 3	45.37 ± 0.01	NA.	2343	20-520	1.76/5.34	0.5	6.14	6.61	-0.1	4.80	4.95	0.6	10.62	8.62

Table 13: Results from a five-day method validation for GC-FID using a BGB 178 30% CD column. Abbreviations correspond as follows: retention time (RT), resolution (R_s), retention index (RI), quality control (QC), intraday and interday imprecision (RSD_R and RSD_T). Bold numbers indicate validation results outside of $\pm 20\%$. Table taken from Raeber et al.¹⁸⁹

#	Analyte	RT [min]	R_s	RI	Range [$\mu\text{g/ml}$]	LoD/LoQ [ng]	QC _{high}			QC _{med}			QC _{low}		
							Bias [%]	RSD_R [%]	RSD_T [%]	Bias [%]	RSD_R [%]	RSD_T [%]	Bias [%]	RSD_R [%]	RSD_T [%]
1	(\pm)- α -pinene	9.24 \pm 0.09	1.27	932	15-875	0.27/0.82	-0.4	2.46	2.55	1.4	2.15	3.14	-9.5	2.17	3.21
2	(\pm)-camphene 1	9.50 \pm 0.07	3.25	938	7-395	0.24/0.72	-0.5	2.36	2.35	1.7	2.20	3.09	-9.4	2.63	3.82
3	(\pm)-camphene 2	9.94 \pm 0.08	7.53	947	6-360	0.24/0.72	-0.6	2.25	2.25	1.4	2.05	2.97	-9.6	1.23	2.95
4	(+)- β -pinene	10.86 \pm 0.08	3.14	967	1-35	0.67/2.03	-0.2	2.65	2.29	1.6	1.33	3.63	-20.5	12.31	18.02
5	(-)- β -pinene	11.15 \pm 0.09	5.71	973	20-1230	0.19/0.57	0.4	3.37	2.58	1.8	2.34	3.14	-8.0	1.58	4.12
6	sabinene	11.74 \pm 0.10	8.18	986	5-300	0.06/0.17	0.0	2.10	2.31	1.6	2.17	2.86	-9.3	1.90	3.01
7	myrcene	12.58 \pm 0.11	20.65	1003	13-770	0.28/0.86	0.2	2.10	2.21	2.5	1.70	2.59	-9.9	1.31	2.89
8	cis-3-hexen-1-ol	14.53 \pm 0.18	10.28	1038	NA	NA	NA	NA	NA	NA	NA	NA	NA	NA	NA
9	α -terpinene	15.75 \pm 0.15	7.14	1059	NA	NA	NA	NA	NA	NA	NA	NA	NA	NA	NA
10	(S)-limonene	15.75 \pm 0.15	7.14	1059	NA	NA	NA	NA	NA	NA	NA	NA	NA	NA	NA
11	(R)-limonene	16.47 \pm 0.14	0.62	1072	30-860	1.21/3.67	0.3	1.95	3.37	2.7	1.43	2.89	-12.1	1.65	4.28
12	p-cymene	16.59 \pm 0.14	12.92	1074	30-830	0.57/1.73	0.6	1.73	1.97	1.5	1.56	2.72	-9.3	1.57	2.70
13	α -terpinolene	19.17 \pm 0.13	1.33	1118	35-1000	0.16/0.49	0.1	1.59	2.22	2.2	1.14	2.34	-10.3	2.02	2.12
14	γ -terpinene	19.38 \pm 0.16	2.40	1122	30-840	0.14/0.44	-0.3	1.88	2.58	2.1	1.30	2.50	-10.8	2.25	2.57
15	(\pm)-cis-rose oxide 1	19.94 \pm 0.11	0.56	1131	15-400	0.39/1.18	1.3	1.76	2.03	3.0	1.03	1.94	-5.3	1.64	3.18
16	(\pm)-cis-rose oxide 2	20.08 \pm 0.11	4.64	1133	15-435	0.46/1.39	1.0	1.72	1.43	2.8	1.42	2.24	-6.5	2.81	3.21
17	(\pm)-trans-rose oxide 1	21.05 \pm 0.11	0.61	1149	1-40	2.69/8.16	1.0	1.69	1.74	3.9	2.48	2.16	5.1	17.81	14.98
18	(\pm)-trans-rose oxide 2	21.20 \pm 0.11	7.30	1152	1-40	2.90/8.78	0.9	1.78	2.02	3.3	2.30	2.88	6.9	28.98	26.45
19	(-)-linalool	22.71 \pm 0.13	1.36	1177	13-390	0.95/2.89	0.6	1.54	1.98	1.9	0.93	1.61	-10.2	1.89	2.90

20	(±)-cis-menthone 1	23.04 ± 0.08	2.38	1182	5-140	1.91/5.80	3.3	2.75	6.15	1.0	7.33	8.32	-0.9	4.07	17.09
21	(±)-cis-menthone 2	23.37 ± 0.14	1.29	1188	NA	NA	NA	NA	NA	NA	NA	NA	NA	NA	NA
22	(+)-linalool	23.37 ± 0.14	1.29	1188	NA	NA	NA	NA	NA	NA	NA	NA	NA	NA	NA
23	(±)-trans-menthone 1	23.61 ± 0.11	0.81	1192	1-320	2.40/7.28	-2.3	6.48	13.08	0.6	1.94	9.56	-11.3	10.10	21.65
24	(±)-trans-menthone 2	23.77 ± 0.09	25.38	1194	4-120	1.36/4.11	5.8	7.49	9.49	-1.6	2.22	10.21	-24.6	3.94	46.18
25	isobornyl acetate	28.86 ± 0.02	7.09	1278	30-930	0.26/0.79	1.0	1.87	1.89	2.2	0.71	1.82	-10.3	1.83	3.44
26	phenylethanol	29.81 ± 0.15	3.17	1293	20-580	0.97/2.94	0.7	1.40	1.83	2.2	0.76	1.89	-9.7	1.11	2.24
27	trans-citral	30.34 ± 0.10	8.55	1301	12-370	1.33/4.04	-0.2	6.29	9.61	1.0	5.12	8.27	-50.5	2.68	93.09
28	(±)-citronellol 1	31.64 ± 0.10	0.61	1323	13-390	0.69/2.10	2.2	2.88	2.58	2.0	2.69	2.32	-4.0	4.63	5.75
29	(±)-citronellol 2	31.74 ± 0.10	1.76	1324	20-530	0.86/2.61	1.7	2.56	2.83	3.0	2.51	2.36	-6.5	2.81	6.38
30	nerol	31.98 ± 0.10	6.31	1328	35-1000	1.22/3.69	1.3	2.24	1.99	2.1	2.04	2.42	-8.5	1.38	1.87
31	cis-citral	32.93 ± 0.09	7.32	1344	15-440	1.30/3.95	1.2	7.42	14.20	8.7	5.70	18.84	-53.0	4.78	95.20
32	geraniol	33.99 ± 0.10	6.65	1361	35-985	0.88/2.66	1.2	3.04	2.57	2.3	1.57	2.49	-7.6	2.22	4.15
33	(±)-citronellyl acetate 1	35.07 ± 0.06	0.61	1379	15-440	0.62/1.88	1.6	2.95	6.02	1.0	6.89	6.26	-1.8	3.09	9.47
34	(±)-citronellyl acetate 2	35.15 ± 0.05	4.48	1381	20-545	0.99/3.01	1.8	6.00	5.42	0.8	6.45	5.36	-11.8	5.36	14.66
35	neryl acetate	35.84 ± 0.05	12.82	1392	30-890	0.56/1.71	1.0	2.29	2.20	-0.2	1.56	2.63	2.7	1.78	7.84
36	geranyl acetate	37.71 ± 0.06	0.87	1423	30-955	0.81/2.46	2.8	1.88	2.68	0.3	0.94	2.89	10.3	1.50	6.14
37	β-caryophyllene	37.88 ± 0.05	9.82	1426	30-990	0.63/1.91	1.1	2.50	1.84	0.3	1.27	1.48	2.2	1.72	7.37
38	eugenol	39.51 ± 0.07	1.05	1454	35-1000	0.35/1.05	1.6	3.75	3.64	1.9	2.64	3.59	-3.7	0.73	4.92
39	α-humulene	39.78 ± 0.03	8.02	1458	30-940	0.80/2.41	0.9	2.82	2.55	-0.3	1.49	2.08	6.2	1.66	8.71
40	methyleugenol	41.12 ± 0.05	12.68	1481	35-1060	1.07/3.24	1.4	2.73	2.11	2.4	1.96	2.77	-7.6	2.26	5.32
41	carvacrol	42.91 ± 0.08	19.12	1511	2-970	0.58/1.77	2.3	3.18	2.52	3.1	2.68	3.08	-10.2	3.95	5.40
42	(±)-cis-nerolidol 1	46.80 ± 0.03	1.02	1578	5-155	2.14/6.49	2.0	3.19	2.37	1.8	2.68	2.96	-20.3	34.24	36.22
43	(±)-cis-nerolidol 2	47.05 ± 0.03	6.78	1583	6-170	2.64/8.00	1.9	3.46	2.70	1.6	2.38	2.98	-13.0	8.32	10.97
44	(±)-trans-nerolidol 1	48.81 ± 0.03	1.06	1614	7-220	2.06/6.26	2.0	3.37	2.50	1.1	3.05	2.88	-8.9	5.92	9.03

45	(±)-trans-nerolidol 2	49.06 ± 0.03	23.66	1618	7-220	1.73/5.25	2.7	3.51	2.99	1.0	8.16	5.92	1.7	5.24	11.23
46	farnesol 1	57.40 ± 0.01	0.54	1770	4-115	3.20/9.70	1.9	4.20	3.29	1.1	3.45	4.74	-9.3	25.77	36.95
47	farnesol 2	57.60 ± 0.02	5.08	1773	10-320	1.93/5.85	-1.4	8.54	9.87	1.0	3.65	4.21	-3.8	7.74	12.70
48	farnesol 3	59.03 ± 0.02	NA	1800	20-520	1.68/5.09	2.1	4.40	3.29	2.1	3.50	4.28	-5.3	4.61	8.23

Table 14: Results from a five-day method validation for GC-FID using a BGB 176 SE column. Abbreviations correspond as follows: retention time (RT), resolution (R_s), retention index (RI), quality control (QC), intraday and interday imprecision (RSD_R and RSD_T). Bold numbers indicate validation results outside of $\pm 20\%$. Table taken from Raeber et al.¹⁸⁹

#	Analyte	RT [min]	R_s	RI	Range [$\mu\text{g/ml}$]	LoD/LoQ [ng]	QC _{high}			QC _{med}			QC _{low}		
							Bias [%]	RSD_R [%]	RSD_T [%]	Bias [%]	RSD_R [%]	RSD_T [%]	Bias [%]	RSD_R [%]	RSD_T [%]
1	(-)- α -pinene	17.18 \pm 0.00	3.02	977	NA	NA	NA	NA	NA	NA	NA	NA	NA	NA	NA
2	(+)- α -pinene	17.56 \pm 0.01	5.61	983	30-875	5.17/15.17	-2.6	1.71	2.30	2.7	2.09	1.98	-12.7	1.60	3.51
3	myrcene	18.32 \pm 0.00	1.18	996	25-780	0.49/1.47	-1.6	1.74	3.47	2.9	2.17	1.97	-10.6	1.94	5.03
4	camphene	18.48 \pm 0.01	0.96	999	15-400	1.10/3.32	-2.7	2.29	2.25	2.8	2.37	3.15	-10.4	2.38	2.47
5	sabinene	18.63 \pm 0.00	1.84	1001	10-300	1.62/4.91	-1.4	2.88	3.87	7.6	10.48	13.61	-12.6	2.22	10.09
6	camphene	18.87 \pm 0.00	5.46	1004	10-360	0.44/1.34	-1.8	1.65	2.47	3.4	3.16	5.00	-12.4	2.32	5.51
7	(+)- β -pinene	19.69 \pm 0.01	4.13	1016	NA	NA	NA	NA	NA	NA	NA	NA	NA	NA	NA
8	cis-hexen-1-ol	19.69 \pm 0.01	4.13	1016	NA	NA	NA	NA	NA	NA	NA	NA	NA	NA	NA
9	(-)- β -pinene	20.09 \pm 0.01	10.18	1022	40-1230	1.47/4.47	-2.1	2.22	2.41	3.4	1.77	2.42	-12.5	2.82	3.83
10	α -terpinene	21.54 \pm 0.01	4.43	1042	25-800	0.59/1.79	-1.8	2.24	2.37	2.5	1.98	2.09	-9.2	2.34	3.31
11	p-cymene	22.14 \pm 0.01	6.42	1051	NA	NA	NA	NA	NA	NA	NA	NA	NA	NA	NA
12	(S)-limonene	22.14 \pm 0.01	6.42	1051	NA	NA	NA	NA	NA	NA	NA	NA	NA	NA	NA
13	(R)-limonene	23.01 \pm 0.01	16.67	1063	30-860	0.44/1.33	-2.1	1.78	2.18	2.4	1.94	2.12	-11.7	2.88	3.70
14	γ -terpinene	25.26 \pm 0.01	1.03	1095	30-840	0.55/1.66	-3.5	2.58	3.65	2.8	3.05	3.58	-9.9	2.29	7.26
15	α -terpinolene	25.40 \pm 0.01	9.28	1097	35-1000	0.54/1.62	-0.5	1.12	1.76	2.9	2.30	2.85	-13.2	6.02	8.03
16	(+/-)-cis-rose oxide 1	26.70 \pm 0.00	5.27	1116	10-415	0.43/1.30	-1.1	2.20	2.08	2.4	1.75	2.48	-9.7	4.84	5.26
17	(+/-)-cis-rose oxide 2	27.37 \pm 0.00	14.07	1126	15-420	0.25/0.76	-1.1	1.94	2.54	1.9	2.60	2.09	-10.0	4.53	5.25
18	(+/-)-trans-rose oxide 1	28.99 \pm 0.00	0.69	1150	3-40	4.71/14.28	2.7	4.75	9.60	3.6	11.38	11.32	-8.6	24.98	56.37
19	(+/-)-trans-rose oxide 1	29.07 \pm 0.00	9.68	1151	3-40	2.07/6.27	-0.3	5.93	13.18	0.9	8.11	8.22	-15.6	39.98	62.80

20	(+/-)-cis-menthone 1	30.30 ± 0.00	3.79	1170	5-140	1.52/4.60	-0.4	2.11	2.65	2.3	3.48	3.45	-10.4	11.60	18.35
21	(+/-)-cis-menthone 2	30.82 ± 0.00	2.05	1177	10-320	0.57/1.74	-1.6	3.29	2.69	3.4	1.32	1.87	-8.5	7.03	10.33
22	(+/-)-trans-menthone 1	31.07 ± 0.00	3.15	1181	10-320	0.34/1.02	-1.2	2.53	2.63	2.7	0.59	1.69	-5.4	6.96	11.06
23	(-)-linalool	31.46 ± 0.00	2.28	1186	15-390	0.41/1.24	-0.9	3.22	3.13	2.6	1.66	1.71	-6.0	7.46	10.60
24	(+/-)-trans-menthone 2	31.77 ± 0.00	1.64	1191	4-120	0.98/1.05	-0.9	4.93	7.00	3.2	3.75	3.92	-3.1	8.00	23.85
25	(+)-linalool	31.98 ± 0.00	28.56	1195	15-390	0.41/1.23	-1.2	2.20	2.55	2.5	1.83	1.95	-8.0	6.87	8.79
26	isobornyl acetate	35.63 ± 0.00	12.04	1252	30-940	0.35/1.05	-1.1	3.53	3.09	1.4	1.61	1.81	-8.5	2.37	8.35
27	phenylethanol	37.12 ± 0.01	19.28	1275	NA	NA	NA	NA	NA	NA	NA	NA	NA	NA	NA
28	trans-citral	37.12 ± 0.01	19.28	1275	NA	NA	NA	NA	NA	NA	NA	NA	NA	NA	NA
29	cis-citral	39.64 ± 0.01	1.96	1316	15-440	0.40/1.22	0.7	6.69	15.72	11.9	9.70	21.72	-52.2	9.12	92.75
30	nerol	39.91 ± 0.01	0.95	1320	NA	NA	NA	NA	NA	NA	NA	NA	NA	NA	NA
31	(+/-)-citronellol 1	39.91 ± 0.01	0.95	1320	NA	NA	NA	NA	NA	NA	NA	NA	NA	NA	NA
32	(+/-)-citronellol 2	40.09 ± 0.01	10.18	1323	15-530	1.40/4.23	-2.6	3.81	4.47	1.4	3.07	5.07	-7.8	10.79	18.72
33	geraniol	41.40 ± 0.01	2.55	1345	35-985	0.46/1.39	-0.5	5.16	5.30	2.2	3.08	3.65	-9.3	2.78	9.03
34	citronellyl acetate	41.83 ± 0.01	1.28	1352	35-980	0.21/0.65	-0.6	2.97	3.41	1.5	2.20	2.20	-9.3	1.88	5.67
35	neryl acetate	42.10 ± 0.00	15.50	1357	30-890	0.56/1.71	-0.2	3.62	3.05	-0.2	3.55	3.96	-8.5	5.08	7.26
36	geranyl acetate	44.11 ± 0.00	7.80	1390	30-955	0.50/1.53	-0.7	4.32	3.79	1.9	1.59	1.86	0.6	1.82	17.86
37	eugenol	45.20 ± 0.01	2.18	1409	35-1000	0.86/2.59	-1.7	4.17	3.64	0.9	2.04	4.32	-5.0	4.87	12.01
38	methyleugenol	45.53 ± 0.01	10.68	1415	NA	NA	NA	NA	NA	NA	NA	NA	NA	NA	NA
39	β-caryophyllene	45.53 ± 0.01	10.68	1415	NA	NA	NA	NA	NA	NA	NA	NA	NA	NA	NA
40	α-humulene	47.06 ± 0.00	37.51	1442	30-940	0.76/2.30	-1.4	4.26	3.53	0.1	1.70	4.78	-7.8	1.47	5.69
41	carvacrol	52.35 ± 0.01	13.25	1538	30-970	0.69/2.10	-0.9	5.23	4.22	0.4	1.24	2.98	-8.0	1.23	5.55
42	(+/-)-cis-nerolidol 1	54.01 ± 0.01	2.00	1569	5-140	1.38/4.19	2.3	7.20	7.04	0.2	4.89	7.51	-5.9	4.96	8.81
43	(+/-)-cis-nerolidol 2	54.30 ± 0.01	10.97	1575	5-150	1.25/3.80	-0.7	7.07	6.13	-0.6	4.37	5.52	-6.0	3.10	8.62
44	(+/-)-trans-nerolidol 1	55.89 ± 0.01	2.42	1605	10-245	0.34/1.03	0.2	6.72	5.40	1.0	2.61	4.32	-7.4	4.94	10.08

45	(+/-)-trans-nerolidol 2	56.24 ± 0.01	45.68	1612	10-230	0.90/2.74	-1.3	7.27	7.08	-0.6	2.11	5.11	-6.4	5.20	6.52
46	farnesol 1	62.86 ± 0.01	10.42	1744	15-450	0.65/1.97	-0.1	7.37	6.57	1.6	2.98	8.16	-6.7	5.44	11.80
47	farnesol 2	64.37 ± 0.01	NA	1775	20-515	0.47/1.41	0.1	8.26	6.91	1.5	2.84	5.47	-2.6	4.23	6.06

Table 15: Results from a five-day method validation for GC-MS using a DB-5 MS column. Abbreviations correspond as follows: retention time (RT), resolution (R_s), retention index (RI), quality control (QC), intraday and interday imprecision (RSD_R and RSD_T). Table taken from Raeber et al.¹⁸⁹

#	Analyte	RT [min]	R_s	RI	Range [µg/ml]	LoD/LoQ [ng]	QC _{high}			QC _{med}			QC _{low}		
							Bias [%]	RSD_R [%]	RSD_T [%]	Bias [%]	RSD_R [%]	RSD_T [%]	Bias [%]	RSD_R [%]	RSD_T [%]
1	cis-hexen-1-ol	3.50 ± 0.02	21.14	856	NA	NA	NA	NA	NA	NA	NA	NA	NA	NA	NA
2	α-pinene	5.10 ± 0.01	4.14	935	15-875	2.49/7.54	-3.2	3.94	11.96	-2.3	8.85	9.36	-12.1	6.93	17.16
3	camphene	5.51 ± 0.00	6.35	951	15-755	4.65/14.09	-2.6	4.99	11.41	2.1	12.57	10.10	-5.8	6.96	19.11
4	sabinene	6.13 ± 0.07	1.59	976	5-300	0.73/2.21	-6.7	7.62	11.76	-0.3	8.49	8.24	-2.4	10.48	10.03
5	β-pinene	6.22 ± 0.01	3.50	980	20-1260	2.87/8.68	-0.7	4.21	10.49	0.9	10.39	10.32	-11.7	12.98	16.37
6	myrcene	6.49 ± 0.09	13.80	990	15-780	1.11/3.36	-1.2	5.40	9.24	2.6	8.58	7.59	-13.2	7.81	8.07
7	α-terpinene	7.29 ± 0.01	4.65	1020	15-790	4.04/12.24	-2.3	5.70	11.14	2.4	11.99	11.00	-5.4	13.87	11.02
8	p-cymene	7.48 ± 0.05	1.97	1026	15-830	4.08/12.36	-1.2	7.32	8.31	0.2	12.26	9.55	-11.2	13.60	11.30
9	limonene	7.57 ± 0.05	14.89	1029	115-860	3.05/9.24	-1.1	6.10	7.92	1.0	12.26	9.88	-15.4	11.23	10.17
10	γ-terpinene	8.41 ± 0.01	1.53	1059	15-840	6.64/20.14	-1.2	4.35	8.77	0.4	13.48	10.06	-7.2	10.99	11.60
11	phenylethanol	8.47 ± 0.01	15.08	1061	10-580	8.97/27.18	5.2	11.71	10.27	0.3	11.60	9.17	-6.7	12.02	13.32
12	α-terpinolene	9.19 ± 0.01	7.87	1086	20-1000	1.62/4.90	1.1	8.24	9.10	0.5	16.05	12.74	-13.9	10.85	9.41
13	linalool	9.67 ± 0.11	5.62	1103	15-770	1.11/3.36	-1.5	8.19	8.12	-4.4	13.90	12.37	-3.2	9.67	13.19
14	cis-rose oxide	9.90 ± 0.01	7.70	1110	15-835	0.98/2.97	-0.9	6.34	5.84	-2.3	15.16	13.45	-9.1	12.36	13.70
15	trans-rose oxide	10.35 ± 0.01	14.26	1126	1-80	1.60/4.85	0.1	6.79	9.33	-4.4	13.28	9.99	-5.4	9.08	13.03
16	trans-menthone	11.23 ± 0.00	4.10	1157	10-640	1.30/3.94	-2.2	8.44	8.02	-1.1	14.09	13.52	-3.9	11.05	13.19
17	cis-menthone	11.48 ± 0.01	33.24	1165	4-255	2.96/8.98	-4.1	5.71	10.76	-3.6	14.24	12.75	-5.7	11.04	12.67
18	nerol	13.21 ± 0.01	1.18	1226	20-1005	6.97/21.13	-0.6	10.78	8.30	-1.9	12.58	10.57	-0.1	12.84	15.11
19	citronellol	13.26 ± 0.01	0.66	1227	30-920	1.35/4.08	-4.0	11.28	11.74	-1.3	11.89	10.46	-1.3	7.59	10.10
20	cis-citral	13.56 ± 0.00	3.17	1238	7-400	6.70/20.30	-4.9	8.61	7.80	-3.2	11.00	11.66	-7.4	12.81	12.97

21	geraniol	13.93 ± 0.01	9.83	1251	16-985	3.22/9.76	-3.9	7.57	7.01	-1.4	14.47	12.94	-3.4	9.23	10.58
22	trans-citral	14.38 ± 0.01	6.93	1267	7-410	2.07/6.28	-2.2	6.51	8.58	-2.4	9.04	13.33	-2.6	5.57	11.86
23	isobornyl acetate	14.94 ± 0.01	4.25	1287	30-930	8.12/24.60	-2.3	9.16	9.51	-0.9	9.48	13.33	-7.1	16.80	14.14
24	carvacrol	15.25 ± 0.01	18.21	1298	30-970	5.76/17.45	-2.5	7.57	7.63	-1.2	12.78	13.36	-4.8	14.85	13.14
25	citronellyl acetate	16.65 ± 0.01	2.62	1350	35-985	2.88/8.72	-2.2	11.26	9.43	-0.5	11.66	12.10	-1.5	13.43	11.57
26	eugenol	16.70 ± 0.02	0.78	1352	20-1000	5.48/16.60	-2.5	6.19	7.65	6.3	4.71	3.94	10.8	6.24	10.16
27	neryl acetate	16.88 ± 0.01	2.04	1360	15-890	3.53/10.69	-3.3	4.24	6.46	0.4	10.31	12.31	-5.3	9.95	9.12
28	geranyl acetate	17.41 ± 0.01	8.06	1379	15-955	1.24/3.77	-3.4	4.91	6.52	-2.0	12.91	13.58	-4.9	9.78	8.80
29	methyleugenol	17.97 ± 0.02	7.05	1397	20-1065	2.838.59	-3.3	5.43	6.79	-1.5	12.06	12.54	-4.0	13.12	12.05
30	β-caryophyllene	18.51 ± 0.01	19.18	1421	20-990	1.80/5.47	-4.6	6.08	7.53	-2.3	12.96	14.17	-4.5	16.62	12.38
31	α-humulene	19.42 ± 0.01	27.11	1457	15-940	7.57/22.95	-1.7	6.36	7.16	1.2	11.97	12.21	-8.8	19.45	17.53
32	cis-nerolidol	21.24 ± 0.01	9.03	1530	5-305	6.91/20.94	-1.2	8.25	7.33	0.6	10.20	11.21	-3.1	13.51	13.44
33	trans-nerolidol	21.99 ± 0.01	28.38	1561	8-460	7.40/22.43	-1.9	4.33	5.75	-2.3	6.46	11.97	-7.2	16.39	15.28
34	farnesol 1	25.01 ± 0.01	3.65	1687	8-460	3.68/11.16	-3.7	5.40	6.67	-0.1	15.42	14.88	1.0	9.50	12.50
35	farnesol 2	25.53 ± 0.00	n.a.	1710	8-500	2.74/8.32	-2.8	5.75	6.87	-1.2	13.89	13.25	-4.3	8.60	6.69

2.3.1.2. Stress testing of single analytes and multi-mix

A mixed effects model was used to assess the individual effects of heat and UV treatment of terpenes present in a multi-mix. The model was fitted with two fixed effects: time and treatment, and an interaction term (time x treatment). Results were considered significant when the P-value was below 0.05. Results from the mixed effects model were consistent across columns (Tables A15-17, Appendix). According to the mixed effects model, time was the main driver of reduced terpene content, with the exception of p-cymene, which increased in concentration (Figure 25 F).

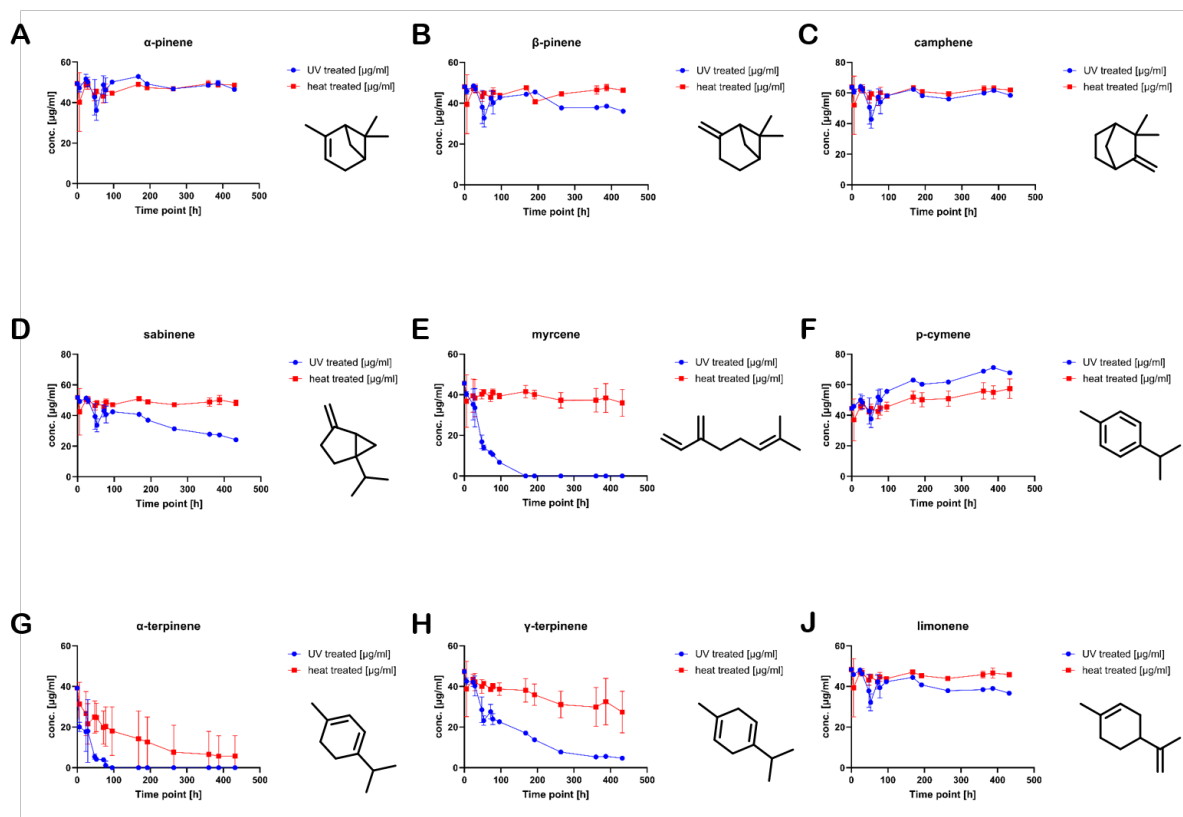


Figure 25: Degradation profiles (n=3) of selected non-oxygenated monoterpenes in a terpene multi-mix after UV (blue) and heat (red) treatment. Data was obtained using GC-FID on a BGB-wax column. Figure taken from Raeber et al.¹⁸⁹

P-cymene is frequently described in the literature as a product of terpene ageing. However, conflicting observations exist: while some studies have reported an increase in concentration, others have reported a decrease. This may be related to the antioxidant effect of terpenes. Depending on the terpene composition, different oxidative reactions can occur.^{58, 190-192} Despite the strong structural similarities among

terpenes, different degradation rates were observed. In particular, rapid degradation was observed for α -terpinene after 72 hours and myrcene after 96 hours (Figure 25, G and E). Myrcene, a common terpene in *C. sativa* L., is linked to more than 40 autoxidation products.¹⁹³ One of these products, hashishene, has recently been identified as a terpene formed from myrcene degradation in *C. sativa* L.¹⁹⁴ However, hashishene formation was not observed in stressed single-analyte samples or in the multi-mix. When exposed to UV light, stressed myrcene samples primarily undergo cyclisation and polymerisation reactions. The formation of α - and β -pinene, as well as *p*-cymene, was confirmed by GC-FID. Additionally, pseudolimonene, trans-geranylgeraniol, geranylgeraniol, 3-carene, geranylgeraniol, and 1-heptatriacontanol were putatively identified by GC-MS (Figure 26). Detailed chromatographic profiles and MS-spectra are available in Figures A18-A23 in the Appendix.

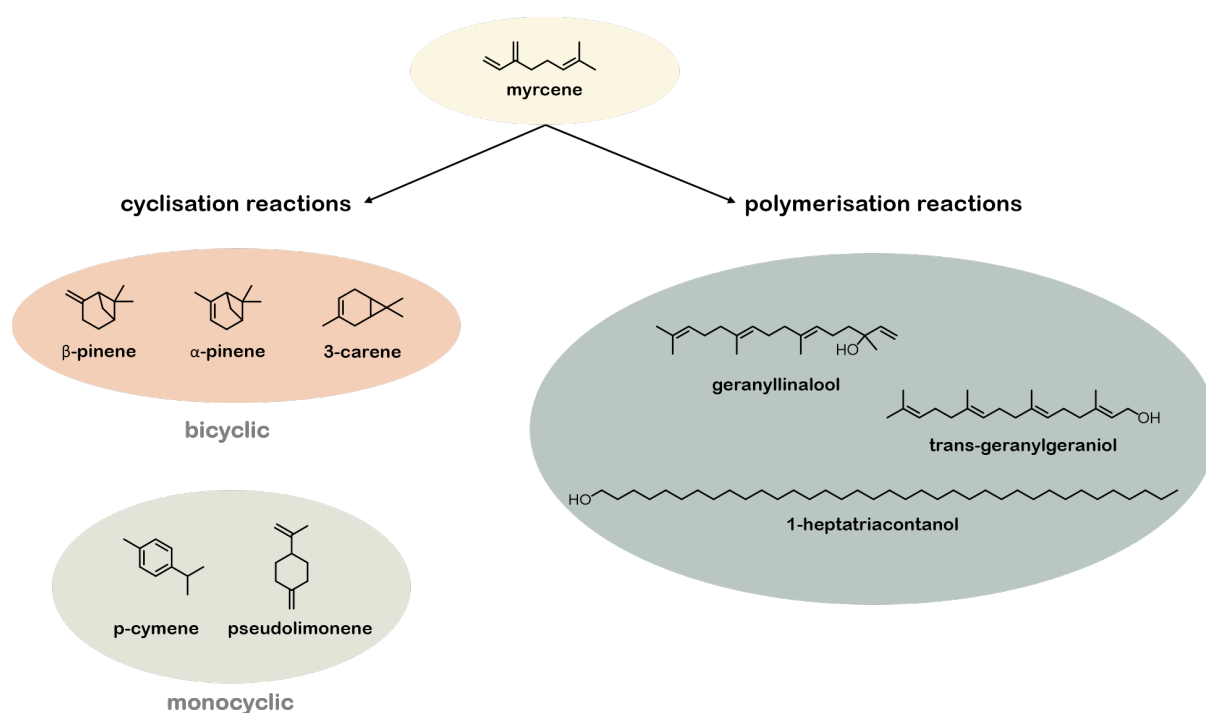


Figure 26: Degradation products observed for myrcene after exposure to UV light.

Even among double bond isomers, highly variable degradation rates can be observed, as demonstrated for α -terpinene, γ -terpinene, and limonene (Figure 25, G-J). α -terpinene is completely degraded after 72 h, whereas γ -terpinene remains detectable at the end of the stress experiment. Furthermore, numerous transformation reactions were observed for stressed α -terpinene samples, as shown in Figure 27, ranging from oxidation to isomerisation, dehydrogenation, and ring opening (Figures

A24-A25, Appendix). In contrast, fewer degradation products were detected in γ -terpinene single analyte experiments. Primarily, p-cymene was formed after UV treatment, but small traces of α -terpinene, α -terpinolene, cis-citral, and carveol were also detected (Figures A26-A27, Appendix). P-cymene was identified as a degradation product of both α -terpinene and γ -terpinene. Limonene, which contains an exocyclic double bond, displayed prolonged stability throughout the entire stress experiment (Figure 25 J). Only traces of myrcene and 3-carene were detected during UV exposure in single analyte experiments of limonene (Figures A45-A46, Appendix). Overall, α -terpinene, γ -terpinene, and limonene were found to be more susceptible to degradation during UV treatment compared to heat treatment.

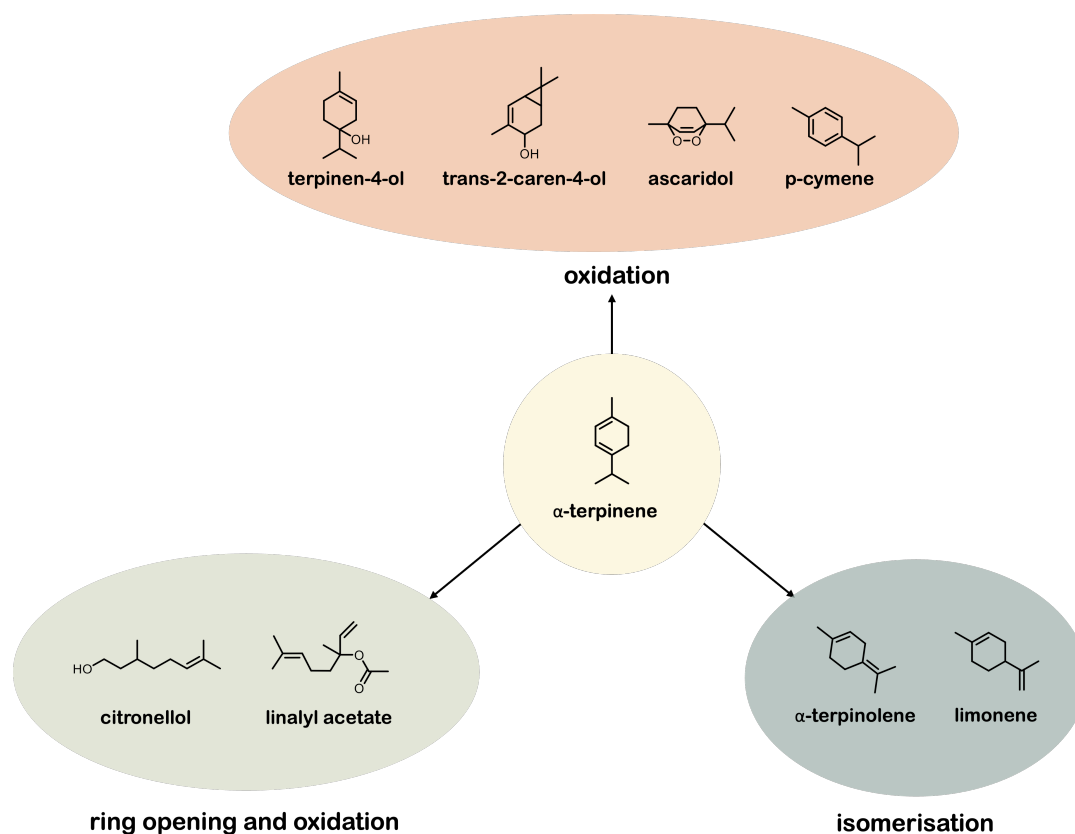


Figure 27: Degradation products of α -terpinene ranging from ring opening and oxidation to isomerisation.

α - and β -pinene, camphene, and sabinene are non-oxygenated bicyclic monoterpenes that maintained stable concentrations throughout the stress study (Figure 25, A-D). However, different degradation rates were also observed. The degradation of α -pinene was primarily time-dependent, whereas sabinene and β -pinene were particularly

sensitive to UV light. After 18 days, α -pinene retained 94% of its initial concentration in solution, whereas β -pinene retained less (75%) in the UV-treated samples. Initial concentration increases were observed for α -pinene, β -pinene, and camphene at the beginning of the stability experiment (Figure 24, A-C). This increase may be explained by rearrangement reactions of other terpenes present in the mixture. Degradation products such as α -pinene, limonene, p-cymene, and camphene have been described for β -pinene after a longer stability testing period (6 months).^{195, 196} A comprehensive overview of all studied concentration profiles are available in Figures A28-A30 in the Appendix.

Two members of the sesquiterpene class, which are also common constituents of *C. sativa* L., were also tested for UV and heat stability. Both α -humulene and β -caryophyllene showed different degradation rates (Figure 28). Both isomers were primarily sensitive to UV light, but α -humulene remained detectable at the end of the study, whereas β -caryophyllene was almost completely degraded.

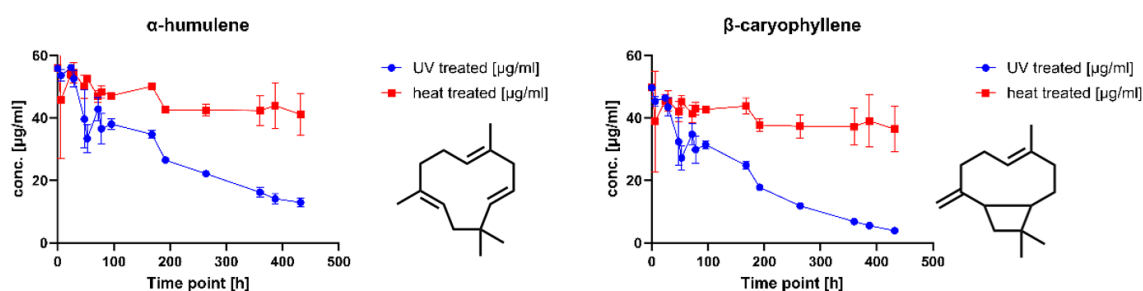


Figure 28: Degradation profiles (n=3) of α -humulene (left) and β -caryophyllene (right) in a terpene multi-mix after UV (blue) and heat (red) treatment. Data was obtained using GC-FID on a BGB-wax column. Figure taken from Raeber et al.¹⁸⁹

For β -caryophyllene, a variety of degradation products were detected following UV exposure. These included isomerisation products such as isocaryophyllene and α -humulene. Additionally, epoxides such as caryophyllene oxide and humulene epoxide II were identified, as well as p-cymene. In contrast, α -humulene exhibited ring opening to cis- α -bisabolene, accompanied by the formation of two epoxide products. Distinctly, β -caryophyllene demonstrated a greater number of degradation products, indicating its lower stability compared to α -humulene, which exhibits a preferred structural configuration. The identities of the degradation products were determined

by comparing their MS spectra and RI with literature values. However, it remains possible that the MS spectra correspond to a different stereoisomer. Definitive stereochemical assignments could be achieved through NMR spectroscopy and chiral chromatography. All observed degradation products are illustrated in Figure 29, with corresponding MS spectra and chromatograms available in Figures A31-A34 in the Appendix.

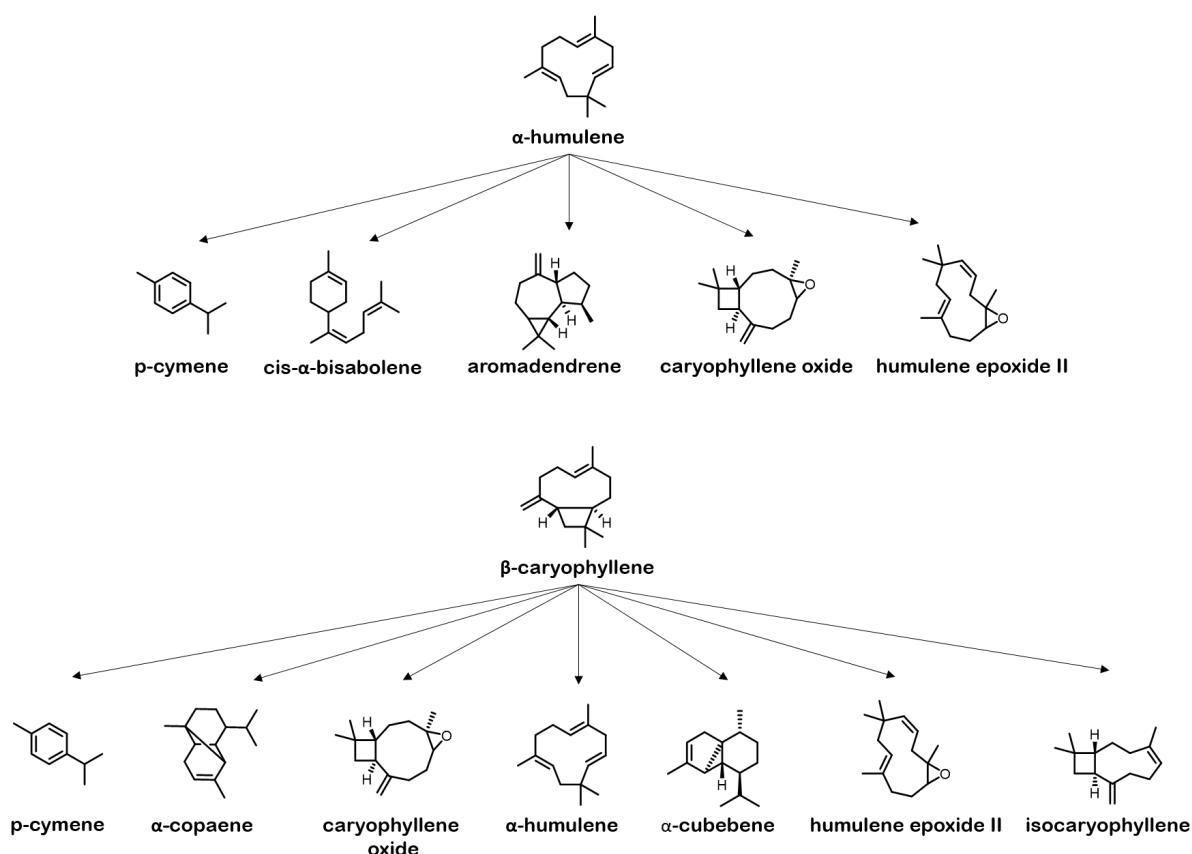


Figure 29: Degradation products for α -humulene and β -caryophyllene after exposure to UV light. Some degradation products overlap, while isomerisation reactions were only observed for β -caryophyllene.

When assessing terpene stability, it is important to favour a quantitative approach over an area-normalised approach. For example, comparing the areas of α -pinene and β -pinene, as well as α -humulene and β -caryophyllene, might suggest transformation reactions (Figure 30). However, β -pinene degrades faster than α -pinene (Figure 25, A and B), similar to the trend observed between α -humulene and β -caryophyllene (Figure 28). Using an area-normalised approach may lead to incorrect conclusions.

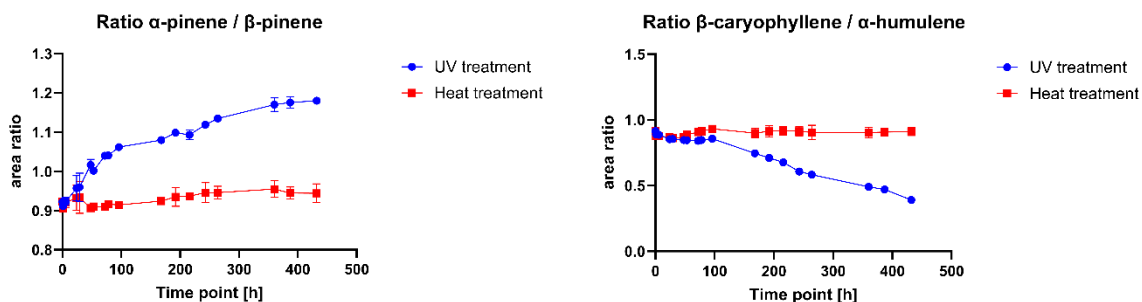


Figure 30: Changing area ratios over time for both α - and β -pinene isomers, as well as β -caryophyllene and α -humulene. For example, UV treatment suggests an increase in the area of α -pinene relative to β -pinene over time. Figure taken from Raeber et al.¹⁸⁹

Not all analytes degraded rapidly under UV light exposure. These unaffected analytes included oxygenated terpenes such as cis- and trans-rose oxide, isobornyl acetate, citronellyl acetate, geranyl acetate, and phenylethanol. In addition, acetylation appears to increase the stability of natural products. For example, geranyl acetate, neryl acetate, and citronellyl acetate showed minimal degradation compared to their non-acetylated counterparts geraniol, nerol, and citronellol. Overall, the analytes included in this study were more susceptible to degradation and transformation reactions under combined exposure of UV light and heat than under heat alone. An exception was observed for citronellol, nerol, and geraniol, three analytes closely related in structure (Figure 31). Their degradation profile in the multi-mix revealed significantly lower rates under UV light than under heat alone. We hypothesise that UV light induces isomerisation of nerol, geraniol, and citronellol, resulting in cis-trans conversions.

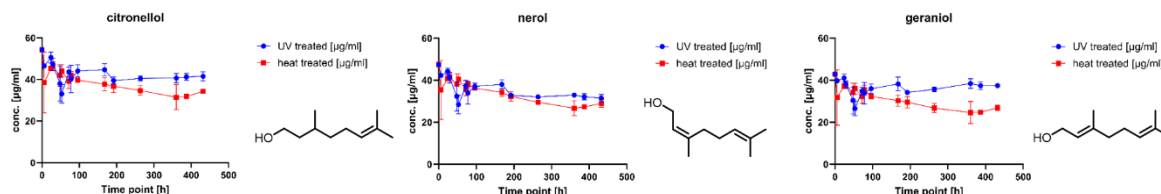


Figure 31: Degradation profiles ($n=3$) of citronellol (left), nerol (middle), and geraniol (right) in a terpene multi-mix after UV (blue) and heat (red) treatment. Data was obtained using GC-FID on a BGB-wax column. Figure taken from Raeber et al.¹⁸⁹

Confirmation of cis-trans isomerisation was investigated by the analysis of stressed single analytes using both GC-MS and GC-FID. UV-treated nerol samples contained geraniol, p-cymene along with epoxides and oxidised compounds, which were putatively identified. Additionally, the formation of citronellol was observed after two weeks of UV treatment (Figures A35-A37, Appendix). In UV-treated geraniol samples, the formation of nerol and citronellol was not observed. Instead, the alcohol group present in geraniol primarily underwent esterification and oxidation to form aldehydes (Figures A38-A39, Appendix). UV treatment of citronellol resulted in less diverse products. Hydrogenation of citronellol resulted in the formation of dihydro-citronellol and isomerisation to α -citronellol. Traces of sabinene, nerol, and geraniol were detected, but citronellol remained the most abundant analyte even after one week of UV exposure (Figures A40-A41, Appendix). As only a small proportion of the compounds analysed showed cis-trans conversions, it is more likely that nerol, geraniol, and citronellol are formed from other terpenes. The study by He et al., investigating the stability of lemon tea, may provide an explanation. They found that linalool was particularly reactive and was converted to α -terpineol, geraniol, and nerol.¹⁹⁰ In this study, linalool demonstrated stability under UV exposure. Traces of limonene, citronellol, nerol, and geraniol were detected after one week of UV exposure, while p-cymene was not detected until two weeks (Figures A42-44, Appendix).

Isomerisation reactions from one enantiomer or diastereomer to another have been postulated numerous times in the literature.^{58, 190} However, we have not been able to confirm this observation. When enantiomers are exposed to the same stressors, their area ratios to each other do not change (Figure 32). The formation of (+)- α -pinene to (-)- α -pinene and (+)- β -pinene to (-)- β -pinene was not observed, confirmed by the lack of detection of (-)- α -pinene and (-)- β -pinene during stability testing. Rose oxide, an important quality marker for *R. damascena* oil, exhibited good stability towards temperature and UV light and the conversion from (+)-cis rose oxide to (-)-cis rose oxide was not recorded (Figure A69, Appendix). The only exception is citronellol, which already showed a strong decrease in its overall degradation profile during heat treatment (Figure 31). The enantiomeric difference may result from the stereoselective conversion of another terpene to the corresponding enantiomer.

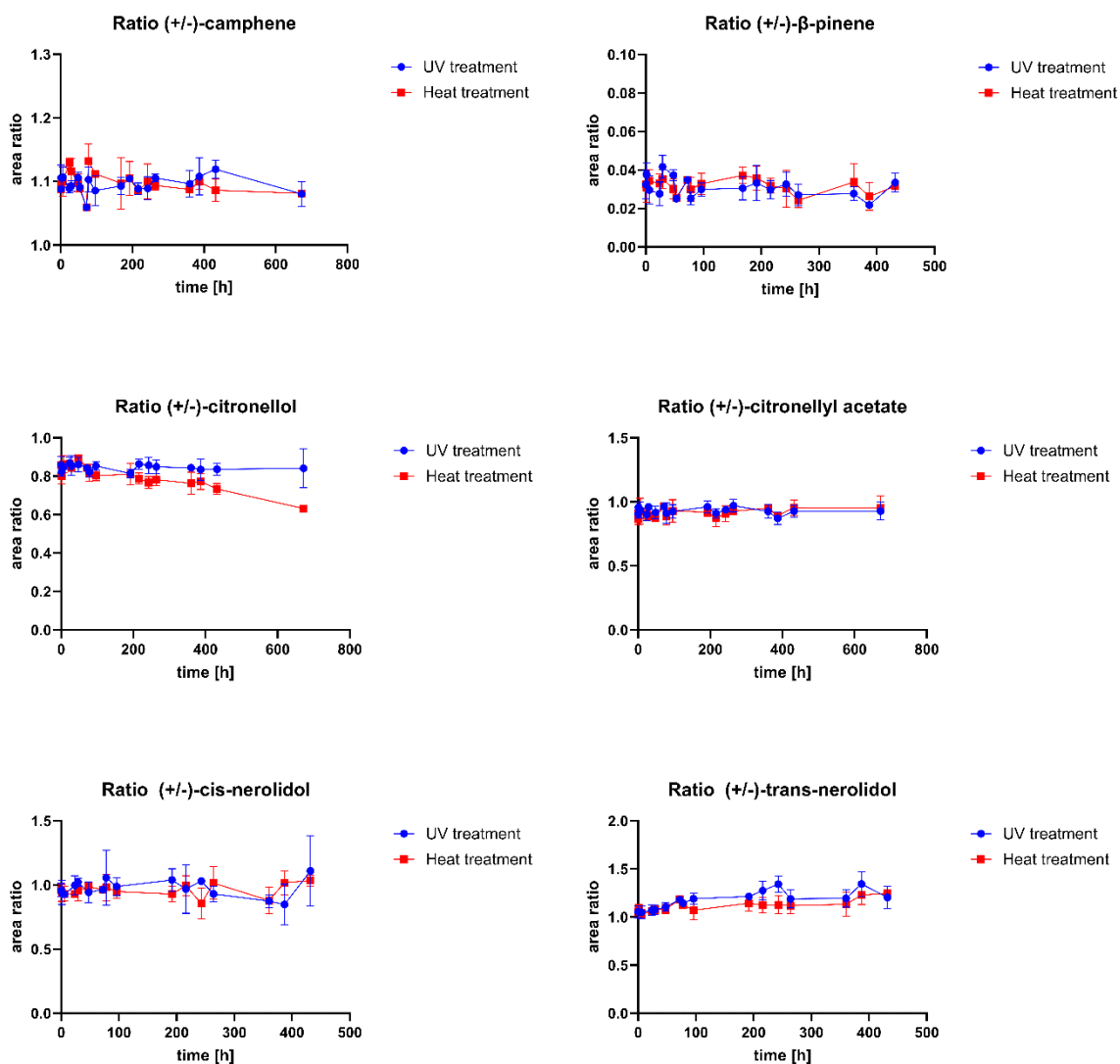


Figure 32: Area ratios (n=3) of six enantiomer pairs present in a terpene multi-mix after UV (blue) and heat (red) treatment. Data was obtained using GC-FID BGB 178 30% CD column. Figure taken from Raeber et al.¹⁸⁹

2.3.1.3. Stress testing of authentic *C. sativa* L. samples

In the previous sections, terpene degradation and conversion has been observed for a controlled terpene mixture and for individual analytes. Thus, specific reactions could be attributed to certain terpenes. How these observed reactions translate to authentic *C. sativa* L. samples requires further investigation. *C. sativa* L. produces and stores terpenes in its glandular trichomes. These specialised cells are broken down when the flowers are crushed, releasing the EO content.¹⁹⁷ The following study is also intended to provide initial guidance on the preferred form of storage for medicinal products

containing *C. sativa* L. For this purpose, three commercially available *C. sativa* L. flowers of the high-CBD type were exposed to UV light and heat, either as whole flowers or as an ethanolic extract. Major terpenes such as α - and β -pinene, sabinene, myrcene, limonene, linalool, β -caryophyllene, and α -humulene were detected in all samples. An initial increase in α - and β -pinene as well as cis-citral was observed in both whole flowers and extracts at the beginning of the stress study, which decreased steadily after about two weeks. Sabinene and p-cymene were detected only as degradation products in the extracts, whereas they were not detected in whole flowers. Myrcene degraded rapidly, similar to previous observations, and was no longer detectable after about one week in extracts and two weeks in whole flowers. Linalool, β -caryophyllene, and α -humulene also experienced rapid degradation. In GC-FID analysis, a signal was observed at the retention time for cis-menthone, which is clearly present in cannabis extracts, however it can be assumed that this is another co-eluting substance, as cis-menthone was not confirmed in GC-MS experiments. An increase in geraniol was only observed for stressed extracts and was not detected in whole flowers. Nerolidol isomers were not detected in all samples. However, cis-nerolidol showed an initial increase at 24 hours and a subsequent decrease for the remainder of the study. Trans-nerolidol only exhibited a decrease. GC-FID chromatograms of the studied authentic *C. sativa* L. samples can be found in Figures A47-A64 in the Appendix. GC-MS analysis of authentic *C. sativa* L. samples provided additional findings. Hashishene was detected exclusively in ethanolic extracts after 48 hours of UV treatment in two of the samples. Further, oxidation products such as fenchol, trans-2-pinanol, phellandral, borneol, α -terpineol, isocaryophyllene, trans-Z- α -bisabolone epoxide, and caryophyllene oxide were observed. Some polymerisation products such as 1-heptatriacontanol were detected. Stressed whole flowers exhibited fenchol as an oxidation product as well as caryophyllene oxide and isoaromadendrene epoxide. Generally, improved stability was observed for whole flowers compared to the ethanolic extract. GC-MS chromatograms and respective MS-spectra are available in Figures A65-A68 in the Appendix. Table 16 shows the evolution of the EE profile over time for the UV-treated authentic flower and extract samples.

Table 16: EE [%] for authentic *C. sativa* L. flowers and ethanolic extracts after UV exposure at seven different times points. Growth conditions are abbreviated as follows: Outdoor (OD) and Indoor (ID). Table taken from Raeber et al.¹⁸⁹

EE [%] of <i>C. sativa</i> L. flowers																														
Analyte	(+)- α -pinene			(+)- β -pinene			(S)-limonene			(+)-linalool			(-)-citronellol			(-)-camphene			cis-nerolidol 2			(+)-trans nerolidol			(-)-cis-menthone					
Sample	1	2	3	1	2	3	1	2	3	1	2	3	1	2	3	1	2	3	1	2	3	1	2	3	1	2	3			
Cond.	OD	ID	ID	OD	ID	ID	OD	ID	ID	OD	ID	ID	OD	ID	ID	OD	ID	ID	OD	ID	ID	OD	ID	ID	OD	ID	ID	OD	ID	ID
0 h	-100	90	47	-45	56	14	86	82	88	88	82	87	n.d.	100	100	100	45	100	n.d.	n.d.	100	100	100	100	100	100	100	100	100	100
24 h	-100	89	43	-68	53	7	77	81	85	100	79	89	-100	100	100	100	33	n.d.	100	100	100	100	n.d.	100	100	100	100	100	100	100
48 h	-63	88	46	-54	53	2	80	86	89	100	100	100	-100	100	100	100	27	100	100	100	100	100	n.d.	100	100	100	100	100	100	100
72 h	-100	88	46	-28	57	-4	79	82	88	100	100	88	100	100	100	100	22	100	100	100	100	100	n.d.	n.d.	100	100	100	100	100	100
1 week	-100	88	47	-66	58	18	85	82	89	100	100	100	n.d.	100	100	100	22	100	100	100	100	100	n.d.	n.d.	100	100	n.d.	100	100	n.d.
2 weeks	-100	88	48	-100	59	25	84	75	87	100	100	100	n.d.	100	100	100	25	100	100	100	100	100	n.d.	n.d.	100	100	n.d.	100	100	n.d.

EE [%] of <i>C. sativa</i> L. extracts																														
Analyte	(+)- α -pinene			(+)- β -pinene			(S)-limonene			(+)-linalool			(-)-citronellol			(-)-camphene			cis-nerolidol 2			(+)-trans nerolidol			(-)-cis-menthone					
Sample	1	2	3	1	2	3	1	2	3	1	2	3	1	2	3	1	2	3	1	2	3	1	2	3	1	2	3			
Cond.	OD	ID	ID	OD	ID	ID	OD	ID	ID	OD	ID	ID	OD	ID	ID	OD	ID	ID	OD	ID	ID	OD	ID	ID	OD	ID	ID	OD	ID	ID
0 h	-100	90	47	-45	56	14	86	82	88	88	82	87	n.d.	100	100	100	45	100	n.d.	n.d.	100	100	100	100	100	100	100	100	100	100
24 h	-100	90	50	-100	50	3	78	83	88	100	100	100	-100	100	100	100	43	100	n.d.	100	100	3	n.d.	100	100	100	100	100	100	100
48 h	-100	90	42	-100	77	10	67	81	89	44	100	100	-100	100	100	100	27	100	n.d.	85	100	-44	100	100	100	100	100	100	100	100
72 h	-100	89	39	-100	51	18	78	83	88	60	100	100	n.d.	100	100	18	4	23	n.d.	100	n.d.	-48	100	n.d.	100	100	100	100	100	100
1 week	-68	86	26	-41	47	8	77	79	86	100	100	100	n.d.	100	100	-36	-8	-40	n.d.	100	100	n.d.	100	n.d.	100	100	n.d.	100	100	n.d.
2 weeks	-80	100	-3	-52	48	11	100	79	89	100	100	100	n.d.	100	100	-13	6	-40	n.d.	0	100	n.d.	100	n.d.	100	100	n.d.	100	100	n.d.

Where pure enantiomeric standards were not available, the enantiomeric identity was determined by literature comparison.^{39, 198-203} Unstressed samples exhibited an excess for (+)- α -pinene, (+)- β -pinene, (S)-limonene, (+)-linalool, (-)-citronellol, (-)-camphene, (+/-)-cis-nerolidol 2, (+)-trans-nerolidol, and (-)-cis-menthone as presented in Table 16. Enantiomeric studies of *C. sativa* L. in the literature are sparse, but some of the enantiomers listed here have also been described in previous studies. As an outlier, sample 1 contained an excess of both (-)- α - and (-)- β -pinene and no citronellol was detected. The EE might depend on the cultivar and/or growth conditions, but none of the studies investigating enantiomeric ratios have compared outdoor and indoor cultivation. Furthermore, details of the growth conditions are mostly not reported.^{200, 202, 204} The EE for most analytes appeared stable throughout the entire study, such as (+)-linalool, (S)-limonene, (-)-citronellol, (+)-trans-nerolidol, (+/-)-cis-nerolidol 2 and (-)-cis-menthone. A conversion into the other enantiomeric form was not observed. However, the areas for (+/-)- α - and (+/-)- β -pinene experienced a dynamic change and were further investigated (Figure A70, Appendix). As sample 1 did not contain (+)- α -pinene, the enantiomeric isomerisation could be studied in detail. No conversion of (-)- α -pinene to (+)- α -pinene was observed in whole flowers. However, a slight increase in (+)- α -pinene and (+)- β -pinene was observed in the UV-treated extracts at the end of the experiment. At the same time, (-)- α -pinene increased strongly, suggesting its formation from another terpene. The UV-treated flowers of sample 2 and 3 exhibited a slight increase for all pinenes and similar degradation profiles. The degradation profiles of α - and β -pinene for UV-treated flowers and extracts are significantly different. In particular, a steep increase in (-)- α -pinene was observed for the extracts obtained from samples 1 and 3. An enantiomeric conversion could not be confirmed from the degradation profile of both stressed whole flowers and extracts. It is more likely that increased enantiomer concentrations result from stereospecific conversions of other terpenes. We assume this can occur through the cyclisation of myrcene, for example. Due to the unusual excess of (-)- α - and (-)- β -pinene in sample 1, which has not yet been described in the literature, an additional 20 authentic *C. sativa* L. extracts were analysed for their EE. A graphical overview of the results is provided in Figure 33.

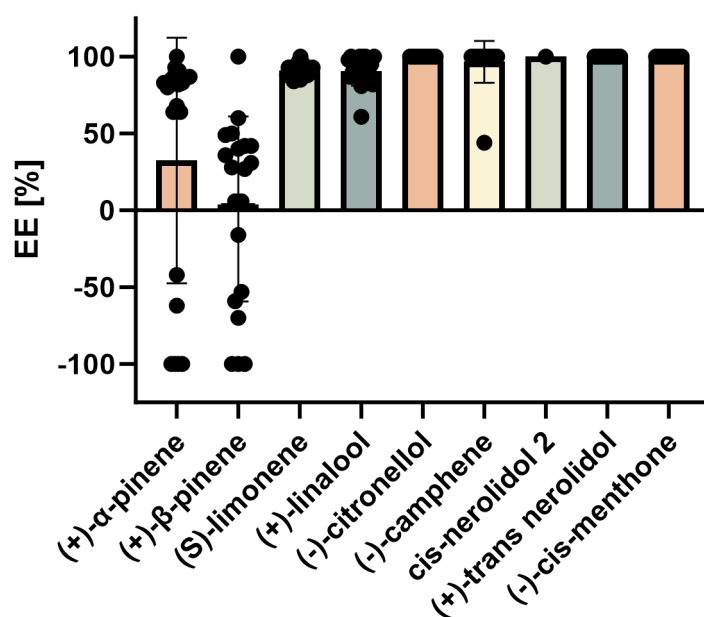


Figure 33: EE [%] present in 20 authentic *C. sativa* L. extracts obtained by chiral GC-FID analysis. Figure taken from Raeber et al.¹⁸⁹

A comprehensive list of EE results and sample specifications can be found in Table A18 in the Appendix. Of the samples analysed, nine were outdoor and eleven were indoor varieties. The distribution of enantiomers was consistent across all samples except for α - and β -pinene and citronellol. Only one sample contained (+)-cis-nerolidol 2. Notably, samples showing an excess of (-)- α - and (-)- β -pinene did not contain any citronellol and were predominantly from indoor varieties. Since plants synthesise terpenes stereospecifically, we state that the variation in the EE of α - and β -pinene is not coincidental but the result of environmental pressure. Different pharmacological effects have been demonstrated for the enantiomers of α - and β -pinene. Both (+)- α -pinene and (+)- β -pinene exhibit higher antibacterial activity than their enantiomeric counterparts. Additionally, (+)- α -pinene is known for its antifungal activity, while (-)- α -pinene exhibits insecticidal properties. Citronellol also possesses both antifungal and herbicidal activity.^{26, 28, 205, 206} The absence of citronellol and reduced or absent levels of (+)- α -pinene and (+)- β -pinene may suggest that the plants do not face an increased risk of fungal and bacterial infections. This could be attributed to the cultivation method or the use of antifungal agents. Furthermore, the detection of citronellol could be used as an indicator to whether a plant contains an excess of either the (+)- or (-)-enantiomer.

2.3.2. Materials and methods

2.3.2.1. Instrumental setup: Chiral analysis

The chemicals and reagents used in this study are listed in Table A10 in the Appendix. Some of the methods used here are extensions of previously published GC methods, which are also discussed in this thesis. The chiral GC-FID analysis was performed based on a method published by Allenspach et al. using a BGB 176 SE (30 m x 0.25 mm x 0.25 μ m, BGB Analytik, Boeckten, Switzerland) and a method published by Raeber et al. using a BGB 178 30% CD column (25 m x 0.25 mm x 0.25 μ m, BGB Analytik, Boeckten, Switzerland), which is further described in *Section 2.1.2.1*. The exact GC parameters can be found in the respective references.^{10, 23} For the measurement of authentic cannabis samples, the split ratio for both methods was reduced to 1:10. A GC Trace 1300 coupled to an AI 3000 autosampler (Thermo Fisher Scientific, Waltham, MA, USA) was installed with the BGB 176 SE chiral column. Data was recorded using ChromCard (Thermo Fisher Scientific, Version: 2.9). A GC Trace 1600 coupled to an AI 3000 autosampler (Thermo Fisher Scientific, Waltham, MA, USA) was installed with the BGB 178 30% CD chiral column. Data was recorded using Chromeleon (Thermo Fisher Scientific, Version: 7.3.1.). For both analyses, helium 6.0 and hydrogen 5.0 (PanGas, Dagmersellen, Switzerland) were used as carrier gas and for the FID detector, respectively. An injection volume of 1 μ l was maintained.

2.3.2.2. Instrumental setup: Polar analysis

The polar GC-FID analysis was performed based on the method published by Raeber et al, which is further described in *Section 2.1.2.1*.¹⁰ A GC Trace 1600 coupled to an AI 3000 autosampler (Thermo Fisher Scientific, Waltham, MA, USA) was installed with a BGB-wax capillary column (30 m x 0.25 mm x 0.25 μ m, BGB Analytik, Boeckten, Switzerland). Data was recorded using Chromeleon (Thermo Fisher Scientific, Version: 7.3.1.). Helium 6.0 and hydrogen 5.0 (PanGas, Dagmersellen, Switzerland) were used as carrier gas and for the FID detector, respectively. An injection volume of 1 μ l was maintained.

2.3.2.3. Instrumental setup: Apolar analysis

The apolar GC-MS analysis was performed by installing a DB-5 MS capillary column (30 m x 0.25 mm x 0.25 μ m) in a Trace GC-Ultra coupled to a Triplus autosampler. The GC was connected to a DSQ II MS (Thermo Fisher Scientific, Waltham, MA, USA). MS settings were as follows: scan mode was set to positive, scan range from 40 - 300 Da, ionisation energy was set to 70 eV with an ion source temperature of 250 °C. The transfer line was heated to 250 °C. The used temperature profile for the GC started with an initial temperature of 60 °C, which was held constant for 3 min and then gradually increased by 5 °C/min to 220 °C. The final temperature was held constant for another 5 min. Inlet temperature was maintained at 250 °C, the GC operated at a constant flow of 1.0 ml/min with a split flow of 20 ml/min and a split ratio of 1:20. Helium 6.0 (PanGas, Dagmersellen, Switzerland) functioned as a carrier gas. Data was recorded using XCalibur (Thermo Fisher Scientific, Version 2.2 SP1.48) GC-MS analysis included a MS spectra library consisting of the NIST MS spectra library, an in-house databank and the Adams library.^{207, 208}

2.3.2.4. Method validation and data analysis

Method validation was conducted according to the ICH Q2(R2) guidelines for the validation of analytical procedures.¹⁷⁸ Six Cals and three QCs were prepared by direct dilution of a terpene stock solution (0.1% m/V) with ethanol. All samples contained a final concentration of 10 mM cis-3-hexen-1-ol as an IS. For the Cals a range of 1 - 600 μ g/ml was obtained and QC samples were placed in the high, medium, and low concentration range. Method validation was performed on five separate days, with QC samples measured in duplicate and Cal samples measured in singlet. Accuracy was expressed in terms of bias by comparing the relative difference between theoretical and experimental determined QC concentrations. Precision was expressed as the imprecision measured for intraday and interday performance following the guidelines outlined by Peters et al.¹⁷⁹ LoD and LoQ were calculated based on the slope and the standard deviation of a linear response. As some of the applied regression models were of quadratic nature, the lower four calibrators were fitted to a linear regression and LoD and LoQ determined.¹⁷⁸ RI values were determined using the van

Den Dool and Kratz equation (Formula 1).⁸⁶ Chromatographic parameters such as the R_s were determined based on the guidelines outlined by the Ph. Eur. 11.5.¹⁸⁸

2.3.2.5. Authentic sample preparation

CBD-rich *C. sativa* L. flowers were purchased online from Swiss vendors. Sample 1 was grown outdoor, while sample 2 and 3 were indoor grown plants. 2 g of whole flowers were placed into clear screw-top vials. Furthermore, ethanolic extracts of the same flowers were prepared. Ethanolic extracts were prepared as outlined in *Section 2.2.2.4*. During UV treatment, six different time points were collected (0 h, 24 h, 48 h, 72 h, 1 week and 2 weeks). In addition, 20 authentic samples were prepared by Swiss Drug Testing Lab (Winterthur, Switzerland) and generously provided to this study.

2.3.2.6. Heat and UV treatment of control samples

As a control sample, a stock solution containing 29 terpenes was prepared with a final concentration of 1 mg/ml. The stock solution was pipetted into 1 ml aliquots into clear screw-top vials. Half of the aliquots were protected from UV-light by wrapping them in aluminium foil. During the accelerated stress test, control samples (in triplicates) and authentic *C. sativa* L. samples were placed into an UV-chamber (SOL 2, Honle UV technology, Gliching, Germany) at an illumination level of 120,000 Lux and 42 °C heat treatment. Control samples were heat and UV-treated over the course of a month and collected at different time points. At each time point, the control samples were diluted 20-fold with ethanol and a final concentration of 10 mM IS was added. Authentic *C. sativa* L. samples were only analysed qualitatively.

2.3.2.7. Data analysis and visualisation

In order to determine the effect of heat and UV-light, a mixed-effect model was employed using GraphPad Prism (Version 10.1.2). For the model, sphericity was assumed and an interaction term included. Data visualisation was conducted using MATLAB (Version: 9.13.0, Release R2022b, The Mathworks Inc.).

Chapter 2: Ionisation Techniques for Terpenes

This chapter is unpublished.

Raeber J, Begley A, Curavic A, Bovens A, Steuer C: Dielectric Barrier Discharge Ionisation Coupled to GC for Structure Elucidation of Terpenes. In preparation.

Contributions: **JR**: conceptualisation, method development, sample preparation, experimental design, data acquisition, analysis and data interpretation, investigation. **AB**: HRMS data acquisition, data interpretation. **AC**: data acquisition, data interpretation and analysis. **AB**: EI-MS spectra data acquisition, data interpretation. **CS**: supervision, resources, conceptualisation.

Licencing:

Unpublished.

3.1. Dielectric Barrier Discharge Ionisation Coupled to GC for Structure Elucidation of Terpenes

The ionisation process of terpenes in DBDI remains poorly understood. Previous studies have either focused on the acquisition of spectra that record the entire volatile fraction of natural products (predominantly terpenes), or have modified the adducts using dopants.^{21, 106, 116, 117, 209} The study by Weber and colleagues is the largest study of terpenes and DBDI to date, including 21 terpenes of varying chemistry. They tested different dopants, modifiers for the in source DBDI environment, and found that $[M+OH]^+$ adducts formed predominantly under all make-up gases with the exception of ammonia which gave rise to $[M-H]^+$.¹¹⁶ In contrast to other ionisation methods like APCI, ESI, and EI, whose mechanisms are well understood, the exact mechanism of DBDI remains a subject of ongoing research. Altering the ionisation environment in the DBDI source gives rise to the formation of different adducts. However, this process does not seem to follow a straightforward pattern. A better understanding of the characteristics of the DBDI source can contribute to improved method development and simplify the method transfer from, for example, GC-EI-MS to GC-DBDI-MS. This chapter focuses on elucidating and recognising patterns derived from terpenes ionised by DBDI. We further hypothesise that the formed adducts can support structure elucidation of terpenes and are stereoselective. The current bottleneck in untargeted analysis is the correct assignment of an analyte identity to an MS spectrum.²¹⁰ Since terpenes are structurally related, they produce similar if not identical MS spectra. EI-MS often results in loss of the molecular ion and APCI-MS produces primarily $[M+H]^+$ molecular ions, which can lead to the formation of the same fragments during fragmentation. The transitions of the APCI-MS method in *Section 2.2.1* serve as an example. Sabinene, isobornyl acetate, myrcene, β -pinene, limonene, and α -pinene form a parent ion at 137.1 Da. This parent ion leads to the formation of the fragments at 81.1 and 77.1 Da, which appear with the highest intensity in the MS spectrum. A distinction between these analytes can only be made based on their retention times. However, this can only be determined if chemical reference standards are available. This is often not the case, leading to incorrect assignments of analyte identities.

3.1.1. Optimising settings for the DBDI source

The ionisation efficiency of the DBDI source for terpenes was evaluated by measuring a multi-mix calibration standard on both GC-DBDI-MS and GC-FID. The DBDI source settings were gradually adjusted until optimal ionisation and a low baseline were achieved. Figure 34 compares the results of GC-FID and GC-DBDI-MS. Several conclusions can be drawn from Figure 34. The peak numbering corresponds to Table 12 in *Section 2.3.1*. The baseline of the GC-DBDI-MS chromatogram is raised, resulting in a reduced signal-to-noise ratio. The split flow had to be decreased from 100 ml/min to 10 ml/min due to lower sensitivity. Differences in detector sensitivity were observed. For instance, sabinene (**4**) showed a lower relative intensity in the GC-FID chromatogram compared to other peaks, whereas in the GC-DBDI-MS chromatogram, sabinene exhibited a higher intensity than α -pinene (**1**), camphene (**2**), and β -pinene (**3**). Notably, α -terpinolene (**10**) was not detected by GC-DBDI-MS. This suggests that the setup might be experiencing sensitivity issues. Despite potential sensitivity problems with the MS, the analysis is currently sufficient to evaluate the ionisation efficiency of the DBDI source. In contrast to the study by Weber and colleagues an amplitude of 1600 V and a frequency of 15,000 Hz was not sufficient to ionise the terpenes studied (Figure A71, Appendix).¹¹⁶ In our experiments, increasing the frequency from 15,000 to 15,500 Hz improved the baseline noise, but did not improve the ionisation efficiency of the terpenes. Steadily increasing the amplitude had the greatest effect on ionisation efficiency. Monoterpenes, particularly the non-oxygenated types, exhibited difficulties in ionising, likely because they have a lower mass compared to sesquiterpenes. Finally, increasing the amplitude from 1800 V to 1900 V resulted in the lowest signal-to-noise ratio and increased the intensity from initially 10^7 cps to 10^8 cps (Figures A72-A76, Appendix).

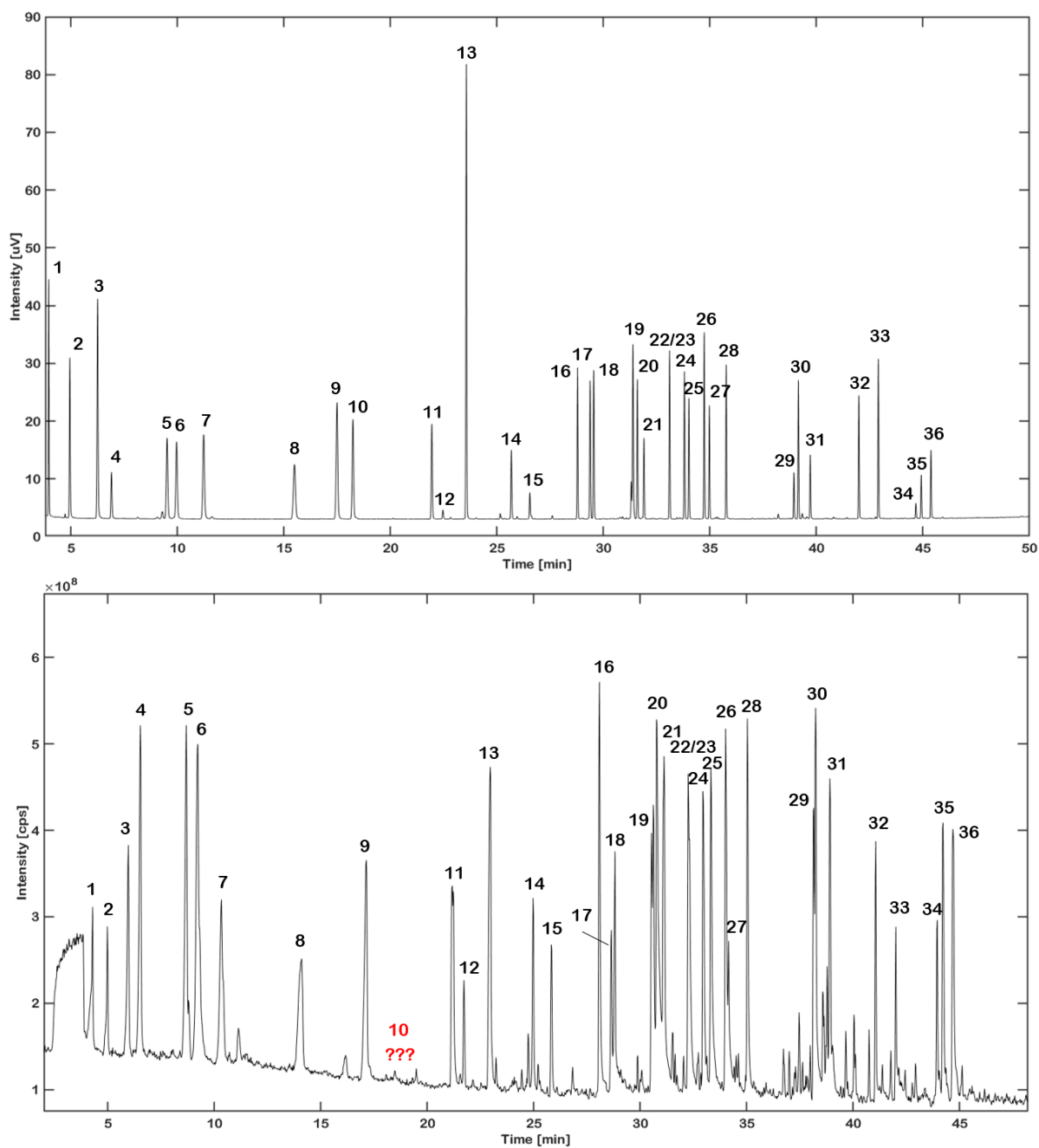


Figure 34: GC-FID chromatogram (top) and GC-DBDI-MS chromatogram (bottom) analysing 29 volatile EO components on a polar wax capillary column. The DBDI source was set to an amplitude of 1900 V and a frequency of 15,000 Hz.

3.1.2. Terpene patterns generated by modifying the ionisation environment

Terpenes from different classes were subjected to ionisation experiments in combination with GC by modifying the ionisation environment with various dopants, including room air, water (H₂O), nitrogen (N₂) and methanol (MeOH). The search for

adducts focused on those previously described in the literature, primarily from studies where DBDI was used as a stand-alone technique.^{106, 112, 113, 116, 211, 212} For the analysis, the ten most intense peaks were selected, and their respective adducts were identified. To differentiate between $[M+H_2O]^+$ and $[M+NH_4]^+$ adducts, an additional experiment was conducted using D₂O-humidified air. These experiments verified the presence of $[M+ND_4]^+$ rather than $[M+D_2O]^+$ adducts. Room air provided the best ionisation efficiency, while N₂ gave rise to a diverse number of adducts. The main adducts observed under all conditions were $[M+NH_4]^+$, $[M+H]^+$, and $[M+H+2O]^+$. Contrary to the study by Weber et al., the $[M-OH]^+$ adduct was observed as the most intense adduct only under N₂-rich ionisation conditions.¹¹⁶ This adduct was primarily formed for linear oxygenated monoterpenes such as nerol, linalool, geraniol, and cis-citral. Similar to Weber et al.'s findings, the highest intensities were generated under room air conditions. Humidifying the air with H₂O lowered intensities and mainly suppressed the formation of the oxygenated adduct $[M+O]^+$ for (+)-fenchol, (-)-borneol, isoborneol, and trans-verbenol. These compounds are structurally related, as they are bicyclic monoterpenes with a functional alcohol group. Similarly, humidifying the ionisation environment with MeOH reduced ionisation efficiency. The adduct pattern changed significantly for only one group of terpenes, which included nerol, linalool, geraniol, citronellol, dihydrolinalool, and citronellal. These linear oxygenated monoterpenes predominantly formed the $[M+H_2O_2]^+$ adduct. Oxygenation plays a major role in determining the types of adducts formed during ionisation. Figure 35 displays the most intense adduct formed under different ionisation conditions. The left plot exclusively features oxygenated monoterpenes, while the right plot includes non-oxygenated monoterpenes, acetylated terpenes, and sesquiterpenes. The predominant adduct for non-oxygenated terpenes was found to be $[M+H+2O]^+$. Humidifying the ionisation environment with MeOH led to the formation of oxygenated derivatives $[M+O]^+$ for α - and β -pinene. A reduced ionisation efficiency for aldehydes, alkanes, and terpenes under MeOH was observed by Weber and colleagues, a finding we were also able to confirm.¹¹⁶ The N₂-enriched plasma favoured the ionisation of non-oxygenated terpenes, particularly camphene and p-cymene, which showed up to 16 times higher intensities compared to other conditions. Guaiazulene, a bicyclic non-oxygenated sesquiterpene, exhibited poor ionisation, with no adducts found under MeOH-enriched conditions and intensities below 1.5×10^7 cps under other conditions. Acetylated derivatives of isoborneol, geraniol, and citronellol underwent deacetylation

as the main reaction during plasma-based ionisation. This reaction was also observed under APCI (Chapter 1, *Section 2.2.1.*, Table 5). Fragmentation products are occasionally observed in the DBDI source; however, they can be controlled by adjusting the frequency and amplitude.

Weber et al. observed the formation of the $[M-H+2O]^+$ adduct for alkanes, whereas this study observed the corresponding adduct for non-oxygenated terpenes.¹¹⁶ Their study included terpenes, but did not distinguish between different terpene classes and their functional groups, which may explain the observed discrepancies. Although room air offers the highest ionisation efficiency, N_2 appears more suitable for terpene analysis. It effectively ionised terpenes that otherwise showed lower intensities and produced a large number of adducts. To establish a relationship among the formed adducts, the dopants used, and the terpene class, PCA was performed. The results are presented in Figures 36-37. The first two PCs captured about 15% of the total variance in the data, indicating its complexity, which suggests that the dataset's variation cannot be fully explained by just two dimensions.

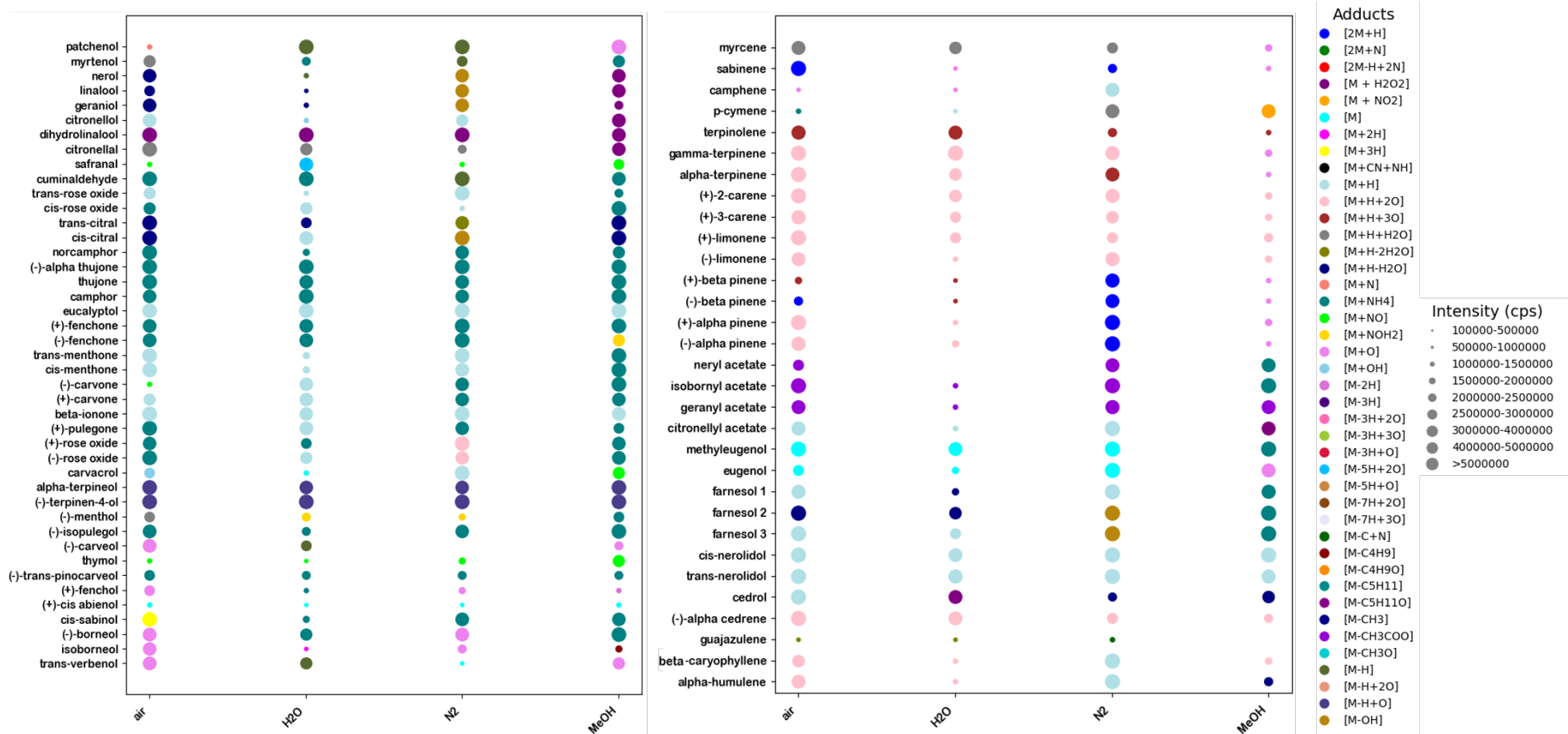


Figure 35: A bubble plot depicting various terpenes and their most abundant adducts, depending on the dopant used (air, H₂O, N₂, and MeOH). The size of each bubble corresponds to the counts per second (cps) of the respective mass peak.

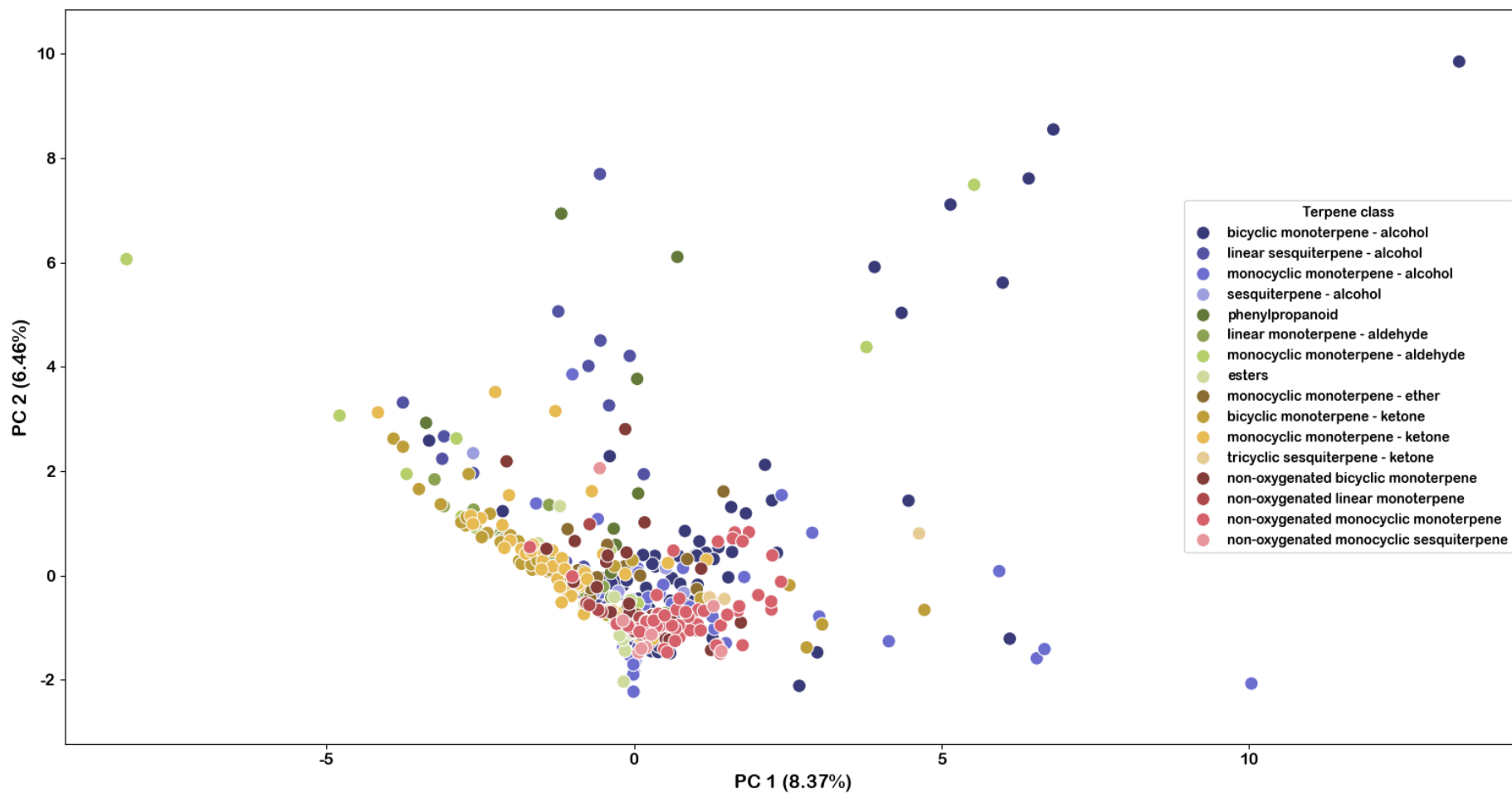


Figure 36: PCA analysis of terpenes ionised under different conditions. The ten most intense mass peaks were assigned to adducts previously described in the literature. Data points are coloured according to their terpene class.

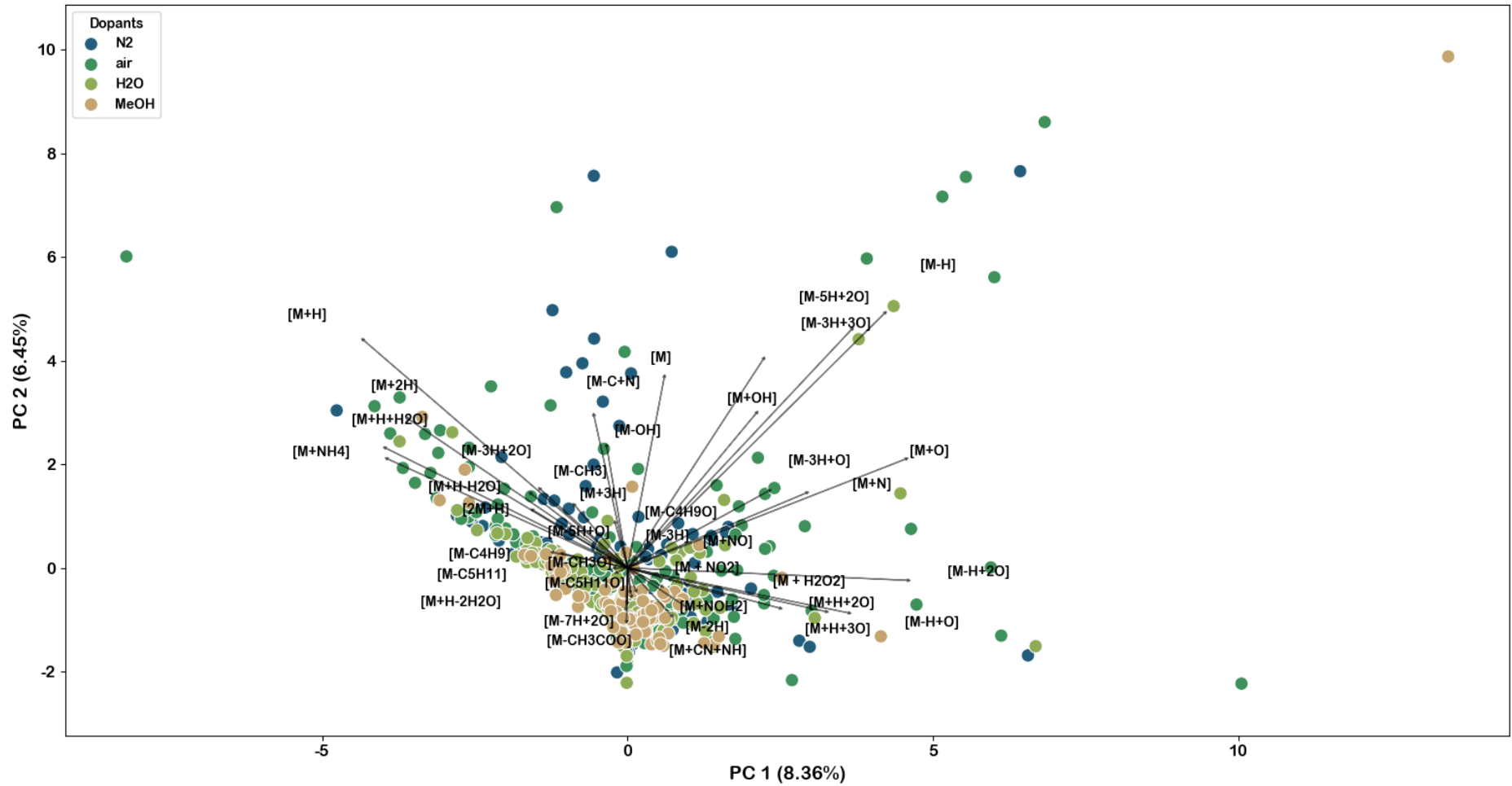


Figure 37: PCA analysis of terpenes ionised under different conditions. The ten most intense mass peaks were assigned to adducts previously described in the literature. Data points are coloured according to the dopant used, and vectors represent the contribution of each studied variable to each PC.

The PCA analysis reveals that one axis in particular accounts for the spatial separation of the points, primarily influenced by the structural properties of the terpenes. Oxygenated and non-oxygenated terpenes appear to be correlated in opposite directions along this axis. Among oxygenated terpenes, adducts such as $[M+H]^+$, $[M+2H]^+$, and $[M+NH_4]^+$ are frequently observed. Non-oxygenated terpenes are characterised mainly by the $[M-H+2O]^+$ adduct and variations thereof such as $[M+H+3O]^+$, $[M+H+2O]^+$, and $[M+H_2O_2]^+$. The use of dopants induces the formation of new adducts for selected analytes. In particular the formation of $[M-C+N]^+$ molecular ions, a reaction observed exclusively under N_2 enrichment. This reaction was observed for cis- and trans-nerolidol, farnesol, carvacrol, α -humulene, β -caryophyllene, menthone, sabinene, citronellyl acetate, methyleugenol, trans- and cis-rose oxide, and camphene. The majority of the aforementioned analytes exhibit a cyclic structure. The $[M]^+$ parent ion, typical of EI, was exclusively present for oxygenated terpenes and consistently formed under all conditions, albeit with a preference for room air. Conversely, the $[M-H]^+$ ion showed no preference for oxygenated or non-oxygenated terpenes and was formed across all analytes in the study. For a comprehensive list of all terpenes, conditions, and detected adducts, refer to Tables A19-A21 in the Appendix. Overall, DBDI forms adducts based on structural features, with (non-)oxygenation being a primary determinant. The choice of dopants significantly influences the ionisation efficiency, with N_2 enrichment generating the widest range of adducts. The study settings did not entirely eliminate in-source fragmentation, which could be mitigated by lowering the frequency but might reduce the ionisation efficiency of monoterpenes. Analysis of terpenes using DBDI thus involves balancing sensitivity loss and in-source fragmentation. While only known adducts have been explored so far, the ionisation process yields characteristic spectra with numerous unidentified fragments and adducts. These spectra potentially offer distinguishing features between structurally related terpenes.

3.1.3. DBDI-MS spectra for structure elucidation of related terpenes

DBDI-MS ionisation and the resulting adducts are highly dependent on structural properties such as (non-)oxygenation, double bond position and/or cyclic and linear conformations. This is illustrated by the comparison of the ionisation patterns of for example α - and β -pinene in Figure 38. Both compounds form similar adducts, although they differ only in the position of their double bonds (endo- vs. exocyclic). The mass observed at 55 Da corresponds to protonated water clusters such as $(\text{H}_2\text{O})_2\text{H}_3\text{O}^+$. Adducts of the form $[\text{M} - (2n + 1)\text{H} + m\text{O}]^+$ are present, which has also been previously observed by Weber et al. for saturated, aliphatic hydrocarbons.¹⁰⁶ However, the biggest difference in the spectra are the masses observed above 180 Da. The double bond position of both pinenes seems to have a large influence on the plasma chemistry. The same analytes were further studied on a custom-made DBDI-source using high resolution MS (HRMS) from the Zenobi group at D-CHAB ETH Zurich. The generated spectra are available in Figures A77-A78 in the Appendix. In comparison to α -pinene, β -pinene again appears to produce additional adducts with higher masses. The spectra for both α -pinene and β -pinene, although varying from those acquired on the MS used in Figure 38, appear significantly different. When using room air as the ionisation environment, factors such as humidity and ambient gases can significantly affect the MS spectra generated. Furthermore, the main factor influencing the residence time of the analyte in the DBDI source is the vacuum of the MS instrument, which is specific to its design and manufacturer. In the DBDI source, competing reactions are observed which can be favoured by controlling both the flow and the composition of the discharge gases.²¹² The ionisation pattern is therefore not only dependent on the analyte, but also on the experimental parameters and the environment. When comparing spectra of α -pinene and β -pinene under different ionisation conditions, major differences are observed (Figure 39). Under the N_2 enriched environment for example, the formation of β -pinene dimers was observed as $[2\text{M}+\text{H}]^+$ ions. Polymerisation and dimerisation reactions have been previously proposed for LTP ionisation in the literature, which we could further verify for DBDI.^{211, 212} The spectra generated under conditions where the air was enriched with MeOH are not clearly interpretable and require further MS^n -experiments for structure elucidation. It appears however, that MeOH suppresses terpene ionisation. Overall, the spectra generated under different conditions appear to be reproducible. This

highlights the importance of understanding the ionisation environment in the DBDI source and suggests that the adducts formed depend on the structure of the analytes, potentially allowing for the distinction of structural isomers, as seen with α - and β -pinene. Figure 40 shows the EI-MS spectra of both α - and β -pinene acquired at 70 eV. The spectra produced are virtually identical, making retention time an indispensable requirement for the correct identity assignment. This necessitates time-consuming chromatography to ensure that the two analytes do not co-elute. In this case, the $[M]^+$ parent ion is detectable in the EI-MS spectrum for both α - and β -pinene, which is often not the case with EI due to complete fragmentation of the parent ion in the ion source.

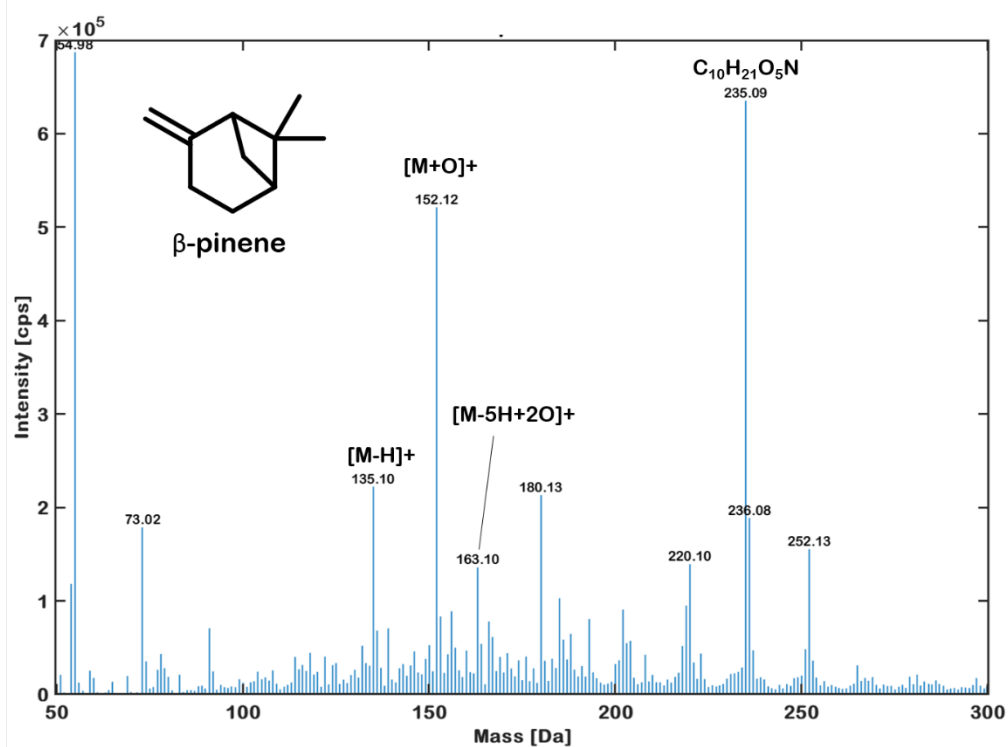
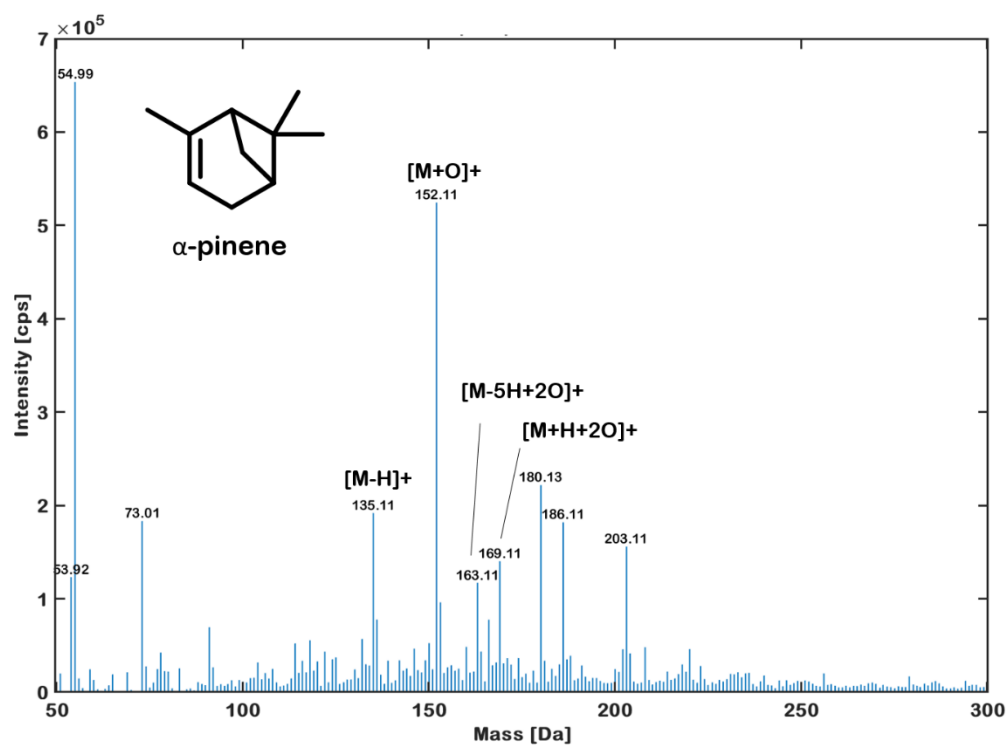


Figure 38: DBDI-Q1-MS spectrum of α - (top) and β -pinene (bottom) acquired at 1900 V and 15,000 Hz. Room air was used for the ionisation process.

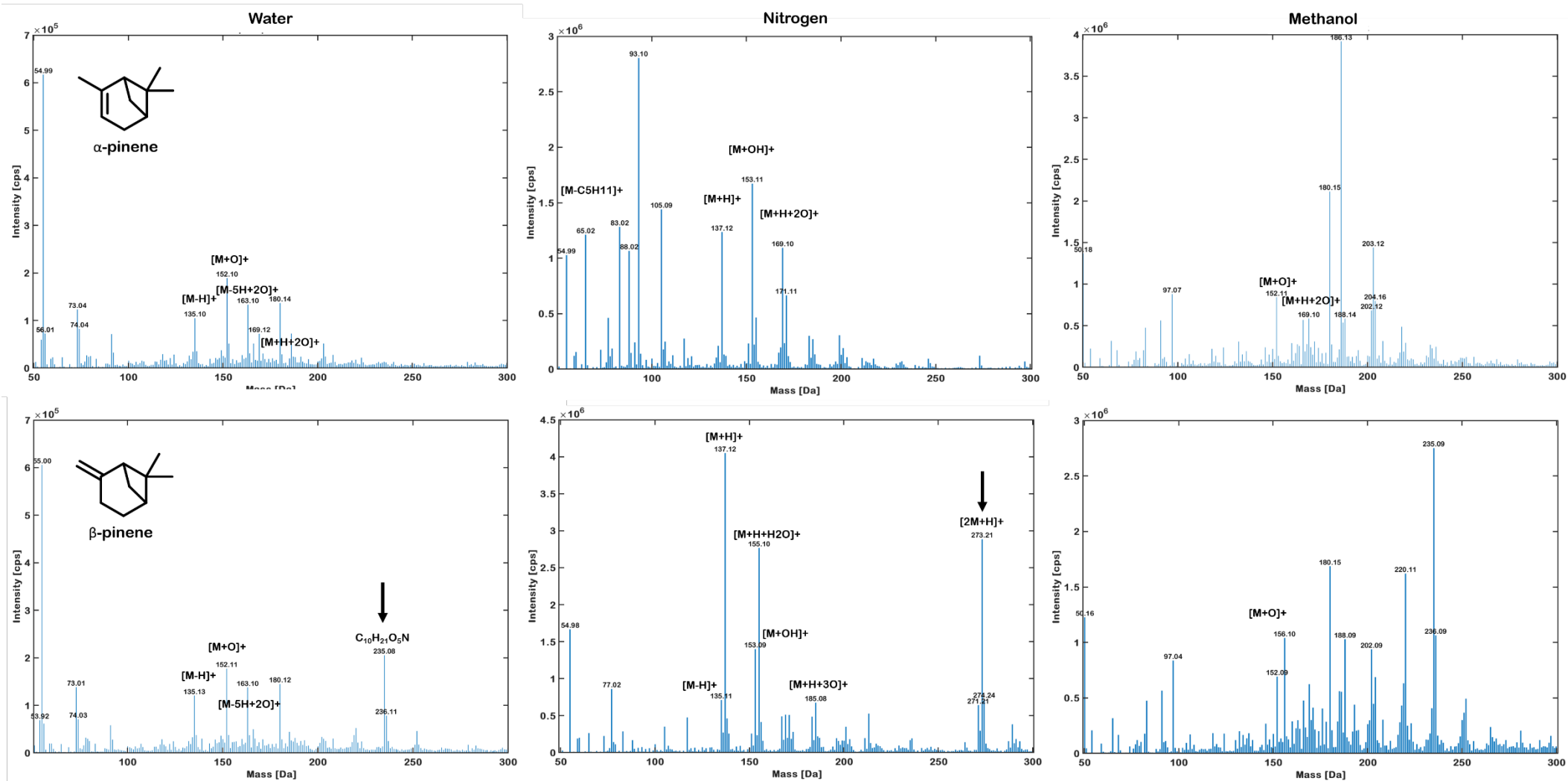


Figure 39: DBDI-Q1-MS spectra of α - (top) and β -pinene (bottom) acquired at 1900 V and 15,000 Hz. Spectra were acquired under different ionisation (from left to right: H₂O, N₂, and MeOH) environments. Arrows indicate significant spectral differences.

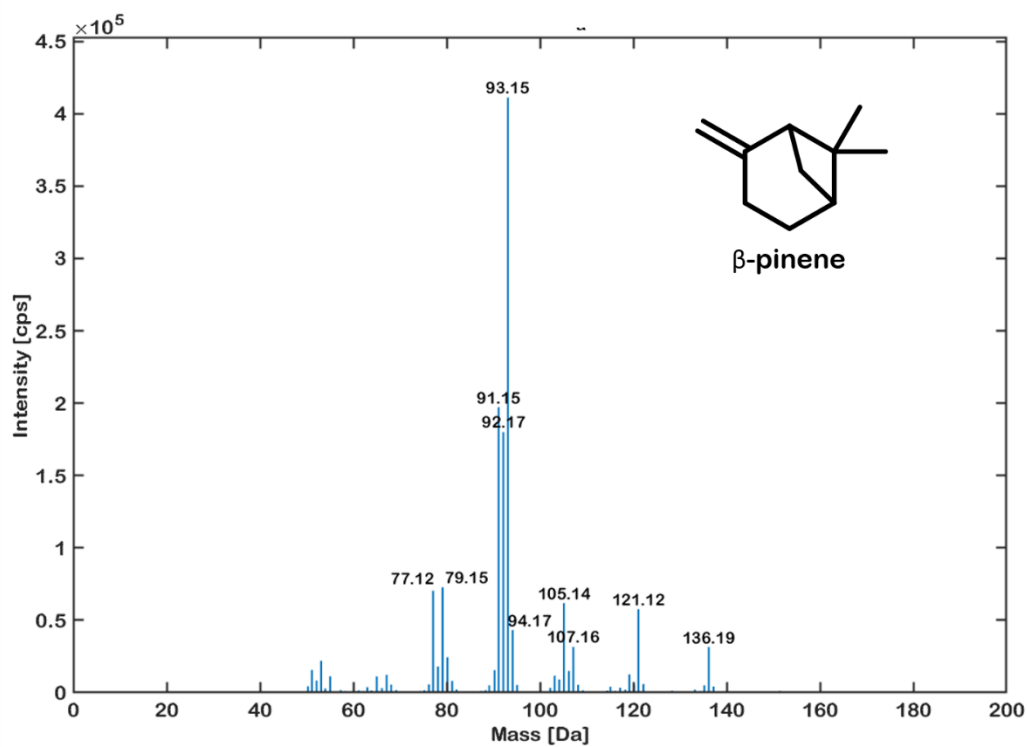
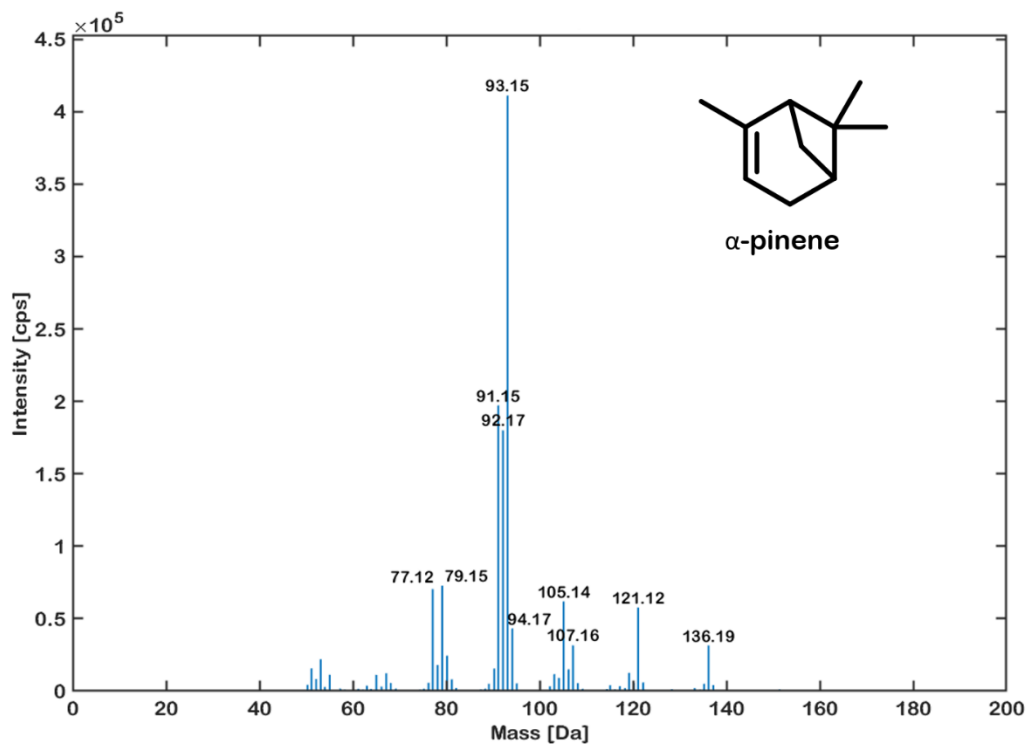


Figure 40: EI-MS spectra acquired at 70 eV for both α - (top) and β -pinene (bottom).

The terpenes α - and γ -terpinene as well as limonene and α -terpinolene are monocyclic double bond isomers. Figure 41 displays their DBDI-Q1-MS spectra acquired at room air. Depending on the position of the double, different adduct patterns are formed. Adducts of the type $[M - (2n + 1)H + mO]^+$ were predominant, $[M-H]^+$ was detected for all analytes and oxygenation was observed. Nørgaard and colleagues observed ozonolysis of limonene in a LTP, giving rise to limonene oxide.²¹¹ Similarly, limonene oxide was also detected under our experimental conditions, suggesting ozonolysis. DBDI-HRMS data of the same analytes is available in Figures A79-A82 in the Appendix. DBDI-HRMS spectra exhibited some in-source fragmentation and the $[M-H]^+$ and $[M+OH]^+$ adducts were predominant. The ionisation patterns observed by DBDI-HRMS and DBDI-Q1-MS are similar. While similar, if not identical adducts are observed for all four analytes, their relative intensities vary greatly. For example, in Figure 41, α -terpinene exhibited the highest intensity for $[M+H+2O]^+$, whereas γ -terpinene showed an unannotated mass at 186.12 Da. The influence of the double bond position on the specific adduct formation remains uncertain for the analytes studied. In this case, two analytes share an endocyclic double bond while the other two share an exocyclic double bond. No discernible ionisation patterns were observed between these exo- and endocyclic structures. All four isomers share common adducts and neither limonene nor α -terpinolene, both of which have an exocyclic double bond, show any distinguishing features compared to α - and γ -terpinene. In a further experiment, the influence of N_2 enrichment on the ionisation patterns was investigated, as it was particularly effective in ionising non-oxygenated monoterpenes. The results are presented in Figure 42. Switching from room air to N_2 significantly altered the adduct patterns. The oxygenated product $[M+O]^+$, previously detected under room air conditions, was no longer detectable and the formation of the $[M+H]^+$ ion was favoured. The exchange of a carbon atom for a nitrogen atom was not observed.

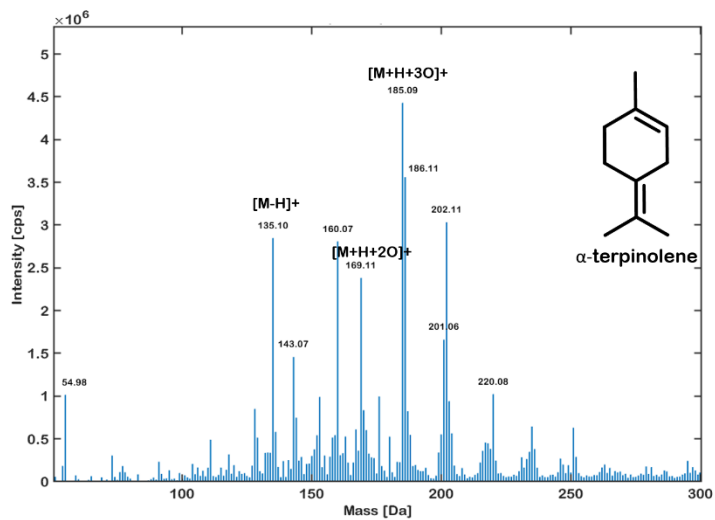
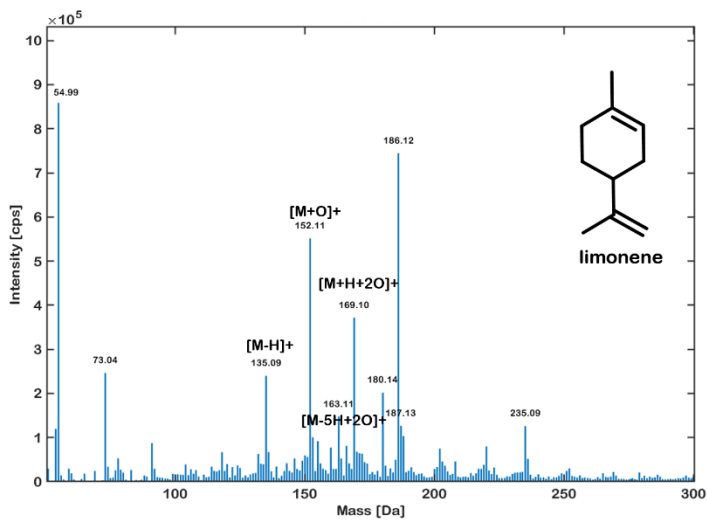
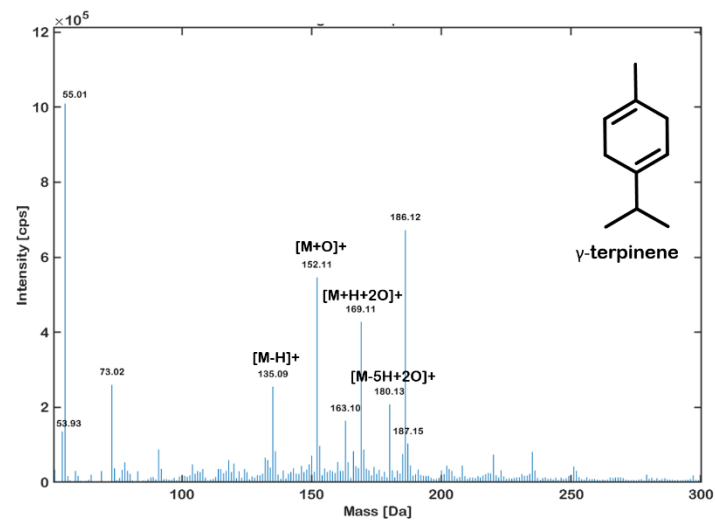
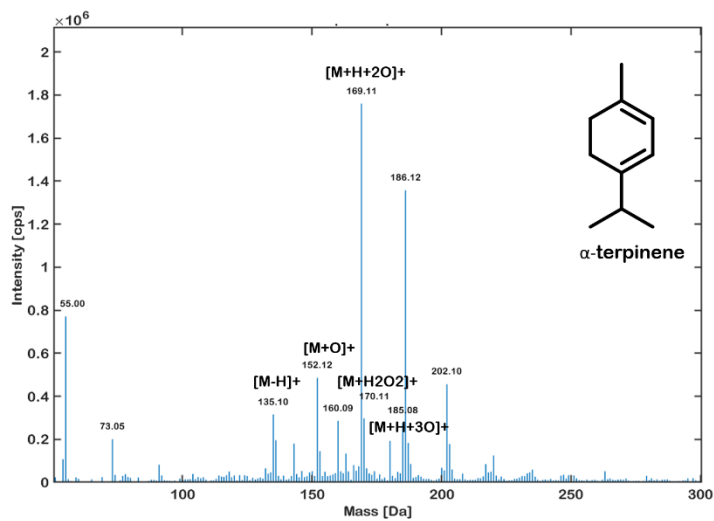


Figure 41: DBDI-Q1-MS spectra of α -terpinene (top, left), γ -terpinene (top, right), limonene (bottom, left), and α -terpinolene (bottom, right) were acquired at 1900 V and 15,000 Hz. Room air was used for the ionisation process.

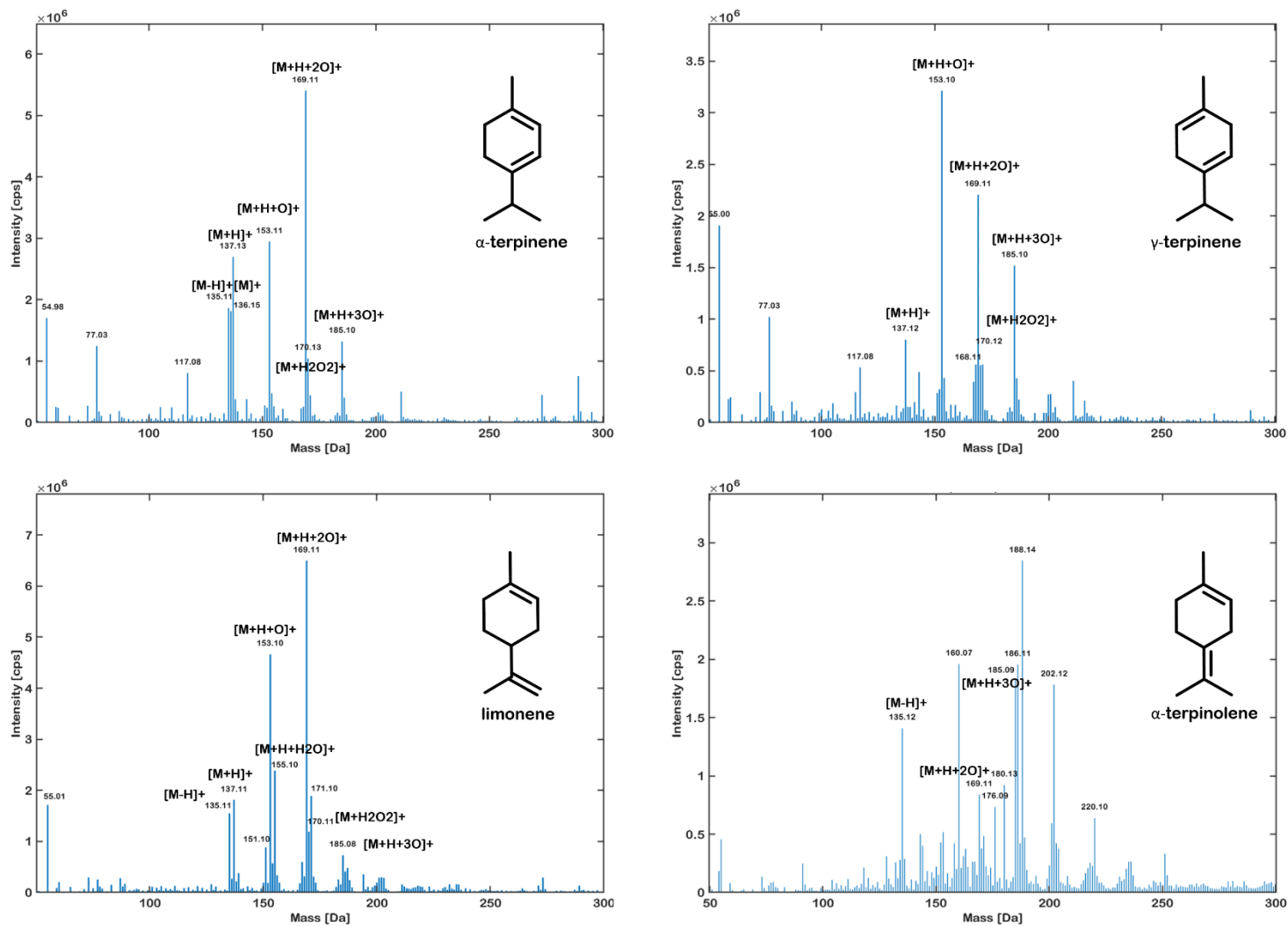


Figure 42: DBDI-Q1-MS spectra of α -terpinene (top, left), γ -terpinene (top, right), limonene (bottom, left), and α -terpinolene (bottom, right) were acquired at 1900 V and 15,000 Hz. N₂ was used for the ionisation process.

Figure 43 presents the state-of-the-art EI-MS spectra for α - and γ -terpinene, as well as limonene and α -terpinolene. The molecular ion $[M]^+$ at 136.20 Da is consistently detected in all spectra. In-source fragmentation produces identical fragments, such as 93.15 and 121.23 Da. However, these fragments exhibit varying intensities and form characteristic patterns. In contrast to α - and β -pinene, the position of the double bond influences the intensity of fragment formations. The spectra generated for α -terpinene and α -terpinolene exhibit the strongest similarity in EI-MS, whereas the DBDI-generated spectra for α -terpinolene show the least resemblance within the same group. For instance, no oxygenation was observed in the DBDI-Q1-MS spectra for α -terpinolene, while limonene, α - and γ -terpinene experienced oxygenation. Not all detected adducts and fragments were successfully annotated in the DBDI-Q1-MS spectra. In addition to proton addition and subtraction and radical formation, various other adducts are also formed. Direct treatment of terpenes with a DBDI source followed by GC-MS analysis revealed conversion and rearrangement reactions of terpenes, induced by an LTP. For example, in a study by Rodrigues et al. the conversion of limonene to α -terpinolene, γ -terpinene, and p-cymene was observed.²¹³ Due to their structural relationship, isomerisation reactions between terpenes are likely. The influence of heat and UV has been discussed in detail for isomerisation in *Section 2.3*.

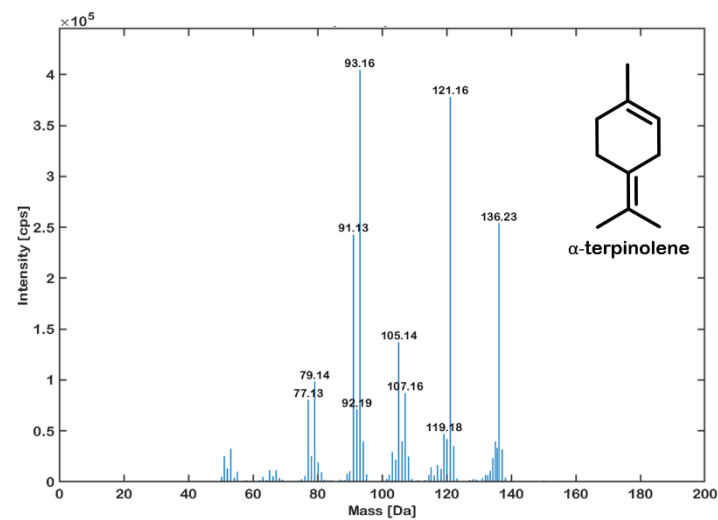
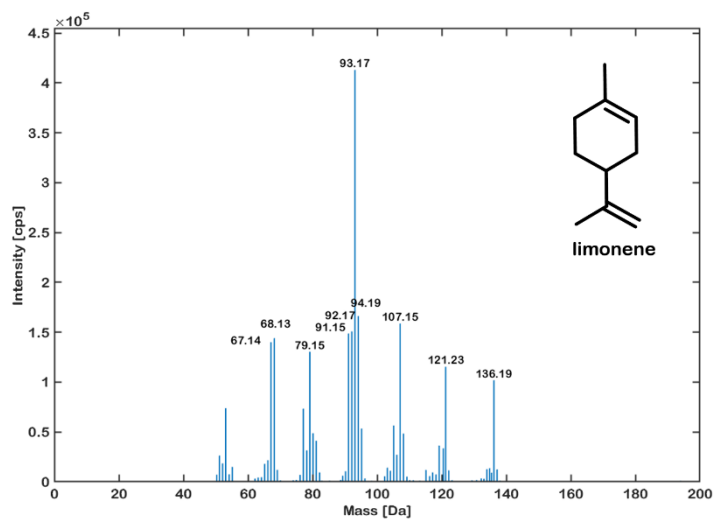
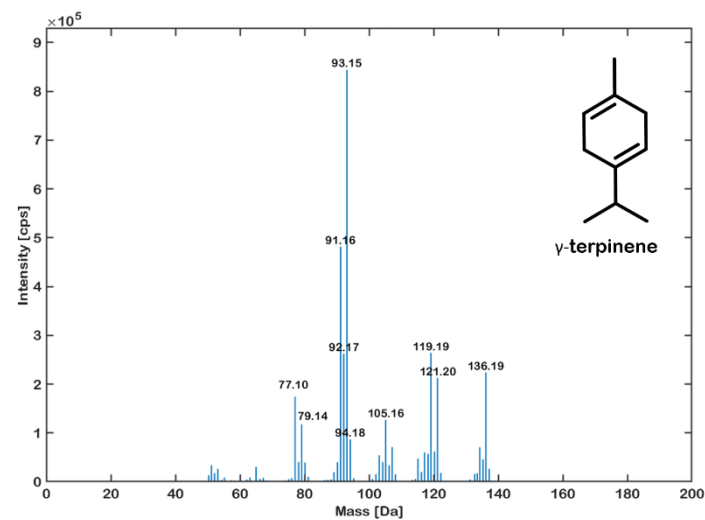
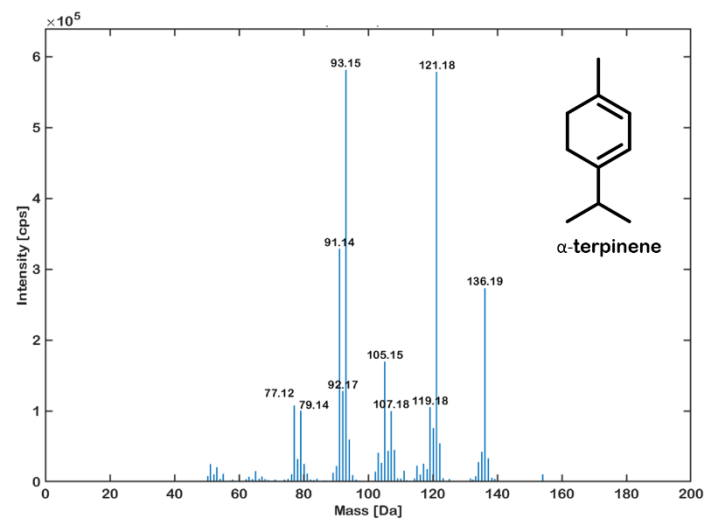


Figure 43: EI-MS spectra of α-terpinene (top, left), γ-terpinene (top, right), limonene (bottom, left), and α-terpinolene (bottom, right) were acquired at 70 eV.

So far, in this section, we have focused on the study of double bond isomers. However, the influence of DBDI on other isomers has also been investigated, such as 2- and 3-carene, which are regioisomers. The DBDI-Q1-MS spectra are shown in Figure 44 under room air conditions. DBDI-HRMS spectra are available in Figures A83-A84 in the Appendix. In DBDI-Q1-MS, the $[M+H+2O]^+$ adduct was predominant for 2-carene, whereas 3-carene showed an unannotated ion at 186.13 Da with the highest intensity. Additionally, the fragment at 118.07 Da and dimerisation $[2M+H]^+$ were exclusively observed for 2-carene. In DBDI-HRMS analysis, the $[M-H]^+$ adduct was predominantly observed for 2-carene, whereas 3-carene exhibited $[M-H+O]^+$ ion formation. The stereochemistry of 3-carene favours oxygenation over hydrogen subtraction. Furthermore, protonation was observed for 3-carene but not for 2-carene in DBDI-HRMS analysis. The observed adducts for both DBDI-Q1-MS and DBDI-HRMS were not congruent; however, they resulted in significantly different MS spectra for both 2-carene and 3-carene. The effects of modifying the ionisation environment with N_2 and H_2O enrichment were further investigated for both compounds using DBDI-Q1-MS, and the results are presented in Figure 45. Humidifying the ionisation environment with H_2O led to the absence of the $[M-H]^+$ adduct for 3-carene (Figure 45). A fragmentation event was observed for 2-carene under N_2 -enriched and room air conditions, which was absent for 3-carene spectra. Additionally humidifying the room air slightly decreased the ionisation efficiency from 7×10^6 cps to 3×10^6 cps. Lastly, DBDI-MS spectra were compared with EI-MS spectra, which are presented in Figure 46. The molecular ion $[M]^+$ was detected for both analytes, and the spectra appear nearly identical. However, there is a noticeable difference in the intensity of the fragment ion at 121.15 Da, which ranks as the second highest peak in the spectrum for 2-carene but only the fourth highest peak for 3-carene. Despite this variation, both analytes produce the same fragments at varying intensities.

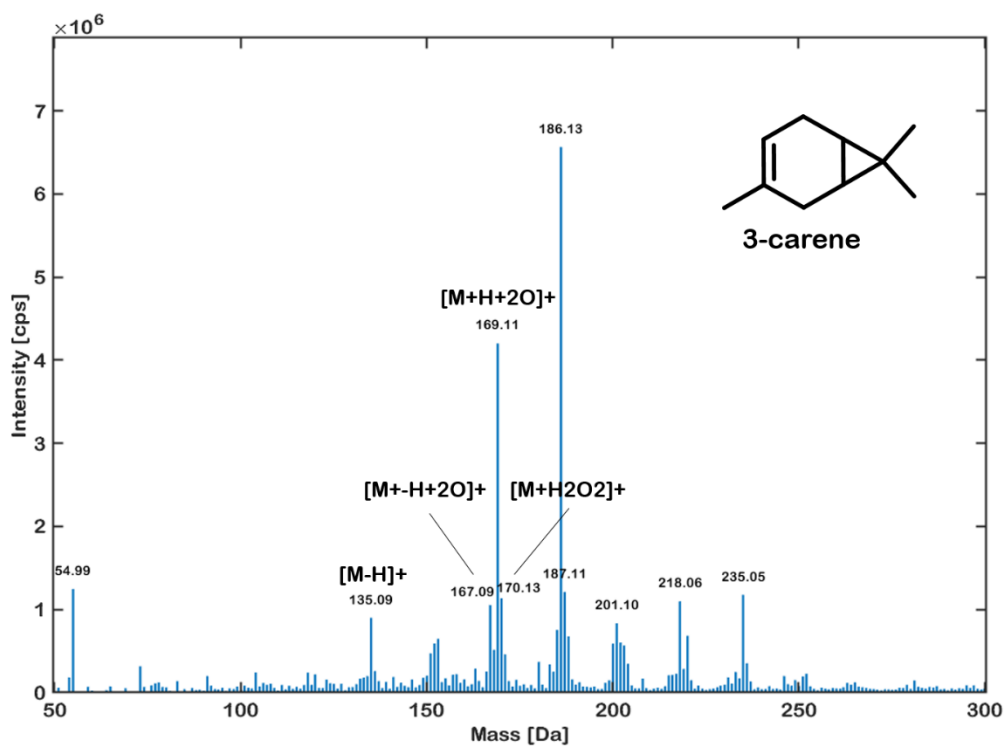
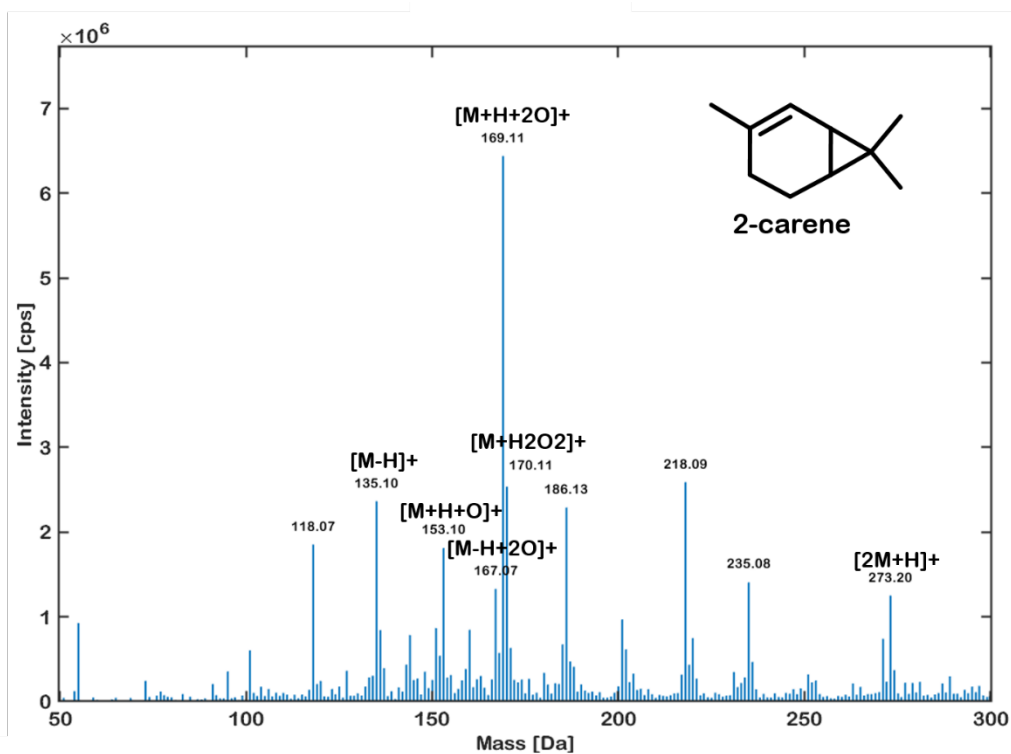


Figure 44: DBDI-Q1-MS spectrum of 2- (top) and 3-carene (bottom) acquired at 1900 V and 15,000 Hz. Room air was used for the ionisation process.

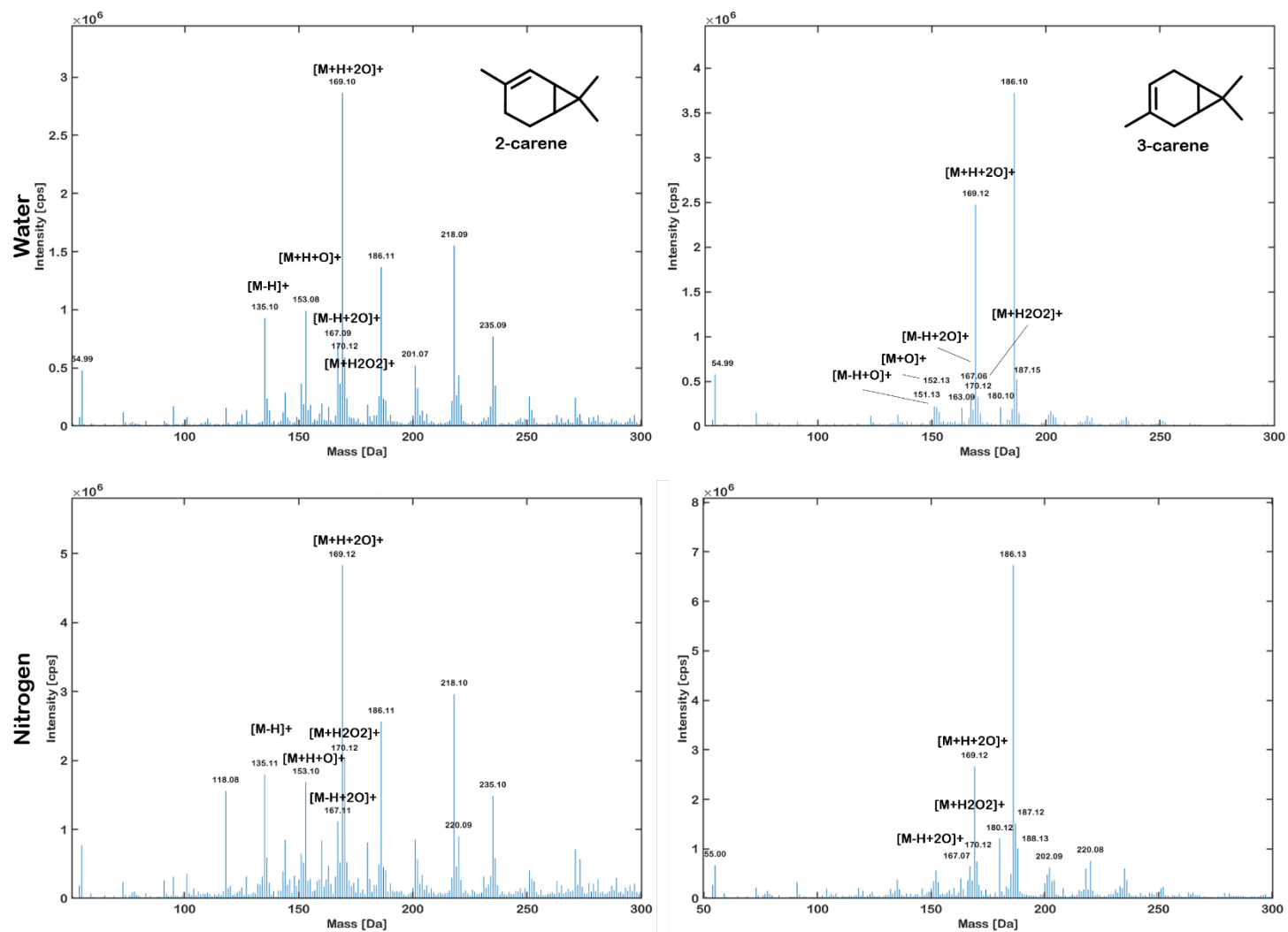


Figure 45: DBDI-Q1-MS spectra of 2- (left) and 3-carene (right) acquired at 1900 V and 15,000 Hz. Spectra were acquired under different ionisation environments: H₂O enrichment on top, N₂ enrichment on the bottom.

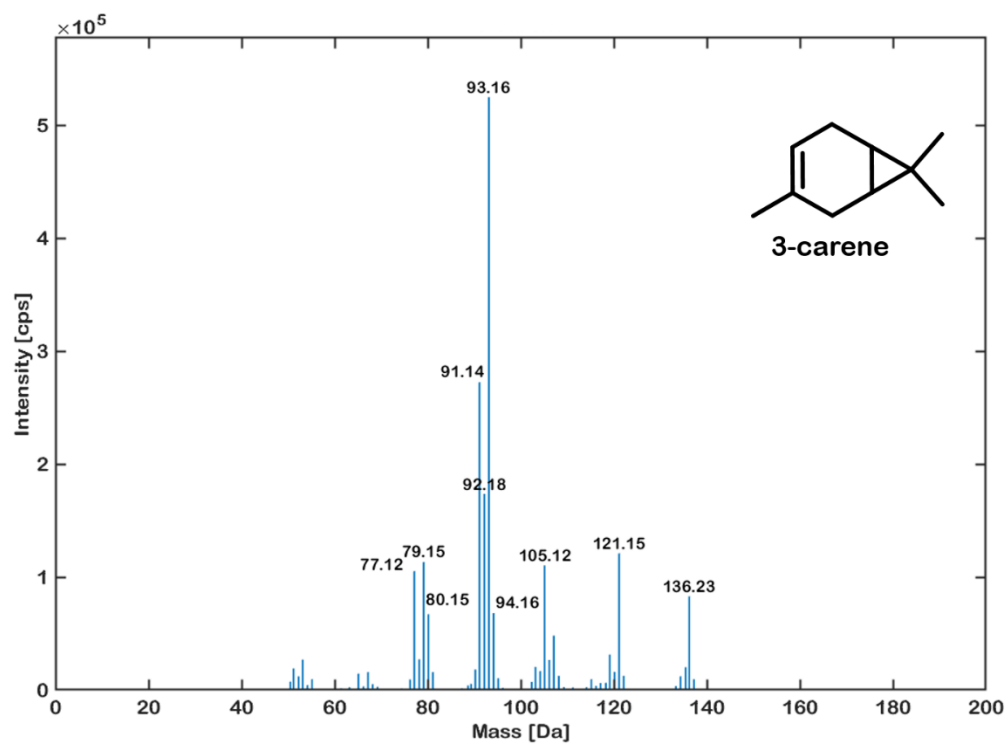
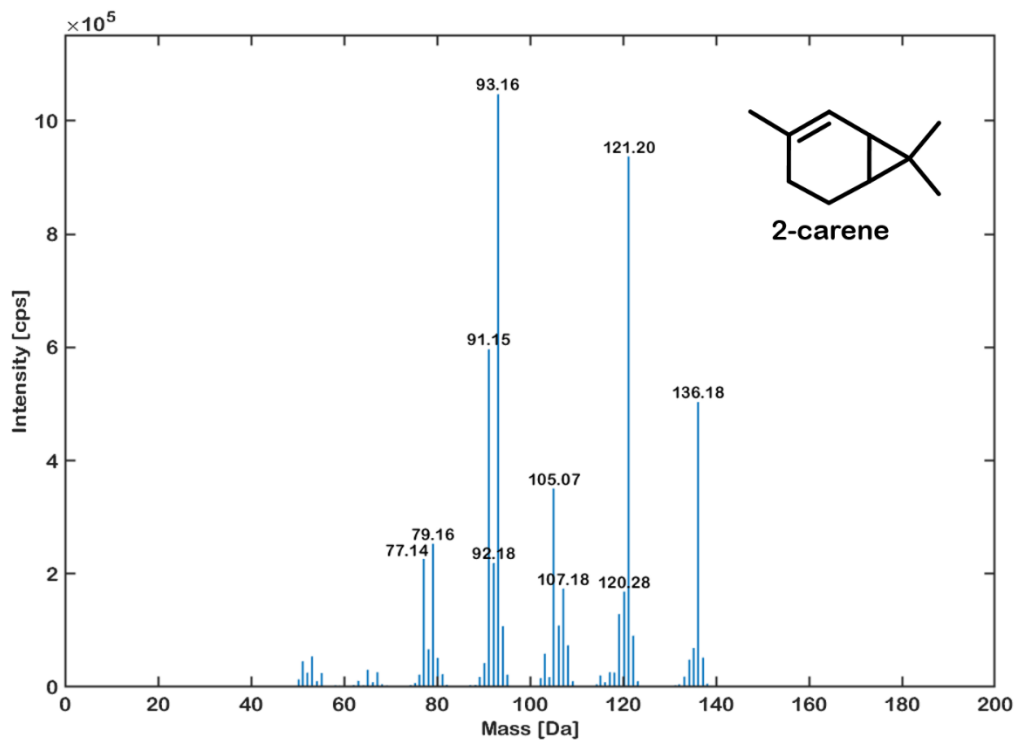


Figure 46: EI-MS spectra acquired at 70 eV for both 2- (top) and 3-carene (bottom).

The sesquiterpenes α -humulene and β -caryophyllene are constitutional isomers that differ in the position of their double bonds. Additionally, β -caryophyllene is bicyclic, whereas α -humulene is monocyclic. Figure 47 shows the DBDI-Q1-MS spectra, while DBDI-HRMS spectra can be found in the Appendix (Figures A85-A86). Notable in DBDI-Q1-MS experiments are the masses at 137.12 Da and 152.09 Da in the β -caryophyllene spectrum. These masses may indicate isomerisation products of β -caryophyllene, possibly converting sesquiterpenes to monoterpenes. However, confirmation would require MS^n experiments. Predominant adducts observed were of the type $[M - (2n + 1)H + mO]^+$, with the $[M+NO]^+$ adduct only present for α -humulene. Both DBDI-Q1-MS and HRMS-DBDI analyses gave rise to unique spectra for α -humulene and β -caryophyllene. Figure 48 compares the DBDI-Q1-MS spectra under two different conditions: humidified air and N_2 enrichment. The formation of water-hydrogen clusters is favoured when the air is humidified. Enriching the source with N_2 led to a significant shift in the MS spectrum. While adducts of the form $[M - (2n + 1)H + mO]^+$ were still primarily formed, the protonated adduct $[M+H]^+$ became dominant. Additionally, the exchange of a carbon atom for a nitrogen atom was observed and isomerisation products are increased, occurring for both α -humulene and β -caryophyllene. EI-MS spectra of both compounds were also compared and are shown in Figure 49. The EI-MS spectra are characteristic for each compound and well distinguishable. Moreover, EI-MS spectra exhibited more unique features compared to DBDI-MS spectra.

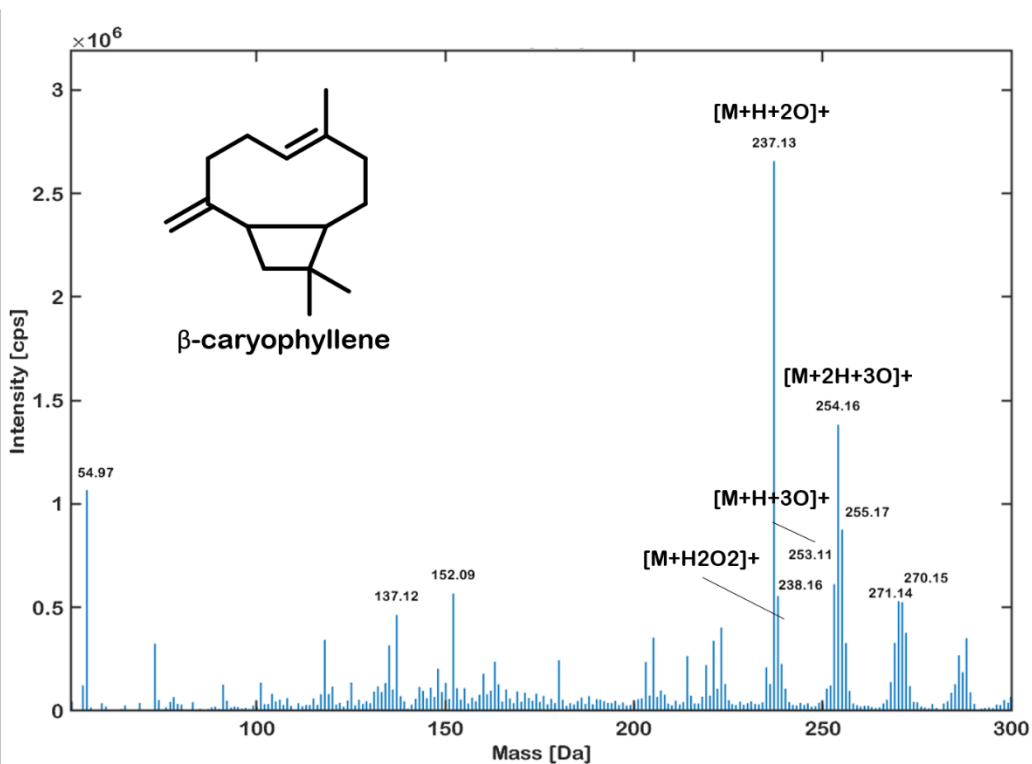
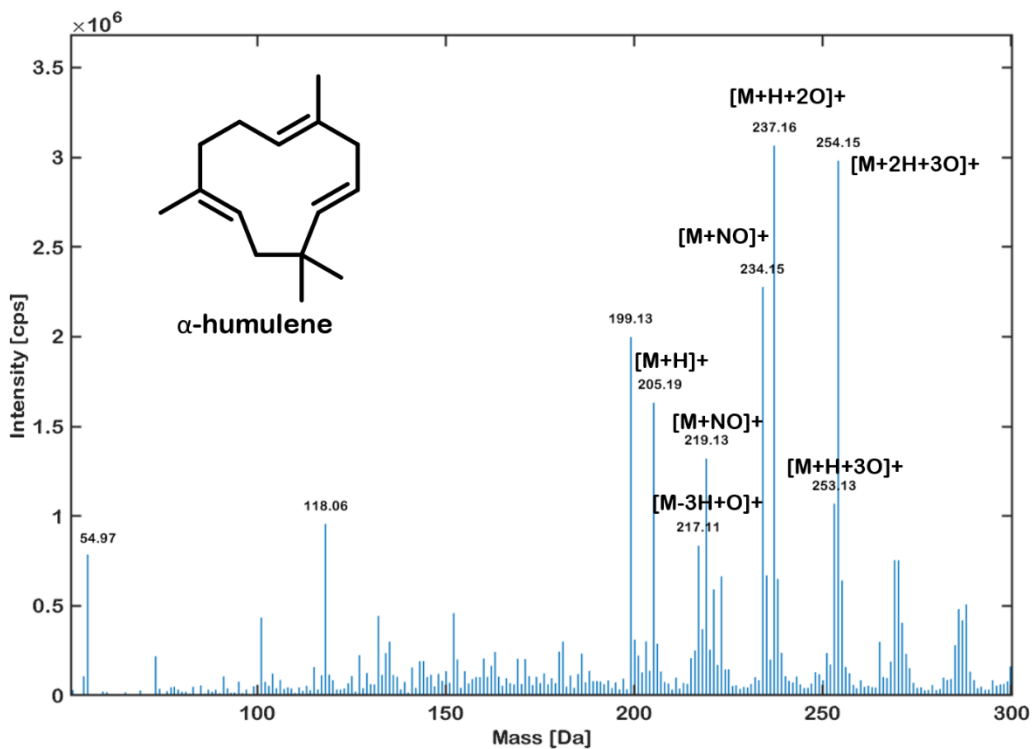


Figure 47: DBDI-Q1-MS spectrum of α -humulene (top) and β -caryophyllene (bottom) acquired at 1900 V and 15,000 Hz. Room air was used for the ionisation process.

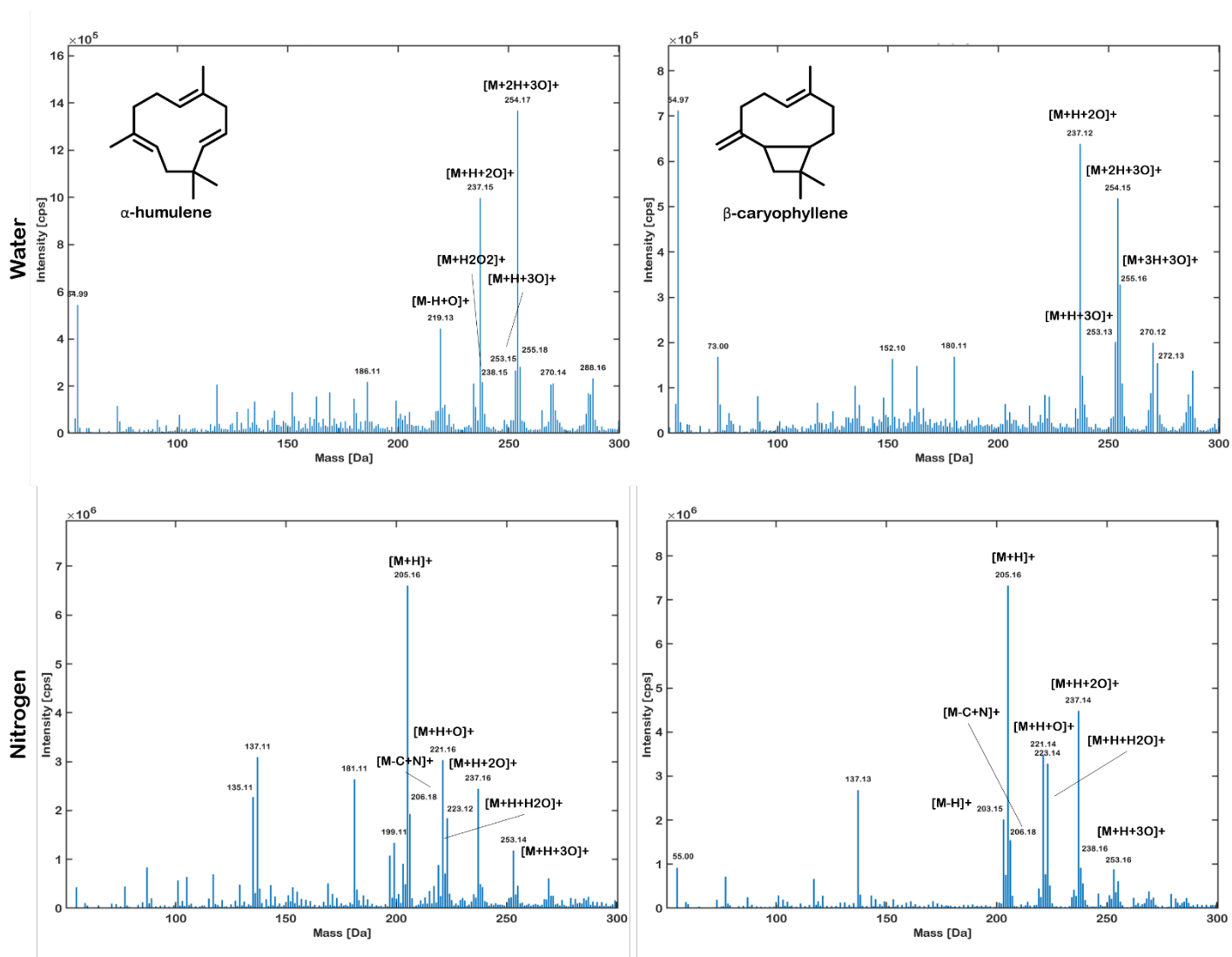


Figure 48: DBDI-Q1-MS spectra of α -humulene (left) and β -caryophyllene (right) acquired at 1900 V and 15,000 Hz. Spectra were acquired under different ionisation environments: H₂O enrichment on top, N₂ enrichment on the bottom.

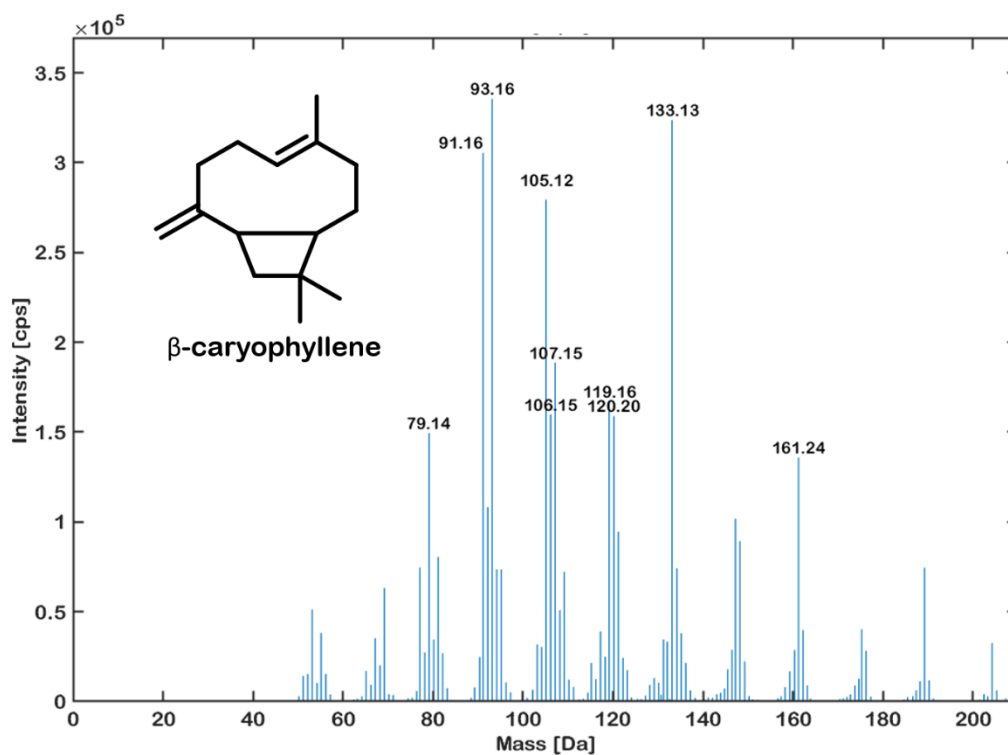
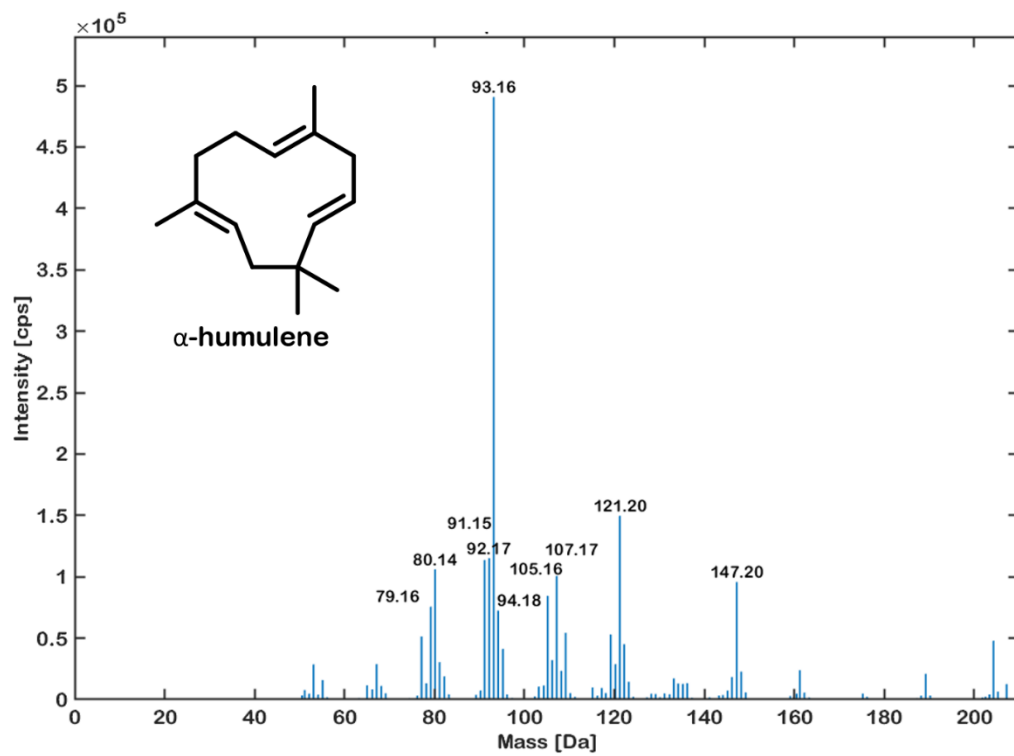


Figure 49: EI-MS spectra acquired at 70 eV for both α -humulene (top) and β -caryophyllene (bottom).

The examples given so far have shown that constitutional isomers, including regioisomers and double bond isomers, can be distinguished by their DBDI-Q1-MS spectra. In the following section, stereoisomers will be discussed. Nerolidol occurs as a diastereomer and exhibits cis-trans isomerism. Figure 50 shows the DBDI-Q1-MS spectrum, which was acquired under room air conditions. Predominantly, the protonated molecular ion was formed, which is characteristic for oxygenated terpenes. In addition, $[M+H+H_2O]^+$ and $[M+2H]^+$ adducts were detected. Overall, cis- and trans-nerolidol were not distinguishable in DBDI-Q1-MS by their adducts; however, the spectra contained slight differences in fragments during in-source fragmentation. Further investigation of these fragments was beyond the scope of this study. However, the spatial orientation of the molecule likely favours certain fragmentation events. Figure 51 shows the DBDI-Q1-MS spectra of the same analytes under N_2 and H_2O enriched environments. Modifying the ionisation environment did not result in a significant shift in adduct patterns for both cis- and trans-nerolidol. However, N_2 enrichment resulted in the exchange of a carbon atom for a nitrogen atom and seemed to promote fragmentation of trans-nerolidol. These subtle differences are significant, especially when comparing the acquired DBDI-Q1-MS spectra with EI-MS spectra of cis- and trans-nerolidol (Figure 52). The EI-MS spectra are identical and do not reveal any differences between the two diastereomers. Furthermore, the molecular ion at 222.37 Da is not detected, indicating complete fragmentation in the ion source.

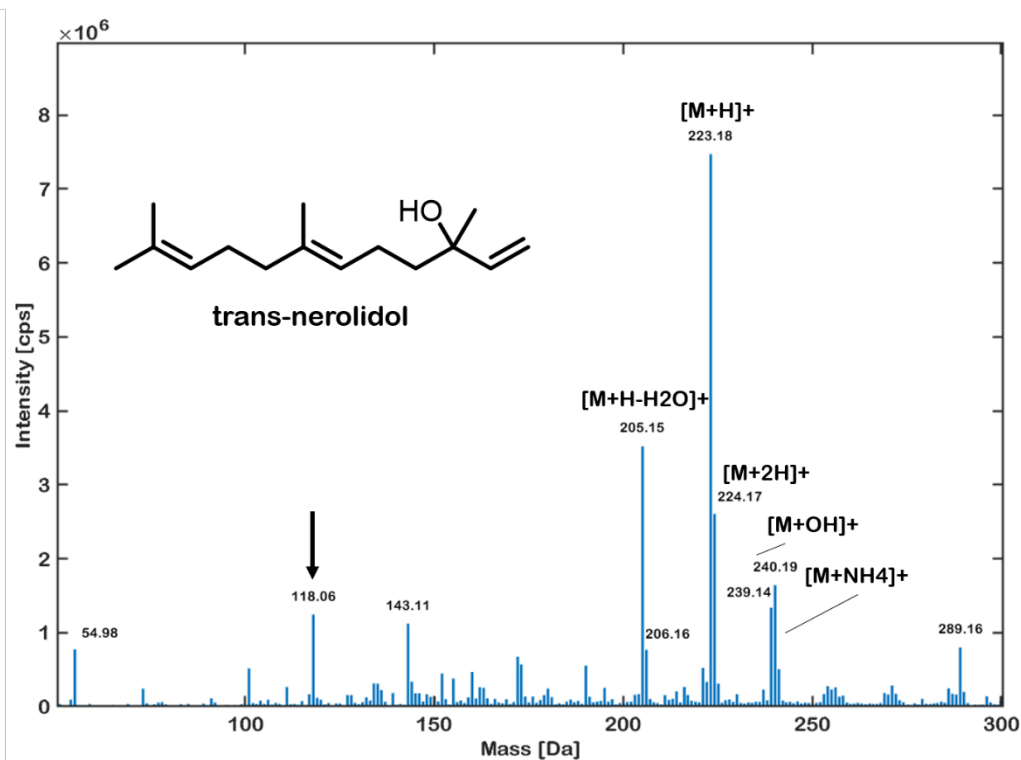
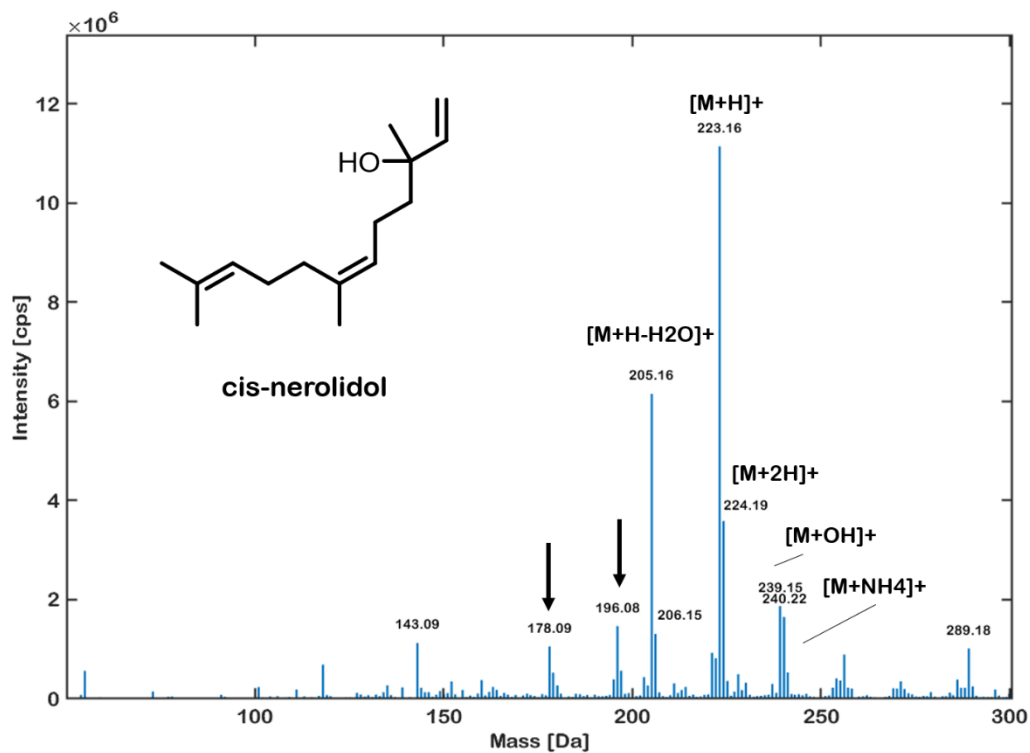


Figure 50: DBDI-Q1-MS spectrum of cis-nerolidol (top) and trans-nerolidol (bottom) acquired at 1900 V and 15,000 Hz. Room air was used for the ionisation process. Differences in spectra are indicated by an arrow.

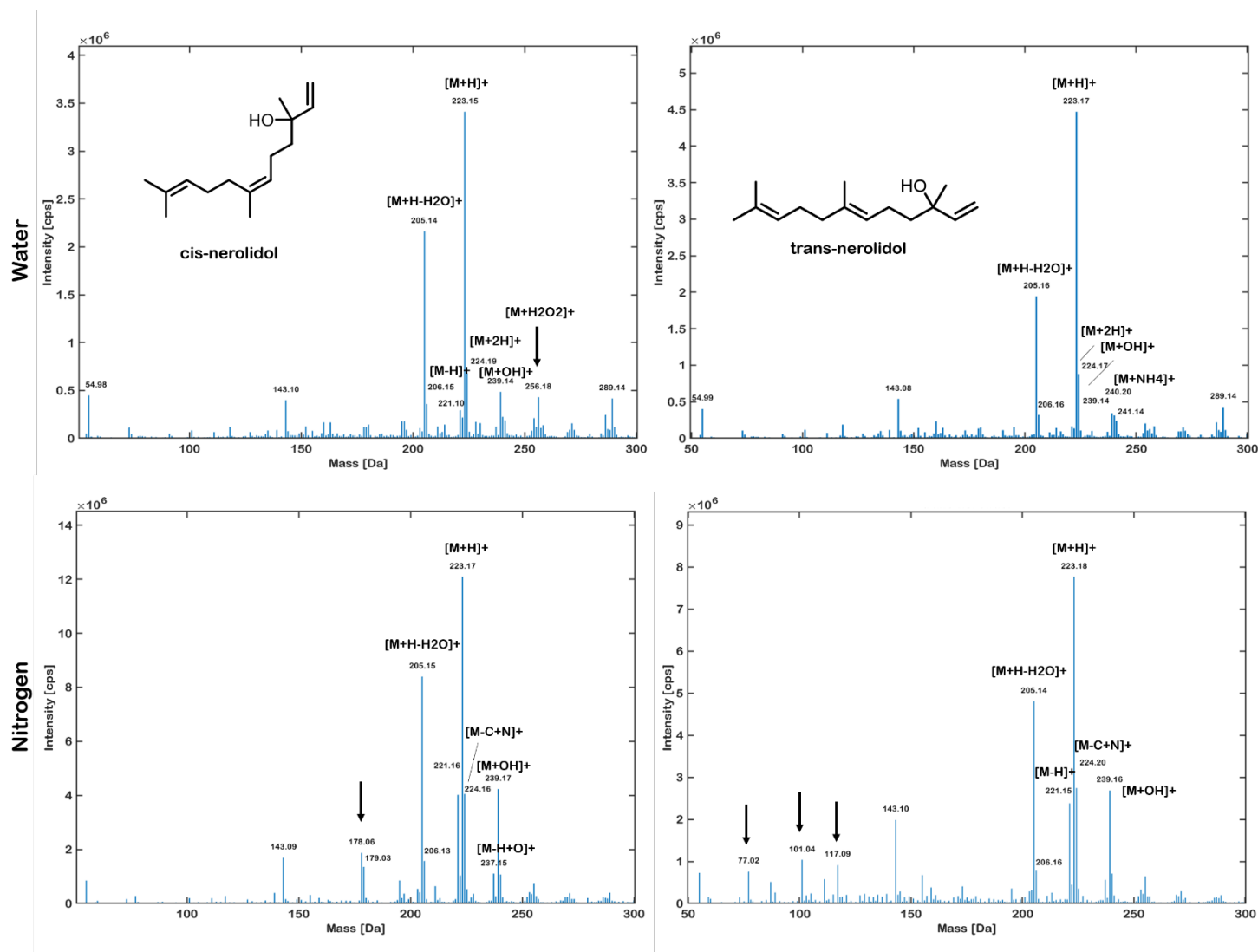


Figure 51: DBDI-Q1-MS spectra of cis-nerolidol (left) and trans-nerolidol (right) acquired at 1900 V and 15,000 Hz. Spectra were acquired under different ionisation environments: H₂O enrichment on top, N₂ enrichment on the bottom. Differences in spectra are indicated by an arrow.

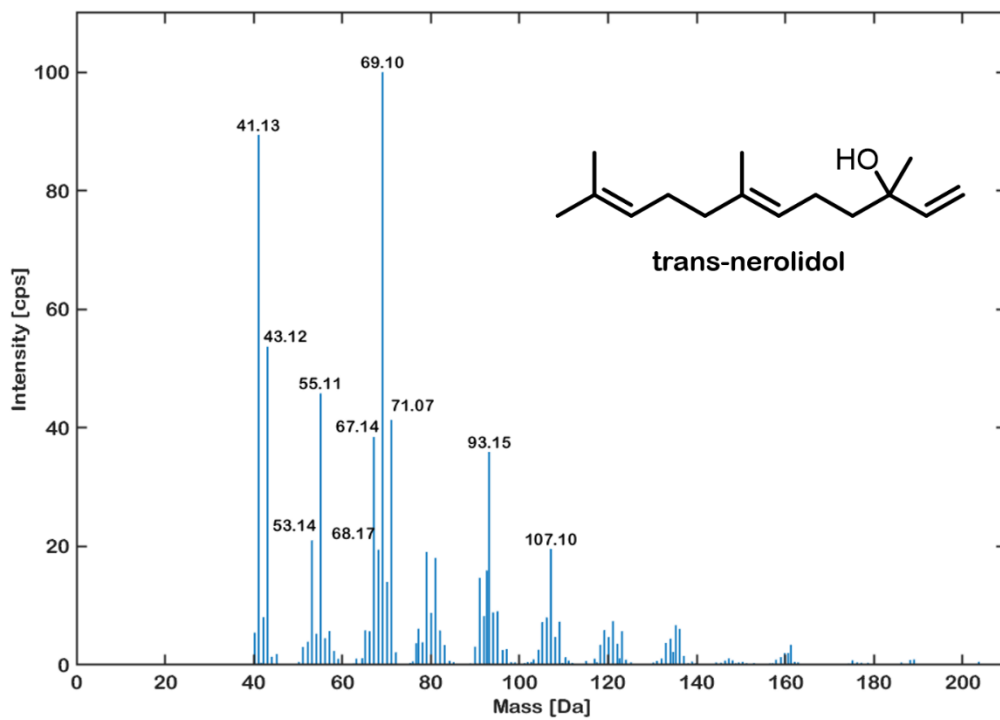
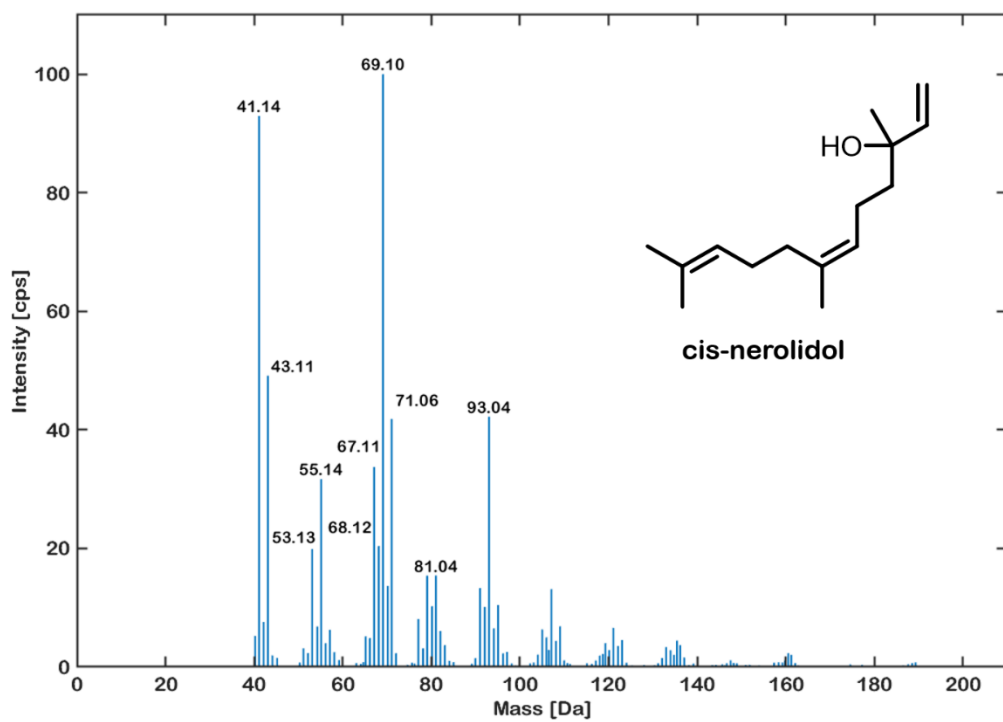


Figure 52: EI-MS spectra acquired at 70 eV for both cis-nerolidol (top) and trans-nerolidol (bottom).

The spectral differences observed in DBDI-Q1-MS between cis- and trans-nerolidol are not unique. Similar observations have been made for cis- and trans-rose oxide, as well as borneol and isoborneol. Figure 53 shows the DBDI-Q1-MS spectra for cis- and trans-rose oxide, recorded under room air conditions. Unlike nerolidol, rose oxide is a monoterpene, and fewer fragmentation events were observed. The experimental ionisation conditions applied are less suitable for sesquiterpenes, which require less energy for efficient ionisation, leading to some in-source fragmentation. The spectra of cis- and trans-rose oxide in Figure 53 exhibit noticeable differences. Specifically, the predominant molecular ion for cis-rose oxide was $[M+NH_4]^+$, whereas for trans-rose oxide it was $[M+H]^+$. Additionally, an unannotated mass at 269.15 Da was observed for cis-rose oxide but not for the trans isomer. Modifying the ionisation environment in the DBDI source by humidifying the air resulted in predominantly the $[M+H]^+$ ion formation for both cis- and trans-rose oxide. Enriching the environment with N_2 led to fragmentation events mainly observed for trans-rose oxide (Figure 54). Similar to cis- and trans-nerolidol, subtle differences were noted in the DBDI-Q1-MS spectra compared to their EI-MS spectra (Figure 55).

Borneol and isoborneol, both hydroxylated bicyclic monoterpenes, represent another diastereomeric structure. Figure 56 displays the DBDI-Q1-MS spectrum recorded under room air conditions. The $[M+NOH_2]^+$ adduct was exclusively observed for borneol. Additionally, relative intensity differences were noted for the $[M+OH]^+$ and $[M+NH_4]^+$ adduct ions in both borneol and isoborneol spectra. Lastly, an unannotated mass at 289.20 Da was found exclusively in the isoborneol spectrum. Figure 57 illustrates the same analytes recorded under modified ionisation environments. The $[M+NOH_2]^+$ adduct is predominantly formed for borneol, but N_2 enrichment also leads to the same adduct formation in isoborneol spectra. However, this adduct is so distinctive of borneol under all ionisation conditions that it can be used as a marker to differentiate borneol from isoborneol. When comparing the EI-MS spectra of borneol and isoborneol (Figure 58), no striking distinguishing features are observed.

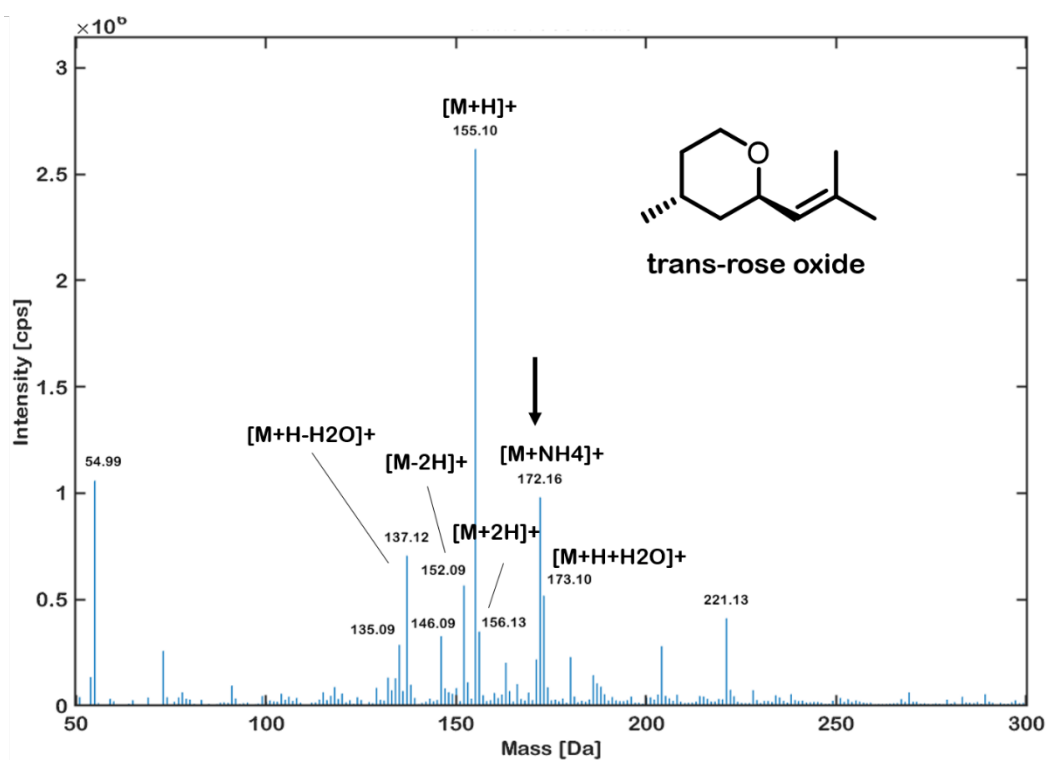
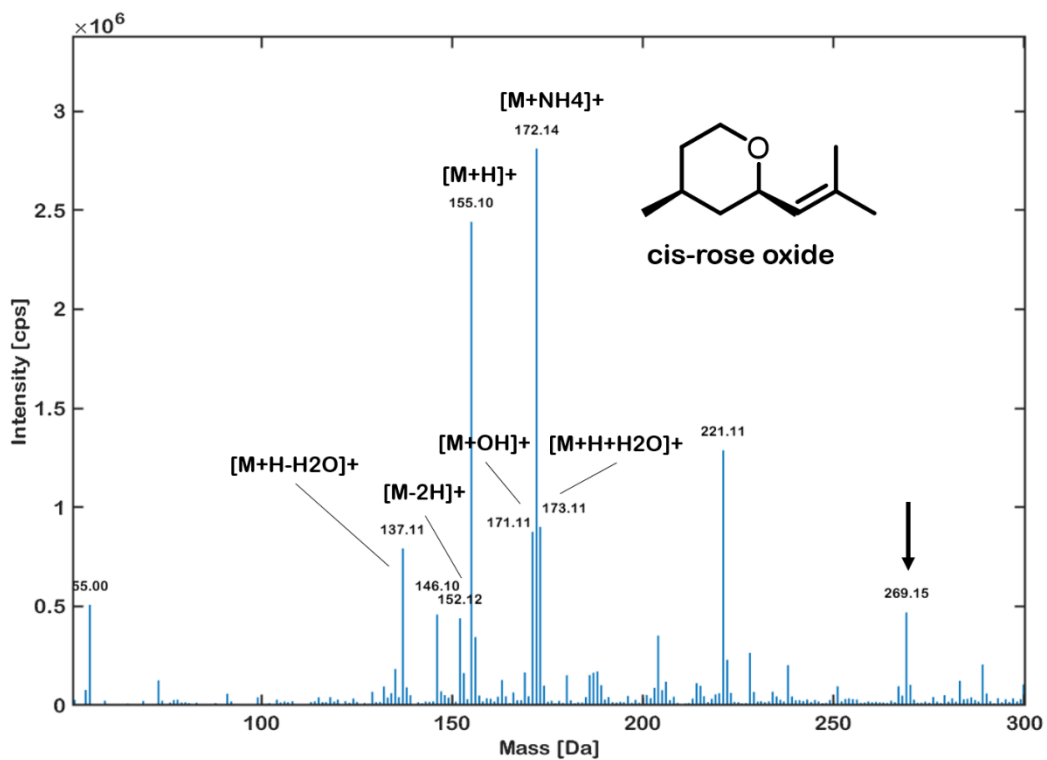


Figure 53: DBDI-Q1-MS spectrum of cis-rose oxide (top) and trans-rose oxide (bottom) acquired at 1900 V and 15,000 Hz. Room air was used for the ionisation process. Differences in spectra are indicated by an arrow.

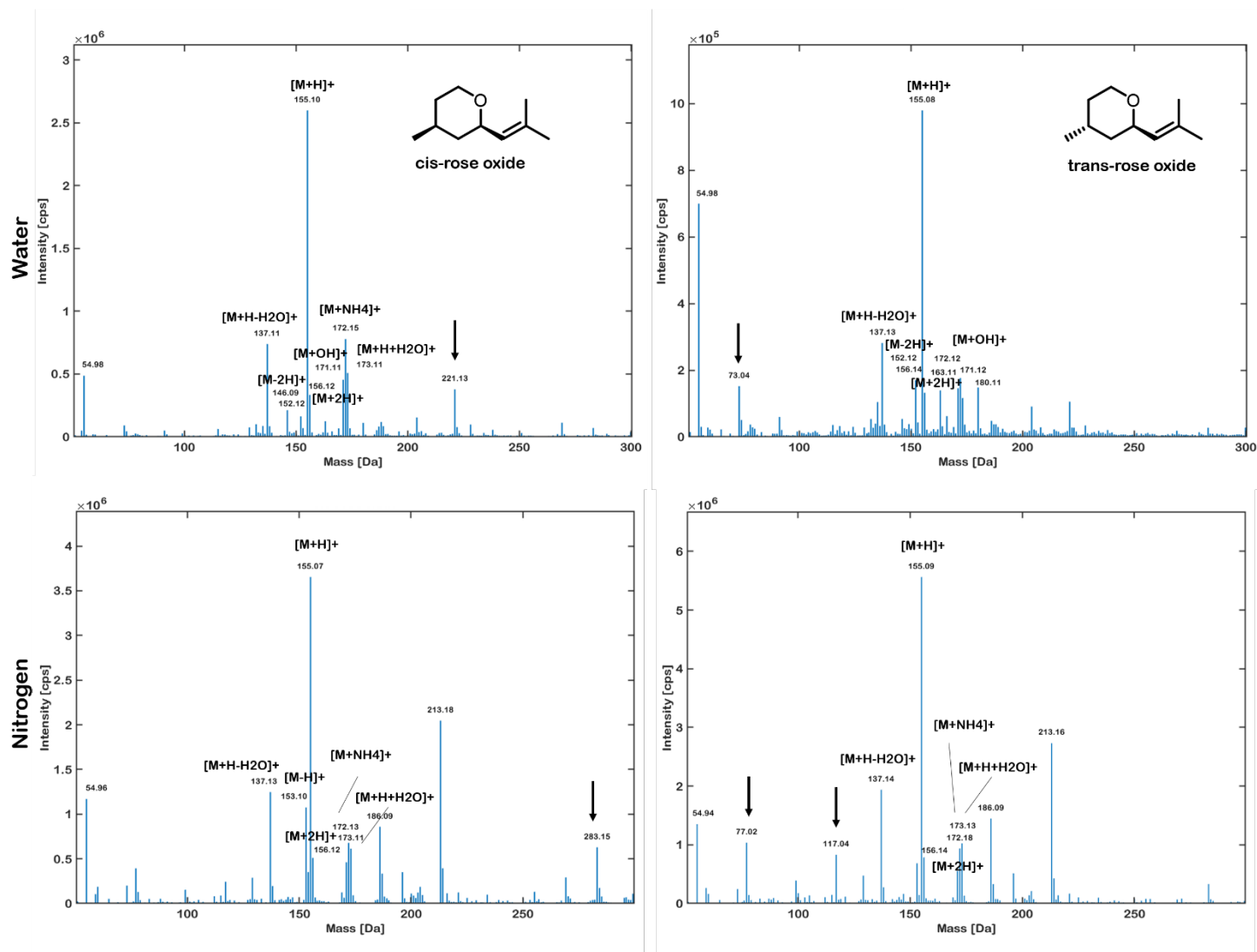


Figure 54: DBDI-Q1-MS spectra of cis-rose oxide (left) and trans-rose oxide (right) acquired at 1900 V and 15,000 Hz. Spectra were acquired under different ionisation environments: H₂O enrichment on top, N₂ enrichment on the bottom. Differences in spectra are indicated by an arrow.

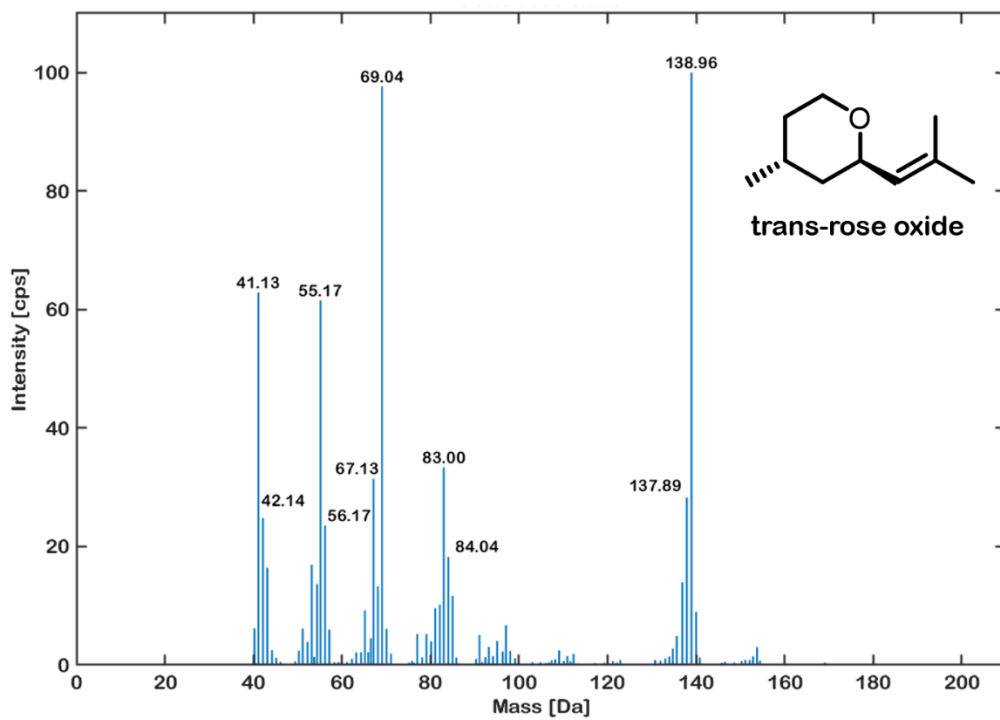
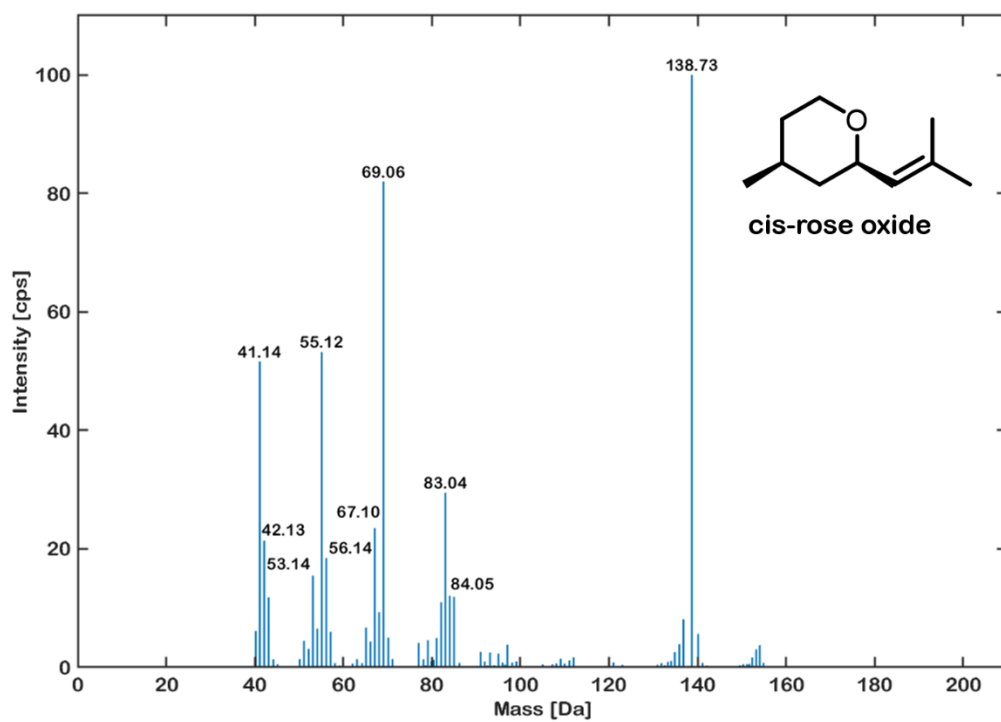


Figure 55: EI-MS spectra acquired at 70 eV for both cis-rose oxide (top) and trans-rose oxide (bottom).

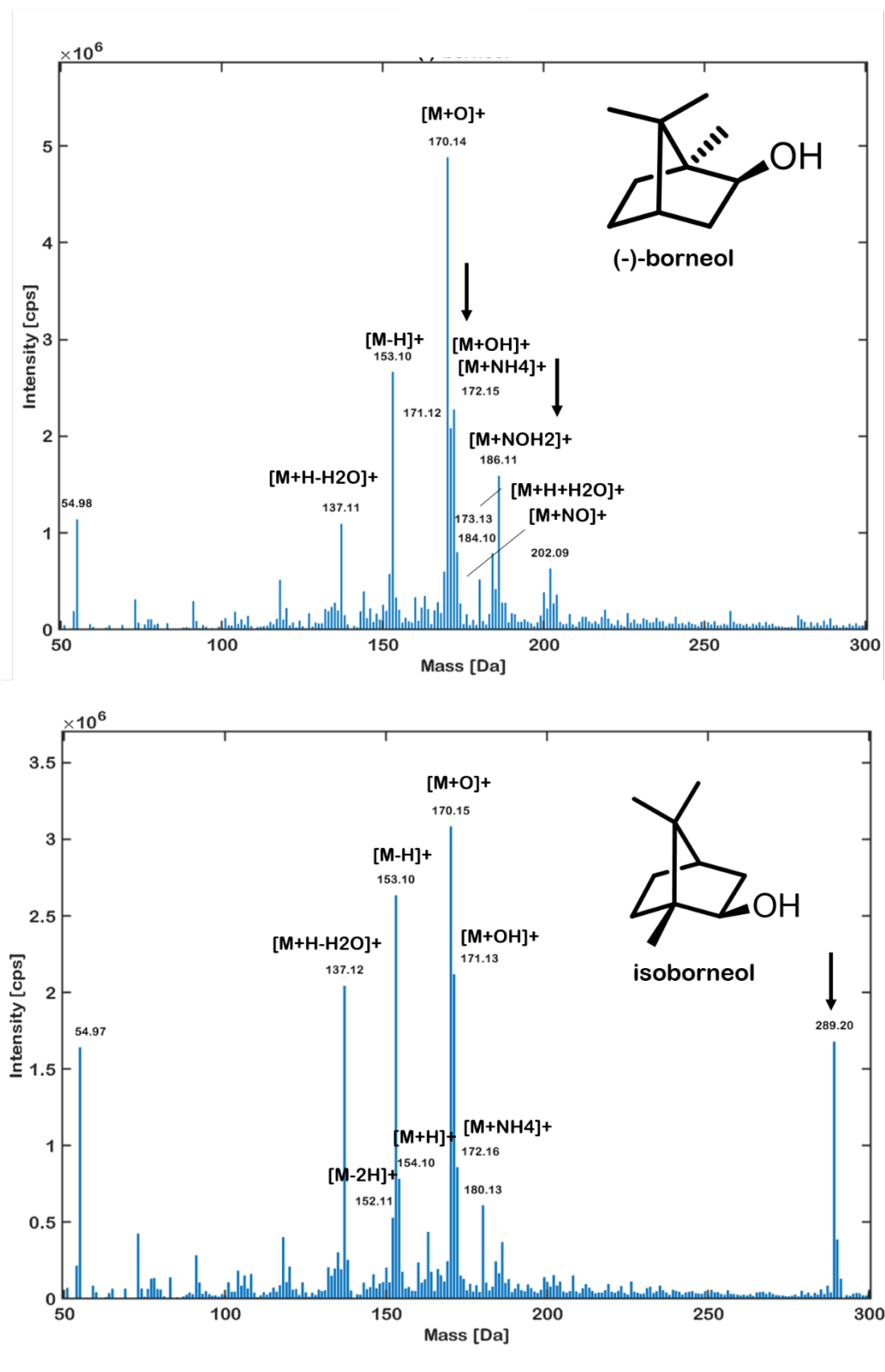


Figure 56: DBDI-Q1-MS spectrum of (-)-borneol (top) and isoborneol (bottom) acquired at 1900 V and 15,000 Hz. Room air was used for the ionisation process. Differences in spectra are indicated by an arrow.

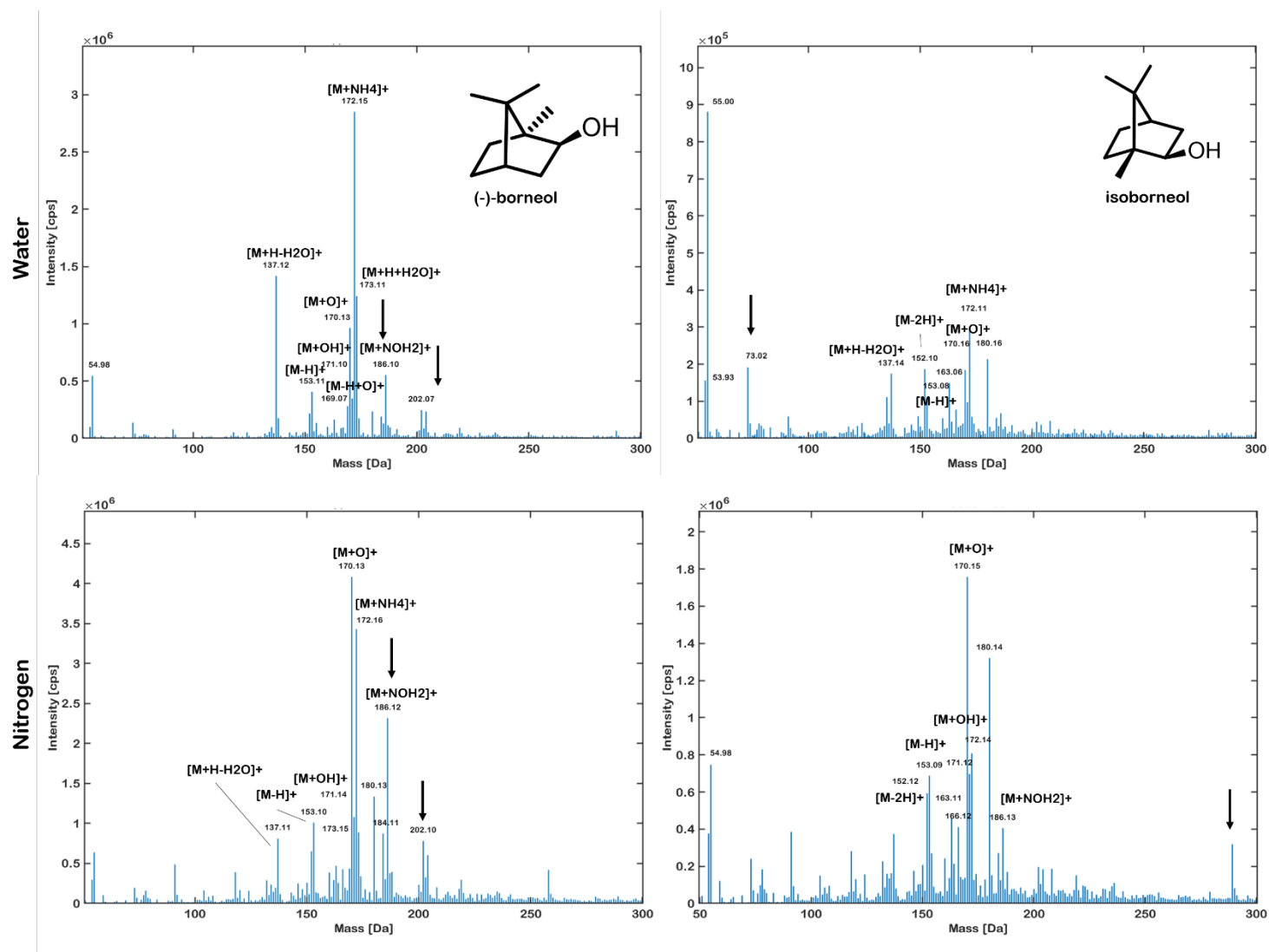


Figure 57: DBDI-Q1-MS spectra of borneol (left) and isoborneol (right) acquired at 1900 V and 15,000 Hz. Spectra were acquired under different ionisation environments: H₂O enrichment on top, N₂ enrichment on the bottom. Differences in spectra are indicated by an arrow.

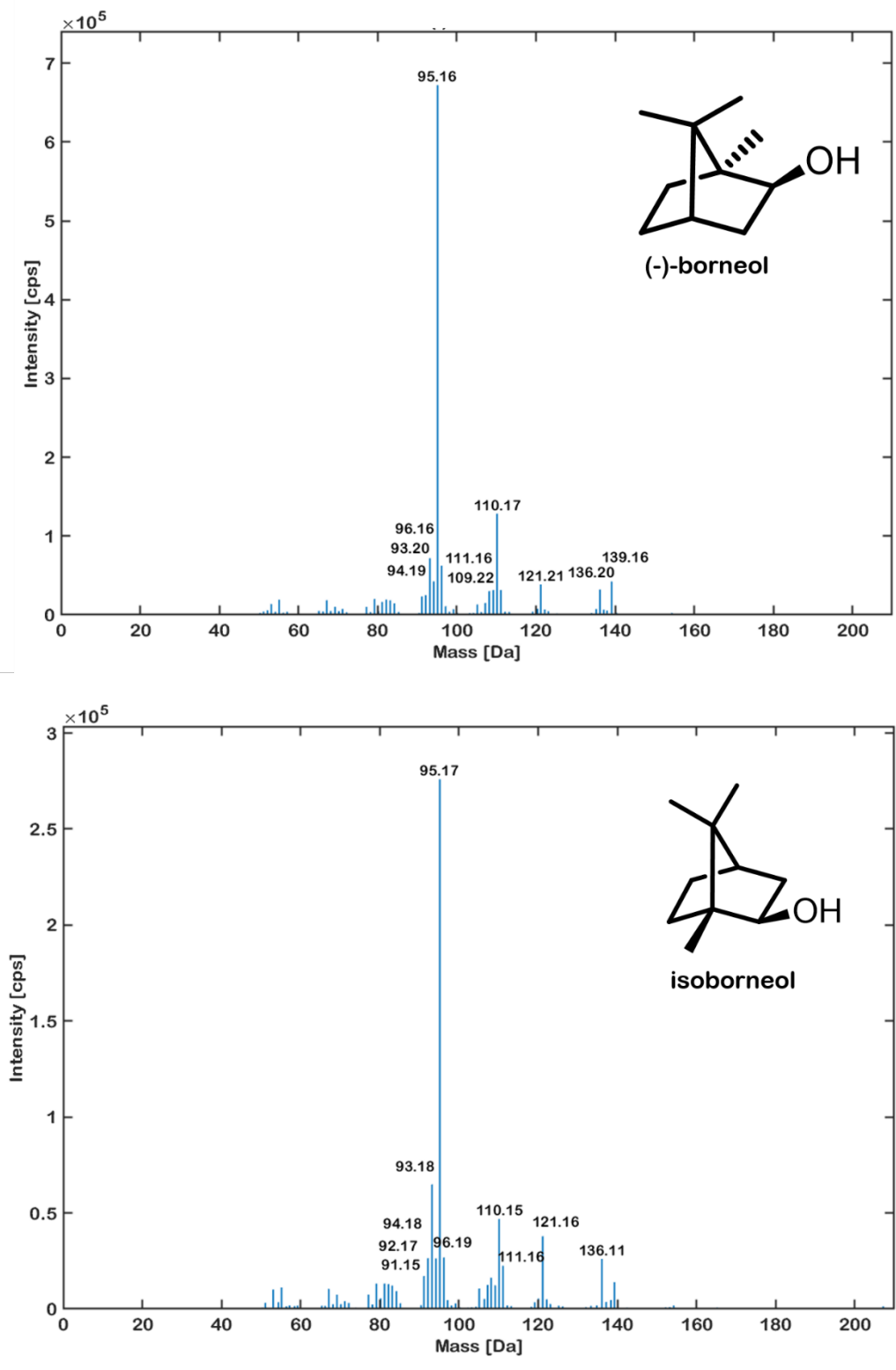


Figure 58: EI-MS spectra acquired at 70 eV for both borneol (top) and isoborneol (bottom).

DBDI-MS generates characteristic spectra for double bond isomers, regioisomers, and diastereomers. However, it remains unclear whether chiral compounds, specifically enantiomers, can be distinguished by their DBDI-induced ionisation patterns. To investigate this, the enantiomers of α -pinene and limonene were subjected to DBDI-Q1-MS analysis. Figures 59 and 60 show the MS spectra recorded under room air, humidified air, and N_2 -enriched conditions. The spectra for both enantiomeric forms of α -pinene show no differences, indicating that ionisation conditions primarily lead to variations in the spectra. Fragmentation is observed, especially in the N_2 -enriched ionisation environment. Additionally, N_2 enrichment promotes the dimerisation of both limonene and α -pinene, with the $[M+H+2O]^+$ adduct ion forming as the main species.

Overall, DBDI-MS is a suitable ionisation method for terpenes and can distinguish between constitutional and stereoisomers by forming characteristic adduct spectra that depend on the stereochemistry of the analyte. However, enantiomers cannot be distinguished by DBDI-MS. Moreover, DBDI-MS spectra are advantageous over EI-MS, which generates almost identical spectra for stereoisomers and requires the retention time as an orthogonal parameter to unambiguously assign compound identities. The most commonly observed ions are $[M+H]^+$, $[M-H]^+$, $[M]^+$, and those of the form $[M - (2n + 1)H + mO]^+$. The formation of adducts depends primarily on the functional group present in the analyte and secondarily on the ionisation environment. Numerous competing chemical reactions seem to occur in the DBDI source, including isomerisation, polymerisation, and oxidation of terpenes. The precise assignment of unannotated adducts and fragments requires further analysis by HRMS and MS^n experiments. In addition, different flow rates should be tested to assess the effect of dwell time in the DBDI source on ionisation efficiency.

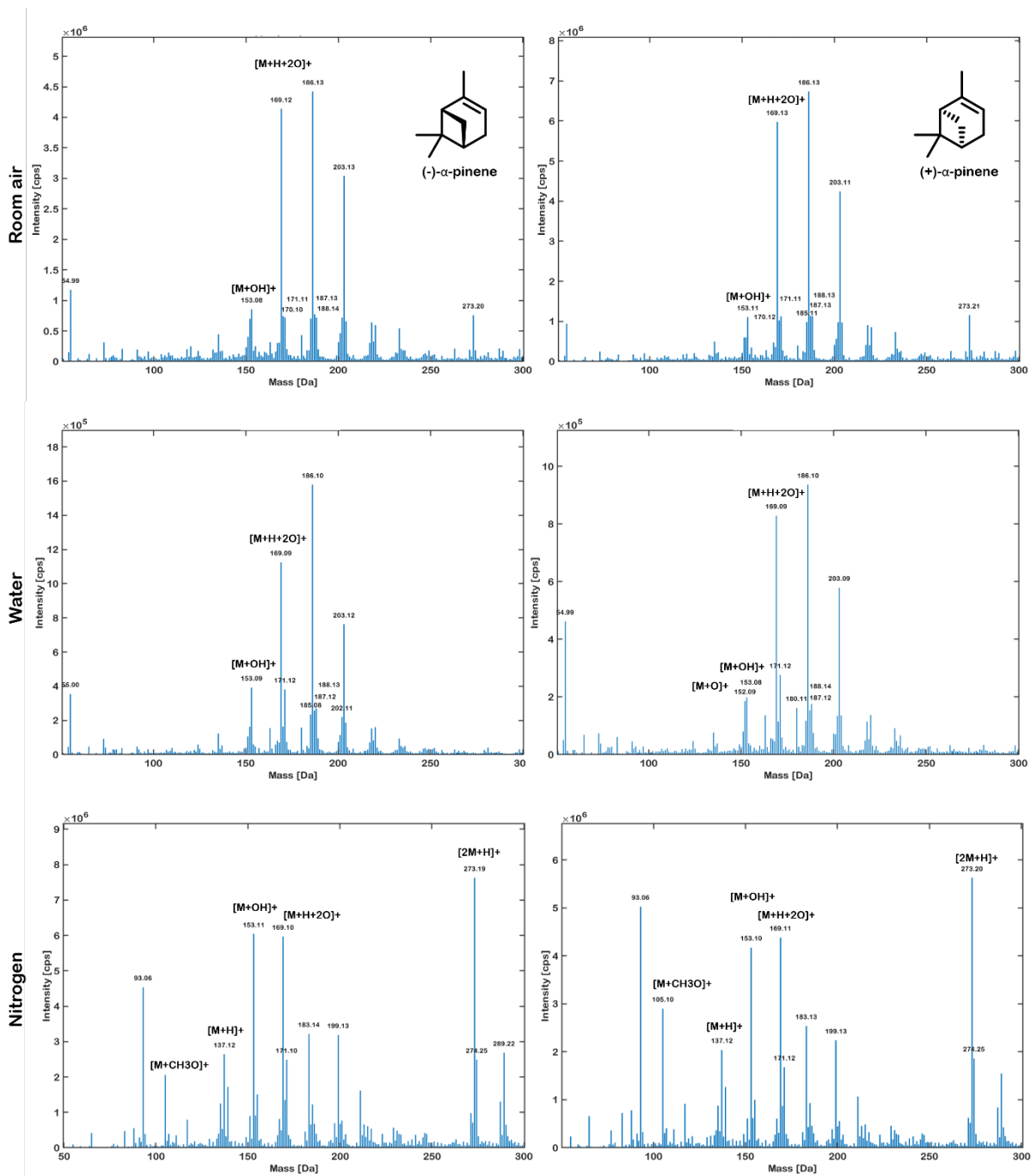


Figure 59: DBDI-Q1-MS spectra of (-)-α-pinene (left) and (+)-α-pinene (right) acquired at 1900 V and 15,000 Hz. Spectra were acquired under different ionisation environments: room air on top, H₂O enrichment in the middle, N₂ enrichment on the bottom.

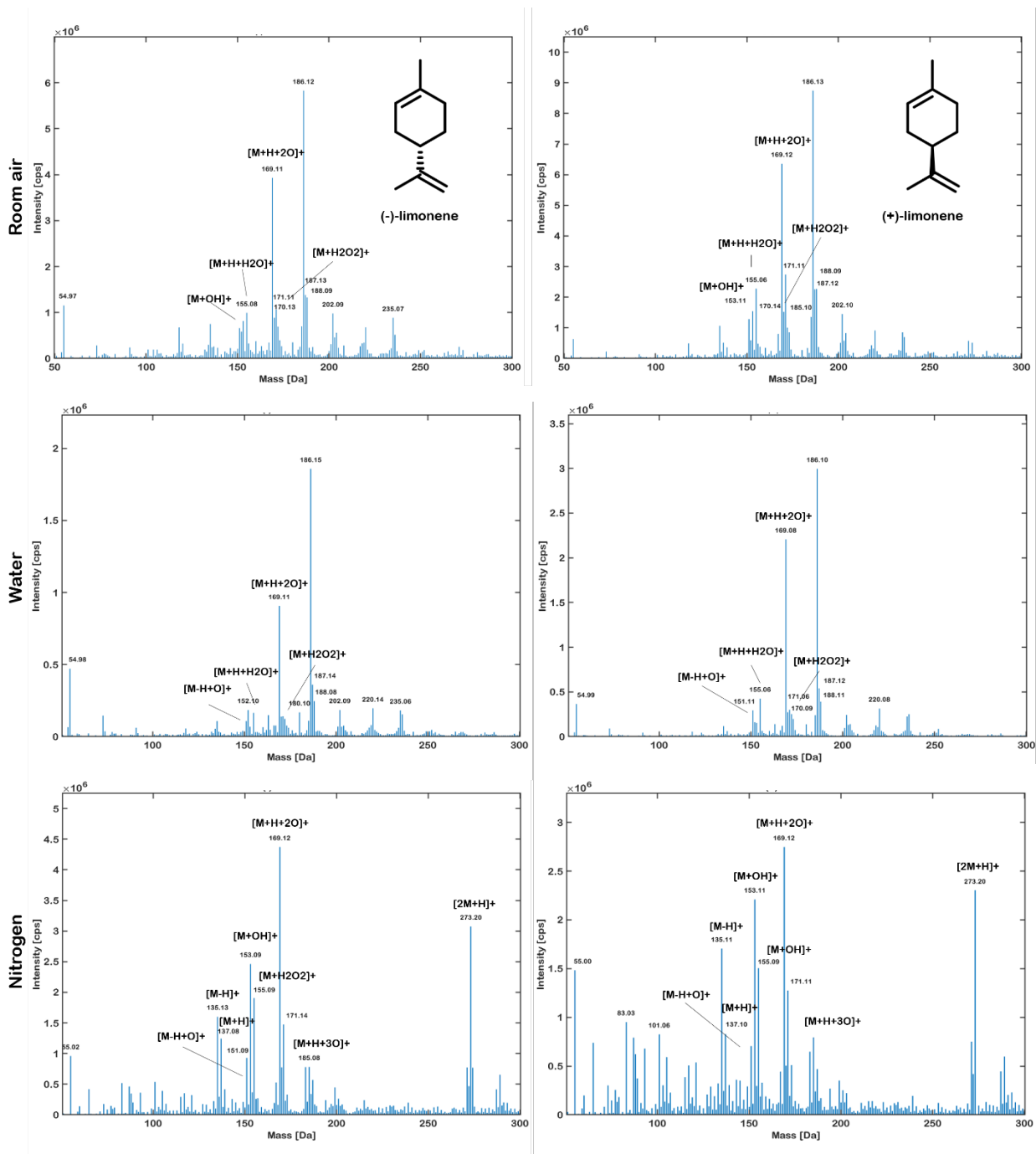


Figure 60: DBDI-Q1-MS spectra of (-)-limonene (left) and (+)-limonene (right) acquired at 1900 V and 15,000 Hz. Spectra were acquired under different ionisation environments: room air on top, H₂O enrichment in the middle, N₂ enrichment on the bottom.

3.2.1. Materials and methods

3.2.2. Instrumental setup

The instrumental setup consisted of a Trace 1310 GC (Thermo Scientific, Waltham, Massachusetts, USA) equipped with a DB-wax column (30 m x 0.25 mm x 0.25 µm, Agilent J&W, Santa Clara, California, USA). The GC settings varied depending on the experiment. Sample injection was controlled by a GC PAL autosampler (CTC Analytics, Zwingen, Switzerland) with an injection volume of 1 µl. The GC was coupled to the MS via a transfer line, a heated GC/SPME module and a commercial DBDI source (SICRIT, Plasmion GmbH, Augsburg, Germany). The GC/SPME module as well as the transfer line were heated to 220 °C and frequency as well as the amplitude were adjusted according to the experiment. Helium 6.0 (PanGas, Dagmersellen, Switzerland) was used as a carrier gas. The MS used for analysis was a TripleQuad 3500 MS (AB Sciex, Redwood City, CA, USA). For data acquisition and processing Analyst® (AB Sciex, Version: 1.7.2.), Sciex OS (AB Sciex, Version: 2.0.0.455330) and XCalibur (Thermo Fisher Scientific, Version 4.4) were used.

3.2.3. Determining optimal settings for the DBDI source

The ionisation efficiency of the DBDI source was evaluated by measuring a calibration standard from *Section 2.3.2.4.*, containing 29 volatile EO components, on the GC-DBDI-MS setup described in *2.1.1.* The GC method used is described in *Section 2.1.2.1.* and further published under Raeber et al.¹⁰ However, the split flow rate was reduced to 10 ml/min, resulting in a split ratio of 5. With regard to the settings of the DBDI source the amplitudes 1500, 1600, 1700, 1800, and 1900 V were tested. For the frequency, 15,000 and 15,500 Hz were evaluated. The MS settings were as follows: Operation in Q1 mode, EP was set to 10 V, the scan range was from 50 - 300 Da and the scan rate was 200 Da/s.

3.2.4. Identifying adducts generated by DBDI

A list of the reagents used in this study is presented in Table A22 in the Appendix. Terpenes were diluted 1000-fold in ethanol before measurement. The following settings were used for the GC: the inlet, transfer line and GC/SPME module were set to a temperature of 220 °C, a constant flow of 2 ml/min was used as well as a split flow of 10 ml/min, resulting in a split ratio of 5. The oven temperature was initially set to 60 °C and gradually increased by 25 °C/min to a final temperature of 220 °C. The total run time was 6.5 min. The DBDI source was set to an amplitude of 1900 V and a frequency of 15,000 Hz. A bubbler was connected to the GC/SPME module and filled with 100 ml of the respective dopant. MS spectra were extracted by forming the sum of the peak area using Sciex OS and exported as txt files by transforming the spectra to centroid view based on peak intensity. Data was further processed using MATLAB (Version: Release R2022b, version: 9.13.0.2126072; The Mathworks Inc.) by extracting the ten most intense peaks. The code can be found the Appendix in Script A5. Further data processing and visualisation was conducted using Python (Version 3.11.9). The individual codes are available in the Appendix in Scripts A7-A10. A comprehensive list of all adducts is available in Table A23 in the Appendix.

3.2.5. High resolution analysis of selected terpenes

HRMS analysis of selected terpenes was conducted in the laboratory of Prof. Dr. Renato Zenobi (Analytical Chemistry, ETH Zurich) under the supervision of Dr. Alina Begley. An LTQ Orbitrap (Thermo Scientific, Waltham, Massachusetts, USA) coupled to a custom built DBDI source was used for spectra acquisition. The recorded spectra were used as a cross reference for the experiments carried out on a GC coupled to a commercial DBDI source. The source settings used varied in both voltage and frequency and are indicated with each experiment.

3.2.6. GC-EI-MS spectra acquisition

GC-EI-MS acquisitions were conducted by Anina Bovens. A Trace GC-Ultra (Thermo Scientific, Waltham, Massachusetts, USA) was equipped with an apolar DB-5 MS capillary column (30 m x 0.25 mm x 0.25 μ m, Agilent Technologies, Santa Clara, USA). A Triplus autosampler was used for automated sampling and the GC was coupled to a DSQ II MS (Thermo Fisher Scientific, Waltham, MA, USA). The GC was operated at isothermal conditions at a temperature of 180 °C, a flow of 1 ml/min, a split ratio of 1:10 and a total duration of 8 min. Injection volume was held at 1 μ l. The MS settings were as follows: scan mode was positive with a range from 40 - 300 Da. The EI source was kept at an energy of 70 eV and an ion source temperature of 250 °C. The MS transfer line was kept at 250 °C. Helium 6.0 (PanGas, Dagmersellen, Switzerland) served as a carrier gas. Data acquisition and processing was performed using XCalibur (Thermo Fisher Scientific, Version 2.2 SP1.48).

Chapter 3: Computational Methods and Data Fusion for Enhanced Classification of Natural Products

This chapter forms part of the following publication:

Raeber J, Steuer C. Exploring new dimensions: Single and multi-block analysis of essential oils using DBDI-MS and FT-IR for enhanced authenticity control. *Analytica Chimica Acta* 2023; 1277: 341657. DOI: <https://doi.org/10.1016/j.aca.2023.341657>.

Contributions: **JR**: conceptualisation, method development, data acquisition and data analysis, computational analysis, study design. **CS**: supervision, resources, conceptualisation.

Licencing:

This article has been published under the terms of the Creative Commons CC-BY 4.0 DEED licence (<https://creativecommons.org/licenses/by/4.0/>), which allows its unrestricted use, provided it is properly cited.

4.1. Exploring New Dimensions: Single and Multi-Block Analysis of Essential Oils using DBDI-MS and FT-IR for Enhanced Authenticity Control

4.1.1. Results and discussion

Chemometrics lies at the intersection of (multivariate) statistics, numerical analysis, machine learning, and deep learning. It offers a versatile toolbox for uncovering hidden information in chemical datasets, ranging from simple data exploration to pattern recognition and prediction/classification of new, unseen samples. These techniques are becoming increasingly valuable as analytical laboratories adopt high-throughput *in-situ* methods. These methods can rapidly process large numbers of samples generating multivariate datasets, sometimes in a matter of seconds. One such method is DBDI coupled to MS. DBDI-MS is a non-destructive, plasma-based ambient ionisation source combined with MS, allowing direct sampling and real-time monitoring of samples.^{93, 214, 215} As an example of its ease of use, Figure 61 shows the setup used in this study.



Figure 61: Exemplary setup for the use of DBDI-MS. An EO is placed in a headspace vial, incubated and directly coupled to the source via a GC liner. Image taken from Raeber et al.²¹

The sample, such as an EO or tea leaves, can be placed in a headspace vial and connected directly to the DBDI source using a GC liner to provide a sealed environment. The source can connect to a GC, or operate without chromatography, making the system faster and easier to use. The spectra generated are full scan spectra acquired either in Q1 mode, which allows the acquisition of ionised but unfragmented species, or in Q3 mode, which detects charged species after fragmentation. The study used a triple quadrupole MS (Figure 62).

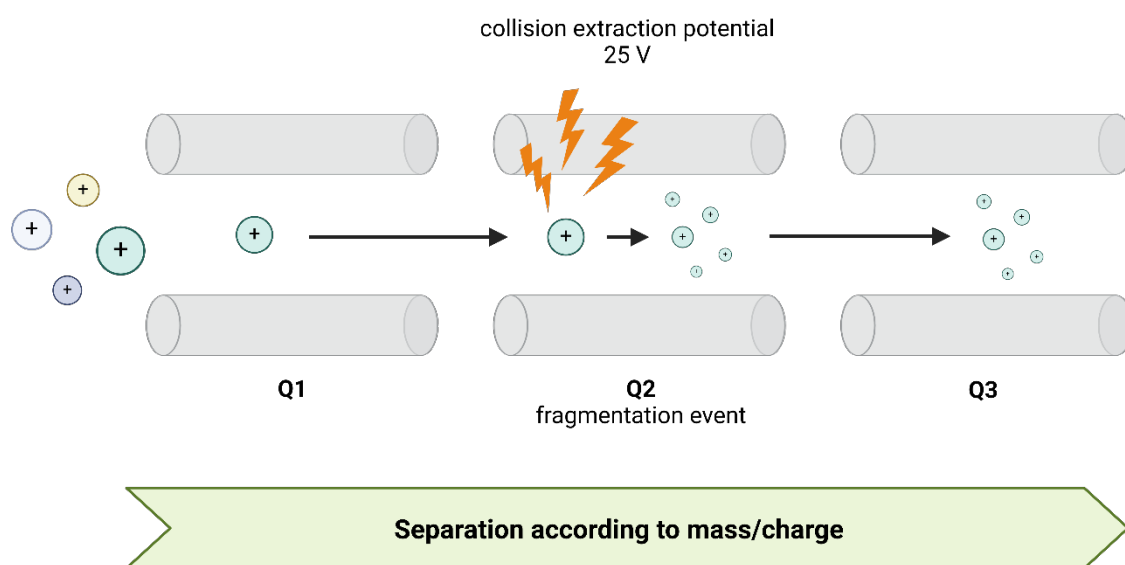


Figure 62: Design of a triple quadrupole MS. The first quadrupole (Q1) acts as a mass filter for the ionised species from the ion source, the second (Q2) as a fragmentation cell and the third (Q3) as a filter for the fragments. Created with BioRender.com.

The analysis of the volatile fraction by DBDI-MS in Q1 and Q3 mode of e.g. *R. damascena* EO results in the spectra shown in Figure 63 and 64, respectively. The spectra are not easy to interpret by manual analysis, represent unique fingerprints and are characterised by noise. The scan range for the spectra presented here was between 50 and 400 Da. There is a noticeable shift from high to low masses from Q1 to Q3 due to the fragmentation event in the MS.

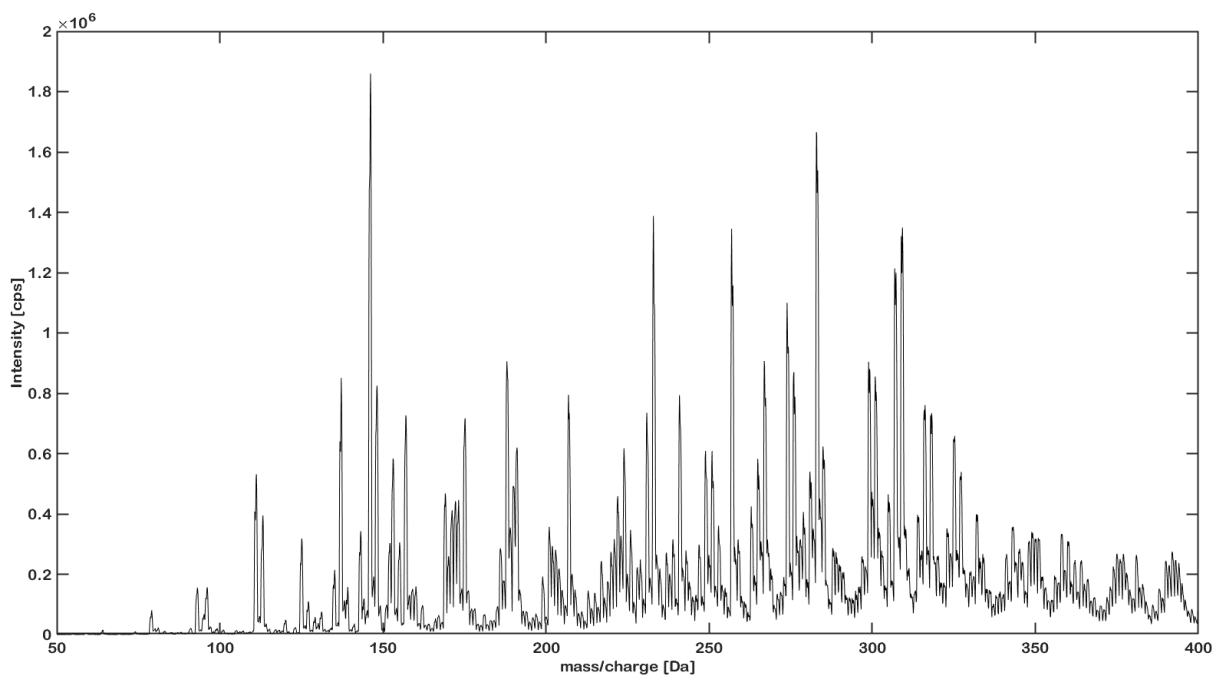


Figure 63: DBDI-MS spectrum in Q1 mode for *R. damascena* EO derived from Bulgaria.

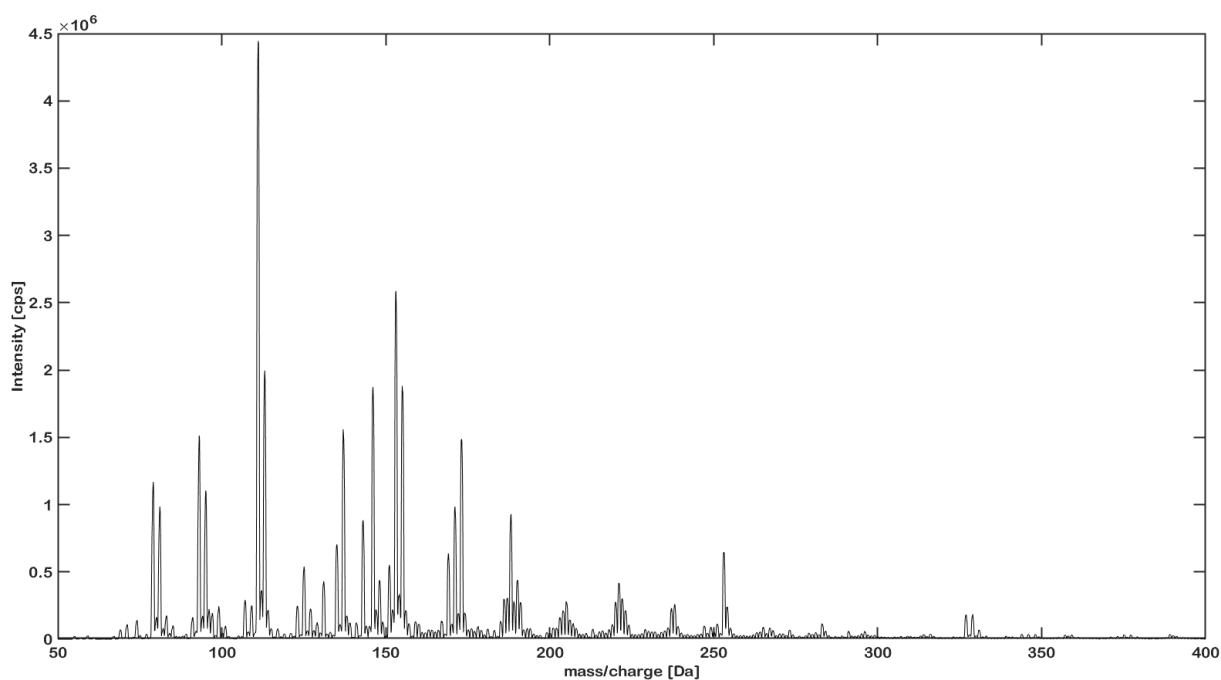


Figure 64: DBDI-MS spectrum in Q3 mode for *R. damascena* EO derived from Bulgaria.

GC-FID is the method of choice for the analysis of EO in regulatory requirements such as the Ph. Eur. and ISO norms.^{155, 188} The high resolution separation allows isomeric forms to be separated and retention time comparison allows direct assignment of compound identities. In addition, chromatographic profiles can be normalised for relative quantification or fully quantified by calibration. The chromatograms obtained

are easy to interpret, but require time-consuming method development and chromatographic expertise. Figure 65 shows the same *R. damascena* EO from Bulgaria, obtained by GC-FID on a polar wax column, as shown in Figure 63 and 64.

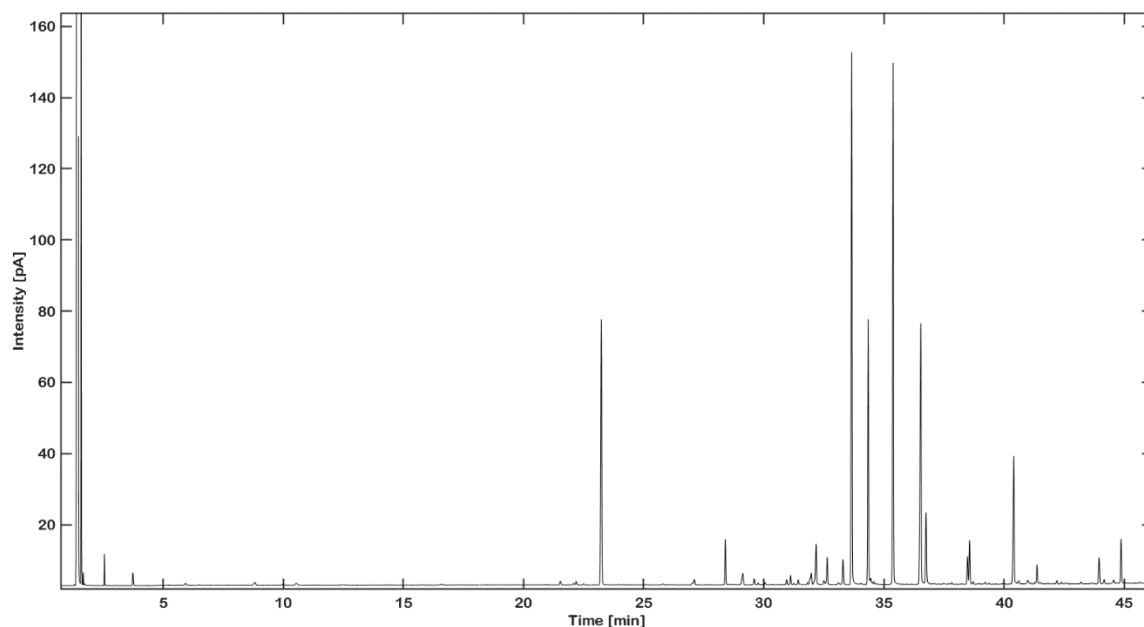


Figure 65: Chromatogram for an *R. damascena* EO from Bulgaria acquired using GC-FID on a DB-wax column.

While the spectra in Figures 63 and 64 were recorded in four minutes, the chromatographic profile took an hour. The monoterpene profile is rather sparse, which can be deduced from the monoterpenes eluting in the first 30 minutes of the chromatographic profile. Terpene patterns for mono-, sesqui- and diterpenes can already be deduced from the chromatographic profile.²² Although chromatography is time-consuming, it allows the use of columns with different polarities and is suitable for the separation of chiral substances, which are commonly found in nature. This makes GC-FID a versatile tool for the analysis of natural products. Another common analytical technique for EO quality control is FT-IR, which is a spectroscopic method. Its advantages are ease of use, economy and time saving, as it requires no sample preparation and can be used *in situ*. Similar to DBDI-MS spectra, the spectroscopic bands result in a characteristic fingerprint-like pattern. These bands can be assigned to functional groups and molecular bonds, facilitating identification. However, to ensure identity, a well-constructed library or reference substances are required to compare the acquired spectra.²¹⁶⁻²¹⁹ Figure 66 shows an example of an FT-IR

spectrum of the same *R. damascena* EO. The fingerprint region, which cannot be directly assigned to specific molecular structures, extends from 600 to 1500 cm^{-1} . There are three bands in the spectrum, at 2922, 2853 and 1793 cm^{-1} , which belong to C-H stretching and C-H bending and/or C=C stretching. The FT-IR spectrum does not contain any unique features. As terpenes are structurally similar, the fingerprint region is the most distinctive section but difficult to interpret.

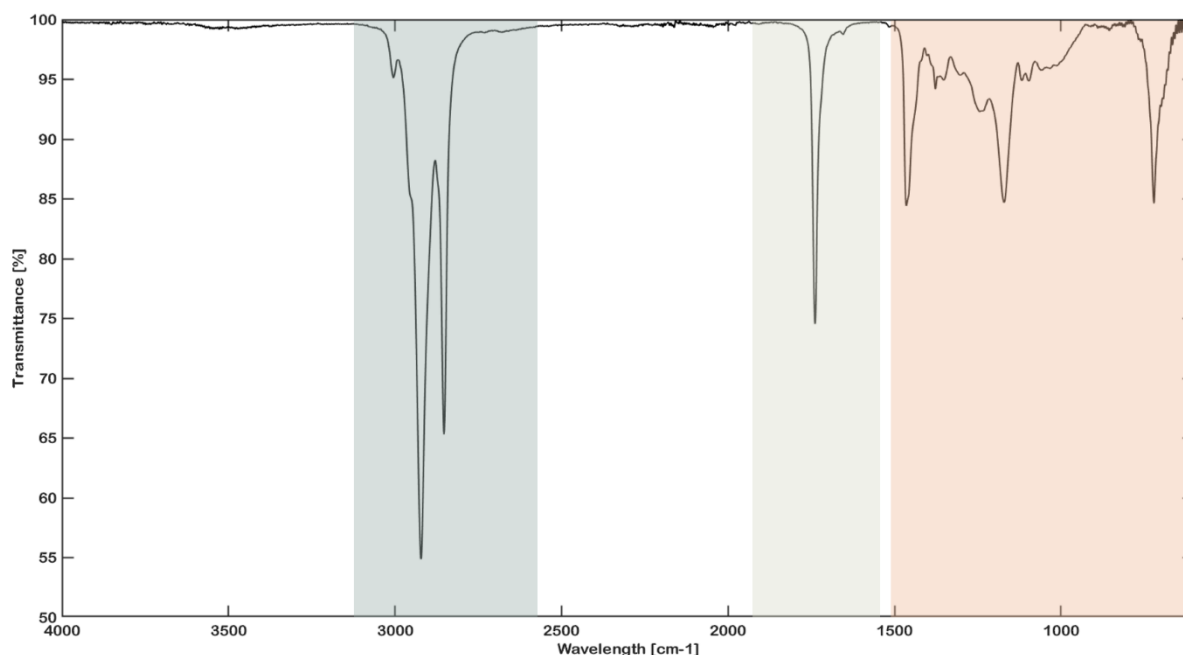


Figure 66: Typical FT-IR spectrum of a *R. damascena* EO. Wavelength in cm^{-1} is plotted on the x-axis and the transmittance in [%] is plotted on the y-axis. The fingerprint region is marked in light orange and ranges from 600-1500 cm^{-1} . C-H stretching is marked in dark green and C-H bending/C=C stretching is marked in light green.

FT-IR spectra share characteristics with DBDI-MS spectra: both are fast to acquire, easy to use, non-destructive and produce characteristic but difficult to interpret spectra. They also provide structural information. Two of the three analytical methods discussed are well established in quality control, while DBDI-MS is a novelty. This study aims to classify and differentiate *R. damascena* EO from three countries, Turkey, Bulgaria and Morocco, creating a classification problem. In most cases, integrating raw data into a classification model is not feasible: numerical functions require well-conditioned matrices, some analytical methods generate noisy data, and depending on the method, more variables are generated than there are observations.

Additionally, variables may be redundant or closely related, requiring operations such as binning. Various pre-processing methods were investigated to convert the collected datasets for 25 EO samples from GC-FID, DBDI-MS, and FT-IR into a suitable form. PCA was used to qualitatively assess the results of these pre-processing techniques. PCA is a dimension reduction technique commonly used in pre-processing. It reduces data from a higher dimensional space to a lower dimensional space by maximising the variance and capturing it in new linear combinations called principal components (PCs).²²⁰ This operation causes data points with positive covariance to align in the same direction in space, while negative covariance corresponds to opposite directions. PCA is well suited for exploratory analysis and outlier identification. For example, FT-IR is particularly susceptible to scattering effects, and because the different wavelengths cover a wide range of 600 - 4000 cm^{-1} , not all wavelengths can be given equal weight. Functions such as Savitzky-Golay smoothing can reduce noise, scattering effects can be reduced using Standard Normal Variate (SNV), and scaling problems can be reduced using various scaling functions.²²¹ Figure 67 shows the 2D and 3D plot of a PCA analysis for FT-IR data after normalisation by the maximum value, scatter correction using SNV, Savitzky-Golay smoothing (3rd order, frame window 11) and auto-scaling.

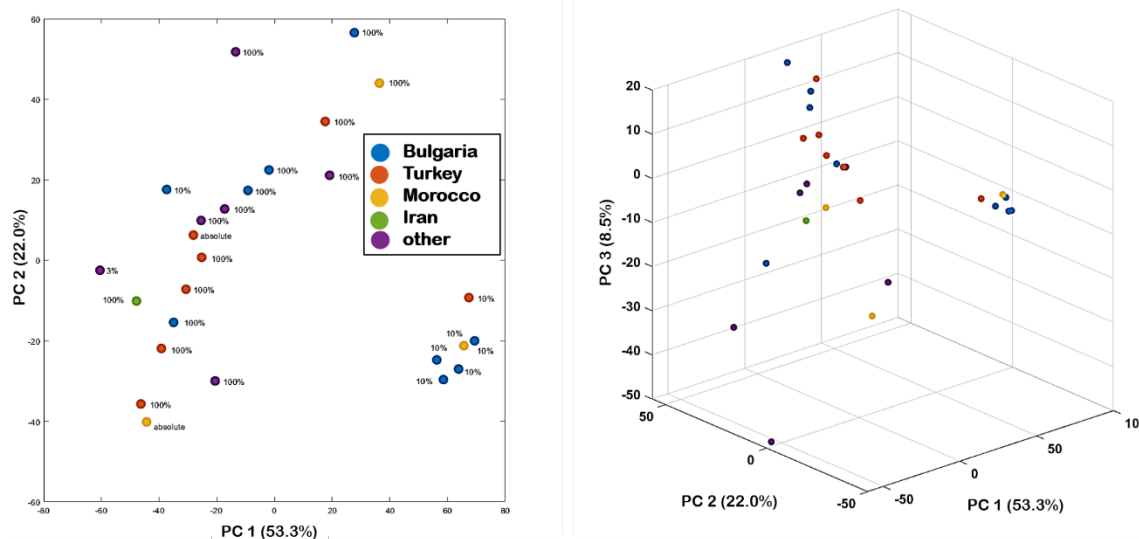


Figure 67: PCA plots for FT-IR data after normalisation by the maximum value, scatter correction using SNV, Savitzky-Golay smoothing at the 3rd order and a frame window of 11 and auto-scaling.

A spatial separation is observed for the different EO concentrations, but no group separation is seen for oils of different origin. Maintaining the same pre-processing as

in Figure 67, but switching from auto-scaling to mean-scaling gives rise to a different outcome. Figure 68 depicts the analysis with the modified pre-processing setup. Authentic EO samples from Bulgaria and Turkey form a distinct cluster. While the separation based on different EO concentrations persists, this adjustment enhances the separation based on origin.

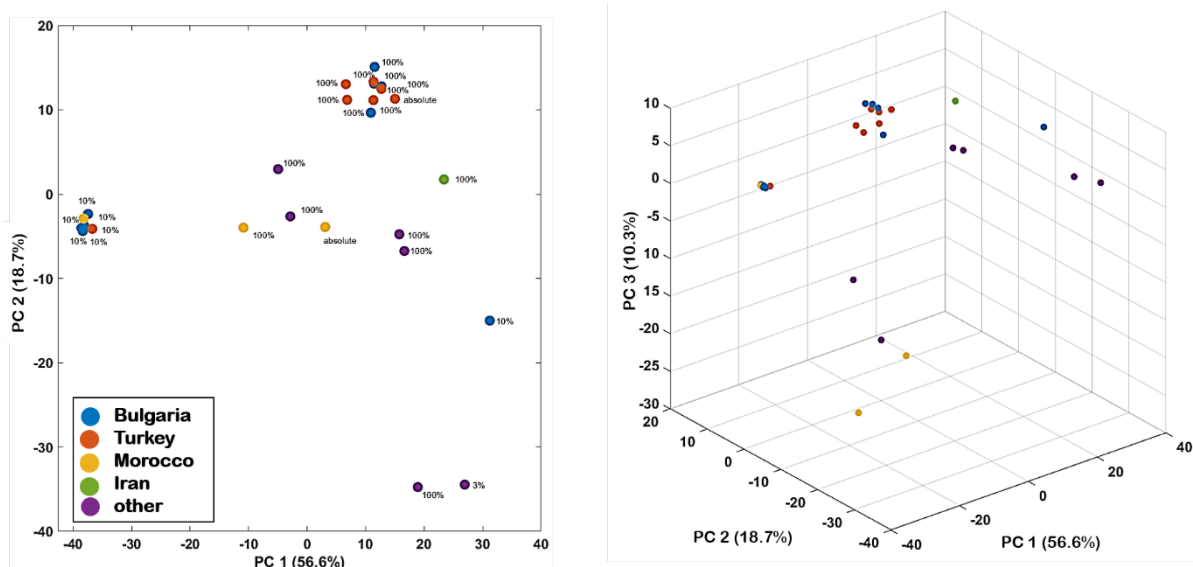


Figure 68: PCA plots for FT-IR data after normalisation by the maximum value, scatter correction using SNV, Savitzky-Golay smoothing at the 3rd order and a frame window of 11 and mean-scaling.

SNV correction and auto-scaling were selected as the final pre-processing method, as it achieved the best separation for both concentration difference and origin in *R. damascena* EO samples. This can be studied in detail in Figure 69. All applied pre-processing combinations can be studied in Table A25 in the Appendix.

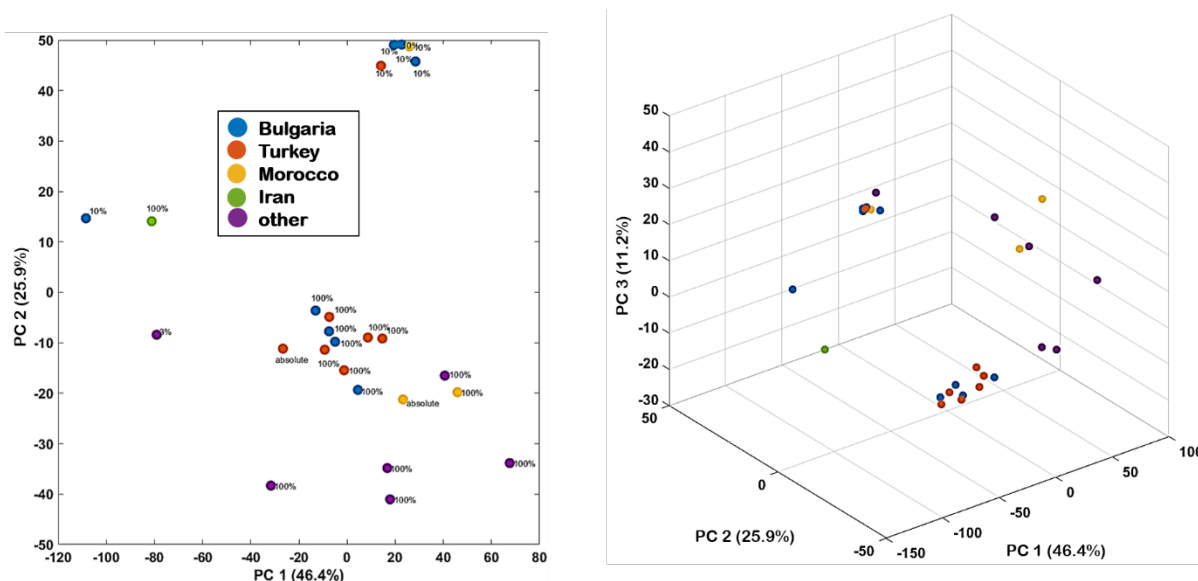


Figure 69: PCA plots for FT-IR data after SNV and auto-scaling.

Pre-processing methods and their effect on DBDI-MS data were also evaluated. Optimal conditions were found after applying sum normalisation, mean-centering, and Savitzky-Golay smoothing (3rd order polynomial, window size 15). Figure 70 illustrates the evolution of the pre-processing methods for data acquired by DBDI-MS in Q3 mode.

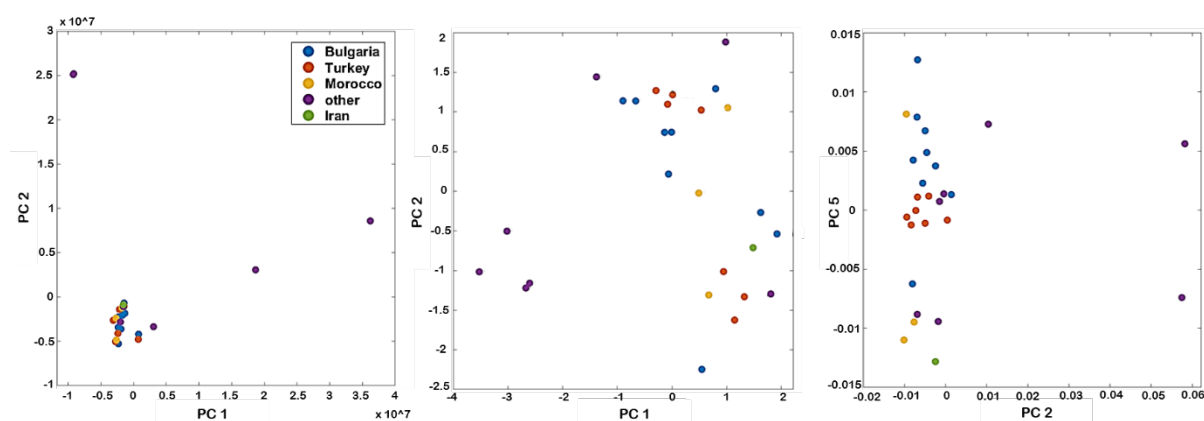


Figure 70: PCA of DBDI-MS Q3 data. From left to right: data without any pre-processing, data after normalisation by the maximum value and data after normalisation by sum, mean-centering and Savitzky-Golay smoothing (3rd order polynomial, window size 15).

Figure 70 reveals scaling issues in the raw data, with no apparent spatial separation for EOs from different origins. Applying a combination of three different pre-processing methods resulted in a separation of origin and resolved the scaling problems. However, this separation was only visible when studying the 2nd and 5th PC. The

loading plot (Figure 71) can be compared in order to see which variables contribute the most to each PC.

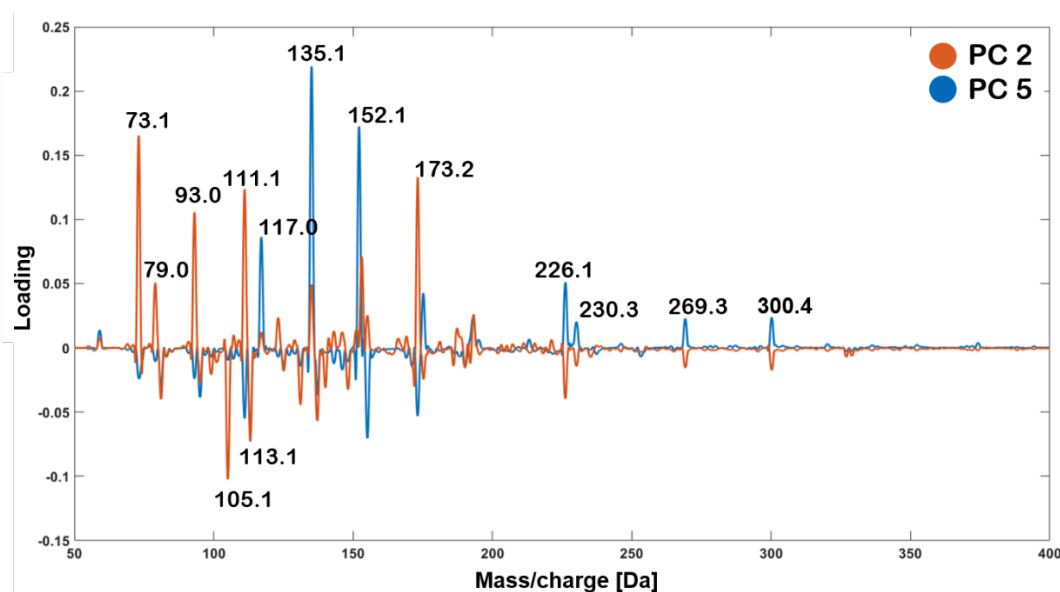


Figure 71: Loading plot comparing PC2 and PC5 of the pre-processed data for DBDI-MS Q3.

From the loading plot, it is apparent that only a few masses contribute to the formation of the PCs. The classification of the individual adducts and fragments is not straightforward, and rearrangement reactions may also play a role. For example, the ion at 135.1 Da may correspond to the $[M-H]^+$ adduct for non-oxygenated monoterpenes. Overall, however, the reduction of the data to its PCs can provide a clearer picture of which variables are unique and can improve the differentiation of samples. After optimising the pre-processing operations, PCA was performed on *R. damascena* EOs analysed by GC-FID equipped with a DB-wax column, chiral column, DBDI-MS Q1, DBDI-MS Q3, and FT-IR. Figure 72 shows the PCA of all EOs and the biplots of *R. damascena* EOs derived from Bulgaria, Turkey and Morocco. In Figure 72 **A**, a group separation is observed for the samples derived from Bulgaria, with limonene, geraniol, citral, β -caryophyllene and nerol being the main drivers of this separation.

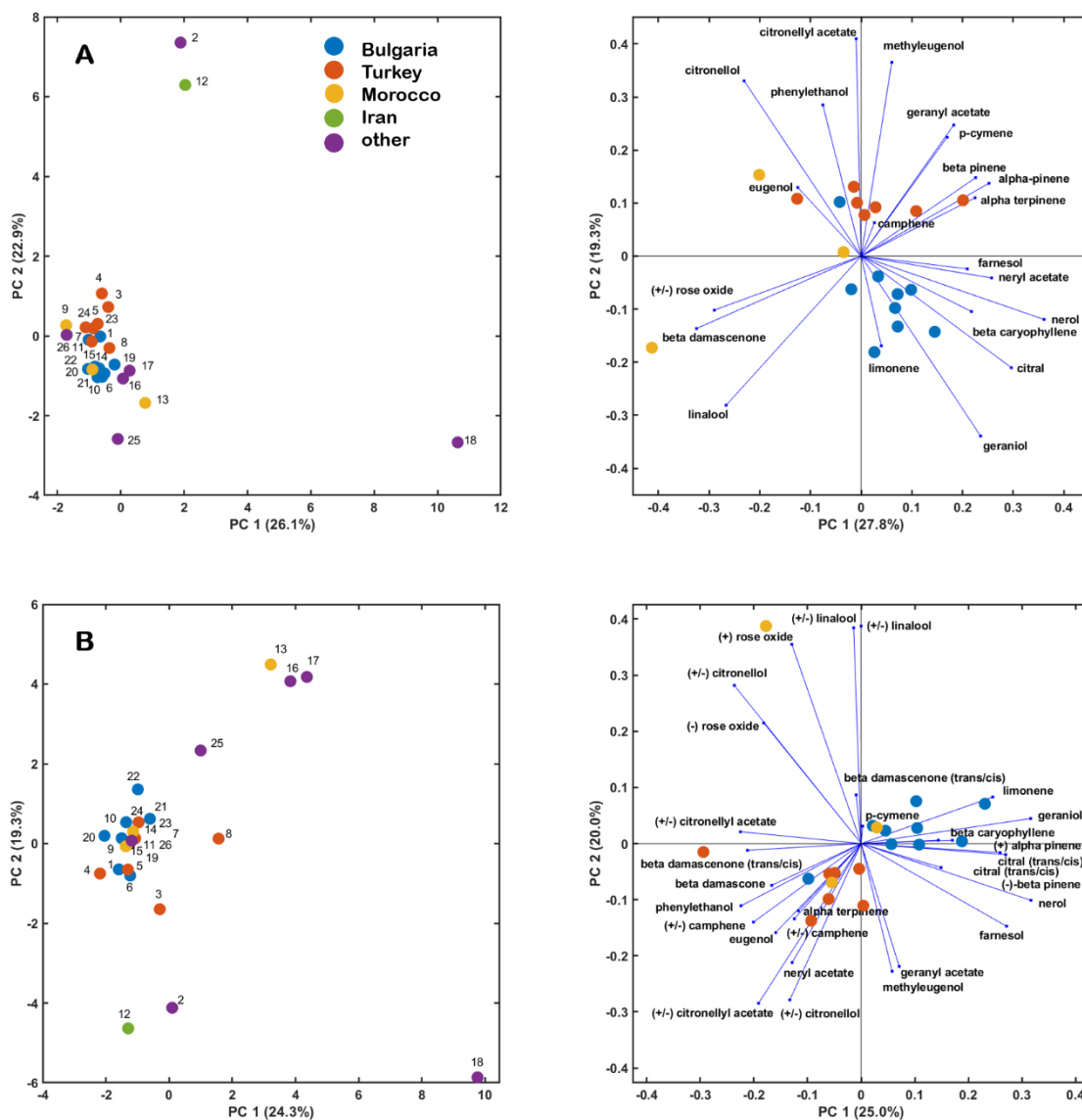


Figure 72: Figure **A** shows samples analysed by GC-FID using a DB-wax column. The left figure shows all analysed EO samples, including samples from Iran (green) and other origins (purple), the right figure only includes samples originating from Bulgaria (blue), Turkey (red) and Morocco (yellow). Figure **B** shows samples analysed by GC-FID using a chiral column. Figure adapted from Raeber et al.²¹

R. damascena EO samples from Turkey are characterised by α -pinene, β -pinene, α -terpinene, p-cymene, geranyl acetate, methyleugenol, citronellyl acetate, phenylethanol, and citronellol. Although Moroccan samples did not cluster closely, they also displayed separation based on linalool, β -damascenone, and rose oxide content, suggesting a different aroma profile. Figure 72 **B** also incorporated chiral information, but it did not enhance group separation. Similar patterns to the analysis on the DB-wax column were observed. PCA of DBDI-MS and FT-IR data did not exhibit the same distinct separation of samples, as presented in Figure 73. Incorporation of

fragmentation data to the analysis resulted in a clearer separation of EOs that were not derived from *R. damascena* (**D**). However, no separation based on origin was observed (**C**, **D**). FT-IR performed well in distinguishing oils from other species and could discriminate between different concentrations of the EO, making it semi-quantitative (**E**). This semi-quantitative approach is likely limited to the concentration of the diluent, such as alcohol or jojoba oil, as terpenes are present at low concentrations and FT-IR is not sensitive enough to detect these minor subtleties. PCA based on DBDI-MS and FT-IR data yields different results as for GC-FID data. FT-IR and DBDI-MS produce high dimensional data with 3401 and 3500 variables, respectively. However, many of these data points are highly correlated and redundant. Methods such as binning can merge data points belonging to the same mass peak or vibration band, reducing the number of variables. However, there is a risk of loss of information as the resolution of overlapping peaks may be reduced or merged to a single peak. In an attempt to improve the group separation by FT-IR, only the fingerprint region (600 - 1500 cm^{-1}) was further analysed. This spectral range contained most of the variability between the individual samples, but did not improve the group separation in PCA. The variables derived from the major components in the EO overpower any contribution from the minor terpenes. Similar difficulties can be observed with the DBDI-MS data. Terpenes have similar, if not identical, masses and isomeric structures. As a result, identical parent and fragment ions can occur, making up the majority of the observed peaks in the MS spectrum. These ions dominate in PCA and obscure the effect of ions present at lower intensities. The complete quantitative profile of *R. damascena* EOs from Bulgaria, Turkey, and Morocco can be studied in Figure 74. Only analytes, that appeared significant in the PCA plots in Figure 72 **A**, are presented. Concentration profiles for the other terpenes is made available in Figure A87 in the Appendix.

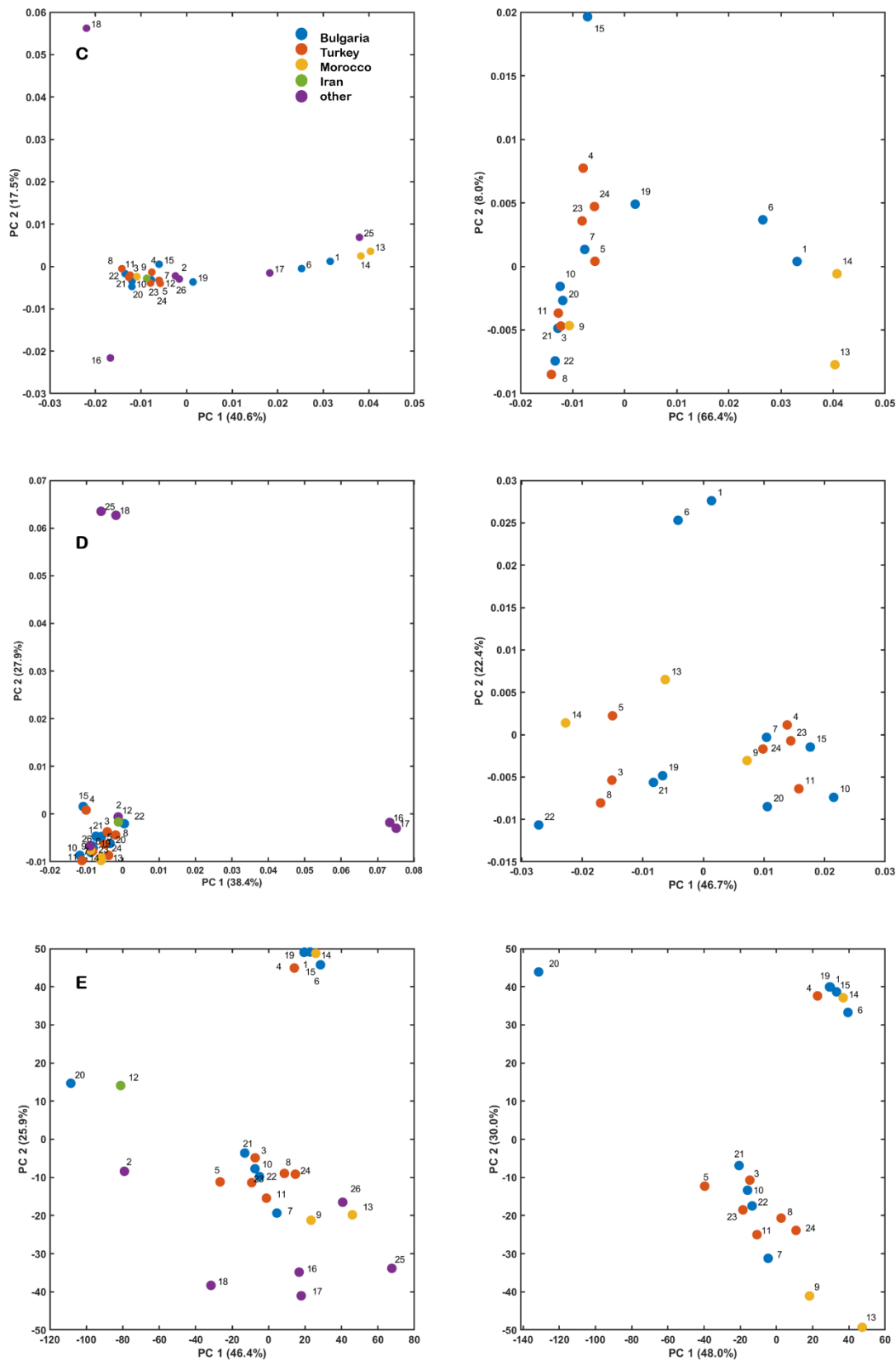


Figure 73: From top to bottom data acquired with DBDI-MS in Q1 mode (C), DBDI-MS in Q3 mode (D) and FT-IR (E). From left to right PCA plots including all studied oils and plots only including oils derived from Turkey (red), Bulgaria (blue), and Morocco (yellow). Figure taken from Ræber et al. ²¹

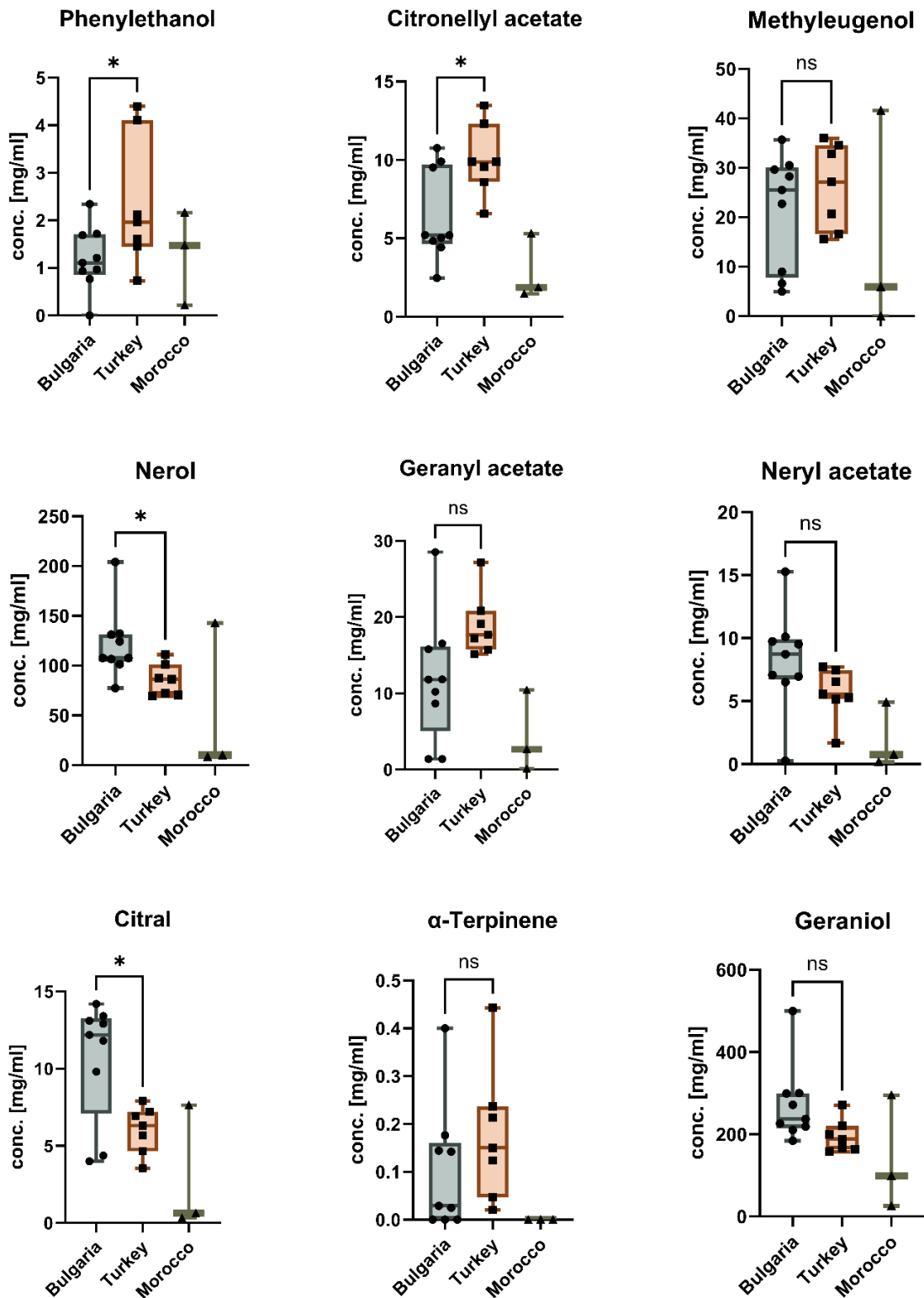


Figure 74: Quantification of selected *R. damascena* EO components by GC-FID equipped with a DB-wax column. Concentrations for different origins (Bulgaria, Turkey and Morocco) are presented as box and whisker plots. The bars show the maximum and minimum values. An unpaired t-test was performed between Bulgarian and Turkish samples. Significance levels were set at ns for $P > 0.05$, * for $P \leq 0.05$, ** for $P \leq 0.01$, *** for $P \leq 0.001$ and **** for $P \leq 0.0001$. Figure was adapted from Raeber et al.²¹

Comparing the terpene profiles for *R. damascena* EO, it appears that phenylethanol, citronellyl acetate, geranyl acetate, and α -terpinene concentrations are elevated in EOs derived from Turkey. On the other hand, oils derived from Bulgaria appear to be rich in nerol, neryl acetate, citral, and geraniol. However, when the components present in the Bulgarian and Turkish oil samples are directly compared by an unpaired t-test, the results do not appear to be significant for most of the components. As group separation was observed in the PCA, the study of individual components is not sufficient to determine the origin of an EO, as the whole terpene pattern seems to be relevant. Due to the small number of samples for Moroccan oils, it is not possible to make clear statements as for the other origins. However, α -terpinene was not detected in any Moroccan oil samples. Enantiomeric profiles in the form of the EE were also investigated and can be studied in Figure 75. *R. damascena* exclusively produces cis-(-)-rose oxide and was detected in all samples except one from Morocco, which was also previously suspected to be an outlier. A comparison of the samples from all three countries with an ordinary one-way ANOVA showed significance only for (+/-)-linalool and (cis/trans)-citral. An unpaired t-test comparing the EE of oils originating from Bulgaria and Turkey resulted in no significant difference.

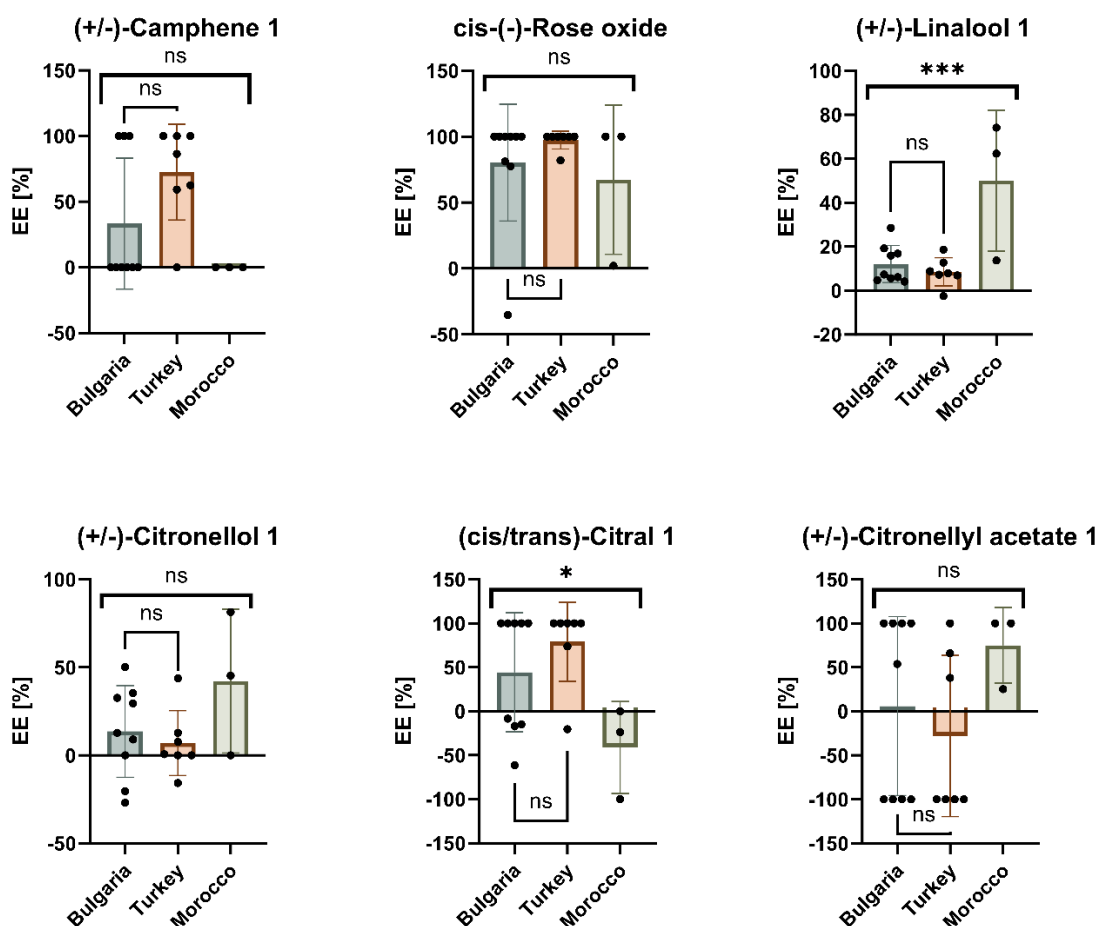


Figure 75: Comparison of the EE in [%] of *R. damascena* EO originating from Bulgaria (n=9), Turkey (n=7) and Morocco (n=3) as a bar plot including the standard deviation. Ordinary one-way ANOVA was performed to identify any significant differences between oils deriving from these three countries, and an unpaired t-test was performed between EOs from Bulgaria and Turkey. Significance was set as follows: ns for $P > 0.05$, * for $P \leq 0.05$, ** for $P \leq 0.01$, *** for $P \leq 0.001$ and **** for $P \leq 0.0001$.

The comparison of the enantiomers does not provide any further insights into the origin of the EOs. However, it reinforces the suspicion that one of the Moroccan oils was adulterated. According to the ISO norm 9842:2003, which distinguishes *R. damascena* EO from different countries, both Bulgarian and Turkish oils match the profile and are compliant.¹⁵⁵

As unsupervised data exploration did not provide sufficient EO classification and there appears to be no single biomarker to classify an EO based on its origin, a PLS-DA prediction model was trained and tested for the above EOs. PLS-DA is a supervised classification method that combines dimensionality reduction with discriminant analysis. PLS-DA constructs latent variables (LV) that attempt to maximise the

covariance between predictor variables (X), such as wavelengths [cm⁻¹] or masses [Da], and a response variable (y), such as an EO originating from Bulgaria, Turkey or Morocco. Because PLS-DA optimises the construction of these LVs and is able to generate decision boundaries in large multivariate datasets, it is prone to overfitting, making cross-validation (CV) essential.^{222, 223} In this study, a double CV procedure was performed due to the small number of samples available. Model selection was performed by 5-fold CV, and accuracy and precision were determined using the leave-one-out CV (LOOCV) procedure, using n-1 samples for training. The number of LVs for each model was selected by optimising for accuracy and precision. Test results for the constructed models using GC-FID, DBDI-MS, and FT-IR data are presented in Table 17. Individual validation results for each class can be viewed in the Table A26 in the Appendix.

Table 17: Test results for optimise PLS-DA models based on five different acquisition methods. Validation results for accuracy, precision, sensitivity and specificity are given in [%]. Root mean square error (RMSE) for Bulgaria (1), Turkey (2) and Morocco (3) is given per country. Table adapted from Raeber et al.²¹

Type of acquisition	# LV	Accuracy [%]	Precision [%]	Sensitivity [%]	Specificity [%]	RMSE		
						1	2	3
Q1	8	63.2	63.9	73.0	75.4	0.44 ± 0.08	0.38 ± 0.05	0.18 ± 0.04
Q3	8	84.2	83.3	88.9	93.6	0.46 ± 0.05	0.36 ± 0.04	0.20 ± 0.02
FT-IR	7	68.4	67.5	68.3	82.3	0.48 ± 0.07	0.36 ± 0.07	0.25 ± 0.03
Wax	2	94.7	95.8	96.3	90.2	0.54 ± 0.02	0.43 ± 0.01	0.27 ± 0.02
Chiral	2	89.5	92.6	85.2	86.6	0.55 ± 0.02	0.47 ± 0.01	0.27 ± 0.02

Results are further presented as confusion matrices in Figure 76. The first two LVs were sufficient as parameters for the classification model based on the GC-FID data using both the DB-wax and the chiral column. Classification accuracy was the highest for the GC-FID data obtained using the polar capillary column.

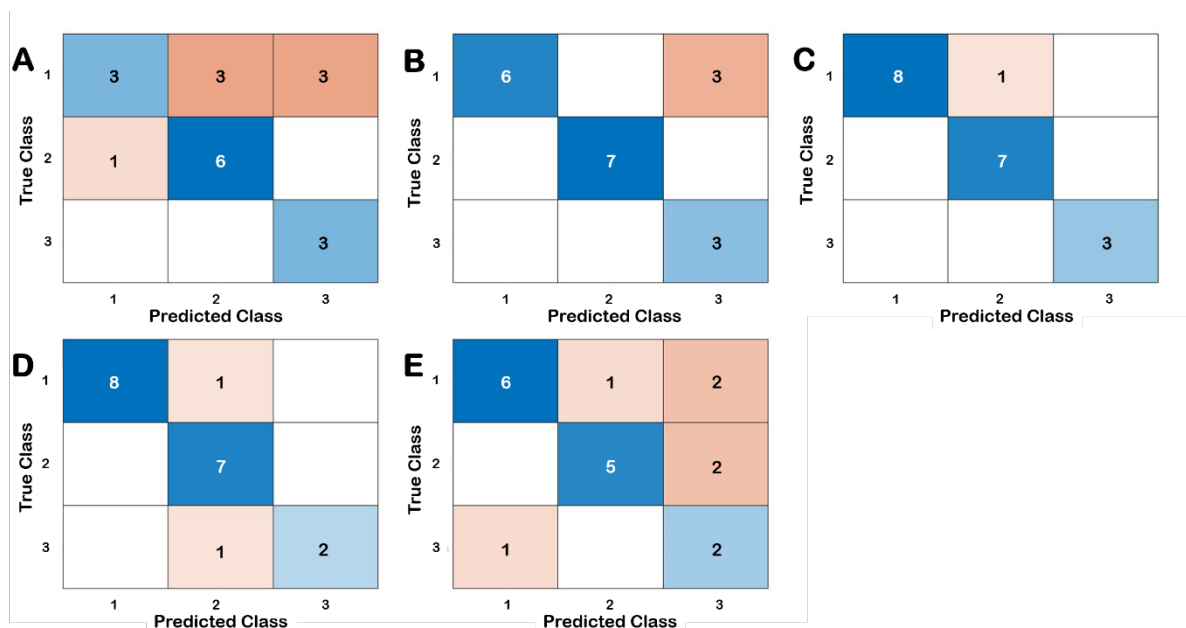


Figure 76: Confusion matrices after model testing for DBDI-MS (Q1) (A), DBDI-MS (Q3) (B), GC-FID on DB-wax column (C), GC-FID on chiral column (D) and FT-IR (E) data. The predicted class labels are plotted against the true class labels and classes correspond to Bulgaria (1), Turkey (2), and Morocco (3). Figure taken from Raeber et al.²¹

The RMSE is not primarily required to determine the goodness of fit of a PLS-DA model, but it does allow comparison between different models. The RMSE was in the same order of magnitude for all models regardless of the data acquisition method. The PLS-DA models for both GC-FID acquisition methods required only the first two LVs for modelling, indicating a simplistic model. The FT-IR and DBDI-MS data models required seven and eight LVs, respectively. A higher number of LVs captures more data variability, which is necessary for improved classification accuracy. Notably, the model based on DBDI-MS (Q3) data achieved an accuracy of 84.2% and a slightly higher specificity compared to the best performing model based on GC-FID data using the DB-wax column. This finding is significant as DBDI-MS (Q3) data acquisition is performed in a fraction of the time compared to GC-FID. It is noteworthy that the PLS-DA model based on GC-FID including chiral information showed a slightly reduced classification accuracy compared to the model based on the DB-wax column. The ratio of enantiomers and diastereomers investigated in this study may be species specific and no significant variation is to be expected. One of the Moroccan samples was considered a potential outlier and may have been mislabelled or adulterated, explaining the misclassification. Both the FT-IR and DBDI-MS (Q1) classification models were able to correctly classify over 60% of all samples, but were far behind

the other methods in terms of accuracy. Considering the time factor, these results are not insignificant. They are sufficient for a rapid screening, but leave plenty of room for misclassification. Since both FT-IR and DBDI-MS benefit from fast data acquisition, the idea of using data fusion approaches to improve classification accuracy is obvious. Combining different datasets from different instruments is only worthwhile if time can be saved. GC-FID is a powerful analytical method for looking at EOs in detail, but method development, calibration, and data analysis are time-consuming and costly. Data fusion is an interesting but not simple approach to improve the classification of e.g. FT-IR data based models. A challenge arises because such datasets are not only multivariate but also multimodal. Fused datasets and the chemometric tools used to analyse them are hereafter referred to as multi-block techniques. PLS-DA is considered a single-block technique because it is an excellent technique for extracting information generated by a single analytical technique, but is unable to identify complementary information generated by two combined datasets.^{142, 224} Considerable effort has been invested in recent years to address this challenge, resulting in the development and application of a large number of new chemometric algorithms.^{142, 148-150, 225} SO-PLS-LDA is an algorithm designed to handle multimodal data and includes a mid-level fusion approach by extracting variables of interest using the SO-PLS approach. It is also invariant to block scaling. Block scaling can be relevant because data derived from different analytical techniques may have different data matrix sizes. In this case, both data blocks were considered balanced with a data matrix of 19 x 3501 and 19 x 3401 for DBDI-MS and FT-IR data, respectively.¹³⁷ As the algorithm sequentially orthogonalises one data block to the other, the order of the blocks can impact model results. This effect was taken into account and investigated. During model development, various pre-treatments, block orders and data types were considered and the results for model performance are summarised in Table 18.

Table 18: Results for the performance of different SO-PLS-LDA models. Latent vectors (LV) were selected separately for each data block. The RMSE was determined individually for the countries Bulgaria (1), Turkey (2), and Morocco (3). Table taken from Raeber et al.²¹

Order (1 st + 2 nd)	# LV	Pre- treatment	Accuracy [%]	Precision [%]	Sensitivity [%]	Specificity [%]	RMSE		
							1	2	3
Q1 + FT-IR	0/3	mean/none	68.4	77.1	69.3	69.0	0.43 ± 0.02	0.38 ± 0.02	0.21 ± 0.03
Q3 + FT-IR	5/5	mean/none	84.2	90.0	81.5	82.6	0.09 ± 0.01	0.08 ± 0.01	0.09 ± 0.02
FT-IR + Q1	6/2	none/mean	73.7	82.2	70.9	72.9	0.13 ± 0.02	0.12 ± 0.01	0.11 ± 0.02
FT-IR + Q3	0/4	none/mean	78.9	87.9	70.4	80.0	0.21 ± 0.02	0.25 ± 0.02	0.21 ± 0.02
Q1 + Q3	0/4	mean/mean	78.9	87.9	70.4	80.0	0.21 ± 0.02	0.25 ± 0.02	0.21 ± 0.02
Q3 + Q1	6/4	mean/mean	84.2	88.9	74.1	83.2	0.11 ± 0.01	0.09 ± 0.01	0.04 ± 0.01

Using the SO-PLS-LDA algorithm, six different models were constructed and their performance evaluated. The number of LVs for model construction was determined by optimising the model performance. Whenever DBDI-MS (Q3) data was selected as the second block, the LVs from the first block were cancelled out and not necessary for model construction. It can be concluded that these data blocks did not contain any relevant variability and that DBDI-MS (Q3) as a data block was the main driver for model construction and performance. The best classification accuracy was observed for the model combining DBDI-MS (Q3) data with FT-IR data, although the results did not surpass the classification accuracy of the PLS-DA model based on DBDI-MS (Q3) data, but showed improved precision. The SO-PLS-LDA models did generally not outperform the PLS-DA models, with the exception of the model integrating both FT-IR and DBDI-MS (Q1) data. Classification accuracy is improved by 5.3% for the FT-IR and 10.5% for the DBDI-MS (Q1) PLS-DA model. The high classification accuracy for the PLS-DA models could also be due to the fact that PLS-DA is particularly susceptible to overfitting, especially when the sample size is small. LDA as a classifier must also be viewed critically: it uses a binary classification approach, assigning a sample to either a 0 or a 1. PLS-DA, on the other hand, uses a dummy matrix and can produce a fuzzy classification.^{137, 226} There are many approaches to avoid overfitting. A larger sample population, CV, selecting only a few LVs and creating confusion matrices can reduce overfitting.²²⁶ Very often, however, a larger sample population is not feasible. For example, the Swiss market for *R. damascena* EO is rather small and the number of actual distributors is even lower. DBDI-MS is proving to be an interesting approach for quality control of EOs, especially when the resulting data is combined with machine learning algorithms. However, it is not only the

algorithm that is crucial, but also the procedure and workflow by which the data is pre-processed for analysis. Validation of these classification models is primarily time-consuming, but so is method development and validation for GC-FID, for example. However, once an algorithm has been developed to discriminate between different oils, it can be used over and over again to classify new samples. Multi-block algorithms are an interesting development that allow the use of fast but less powerful methods such as FT-IR. On their own, these methods struggle to detect subtle differences in samples. However, when combined with other data sets, they can make a significant contribution to classification tasks. The overall objective of this study was based on the classification of an oil according to its origin. Other classification tasks such as concentration, ageing, or chemotype are also possible, demonstrating the flexibility and broad applicability of the study presented here. It is conceivable that the FT-IR datasets for determining the concentration could have performed significantly better in a classification model. Multi-block analysis opens up new dimensions by extracting new information from additional datasets. Ultimately, the choice of analytical methods and datasets depends on the overall objective and question.

4.2.1. Materials and methods

4.2.1.1. Authentic samples

A total of 26 authentic EOs of different origins and partly of other species (*Pelargonium graveolens*, *Rosa centifolia*) were purchased in Swiss pharmacies. A detailed list of all samples and their corresponding numbering can be found in Table A26 in the Appendix. Of the *R. damascena* samples, nine originated from Bulgaria, seven from Turkey and three from Morocco.

4.2.1.2. FT-IR analysis and data acquisition

FT-IR spectra were collected using a PerkinElmer Spectrum 100 FT-IR spectrometer (PerkinElmer, Waltham MA, USA) equipped with a triglycine sulphate detector and an universal attenuated total reflectance (UATR) accessory. The spectra were acquired over the range of 600 - 4000 cm^{-1} at a scan rate of 0.2 cm/s with a resolution of 4 cm^{-1} . Each measurement consisted of four scans each. Prior to analysis, the

background was recorded by exposing the crystal to air. For each measurement, 20 µl of EO was placed on top of the diamond crystal, and the UATR was set to a pressure force of 100. Data acquisition was performed at room temperature. Data processing and baseline correction were performed using Spectrum software (PerkinElmer, Version 10.5.0). After each measurement, the UATR was cleaned with ethanol and air dried. The acquired spectra can be viewed in Figure A88 in the Appendix.

4.2.1.3. DBDI-MS analysis and data acquisition

DBDI-MS spectra were collected using a TripleQuad 3500 MS (AB Sciex, Redwood City, CA, USA) coupled to a DBDI source (Plasmion GmbH, Augsburg, Germany). Spectra were recorded in both the first (Q1) and third quadrupoles (Q3). For Q1 acquisition, the scan range was set from 50 - 400 Da, with a scan rate of 200 Da/s, a DP of 140 V, and an EP of 10 V. Q3 settings were similar to Q1 but also included a CXP of 25 V. The DBDI source was set to an amplitude of 1500 V and a frequency of 15,000 Hz. A GC-liner (Topaz, straight liner, 4 mm x 6.3 mm x 78.5 mm, Restek, Bellefonte, PA, USA) was attached to the top of the DBDI source. Prior to data acquisition, 20 µl of an EO was added to a headspace vial and incubated for 10 min at room temperature. During data acquisition, the GC-liner was inserted two-thirds into the headspace vial, allowing volatile components of the EOs to be drawn into the DBDI source by the MS vacuum. Samples were analysed randomly and a blank, consisting of an air-filled headspace vial, was measured after every seven measurements. The total data acquisition time was four minutes and the headspace vials were cleaned with ethanol and air dried after each measurement. Data acquisition was performed using Analyst® software (AB Sciex, Version: 1.7.2.) and processed using Sciex OS (AB Sciex, Version: 2.0.0.455330). Data was pre-processed by averaging MS spectra from 1.5 to 2.5 minutes and exporting them as txt files for further analysis. The acquired spectra can be seen in Figures A89-90 in the Appendix.

4.2.1.4. GC-FID analysis and data acquisition

Prior to analysis, EO samples were diluted 1:10 and 1:500 with n-heptane (99.9%, Carl Roth GmbH, Karlsruhe, Germany). Samples contained a final concentration of 10 mM cis-hexen-1-ol (98.0%, Sigma Aldrich, St. Louis, MO, USA), which served as an IS. Each sample was acquired in triplicates using a Thermo Scientific Trace 1600 GC-FID (Thermo Scientific, Waltham, Massachusetts, USA) equipped with either a DB-wax capillary column (30 m x 0.25 mm x 0.25 μ m, Agilent J&W, Santa Clara, CA, USA) or a chiral BGB 178 30% CD capillary column (25 m x 0.25 mm x 0.25 μ m, BGB Analytik AG, Boeckten, Switzerland). Helium 6.0 functioned as a carrier gas and hydrogen 5.0 was used for the FID flame (PanGas, Dagmersellen, Switzerland). The temperature gradient and GC-FID settings are presented in Chapter 1, *Section 2.1.2.1*, and were further published under Raeber et al.¹⁰ A total of 21 analytes were quantified on the DB-wax and 29 analytes on the chiral column. Quality control samples covering the high, medium and low concentration range were also recorded during data acquisition. Data was acquired and processed using Chromeleon software (Thermo Scientific, Version 7.3.1.). The acquired spectra can be viewed in the Figures A91-92 in the Appendix.

4.2.1.5. Data pre-processing and computational analysis

Data pre-processing and chemometric studies were performed using MATLAB (Release R2022b, Version: 9.13.0; The Mathworks Inc.). The code used required the “Statistics and Machine Learning Toolbox” (Version: 12.3) and the “Signal Processing Toolbox” (Version: 9.1). Code for pre-processing such as mean-centering, normalisation, auto-scaling, SNV and PCA can be found in Script A11 in the Appendix. The code for the PLS-DA and SO-PLS-DA analysis is publicly available at Rome Chemometrics at <https://www.chem.uniroma1.it/romechemometrics/research/algorithms/>.^{227, 228} All files contained in the ZIP file must be opened using the MATLAB API. The pre-processing was evaluated individually for each data type and set to normalisation by sum, mean-centering, and Savitzky-Golay smoothing using a 3rd order polynomial and a window size of 15 for DBDI-MS data, SNV and auto-scaling for FT-IR data. The PLS-DA analysis was carried out using the SIMPLS

algorithm.^{229, 230} Model parameters were optimise through 5-fold CV and the models were tested by LOOCV, due to small sample size.²³¹ Model performance was evaluated based on accuracy, precision, sensitivity, and specificity based on the publication by Sokolova et al.²³² In addition, the RMSE was determined for each model. Further data exploration was conducted using GraphPad Prism (Version 9.4.1.).

5. Conclusion and Outlook

In this thesis, we explored multiple analytical techniques for the separation, detection, and computational analysis of secondary metabolites in plants, with particular emphasis on terpenes. The overall aim was to achieve a holistic characterisation of natural products to assess their authenticity, origin, ageing, cultivar, and chemovar. Hypothesis 1 addressed chromatographic separation science to identify major, minor, and chiral components in two model plants, *R. damascena* and *C. sativa* L. Both LC and GC were explored as separation techniques. Although LC has traditionally been considered unsuitable for analysing volatile compounds such as terpenes, we demonstrate that LC can effectively analyse the major terpenes present in *C. sativa* L. In addition, LC offers the advantage of simultaneously quantifying cannabinoids and their acids without prior derivatisation reactions. This simplifies the analysis of *C. sativa* L. based products by covering a wide range of secondary metabolites in a single chromatographic run. In addition to determining CBD and THC ratios, the methodology also allows for extended chemotype classifications by including the analysis of terpene and minor cannabinoid patterns. While the entourage effect remains a topic of debate, well-characterised *C. sativa* L. products facilitate improved clinical trial designs, allowing specific strains to be linked to pharmacological effects. Additionally, four GC-based methods using chiral, polar, and apolar separation were developed and validated. Natural products such as EOs are often targets of adulteration, which can include blending with other EOs or adding natural or synthetic components. These adulterations can alter the enantiomeric ratios in the product, as plants produce enantiomers in species-specific ratios. Furthermore, the effects of heat and UV exposure on terpene isomerisation were explored, as these transformation reactions have been previously described in the literature and have also been reported to change the enantiomeric patterns in natural products. Rearrangement reactions from one enantiomer to the other were not observed. However, isomerisation, polymerisation, oxidation, dehydrogenation, and cyclisation reactions are common and can significantly alter the terpene profile. We discovered an excess of (-)-cis rose oxide, (-)-linalool and (-)-citronellol in *R. damascena*. In *C. sativa* L., there was an excess of (+)- α -pinene, (+)- β -pinene, (S)-limonene, (+)-linalool, (-)-citronellol,

(-)-camphene, (+)-trans-nerolidol, and (-)-cis-menthone. However, in some samples, we found an excess of (-)- α -pinene and (-)- β -pinene without any citronellol present. We suspect that growth conditions (indoor vs. outdoor) and the use of plant protective agents can influence enantiomer production. This observation requires further investigation by comparing enantiomeric ratios of the same cultivar grown under different conditions. Given that enzymes are enantio-specific, this finding could offer a further explanation for the contradictory results of the entourage effect. Limitations of the study include the focus solely on the CBD-high chemotype of *C. sativa* L. The enantiomer ratios in high THC and balanced THC:CBD chemotypes remain subjects of ongoing investigation.

Hypothesis 2 addressed MS as a detection method for terpenes, as it provides structural information and stands out for its speed. Terpenes share a common biosynthetic pathway, consist of identical repeating units and are the largest class of secondary metabolites in plants. Within the class, numerous isomeric structures exist, leading to identical MS spectra when analysed by EI. This similarity can complicate the annotation of analytes, particularly when relying merely on comparison with spectral libraries. APCI and DBDI are soft ionisation methods that provide an alternative to state-of-the-art EI. We demonstrate that APCI effectively ionises terpenes. DBDI, a novel ionisation method, can be coupled to both GC and LC. In this thesis, we explore the application of DBDI hyphenated to GC or as a stand-alone technique. Unlike techniques such as APCI or ESI, which typically produce $[M+H]^+$ adducts in the positive mode, ionisation events in DBDI are not straightforward. Moreover, the ionisation environment in the source can be customised by using different discharge gases like N_2 or by adding dopants. We observed different adduct patterns depending on the terpene class. Oxygenated terpenes formed adducts such as $[M]^+$, $[M+H]^+$, $[M+2H]^+$, and $[M+NH_4]^+$, while non-oxygenated terpenes formed adducts like $[M-H+2O]^+$, $[M+H+3O]^+$, $[M+H+2O]^+$, and $[M+H_2O_2]^+$. In a few cases, we observed an unusual exchange of a carbon atom for a nitrogen atom under N_2 enrichment. Fragmentation and isomerisation were also observed in the source. The individual DBDI-Q1-MS spectra for terpenes were identical for enantiomers, but other isomers such as diastereomers yielded significantly different spectra. For instance, while the EI-MS spectra of α - and β -pinene are nearly identical, DBDI-MS spectra exhibit notable differences and can distinguish between the double bond isomer pair.

This observation was consistent across numerous terpenes and suggests potential improvements in peak annotation. Not all MS peaks were annotated, and further investigation is needed for some reactions occurring in the DBDI source. We suggest a comprehensive study of fragmentation events using HRMS. Additionally, using deuterated terpenes could aid in assigning individual fragments. As slight changes in the ionisation environment can lead to significantly different spectra, a thorough understanding and control of this environment is essential. This can be achieved by using high purity gases and consistent heating in the bubbler. Although room air provides the highest ionisation efficiency, it is sensitive to fluctuations, rendering the ionisation patterns unpredictable. Using the DBDI source independently of chromatography allows for the recording of unique spectra of natural products, effectively serving as a fingerprint. Moreover, these spectra can enhance terpene structure elucidation by distinguishing between isomers, thereby improving natural product screening.

Lastly, hypothesis 3 postulated that the integration of chemometrics with data fusion from multiple analytical techniques could improve the classification performance of predictive machine learning models. Several models were trained to classify the originality of *R. damascena* EOs. These models were either based on data generated by a single analytical technique or combined datasets from multiple platforms. While single-block methods based on targeted EO quantification data outperformed all other models in terms of accuracy, they were time-consuming in terms of data acquisition. DBDI-MS single-block models showed high accuracy, did not require complex sample preparation and data acquisition took only a few minutes. Adding DBDI-MS data to a fusion model did not improve prediction. By optimising the number of LVs used in the model, we observed a tendency to rely only on the LVs from the DBDI-MS data, rather than those from other datasets. This underlines the importance and uniqueness of the DBDI-MS data compared to, for example, FT-IR data. FT-IR did not provide enough novel information to improve model performance. The study was limited to a specific question (originality) and species (*R. damascena*), further studies with other natural products and species are possible. An improvement in model performance was observed when Q1 DBDI-MS data was combined with FT-IR data as the training set compared to the respective single-block methods. Multi-block analyses have primarily been developed for spectroscopic investigations, such as FT-IR and NIR, which offer

similar information content. Multi-block methods are capable of extracting redundant information, thereby enhancing prediction accuracy. However, it is improbable that FT-IR would yield additional insights compared to, for instance, Q3 DBDI-MS, making the single block method satisfactory. Since interpreting the MS spectra generated by DBDI is challenging, chemometrics is well suited for uncovering hidden information. Multi-block analysis is an interesting approach, especially when the same samples can be measured rapidly using different methods. In addition, data fusion can enhance the information content. Other potential models could include data on density or boiling point. Raman spectroscopy and NMR are also conceivable, although the effort involved should be minimal compared to state-of-the-art methods.

Understanding the composition of natural products remains challenging. Secondary metabolites such as terpenes often contain chiral centres, leading to multiple stereochemistries within the same sample. This complexity complicates both separation techniques and the acquisition of MS spectra. Moreover, terpene patterns in plants are influenced by various factors such as growth conditions, ageing, processing methods, environmental factors, heating, and cultivar type, rendering them dynamic and subject to change over time. This thesis aims to provide new insights into addressing these challenges and enhancing the comprehensive analysis of terpenes. It also investigates whether current methods can be simplified to allow a high-throughput approach. While the primary focus of this thesis has been on terpenes, other secondary metabolites such as flavonoids and lignins could also benefit from similar analytical approaches. Moreover, these methods hold potential for drug discovery by enabling rapid classification and chemical profiling of natural products.

6. Acknowledgments

There are numerous people to whom I owe gratitude for their support over the past few years. This thesis and the experience would not have been the same without them. Firstly, I would like to thank my committee and examiners Prof. Dr. Gisbert Schneider, Prof. Dr. Robin Teufel and Dr. Christian Steuer for evaluating my work. In particular, I would like to thank Christian for offering me the opportunity to conduct my thesis under his supervision and for his unwavering support throughout. I will be forever grateful for the wonderful time in and outside the lab that I got to experience with Vanessa Erckes, Alessandro Streuli and Mattis Hilleke. Ski slopes, Superkondi lessons, singing performances and shared lunch breaks will be greatly missed. I extend my gratitude to all the master students with whom I had the pleasure of working with during my PhD, especially, Bryan Bajor, Pia Ostertag, Ana Cuarvic, Annina Bovens, Anina Schmidli, Sina Favrod, and Teresa Denfile. Special thanks are also due to Benj Oberlin, Dani Lüthi, Ina Schmidt, Dr. Jan-Christoph Wolf and Dr. Jan Bucek for the technical support in the lab. I am also thankful to collaborators and colleagues who contributed to the projects presented here, particularly, Dr. Alina Begley, Dr. Julian Harrison, Prof. Dr. Renato Zenobi, Dr. Michael Pöttsch, Jens Settelmeier and Dr. Sebastian Orth. I really appreciated the insightful discussions and easy going collaborations! Lastly, I would like to thank the people outside of my academic environment. Especially to my parents Ingrid and André for always being there and supporting me in whatever I set out to do. Thanks to my brothers Michele, Fabian and Dominic for always lending a helping hand and to our cat Yuka. A special thanks to Matthew Mirman for sticking by me and supporting me in my ventures. Lastly, I extend my heartfelt thanks to my friends for their constant presence and support.

7. References

- (1) Chen, F.; Tholl, D.; Bohlmann, J.; Pichersky, E. The family of terpene synthases in plants: a mid-size family of genes for specialized metabolism that is highly diversified throughout the kingdom. *The Plant Journal* **2011**, *66* (1), 212-229. DOI: <https://doi.org/10.1111/j.1365-313X.2011.04520.x>.
- (2) Cox-Georgian, D.; Ramadoss, N.; Dona, C.; Basu, C. Therapeutic and Medicinal Uses of Terpenes. In *Medicinal Plants: From Farm to Pharmacy*, Joshee, N., Dhekney, S. A., Parajuli, P. Eds.; Springer International Publishing, **2019**; pp 333-359. DOI: 10.1007/978-3-030-31269-5_15.
- (3) Abdel-Azeem, A. M.; Abdel-Azeem, M. A.; Khalil, W. F. Chapter 21 - Endophytic Fungi as a New Source of Antirheumatoid Metabolites. In *Bioactive Food as Dietary Interventions for Arthritis and Related Inflammatory Diseases (Second Edition)*, Watson, R. R., Preedy, V. R. Eds.; Academic Press, **2019**; pp 355-384.
- (4) Sticher, O.; Heilmann, J.; Zündorf, I. *Pharmakognosie phytopharmazie*; Springer, **2015**.
- (5) Hüsni, K.; Başer, C.; Demirci, F. Chemistry of essential oils. In *Flavours and fragrances: chemistry, bioprocessing and sustainability*, Springer, **2007**; pp 43-86.
- (6) Maimone, T. J.; Baran, P. S. Modern synthetic efforts toward biologically active terpenes. *Nature Chemical Biology* **2007**, *3* (7), 396-407. DOI: 10.1038/nchembio.2007.1.
- (7) Zhou, F.; Pichersky, E. More is better: the diversity of terpene metabolism in plants. *Current Opinion in Plant Biology* **2020**, *55*, 1-10. DOI: <https://doi.org/10.1016/j.pbi.2020.01.005>.
- (8) Noriega, P. Terpenes in essential oils: Bioactivity and applications. *Terpenes and Terpenoids—Recent Advances* **2020**.
- (9) Pichersky, E.; Raguso, R. A. Why do plants produce so many terpenoid compounds? *New Phytologist* **2018**, *220* (3), 692-702. DOI: <https://doi.org/10.1111/nph.14178>.
- (10) Raeber, J.; Favrod, S.; Steuer, C. Determination of Major, Minor and Chiral Components as Quality and Authenticity Markers of Rosa damascena Oil by GC-FID. *Plants* **2023**, *12* (3). DOI: 10.3390/plants12030506.
- (11) Shen, B. A new golden age of natural products drug discovery. *Cell* **2015**, *163* (6), 1297-1300. DOI: <http://dx.doi.org/10.1016/j.cell.2015.11.031>.
- (12) Rodrigues, T.; Reker, D.; Schneider, P.; Schneider, G. Counting on natural products for drug design. *Nature Chemistry* **2016**, *8* (6), 531-541. DOI: 10.1038/nchem.2479.
- (13) Dubey, V. S.; Bhalla, R.; Luthra, R. An overview of the non-mevalonate pathway for terpenoid biosynthesis in plants. *Journal of Biosciences* **2003**, *28* (5), 637-646. DOI: 10.1007/BF02703339.
- (14) Ruzicka, L. The isoprene rule and the biogenesis of terpenic compounds. *Experientia* **1953**, *9* (10), 357-367. DOI: <https://doi.org/10.1007/BF02167631>.
- (15) Ninkuu, V.; Zhang, L.; Yan, J.; Fu, Z.; Yang, T.; Zeng, H. Biochemistry of Terpenes and Recent Advances in Plant Protection. *International Journal of Molecular Sciences* **2021**, *22* (11). DOI: 10.3390/ijms22115710.

- (16) De los Santos, Z. A.; Wolf, C. Optical Terpene and Terpenoid Sensing: Chiral Recognition, Determination of Enantiomeric Composition and Total Concentration Analysis with Late Transition Metal Complexes. *Journal of the American Chemical Society* **2020**, *142* (9), 4121-4125. DOI: 10.1021/jacs.9b13910.
- (17) Ruiz del Castillo, M. L.; Blanch, G. P.; Herraiz, M. Natural variability of the enantiomeric composition of bioactive chiral terpenes in *Mentha piperita*. *Journal of Chromatography A* **2004**, *1054* (1), 87-93. DOI: <https://doi.org/10.1016/j.chroma.2004.08.055>.
- (18) Wong, Y. F.; Davies, N. W.; Chin, S.-T.; Larkman, T.; Marriott, P. J. Enantiomeric distribution of selected terpenes for authenticity assessment of Australian *Melaleuca alternifolia* oil. *Industrial Crops and Products* **2015**, *67*, 475-483. DOI: <https://doi.org/10.1016/j.indcrop.2015.01.066>.
- (19) Sadgrove, N. J.; Padilla-González, G. F.; Phumthum, M. Fundamental Chemistry of Essential Oils and Volatile Organic Compounds, Methods of Analysis and Authentication. *Plants* **2022**, *11* (6). DOI: 10.3390/plants11060789.
- (20) Perveen, S.; Al-Taweel, A. *Terpenes and terpenoids*; BoD—Books on Demand, **2018**.
- (21) Raeber, J.; Steuer, C. Exploring new dimensions: Single and multi-block analysis of essential oils using DBDI-MS and FT-IR for enhanced authenticity control. *Analytica Chimica Acta* **2023**, *1277*, 341657. DOI: <https://doi.org/10.1016/j.aca.2023.341657>.
- (22) Allenspach, M.; Valder, C.; Flamm, D.; Grisoni, F.; Steuer, C. Verification of Chromatographic Profile of Primary Essential Oil of *Pinus sylvestris* L. Combined with Chemometric Analysis. *Molecules* **2020**, *25* (13). DOI: 10.3390/molecules25132973.
- (23) Allenspach, M.; Valder, C.; Flamm, D.; Steuer, C. Authenticity control of pine *sylyvestris* essential oil by chiral gas chromatographic analysis of α -pinene. *Scientific Reports* **2021**, *11* (1), 16923. DOI: 10.1038/s41598-021-96356-x.
- (24) André, A.; Leupin, M.; Kneubühl, M.; Pedan, V.; Chetschik, I. Evolution of the Polyphenol and Terpene Content, Antioxidant Activity and Plant Morphology of Eight Different Fiber-Type Cultivars of *Cannabis sativa* L. Cultivated at Three Sowing Densities. *Plants* **2020**, *9* (12). DOI: 10.3390/plants9121740.
- (25) de Carvalho, C. C. C. R.; da Fonseca, M. M. R. Biotransformation of terpenes. *Biotechnology Advances* **2006**, *24* (2), 134-142. DOI: <https://doi.org/10.1016/j.biotechadv.2005.08.004>.
- (26) Allenspach, M.; Steuer, C. α -Pinene: A never-ending story. *Phytochemistry* **2021**, *190*, 112857. DOI: <https://doi.org/10.1016/j.phytochem.2021.112857>.
- (27) Geithe, C.; Krautwurst, D. Chirality Matters – Enantioselective Orthologous Odorant Receptors for Related Terpenoid Structures. In *Importance of Chirality to Flavor Compounds*, ACS Symposium Series, Vol. 1212; American Chemical Society, **2015**; pp 161-181.
- (28) Silva, A. C. R. d.; Lopes, P. M.; Azevedo, M. M. B. d.; Costa, D. C. M.; Alviano, C. S.; Alviano, D. S. Biological Activities of α -Pinene and β -Pinene Enantiomers. *Molecules* **2012**, *17* (6), 6305-6316. DOI: 10.3390/molecules17066305.
- (29) Baser, K. Turkish rose oil. *Perfumer and Flavorist* **1992**, *17*, 45-45.
- (30) Do, T. K. T.; Hadji-Minaglou, F.; Antoniotti, S.; Fernandez, X. Authenticity of essential oils. *TrAC Trends in Analytical Chemistry* **2015**, *66*, 146-157. DOI: <https://doi.org/10.1016/j.trac.2014.10.007>.

- (31) Jalali-Heravi, M.; Parastar, H.; Sereshti, H. Development of a method for analysis of Iranian damask rose oil: Combination of gas chromatography–mass spectrometry with Chemometric techniques. *Analytica Chimica Acta* **2008**, *623* (1), 11-21. DOI: <https://doi.org/10.1016/j.aca.2008.05.078>.
- (32) Boren, K.; Young, D.; Woolley, C.; Smith, B.; Carlson, R. Detecting essential oil adulteration. *Journal of Environmental Analytical Chemistry* **2015**, *2* (1000132), 2380-2391.1000132. DOI: <http://dx.doi.org/10.4172/jreac.1000132>.
- (33) Gafner, S.; Blumenthal, M.; Foster, S.; Cardellina, J. H., II; Khan, I. A.; Upton, R. Botanical Ingredient Forensics: Detection of Attempts to Deceive Commonly Used Analytical Methods for Authenticating Herbal Dietary and Food Ingredients and Supplements. *Journal of Natural Products* **2023**, *86* (2), 460-472. DOI: 10.1021/acs.jnatprod.2c00929.
- (34) Council of Europe. *European Pharmacopeia*; EDQM, **2023**.
- (35) Satyal, P.; Setzer, W. N. Adulteration Analysis in Essential Oils. In *Essential Oil Research: Trends in Biosynthesis, Analytics, Industrial Applications and Biotechnological Production*, Malik, S. Ed.; Springer International Publishing, **2019**; pp 261-273.
- (36) Korir, N. K.; Han, J.; Shangguan, L.; Wang, C.; Kayesh, E.; Zhang, Y.; Fang, J. Plant variety and cultivar identification: advances and prospects. *Critical Reviews in Biotechnology* **2013**, *33* (2), 111-125. DOI: 10.3109/07388551.2012.675314.
- (37) Clarke, R. C.; Merlin, M. D. Cannabis Domestication, Breeding History, Present-day Genetic Diversity, and Future Prospects. *Critical Reviews in Plant Sciences* **2016**, *35* (5-6), 293-327. DOI: 10.1080/07352689.2016.1267498.
- (38) Grof, C. P. L. Cannabis, from plant to pill. *British Journal of Clinical Pharmacology* **2018**, *84* (11), 2463-2467. DOI: 10.1111/bcp.13618.
- (39) Booth, J. K.; Bohlmann, J. Terpenes in Cannabis sativa – From plant genome to humans. *Plant Science* **2019**, *284*, 67-72. DOI: <https://doi.org/10.1016/j.plantsci.2019.03.022>.
- (40) Corps, M. G. *Kannapedia - Library of Cannabis and Genetics*. Medicinal Genomics Corps, **2024**. <https://www.kannapedia.net/strains> (accessed 04.04.2024).
- (41) Hazekamp, A.; Fishedick, J. T. Cannabis - from cultivar to chemovar. *Drug Testing and Analysis* **2012**, *4* (7-8), 660-667. DOI: <https://doi.org/10.1002/dta.407>.
- (42) Hazekamp, A.; Tejkalová, K.; Papadimitriou, S. Cannabis: From Cultivar to Chemovar II—A Metabolomics Approach to Cannabis Classification. *Cannabis and Cannabinoid Research* **2016**, *1* (1), 202-215. DOI: 10.1089/can.2016.0017.
- (43) European Directorate for the Quality of Medicines & HealthCare; (EDQM), Monograph Cannabis flower. In *European Pharmacopeia*, Vol. 11.5; Council of Europe, **2023**.
- (44) Jin, D.; Henry, P.; Shan, J.; Chen, J. Identification of Phenotypic Characteristics in Three Chemotype Categories in the Genus Cannabis. *HortScience* **2021**, *56* (4), 481-490. DOI: 10.21273/HORTSCI15607-20.
- (45) Barcaccia, G.; Palumbo, F.; Scariolo, F.; Vannozzi, A.; Borin, M.; Bona, S. Potentials and Challenges of Genomics for Breeding Cannabis Cultivars. *Frontiers in Plant Science* **2020**, *11*, Review. DOI: 10.3389/fpls.2020.573299.

- (46) Dias, K. J. S. D. O.; Miranda, G. M.; Bessa, J. R.; Araújo, A. C. J. D.; Freitas, P. R.; Almeida, R. S. D.; Paulo, C. L. R.; Neto, J. B. D. A.; Coutinho, H. D. M.; Ribeiro-Filho, J. Terpenes as bacterial efflux pump inhibitors: A systematic review. *Frontiers in Pharmacology* **2022**, *13*, Systematic Review. DOI: 10.3389/fphar.2022.953982.
- (47) Douafer, H.; Andrieu, V.; Phanstiel, O. I. V.; Brunel, J. M. Antibiotic Adjuvants: Make Antibiotics Great Again! *Journal of Medicinal Chemistry* **2019**, *62* (19), 8665-8681. DOI: 10.1021/acs.jmedchem.8b01781.
- (48) Sieniawska, E.; Swatko-Ossor, M.; Sawicki, R.; Skalicka-Woźniak, K.; Ginalska, G. Natural Terpenes Influence the Activity of Antibiotics against Isolated Mycobacterium tuberculosis. *Medical Principles and Practice* **2016**, *26* (2), 108-112. DOI: 10.1159/000454680.
- (49) Ben-Shabat, S.; Fride, E.; Sheskin, T.; Tamiri, T.; Rhee, M.-H.; Vogel, Z.; Bisogno, T.; De Petrocellis, L.; Di Marzo, V.; Mechoulam, R. An entourage effect: inactive endogenous fatty acid glycerol esters enhance 2-arachidonoyl-glycerol cannabinoid activity. *European Journal of Pharmacology* **1998**, *353* (1), 23-31. DOI: [https://doi.org/10.1016/S0014-2999\(98\)00392-6](https://doi.org/10.1016/S0014-2999(98)00392-6).
- (50) Gertsch, J.; Leonti, M.; Raduner, S.; Racz, I.; Chen, J.-Z.; Xie, X.-Q.; Altmann, K.-H.; Karsak, M.; Zimmer, A. Beta-caryophyllene is a dietary cannabinoid. *Proceedings of the National Academy of Sciences* **2008**, *105* (26), 9099-9104. DOI: 10.1073/pnas.0803601105.
- (51) Finlay, D. B.; Sircombe, K. J.; Nimick, M.; Jones, C.; Glass, M. Terpenoids From Cannabis Do Not Mediate an Entourage Effect by Acting at Cannabinoid Receptors. *Frontiers in Pharmacology* **2020**, *11*, Original Research. DOI: 10.3389/fphar.2020.00359.
- (52) Santiago, M.; Sachdev, S.; Arnold, J. C.; McGregor, I. S.; Connor, M. Absence of Entourage: Terpenoids Commonly Found in Cannabis sativa Do Not Modulate the Functional Activity of Δ9-THC at Human CB1 and CB2 Receptors. *Cannabis and Cannabinoid Research* **2019**, *4* (3), 165-176. DOI: 10.1089/can.2019.0016.
- (53) Russo, E. B. The Case for the Entourage Effect and Conventional Breeding of Clinical Cannabis: No "Strain," No Gain. *Frontiers in Plant Science* **2019**, *9*, Perspective. DOI: 10.3389/fpls.2018.01969.
- (54) Russo, E. B. Taming THC: potential cannabis synergy and phytocannabinoid-terpenoid entourage effects. *British Journal of Pharmacology* **2011**, *163* (7), 1344-1364. DOI: <https://doi.org/10.1111/j.1476-5381.2011.01238.x>.
- (55) Worth, T. Cannabis's chemical synergies. *Nature* **2019**, *572* (7771), S12-s13. DOI: 10.1038/d41586-019-02528-1
- (56) Wagner, H.; Ulrich-Merzenich, G. Synergy research: Approaching a new generation of phytopharmaceuticals. *Phytomedicine* **2009**, *16* (2), 97-110. DOI: <https://doi.org/10.1016/j.phymed.2008.12.018>.
- (57) Olmedo, R. H.; Asensio, C. M.; Grosso, N. R. Thermal stability and antioxidant activity of essential oils from aromatic plants farmed in Argentina. *Industrial Crops and Products* **2015**, *69*, 21-28. DOI: <https://doi.org/10.1016/j.indcrop.2015.02.005>.
- (58) Turek, C.; Stintzing, F. C. Stability of Essential Oils: A Review. *Comprehensive Reviews in Food Science and Food Safety* **2013**, *12* (1), 40-53. DOI: <https://doi.org/10.1111/1541-4337.12006>.

- (59) Bueno, J.; Alborzi, S.; Greenbaum, E. A. Vapor Phase Terpenes Mitigate Oxidative Degradation of Cannabis sativa Inflorescence Cannabinoid Content in an Accelerated Stability Study. *Cannabis and Cannabinoid Research* **2022**, *8* (5), 887-898. DOI: 10.1089/can.2021.0207.
- (60) Hanuš, L. O.; Hod, Y. Terpenes/Terpenoids in Cannabis: Are They Important? *Medical Cannabis and Cannabinoids* **2020**, *3* (1), 25-60. DOI: 10.1159/000509733.
- (61) Kovalchuk, O.; Li, D.; Rodriguez-Juarez, R.; Golubov, A.; Hudson, D.; Kovalchuk, I. The effect of cannabis dry flower irradiation on the level of cannabinoids, terpenes and anti-cancer properties of the extracts. *Biocatalysis and Agricultural Biotechnology* **2020**, *29*, 101736. DOI: <https://doi.org/10.1016/j.bcab.2020.101736>.
- (62) Addo, P. W.; Desaulniers Brousseau, V.; Morello, V.; MacPherson, S.; Paris, M.; Lefsrud, M. Cannabis chemistry, post-harvest processing methods and secondary metabolite profiling: A review. *Industrial Crops and Products* **2021**, *170*, 113743. DOI: <https://doi.org/10.1016/j.indcrop.2021.113743>.
- (63) Thurman, E. M. Chapter Seven - Analysis of terpenes in hemp (Cannabis sativa) by gas chromatography/mass spectrometry: Isomer identification analysis. In *Comprehensive Analytical Chemistry*, Ferrer, I., Thurman, E. M. Eds.; Vol. 90; Elsevier, **2020**; pp 197-233.
- (64) Calvi, L.; Pentimalli, D.; Panseri, S.; Giupponi, L.; Gelmini, F.; Beretta, G.; Vitali, D.; Bruno, M.; Zilio, E.; Pavlovic, R.; et al. Comprehensive quality evaluation of medical Cannabis sativa L. inflorescence and macerated oils based on HS-SPME coupled to GC-MS and LC-HRMS (q-exactive orbitrap®) approach. *Journal of Pharmaceutical and Biomedical Analysis* **2018**, *150*, 208-219. DOI: <https://doi.org/10.1016/j.jpba.2017.11.073>.
- (65) Marriott, P. J.; Shellie, R.; Cornwell, C. Gas chromatographic technologies for the analysis of essential oils. *Journal of Chromatography A* **2001**, *936* (1), 1-22. DOI: [https://doi.org/10.1016/S0021-9673\(01\)01314-0](https://doi.org/10.1016/S0021-9673(01)01314-0).
- (66) McNair, H. M.; Miller, J. M.; Snow, N. H. *Basic gas chromatography*; John Wiley & Sons, **2019**.
- (67) Nahar, L.; Gavril, G. L.; Sarker, S. D. Application of gas chromatography in the analysis of phytocannabinoids: An update (2020–2023). *Phytochemical Analysis* **2023**, *34* (8), 903-924. DOI: <https://doi.org/10.1002/pca.3303>.
- (68) Micalizzi, G.; Vento, F.; Alibrando, F.; Donnarumma, D.; Dugo, P.; Mondello, L. Cannabis Sativa L.: a comprehensive review on the analytical methodologies for cannabinoids and terpenes characterization. *Journal of Chromatography A* **2021**, *1637*, 461864. DOI: <https://doi.org/10.1016/j.chroma.2020.461864>.
- (69) Zivovinic, S.; Alder, R.; Allenspach, M. D.; Steuer, C. Determination of cannabinoids in Cannabis sativa L. samples for recreational, medical, and forensic purposes by reversed-phase liquid chromatography-ultraviolet detection. *Journal of Analytical Science and Technology* **2018**, *9* (1), 1-10. DOI: <https://doi.org/10.1186/s40543-018-0159-8>.
- (70) Raeber, J.; Poetzsch, M.; Schmidli, A.; Favrod, S.; Steuer, C. Simultaneous quantification of terpenes and cannabinoids by reversed-phase LC-APCI-MS/MS in Cannabis sativa L. samples combined with a subsequent chemometric analysis. *Analytical and Bioanalytical Chemistry* **2024**. DOI: 10.1007/s00216-024-05349-y.

- (71) Mudge, E. M.; Brown, P. N.; Murch, S. J. The terroir of Cannabis: terpene metabolomics as a tool to understand Cannabis sativa selections. *Planta Medica* **2019**, *85* (09/10), 781-796. DOI: 10.1055/a-0915-2550.
- (72) Fodor, B.; Molnár-Perl, I. The role of derivatization techniques in the analysis of plant cannabinoids by gas chromatography mass spectrometry. *TrAC Trends in Analytical Chemistry* **2017**, *95*, 149-158. DOI: <https://doi.org/10.1016/j.trac.2017.07.022>.
- (73) Ibrahim, E. A.; Gul, W.; Gul, S. W.; Stamper, B. J.; Hadad, G. M.; Salam, R. A. A.; Ibrahim, A. K.; Ahmed, S. A.; Chandra, S.; Lata, H. Determination of acid and neutral cannabinoids in extracts of different strains of Cannabis sativa using GC-FID. *Planta Medica* **2018**, *84* (04), 250-259. DOI: 10.1055/s-0043-124088.
- (74) Jin, D.; Jin, S.; Yu, Y.; Lee, C.; Chen, J. Classification of Cannabis cultivars marketed in Canada for medical purposes by quantification of cannabinoids and terpenes using HPLC-DAD and GC-MS. *Journal of Analytical and Bioanalytical Techniques* **2017**, *8* (2). DOI: 10.4172/2155-9872.1000349.
- (75) Hyland, K.; Borton, C.; Winkler, P.; Roberts, S.; Noestheden, M. Quantitation of Terpenes in Cannabis Products Using the Triple Quad™ 3500 LC-MS/MS System. *SCIEX, Redwood City, Calif* **2017**, *2*.
- (76) Caruso, S. J.; Acquaviva, A.; Müller, J. L.; Castells, C. B. Simultaneous analysis of cannabinoids and terpenes in Cannabis sativa inflorescence using full comprehensive two-dimensional liquid chromatography coupled to smart active modulation. *Journal of Chromatography A* **2024**, *1720*, 464810. DOI: <https://doi.org/10.1016/j.chroma.2024.464810>.
- (77) Li, W.; Fitzloff, J. F. Simultaneous determination of terpene lactones and flavonoid aglycones in Ginkgo biloba by high-performance liquid chromatography with evaporative light scattering detection. *Journal of Pharmaceutical and Biomedical Analysis* **2002**, *30* (1), 67-75. DOI: [https://doi.org/10.1016/S0731-7085\(02\)00201-7](https://doi.org/10.1016/S0731-7085(02)00201-7).
- (78) Rudbäck, J.; Islam, N.; Nilsson, U.; Karlberg, A.-T. A sensitive method for determination of allergenic fragrance terpene hydroperoxides using liquid chromatography coupled with tandem mass spectrometry. *Journal of Separation Science* **2013**, *36* (8), 1370-1378. DOI: <https://doi.org/10.1002/jssc.201200855>.
- (79) Mauri, P.; Simonetti, P.; Gardana, C.; Minoggio, M.; Morazzoni, P.; Bombardelli, E.; Pietta, P. Liquid chromatography/atmospheric pressure chemical ionization mass spectrometry of terpene lactones in plasma of volunteers dosed with Ginkgo biloba L. extracts. *Rapid Communications in Mass Spectrometry* **2001**, *15* (12), 929-934. DOI: <https://doi.org/10.1002/rcm.316>.
- (80) Glasius, M.; Duane, M.; Larsen, B. R. Determination of polar terpene oxidation products in aerosols by liquid chromatography-ion trap mass spectrometry. *Journal of Chromatography A* **1999**, *833* (2), 121-135. DOI: [https://doi.org/10.1016/S0021-9673\(98\)01042-5](https://doi.org/10.1016/S0021-9673(98)01042-5).
- (81) Turek, C.; Stintzing, F. C. Application of high-performance liquid chromatography diode array detection and mass spectrometry to the analysis of characteristic compounds in various essential oils. *Analytical and Bioanalytical Chemistry* **2011**, *400*, 3109-3123. DOI: <https://doi.org/10.1007/s00216-011-4976-5>.

- (82) Tranchida, P. Q.; Zoccali, M.; Bonaccorsi, I.; Dugo, P.; Mondello, L.; Dugo, G. The off-line combination of high performance liquid chromatography and comprehensive two-dimensional gas chromatography–mass spectrometry: a powerful approach for highly detailed essential oil analysis. *Journal of Chromatography A* **2013**, *1305*, 276-284. DOI: <https://doi.org/10.1016/j.chroma.2013.07.042>.
- (83) Nicolau, E. d. S.; Ribeiro, L. d. P.; Ansante, T. F.; Fernandes, J. B.; Forim, M. R.; Vieira, P. C.; Vendramim, J. D.; Da Silva, M. F. d. G. F. Isolation of chavibetol and methyleugenol from essential oil of *Pimenta pseudocaryophyllus* by high performance liquid chromatography. *Molecules* **2018**, *23* (11), 2909. DOI: <https://doi.org/10.3390/molecules23112909>.
- (84) Allenspach, M. D.; Valder, C.; Steuer, C. Absolute quantification of terpenes in conifer-derived essential oils and their antibacterial activity. *Journal of Analytical Science and Technology* **2020**, *11*, 1-10. DOI: <https://doi.org/10.1186/s40543-020-00212-y>.
- (85) Holm, T. Aspects of the mechanism of the flame ionization detector. *Journal of Chromatography A* **1999**, *842* (1), 221-227. DOI: [https://doi.org/10.1016/S0021-9673\(98\)00706-7](https://doi.org/10.1016/S0021-9673(98)00706-7).
- (86) van Den Dool, H.; Dec. Kratz, P. A generalization of the retention index system including linear temperature programmed gas–liquid partition chromatography. *Journal of Chromatography A* **1963**, *11*, 463-471. DOI: [https://doi.org/10.1016/S0021-9673\(01\)80947-X](https://doi.org/10.1016/S0021-9673(01)80947-X).
- (87) Gonzalez, F. R.; Nardillo, A. M. Retention index in temperature-programmed gas chromatography. *Journal of Chromatography A* **1999**, *842* (1), 29-49. DOI: [https://doi.org/10.1016/S0021-9673\(99\)00158-2](https://doi.org/10.1016/S0021-9673(99)00158-2).
- (88) Garcia, A.; Barbas, C. Gas Chromatography-Mass Spectrometry (GC-MS)-Based Metabolomics. In *Metabolic Profiling: Methods and Protocols*, Metz, T. O. Ed.; Humana Press, **2011**; pp 191-204.
- (89) National Institute of Standards and Technology (NIST). *NIST Chemistry WebBook*. U.S. Secretary of Commerce **2023**. <https://webbook.nist.gov/>.
- (90) Adams, R. P. Identification of essential oil components by gas chromatography/mass spectrometry. 5 online ed. *Gruver, TX USA: Texensis Publishing* **2017**.
- (91) Scheubert, K.; Hufsky, F.; Böcker, S. Computational mass spectrometry for small molecules. *Journal of Cheminformatics* **2013**, *5* (1), 12. DOI: [10.1186/1758-2946-5-12](https://doi.org/10.1186/1758-2946-5-12).
- (92) Li, D.-X.; Gan, L.; Bronja, A.; Schmitz, O. J. Gas chromatography coupled to atmospheric pressure ionization mass spectrometry (GC-API-MS): Review. *Analytica Chimica Acta* **2015**, *891*, 43-61. DOI: <https://doi.org/10.1016/j.aca.2015.08.002>.
- (93) Weidner, L.; Hemmler, D.; Rychlik, M.; Schmitt-Kopplin, P. Real-Time Monitoring of Miniaturized Thermal Food Processing by Advanced Mass Spectrometric Techniques. *Analytical Chemistry* **2023**, *95* (2), 1694-1702. DOI: [10.1021/acs.analchem.2c04874](https://doi.org/10.1021/acs.analchem.2c04874).
- (94) Venter, A. R.; Douglass, K. A.; Shelley, J. T.; Hasman, G., Jr.; Honarvar, E. Mechanisms of Real-Time, Proximal Sample Processing during Ambient Ionization Mass Spectrometry. *Analytical Chemistry* **2014**, *86* (1), 233-249. DOI: [10.1021/ac4038569](https://doi.org/10.1021/ac4038569).
- (95) You, X.; Lu, Q.; Guan, X.; Xu, Z.; Zenobi, R. Pesticide uptake and translocation in plants monitored in situ via laser ablation dielectric barrier discharge ionization mass spectrometry imaging. *Sensors and Actuators B: Chemical* **2024**, *409*, 135532. DOI: <https://doi.org/10.1016/j.snb.2024.135532>.

- (96) Funke, S. K. I.; Brückel, V. A.; Weber, M.; Lützen, E.; Wolf, J.-C.; Haisch, C.; Karst, U. Plug-and-play laser ablation-mass spectrometry for molecular imaging by means of dielectric barrier discharge ionization. *Analytica Chimica Acta* **2021**, *1177*, 338770. DOI: <https://doi.org/10.1016/j.aca.2021.338770>.
- (97) Plasmion. *About Plasmion*. **2024**. <https://plasmion.com/about-us/> (accessed 2024 08.04.2024).
- (98) Meyer, C.; Müller, S.; Gurevich, E. L.; Franzke, J. Dielectric barrier discharges in analytical chemistry. *Analyst* **2011**, *136* (12), 2427-2440, 10.1039/C0AN00994F. DOI: 10.1039/C0AN00994F.
- (99) Gyr, L.; Wolf, J.-C.; Franzke, J.; Zenobi, R. Mechanistic Understanding Leads to Increased Ionization Efficiency and Selectivity in Dielectric Barrier Discharge Ionization Mass Spectrometry: A Case Study with Perfluorinated Compounds. *Analytical Chemistry* **2018**, *90* (4), 2725-2731. DOI: 10.1021/acs.analchem.7b04711.
- (100) Gilbert-López, B.; García-Reyes, J. F.; Meyer, C.; Michels, A.; Franzke, J.; Molina-Díaz, A.; Hayen, H. Simultaneous testing of multiclass organic contaminants in food and environment by liquid chromatography/dielectric barrier discharge ionization-mass spectrometry. *Analyst* **2012**, *137* (22), 5403-5410, 10.1039/C2AN35705D. DOI: 10.1039/C2AN35705D.
- (101) Lara-Ortega, F. J.; Robles-Molina, J.; Brandt, S.; Schütz, A.; Gilbert-López, B.; Molina-Díaz, A.; García-Reyes, J. F.; Franzke, J. Use of dielectric barrier discharge ionization to minimize matrix effects and expand coverage in pesticide residue analysis by liquid chromatography-mass spectrometry. *Analytica Chimica Acta* **2018**, *1020*, 76-85. DOI: <https://doi.org/10.1016/j.aca.2018.02.077>.
- (102) Hayen, H.; Michels, A.; Franzke, J. Dielectric Barrier Discharge Ionization for Liquid Chromatography/Mass Spectrometry. *Analytical Chemistry* **2009**, *81* (24), 10239-10245. DOI: 10.1021/ac902176k.
- (103) Mirabelli, M. F.; Wolf, J.-C.; Zenobi, R. Atmospheric pressure soft ionization for gas chromatography with dielectric barrier discharge ionization-mass spectrometry (GC-DBDI-MS). *Analyst* **2017**, *142* (11), 1909-1915, 10.1039/C7AN00245A. DOI: 10.1039/C7AN00245A.
- (104) Mirabelli, M. F.; Wolf, J.-C.; Zenobi, R. Direct Coupling of Solid-Phase Microextraction with Mass Spectrometry: Sub-pg/g Sensitivity Achieved Using a Dielectric Barrier Discharge Ionization Source. *Analytical Chemistry* **2016**, *88* (14), 7252-7258. DOI: 10.1021/acs.analchem.6b01507.
- (105) Mirabelli, M. F.; Wolf, J.-C.; Zenobi, R. Pesticide analysis at ppt concentration levels: coupling nano-liquid chromatography with dielectric barrier discharge ionization-mass spectrometry. *Analytical and Bioanalytical Chemistry* **2016**, *408* (13), 3425-3434. DOI: 10.1007/s00216-016-9419-x.
- (106) Weber, M.; Wolf, J.-C.; Haisch, C. Gas Chromatography–Atmospheric Pressure Inlet–Mass Spectrometer Utilizing Plasma-Based Soft Ionization for the Analysis of Saturated, Aliphatic Hydrocarbons. *Journal of the American Society for Mass Spectrometry* **2021**, *32* (7), 1707-1715. DOI: 10.1021/jasms.0c00476.
- (107) Hagenhoff, S.; Franzke, J.; Hayen, H. Determination of Peroxide Explosive TATP and Related Compounds by Dielectric Barrier Discharge Ionization-Mass Spectrometry (DBDI-MS). *Analytical Chemistry* **2017**, *89* (7), 4210-4215. DOI: 10.1021/acs.analchem.7b00233.
- (108) Wolf, J.-C.; Schaer, M.; Siegenthaler, P.; Zenobi, R. Direct Quantification of Chemical Warfare Agents and Related Compounds at Low ppt Levels: Comparing Active Capillary Dielectric Barrier 173

- Discharge Plasma Ionization and Secondary Electrospray Ionization Mass Spectrometry. *Analytical Chemistry* **2015**, *87* (1), 723-729. DOI: 10.1021/ac5035874.
- (109) Liu, Q.; Lan, J.; Wu, R.; Begley, A.; Ge, W.; Zenobi, R. Hybrid Ionization Source Combining Nanoelectrospray and Dielectric Barrier Discharge Ionization for the Simultaneous Detection of Polar and Nonpolar Compounds in Single Cells. *Analytical Chemistry* **2022**, *94* (6), 2873-2881. DOI: 10.1021/acs.analchem.1c04759.
- (110) Huba, A. K.; Mirabelli, M. F.; Zenobi, R. Understanding and Optimizing the Ionization of Polycyclic Aromatic Hydrocarbons in Dielectric Barrier Discharge Sources. *Analytical Chemistry* **2019**, *91* (16), 10694-10701. DOI: 10.1021/acs.analchem.9b02044.
- (111) Gyr, L.; Klute, F. D.; Franzke, J.; Zenobi, R. Characterization of a Nitrogen-Based Dielectric Barrier Discharge Ionization Source for Mass Spectrometry Reveals Factors Important for Soft Ionization. *Analytical Chemistry* **2019**, *91* (10), 6865-6871. DOI: 10.1021/acs.analchem.9b01132.
- (112) Begley, A.; Zenobi, R. Discriminating alkylbenzene isomers with tandem mass spectrometry using a dielectric barrier discharge ionization source. *Journal of Mass Spectrometry* **2023**, *58* (3), e4910. DOI: <https://doi.org/10.1002/jms.4910>.
- (113) Begley, A. I.; Shuman, N. S.; Long, B. A.; Kämpf, R.; Gyr, L.; Viggiano, A. A.; Zenobi, R. Excited-State N Atoms Transform Aromatic Hydrocarbons into N-Heterocycles in Low-Temperature Plasmas. *The Journal of Physical Chemistry A* **2022**, *126* (10), 1743-1754. DOI: 10.1021/acs.jpca.1c10657.
- (114) Wolf, J.-C.; Gyr, L.; Mirabelli, M. F.; Schaer, M.; Siegenthaler, P.; Zenobi, R. A Radical-Mediated Pathway for the Formation of $[M + H]^+$ in Dielectric Barrier Discharge Ionization. *Journal of the American Society for Mass Spectrometry* **2016**, *27* (9), 1468-1475. DOI: 10.1007/s13361-016-1420-2.
- (115) Liu, Q.; Zenobi, R. Rapid analysis of fragrance allergens by dielectric barrier discharge ionization mass spectrometry. *Rapid Communications in Mass Spectrometry* **2021**, *35* (6), e9021. DOI: <https://doi.org/10.1002/rcm.9021>.
- (116) Weber, M.; Wolf, J.-C.; Haisch, C. Effect of Dopants and Gas-Phase Composition on Ionization Behavior and Efficiency in Dielectric Barrier Discharge Ionization. *Journal of the American Society for Mass Spectrometry* **2023**, *34* (4), 538-549. DOI: 10.1021/jasms.2c00279.
- (117) Massaro, A.; Zacometti, C.; Bragolusi, M.; Buček, J.; Piro, R.; Tata, A. Authentication of the botanical origin of monofloral honey by dielectric barrier discharge ionization high resolution mass spectrometry (DBDI-HRMS). Breaching the 6 s barrier of analysis time. *Food Control* **2024**, *160*, 110330. DOI: <https://doi.org/10.1016/j.foodcont.2024.110330>.
- (118) Xuesong, H.; Pu, C.; Jingyan, L.; Yupeng, X.; Dan, L.; Xiaoli, C. Commentary on the review articles of spectroscopy technology combined with chemometrics in the last three years. *Applied Spectroscopy Reviews* **2024**, *59* (4), 423-482. DOI: 10.1080/05704928.2023.2204946.
- (119) Vervoort, N.; Goossens, K.; Baeten, M.; Chen, Q. Recent advances in analytical techniques for high throughput experimentation. *Analytical Science Advances* **2021**, *2* (3-4), 109-127. DOI: <https://doi.org/10.1002/ansa.202000155>.
- (120) Engel, J.; Gerretzen, J.; Szymańska, E.; Jansen, J. J.; Downey, G.; Blanchet, L.; Buydens, L. M. C. Breaking with trends in pre-processing? *TrAC Trends in Analytical Chemistry* **2013**, *50*, 96-106. DOI: <https://doi.org/10.1016/j.trac.2013.04.015>.

- (121) Guo, J.; Yu, H.; Xing, S.; Huan, T. Addressing big data challenges in mass spectrometry-based metabolomics. *Chemical Communications* **2022**, *58* (72), 9979-9990, 10.1039/D2CC03598G. DOI: 10.1039/D2CC03598G.
- (122) Wold, S. Chemometrics; what do we mean with it, and what do we want from it? *Chemometrics and Intelligent Laboratory Systems* **1995**, *30* (1), 109-115. DOI: [https://doi.org/10.1016/0169-7439\(95\)00042-9](https://doi.org/10.1016/0169-7439(95)00042-9).
- (123) Wold, S.; Sjöström, M. Chemometrics, present and future success. *Chemometrics and Intelligent Laboratory Systems* **1998**, *44* (1), 3-14. DOI: [https://doi.org/10.1016/S0169-7439\(98\)00075-6](https://doi.org/10.1016/S0169-7439(98)00075-6).
- (124) Houhou, R.; Bocklitz, T. Trends in artificial intelligence, machine learning, and chemometrics applied to chemical data. *Analytical Science Advances* **2021**, *2* (3-4), 128-141. DOI: <https://doi.org/10.1002/ansa.202000162>.
- (125) Xu, G.; Stupak, J.; Yang, L.; Hu, L.; Guo, B.; Li, J. Deconvolution in mass spectrometry based proteomics. *Rapid Communications in Mass Spectrometry* **2018**, *32* (10), 763-774. DOI: <https://doi.org/10.1002/rcm.8103>.
- (126) Guo, Z.; Fan, Y.; Yu, C.; Lu, H.; Zhang, Z. GCMSFormer: A Fully Automatic Method for the Resolution of Overlapping Peaks in Gas Chromatography–Mass Spectrometry. *Analytical Chemistry* **2024**. DOI: 10.1021/acs.analchem.3c05772.
- (127) Yi, L.; Dong, N.; Yun, Y.; Deng, B.; Ren, D.; Liu, S.; Liang, Y. Chemometric methods in data processing of mass spectrometry-based metabolomics: A review. *Analytica Chimica Acta* **2016**, *914*, 17-34. DOI: <https://doi.org/10.1016/j.aca.2016.02.001>.
- (128) Dayananda, B.; Owen, S.; Kolobaric, A.; Chapman, J.; Cozzolino, D. Pre-processing Applied to Instrumental Data in Analytical Chemistry: A Brief Review of the Methods and Examples. *Critical Reviews in Analytical Chemistry*, 1-9. DOI: 10.1080/10408347.2023.2199864.
- (129) Rinnan, Å.; Berg, F. v. d.; Engelsen, S. B. Review of the most common pre-processing techniques for near-infrared spectra. *TrAC Trends in Analytical Chemistry* **2009**, *28* (10), 1201-1222. DOI: <https://doi.org/10.1016/j.trac.2009.07.007>.
- (130) Mishra, P.; Rutledge, D. N.; Roger, J.-M.; Wali, K.; Khan, H. A. Chemometric pre-processing can negatively affect the performance of near-infrared spectroscopy models for fruit quality prediction. *Talanta* **2021**, *229*, 122303. DOI: <https://doi.org/10.1016/j.talanta.2021.122303>.
- (131) Oliveri, P.; Malegori, C.; Simonetti, R.; Casale, M. The impact of signal pre-processing on the final interpretation of analytical outcomes – A tutorial. *Analytica Chimica Acta* **2019**, *1058*, 9-17. DOI: <https://doi.org/10.1016/j.aca.2018.10.055>.
- (132) Kumar, N.; Bansal, A.; Sarma, G. S.; Rawal, R. K. Chemometrics tools used in analytical chemistry: An overview. *Talanta* **2014**, *123*, 186-199. DOI: <https://doi.org/10.1016/j.talanta.2014.02.003>.
- (133) Biancolillo, A.; Marini, F. Chemometric Methods for Spectroscopy-Based Pharmaceutical Analysis. *Frontiers in Chemistry* **2018**, *6*, Review. DOI: 10.3389/fchem.2018.00576.
- (134) Cocchi, M.; Biancolillo, A.; Marini, F. Chapter Ten - Chemometric Methods for Classification and Feature Selection. In *Comprehensive Analytical Chemistry*, Jaumot, J., Bedia, C., Tauler, R. Eds.; Vol. 82; Elsevier, **2018**; pp 265-299.

- (135) Mishra, P.; Liland, K. H. An algorithm for robust multiblock partial least squares predictive modelling. *Journal of Chemometrics* **2023**, *37* (6), e3480. DOI: <https://doi.org/10.1002/cem.3480>.
- (136) Spink, J.; Moyer, D. C. Defining the Public Health Threat of Food Fraud. *Journal of Food Science* **2011**, *76* (9), R157-R163. DOI: <https://doi.org/10.1111/j.1750-3841.2011.02417.x>.
- (137) Biancolillo, A.; Måge, I.; Næs, T. Combining SO-PLS and linear discriminant analysis for multi-block classification. *Chemometrics and Intelligent Laboratory Systems* **2015**, *141*, 58-67. DOI: <https://doi.org/10.1016/j.chemolab.2014.12.001>.
- (138) Skov, T.; Honoré, A. H.; Jensen, H. M.; Næs, T.; Engelsen, S. B. Chemometrics in foodomics: Handling data structures from multiple analytical platforms. *TrAC Trends in Analytical Chemistry* **2014**, *60*, 71-79. DOI: <https://doi.org/10.1016/j.trac.2014.05.004>.
- (139) Mishra, P.; Liland, K. H.; Indahl, U. G. Swiss knife covariates selection: A unified algorithm for covariates selection in single block, multiblock, multiway, multiway multiblock cases including multiple responses. *Journal of Chemometrics* **2022**, *36* (10), e3441. DOI: <https://doi.org/10.1002/cem.3441>.
- (140) Smilde, A. K.; Westerhuis, J. A.; de Jong, S. A framework for sequential multiblock component methods. *Journal of Chemometrics* **2003**, *17* (6), 323-337. DOI: <https://doi.org/10.1002/cem.811>.
- (141) Biancolillo, A.; Liland, K. H.; Måge, I.; Næs, T.; Bro, R. Variable selection in multi-block regression. *Chemometrics and Intelligent Laboratory Systems* **2016**, *156*, 89-101. DOI: <https://doi.org/10.1016/j.chemolab.2016.05.016>.
- (142) Mishra, P.; Roger, J.-M.; Jouan-Rimbaud-Bouveresse, D.; Biancolillo, A.; Marini, F.; Nordon, A.; Rutledge, D. N. Recent trends in multi-block data analysis in chemometrics for multi-source data integration. *TrAC Trends in Analytical Chemistry* **2021**, *137*, 116206. DOI: <https://doi.org/10.1016/j.trac.2021.116206>.
- (143) Borràs, E.; Ferré, J.; Boqué, R.; Mestres, M.; Aceña, L.; Busto, O. Data fusion methodologies for food and beverage authentication and quality assessment – A review. *Analytica Chimica Acta* **2015**, *891*, 1-14. DOI: <https://doi.org/10.1016/j.aca.2015.04.042>.
- (144) Acar, E.; Rasmussen, M. A.; Savorani, F.; Næs, T.; Bro, R. Understanding data fusion within the framework of coupled matrix and tensor factorizations. *Chemometrics and Intelligent Laboratory Systems* **2013**, *129*, 53-63. DOI: <https://doi.org/10.1016/j.chemolab.2013.06.006>.
- (145) Mishra, P.; Metz, M.; Marini, F.; Biancolillo, A.; Rutledge, D. N. Response oriented covariates selection (ROCS) for fast block order- and scale-independent variable selection in multi-block scenarios. *Chemometrics and Intelligent Laboratory Systems* **2022**, *224*, 104551. DOI: <https://doi.org/10.1016/j.chemolab.2022.104551>.
- (146) Biancolillo, A.; Boqué, R.; Cocchi, M.; Marini, F. Chapter 10 - Data Fusion Strategies in Food Analysis. In *Data Handling in Science and Technology*, Cocchi, M. Ed.; Vol. 31; Elsevier, **2019**; pp 271-310.
- (147) Kohonen, J.; Reinikainen, S.-P.; Aaljoki, K.; Perkiö, A.; Väänänen, T.; Höskuldsson, A. Multi-block methods in multivariate process control. *Journal of Chemometrics* **2008**, *22* (3-4), 281-287. DOI: <https://doi.org/10.1002/cem.1120>.
- (148) Biancolillo, A.; Preys, S.; Gaci, B.; Le-Quere, J.-L.; Laboure, H.; Deuscher, Z.; Cheynier, V.; Sommerer, N.; Fayeulle, N.; Costet, P.; et al. Multi-block classification of chocolate and cocoa samples

into sensory poles. *Food Chemistry* **2021**, *340*, 127904. DOI: <https://doi.org/10.1016/j.foodchem.2020.127904>.

(149) Foschi, M.; Biancolillo, A.; Marini, F.; Cosentino, F.; Di Donato, F.; D'Archivio, A. A. Multi-block approach for the characterization and discrimination of Italian chickpeas landraces. *Food Control* **2024**, *157*, 110170. DOI: <https://doi.org/10.1016/j.foodcont.2023.110170>.

(150) Firmani, P.; Nardecchia, A.; Nocente, F.; Gazza, L.; Marini, F.; Biancolillo, A. Multi-block classification of Italian semolina based on Near Infrared Spectroscopy (NIR) analysis and alveographic indices. *Food Chemistry* **2020**, *309*, 125677. DOI: <https://doi.org/10.1016/j.foodchem.2019.125677>.

(151) Mishra, P.; Brouwer, B.; Meesters, L. Improved understanding and prediction of pear fruit firmness with variation partitioning and sequential multi-block modelling. *Chemometrics and Intelligent Laboratory Systems* **2022**, *222*, 104517. DOI: <https://doi.org/10.1016/j.chemolab.2022.104517>.

(152) Bajoub, A.; Medina-Rodríguez, S.; Gómez-Romero, M.; Ajal, E. A.; Bagur-González, M. G.; Fernández-Gutiérrez, A.; Carrasco-Pancorbo, A. Assessing the varietal origin of extra-virgin olive oil using liquid chromatography fingerprints of phenolic compound, data fusion and chemometrics. *Food Chemistry* **2017**, *215*, 245-255. DOI: <https://doi.org/10.1016/j.foodchem.2016.07.140>.

(153) Ballabio, D.; Robotti, E.; Grisoni, F.; Quasso, F.; Bobba, M.; Vercelli, S.; Gosetti, F.; Calabrese, G.; Sangiorgi, E.; Orlandi, M.; et al. Chemical profiling and multivariate data fusion methods for the identification of the botanical origin of honey. *Food Chemistry* **2018**, *266*, 79-89. DOI: <https://doi.org/10.1016/j.foodchem.2018.05.084>.

(154) Márquez, C.; López, M. I.; Ruisánchez, I.; Callao, M. P. FT-Raman and NIR spectroscopy data fusion strategy for multivariate qualitative analysis of food fraud. *Talanta* **2016**, *161*, 80-86. DOI: <https://doi.org/10.1016/j.talanta.2016.08.003>.

(155) International Standard. Oil of rose (*Rosa x damascena* Miller). ISO, Ed.; Switzerland, **2003**.

(156) Venkatesha, K. T.; Gupta, A.; Rai, A. N.; Jambhulkar, S. J.; Bisht, R.; Padalia, R. C. Recent developments, challenges, and opportunities in genetic improvement of essential oil-bearing rose (*Rosa damascena*): A review. *Industrial Crops and Products* **2022**, *184*, 114984. DOI: <https://doi.org/10.1016/j.indcrop.2022.114984>.

(157) Botelho, G.; Caldeira, I.; Mendes-Faia, A.; Clímaco, M. C. Evaluation of two quantitative gas chromatography–olfactometry methods for clonal red wines differentiation. *Flavour and Fragrance Journal* **2007**, *22* (5), 414-420. DOI: <https://doi.org/10.1002/ffj.1815>.

(158) Osorio, C.; Alarcon, M.; Moreno, C.; Bonilla, A.; Barrios, J.; Garzon, C.; Duque, C. Characterization of odor-active volatiles in Champa (*Campomanesia lineatifolia* R. & P.). *Journal of agricultural and food chemistry* **2006**, *54* (2), 509-516. DOI: <https://doi.org/10.1021/jf052098c>.

(159) Seo, W. H.; Baek, H. H. Identification of characteristic aroma-active compounds from water dropwort (*Oenanthe javanica* DC.). *Journal of Agricultural and Food Chemistry* **2005**, *53* (17), 6766-6770. DOI: <https://doi.org/10.1021/jf050150z>.

(160) Gancel, A.-L.; Ollitrault, P.; Froelicher, Y.; Tomi, F.; Jacquemond, C.; Luro, F.; Brillouet, J.-M. Leaf volatile compounds of six citrus somatic allotetraploid hybrids originating from various combinations of lime, lemon, citron, sweet orange, and grapefruit. *Journal of agricultural and food chemistry* **2005**, *53* (6), 2224-2230. DOI: <https://doi.org/10.1021/jf048315b>.

- (161) Fanciullino, A.-L.; Gancel, A.-L.; Froelicher, Y.; Luro, F.; Ollitrault, P.; Brillouet, J.-M. Effects of nucleo-cytoplasmic interactions on leaf volatile compounds from citrus somatic diploid hybrids. *Journal of agricultural and food chemistry* **2005**, *53* (11), 4517-4523. DOI: <https://doi.org/10.1021/jf0502855>.
- (162) Zheng, C. H.; Kim, T. H.; Kim, K. H.; Leem, Y. H.; Lee, H. J. Characterization of potent aroma compounds in *Chrysanthemum coronarium* L.(Garland) using aroma extract dilution analysis. *Flavour and Fragrance Journal* **2004**, *19* (5), 401-405. DOI: <https://doi.org/10.1002/ffj.1447>.
- (163) Yu, E. J.; Kim, T. H.; Kim, K. H.; Lee, H. J. Characterization of aroma-active compounds of *Abies nephrolepis* (Khingnan fir) needles using aroma extract dilution analysis. *Flavour and Fragrance Journal* **2004**, *19* (1), 74-79. DOI: <https://doi.org/10.1002/ffj.1314>.
- (164) Varming, C.; Andersen, M. L.; Poll, L. Influence of thermal treatment on black currant (*Ribes nigrum* L.) juice aroma. *Journal of Agricultural and Food Chemistry* **2004**, *52* (25), 7628-7636. DOI: <https://doi.org/10.1021/jf049435m>.
- (165) Ledauphin, J.; Saint-Clair, J.-F.; Lablanquie, O.; Guichard, H.; Fournier, N.; Guichard, E.; Barillier, D. Identification of trace volatile compounds in freshly distilled calvados and cognac using preparative separations coupled with gas chromatography– mass spectrometry. *Journal of Agricultural and Food Chemistry* **2004**, *52* (16), 5124-5134. DOI: <https://doi.org/10.1021/jf040052y>.
- (166) Bertoli, A.; Menichini, F.; Noccioli, C.; Morelli, I.; Pistelli, L. Volatile constituents of different organs of *Psoralea bituminosa* L. *Flavour and Fragrance Journal* **2004**, *19* (2), 166-171. DOI: <https://doi.org/10.1002/ffj.1315>.
- (167) Kim, T. H.; Thuy, N. T.; Shin, J. H.; Baek, H. H.; Lee, H. J. Aroma-active compounds of miniature beefsteakplant (*Mosla dianthera* Maxim.). *Journal of Agricultural and Food Chemistry* **2000**, *48* (7), 2877-2881. DOI: <https://doi.org/10.1021/jf000219x>.
- (168) Möllenbeck, S.; König, T.; Schreier, P.; Schwab, W.; Rajaonarivony, J.; Ranarivelo, L. Chemical composition and analyses of enantiomers of essential oils from Madagascar. *Flavour and Fragrance Journal* **1997**, *12* (2), 63-69. DOI: [https://doi.org/10.1002/\(SICI\)1099-1026\(199703\)12:2<63::AID-FFJ614>3.0.CO;2-Z](https://doi.org/10.1002/(SICI)1099-1026(199703)12:2<63::AID-FFJ614>3.0.CO;2-Z).
- (169) Beale, D. J.; Morrison, P. D.; Karpe, A. V.; Dunn, M. S. Chemometric analysis of lavender essential oils using targeted and untargeted GC-MS acquired data for the rapid identification and characterization of oil quality. *Molecules* **2017**, *22* (8), 1339. DOI: <https://doi.org/10.3390/molecules22081339>.
- (170) Krupčík, J.; Gorovenko, R.; Špánik, I.; Armstrong, D. W.; Sandra, P. Enantioselective comprehensive two-dimensional gas chromatography of lavender essential oil. *Journal of Separation Science* **2016**, *39* (24), 4765-4772. DOI: <https://doi.org/10.1002/jssc.201600986>.
- (171) Salek, R. M.; Steinbeck, C.; Viant, M. R.; Goodacre, R.; Dunn, W. B. The role of reporting standards for metabolite annotation and identification in metabolomic studies. *GigaScience* **2013**, *2* (1), 2047-2217X-2042-2013. DOI: 10.1186/2047-217X-2-13.
- (172) Cebi, N. Quantification of the Geranium Essential Oil, Palmarosa Essential Oil and Phenylethyl Alcohol in *Rosa damascena* Essential Oil Using ATR-FTIR Spectroscopy Combined with Chemometrics. *Foods* **2021**, *10* (8). DOI: 10.3390/foods10081848.

- (173) Fanali, C.; D'Orazio, G.; Gentili, A.; Fanali, S. Analysis of enantiomers in products of food interest. *Molecules* **2019**, *24* (6), 1119. DOI: <https://doi.org/10.3390/molecules24061119>.
- (174) Mosandl, A. Enantioselective capillary gas chromatography and stable isotope ratio mass spectrometry in the authenticity control of flavors and essential oils. *Food Reviews International* **1995**, *11* (4), 597-664. DOI: 10.1080/87559129509541063.
- (175) Schmidt, E.; Wanner, J. Adulteration of essential oils. In *Handbook of Essential Oils*, CRC Press, **2020**; pp 543-580.
- (176) Bardarov, V.; Veltcheva, A. Comparison of the chiral selectivity of two GC columns for the separation of enantiomers in rose oil. *Journal of the University of Chemical Technology and Metallurgy* **2011**, *46* (3), 320-328.
- (177) Krupčík, J.; Gorovenko, R.; Špánik, I.; Sandra, P.; Armstrong, D. W. Enantioselective comprehensive two-dimensional gas chromatography. A route to elucidate the authenticity and origin of *Rosa damascena* Miller essential oils. *Journal of Separation Science* **2015**, *38* (19), 3397-3403. DOI: <https://doi.org/10.1002/jssc.2015007443>.
- (178) European Medicines Agency. ICH guideline Q2(R2) on validation of analytical procedures. *ICH Guidelines* **2022**, Q2(R2).
- (179) Peters, F. T.; Hartung, M.; Herbold, M.; Schmitt, G. Requirements for the validation of analytical methods. *To the GTFCh Guidelines for quality assurance in forensic-toxicological analyses* **2009**, Appendix B.
- (180) Council of Europe. *European Pharmacopeia*; EDQM, **2021**.
- (181) Souverain, S.; Rudaz, S.; Veuthey, J.-L. Matrix effect in LC-ESI-MS and LC-APCI-MS with off-line and on-line extraction procedures. *Journal of Chromatography A* **2004**, *1058* (1), 61-66. DOI: <https://doi.org/10.1016/j.chroma.2004.08.118>.
- (182) Filer, C. N. Acidic Cannabinoid Decarboxylation. *Cannabis and Cannabinoid Research* **2021**, *7* (3), 262-273. DOI: 10.1089/can.2021.0072.
- (183) Nuutinen, T. Medicinal properties of terpenes found in *Cannabis sativa* and *Humulus lupulus*. *European Journal of Medicinal Chemistry* **2018**, *157*, 198-228. DOI: <https://doi.org/10.1016/j.ejmech.2018.07.076>.
- (184) Gülck, T.; Møller, B. L. Phytocannabinoids: Origins and Biosynthesis. *Trends in Plant Science* **2020**, *25* (10), 985-1004. DOI: <https://doi.org/10.1016/j.tplants.2020.05.005>.
- (185) Tahir, M. N.; Shahbazi, F.; Rondeau-Gagné, S.; Trant, J. F. The biosynthesis of the cannabinoids. *Journal of Cannabis Research* **2021**, *3* (1), 7. DOI: 10.1186/s42238-021-00062-4.
- (186) Pavlovic, R.; Nenna, G.; Calvi, L.; Panseri, S.; Borgonovo, G.; Giupponi, L.; Cannazza, G.; Giorgi, A. Quality Traits of "Cannabidiol Oils": Cannabinoids Content, Terpene Fingerprint and Oxidation Stability of European Commercially Available Preparations. *Molecules* **2018**, *23* (5). DOI: 10.3390/molecules23051230.
- (187) Sannikova, N. The Effect of Storage Conditions on Cannabinoid Stability. Ascension Sciences Inc.: Vancouver, Canada, **2020**.
- (188) Council of Europe. *European Pharmacopeia*; EDQM, **2024**.

- (189) Raeber, J.; Bajor, B.; Poetzsch, M.; Steuer, C. Comprehensive analysis of chemical and enantiomeric stability of terpenes in *L.* flowers. *Phytochemical Analysis* **2024**, DOI: <https://doi.org/10.1002/pca.3432>.
- (190) He, F.; Qian, Y. L.; Qian, M. C. Flavor and chiral stability of lemon-flavored hard tea during storage. *Food Chemistry* **2018**, *239*, 622-630. DOI: <https://doi.org/10.1016/j.foodchem.2017.06.136>.
- (191) Mehdizadeh, L.; Ghasemi Pirbalouti, A.; Moghaddam, M. Storage stability of essential oil of cumin (*Cuminum Cyminum* L.) as a function of temperature. *International Journal of Food Properties* **2017**, *20* (sup2), 1742-1750. DOI: [10.1080/10942912.2017.1354018](https://doi.org/10.1080/10942912.2017.1354018).
- (192) Al-Harrasi, A.; Bhatia, S.; Behl, T.; Anwer, K. Essential oil stability. In *Role of Essential Oils in the Management of COVID-19*, CRC Press, **2022**; pp 159-168.
- (193) Dieckmann, R. H.; Palamand, S. R. Autoxidation of some constituents of hops. I. Monoterpene hydrocarbon, myrcene. *Journal of Agricultural and Food Chemistry* **1974**, *22* (3), 498-503.
- (194) Marchini, M.; Charvoz, C.; Dujourdy, L.; Baldovini, N.; Filippi, J.-J. Multidimensional analysis of cannabis volatile constituents: Identification of 5,5-dimethyl-1-vinylbicyclo[2.1.1]hexane as a volatile marker of hashish, the resin of *Cannabis sativa* L. *Journal of Chromatography A* **2014**, *1370*, 200-215. DOI: <https://doi.org/10.1016/j.chroma.2014.10.045>.
- (195) Rhoderick, G. C. Stability assessment of gas mixtures containing terpenes at nominal 5 nmol/mol contained in treated aluminum gas cylinders. *Analytical and Bioanalytical Chemistry* **2010**, *398* (3), 1417-1425. DOI: [10.1007/s00216-010-4058-0](https://doi.org/10.1007/s00216-010-4058-0).
- (196) Rhoderick, G. C.; Lin, J. Stability Assessment of Gas Mixtures Containing Monoterpenes in Varying Cylinder Materials and Treatments. *Analytical Chemistry* **2013**, *85* (9), 4675-4685. DOI: [10.1021/ac400324v](https://doi.org/10.1021/ac400324v).
- (197) Livingston, S. J.; Quilichini, T. D.; Booth, J. K.; Wong, D. C. J.; Rensing, K. H.; Laflamme-Yonkman, J.; Castellarin, S. D.; Bohlmann, J.; Page, J. E.; Samuels, A. L. Cannabis glandular trichomes alter morphology and metabolite content during flower maturation. *The Plant Journal* **2020**, *101* (1), 37-56. DOI: <https://doi.org/10.1111/tpj.14516>.
- (198) Fiorini, D.; Scortichini, S.; Bonacucina, G.; Greco, N. G.; Mazzara, E.; Petrelli, R.; Torresi, J.; Maggi, F.; Cespi, M. Cannabidiol-enriched hemp essential oil obtained by an optimized microwave-assisted extraction using a central composite design. *Industrial Crops and Products* **2020**, *154*, 112688. DOI: <https://doi.org/10.1016/j.indcrop.2020.112688>.
- (199) Wang, M.; Lee, J.; Zhao, J.; Chatterjee, S.; Chittiboyina, A. G.; Ali, Z.; Khan, I. A. Comprehensive quality assessment of peppermint oils and commercial products: An integrated approach involving conventional and chiral GC/MS coupled with chemometrics. *Journal of Chromatography B* **2024**, *1232*, 123953. DOI: <https://doi.org/10.1016/j.jchromb.2023.123953>.
- (200) Cucinotta, L.; De Grazia, G.; Micalizzi, G.; Bontempo, L.; Camin, F.; Mondello, L.; Sciarrone, D. Simultaneous evaluation of the enantiomeric and carbon isotopic ratios of *Cannabis sativa* L. essential oils by multidimensional gas chromatography. *Analytical and Bioanalytical Chemistry* **2022**, *414* (18), 5643-5656. DOI: [10.1007/s00216-022-04035-1](https://doi.org/10.1007/s00216-022-04035-1).

- (201) Ruiz Del Castillo, M. L.; Caja, M. M.; Blanch, G. P.; Herraiz, M. Enantiomeric Distribution of Chiral Compounds in Orange Juices according to Their Geographical Origins. *Journal of Food Protection* **2003**, *66* (8), 1448-1454. DOI: <https://doi.org/10.4315/0362-028X-66.8.1448>.
- (202) Micalizzi, G.; Alibrando, F.; Vento, F.; Trovato, E.; Zoccali, M.; Guarnaccia, P.; Dugo, P.; Mondello, L. Development of a Novel Microwave Distillation Technique for the Isolation of Cannabis sativa L. Essential Oil and Gas Chromatography Analyses for the Comprehensive Characterization of Terpenes and Terpenoids, Including Their Enantio-Distribution. *Molecules* **2021**, *26* (6). DOI: 10.3390/molecules26061588.
- (203) Wüst, M.; Mosandl, A. Important chiral monoterpenoid ethers in flavours and essential oils – enantioselective analysis and biogenesis. *European Food Research and Technology* **1999**, *209* (1), 3-11. DOI: 10.1007/s002170050447.
- (204) Booth, J. K.; Page, J. E.; Bohlmann, J. Terpene synthases from Cannabis sativa. *PLOS ONE* **2017**, *12* (3), e0173911. DOI: 10.1371/journal.pone.0173911.
- (205) Kaur, S.; Rana, S.; Singh, H. P.; Batish, D. R.; Kohli, R. K. Citronellol Disrupts Membrane Integrity by Inducing Free Radical Generation. **2011**, *66* (5-6), 260-266. DOI: doi:10.1515/znc-2011-5-609.
- (206) Yamasaki, Y.; Kunoh, H.; Yamamoto, H.; Akimitsu, K. Biological roles of monoterpene volatiles derived from rough lemon (Citrus jambhiri Lush) in citrus defense. *Journal of General Plant Pathology* **2007**, *73* (3), 168-179. DOI: 10.1007/s10327-007-0013-0.
- (207) Adams, R. *Identification of Essential Oil Components by Gas Chromatography/Quadrupole Mass Spectroscopy*; Allured publishing corporation, **2007**.
- (208) Wallace, W. E. In *NIST Chemistry WebBook, NIST Standard Reference Database Number 69*, Eds. P.J. Linstrom and W.G. Mallard.
- (209) Heffernan, D.; Pilz, M.; Klein, M.; Haack, M.; Race, A. M.; Brück, T.; Qoura, F.; Strittmatter, N. Screening of volatile organic compounds (VOCs) from liquid fungal cultures using ambient mass spectrometry. *Analytical and Bioanalytical Chemistry* **2023**, *415* (18), 4615-4627. DOI: 10.1007/s00216-023-04769-6.
- (210) Vaniya, A.; Fiehn, O. Using fragmentation trees and mass spectral trees for identifying unknown compounds in metabolomics. *TrAC Trends in Analytical Chemistry* **2015**, *69*, 52-61. DOI: <https://doi.org/10.1016/j.trac.2015.04.002>.
- (211) Nørgaard, A. W.; Vibenholt, A.; Benassi, M.; Clausen, P. A.; Wolkoff, P. Study of Ozone-Initiated Limonene Reaction Products by Low Temperature Plasma Ionization Mass Spectrometry. *Journal of the American Society for Mass Spectrometry* **2013**, *24* (7), 1090-1096. DOI: 10.1007/s13361-013-0648-3.
- (212) Nørgaard, A. W.; Kofoed-Sørensen, V.; Svensmark, B.; Wolkoff, P.; Clausen, P. A. Gas Chromatography Interfaced with Atmospheric Pressure Ionization-Quadrupole Time-of-Flight-Mass Spectrometry by Low-Temperature Plasma Ionization. *Analytical Chemistry* **2013**, *85* (1), 28-32. DOI: 10.1021/ac301859r.
- (213) Rodrigues, S.; Fernandes, F. A. N. Effect of Dielectric Barrier Discharge Plasma Treatment in Pasteurized Orange Juice: Changes in Volatile Composition, Aroma, and Mitigation of Off-flavors. *Food and Bioprocess Technology* **2023**, *16* (4), 930-939. DOI: 10.1007/s11947-022-02976-0.

- (214) Nudnova, M. M.; Zhu, L.; Zenobi, R. Active capillary plasma source for ambient mass spectrometry. *Rapid Communications in Mass Spectrometry* **2012**, *26* (12), 1447-1452. DOI: <https://doi.org/10.1002/rcm.6242>.
- (215) Bartella, L.; Bouza, M.; Rocío-Bautista, P.; Di Donna, L.; Garcia-Reyes, J. F.; Molina-Díaz, A. Direct wine profiling by mass spectrometry (MS): A comparison of different ambient MS approaches. *Microchemical Journal* **2022**, *179*, 107479. DOI: <https://doi.org/10.1016/j.microc.2022.107479>.
- (216) Krysa, M.; Szymańska-Chargot, M.; Zdunek, A. FT-IR and FT-Raman fingerprints of flavonoids – A review. *Food Chemistry* **2022**, *393*, 133430. DOI: <https://doi.org/10.1016/j.foodchem.2022.133430>.
- (217) Thygesen, L. G.; Løkke, M. M.; Micklander, E.; Engelsen, S. B. Vibrational microspectroscopy of food. Raman vs. FT-IR. *Trends in Food Science & Technology* **2003**, *14* (1), 50-57. DOI: [https://doi.org/10.1016/S0924-2244\(02\)00243-1](https://doi.org/10.1016/S0924-2244(02)00243-1).
- (218) Agatonovic-Kustrin, S.; Ristivojevic, P.; Gegechkori, V.; Litvinova, T. M.; W. Morton, D. Essential Oil Quality and Purity Evaluation via FT-IR Spectroscopy and Pattern Recognition Techniques. *Applied Sciences* **2020**, *10* (20). DOI: 10.3390/app10207294.
- (219) Rather, M. A.; Dar, B. A.; Shah, W. A.; Prabhakar, A.; Bindu, K.; Banday, J. A.; Qurishi, M. A. Comprehensive GC–FID, GC–MS and FT-IR spectroscopic analysis of the volatile aroma constituents of *Artemisia indica* and *Artemisia vestita* essential oils. *Arabian Journal of Chemistry* **2017**, *10*, S3798-S3803. DOI: <https://doi.org/10.1016/j.arabjc.2014.05.017>.
- (220) Granato, D.; Putnik, P.; Kovačević, D. B.; Santos, J. S.; Calado, V.; Rocha, R. S.; Cruz, A. G. D.; Jarvis, B.; Rodionova, O. Y.; Pomerantsev, A. Trends in Chemometrics: Food Authentication, Microbiology, and Effects of Processing. *Comprehensive Reviews in Food Science and Food Safety* **2018**, *17* (3), 663-677. DOI: <https://doi.org/10.1111/1541-4337.12341>.
- (221) Chu, X.; Huang, Y.; Yun, Y.-H.; Bian, X. *Chemometric methods in analytical spectroscopy technology*; Springer, **2022**. DOI: <https://doi.org/10.1007/978-981-19-1625-0>.
- (222) Lee, L. C.; Liong, C.-Y.; Jemain, A. A. Partial least squares-discriminant analysis (PLS-DA) for classification of high-dimensional (HD) data: a review of contemporary practice strategies and knowledge gaps. *Analyst* **2018**, *143* (15), 3526-3539. DOI: 10.1039/C8AN00599K.
- (223) Ruiz-Perez, D.; Guan, H.; Madhivanan, P.; Mathee, K.; Narasimhan, G. So you think you can PLS-DA? *BMC Bioinformatics* **2020**, *21*, 1-10. DOI: <https://doi.org/10.1186/s12859-019-3310-7>.
- (224) Smilde, A. K.; Måge, I.; Naes, T.; Hankemeier, T.; Lips, M. A.; Kiers, H. A.; Acar, E.; Bro, R. Common and distinct components in data fusion. *Journal of Chemometrics* **2017**, *31* (7), e2900. DOI: <https://doi.org/10.1002/cem.2900>.
- (225) Schiavone, S.; Marchionni, B.; Bucci, R.; Marini, F.; Biancolillo, A. Authentication of Grappa (Italian grape marc spirit) by Mid and Near Infrared spectroscopies coupled with chemometrics. *Vibrational Spectroscopy* **2020**, *107*, 103040. DOI: <https://doi.org/10.1016/j.vibspec.2020.103040>.
- (226) Westerhuis, J. A.; Hoefsloot, H. C.; Smit, S.; Vis, D. J.; Smilde, A. K.; van Velzen, E. J.; van Duijnhoven, J. P.; van Dorsten, F. A. Assessment of PLS-DA cross validation. *Metabolomics* **2008**, *4*, 81-89. DOI: <https://doi.org/10.1007/s11306-007-0099-6>.
- (227) *Sequential and orthogonalized Partial Least Squares (SO-PLS)*; Rome Chemometrics, **2020**. <https://www.chem.uniroma1.it/romechemometrics/research/algorithms/so-pls/> (accessed 22.03.2023).

- (228) *PLS-DA: Partial Least Squares-Discriminant Analysis*; Rome Chemometrics <https://www.chem.uniroma1.it/romechemometrics/research/algorithms/plsda/> (accessed 22.03.2023).
- (229) Sjöström, M.; Wold, S.; Söderström, B. PLS discriminant plots. In *Pattern recognition in practice*, Elsevier, **1986**; pp 461-470.
- (230) Ståhle, L.; Wold, S. Partial least squares analysis with cross-validation for the two-class problem: A Monte Carlo study. *Journal of Chemometrics* **1987**, *1* (3), 185-196. DOI: <https://doi.org/10.1002/cem.1180010306>.
- (231) Wong, T.-T. Performance evaluation of classification algorithms by k-fold and leave-one-out cross validation. *Pattern recognition* **2015**, *48* (9), 2839-2846. DOI: <https://doi.org/10.1016/j.patcog.2015.03.009>.
- (232) Sokolova, M.; Lapalme, G. A systematic analysis of performance measures for classification tasks. *Information Processing & Management* **2009**, *45* (4), 427-437. DOI: <https://doi.org/10.1016/j.ipm.2009.03.002>.

Curriculum Vitae

EDUCATION

PhD ETH Zurich – Institute of Pharmaceutical Sciences July 2021 - July 2024
Pharmaceutical Analytics

Thesis: “Terpene Patterns Across Analytical Techniques for Advanced Authenticity Control of Natural Products”

Advisors: Prof. Dr. Gisbert Schneider
Prof. Dr. Robin Teufel
Dr. Christian Steuer

MS ETH Zurich, Pharmacy September 2017 - October 2019

Thesis: “Untargeted Metabolomics Analysis of Gamma-Hydroxybutyric Acid (GHB) in Human Serum and Urine Samples from a Randomized Placebo-Controlled Crossover Study”

Advisors: Prof. Dr. Gisbert Schneider
PD Dr. Andrea Steuer
Dr. Christian Steuer

BS ETH Zurich, Pharmaceutical Sciences September 2014 - August 2017

PUBLICATIONS

Journal Publications

Raeber J, Bajor B, Poetzsch M, Steuer C. Comprehensive analysis of chemical and enantiomeric stability of terpenes in *Cannabis sativa* L. flowers. *Phytochemical Analysis* 2024.

Raeber J, Poetzsch M, Schmidli A, Favrod S, Steuer C. Simultaneous quantification of terpenes and cannabinoids by reversed-phase LC-APCI-MS/MS in *Cannabis sativa* L. samples combined with a subsequent chemometric analysis. *Analytical and Bioanalytical Chemistry* 2024.

Raeber J, Steuer C. Exploring new dimensions: Single and multi-block analysis of essential oils using DBDI-MS and FT-IR for enhanced authenticity control. *Analytica Chimica Acta* 2023, 1277, 341657.

Raeber J, Favrod S, Steuer C. Determination of Major, Minor and Chiral Components as Quality and Authenticity Markers of *Rosa damascena* Oil by GC-FID. *Plants*. 2023; 12(3):506.

Steuer C, Quattrini D, **Raeber J**, Waser P, Steuer AE. Easy and convenient millimole-scale synthesis of new, potential biomarkers for gamma-hydroxybutyric acid (GHB) intake: Feasible for analytical laboratories. *Drug Test Anal.* 2022; 14(8): 1460- 1470.

Steuer AE, **Raeber J**, Simbuerger F, Dornbierer DA, Bosch OG, Quednow BB, Seifritz E, Kraemer T. Towards Extending the Detection Window of Gamma-Hydroxybutyric Acid – An Untargeted Metabolomics Study in Serum and Urine Following Controlled Administration in Healthy Men. *Metabolites.* 2021; 11(3):166.

Steuer AE, **Raeber J**, Steuer C, Boxler MI, Dornbierer DA, Bosch OG, Quednow BB, Seifritz E, Kraemer T. Identification of new urinary gamma-hydroxybutyric acid markers applying untargeted metabolomics analysis following placebo-controlled administration to humans. *Drug Test Anal.* 2019; 11: 813– 823.

CONFERENCES AND POSTERS

International Congress on Natural Products Research, Krakow, Poland, July 2024, Poster presentation: “Simultaneous Quantification of Terpenes and Cannabinoids in *Cannabis Sativa* L. by Reversed Phase LC-APCI-MS/MS”

International Congress and Annual Meeting of the Society for Medicinal Plant and Natural Product Research (GA), Trinity College Dublin, July 2023, Poster presentation: “Exploring New Dimensions : Single and Multi-Block Analysis of Essential Oils Using DBDI-MS and FT-IR for Enhanced Authenticity Control”

Chemometrics in Analytical Chemistry (CAC), University of Rome, August 2022
Poster presentation: “Fast and Convenient Authenticity Control of Natural Products Using Mass Spectrometry and Chemometrics”

Swiss Pharma Science Day (SPhSD), University of Berne, August 2022
Poster presentation: “Terpenomics for Authenticity Control of Natural Products Using Mass Spectrometry and Chemometrics”

Ions and Photons in Analytical Science (IPAS), ETH Zurich, April 2022
Poster presentation: “Authenticity Control of Natural Products using Mass Spectrometry combined with Chemometrics”

HONORS AND AWARDS

Society for Medicinal Plant and Natural Product Research Travel Award 2024
Travel award towards participating at the International Congress on Natural Products Research in Krakow, Poland

Swiss Group for Mass Spectrometry (SGMS) Student Travel Award 2023
Award to students working in mass spectrometry

FeMS Empowerment Award 2022
Award towards women working in mass spectrometry

TopPharm Award 2019
Yearly awarded to pharmacy students achieving the best overall result in the federal exam for pharmacists in Switzerland

Appendix

Chapter 1: Separation techniques for terpenes covering minor, major and chiral components

2.1. Determination of Major, Minor and Chiral Components as Quality and Authenticity Markers of *Rosa damascena* Oil by GC-FID

Some of the data presented here was published in the following publication:

Raeber J, Favrod S, Steuer C. Determination of Major, Minor and Chiral Components as Quality and Authenticity Markers of *Rosa damascena* Oil by GC-FID. *Plants* 2023; 12. DOI: 10.3390/plants12030506

Table A1: Chemicals and reagents. Adapted from Raeber et al.¹⁰

Chemical	Purity	Manufacturer	Origin
phenylethanol	NA	Fluka Chemie GmbH	Buchs, Switzerland
limonene	NA	Fluka Chemie GmbH	Buchs, Switzerland
α -terpinene	pract	Fluka Chemie GmbH	Buchs, Switzerland
camphene	95%	Sigma Aldrich	St. Louis, MO, USA
β -damascone	>95%	Sigma Aldrich	St. Louis, MO, USA
citronellyl acetate	>95%	Sigma Aldrich	St. Louis, MO, USA
β -damascenone	natural	Sigma Aldrich	St. Louis, MO, USA
(+)- β -pinene	analytical standard	Sigma Aldrich	St. Louis, MO, USA
(-)- β -pinene	99%	Sigma Aldrich	St. Louis, MO, USA
(+)- α -pinene	\geq 99%	Sigma Aldrich	St. Louis, MO, USA
(-)- α -pinene	analytical standard	Sigma Aldrich	St. Louis, MO, USA
farnesol	95%	Sigma Aldrich	St. Louis, MO, USA
geranyl acetate	>99%	Sigma Aldrich	St. Louis, MO, USA
linalool	97%	Sigma Aldrich	St. Louis, MO, USA
p-cymene	99%	Sigma Aldrich	St. Louis, MO, USA
rose oxide	cis/trans mixture	Sigma Aldrich	St. Louis, MO, USA
cis-3-hexen-1-ol internal standard (IS)	98%	Sigma Aldrich	St. Louis, MO, USA
n-alkanes	C8-C20, C21-C40, analytical standard	Sigma Aldrich	St. Louis, MO, USA
eugenol	NA	Systema Natura GmbH	Flintbek, Germany
β -caryophyllene	NA	Systema Natura GmbH	Flintbek, Germany
citral	cis/trans mixture, >98%	TCI Chemical	Eschborn, Germany
neryl acetate	>95%	TCI Chemical	Eschborn, Germany
citronellol	95%	Acros Organics	Geel, Belgium
geraniol	99%	Acros Organics	Geel, Belgium
nerol	97%	Acros Organics	Geel, Belgium
methyleugenol	NA	Carl Roth GmbH	Karlsruhe, Germany
n-heptane	99.9%	VWR chemicals	Schlieren, Switzerland
helium	6.0	PanGas	Dagmersellen, Switzerland
hydrogen	5.0	PanGas	Dagmersellen, Switzerland

Script A1: MATLAB code for the integration of chromatographic peaks acquired with ChromCard and exported as ASCII files. Code was published by Raeber et al.¹⁰

```
% Script can be used to plot chromatogram data from ChromCard. Download data as a
.txt file to insert (export to ASCII)
% Select retention times and place them as a .txt file
```

```
peak_width          = 0.1; % determine the desired peak width
peak_width_half     = peak_width/2;
retention_times     = [45.35] % Data array of desired Retention times
peak_bounds_start   = abs(retention_times - peak_width_half);
peak_bounds_end     = abs(retention_times + peak_width_half);
peak_bounds         = zeros(1, length(retention_times)*2);
npeaks              = length(peak_bounds)/2;

for i=1:npeaks

    peak_bounds(2*i-1) = peak_bounds_start(i);
    peak_bounds(2*i)   = peak_bounds_end(i);

end

idx_peak_bounds = zeros(1, length(peak_bounds)); % zero vector with number of Peak
bounds
peaks           = zeros(1, npeaks); % zero vector with amount of peaks -> used to
store area under the curve

% upload data as .txt file

Chrom_Data      = readmatrix("Data.txt"); % Data import from ChromCard -
Exportation in Software as ASCII Files
time            = Chrom_Data(:,1); % extract time as vector in minutes
uV              = Chrom_Data(:, end); % extract uV as vector
noiseThresh    = 1100; % read from chromatogram where the noise is about
Ts              = time(2)-time(1); % sampling interval (in what amount of time
is a data point constructed in [min])

noise           = uV;
noise(noise > noiseThresh) = NaN; % NaN=not a number, defines value not as zero
but not defined yet, defines noise as all values below the noise

% Moving Average for noise filtering
T_window       = 1; % min ... width over which the moving average is taken
nSamples       = T_window / Ts; % amounts of data points that are collected over a
minute
noise_avg      = movmean(noise, nSamples, 'omitnan'); % movmean -> returns mean
values over an array -> sliding window. Noise (is uV below threshold), nSamples is
data points for a certain time frame and omitnan a function which jumps over NaN
values
```

```

% Determine Peak Index and Integration

for i=1:npeaks
    timeDiffStart      = abs(time - peak_bounds(2*i - 1)); % find minimum
difference between peak bounds and time
    timeDiffMinStart   = min(timeDiffStart);
    idxPkStart         = find(timeDiffStart == timeDiffMinStart); % find index of
minimum (equal to index of startpeak)
    timeDiffEnd        = abs(time - peak_bounds(2*i));
    timeDiffMinEnd     = min(timeDiffEnd);
    idxPkEnd           = find(timeDiffEnd == timeDiffMinEnd);
    idx_peak_bounds(2*i-1) = idxPkStart;
    idx_peak_bounds(2*i)   = idxPkEnd;
    peaks(i)            = trapz(time(idxPkStart:idxPkEnd,1),
uV(idxPkStart:idxPkEnd,1) - noise_avg(idxPkStart))*60; % Integration + Offset
correction, Unit is s*uV

    meep = noise_avg(idxPkStart);
    if (isscalar(meep) && isfinite(meep))
        % Plot area of peaks
        plot(time,uV)
        xlabel('time [min]');
        ylabel('uV');
        legend('Data');
        hold on;
    %     area(time(idxPkStart:idxPkEnd,1),uV(idxPkStart:idxPkEnd,1),
noise_avg(idxPkStart))

        area(time(idxPkStart:idxPkEnd,1),uV(idxPkStart:idxPkEnd,1), meep)

        colororder('red')
    end
end

area = transpose(peaks);
area_RT = [retention_times(:), area(:)];

% Exportation of data

filename = 'Filename.xlsx'
xlswrite(filename, area_RT)

```

Table A2: Results for testing the robustness of a GC-FID method using a DB-wax column. Taken from Raeber et al.¹⁰

Analyte		α -pinene	camphene	(-)- β -pinene	α -terpinene	limonene	p-cymene	(+/-)-rose oxide	cis-3-hexen-1-ol	linalool	β -caryophyllene	β -damascenone
Standard method	RT [min]	4.25	5.36	6.84	10.98	12.43	18.28	22.52	24.03	29.00	29.83	31.17
	R _s	16.1	12.3	22.7	6.0	28.3	34.1	17.6	85.8	11.3	16.8	6.3
FID temp. 275 °C	Fold change	1.02	1.03	1.01	1.03	1.01	1.01	1.04	1.00	1.04	1.04	1.18
FID temp. 225 °C	Fold change	0.95	0.96	0.95	0.94	0.96	0.93	0.92	1.00	0.92	0.88	0.87
Inlet temp. 240 °C	Fold change	1.05	1.05	1.06	1.06	1.07	1.05	1.06	1.00	1.07	1.09	1.08
Inlet. temp. 220 °C	Fold change	0.94	0.96	0.93	0.93	0.93	0.92	0.91	1.00	0.92	0.89	0.88
Split ratio 1:100	Fold change	1.07	1.06	1.08	1.07	1.09	1.08	1.11	1.00	1.10	1.13	1.10
Split ratio 1:25	Fold change	1.10	1.11	1.10	1.18	1.14	1.12	1.14	1.00	1.13	1.16	1.15
Flow 2.5 ml/min	RT [min]	3.67	4.65	5.90	9.43	10.67	16.78	21.54	23.20	28.27	28.99	30.45
	R _s	12.2	12.9	27.2	7.2	35.3	35.1	17.5	68.8	8.4	14.4	5.0
Flow 1.5 ml/min	RT [min]	5.16	6.54	8.31	13.31	15.07	19.93	23.74	25.12	29.93	30.86	32.11
	R _s	11.6	13.1	34.7	8.7	27.3	35.7	18.4	73.2	11.8	15.4	6.5
Temperature ramp 7.5 °C/min	RT [min]	4.24	5.37	6.82	10.91	12.35	17.82	21.04	22.12	25.56	26.26	27.09
	R _s	12.3	11.9	22.3	6.7	33.4	35.3	14.8	70.0	14.2	16.9	7.1
Temperature ramp 2.5 °C/min	RT [min]	4.24	5.37	6.82	10.92	12.36	18.87	25.39	28.13	37.31	38.24	41.33
	R _s	13.3	12.2	26.9	7.7	48.0	27.1	15.2	70.3	8.4	23.7	7.4

Analyte		citronellyl acetate	citral	neryl acetate	geranyl acetate	citronellol	nerol	phenylethanol	geraniol	methyl Eugenol	eugenol	farnesol
Standard method	RT [min]	31.70	32.00	33.17	33.86	34.17	34.87	35.00	35.89	39.10	41.92	45.38
	R _s	4.0	14.2	8.5	4.8	10.6	2.4	13.0	44.0	38.6	47.6	NA
FID temp. 275 °C	Fold change	1.08	1.10	1.06	1.04	1.05	1.05	1.05	1.05	1.04	1.20	1.06
FID temp. 225 °C	Fold change	0.88	0.89	0.89	0.88	0.90	0.92	0.91	0.91	0.89	0.84	0.85
Inlet temp. 240 °C	Fold change	1.02	1.08	1.07	1.07	1.10	1.09	1.10	1.08	1.04	1.06	1.02
Inlet. temp. 220 °C	Fold change	0.95	0.89	0.87	0.88	0.92	0.94	0.90	0.88	0.85	0.88	0.95
Split ratio 1:100	Fold change	1.07	0.94	1.11	1.07	1.17	1.16	1.17	1.13	1.13	1.19	1.14
Split ratio 1:1:25	Fold change	1.13	1.20	1.14	1.14	1.13	1.17	1.17	1.14	1.16	1.10	1.16
Flow 2.5 ml/min	RT [min]	30.96	31.25	32.44	33.13	33.47	34.16	34.30	35.19	38.37	41.17	44.65
	R _s	2.9	11.7	6.8	4.5	10.9	1.6	10.0	37.0	28.5	43.2	NA
Flow 1.5 ml/min	RT [min]	32.64	33.00	34.11	34.79	35.08	35.80	35.99	36.81	40.04	42.88	46.31
	R _s	4.4	13.6	8.4	4.1	11.8	2.7	10.8	42.3	37.2	45.0	NA
Temperature ramp 7.5 °C/min	RT [min]	27.44	27.72	28.45	28.91	29.10	29.60	29.74	30.77	32.47	34.41	36.68
	R _s	5.7	11.0	7.0	3.4	11.3	2.5	9.6	44.8	39.5	46.2	NA
Temperature ramp 2.5 °C/min	RT [min]	42.29	42.75	45.11	46.47	47.22	48.47	48.67	50.54	56.63	62.00	69.07
	R _s	3.5	16.6	9.6	5.3	8.8	1.4	13.1	64.2	37.7	54.5	NA

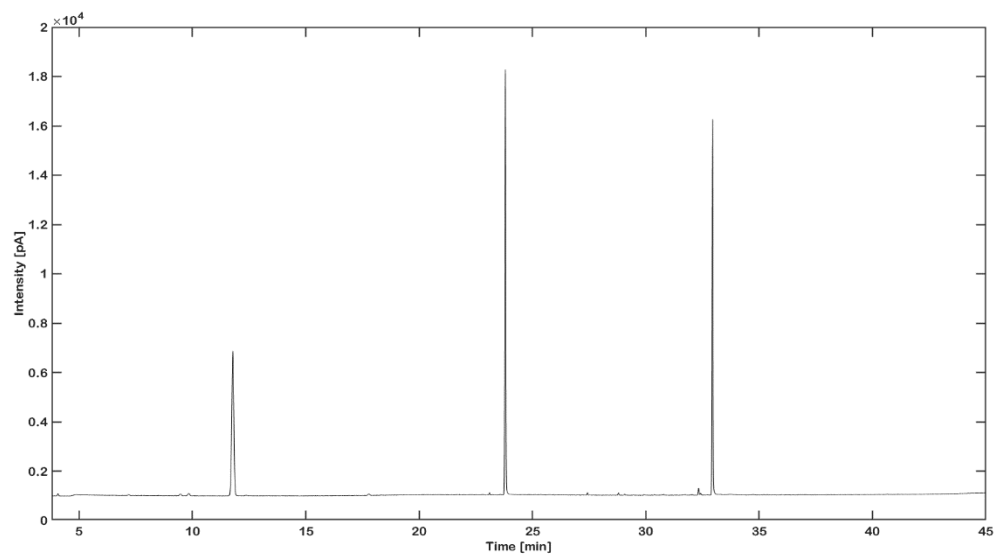
Table A3: Results for testing the robustness of a GC-FID method using a BGB 178 30 % CD column. Taken from Raeber et al.¹⁰

Analyte		α -pinene	camphene	camphene	(-)- β -pinene	cis-3-hexen-1-ol	α -terpinene	limonene	p-cymene	(+)-rose oxide	(-)-rose oxide	linalool	linalool	phenylethanol	cis/trans-citral	citronellol
Standard method	RT [min]	9.58	9.77	10.27	11.49	15.21	16.26	17.06	17.16	20.28	20.43	23.18	23.87	29.8 ₂	30.66	31.95
	R _s	2.4	5.9	12.0	28.6	8.3	7.9	1.2	30.6	1.5	27.1	6.7	58.4	6.7	9.0	0.9
FID temp. 280 °C	Fold change	1.06	1.10	1.07	1.07	1.00	1.07	1.09	1.05	1.10	1.10	1.14	1.13	1.09	1.13	1.07
FID temp. 240 °C	Fold change	1.03	1.02	1.05	1.04	1.00	1.04	1.07	0.98	1.09	1.07	1.08	1.07	1.04	1.06	1.08
Inlet temp. 260 °C	Fold change	1.02	1.07	1.02	1.02	1.00	1.04	1.02	1.07	1.06	1.07	1.05	1.05	1.03	1.05	0.99
Inlet temp. 220 °C	Fold change	0.94	0.93	0.94	0.92	1.00	0.86	0.91	0.93	0.91	0.89	0.95	0.95	0.92	0.91	0.91
Split flow 200 ml/min	Fold change	1.07	1.08	1.07	1.08	1.00	1.09	1.09	1.10	1.14	1.14	1.14	1.14	1.09	1.17	1.09
Split flow 80 ml/min	Fold change	0.98	1.00	0.98	0.98	1.00	0.95	1.00	0.94	0.98	0.97	1.01	1.01	0.99	1.00	1.01
Constant flow 120 kPa	RT [min]	8.51	8.67	9.17	10.29	13.99	14.90	15.67	15.75	18.74	18.89	21.71	22.41	28.3 ₅	28.99	30.35
	R _s	1.4	4.5	10.0	27.1	6.7	5.6	0.6	24.0	1.4	22.6	5.6	43.8	41.6	11.8	0.9
Flow const. Pressure 80 kPa	RT [min]	11.05	11.30	11.83	13.13	16.82	18.09	18.89	19.02	22.28	22.43	25.07	25.74	31.6 ₇	32.79	33.98
	R _s	2.3	4.8	11.8	30.03	8.6	6.5	1.3	26.7	1.2	19.5	4.9	43.7	8.3	8.8	0.7
Temperature ramp 4 °C/min	RT [min]	8.09	8.28	8.59	9.38	11.20	12.12	12.57	12.66	14.49	14.57	15.78	16.09	19.0 ₄	19.19	20.40
	R _s	2.6	4.2	10.7	19.2	9.7	5.5	1.1	27.7	1.2	17.8	4.6	45.8	1.6	10.6	0.7
Temperature ramp 1 °C/min	RT [min]	10.90	11.06	11.81	13.51	20.12	21.17	22.52	22.52	27.66	27.92	33.71	35.16	46.8 ₇	49.46	50.26
	R _s	1.3	6.1	11.9	31.5	5.0	7.1	24.1	24.1	1.4	30.5	6.4	51.6	12.7	4.4	1.2

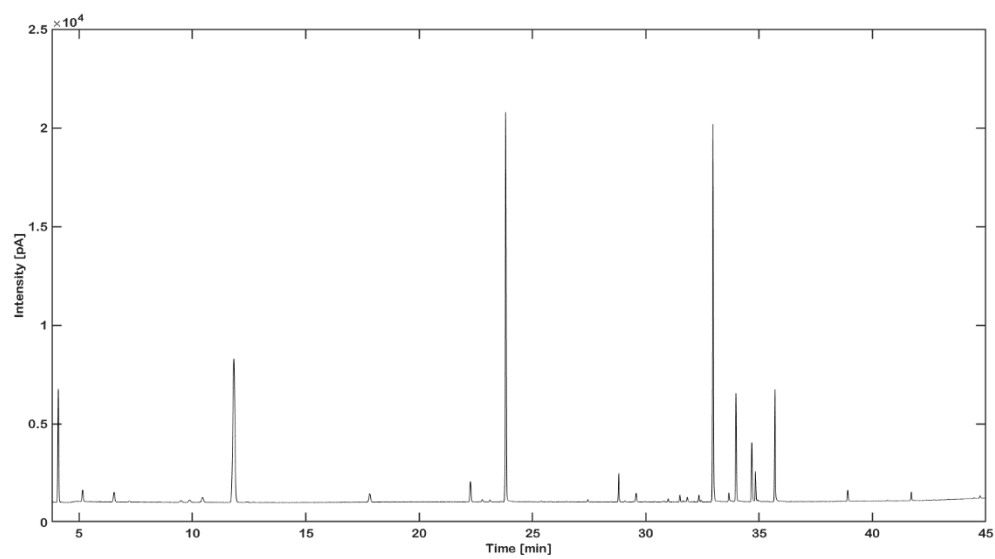
Analyte		citronellol	nerol	cis/trans-citral	geraniol	citronellyl acetate	citronellyl acetate	neryl acetate	(cis/trans)- β -damascenone	geranyl acetate	β -caryophyllene	(cis/trans)- β -damascenone	β -damascenone	eugenol	methyleugenol	farnesol
Standard method	RT [min]	32.06	32.35	33.26	34.30	35.16	35.27	35.87	36.70	37.78	37.87	38.11	38.64	39.61	41.11	58.67
	R _s	2.2	7.7	7.3	5.9	0.8	4.1	6.5	8.4	0.7	1.9	4.0	7.6	11.6	76.1	-
FID temp. 280 °C	RT [min]	32.06	32.35	33.26	34.30	35.16	35.27	35.87	36.70	37.78	37.87	38.11	38.64	39.61	41.11	58.67
	Fold change	1.02	1.11	1.11	1.13	1.16	1.12	1.13	1.13	1.05	1.03	1.16	1.14	1.14	1.12	1.15
FID temp. 240 °C	RT [min]	32.06	32.35	33.26	34.30	35.16	35.27	35.87	36.70	37.78	37.87	38.11	38.64	39.61	41.11	58.67
	Fold change	1.04	1.06	1.06	1.07	1.14	1.09	1.07	1.09	1.01	0.96	1.10	1.09	1.15	1.12	1.08
Inlet temp. 260 °C	RT [min]	32.06	32.35	33.26	34.30	35.16	35.27	35.87	36.70	37.78	37.87	38.11	38.64	39.61	41.11	58.67
	Fold change	0.97	1.05	1.04	1.05	1.19	1.20	1.05	1.09	0.98	1.01	1.06	1.03	1.08	1.08	1.04
Inlet. temp. 220 °C	RT [min]	32.06	32.35	33.26	34.30	35.16	35.27	35.87	36.70	37.78	37.87	38.11	38.64	39.61	41.11	58.67
	Fold change	0.89	0.91	0.90	0.90	0.94	0.91	0.89	0.89	0.89	0.87	0.91	0.88	0.89	0.90	0.84
Split flow 200 ml/min	Fold change	1.05	1.13	1.13	1.16	1.29	1.28	1.13	1.14	1.17	1.18	1.17	1.16	1.19	1.17	1.31
Split flow 80 ml/min	Fold change	1.00	0.92	0.98	1.01	1.06	1.03	0.97	0.96	1.04	1.03	1.00	0.98	1.03	1.00	0.99
Constant flow 120 kPa	RT [min]	30.47	30.75	31.55	32.69	33.38	33.51	34.06	34.76	35.97	35.97	36.35	36.70	37.79	39.28	56.67
	R _s	1.9	6.2	7.7	4.8	1.0	4.3	5.4	7.3	2.4	NA	2.3	7.5	11.2	123.6	NA
Flow const. Pressure 80 kPa	RT [min]	34.07	34.36	35.41	36.34	37.40	37.50	38.15	39.16	40.05	40.34	40.34	41.10	41.93	43.45	61.16
	R _s	2.1	7.4	6.5	7.4	0.7	4.6	7.1	6.3	1.9	5.0	NA	5.4	10.0	130.6	NA
Temperature ramp 4 °C/min	RT [min]	20.45	20.6	21.27	21.61	22.38	22.38	22.82	23.53	23.76	23.85	24.14	24.50	24.75	25.54	34.12
	R _s	2.0	8.2	4.2	7.6	3.6	3.6	6.3	2.5	1.1	3.6	4.4	2.7	9.3	68.9	NA
Temperature ramp 1 °C/min	RT [min]	50.52	51.08	52.03	54.83	55.23	55.54	56.36	57.08	59.49	60.26	60.92	61.17	63.68	66.56	100.56
	R _s	2.3	3.9	11.5	1.6	1.3	3.4	3.1	10.3	3.3	2.8	1.1	9.0	11.4	120.1	NA

Figure A1: Spiking experiments on DB-wax column.

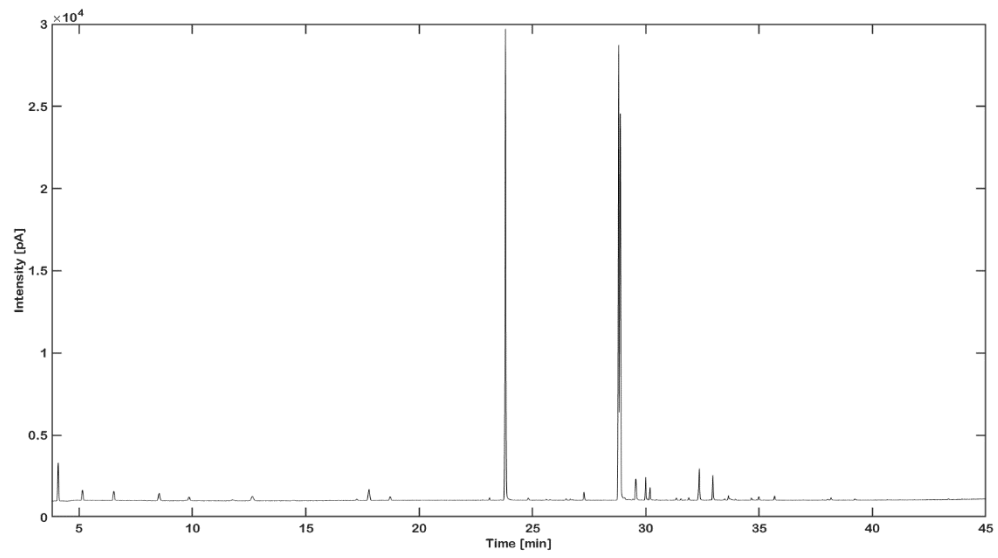
Caraway EO unspiked



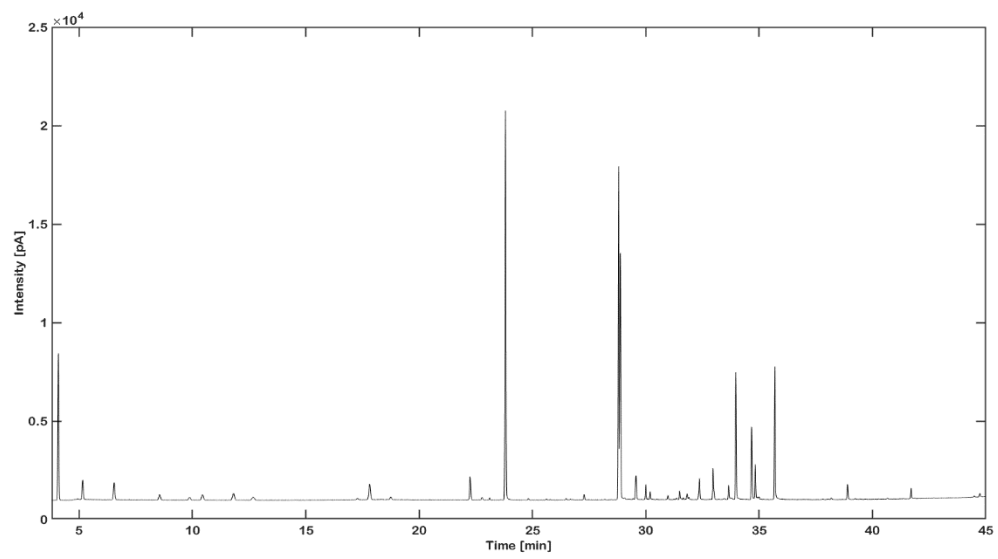
Caraway EO spiked



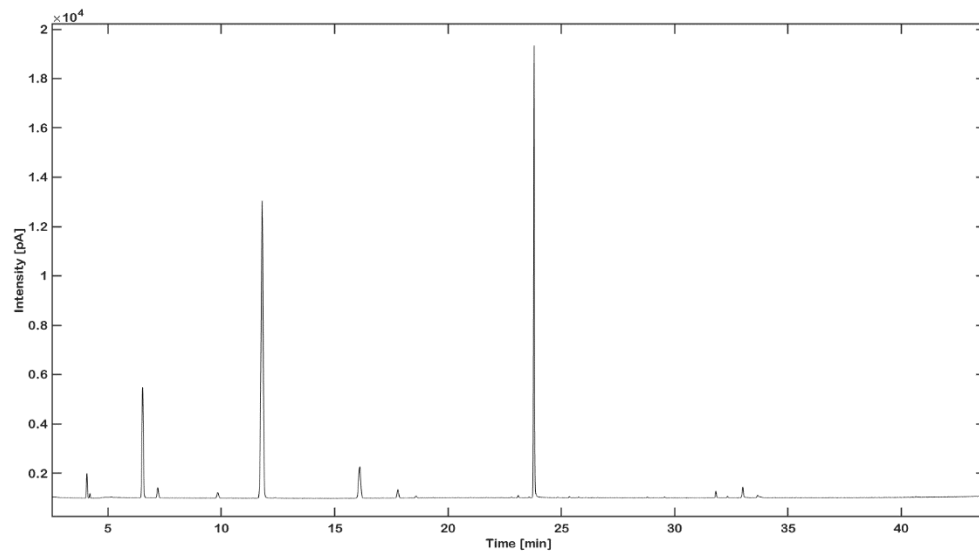
Lavender EO unspiked



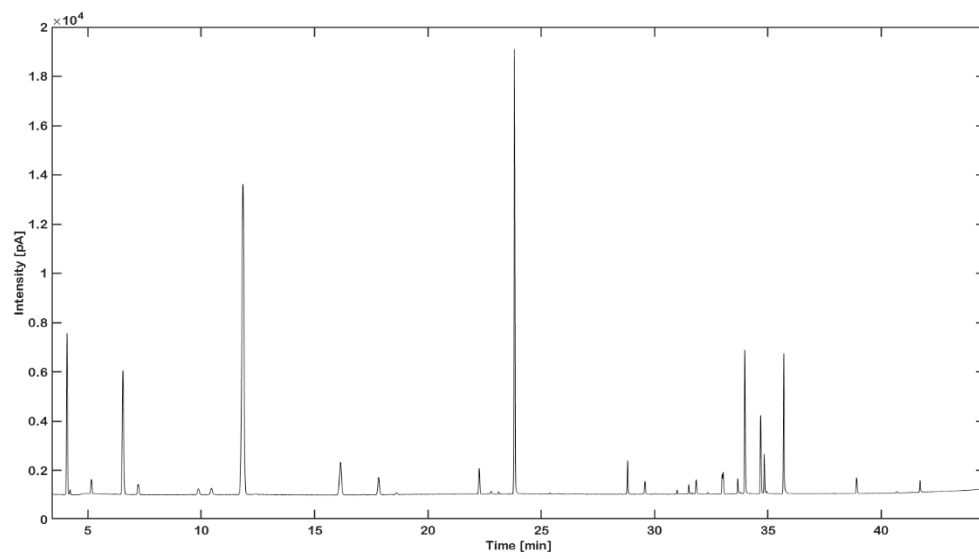
Lavender EO spiked



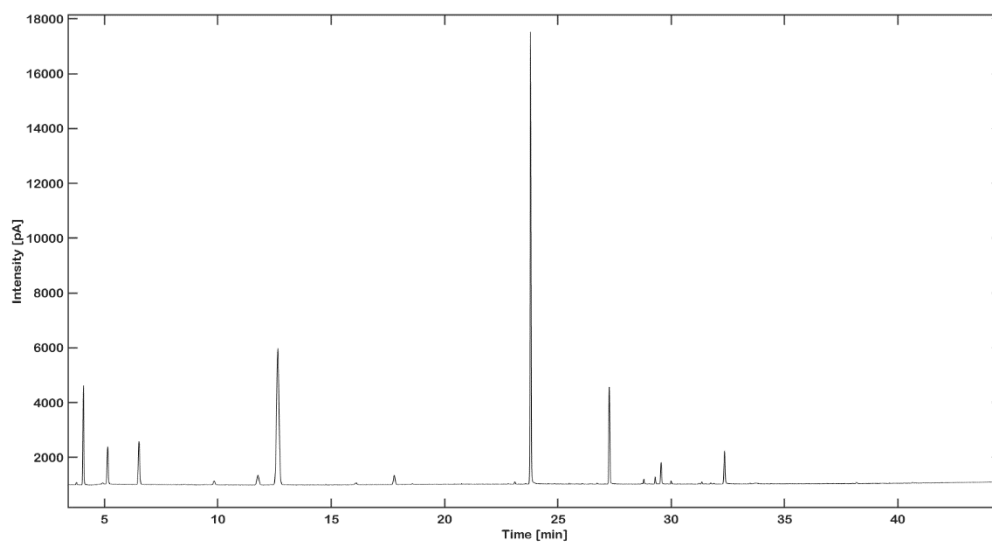
Lemon EO unspiked



Lemon EO spiked



Rosmary EO unspiked



Rosmary EO spiked

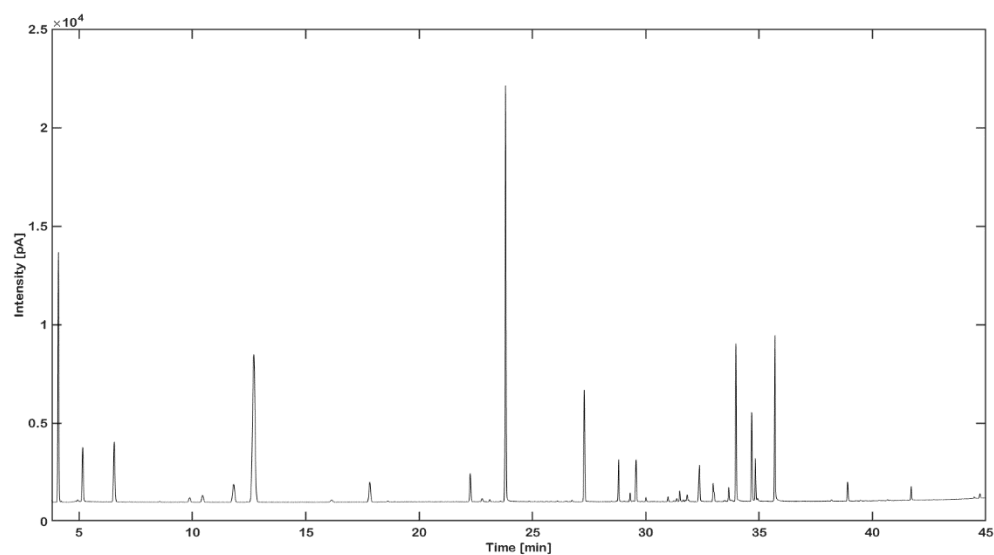
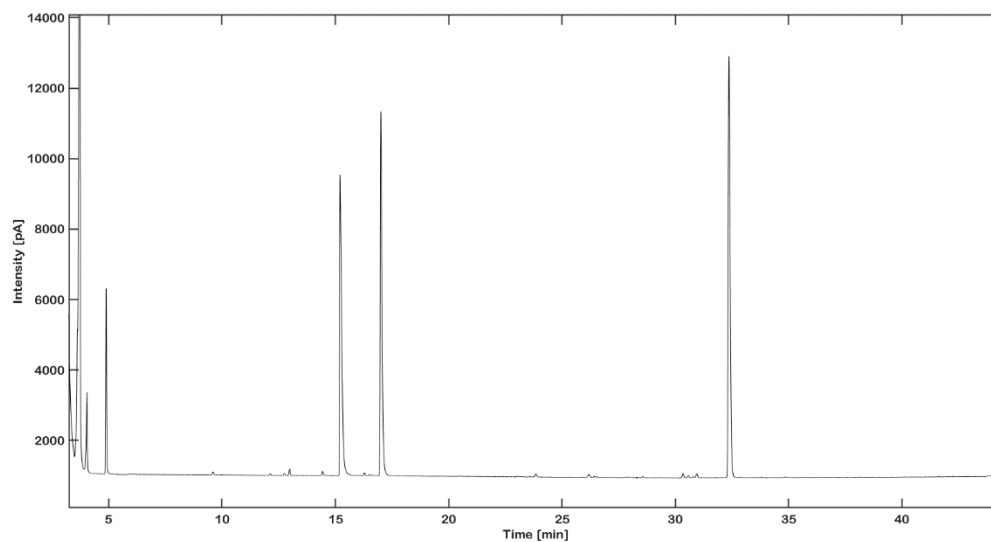
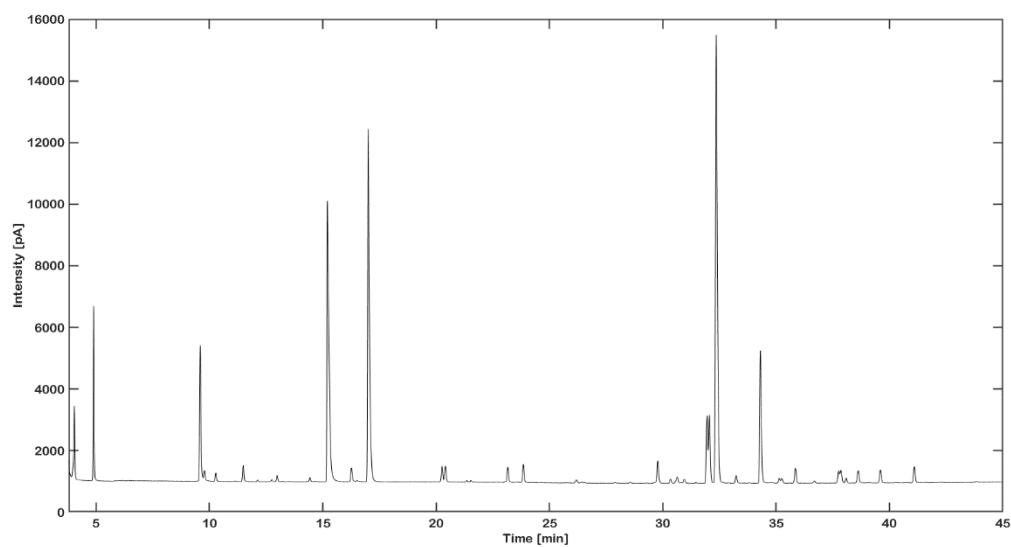


Figure A2: Spiking experiments on BGB 178 30% CD column.

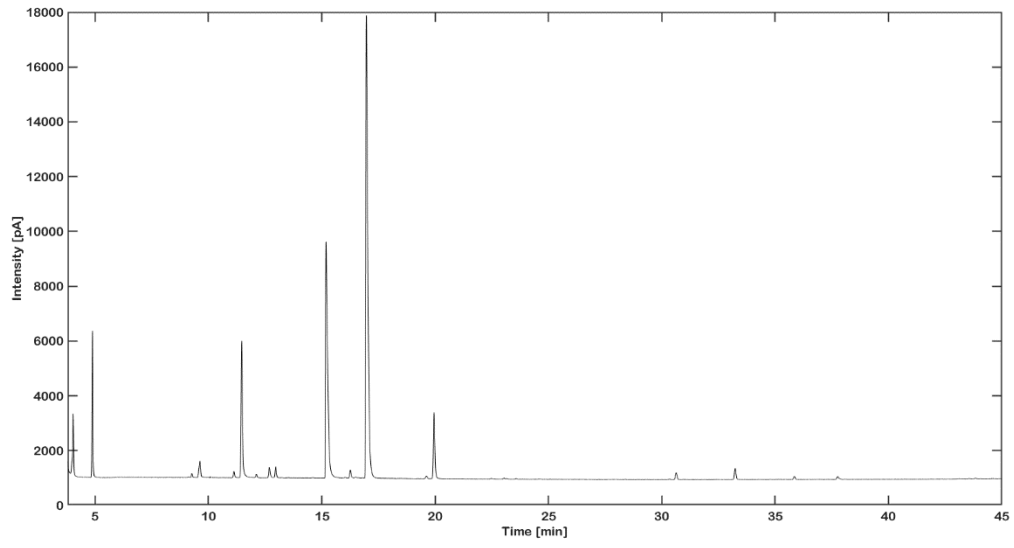
Caraway EO unspiked



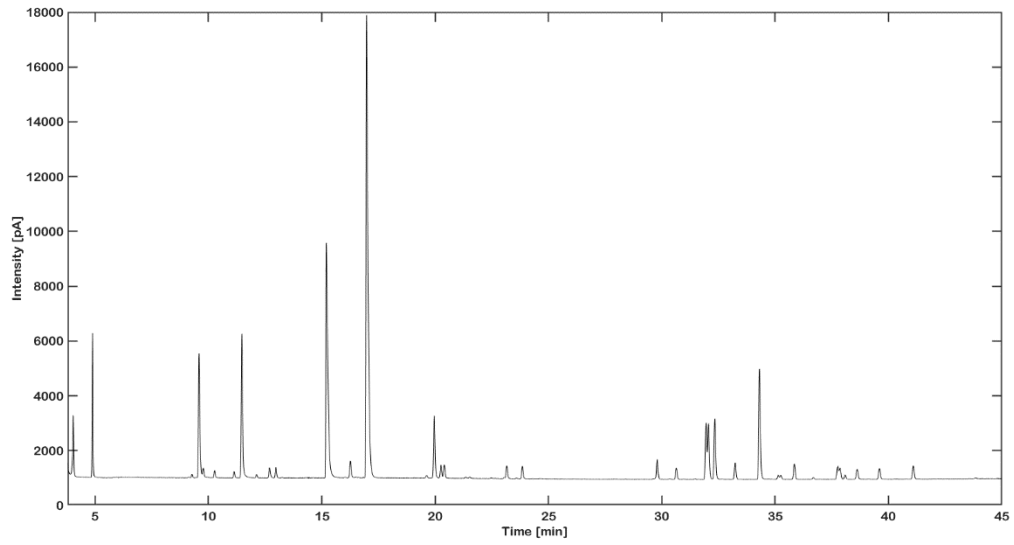
Caraway EO spiked



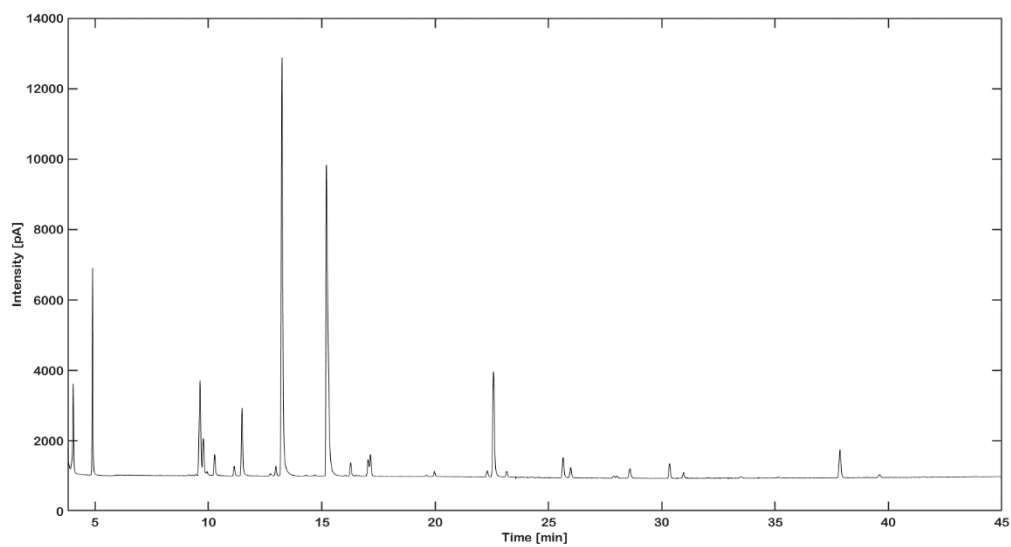
Lemon EO unspiked



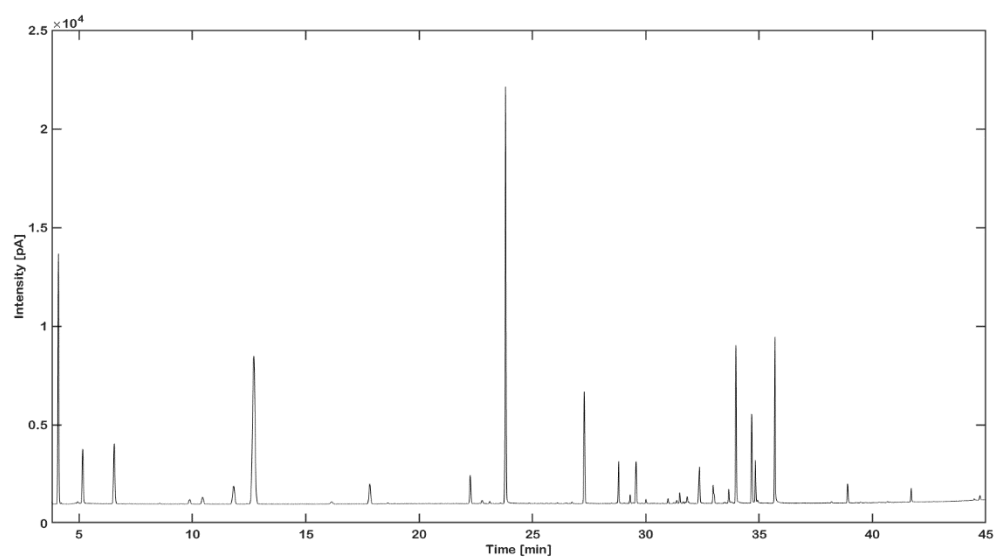
Lemon EO spiked



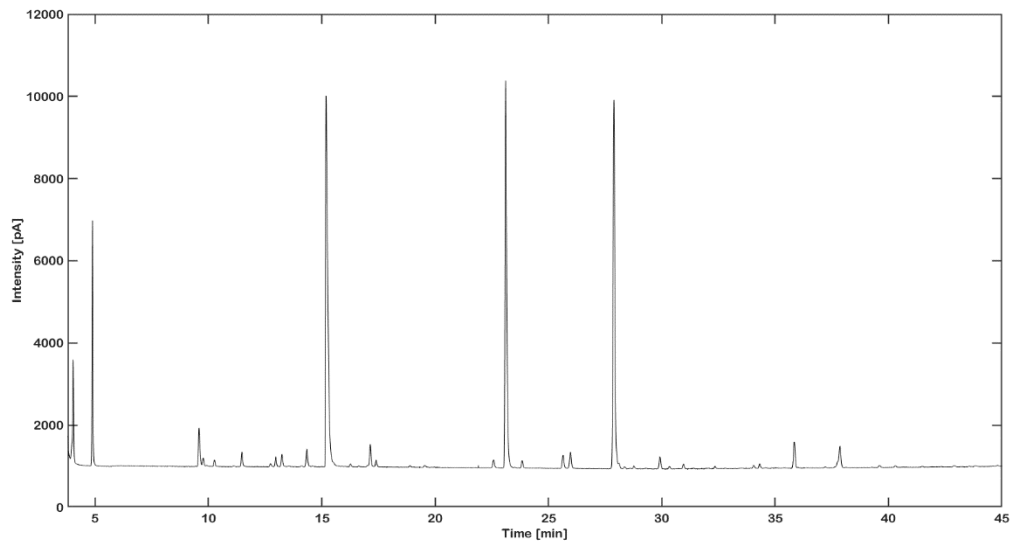
Rosmary EO unspiked



Rosmary EO spiked



Lavender EO unspiked



Lavender EO spiked

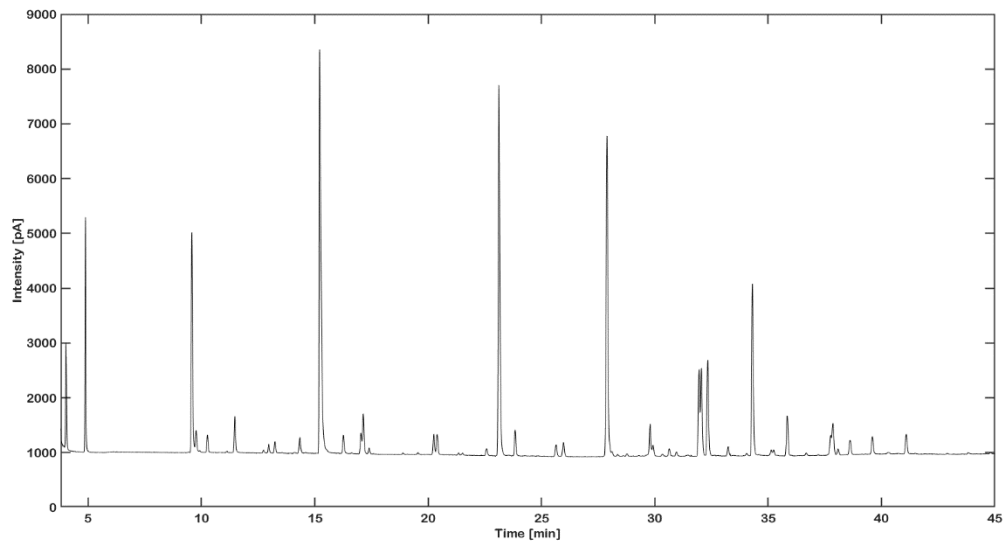


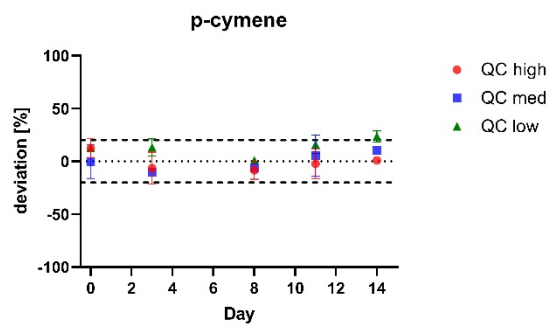
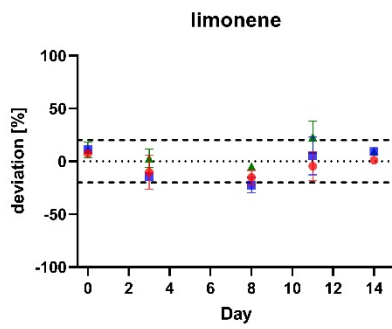
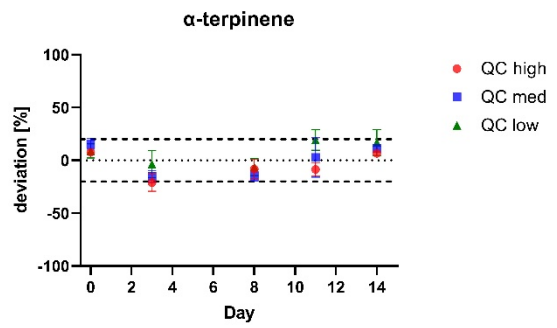
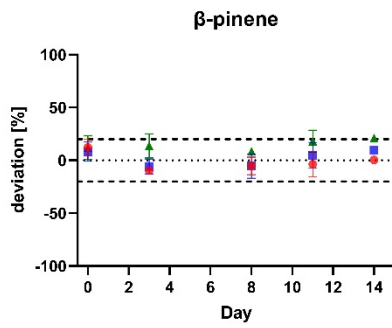
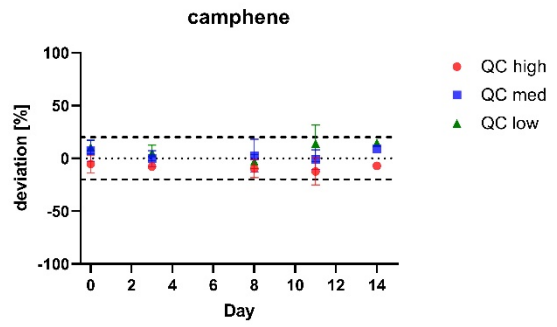
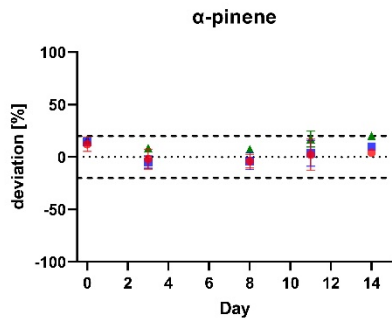
Table A4: Concentration profile incl. standard deviation (n=3) for terpenes acquired on DB-wax column using GC-FID. Table taken from Raeber et al.¹⁰

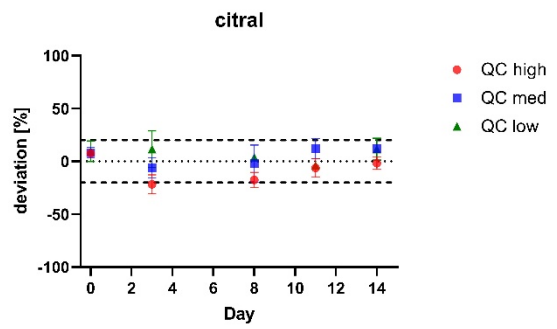
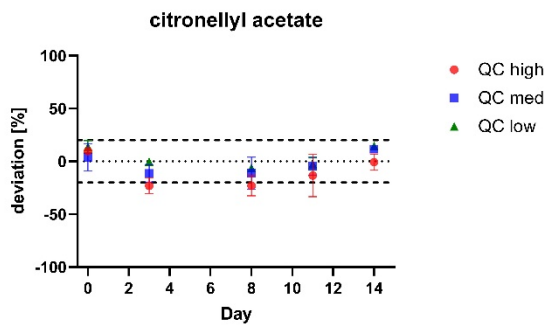
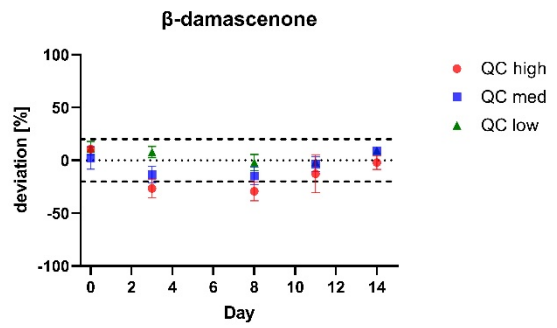
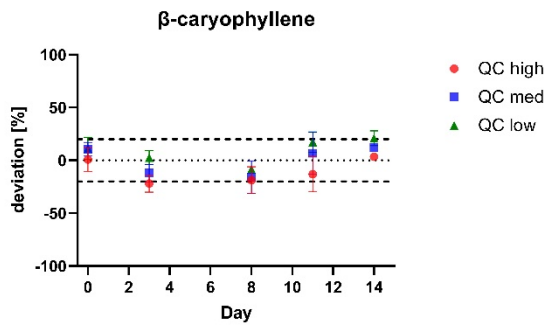
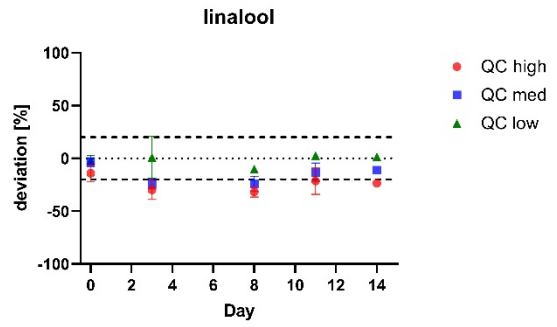
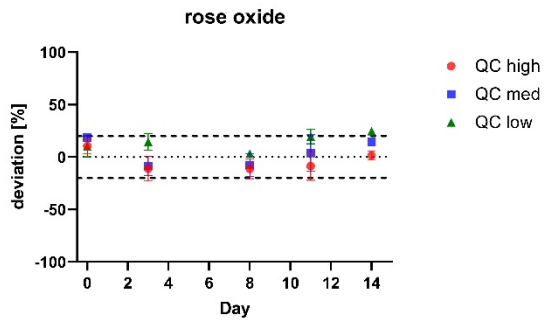
Species	<i>R. damascena</i>	<i>P. graveolens</i>	<i>P. graveolens</i>	<i>R. damascena</i>	<i>R. damascena</i>	<i>R. damascena</i>	<i>R. damascena</i>	<i>R. damascena</i>	<i>R. damascena</i>	<i>R. damascena</i>
Quality Origin	pure Bulgaria	pure NA	pure NA	10% Morocco	pure Turkey	pure Bulgaria	pure Bulgaria	pure Turkey	pure Turkey	10% Bulgaria
	Conc. [mg/ml]	Conc. [mg/ml]	Conc. [mg/ml]	Conc. [mg/ml]	Conc. [mg/ml]	Conc. [mg/ml]	Conc. [mg/ml]	Conc. [mg/ml]	Conc. [mg/ml]	Conc. [mg/ml]
α-pinene	1.62 ± 0.00	1.99 ± 0.02	3.24 ± 0.02	0.51 ± 0.01	5.11 ± 0.01	6.24 ± 0.04	2.94 ± 0.01	3.60 ± 0.02	14.24 ± 0.05	0.58 ± 0.03
camphene	0.03 ± 0.00	0.04 ± 0.00	0.05 ± 0.00	n.d.	0.04 ± 0.00	0.05 ± 0.00	0.04 ± 0.00	0.04 ± 0.00	0.05 ± 0.00	0.03 ± 0.00
β-pinene	0.41 ± 0.00	0.04 ± 0.00	0.06 ± 0.00	0.16 ± 0.00	2.05 ± 0.08	2.19 ± 0.01	0.70 ± 0.00	1.45 ± 0.03	2.78 ± 0.08	0.16 ± 0.01
α-terpinene	0.02 ± 0.00	0.04 ± 0.00	0.07 ± 0.00	n.d.	0.05 ± 0.00	0.14 ± 0.00	0.03 ± 0.00	0.12 ± 0.00	0.21 ± 0.02	0.02 ± 0.00
limonene	0.12 ± 0.00	1.46 ± 0.05	1.99 ± 0.09	0.25 ± 0.01	0.28 ± 0.00	0.33 ± 0.00	0.23 ± 0.00	0.25 ± 0.00	0.40 ± 0.00	0.23 ± 0.91
p-cymene	0.21 ± 0.00	0.42 ± 0.01	1.06 ± 0.01	0.09 ± 0.00	0.55 ± 0.01	0.25 ± 0.00	0.49 ± 0.00	0.38 ± 0.00	0.67 ± 0.00	0.03 ± 0.00
rose oxide	6.18 ± 0.03	16.12 ± 0.20	18.46 ± 0.14	0.26 ± 0.00	2.67 ± 0.07	1.75 ± 0.04	2.83 ± 0.05	4.92 ± 0.00	2.12 ± 0.02	0.20 ± 0.01
linalool	14.79 ± 0.09	63.94 ± 0.34	69.88 ± 0.16	1.84 ± 0.04	8.85 ± 0.08	14.27 ± 0.19	17.79 ± 0.09	6.78 ± 0.05	10.51 ± 0.11	1.19 ± 0.04
β-caryophyllene	12.42 ± 0.32	11.12 ± 0.10	13.11 ± 0.09	0.63 ± 0.02	8.90 ± 0.31	8.22 ± 0.14	5.74 ± 0.08	10.13 ± 0.30	8.62 ± 0.90	0.32 ± 0.02
β-damascenone	1.51 ± 0.22	6.45 ± 0.25	6.86 ± 0.10	0.37 ± 0.05	2.41 ± 0.08	1.81 ± 0.14	1.69 ± 0.08	2.12 ± 0.16	2.08 ± 0.01	0.31 ± 0.01
citronellyl acetate	9.89 ± 0.17	8.27 ± 0.07	9.34 ± 0.31	0.53 ± 0.01	9.90 ± 0.17	4.42 ± 0.07	5.21 ± 0.19	9.57 ± 0.11	9.88 ± 0.32	0.25 ± 0.01
citral	11.81 ± 0.23	9.19 ± 0.06	10.66 ± 0.06	0.76 ± 0.08	5.68 ± 0.12	12.89 ± 0.22	13.07 ± 0.02	6.93 ± 0.14	7.92 ± 0.30	0.98 ± 0.04
neryl acetate	15.27 ± 0.24	12.74 ± 0.13	13.36 ± 0.08	0.49 ± 0.01	7.47 ± 0.12	9.52 ± 0.16	10.11 ± 0.07	6.53 ± 0.08	7.73 ± 0.24	0.65 ± 0.02
geranyl acetate	28.54 ± 0.65	7.23 ± 0.06	7.90 ± 0.06	1.04 ± 0.03	15.74 ± 0.27	15.79 ± 0.26	11.82 ± 0.09	20.84 ± 0.15	27.20 ± 0.16	0.87 ± 0.04
citronellol	503.42 ± 8.22	479.94 ± 3.50	496.13 ± 2.97	55.38 ± 1.40	433.24 ± 5.56	300.10 ± 4.18	297.12 ± 2.21	419.55 ± 4.16	378.10 ± 2.23	33.81 ± 1.49
nerol	204.05 ± 3.53	4.39 ± 0.18	4.11 ± 0.10	14.28 ± 0.20	101.25 ± 1.29	124.17 ± 1.69	107.74 ± 1.00	86.26 ± 0.84	111.13 ± 0.64	10.65 ± 0.23
phenylethanol	0.97 ± 0.02	0.19 ± 0.01	0.18 ± 0.01	0.22 ± 0.01	2.12 ± 0.06	0.93 ± 0.05	1.11 ± 0.31	4.11 ± 0.05	4.40 ± 0.04	0.12 ± 0.00
geraniol	499.85 ± 9.12	221.04 ± 1.78	209.02 ± 1.00	29.52 ± 0.55	220.03 ± 2.75	300.28 ± 4.29	210.33 ± 1.57	199.17 ± 2.21	270.95 ± 2.09	23.73 ± 0.50
methyleugenol	28.25 ± 0.69	8.14 ± 0.75	6.27 ± 0.06	4.16 ± 0.07	32.84 ± 0.38	8.97 ± 0.17	29.63 ± 0.29	34.61 ± 0.61	35.98 ± 0.55	0.50 ± 0.02
eugenol	21.93 ± 0.72	3.39 ± 0.07	3.02 ± 0.04	3.19 ± 0.06	15.32 ± 0.45	12.25 ± 0.34	8.00 ± 0.11	13.31 ± 0.12	22.19 ± 1.47	0.73 ± 0.01
farnesol	81.18 ± 5.82	2.95 ± 0.27	0.49 ± 0.07	3.73 ± 0.19	23.16 ± 0.57	30.92 ± 0.57	40.26 ± 0.47	23.53 ± 0.52	29.20 ± 1.25	3.21 ± 0.15

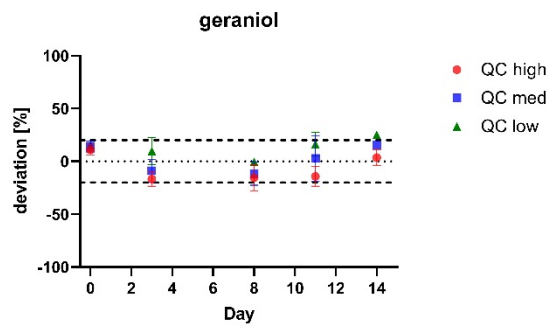
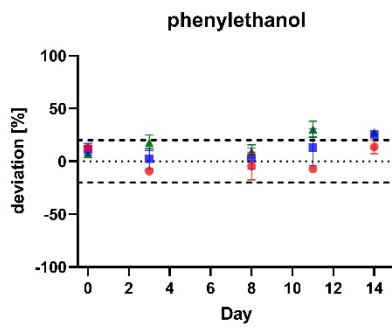
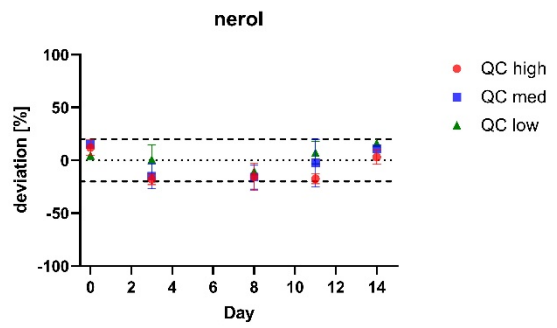
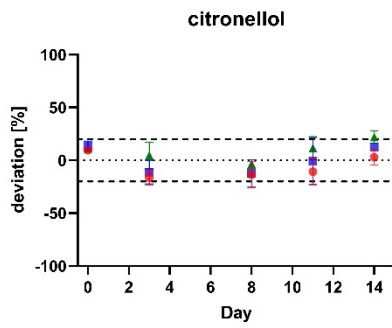
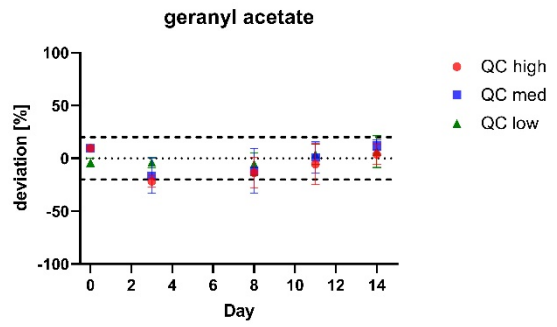
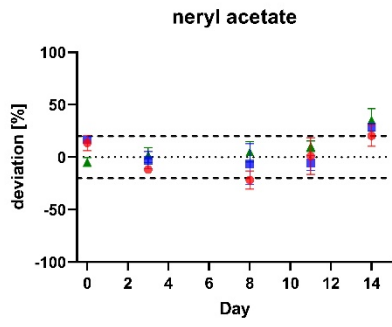
Table A5: Concentration profile incl. standard deviation (n=3) for terpenes acquired on BGB 178 30% CD column using GC-FID.

Table taken from Raeber et al.¹⁰

Species	R. damascena	P. graveolens	P. graveolens	R. damascena	R. damascena	R. damascena	R. damascena	R. damascena	R. damascena	R. damascena
Quality	pure	pure	pure	10%	pure	pure	pure	pure	pure	10%
Origin	Bulgaria	NA	NA	Morocco	Turkey	Bulgaria	Bulgaria	Turkey	Turkey	Bulgaria
	Conc. [mg/ml]	Conc. [mg/ml]	Conc. [mg/ml]	Conc. [mg/ml]	Conc. [mg/ml]	Conc. [mg/ml]	Conc. [mg/ml]	Conc. [mg/ml]	Conc. [mg/ml]	Conc. [mg/ml]
α-pinene	0.21 ± 0.00	0.21 ± 0.00	0.23 ± 0.00	0.15 ± 0.00	4.84 ± 0.03	7.15 ± 0.01	0.45 ± 0.00	0.34 ± 0.00	16.60 ± 0.08	0.75 ± 0.04
β-pinene	0.36 ± 0.00	0.04 ± 0.00	0.05 ± 0.00	0.16 ± 0.01	2.22 ± 0.06	2.28 ± 0.09	0.64 ± 0.00	1.73 ± 0.10	2.76 ± 0.02	0.18 ± 0.01
α-terpinene	0.08 ± 0.00	0.25 ± 0.00	0.37 ± 0.00	0.03 ± 0.00	0.15 ± 0.00	0.31 ± 0.00	0.13 ± 0.00	0.23 ± 0.01	0.35 ± 0.00	0.04 ± 0.00
limonene	0.07 ± 0.00	0.43 ± 0.00	0.63 ± 0.00	0.20 ± 0.02	0.09 ± 0.00	0.33 ± 0.00	0.12 ± 0.00	0.22 ± 0.05	0.20 ± 0.00	0.29 ± 0.02
p-cymene	0.15 ± 0.00	0.23 ± 0.00	0.29 ± 0.00	0.05 ± 0.00	0.30 ± 0.00	0.10 ± 0.00	0.15 ± 0.00	0.17 ± 0.04	0.32 ± 0.00	0.04 ± 0.01
phenylethanol	n.d.	n.d.	n.d.	n.d.	n.d.	n.d.	n.d.	n.d.	0.11 ± 0.00	n.d.
nerol	174.27 ± 5.82	16.78 ± 0.82	14.56 ± 0.51	17.44 ± 0.76	99.35 ± 0.09	103.05 ± 1.29	140.88 ± 1.57	82.69 ± 1.43	104.22 ± 1.27	13.51 ± 0.16
neryl acetate	0.96 ± 0.02	0.09 ± 0.01	0.07 ± 0.01	0.18 ± 0.01	2.93 ± 0.06	0.93 ± 0.00	0.71 ± 0.01	1.09 ± 0.01	1.19 ± 0.01	0.15 ± 0.01
geraniol	429.48 ± 2.45	206.47 ± 1.25	197.30 ± 0.74	34.13 ± 0.76	222.15 ± 0.90	253.16 ± 4.94	286 ± 3.39	189.39 ± 3.46	253.27 ± 3.47	26.75 ± 0.30
geranyl acetate	21.61 ± 0.20	6.91 ± 0.37	4.53 ± 0.26	1.19 ± 0.06	15.95 ± 0.19	13.06 ± 0.24	16.29 ± 0.24	18.48 ± 0.13	23.26 ± 0.12	1.04 ± 0.07
β-caryophyllene	6.97 ± 0.21	9.08 ± 0.20	12.19 ± 0.92	1.02 ± 0.04	3.74 ± 0.15	4.28 ± 0.03	4.58 ± 0.07	5.29 ± 0.16	8.38 ± 0.24	0.32 ± 0.01
β-damascone	n.d.	2.65 ± 0.20	3.41 ± 0.10	n.d.	n.d.	0.09 ± 0.01	0.13 ± 0.00	n.d.	n.d.	n.d.
eugenol	42.71 ± 0.64	15.82 ± 0.15	17.04 ± 0.44	2.08 ± 0.05	37.24 ± 0.86	23.53 ± 1.00	28.97 ± 0.51	37.20 ± 0.43	52.64 ± 0.53	1.60 ± 0.07
methyleugenol	22.61 ± 0.21	1.01 ± 0.02	0.70 ± 0.01	4.02 ± 0.21	30.47 ± 0.38	7.97 ± 0.12	38.90 ± 0.51	31.32 ± 0.15	31.56 ± 0.11	0.58 ± 0.02
farnesol	67.50 ± 1.30	n.d.	n.d.	3.74 ± 0.69	25.47 ± 0.33	25.40 ± 0.49	55.54 ± 1.81	25.14 ± 0.55	29.74 ± 0.91	2.80 ± 0.06
Enantiomeric excess (EE)/ diastereomeric excess (DE) [%]										
camphene 1	n.d.	100	100	n.d.	100	100	100	100	100	n.d.
camphene 2	n.d.	n.d.	n.d.	n.d.	n.d.	n.d.	n.d.	n.d.	n.d.	n.d.
(+)-cis rose oxide	n.d.	NA	NA	n.d.	n.d.	NA	n.d.	n.d.	n.d.	NA
(-)-cis rose oxide	100	16	15	100	100	81	100	100	100	78
(-)-linalool	6	0	NA	16	16	19	5	12	9	19
(+)-linalool	NA	NA	11	NA	NA	NA	NA	NA	NA	NA
(+)-citronellol	29	24	NA	n.d.	n.d.	n.d.	NA	n.d.	n.d.	n.d.
(-)-citronellol	NA	NA	23	100	100	100	99	100	100	100
cis-citral	NA	NA	NA	NA	NA	NA	NA	NA	NA	NA
trans-citral	44	27	17	9	52	21	33	29	28	52
(+/-)-citronellyl acetate 1	n.d.	27	22	100	100	100	86	68	69	100
(+/-)-citronellyl acetate 2	100	NA	NA	n.d.	n.d.	n.d.	NA	NA	NA	n.d.
β-damasconone 1	100	19	10	100	n.d.	57	85	n.d.	n.d.	n.d.
β-damasconone 2	n.d.	NA	NA	n.d.	n.d.	NA	NA	n.d.	n.d.	n.d.







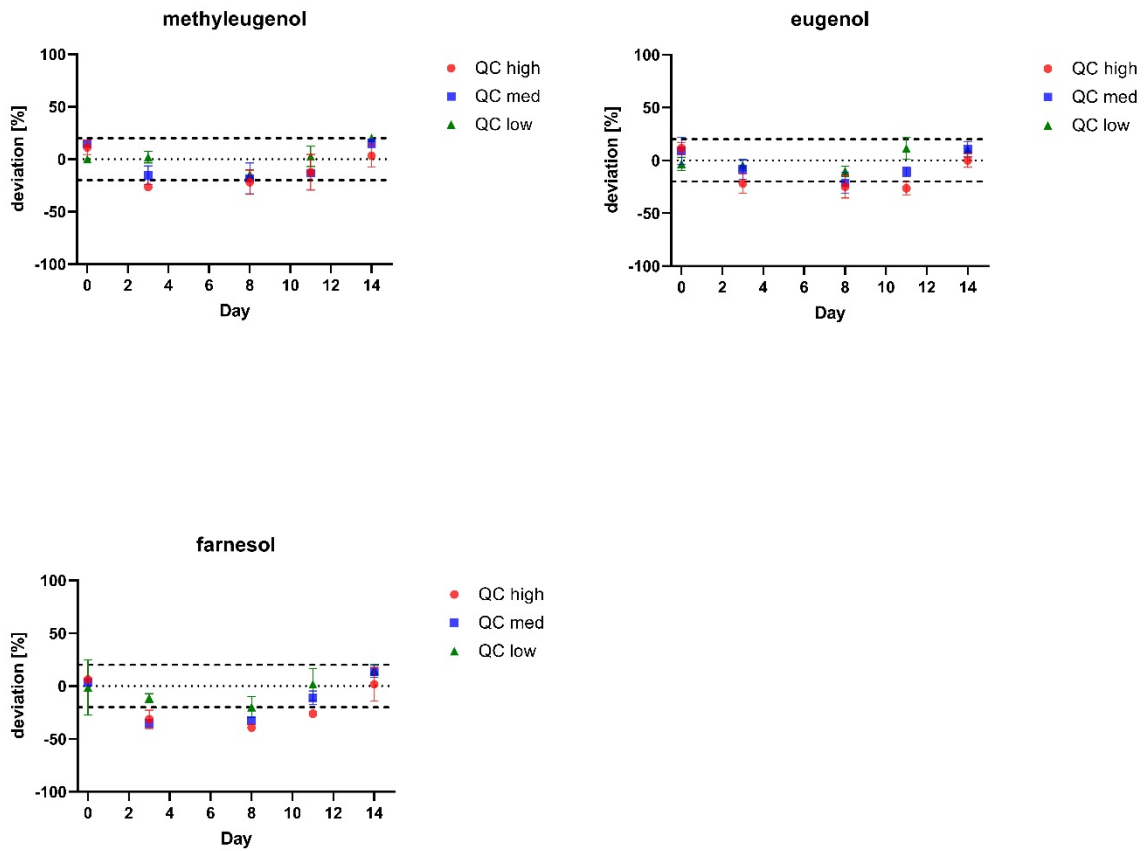
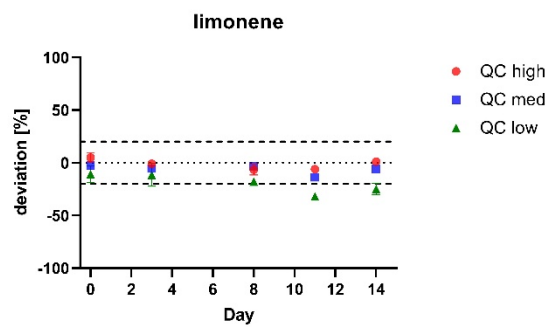
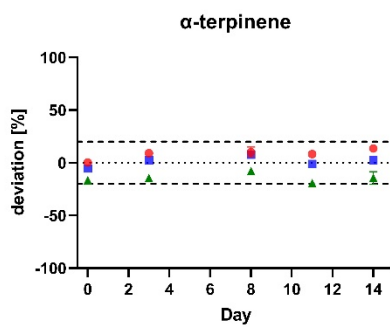
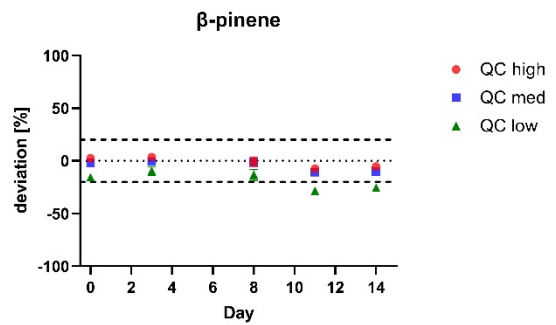
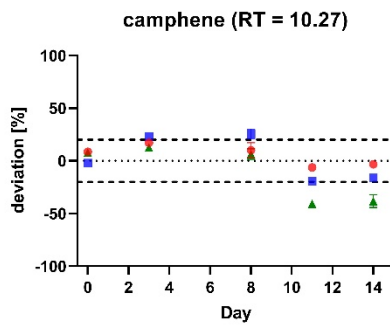
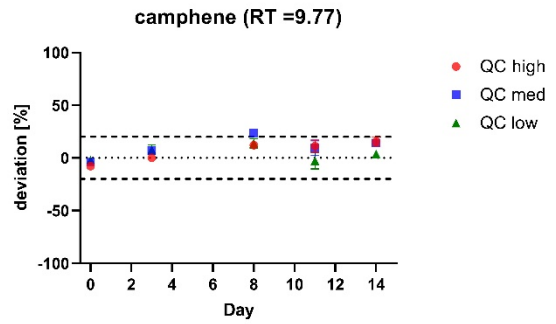
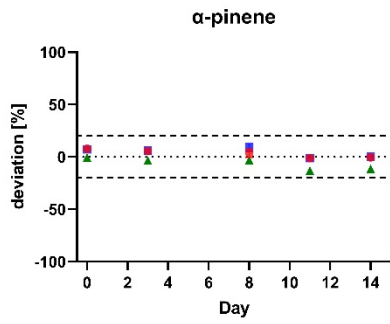
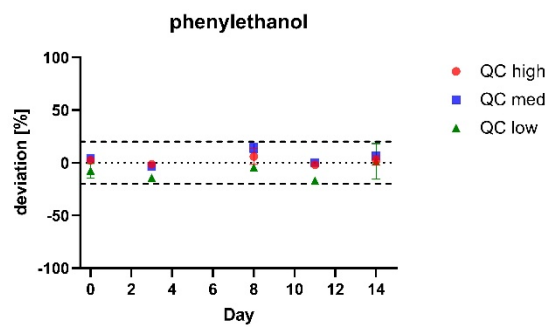
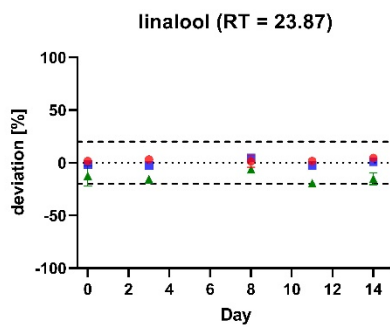
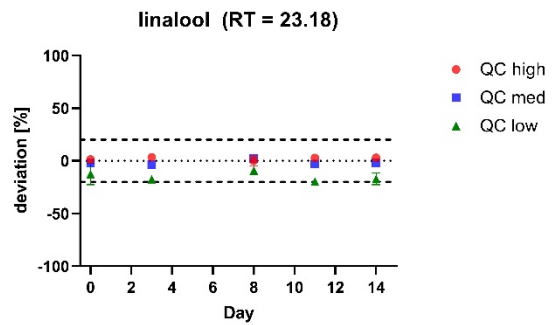
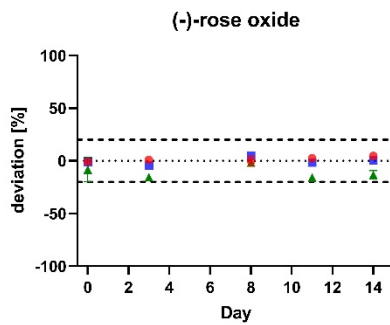
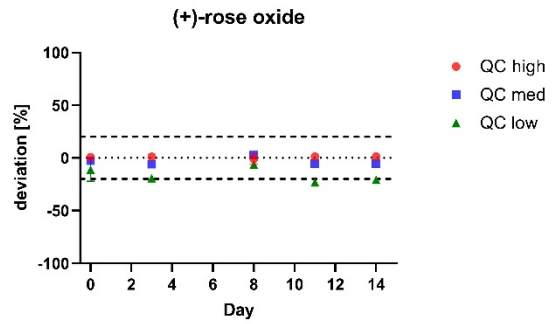
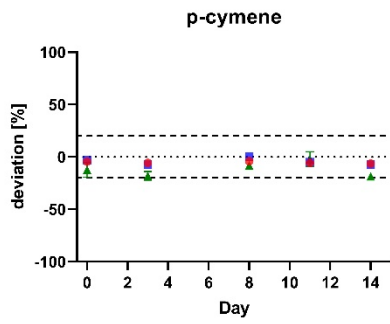
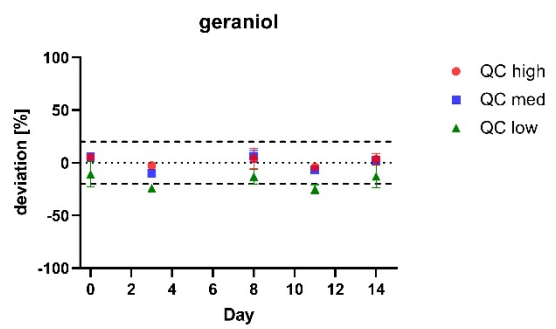
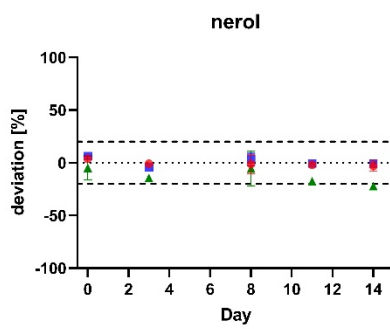
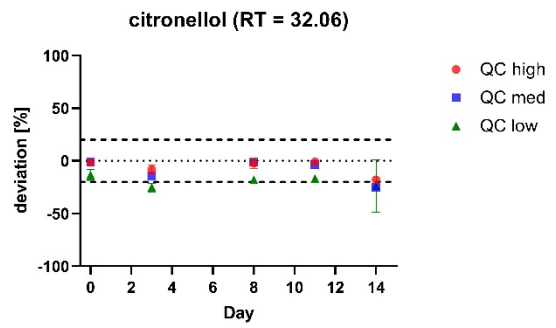
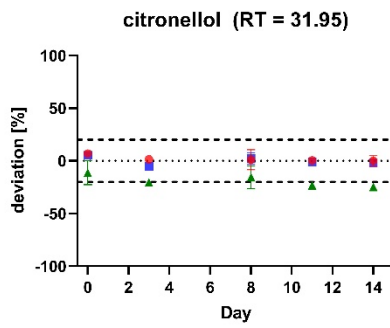
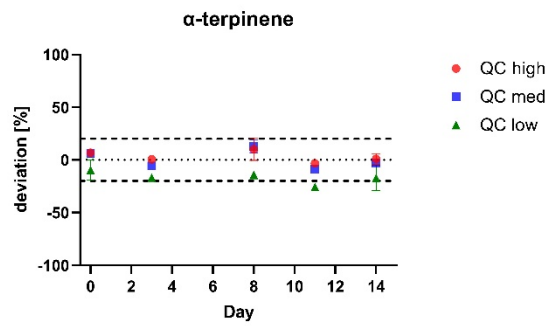
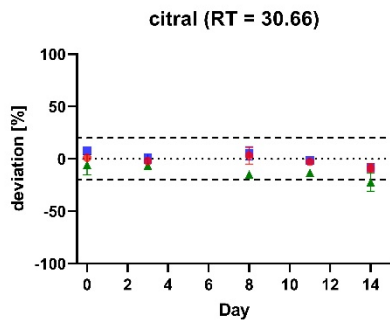
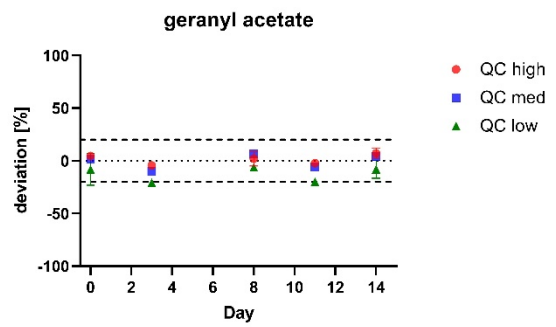
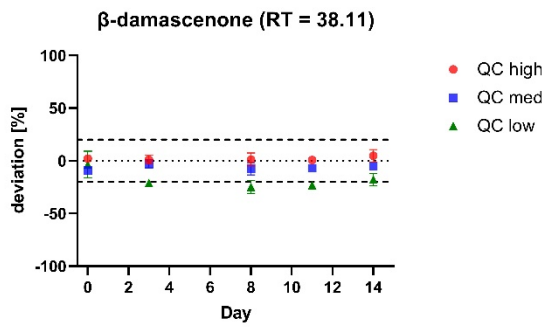
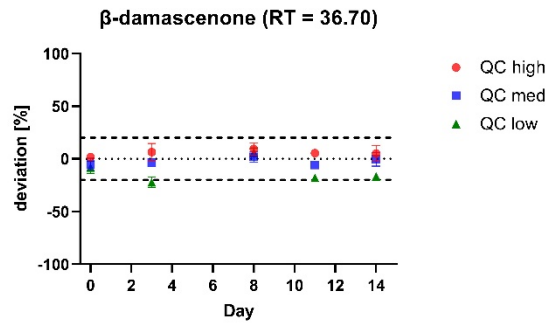
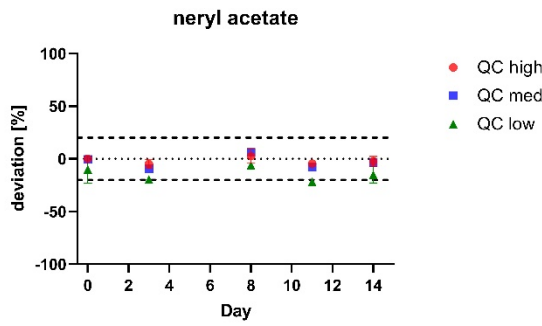
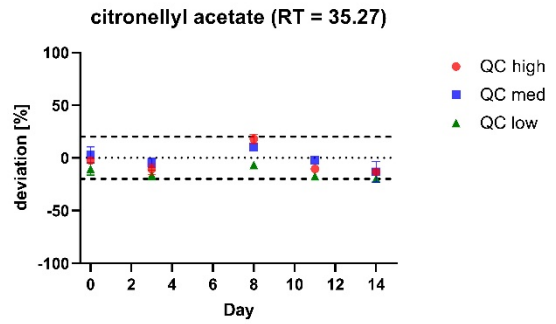
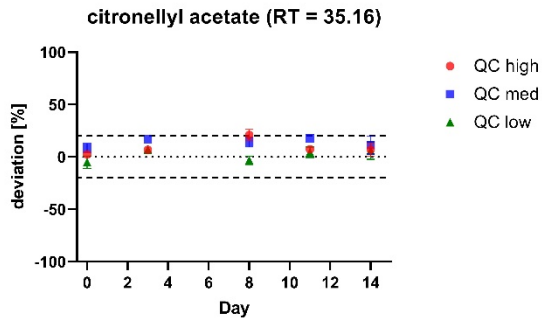


Figure A3: Calibration stability using QC samples from the five validation days and calculating their concentration using the calibration curve from the first validation day. Results are presented for the DB-wax column. Figure taken from Raeber et al.¹⁰









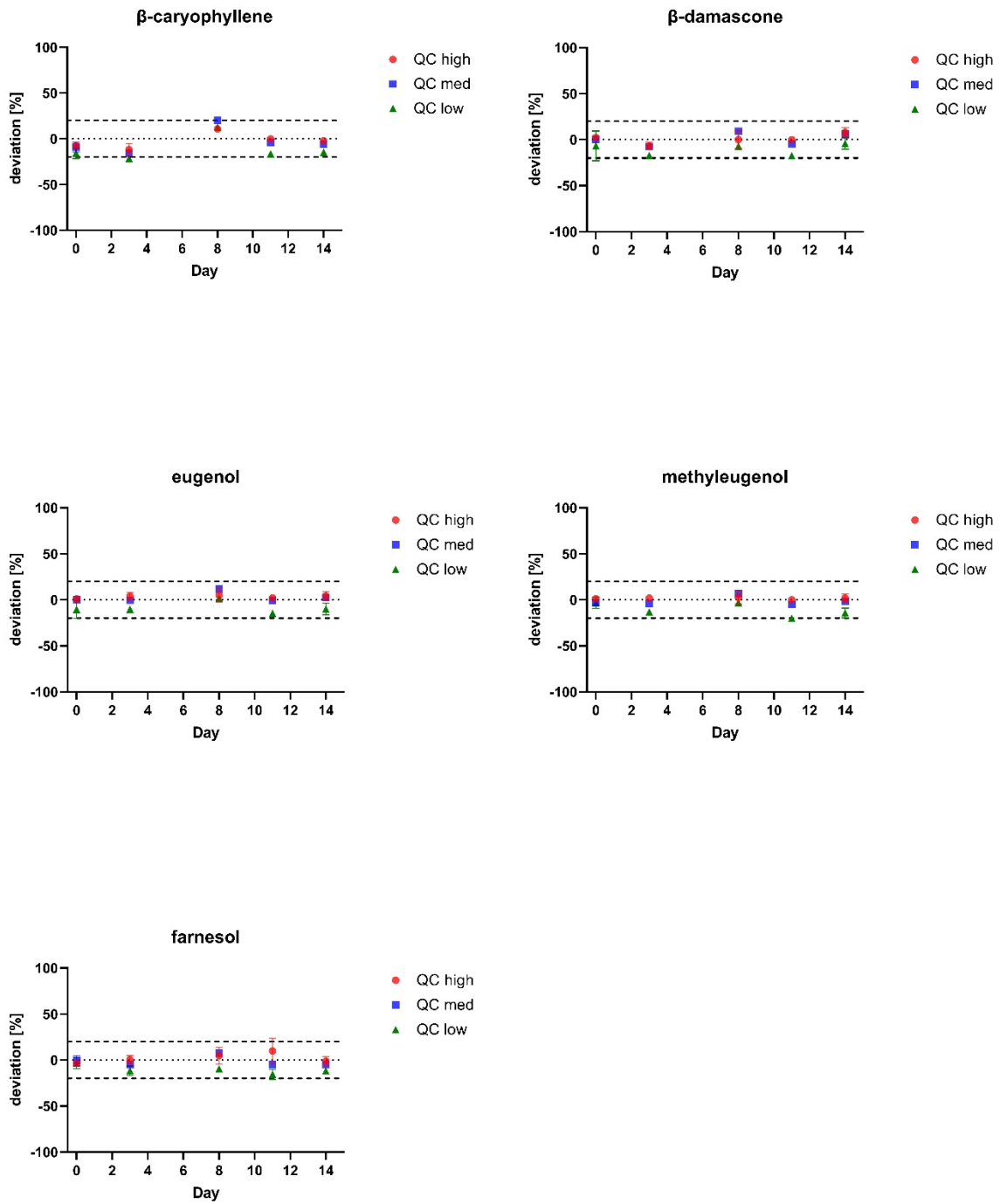
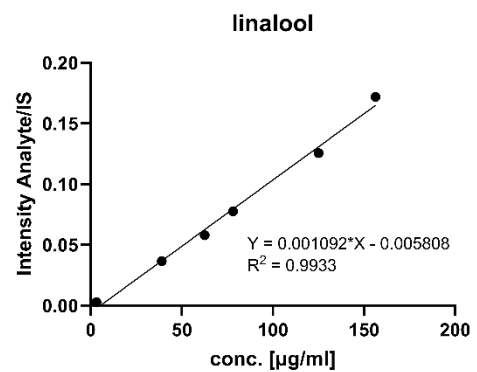
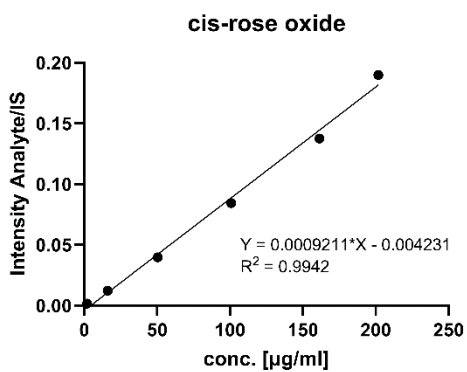
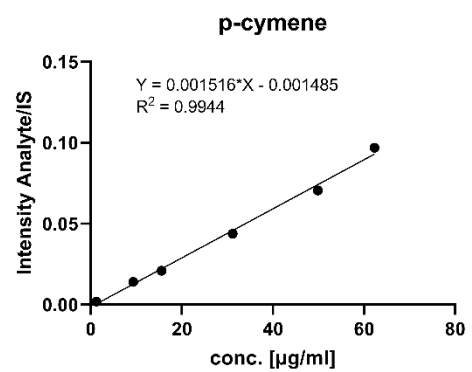
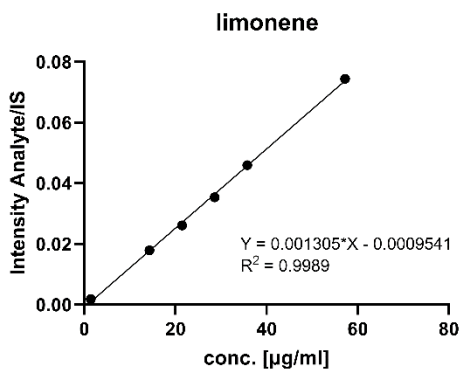
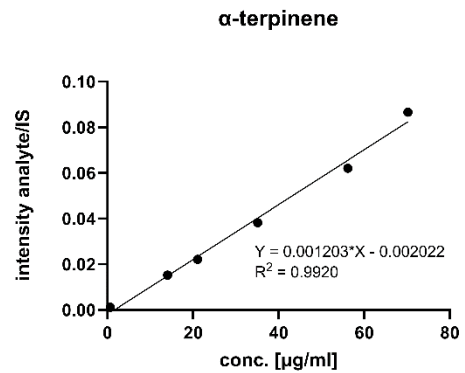
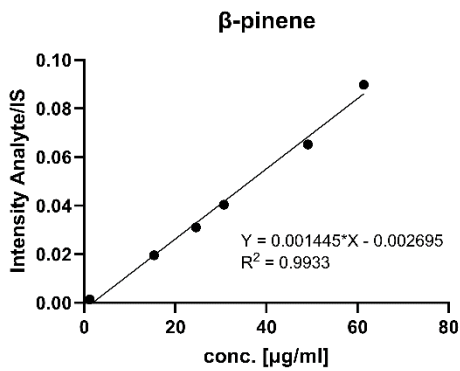
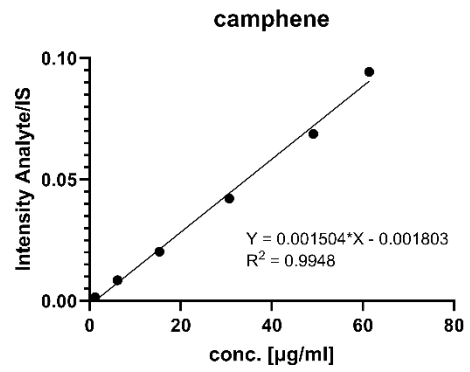
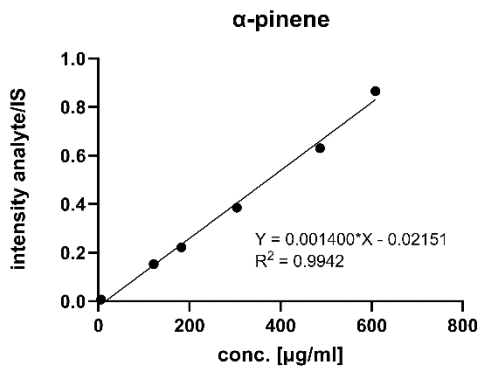
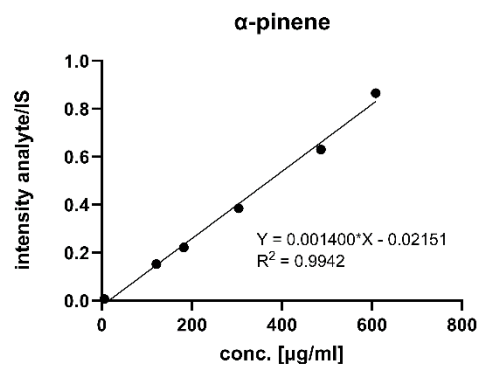
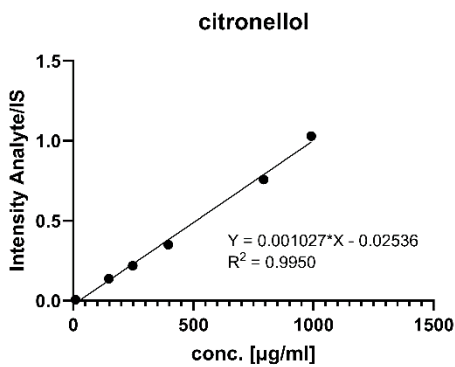
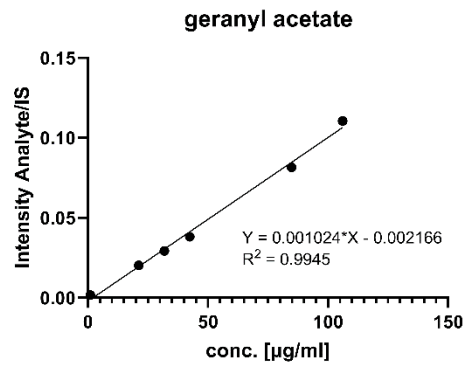
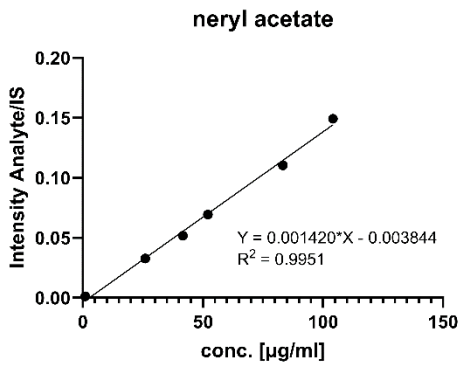
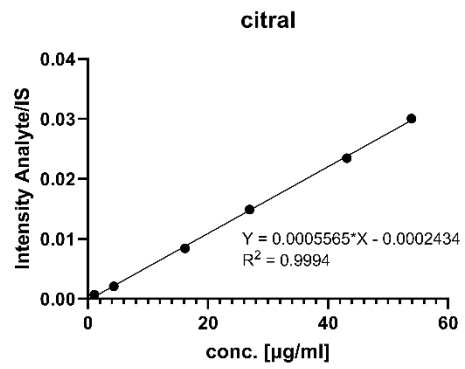
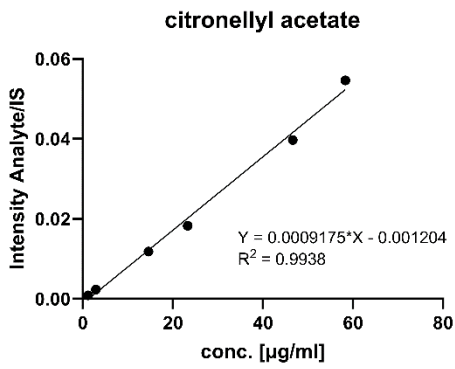
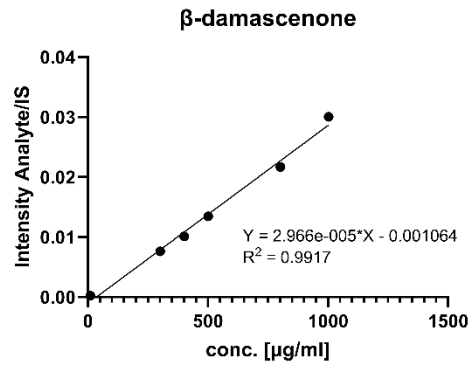
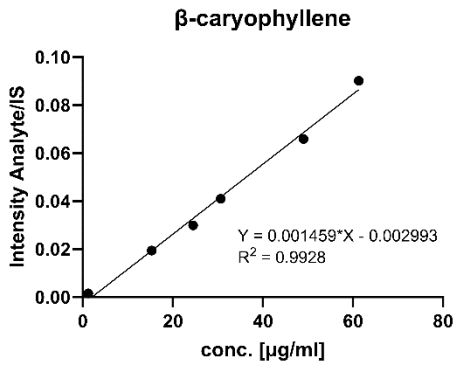


Figure A4: Calibration stability using QC samples from the five validation days and calculating their concentration using the calibration curve from the first validation day. Results are presented for the BGB 178 30% CD column. Figure taken from Raeber et al.¹⁰





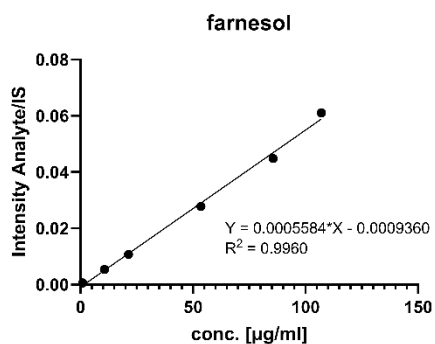
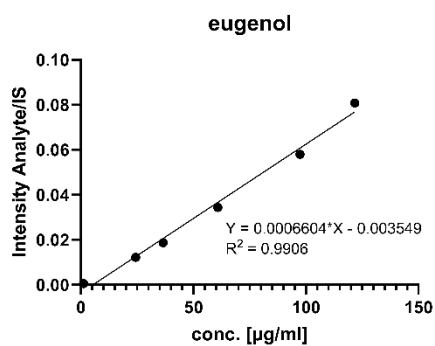
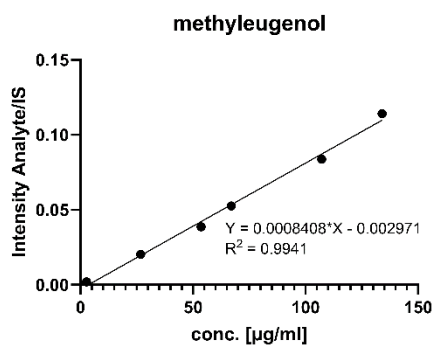
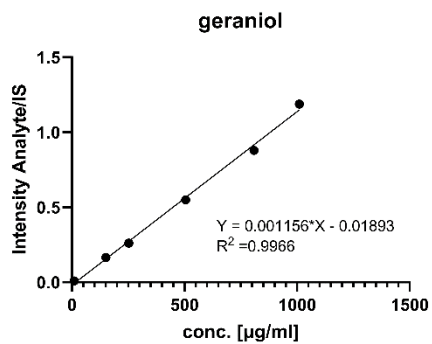
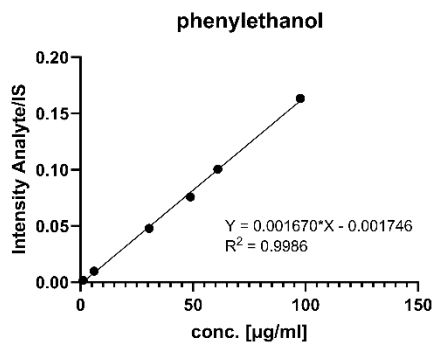
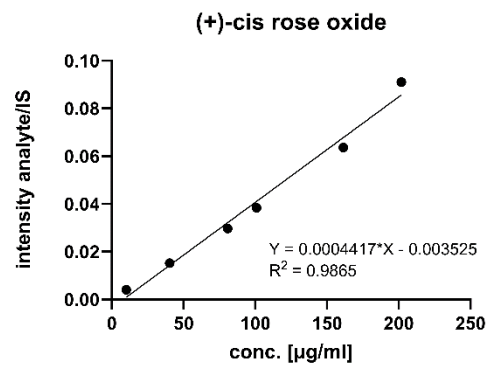
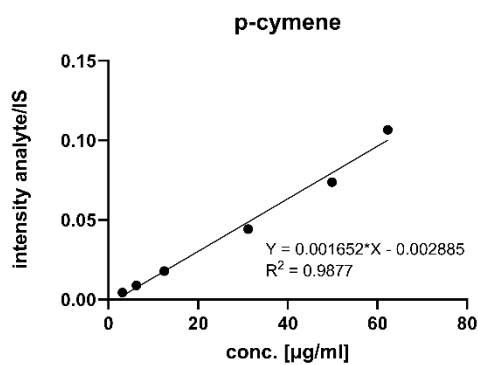
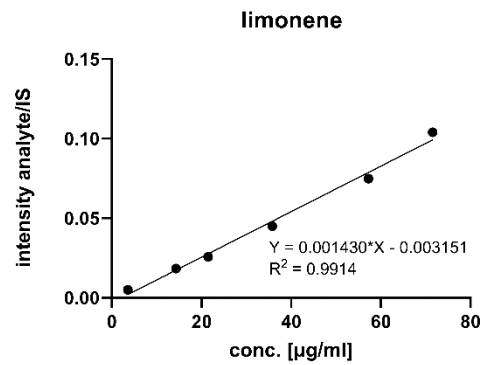
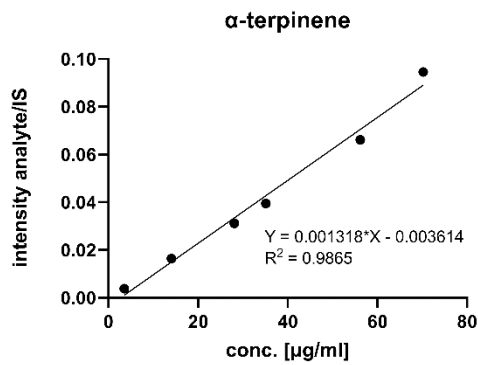
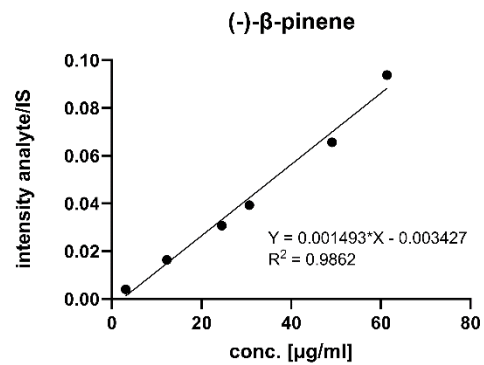
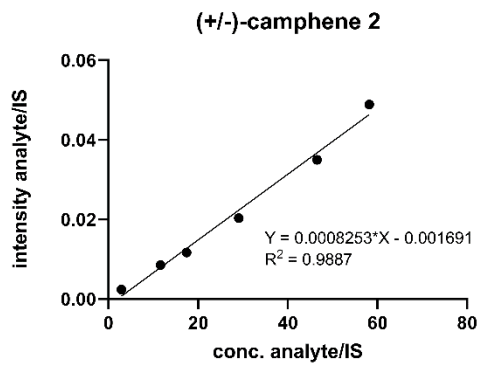
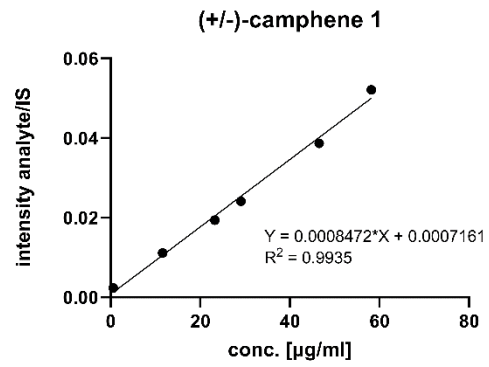
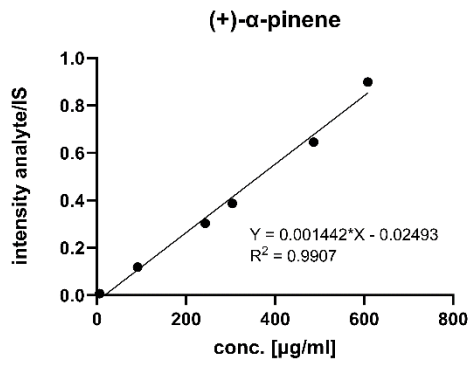
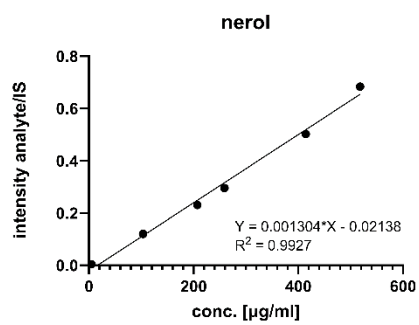
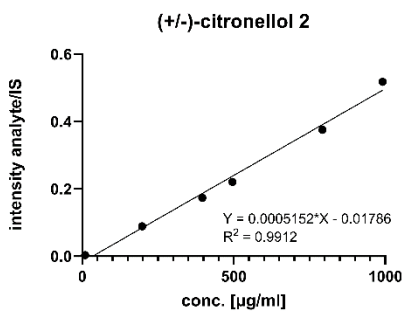
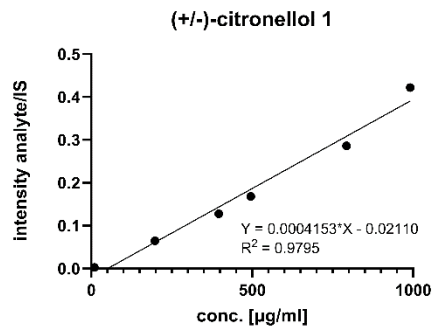
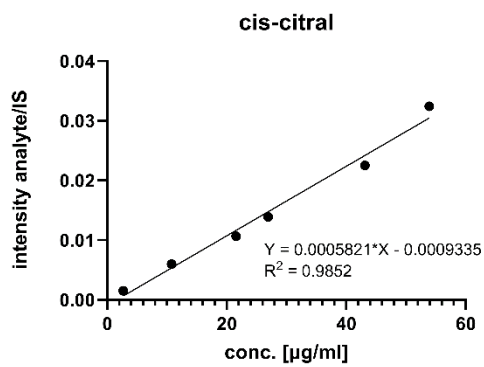
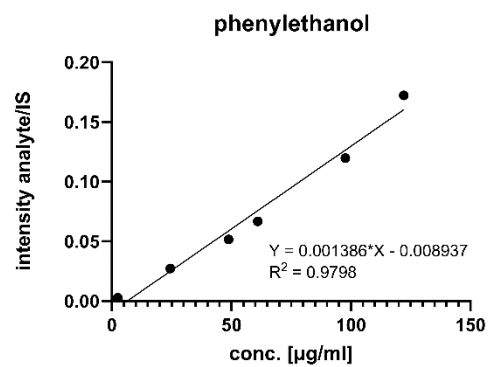
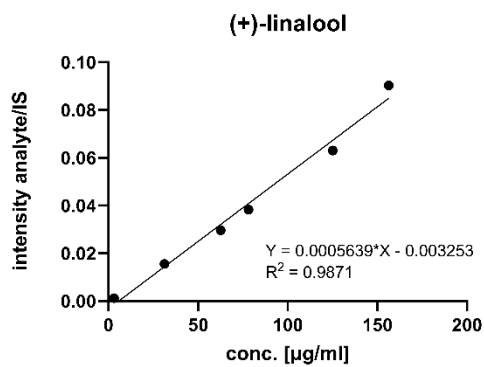
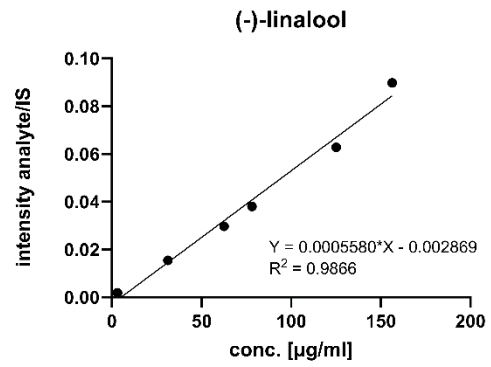
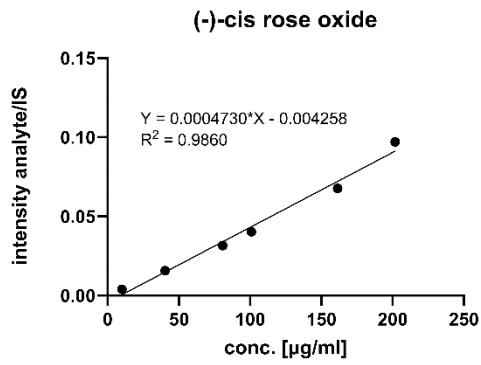
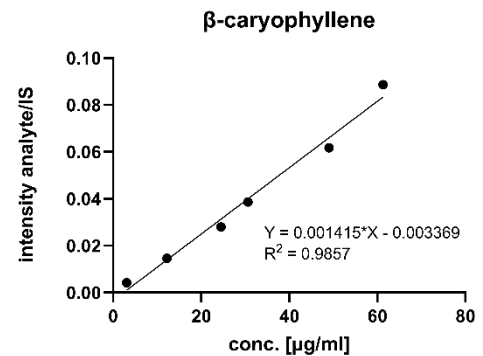
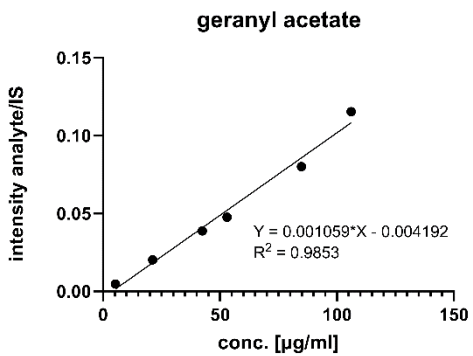
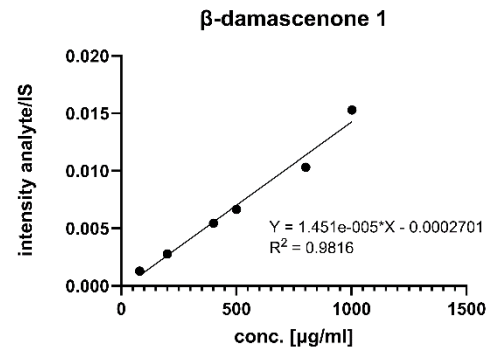
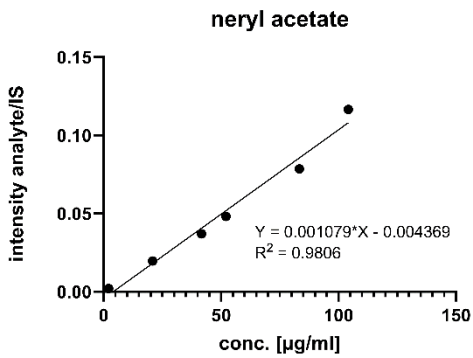
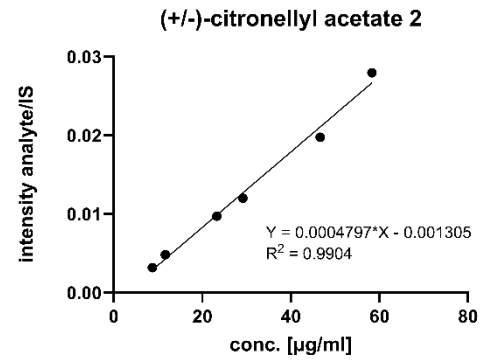
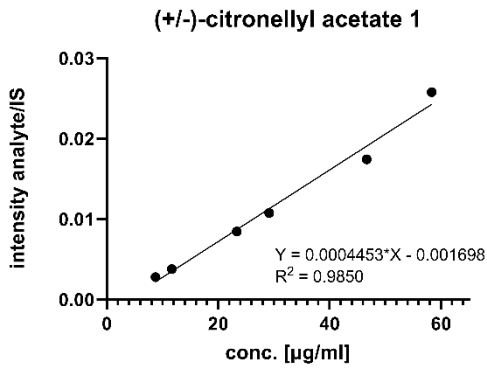
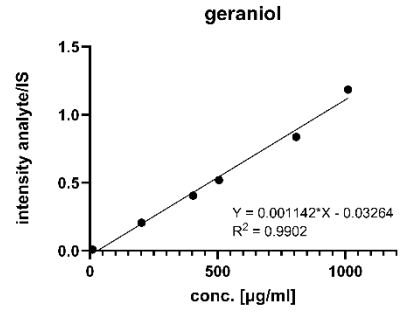
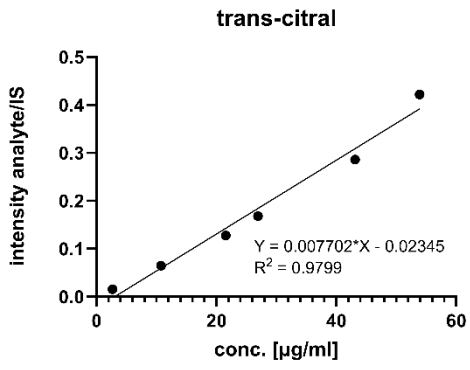


Figure A5: Calibration plots for analytes on DB-wax column.







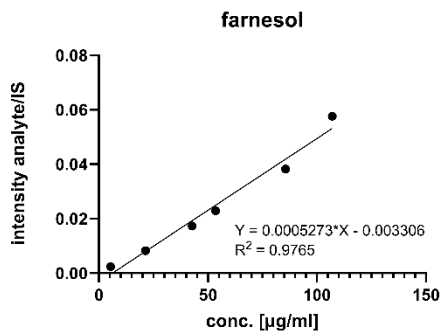
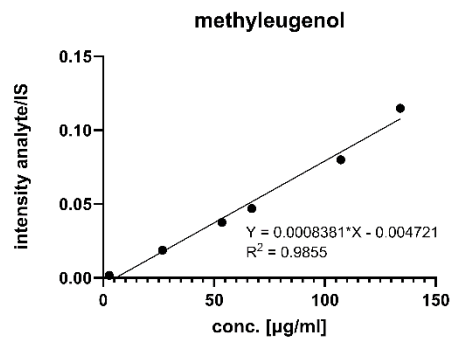
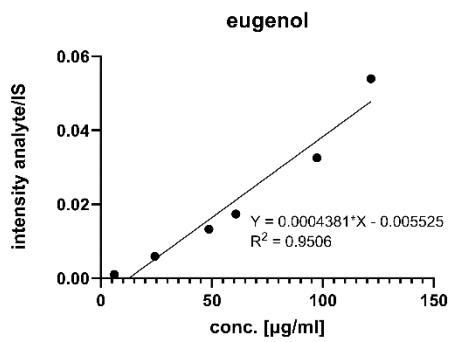
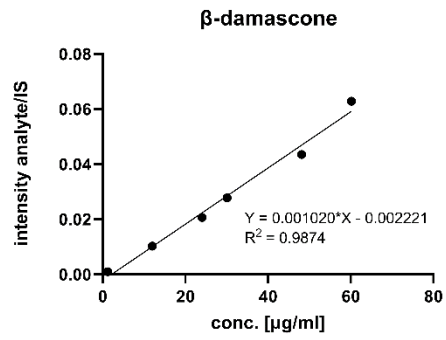
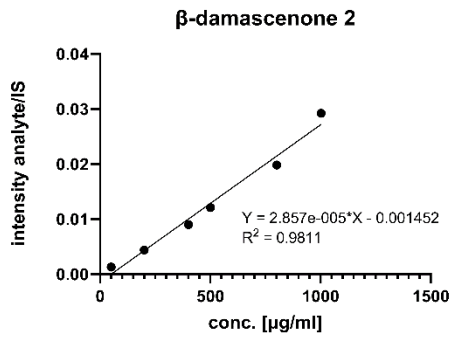


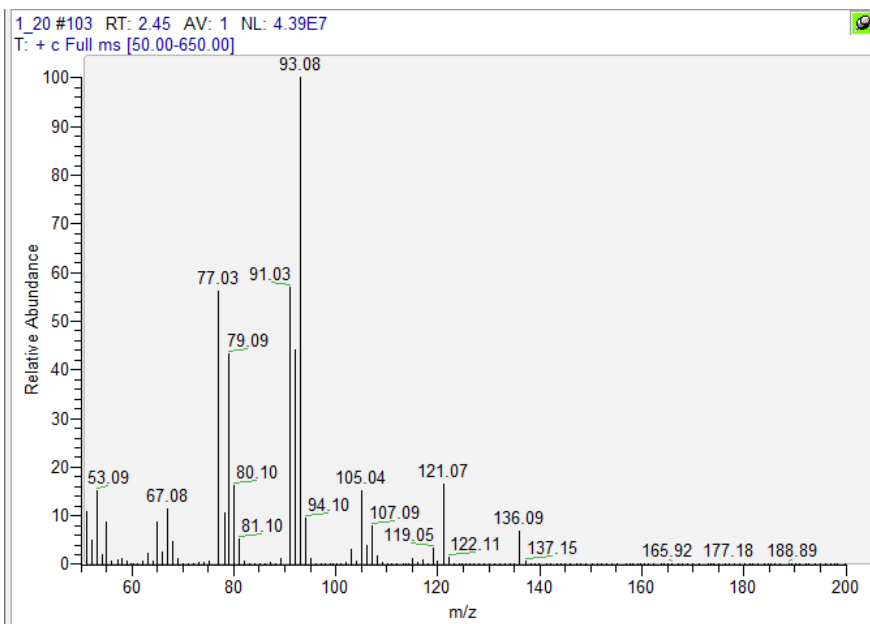
Figure A6: Calibration plots for analytes on BGB 178 30% CD column.

Table A6: Authentic *R. damascena* samples. Table taken from Raeber et al.¹⁰

Number	3018	3057	3058	3053	3021	3072	3073	3075	3074	3070
Species	<i>R. damascena</i>	<i>P. graveolens</i>	<i>P. graveolens</i>	<i>R. damascena</i>	<i>R. damascena</i>	<i>R. damascena</i>	<i>R. damascena</i>	<i>R. damascena</i>	<i>R. damascena</i>	<i>R. damascena</i>
Quality	pure	pure	pure	10%	pure	pure	pure	pure	pure	10%
Origin	Bulgaria	NA	NA	Morocco	Turkey	Bulgaria	Bulgaria	Turkey	Turkey	Bulgaria

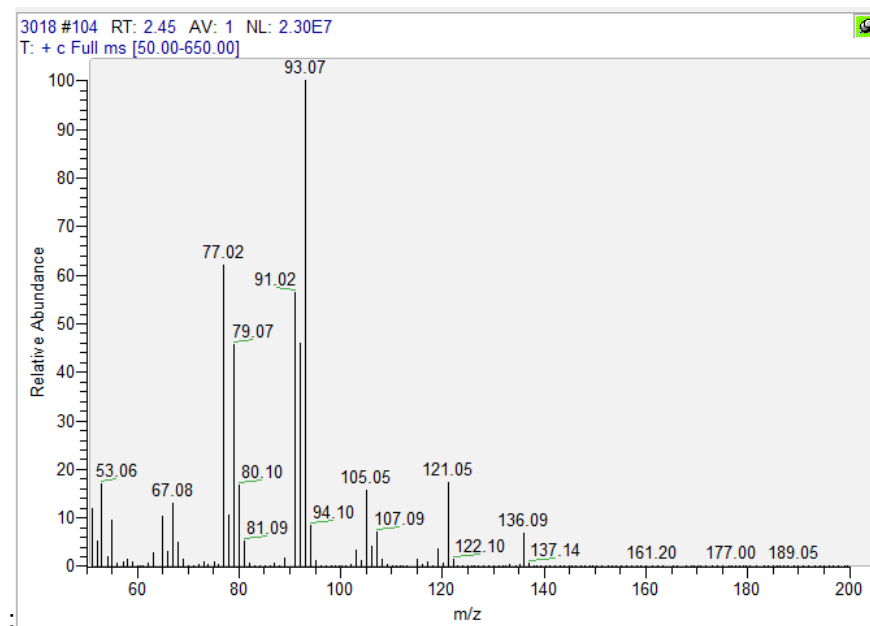
Figure A7: MS spectra from reference compounds and authentic samples in *R. damascena* oils. Figures taken from Raeber et al.¹⁰

Reference of α -pinene

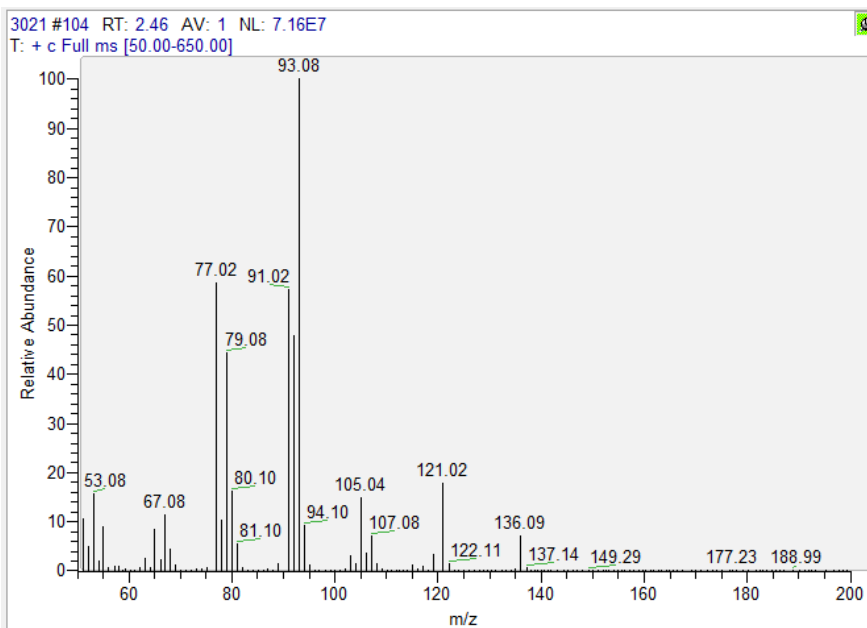


Authentic samples:

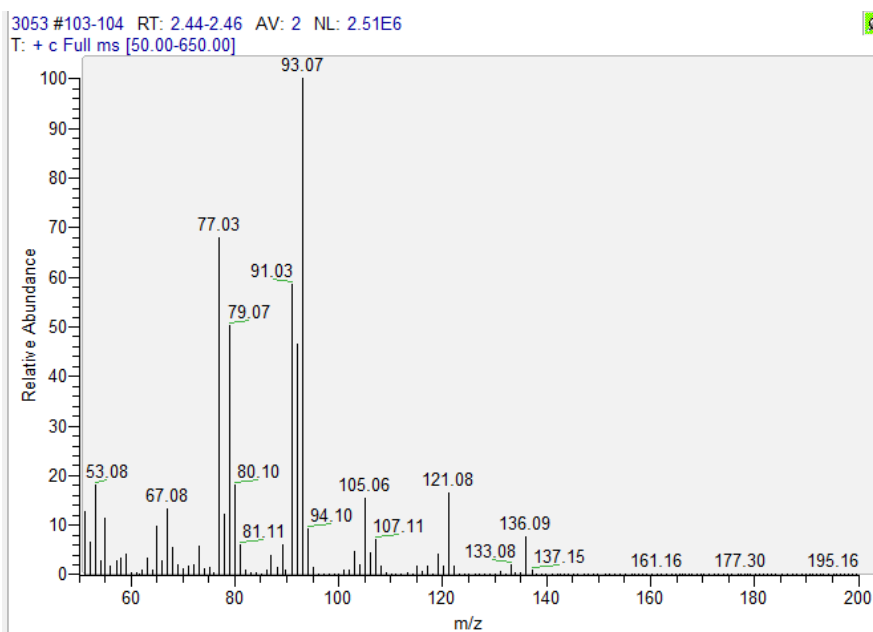
Sample 3018



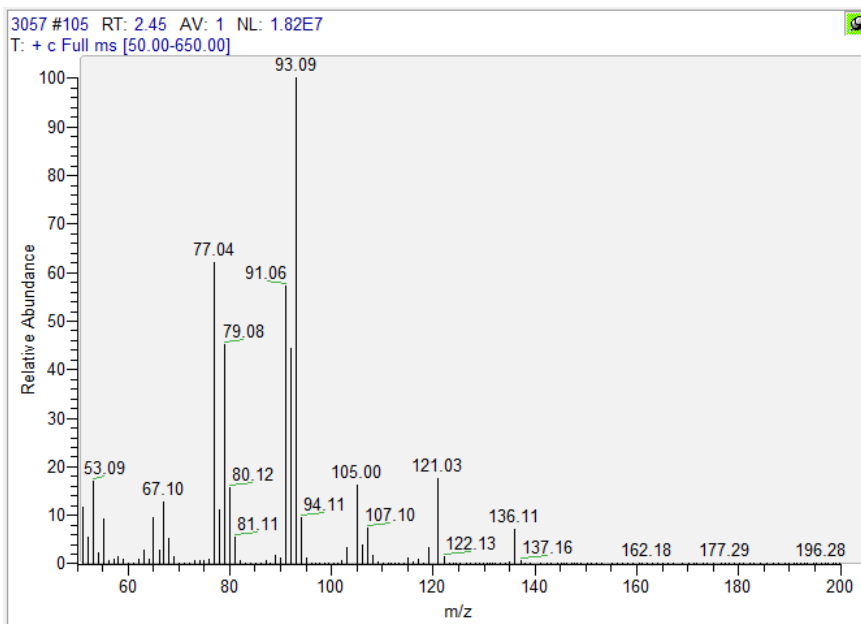
Sample 3021



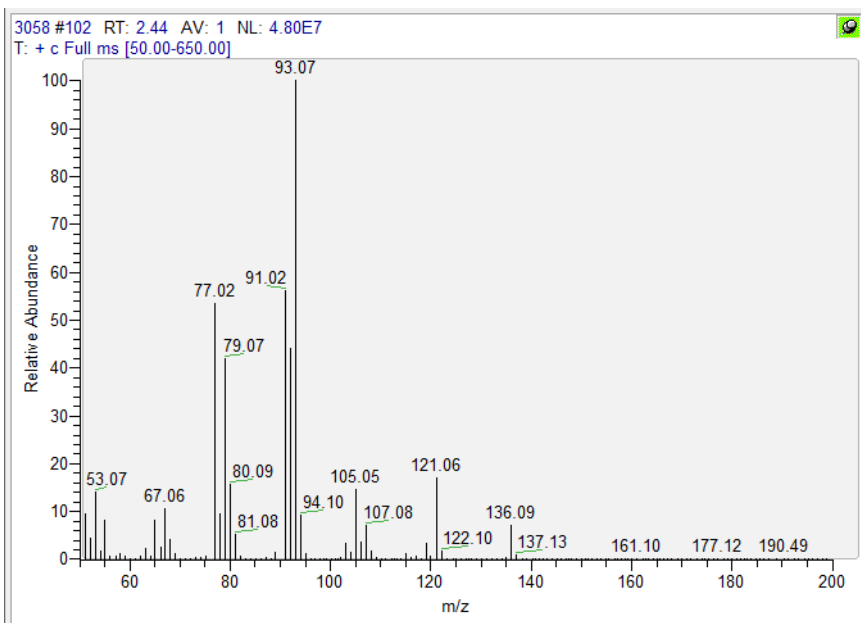
Sample 3053



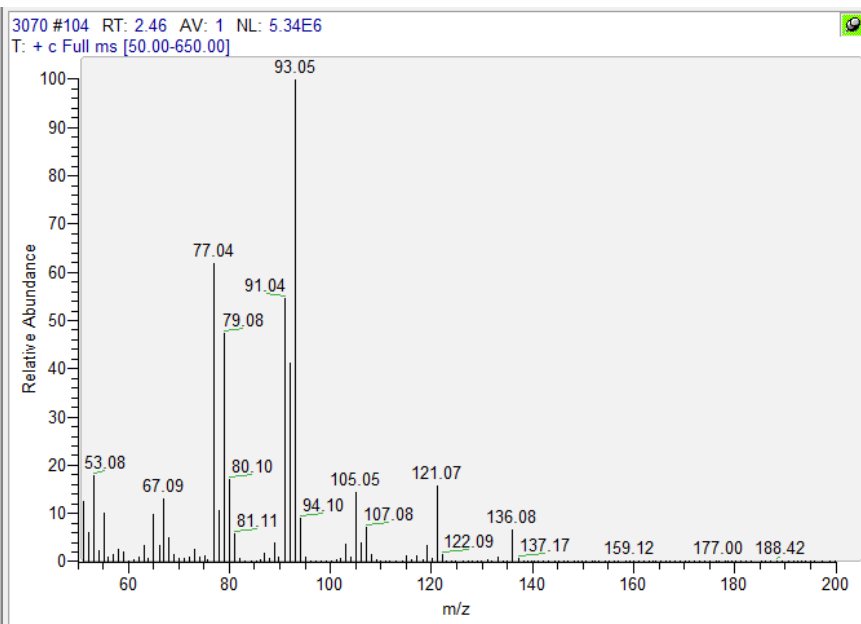
Sample 3057



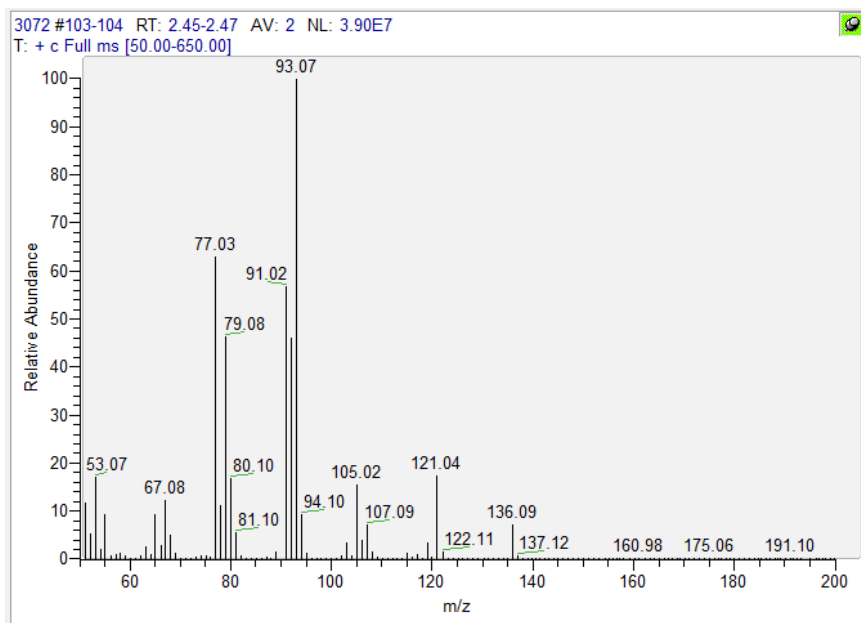
Sample 3058



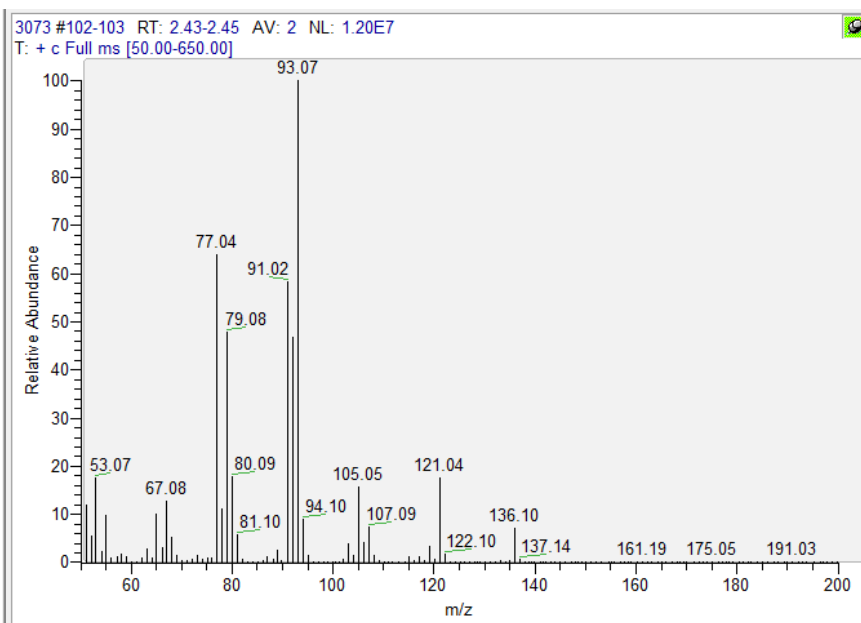
Sample 3070



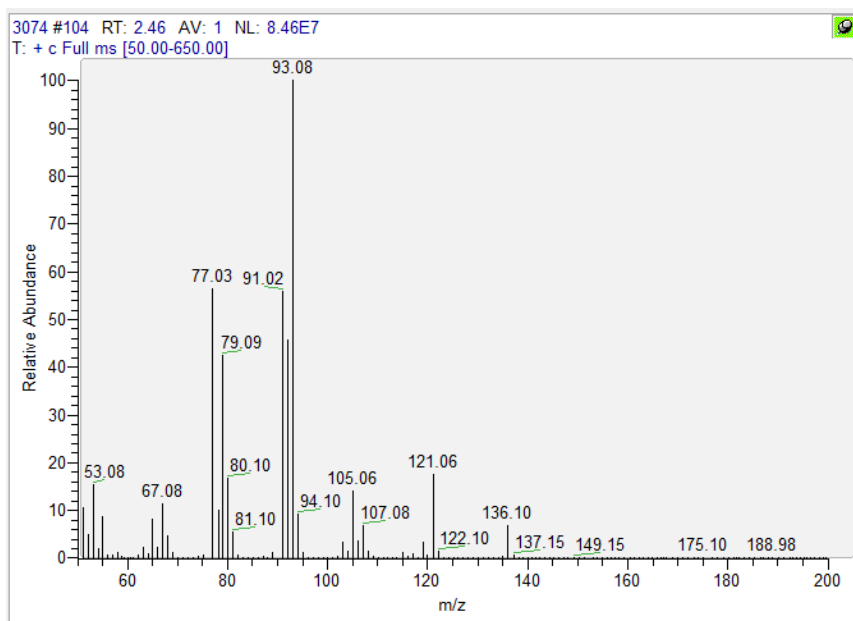
Sample 3072



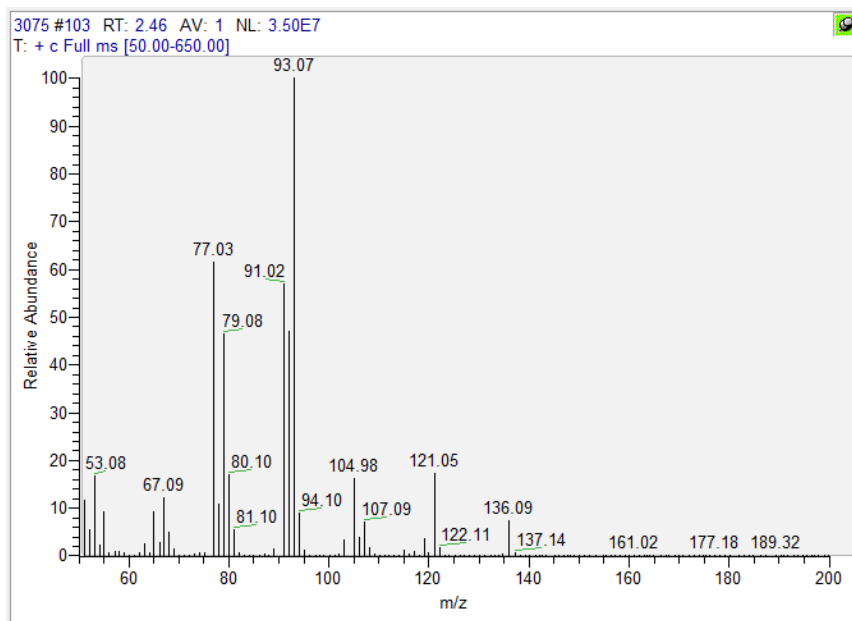
Sample 3073



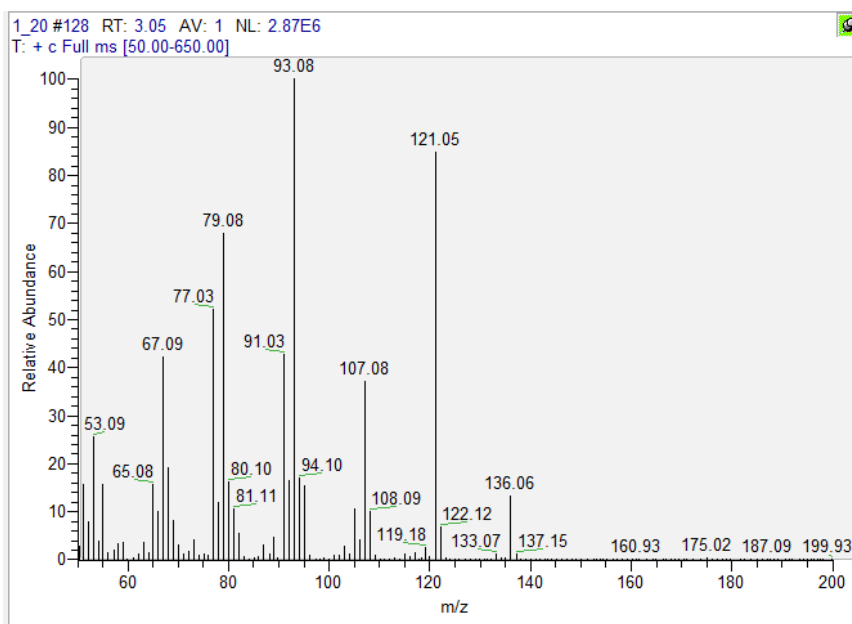
Sample 3074



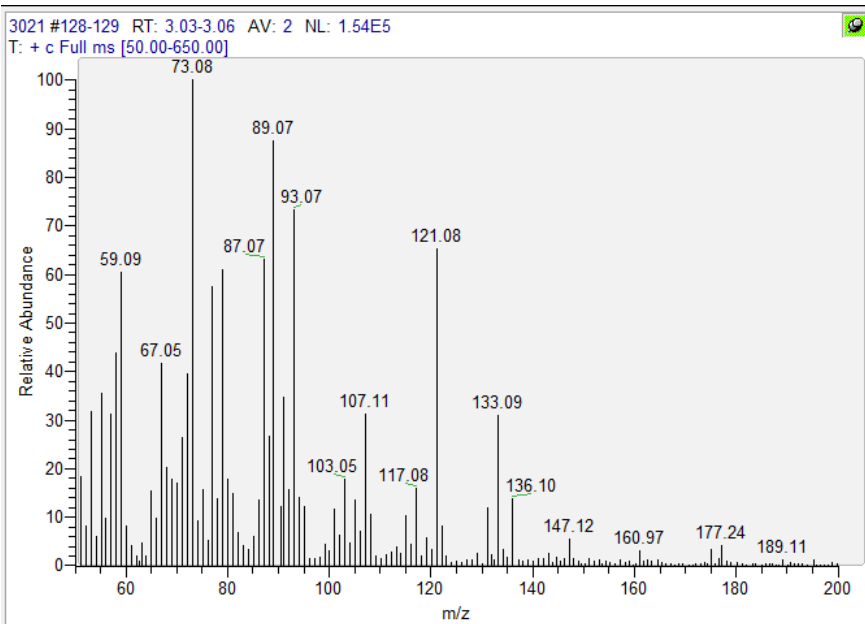
Sample 3075



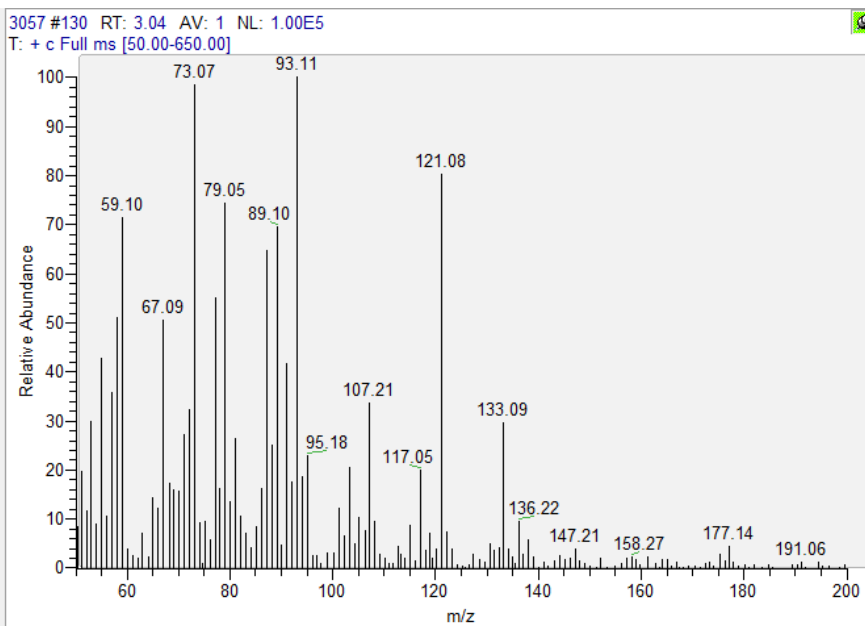
Reference of camphene



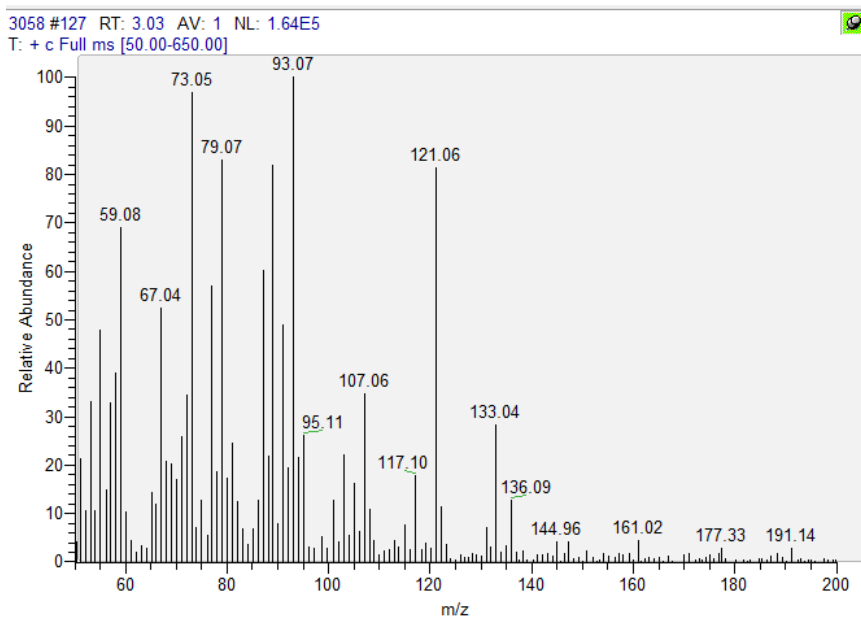
Sample 3021



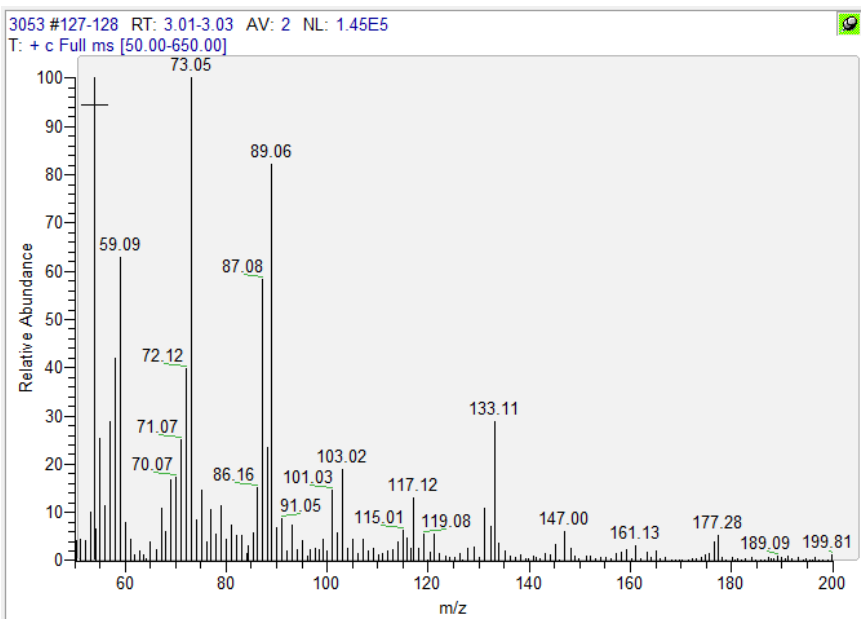
Sample 3057



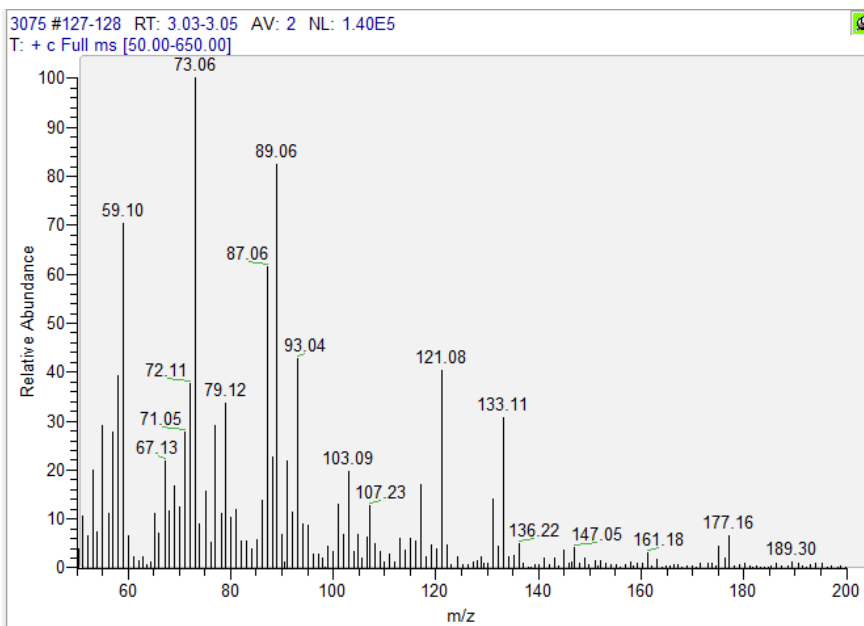
Sample 3058



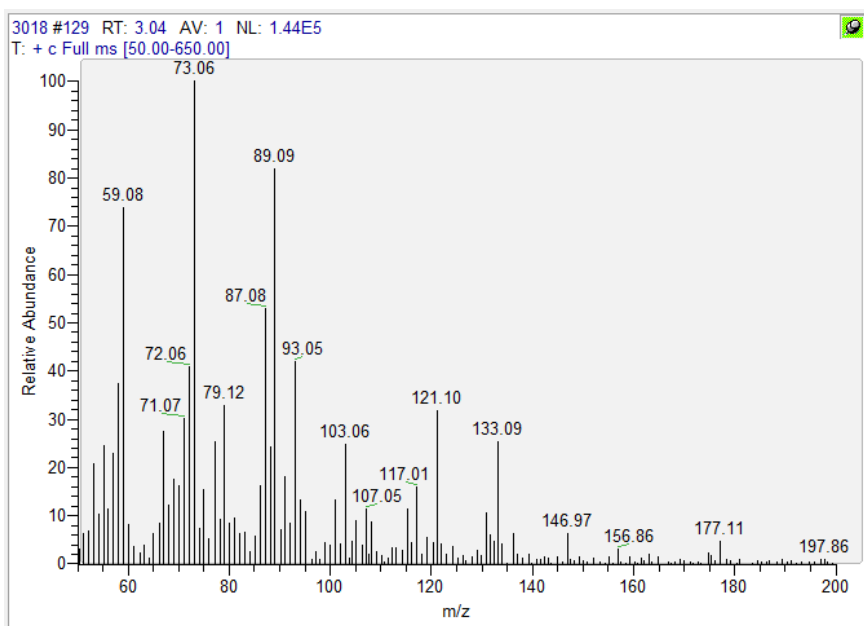
Sample 3053



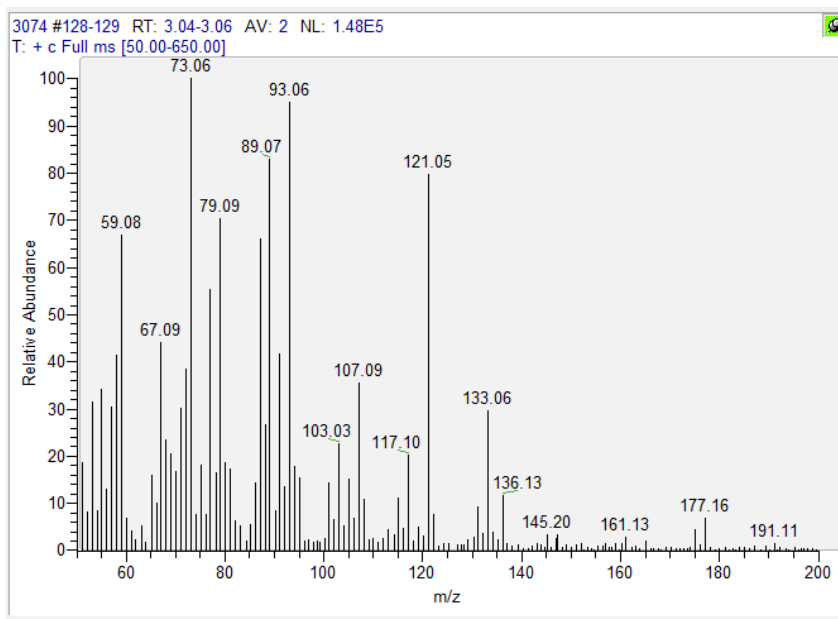
Sample 3075



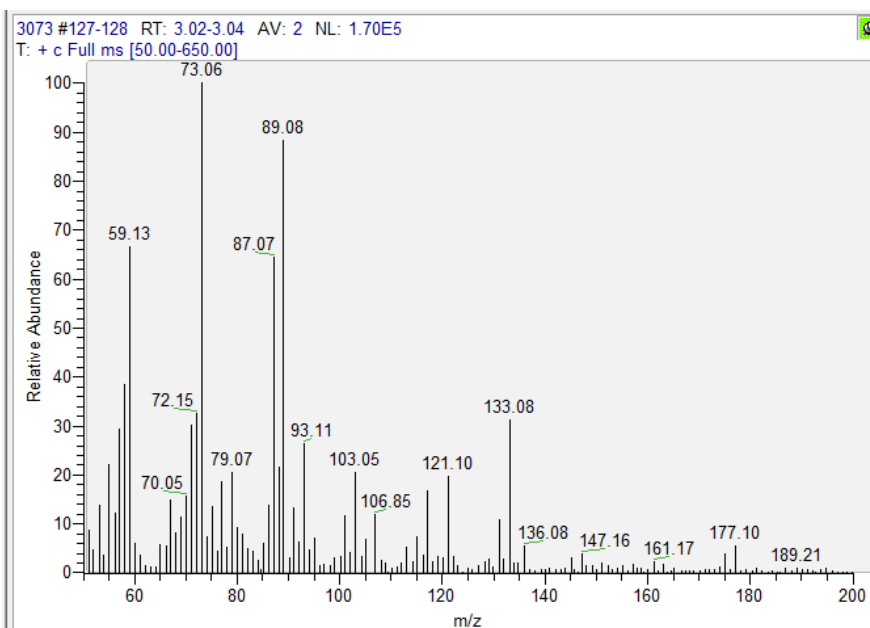
Sample 3018



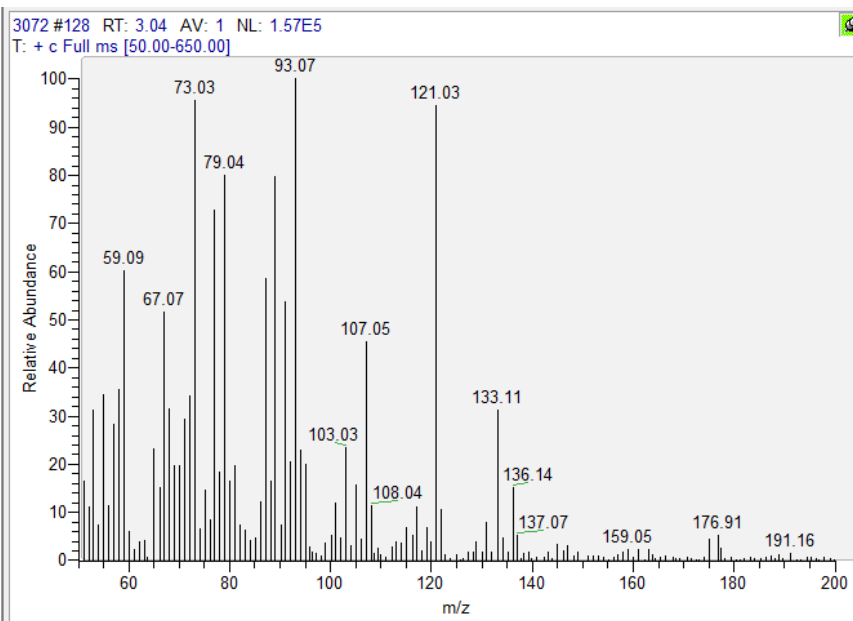
Sample 3074



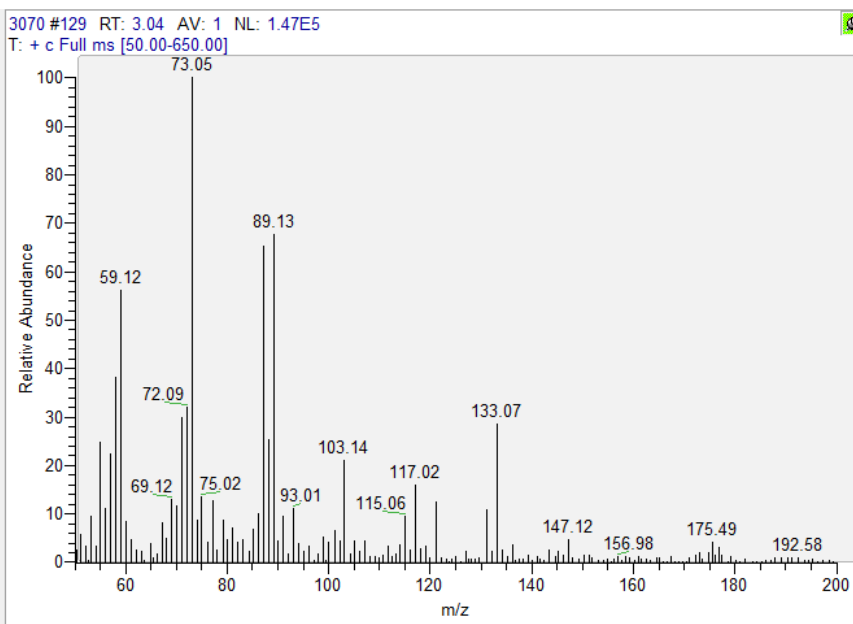
Sample 3073



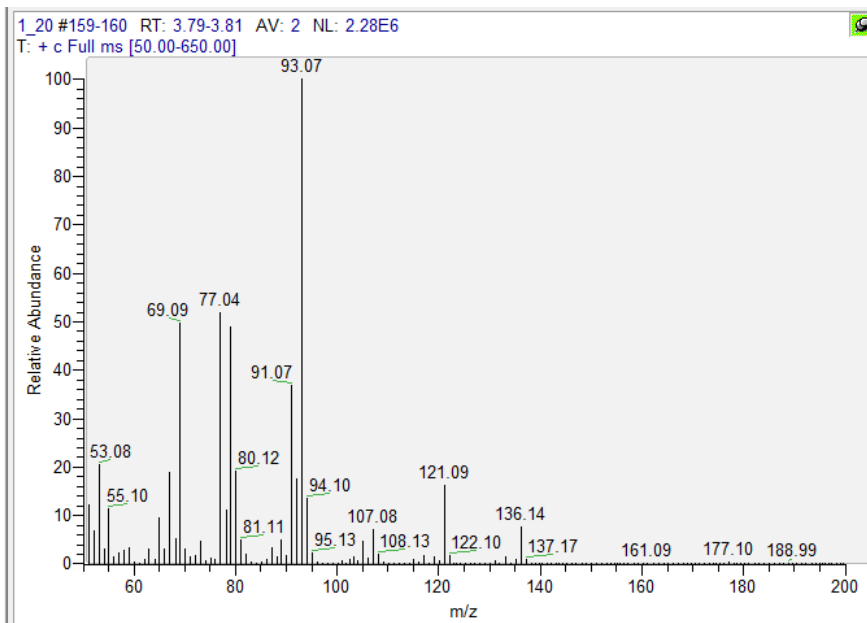
Sample 3072



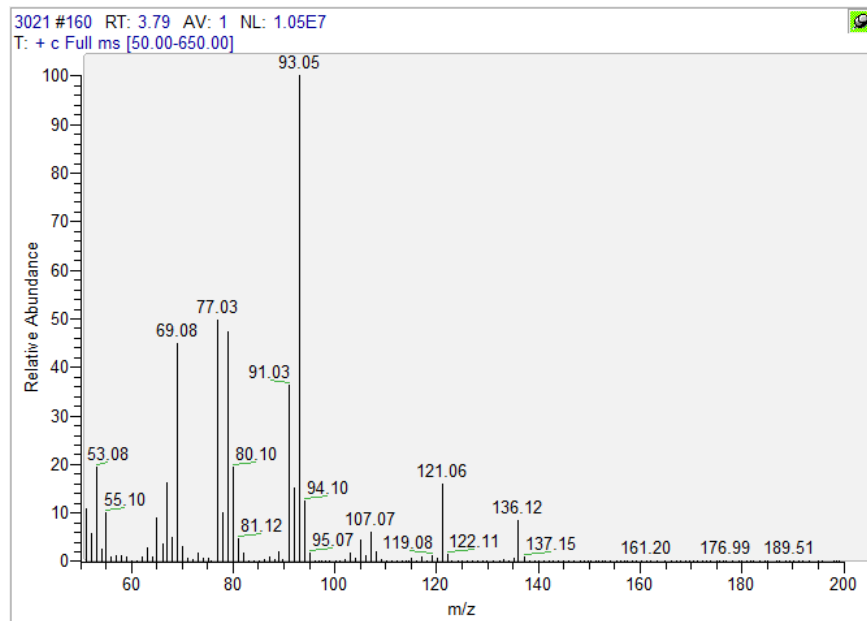
Sample 3075



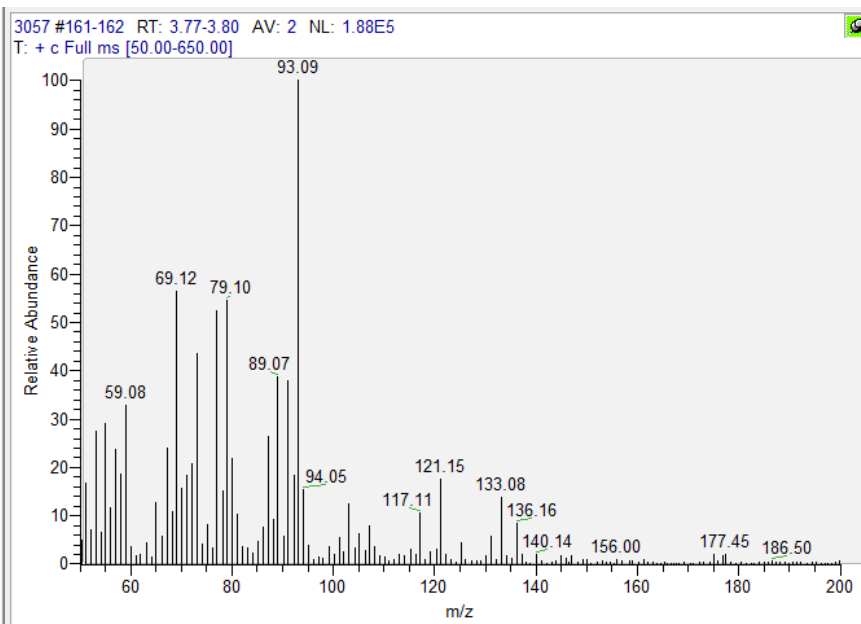
Reference of β -pinene



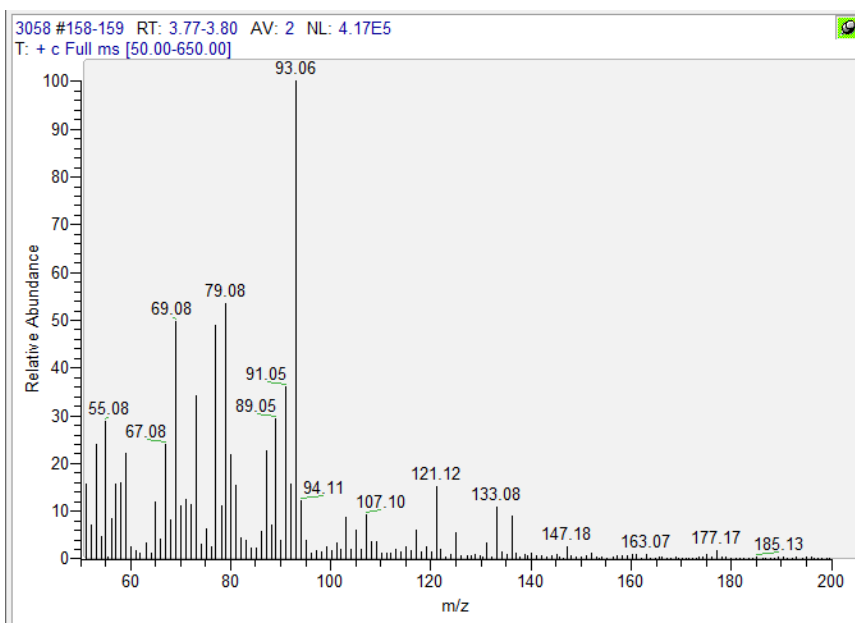
Sample 3075



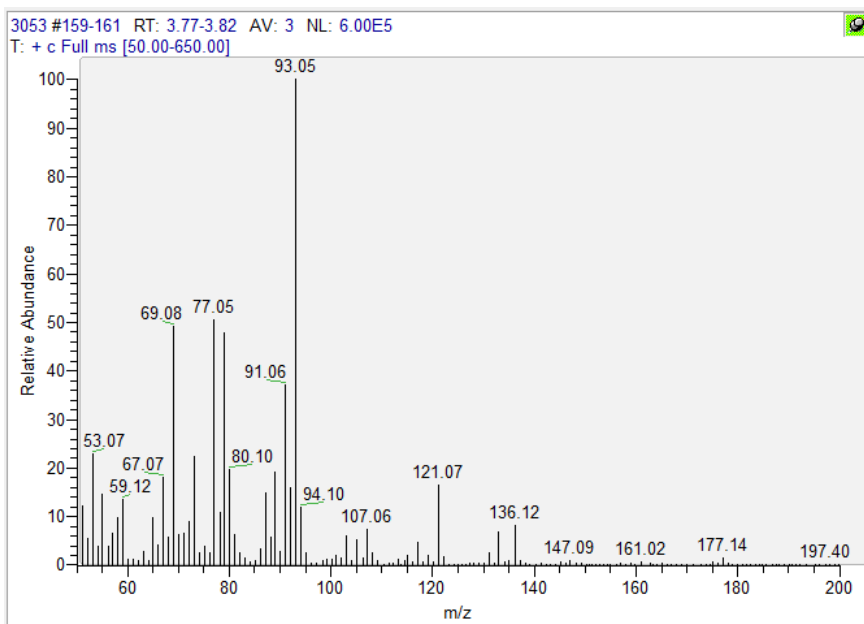
Sample 3057



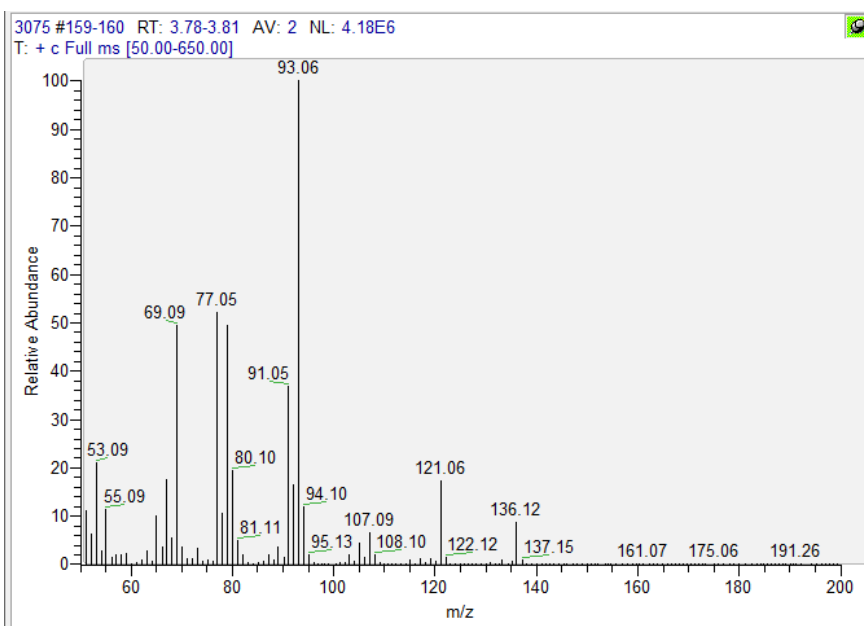
Sample 3058



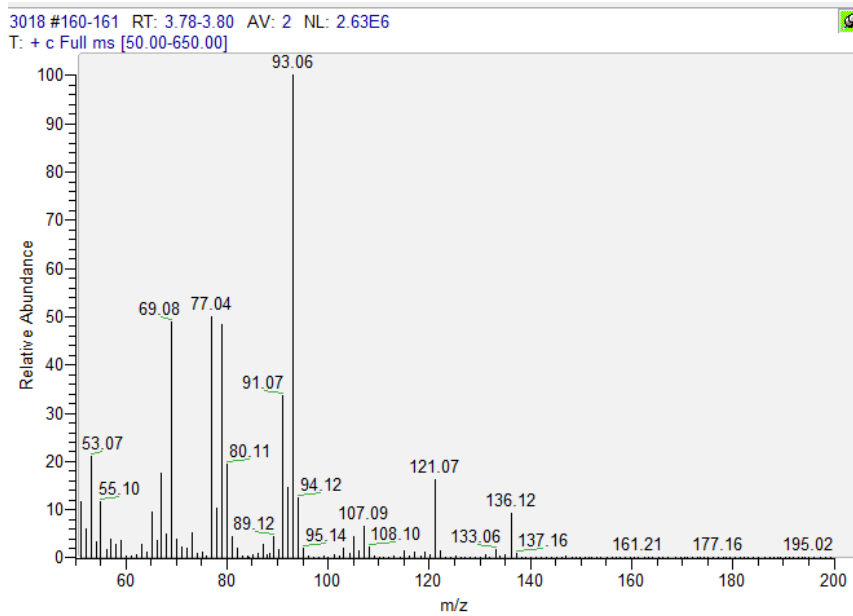
Sample 3053



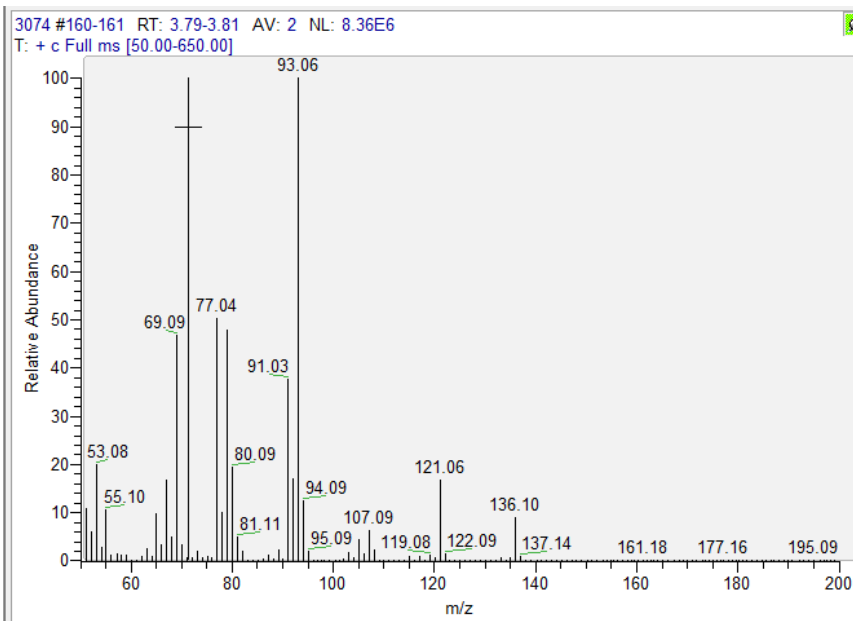
Sample 3075



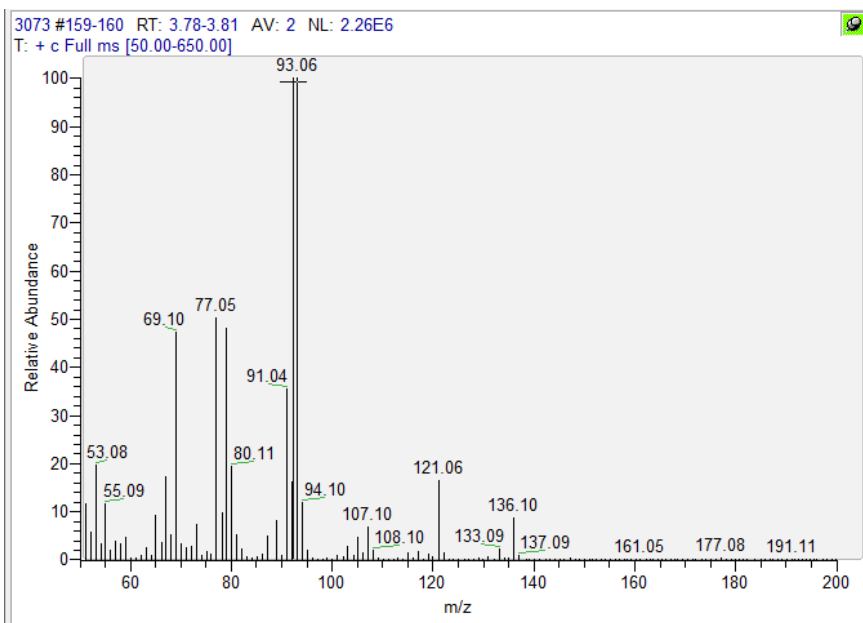
Sample 3018



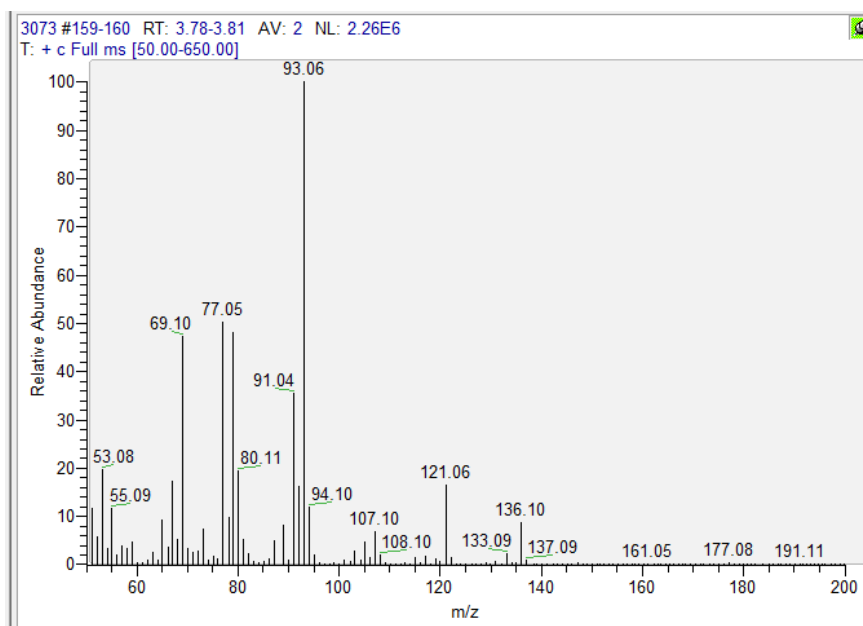
Sample 3074



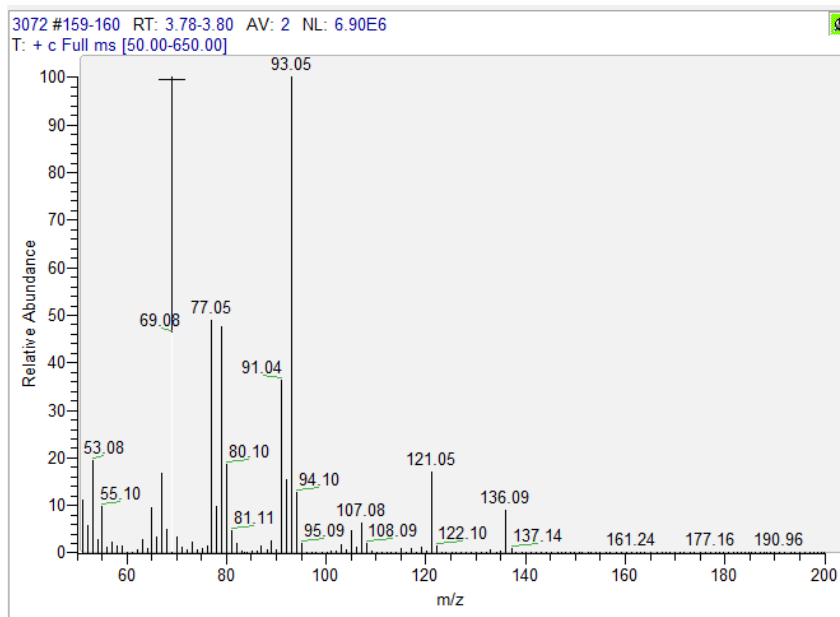
Sample 3073



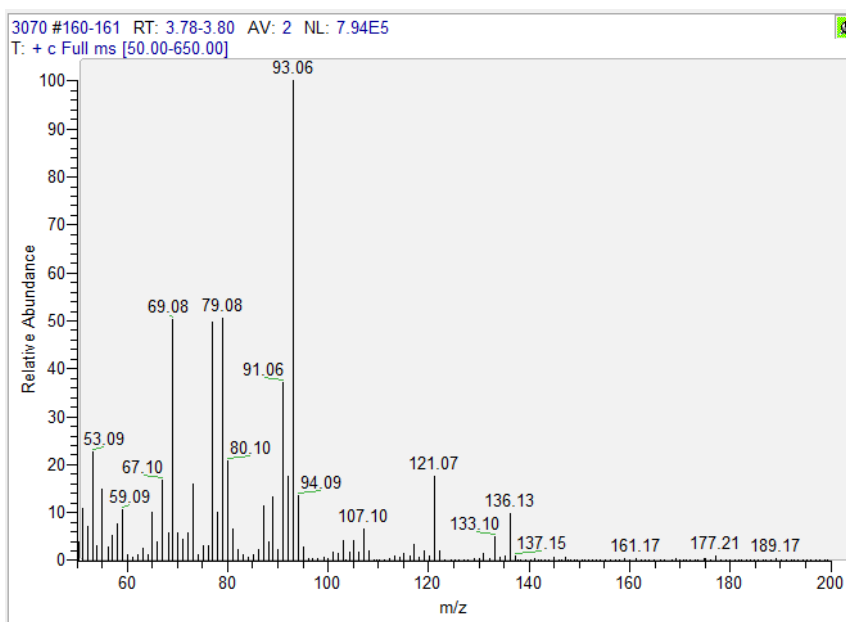
Sample 3073



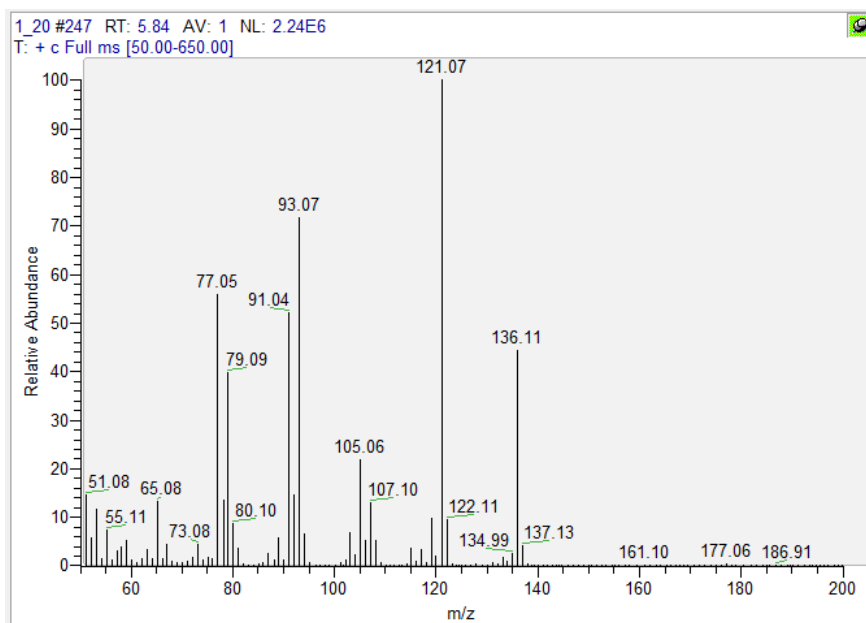
Sample 3072



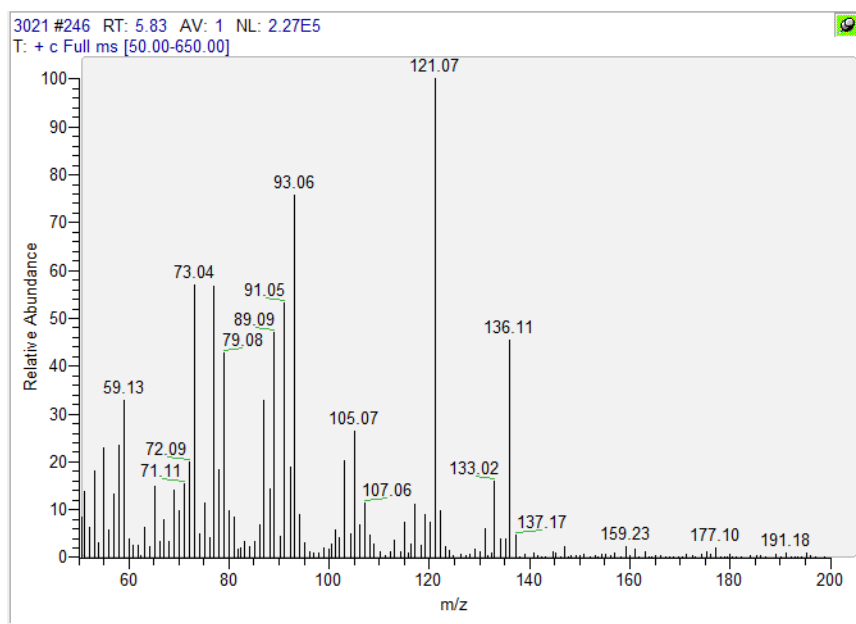
Sample 3070



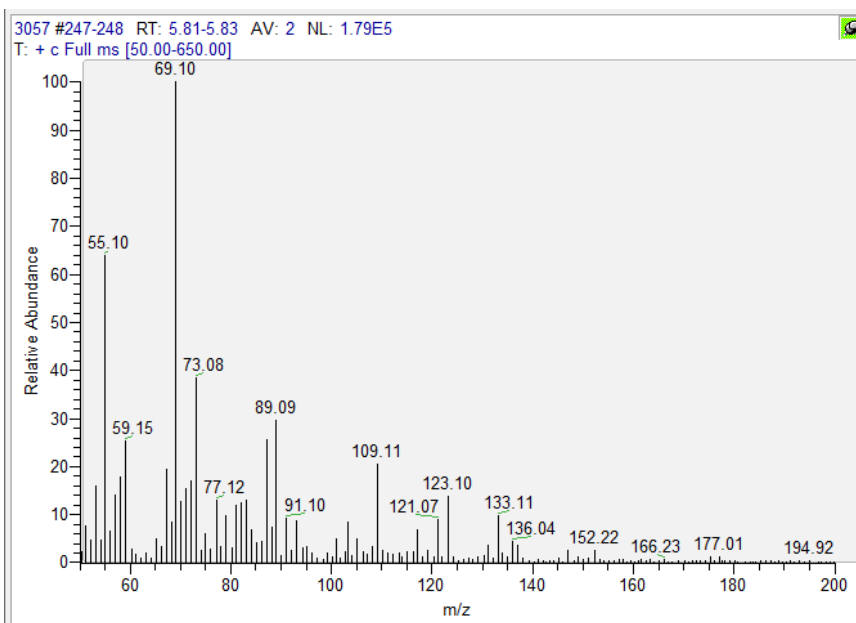
Reference of α -terpinene



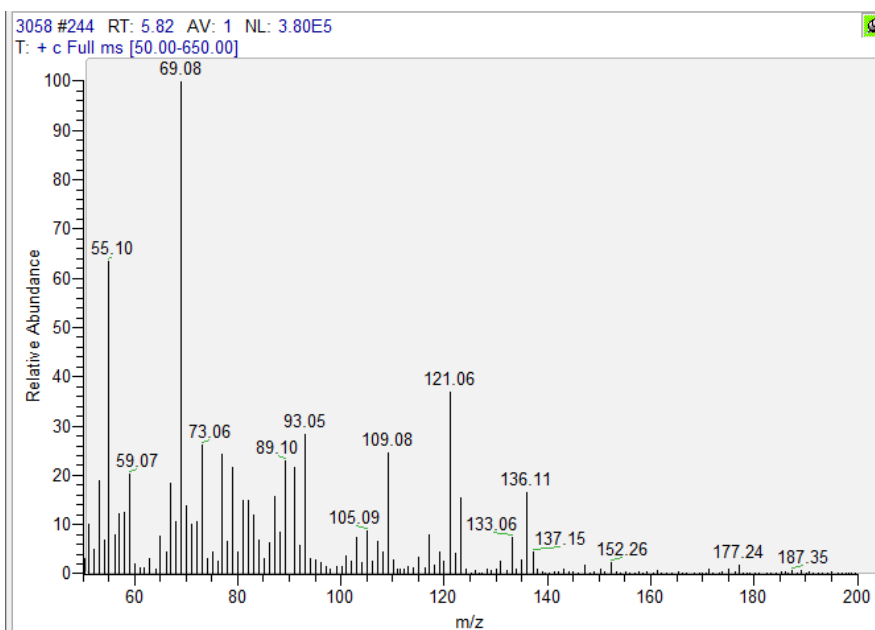
Sample 3021



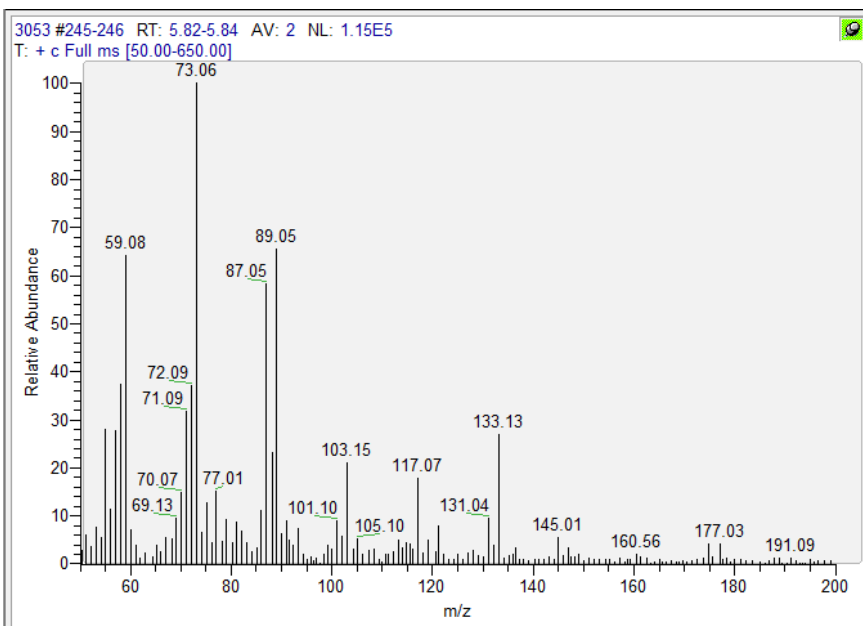
Sample 3057



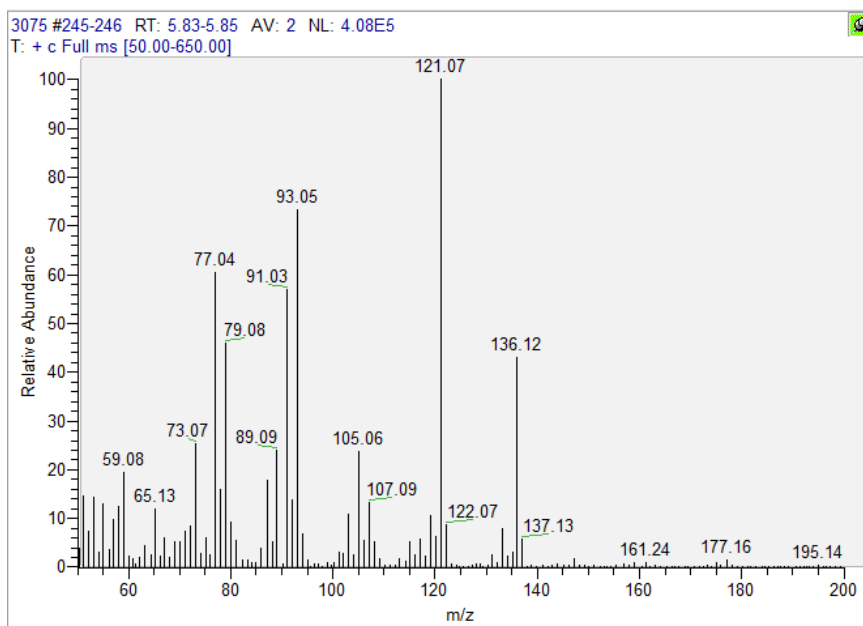
Sample 3058



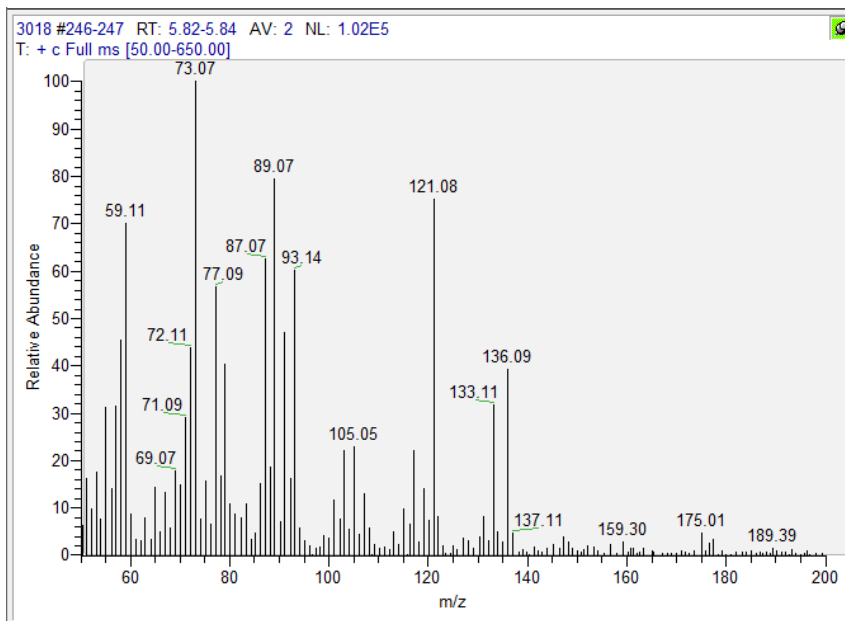
Sample 3053



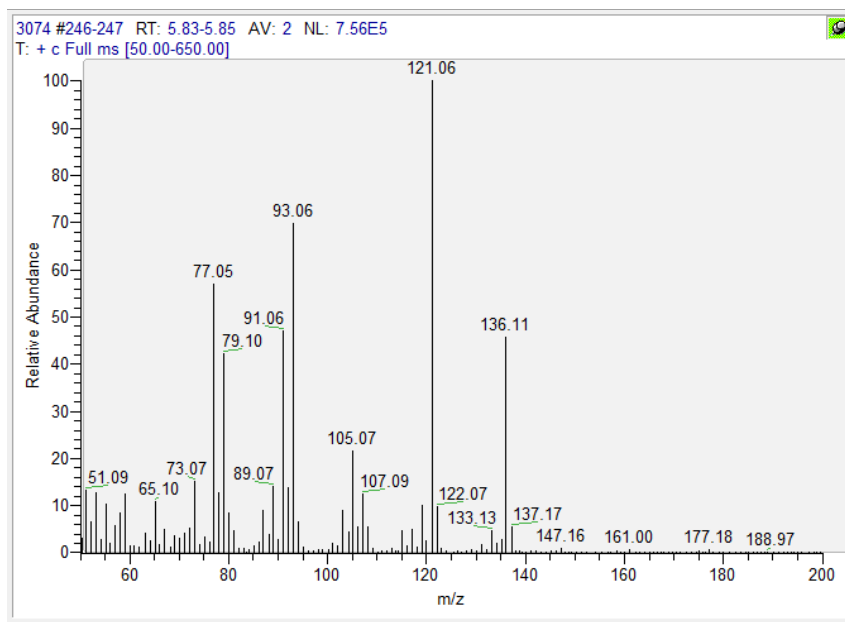
Sample 3075



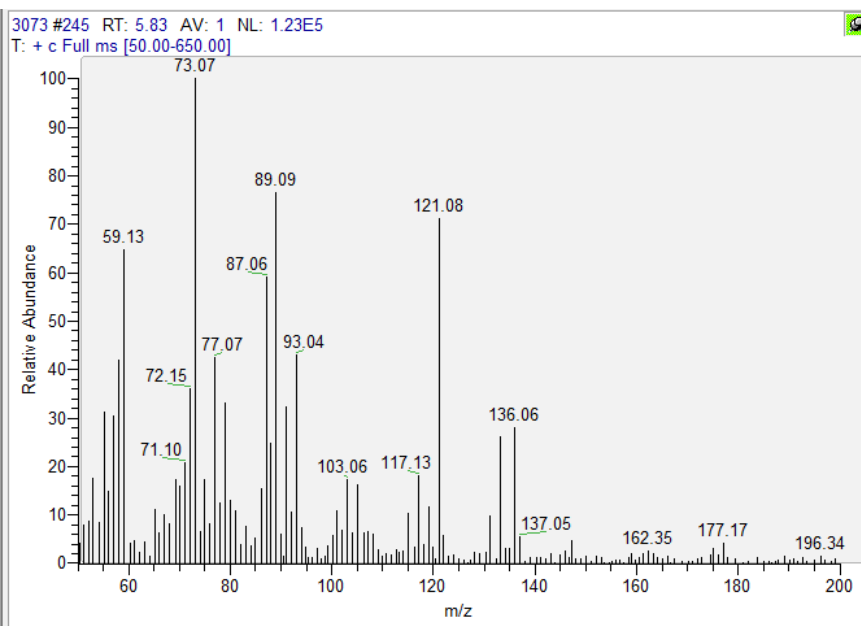
Sample 3018



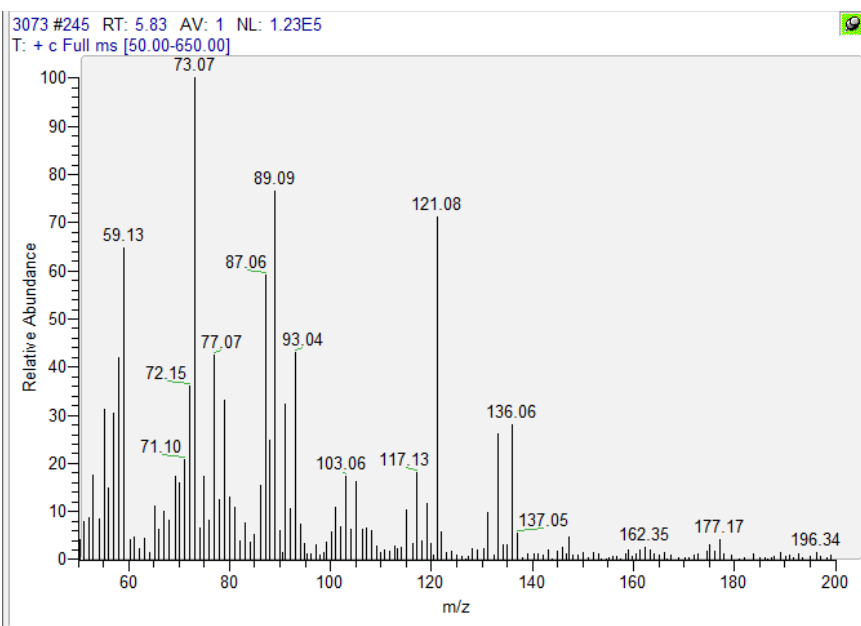
Sample 3074



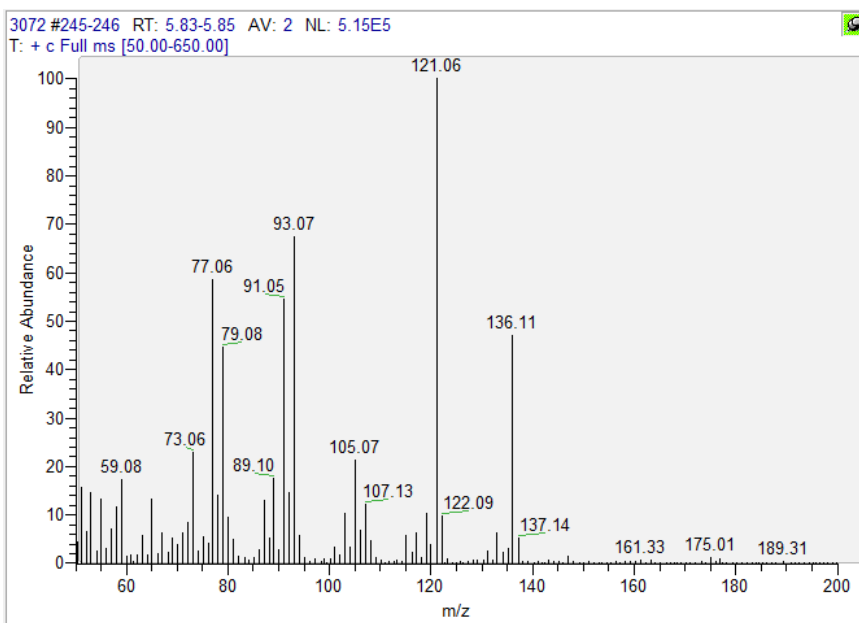
Sample 3073



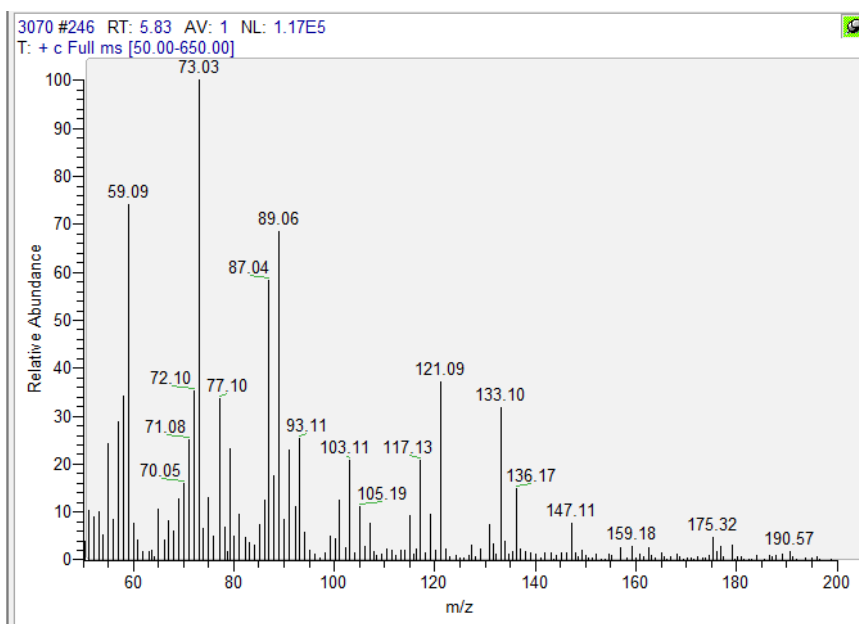
Sample 3073



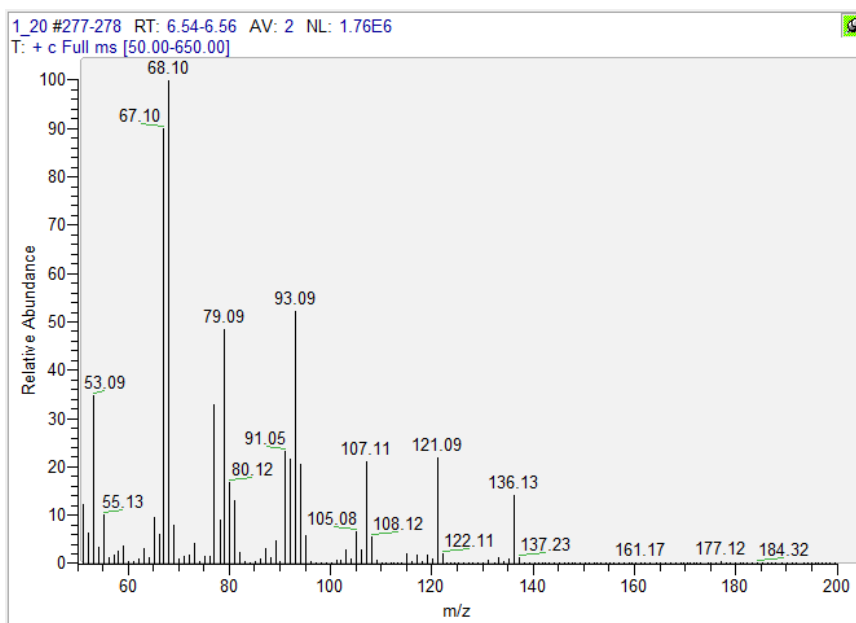
Sample 3072



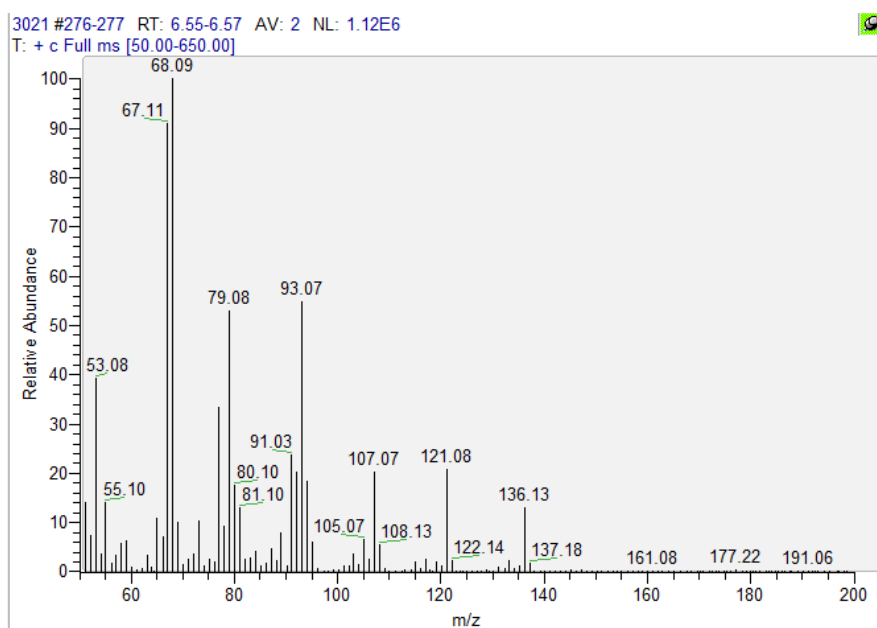
Sample 3070



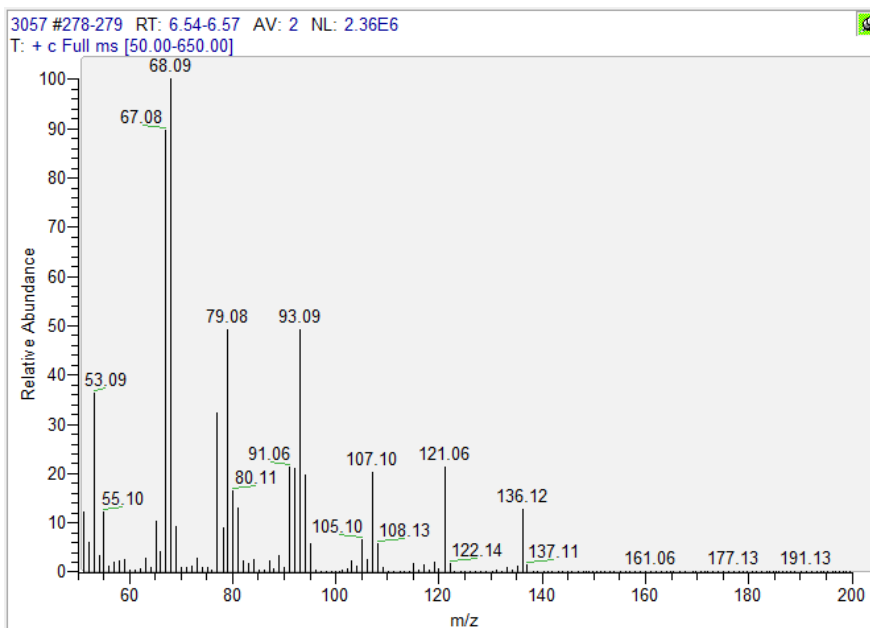
Reference of limonene:



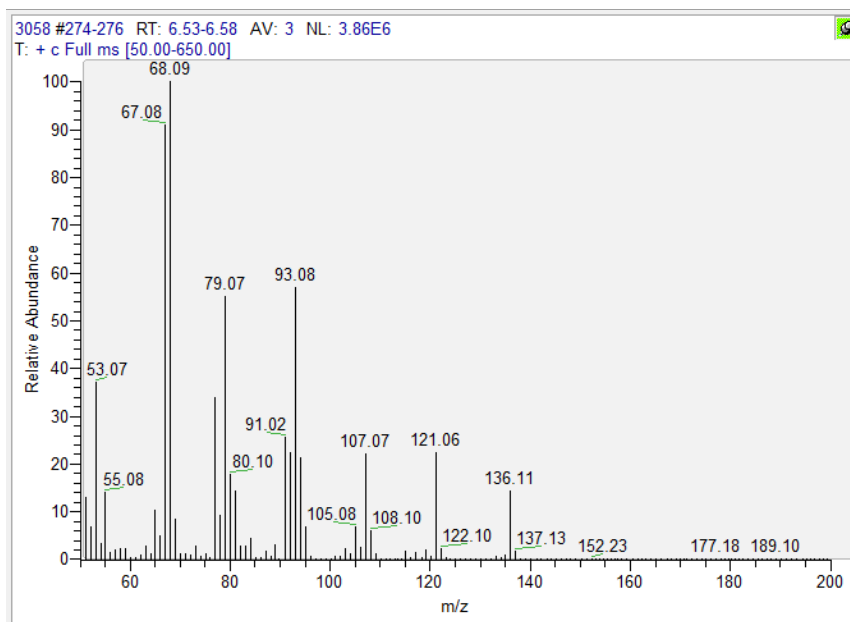
Sample 3021



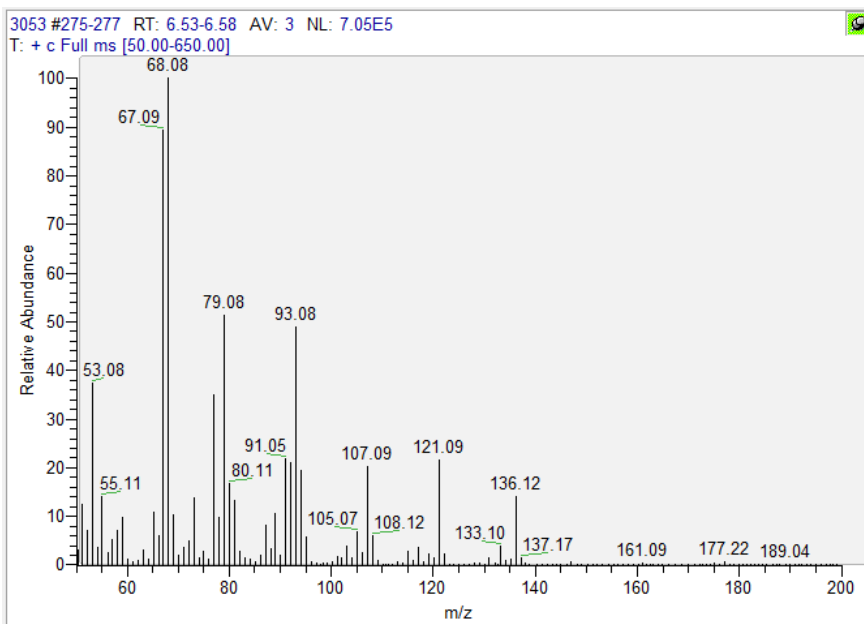
Sample 3057



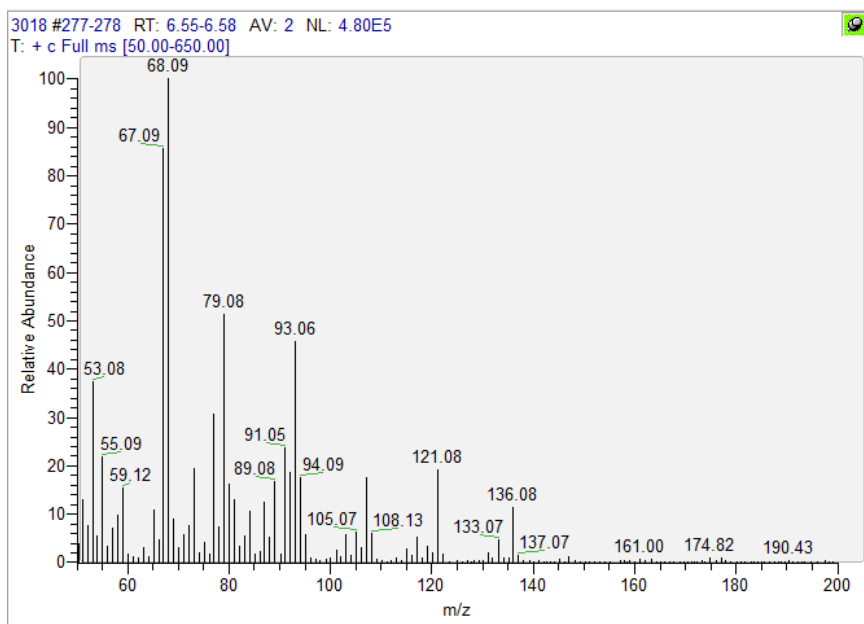
Sample 3058



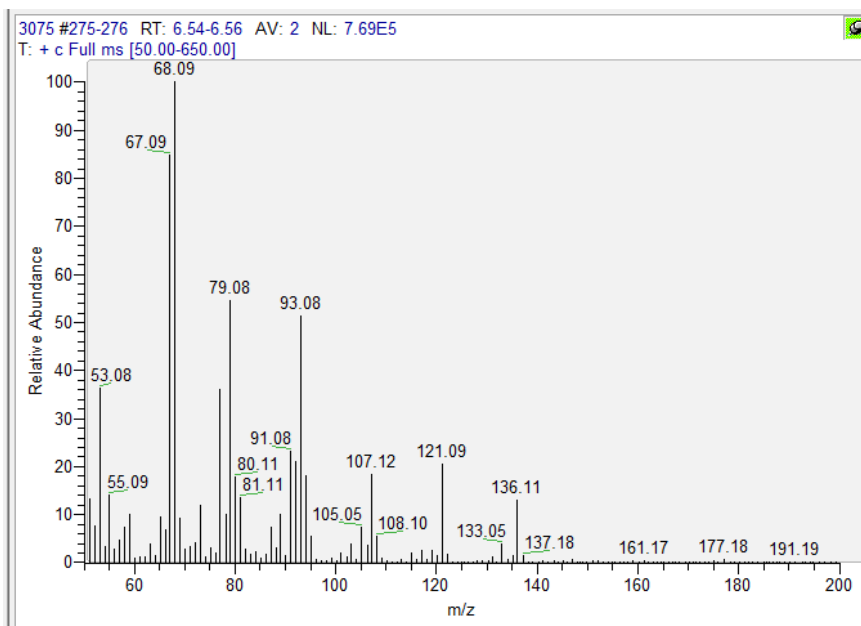
Sample 3053



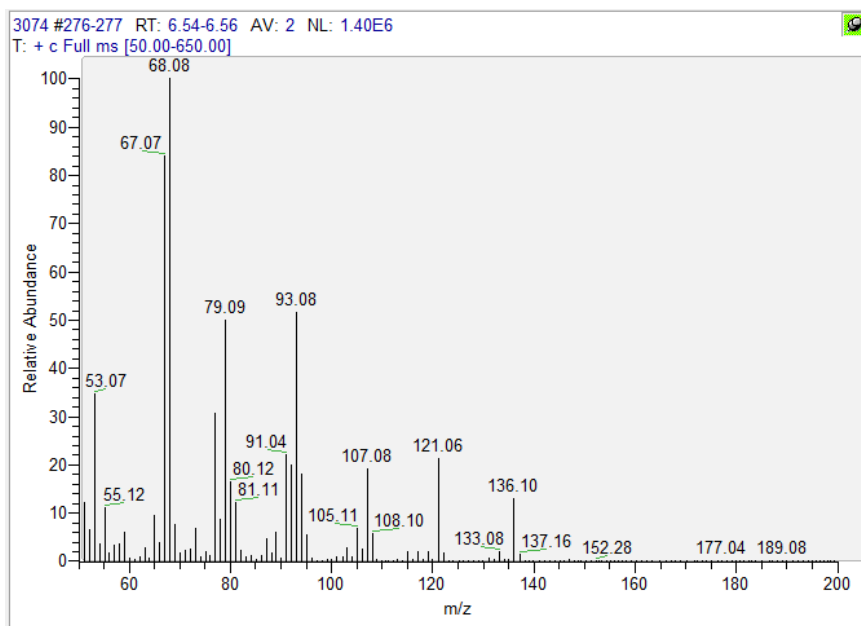
Sample 3018



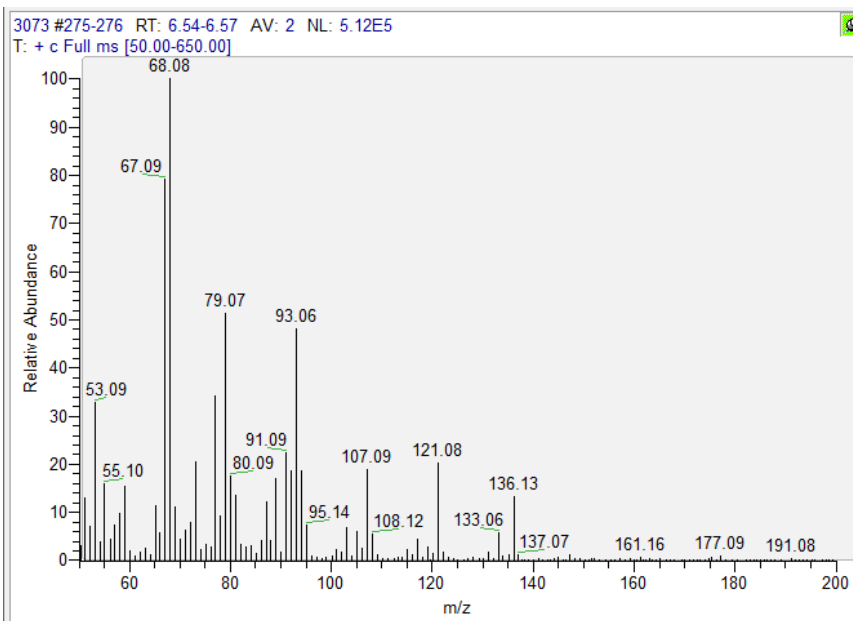
Sample 3075



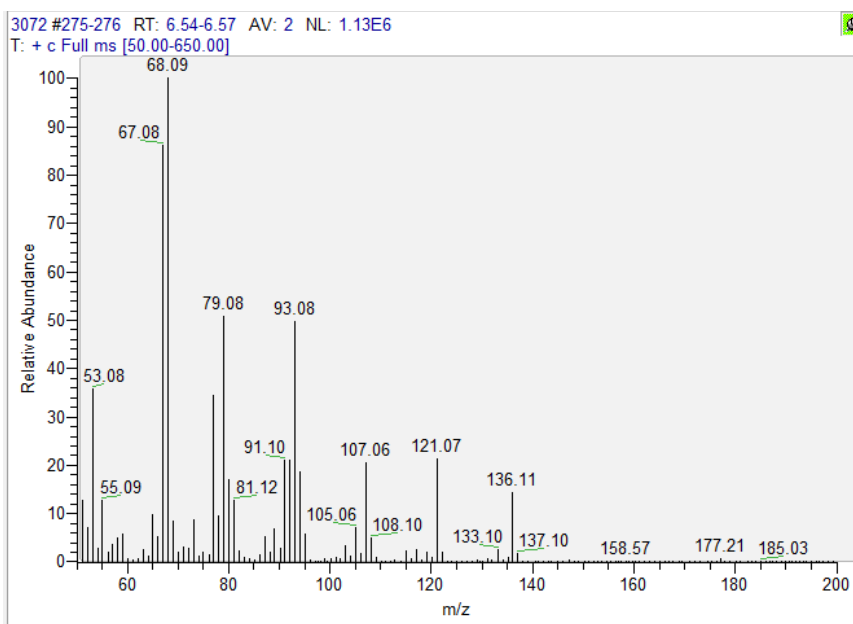
Sample 3074



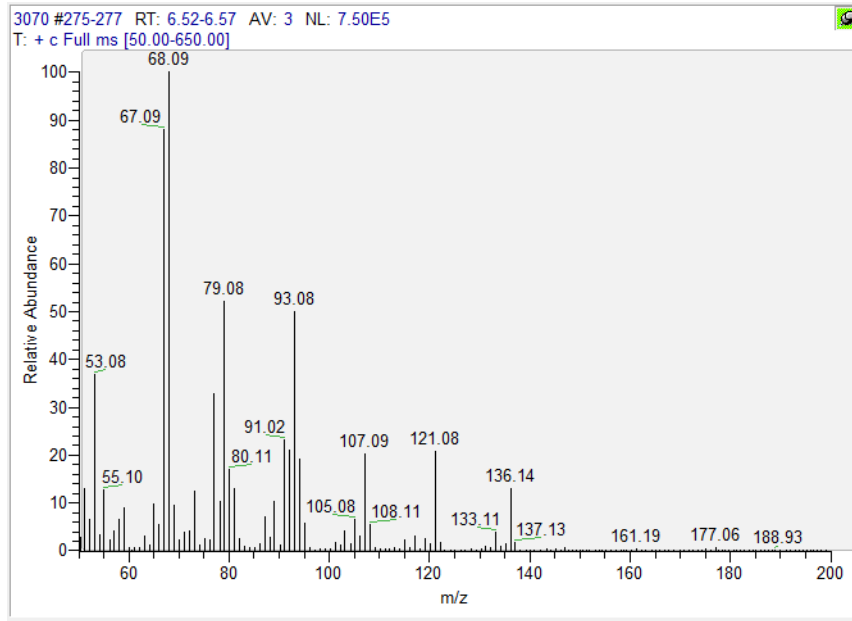
Sample 3073



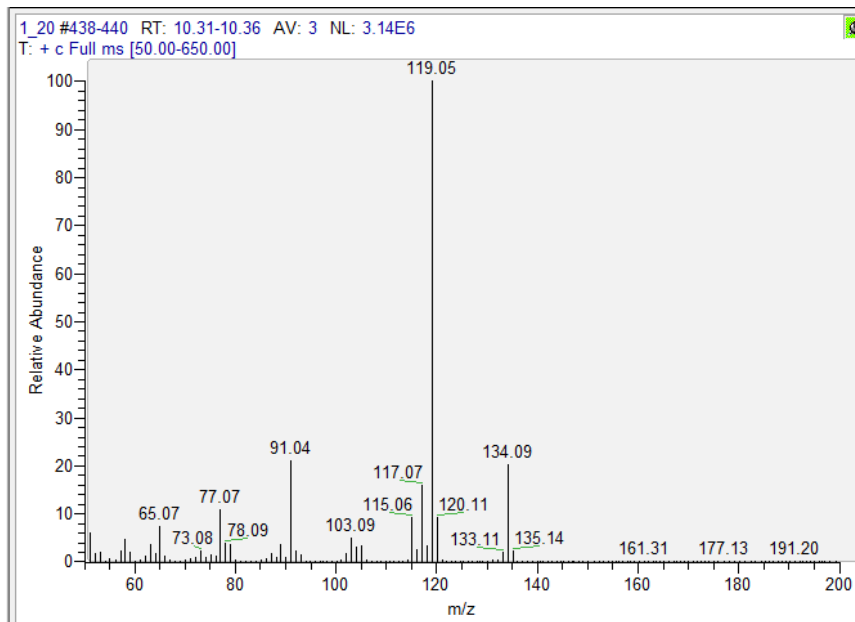
Sample 3072



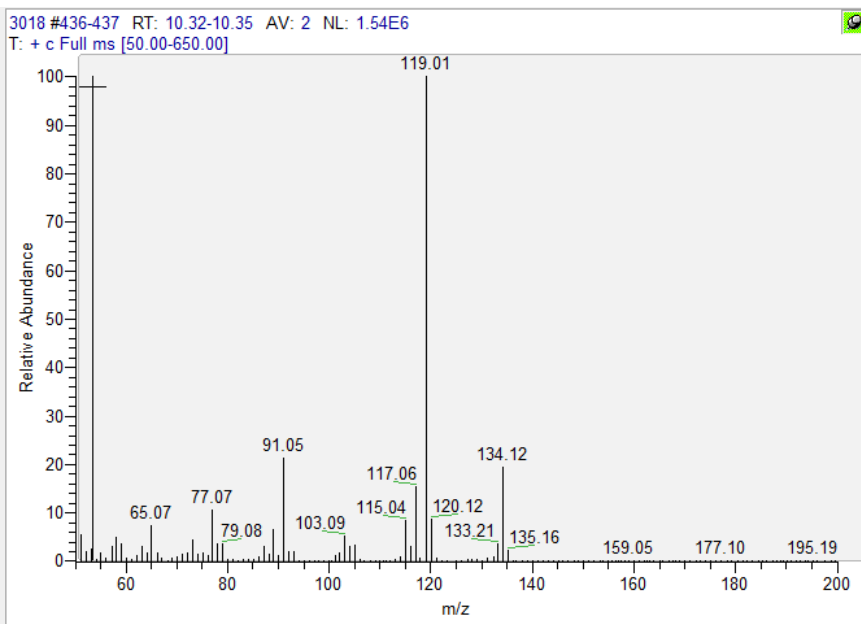
Sample 3070



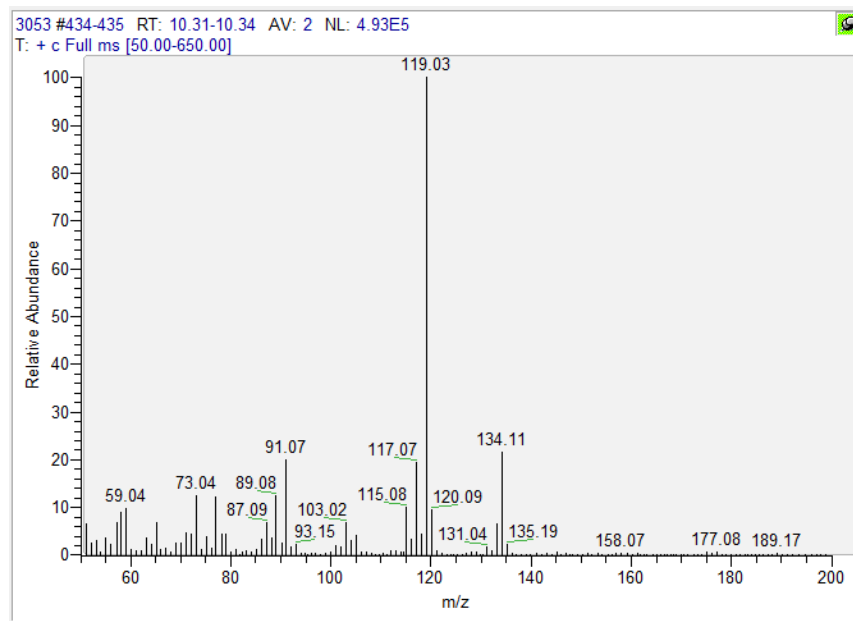
Reference of p-cymene



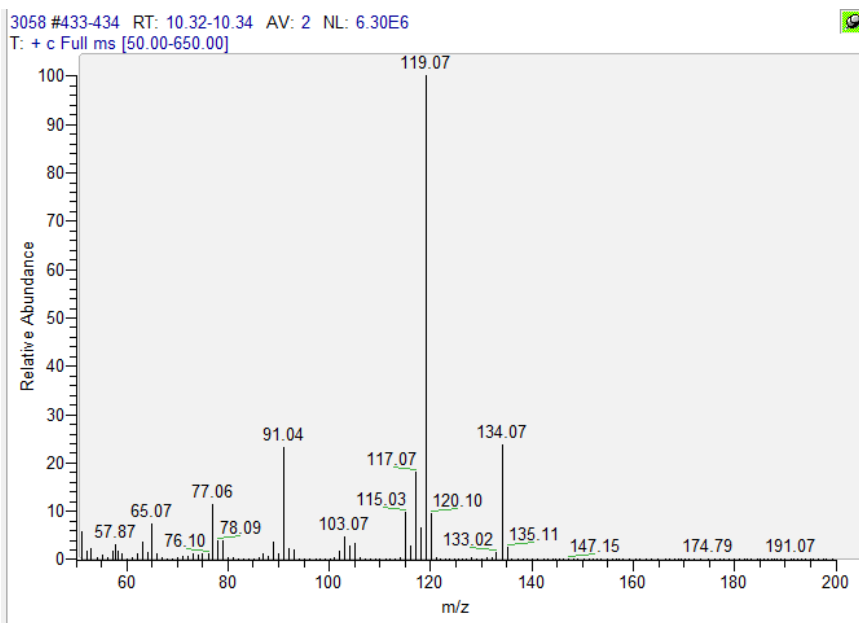
Sample 3018



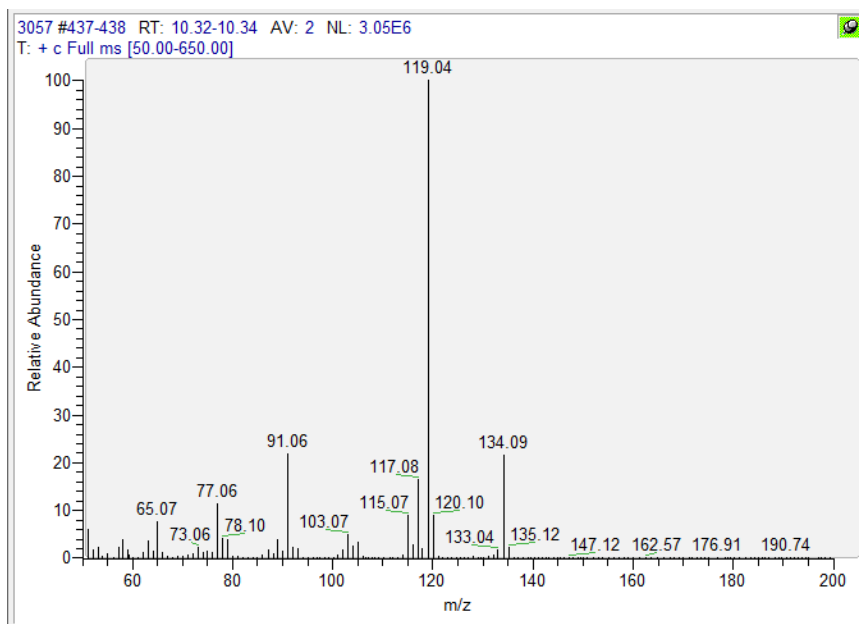
Sample 3053



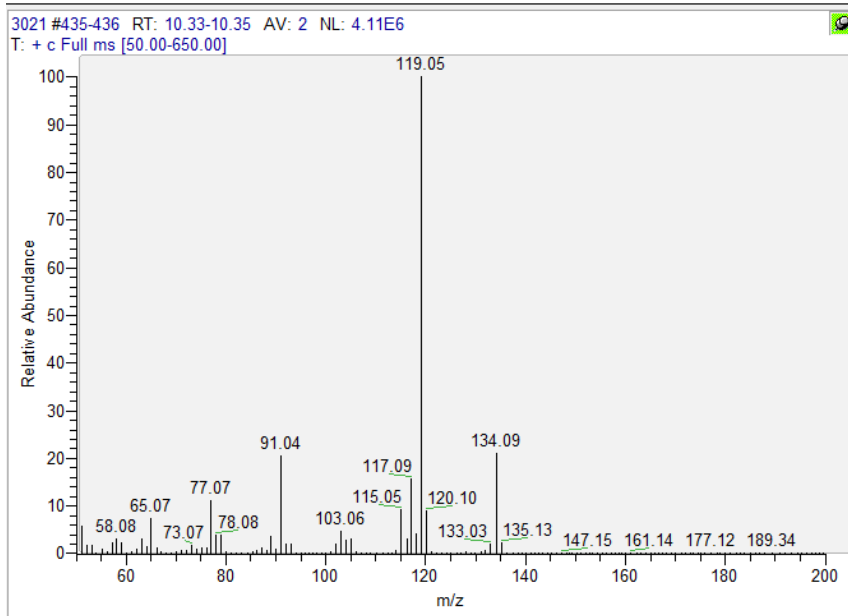
Sample 3058



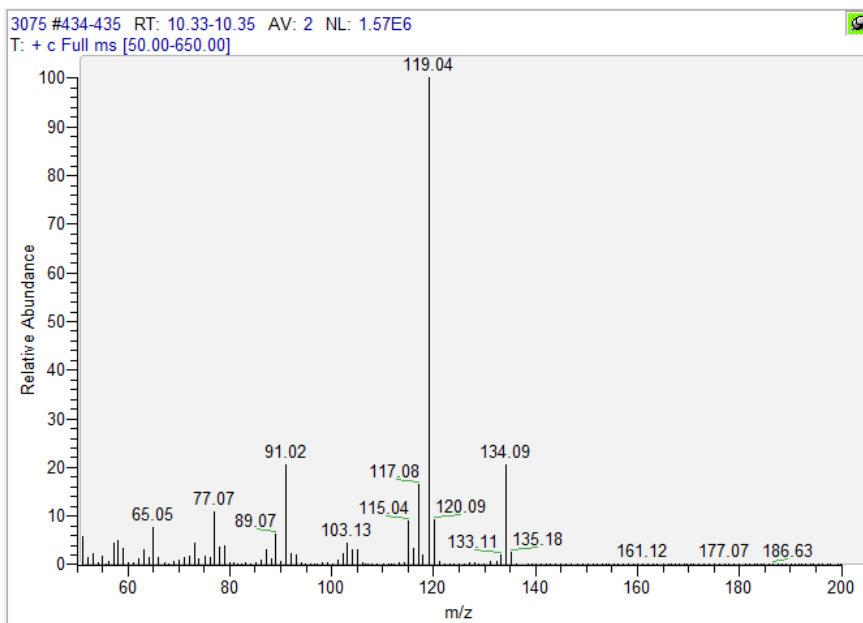
Sample 3057



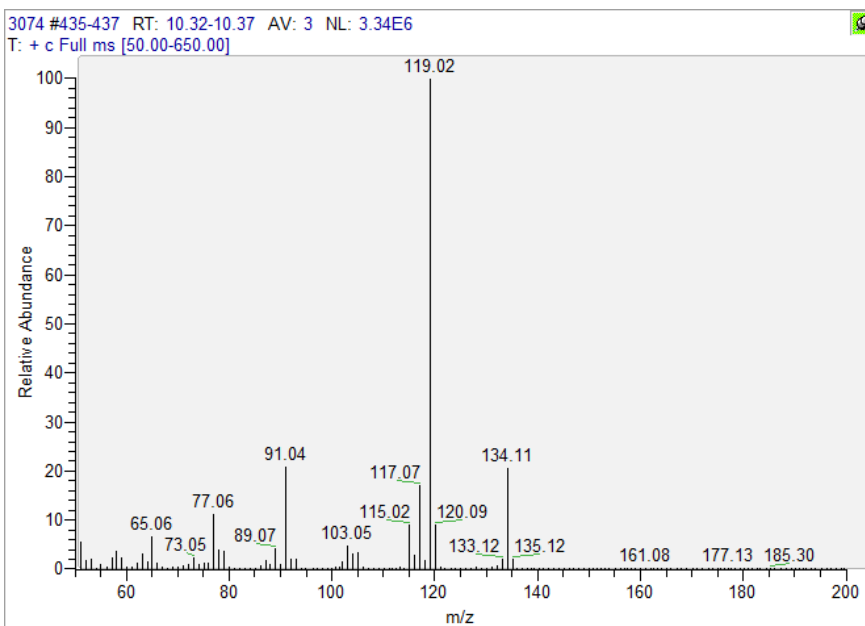
Sample 3021



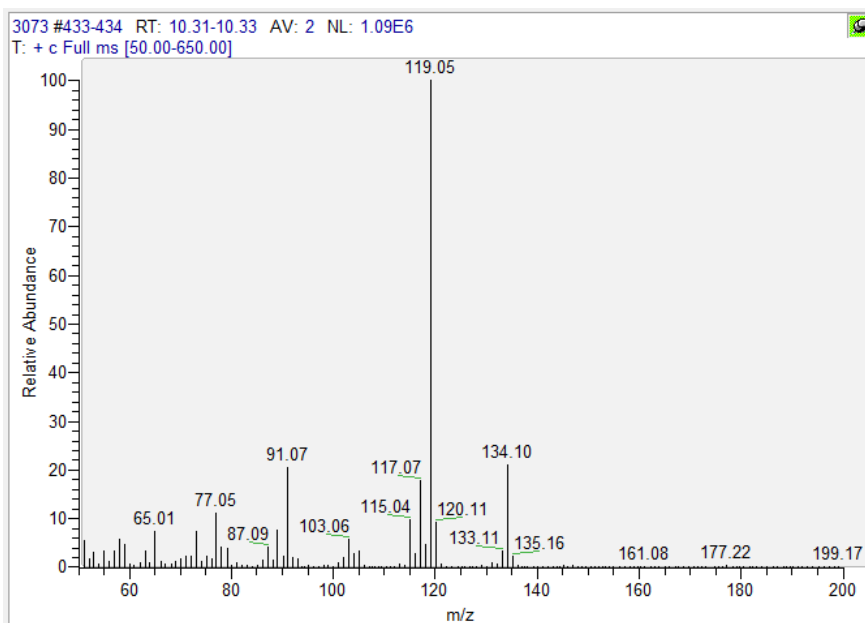
Sample 3075



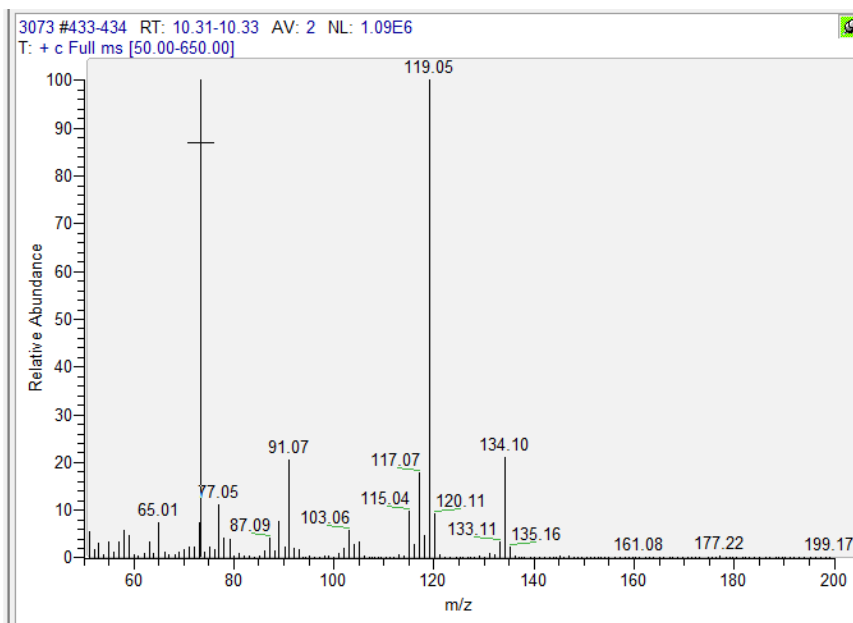
Sample 3074



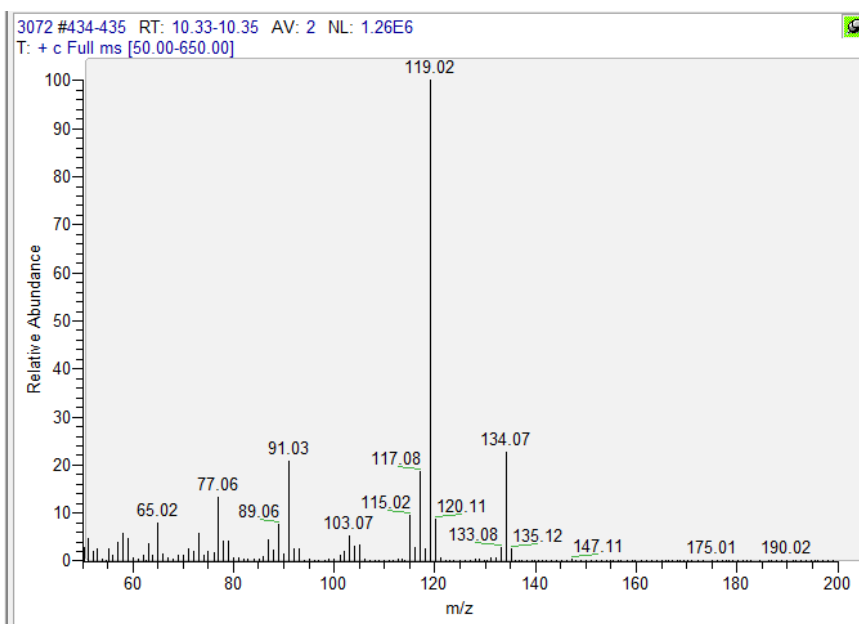
Sample 3073



Sample 3073

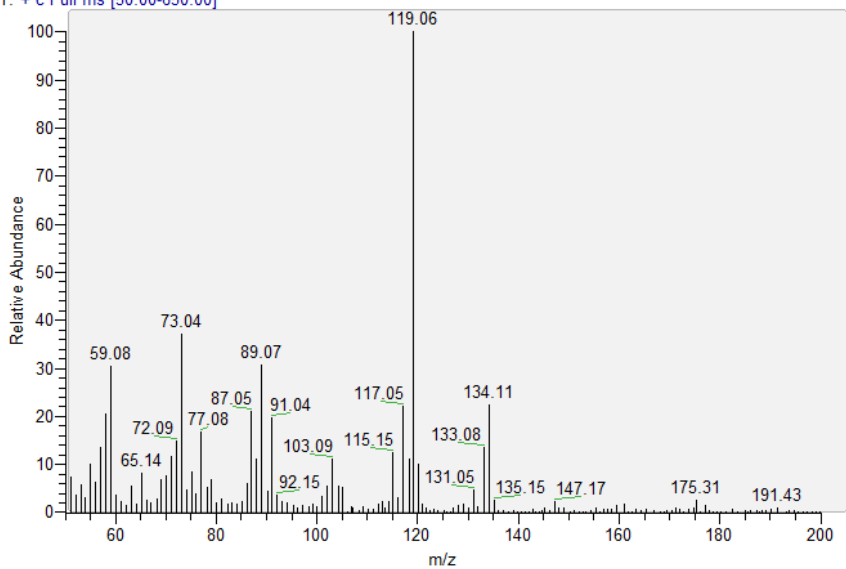


Sample 3072



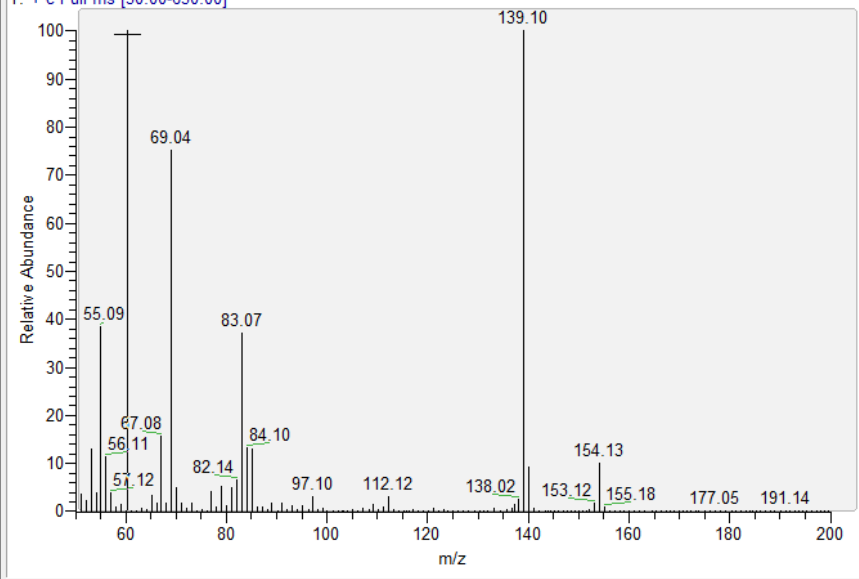
Sample 3070

3070 #436-437 RT: 10.33-10.35 AV: 2 NL: 1.75E5
T: + c Full ms [50.00-650.00]

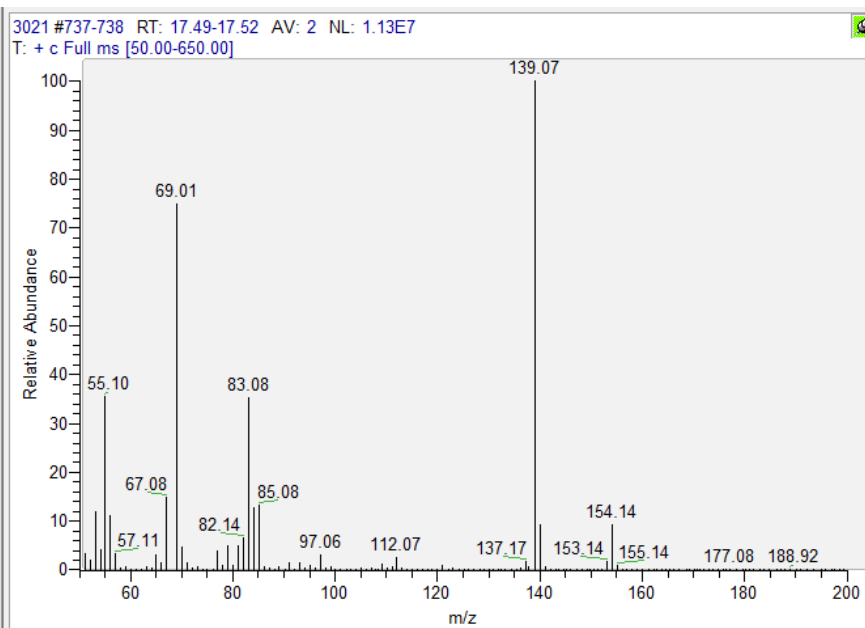


Reference of rose oxide

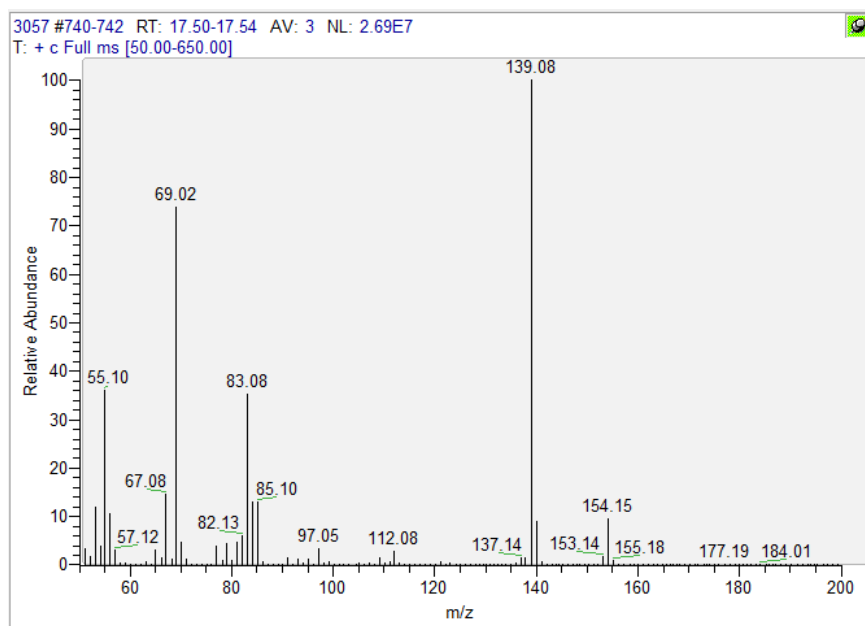
1_20 #740-742 RT: 17.45-17.50 AV: 3 NL: 3.89E6
T: + c Full ms [50.00-650.00]



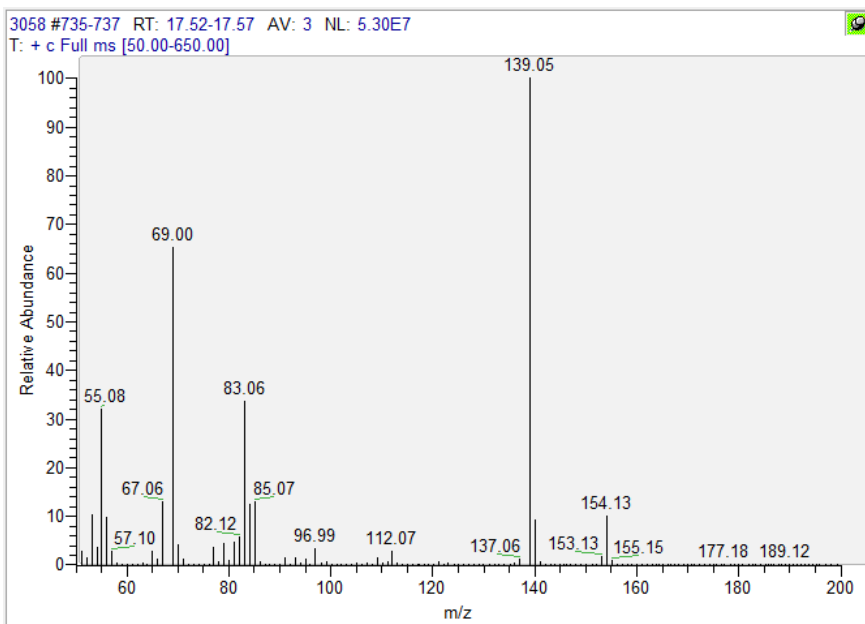
Sample 3021



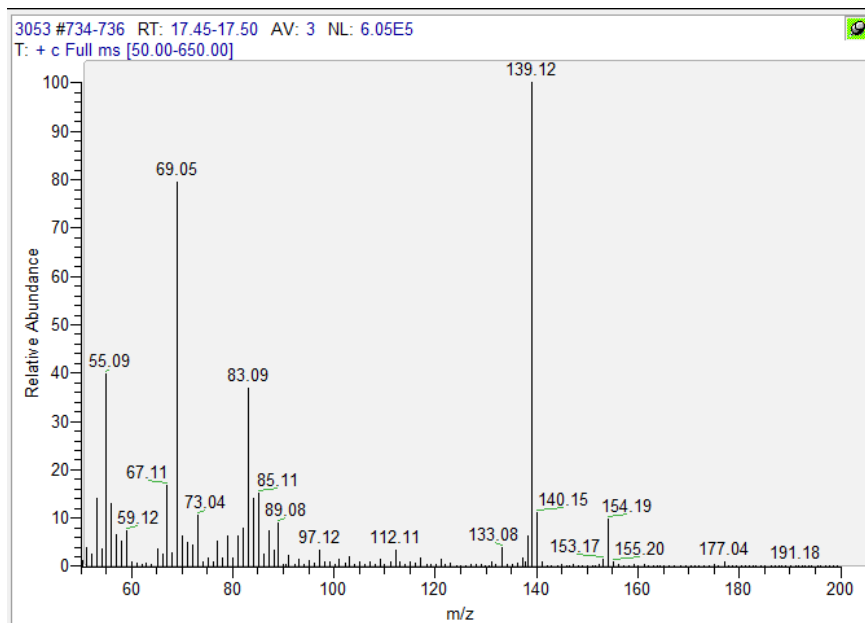
Sample 3057



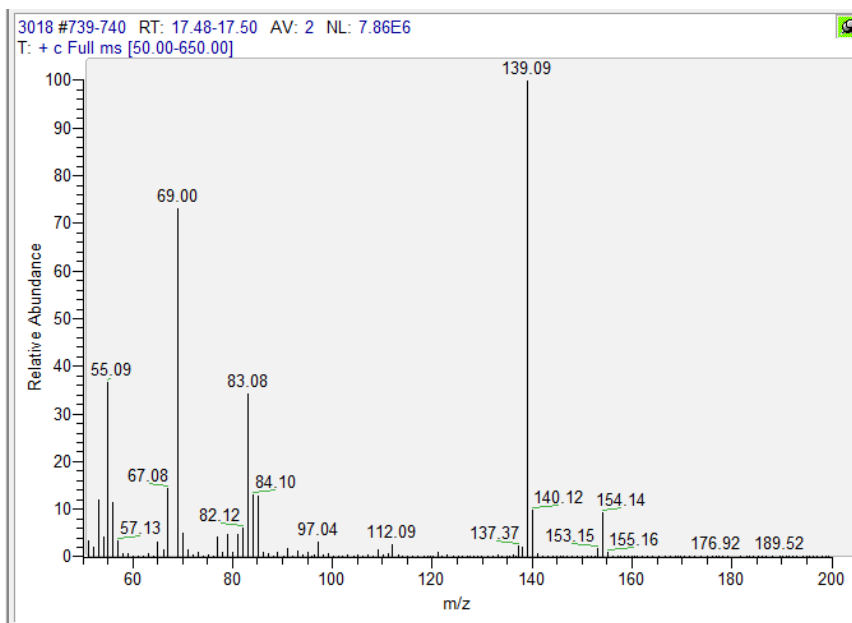
Sample 3058



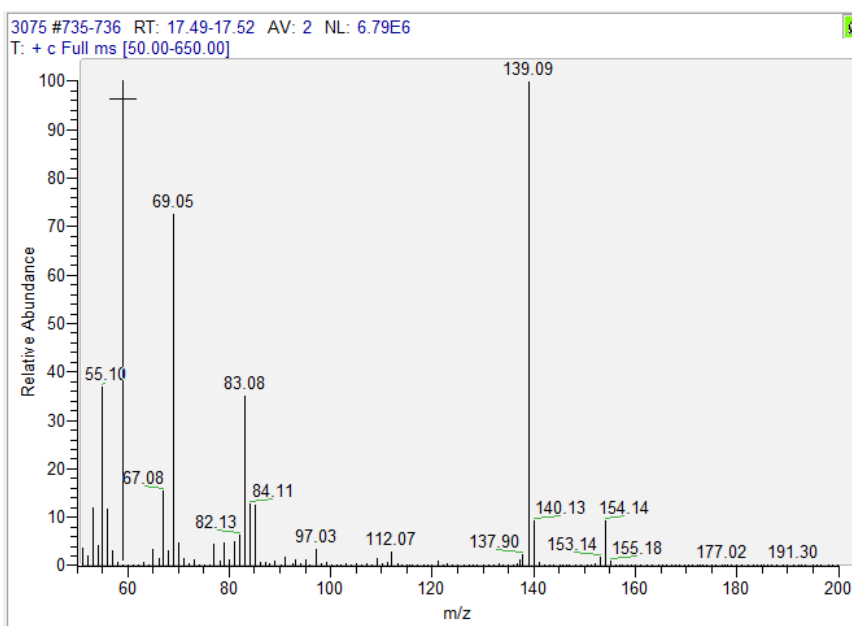
Sample 3053



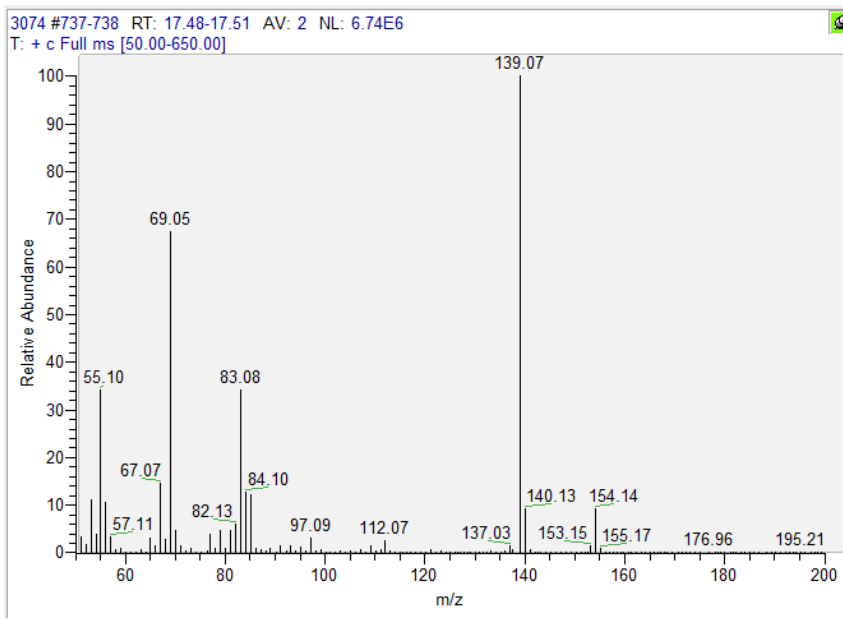
Sample 3018



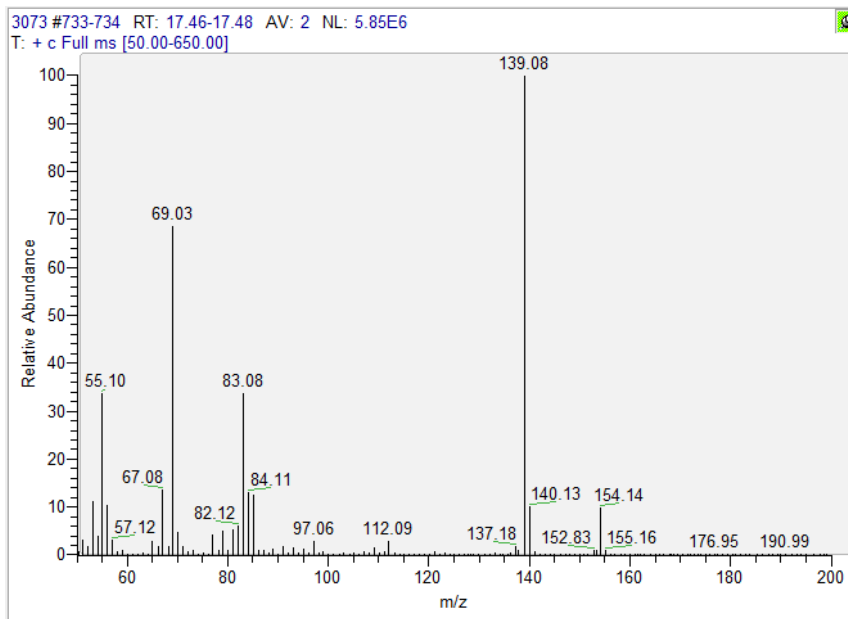
Sample 3075



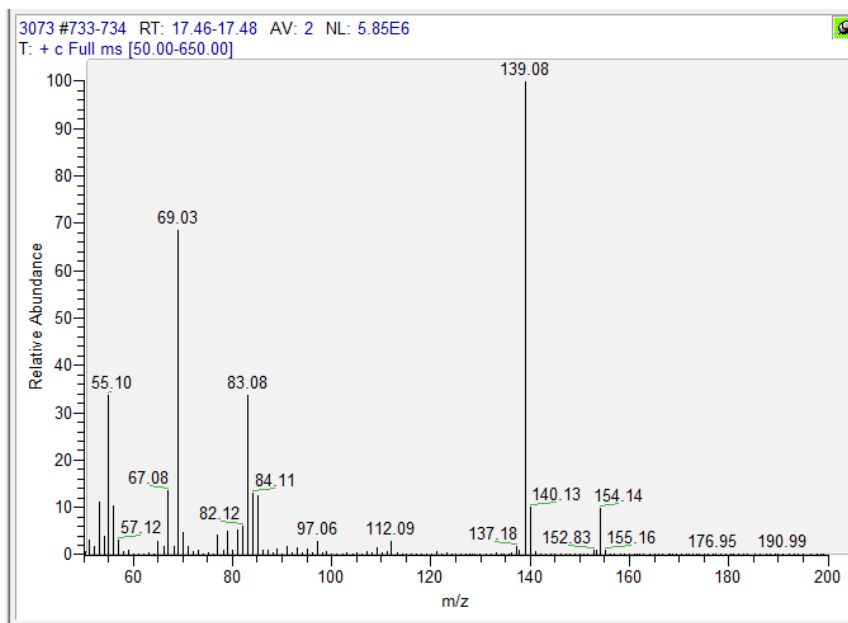
Sample 3074



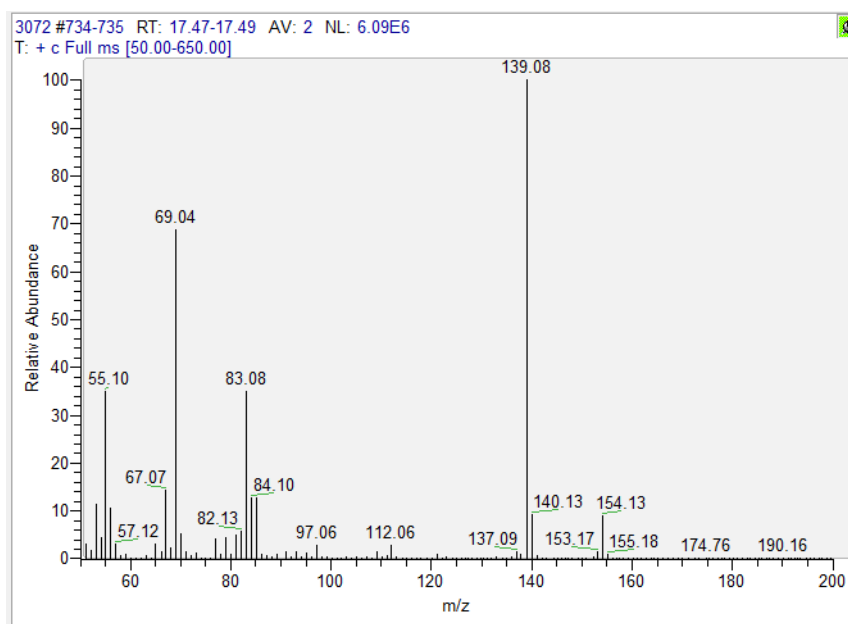
Sample 3073



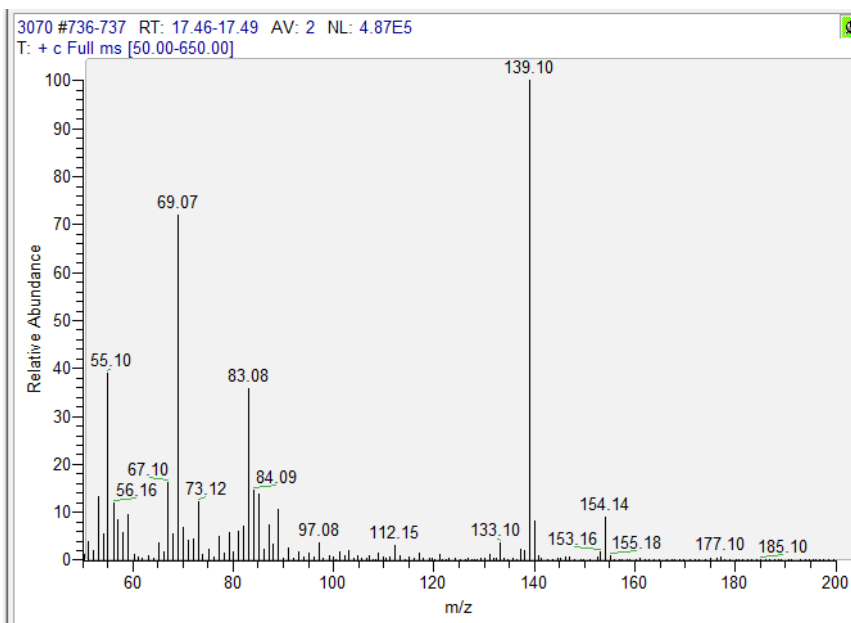
Sample 3073



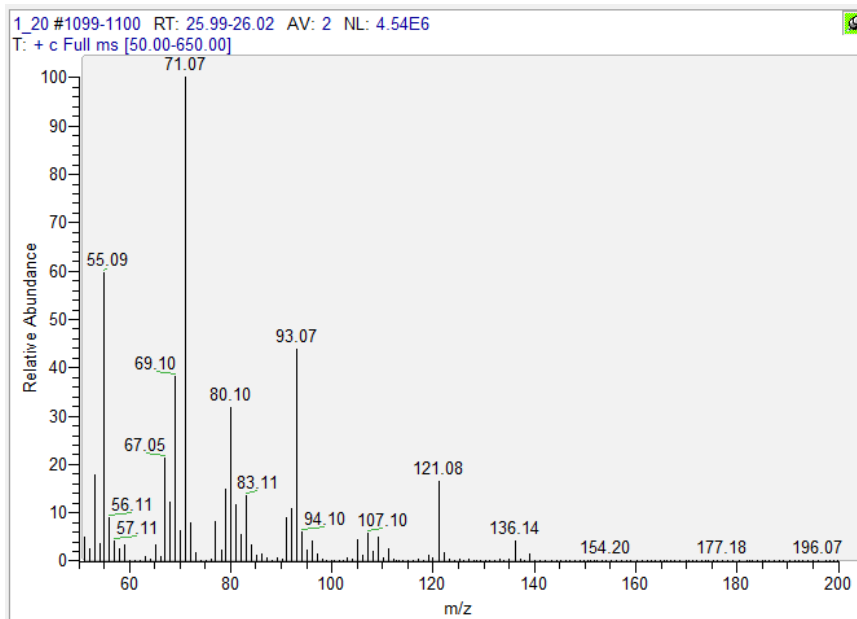
Sample 3072



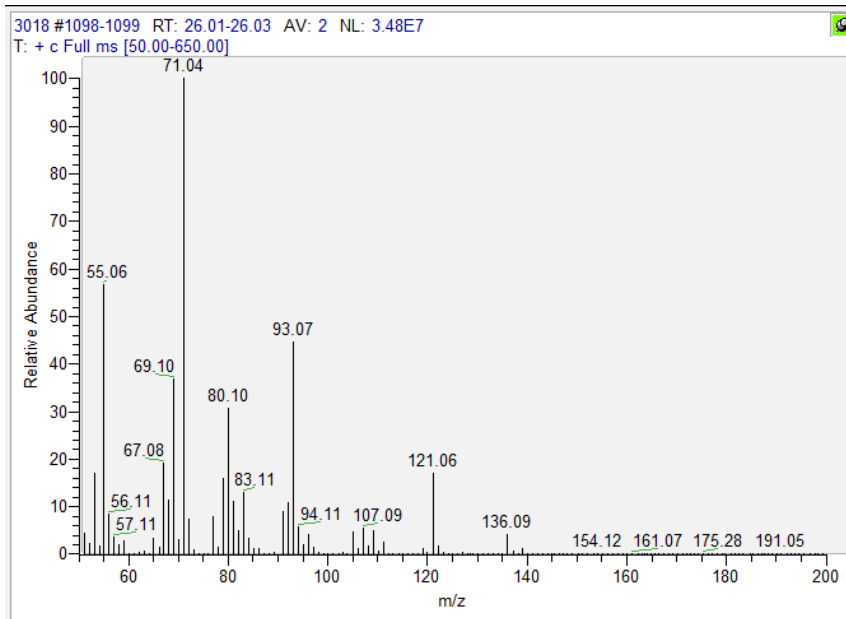
Sample 3070



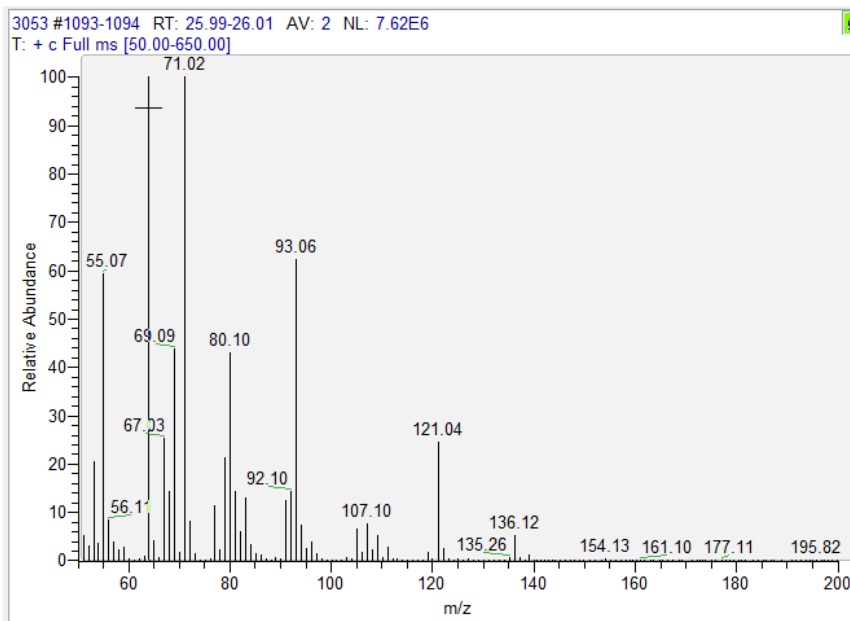
Reference of linalool



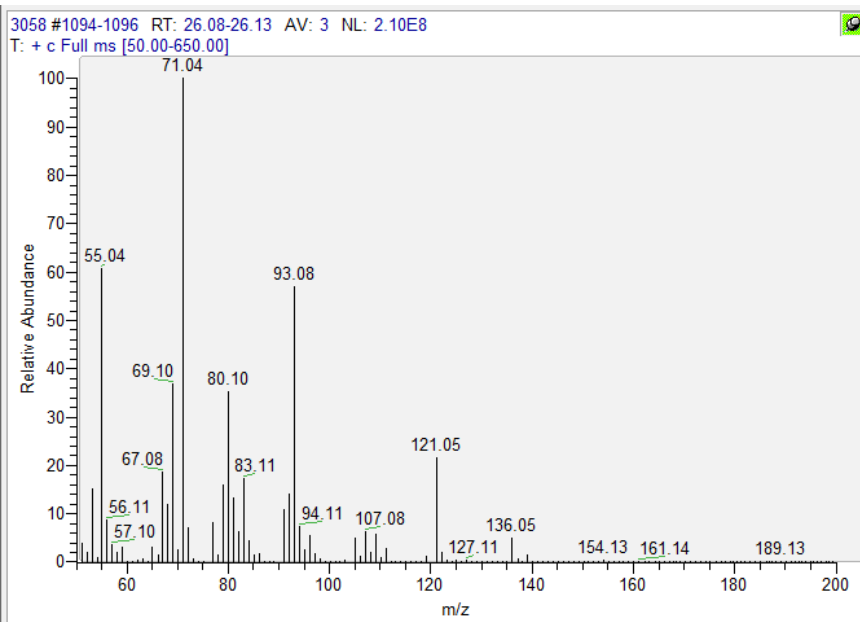
Sample 3018



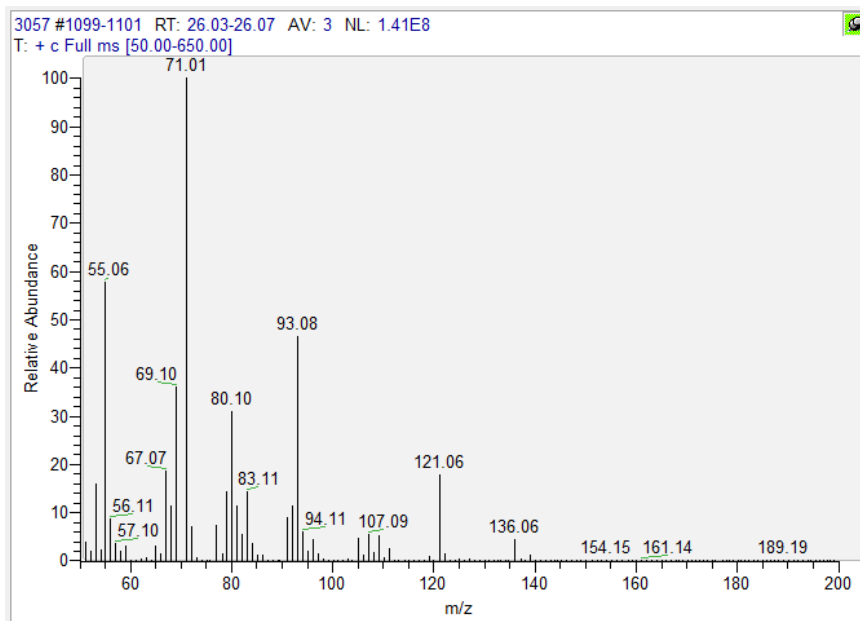
Sample 3053



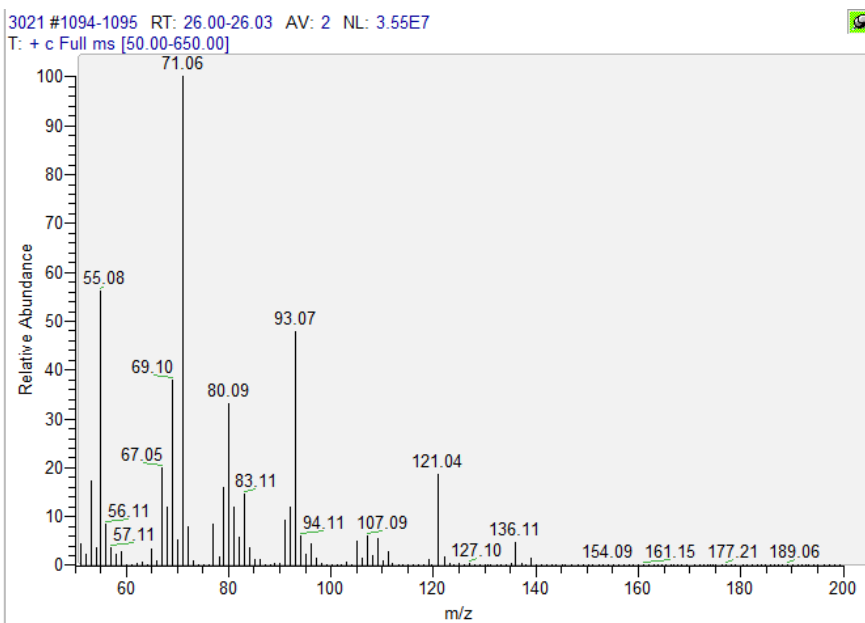
Sample 3058



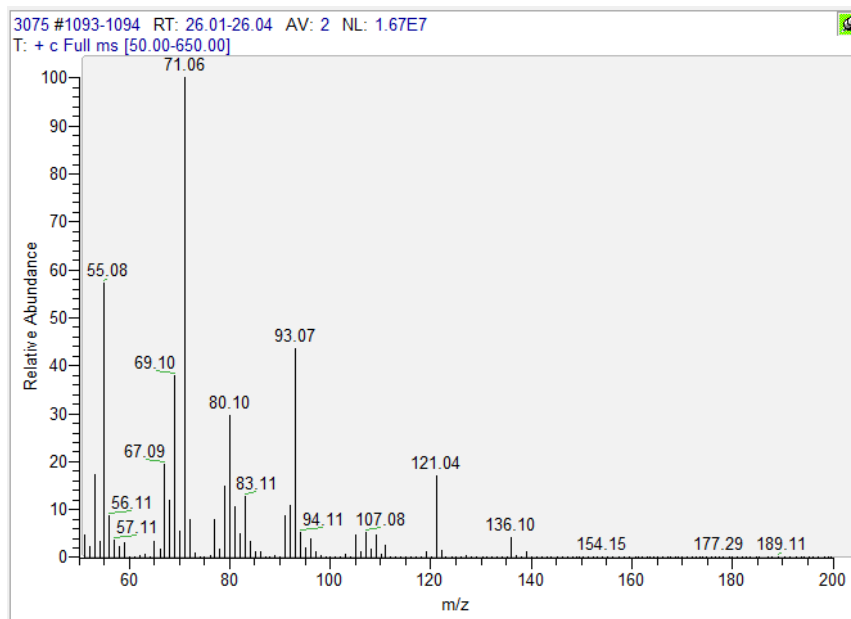
Sample 3057



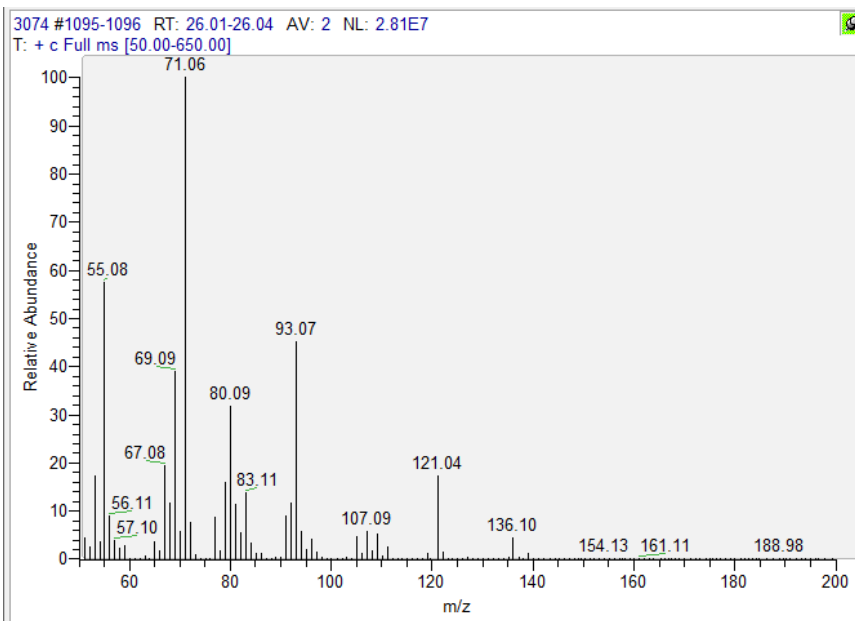
Sample 3021



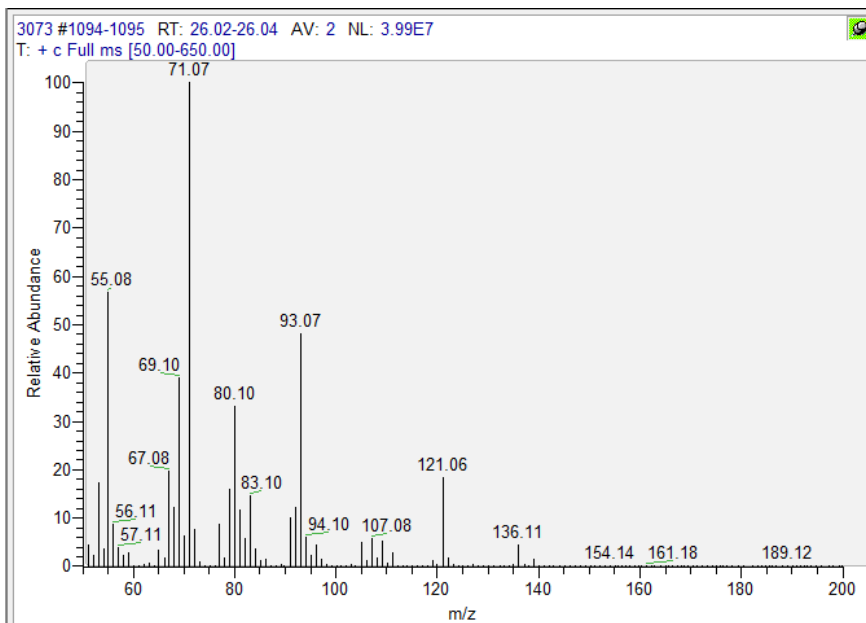
Sample 3075



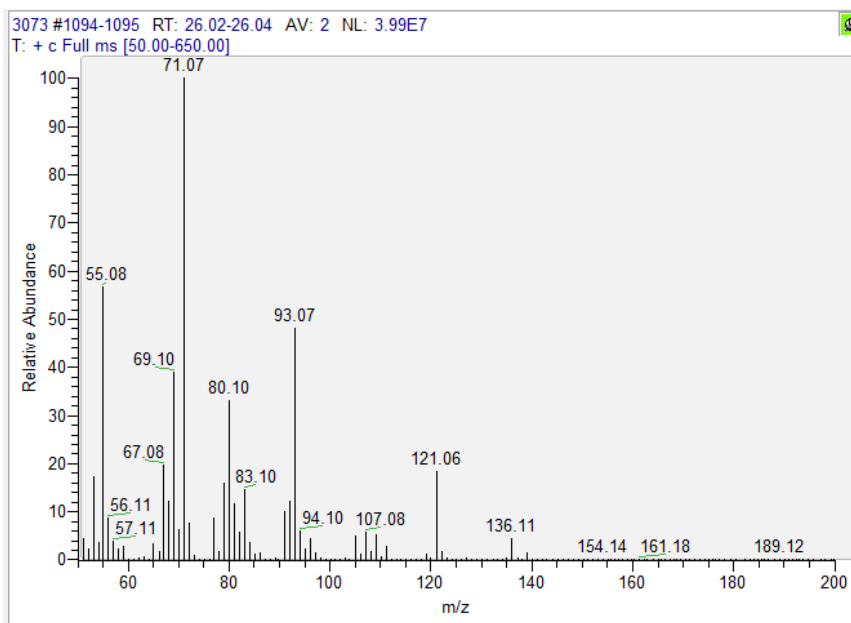
Sample 3074



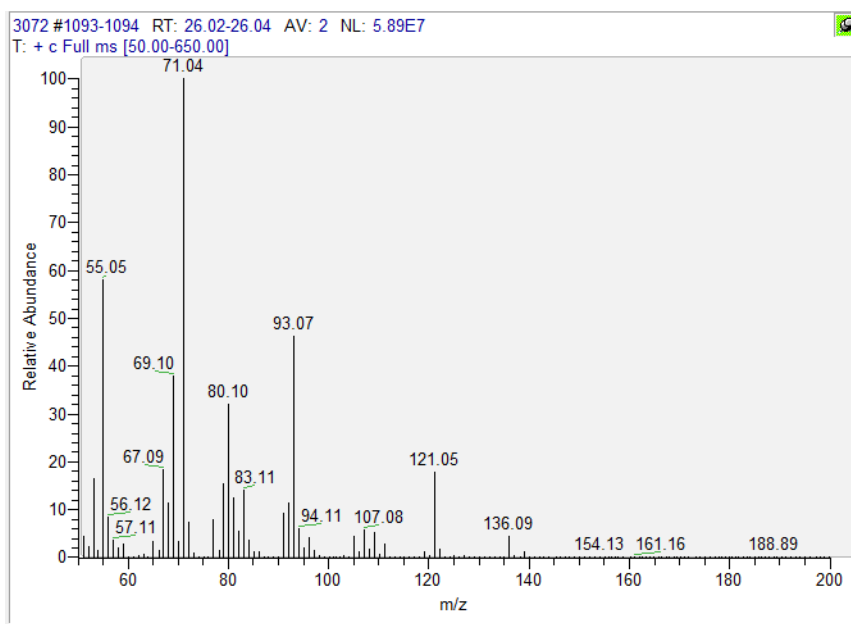
Sample 3073



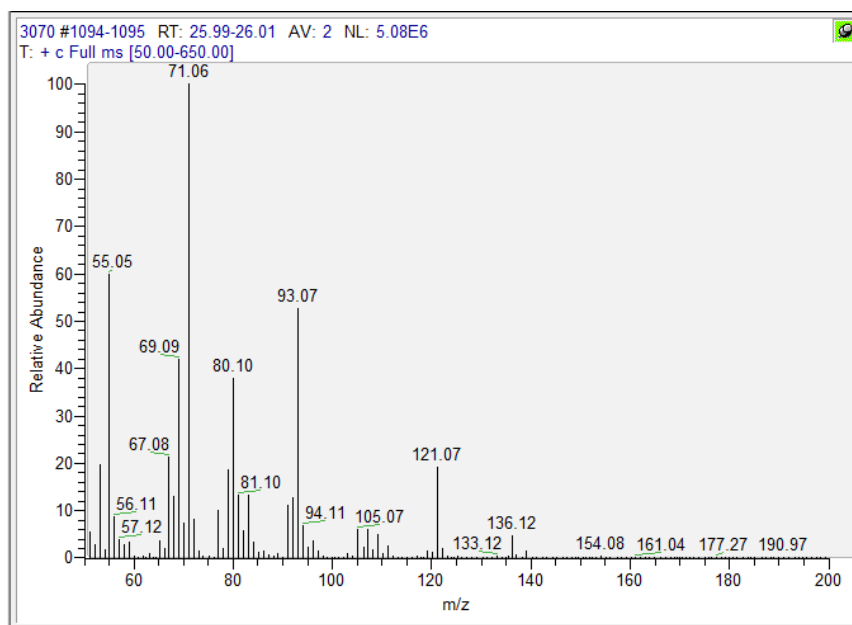
Sample 3073



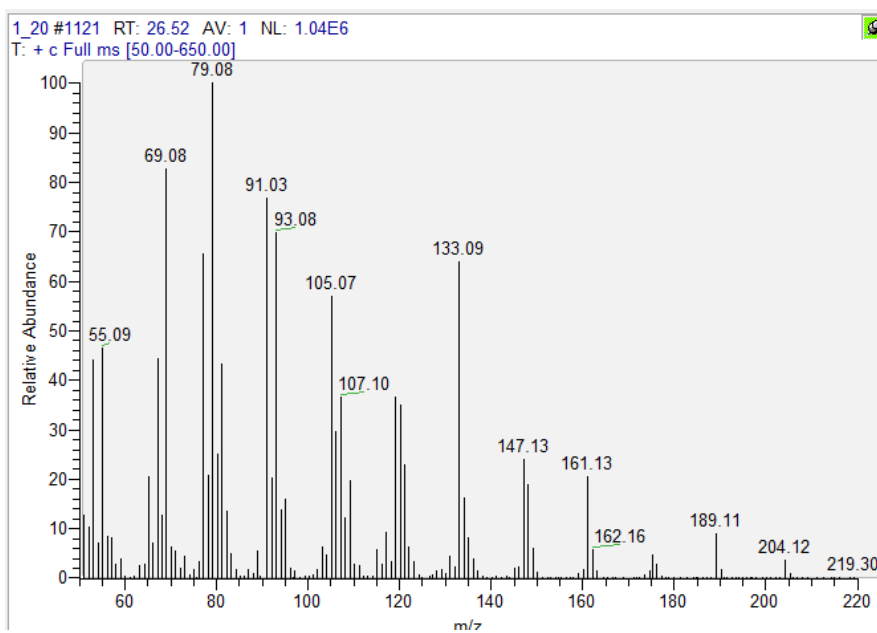
Sample 3072



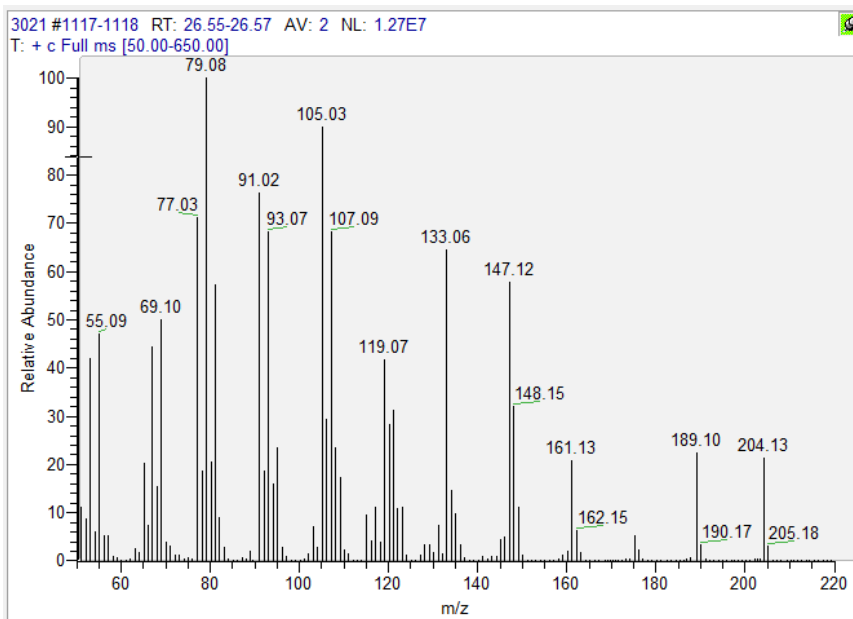
Sample 3070



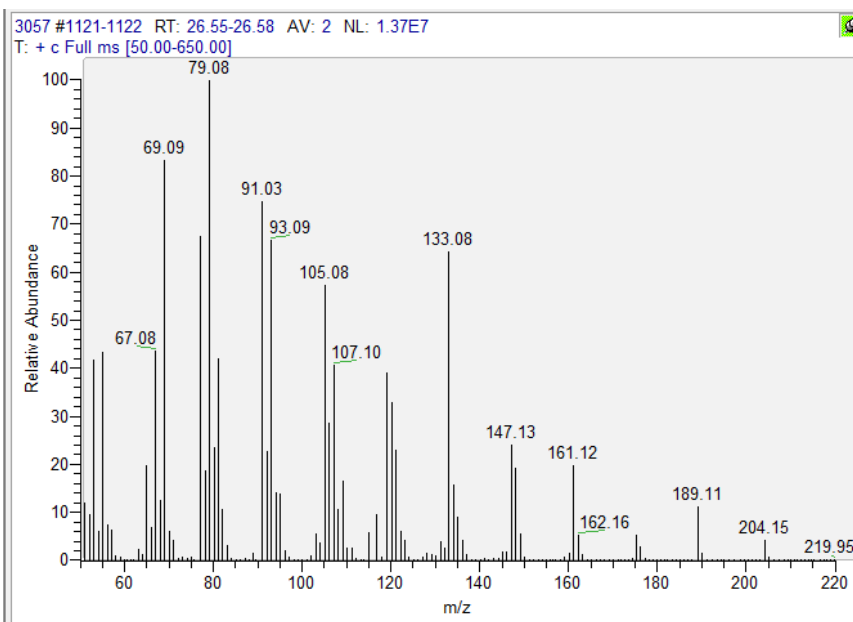
Reference of β -caryophyllene



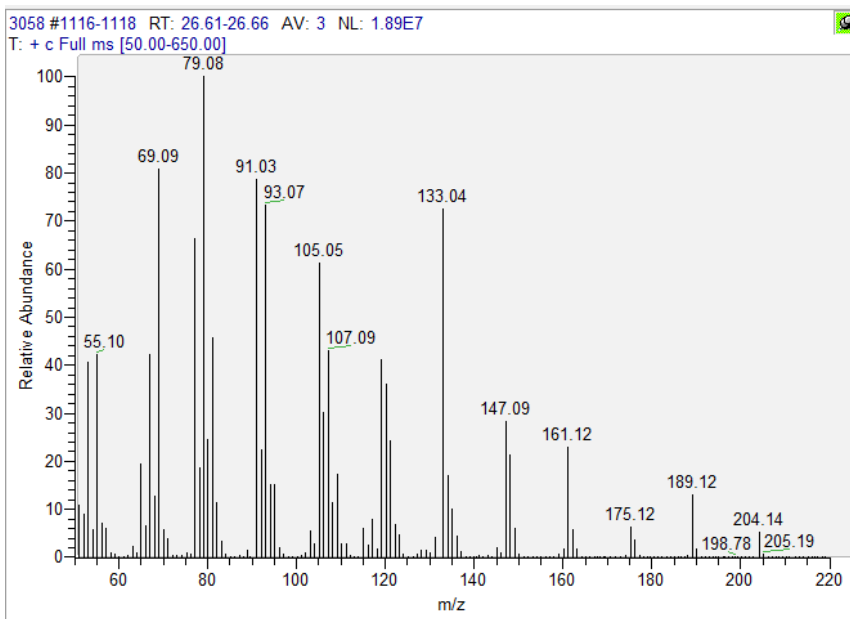
Sample 3021



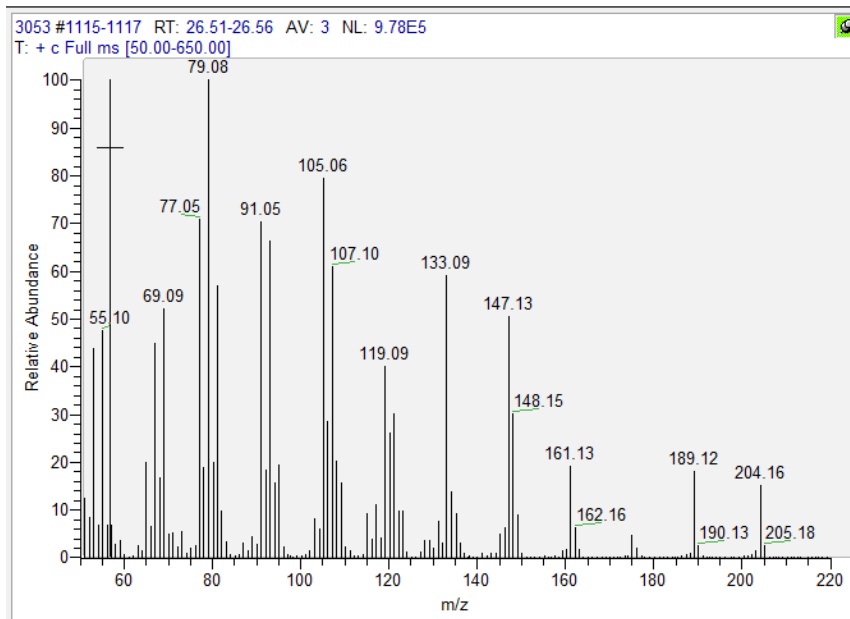
Sample 3057



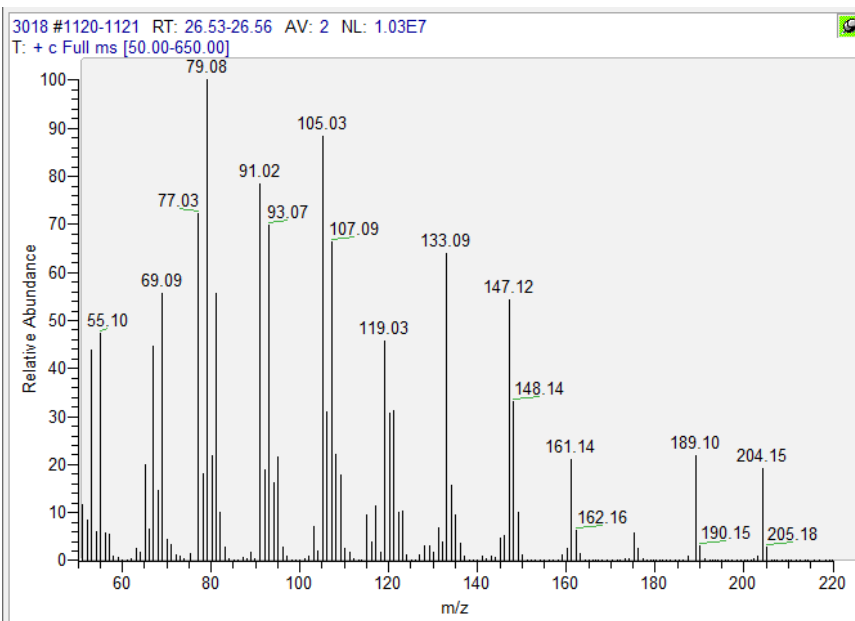
Sample 3058



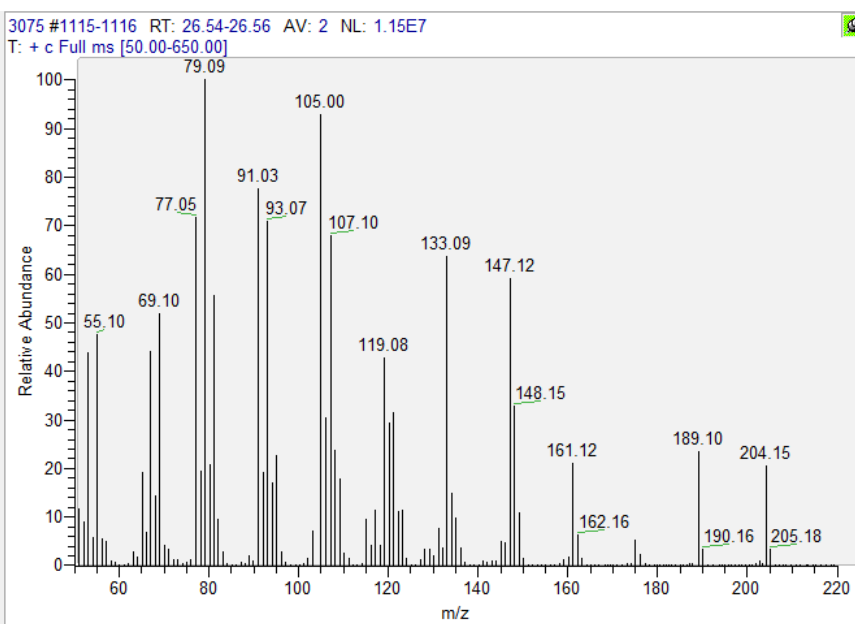
Sample 3053



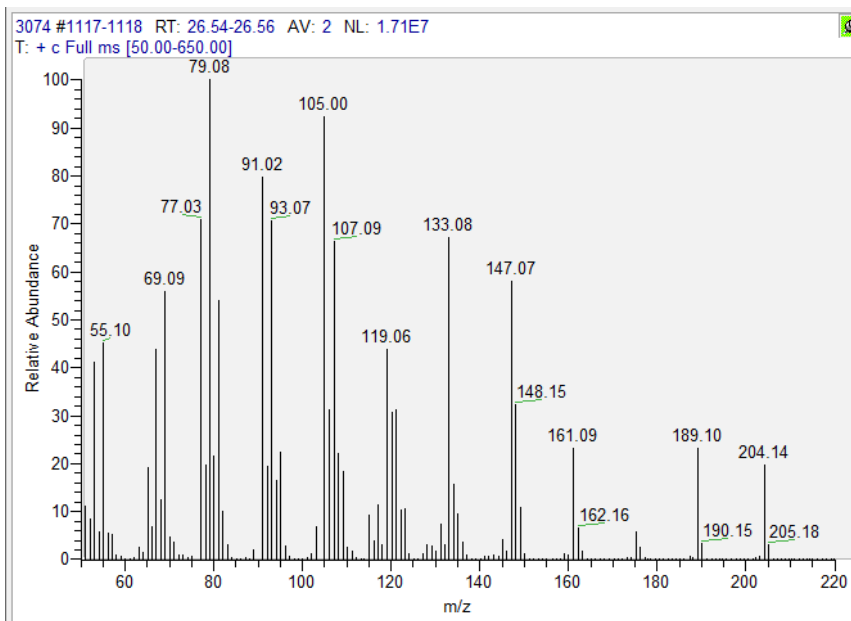
Sample 3018



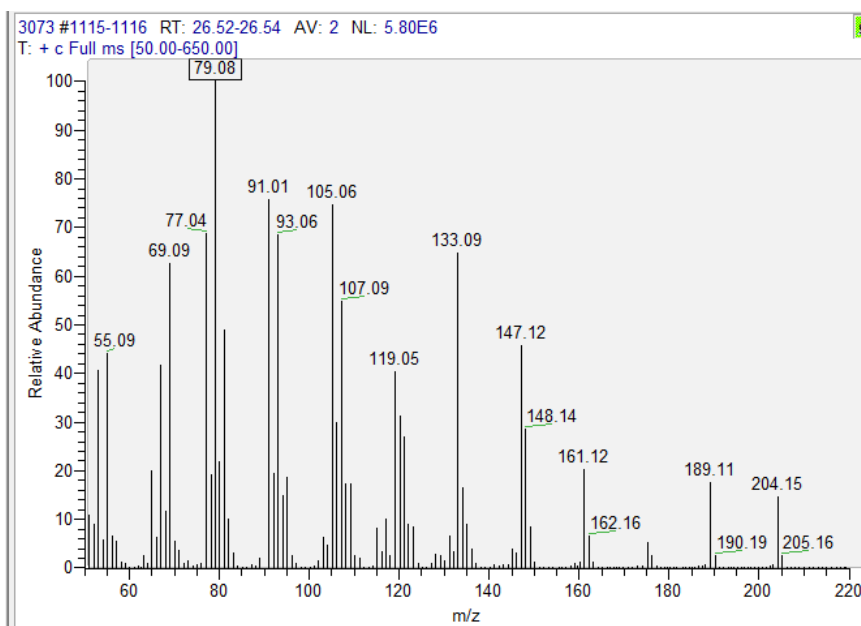
Sample 3075



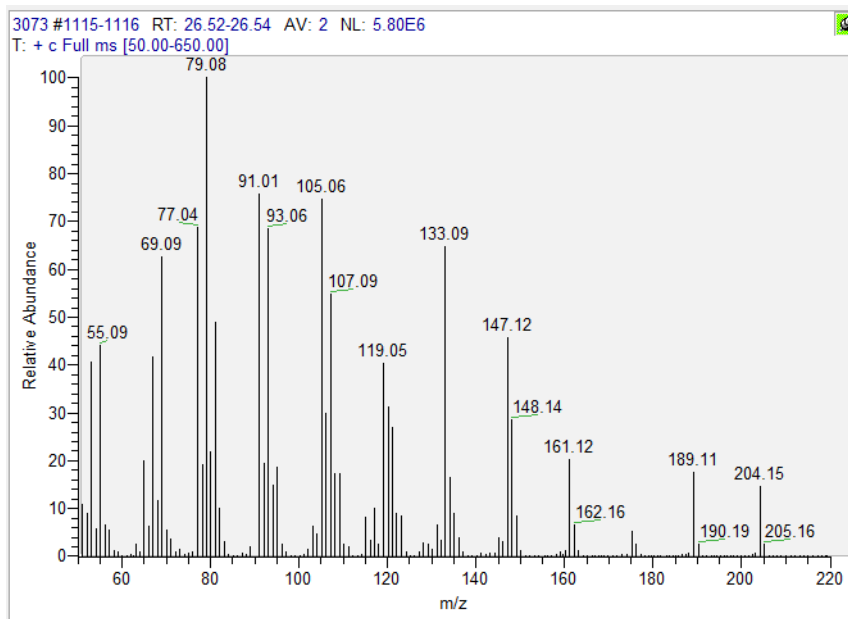
Sample 3074



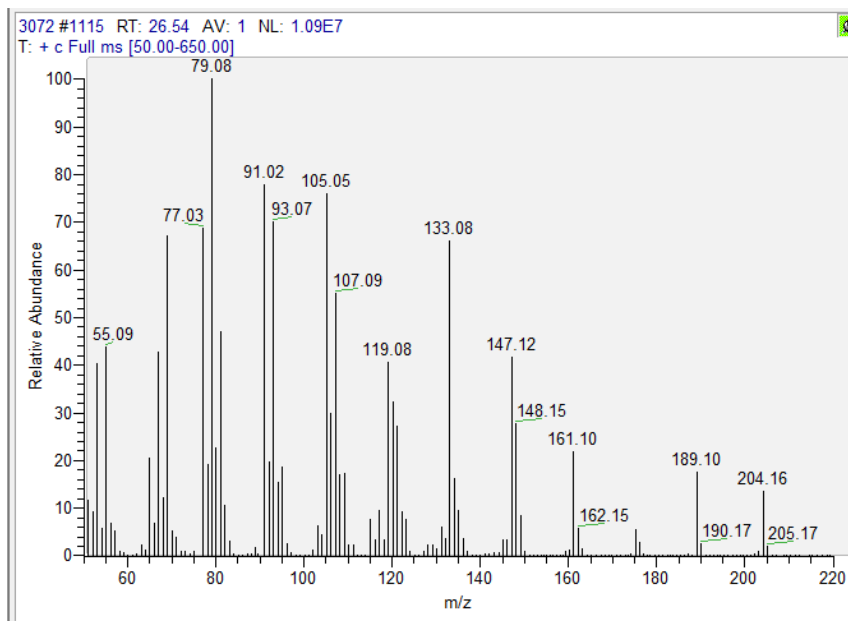
Sample 3073



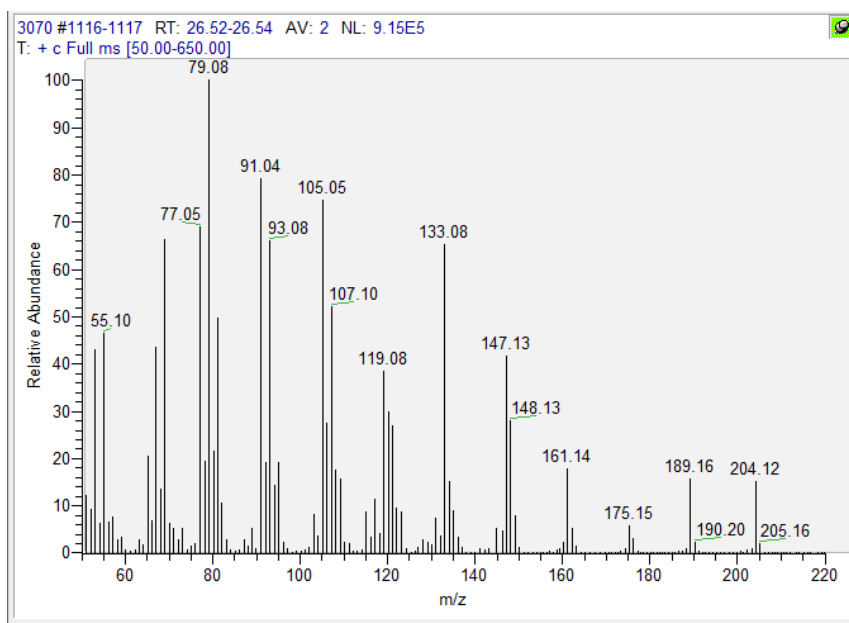
Sample 3073



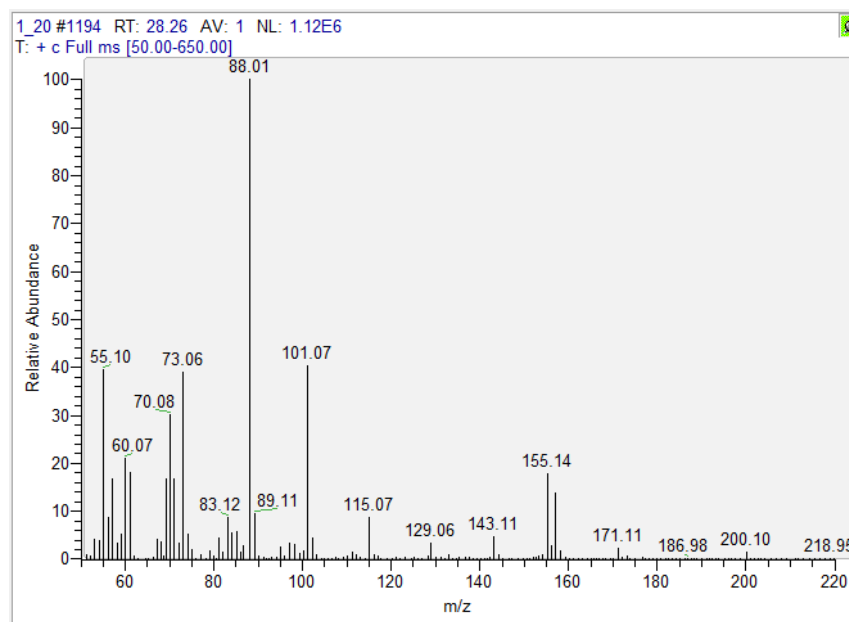
Sample 3072



Sample 3070

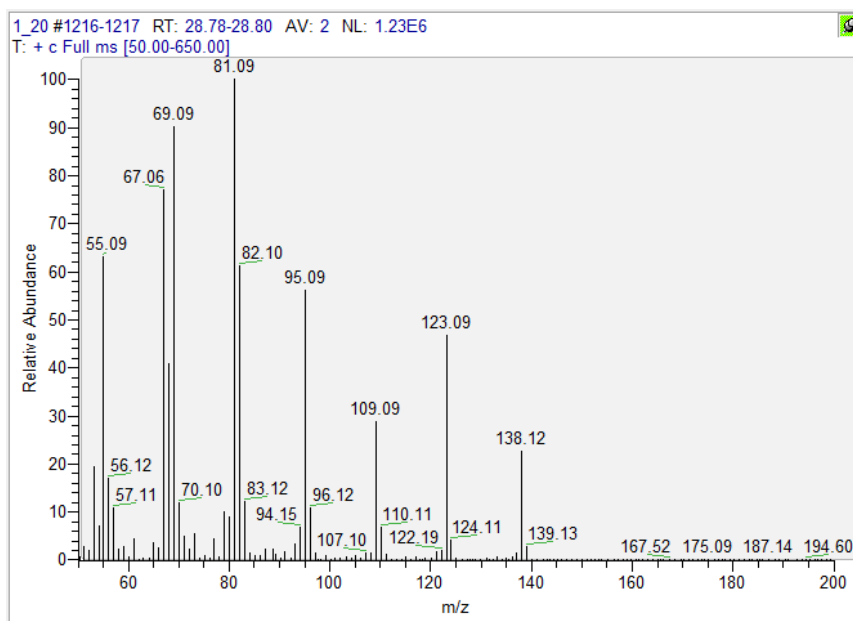


Reference of β -damascenone

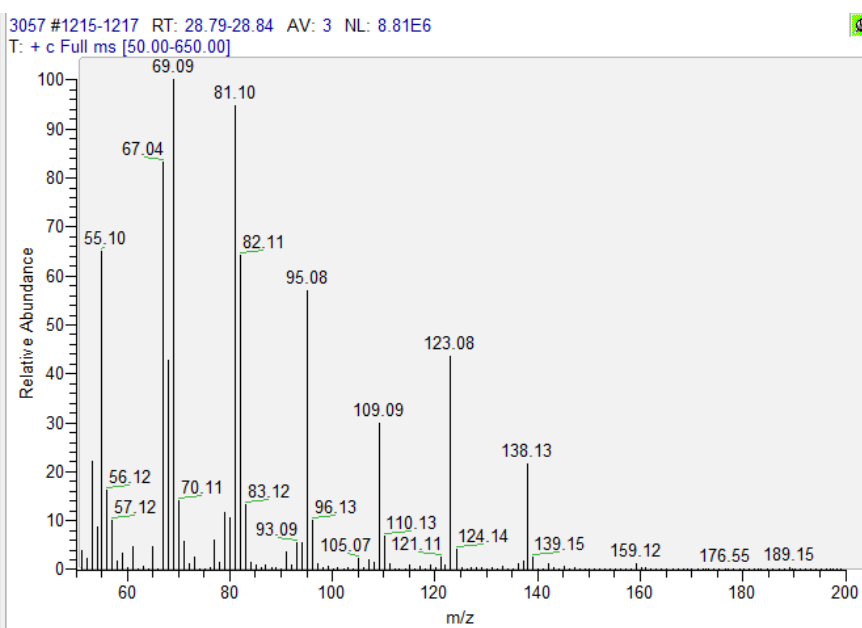


Not detected in any of the acquired samples.

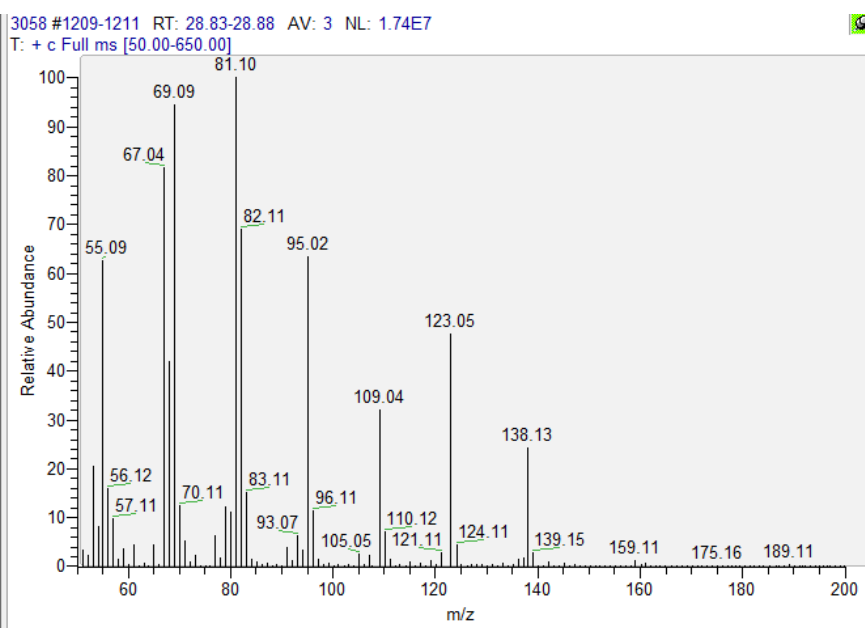
Reference of citronellyl acetate



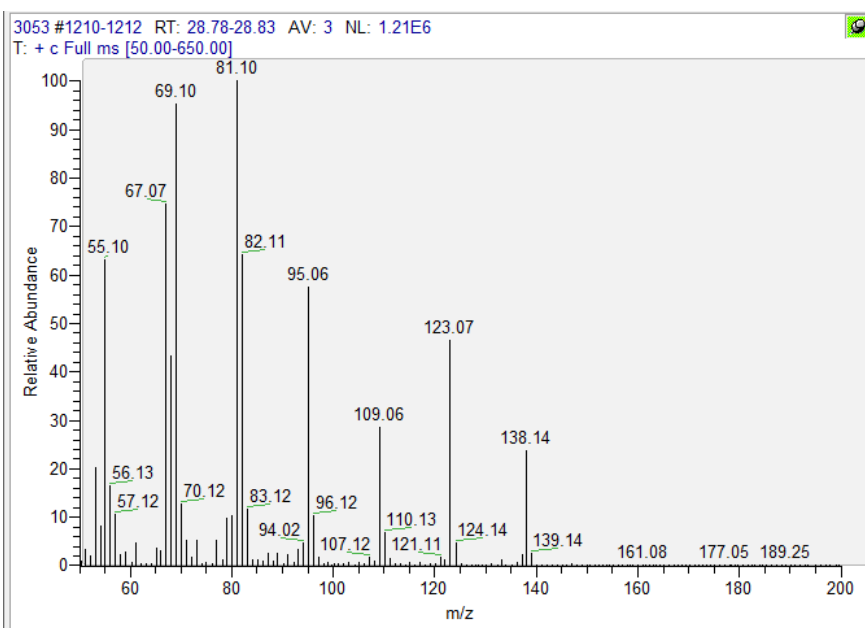
Sample 3057



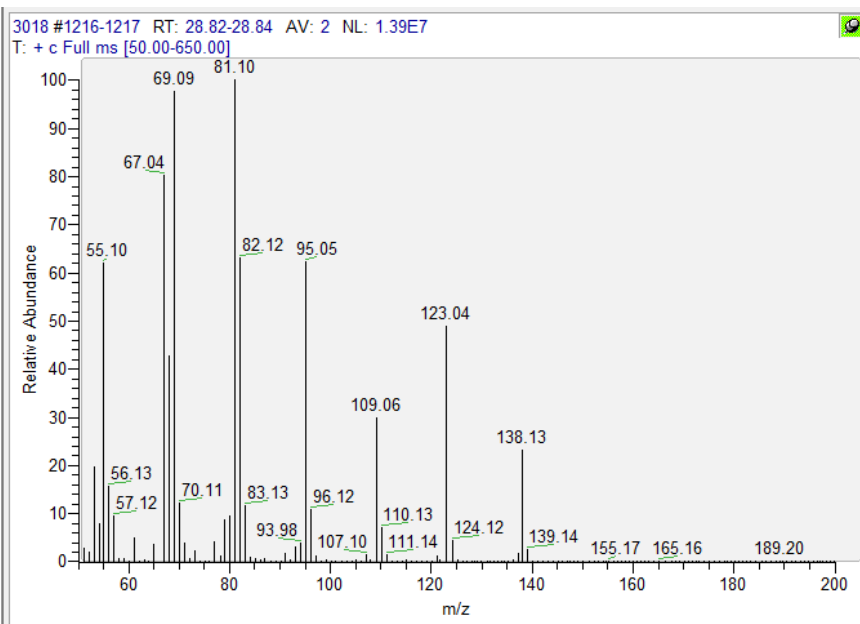
Sample 3058



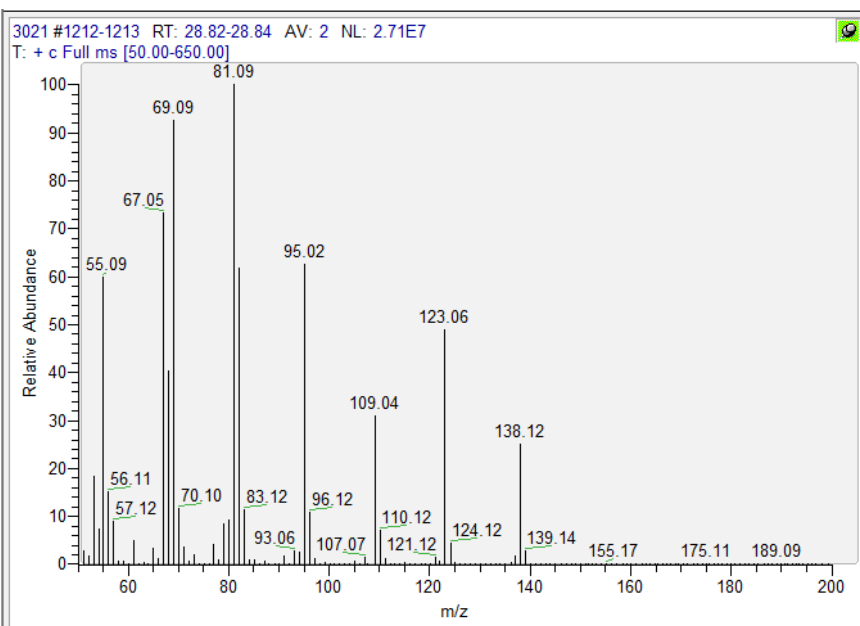
Sample 3053



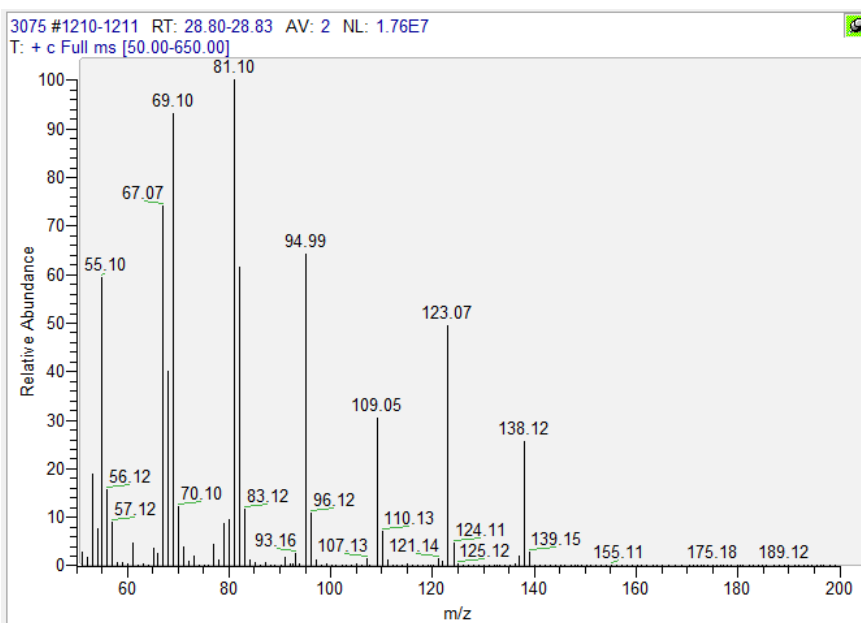
Sample 3018



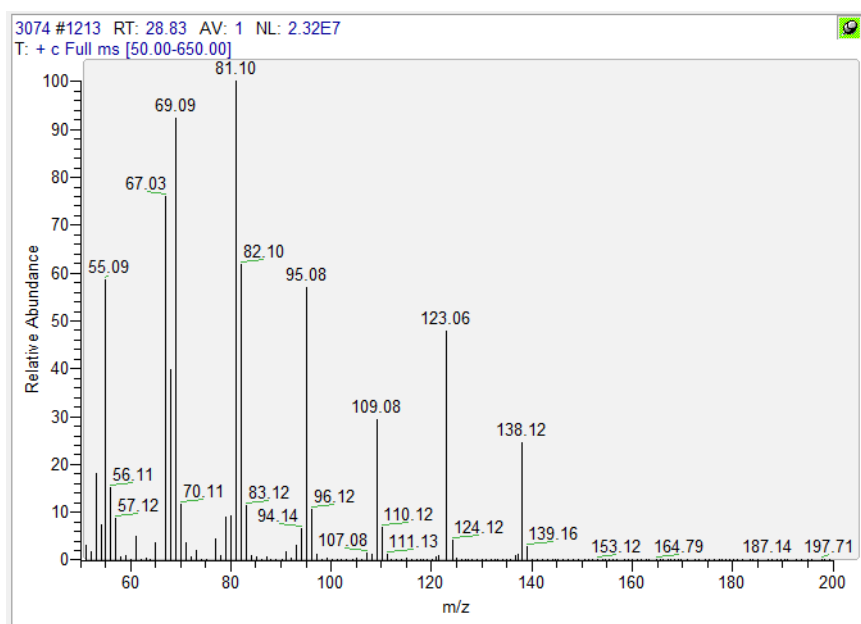
Sample 3021



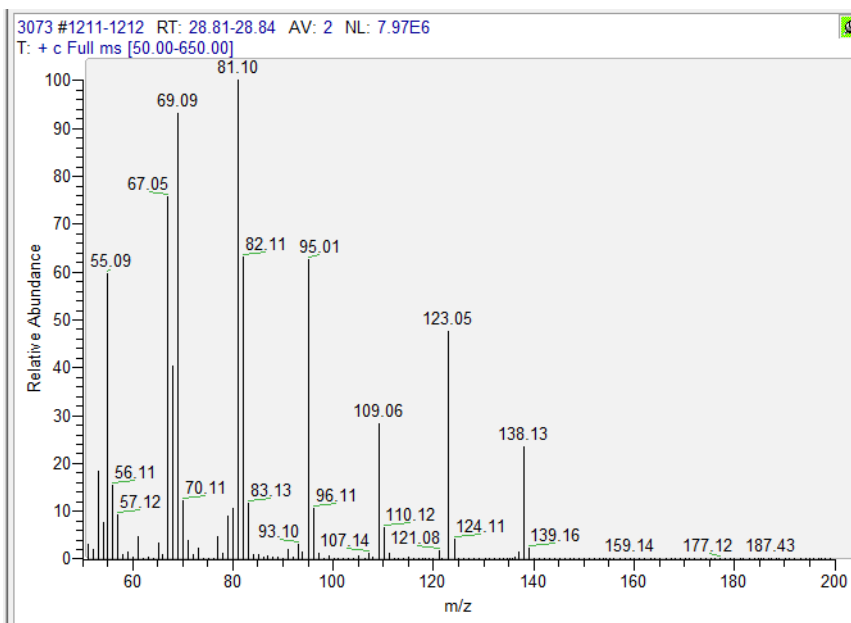
Sample 3075



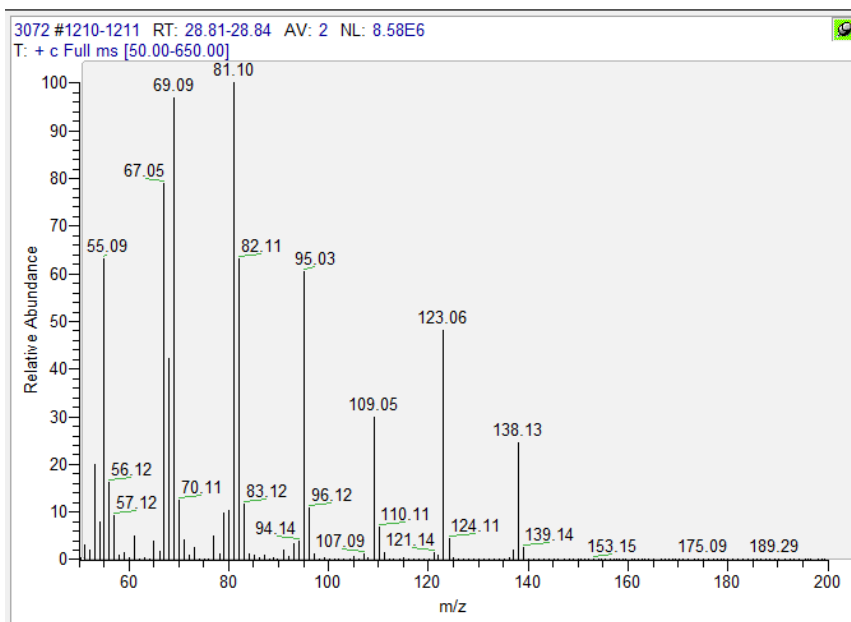
Sample 3074



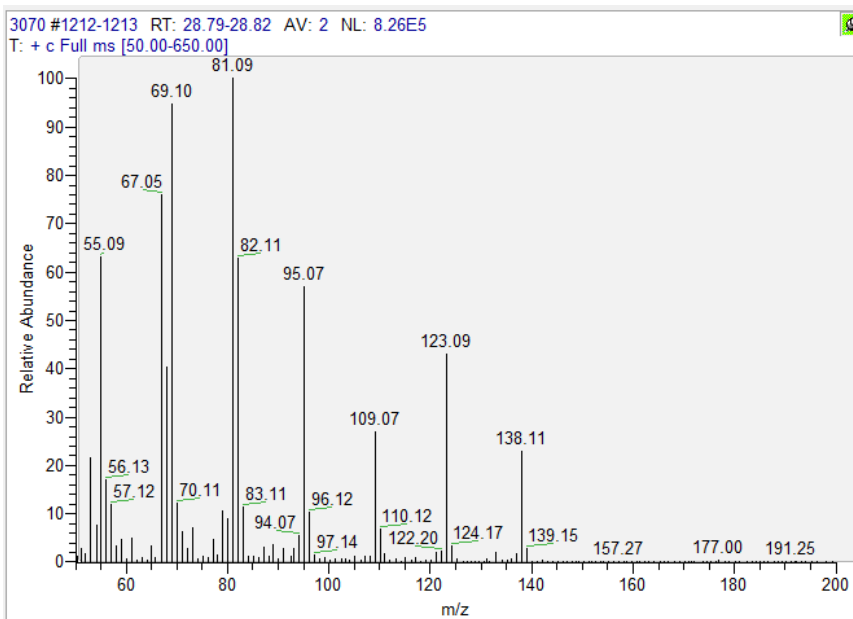
Sample 3073



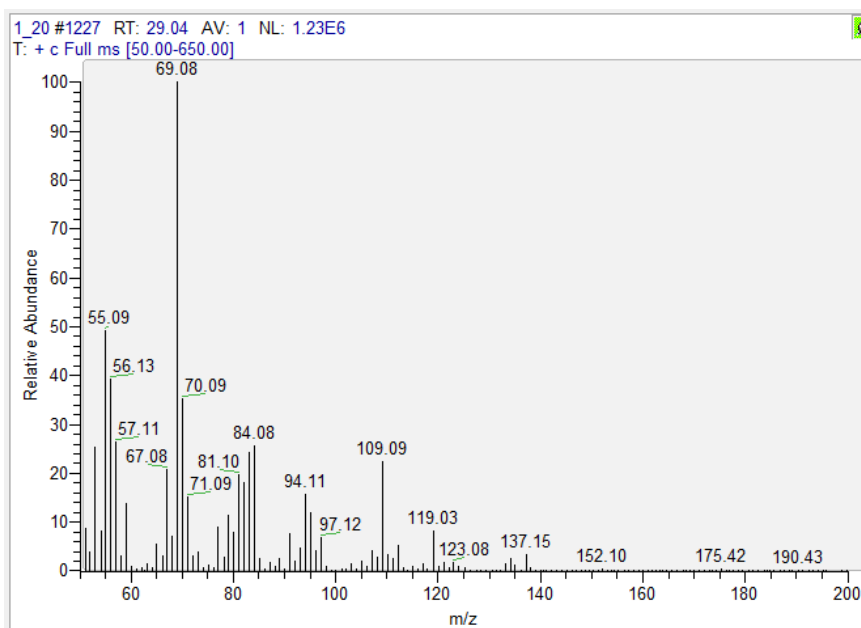
Sample 3072



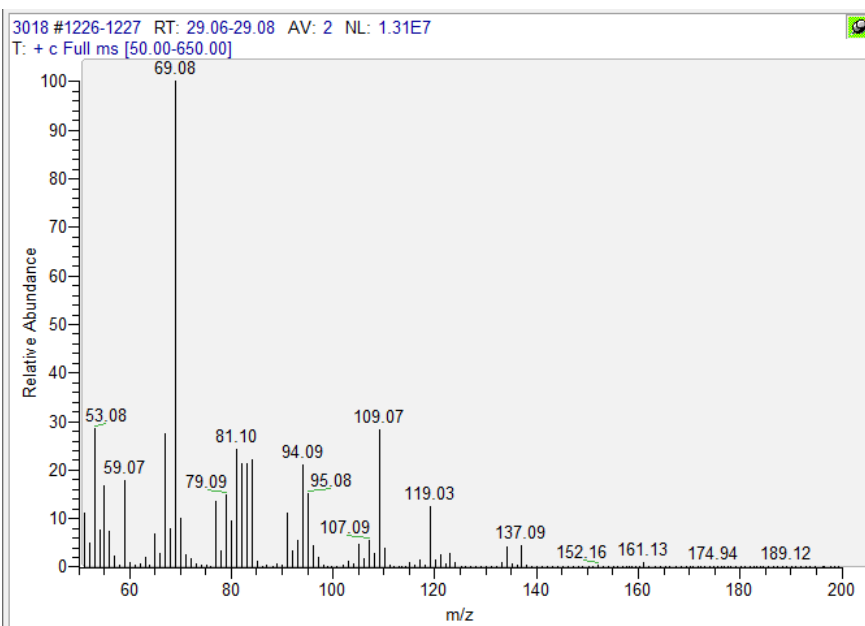
Sample 3070



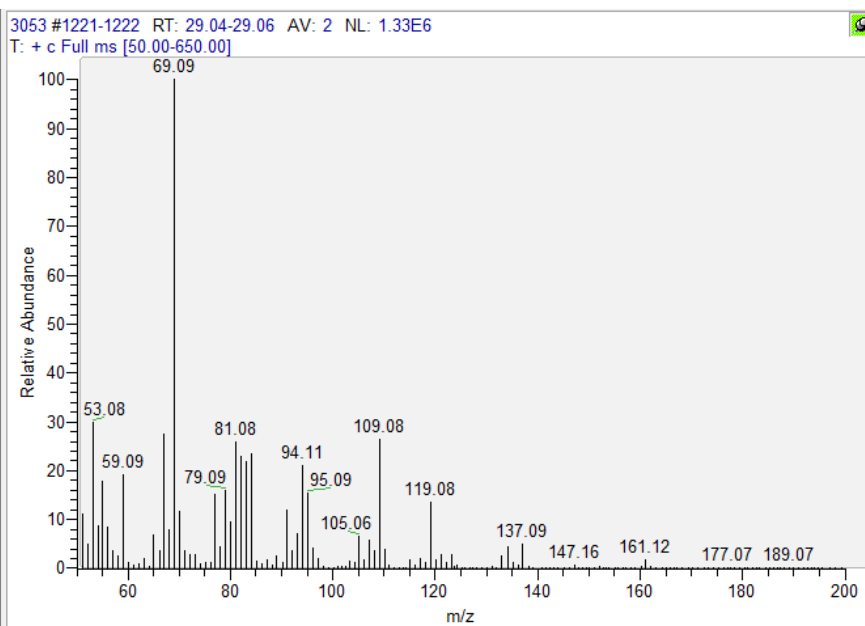
Reference of citral



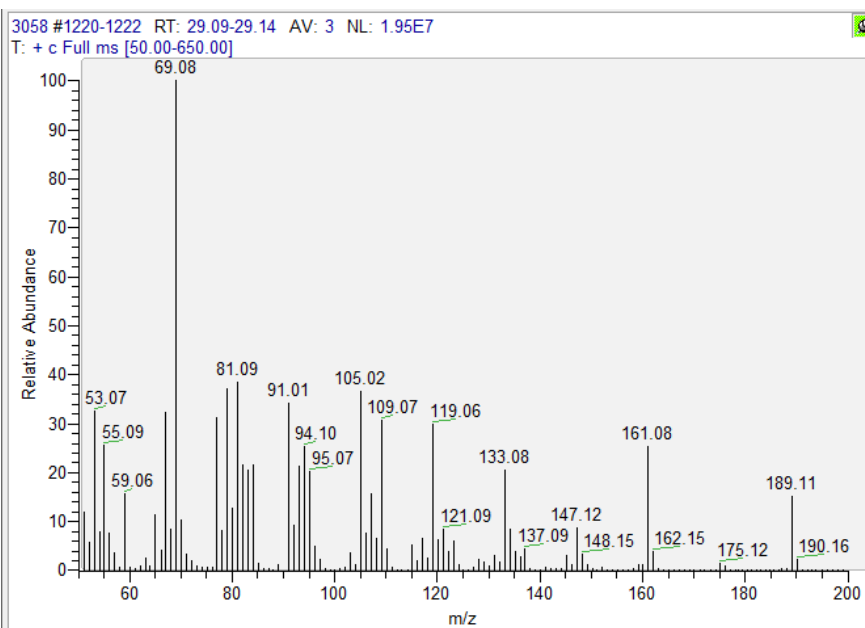
Sample 3018



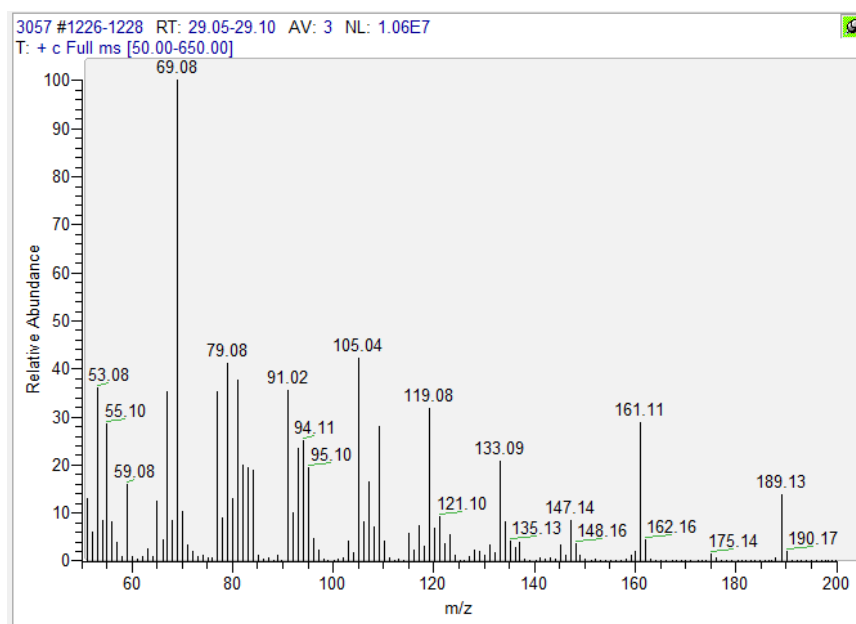
Sample 3053



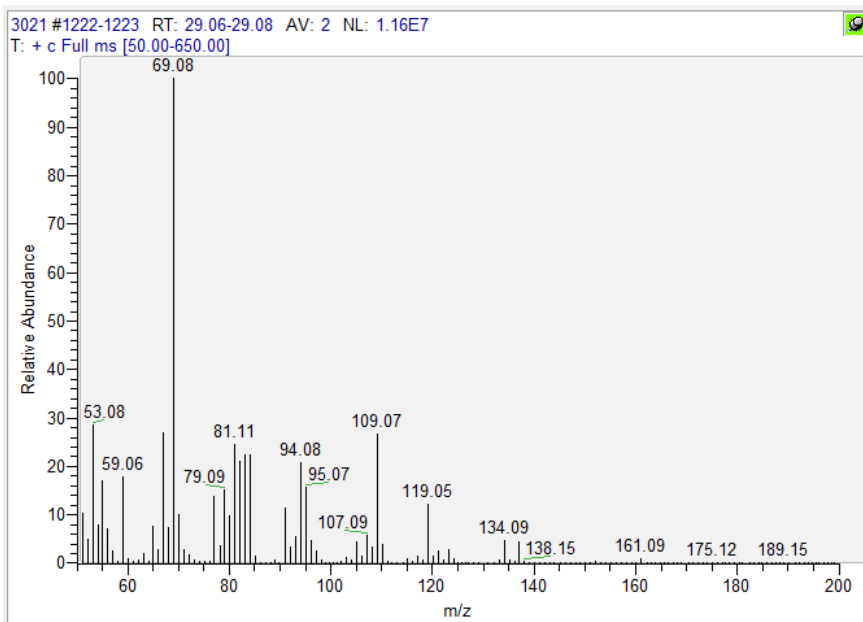
Sample 3058



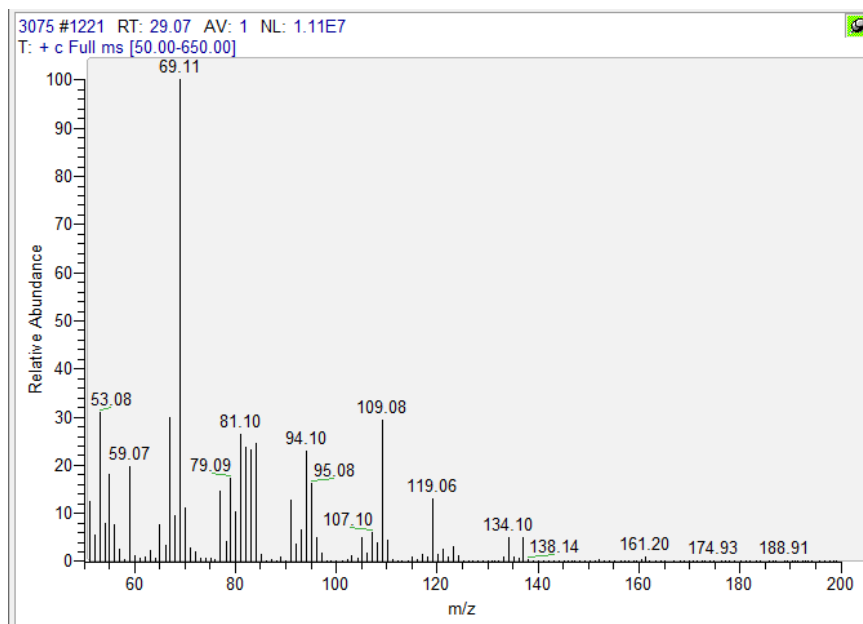
Sample 3057



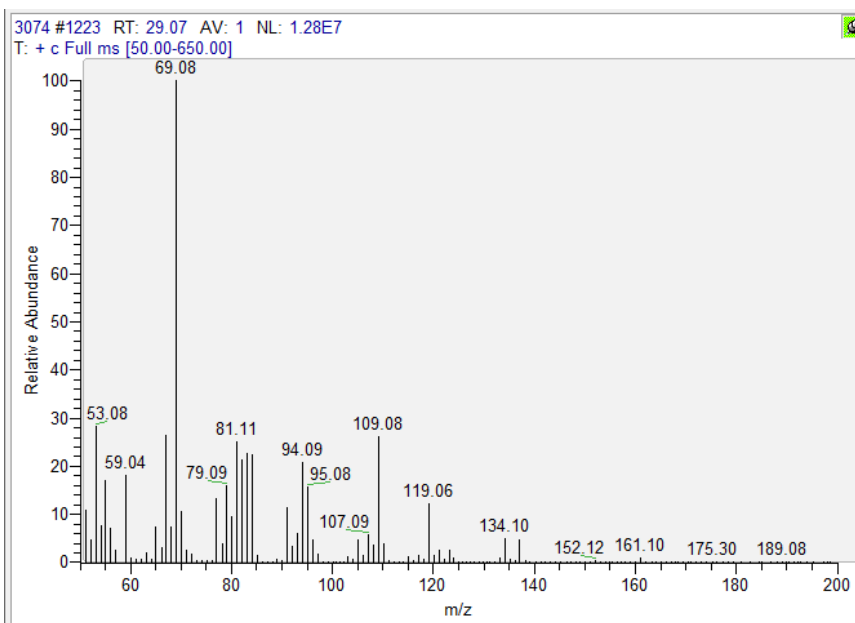
Sample 3021



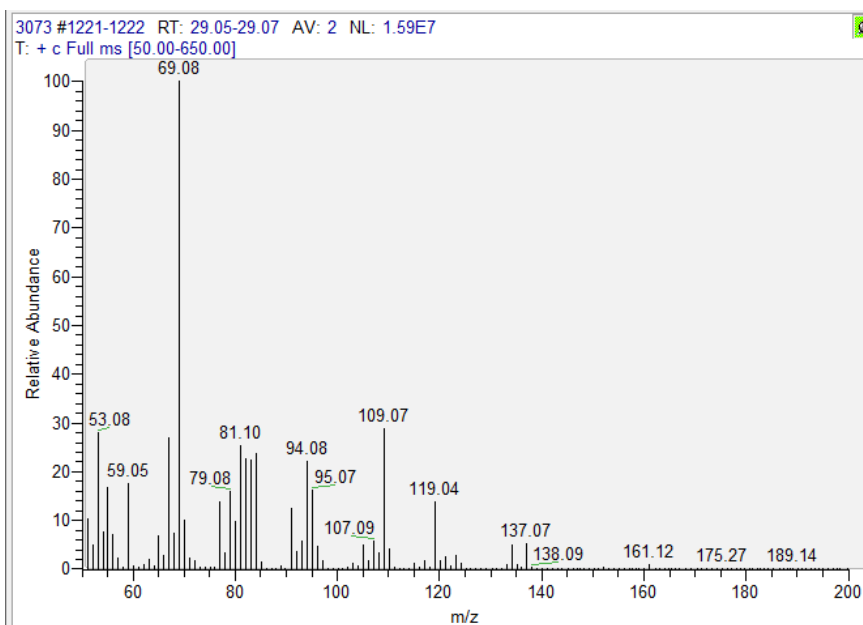
Sample 3075



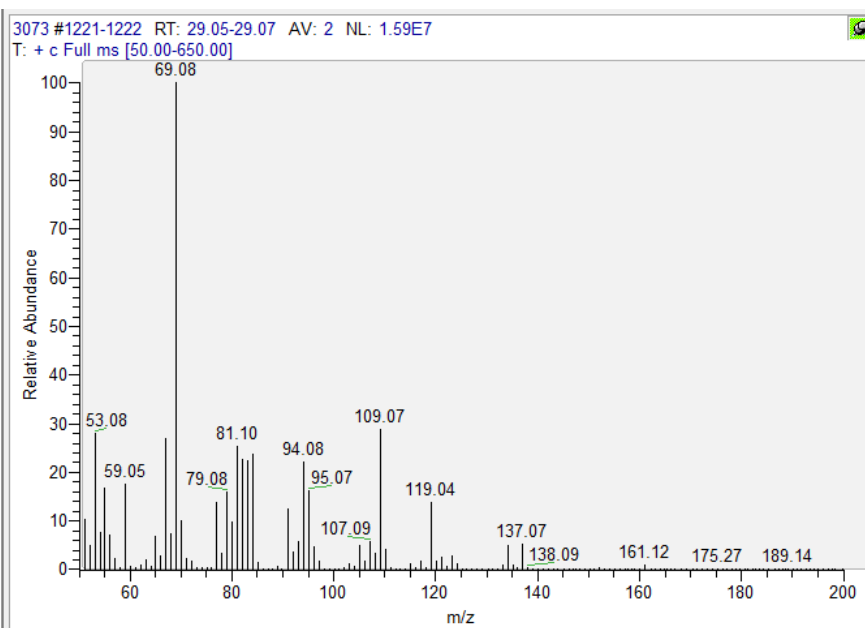
Sample 3074



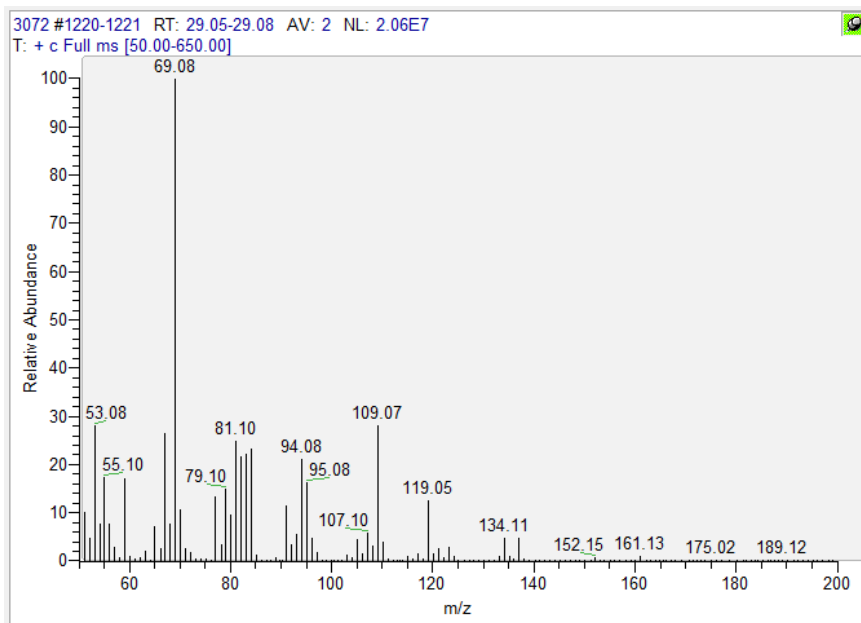
Sample 3073



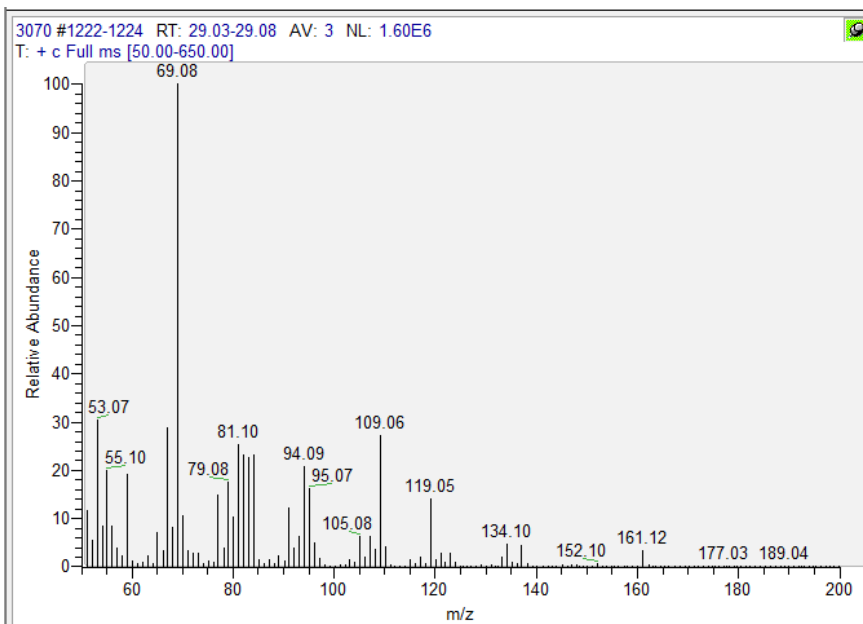
Sample 3073



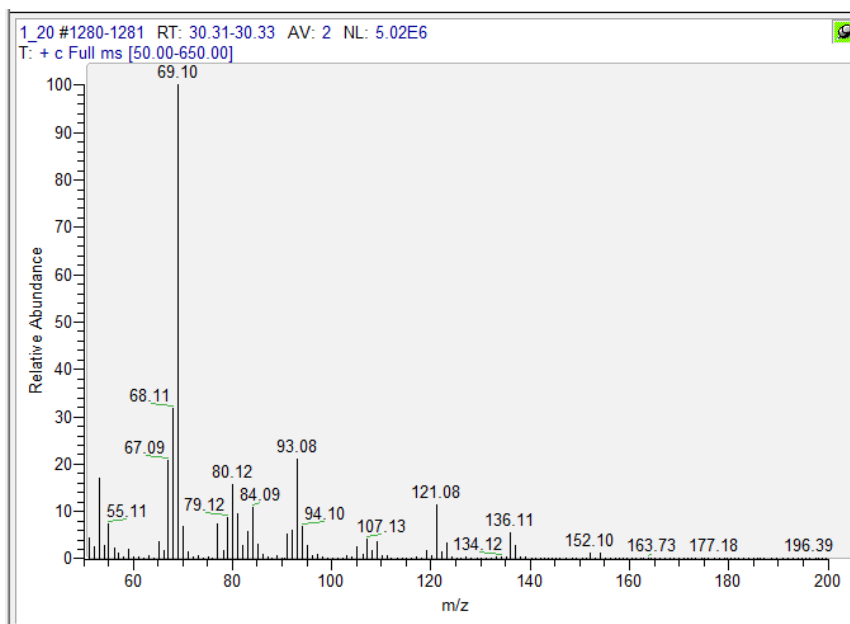
Sample 3072



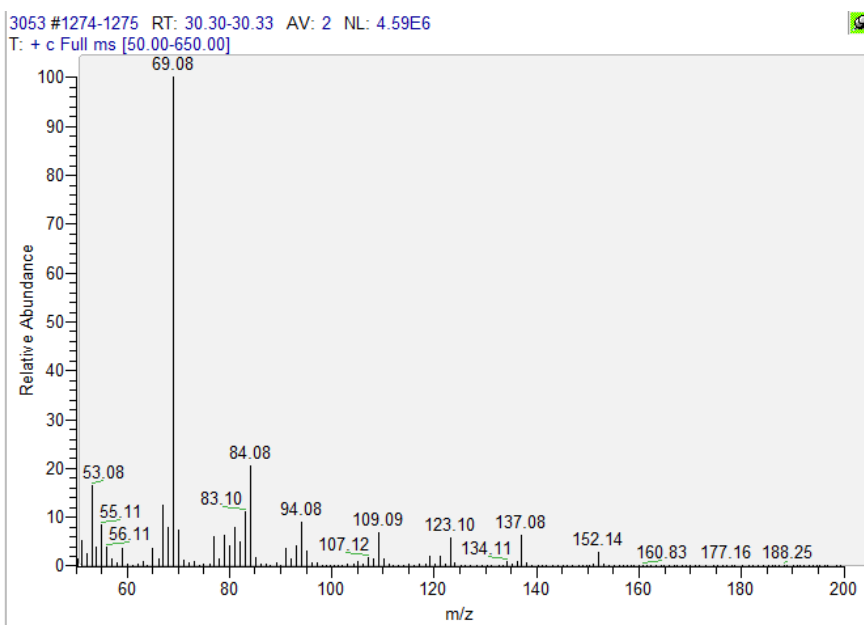
Sample 3070



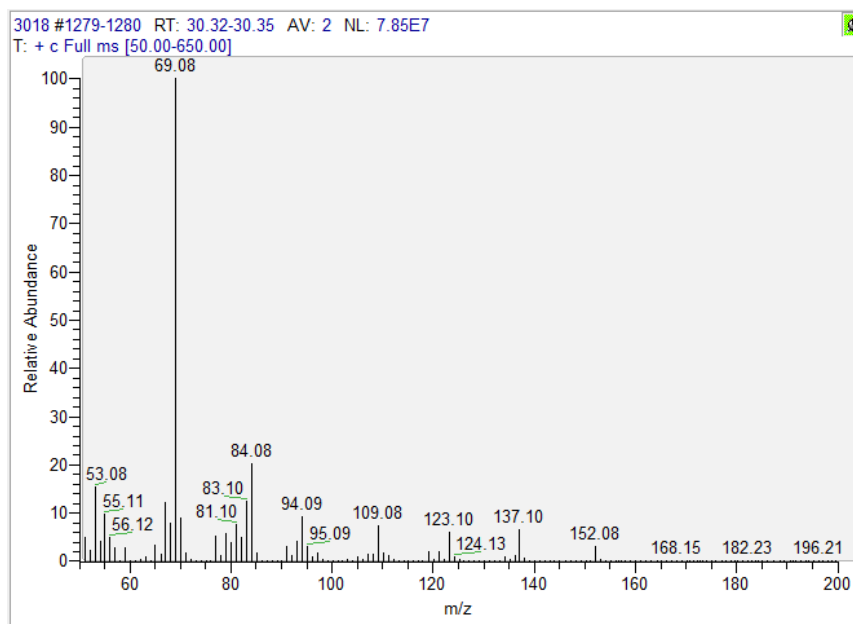
Reference of neryl acetate



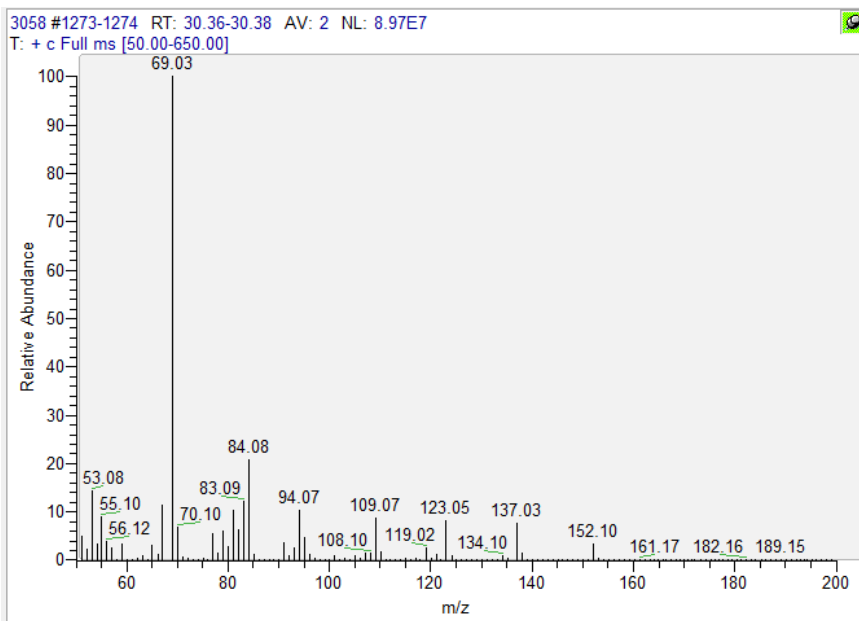
Sample 3053



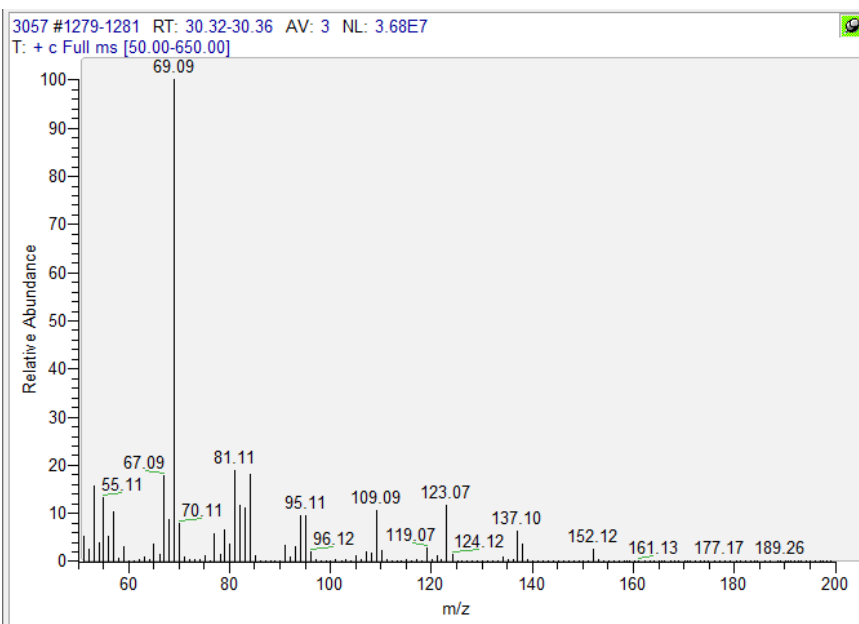
Sample 3018



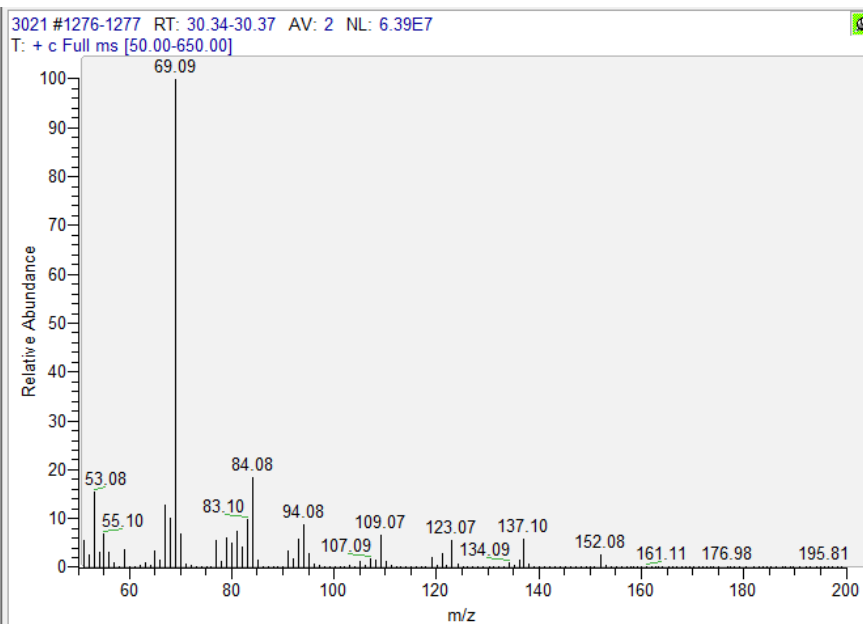
Sample 3058



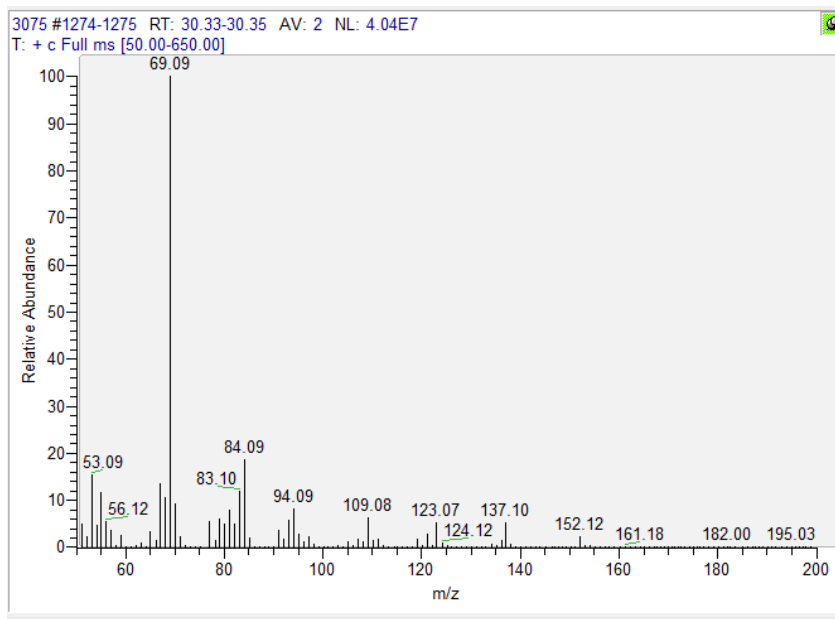
Sample 3057



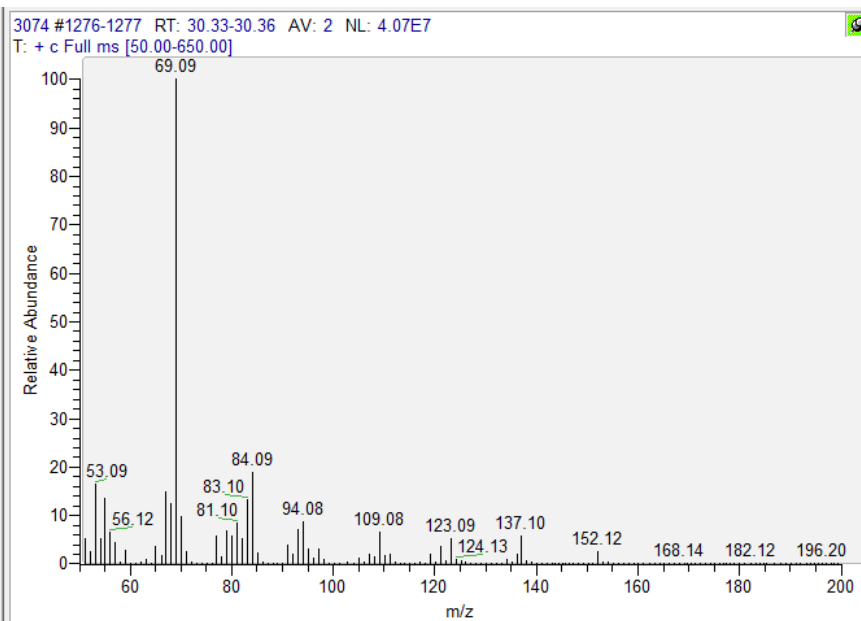
Sample 3021



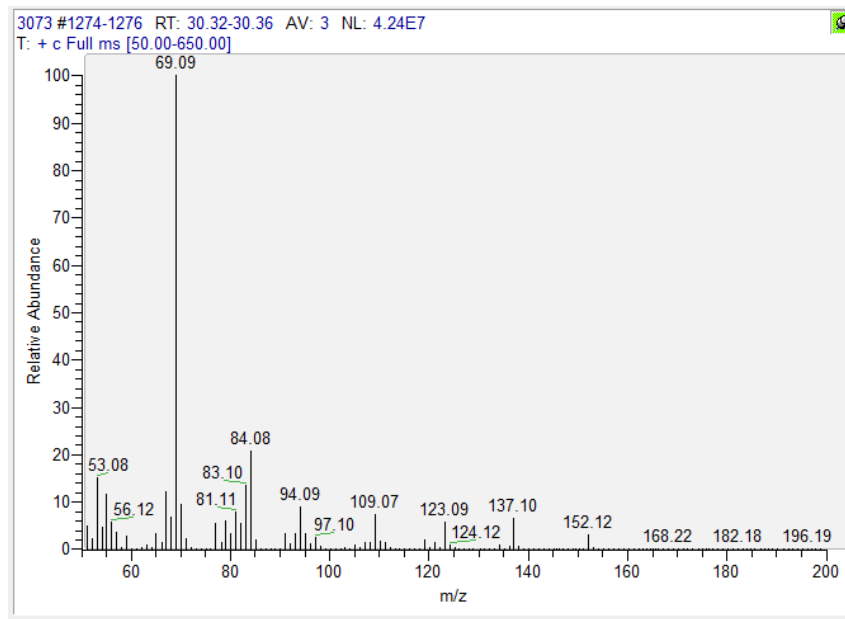
Sample 3075



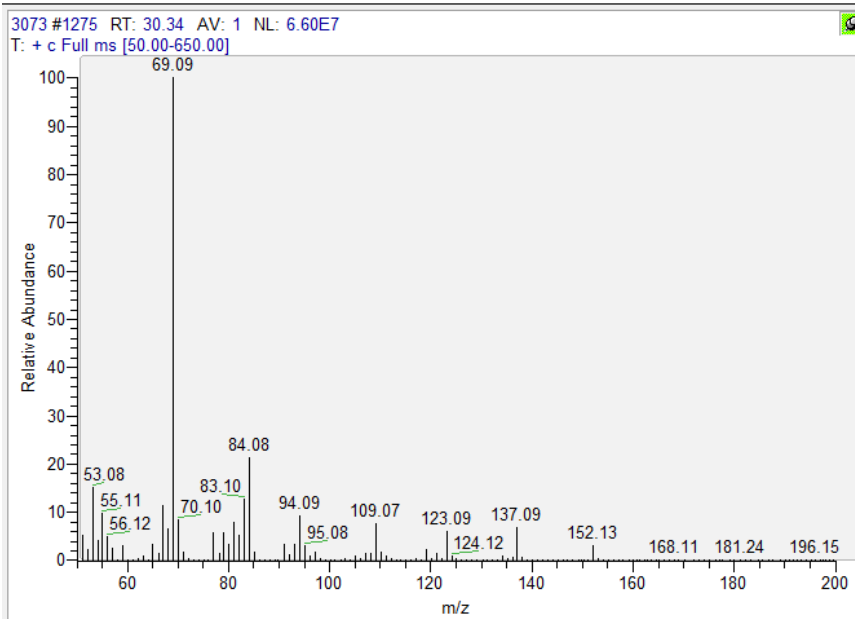
Sample 3074



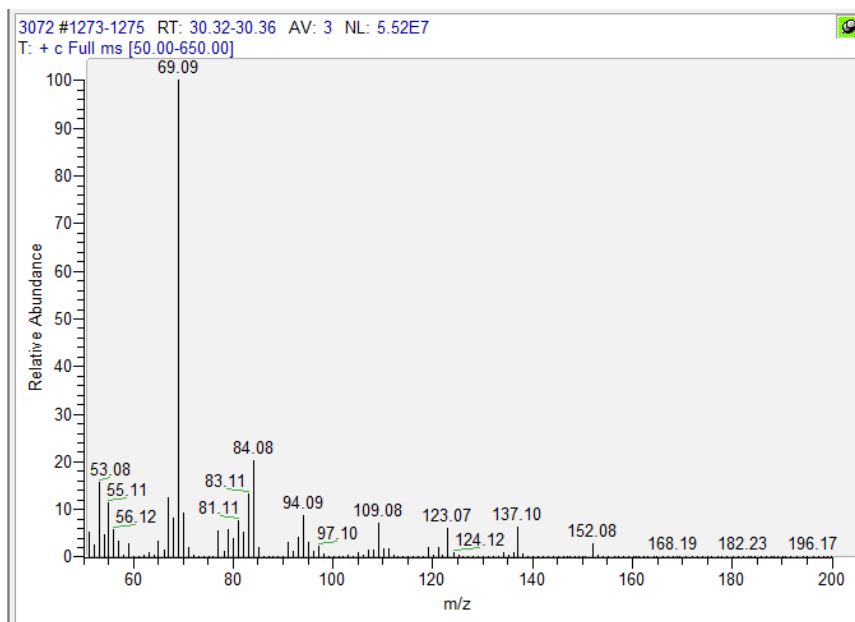
Sample 3073



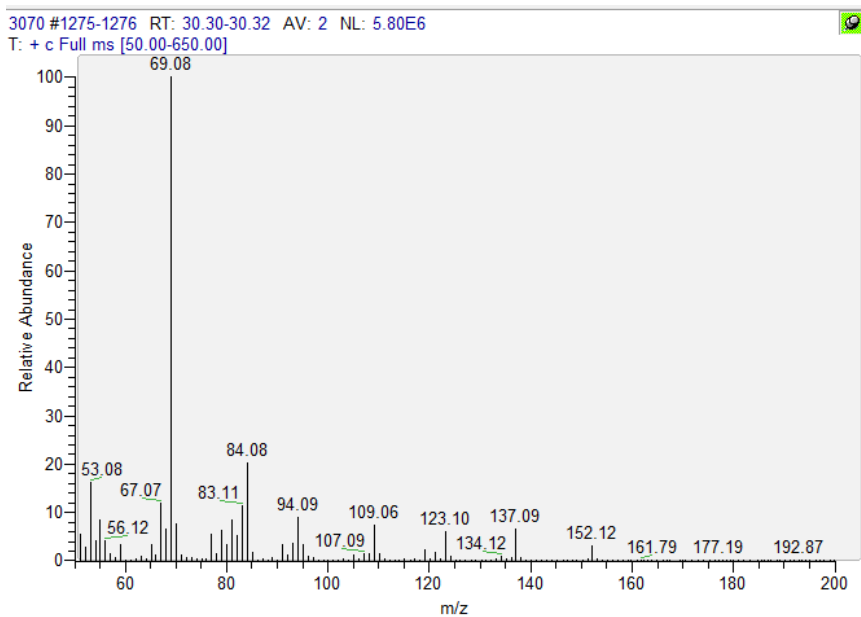
Sample 3073



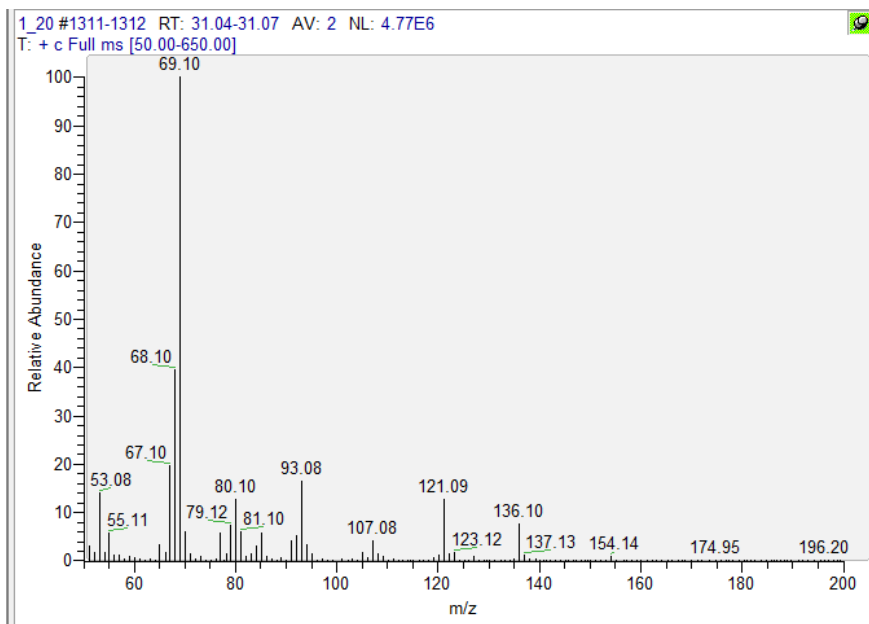
Sample 3072



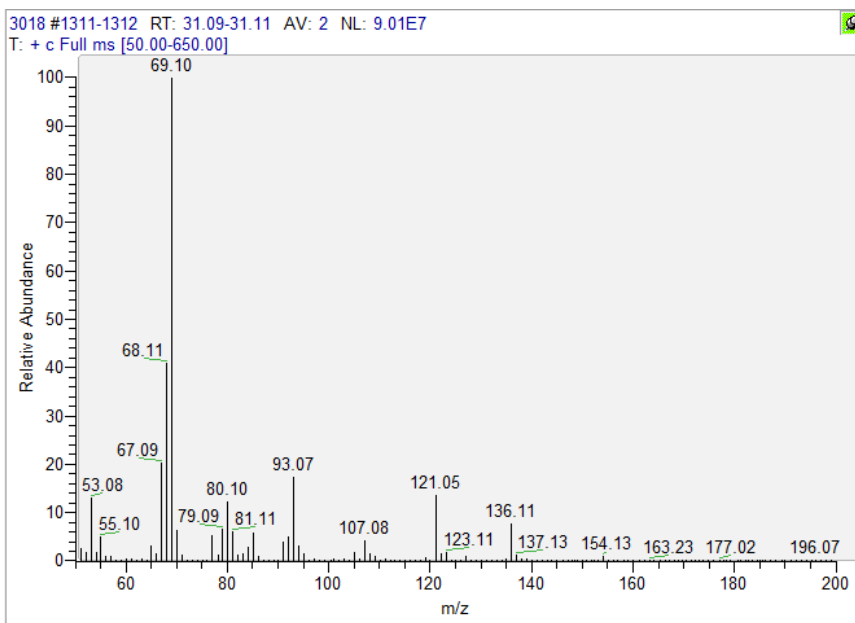
Sample 3070



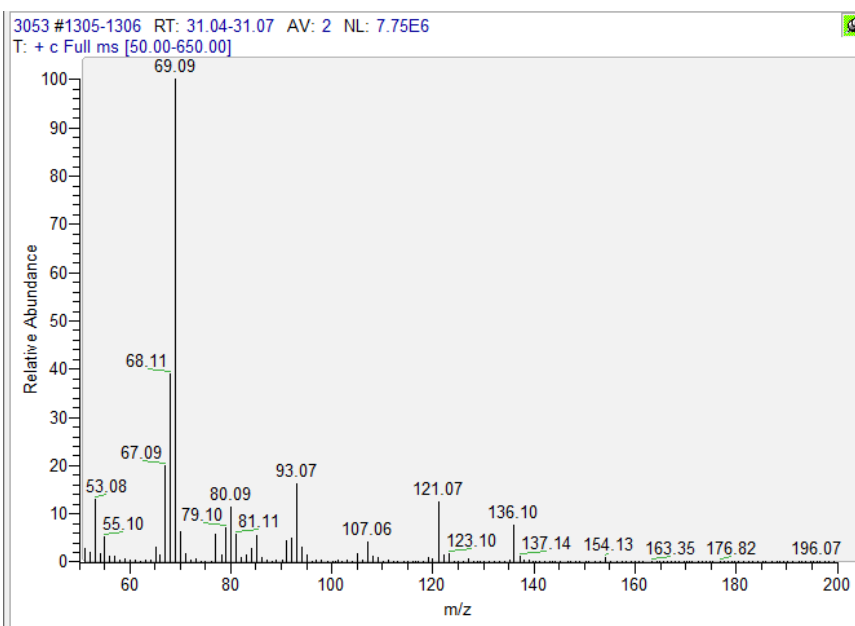
Reference geranyl acetate



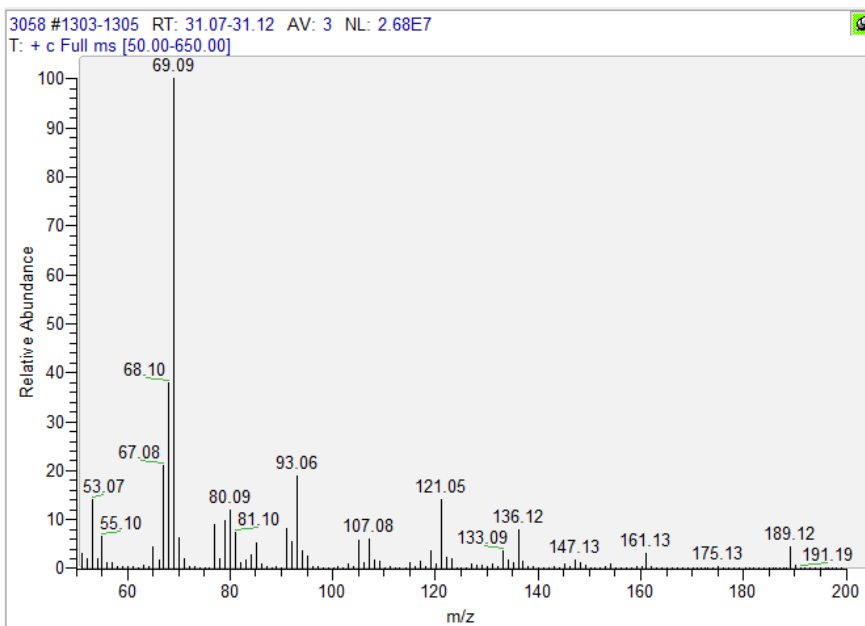
Sample 3018



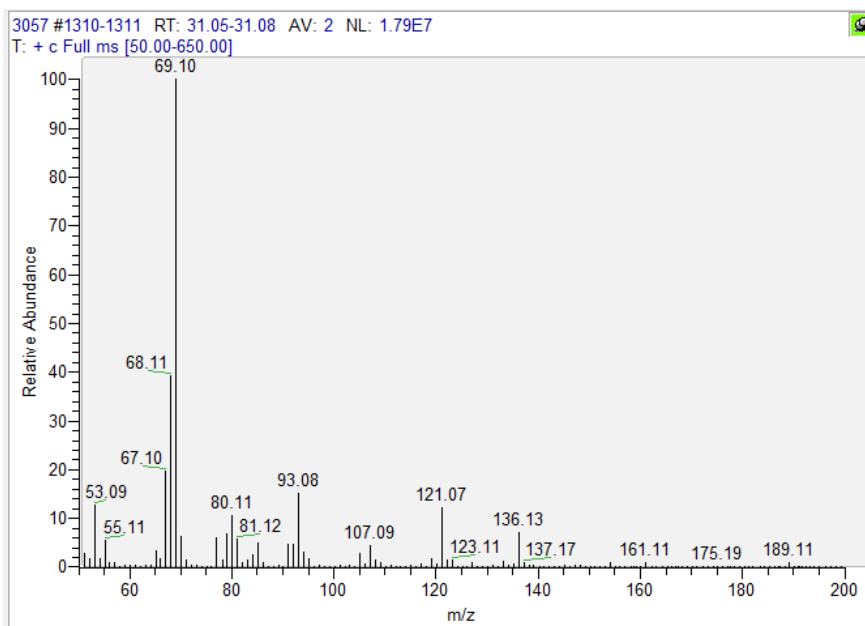
Sample 3053



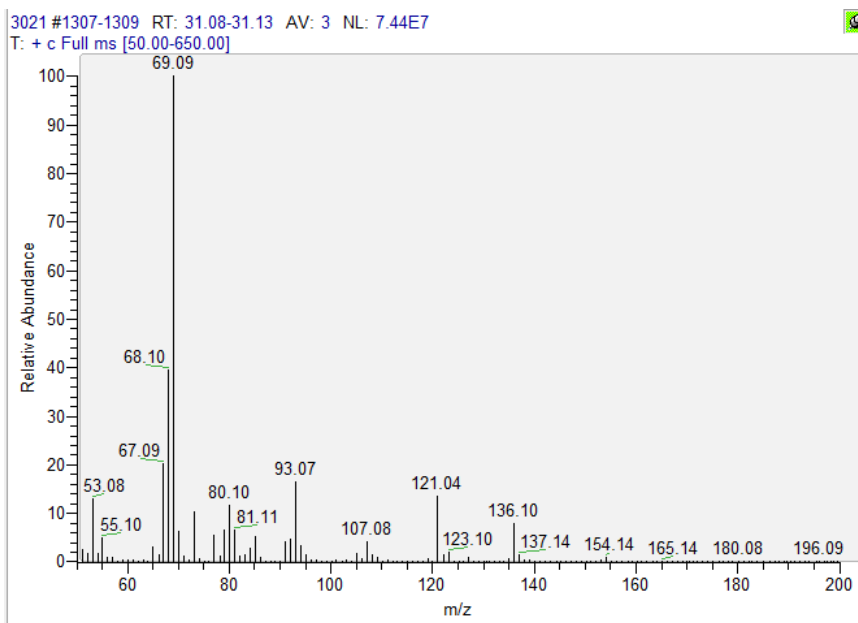
Sample 3058



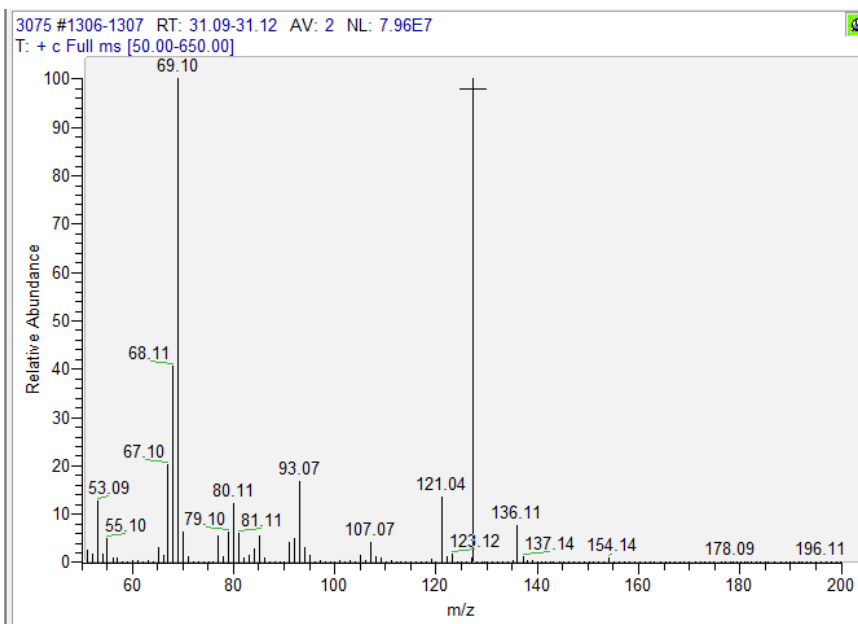
Sample 3057



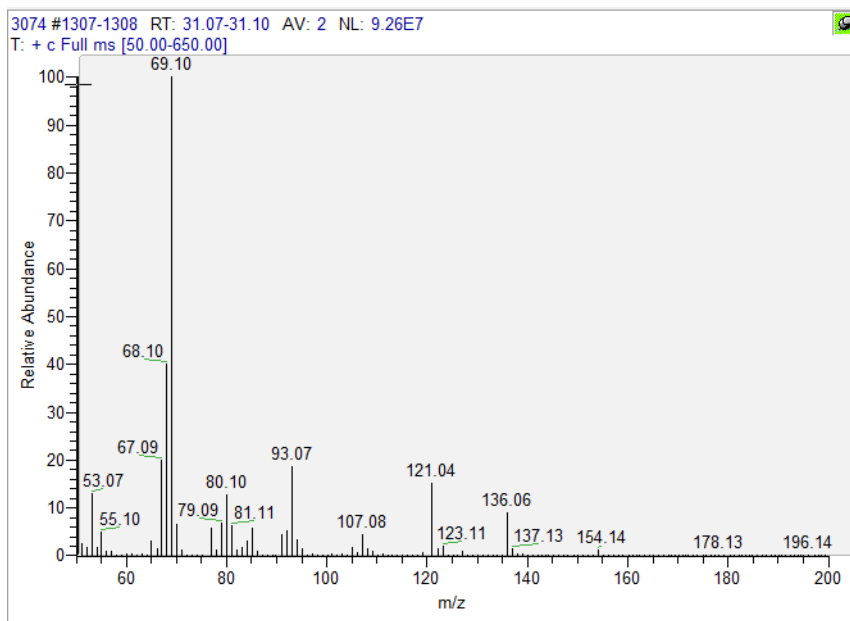
Sample 3021



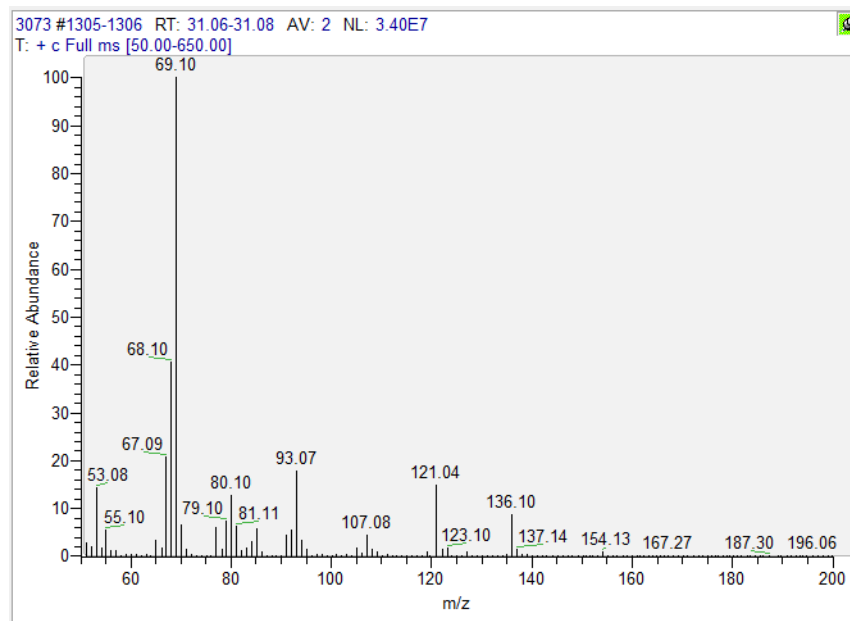
Sample 3075



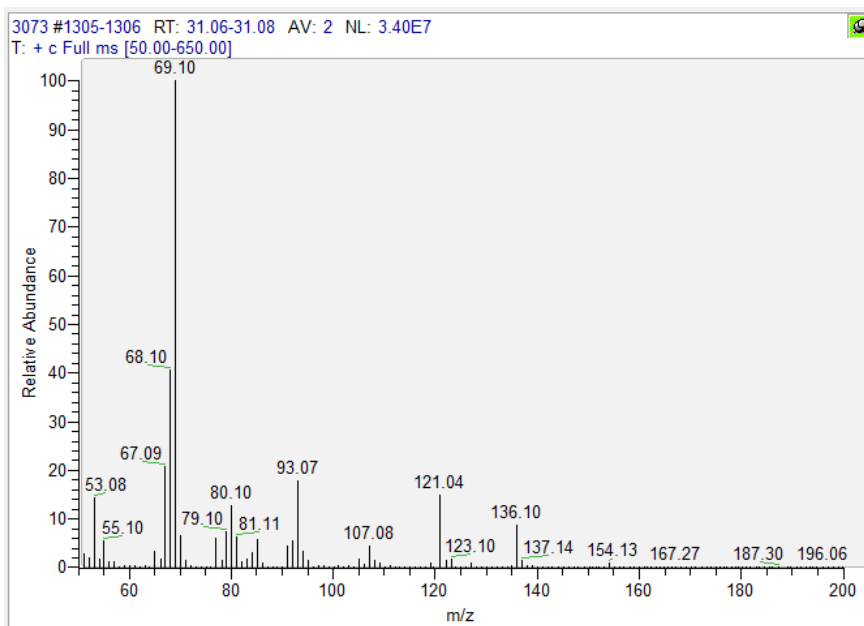
Sample 3074



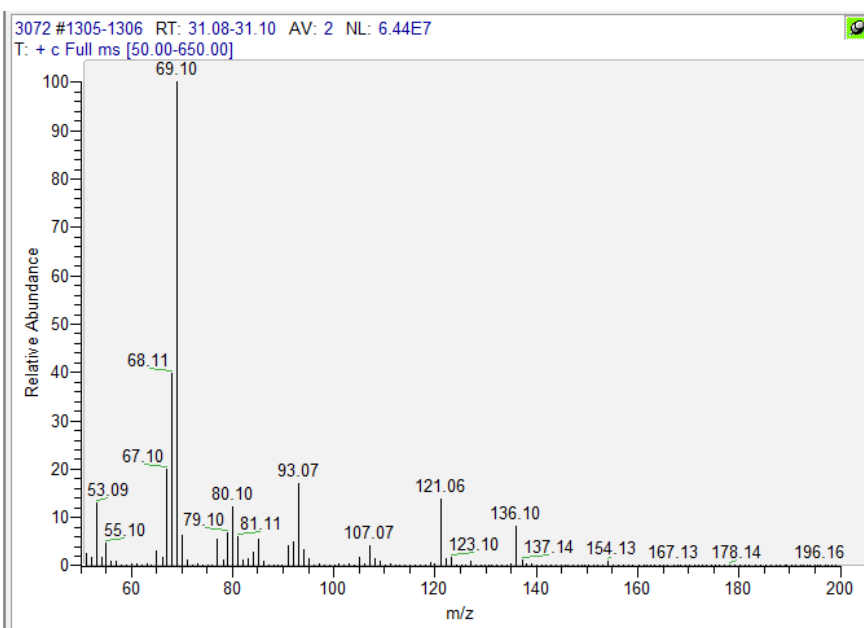
Sample 3073



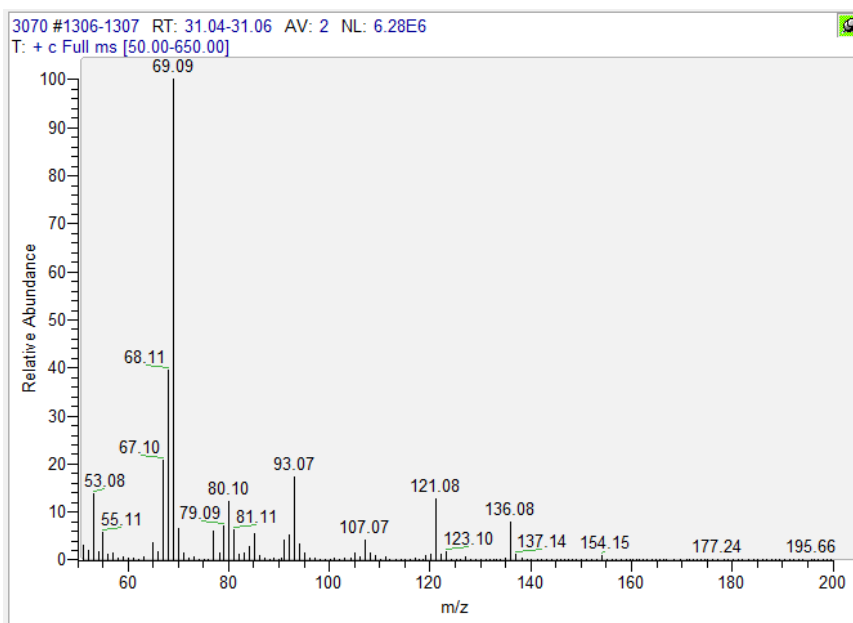
Sample 3073



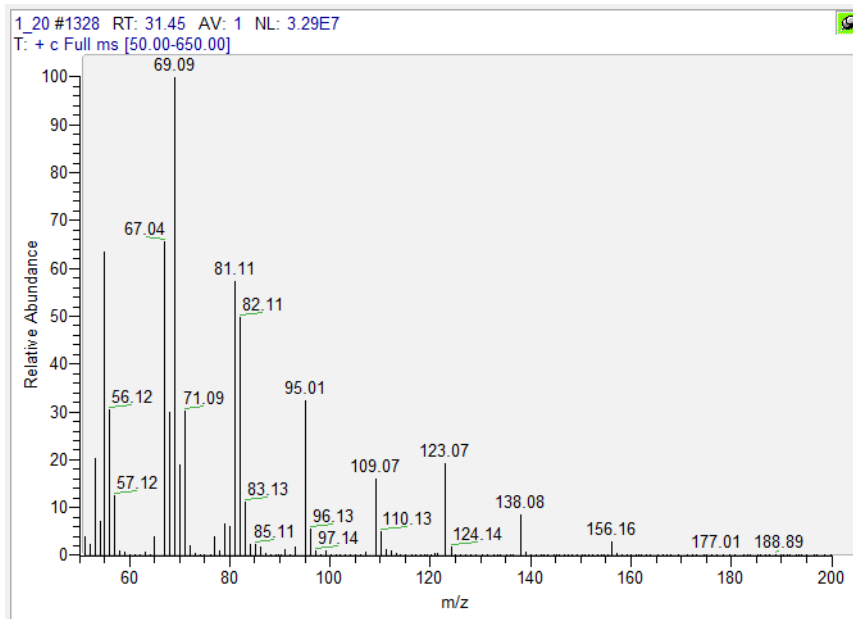
Sample 3072



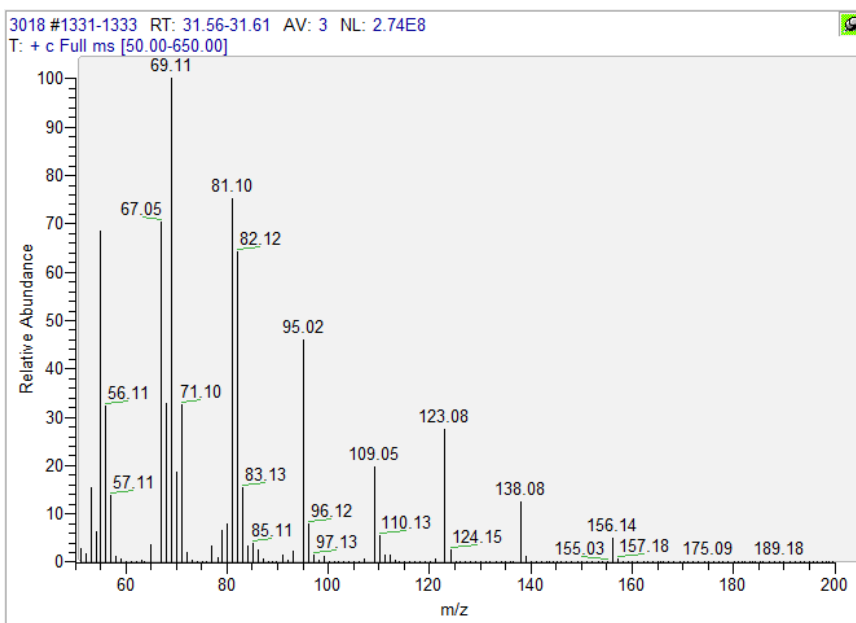
Sample 3070



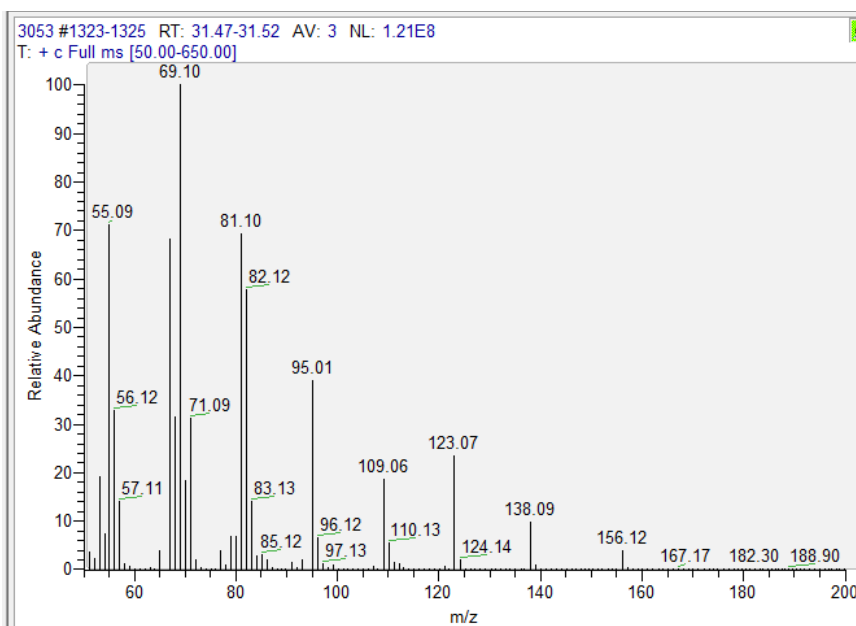
Reference of citronellol



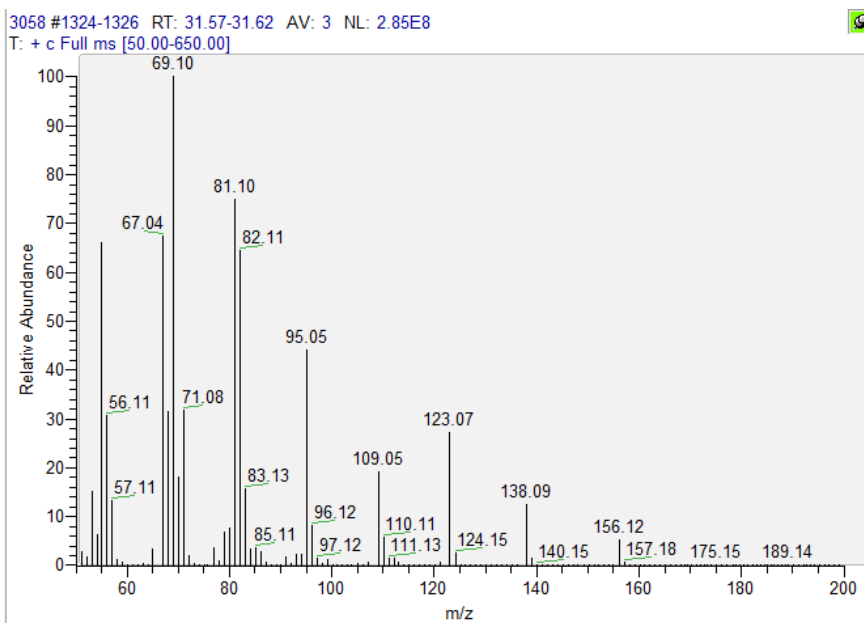
Sample 3018



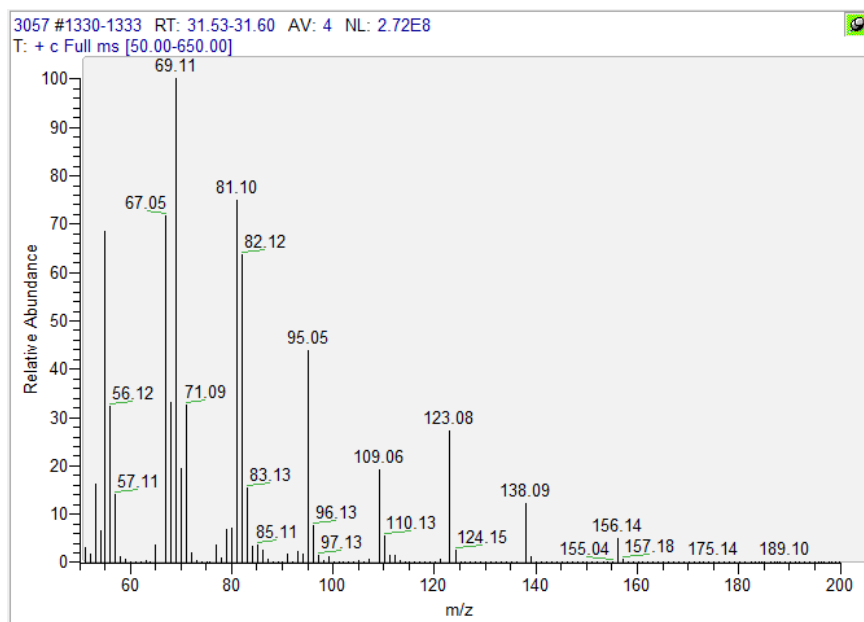
Sample 3053



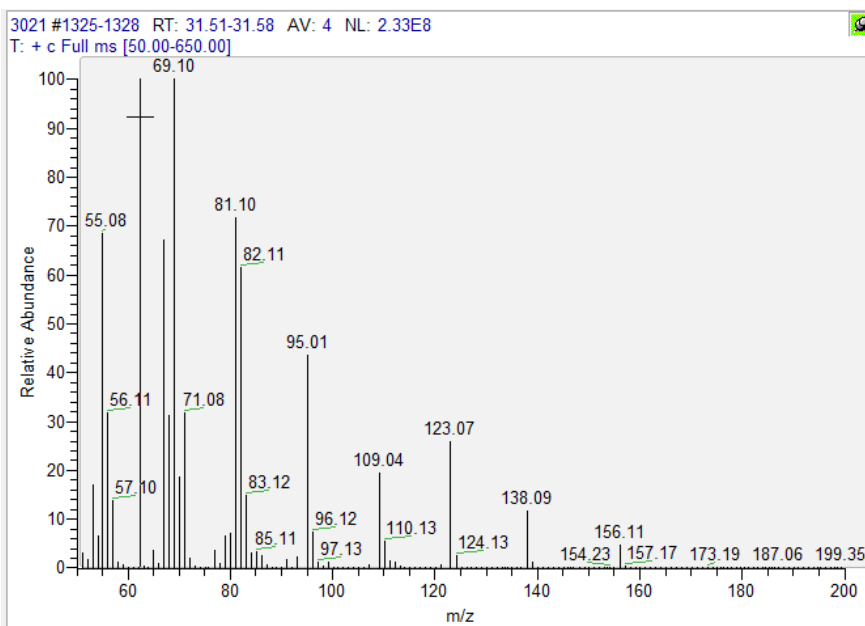
Sample 3058



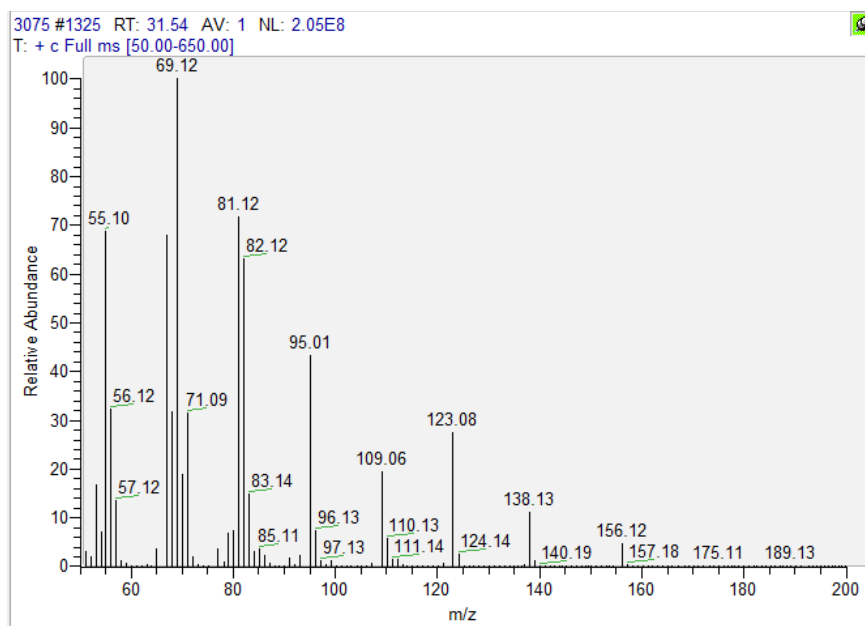
Sample 3057



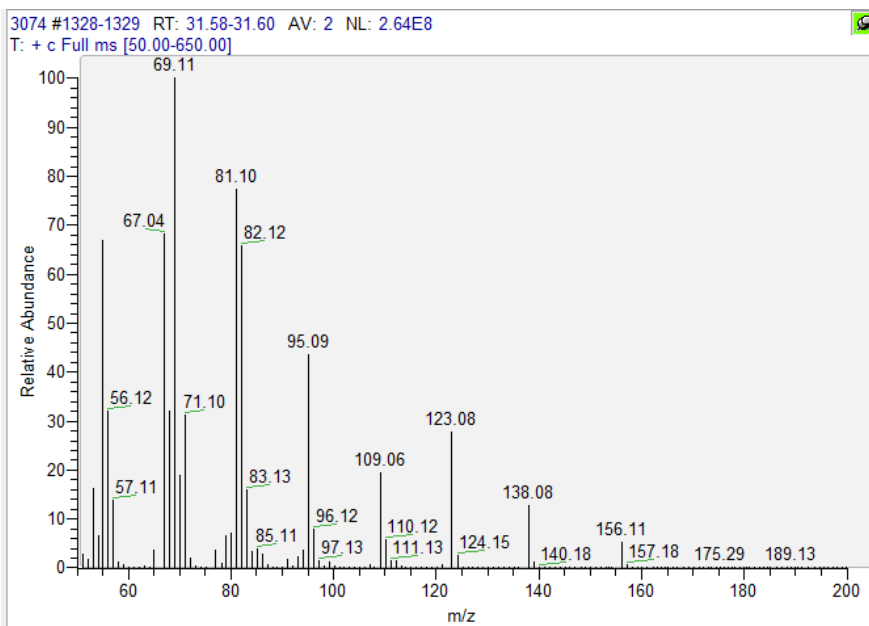
Sample 3021



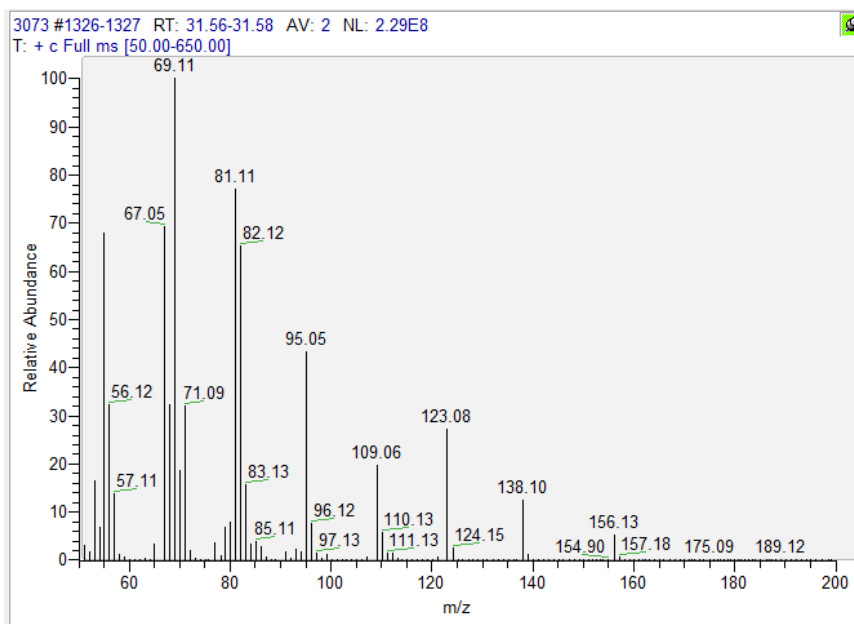
Sample 3075



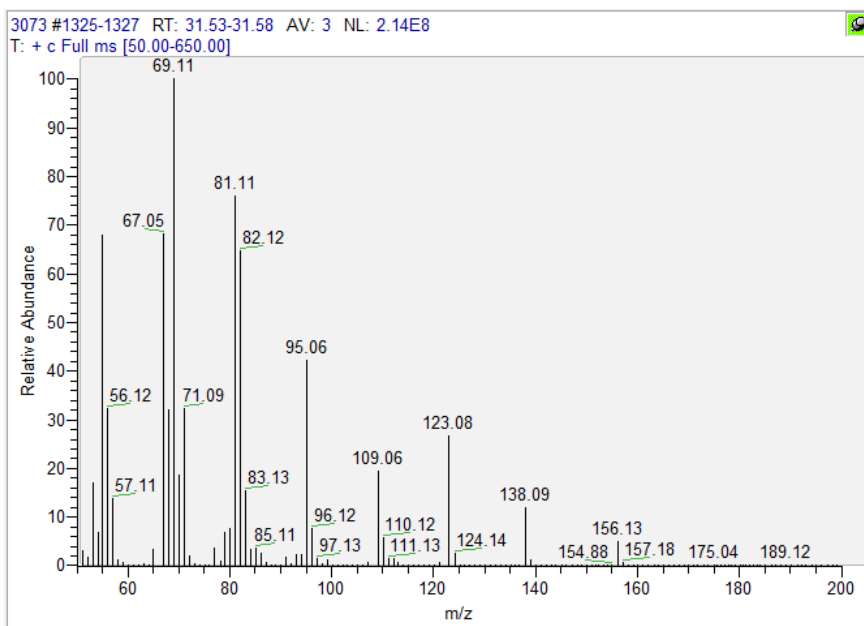
Sample 3074



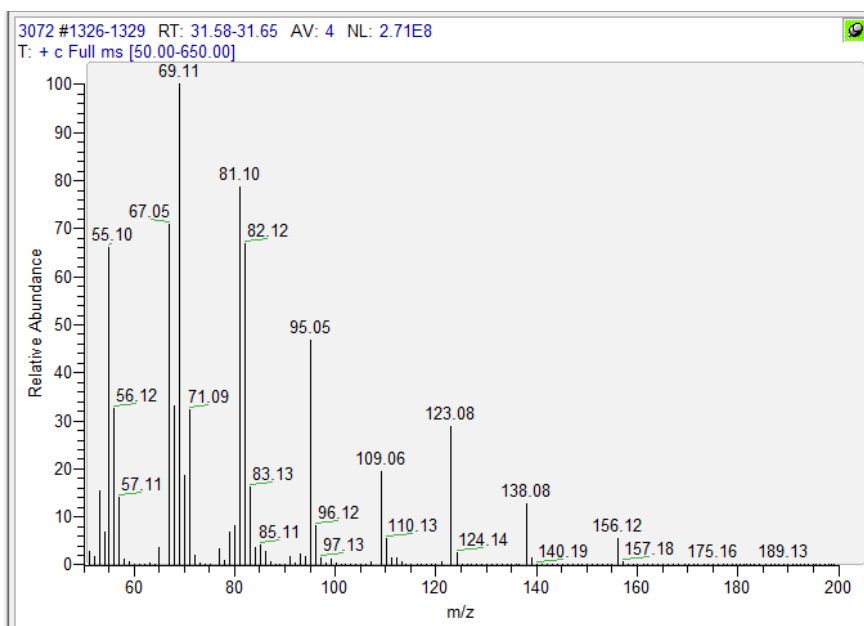
Sample 3073



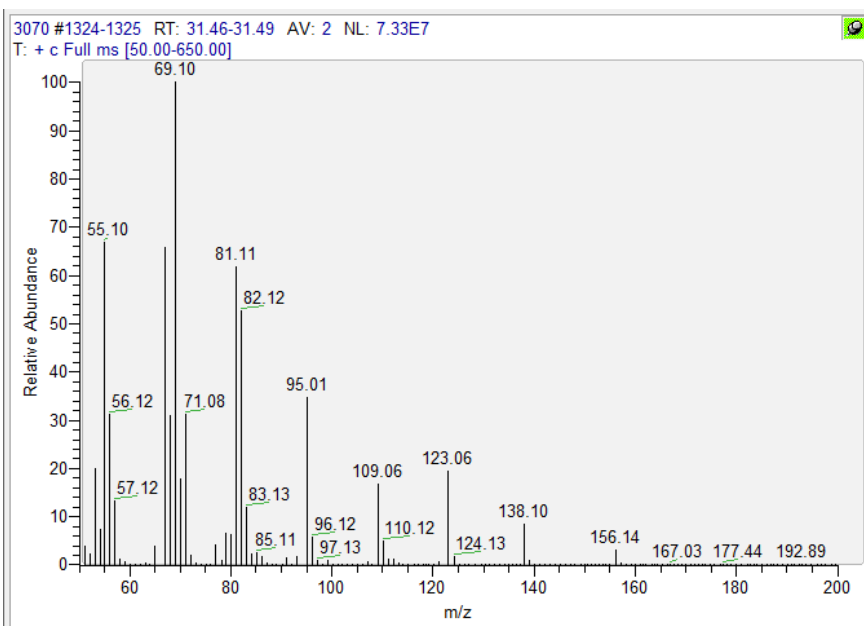
Sample 3073



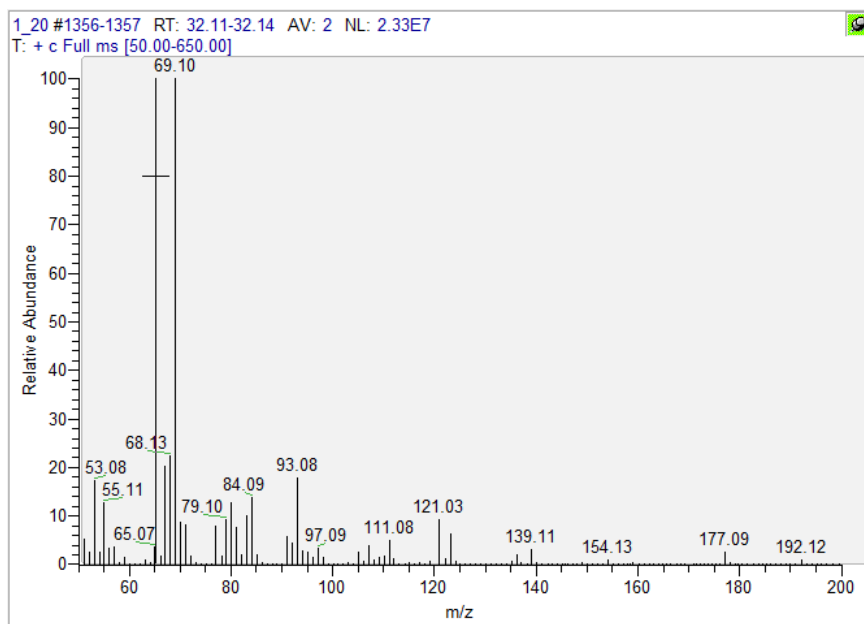
Sample 3072



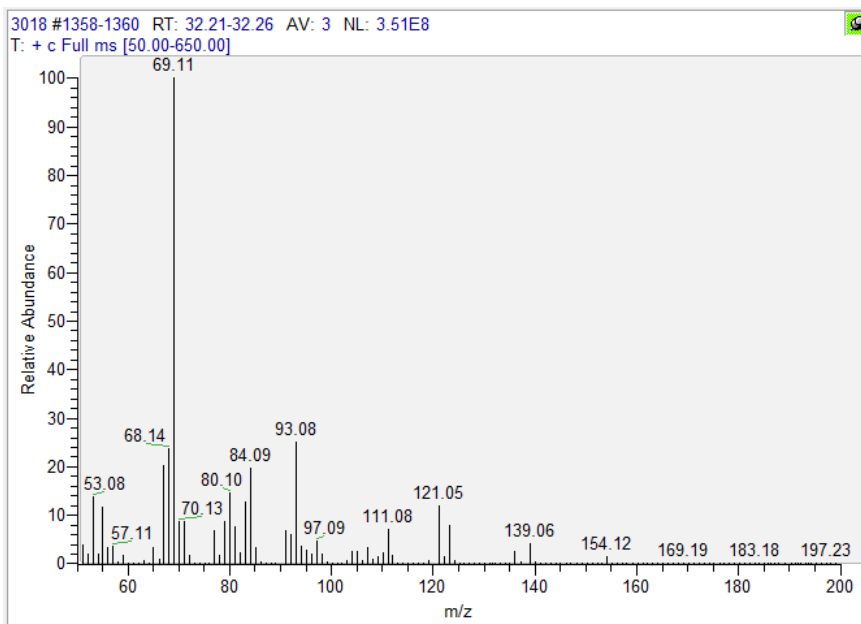
Sample 3070



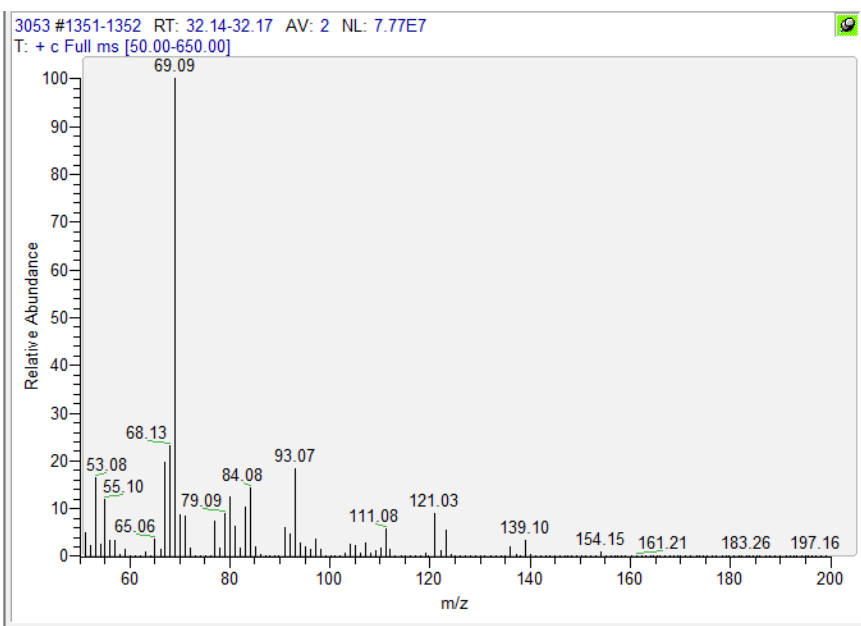
Reference of nerol



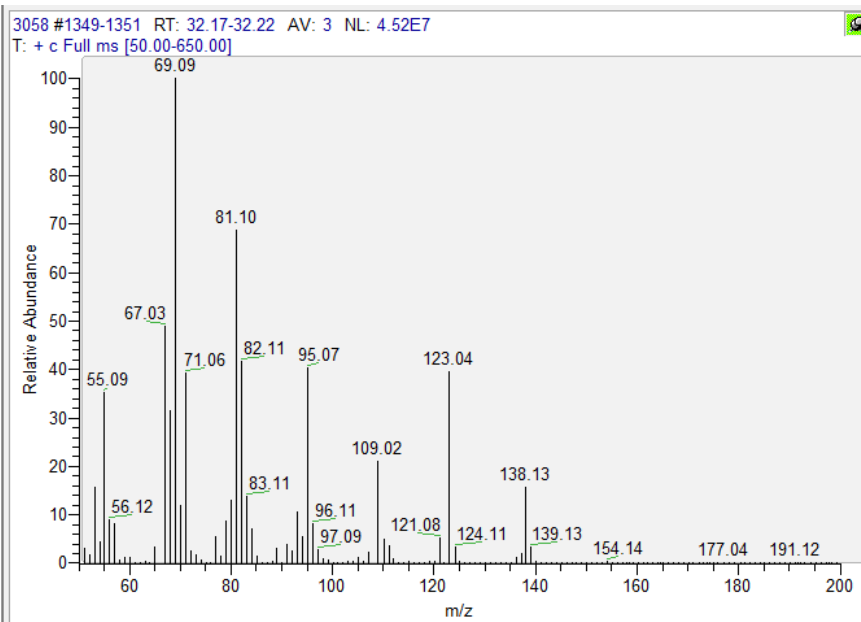
Sample 3018



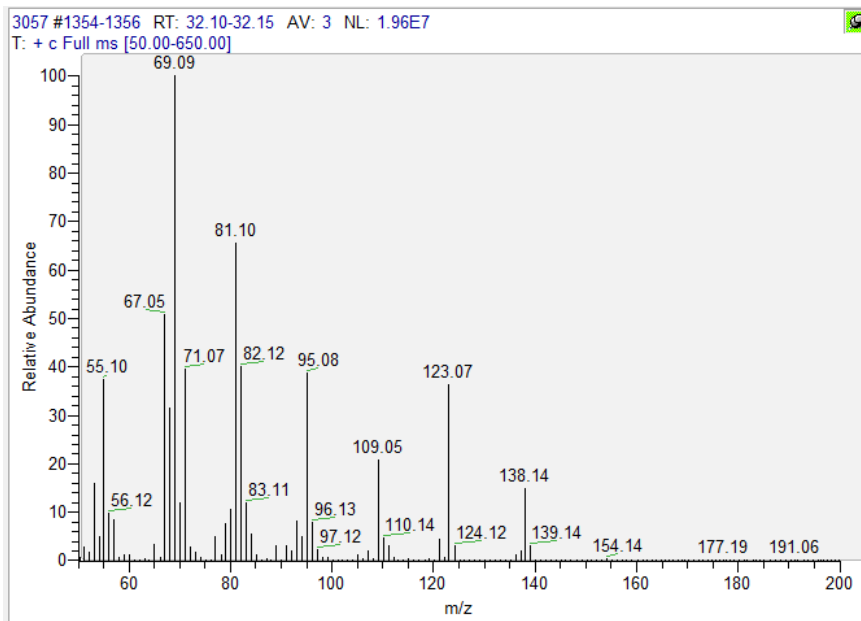
Sample 3053



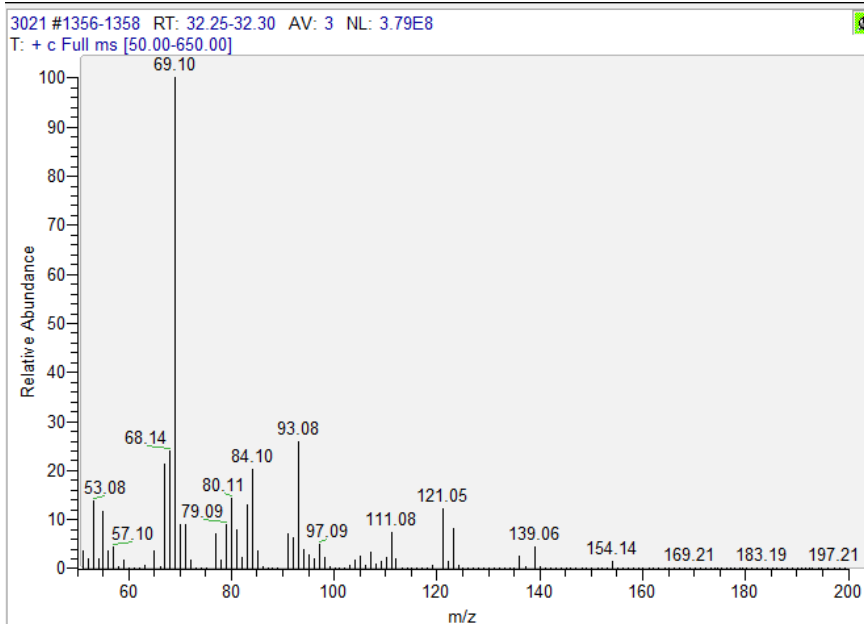
Sample 3058



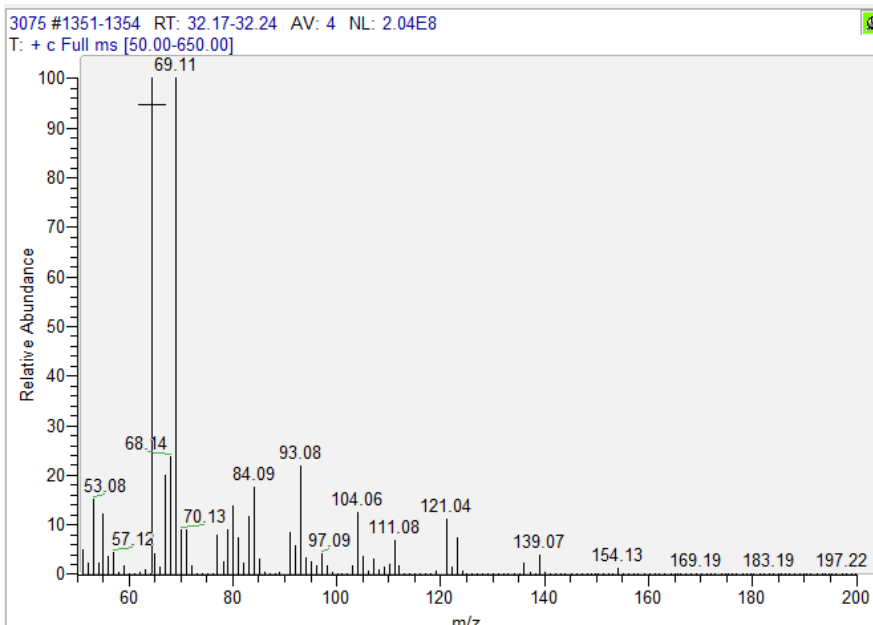
Sample 3057



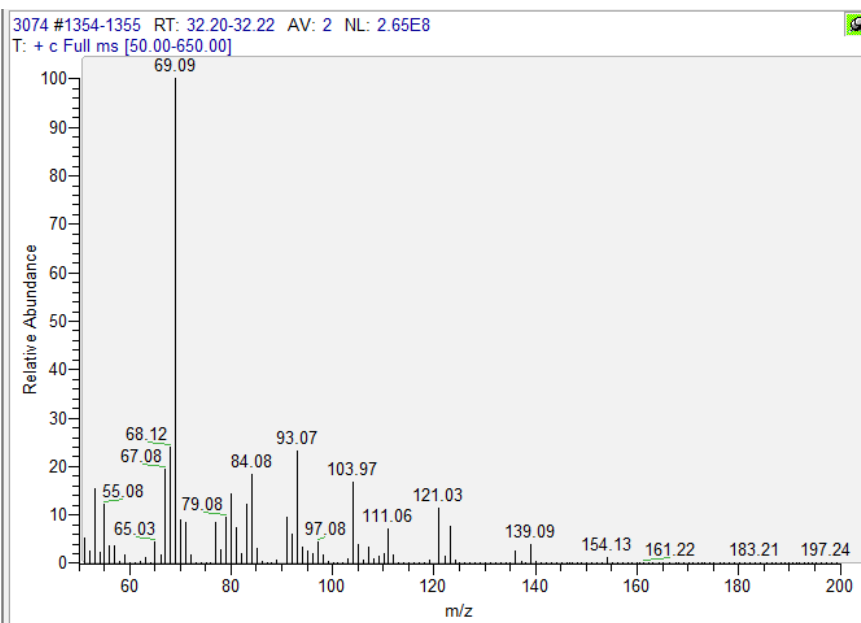
Sample 3021



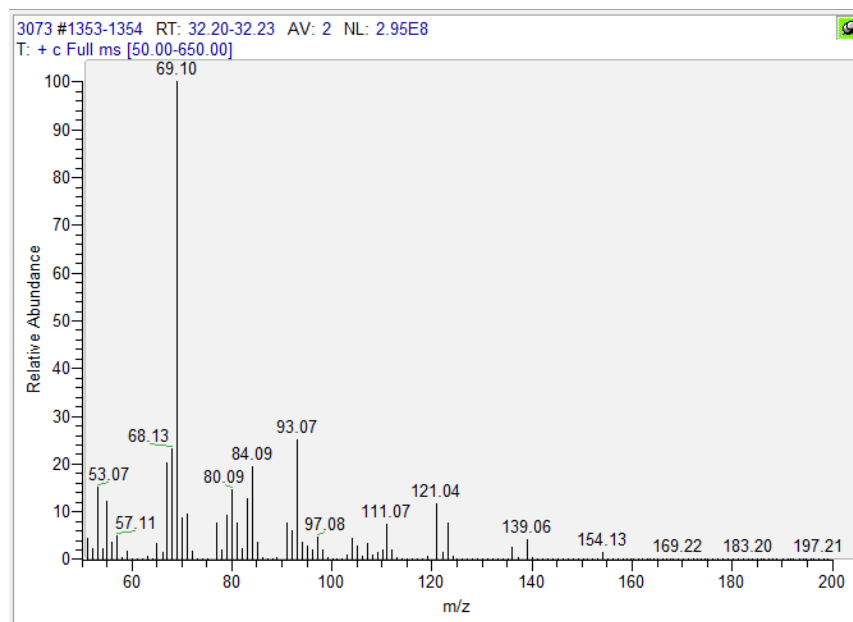
Sample 3075



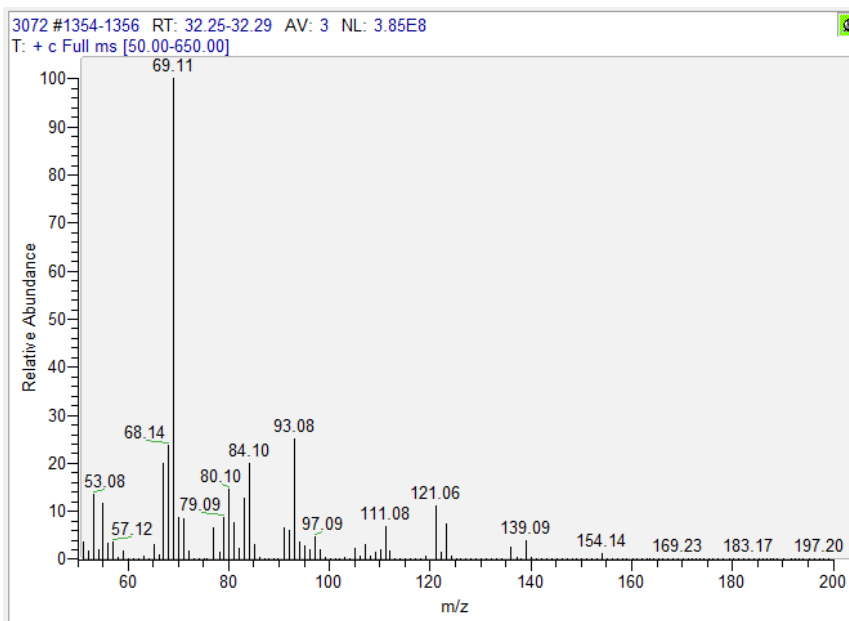
Sample 3074



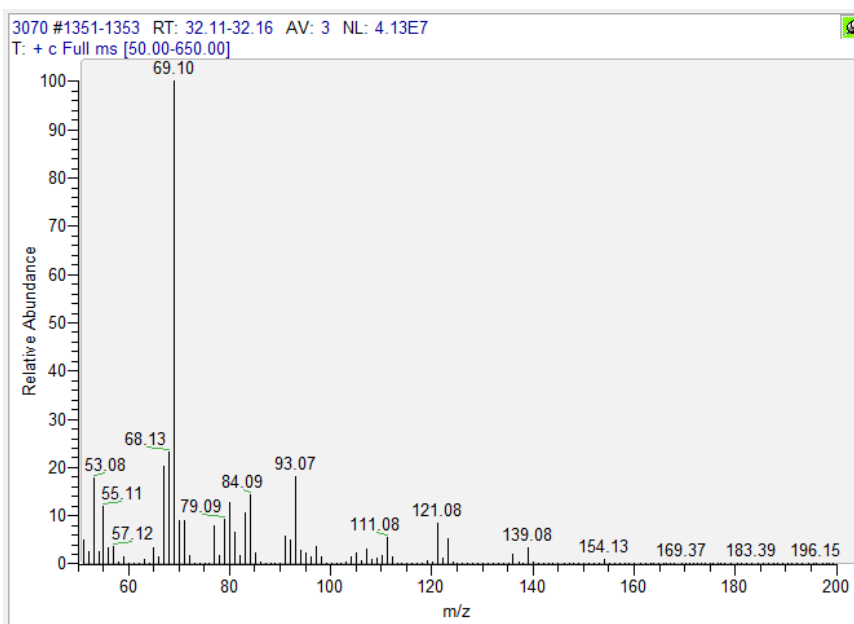
Sample 3073



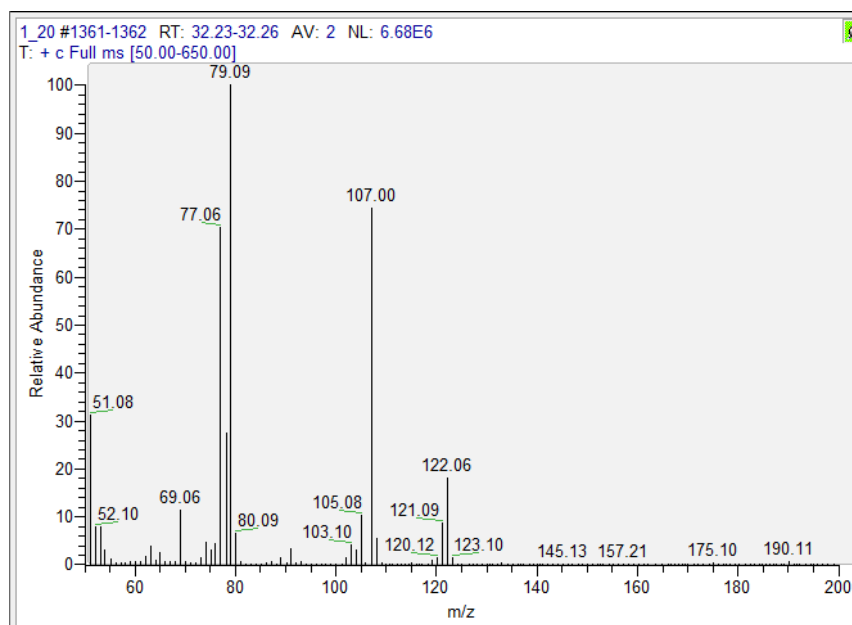
Sample 3072



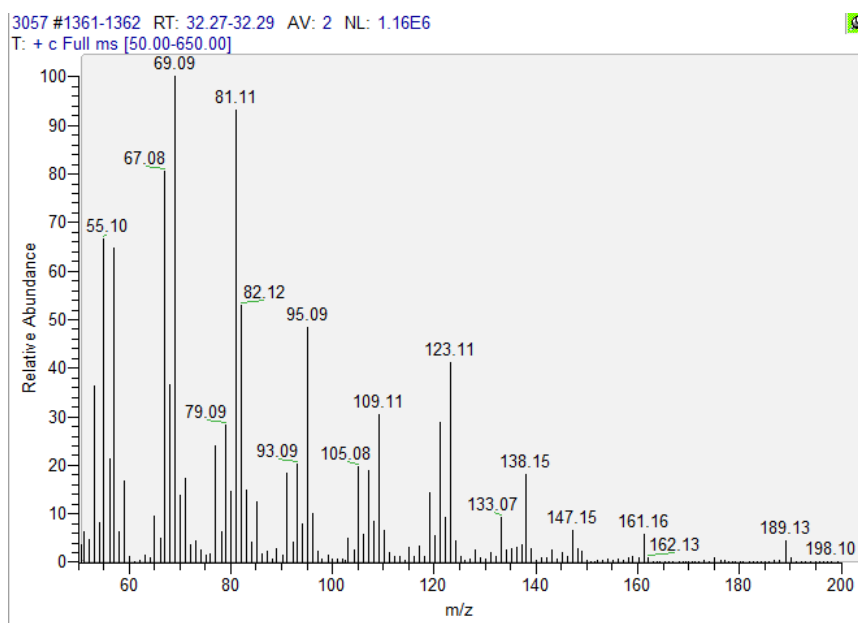
Sample 3070



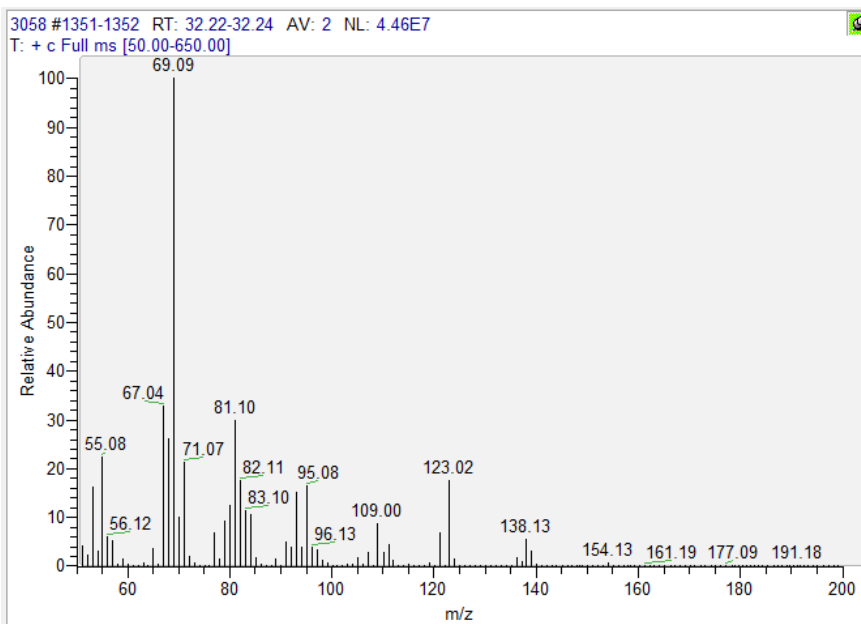
Reference of phenylethanol



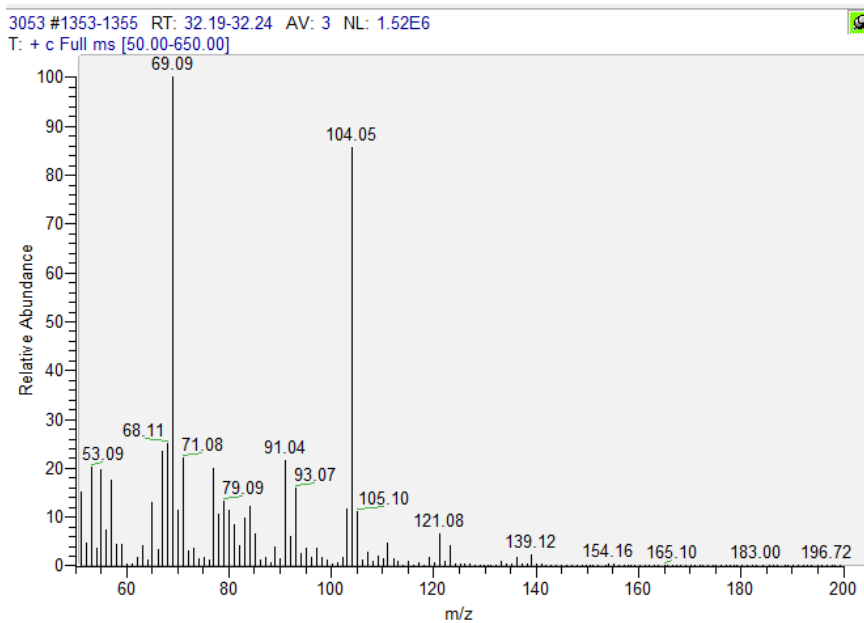
Sample 3057



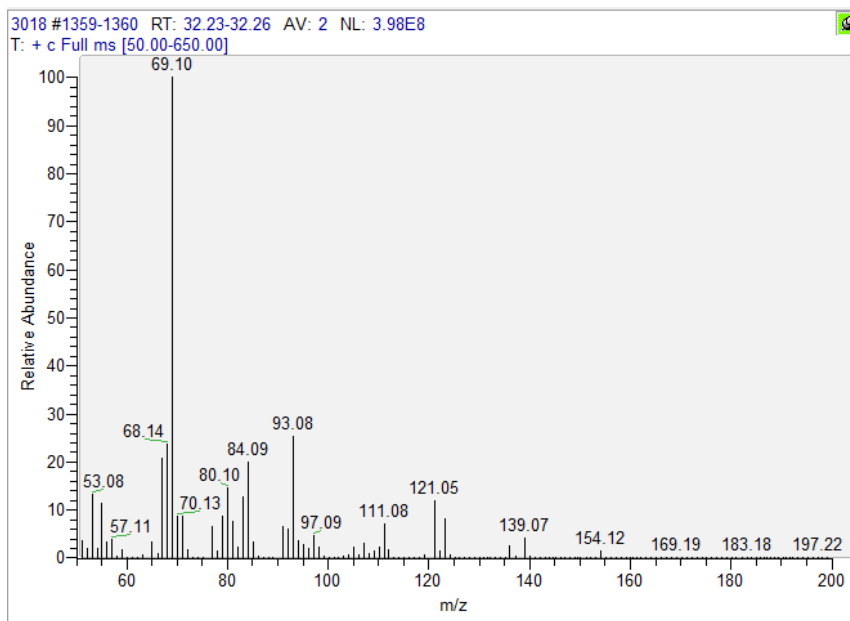
Sample 3058



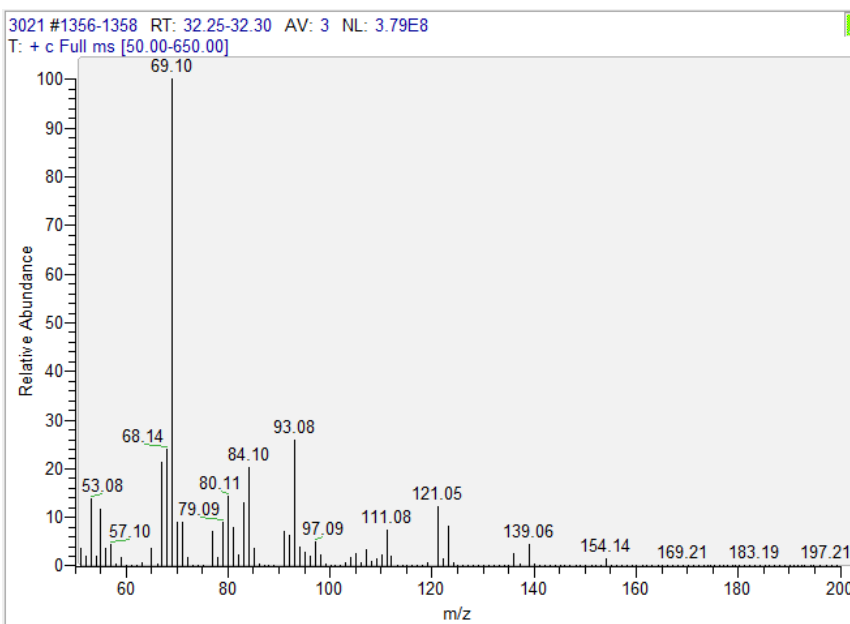
Sample 3053



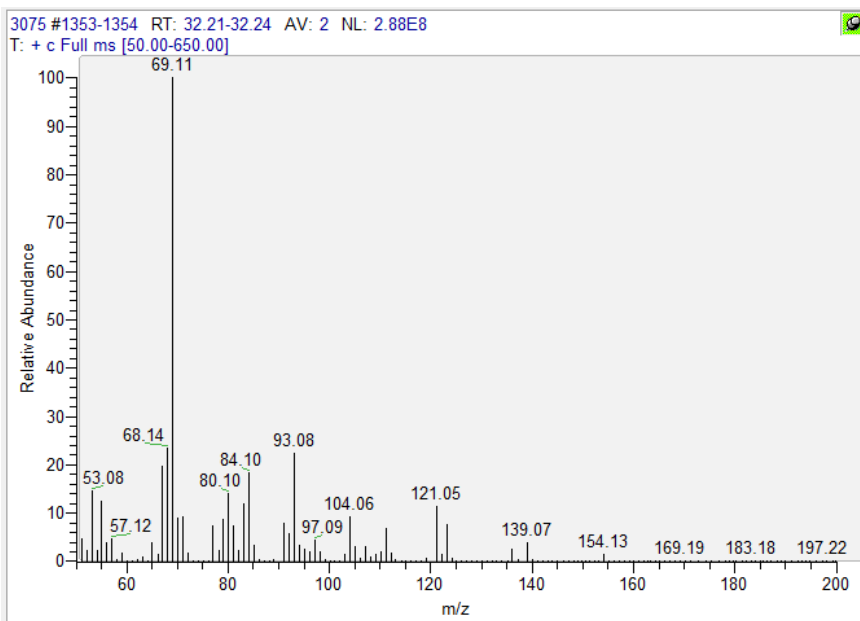
Sample 3018



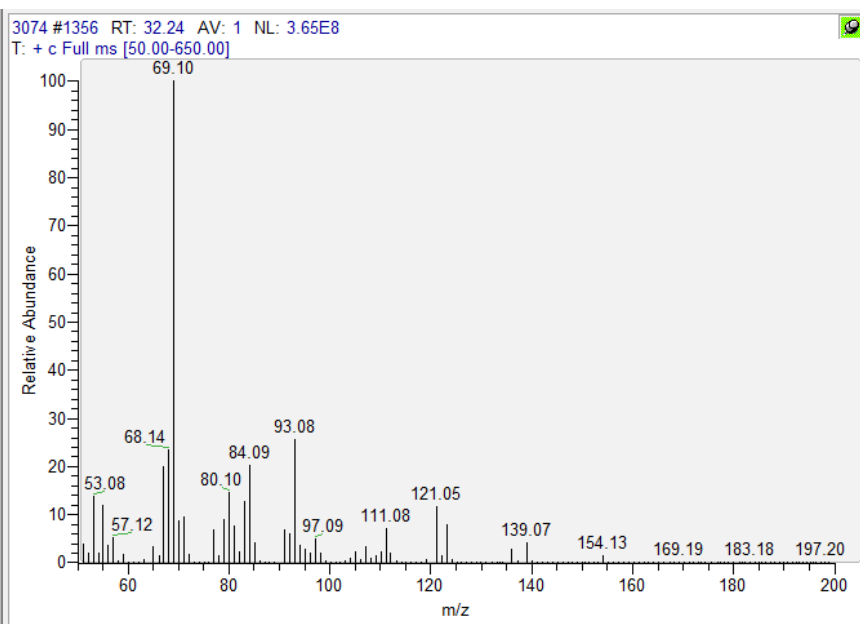
Sample 3021



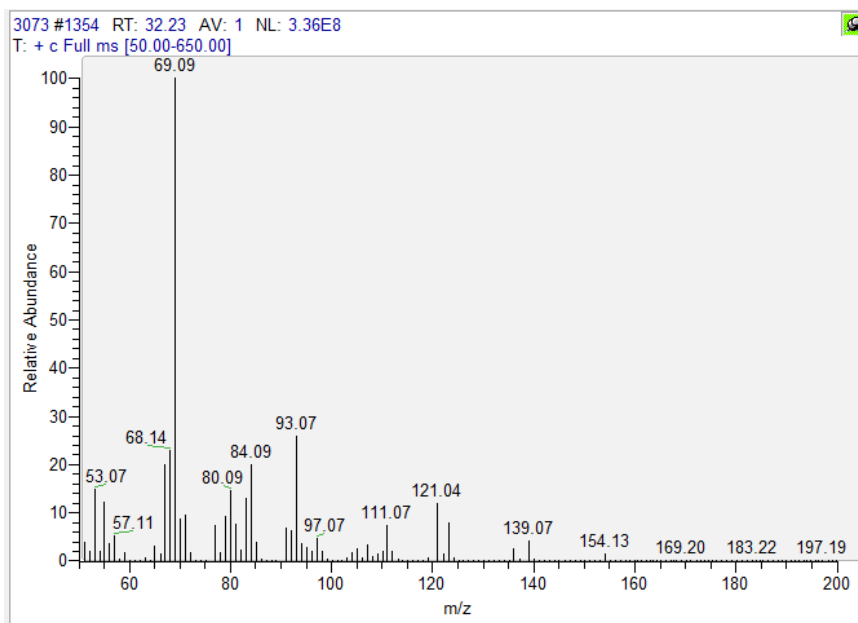
Sample 3075



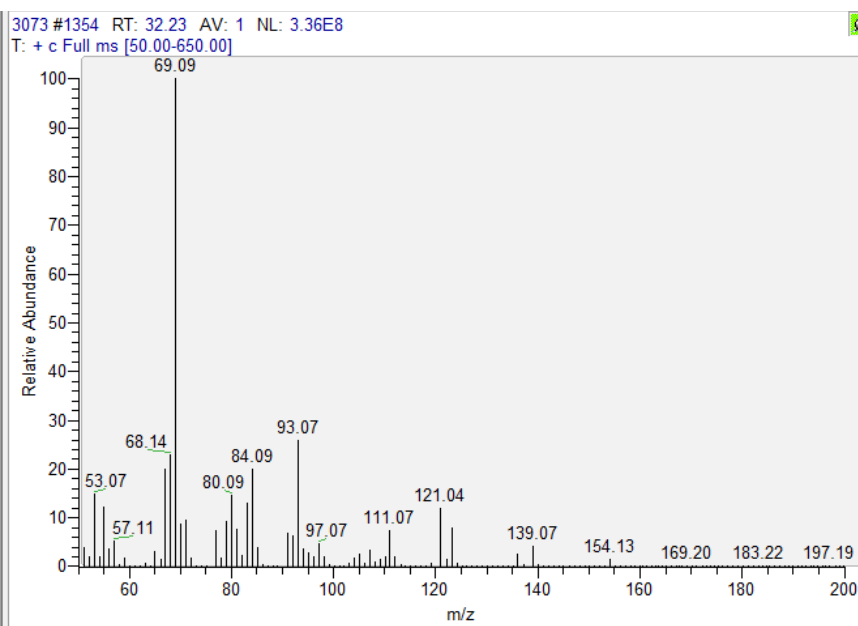
Sample 3074



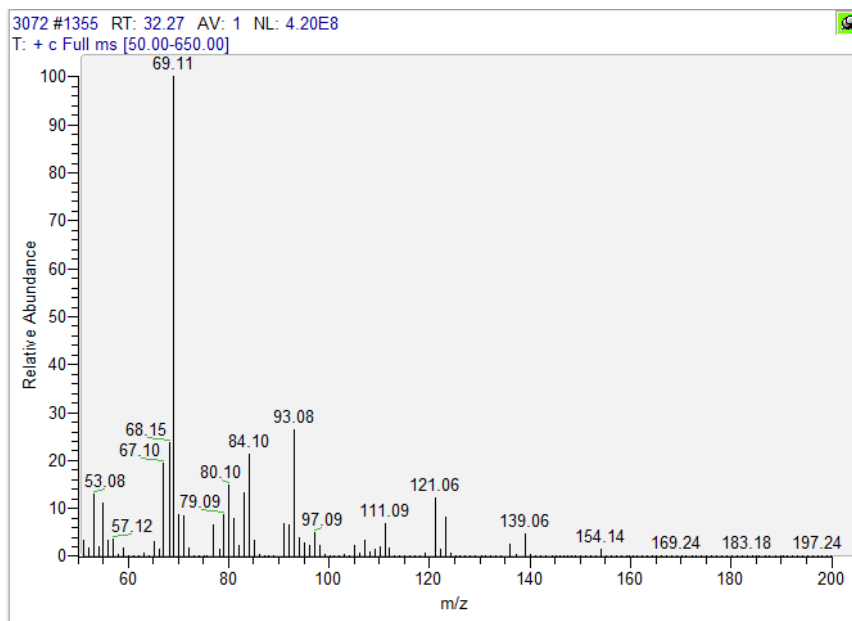
Sample 3073



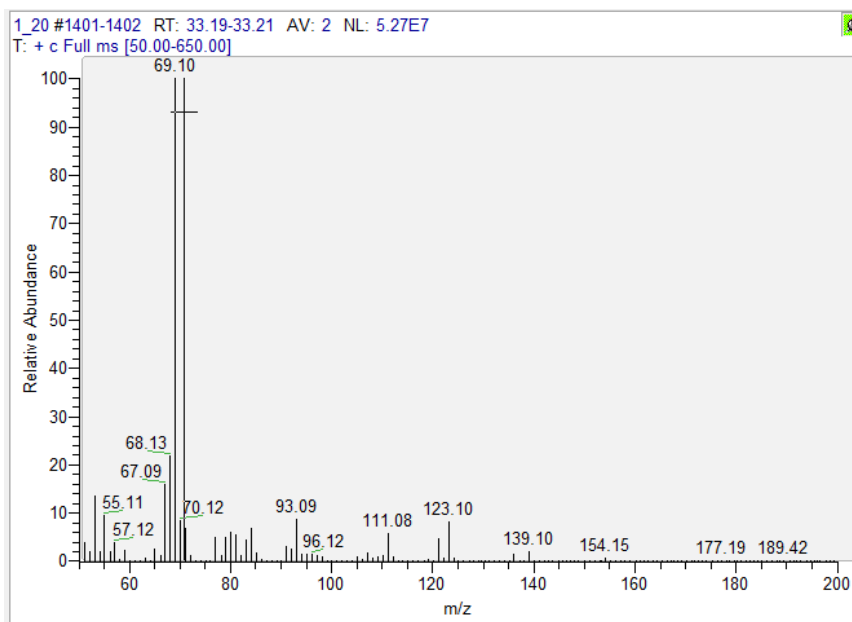
Sample 3073



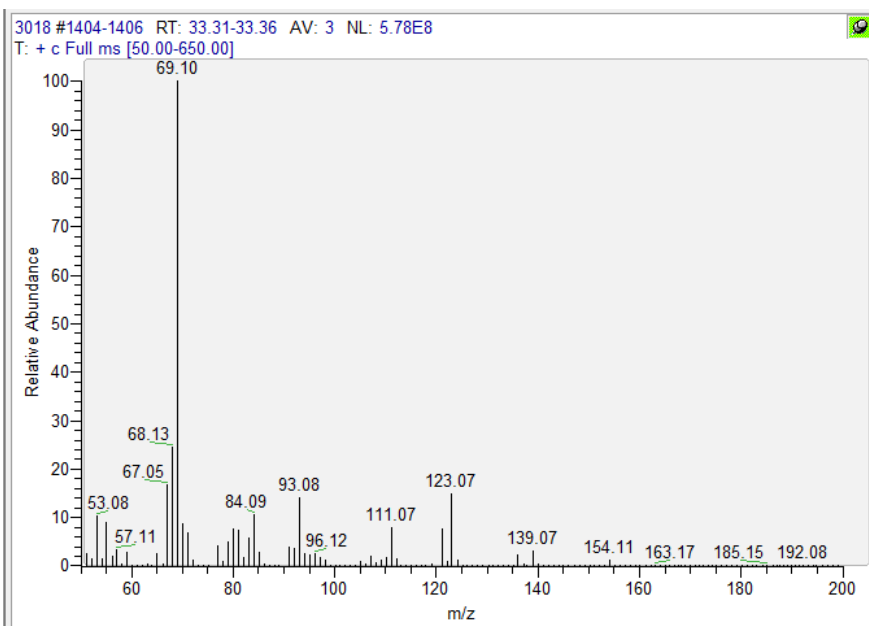
Sample 3072



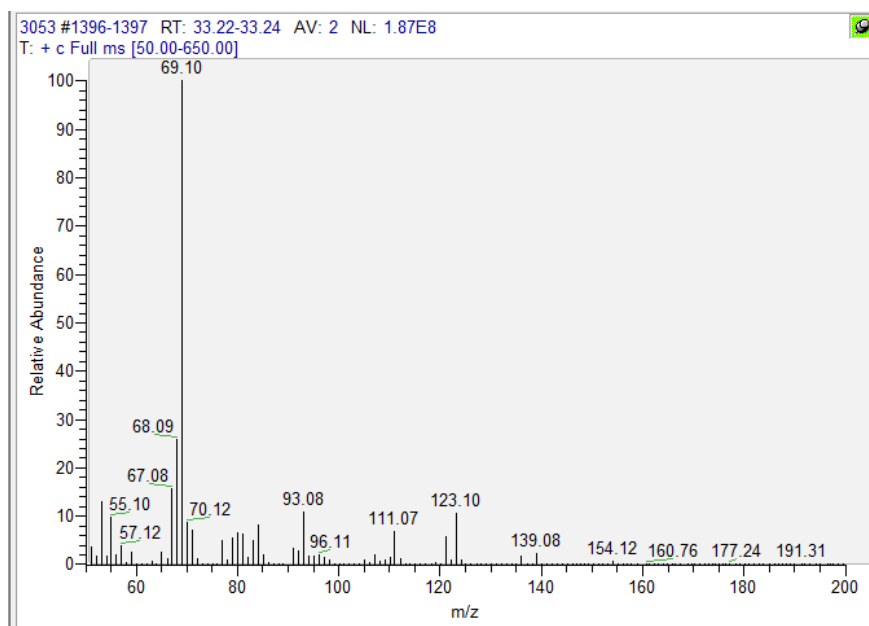
Reference of geraniol



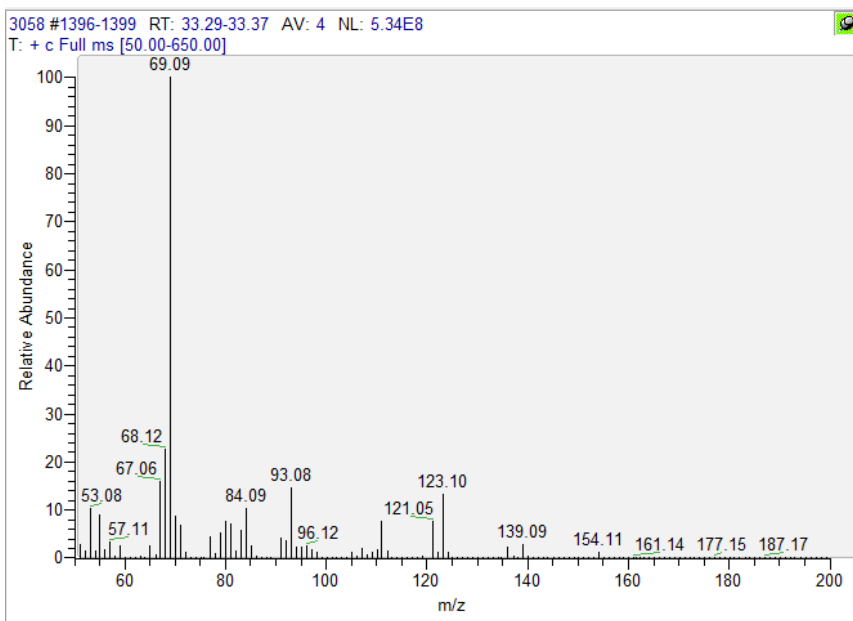
Sample 3018



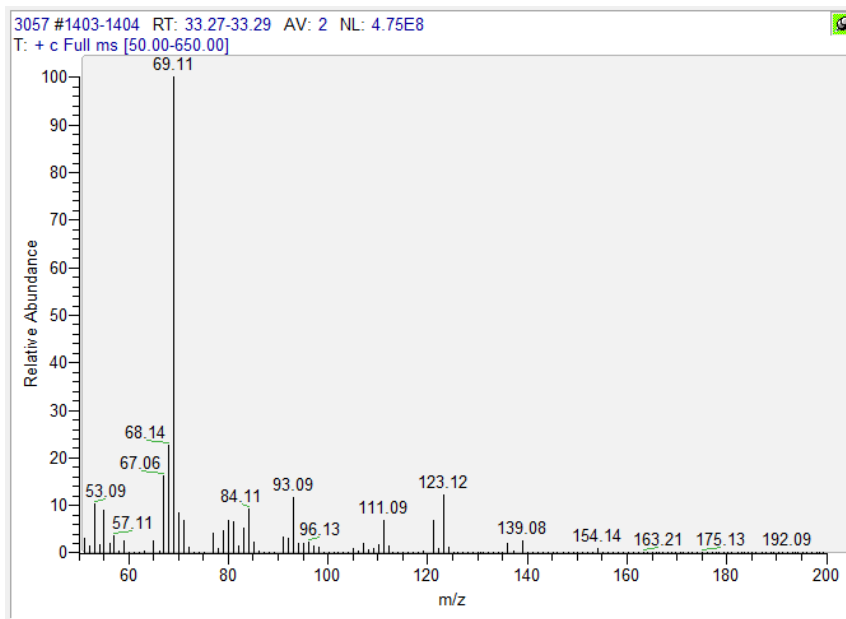
Sample 3053



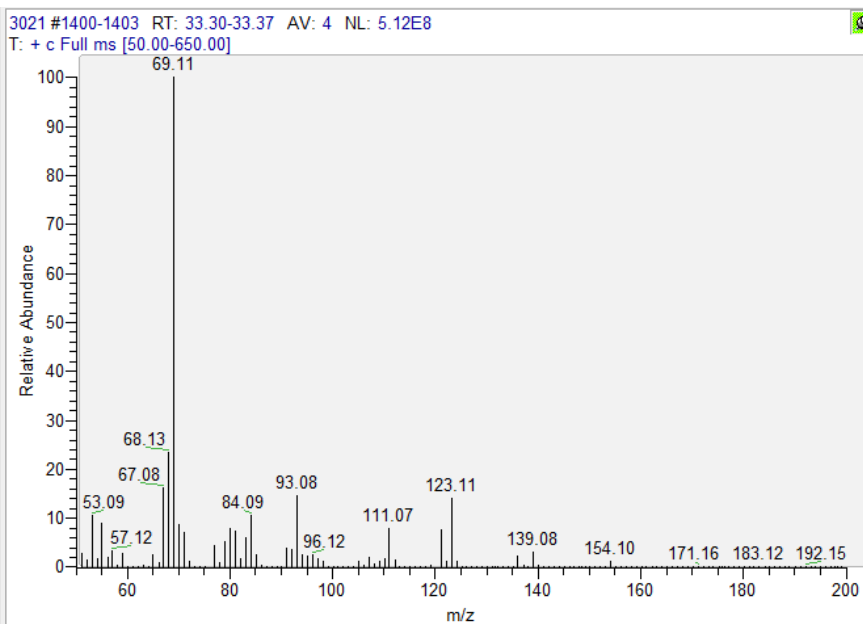
Sample 3058



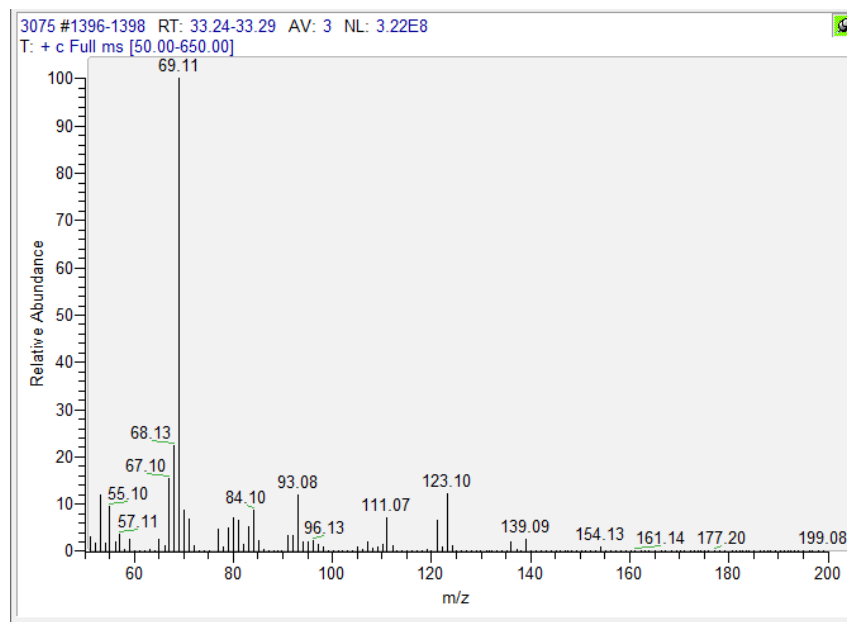
Sample 3057



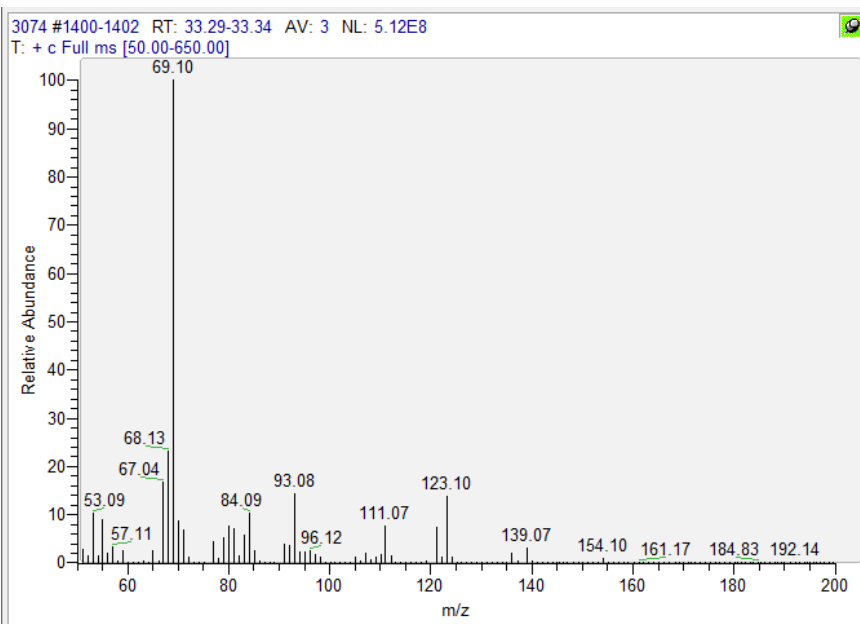
Sample 3021



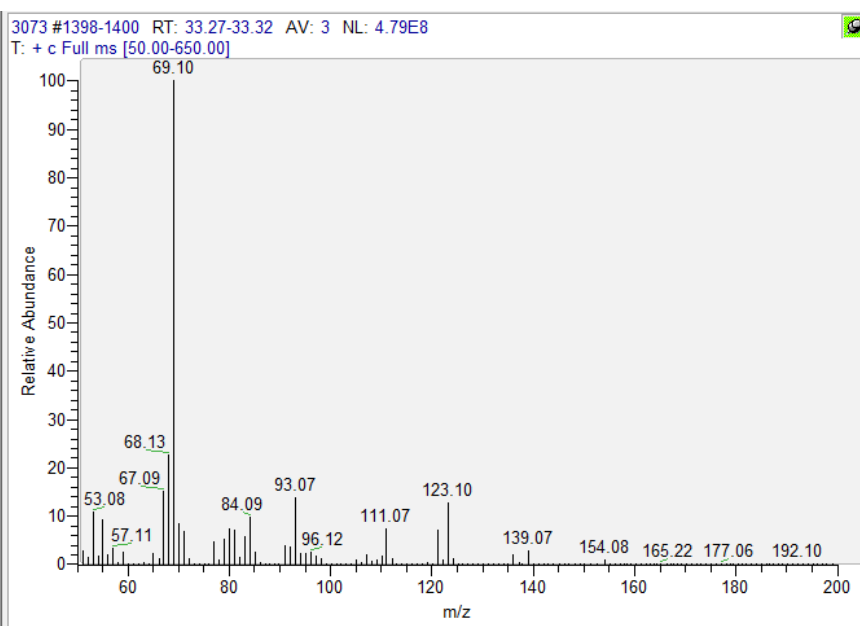
Sample 3075



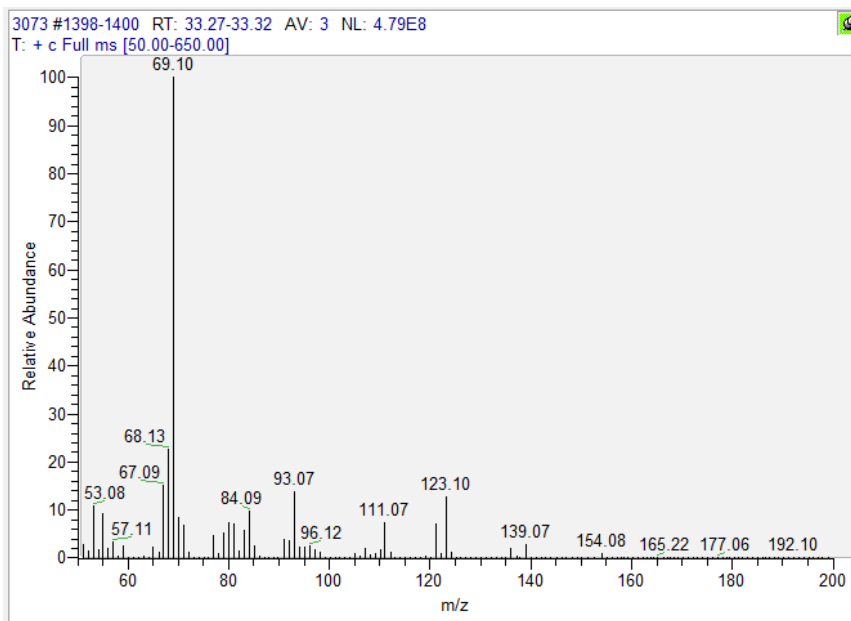
Sample 3074



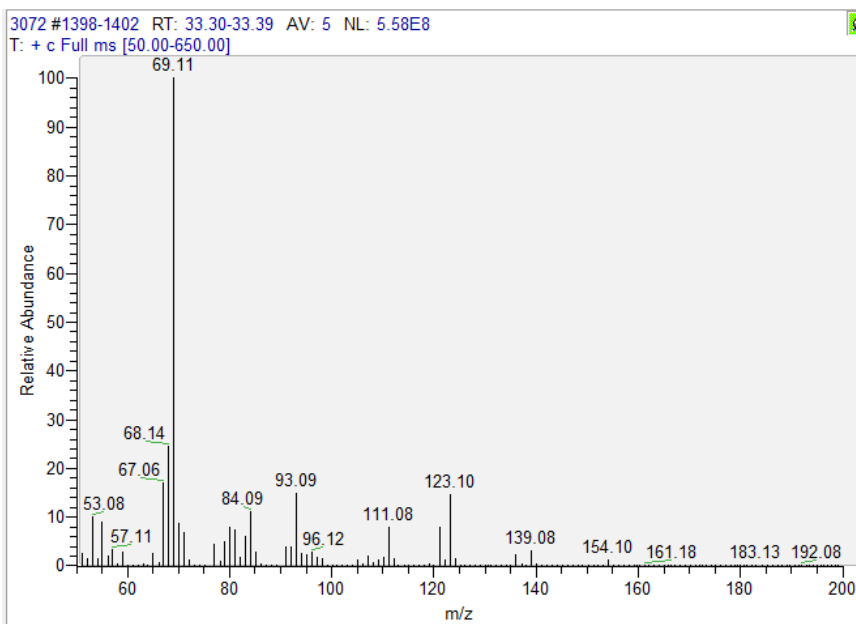
Sample 3073



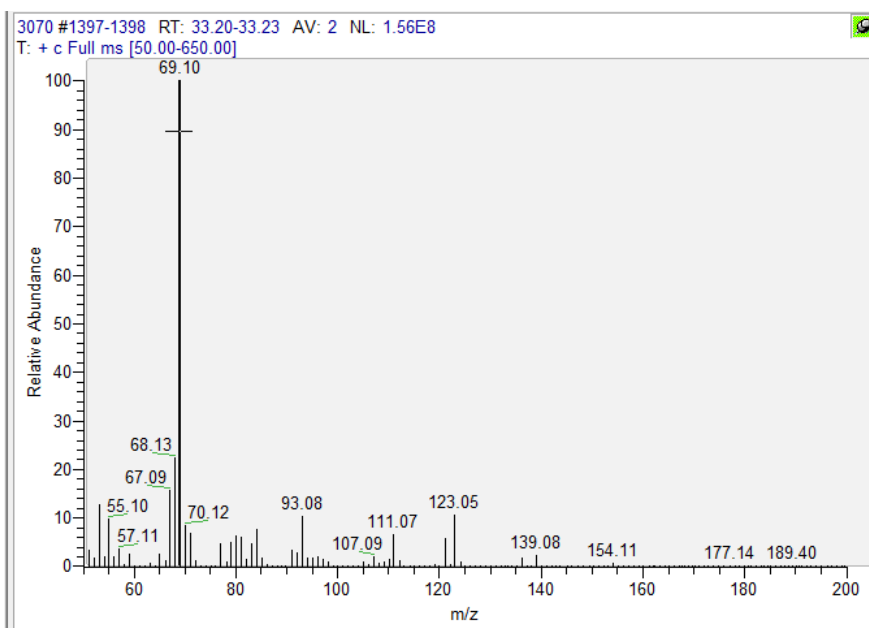
Sample 3073



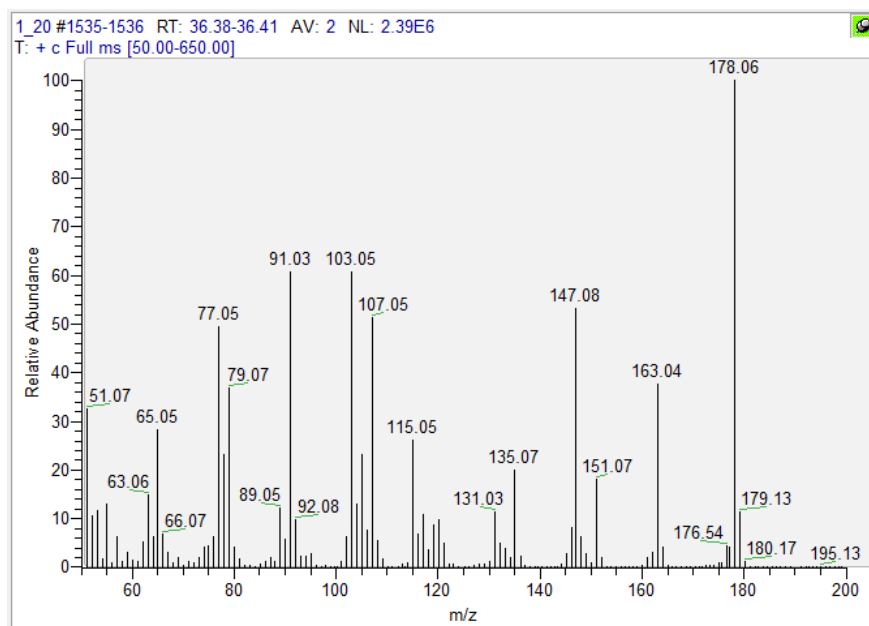
Sample 3072



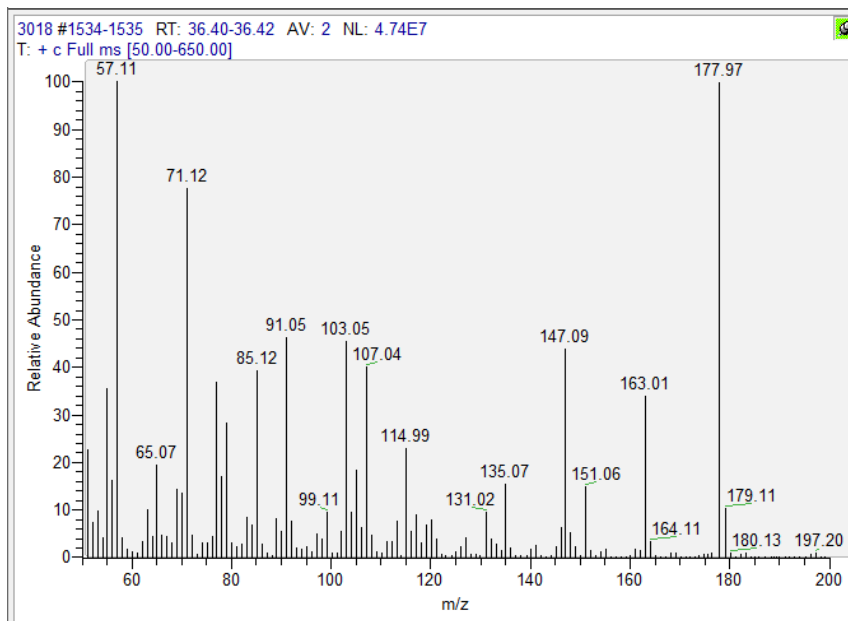
Sample 3070



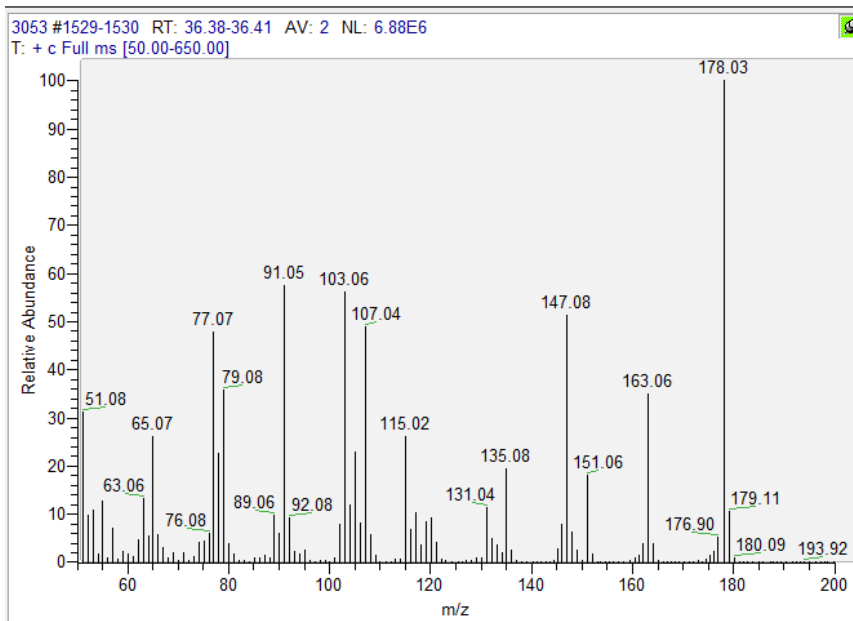
Reference of methyleugenol



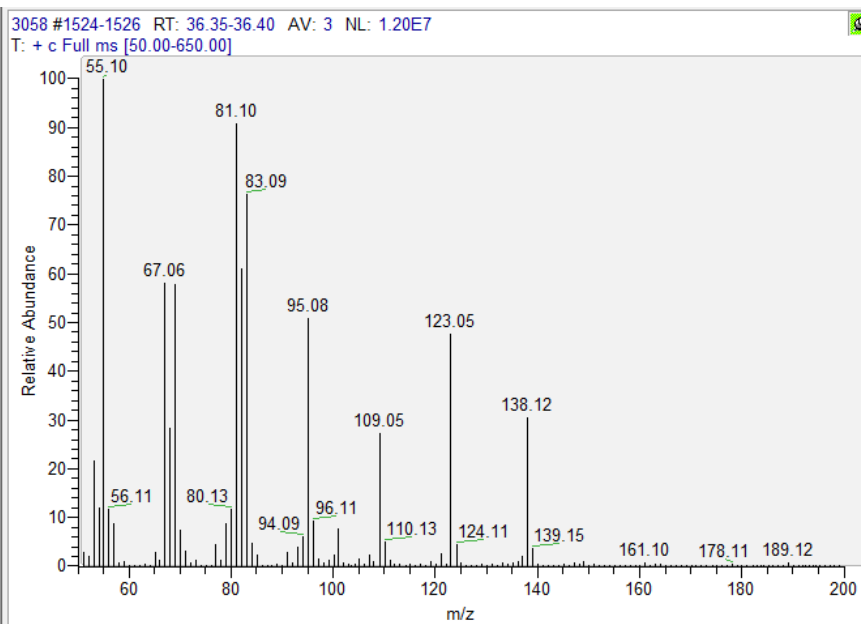
Sample 3018



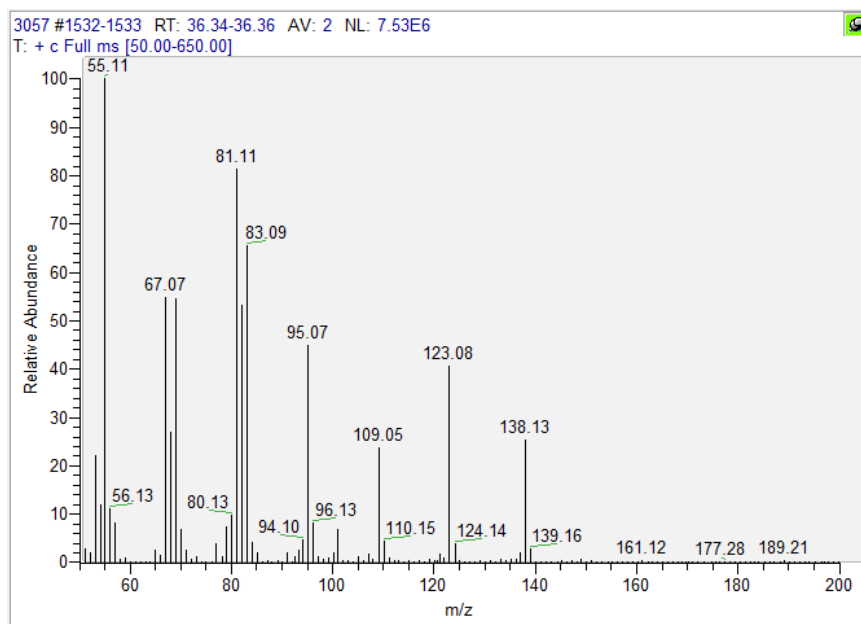
Sample 3053



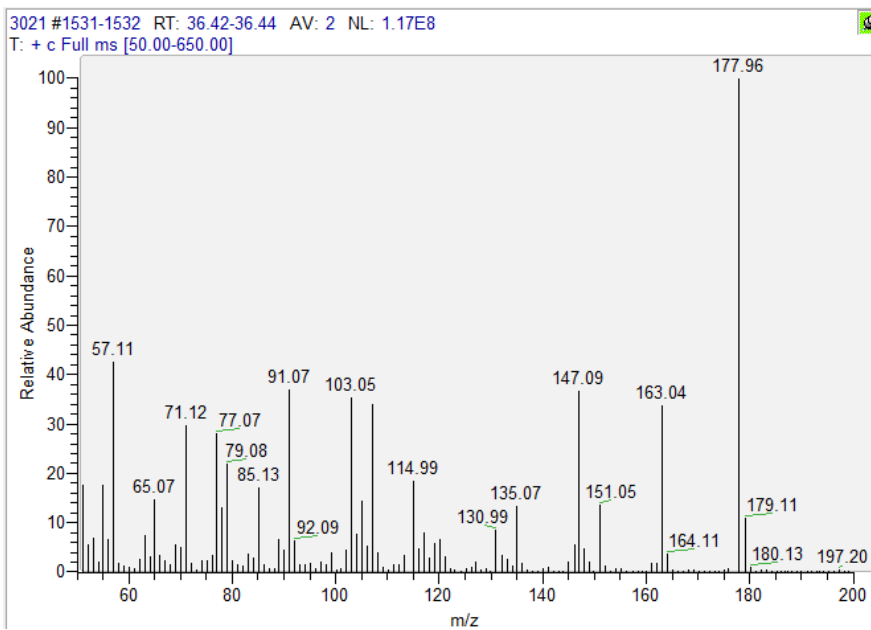
Sample 3058



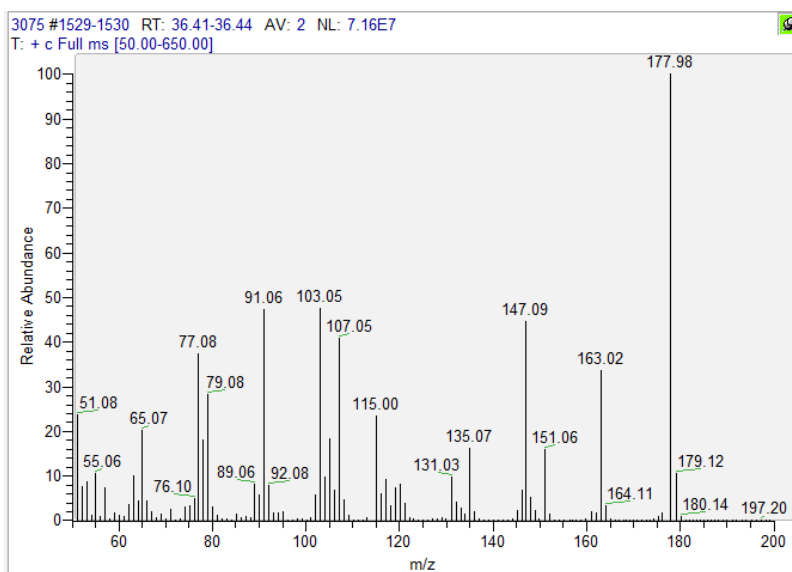
Sample 3057



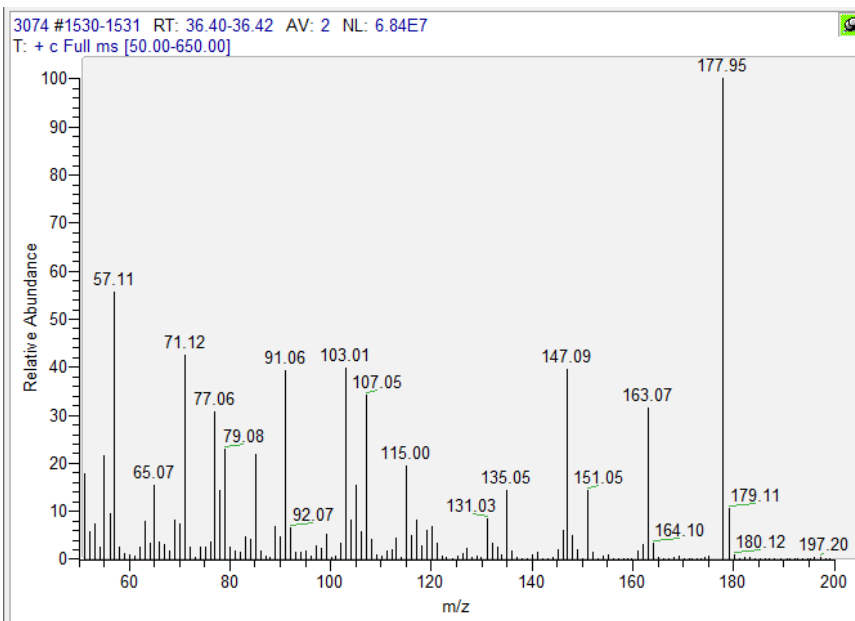
Sample 3021



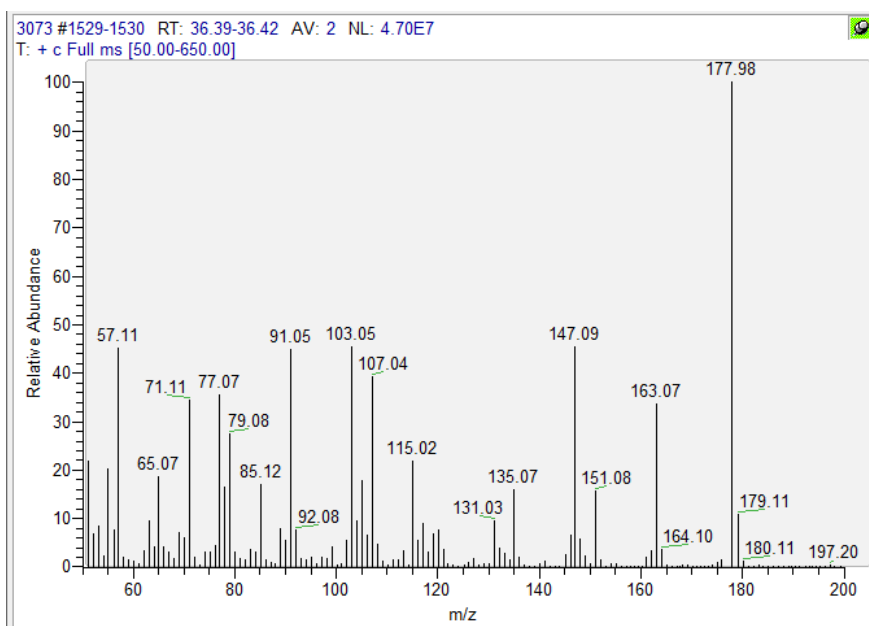
Sample 3075



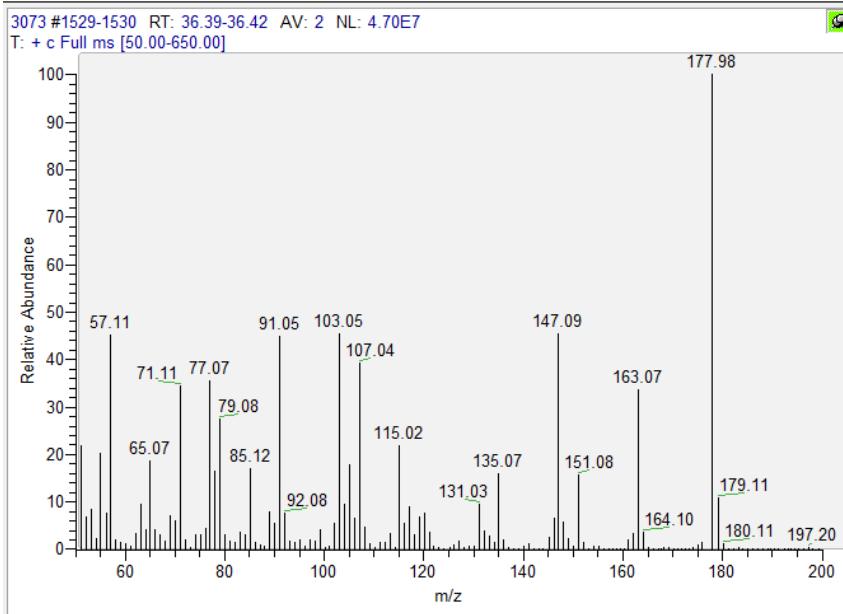
Sample 3074



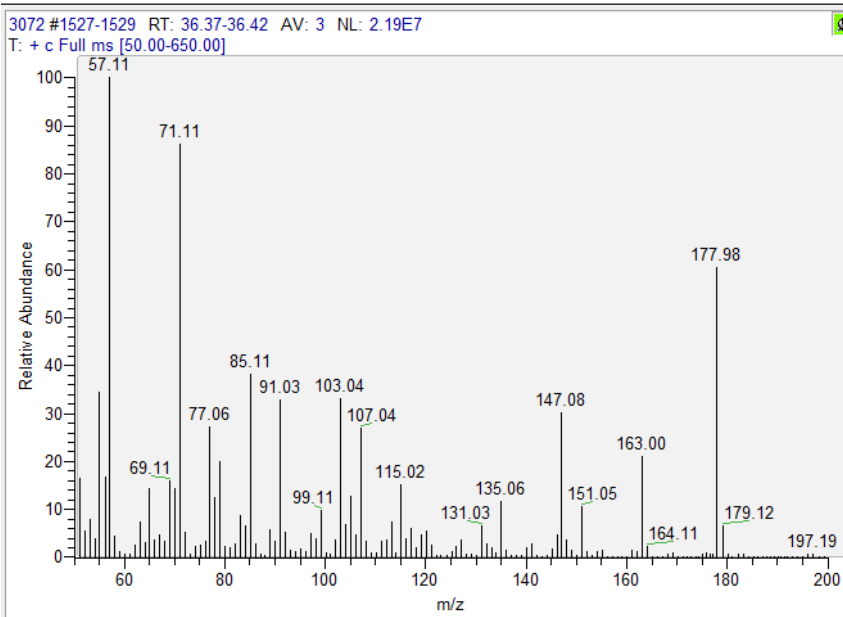
Sample 3073



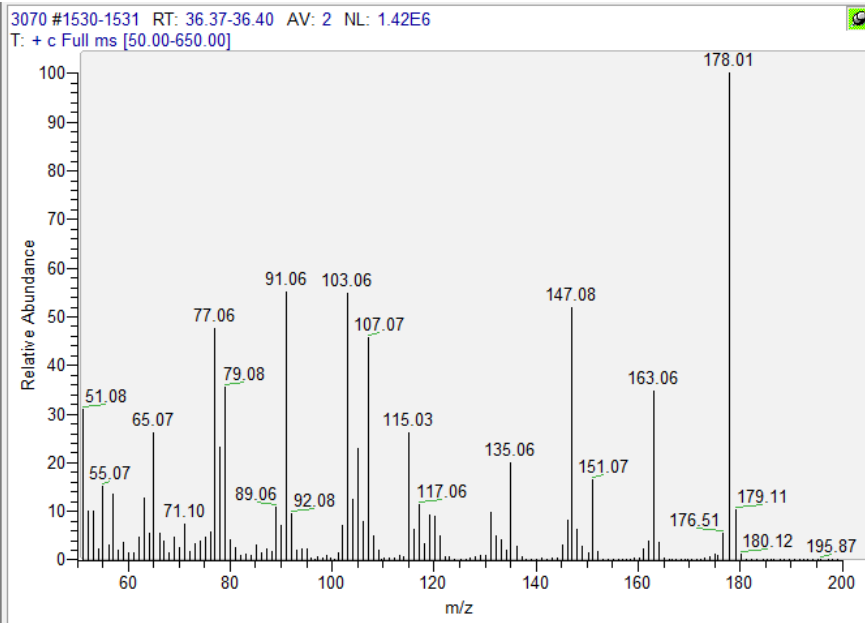
Sample 3073



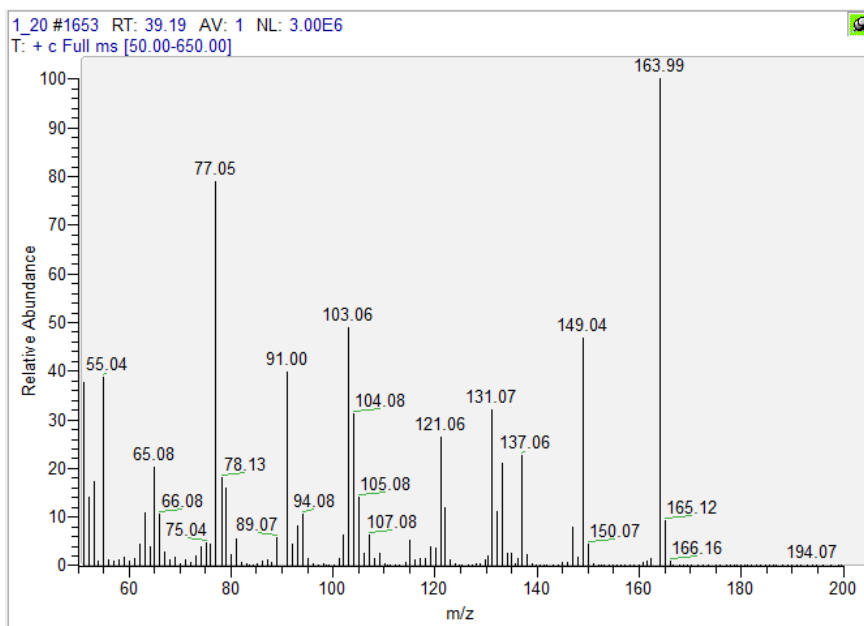
Sample 3072



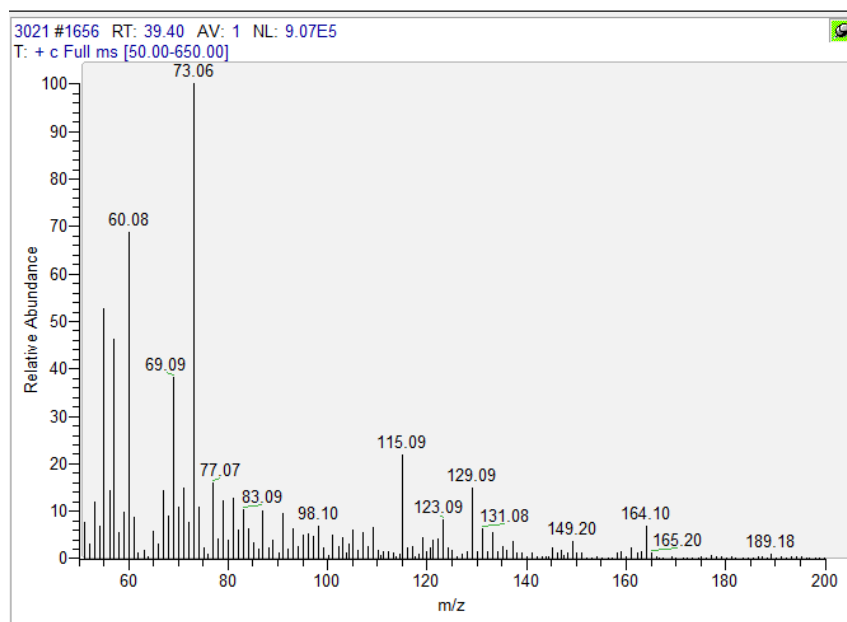
Sample 3070



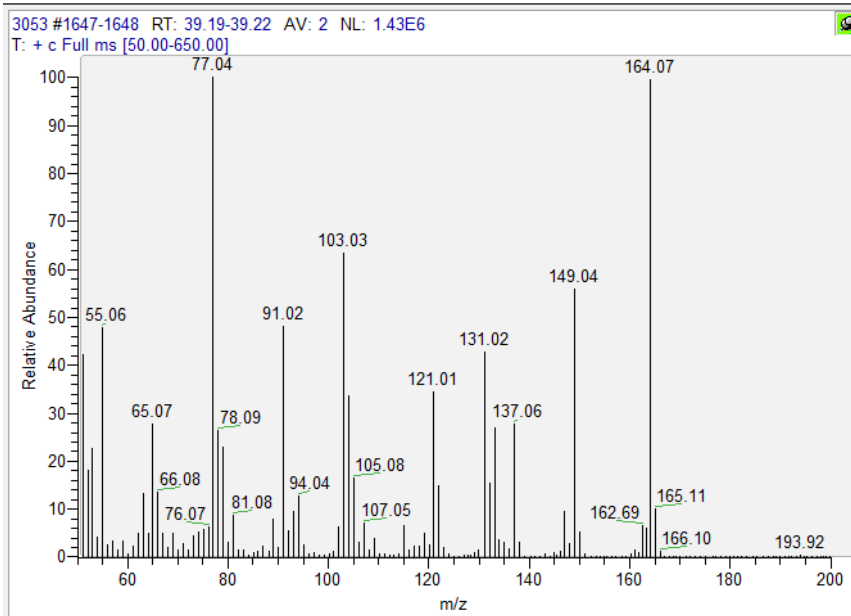
Reference of eugenol



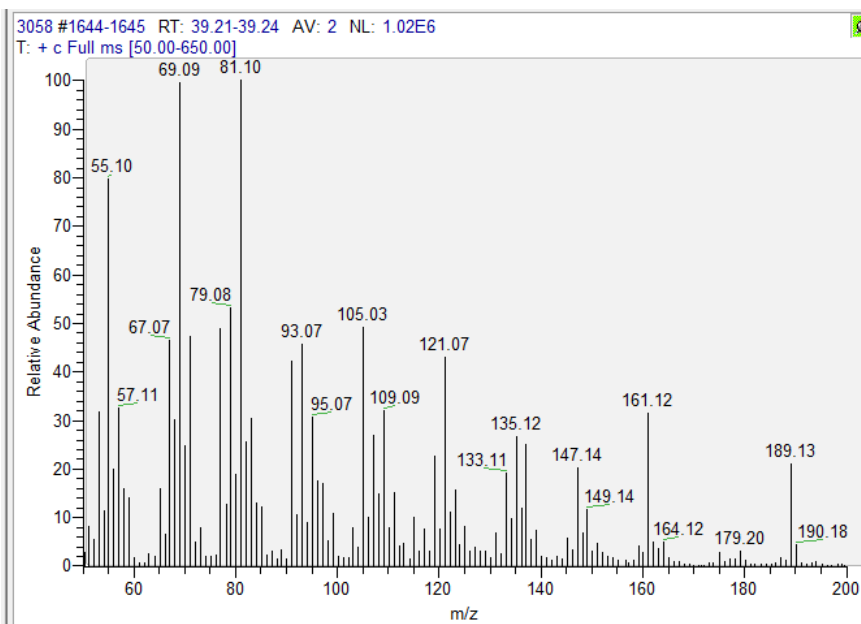
Sample 3021



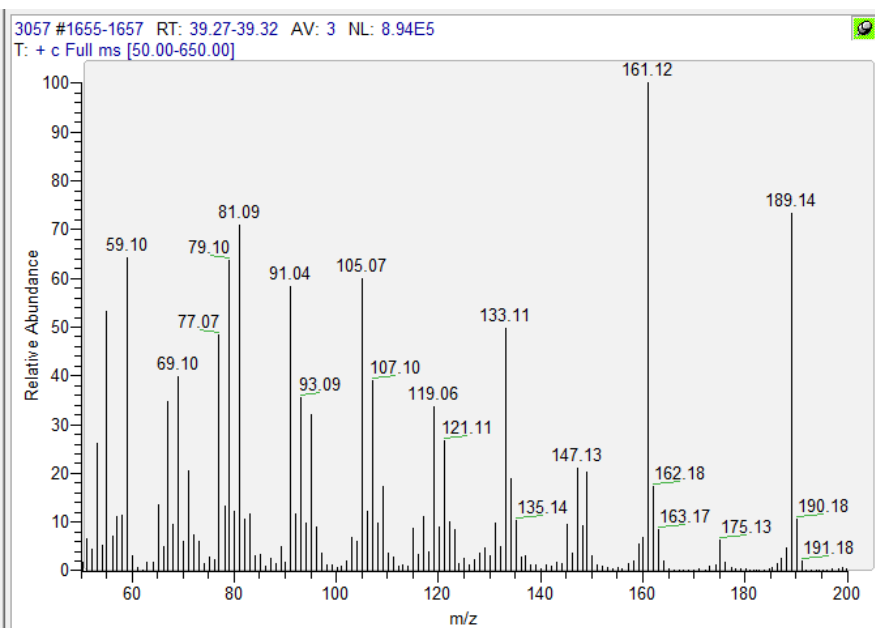
Sample 3053



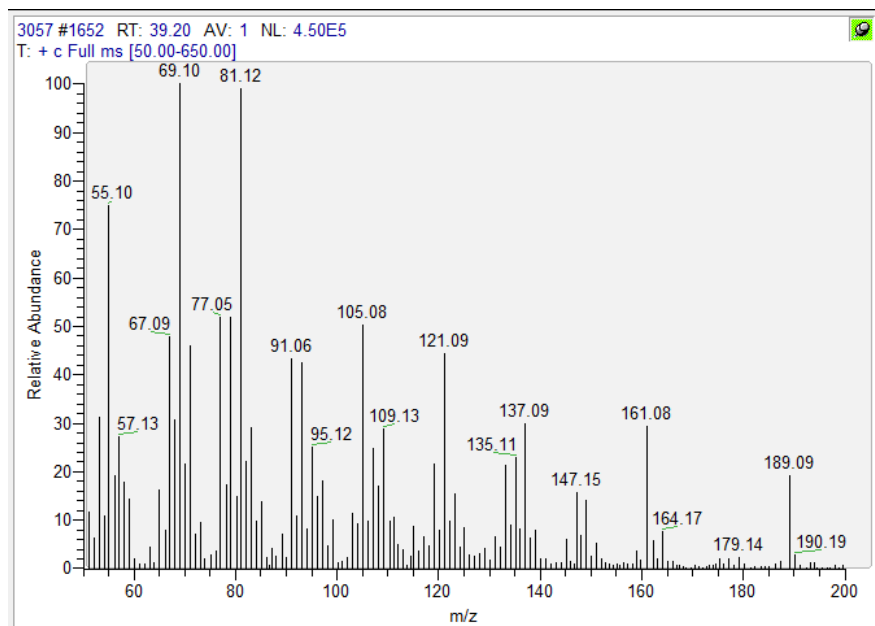
Sample 3058



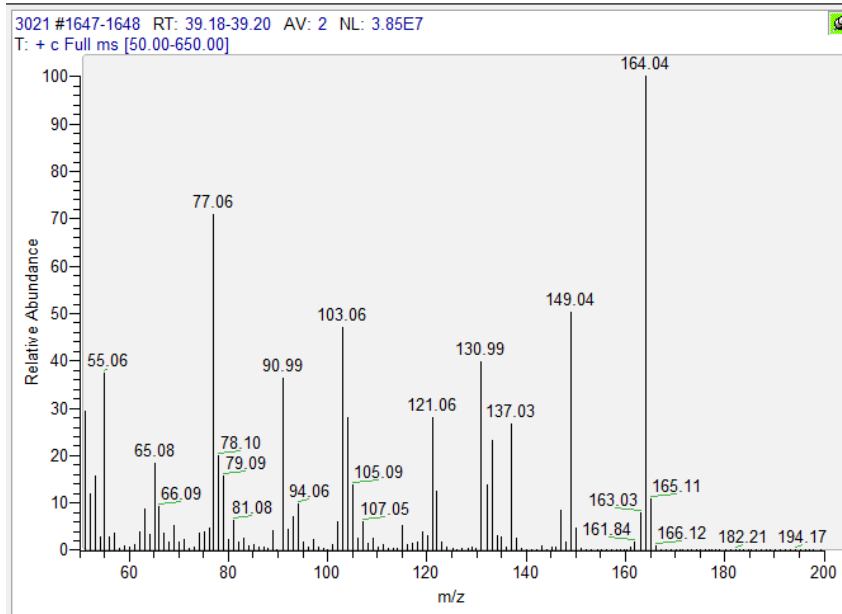
Sample 3057



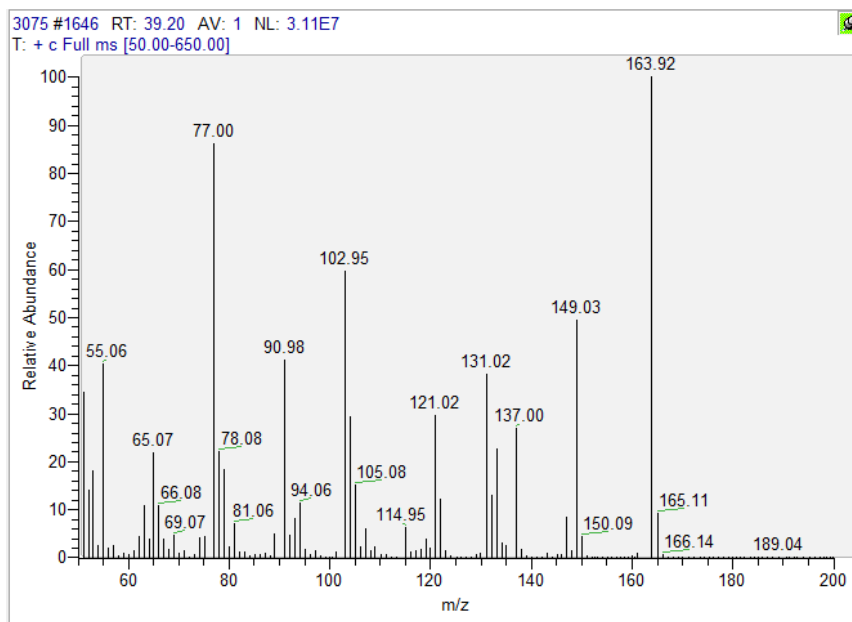
Sample 3057



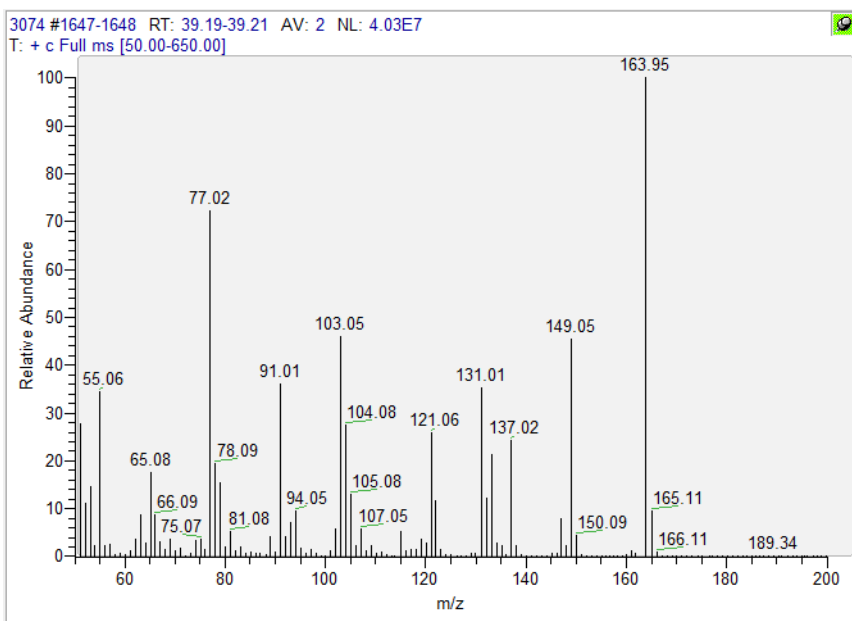
Sample 3021



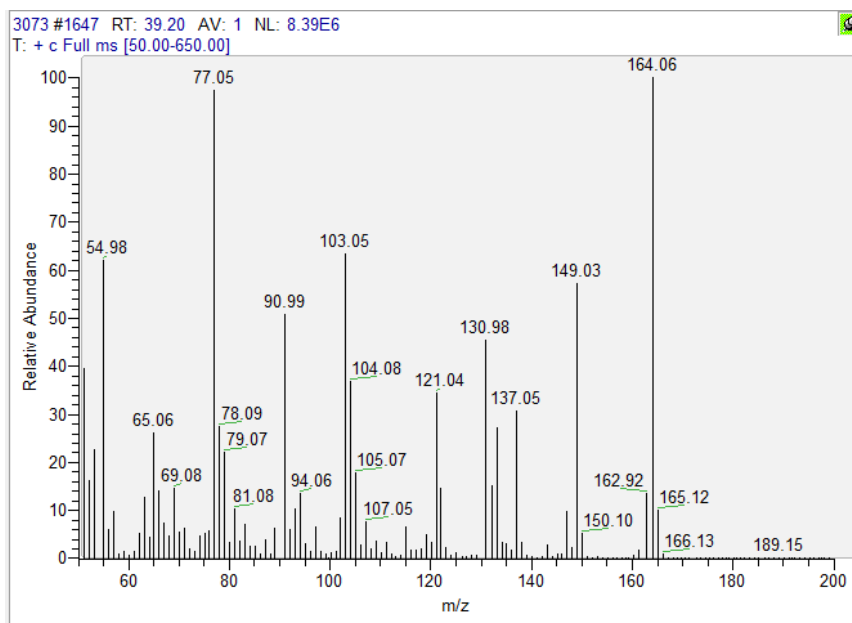
Sample 3075



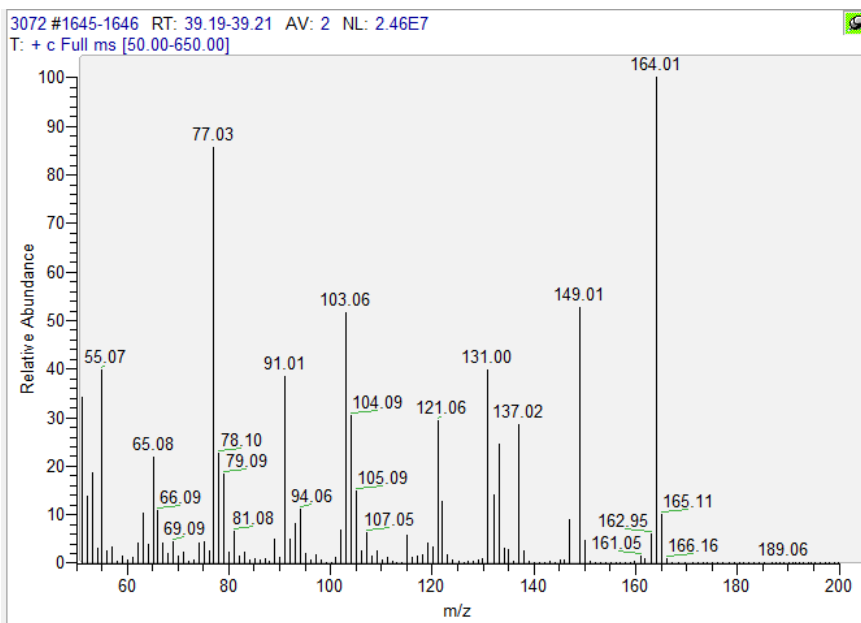
Sample 3074



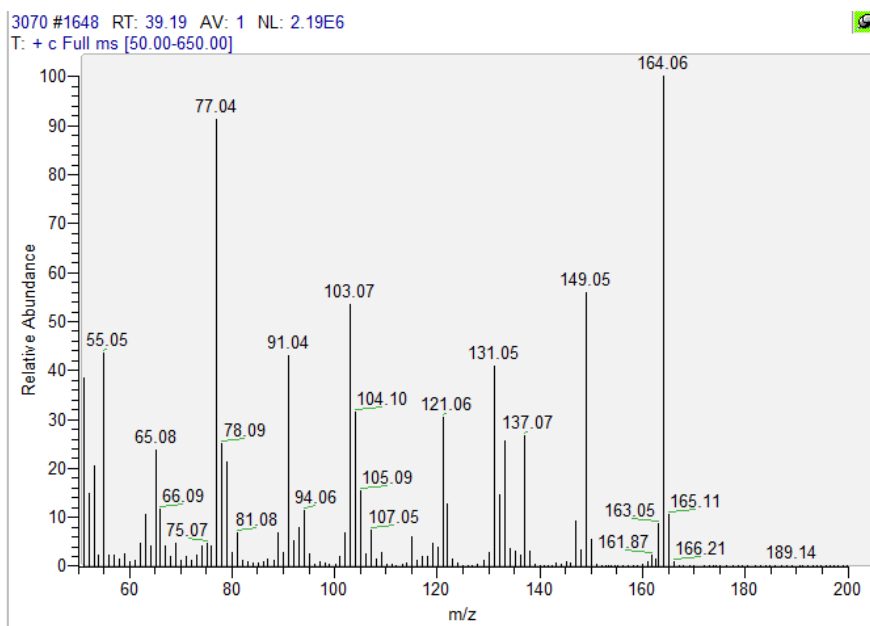
Sample 3073



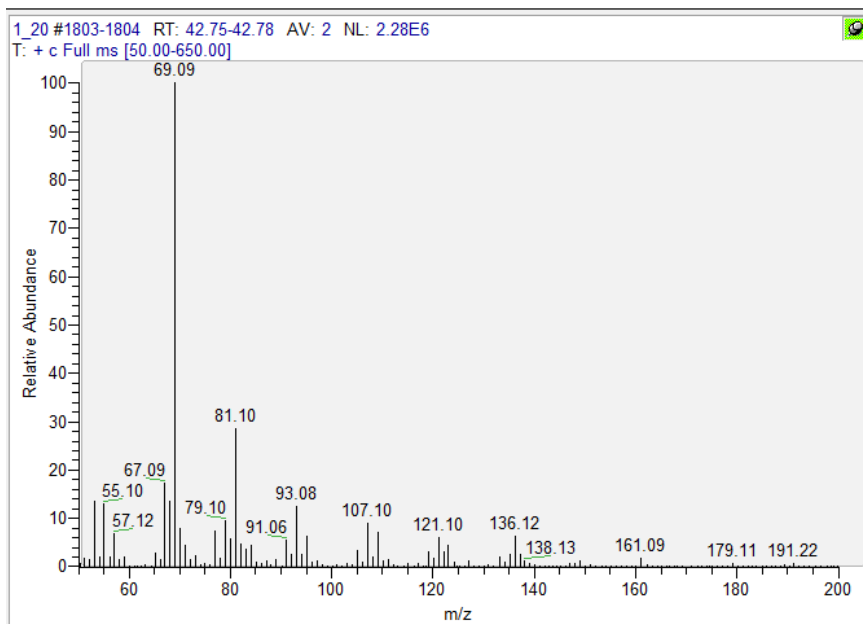
Sample 3072



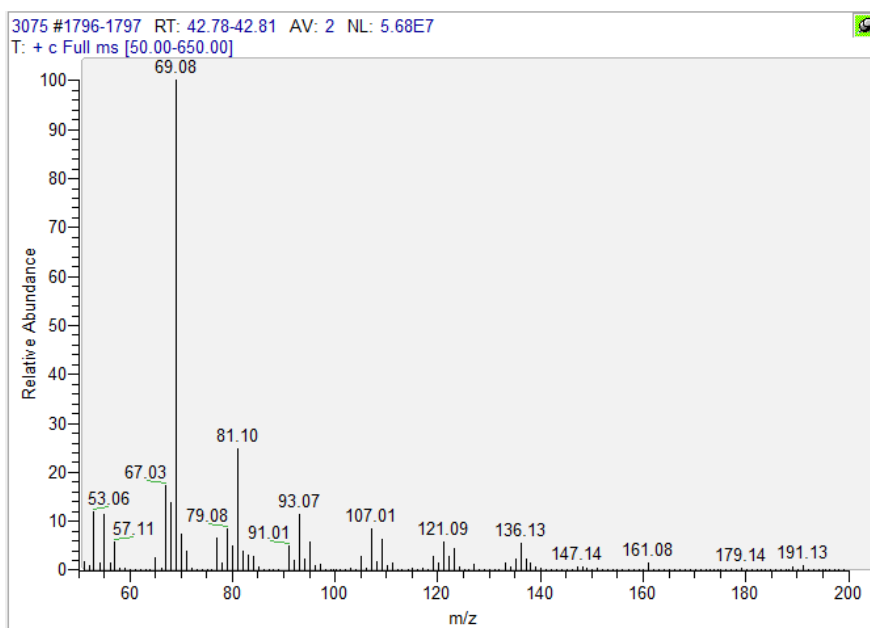
Sample 3070



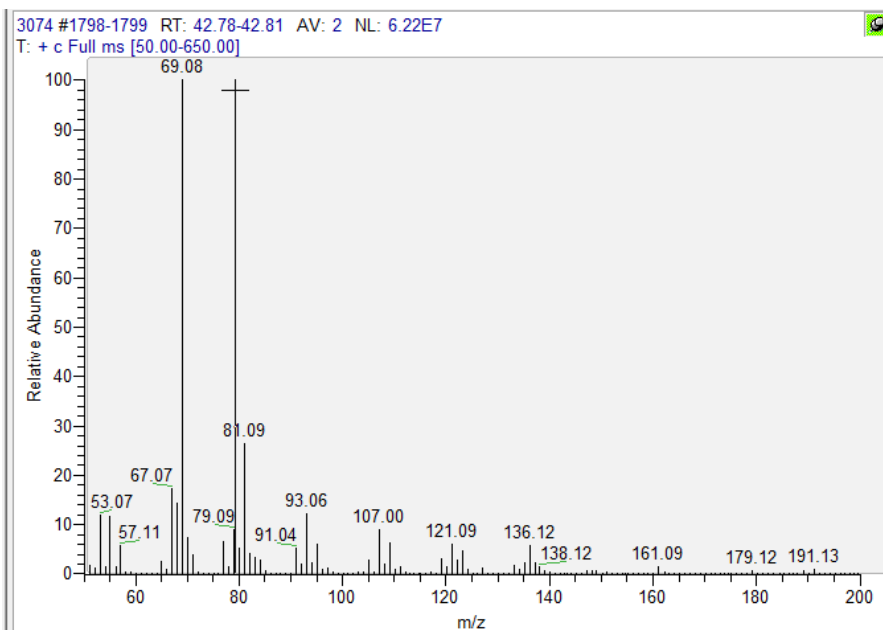
Reference of farnesol



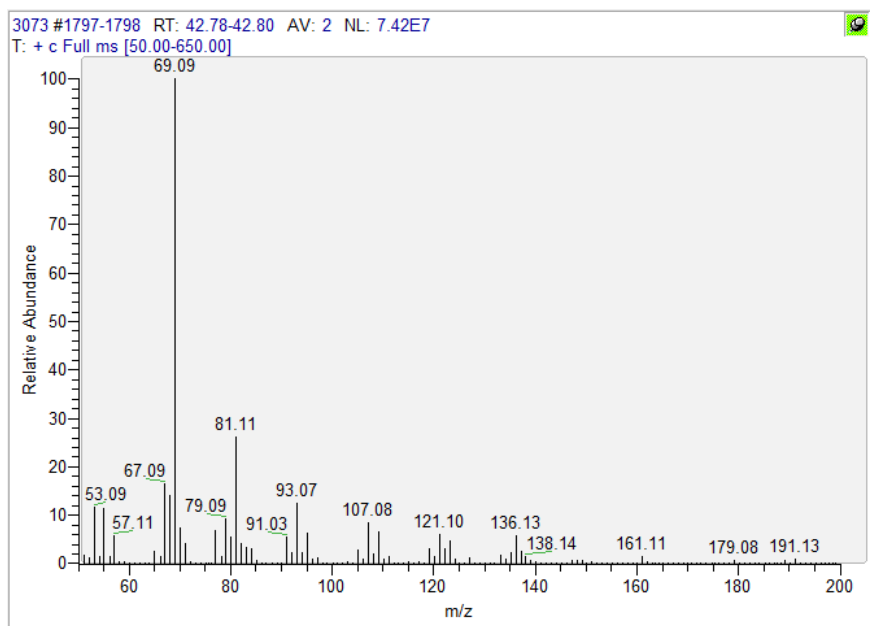
Sample 3075



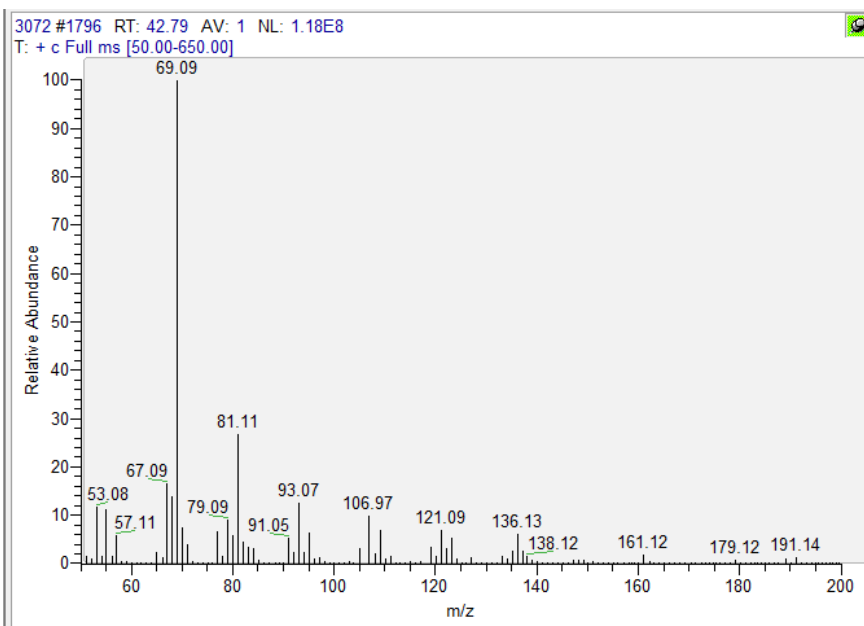
Sample 3074



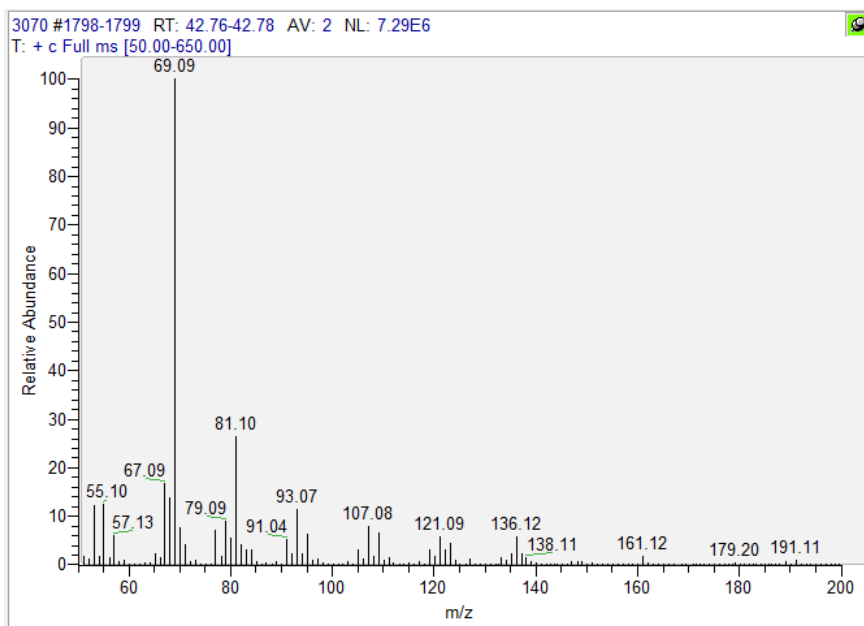
Sample 3073



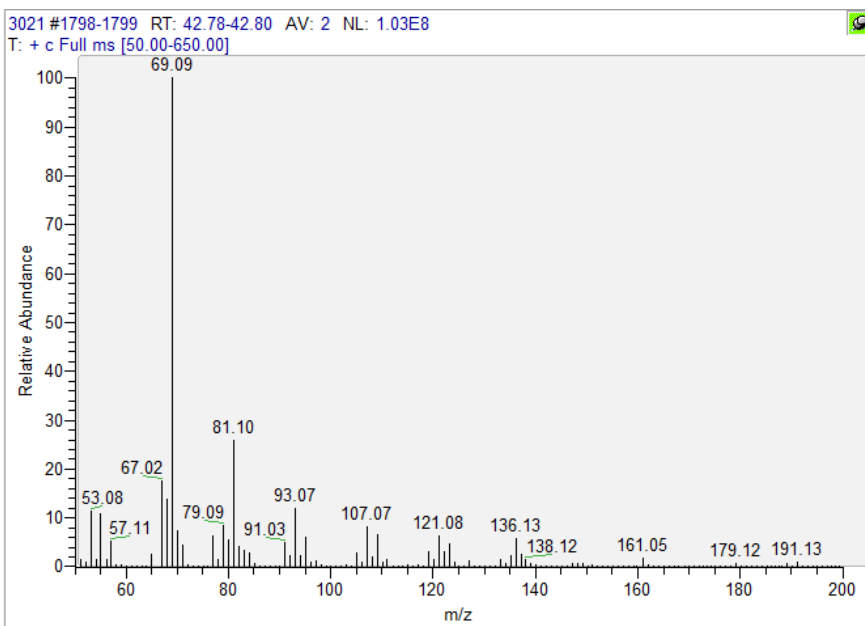
Sample 3072



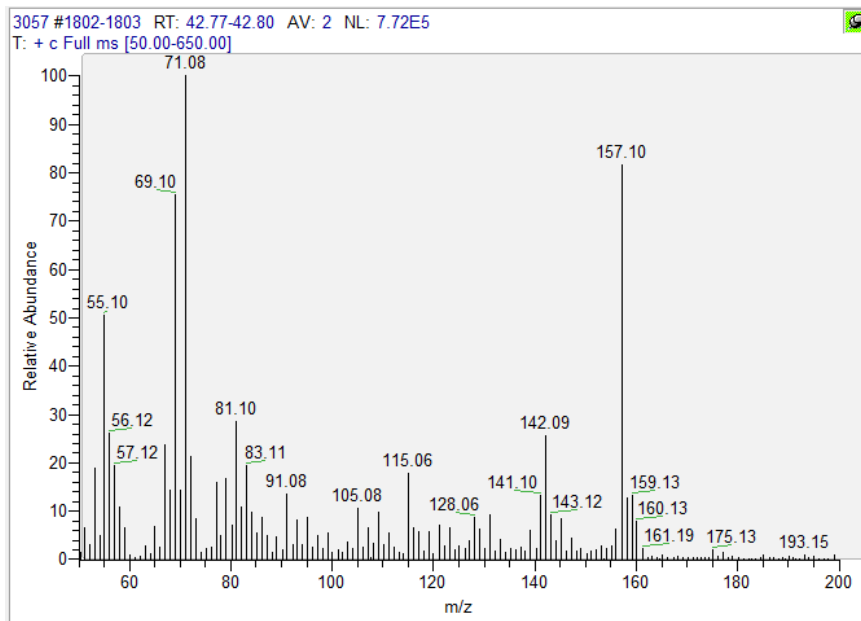
Sample 3070



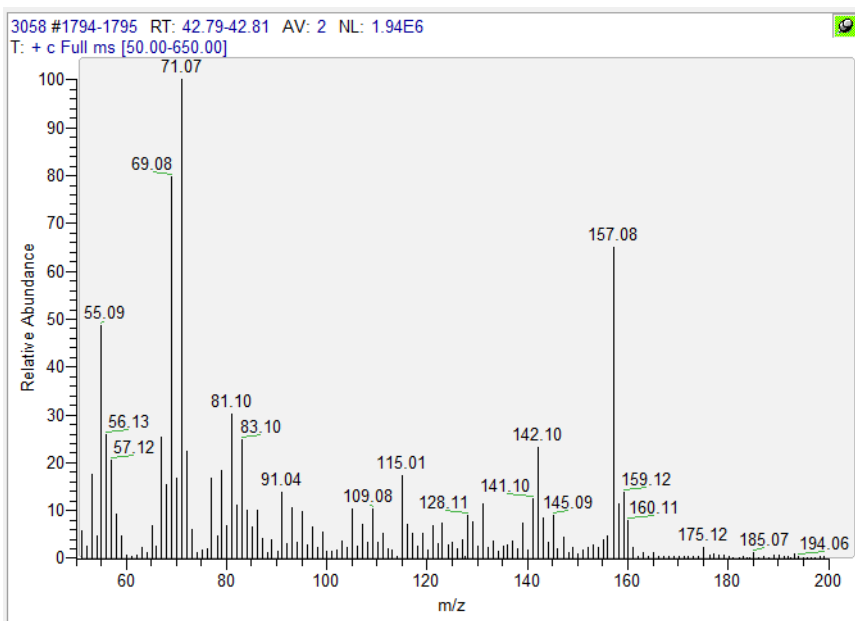
Sample 3021



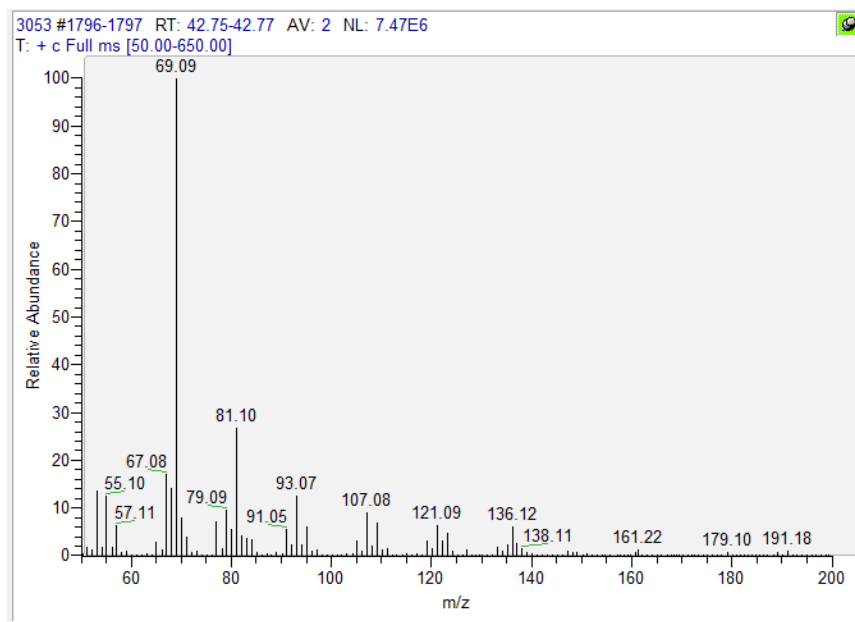
Sample 3057



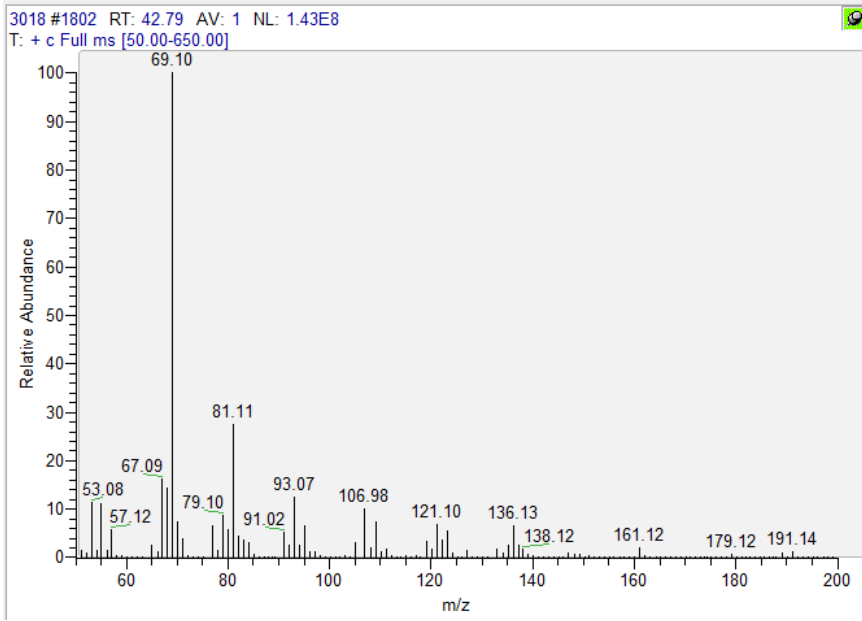
Sample 3058



Sample 3053



Sample 3018



2.2. Simultaneous Quantification of Terpenes and Cannabinoids by Reversed-Phase LC-APCI-MS/MS in *Cannabis sativa* L. Samples Combined with a Subsequent Chemometric Analysis

Some of the data presented here was published in the following publication:

Raeber J, Poetzsch M, Schmidli, Favrod S, Steuer C. Simultaneous quantification of terpenes and cannabinoids by reversed-phase LC-APCI-MS/MS in *Cannabis sativa* L. samples combined with a subsequent chemometric analysis. *Analytical and Bioanalytical Chemistry* 2024. DOI: 10.1007/s00216-024-05349-y

Table A7: Chemicals and reagents. Adapted from Raeber et al.⁷⁰

Chemical	Purity	Manufacturer	Origin
Sabinene	98%	abcr	Karlsruhe, Germany
citronellol	95%,	Acros Organics™, Thermo Fisher Scientific	Reinach, Switzerland
ammonium acetate	>99%	Fisher Chemicals	Loughborough, United Kingdom
methanol	Optima™, LC-MS grade	Fisher Chemicals	Loughborough, United Kingdom
menthone	purum	Fluka	Buchs, Switzerland
limonene	purum	Fluka	Buchs, Switzerland
propylparaben	purum	Fluka	Buchs, Switzerland
β-caryophyllene	NA	Frey + Lau	Henstedt-Ulzburg, Germany
THCA	1 mg/mL in isopropanol	Lipomed	Arlesheim, Switzerland
CBD	1 mg/mL in methanol	Lipomed	Arlesheim, Switzerland
CBDA	1 mg/mL in acetonitrile	Lipomed	Arlesheim, Switzerland
CBDV	1 mg/ml in ethanol	Lipomed	Arlesheim, Switzerland
CBG	1 mg/ml in ethanol	Lipomed	Arlesheim, Switzerland
Δ ⁸ -THC	1 mg/mL in methanol	Lipomed	Arlesheim, Switzerland
Δ ⁹ -THC-D3	0.1 mg/mL in ethanol	Lipomed	Arlesheim, Switzerland
Ethanol	Emsure®, ISO, Reag. Ph. Eur., absolute for analysis	Merck	Darmstadt, Germany
carvacrol	SAFC®, ≥ 98%	Merck	Darmstadt, Germany
isobornyl acetate	SAFC®, ≥90	Merck	Darmstadt, Germany
myrcene	Sigma, analytical standard	Merck	Darmstadt, Germany
linalool	Sigma, 97%	Merck	Darmstadt, Germany
geranyl acetate	Sigma, analytical standard	Merck	Darmstadt, Germany
THC	Supelco, Cerilliant®, 1 mg/mL in methanol	Merck	Darmstadt, Germany
CBN	Supelco, Cerilliant®, 1 mg/mL in methanol	Merck	Darmstadt, Germany
Citral	>98%	TCI	Eschborn, Germany
α-humulene	>93%	TCI	Eschborn, Germany
formic acid	99-100%, Ph. Eur.	VWR	Dietikon, Switzerland
water	Purified, 18.2 MΩ	ELGA Labwater, PURELAB flex 3	in-house

Script A2: MATLAB code for PCA and visualisation of the biplot.

```
% Step 1: Import dataframe with observations in each row and variables
% in each column

df = readmatrix("data.xlsx");

variable_names = readcell("variableNames.xlsx");
variable_names = variable_names(2:16);

sample_names = readcell("sampleLabel.xlsx");
sample_names = sample_names(2:end, 1);

% Step 2: Pre-processing of data and PCA analysis

% Mean Centering and autoscaling
mean_centered_data = bsxfun(@minus, df, mean(df));
auto_scaled_data = bsxfun(@rdivide, mean_centered_data, std(df));

% PCA
[coeff, score, latent, tsquared, explained, mu] = pca(auto_scaled_data);

% Step 3: Extract loadings
loadings = coeff(:,1:2); % Adjust based on how many components you want to
visualize

% Step 4: Plot loadings
biplot(loadings, 'Scores', score(:,1:2), 'VarLabels', variable_names,
'MarkerSize', 15);
title('PCA Loading Plot');
xlabel('PC1 ('' %)\');
ylabel('PC2 ('' %)\');
```

Script A3: Python code for the generation of the 3D MRM plot.

```
import os
import numpy as np
import matplotlib.pyplot as plt
from matplotlib.colors import ListedColormap
from matplotlib.lines import Line2D

# Directory containing your .txt files
data_dir = 'Include Directory that contains your files - files should be in
the txt format'

# Initialize empty lists to store data
data = []

# Initialize a list to store the legend labels in the order of appearance
legend_labels = []

# Initialize a list to store the legend handles with correct colors
legend_handles = []

# Loop through .txt files in the directory
for filename in os.listdir(data_dir):
    if filename.endswith('.txt'):
        filepath = os.path.join(data_dir, filename)
        name = os.path.splitext(filename)[0] # Extract the name from the
filename
        retention_times, intensities = [], []
        with open(filepath, 'r') as file:
            # Skip lines until the header is found
            for line in file:
                if line.startswith("Time"):
                    break
            # Read data after the header
            for line in file:
                time, intensity = map(float, line.strip().split())
                retention_times.append(time)
                intensities.append(intensity)

        # Determine the retention time corresponding to the maximum intensity
(peaks)
        max_intensity_index = np.argmax(intensities)
        max_intensity_time = retention_times[max_intensity_index]

        # Define a time range (+/- 1 second) around the peak
        min_time = max_intensity_time - 1.5
        max_time = max_intensity_time + 1.5
```

```

        # Filter data to include only the specified time range
        filtered_retention_times = [t for t in retention_times if min_time <=
t <= max_time]
        filtered_intensities = [i for i, t in zip(intensities,
retention_times) if min_time <= t <= max_time]

        max_intensity = max(filtered_intensities)
        filtered_intensities = [(i / max_intensity) * 100 for i in
filtered_intensities] # Convert to percentage

        data.append((name, filtered_retention_times, filtered_intensities))
        legend_labels.append(name) # Add the legend label in order of
appearance

# Sort the data based on the earliest retention time
data.sort(key=lambda x: min(x[1]))

# Create a color map for differentiating files
colors = plt.cm.tab20.colors
cmap = ListedColormap(colors[:len(data)])

# Create a larger 3D plot
fig = plt.figure(figsize=(15, 10))
ax = fig.add_subplot(111, projection='3d')

for i, (name, retention_times, intensities) in enumerate(data[:-3]):
    ax.plot(retention_times, [i] * len(retention_times), intensities,
label=name, color=cmap(i))
    legend_handles.append(Line2D([0], [0], color=cmap(i), label=name)) #
Create legend handles

# Assign different colors to the last three chromatograms
last_three_chromatograms = data[-3:]
last_three_colors = ['purple', 'brown', 'olive']

for i, (name, retention_times, intensities) in
enumerate(last_three_chromatograms):
    ax.plot(retention_times, [i + len(data) - 3] * len(retention_times),
intensities, label=name, color=last_three_colors[i])
    legend_handles.append(Line2D([0], [0], color=last_three_colors[i],
label=name)) # Create legend handles

# Set axis labels and title
ax.set_xlabel('Retention Time [min]')
ax.set_zlabel('Relative Intensity [%]')
plt.title('Chromatogram')

```



```
# Show legend on the far right, ordered by appearance
ax.legend(handles=legend_handles, loc=3, bbox_to_anchor=(1, 1))

# Adjust layout
plt.tight_layout()

# Show the plot
plt.show()
```

Script A4: Python code for the 2D plotting of the TIC.

```
import matplotlib.pyplot as plt
import seaborn as sns

# Set a colorblind-friendly color palette from Seaborn
palette = sns.color_palette("colorblind")

# Specify the path to your chromatogram file
chromatogram_file = "Add your Directory with the filename. Should be .txt"

# Initialize lists to store time and intensity data
time = []
intensity = []

# Read the data from the file, skipping the header line
with open(chromatogram_file, "r") as file:
    lines = file.readlines()
    for line in lines[1:]: # Skip the first line (header)
        data = line.strip().split()
        time.append(float(data[0]))
        intensity.append(float(data[1]))

# Create the chromatogram plot
plt.figure(figsize=(10, 6)) # Set the figure size

# Plot the chromatogram with a colorblind-friendly color
plt.plot(time, intensity, color=palette[0], label="TIC")

# Set axis labels and a title
plt.xlabel("Time [min]", fontsize =14)
plt.ylabel("Intensity [cps]", fontsize = 14)

plt.xticks(fontsize = 14)
plt.yticks(fontsize = 14)

# Show the legend
plt.legend()

# Show the plot
plt.grid(True)
plt.show()
```

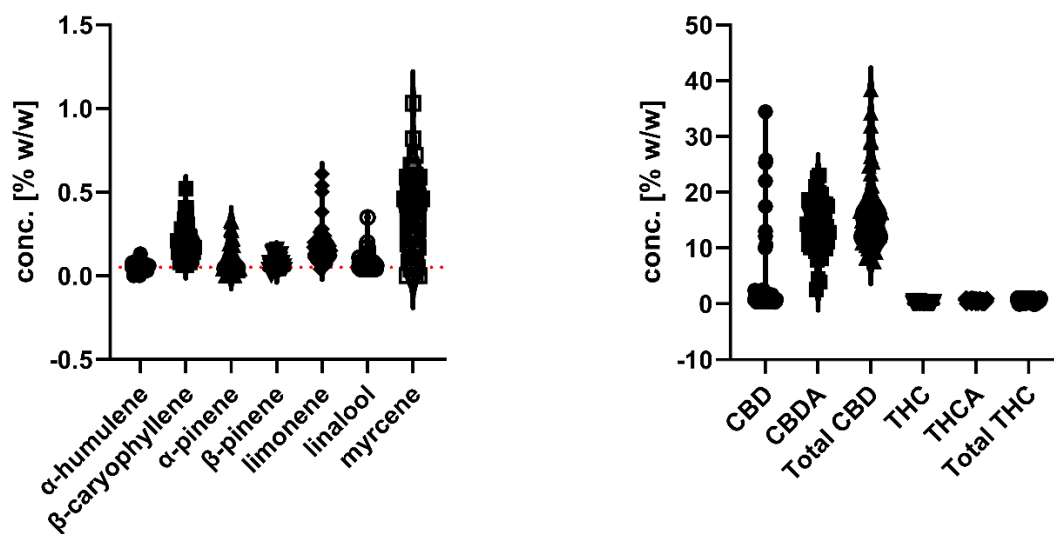


Figure A8: Violin plots with the individual samples for both the terpene as well as the major cannabinoid profile. Figure adapted from Raeber et al. ⁷⁰

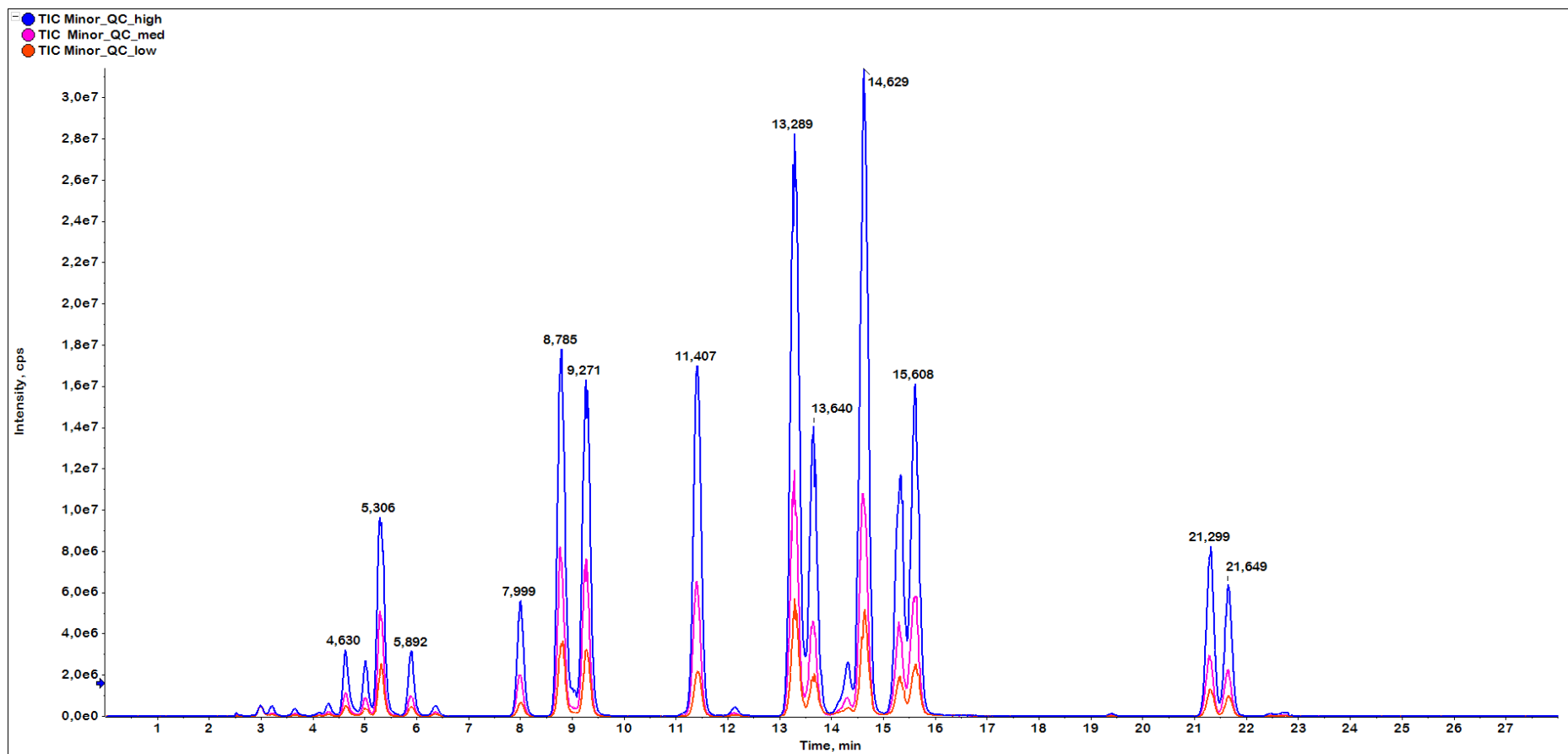


Figure A9: TIC overlay QC samples from the first validation day for the minor calibration range.

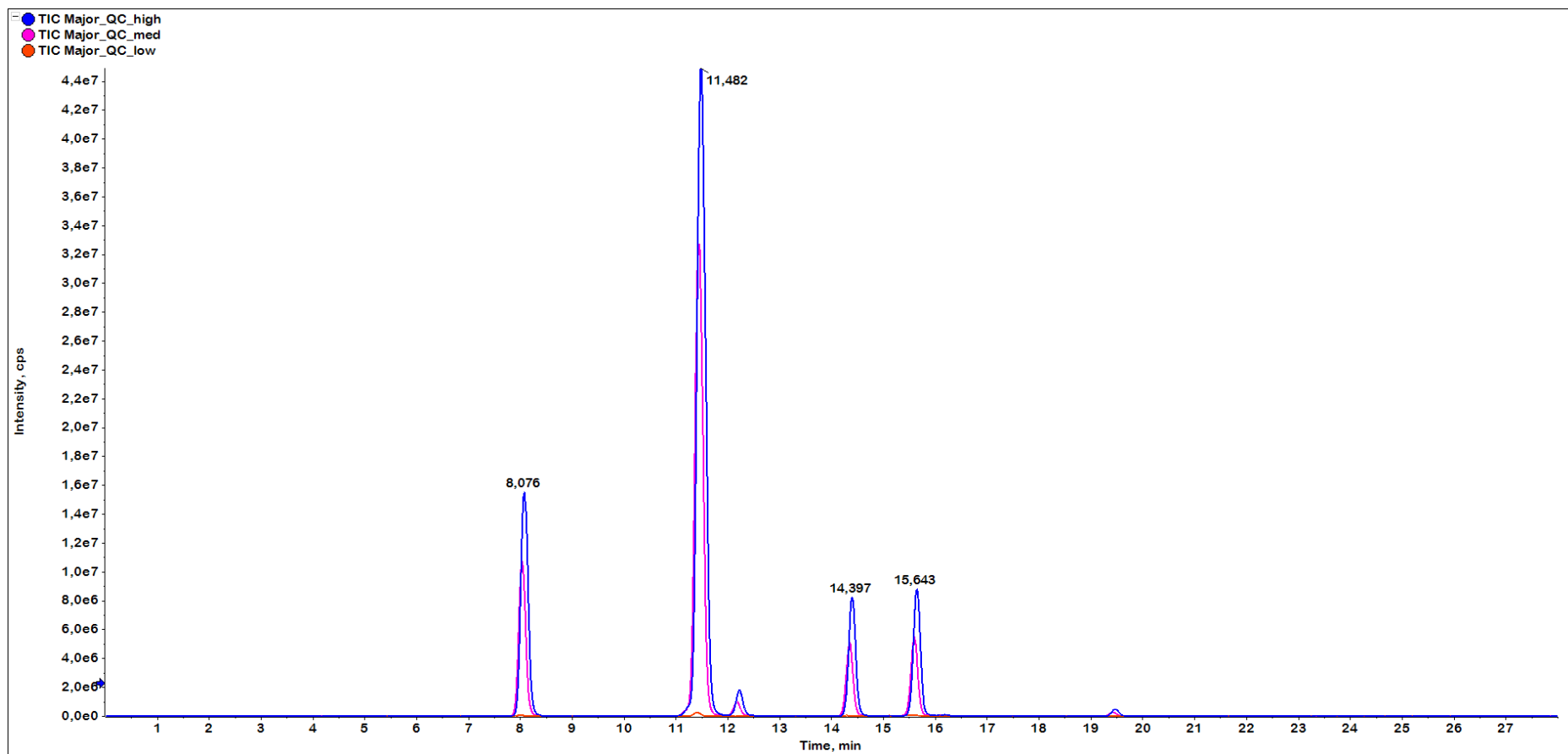
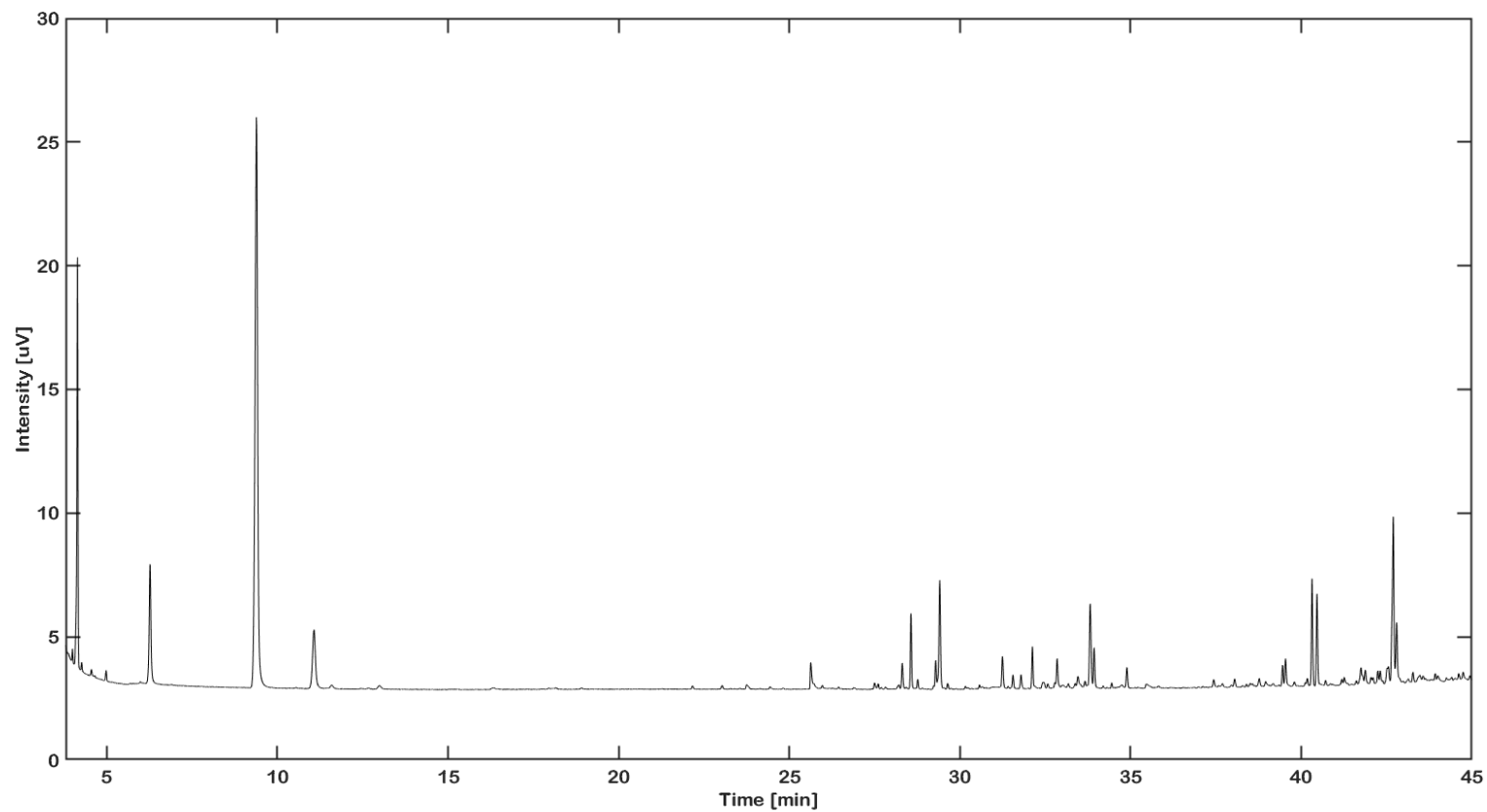


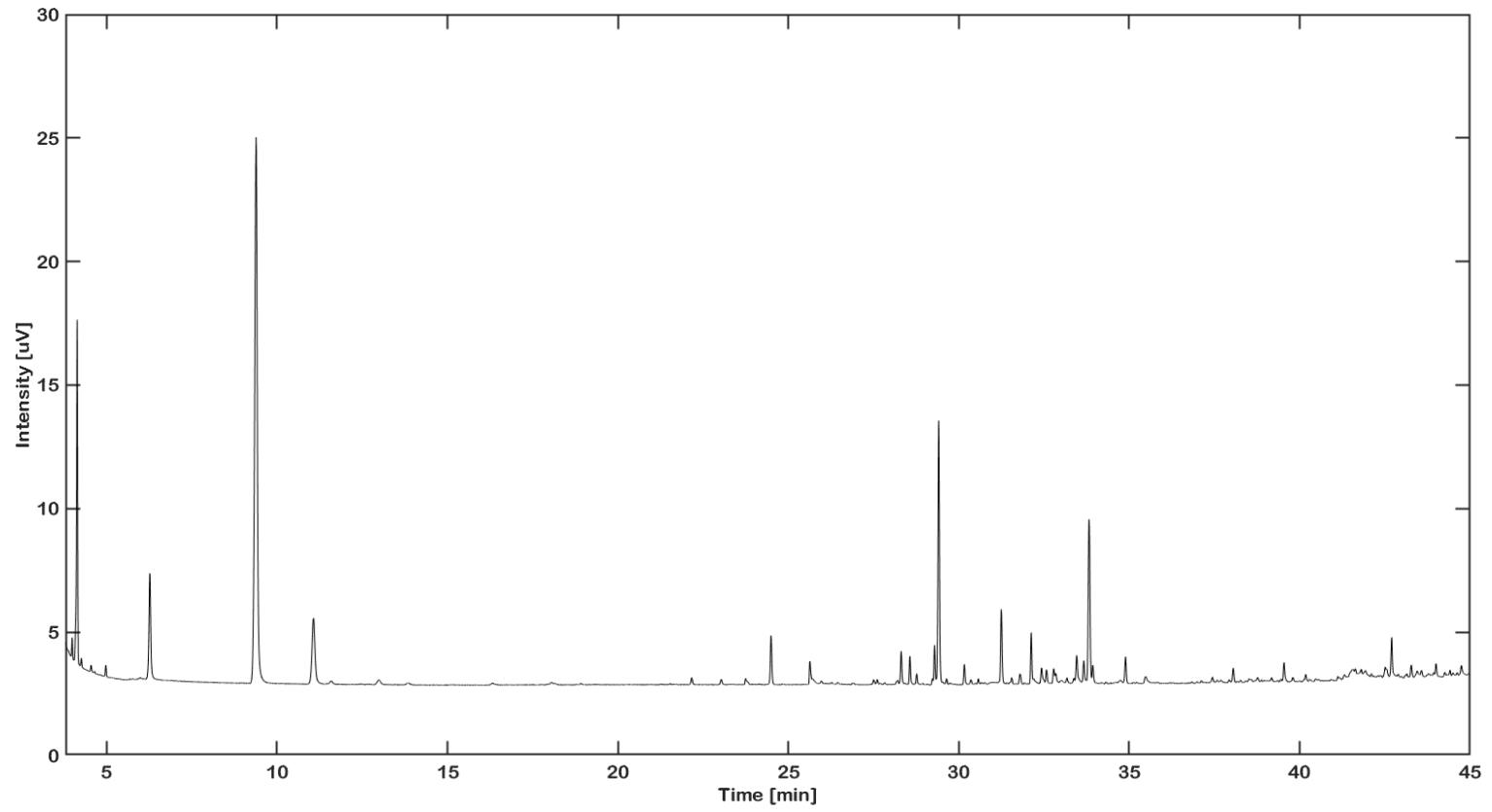
Figure A10: TIC overlay QC samples from the first validation day for the major calibration range.

Figure A11: GC-FID chromatograms acquired for method comparison to LC-APCI-MS/MS for 15 randomly selected samples.

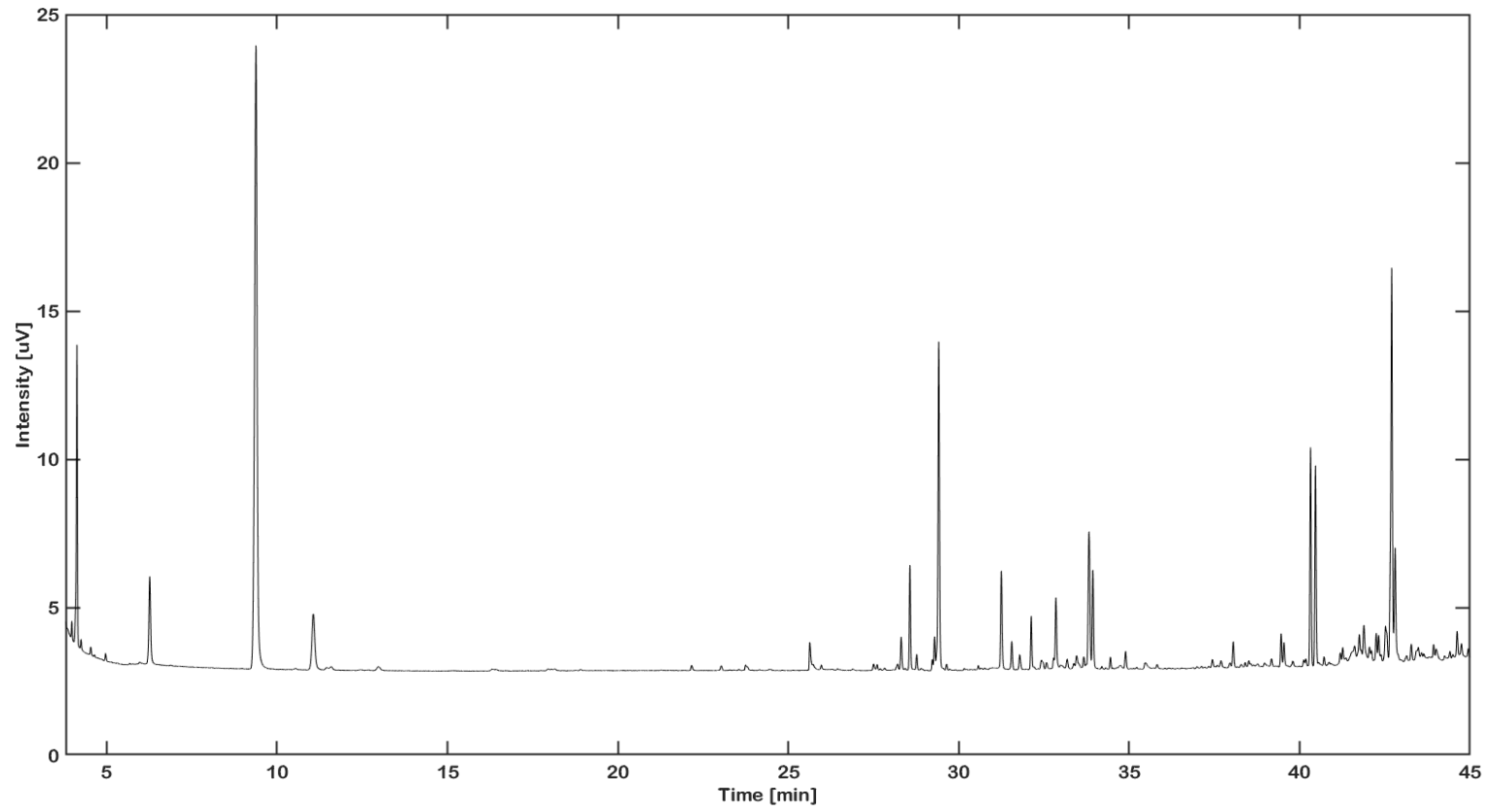
C. sativa L. sample 1



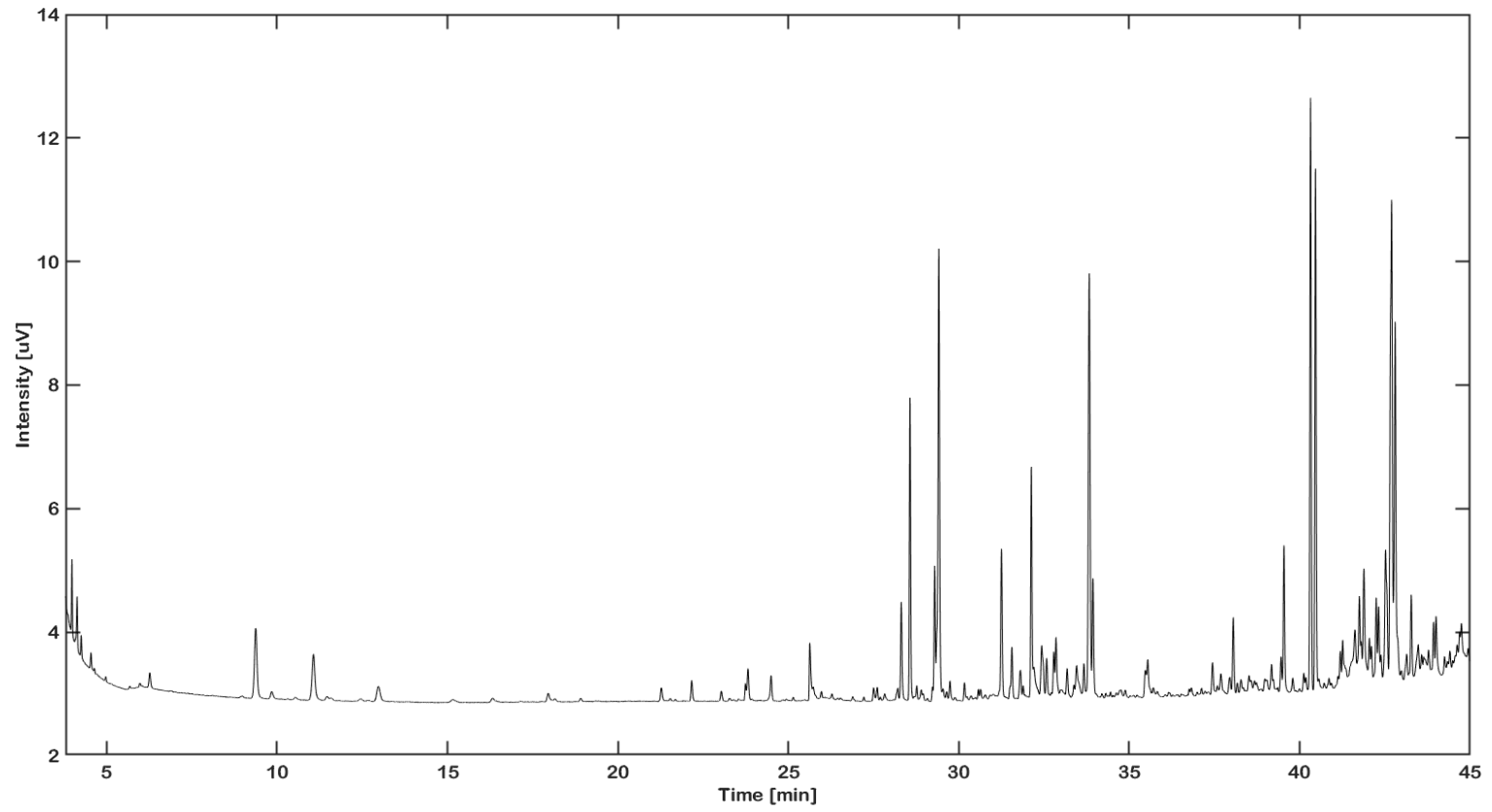
C. sativa L. sample 2



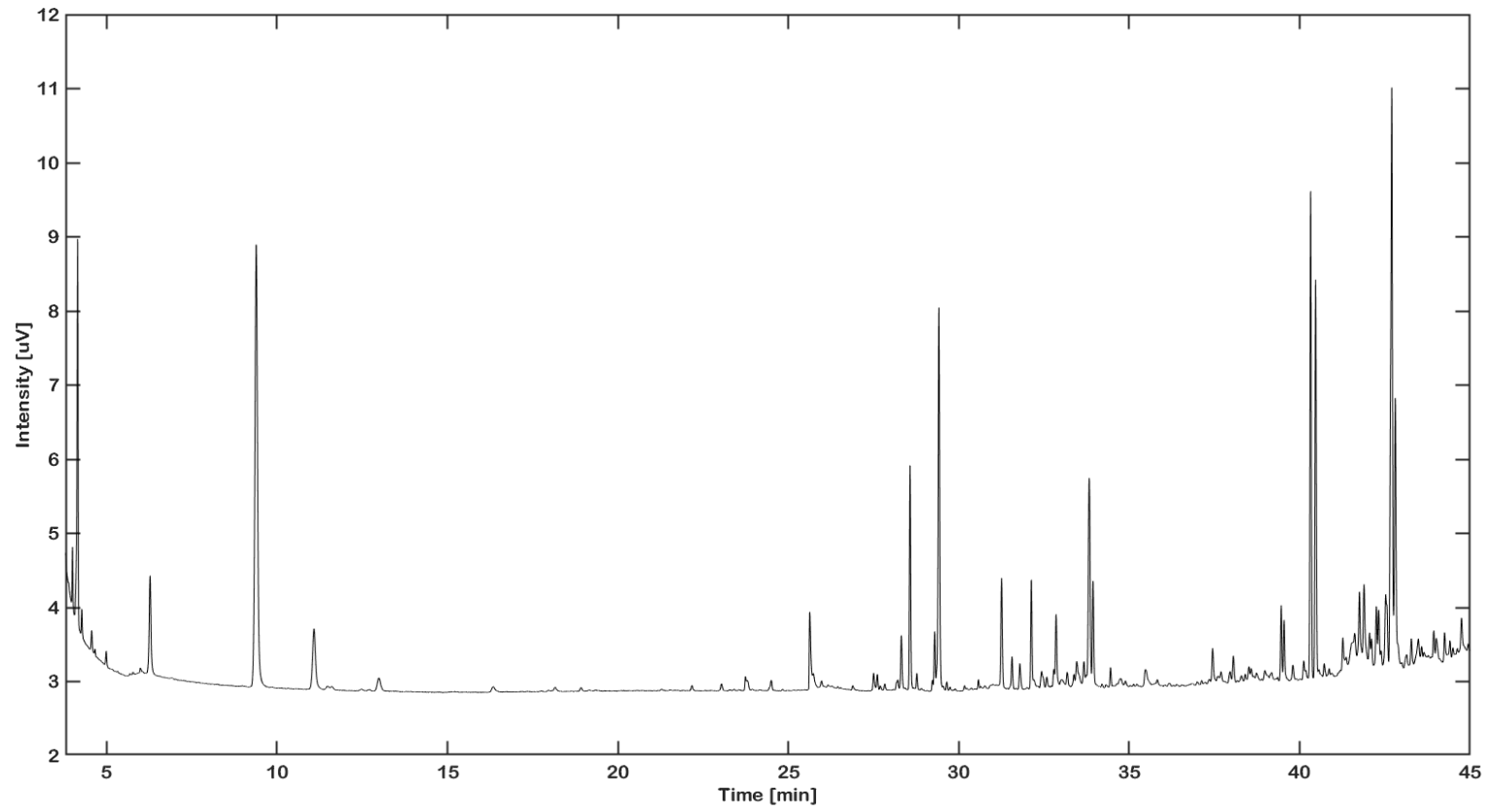
C. sativa L. sample 3



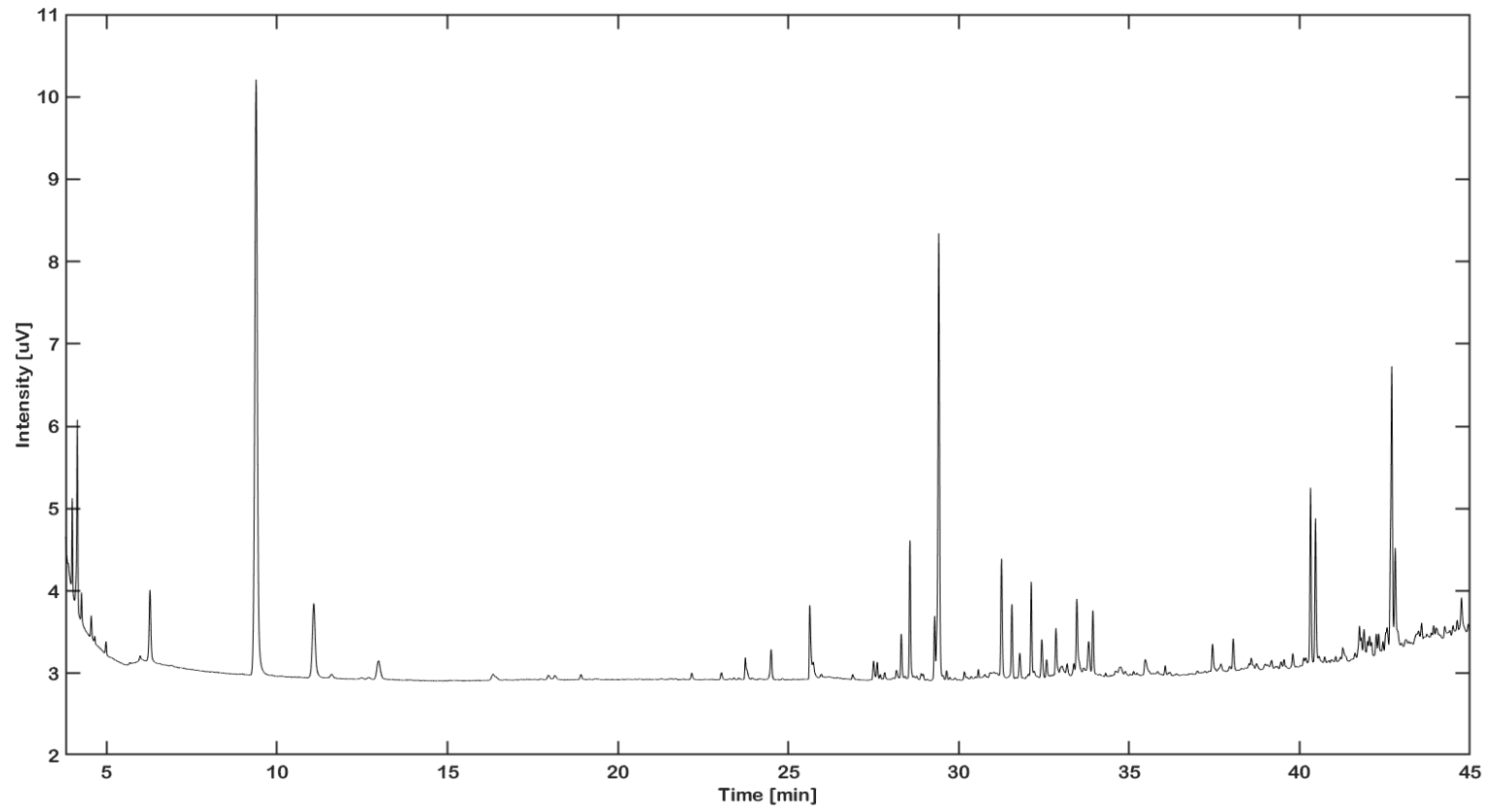
C. sativa L. sample 4



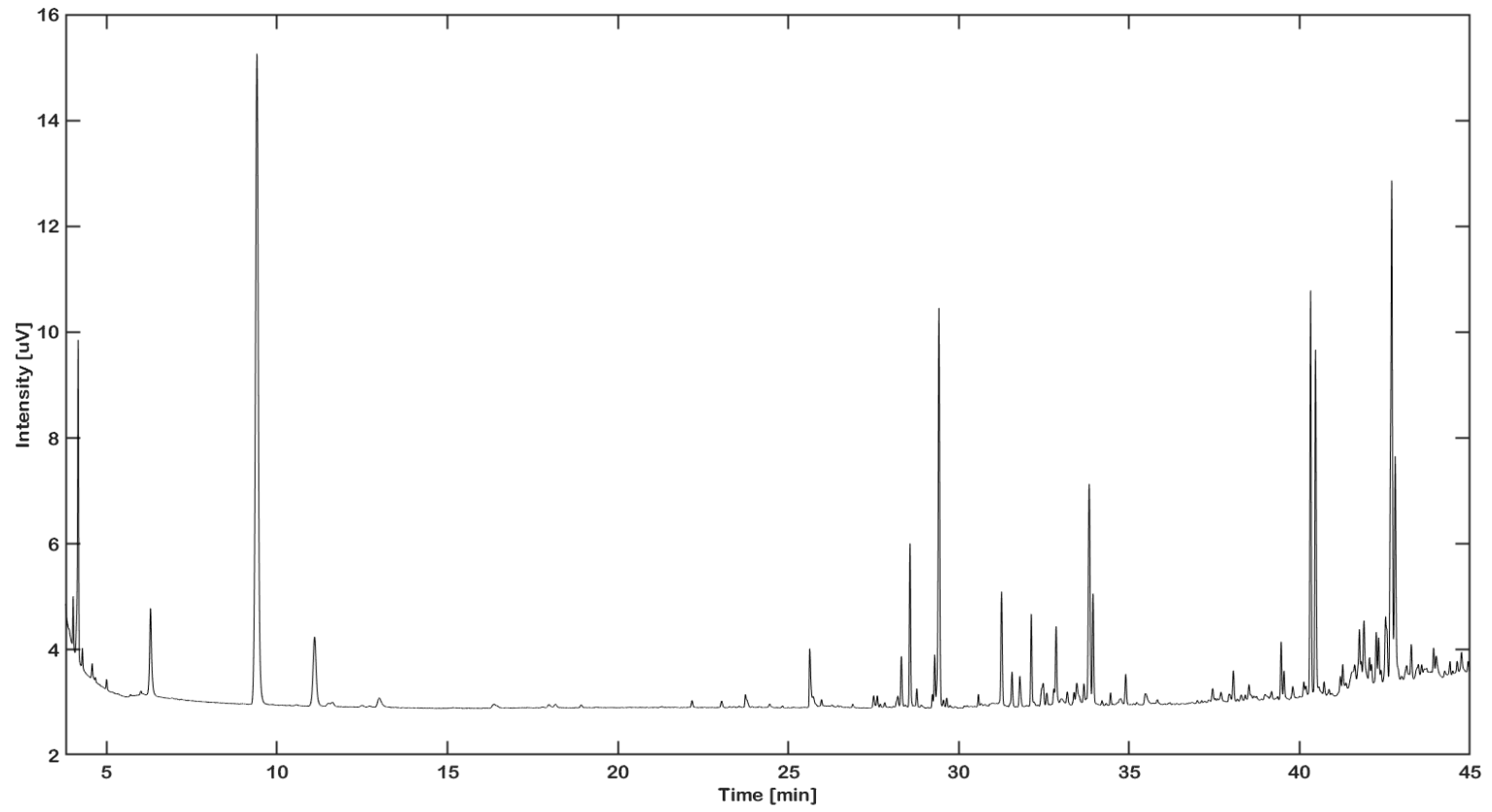
C. sativa L. sample 5



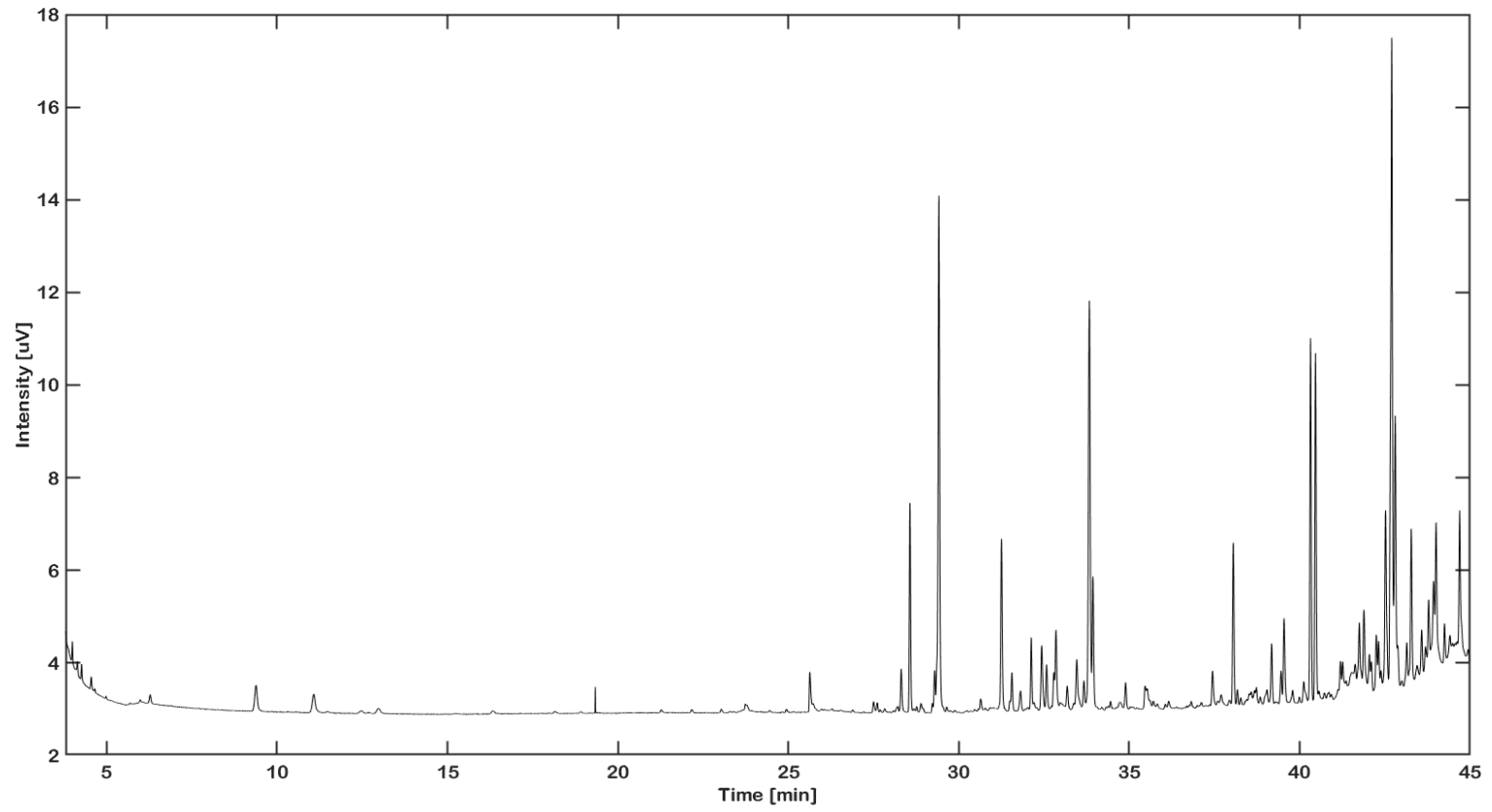
C. sativa L. sample 6



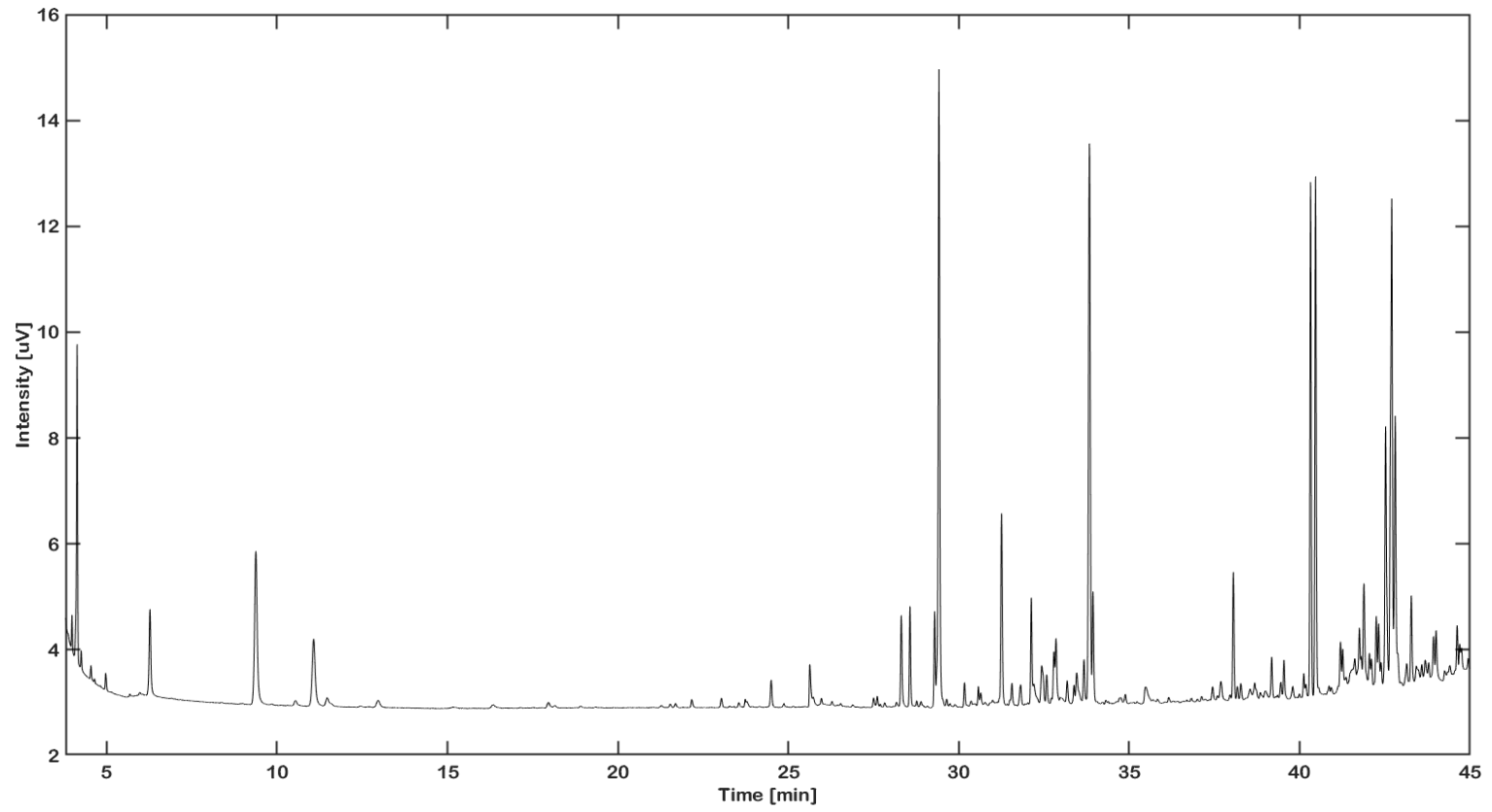
C. sativa L. sample 7



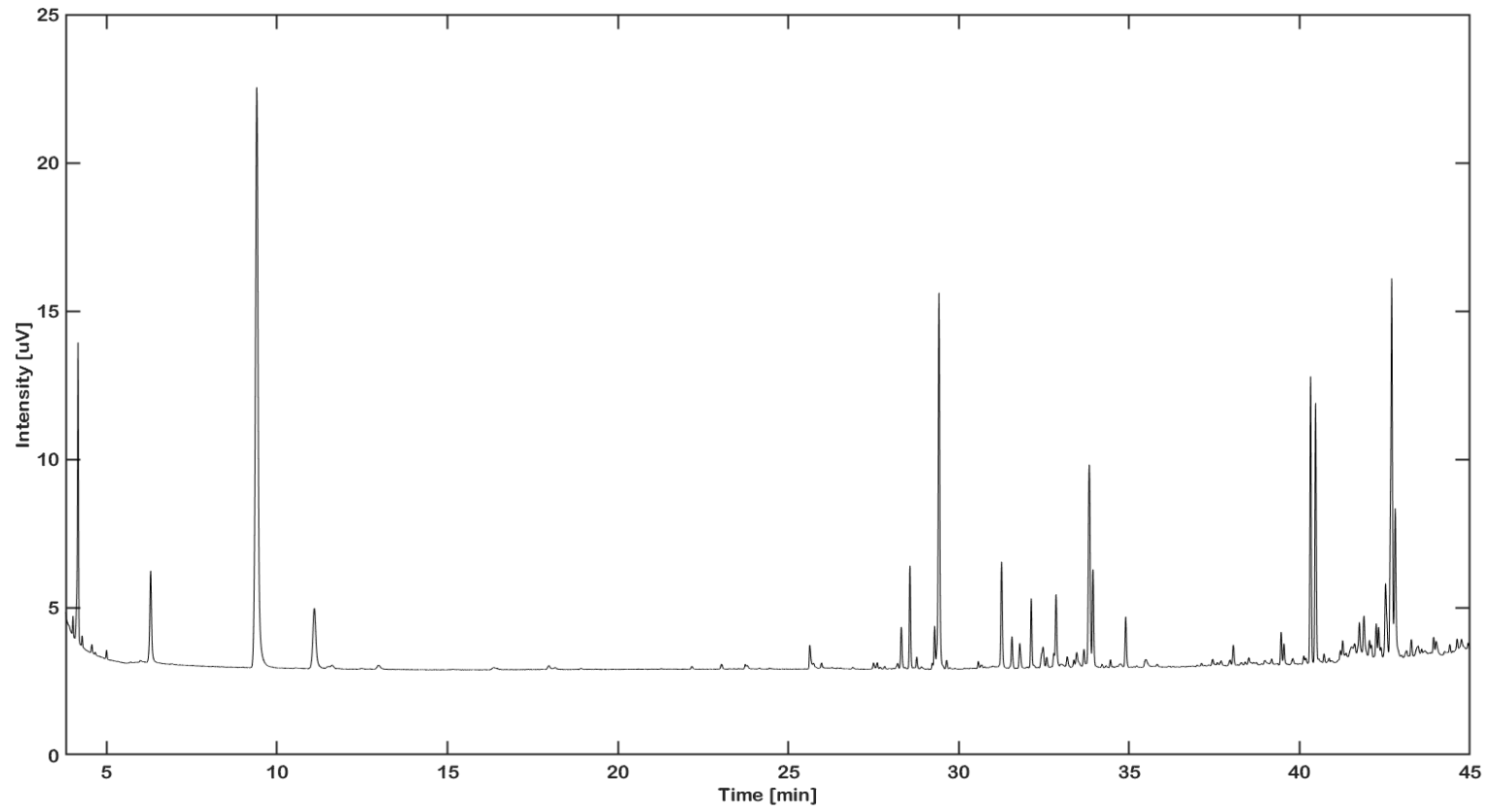
C. sativa L. sample 8



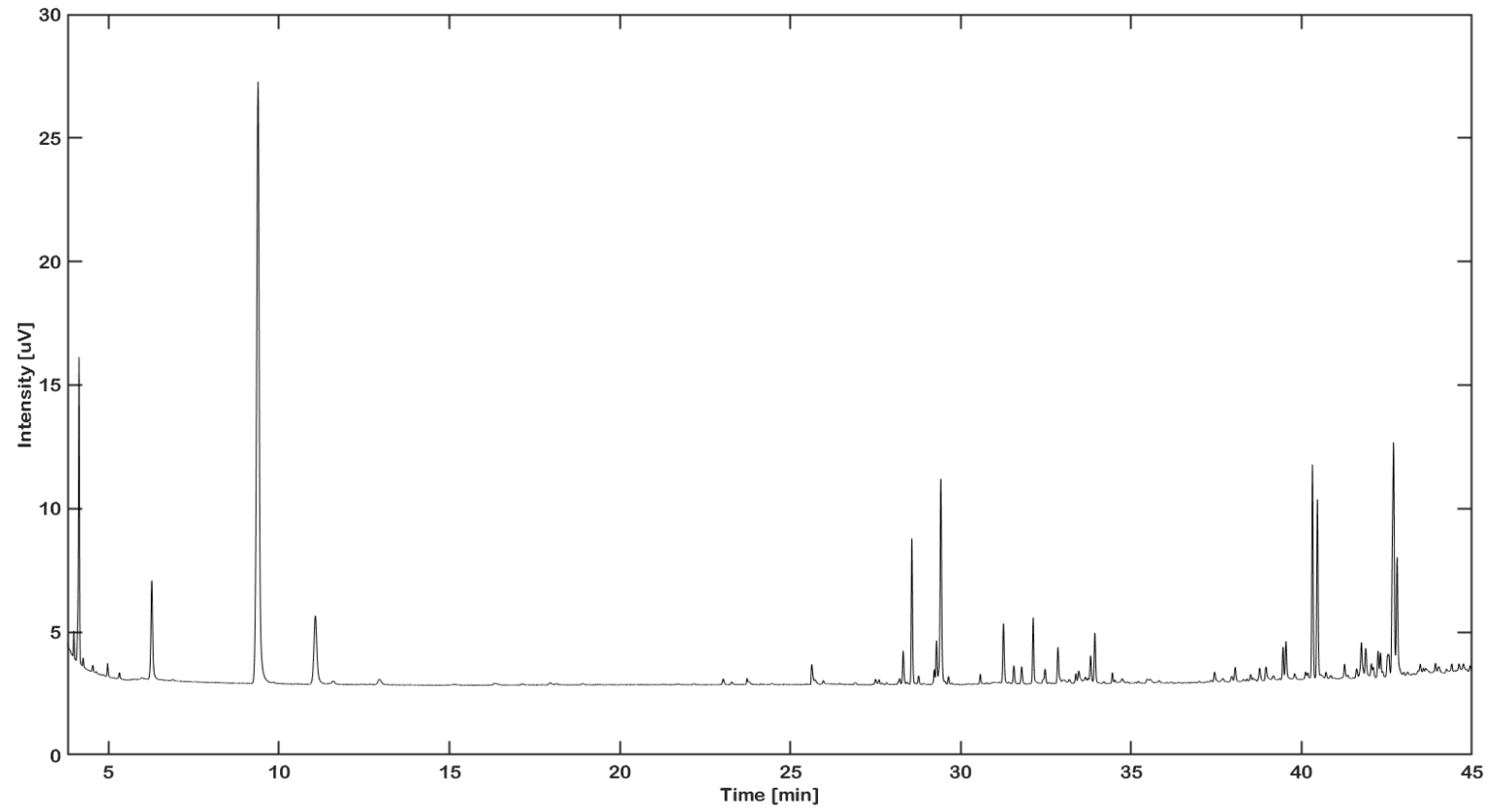
C. sativa L. sample 9



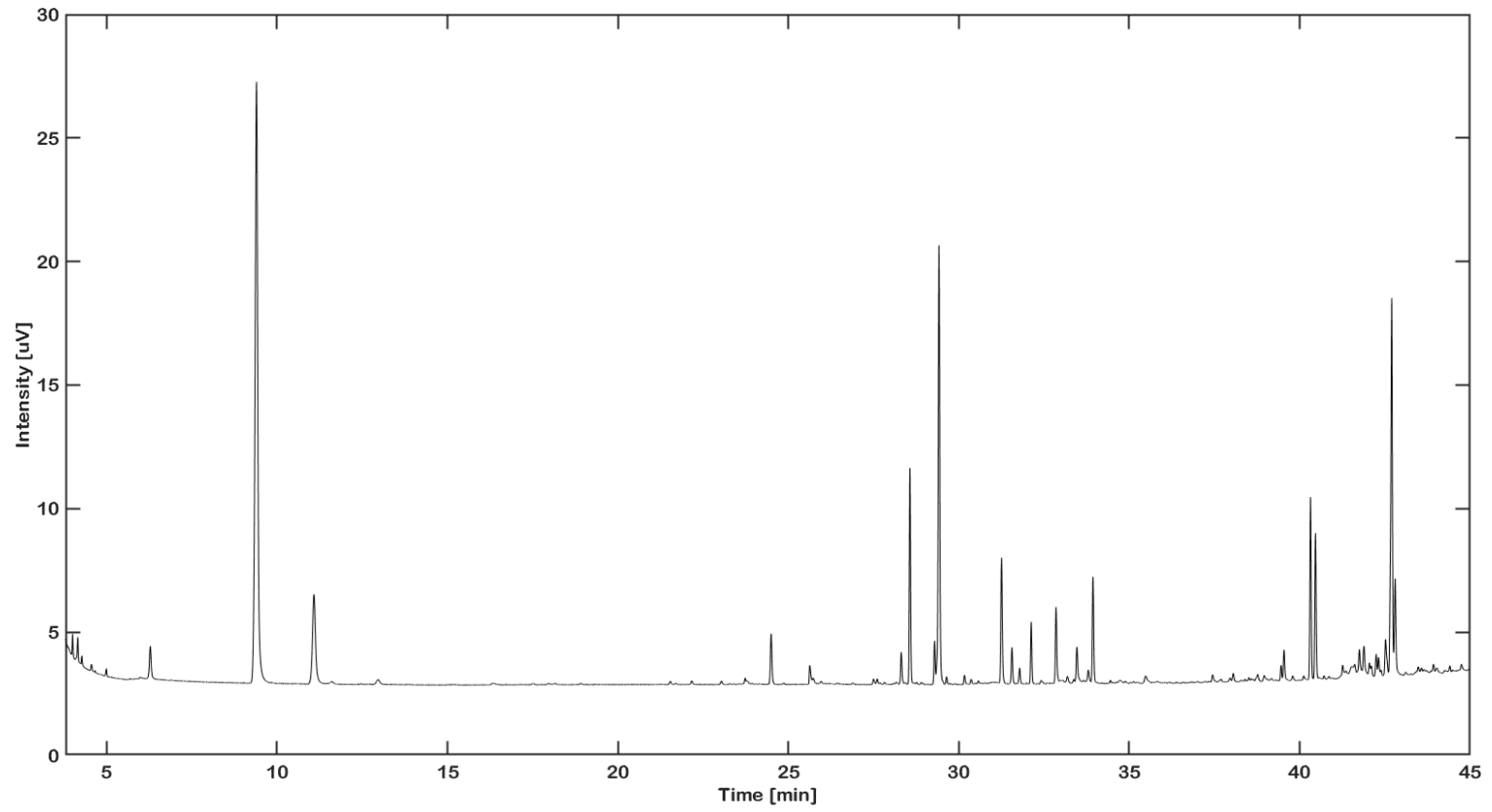
C. sativa L. sample 10



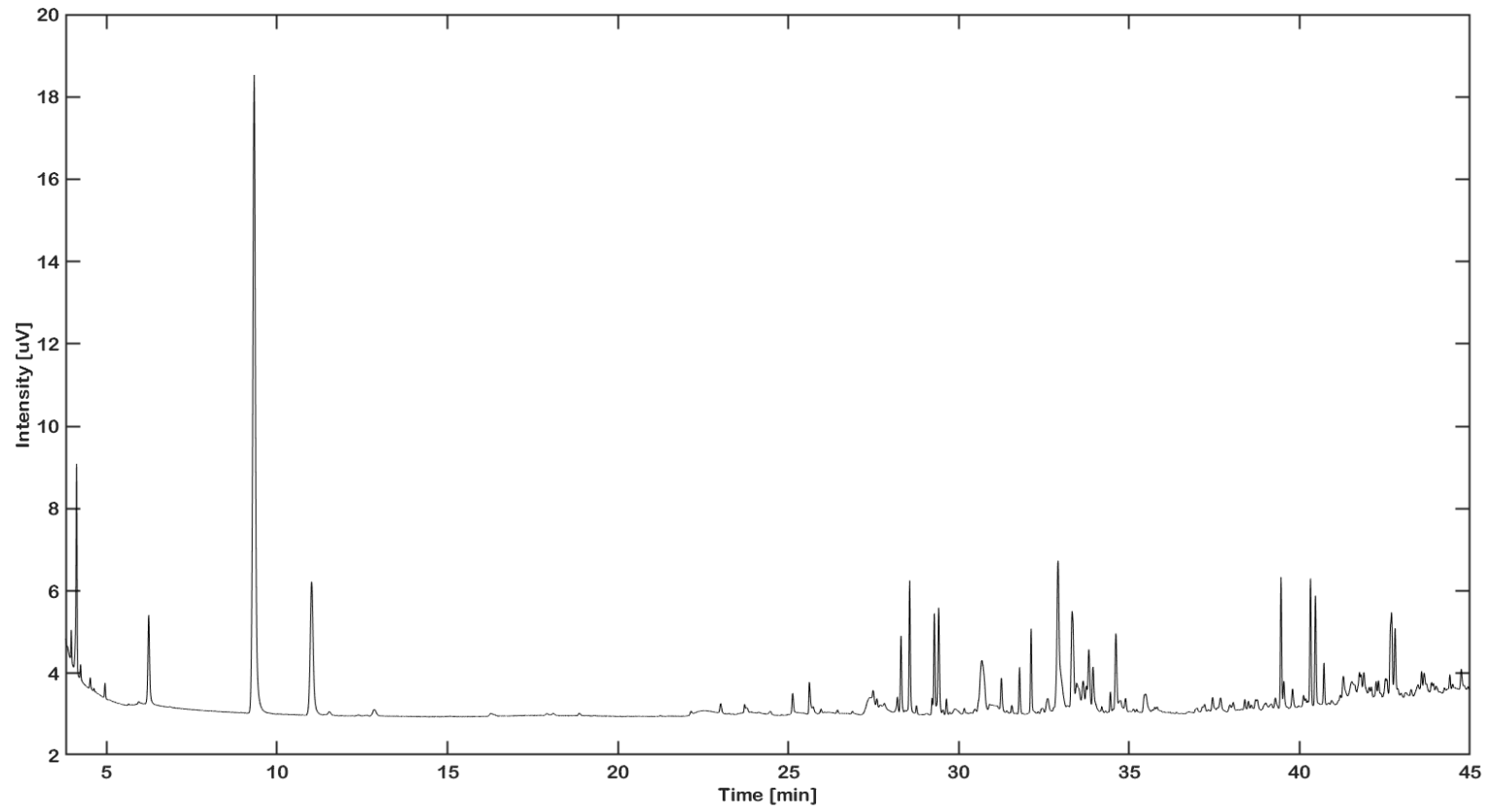
C. sativa L. sample 11



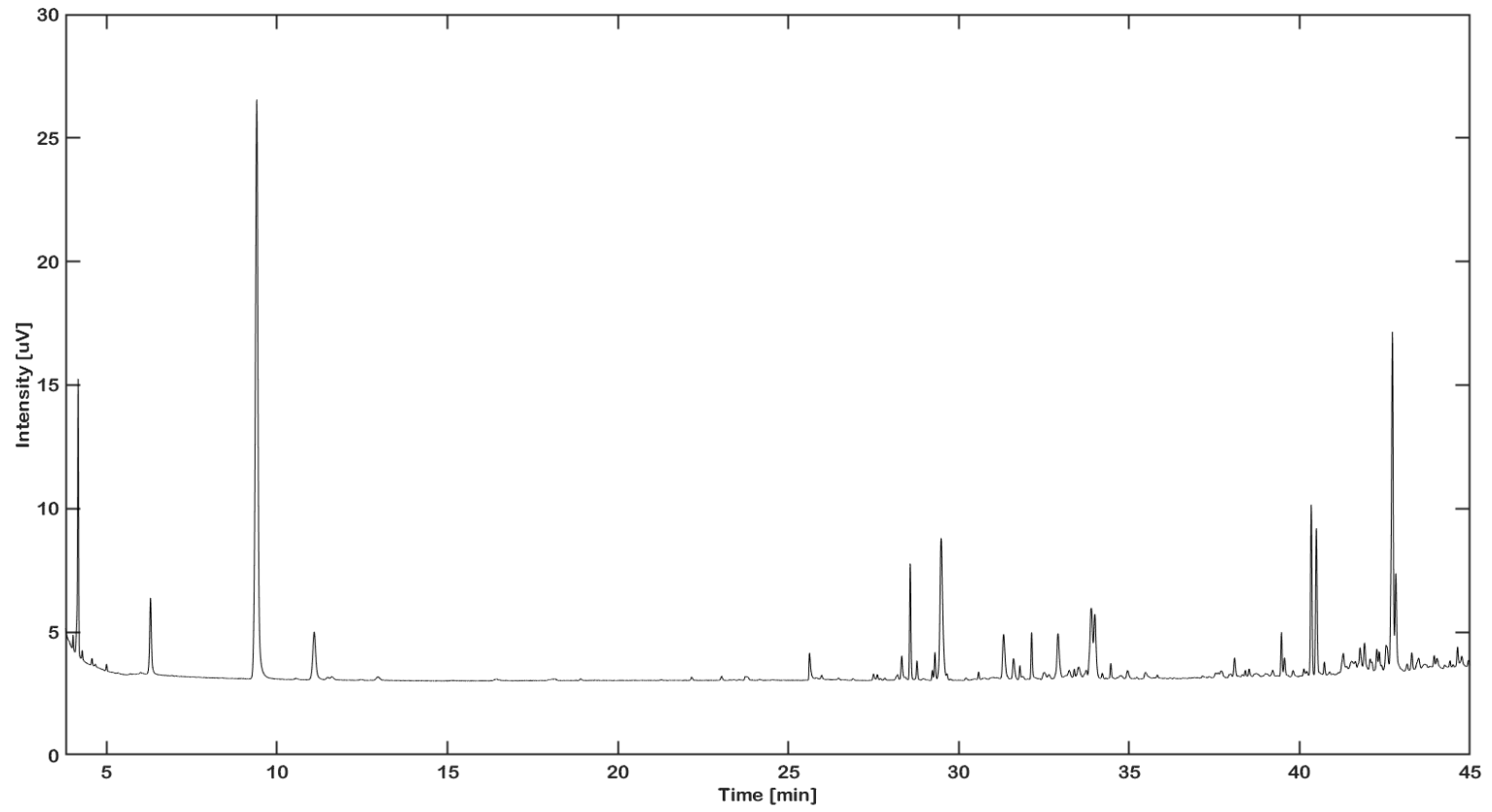
C. sativa L. sample 12



C. sativa L. sample 13



C. sativa L. sample 14



C. sativa L. sample 15

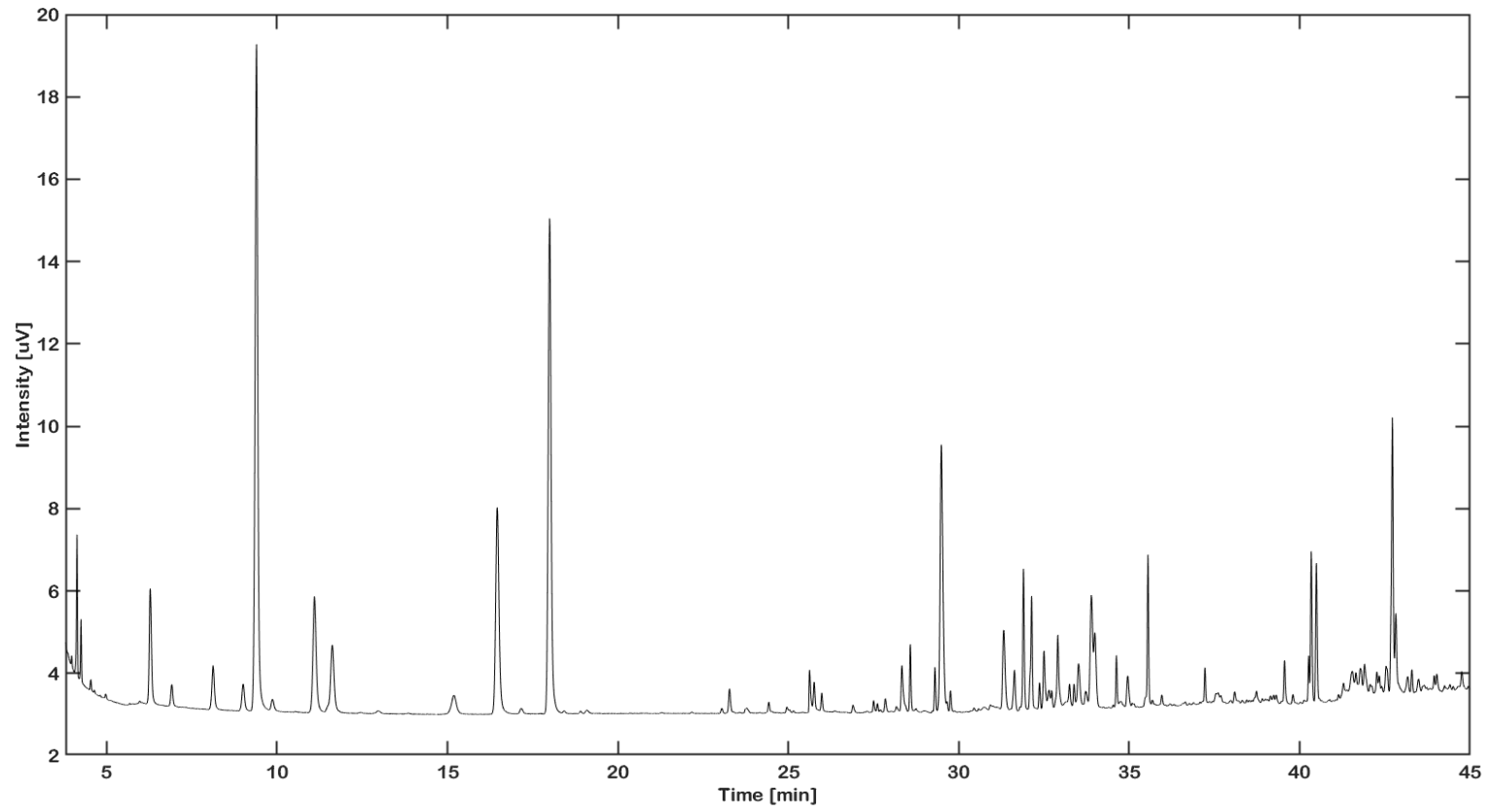
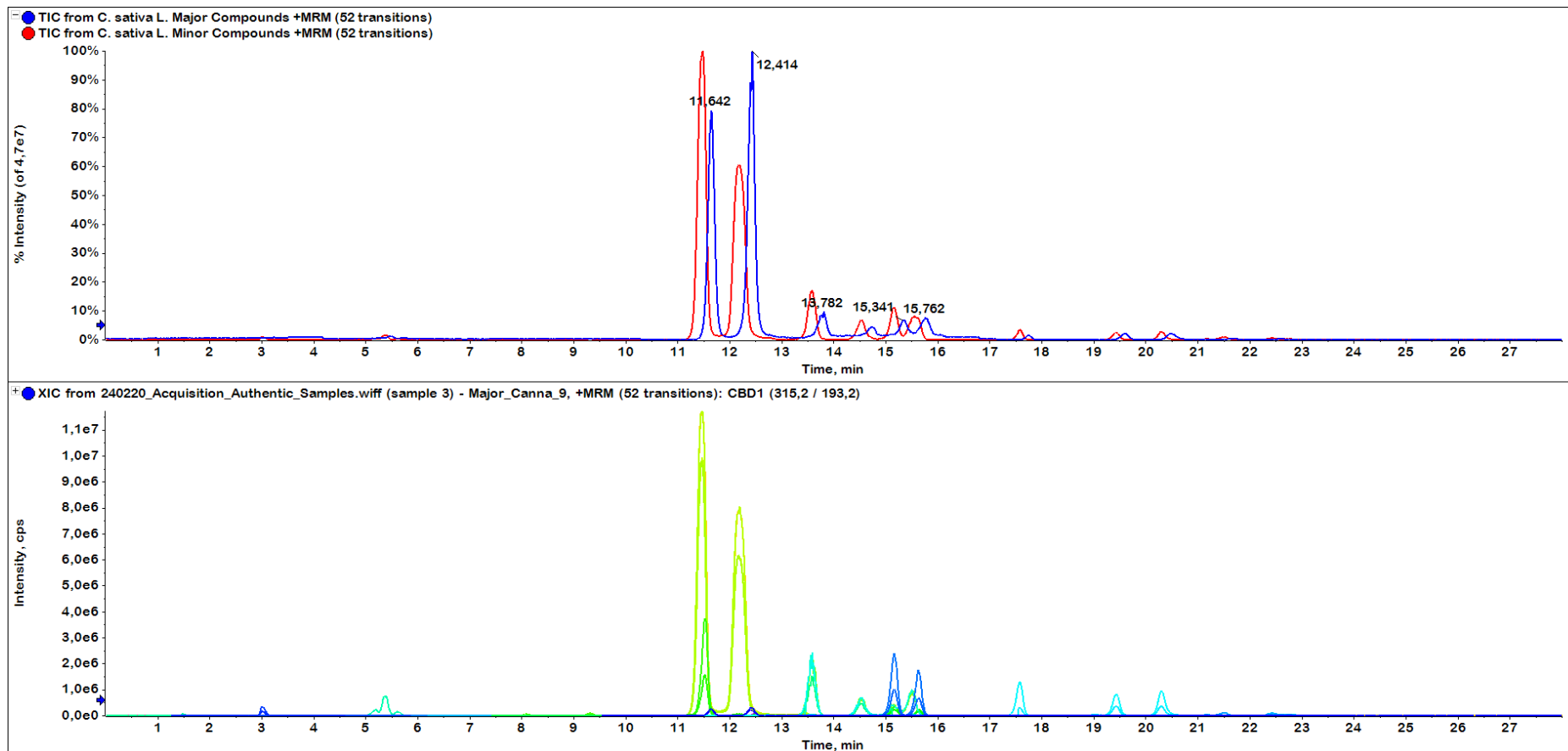
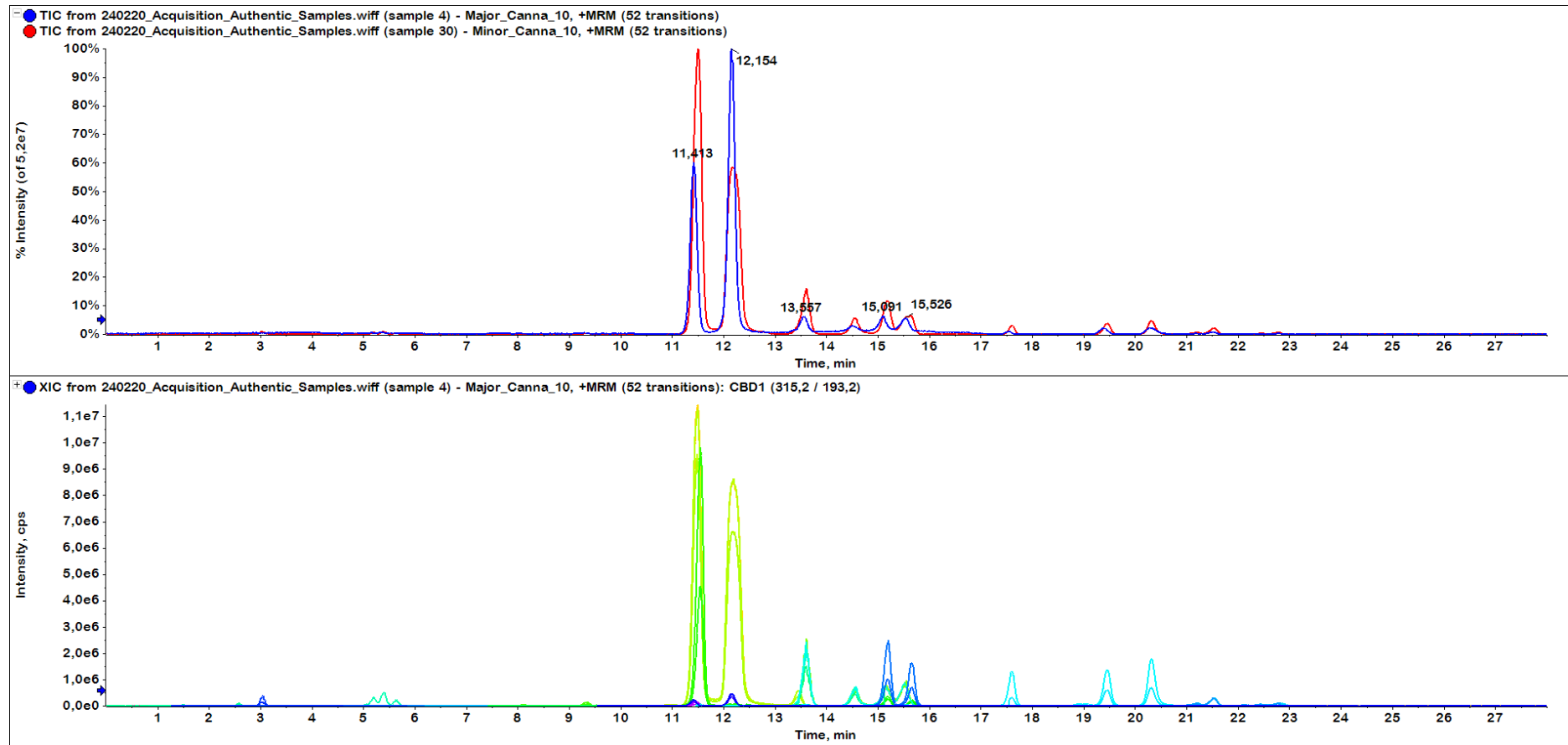


Figure A12: TIC and XIC of 55 authentic *C. sativa* L. samples for the quantification of major and minor compounds. The top chromatogram contains the TIC, with dark blue showing the 100-fold diluted *C. sativa* L. sample and red the undiluted sample.

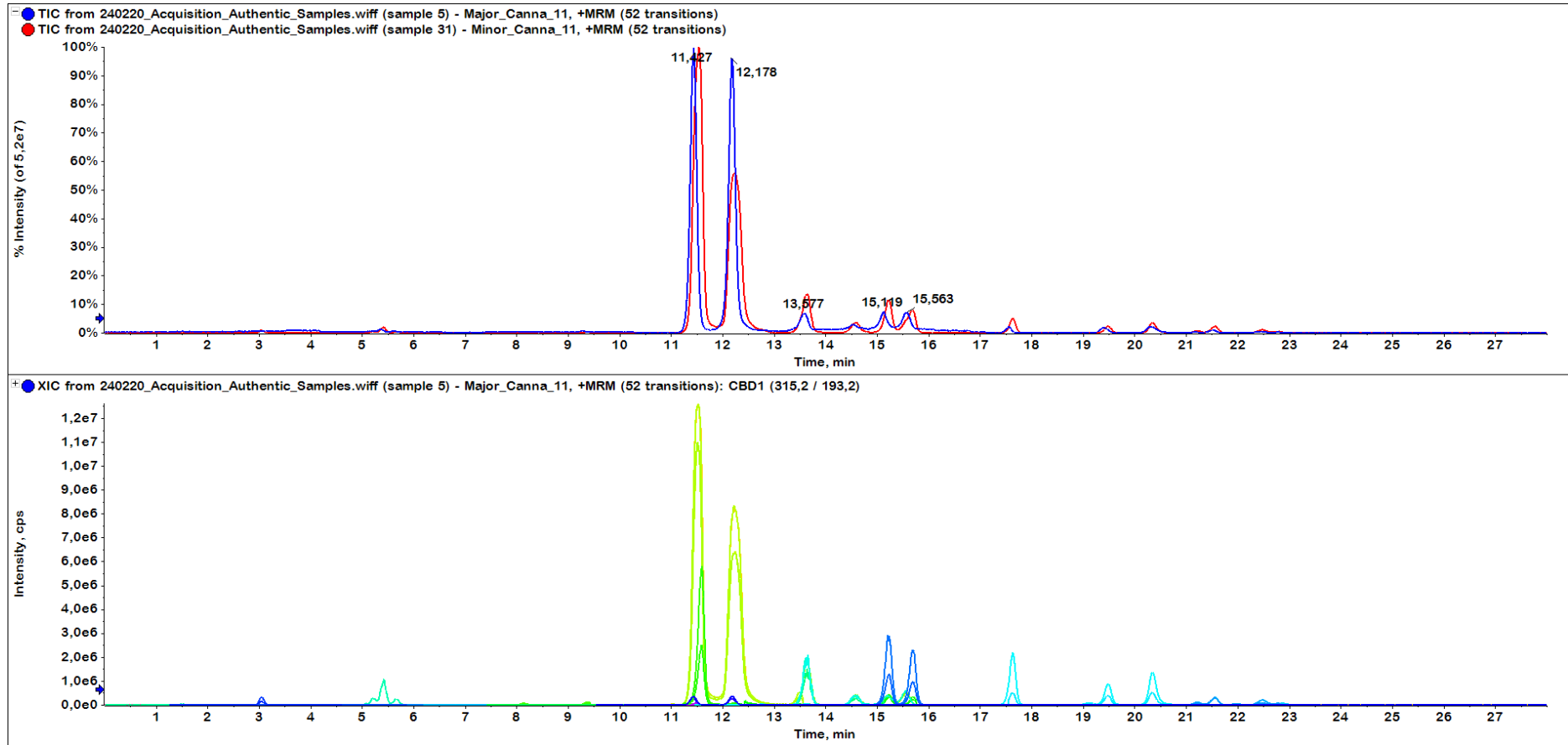
C. sativa L. sample 1



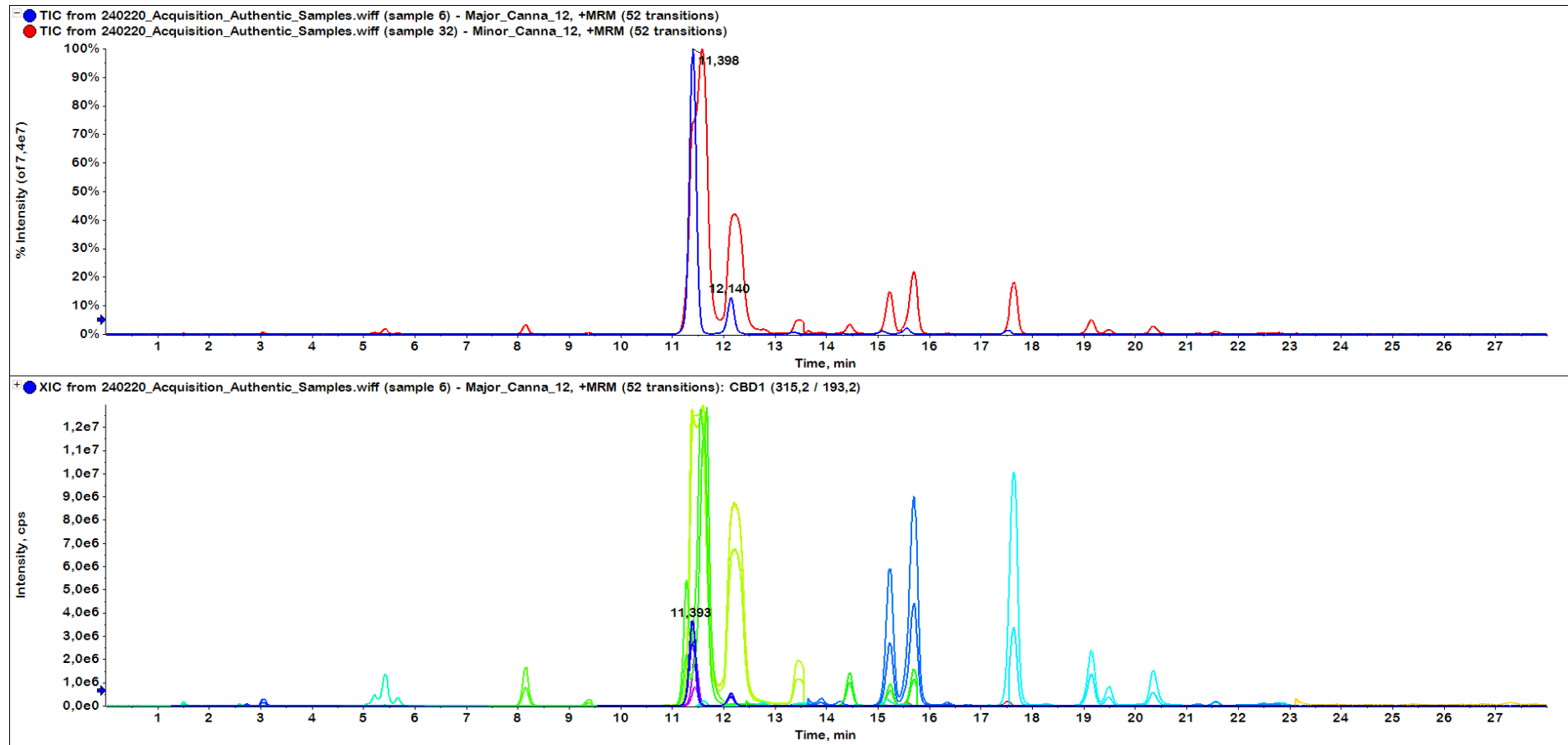
C. sativa L. sample 2



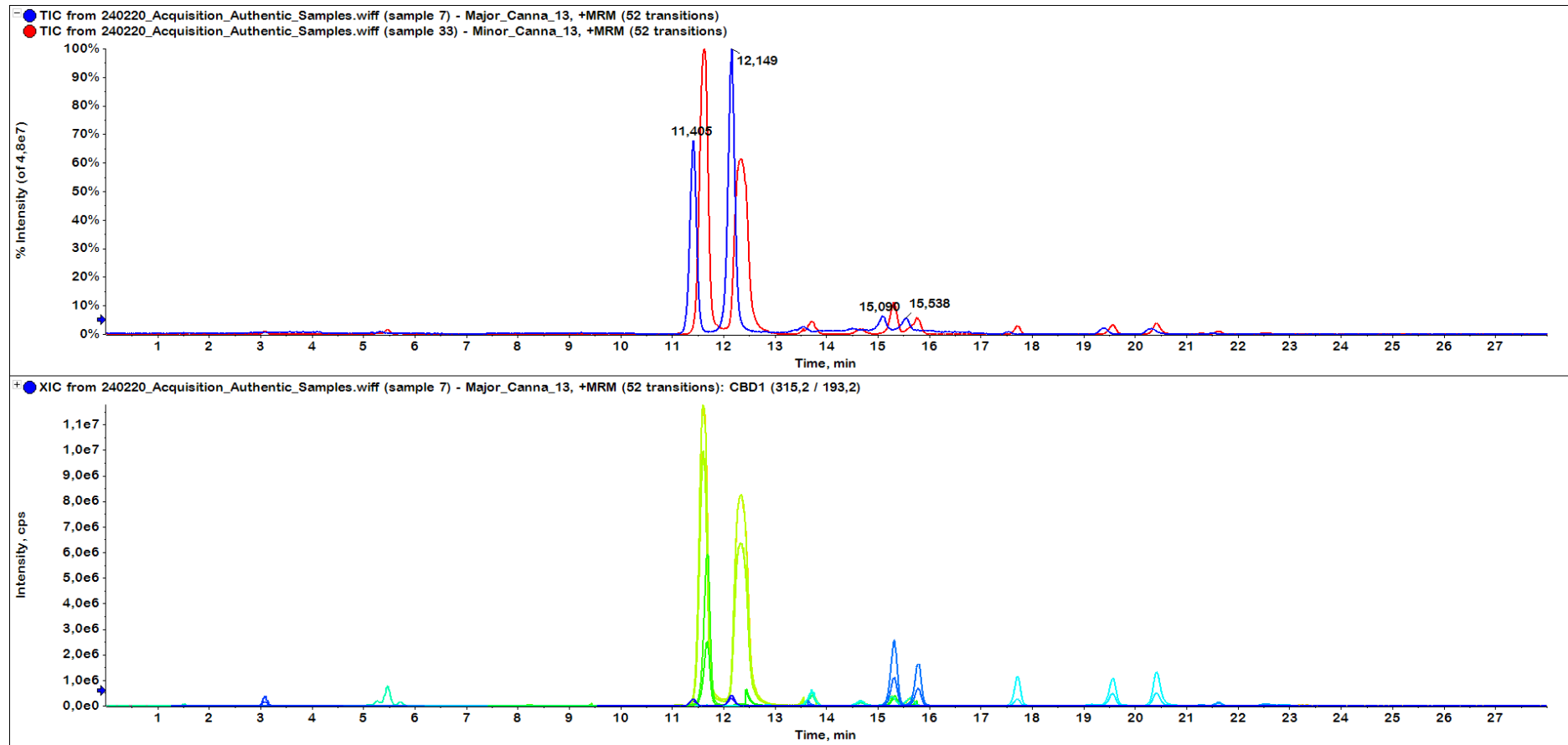
C. sativa L. sample 3



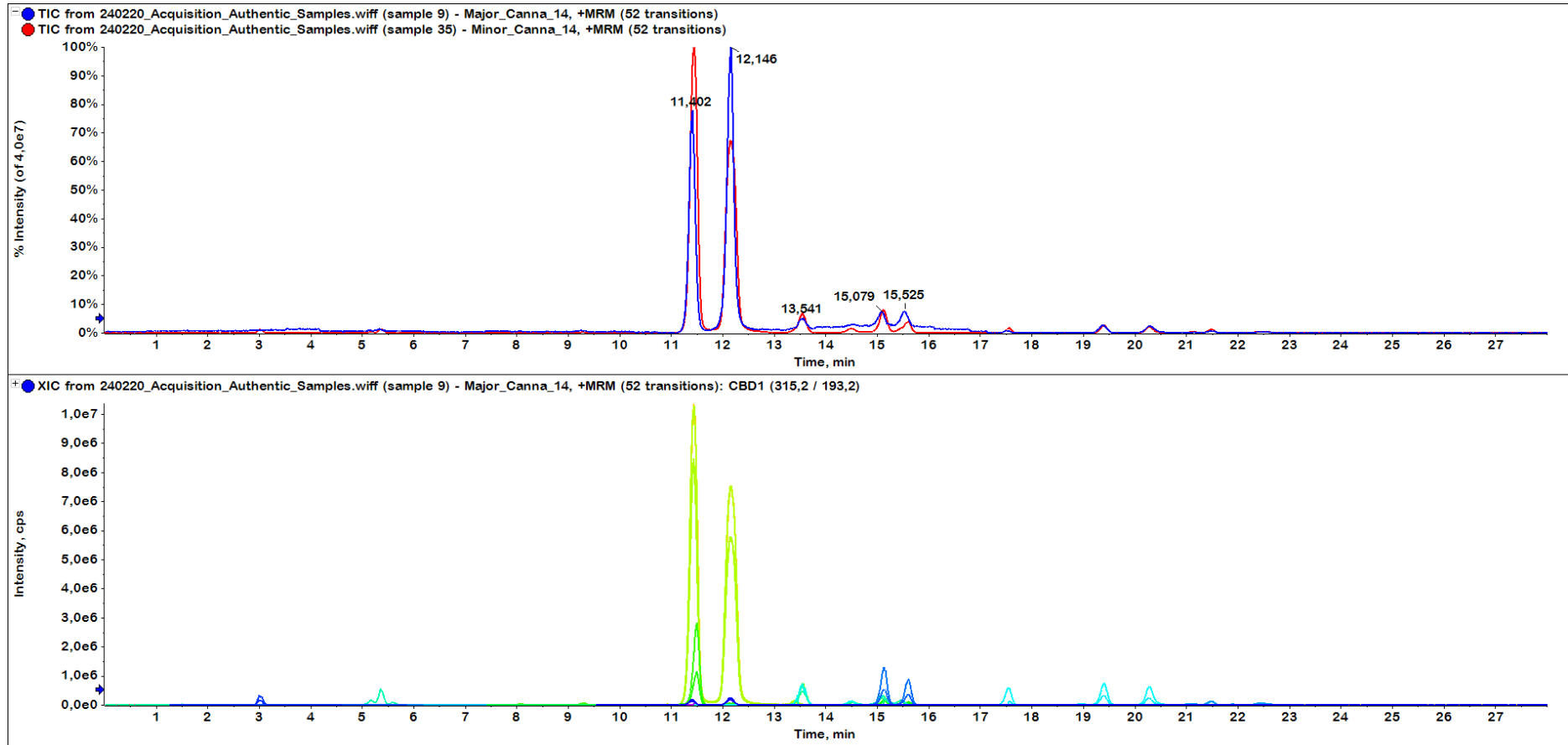
C. sativa L. sample 4



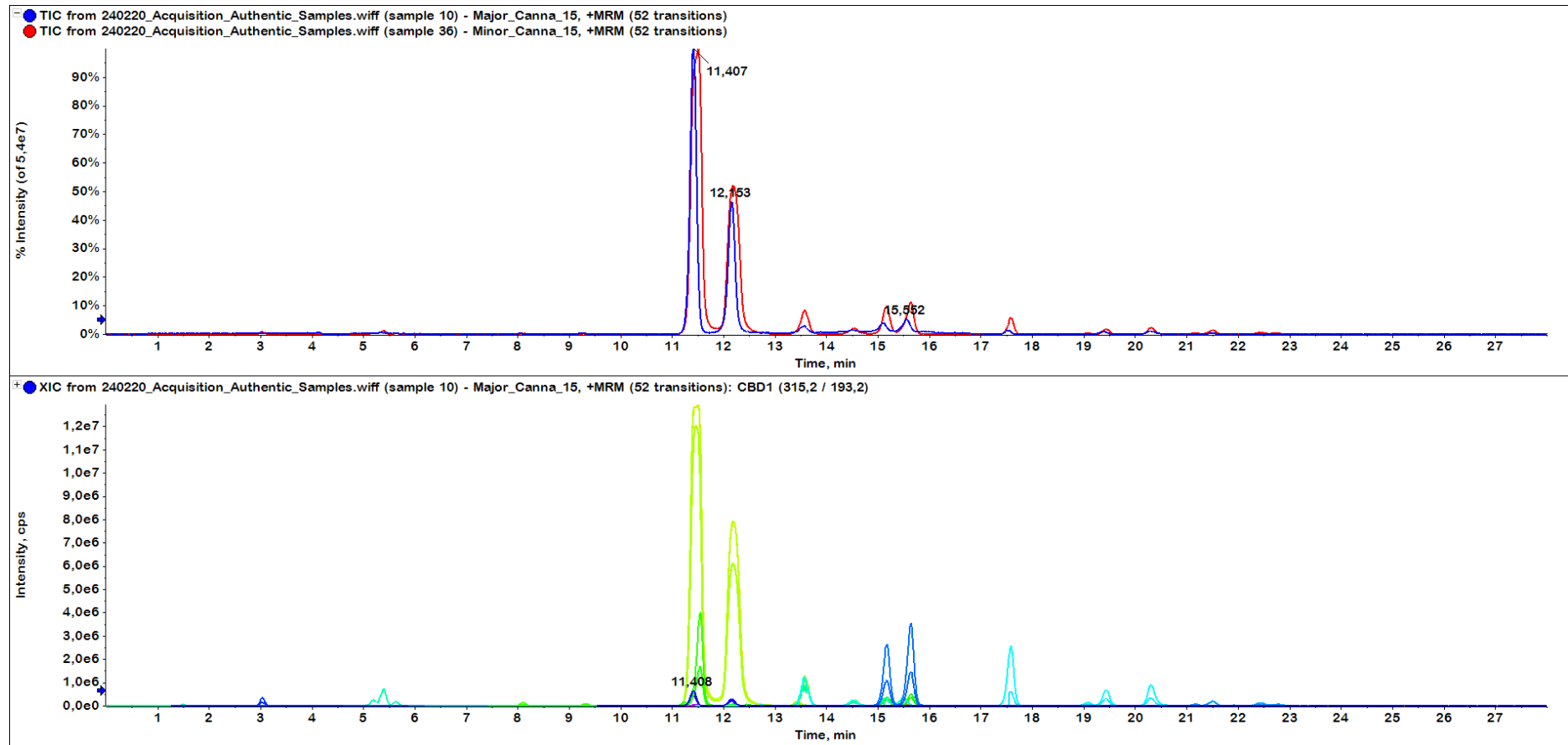
C. sativa L. sample 5



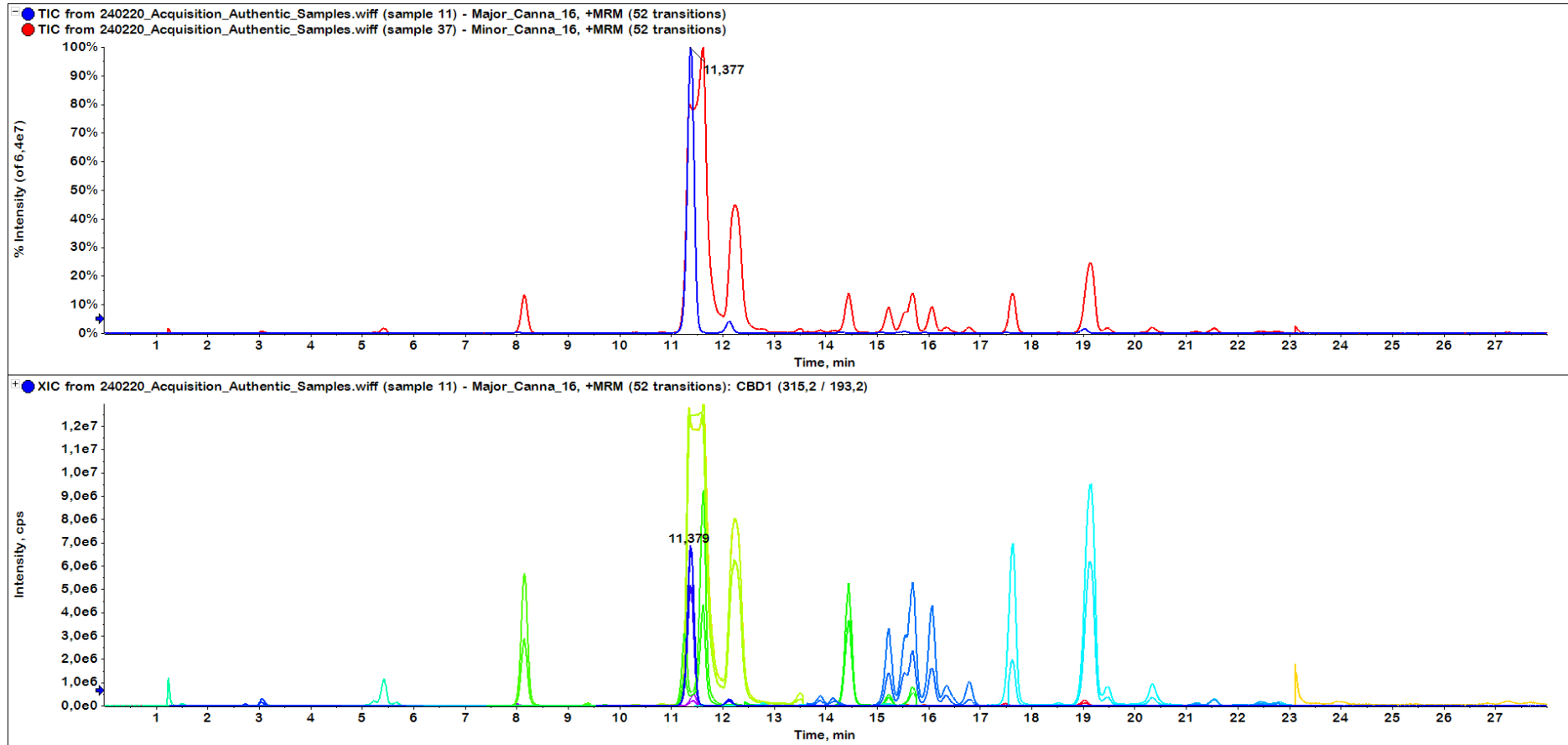
C. sativa L. sample 6



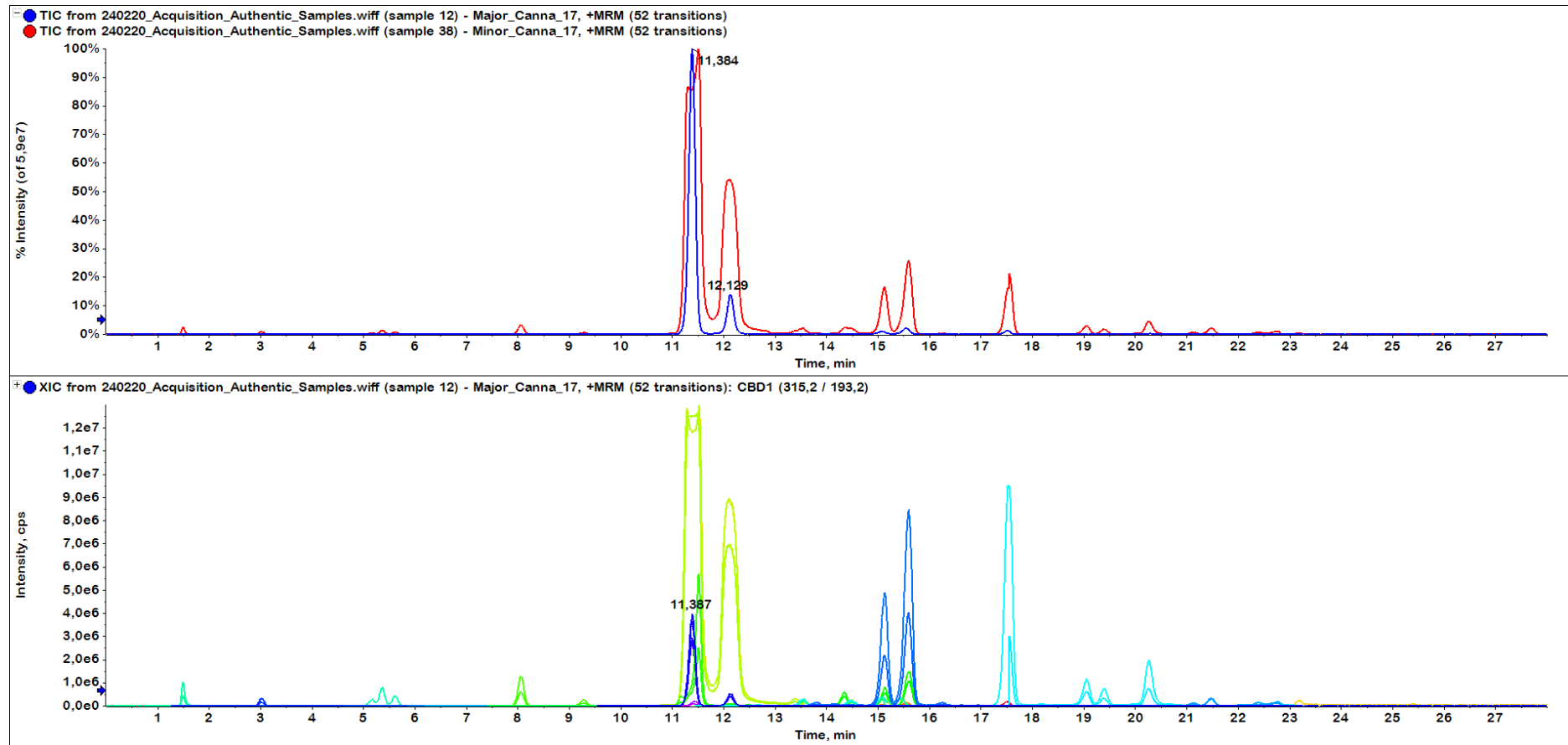
C. sativa L. sample 7



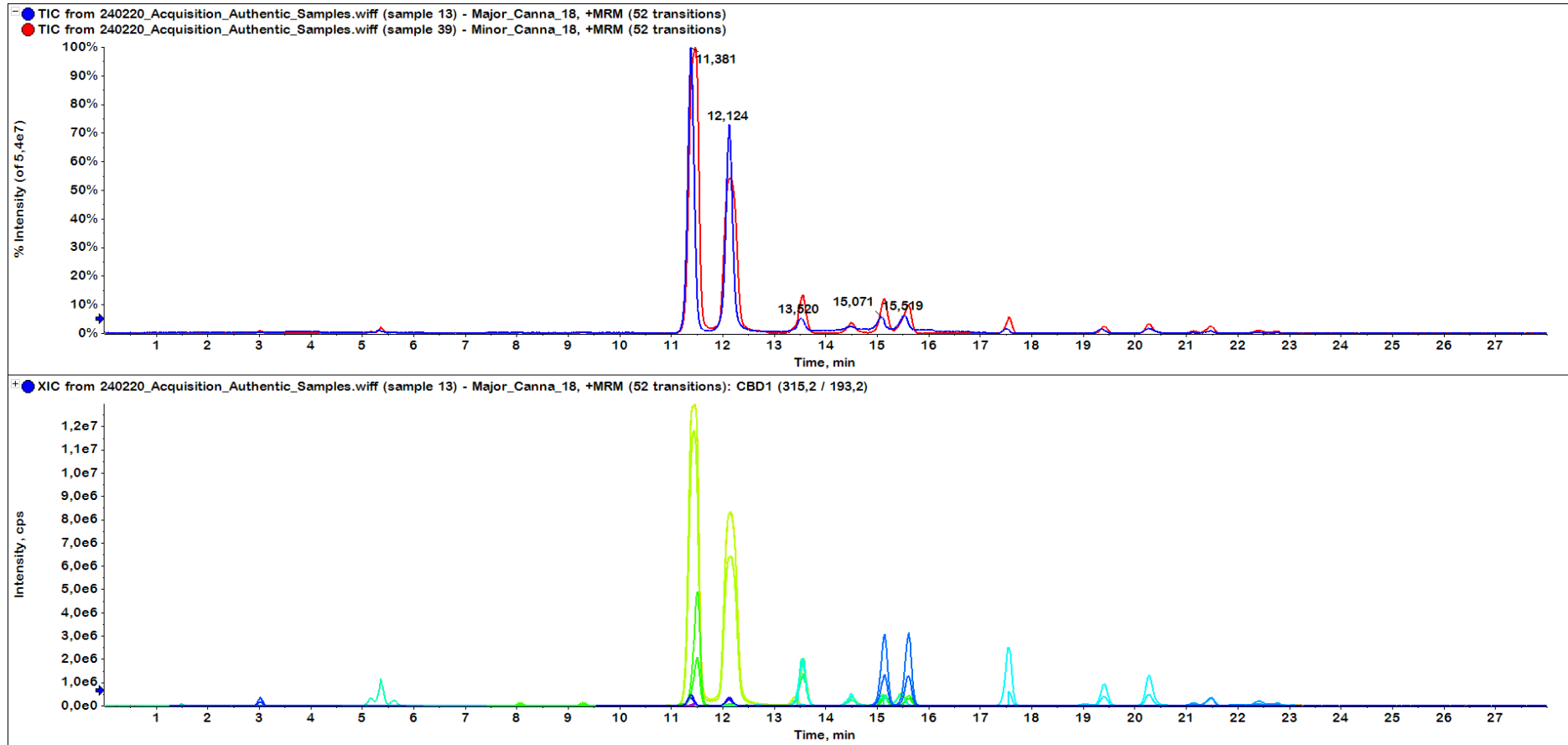
C. sativa L. sample 8



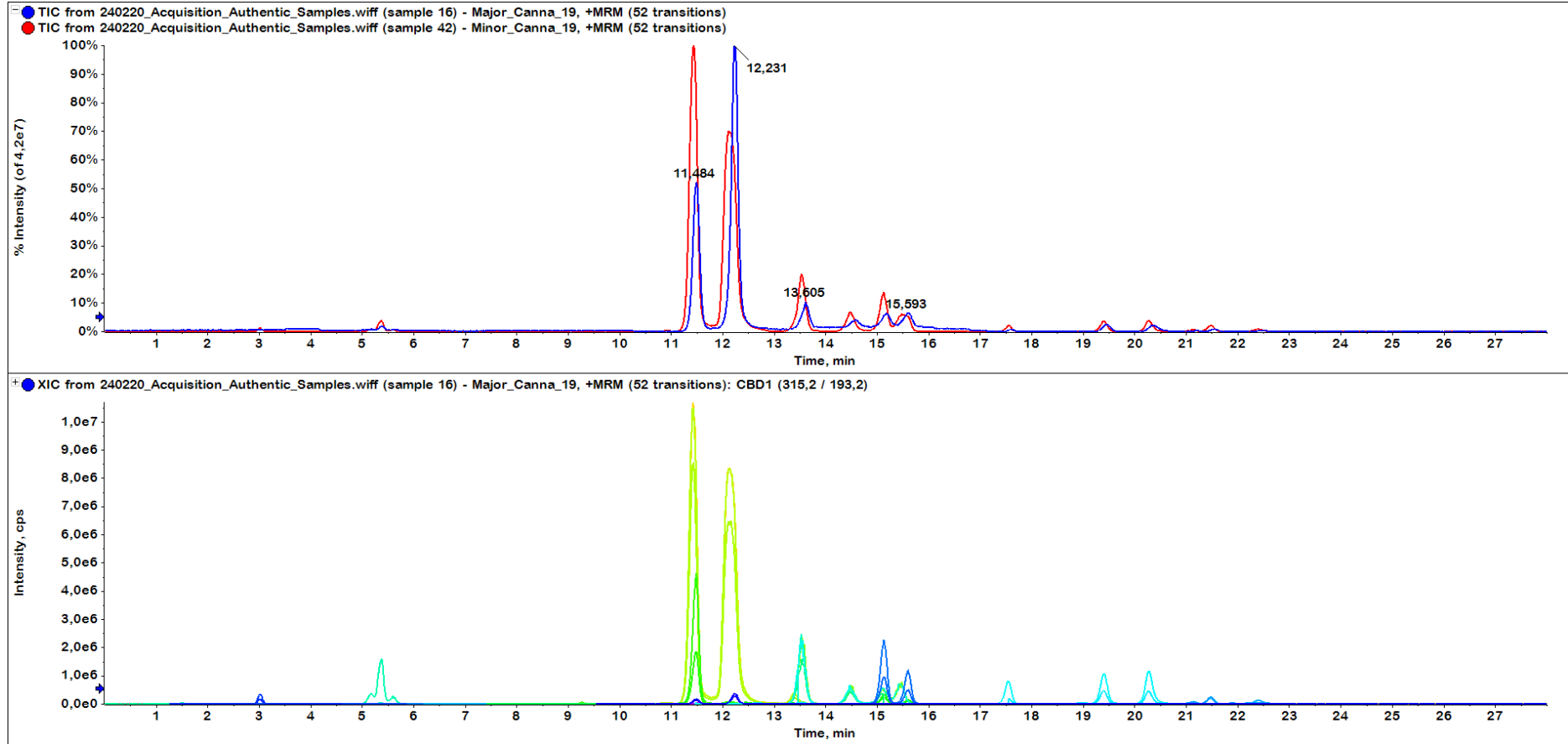
C. sativa L. sample 9



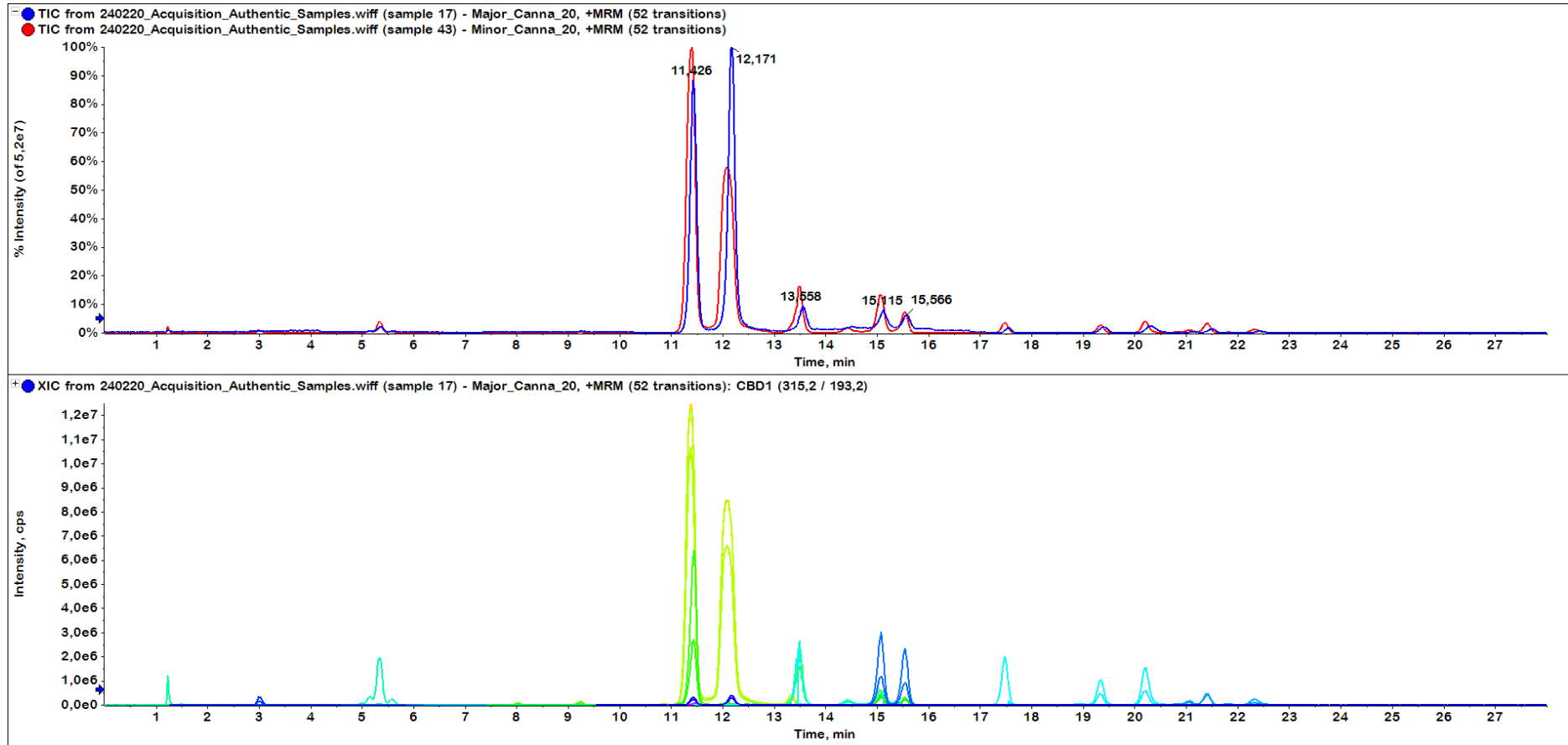
C. sativa L. sample 10



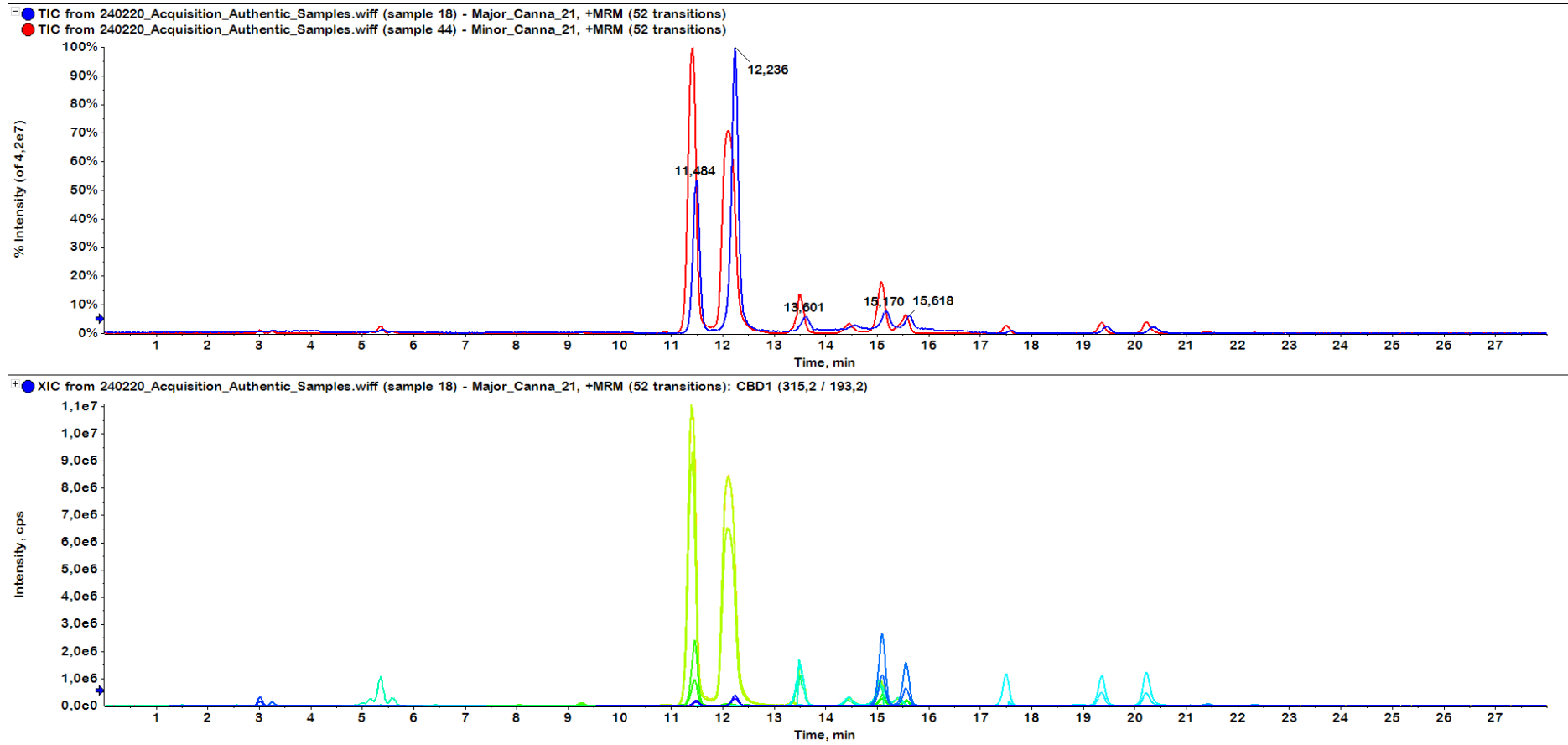
C. sativa L. sample 11



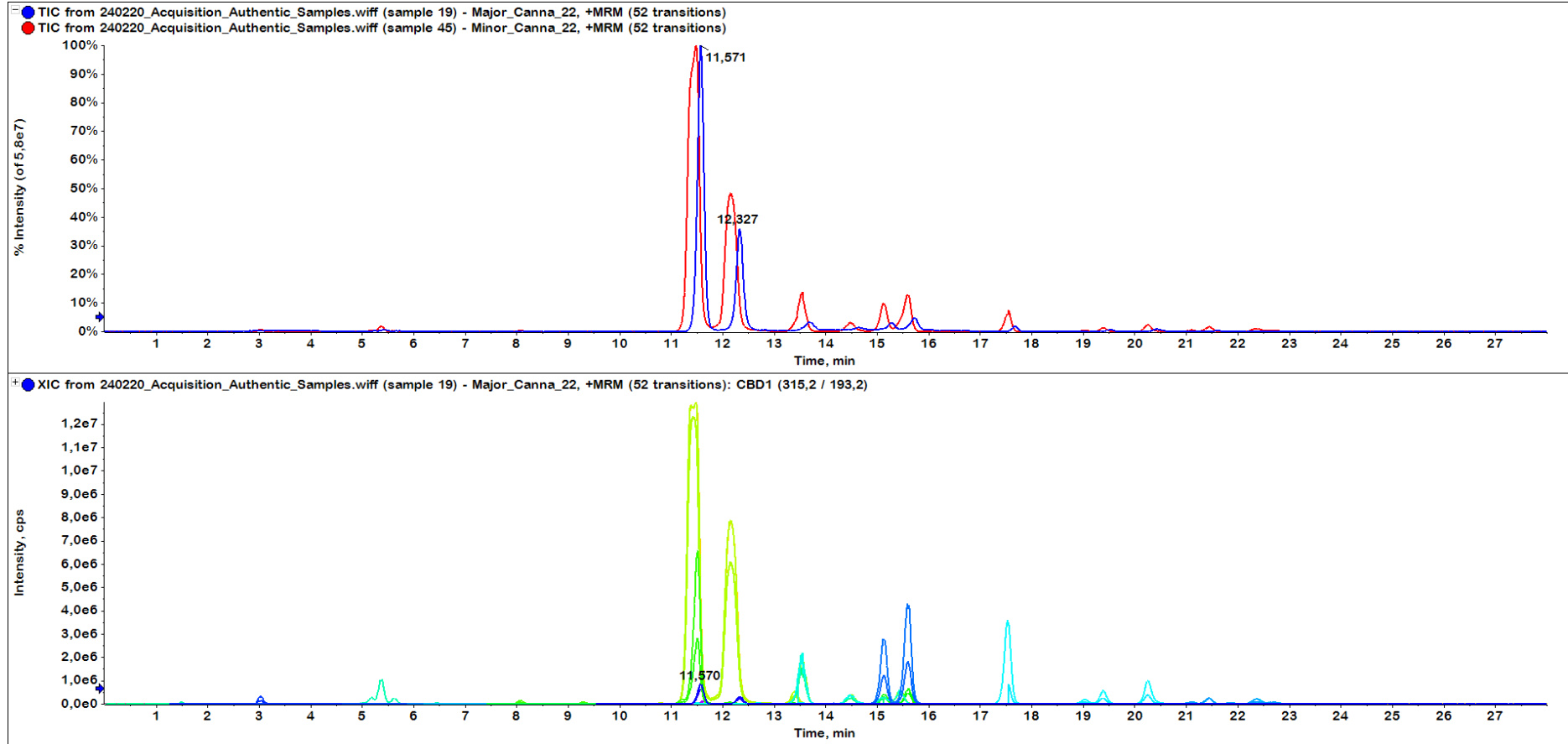
C. sativa L. sample 12



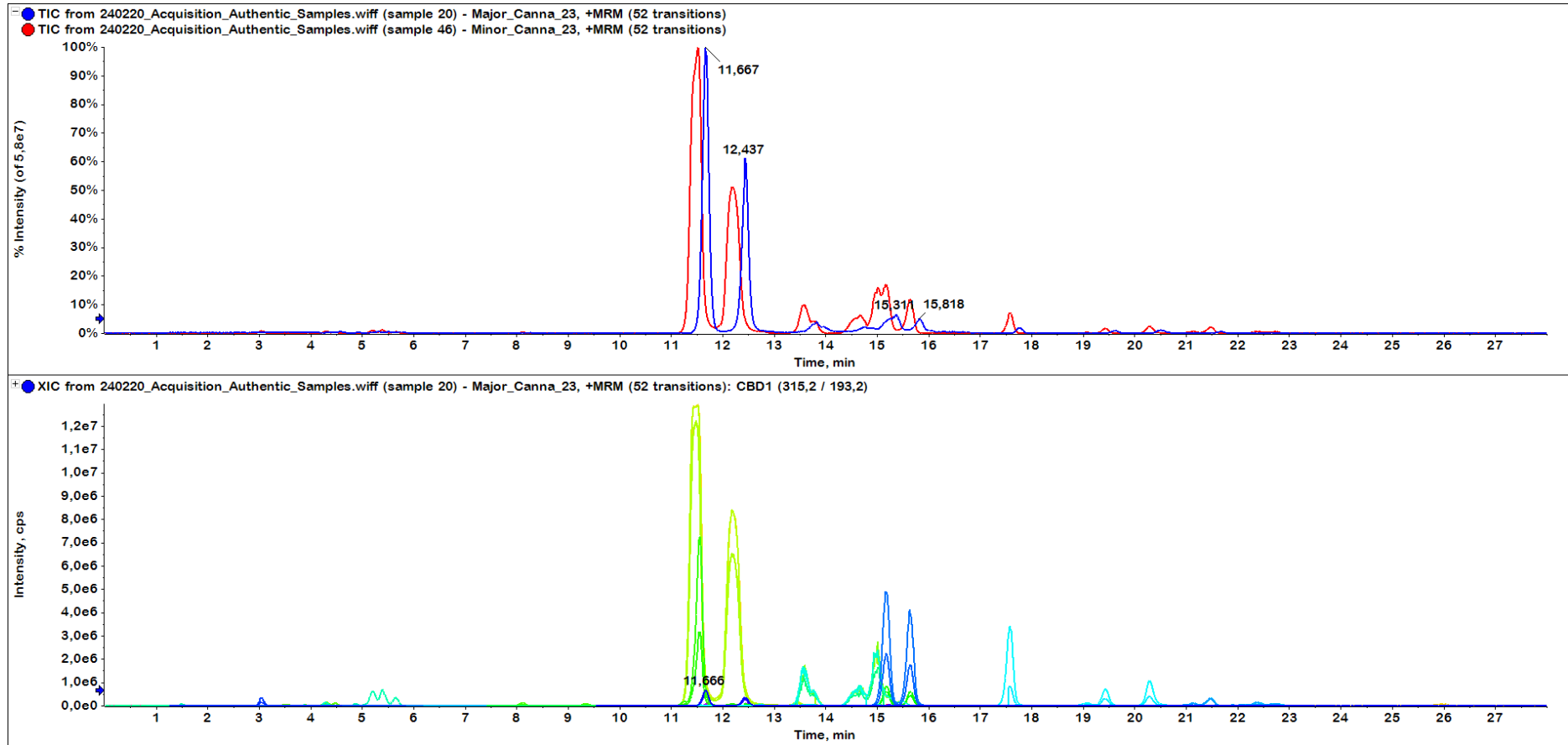
C. sativa L. sample 13



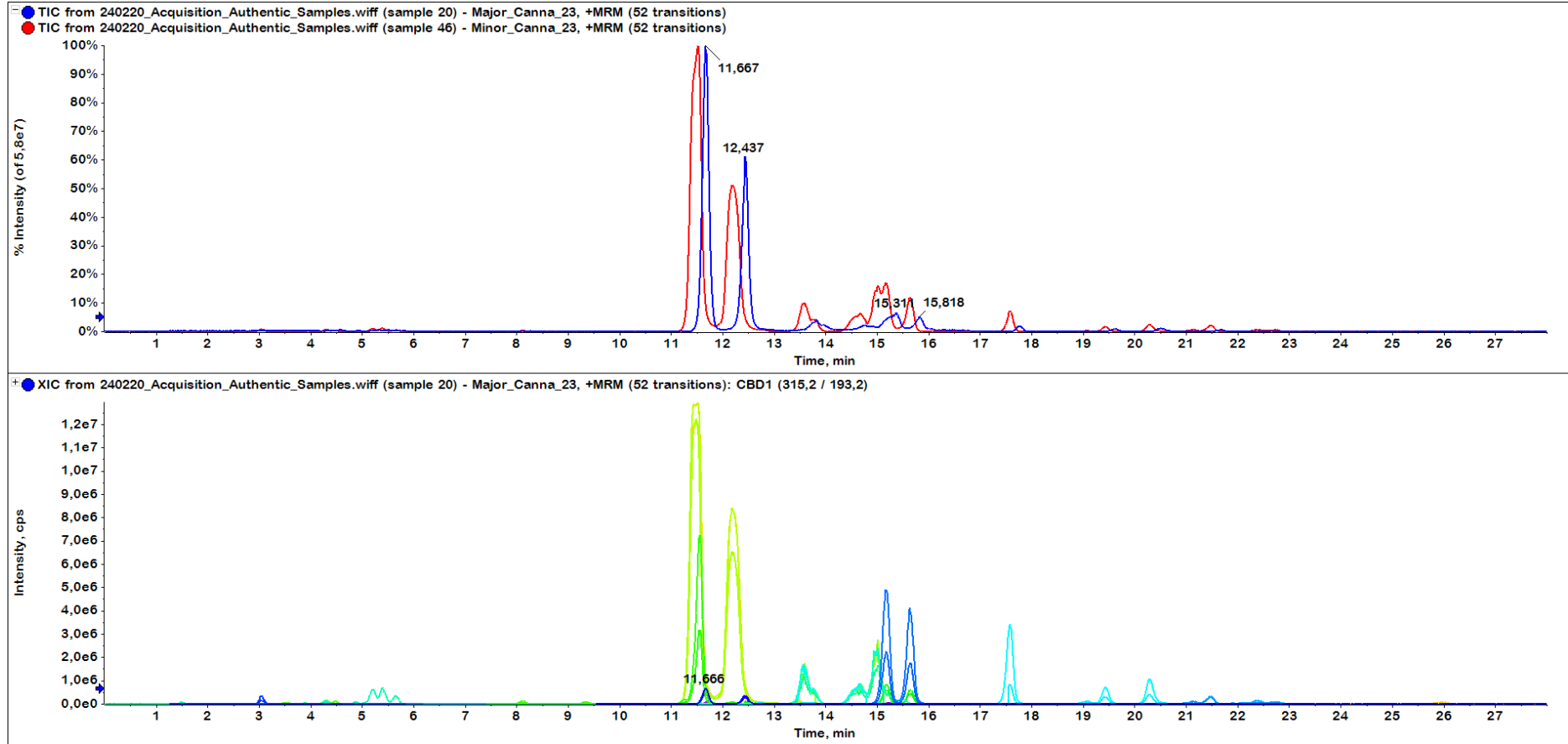
C. sativa L. sample 14



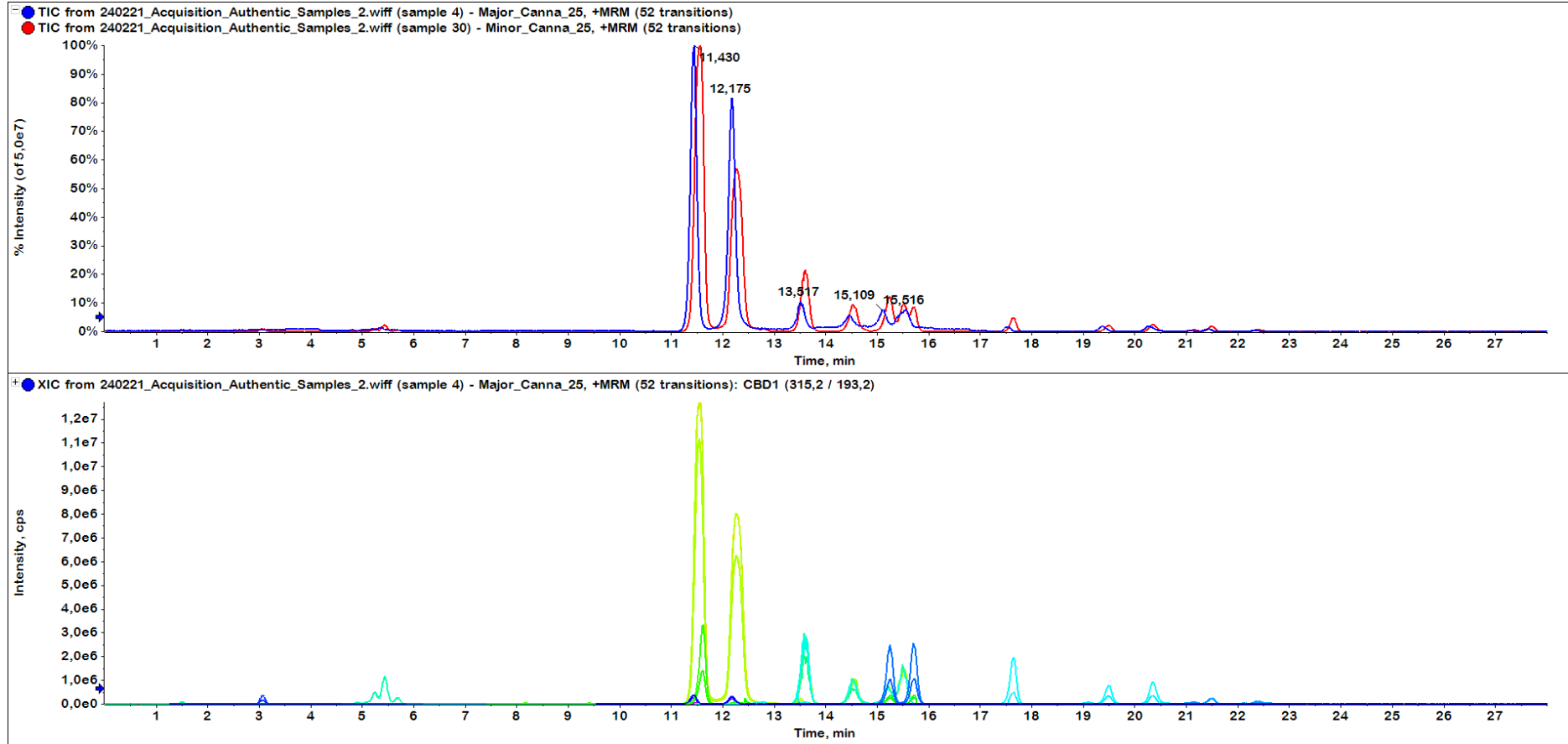
C. sativa L. sample 15



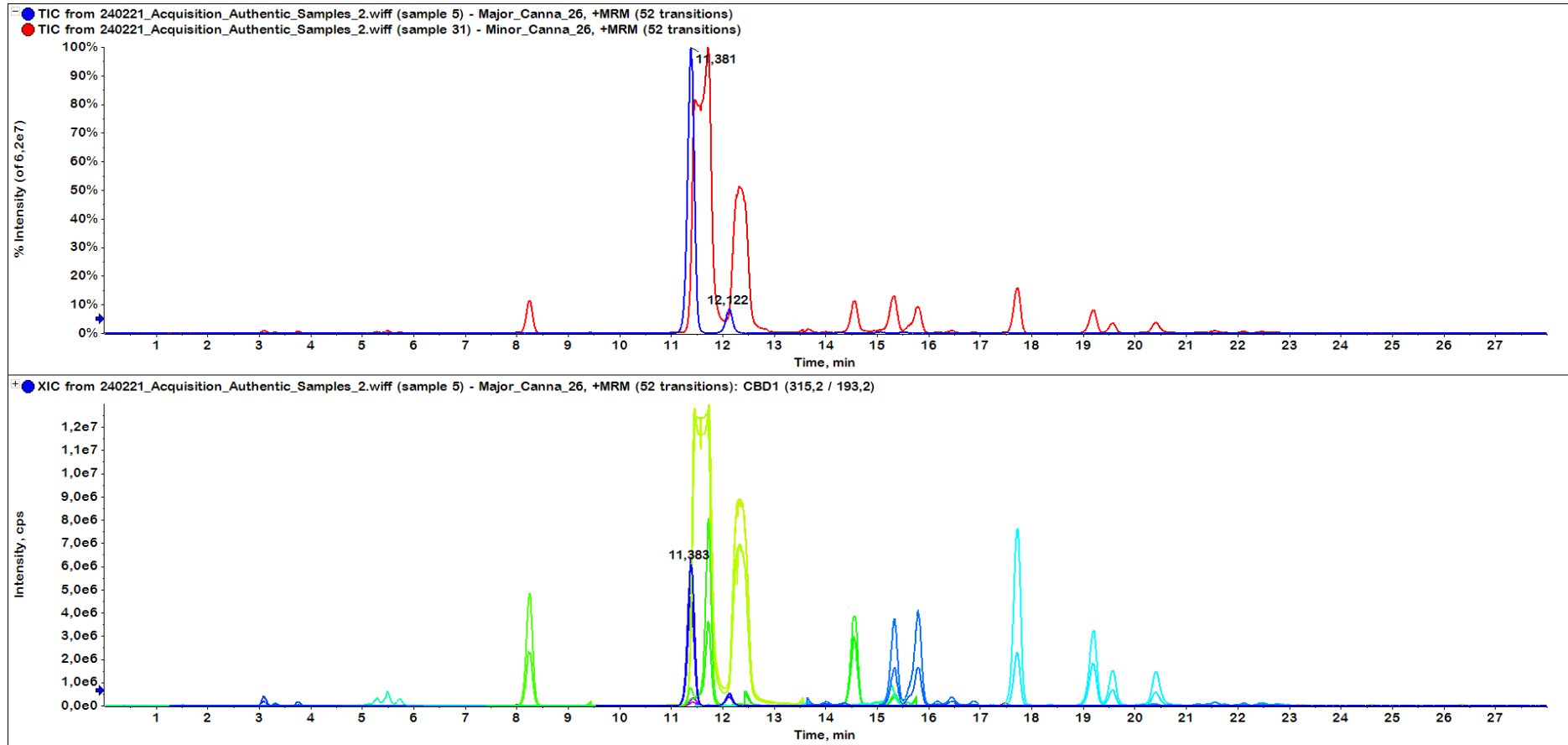
C. sativa L. sample 16



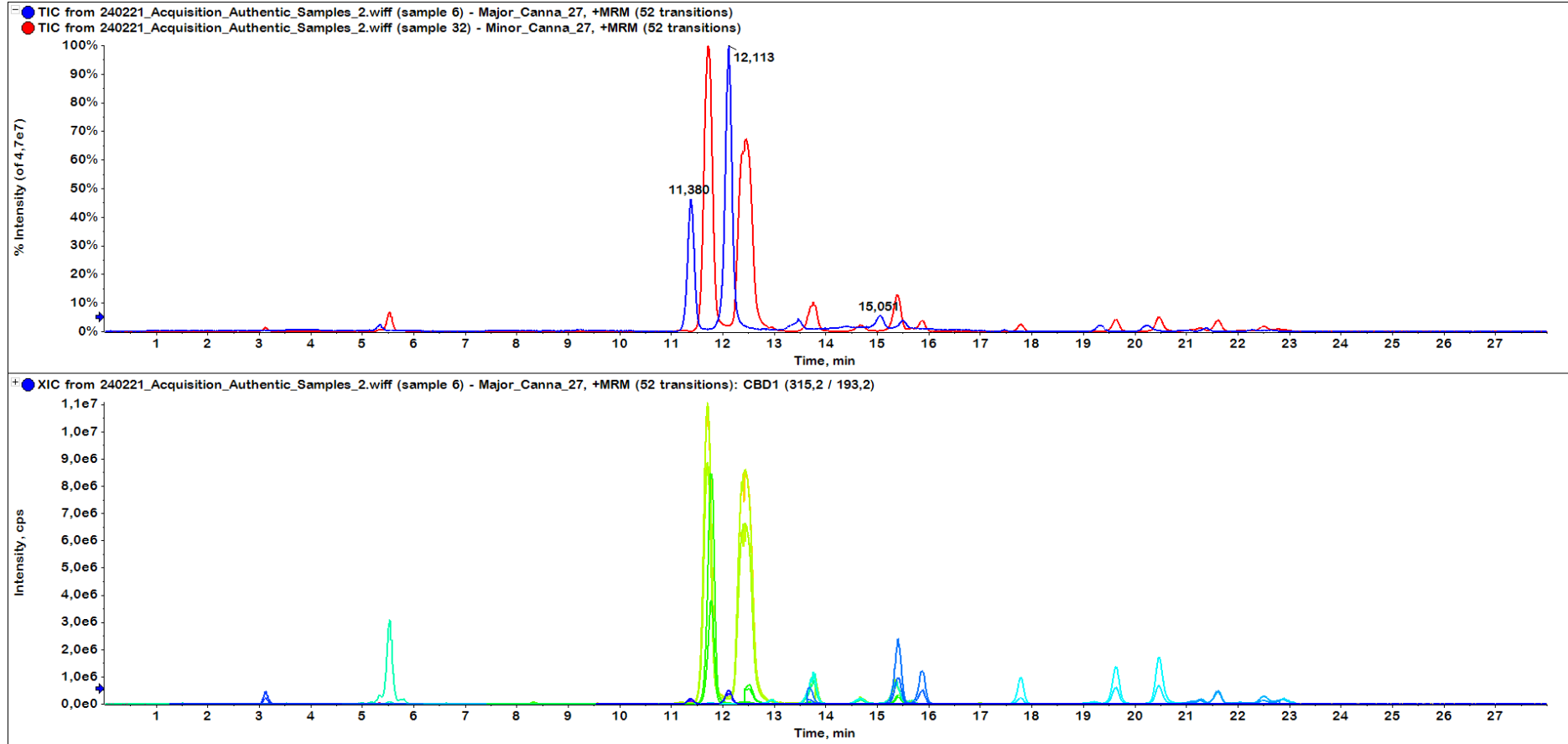
C. sativa L. sample 17



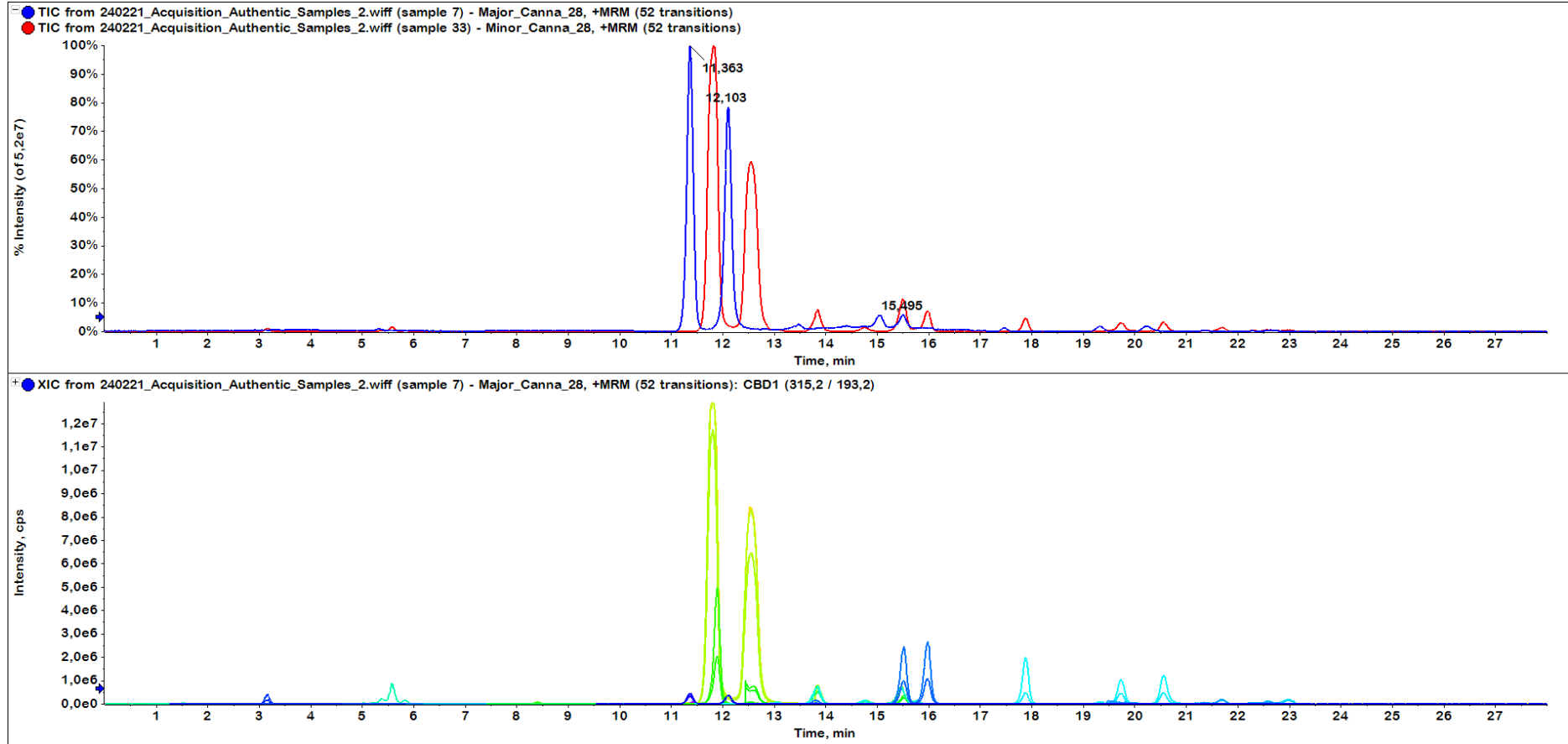
C. sativa L. sample 18



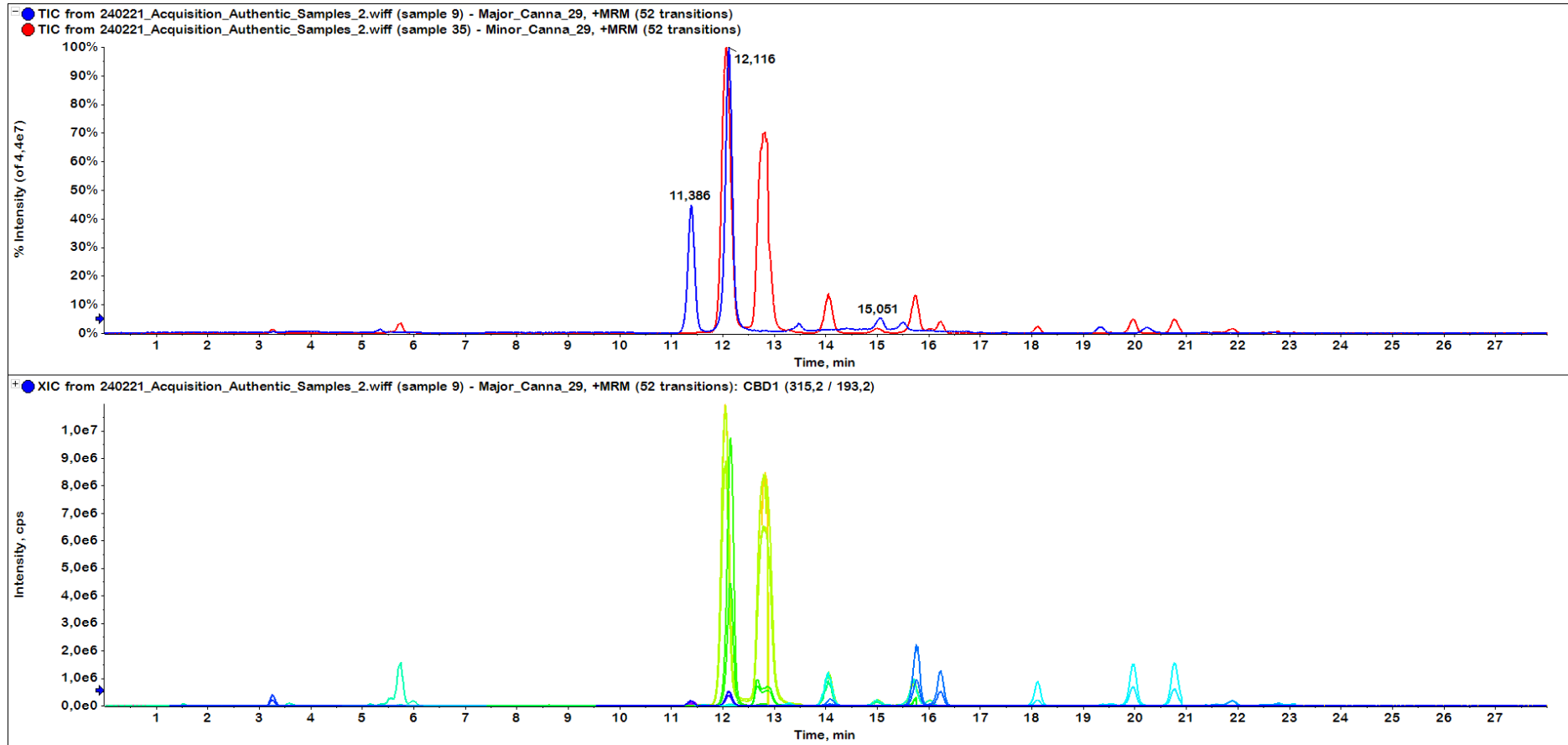
C. sativa L. sample 19



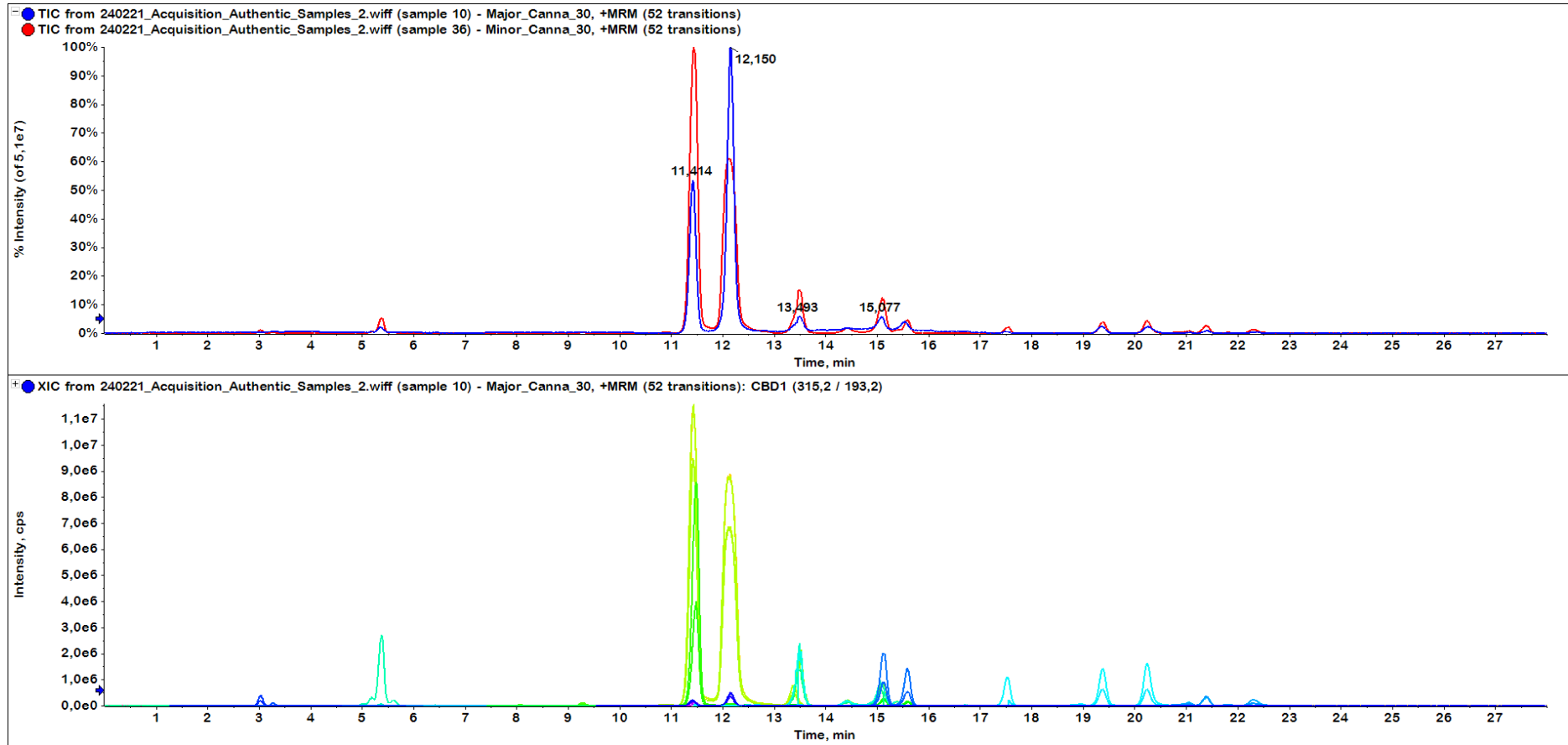
C. sativa L. sample 20



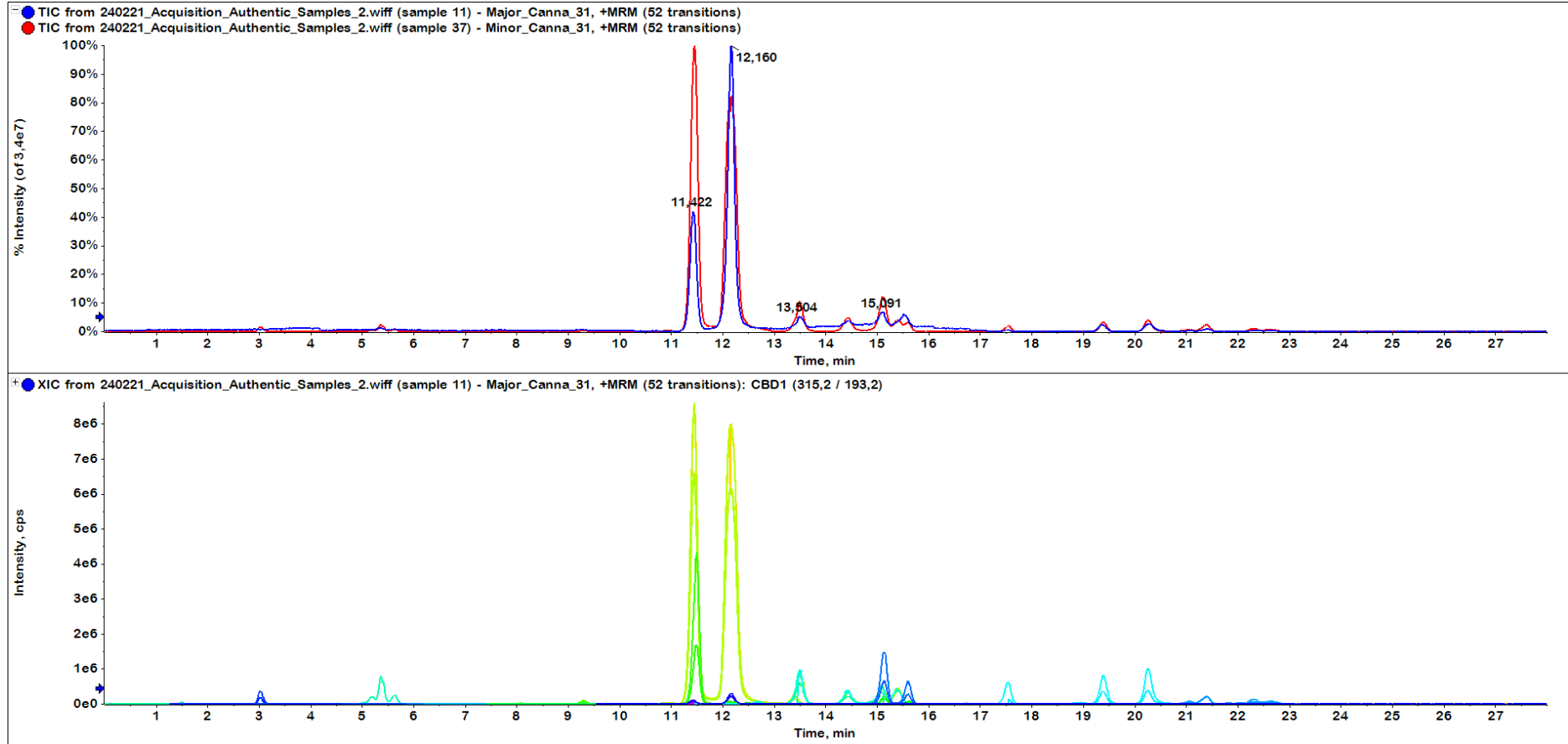
C. sativa L. sample 21



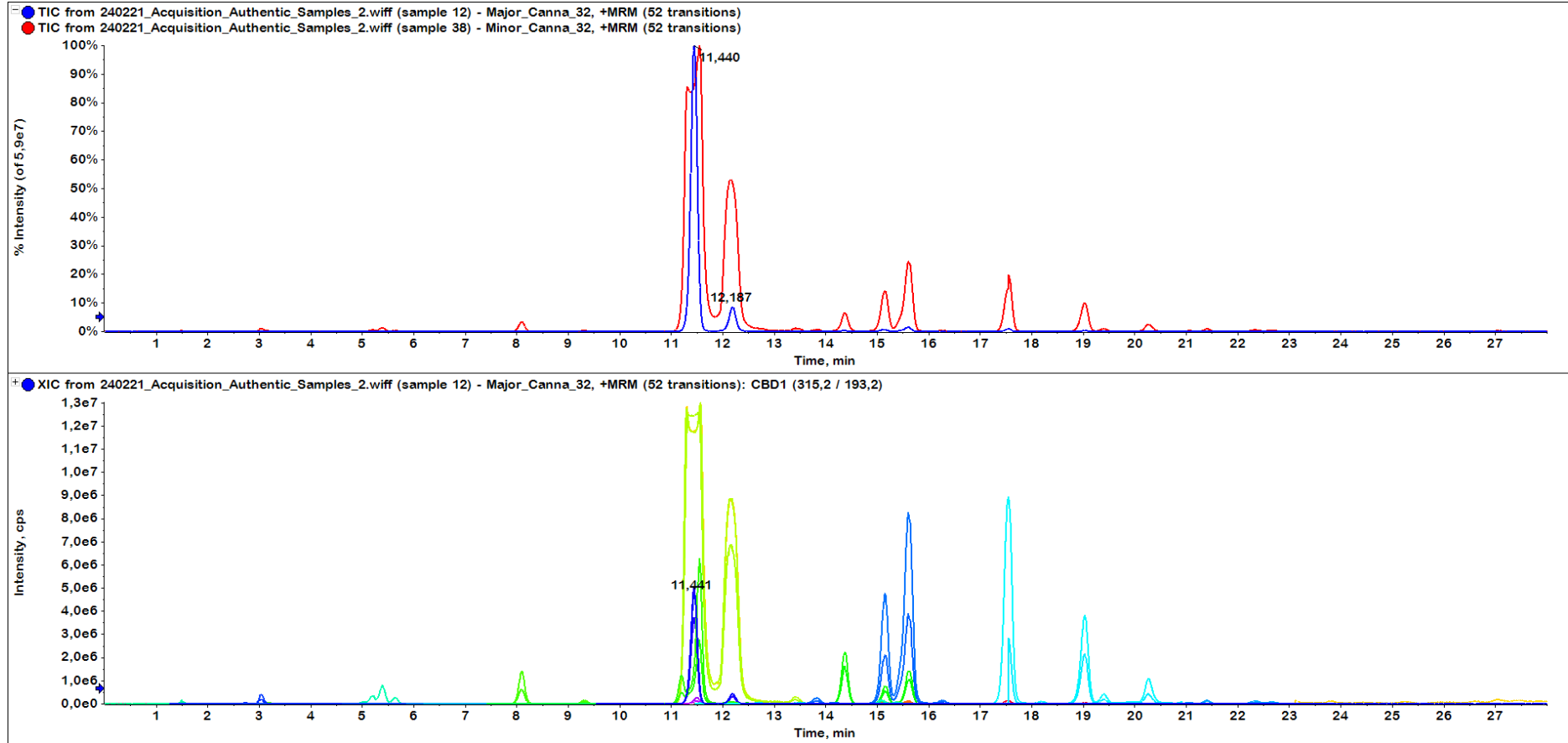
C. sativa L. sample 22



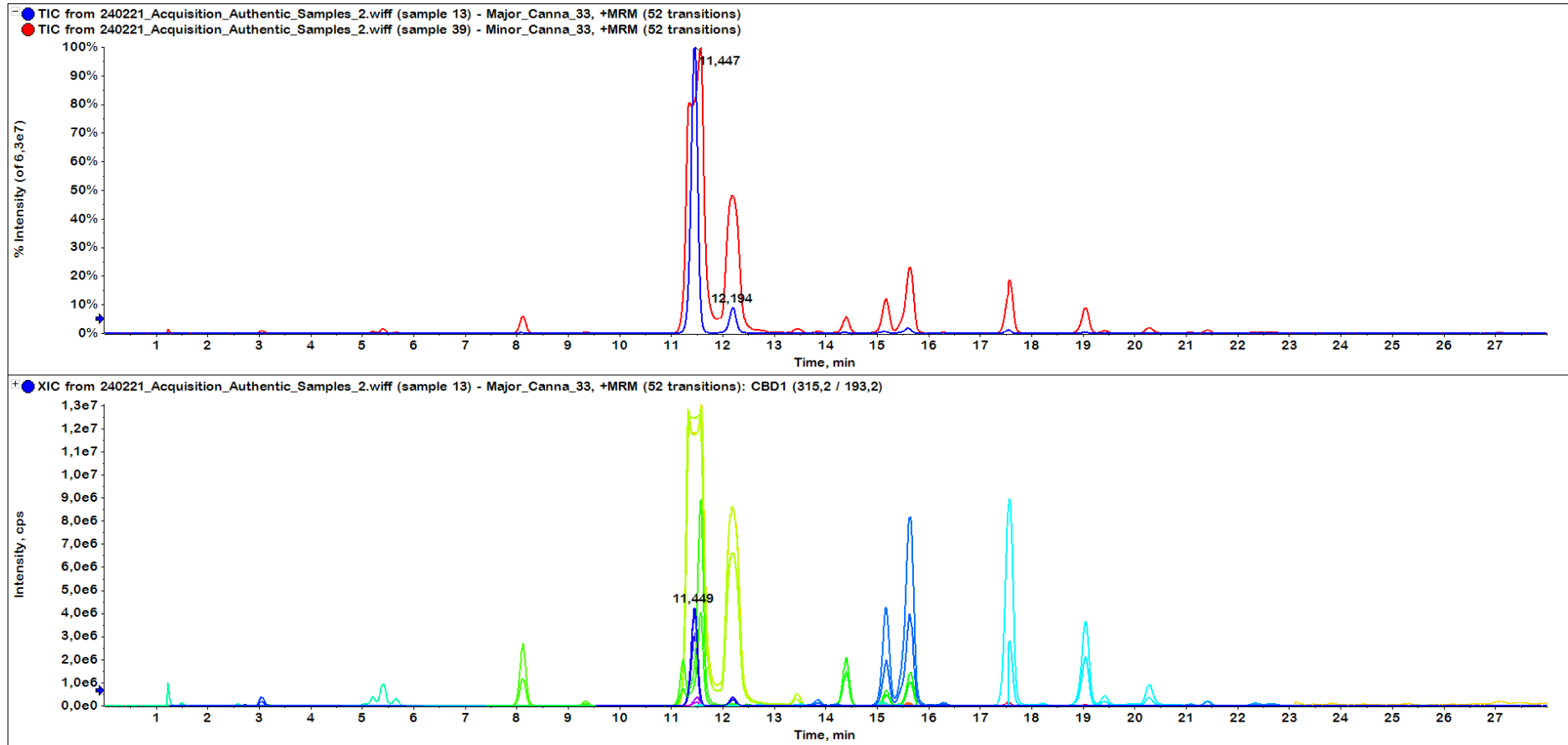
C. sativa L. sample 23



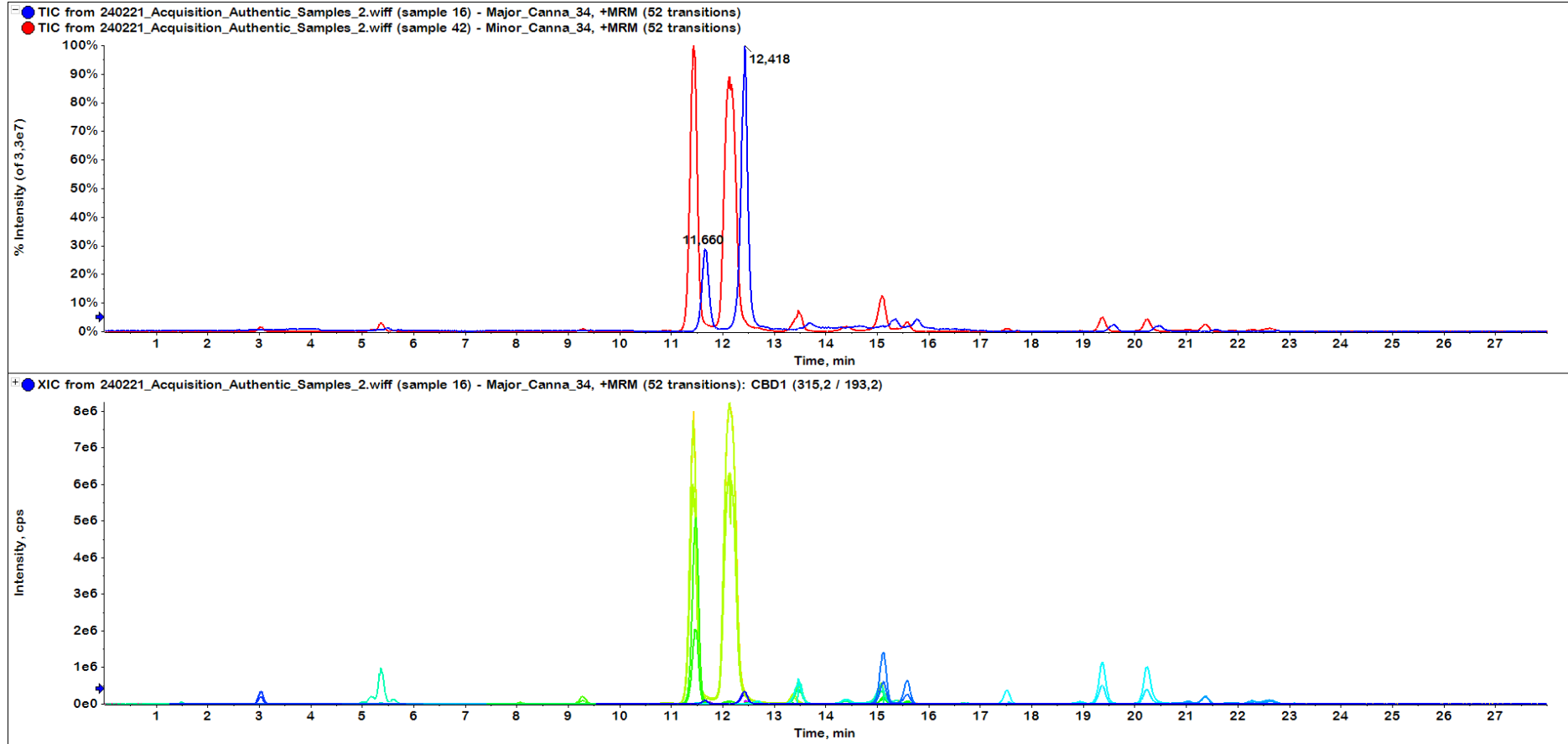
C. sativa L. sample 24



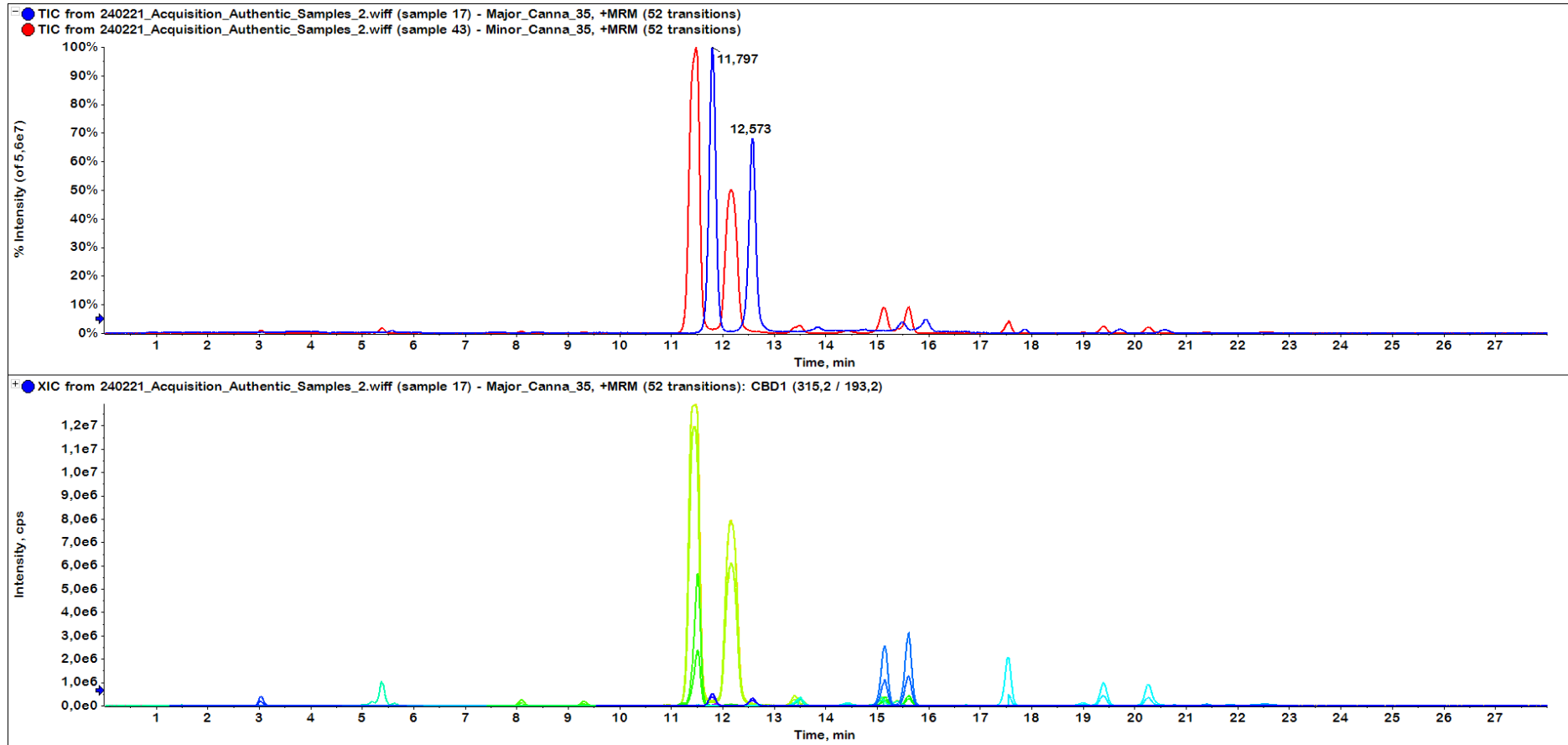
C. sativa L. sample 25



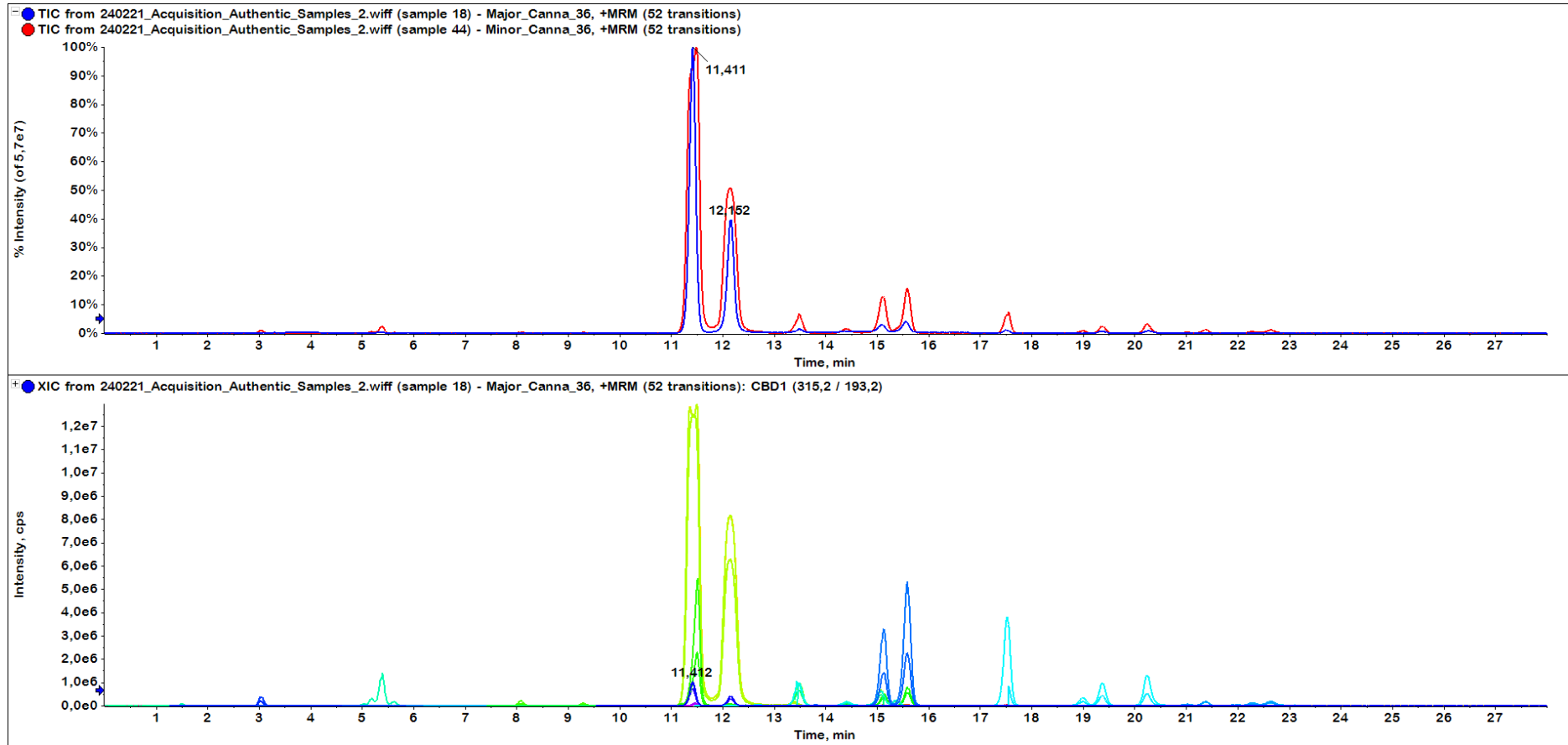
C. sativa L. sample 26



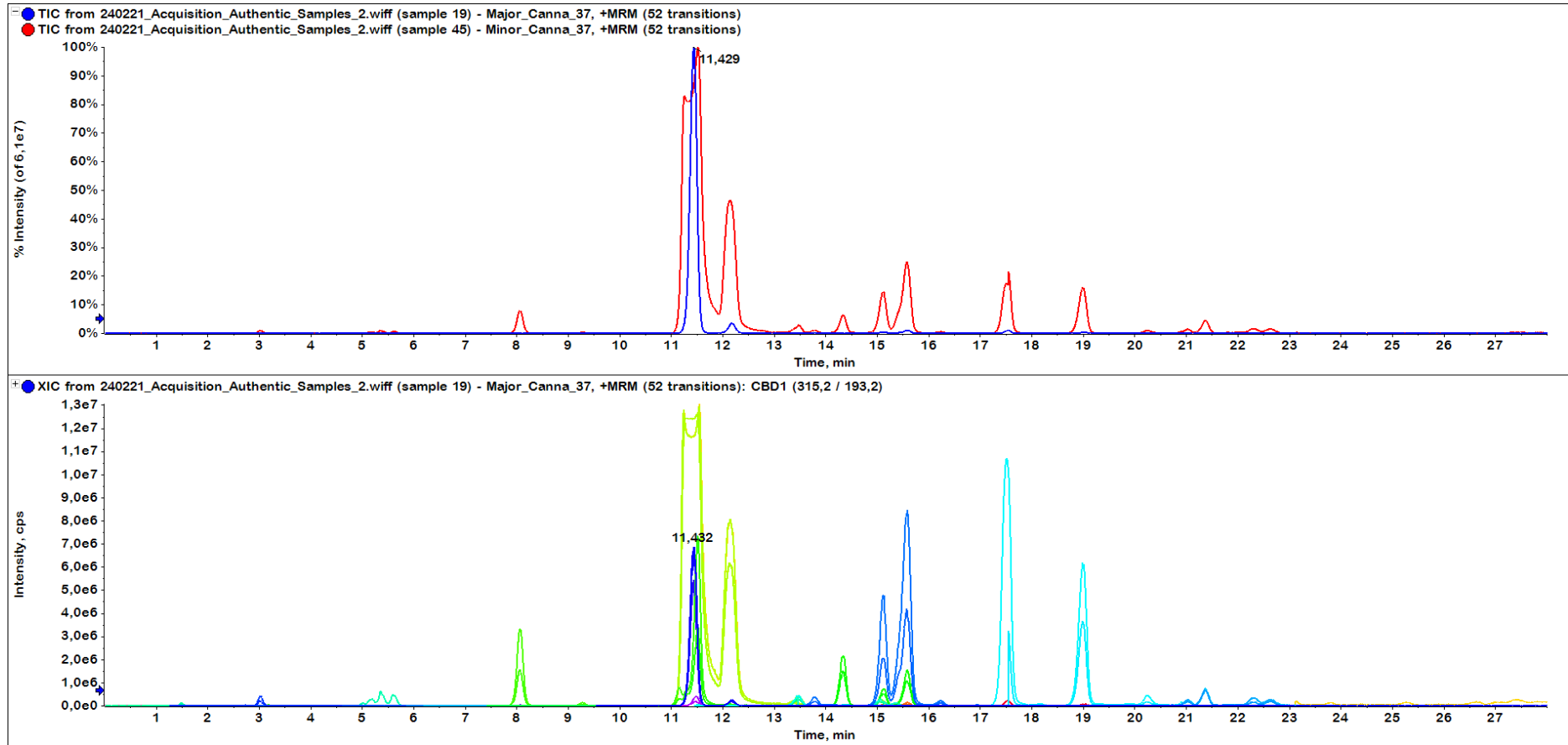
C. sativa L. sample 27



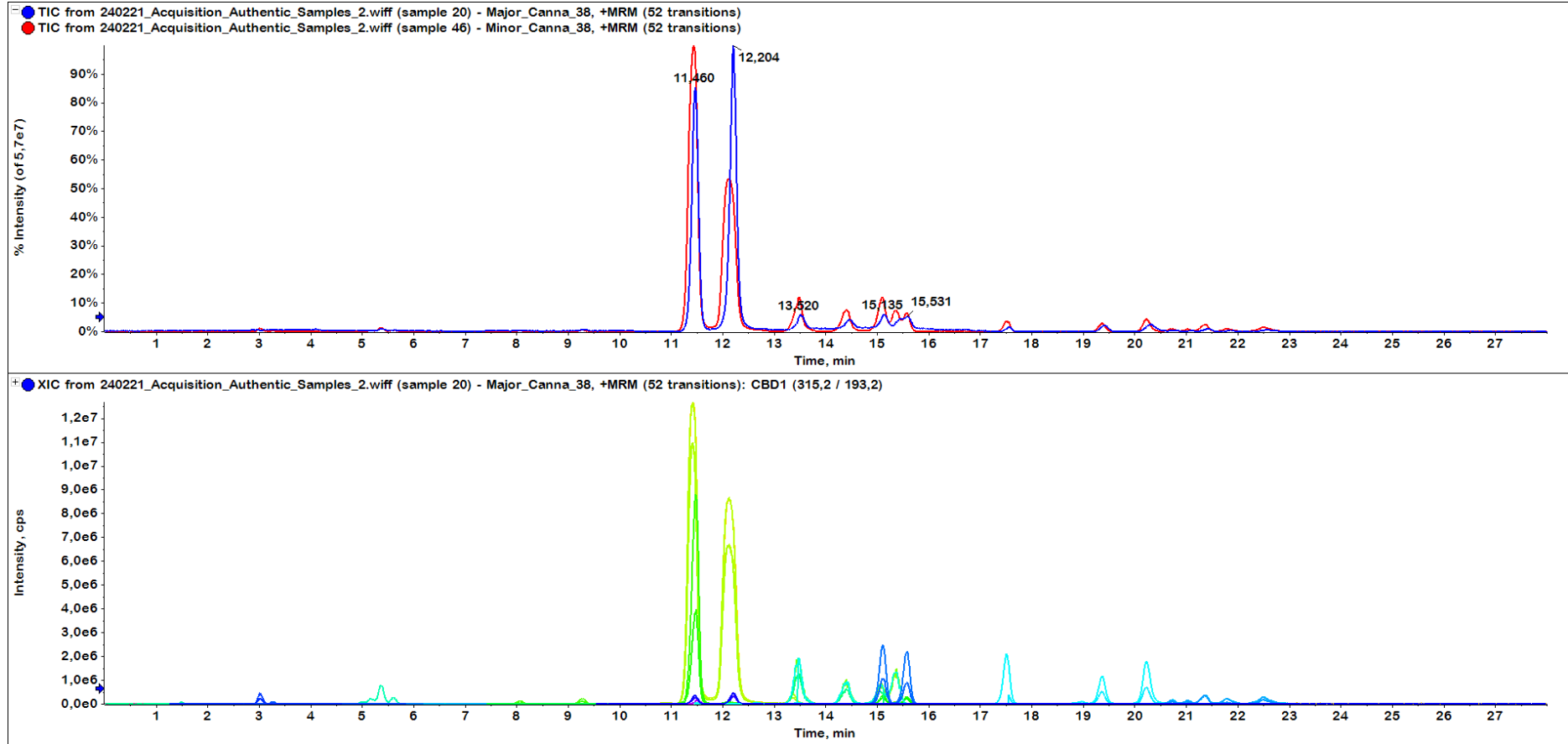
C. sativa L. sample 28



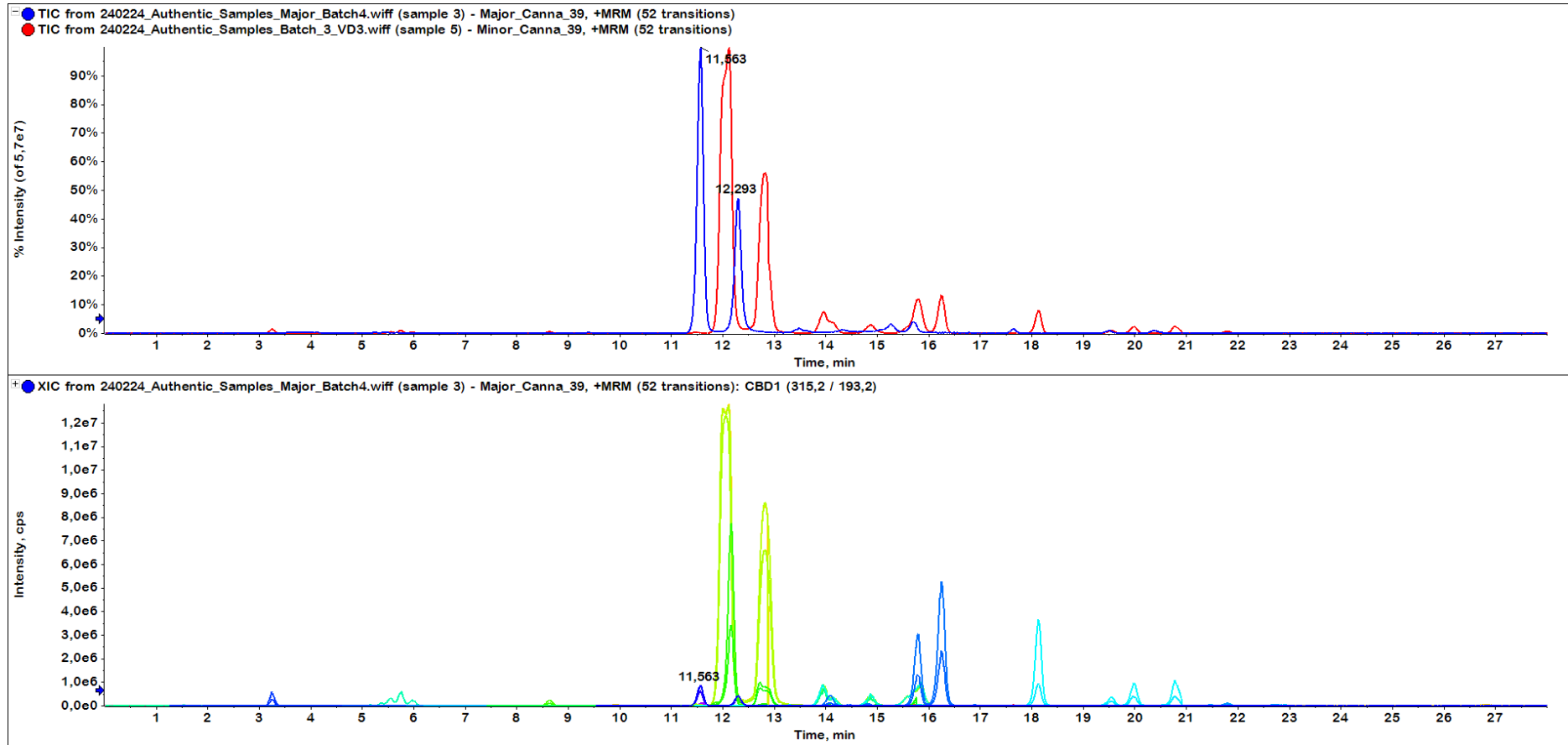
C. sativa L. sample 29



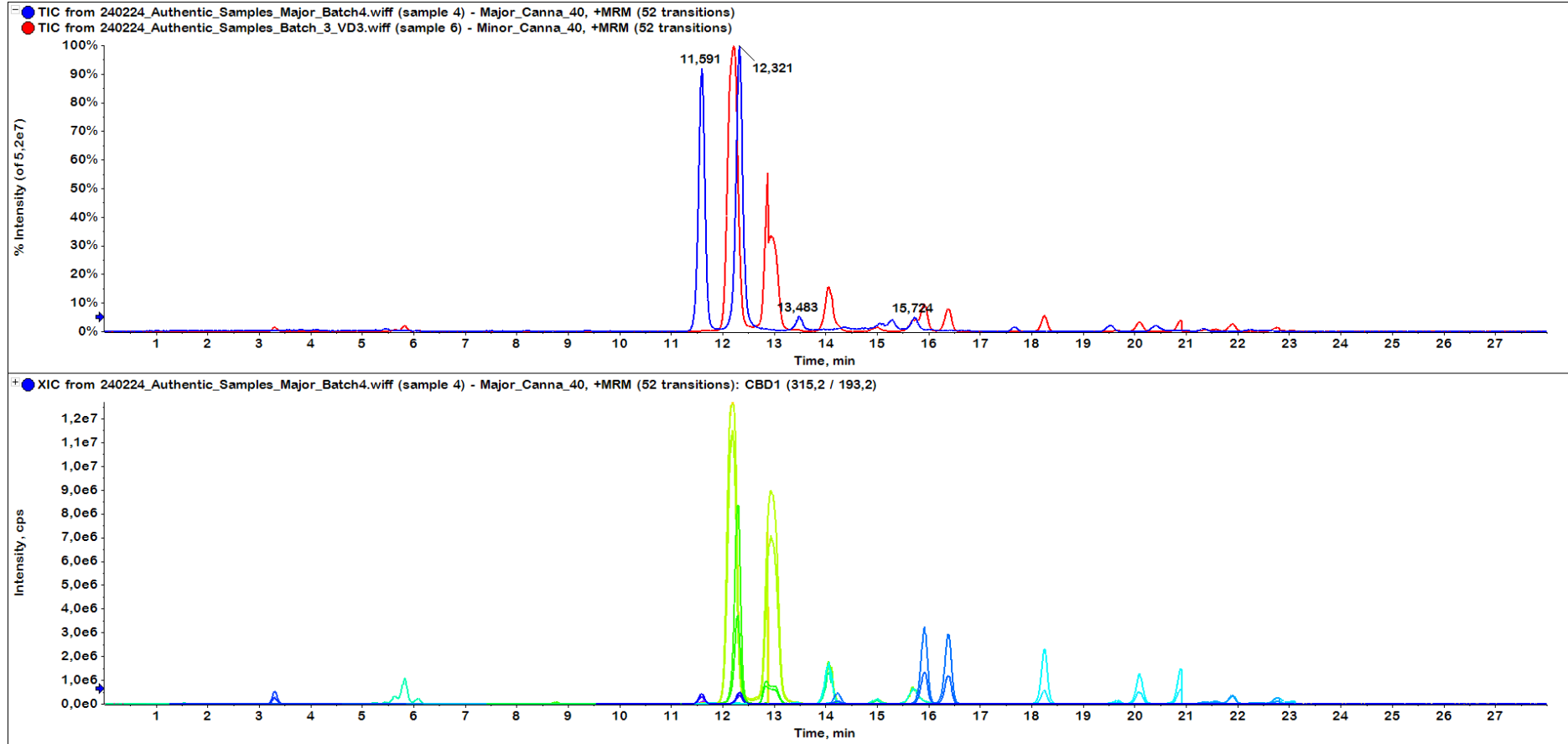
C. sativa L. sample 30



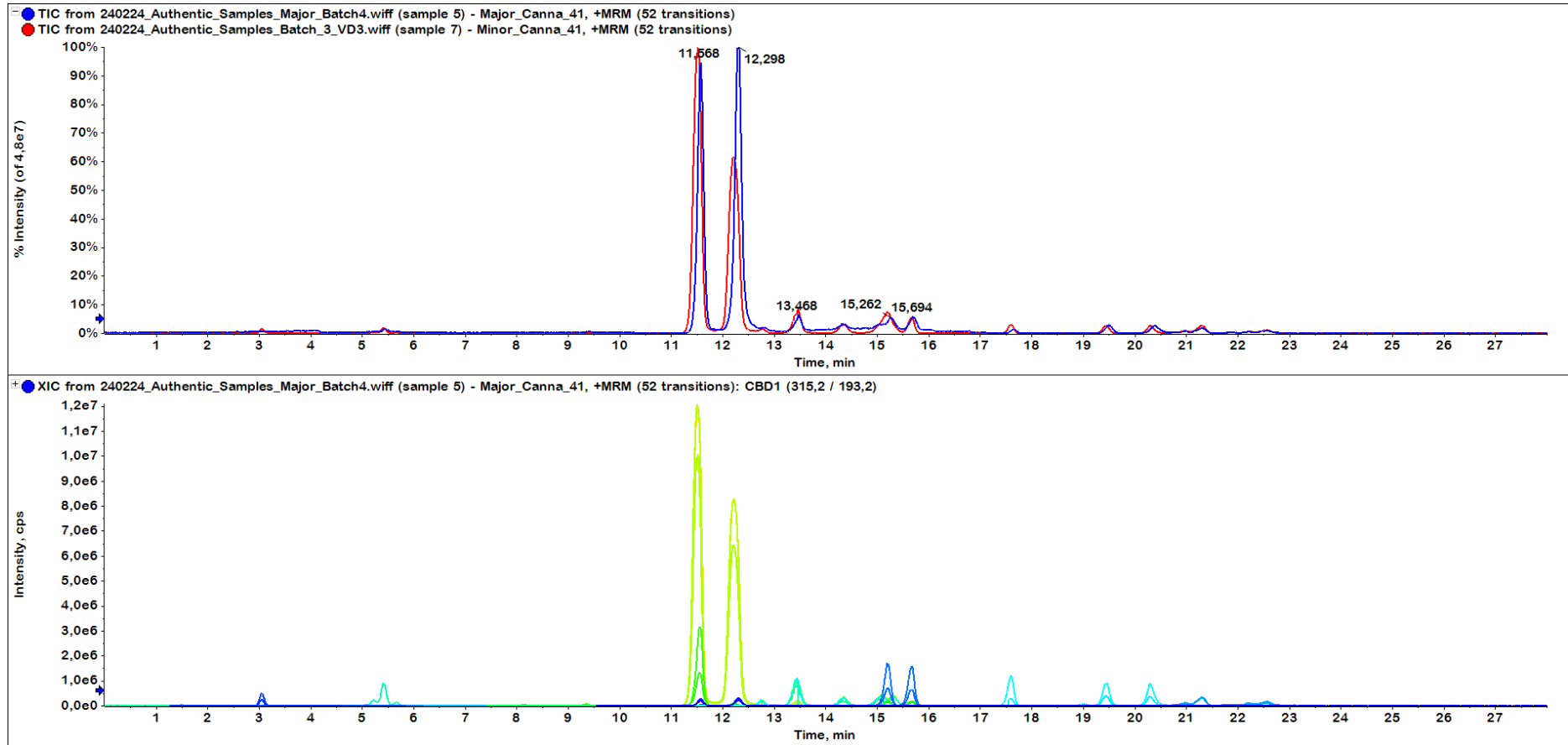
C. sativa L. sample 31



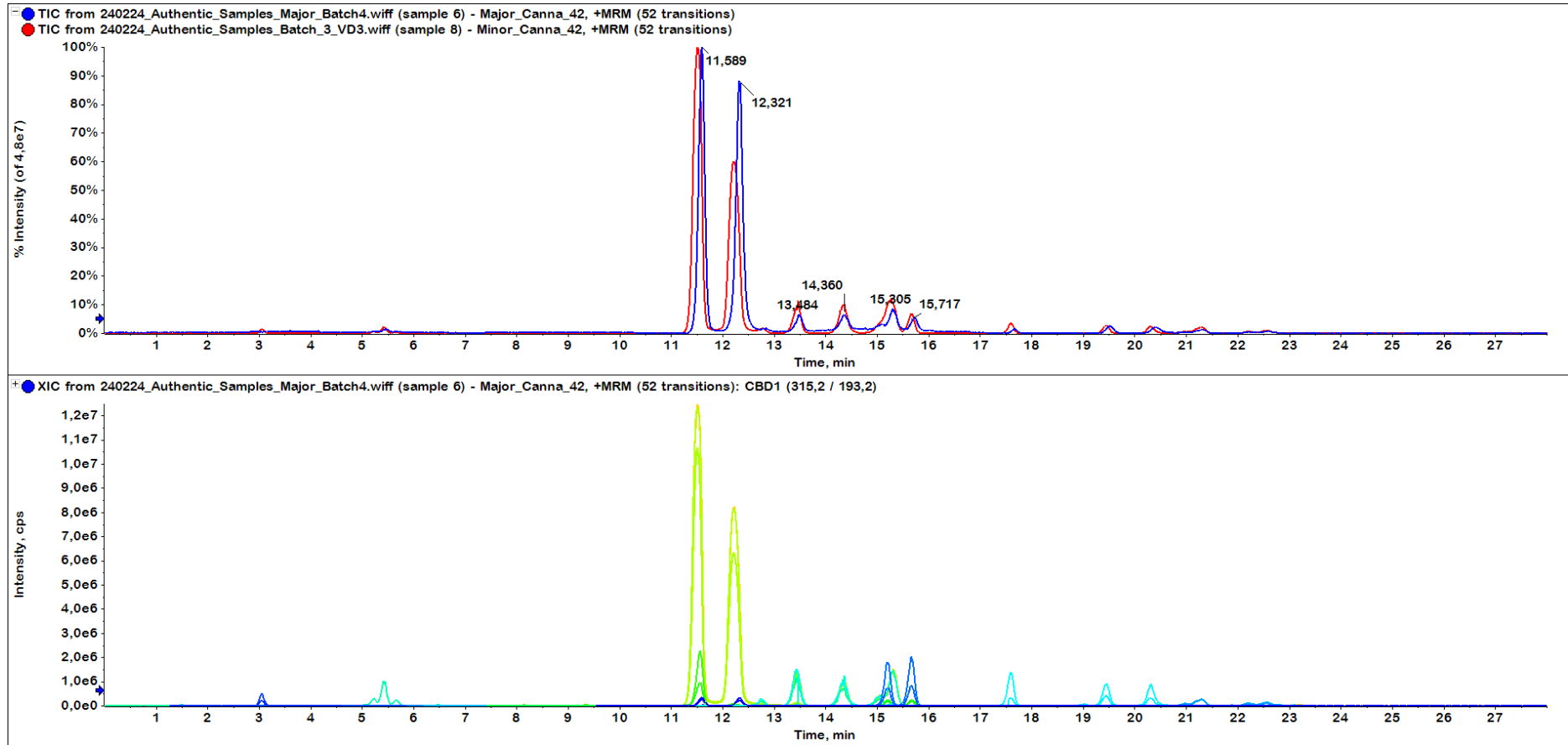
C. sativa L. sample 32



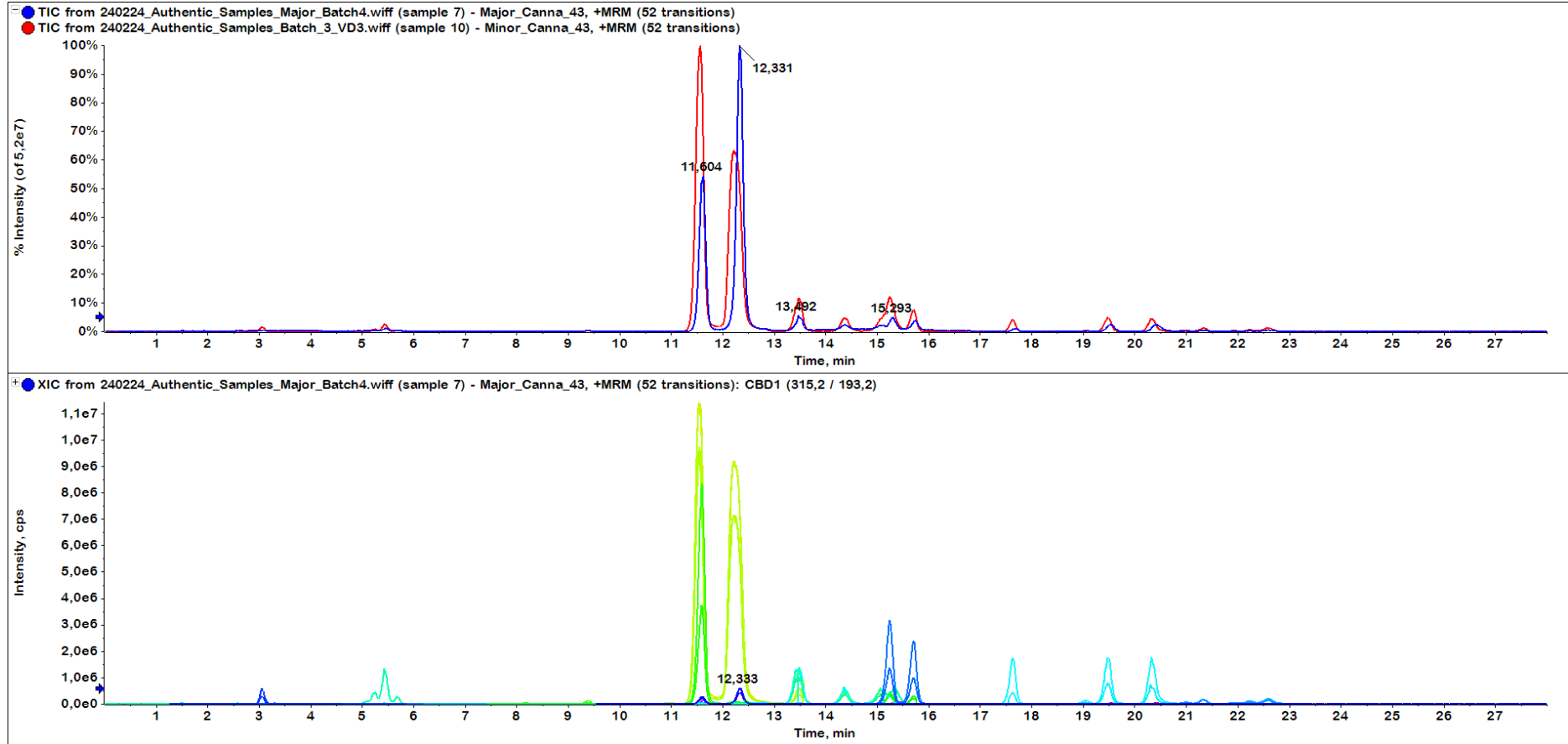
C. sativa L. sample 33



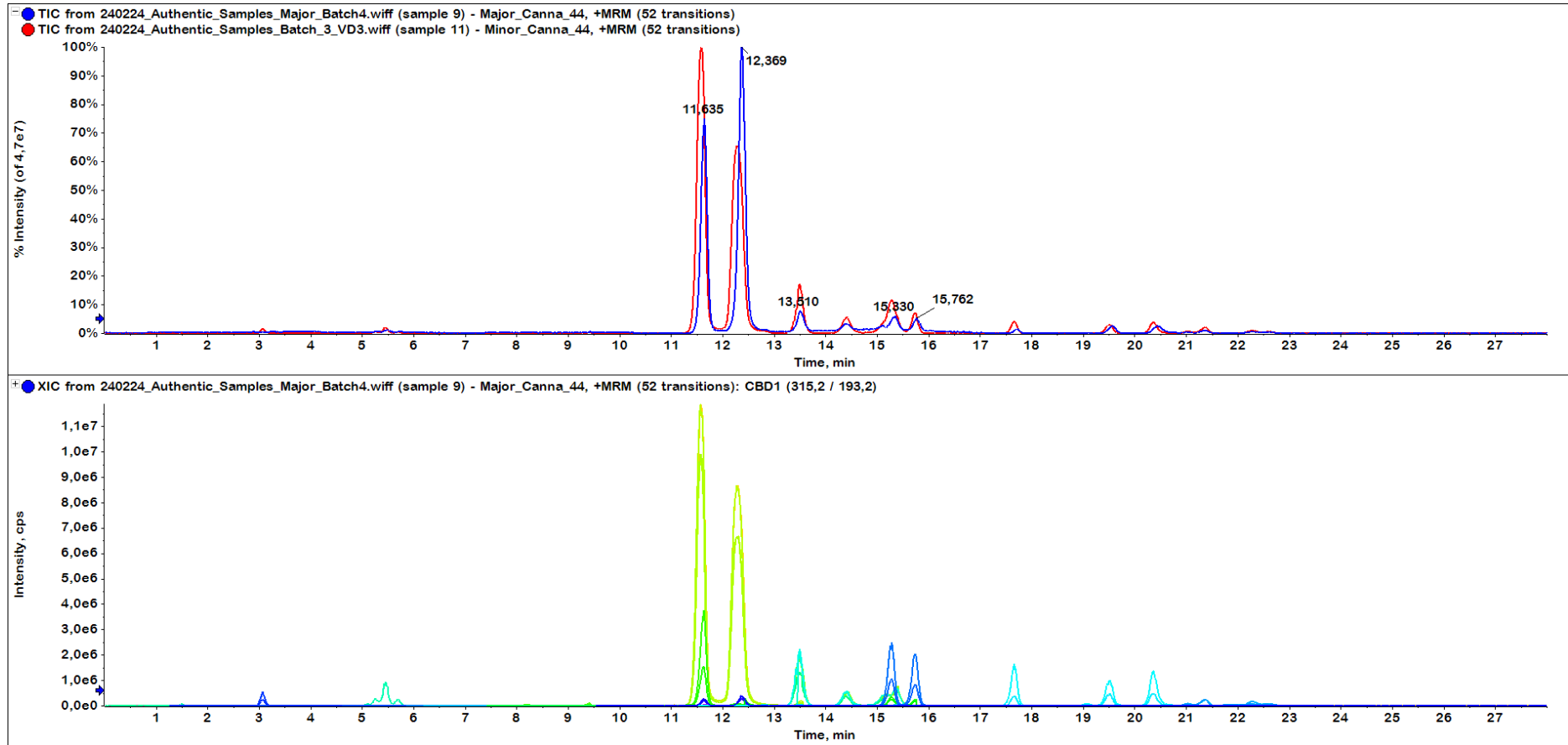
C. sativa L. sample 34



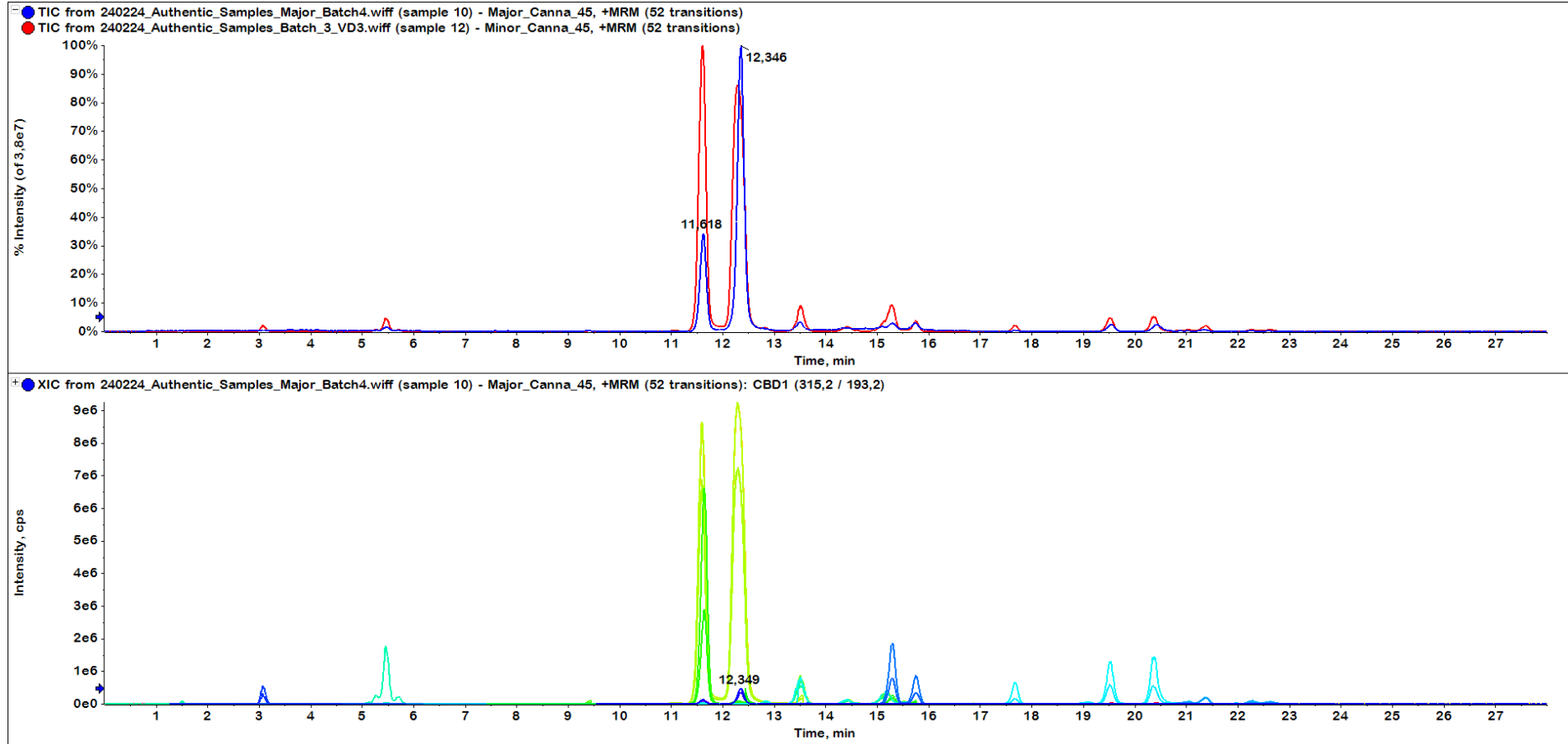
C. sativa L. sample 35



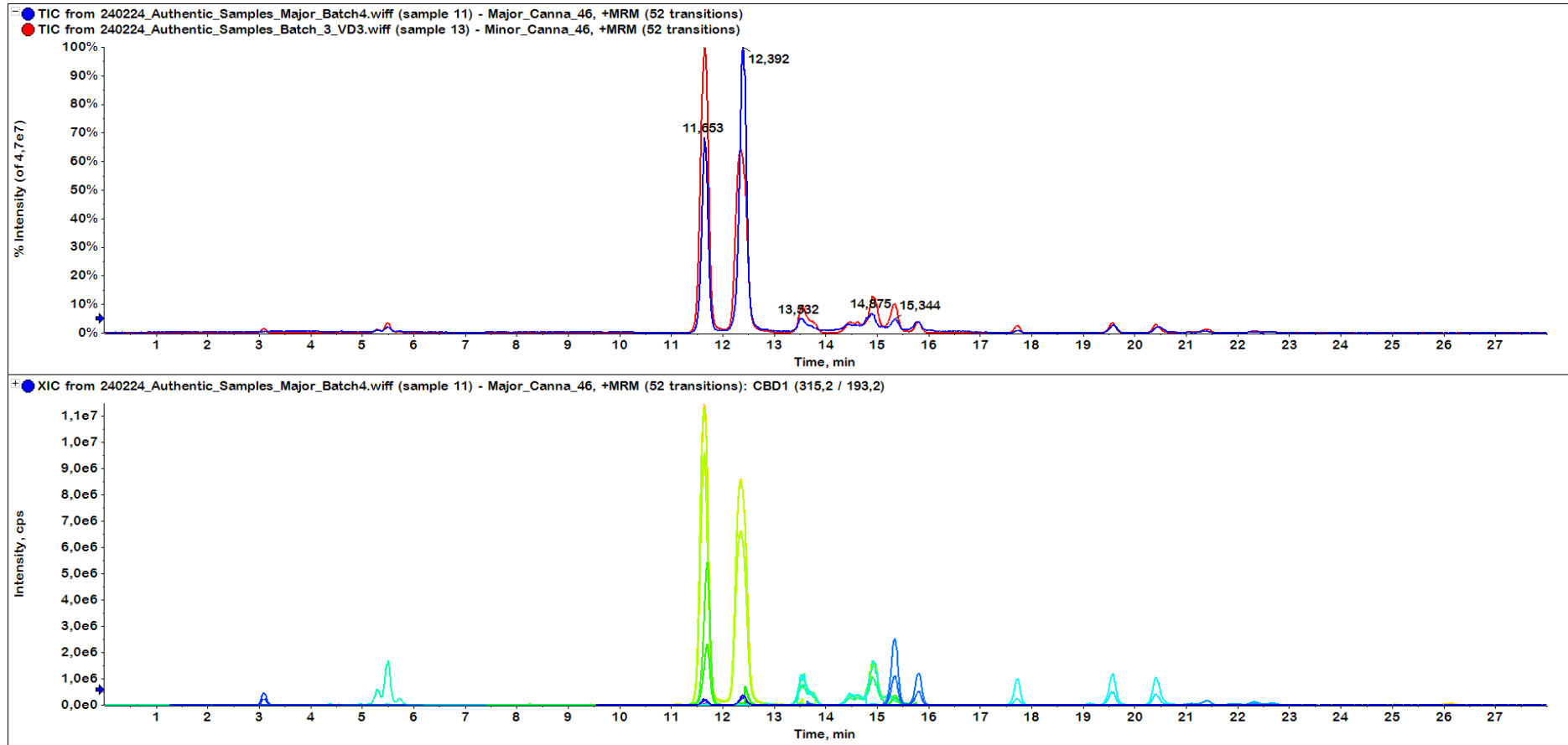
C. sativa L. sample 36



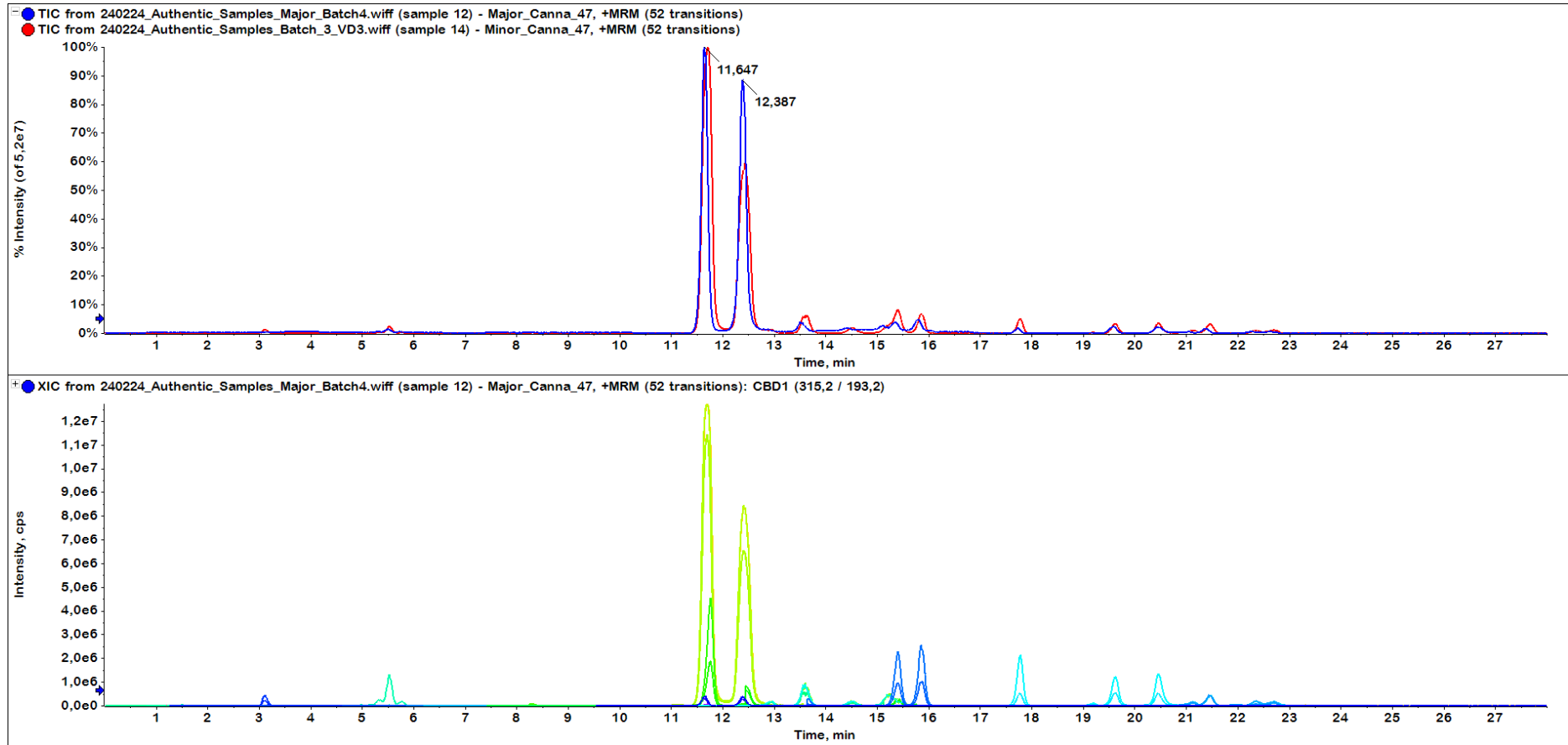
C. sativa L. sample 37



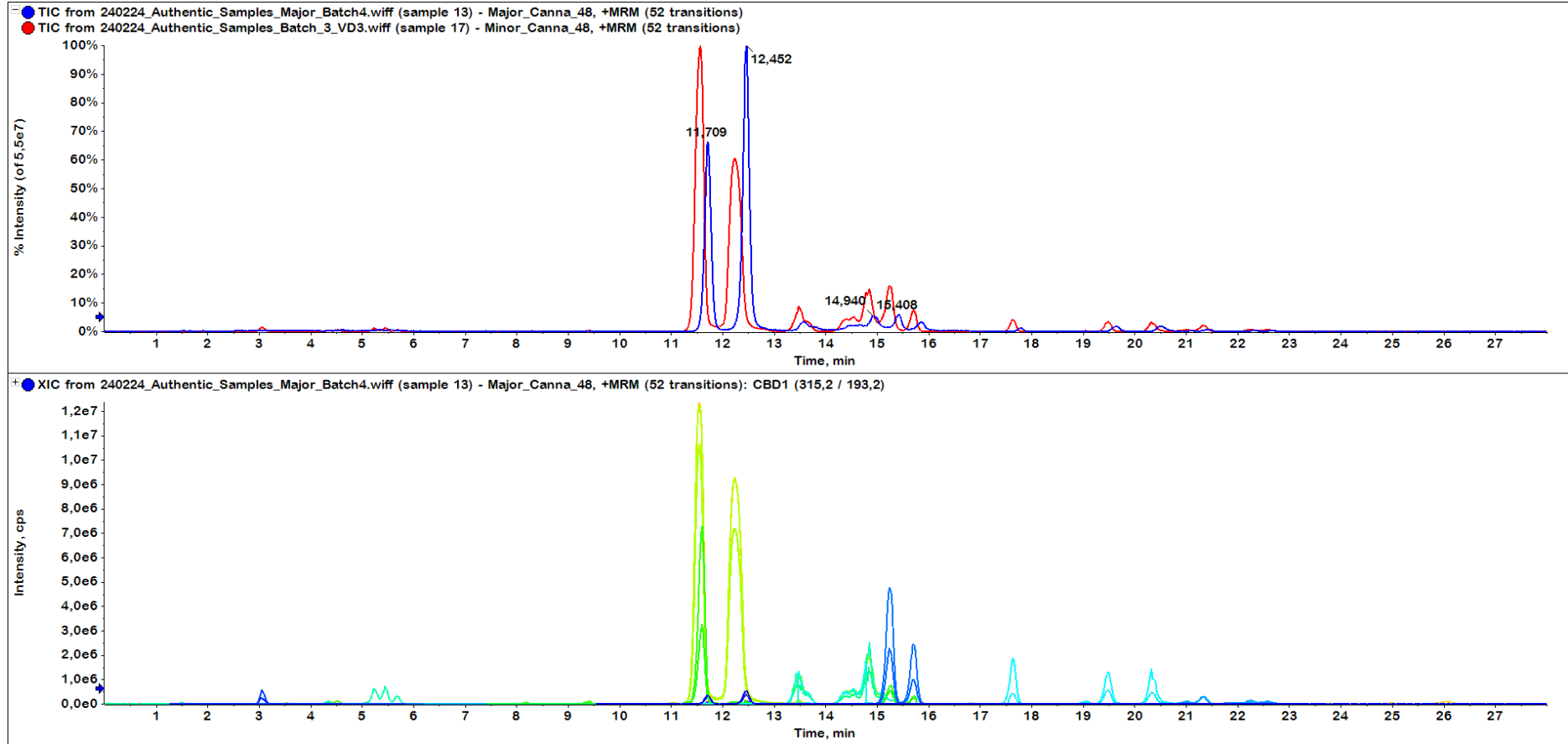
C. sativa L. sample 38



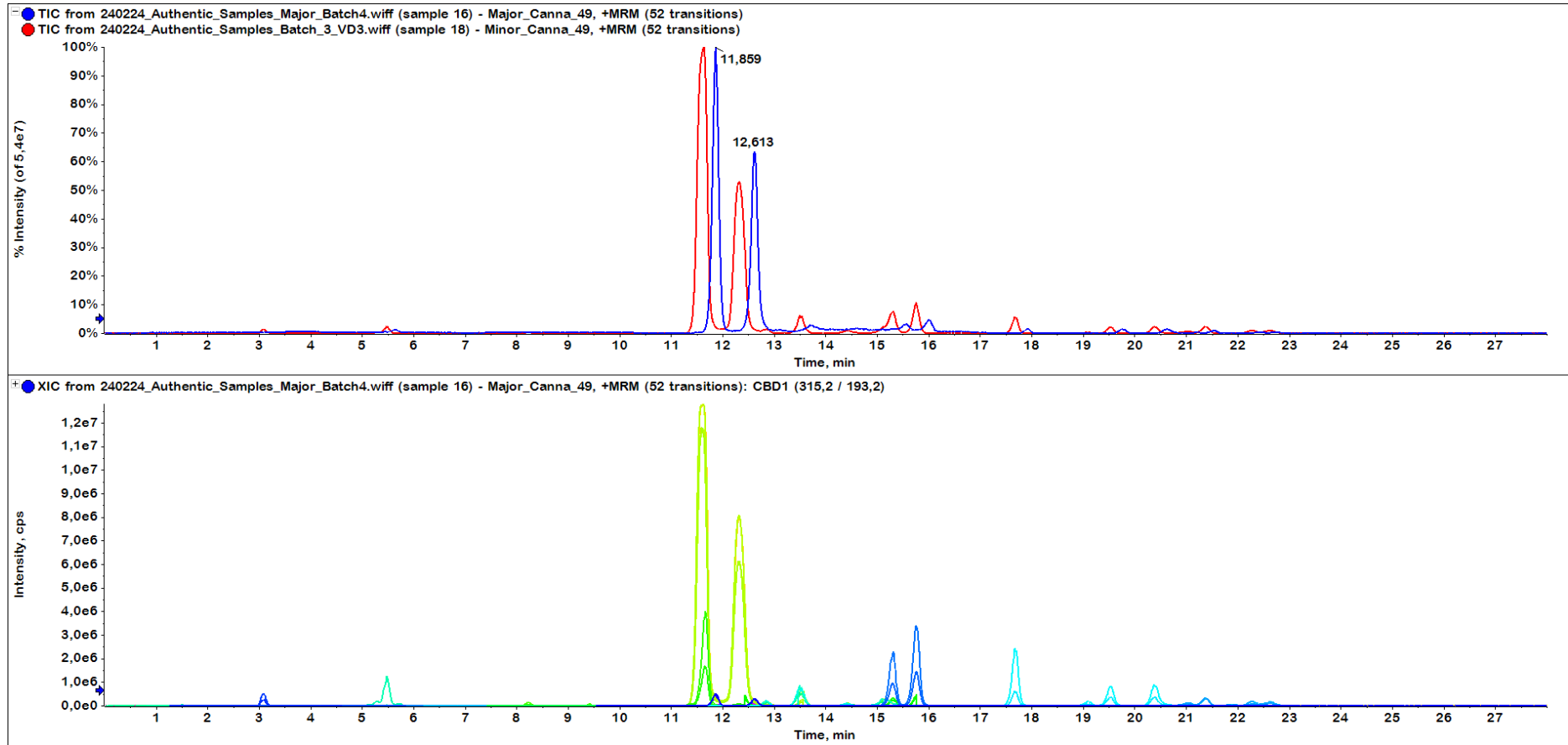
C. sativa L. sample 39



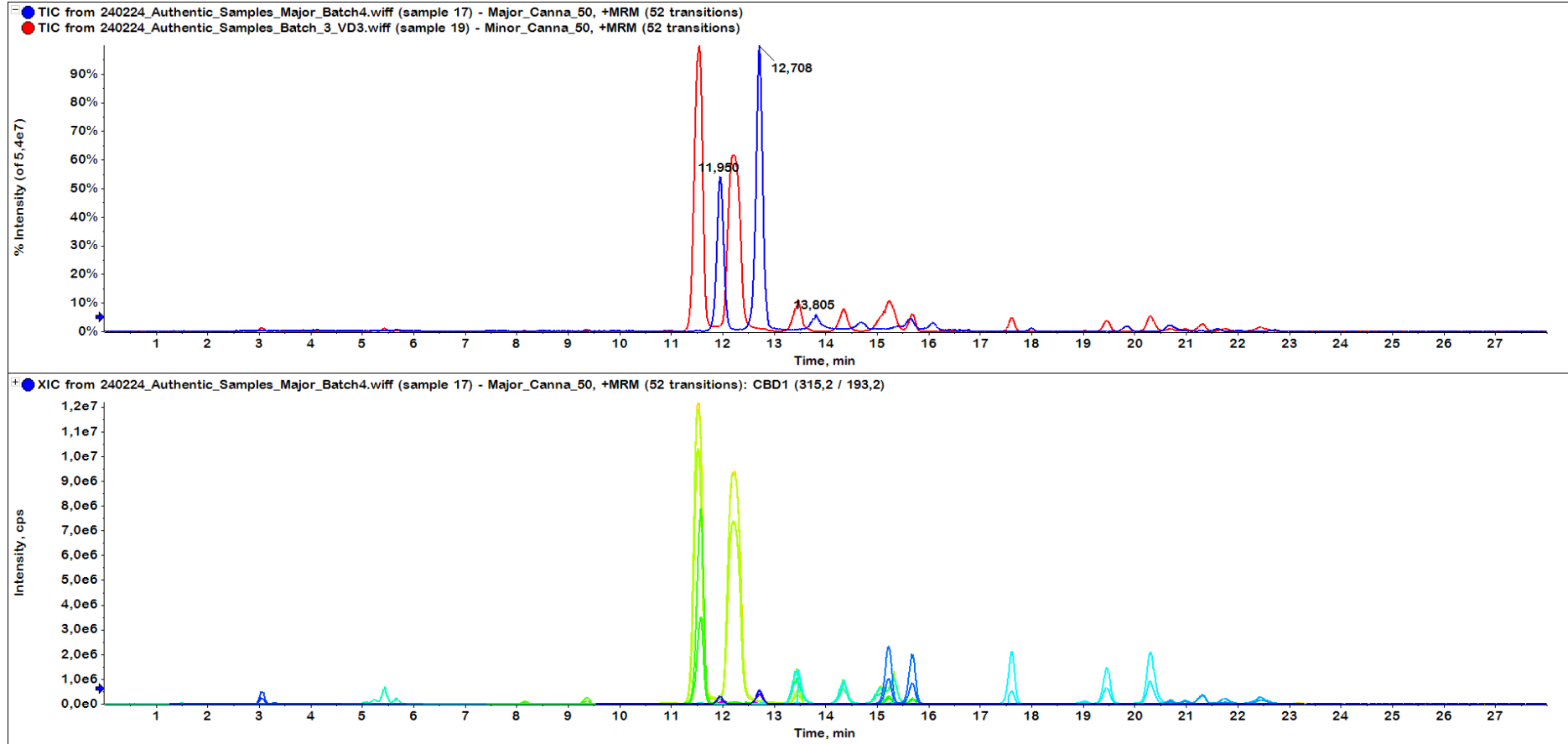
C. sativa L. sample 40



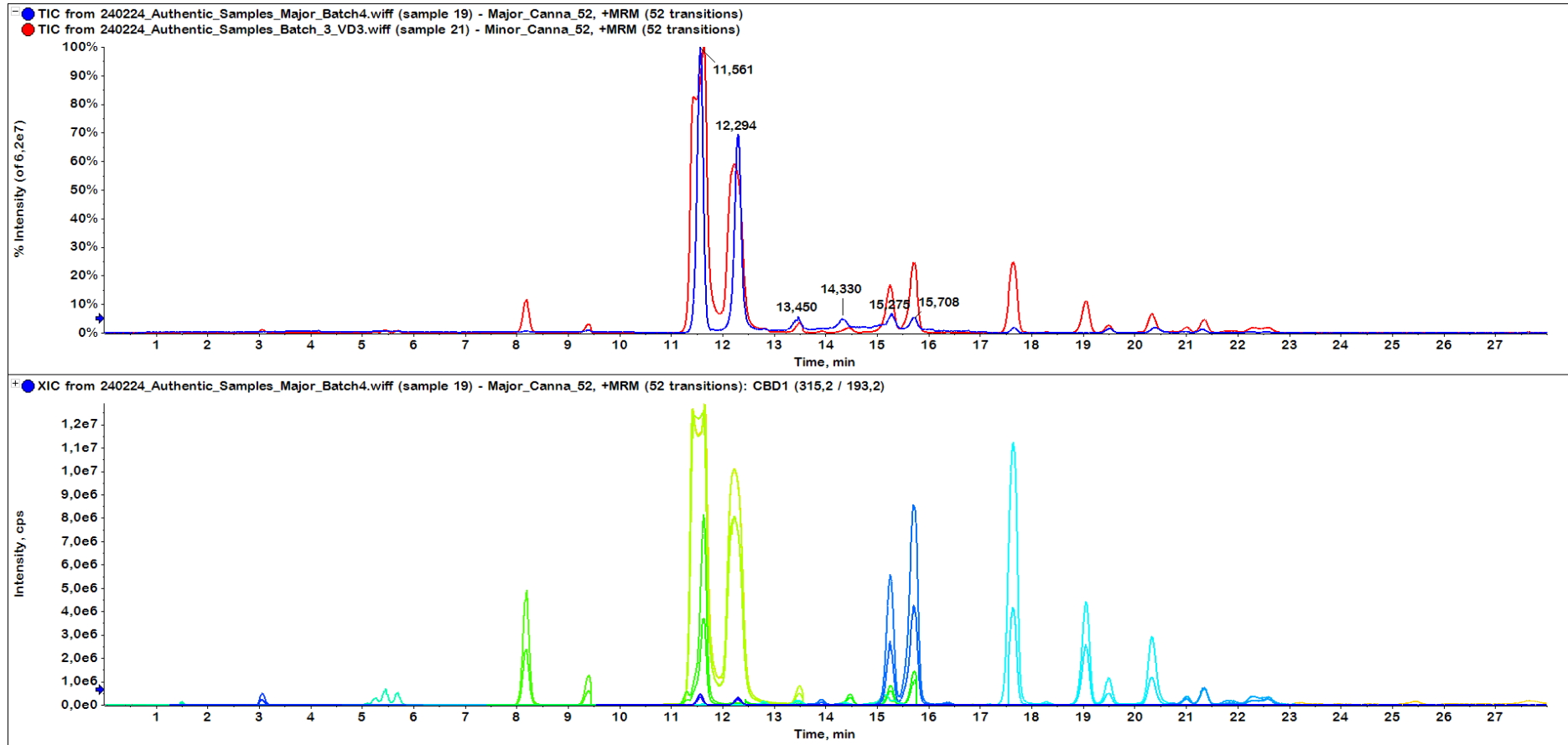
C. sativa L. sample 41



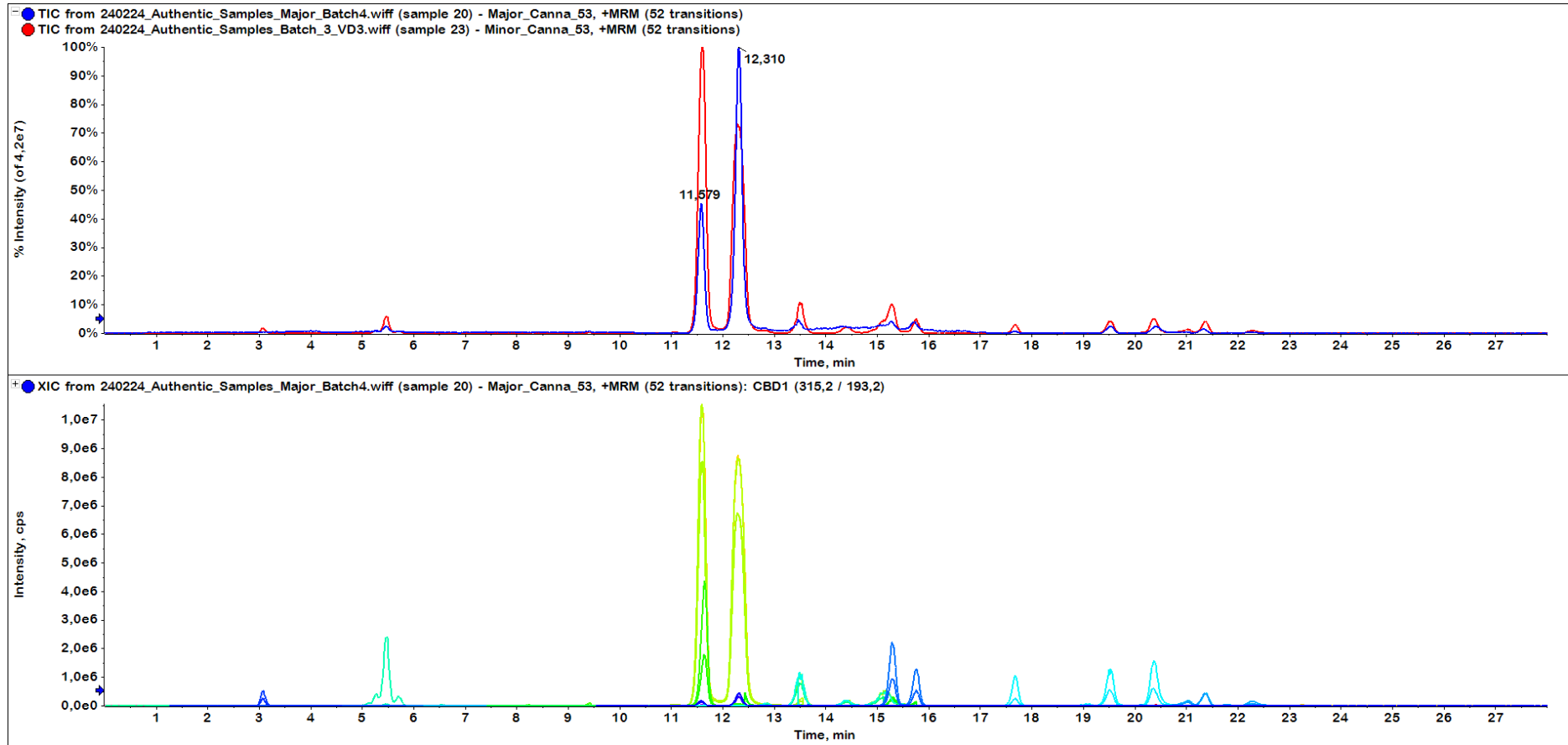
C. sativa L. sample 42



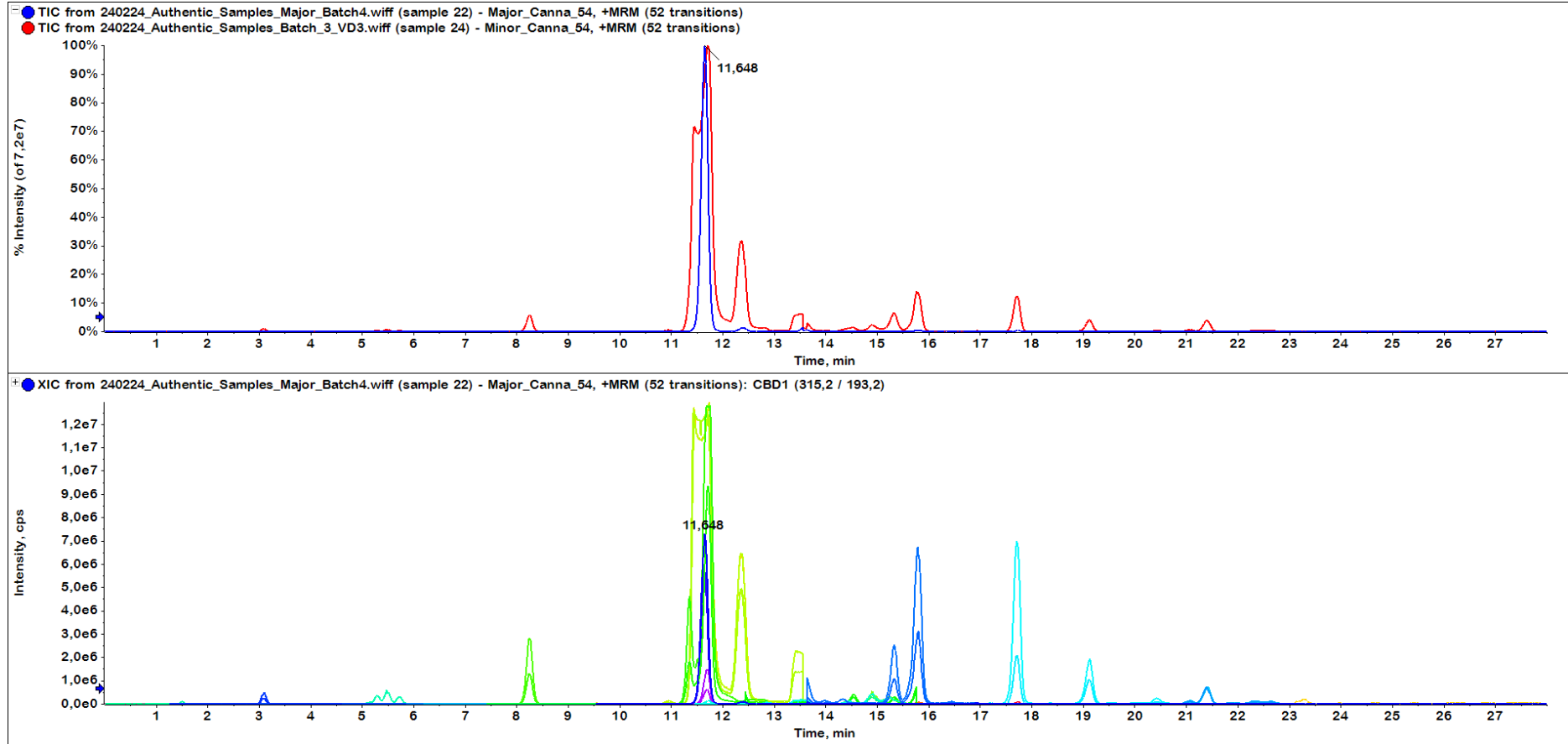
C. sativa L. sample 43



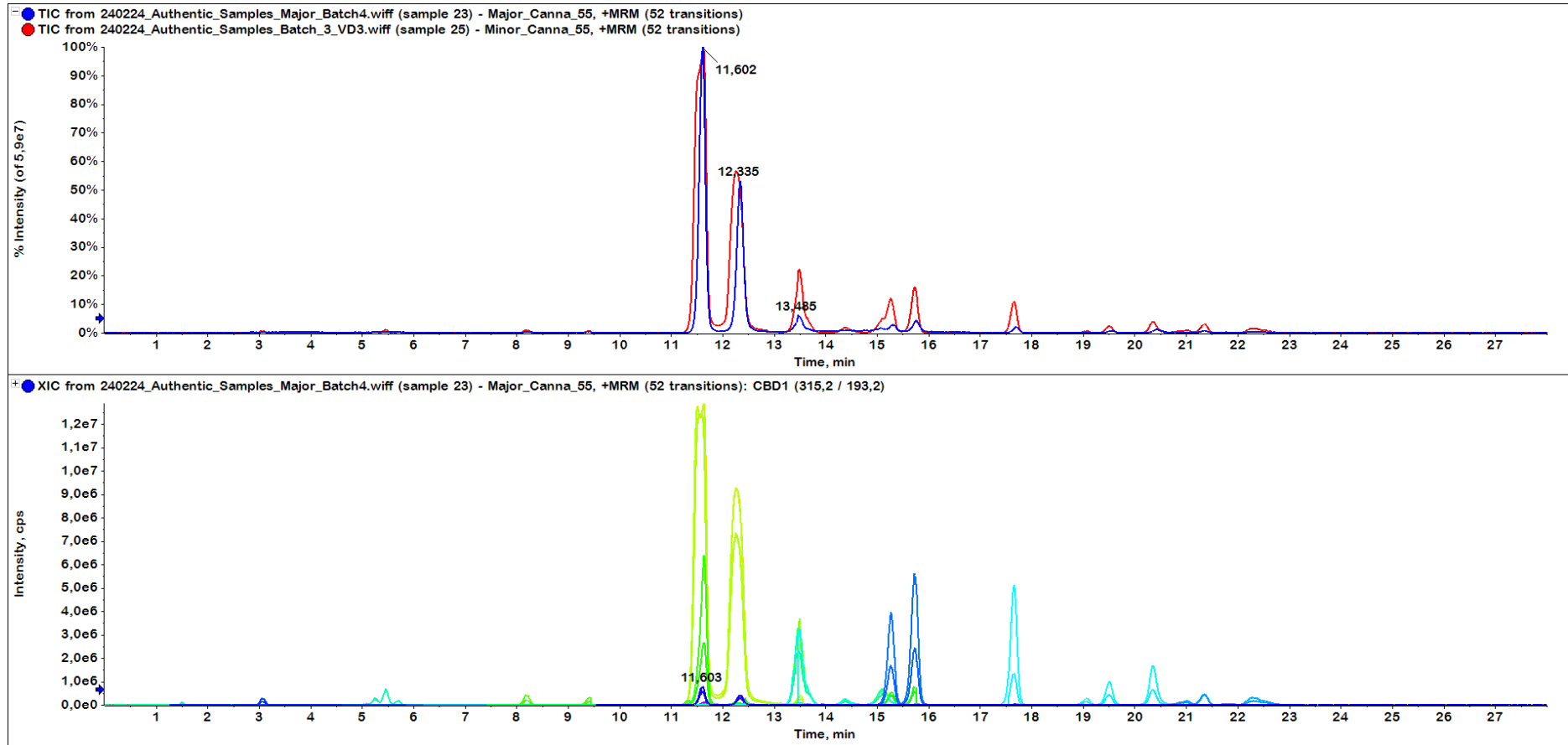
C. sativa L. sample 44



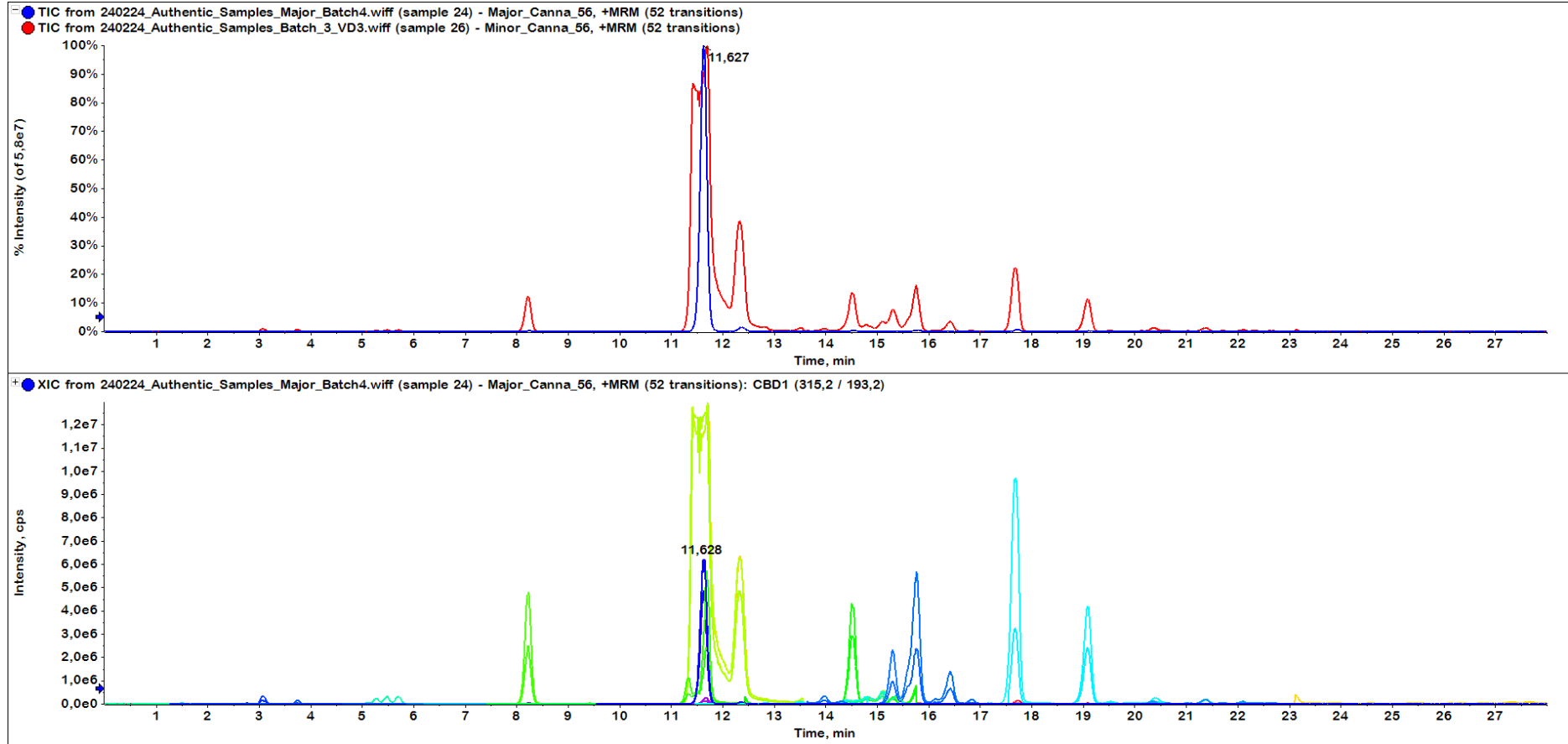
C. sativa L. sample 45



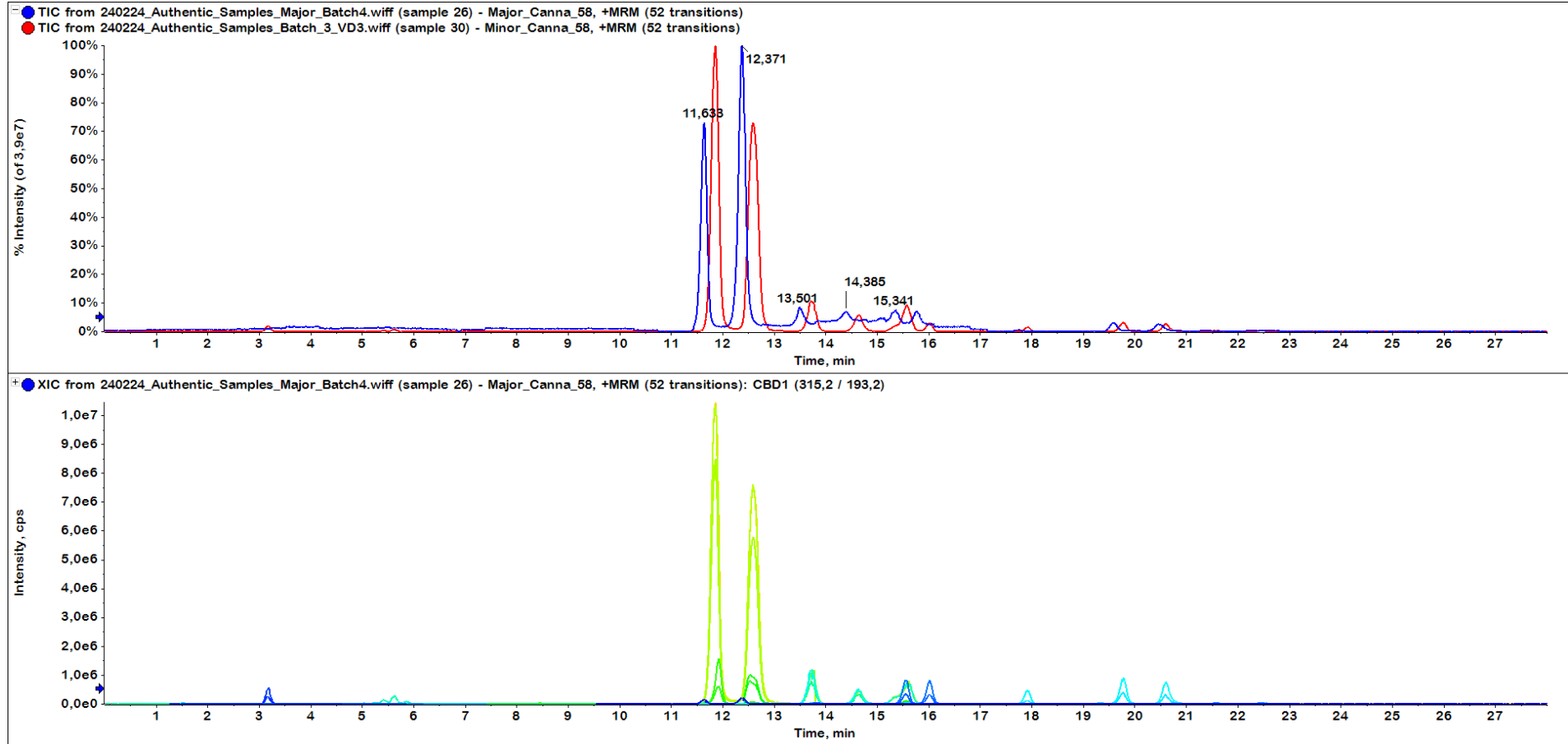
C. sativa L. sample 46



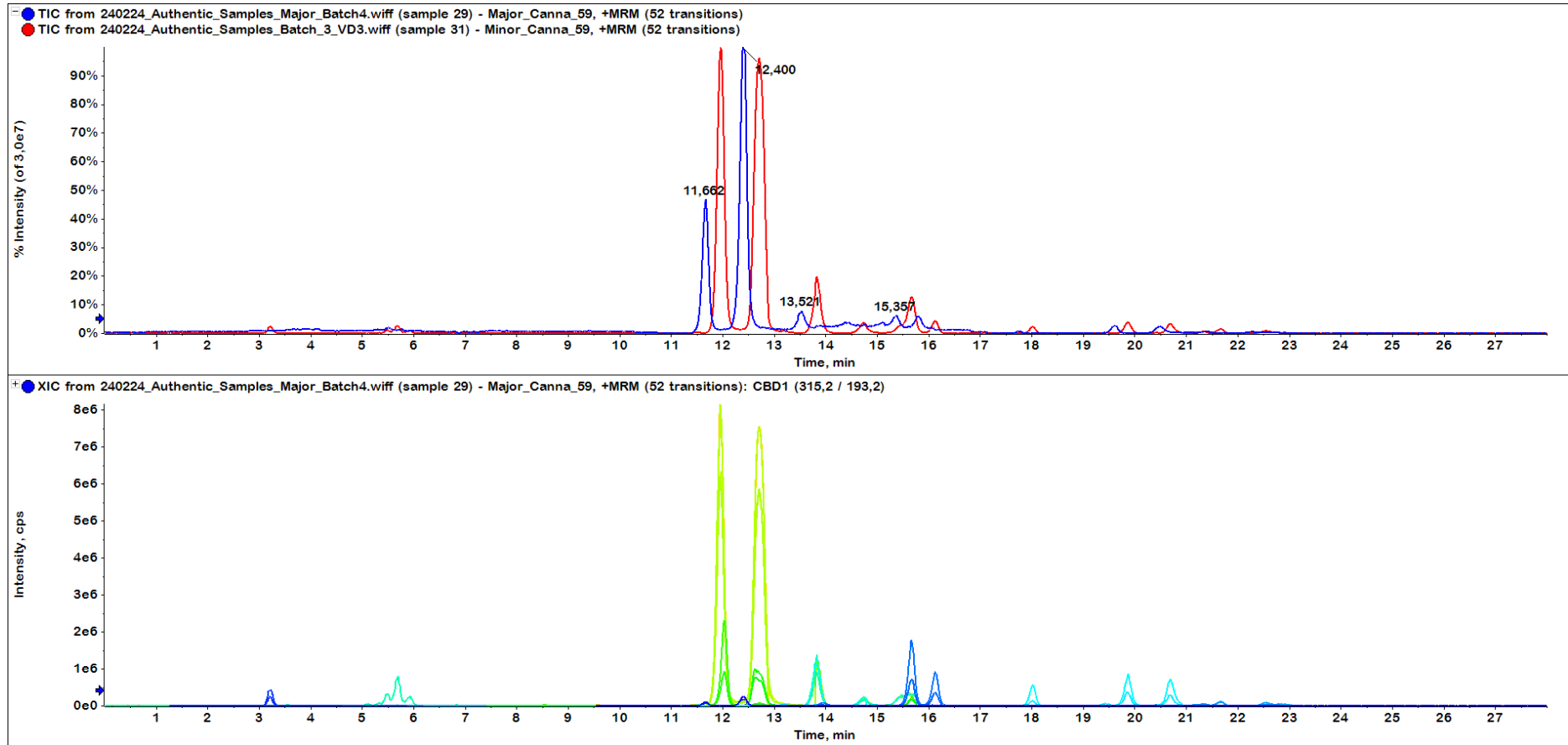
C. sativa L. sample 47



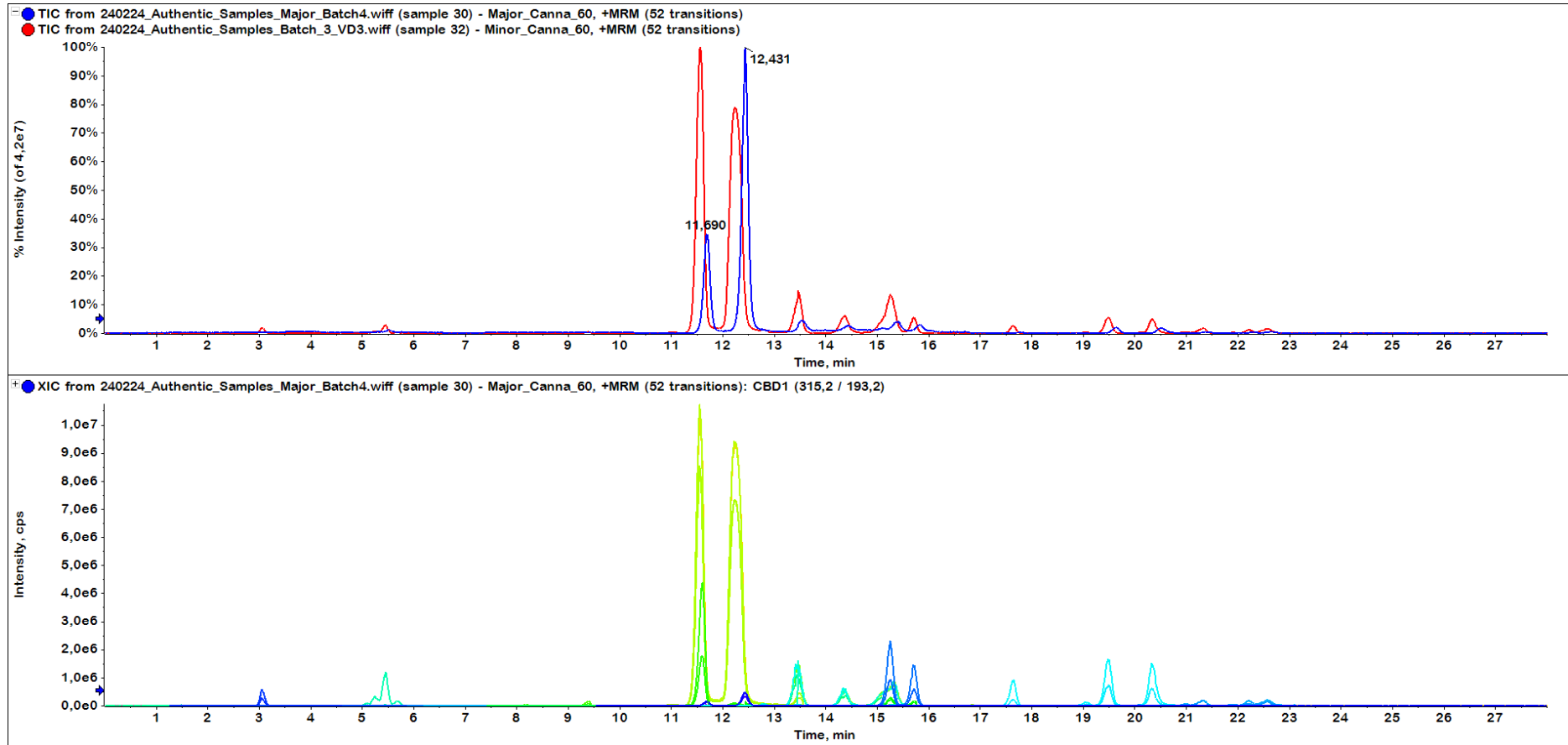
C. sativa L. sample 48



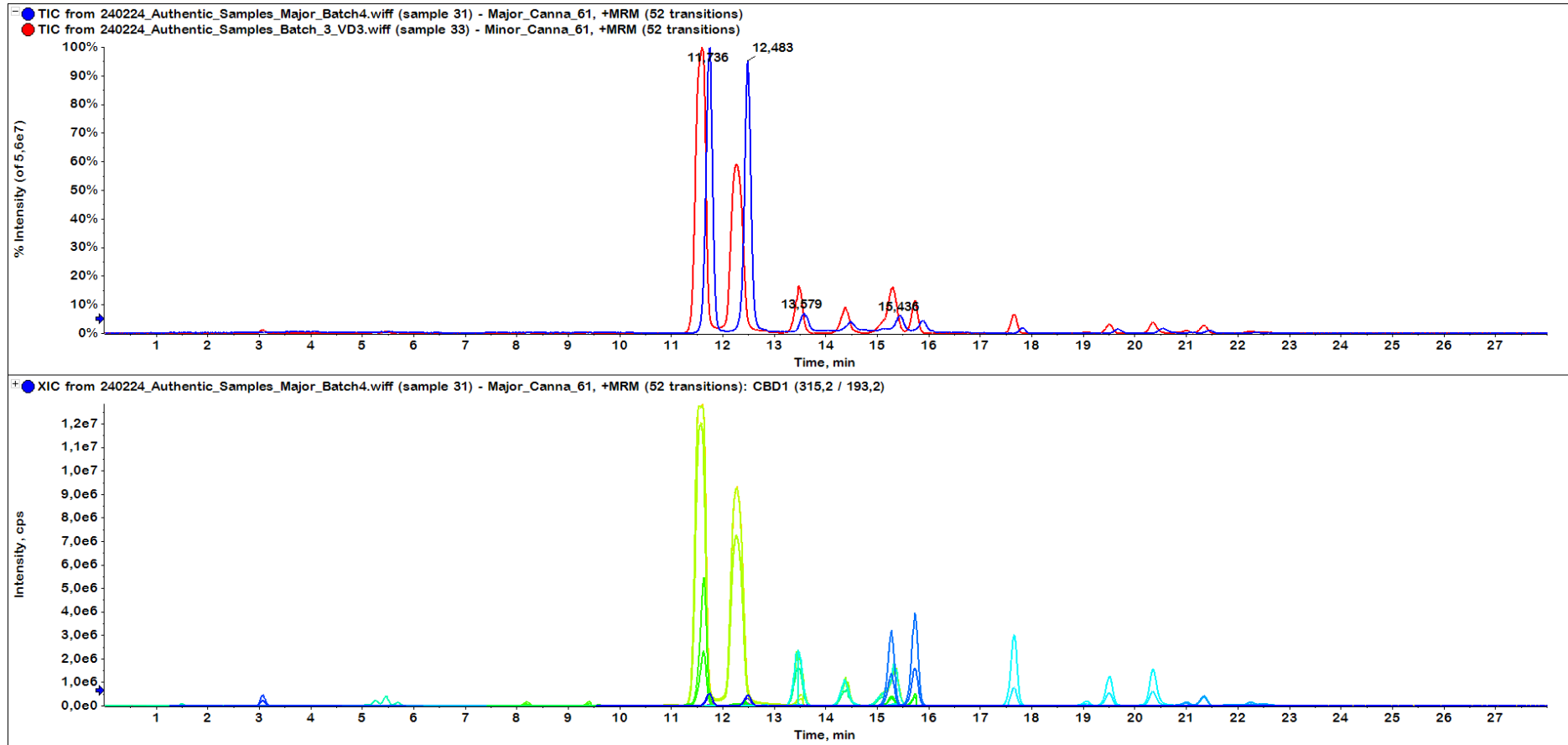
C. sativa L. sample 49



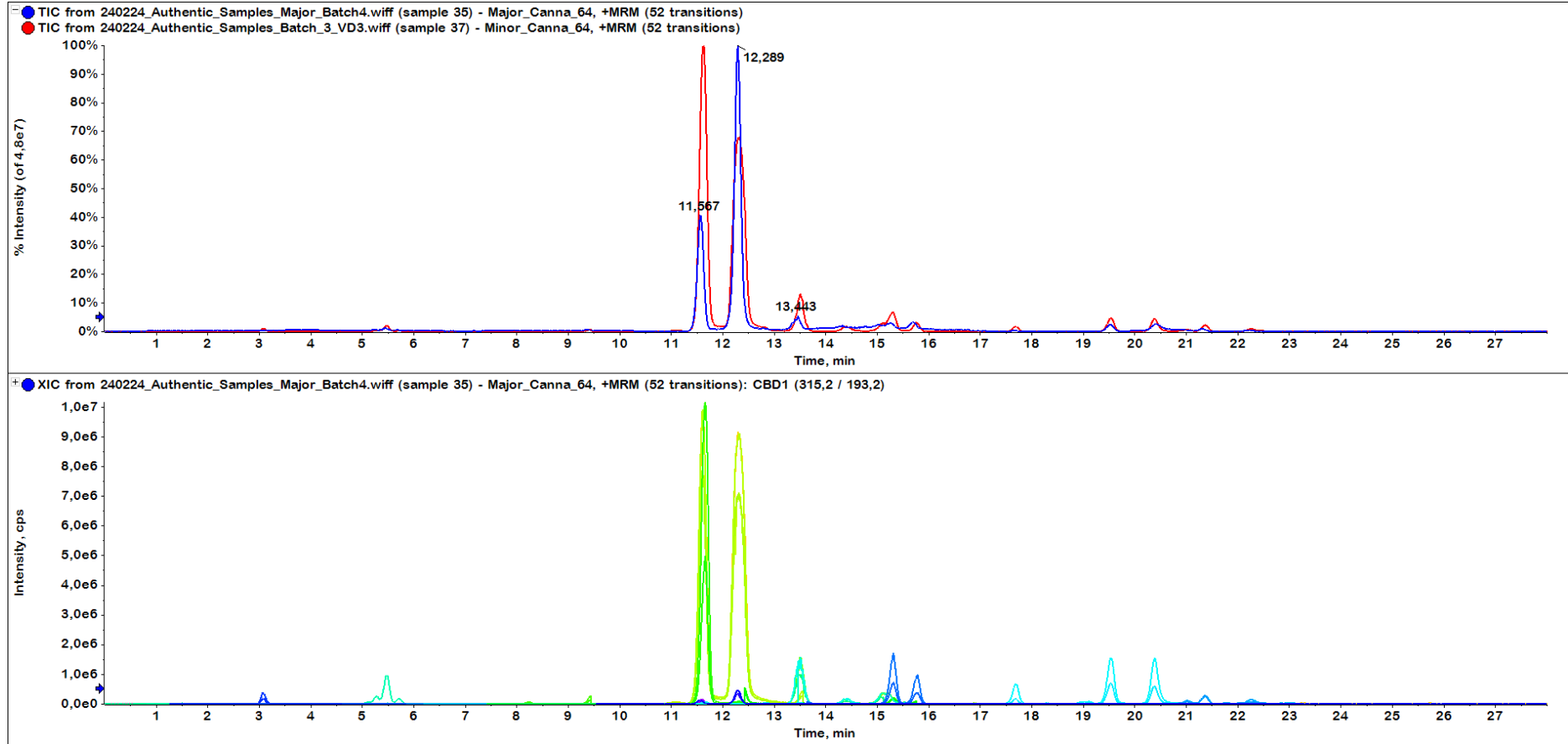
C. sativa L. sample 50



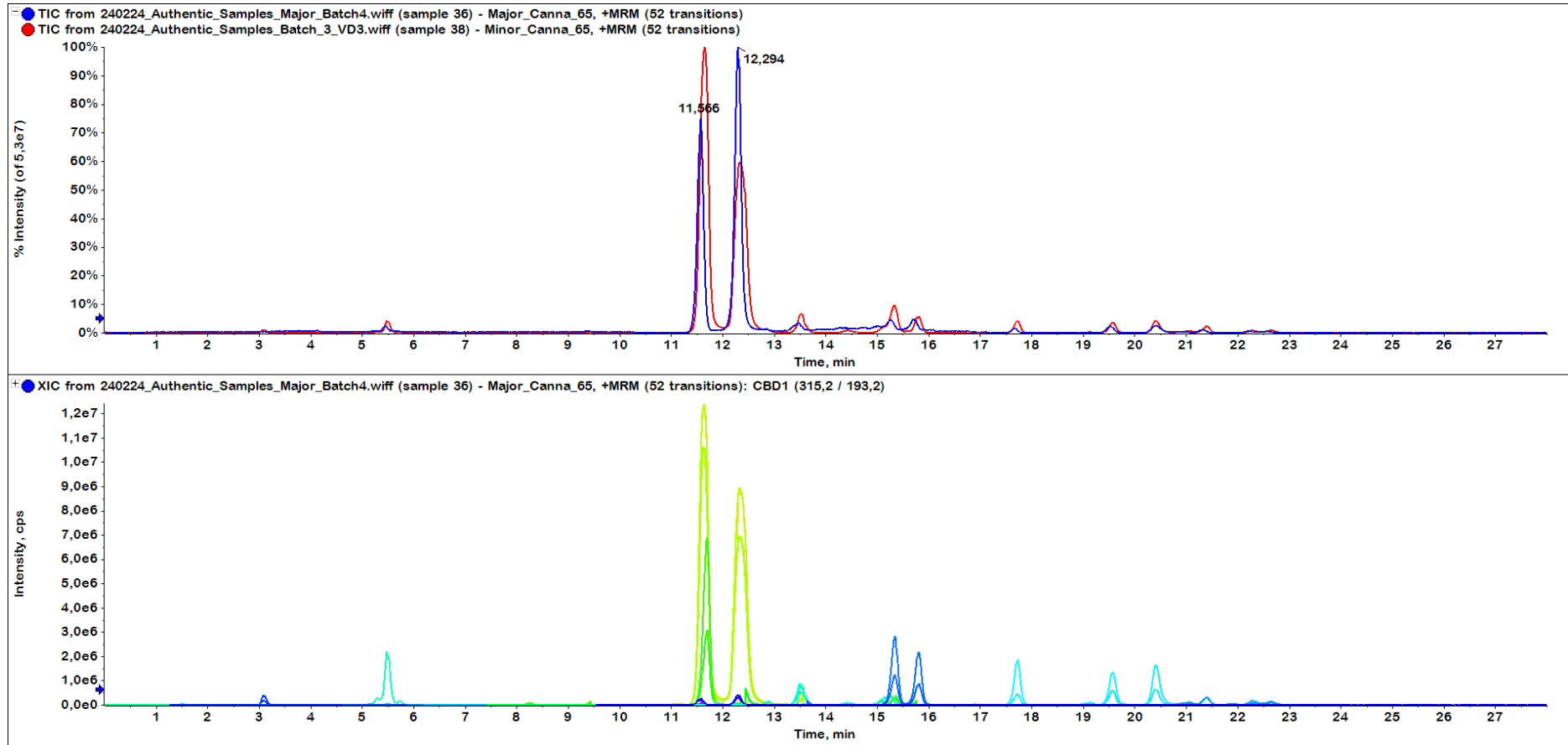
C. sativa L. sample 51



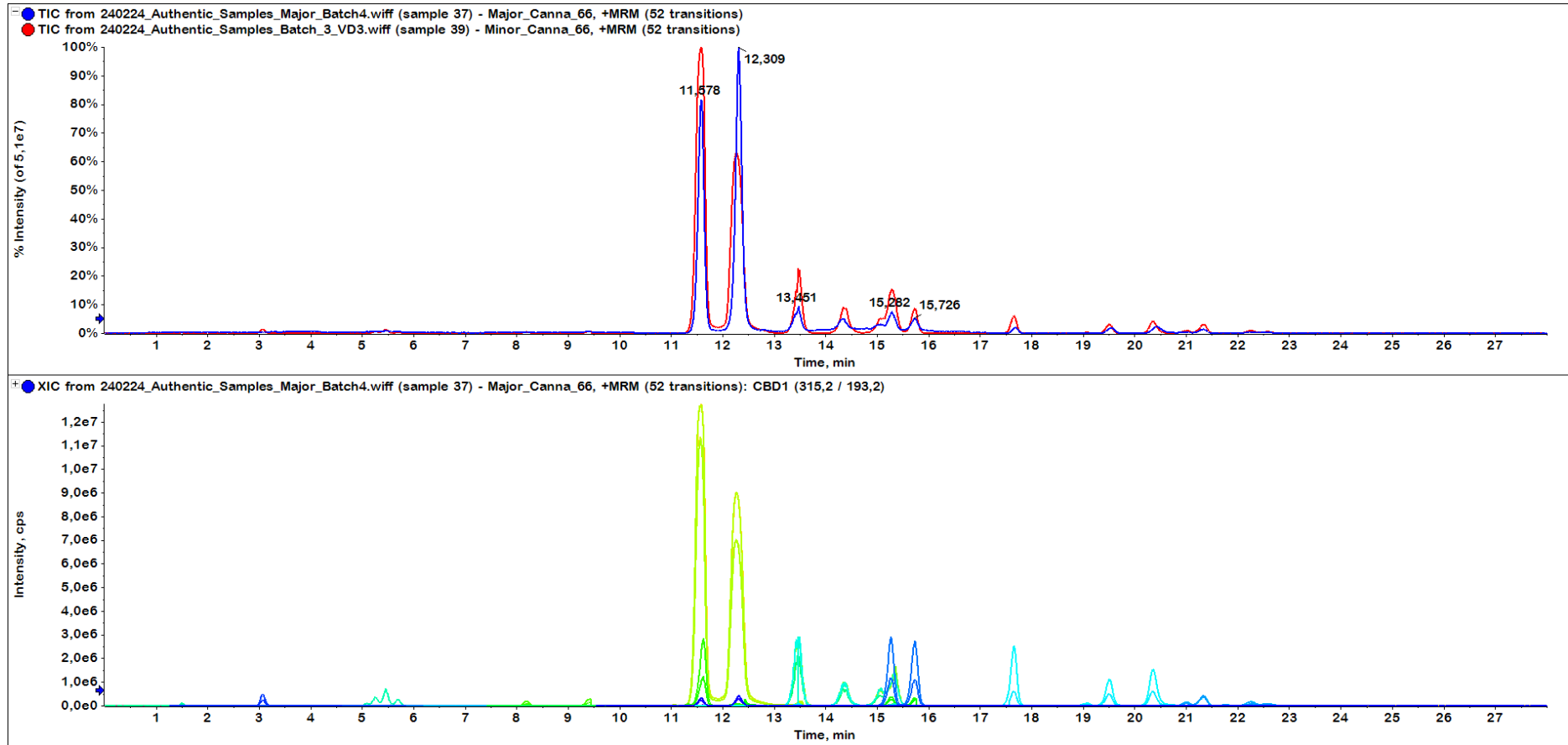
C. sativa L. sample 52



C. sativa L. sample 53



C. sativa L. sample 54



C. sativa L. sample 55

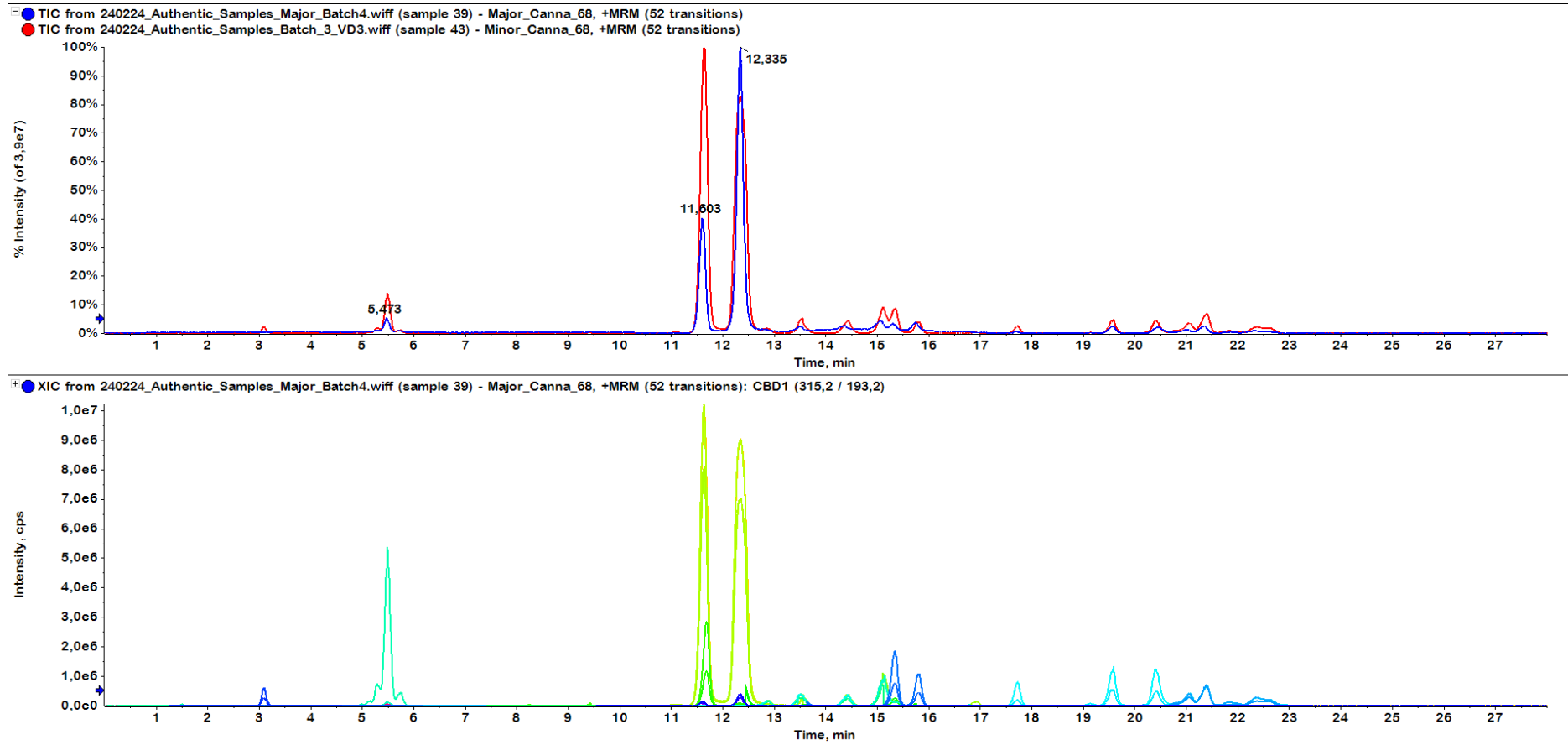
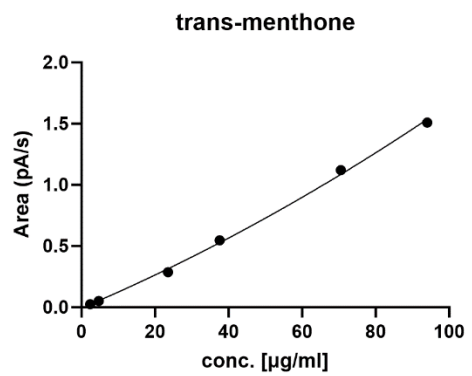
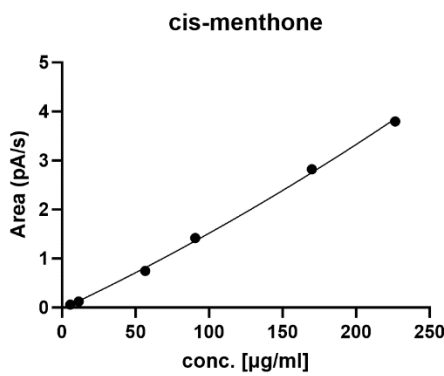
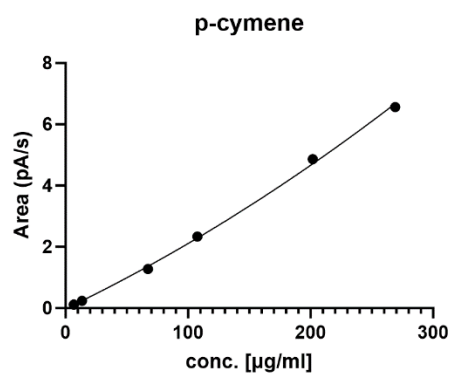
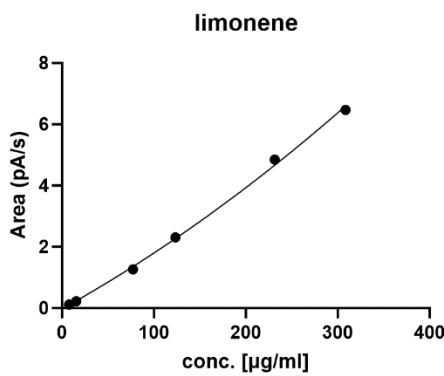
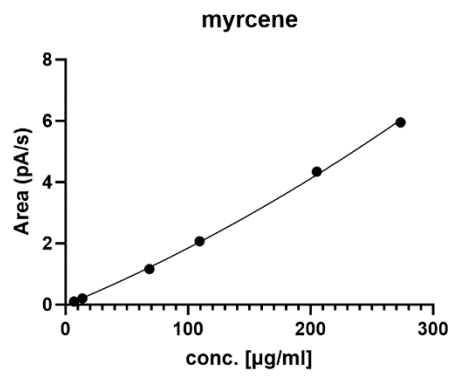
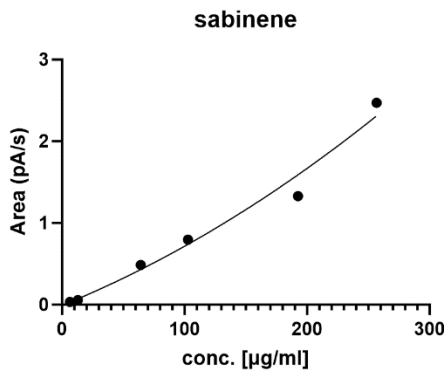
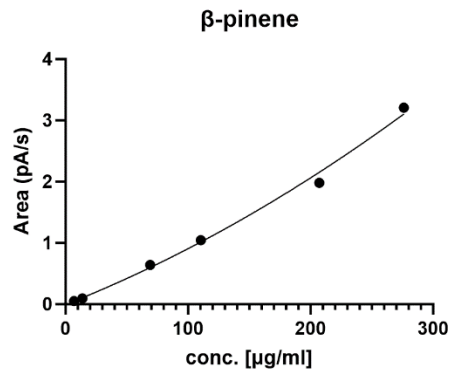
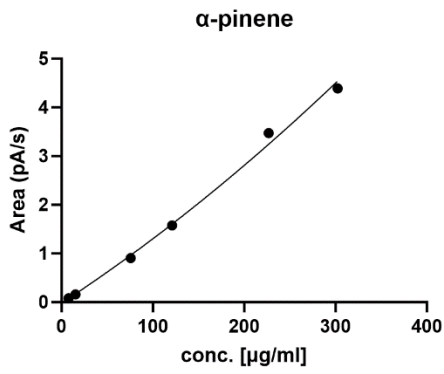
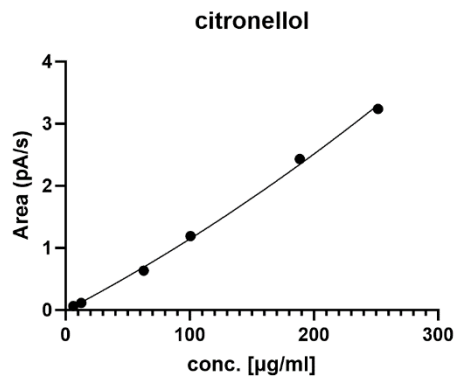
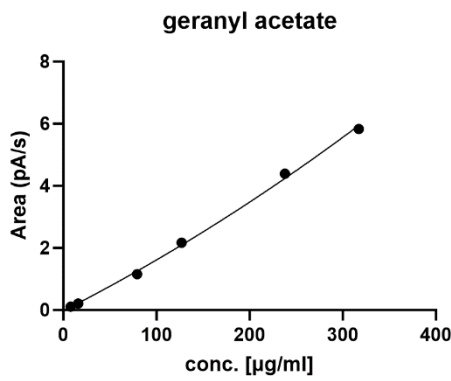
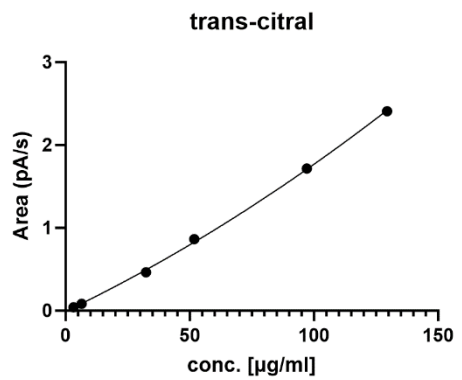
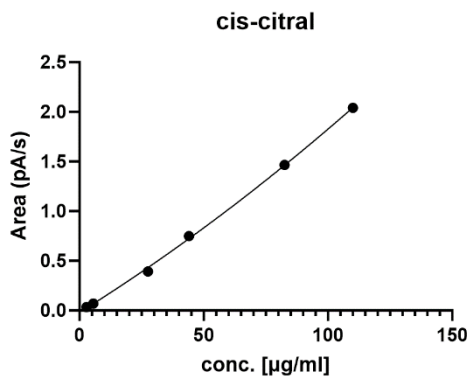
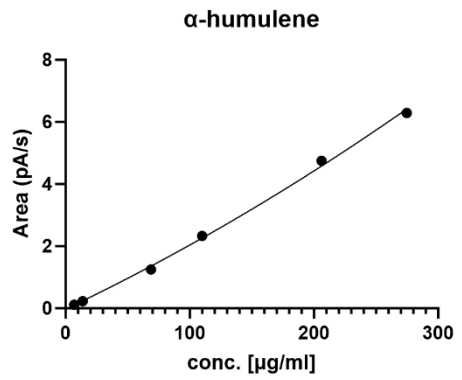
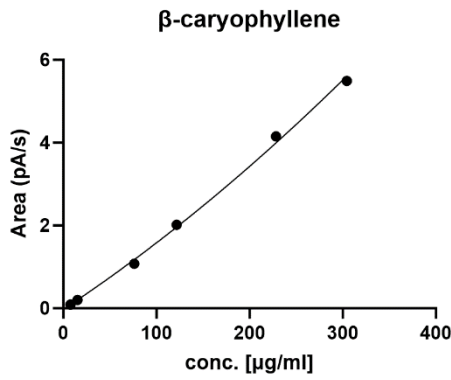
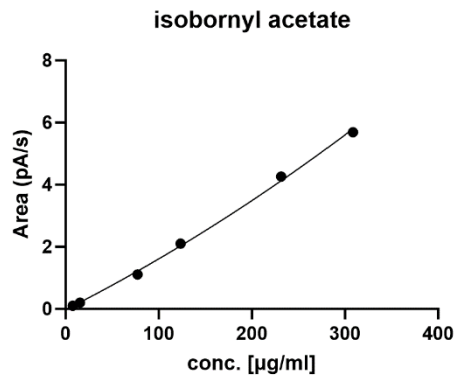
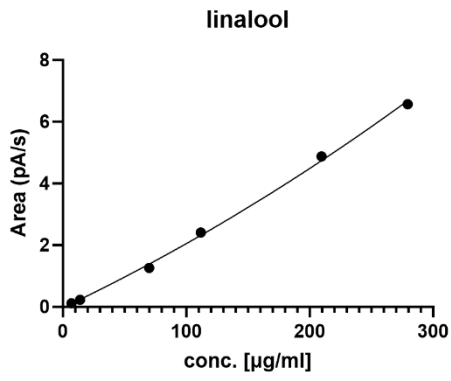


Table A8: Calibration models used for quantification of *C. sativa* L. samples using GC-FID. Table adapted from Raeber et al. ⁷⁰

Analyte	Range [ug/ml]	Calibration model	Weight	Equation	R ²
α-pinene	5 - 250	Quadratic	1/x	$Y = -0.02 + 0.01*X + 0.00001*X^2$	0.9971
β-pinene	5 - 250	Quadratic	1/x	$Y = -0.006 + 0.008*X + 0.00001*X^2$	0.9963
sabinene	5 - 250	Quadratic	1/x	$Y = -0.009 + 0.006*X + 0.00001*X^2$	0.9850
myrcene	5 - 250	Quadratic	1/x	$Y = -0.02 + 0.02*X + 0.00002*X^2$	0.9994
limonene	5 - 250	Quadratic	1/x	$Y = -0.02 + 0.02*X + 0.00002*X^2$	0.9987
cis-menthone	5 - 225	Quadratic	1/x	$Y = -0.03 + 0.01*X + 0.00001*X^2$	0.9986
trans-menthone	2 - 95	Quadratic	1/x	$Y = -0.006 + 0.01*X + 0.00004*X^2$	0.9985
linalool	5 - 250	Quadratic	1/x	$Y = -0.03 + 0.02*X + 0.00002*X^2$	0.9985
isobornyl acetate	5 - 250	Quadratic	1/x	$Y = -0.02 + 0.02*X + 0.00001*X^2$	0.9983
β-caryophyllene	5 - 250	Quadratic	1/x	$Y = -0.03 + 0.01*X + 0.00001*X^2$	0.9983
α-humulene	5 - 250	Quadratic	1/x	$Y = -0.02 + 0.02*X + 0.00002*X^2$	0.9983
cis-citral	2.5 - 110	Quadratic	1/x	$Y = -0.02 + 0.02*X + 0.00003*X^2$	0.9993
trans-citral	2.5 - 110	Quadratic	1/x	$Y = -0.007 + 0.01*X + 0.00003*X^2$	0.9993
geranyl acetate	5 - 250	Quadratic	1/x	$Y = -0.02 + 0.02*X + 0.00001*X^2$	0.9983
citronellol	5 - 250	Quadratic	1/x	$Y = -0.009 + 0.01*X + 0.00001*X^2$	0.9983
carvacrol	5 - 250	Quadratic	1/x	$Y = -0.03 + 0.02*X + 0.00001*X^2$	0.9975





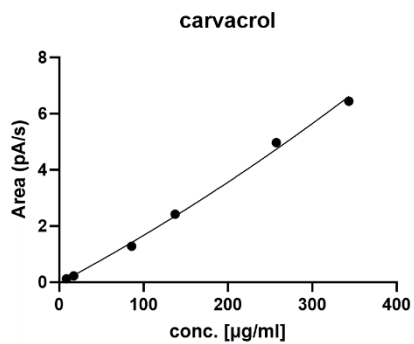


Figure A13: Six calibration standards at different concentrations [µg/ml] plotted against the area [pA/s] after GC-FID acquisition (n=1). Respective calibration models from Table A8 were fitted.

Table A9: Analyte concentrations for all 55 authentic *C. sativa* L. samples. Table taken from Raeber et al.⁷⁰

Sample	CBD [% w/w]	CBDa [% w/w]	Total CBD [% w/w]	CBDv [% w/w]	CBG [% w/w]	CBN [% w/w]	THC [% w/w]	THCA [% w/w]	Total THC [% w/w]	α -humulene [% w/w]	β -pinene [% w/w]	α -pinene [% w/w]	carvacrol [% w/w]	β -caryo- phyllene [% w/w]	cis-citral [% w/w]	trans- menthone [% w/w]	Citronellol [% w/w]	geranyl acetate [% w/w]	isobornyl acetate [% w/w]	limonene [% w/w]	linalool [% w/w]	myrcene [% w/w]	sabinene [% w/w]	trans-citral [% w/w]	cis-menthone [% w/w]
C. Sativa 1	0,65	10,48	9,84	0,001	0,04	0,0006	0,08	0,58	0,59	< LoQ	0,13	0,22	n.d.	0,08	n.d.	n.d.	0,0277	n.d.	n.d.	0,13	0,04	0,60	n.d.	n.d.	n.d.
C. Sativa 2	0,64	17,51	16,00	0,001	0,18	> LoQ	0,08	0,91	0,88	0,04	0,15	0,20	n.d.	0,21	n.d.	n.d.	> LoQ	n.d.	n.d.	0,21	0,05	0,59	n.d.	n.d.	n.d.
C. Sativa 3	0,95	12,65	12,04	0,002	0,07	0,0008	0,12	0,60	0,64	0,05	0,10	0,15	n.d.	0,21	n.d.	n.d.	> LoQ	n.d.	n.d.	0,12	0,05	0,58	n.d.	n.d.	n.d.
C. Sativa 4	10,02	17,52	25,39	0,027	2,05	0,0716	0,33	0,43	0,71	0,03	> LoQ	> LoQ	n.d.	0,12	n.d.	n.d.	> LoQ	n.d.	> LoQ	0,07	0,06	n.d.	n.d.	n.d.	n.d.
C. Sativa 5	0,69	14,26	13,20	0,001	0,07	0,0009	0,08	0,81	0,79	> LoQ	0,04	0,08	n.d.	0,09	n.d.	n.d.	< LoQ	n.d.	n.d.	0,10	0,04	0,17	n.d.	n.d.	n.d.
C. Sativa 6	0,50	8,73	8,16	0,001	0,03	< LoQ	0,04	0,58	0,55	< LoQ	0,04	0,05	n.d.	0,10	n.d.	n.d.	n.d.	n.d.	n.d.	0,11	> LoQ	0,22	n.d.	n.d.	n.d.
C. Sativa 7	1,75	10,68	11,11	0,003	0,05	0,0023	0,19	0,52	0,65	0,03	0,08	0,09	n.d.	0,14	n.d.	n.d.	n.d.	n.d.	n.d.	0,09	0,05	0,38	n.d.	n.d.	n.d.
C. Sativa 8	25,29	10,06	34,12	0,165	0,54	0,3627	0,32	0,13	0,44	0,06	> LoQ	> LoQ	n.d.	0,19	n.d.	n.d.	n.d.	n.d.	n.d.	0,04	0,06	< LoQ	n.d.	n.d.	n.d.
C. Sativa 9	10,54	18,08	26,40	0,020	0,20	0,0265	0,63	0,39	0,98	0,05	0,05	0,08	n.d.	0,19	n.d.	n.d.	n.d.	n.d.	n.d.	0,12	0,04	0,08	n.d.	n.d.	n.d.
C. Sativa 10	1,21	12,05	11,78	0,003	0,06	0,0007	0,15	0,60	0,68	0,06	0,11	0,14	n.d.	0,24	n.d.	n.d.	n.d.	n.d.	n.d.	0,15	0,06	0,53	n.d.	n.d.	n.d.
C. Sativa 11	0,47	12,89	11,78	0,001	0,05	0,0005	0,06	0,79	0,76	0,04	0,13	0,18	n.d.	0,17	n.d.	n.d.	0,0341	n.d.	n.d.	0,18	0,09	0,65	n.d.	n.d.	n.d.
C. Sativa 12	0,79	13,07	12,25	0,002	0,08	< LoQ	0,11	0,72	0,74	0,07	0,06	0,03	n.d.	0,30	n.d.	n.d.	n.d.	n.d.	n.d.	0,20	0,11	0,60	n.d.	n.d.	n.d.
C. Sativa 13	0,53	13,60	12,46	0,001	0,02	< LoQ	0,08	0,78	0,76	< LoQ	0,08	0,08	n.d.	0,06	n.d.	n.d.	< LoQ	n.d.	n.d.	0,28	0,06	0,46	n.d.	n.d.	n.d.
C. Sativa 14	2,32	11,38	12,30	0,003	0,09	0,0014	0,28	0,12	0,39	0,05	0,10	0,16	n.d.	0,17	n.d.	n.d.	< LoQ	n.d.	n.d.	0,09	0,07	0,59	n.d.	n.d.	n.d.
C. Sativa 15	1,65	12,29	12,43	0,003	0,10	0,0008	0,22	0,46	0,62	0,06	0,12	0,05	n.d.	0,23	n.d.	n.d.	n.d.	n.d.	n.d.	0,61	0,04	0,45	n.d.	n.d.	n.d.
C. Sativa 16	> Range	2,59	> 30 %	0,148	1,33	6,4436	0,19	0,01	0,20	0,04	< LoQ	< LoQ	n.d.	0,34	n.d.	n.d.	n.d.	n.d.	n.d.	0,06	< LoQ	n.d.	n.d.	n.d.	n.d.
C. Sativa 17	0,89	9,88	9,55	0,001	0,03	0,0008	0,12	0,49	0,55	0,05	0,16	0,32	n.d.	0,16	n.d.	n.d.	0,0464	n.d.	n.d.	0,19	0,08	0,82	n.d.	n.d.	n.d.
C. Sativa 18	17,45	16,46	31,89	0,103	0,08	0,2058	0,20	0,79	0,89	< LoQ	< LoQ	0,03	n.d.	0,10	n.d.	n.d.	n.d.	n.d.	n.d.	0,17	0,04	0,05	n.d.	n.d.	n.d.
C. Sativa 19	0,51	17,99	16,29	0,002	0,13	< LoQ	0,06	0,95	0,89	0,07	0,04	0,04	n.d.	0,31	n.d.	n.d.	n.d.	n.d.	n.d.	0,22	0,20	0,36	< LoQ	n.d.	n.d.
C. Sativa 20	1,10	11,87	11,51	0,002	0,05	0,0015	0,12	0,68	0,72	< LoQ	< LoQ	0,04	n.d.	0,12	n.d.	n.d.	n.d.	n.d.	n.d.	0,18	0,06	0,22	< LoQ	n.d.	n.d.
C. Sativa 21	0,46	17,55	15,86	n.d.	0,13	n.d.	0,06	0,94	0,88	n.d.	0,04	0,05	n.d.	0,14	n.d.	n.d.	n.d.	n.d.	n.d.	0,21	0,11	0,34	< LoQ	n.d.	n.d.
C. Sativa 22	0,58	17,51	15,94	0,001	0,14	< LoQ	0,07	1,00	0,94	0,06	0,04	0,05	n.d.	0,23	n.d.	n.d.	n.d.	n.d.	n.d.	0,26	0,17	0,56	n.d.	n.d.	n.d.
C. Sativa 23	0,32	10,12	9,20	0,001	0,05	< LoQ	0,03	0,56	0,52	0,04	0,06	0,10	n.d.	0,17	n.d.	n.d.	n.d.	n.d.	n.d.	0,14	0,05	0,26	n.d.	n.d.	n.d.
C. Sativa 24	13,00	13,27	24,64	0,022	0,05	0,1183	0,57	0,18	0,73	< LoQ	< LoQ	< LoQ	n.d.	0,08	n.d.	n.d.	n.d.	n.d.	n.d.	0,05	0,05	< LoQ	n.d.	n.d.	n.d.
C. Sativa 25	12,10	12,81	23,33	0,062	0,09	0,1189	0,63	0,22	0,83	0,04	< LoQ	n.d.	n.d.	0,13	n.d.	n.d.	n.d.	n.d.	n.d.	0,05	0,06	< LoQ	n.d.	n.d.	n.d.
C. Sativa 26	0,29	11,54	10,41	0,001	0,06	< LoQ	0,03	0,72	0,66	0,04	< LoQ	< LoQ	n.d.	0,17	n.d.	n.d.	n.d.	n.d.	n.d.	0,15	0,07	0,19	n.d.	n.d.	n.d.
C. Sativa 27	1,34	11,14	11,11	0,005	0,07	0,0021	0,15	0,64	0,71	n.d.	< LoQ	0,06	n.d.	0,06	n.d.	n.d.	n.d.	n.d.	n.d.	0,10	0,07	0,11	n.d.	n.d.	n.d.
C. Sativa 28	2,54	13,80	14,64	0,004	0,06	0,0038	0,28	0,65	0,85	< LoQ	< LoQ	0,06	n.d.	0,12	n.d.	n.d.	n.d.	n.d.	n.d.	0,17	0,08	0,27	n.d.	n.d.	n.d.
C. Sativa 29	22,01	7,80	28,86	0,074	0,07	0,1165	0,67	0,00	0,67	0,08	< LoQ	< LoQ	n.d.	0,37	n.d.	n.d.	n.d.	n.d.	n.d.	0,08	0,04	0,11	n.d.	n.d.	n.d.
C. Sativa 30	0,89	15,40	14,40	0,003	0,16	< LoQ	0,11	0,80	0,81	0,05	0,15	0,28	n.d.	0,26	n.d.	n.d.	n.d.	n.d.	n.d.	0,22	0,05	0,54	n.d.	n.d.	n.d.
C. Sativa 31	2,42	16,09	16,53	0,005	0,09	n.d.	0,29	0,71	0,92	< LoQ	0,07	n.d.	n.d.	0,07	n.d.	n.d.	n.d.	n.d.	n.d.	0,38	0,05	n.d.	n.d.	n.d.	n.d.
C. Sativa 32	1,21	19,91	18,67	0,002	0,10	n.d.	0,15	0,96	0,99	0,04	< LoQ	n.d.	n.d.	0,23	n.d.	n.d.	n.d.	n.d.	n.d.	0,21	0,08	0,50	n.d.	n.d.	n.d.
C. Sativa 33	0,74	11,52	10,85	0,001	0,03	0,0010	0,07	0,76	0,74	0,05	0,05	0,10	n.d.	0,24	n.d.	n.d.	n.d.	n.d.	n.d.	0,12	0,06	0,33	n.d.	n.d.	n.d.
C. Sativa 34	1,00	12,43	11,90	0,001	0,02	0,0017	0,10	0,82	0,82	0,05	0,16	0,33	n.d.	0,20	n.d.	n.d.	n.d.	n.d.	< LoQ	0,12	0,07	0,43	n.d.	n.d.	n.d.
C. Sativa 35	0,73	22,57	20,53	0,001	0,15	0,0006	0,11	0,89	0,89	< LoQ	0,08	0,14	n.d.	0,11	n.d.	n.d.	< LoQ	n.d.	n.d.	0,17	0,08	0,45	n.d.	n.d.	n.d.
C. Sativa 36	0,78	15,01	13,94	0,001	0,04	< LoQ	0,11	0,91	0,90	0,04	0,09	0,16	n.d.	0,17	n.d.	n.d.	< LoQ	n.d.	n.d.	0,17	0,06	0,56	n.d.	n.d.	n.d.
C. Sativa 37	0,37	18,69	16,76	0,0005	0,08	< LoQ	0,04	0,95	0,87	0,04	< LoQ	< LoQ	n.d.	0,15	n.d.	n.d.	n.d.	n.d.	n.d.	0,12	0,11	0,25	n.d.	n.d.	n.d.
C. Sativa 38	0,71	16,37	15,07	0,001	0,06	< LoQ	0,06	1,00	0,93	< LoQ	0,04	< LoQ	n.d.	0,14	n.d.	n.d.	n.d.	n.d.	n.d.	0,50	0,11	0,46	n.d.	n.d.	n.d.
C. Sativa 39	1,19	15,63	14,90	0,002	0,05	0,0018	0,13	0,91	0,93	0,07	0,04	0,05	n.d.	0,28	n.d.	n.d.	n.d.	n.d.	n.d.	0,16	0,08	0,27	n.d.	n.d.	n.d.
C. Sativa 40	0,98	21,07	19,46	0,001	0,08	0,0007	0,12	0,90	0,91	0,04	n.d.	0,04	n.d.	0,19	n.d.	n.d.	n.d.	n.d.	n.d.	0,54	0,04	0,43	n.d.	n.d.	n.d.
C. Sativa 41	1,64	13,56	13,53	0,003	0,04	0,0024	0,19	0,80	0,90	0,06	< LoQ	< LoQ	n.d.	0,21	n.d.	n.d.	n.d.	n.d.	n.d.	0,11	0,08	0,24	n.d.	n.d.	n.d.
C. Sativa 42	0,90	23,04	21,10	0,002	0,16	0,0006	0,10	0,00	0,10	0,06	0,13	0,23	n.d.	0,23	n.d.	n.d.	n.d.	n.d.	n.d.	0,22	0,04	0,46	n.d.	n.d.	n.d.
C. Sativa 43	1,27	12,65	12,36	0,078	0,08	0,0205	0,15	0,60	0,67	0,11	< LoQ	0,04	n.d.	0,41	n.d.	n.d.	n.d.	n.d.	n.d.	0,12	0,04	0,06	n.d.	n.d.	n.d.
C. Sativa 44	0,55	19,65	17,79	0,001	0,05	< LoQ	0,06	0,71	0,68	0,09	0,04	< LoQ	n.d.	0,30	n.d.	n.d.	n.d.	n.d.	n.d.	0,20	0,17	0,35	n.d.	n.d.	n.d.
C. Sativa 45	34,43	4,46	38,35	0,077	1,99	0,0188	0,44	0,00	0,44	0,05	< LoQ	< LoQ	n.d.	0,41	n.d.	n.d.	n.d.	n.d.	n.d.	0,12	0,04	0,11	n.d.	n.d.	n.d.
C. Sativa 46	2,34	17,94	18,08	0,008	0,07	0,0010	0,29	0,58	0,80	0,08	< LoQ	< LoQ	n.d.	0,28	n.d.	n.d.	n.d.	n.d.	n.d.	0,18	0,04	1,03	n.d.	n.d.	n.d.
C. Sativa 47	25,76	3,94	29,22	0,118	0,05	0,2536	0,35	0,02	0,37	< LoQ	< LoQ	0,08	n.d.	0,12	n.d.	n.d.	n.d.	n.d.	n.d.	0,14	< LoQ	0,04	n.d.	n.d.	n.d.
C. Sativa 48	0,44	8,07	7,52	0,001	0,01	n.d.	0,04	0,01	0,04	< LoQ	0,08	n.d.	n.d.	< LoQ	n.d.	n.d.	n.d.	n.d.	n.d.	0,08	< LoQ	0,31	n.d.	n.d.	n.d.
C. Sativa 49	0,31	9,36	8,51	0,001	0,02	n.d.	0,04	0,55	0,53	< LoQ	0,04	0,09	n.d.	0,08	n.d.	n.d.	< LoQ	n.d.	n.d.	0,09	0,06	0,34	n.d.	n.d.	n.d.
C. Sativa 50	0,52	19,74	17,83	0,001	0,04	< LoQ	0,06	1,02	0,96	< LoQ	0,09	0,19	n.d.	0,14	n.d.	n.d.	< LoQ	n.d.	n.d.	0,24	0,07	0,43	n.d.	n.d.	n.d.
C. Sativa 51	1,62	18,11	17,50	0,003	0,06	0,0009	0,19	0,78	0,87	0,07	0,15	n.d.	n.d.	0,23	n.d.	n.d.	0,0354	n.d.	n.d.	0,18	< LoQ	0,66	n.d.	n.d.	n.d.
C. Sativa 52	0,39	18,17	16,33	0,001	0,16	< LoQ	0,04	1,01	0,93	0,05	0,04	< LoQ	n.d.	0,18	n.d.	n.d.	n.d.	n.d.	n.d.	0,15	0,07	0,43	n.d.	n.d.	n.d.
C. Sativa 53	0,87	17,93	16,59	0,002	0,08	0,0005	0,12	0,95	0,95	0,06	< LoQ	n.d.	n.d.	0,20	n.d.	n.d.	n.d.	n.d.	n.d.	0,13	0,14	0,24	n.d.	n.d.	n.d.
C. Sativa 54	0,98	16,77	15,68	0,003	0,03	< LoQ	0,13	0,73	0,77	0,06	0,14	0,27	n.d.	0,25	n.d.	n.d.	< LoQ	n.d.	n.d.	0,18	0,04	0,72	n.d.	n.d.	n.d.
C. Sativa 55	0,45	16,28	14,73	0,001	0,03	0,0005	0,05																		

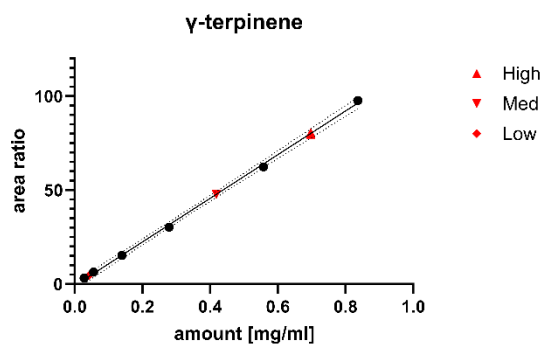
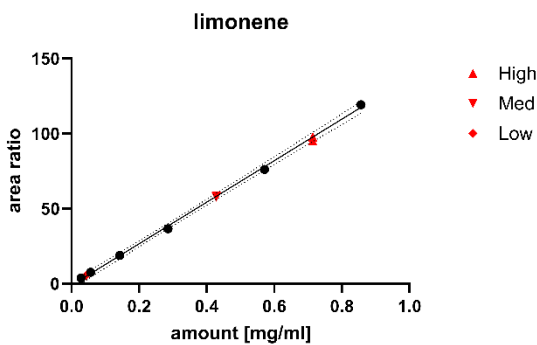
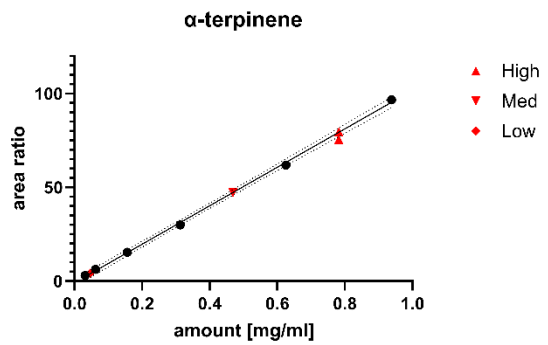
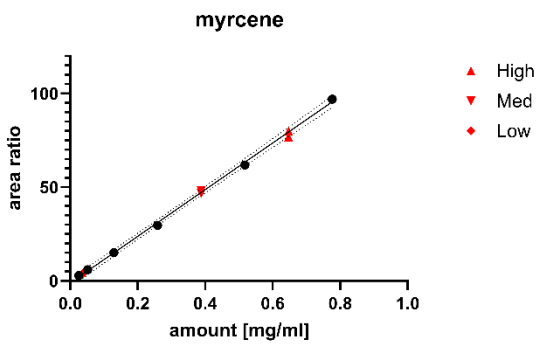
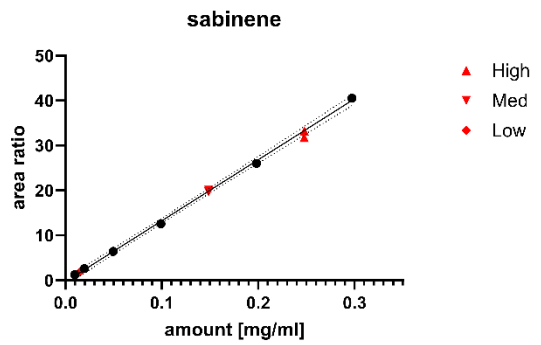
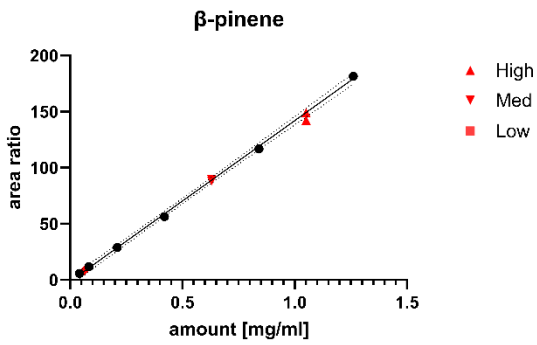
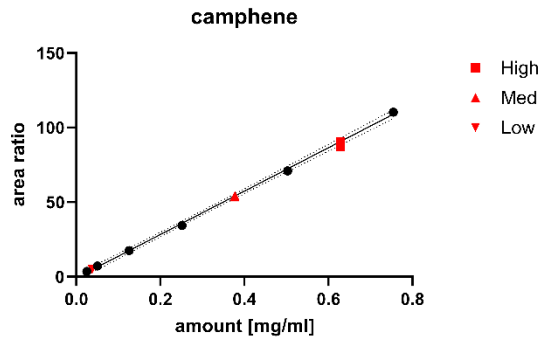
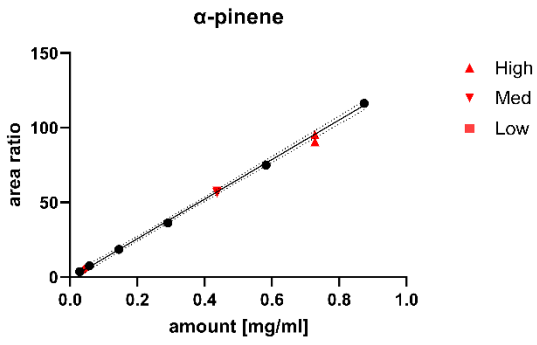
2.3. Comprehensive Analysis of Chemical and Enantiomeric Stability of Terpenes in *Cannabis sativa* L. flowers

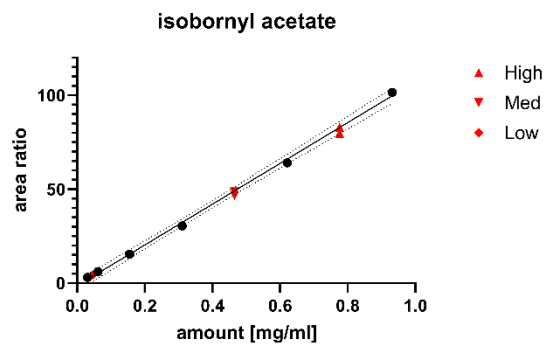
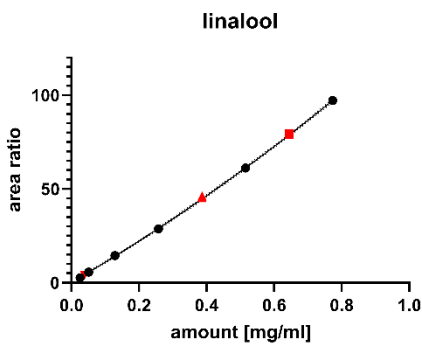
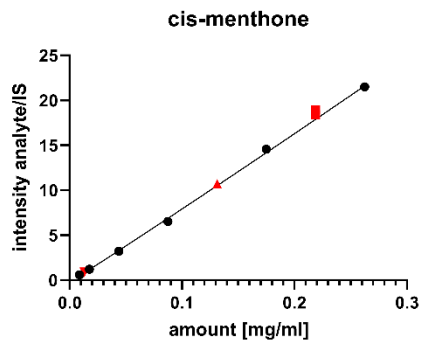
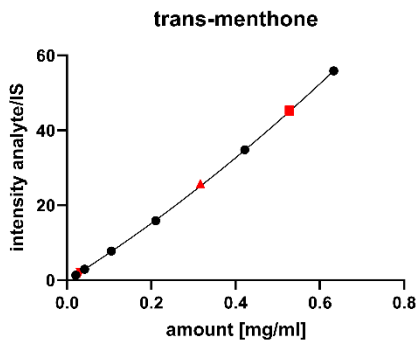
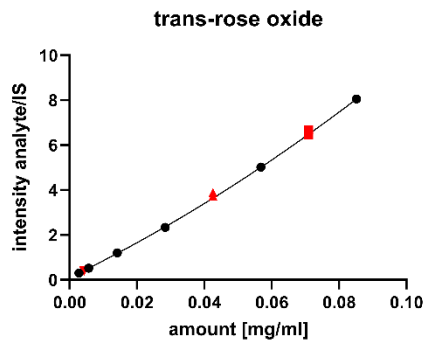
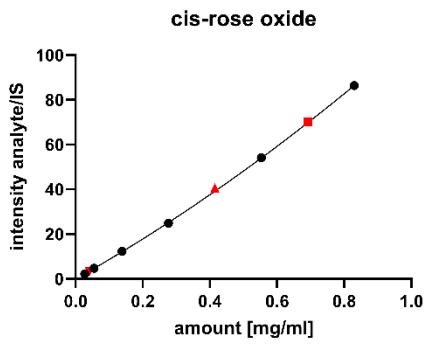
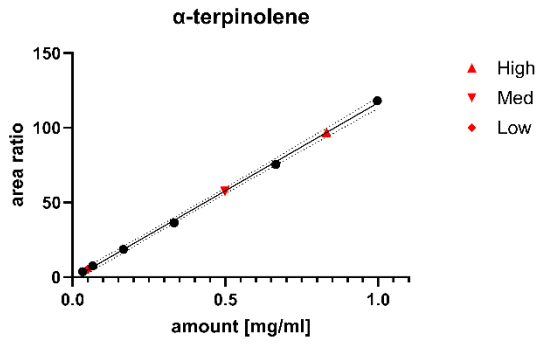
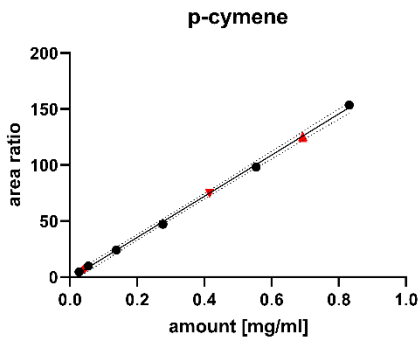
Some of the data presented here was published in the following publication:

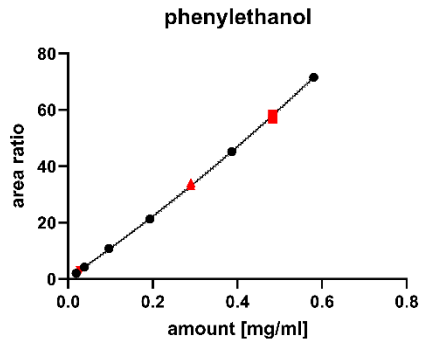
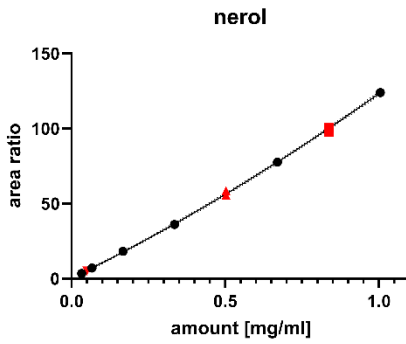
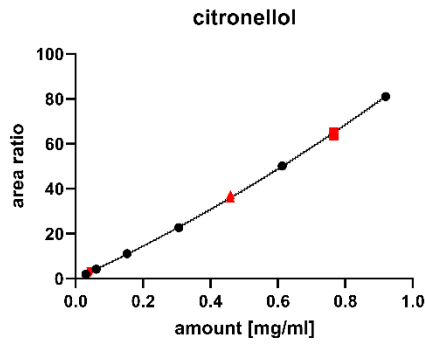
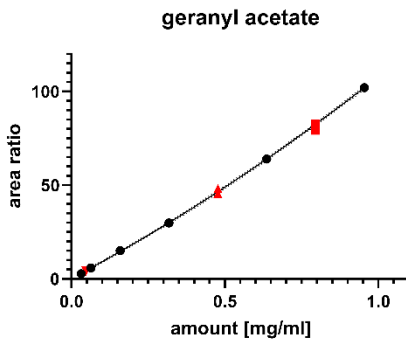
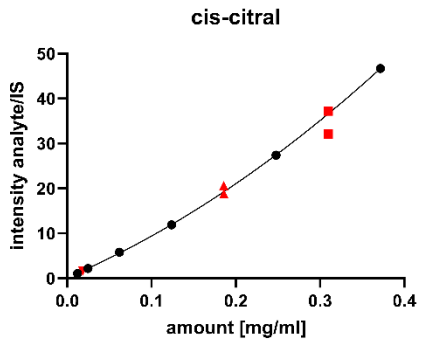
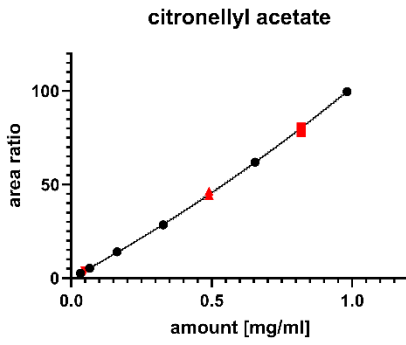
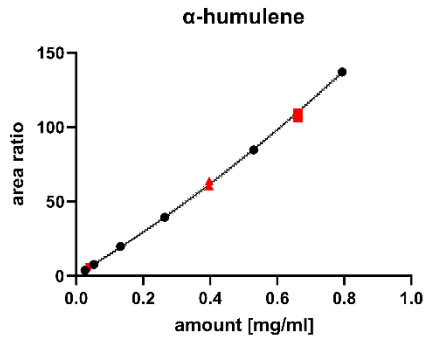
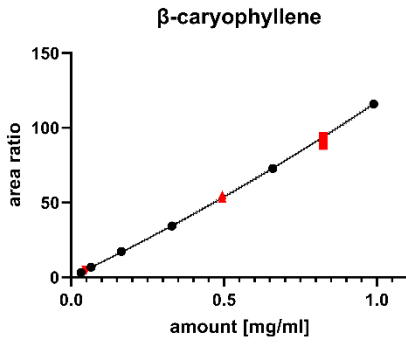
Raeber J, Bajor B, Poetzsch M, Steuer C. Comprehensive analysis of chemical and enantiomeric stability of terpenes in *Cannabis sativa* L. flowers. *Phytochemical Analysis* 2024; 1-13. DOI:10.1002/pca.3432.

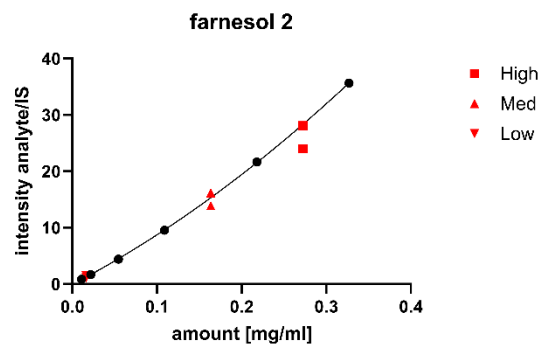
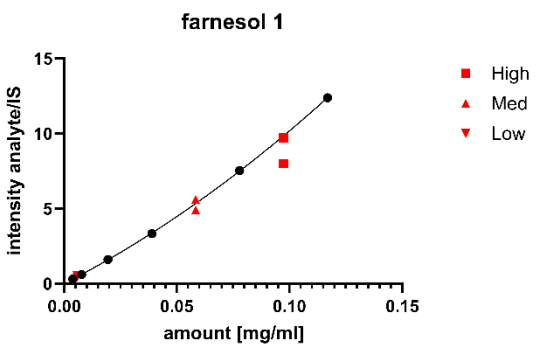
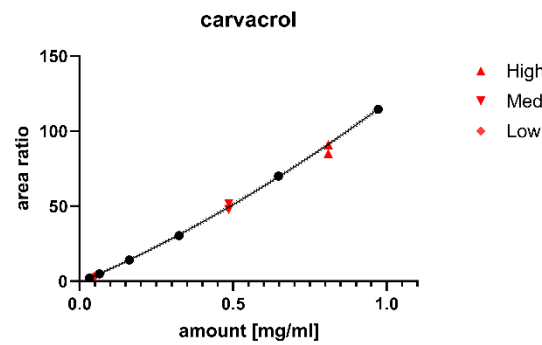
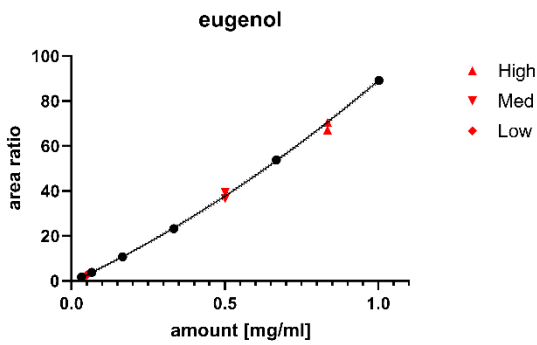
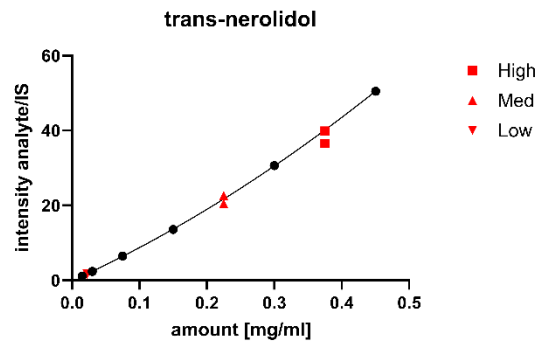
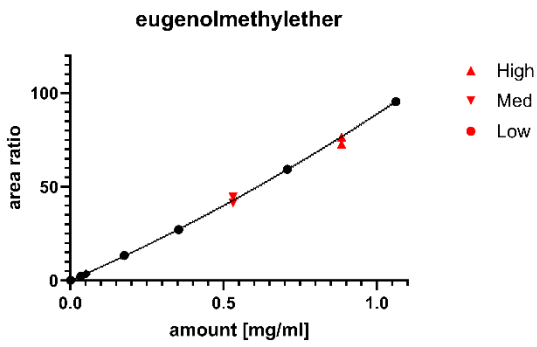
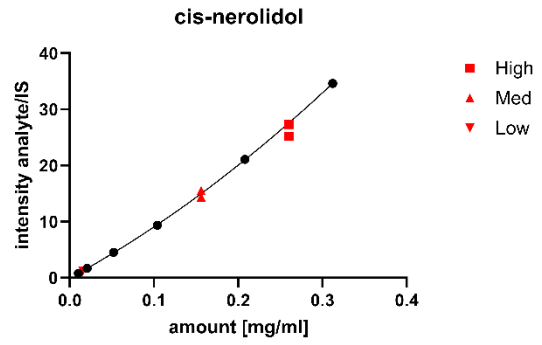
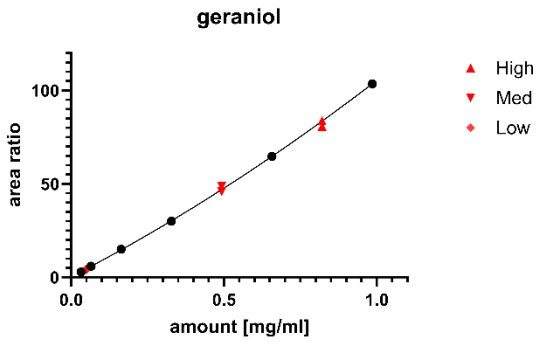
Table A10: Chemicals and reagents.

Chemical	Purity	Manufacturer	Origin
nerol	97%	Acros Organics	Geel, Belgium
geraniol	99%	Acros Organics	Geel, Belgium
eugenol	NA	Essencia	Winterthur, Switzerland
nerolidol	NA	Essencia	Winterthur, Switzerland
α -terpinene	95%	Fluka Chemie GmbH	Buchs, Switzerland
limonene	98%	Fluka Chemie GmbH	Buchs, Switzerland
phenylethanol	>99%	Fluka Chemie GmbH	Buchs, Switzerland
menthone	97%	Fluka Chemie GmbH	Buchs, Switzerland
β -caryophyllene	NA	Frey & Lau	Henstedt-Ulzberg, Germany
γ -terpinene	NA	Frey & Lau	Henstedt-Ulzberg, Germany
citronellol	97%	Merck	Darmstadt, Germany
C8-C40 n-alkane mix	calibration standard	Merck	Darmstadt, Germany
sabinene	analytical standard	Carl Roth GmbH	Karlsruhe, Germany
methyleugenol	>98%	SAFC	St. Louis, MO, USA
camphene	95%	Sigma Aldrich	St. Louis, MO, USA
p-cymene	99%	Sigma Aldrich	St. Louis, MO, USA
rose oxide	\geq 98%, isomer mix	Sigma Aldrich	St. Louis, MO, USA
cis-hexen-1-ol	>98%	Sigma Aldrich	St. Louis, MO, USA
linalool	97%	Sigma Aldrich	St. Louis, MO, USA
citronellyl acetate	>95%	Sigma Aldrich	St. Louis, MO, USA
geranyl acetate	analytical standard	Sigma Aldrich	St. Louis, MO, USA
farnesol	95%	Sigma Aldrich	St. Louis, MO, USA
carvacrol	>98%	Sigma Aldrich	St. Louis, MO, USA
isobornyl acetate	>90%	Sigma Aldrich	St. Louis, MO, USA
myrcene	95%	Sigma Aldrich	St. Louis, MO, USA
α -terpinolene	>90%	Sigma Aldrich	St. Louis, MO, USA
(-)- α -pinene	>99%	Sigma Aldrich	St. Louis, MO, USA
(+)- α -pinene	>99%	Sigma Aldrich	St. Louis, MO, USA
(-)- β -pinene	99%	Sigma Aldrich	St. Louis, MO, USA
(+)- β -pinene	analytical standard	Sigma Aldrich	St. Louis, MO, USA
citral	>98%, isomer mix	TCI Chemical	Eschborn, Germany
neryl acetate	>95%	TCI Chemical	Eschborn, Germany
α -humulene	>93%	TCI Chemical	Eschborn, Germany









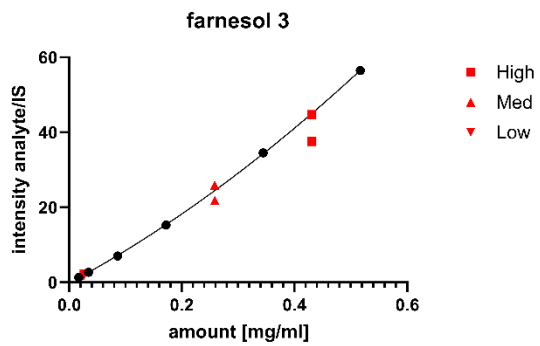
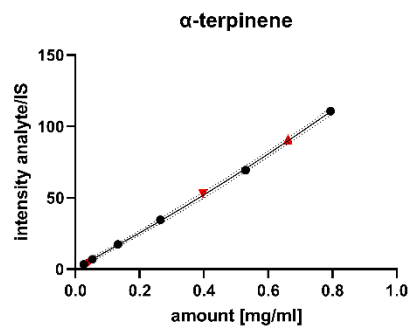
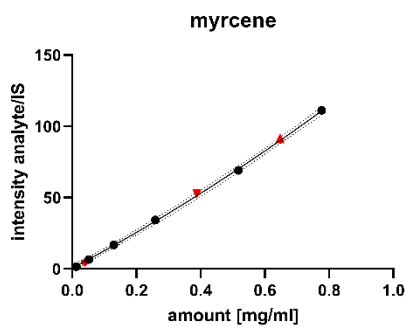
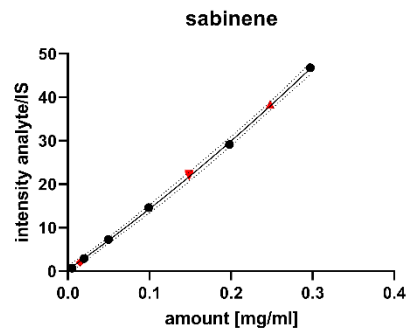
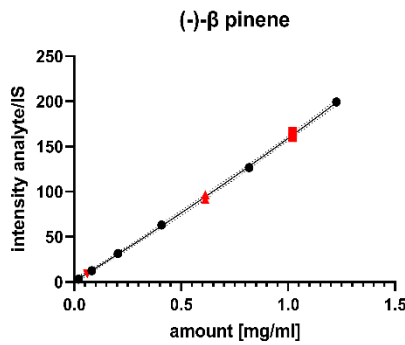
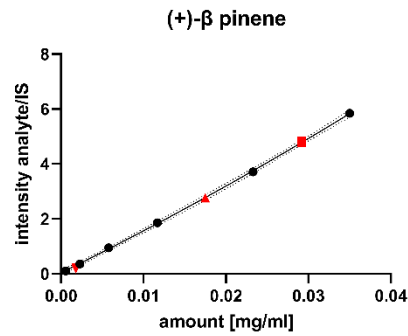
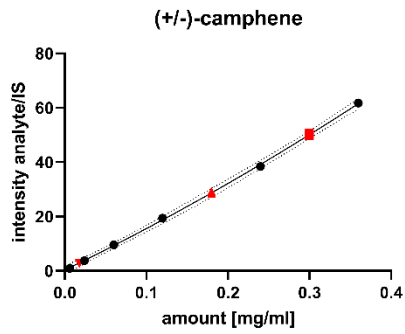
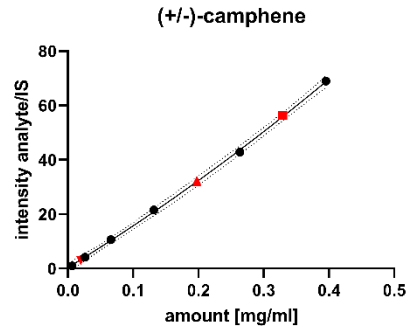
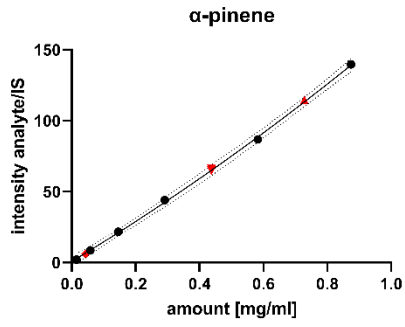
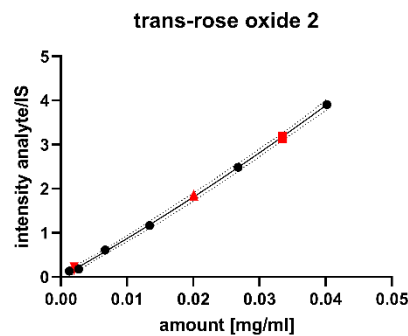
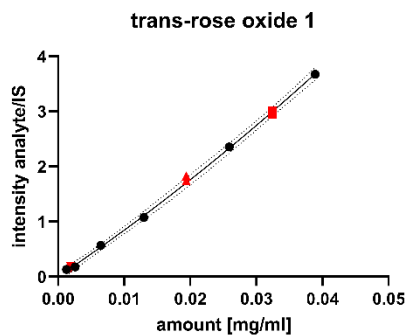
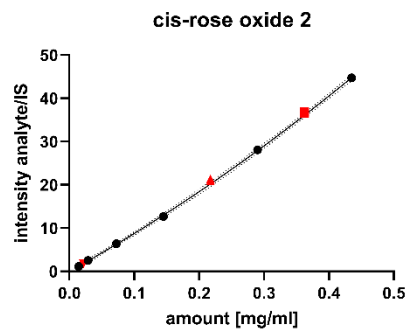
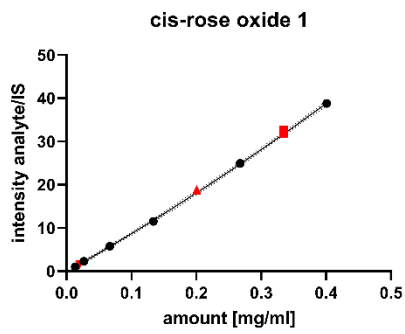
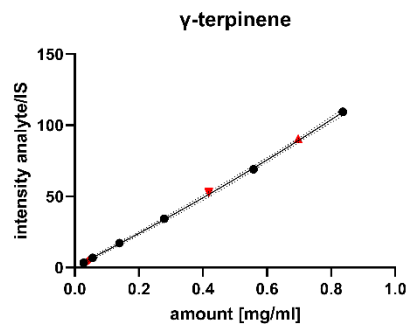
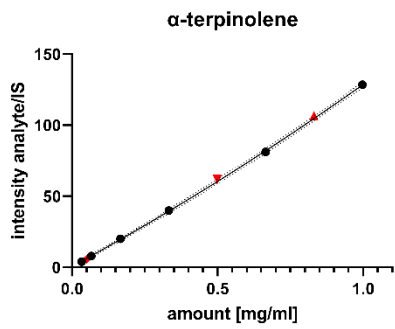
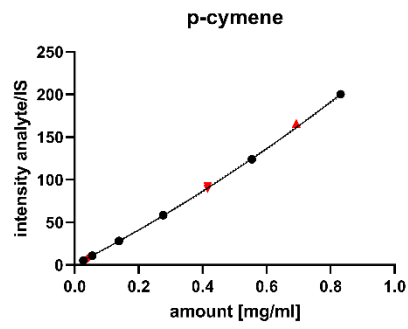
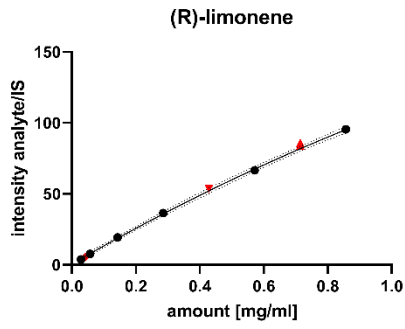


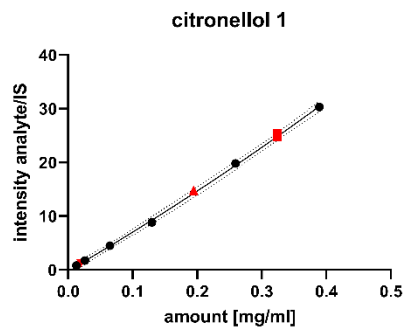
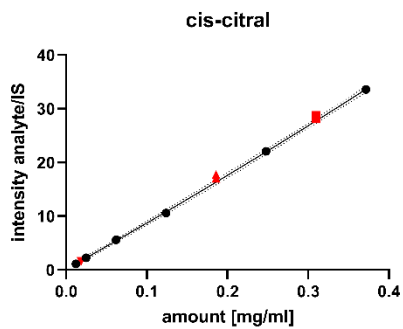
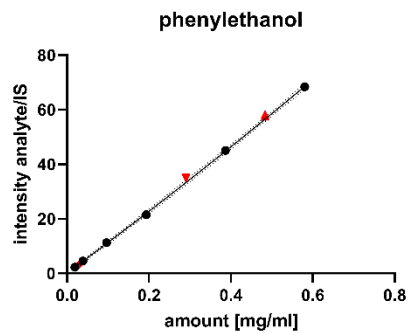
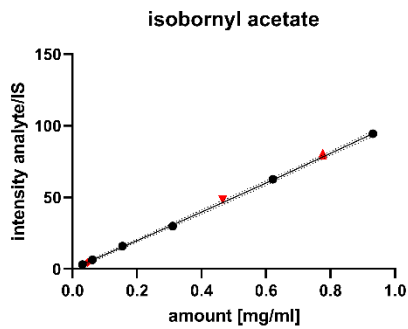
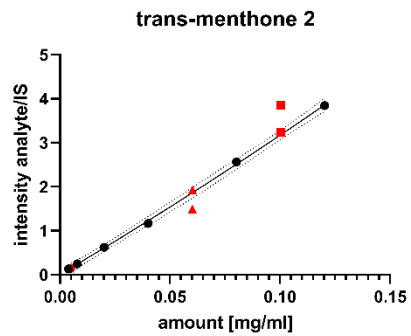
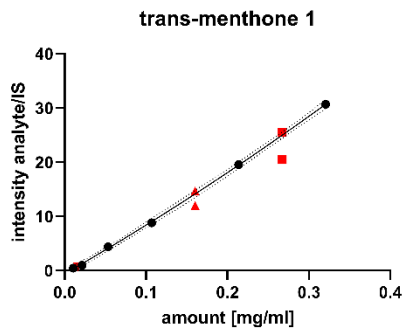
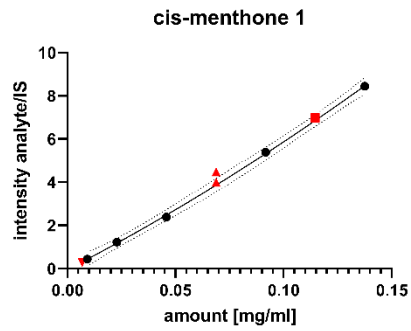
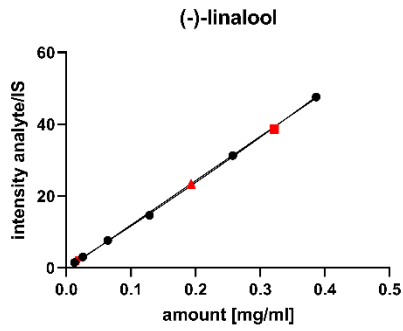
Figure A14: Calibration plots for analytes analysed on the BGB-wax column. Figure taken from Raeber et al.¹⁸⁹

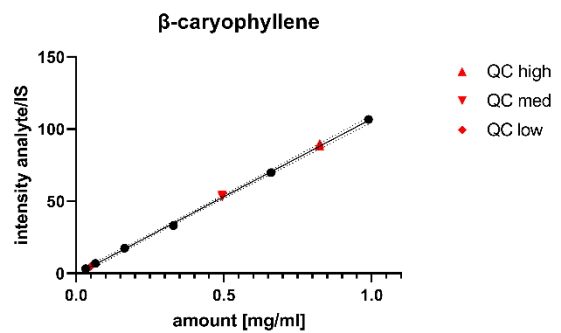
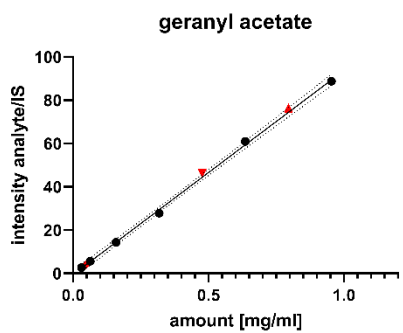
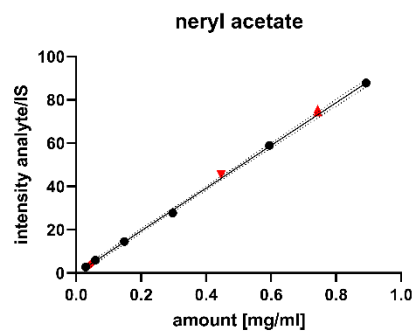
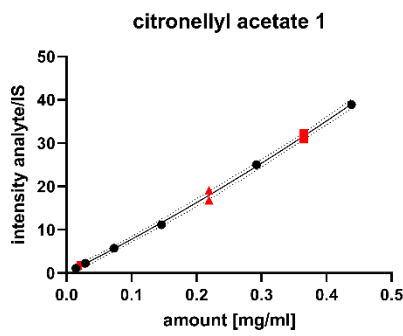
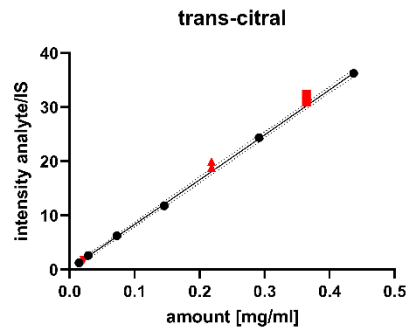
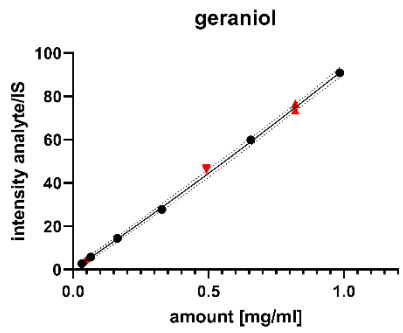
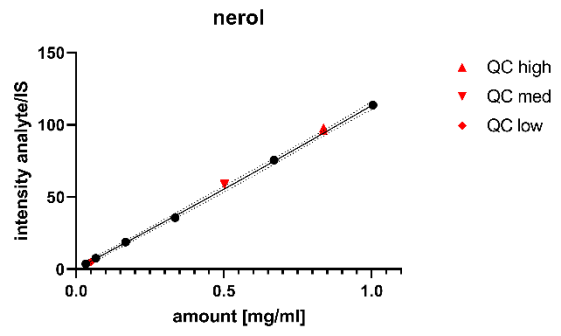
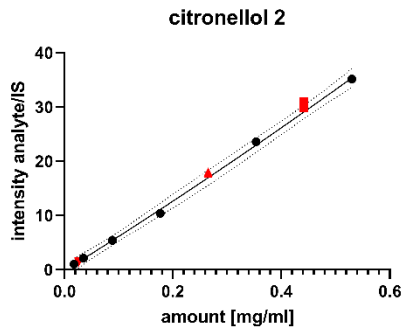
Table A11: Regression functions acquired for the GC-FID method using the BGB-wax column. Table adapted from Raeber et al.¹⁸⁹

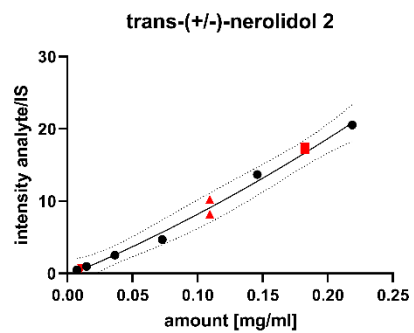
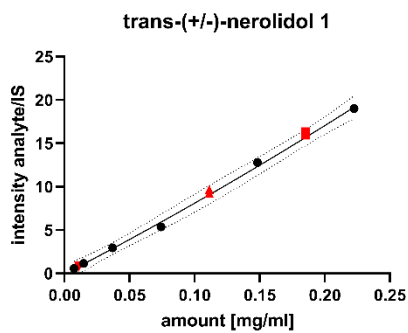
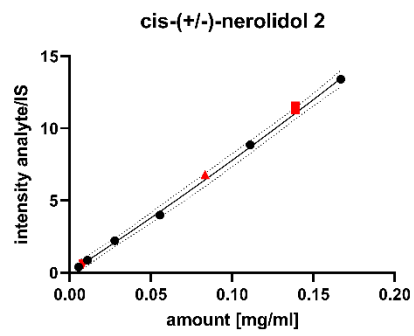
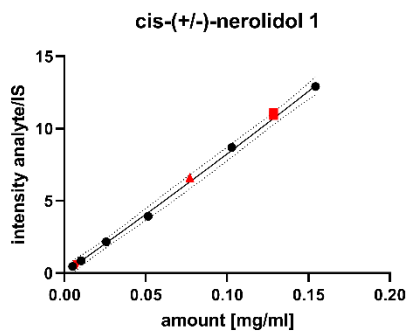
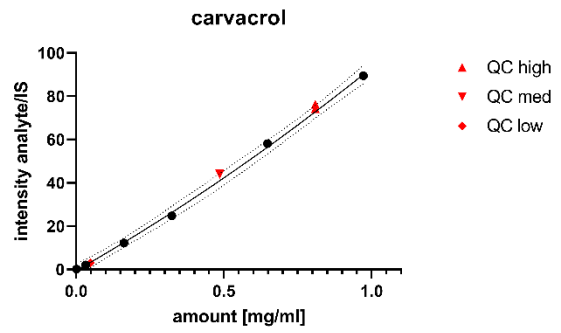
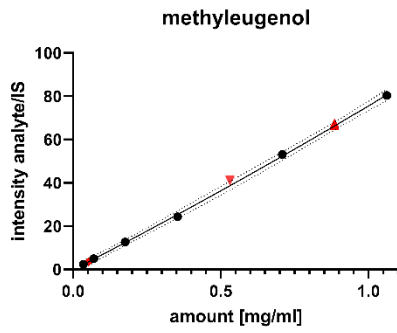
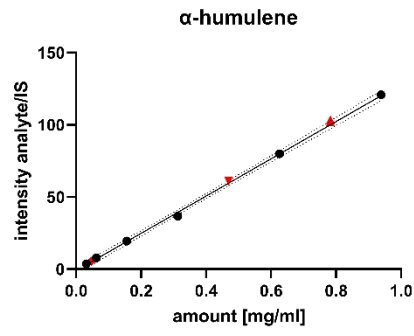
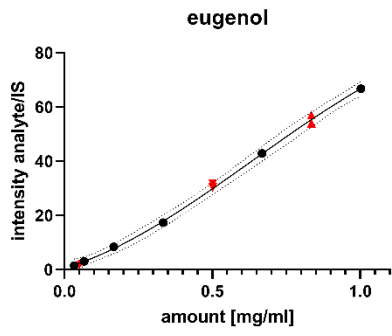
#	Analyte	Equation type	Equation	Goodness of fit R ²
1	α-pinene	Linear	Y = 132.5*X - 0.8395	0.9993
2	camphene	Linear	Y = 145.4*X - 0.8251	0.9993
3	β-pinene	Linear	Y = 143.3*X - 1.403	0.9992
4	sabinene	Linear	Y = 135.7*X - 0.3343	0.9991
5	myrcene	Linear	Y = 124.5*X - 1.165	0.9989
6	α-terpinene	Linear	Y = 102.5*X - 0.8582	0.9991
7	limonene	Linear	Y = 138.4*X - 1.155	0.9989
8	γ-terpinene	Linear	Y = 116.2*X - 0.8975	0.9990
9	p-cymene	Linear	Y = 183.8*X - 1.396	0.9990
10	α-terpinolene	Linear	Y = 117.8*X - 1.100	0.9990
11	cis-rose oxide	Quadratic	Y = -0.1098 + 84.77*X + 23.40*X ²	1.000
12	trans-rose-oxide	Quadratic	Y = 0.09979 + 72.77*X + 241.7*X ²	1.000
13	cis-3-hexen-1-ol	NA	NA	NA
14	trans-menthone	Quadratic	Y = -0.1208 + 70.69*X + 28.08*X ²	1.000
15	cis-menthone	Quadratic	Y = -0.2583 + 80.84 *X + 9.686 *X ²	0.9991
16	linalool	Quadratic	Y = 0.1644 + 104.6*X + 26.78*X ²	1.000
17	isobornyl acetate	Linear	Y = 108.6*X - 1.437	0.9983
18	β-caryophyllene	Quadratic	Y = 0.2940 + 96.90*X + 20.16*X ²	1.000
19	α-humulene	Quadratic	Y = 0.4305 + 135.4*X + 45.80*X ²	1.000
20	citronellyl acetate	Quadratic	Y = -0.04279 + 80.54*X + 21.35*X ²	1.000
21	cis-citral	Quadratic	Y = 0.1592 + 80.23*X + 120.7*X ²	1.000
22	neryl acetate	NA	NA	NA
23	trans-citral	NA	NA	NA
24	geranyl acetate	Quadratic	Y = 0.2051 + 87.10*X + 20.53*X ²	1.000
25	citronellol	Quadratic	Y = -0.1001 + 68.59*X + 21.43*X ²	1.000
26	nerol	Quadratic	Y = 0.2810 + 100.3*X + 22.66*X ²	1.000
27	phenylethanol	Quadratic	Y = 0.1957 + 103.3*X + 33.86*X ²	1.000
28	geraniol	Quadratic	Y = 0.2671 + 84.59*X + 20.54*X ²	1.000
29	cis-nerolidol	Quadratic	Y = -0.06779 + 81.74*X + 94.08*X ²	1.000
30	methyleugenol	Quadratic	Y = -0.05093 + 71.12*X + 17.69*X ²	1.000
31	trans-nerolidol	Quadratic	Y = -0.1165 + 81.59*X + 68.44*X ²	1.000
32	eugenol	Quadratic	Y = -0.5610 + 63.24*X + 26.30*X ²	1.000
33	carvacrol	Quadratic	Y = -0.9395 + 88.25*X + 31.59*X ²	0.9999
34	farnesol 1	Quadratic	Y = -0.004047 + 76.99*X + 248.1*X ²	1.000
35	farnesol 2	Quadratic	Y = -0.08291 + 78.77*X + 93.47*X ²	1.000
36	farnesol 3	Quadratic	Y = -0.2010 + 81.00*X + 55.65*X ²	1.000











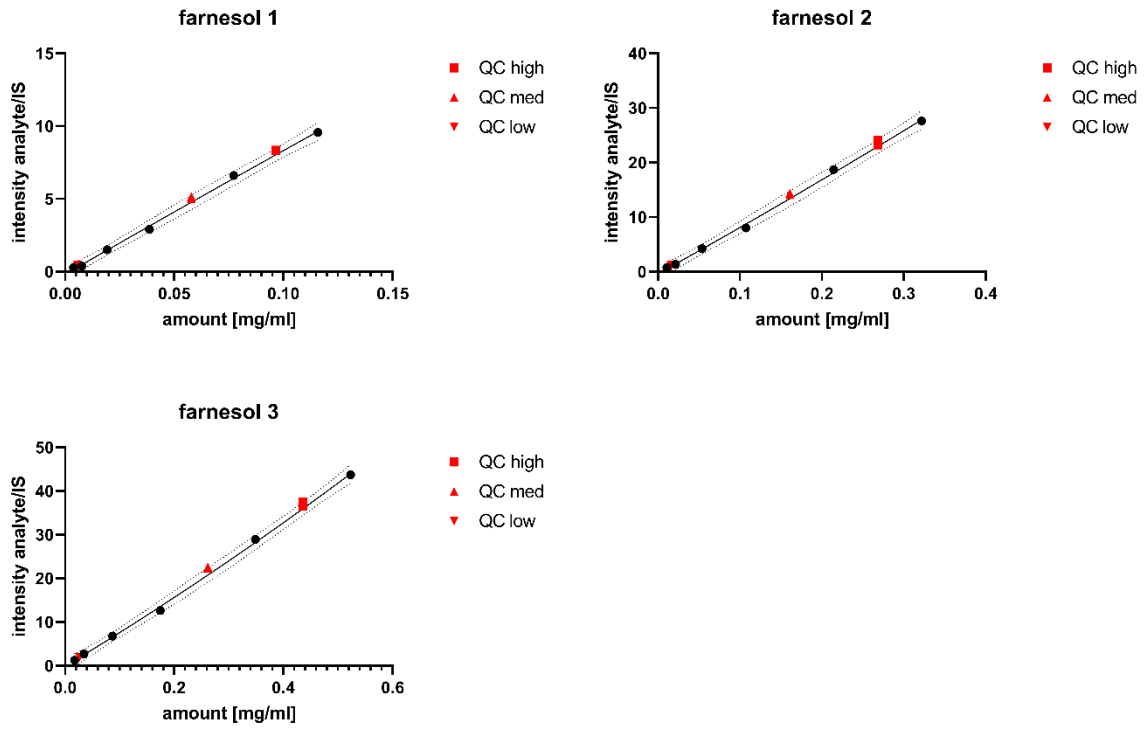
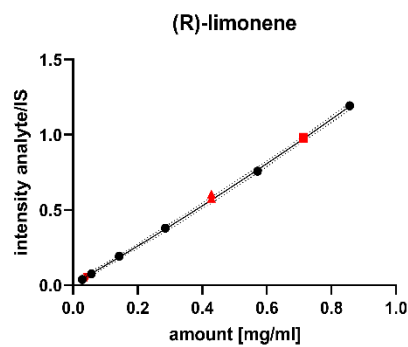
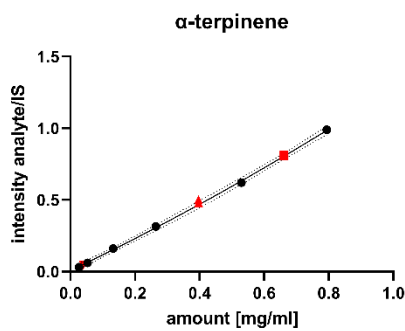
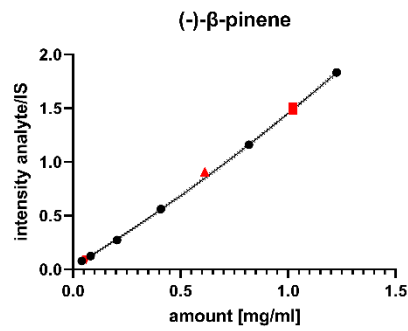
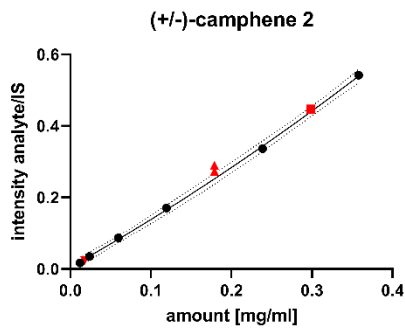
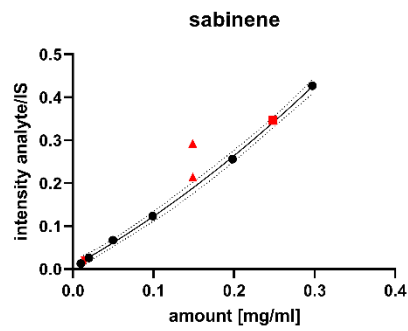
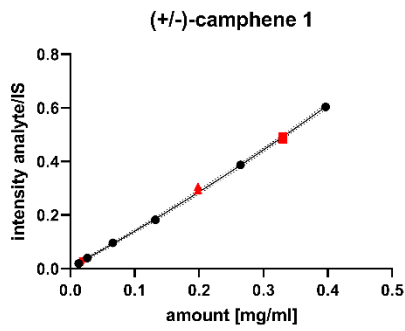
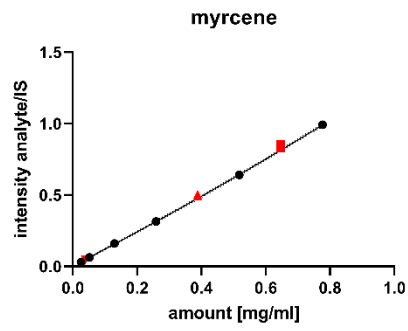
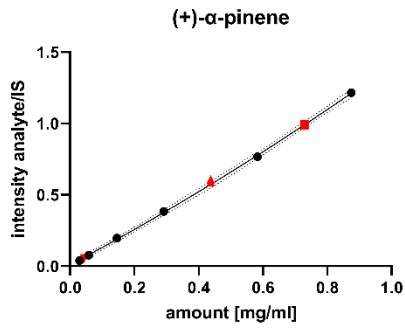
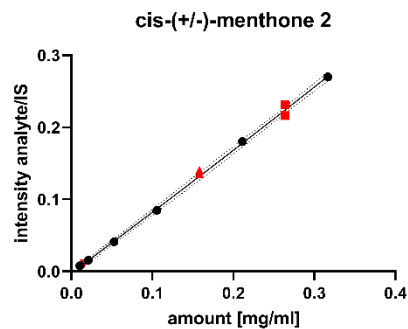
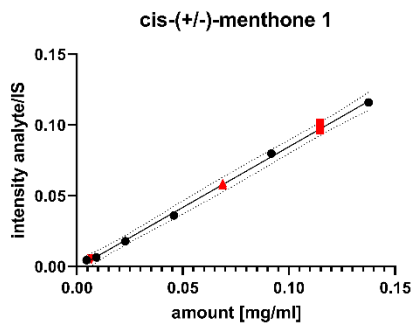
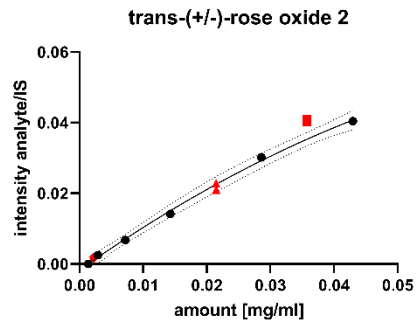
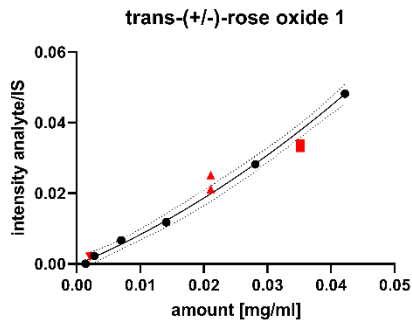
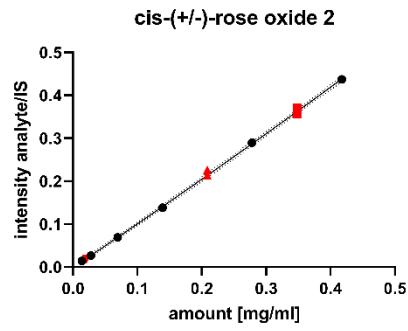
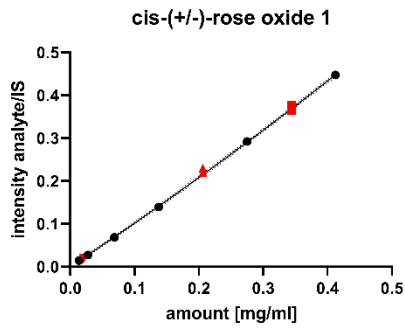
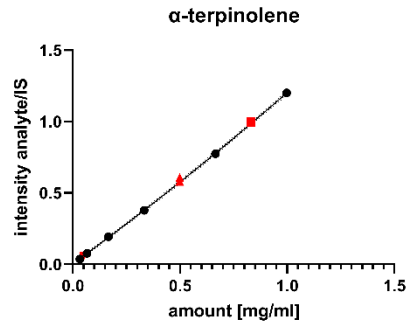
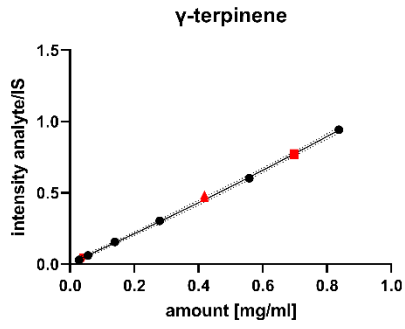


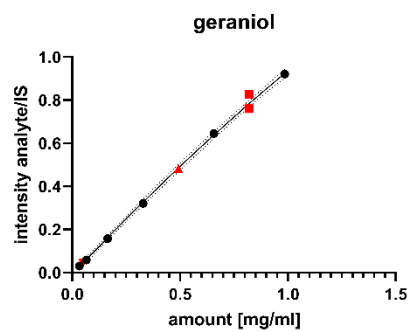
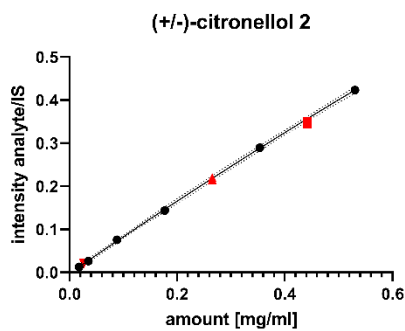
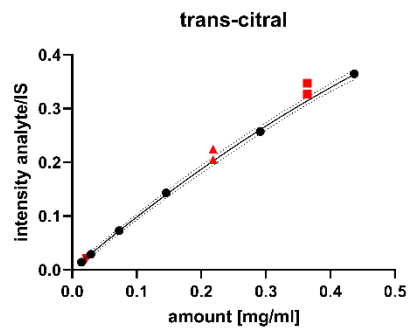
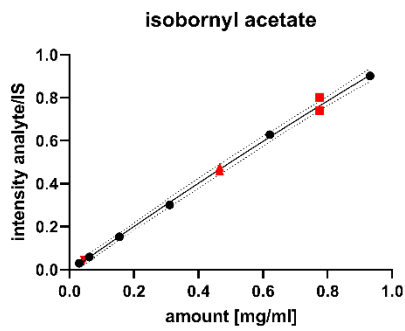
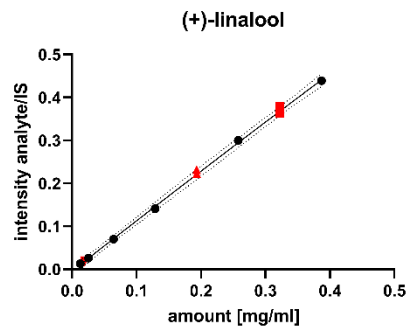
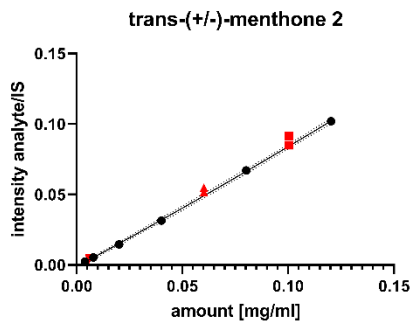
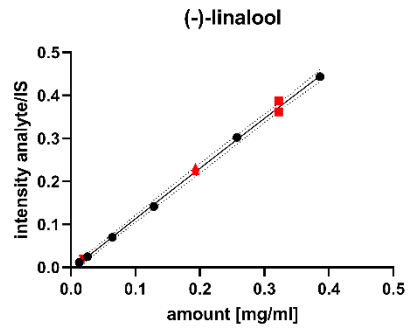
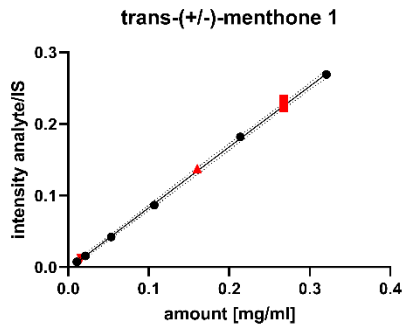
Figure A15: Calibration plots for analytes analysed on the BGB 178 30% CD column. Figure taken from Raeber et al.¹⁸⁹

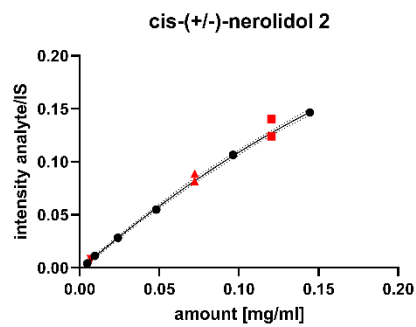
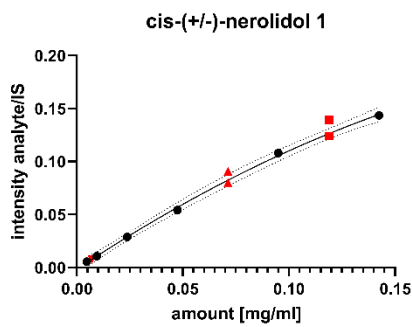
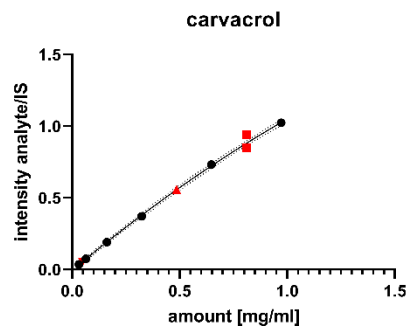
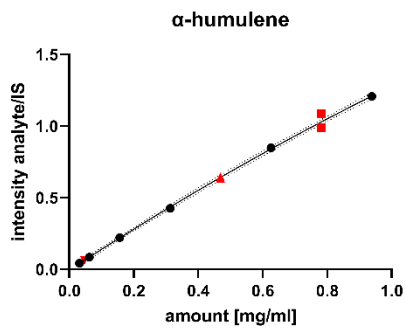
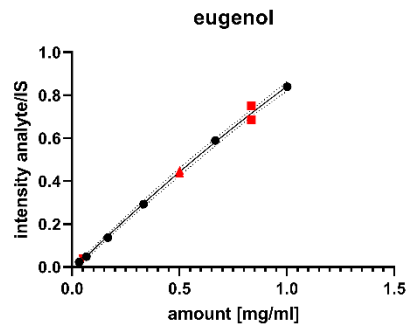
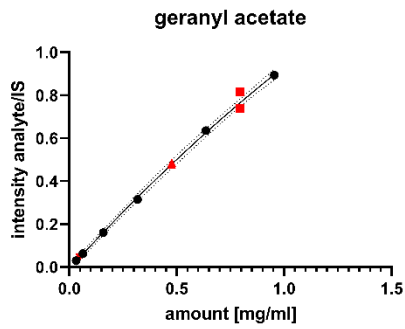
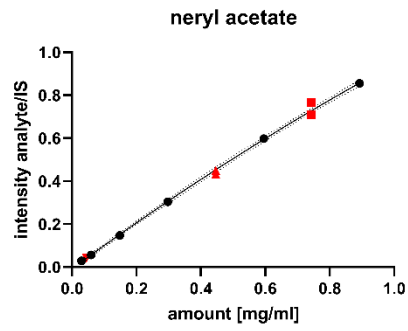
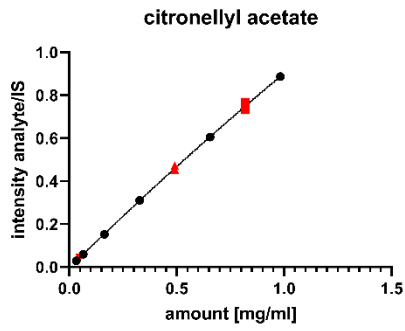
Table A12: Regression functions acquired for the GC-FID method using the BGB 178 30% CD chiral column. Table adapted from Raeber et al.¹⁸⁹

#	Analyte	Equation type	Equation	Goodness of fit R ²
1	(±)-α-pinene	Quadratic	$Y = 0.7825 + 135.4 \cdot X + 25.95 \cdot X^2$	0.9995
2	(±)-camphene 1	Quadratic	$Y = 0.3554 + 146.9 \cdot X + 65.79 \cdot X^2$	0.9996
3	(±)-camphene 2	Quadratic	$Y = 0.3159 + 145.4 \cdot X + 68.57 \cdot X^2$	0.9996
4	(+)-β-pinene	Quadratic	$Y = 0.03157 + 147.8 \cdot X + 509.1 \cdot X^2$	0.9998
5	(-)-β-pinene	Quadratic	$Y = 0.6740 + 144.2 \cdot X + 14.06 \cdot X^2$	0.9999
6	sabinene	Quadratic	$Y = 0.2709 + 132.6 \cdot X + 78.20 \cdot X^2$	0.9996
7	myrcene	Quadratic	$Y = 0.4370 + 119.9 \cdot X + 28.42 \cdot X^2$	0.9997
8	cis-3-hexen-1-ol	NA	NA	NA
9	α-terpinene	Quadratic	$Y = 0.6571 + 118.6 \cdot X + 24.53 \cdot X^2$	0.9997
10	(S)-limonene	NA	NA	NA
11	(R)-limonene	Quadratic	$Y = 0.5530 + 130.0 \cdot X - 22.87 \cdot X^2$	0.9997
12	p-cymene	Quadratic	$Y = 0.2506 + 192.3 \cdot X + 57.74 \cdot X^2$	1.000
13	α-terpinolene	Quadratic	$Y = 0.6541 + 111.1 \cdot X + 16.80 \cdot X^2$	0.9999
14	γ-terpinene	Quadratic	$Y = 0.6025 + 112.9 \cdot X + 20.08 \cdot X^2$	0.9998
15	(±)-cis-rose oxide 1	Quadratic	$Y = -0.09524 + 84.60 \cdot X + 31.31 \cdot X^2$	0.9999
16	(±)-cis-rose oxide 2	Quadratic	$Y = 0.00322 + 82.77 \cdot X + 46.28 \cdot X^2$	0.9999
17	(±)-trans-rose oxide 1	Quadratic	$Y = -0.00027 + 80.80 \cdot X + 357.2 \cdot X^2$	0.9996
18	(±)-trans-rose oxide 2	Quadratic	$Y = -0.0031 + 83.92 \cdot X + 331.5 \cdot X^2$	0.9996
19	(-)-linalool	Quadratic	$Y = -0.0047 + 113.8 \cdot X + 24.84 \cdot X^2$	0.9998
20	(±)-cis-menthone 1	Quadratic	$Y = -0.0460 + 51.87 \cdot X + 72.89 \cdot X^2$	0.9996
21	(±)-cis-menthone 2	NA	NA	NA
22	(+)-linalool	NA	NA	NA
23	(±)-trans-menthone 1	Quadratic	$Y = -0.6049 + 86.27 \cdot X + 35.26 \cdot X^2$	0.9997
24	(±)-trans-menthone 2	Quadratic	$Y = 0.00490 + 29.66 \cdot X + 19.80 \cdot X^2$	0.9993
25	isobornyl acetate	Quadratic	$Y = 0.2646 + 96.67 \cdot X + 4.814 \cdot X^2$	0.9998
26	phenylethanol	Quadratic	$Y = 0.1396 + 110.4 \cdot X + 12.68 \cdot X^2$	0.9999
27	trans-citral	Quadratic	$Y = 0.1328 + 84.20 \cdot X + 15.86 \cdot X^2$	0.9999
28	(±)-citronellol 1	Quadratic	$Y = -0.1495 + 69.45 \cdot X + 23.46 \cdot X^2$	0.9995
29	(±)-citronellol 2	Quadratic	$Y = -0.2119 + 62.38 \cdot X + 8.864 \cdot X^2$	0.9990
30	nerol	Quadratic	$Y = 0.1430 + 107.8 \cdot X + 5.424 \cdot X^2$	0.9998
31	cis-citral	Quadratic	$Y = 0.1284 + 81.80 \cdot X + 2.31 \cdot X^2$	0.9998
32	geraniol	Quadratic	$Y = -0.0217 + 85.13 \cdot X + 7.404 \cdot X^2$	0.9997
33	(±)-citronellyl acetate 1	Quadratic	$Y = -0.0383 + 75.04 \cdot X + 32.04 \cdot X^2$	0.9996
34	(±)-citronellyl acetate 2	Quadratic	$Y = -0.2604 + 77.40 \cdot X + 4.660 \cdot X^2$	0.9995
35	neryl acetate	Linear	$Y = 98.69 \cdot X - 0.3525$	0.9996
36	geranyl acetate	Linear	$Y = 94.17 \cdot X - 0.5369$	0.9991
37	β-caryophyllene	Linear	$Y = 107.7 \cdot X - 0.7075$	0.9995
38	eugenol	3 rd order polynomial	$Y = 0.5412 + 32.19 \cdot X + 70.99 \cdot X^2 - 37.12 \cdot X^3$	0.9998
39	α-humulene	Linear	$Y = 129.1 \cdot X - 1.059$	0.9992
40	methyleugenol	Quadratic	$Y = -0.2062 + 70.23 \cdot X + 5.484 \cdot X^2$	0.9996
41	carvacrol	Quadratic	$Y = -0.5830 + 77.68 \cdot X + 15.96 \cdot X^2$	0.9991
42	(±)-cis-nerolidol 1	Quadratic	$Y = 0.0244 + 79.33 \cdot X + 28.88 \cdot X^2$	0.9990
43	(±)-cis-nerolidol 2	Quadratic	$Y = 0.0168 + 73.41 \cdot X + 42.65 \cdot X^2$	0.9992
44	(±)-trans-nerolidol 1	Quadratic	$Y = -0.0780 + 77.79 \cdot X + 38.88 \cdot X^2$	0.9979
45	(±)-trans-nerolidol 2	Quadratic	$Y = -0.3098 + 75.21 \cdot X + 97.86 \cdot X^2$	0.9938
46	farnesol 1	Quadratic	$Y = -0.1919 + 86.54 \cdot X - 14.82 \cdot X^2$	0.9982
47	farnesol 2	Quadratic	$Y = -0.3887 + 83.48 \cdot X + 12.75 \cdot X^2$	0.9983
48	farnesol 3	Quadratic	$Y = -0.1247 + 75.27 \cdot X + 17.18 \cdot X^2$	0.9990









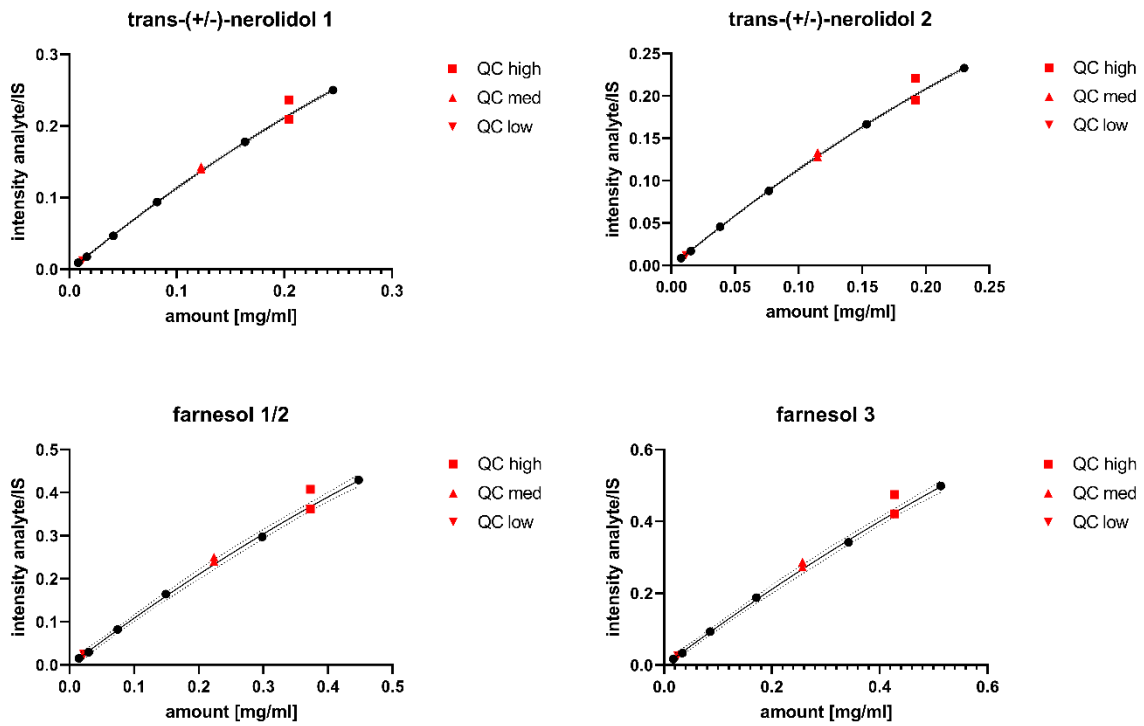
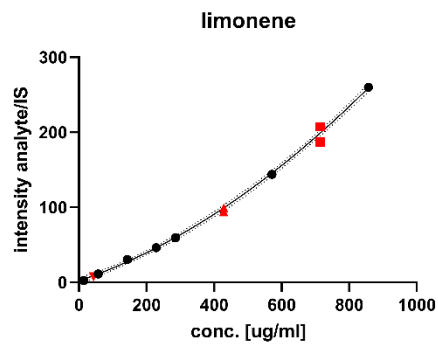
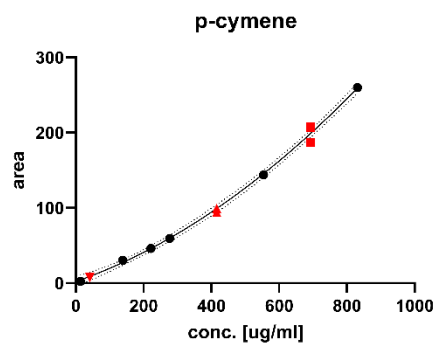
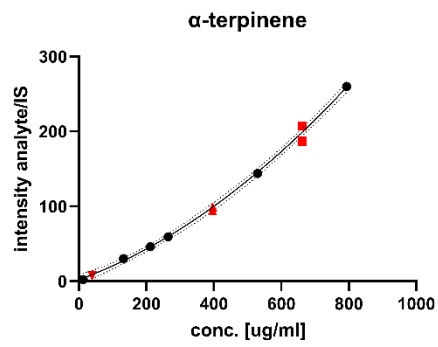
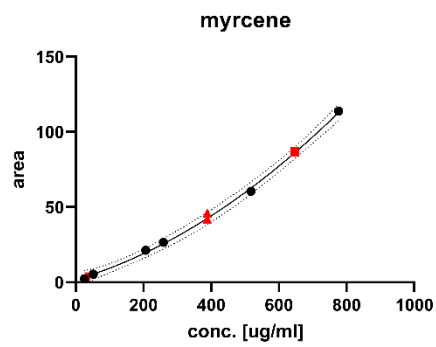
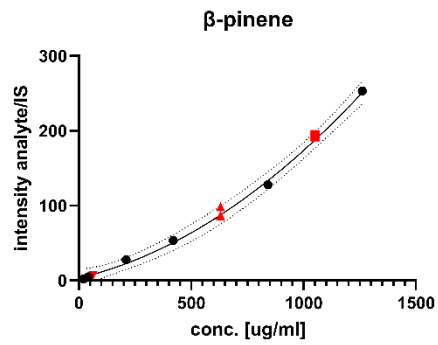
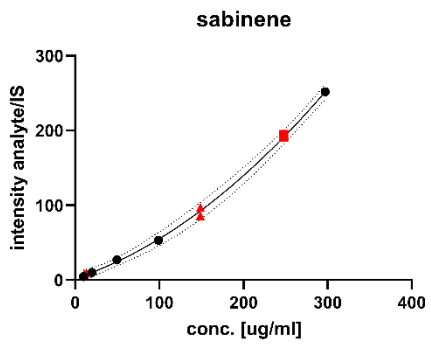
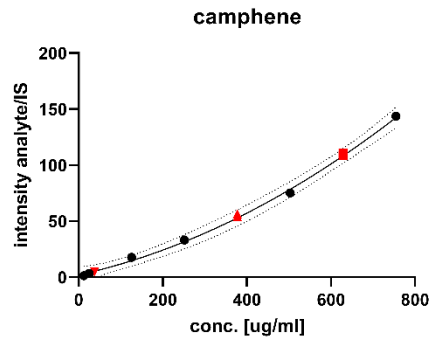
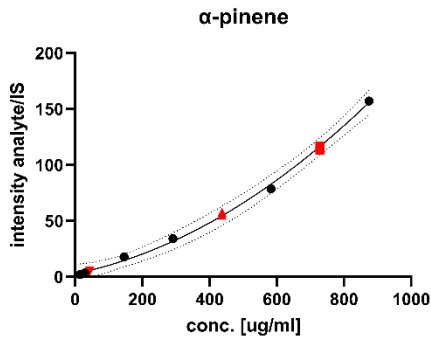


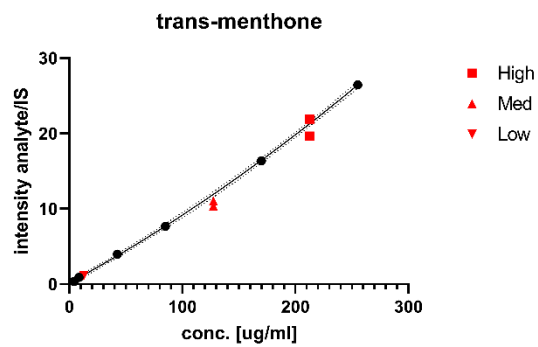
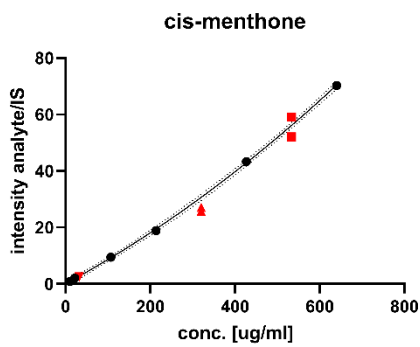
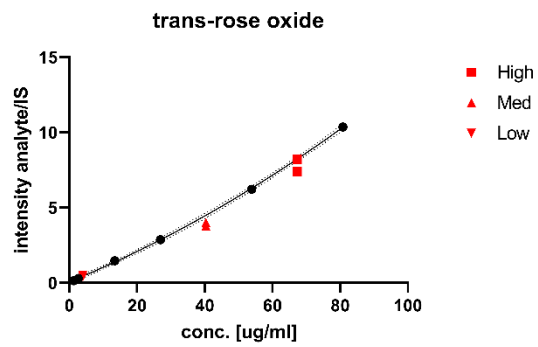
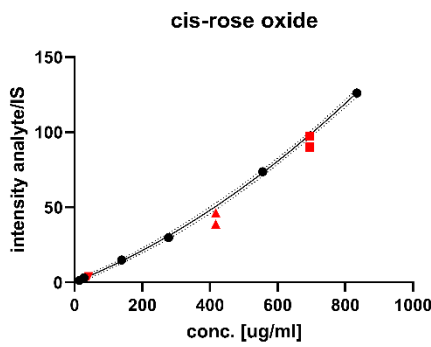
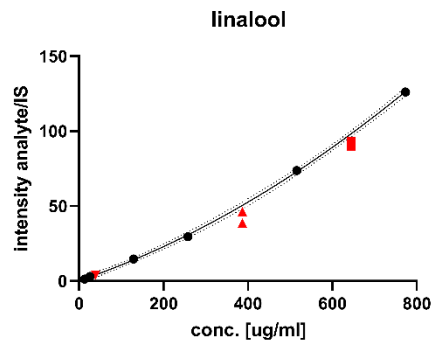
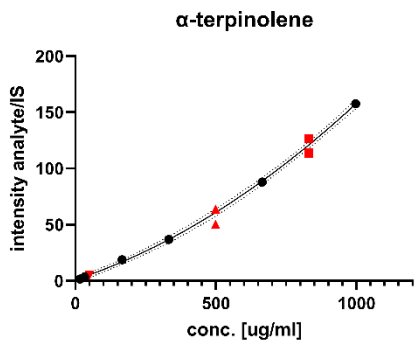
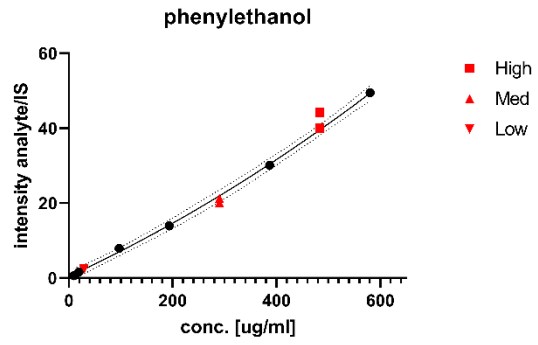
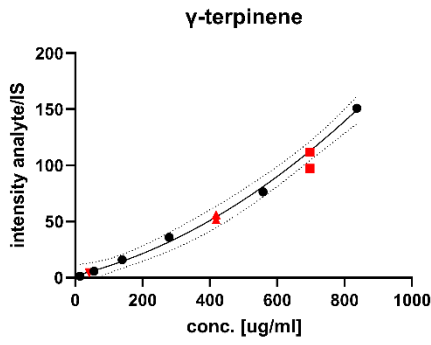
Figure A16: Calibration plots for analytes analysed on the BGB 176 SE column.

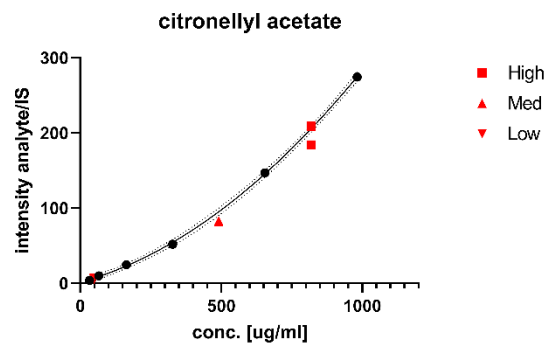
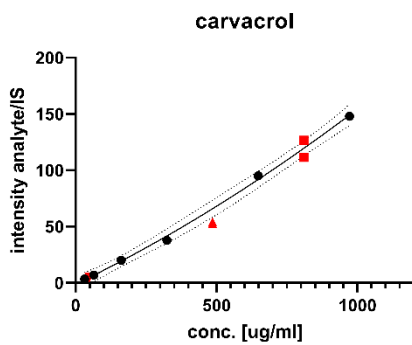
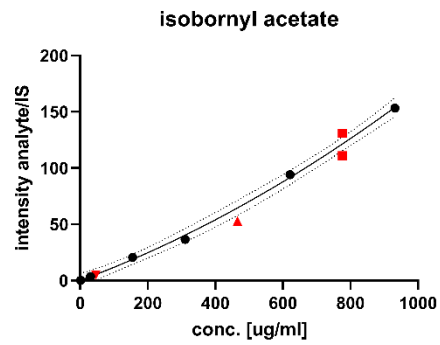
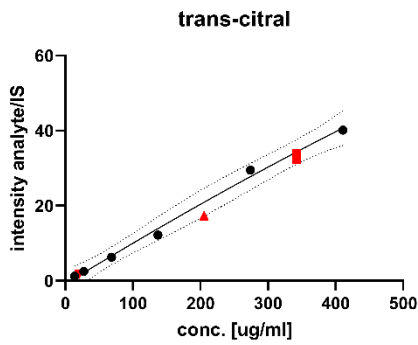
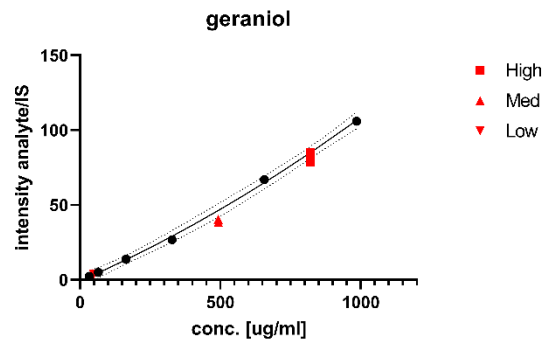
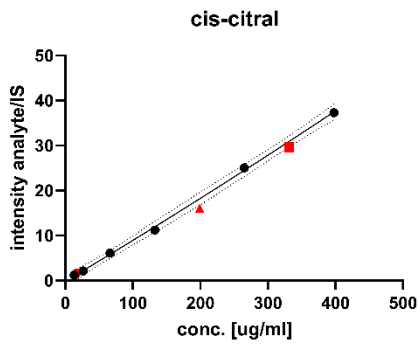
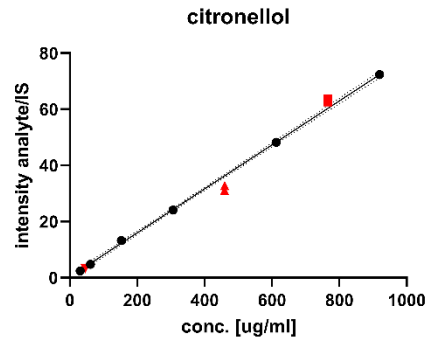
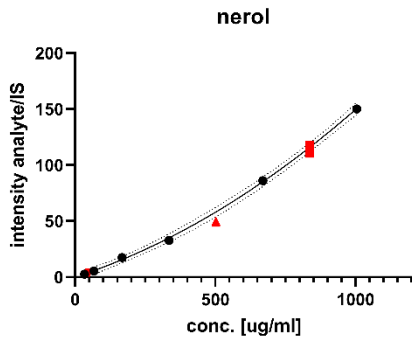
Figure taken from Raeber et al.¹⁸⁹

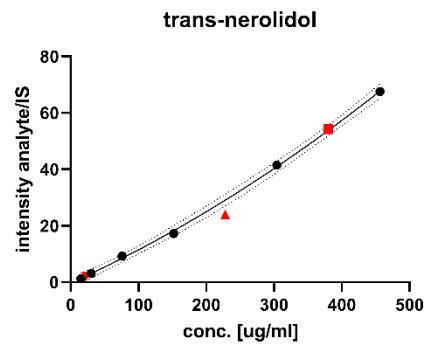
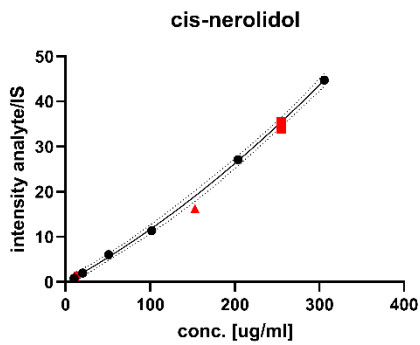
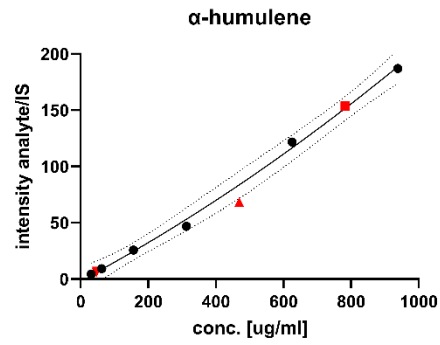
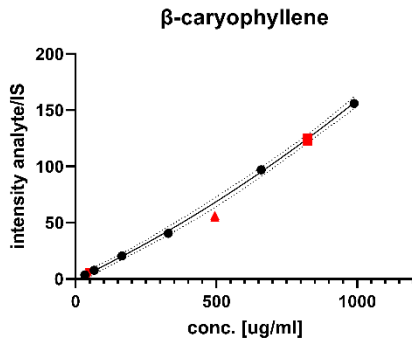
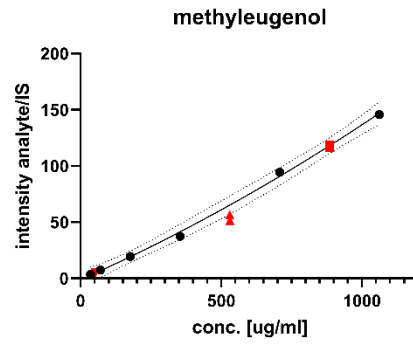
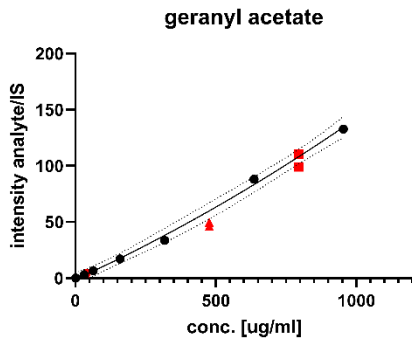
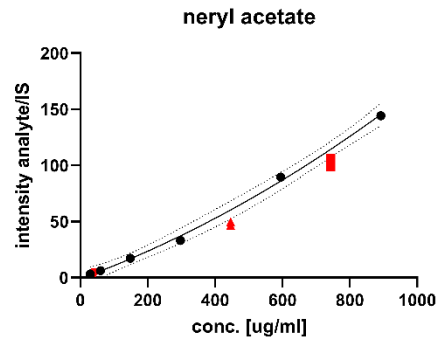
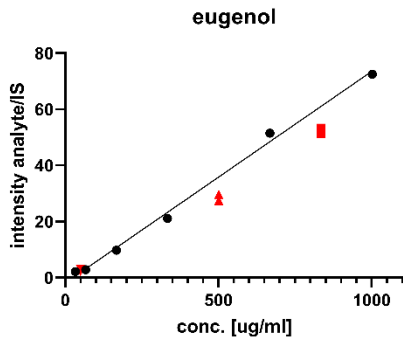
Table A13: Regression functions acquired for the GC-FID method using the BGB 176 SE chiral column. Table adapted from Raeber et al.¹⁸⁹

#	Analyte	Equation type	Equation	Goodness of fit R ²
1	(-)- α -pinene	NA	NA	NA
2	(+)- α -pinene	Quadratic	$Y = 0.0092 + 1.202*X + 0.1978*X^2$	0.9997
3	myrcene	Quadratic	$Y = 0.0030 + 1.163*X + 0.1382*X^2$	1.000
4	camphene	Quadratic	$Y = 0.0037 + 1.309*X + 0.5136*X^2$	0.9999
5	sabinene	Quadratic	$Y = 0.0060 + 1.044*X + 1.227*X^2$	0.9993
6	camphene	Quadratic	$Y = 0.0051 + 1.265*X + 0.6325*X^2$	0.9995
7	(+)- β -pinene	NA	NA	NA
8	cis-hexen-1-ol	NA	NA	NA
9	(-)- β -pinene	Quadratic	$Y = 0.0231 + 1.217*X + 0.2105*X^2$	0.9999
10	α -terpinene	Quadratic	$Y = 0.0068 + 1.078*X + 0.1934*X^2$	0.9996
11	p-cymene	NA	NA	NA
12	(S)-limonene	NA	NA	NA
13	(R)-limonene	Quadratic	$Y = 0.0071 + 1.231*X + 0.1732*X^2$	0.9998
14	γ -terpinene	Quadratic	$Y = 0.0058 + 1.013*X + 0.1228*X^2$	0.9998
15	α -terpinolene	Quadratic	$Y = 0.0036 + 1.091*X + 0.1081*X^2$	0.9999
16	(+/-)-cis-rose oxide 1	Quadratic	$Y = -0.0003 + 0.9987*X + 0.2129*X^2$	0.9999
17	(+/-)-cis-rose oxide 2	Quadratic	$Y = -0.0014 + 1.005*X + 0.1141*X^2$	0.9999
18	(+/-)-trans-rose oxide 1	Quadratic	$Y = -0.0002 + 0.7599*X + 9.119*X^2$	0.9986
19	(+/-)-trans-rose oxide 1	Quadratic	$Y = -0.0017 + 1.271*X - 6.579*X^2$	0.9983
20	(+/-)-cis-menthone 1	Quadratic	$Y = -0.0011 + 0.8567*X + 0.0028*X^2$	0.9987
21	(+/-)-cis-menthone 2	Quadratic	$Y = -0.0023 + 0.8346*X + 0.0873*X^2$	0.9998
22	(+/-)-trans-menthone 1	Quadratic	$Y = -0.0029 + 0.8588*X - 0.0258*X^2$	0.9998
23	(-)-linalool	Quadratic	$Y = -0.0062 + 1.196*X - 0.0709*X^2$	0.9996
24	(+/-)-trans-menthone 2	Quadratic	$Y = -0.0013 + 0.8118*X + 0.3995*X^2$	0.9998
25	(+)-linalool	Quadratic	$Y = -0.0045 + 1.177*X - 0.0681*X^2$	0.9995
26	isobornyl acetate	Quadratic	$Y = -0.0076 + 1.057*X - 0.0831*X^2$	0.9995
27	phenylethanol	NA	NA	NA
28	trans-citral	NA	NA	NA
29	cis-citral	Quadratic	$Y = 0.0005 + 1.018*X - 0.4312*X^2$	0.9997
30	nerol	NA	NA	NA
31	(+/-)-citronellol 1	NA	NA	NA
32	(+/-)-citronellol 2	Quadratic	$Y = -0.0026 + 0.862*X - 0.1112*X^2$	0.9999
33	geraniol	Quadratic	$Y = -0.0093 + 1.060*X - 0.1148*X^2$	0.9998
34	citronellyl acetate	Quadratic	$Y = -0.0041 + 0.9796*X - 0.0738*X^2$	1.000
35	neryl acetate	Quadratic	$Y = -0.0083 + 1.097*X - 0.1433*X^2$	0.9999
36	geranyl acetate	Quadratic	$Y = -0.0080 + 1.092*X - 0.1516*X^2$	0.9997
37	eugenol	Quadratic	$Y = -0.0152 + 0.9727*X - 0.1171*X^2$	0.9997
38	methyleugenol	NA	NA	NA
39	β -caryophyllene	NA	NA	NA
40	α -humulene	Quadratic	$Y = -0.0061 + 1.465*X - 0.1811*X^2$	0.9998
41	carvacrol	Quadratic	$Y = -0.0066 + 1.253*X - 0.1969*X^2$	0.9998
42	(+/-)-cis-nerolidol 1	Quadratic	$Y = -0.0017 + 1.336*X - 2.177*X^2$	0.9991
43	(+/-)-cis-nerolidol 2	Quadratic	$Y = -0.0017 + 1.286*X - 1.795*X^2$	0.9998
44	(+/-)-trans-nerolidol 1	Quadratic	$Y = -0.0019 + 1.238*X - 0.8563*X^2$	1.000
45	(+/-)-trans-nerolidol 2	Quadratic	$Y = -0.0012 + 1.244*X - 0.9862*X^2$	1.000
46	farnesol 1	Quadratic	$Y = -0.0014 + 1.136*X - 0.3948*X^2$	0.9995
47	farnesol 2	Quadratic	$Y = -0.0016 + 1.121*X - 0.2924*X^2$	0.9995









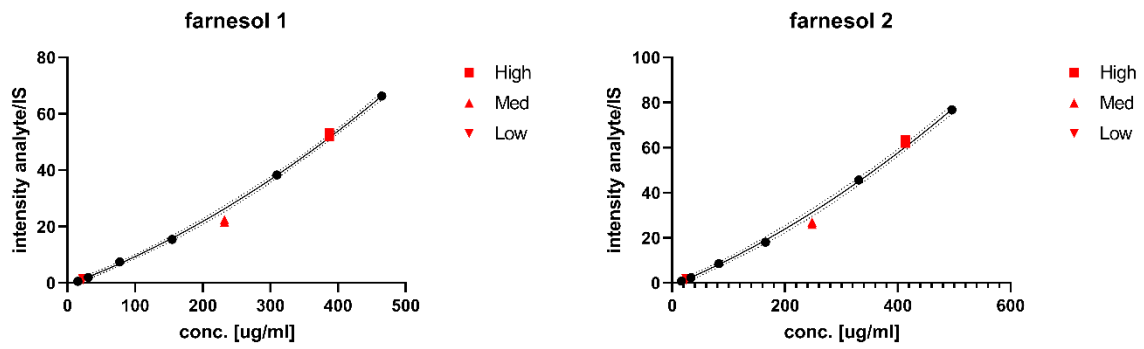


Figure A17: Calibration plots for analytes analysed on the BGB 176 SE column. Figure taken from Raeber et al.¹⁸⁹

Table A14: Regression functions acquired for the GC-MS method using the DB-5 MS.Table adapted from Raeber et al.¹⁸⁹

#	Analyte	Equation type	Equation	Goodness of fit R ²
1	cis-hexen-1-ol	NA	NA	NA
2	α-pinene	Quadratic	$Y = 2.826 + 0.0618*X + 0.0001*X^2$	0.9979
3	camphene	Quadratic	$Y = 2.081 + 0.0835*X + 0.0001*X^2$	0.9982
4	sabinene	Quadratic	$Y = 2.139 + 0.3737*X + 0.0016*X^2$	0.9997
5	β-pinene	Quadratic	$Y = 3.295 + 0.0708*X + 0.0001*X^2$	0.9984
6	myrcene	Quadratic	$Y = 1.743 + 0.0665*X + 0.0001*X^2$	0.9989
7	α-terpinene	Quadratic	$Y = 2.108 + 0.1647*X + 0.0002*X^2$	0.9997
8	p-cymene	Quadratic	$Y = 2.096 + 0.1573*X + 0.0002*X^2$	0.9997
9	limonene	Quadratic	$Y = 2.014 + 0.1530*X + 0.0002*X^2$	0.9997
10	γ-terpinene	Quadratic	$Y = 1.881 + 0.0730*X + 0.0001*X^2$	0.9972
11	phenylethanol	Quadratic	$Y = 0.4674 + 0.0638*X + 0.00004*X^2$	0.9993
12	α-terpinolene	Quadratic	$Y = 1.002 + 0.0830*X + 0.00007*X^2$	0.9997
13	linalool	Quadratic	$Y = 0.2186 + 0.0964*X + 0.00009*X^2$	0.9998
14	cis-rose oxide	Quadratic	$Y = 0.2252 + 0.0904*X + 0.00007*X^2$	0.9998
15	trans-rose oxide	Quadratic	$Y = 0.0631 + 0.0920*X + 0.0004*X^2$	0.9998
16	trans-menthone	Quadratic	$Y = 0.0657 + 0.0811*X + 0.0004*X^2$	0.9998
17	cis-menthone	Quadratic	$Y = 0.1423 + 0.0816*X + 0.00008*X^2$	0.9999
18	nerol	Quadratic	$Y = 0.0090 + 0.0812*X + 0.00007*X^2$	0.9994
19	citronellol	Linear	$Y = 0.0783*X + 0.3081$	0.9997
20	cis-citral	Quadratic	$Y = -0.1870 + 0.0896*X + 0.00001*X^2$	0.9990
21	geraniol	Quadratic	$Y = -0.7550 + 0.0821*X + 0.00003*X^2$	0.9988
22	trans-citral	Quadratic	$Y = -0.8626 + 0.1108*X - 0.00002*X^2$	0.9947
23	isobornyl acetate	Quadratic	$Y = 0.0272 + 0.1118*X + 0.00006*X^2$	0.9987
24	carvacrol	Quadratic	$Y = -1.309 + 0.1216*X + 0.00003*X^2$	0.9983
25	citronellyl acetate	Quadratic	$Y = 1.340 + 0.1034*X + 0.0002*X^2$	0.9998
26	eugenol	Linear	$Y = 0.0754*X - 1.910$	0.9956
27	neryl acetate	Quadratic	$Y = -0.9481 + 0.1104*X + 0.00006*X^2$	0.9980
28	geranyl acetate	Quadratic	$Y = -1.182 + 0.1141*X + 0.00003*X^2$	0.9969
29	methyleugenol	Quadratic	$Y = -1.199 + 0.1107*X + 0.00003*X^2$	0.9980
30	β-caryophyllene	Quadratic	$Y = -0.6273 + 0.1178*X + 0.00004*X^2$	0.9995
31	α-humulene	Quadratic	$Y = -1.578 + 0.1607*X + 0.00004*X^2$	0.9973
32	cis-nerolidol	Quadratic	$Y = -0.1256 + 0.1036*X + 0.0001*X^2$	0.9995
33	trans-nerolidol	Quadratic	$Y = -0.3046 + 0.1085*X + 0.00009*X^2$	0.9994
34	farnesol 1	Quadratic	$Y = -0.7394 + 0.0888*X + 0.0001*X^2$	0.9998
35	farnesol 2	Quadratic	$Y = -1.130 + 0.1033*X + 0.00001*X^2$	0.9997

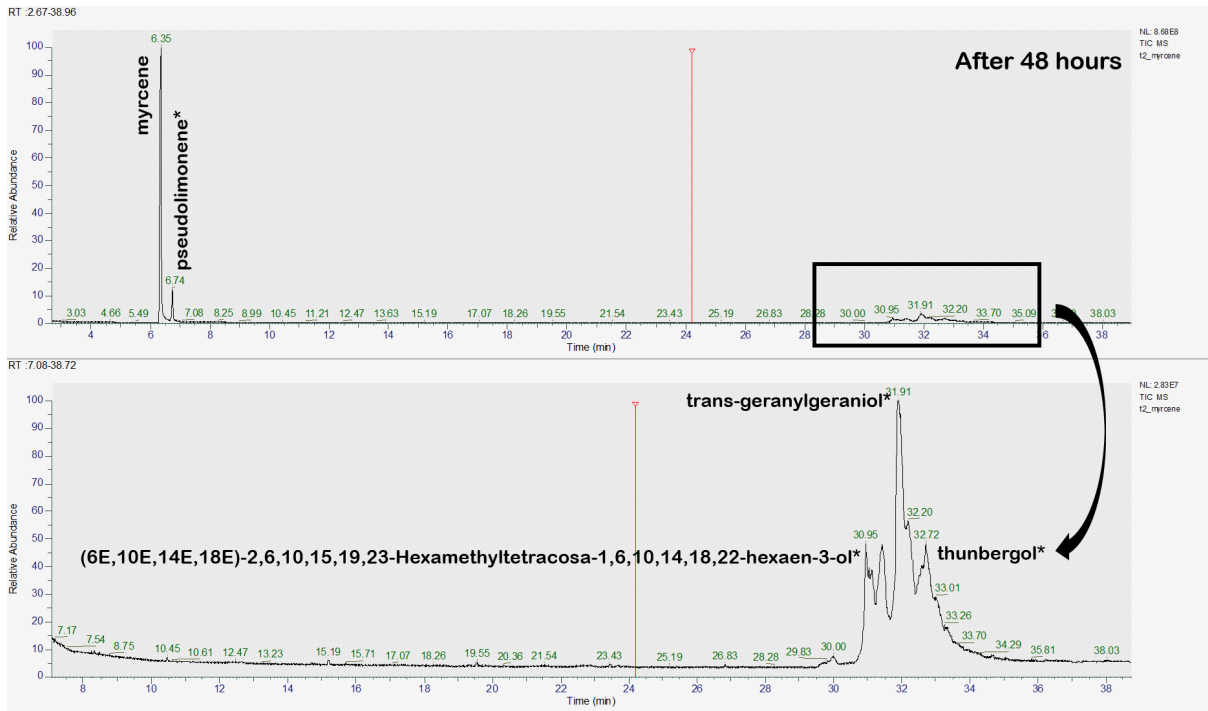


Figure A18: GC-MS chromatogram after stressing a 1 mg/ml myrcene solution for 48 hours. Compound names marked with an asterisk (*) have been putatively identified. Figure taken from Raeber et al.¹⁸⁹

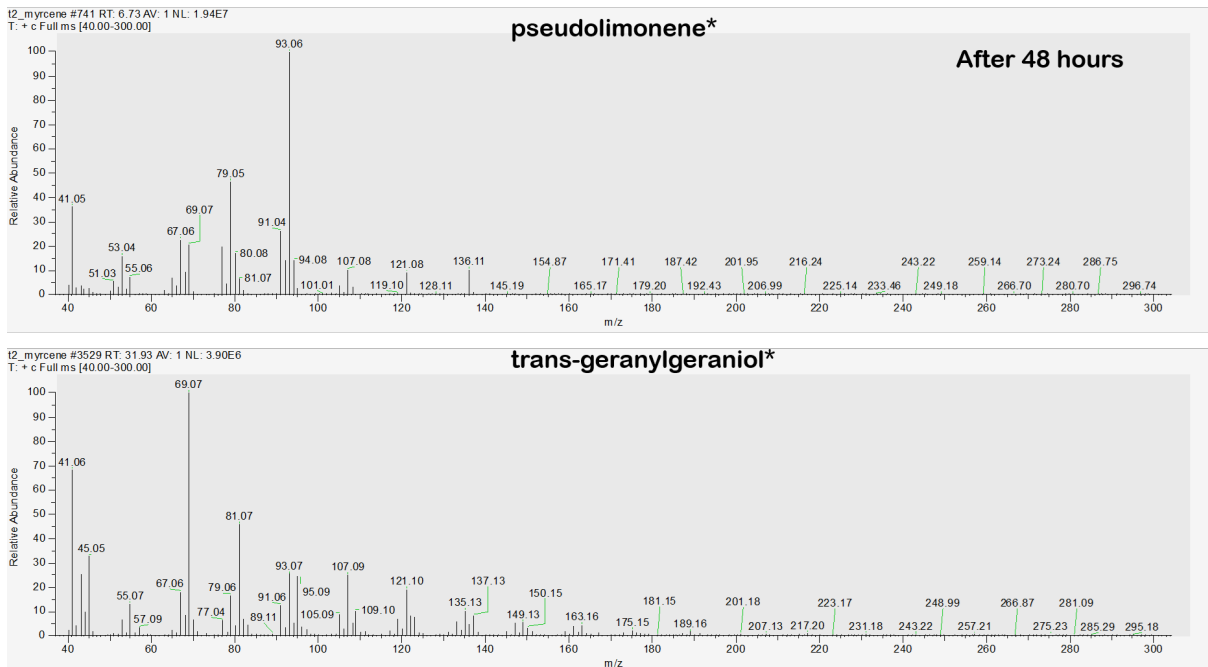


Figure A19: MS-spectra of pseudolimonene and trans-geranylgeraniol. Compound names marked with an asterisk (*) have been putatively identified. Figure taken from Raeber et al.¹⁸⁹

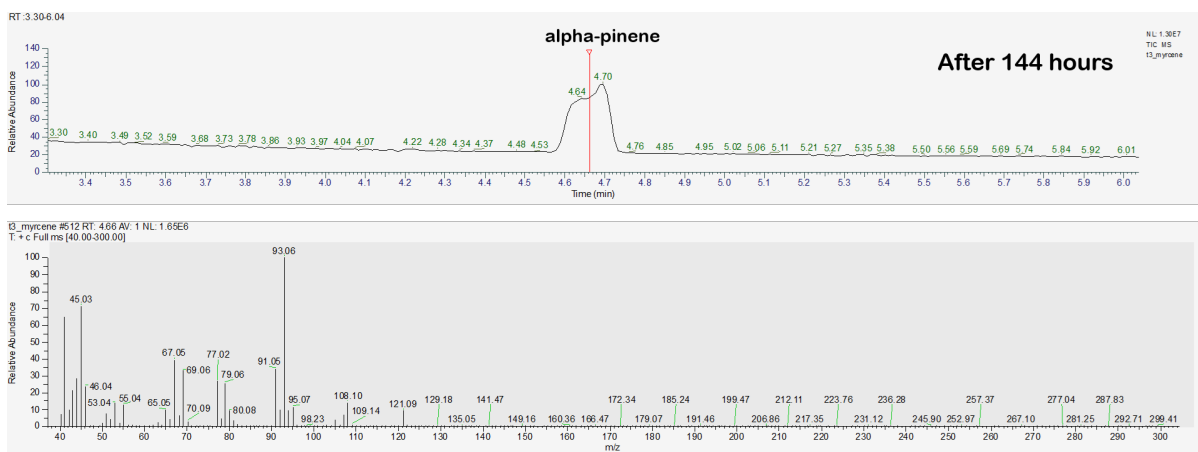


Figure A20: Chromatogram and MS-spectrum of α -pinene found in 144 hours UV-stressed myrcene sample. Figure taken from Raeber et al.¹⁸⁹

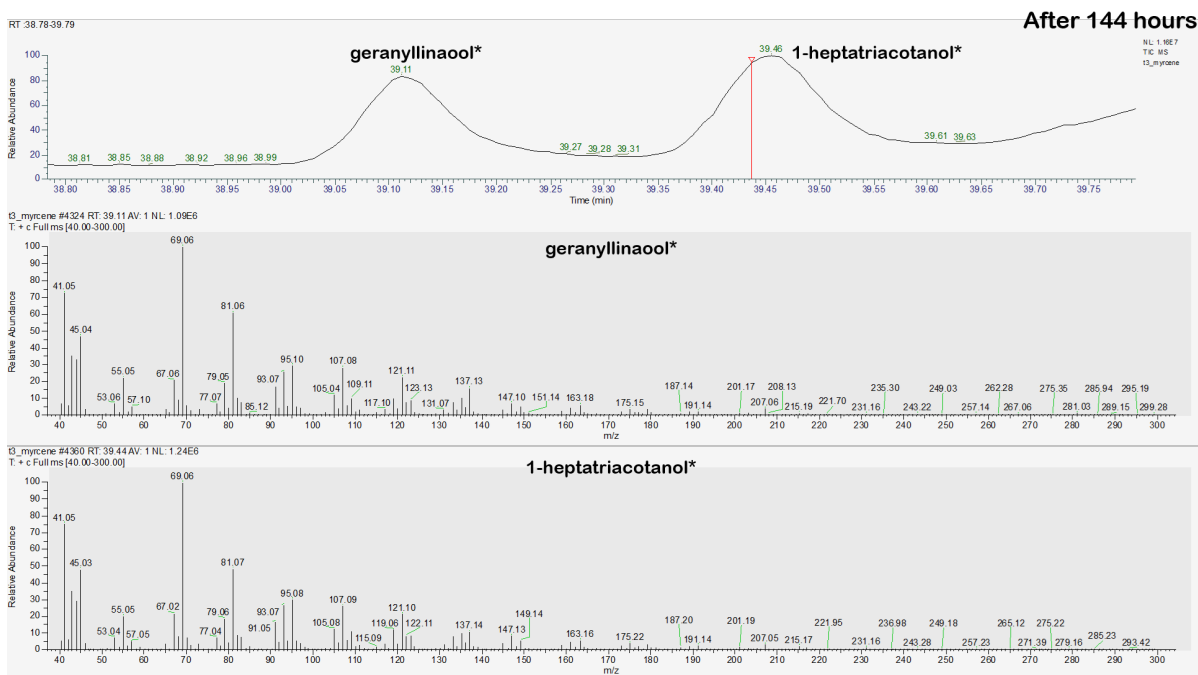


Figure A21: Chromatogram and MS-spectrum of geranyllinalool and 1-heptatriacotanol found in 144 hours UV-stressed myrcene sample. Compound names marked with an asterisk (*) have been putatively identified. Figure taken from Raeber et al.¹⁸⁹

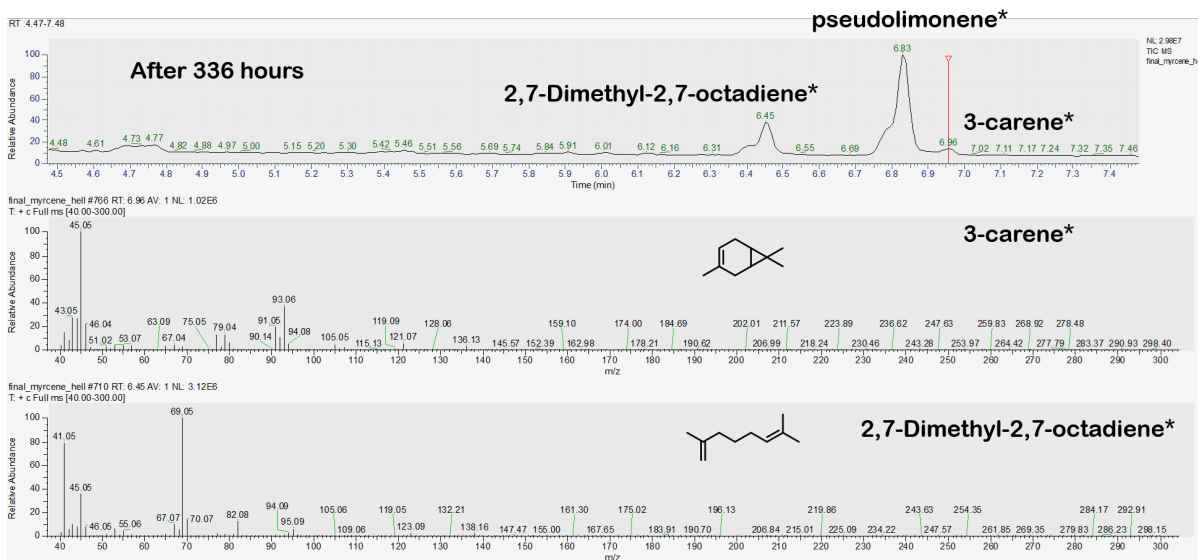


Figure A22: Chromatogram and MS-spectrum of 2,7-dimethyl-2,7-octadiene and 3-carene found in 336 hours UV-stressed myrcene sample. Compound names marked with an asterisk (*) have been putatively identified. Figure taken from Raeber et al.¹⁸⁹

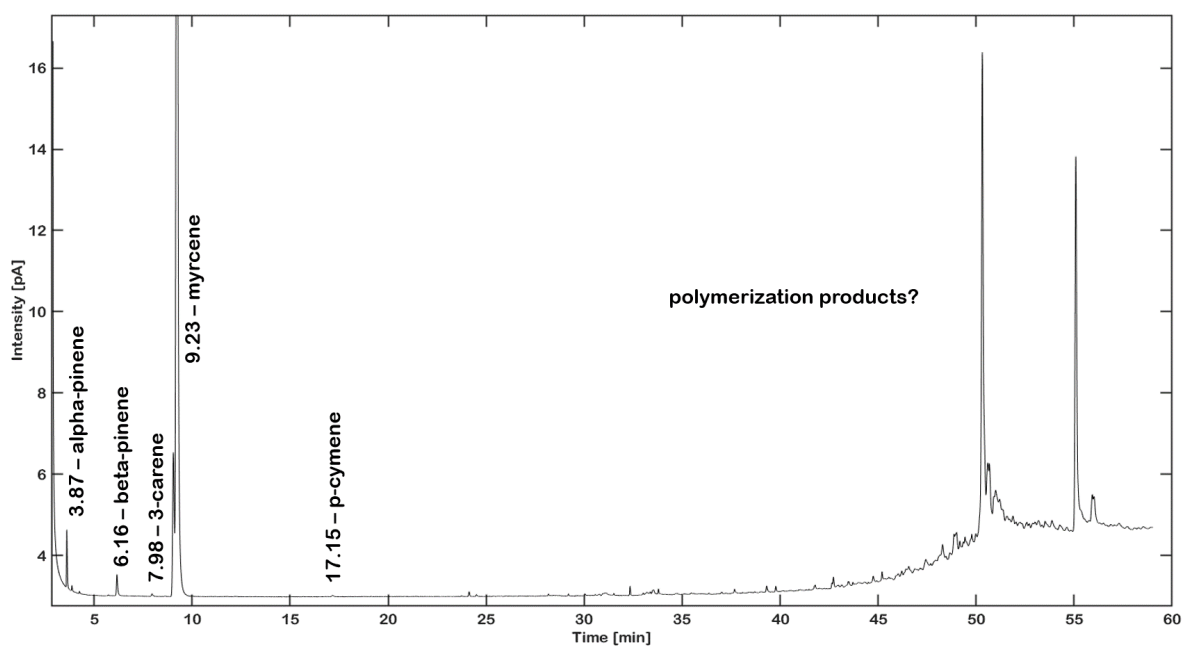


Figure A23: GC-FID chromatogram on a BGB wax column of a UV-treated sample containing 1 mg/ml myrcene after 48 hours. Figure taken from Raeber et al.¹⁸⁹

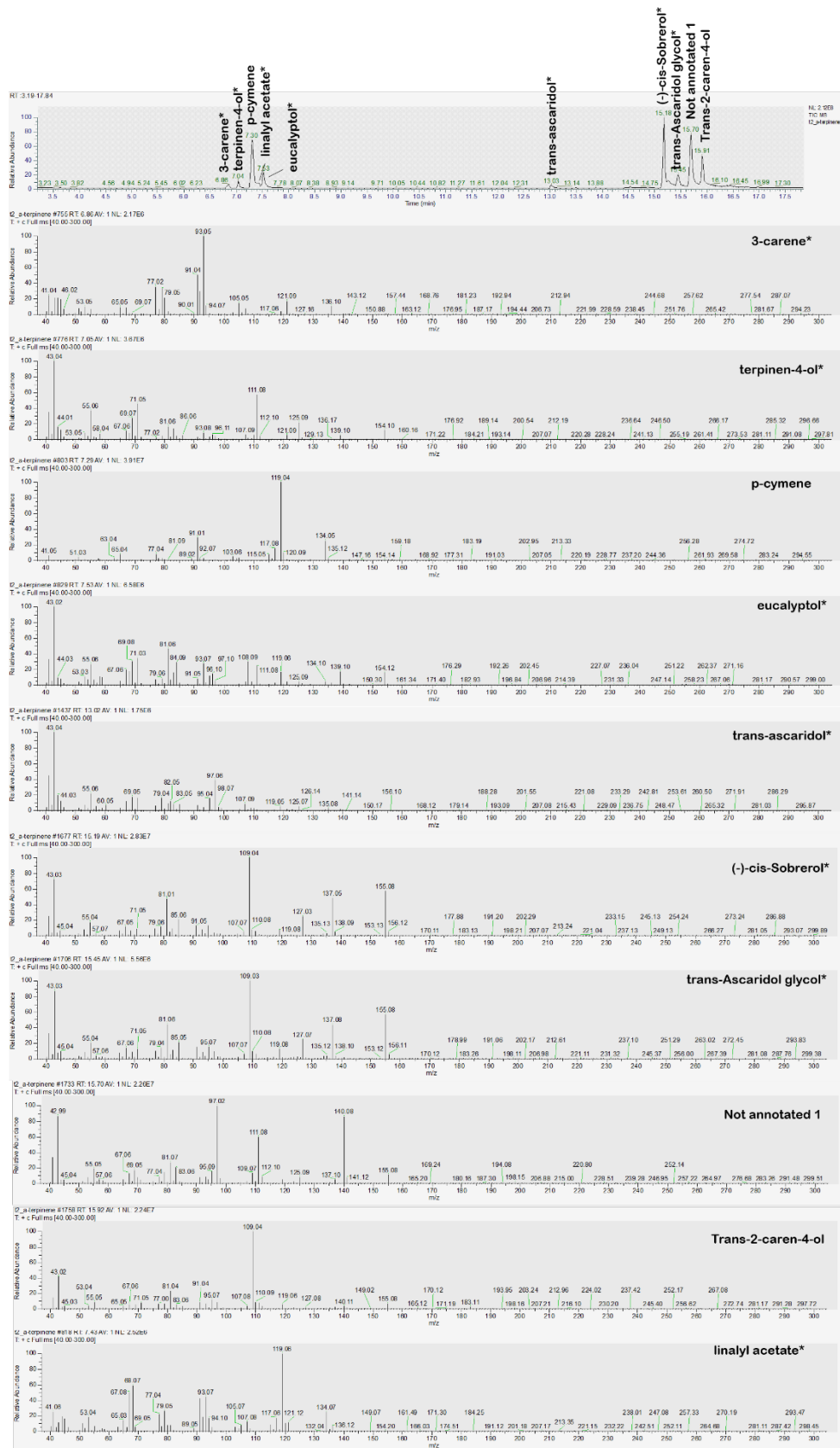


Figure A24: Chromatographic profile with associated MS spectra of a 1 mg/ml α -terpinene solution. Sample was treated with UV-light for 48 hours. Figure taken from Raeber et al.¹⁸⁹

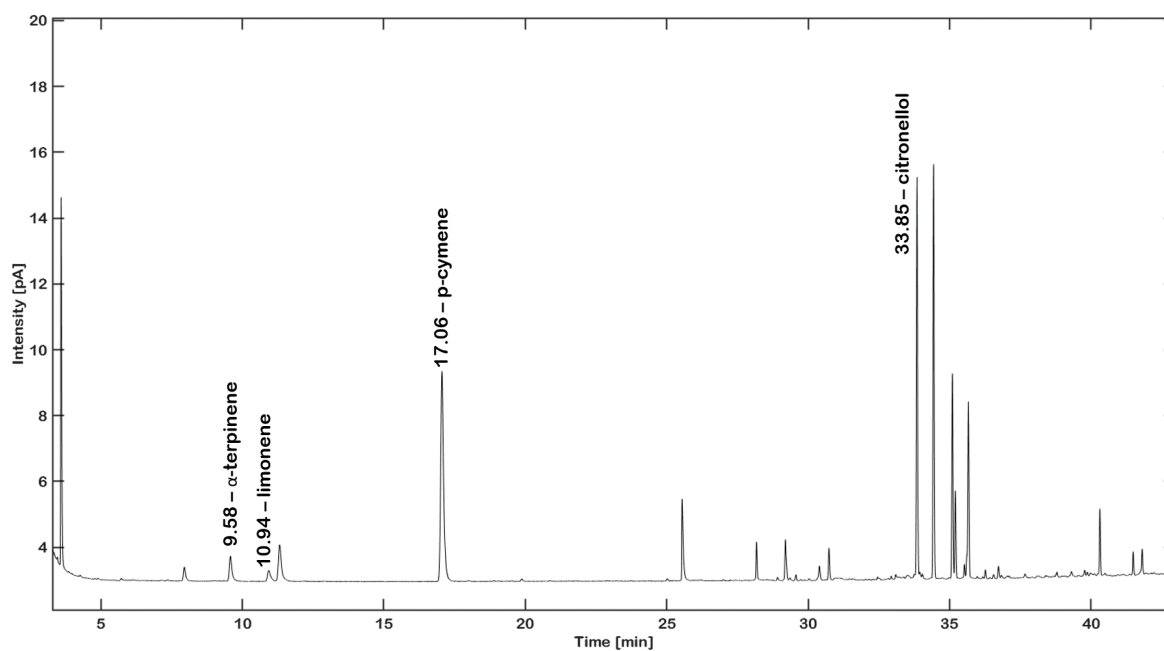


Figure A25: Chromatographic profile acquired with GC-FID on a BGB-wax column of a 1 mg/ml α -terpinene solution. Sample was treated with UV-light for 48 hours. Figure taken from Raeber et al.¹⁸⁹

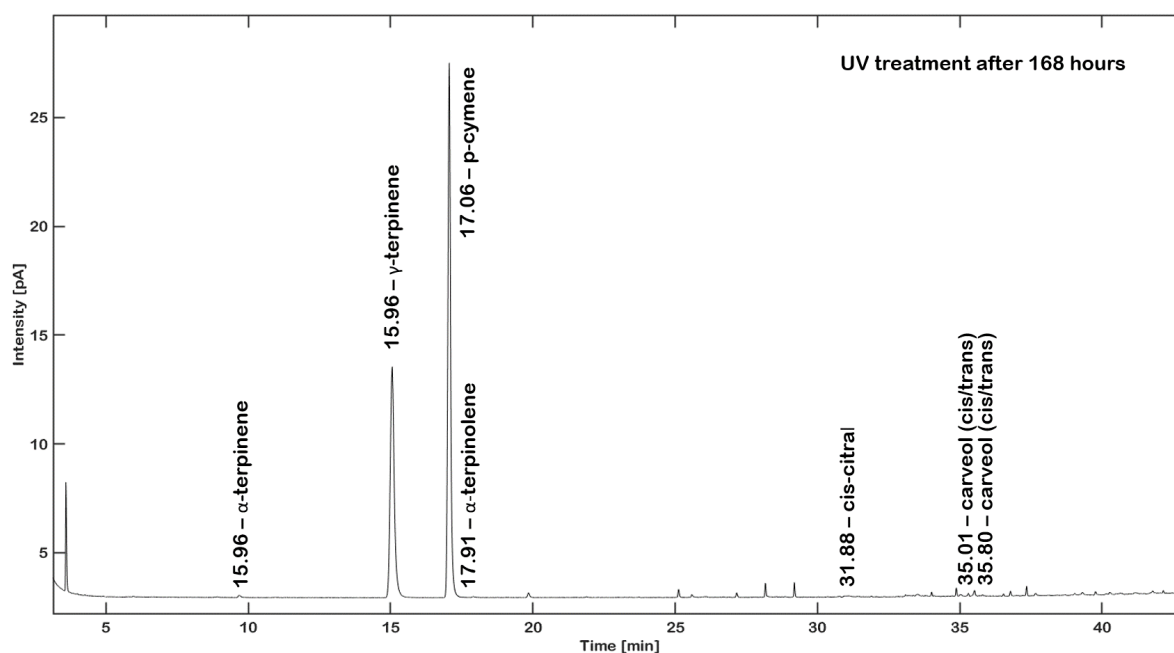


Figure A26: Chromatographic profile acquired with GC-FID on a BGB-wax column of a 1 mg/ml γ -terpinene solution. Sample was treated with UV-light for 168 hours. Figure taken from Raeber et al.¹⁸⁹

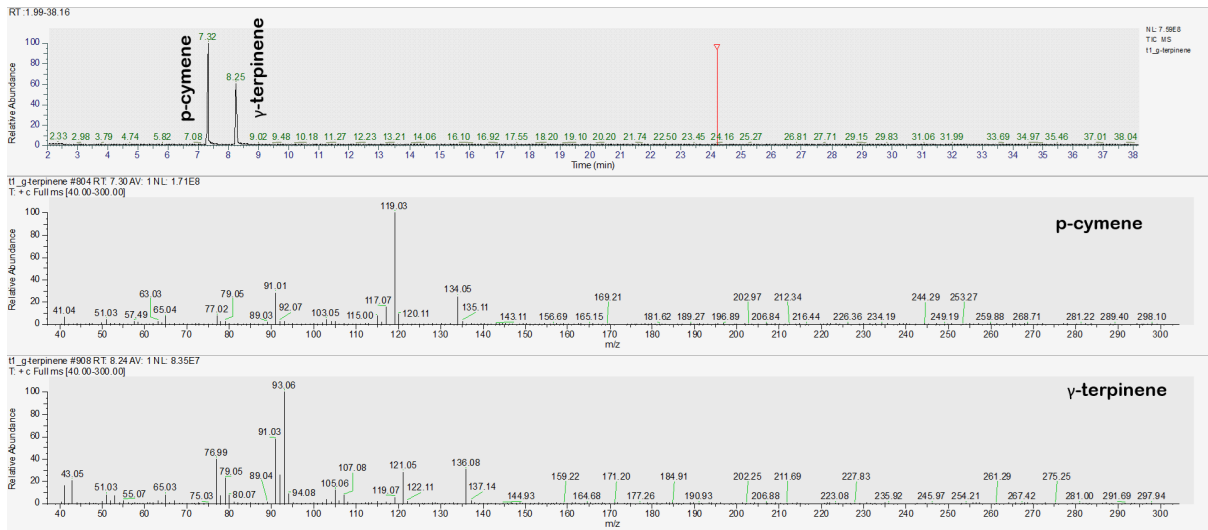
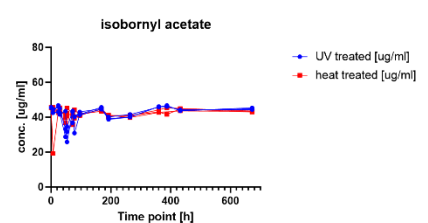
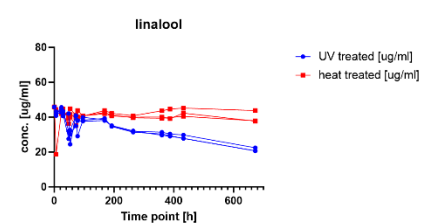
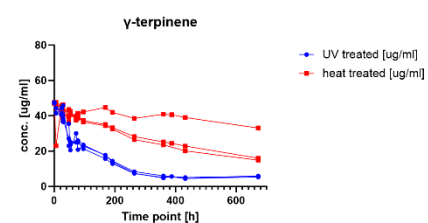
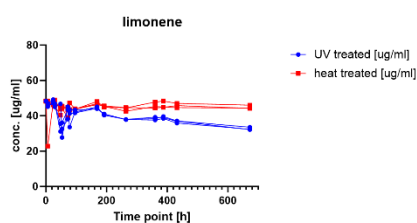
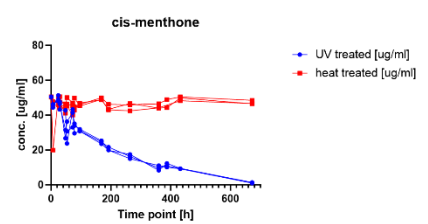
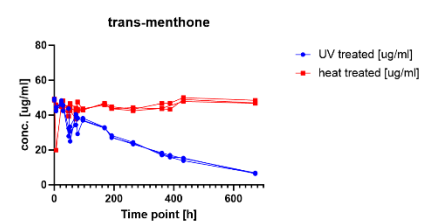
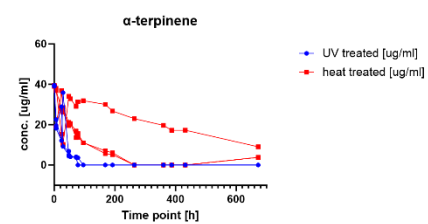
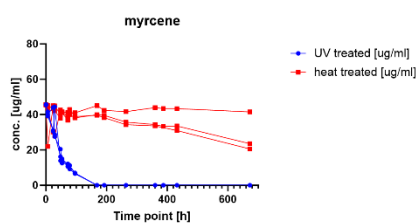
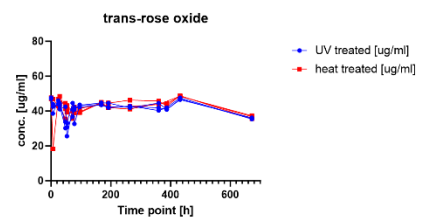
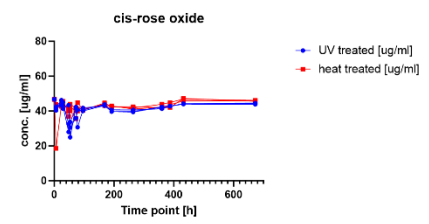
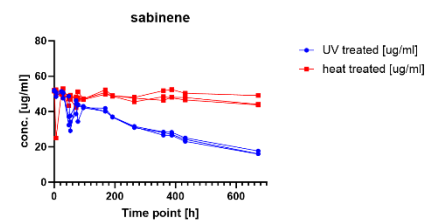
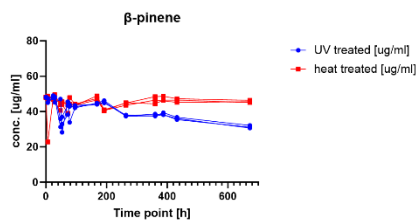
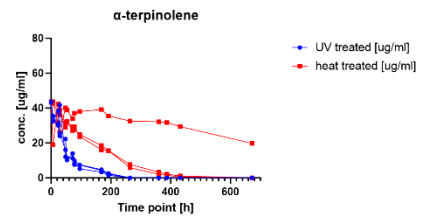
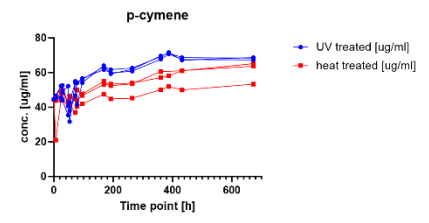
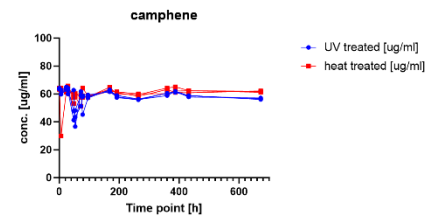
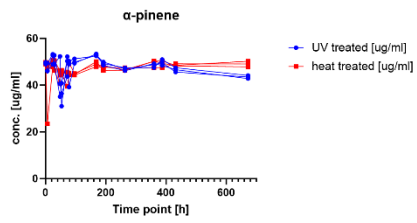
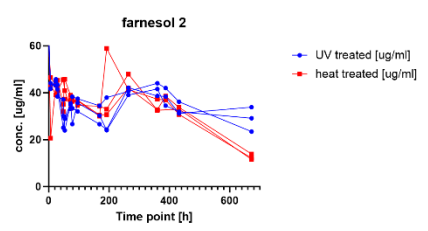
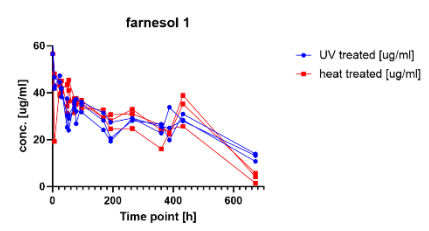
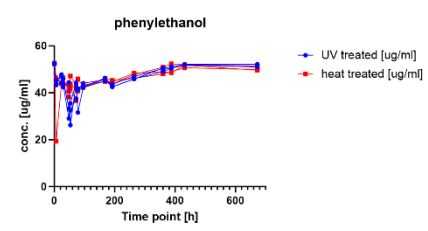
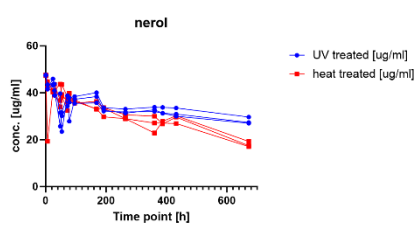
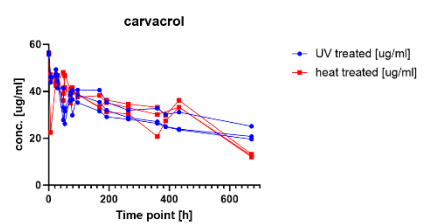
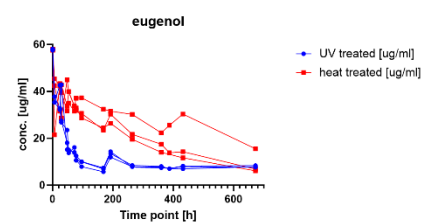
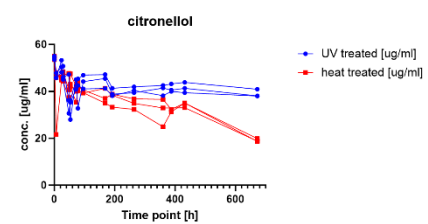
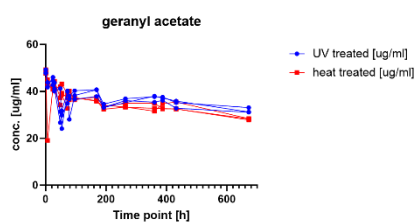
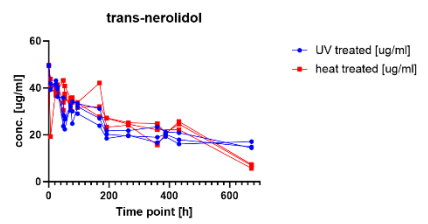
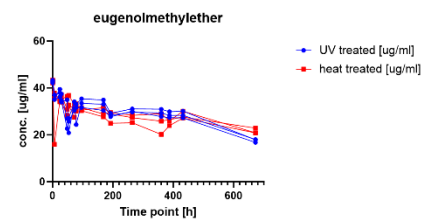
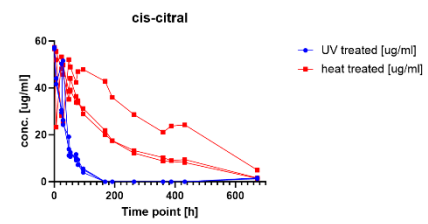
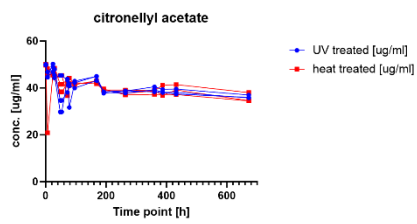
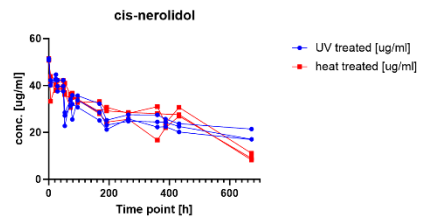
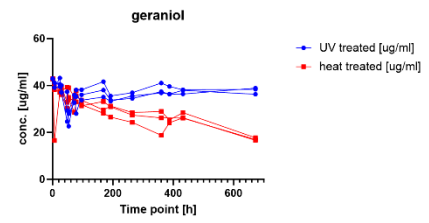
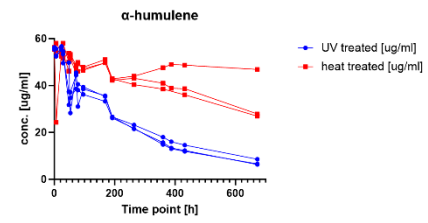
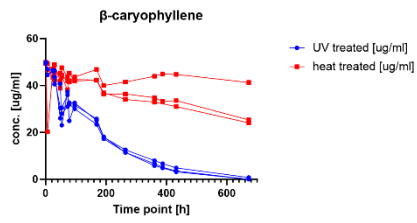


Figure A27: Chromatographic profile acquired with GC-MS of a 1 mg/ml γ -terpinene solution. Sample was treated with UV-light for 168 hours. Figure taken from Raeber et al.¹⁸⁹





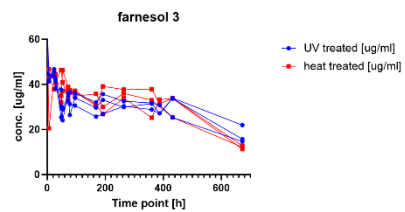
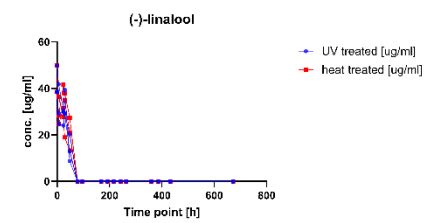
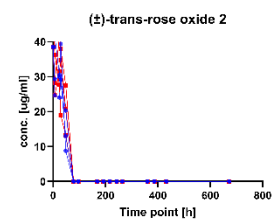
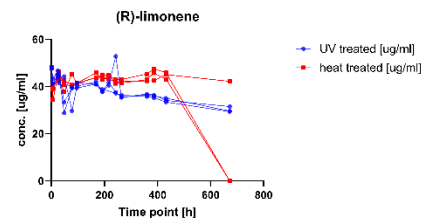
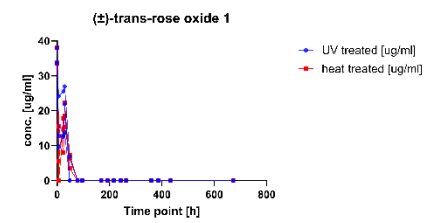
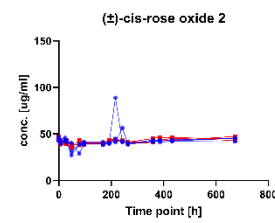
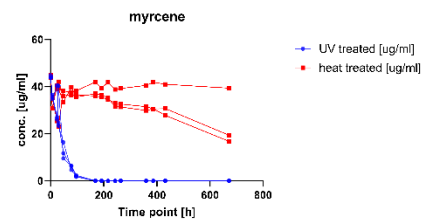
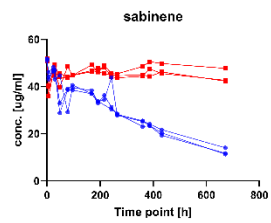
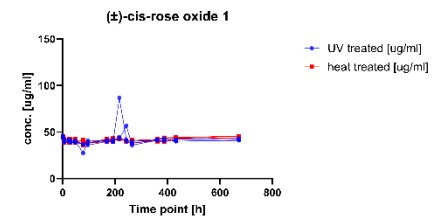
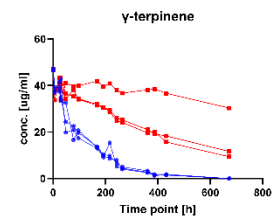
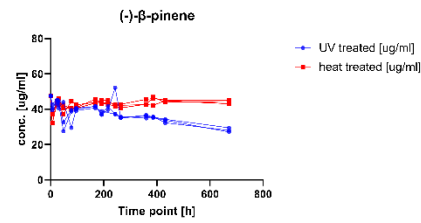
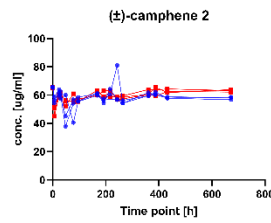
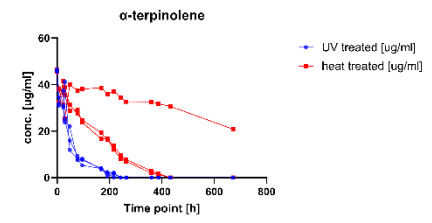
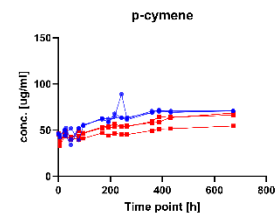
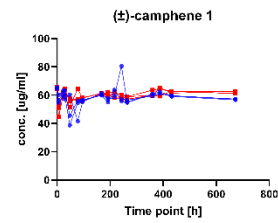
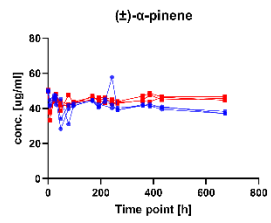
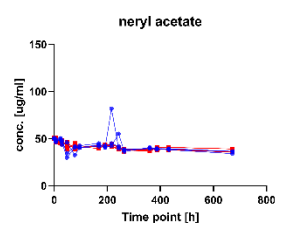
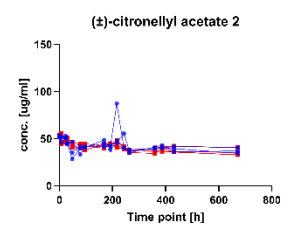
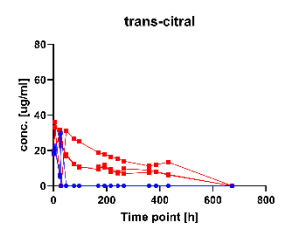
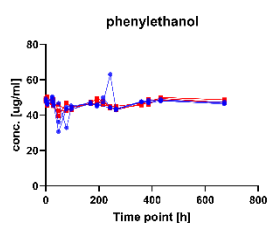
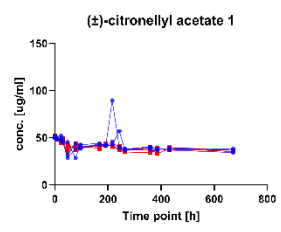
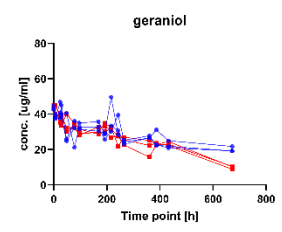
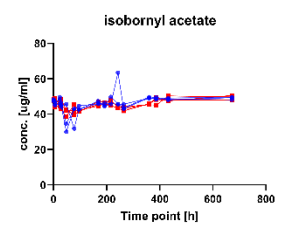
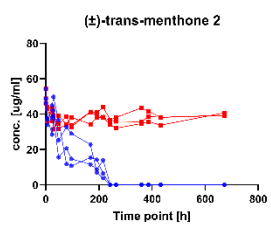
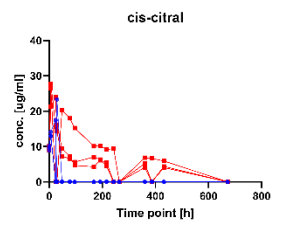
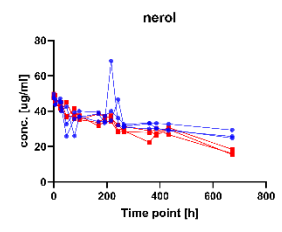
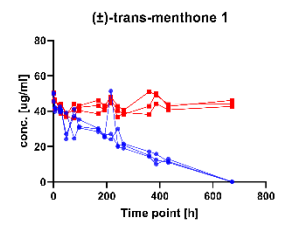
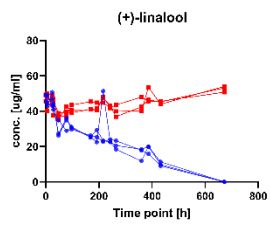
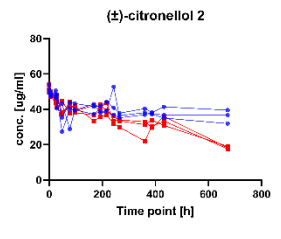
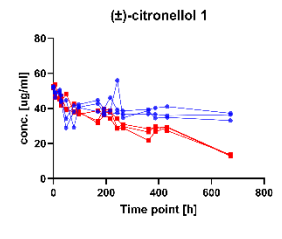
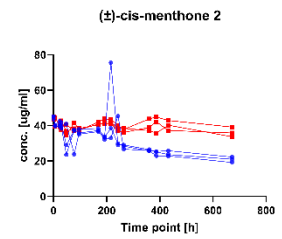
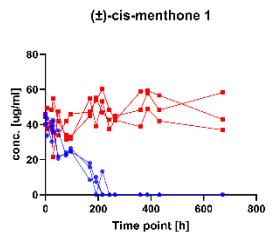


Figure A28: Concentration profiles of terpenes analysed on a BGB-wax column with GC-FID. Analytical replicates were performed (n=3). Figure taken from Raeber et al.¹⁸⁹





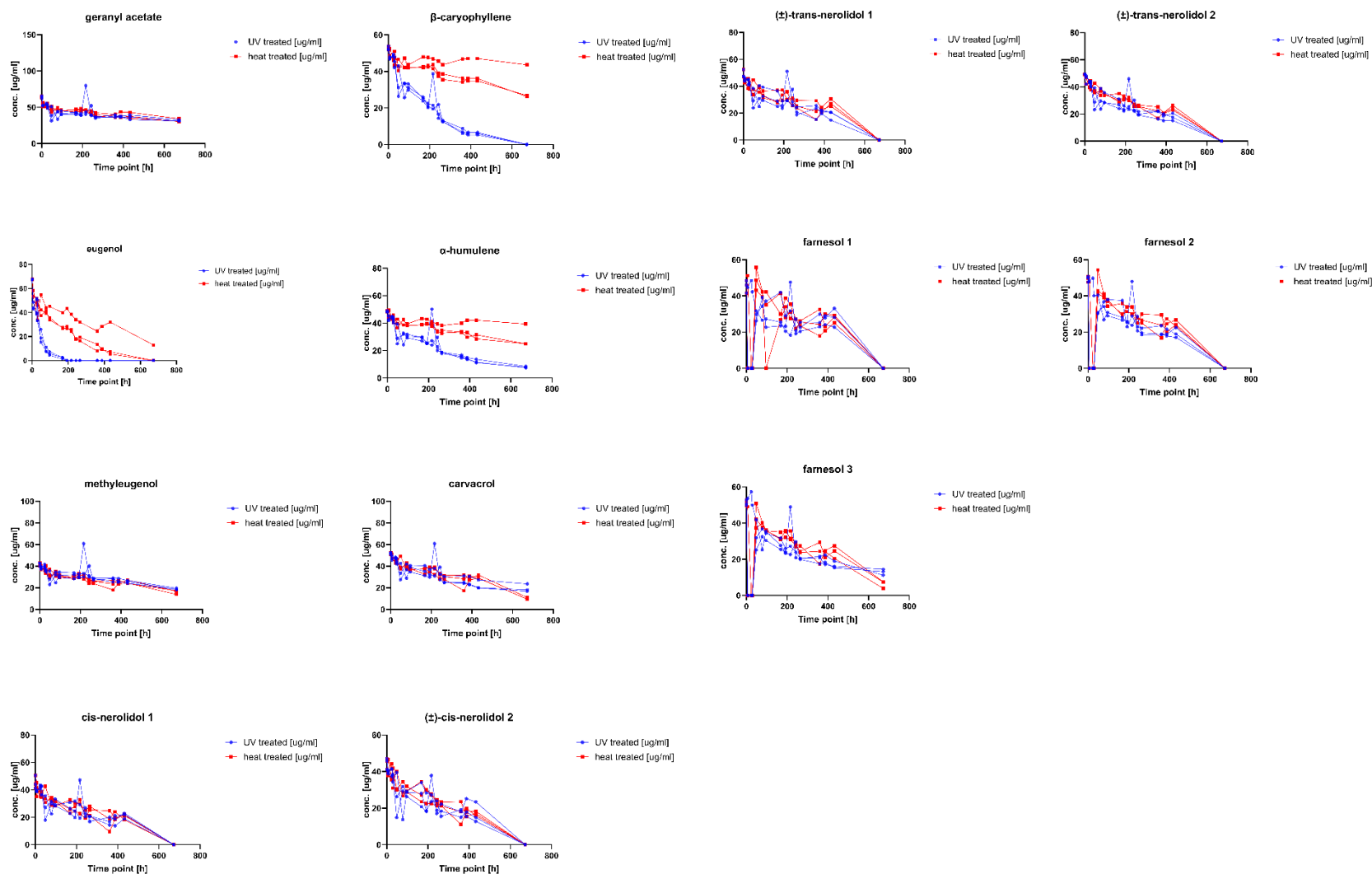
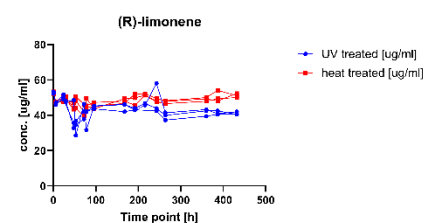
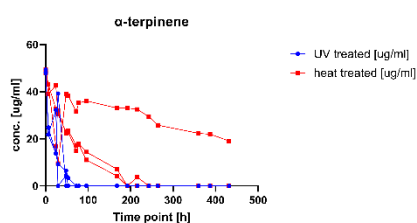
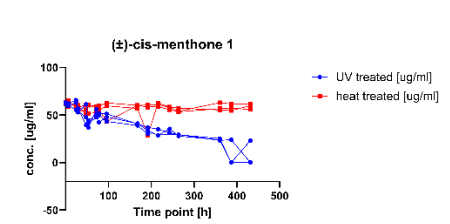
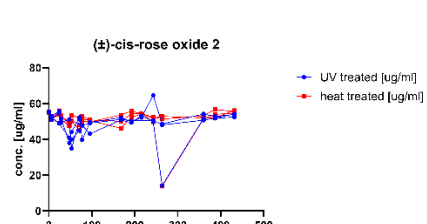
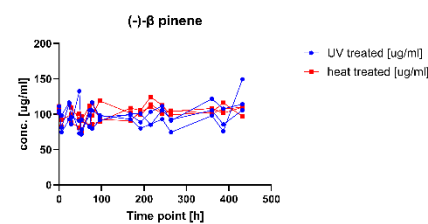
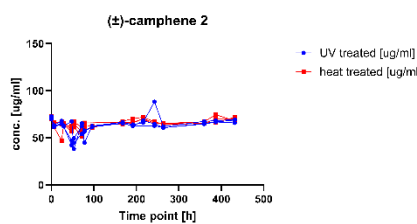
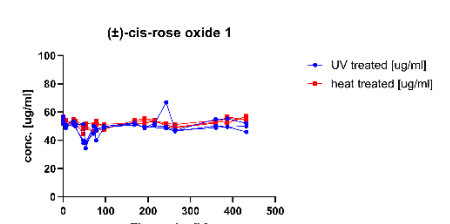
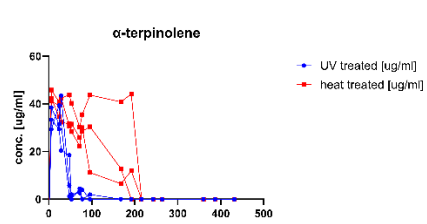
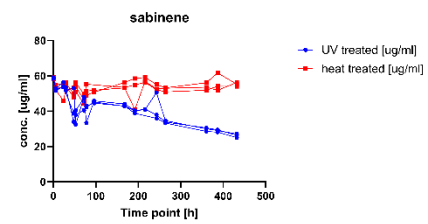
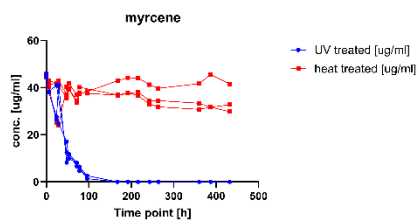
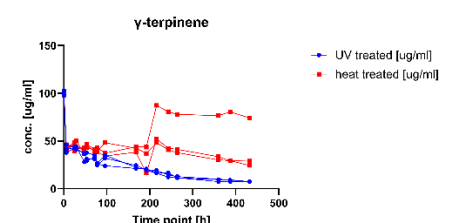
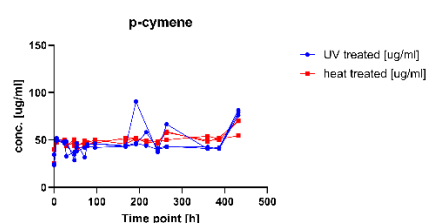
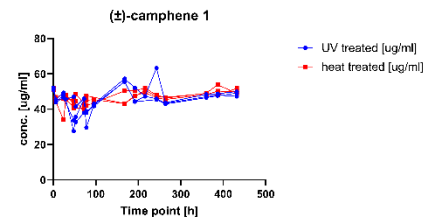
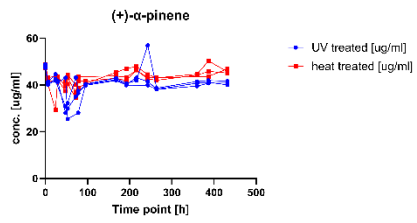
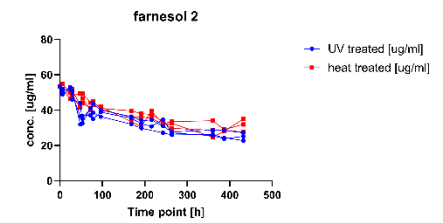
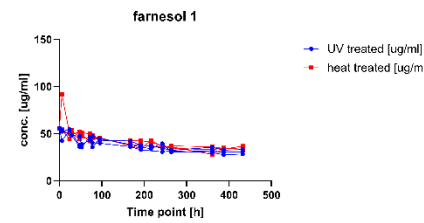
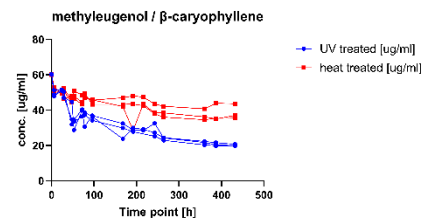
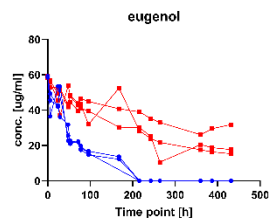
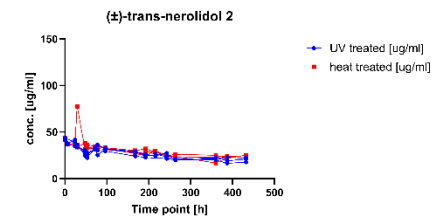
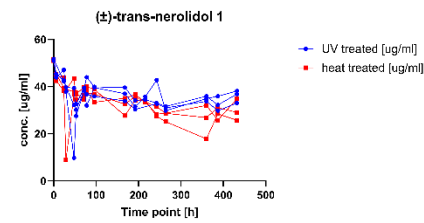
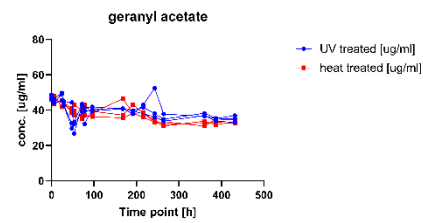
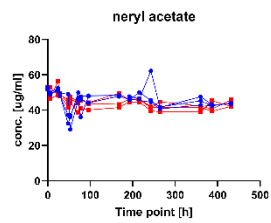
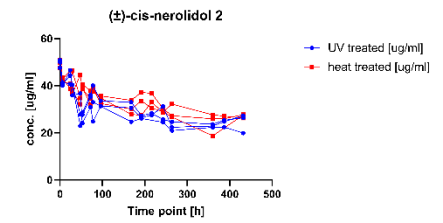
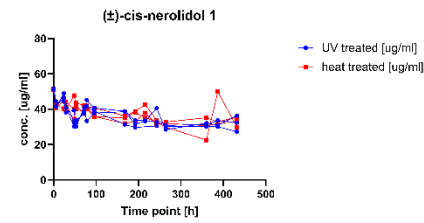
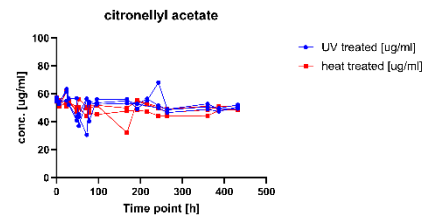
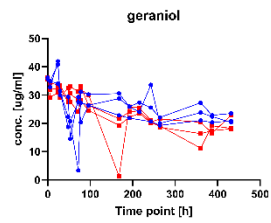
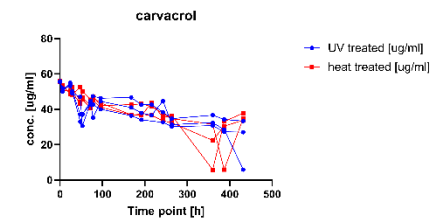
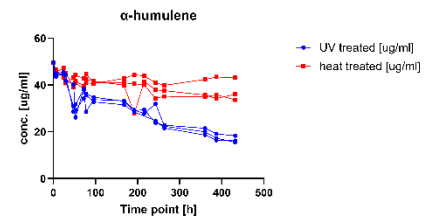
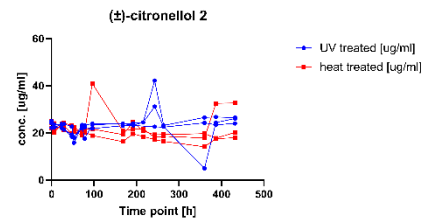
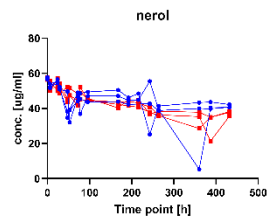


Figure A29: Concentration profiles of terpenes analysed on a BGB 178 30% CD chiral column with GC-FID. Analytical replicates were performed ($n=3$). Figure taken from Raeber et al.¹⁸⁹





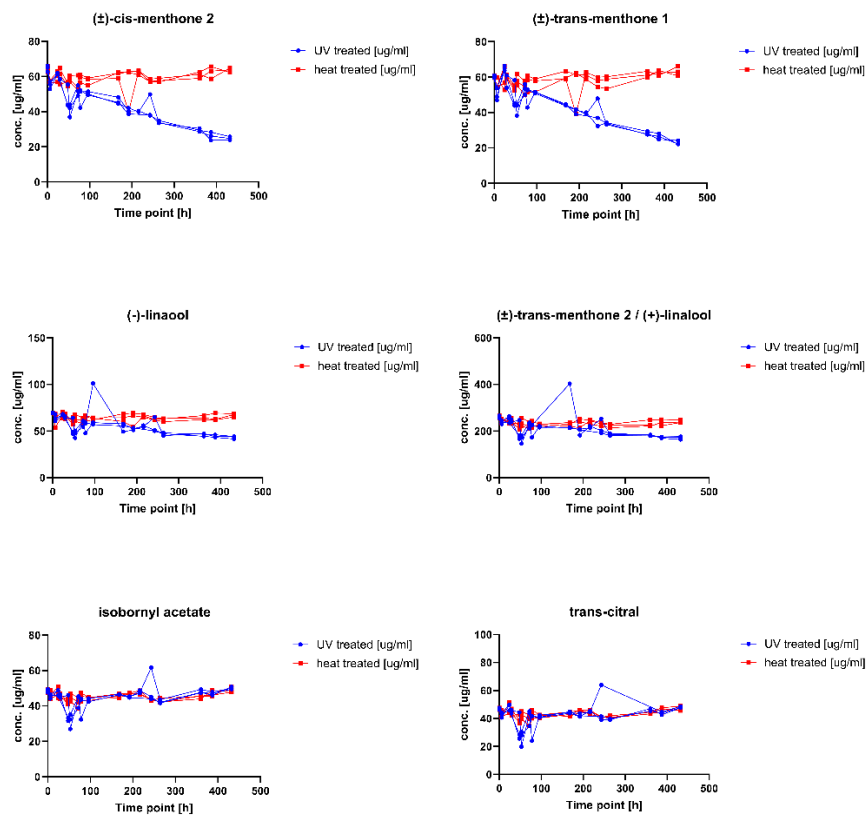


Figure A30: Concentration profiles of terpenes analysed on a BGB 176 SE chiral column with GC-FID. Analytical replicates were performed ($n=3$). Figure taken from Raeber et al.¹⁸⁹

Table A15: Results derived from the mixed effects model based on GC-FID data using a BGB-wax column. Significance levels were set at ns for $P > 0.05$, * for ≤ 0.5 , ** for $P \leq 0.01$, *** for $P \leq 0.001$ and **** for $P \leq 0.0001$. Table adapted from Raeber et al.¹⁸⁹

Analyte	P-value time	P-value Treatment	P-value Time x Treatment
α -pinene	0,0003, ***	0,4442, ns.	0,0371, *
camphene	0,0002, ***	0,0180, *	0,0319, *
β -pinene	<0,0001, ****	<0,0001, ****	<0,0001, ****
sabinene	<0,0001, ****	<0,0001, ****	<0,0001, ****
myrcene	<0,0001, ****	<0,0001, ****	<0,0001, ****
α -terpinene	<0,0001, ****	0,0451, *	0,1461, ns
limonene	<0,0001, ****	<0,0001, ****	0,0004, ***
γ -terpinene	<0,0001, ****	0,0038, **	<0,0001, ****
p-cymene	<0,0001, ****	0,0102, *	0,0001, ***
α -terpinolene	<0,0001, ****	0,0384, *	0,0050, **
cis-rose oxide	<0,0001, ****	0,0424, *	0,0282, *
trans-rose-oxide	<0,0001, ****	0,1297, ns	0,1273, ns
cis-3-hexen-1-ol	n.a.	n.a.	n.a.
trans-menthone	<0,0001, ****	<0,0001, ****	<0,0001, ****
cis-menthone	<0,0001, ****	<0,0001, ****	<0,0001, ****
linalool	<0,0001, ****	0,0025, **	<0,0001, ****
isobornyl acetate	<0,0001, ****	0,7592, n.s.	0,0178, *
β -caryophyllene	<0,0001, ****	0,0006, ***	<0,0001, ****
α -humulene	<0,0001, ****	0,0012, **	<0,0001, ****
citronellyl acetate	<0,0001, ****	0,8992, ns	0,4992, ns
cis-citral	<0,0001, ****	0,0037, **	<0,0001, ****
neryl acetate	n.a.	n.a.	n.a.
trans-citral	n.a.	n.a.	n.a.
geranyl acetate	<0,0001, ****	0,4131, ns	0,0116, *
citronellol	<0,0001, ****	0,0205, *	<0,0001, ****
nerol	<0,0001, ****	0,2029, ns	0,0004, ***
phenylethanol	<0,0001, ****	0,3339, ns	0,0191, *
geraniol	<0,0001, ****	0,0064, **	<0,0001, ****
cis-nerolidol	<0,0001, ****	0,4601, ns	<0,0001, ****
methyleugenol	<0,0001, ****	0,4672, ns	0,0104, *
trans-nerolidol	<0,0001, ****	0,1072, ns	0,0012, **
eugenol	<0,0001, ****	0,0025, **	<0,0001, ****
carvacrol	<0,0001, ****	0,4357, ns	0,0008, ***
farnesol 1	<0,0001, ****	0,5578, ns	0,0173, *
farnesol 2	<0,0001, ****	0,6077, ns	0,0010, ***
farnesol 3	<0,0001, ****	0,2118, ns	0,0377, *

Table A16: Results derived from the mixed effects model based on GC-FID data using a BGB 178 30% CD chiral column. Significance levels were set at ns for $P > 0.05$, * for ≤ 0.5 , ** for $P \leq 0.01$, *** for $P \leq 0.001$ and **** for $P \leq 0.0001$. Table adapted from Raeber et al.¹⁸⁹

Analyte	P-value time	P-value Treatment	P-value Time x Treatment
(±)-α-pinene	<0,0001, ****	0,0004, ***	0,0062, **
(±)-camphene 1	<0,0001, ****	0,1100, ns	0,0918, ns
(±)-camphene 2	<0,0001, ****	0,1809, ns	0,1809, ns
(-)-β-pinene	<0,0001, ****	<0,0001, ****	<0,0001, ****
sabinene	<0,0001, ****	<0,0001, ****	<0,0001, ****
myrcene	<0,0001, ****	<0,0001, ****	<0,0001, ****
α-terpinene	<0,0001, ****	0,0798, ns	0,4357, ns
(R)-limonene	<0,0001, ****	0,0993, ns	0,0195, *
p-cymene	<0,0001, ****	0,0174, *	0,0001, ***
α-terpinolene	<0,0001, ****	0,0526, ns	0,0078, **
γ-terpinene	<0,0001, ****	0,0044, **	<0,0001, ****
(±)-cis-rose oxide 1	<0,0001, ****	0,9266, ns	0,3539, ns
(±)-cis-rose oxide 2	<0,0001, ****	0,9706, ns	0,4862, ns
(±)-cis-menthone 1	<0,0001, ****	<0,0001, ****	<0,0001, ****
(±)-cis-menthone 2	<0,0001, ****	<0,0001, ****	0,0043, **
(+)-linalool	<0,0001, ****	<0,0001, ****	<0,0001, ****
(±)-trans-menthone 1	<0,0001, ****	<0,0001, ****	<0,0001, ****
(±)-trans-menthone 2	<0,0001, ****	<0,0001, ****	<0,0001, ****
isobornyl acetate	<0,0001, ****	0,7286, ns	0,3912, ns
phenylethanol	<0,0001, ****	0,5227, ns	0,6731, ns
trans-citral	<0,0001, ****	<0,0001, ****	0,0849, ns
(±)-citronellol 1	<0,0001, ****	0,0059, **	<0,0001, ****
(±)-citronellol 2	<0,0001, ****	0,0527, ns	0,0003, ***
nerol	<0,0001, ****	0,0408, *	0,0619, ns
cis-citral	<0,0001, ****	<0,0001, ****	0,2699, ns
geraniol	<0,0001, ****	0,0446, *	0,0252, *
(±)-citronellyl acetate 1	<0,0001, ****	0,2532, ns	0,2818, ns
(±)-citronellyl acetate 2	<0,0001, ****	0,6076, ns	0,2387, ns
neryl acetate	<0,0001, ****	0,6205, ns	0,3278, ns
geranyl acetate	<0,0001, ****	0,1040, ns	0,6843, ns
β-caryophyllene	<0,0001, ****	0,0004, ***	<0,0001, ****
eugenol	<0,0001, ****	0,0031, **	<0,0001, ****
α-humulene	<0,0001, ****	0,0010, **	<0,0001, ****
methyleugenol	<0,0001, ****	0,0670, ns	0,1874, ns
carvacrol	<0,0001, ****	0,5948, ns	0,1619, ns
(±)-cis-nerolidol 1	<0,0001, ****	0,3648, ns	0,7494, ns
(±)-cis-nerolidol 2	<0,0001, ****	0,2957, ns	0,9502, ns
(±)-trans-nerolidol 1	<0,0001, ****	0,1627, ns	0,3244, ns
(±)-trans-nerolidol 2	<0,0001, ****	0,0009, ***	0,4956, ns
farnesol 1	<0,0001, ****	0,7331, ns	0,7122, ns
farnesol 2	<0,0001, ****	0,5571, ns	0,6959, ns
farnesol 3	<0,0001, ****	0,9073, ns	0,9972, ns

Table A17: Results derived from the mixed effects model based on GC-FID data using a BGB 176 SE chiral column. Significance levels were set at ns for $P > 0.05$, * for ≤ 0.5 , ** for $P \leq 0.01$, *** for $P \leq 0.001$ and **** for $P \leq 0.0001$. Table adapted from Raeber et al.¹⁸⁹

Analyte	P-value time	P-value Treatment	P-value Time x Treatment
(+)- α -pinene	<0,0001, ****	0,0267, *	0,0226, *
myrcene	<0,0001, ****	<0,0001, ****	<0,0001, ****
camphene	<0,0001, ****	0,425ns	0,0056, **
sabinene	<0,0001, ****	<0,0001, ****	<0,0001, ****
camphene	<0,0001, ****	<0,0001, ****	0,0151, *
(-)- β -pinene	<0,0001, ****	0,1429, ns	0,5976, ns
α -terpinene	<0,0001, ****	0,0471, *	0,1925, ns
(R)-limonene	<0,0001, ****	0,005, **	0,0052, **
γ -terpinene	<0,0001, ****	0,0211, *	<0,0001, ****
α -terpinolene	<0,0001, ****	0,0067, **	<0,0001, ****
(+/-)-cis-rose oxide 1	<0,0001, ****	0,0126, *	0,0158, *
(+/-)-cis-rose oxide 2	<0,0001, ****	0,2284, ns	0,9036, ns
(+/-)-cis-menthone 1	<0,0001, ****	<0,0001, ****	<0,0001, ****
(+/-)-cis-menthone 2	<0,0001, ****	<0,0001, ****	<0,0001, ****
(+/-)-trans-menthone 1	<0,0001, ****	<0,0001, ****	<0,0001, ****
(-)-linalool	<0,0001, ****	<0,0001, ****	0,0005, ***
(+/-)-trans-menthone 2	<0,0001, ****	<0,0001, ****	0,0134, *
isobornyl acetate	<0,0001, ****	0,3052, ns	0,0099, **
nerol	<0,0001, ****	<0,0001, ****	0,3256, ns
(+/-)-citronellol 2	0,0142, *	0,2469, ns	0,1478, ns
geraniol	<0,0001, ****	0,5879, ns	0,0012, **
citronellyl acetate	<0,0001, ****	0,3559, ns	0,2182, ns
neryl acetate	<0,0001, ****	0,4745, ns	0,0099, **
geranyl acetate	<0,0001, ****	0,4005, ns	0,0186, *
eugenol	<0,0001, ****	0,0005, ***	<0,0001, ****
α -humulene	<0,0001, ****	0,0003, ***	<0,0001, ****
carvacrol	<0,0001, ****	0,5379, ns	0,026, *
(+/-)-cis-nerolidol 1	<0,0001, ****	0,0301, *	0,1557, ns
(+/-)-cis-nerolidol 2	<0,0001, ****	0,0187, *	0,1651, ns
(+/-)-trans-nerolidol 1	<0,0001, ****	0,217, ns	0,0824, ns
(+/-)-trans-nerolidol 2	<0,0001, ****	0,0664, ns	0,7051, ns
farnesol 1	<0,0001, ****	0,0491, *	0,2899, ns
farnesol 2	<0,0001, ****	0,0175, *	0,219, ns

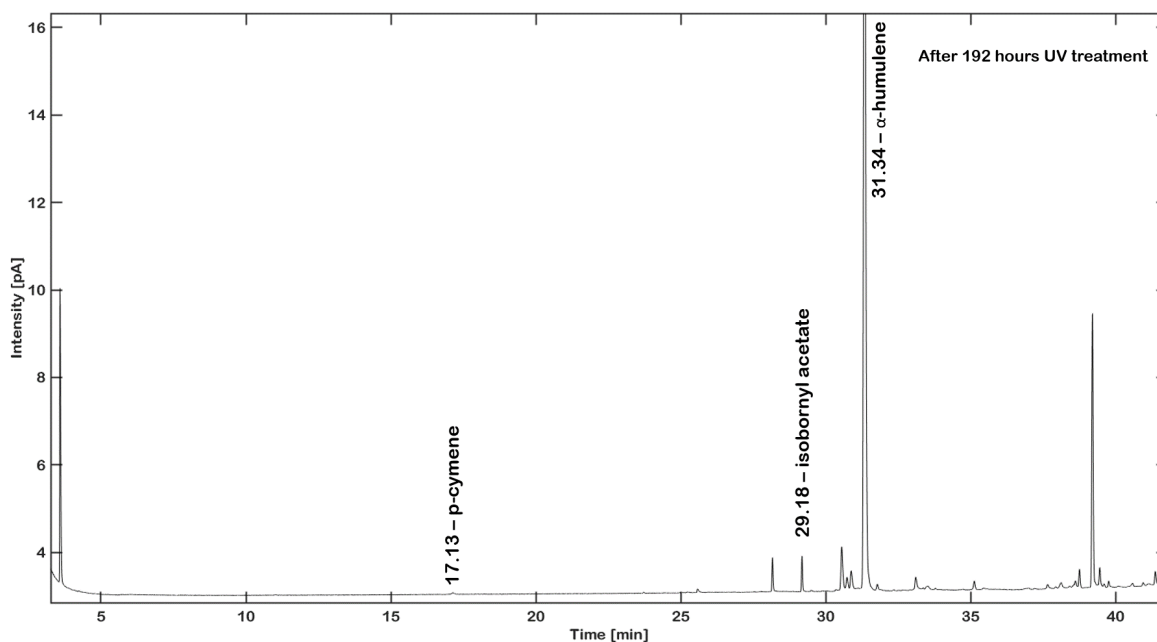


Figure A31: Chromatogram was acquired using GC-FID and a BGB-wax column. A 1 mg/ml α -humulene sample was treated with UV-light for 192 hours. Figure taken from Raeber et al.¹⁸⁹

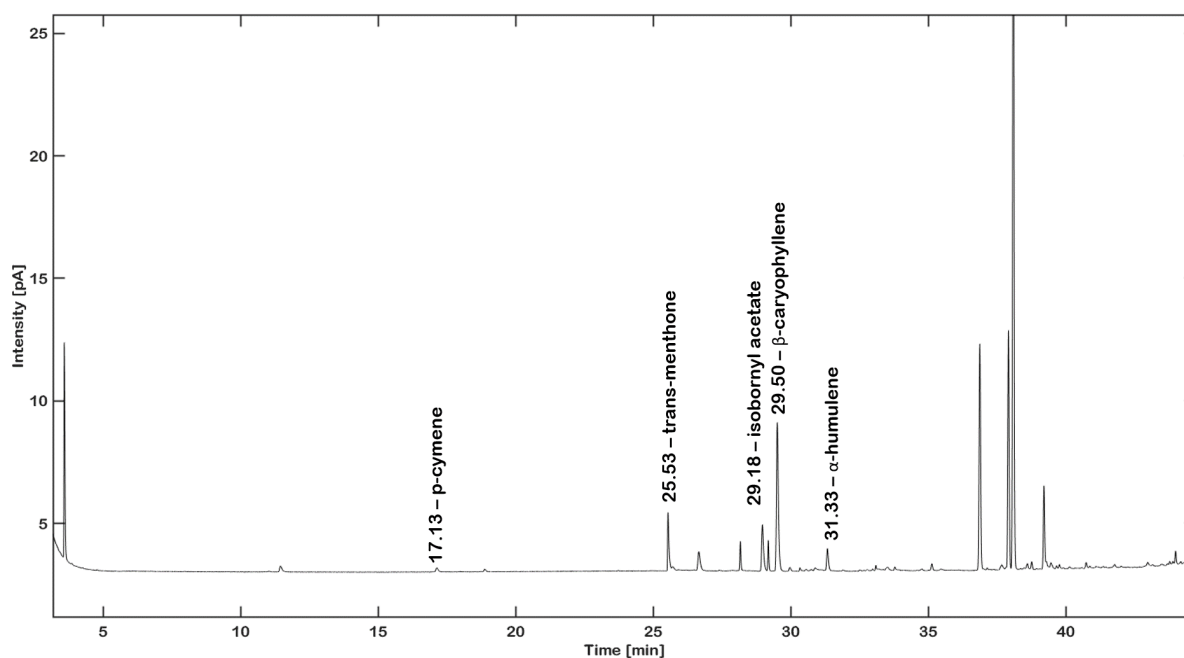


Figure A32: Chromatogram was acquired using GC-FID and a BGB-wax column. A 1 mg/ml β -caryophyllene sample was treated with UV-light for 192 hours. Figure taken from Raeber et al.¹⁸⁹

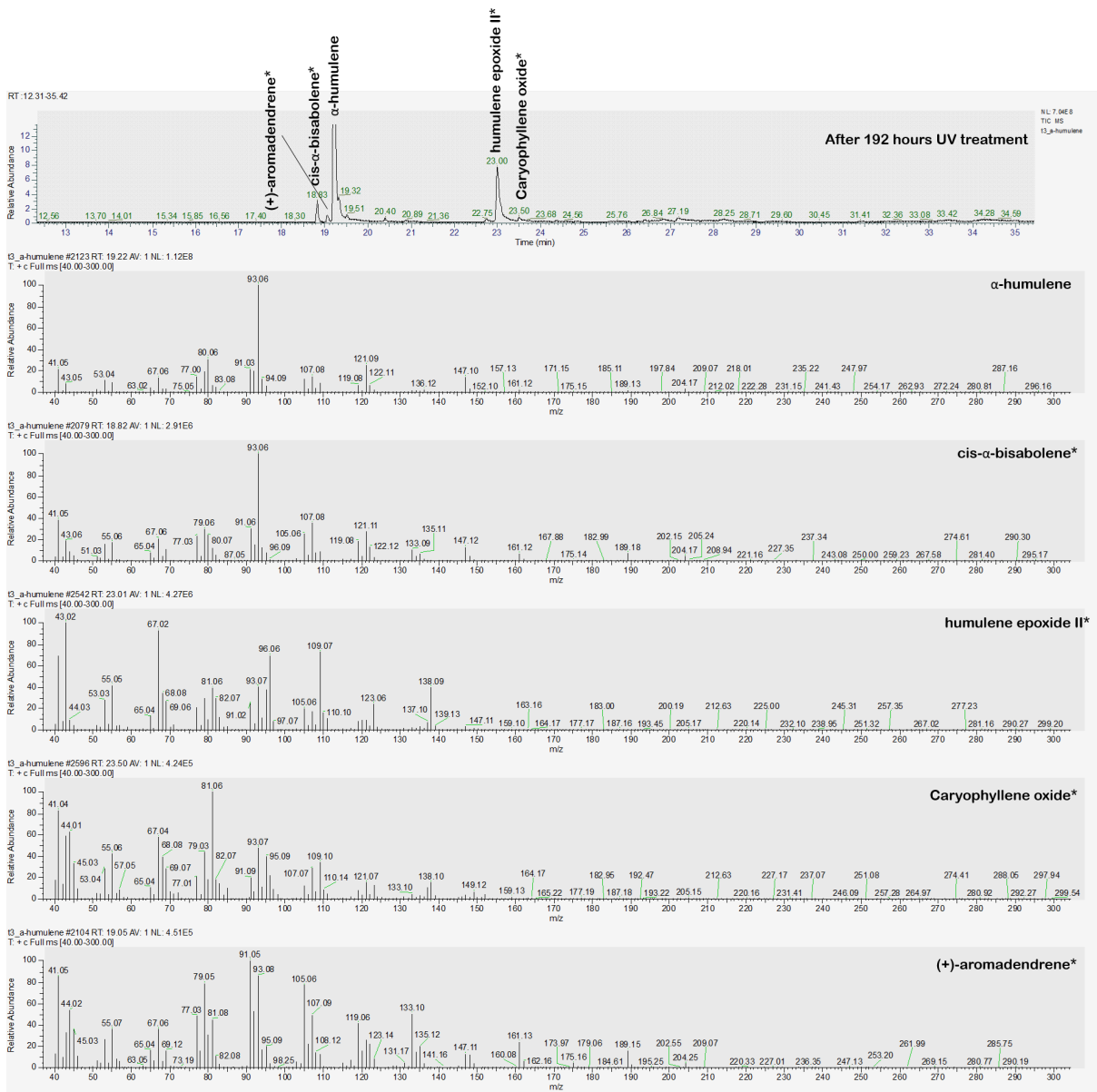


Figure A33: Chromatogram and spectra were acquired using GC-MS. A 1 mg/ml α-humulene sample was treated with UV-light for 192 hours. Figure taken from Ræber et al.¹⁸⁹

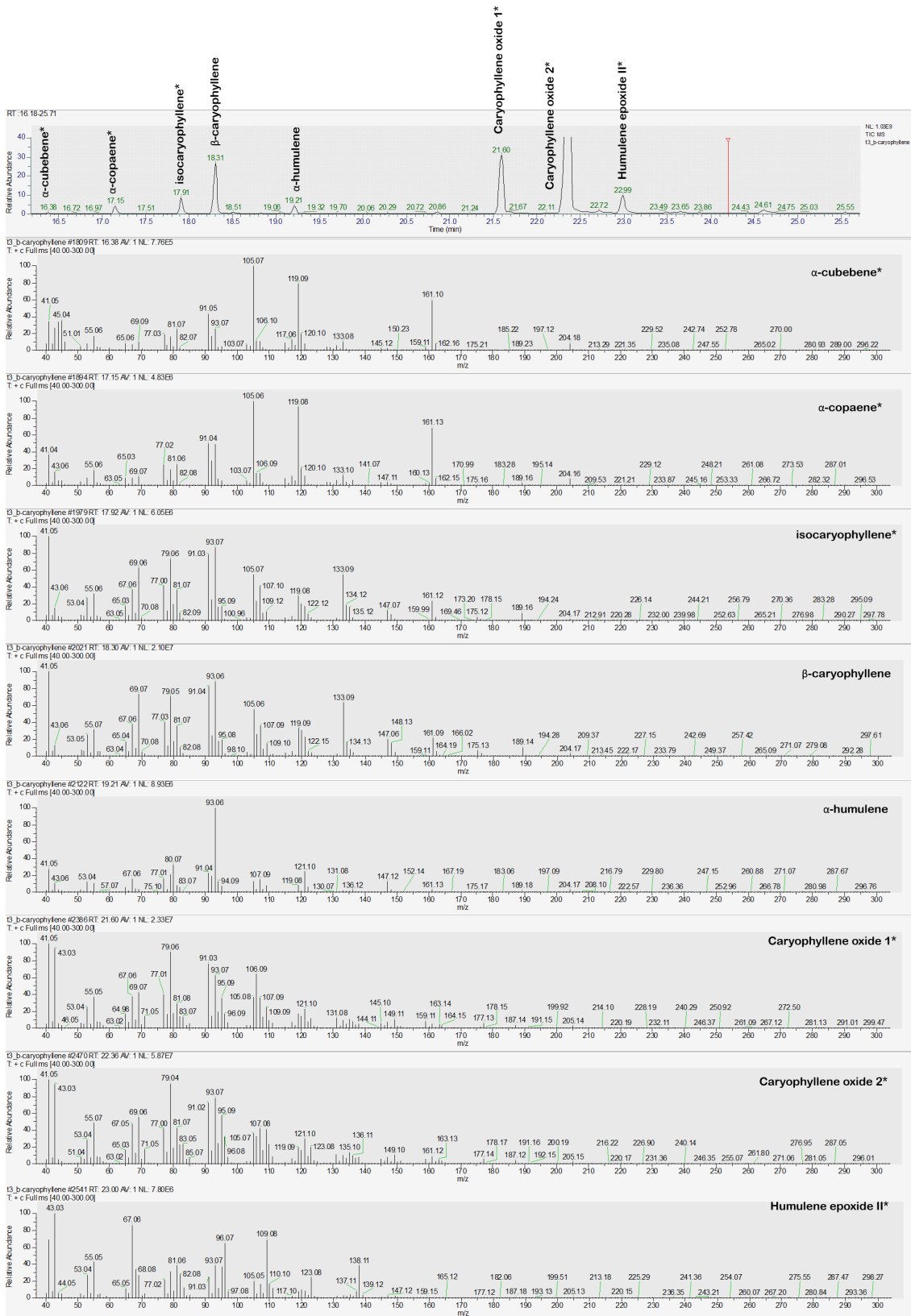


Figure A34: Chromatogram and spectra were acquired using GC-MS. A 1 mg/ml β-caryophyllene sample was treated with UV-light for 192 hours. Figure taken from Raeber et al.¹⁸⁹

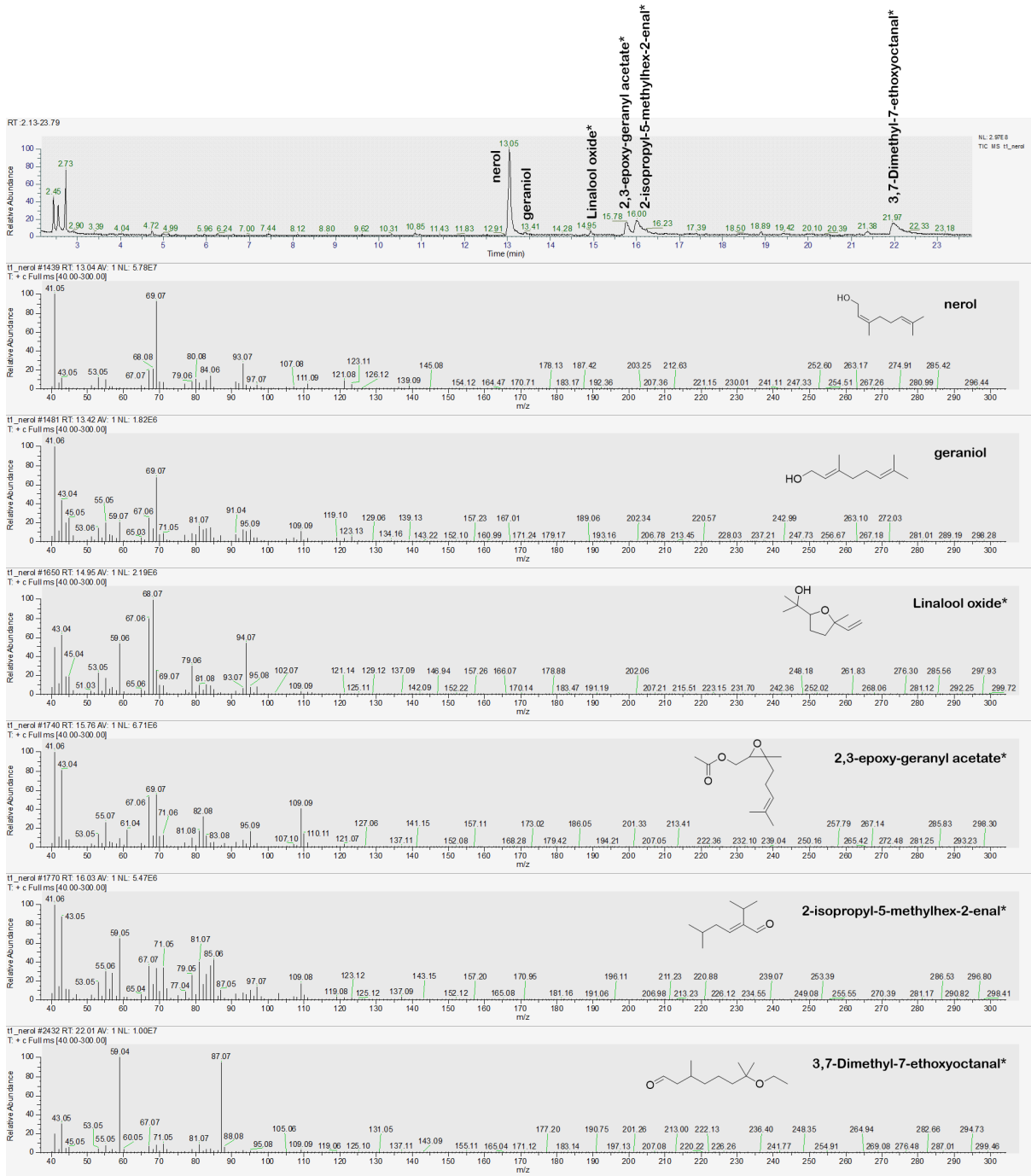


Figure A35: Chromatogram and spectra were acquired using GC-MS. A 1 mg/ml nerol sample was treated with UV-light for 192 hours. Figure taken from Raeber et al.¹⁸⁹

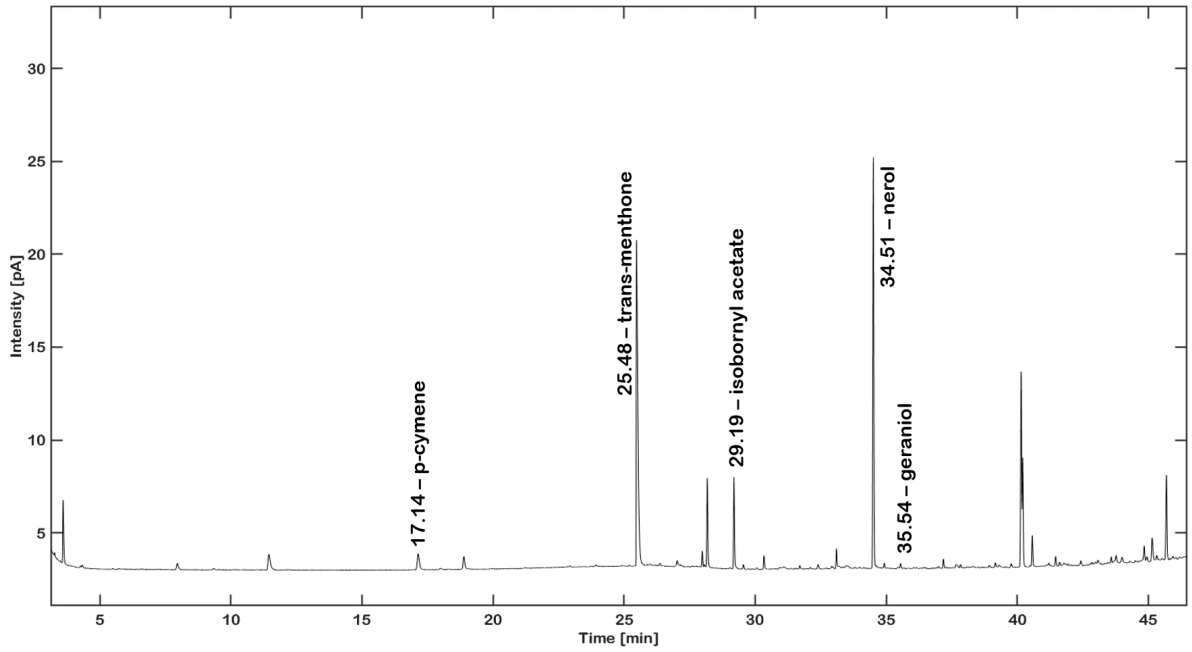


Figure A36: Chromatogram was acquired using GC-FID equipped with a BGB-wax column. A 1 mg/ml nerol sample was treated with UV-light for 192 hours. Figure taken from Raeber et al.¹⁸⁹

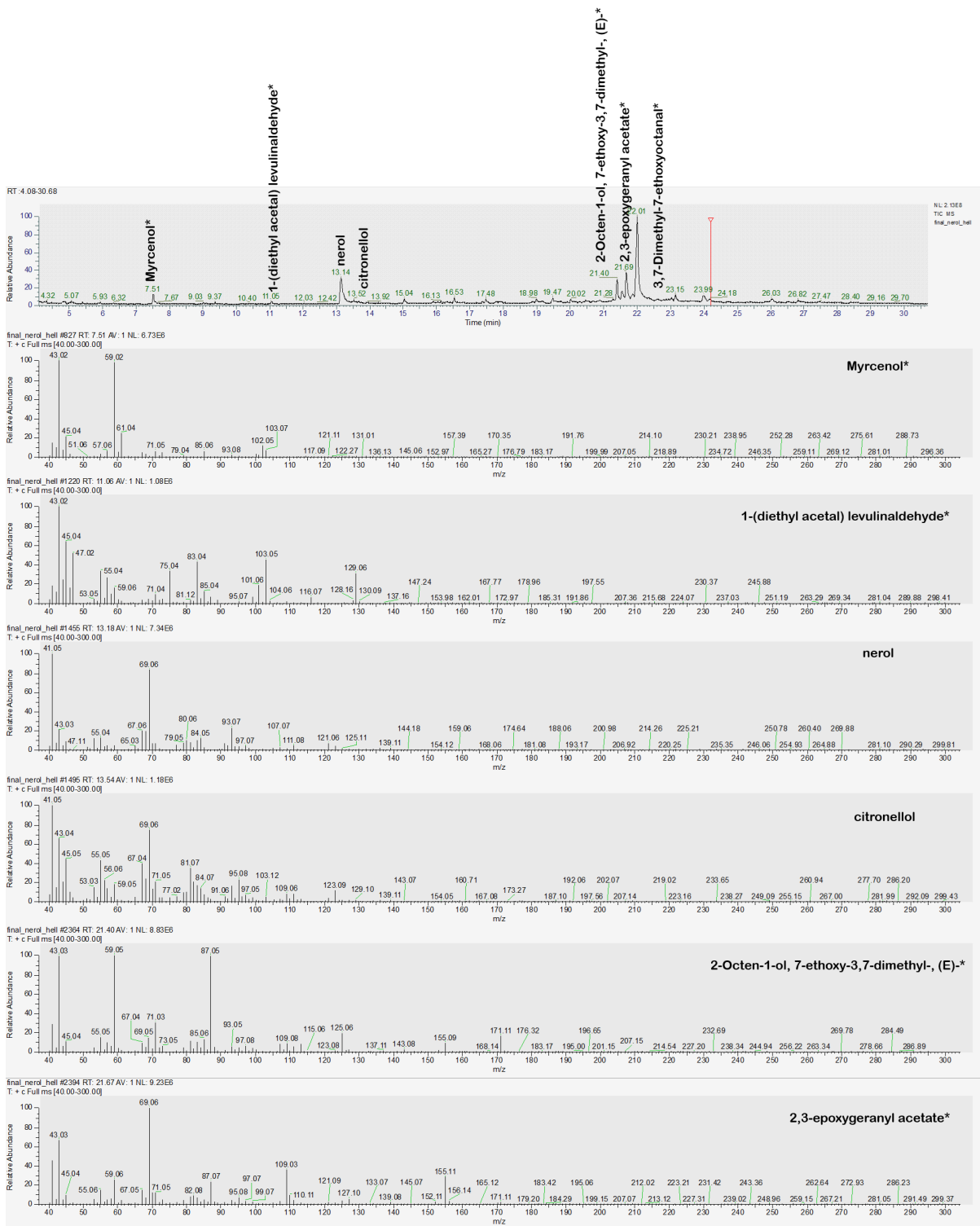


Figure A37: Chromatogram and spectra were acquired using GC-MS. A 1 mg/ml nerol sample was treated with UV-light for 336 hours. Figure taken from Raeber et al.¹⁸⁹

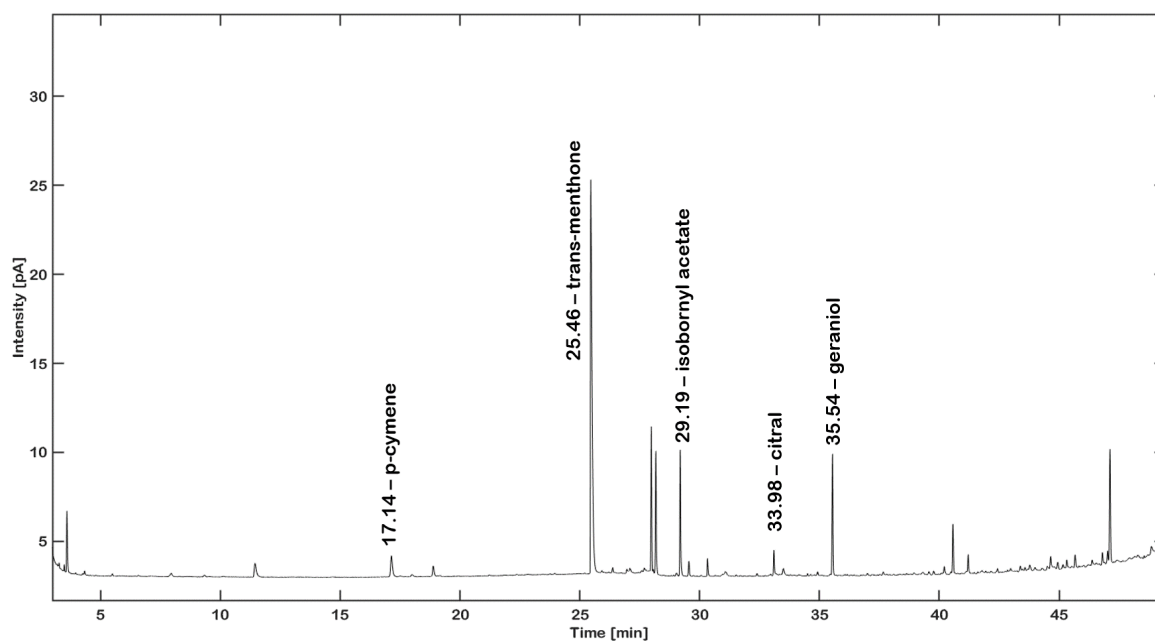


Figure A38: Chromatogram was acquired using GC-FID equipped with a BGB-wax column. A 1 mg/ml geraniol sample was treated with UV-light for 192 hours. Figure taken from Raeber et al.¹⁸⁹

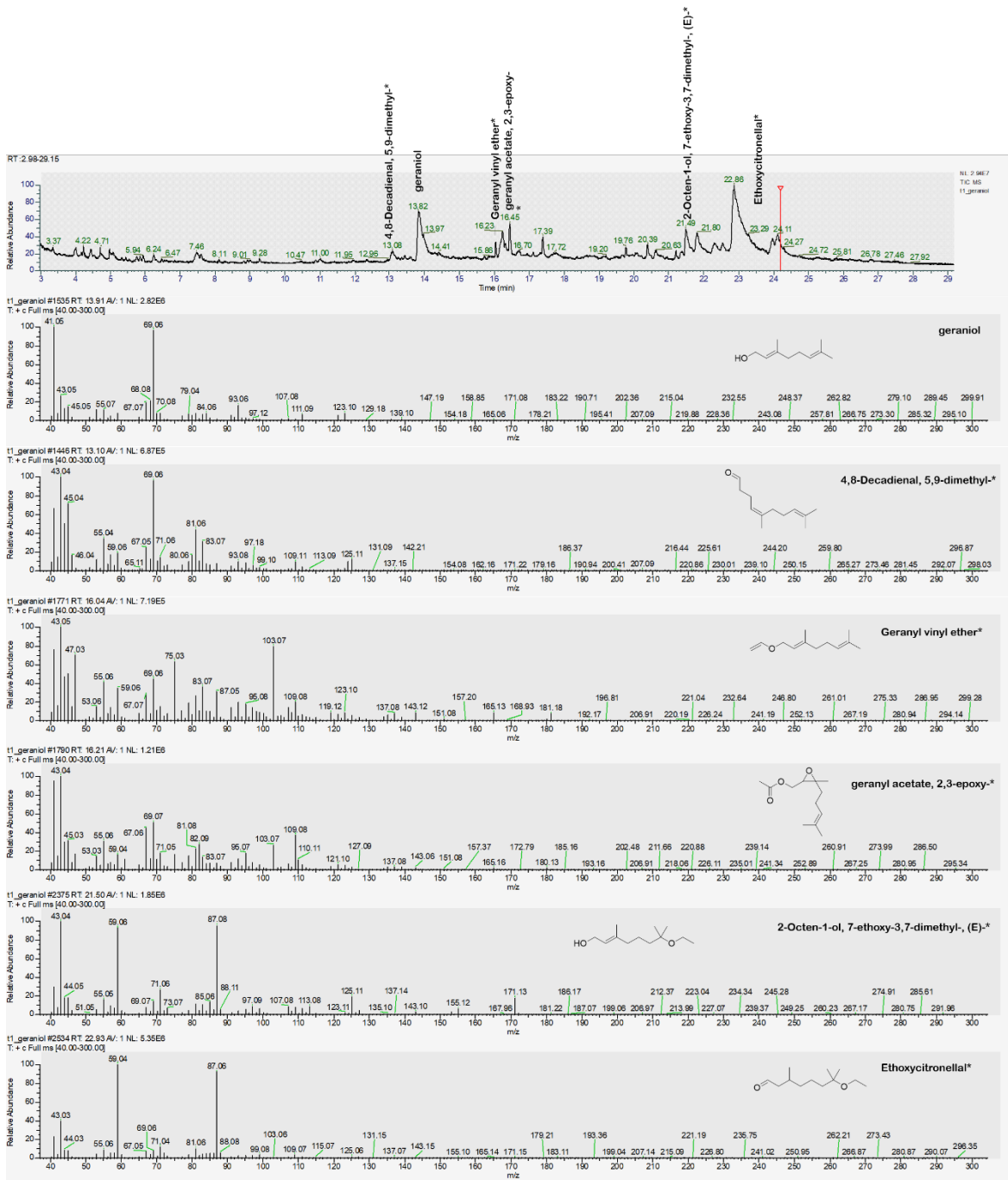


Figure A39: Chromatogram and spectra were acquired using GC-MS. A 1 mg/ml geraniol sample was treated with UV-light for 192 hours. Figure taken from Raeber et al.¹⁸⁹

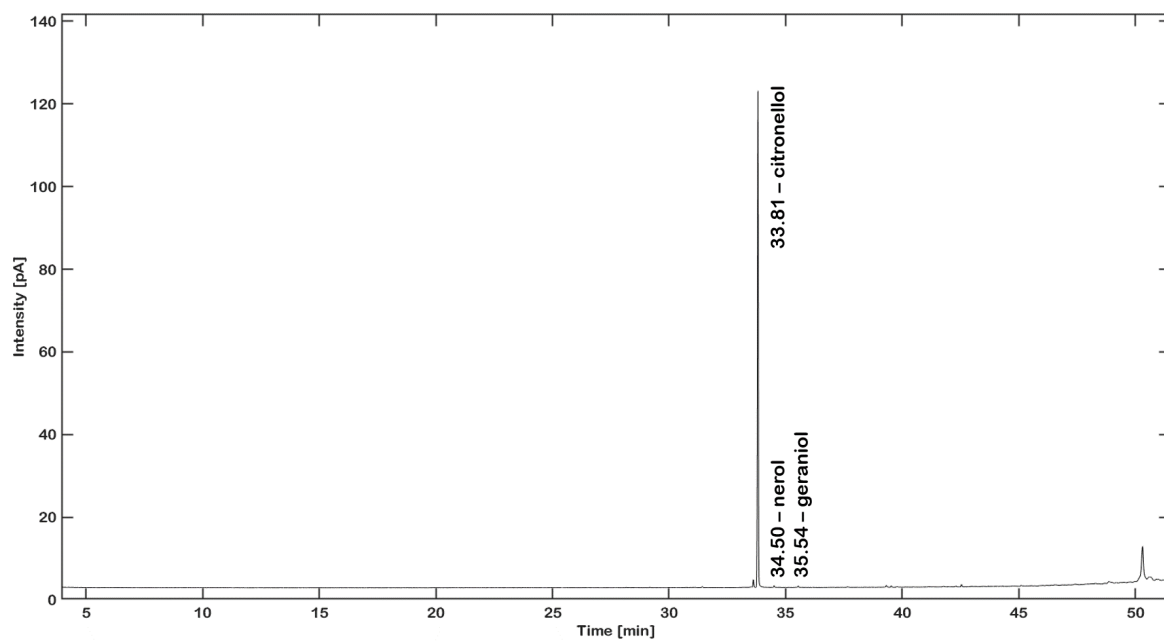


Figure A40: Chromatogram was acquired using GC-FID equipped with a BGB-wax column. A 1 mg/ml citronellol sample was treated with UV-light for 192 hours. Figure taken from Raeber et al.¹⁸⁹

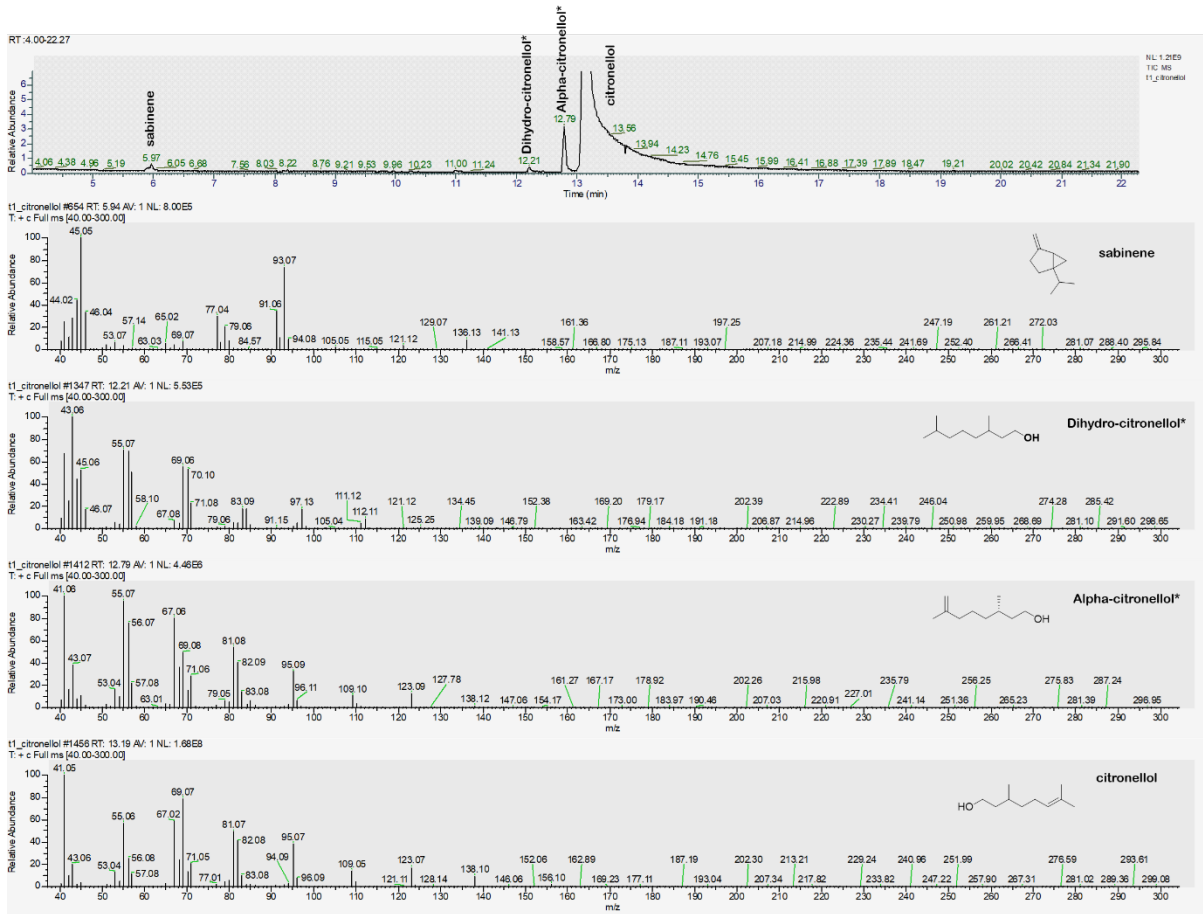


Figure A41: Chromatogram and spectra were acquired using GC-MS. A 1 mg/ml citronellol sample was treated with UV-light for 192 hours. Figure taken from Raeber et al.¹⁸⁹

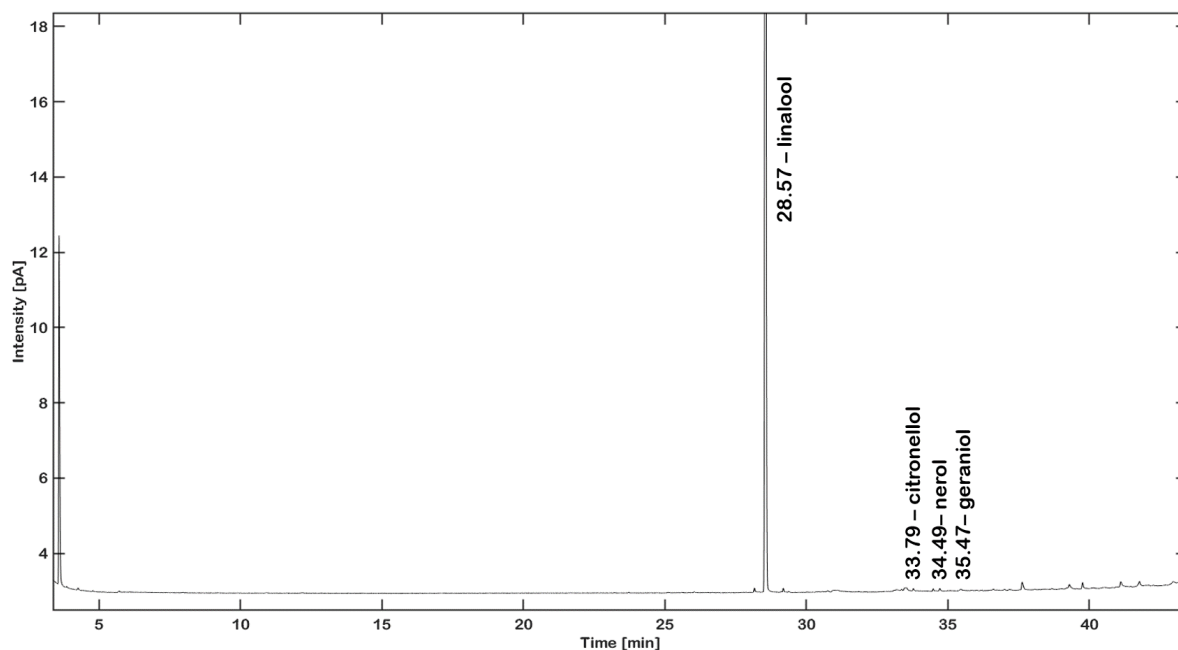


Figure A42: Chromatogram was acquired using GC-FID equipped with a BGB-wax column. A 1 mg/ml linalool sample was treated with UV-light for 192 hours. Figure taken from Raeber et al.¹⁸⁹

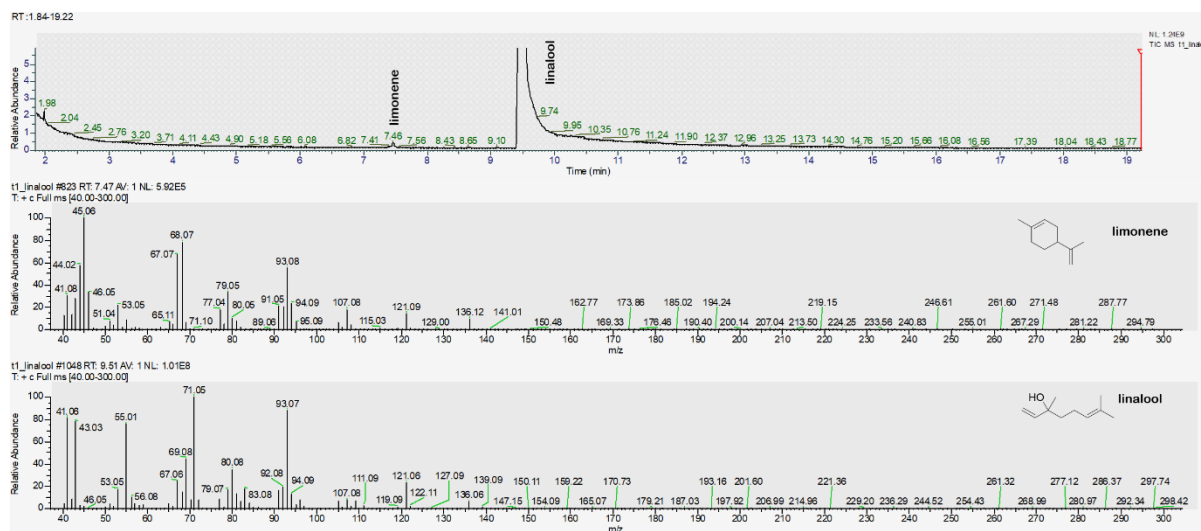


Figure A43: Chromatogram and spectra were acquired using GC-MS. A 1 mg/ml linalool sample was treated with UV-light for 192 hours. Figure taken from Raeber et al.¹⁸⁹

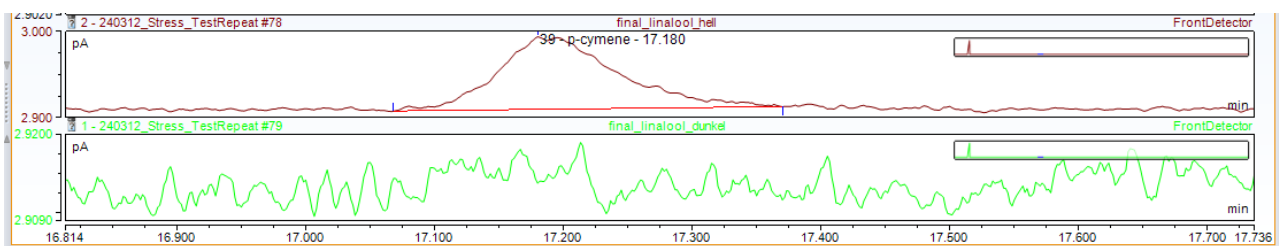


Figure A44: Chromatogram of a UV-stressed 1 mg/ml linalool solution acquired with GC-FID on a BGB-wax column after 336 hours exposure time. The chromatogram on top displays the formation of p-cymene of the UV-exposed sample, while the bottom chromatogram does not show p-cymene formation and was protected from UV-light. Figure taken from Raeber et al.¹⁸⁹

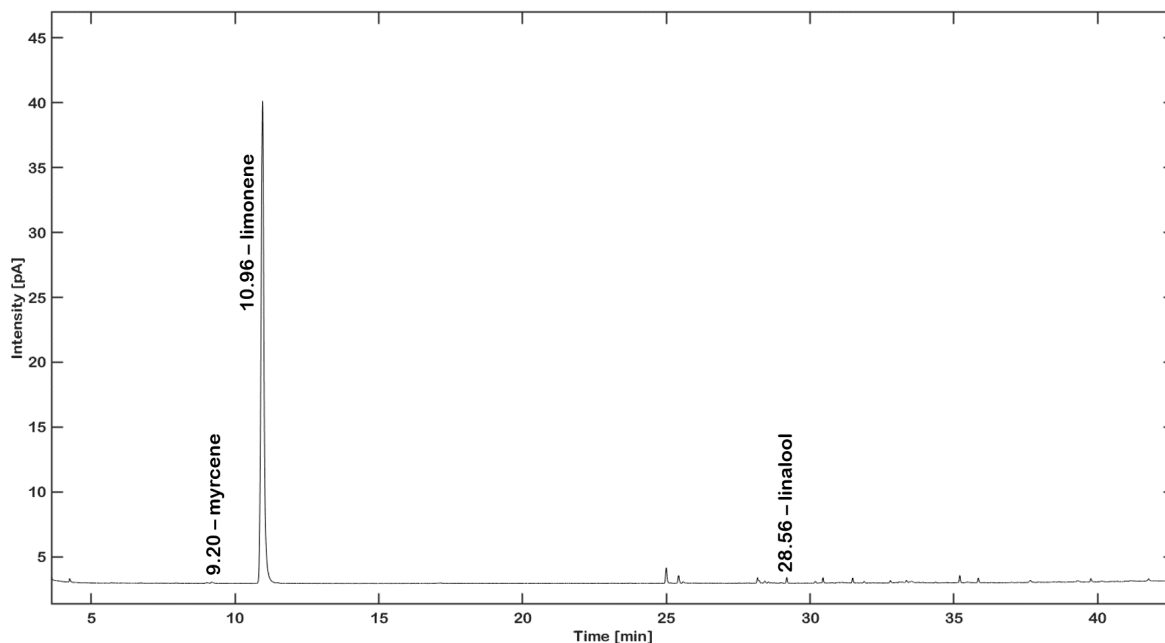


Figure A45: Chromatogram was acquired using GC-FID equipped with a BGB-wax column. A 1 mg/ml limonene sample was treated with UV-light for 192 hours. Figure taken from Raeber et al.¹⁸⁹

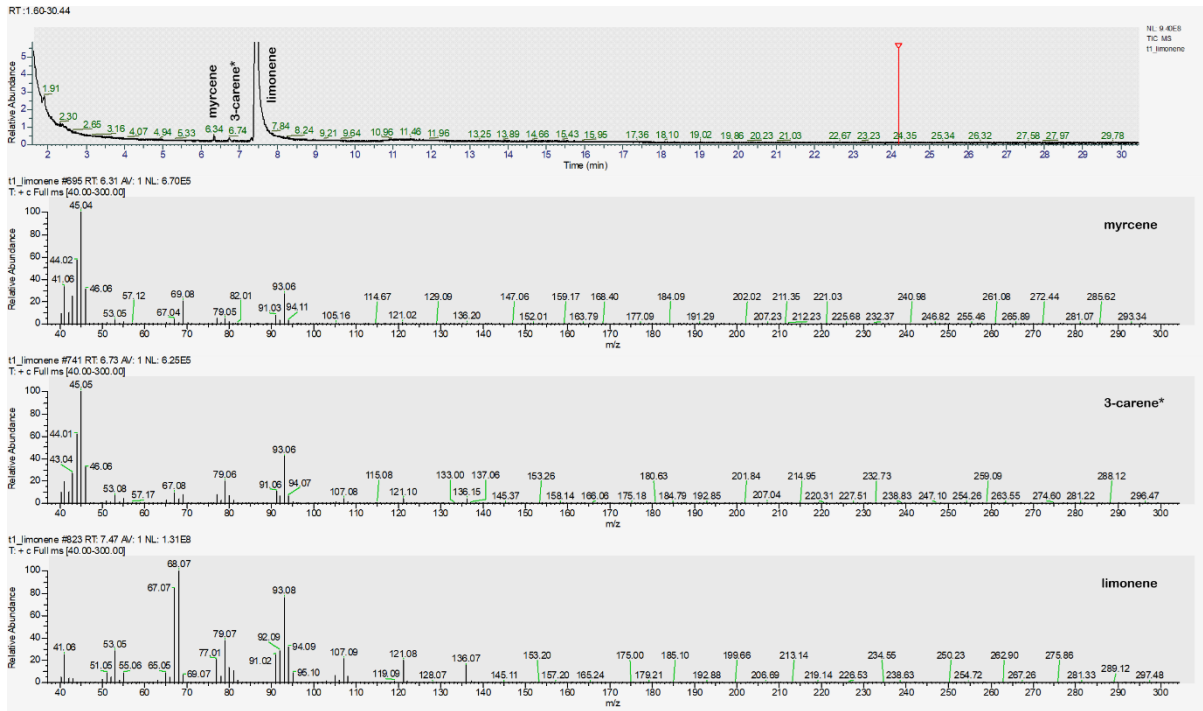


Figure A46: Chromatogram and spectra were acquired using GC-MS. A 1 mg/ml limonene sample was treated with UV-light for 192 hours. Figure taken from Raeber et al.¹⁸⁹

Chromatograms using GC-FID equipped with a BGB-wax capillary column.

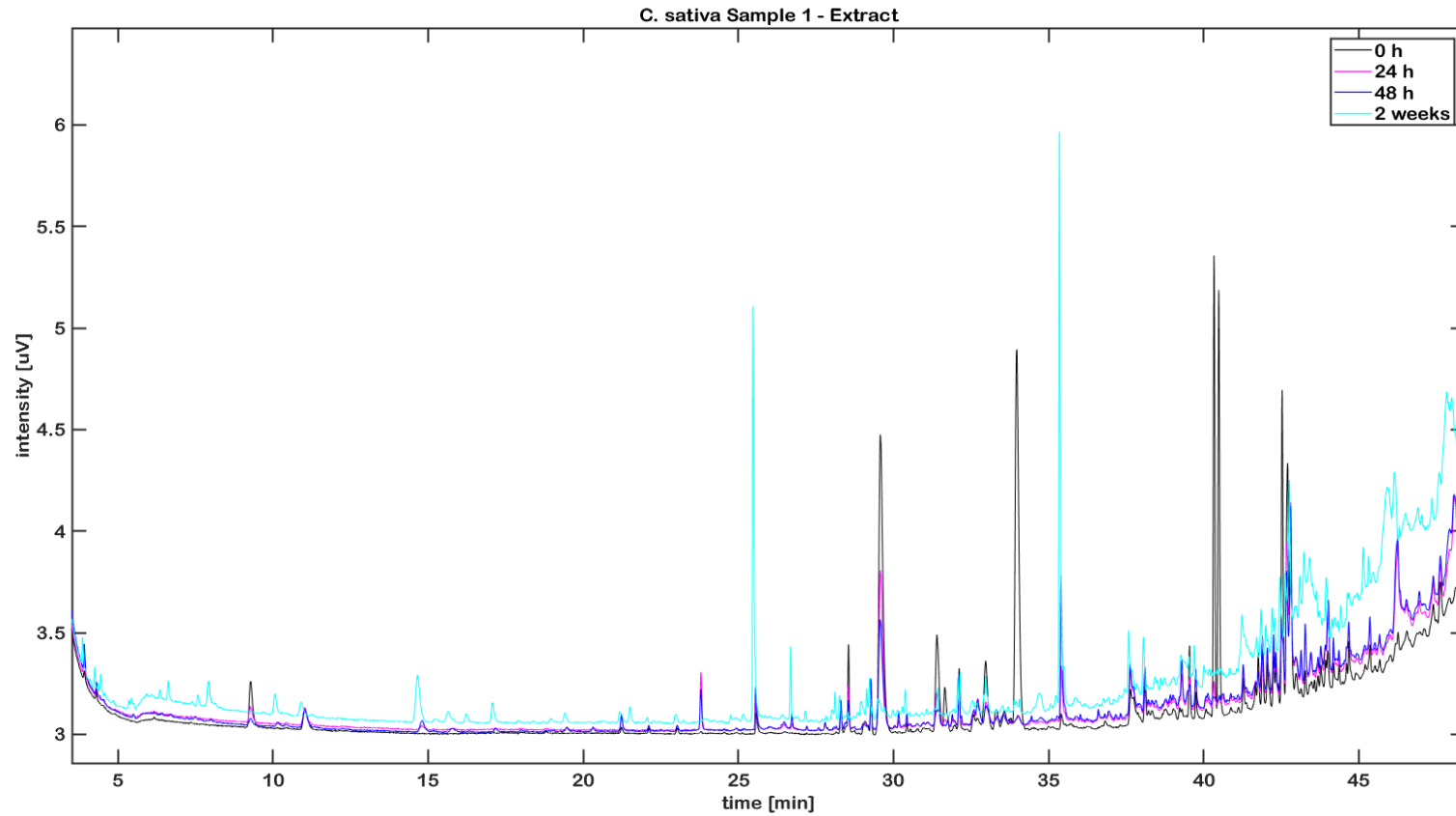


Figure A47: UV-stressed *C. sativa* L. sample 1 as an extract. The overlay shows the chromatogram at time point 0, 24 h, 48 h and 2 weeks of treatment. Figure taken from Raeber et al.¹⁸⁹

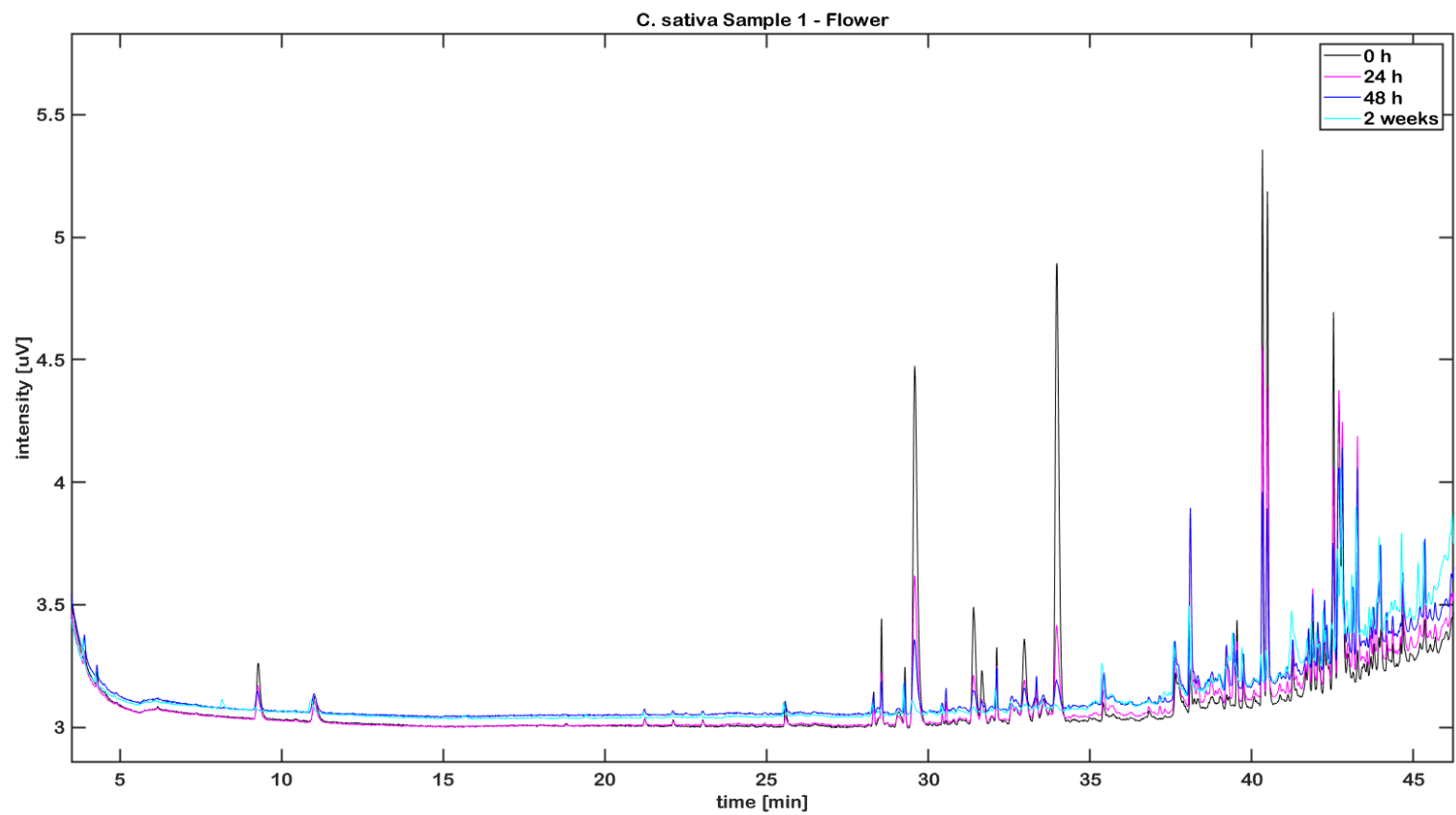


Figure A48: UV-stressed *C. sativa* L. sample 1 as a flower. The overlay shows the chromatogram at time point 0, 24 h, 48 h and 2 weeks of treatment. Figure taken from Raeber et al.¹⁸⁹

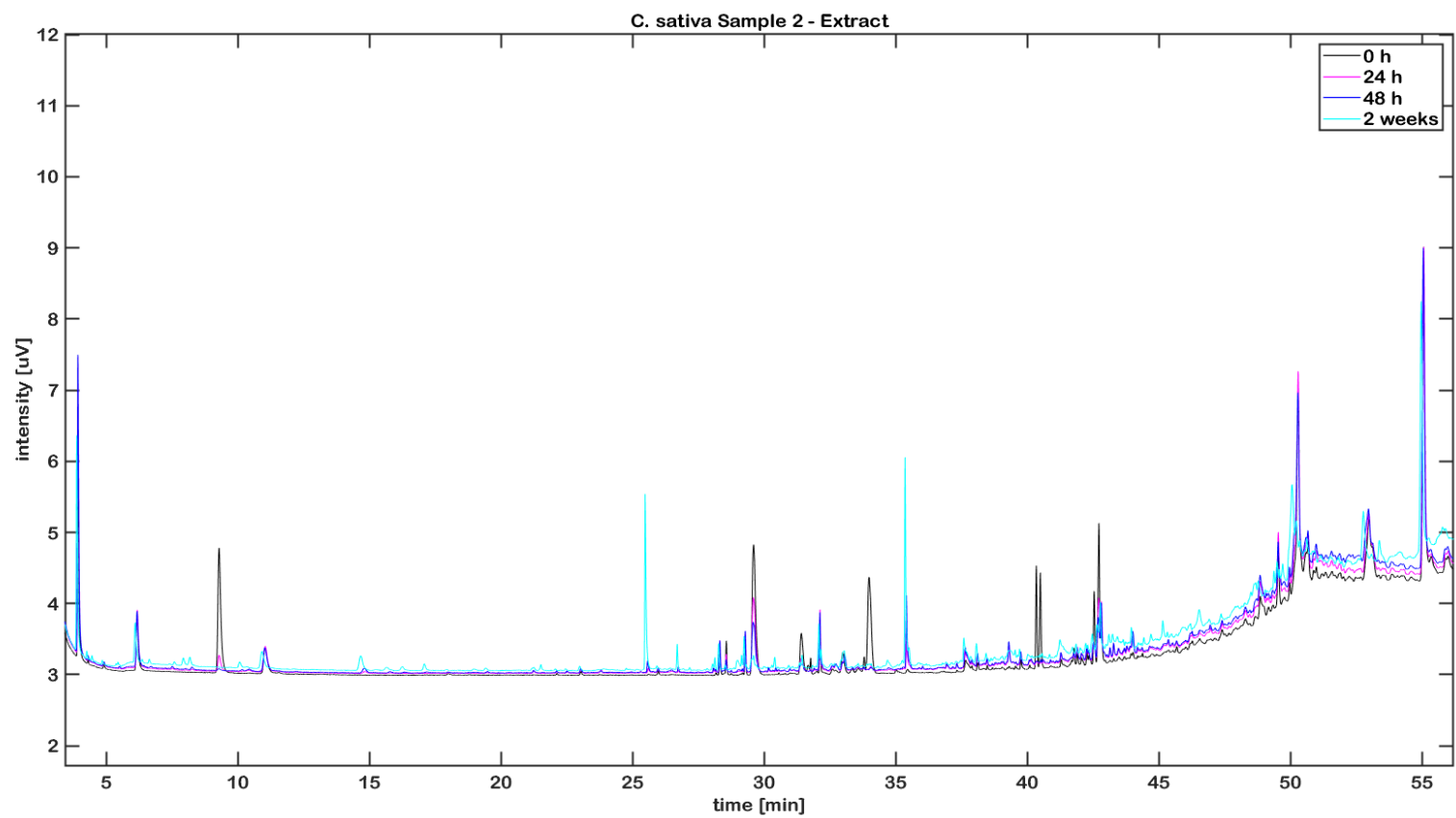


Figure A49: UV-stressed *C. sativa* L. sample 2 as an extract. The overlay shows the chromatogram at time point 0, 24 h, 48 h and 2 weeks of treatment. Figure taken from Raeber et al.¹⁸⁹

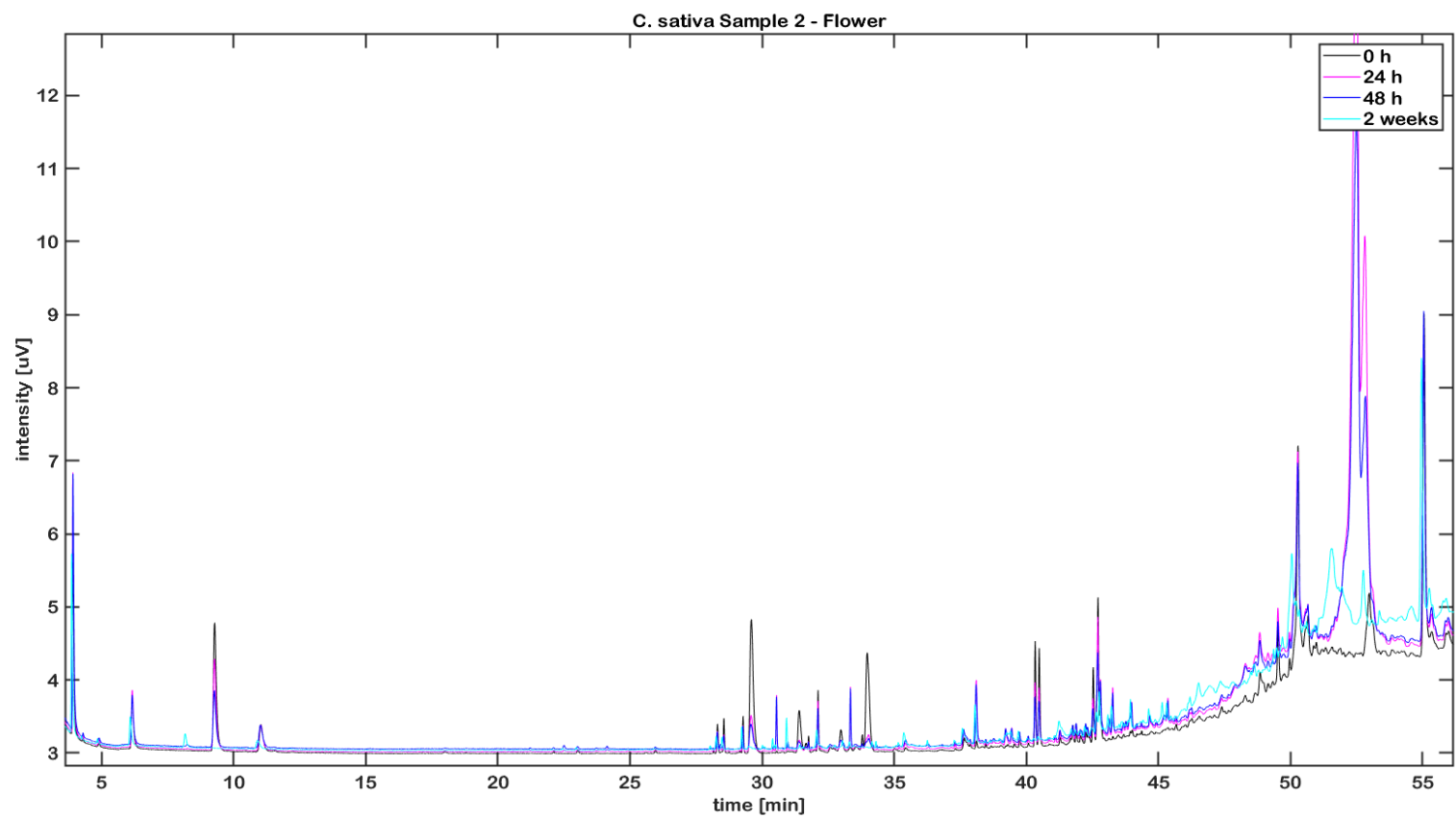


Figure A50: UV-stressed *C. sativa* L. sample 2 as a flower. The overlay shows the chromatogram at time point 0, 24 h, 48 h and 2 weeks of treatment. Figure taken from Raeber et al.¹⁸⁹

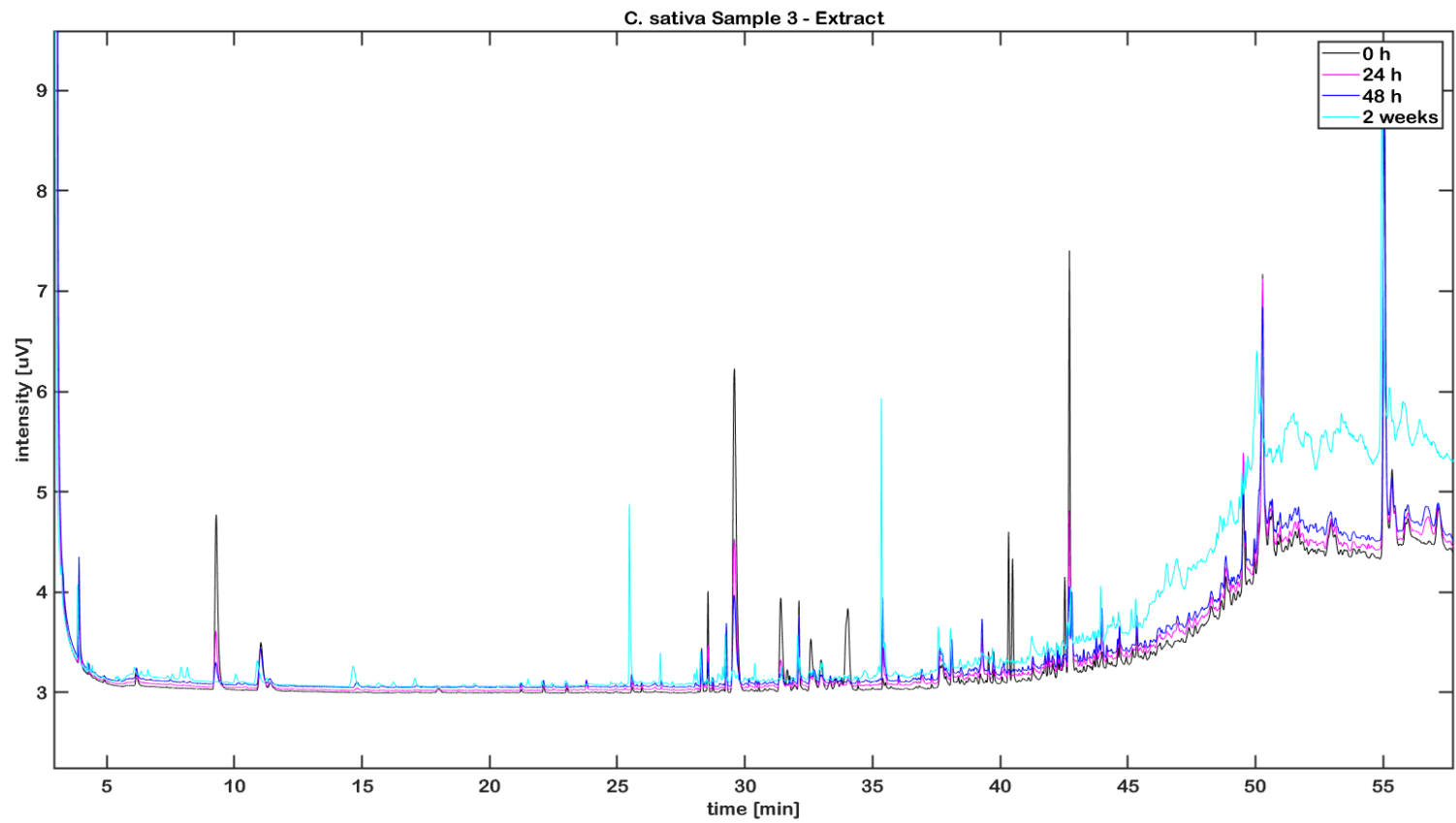


Figure A51: UV-stressed *C. sativa* L. sample 3 as an extract. The overlay shows the chromatogram at time point 0, 24 h, 48 h and 2 weeks of treatment. Figure taken from Raeber et al.¹⁸⁹

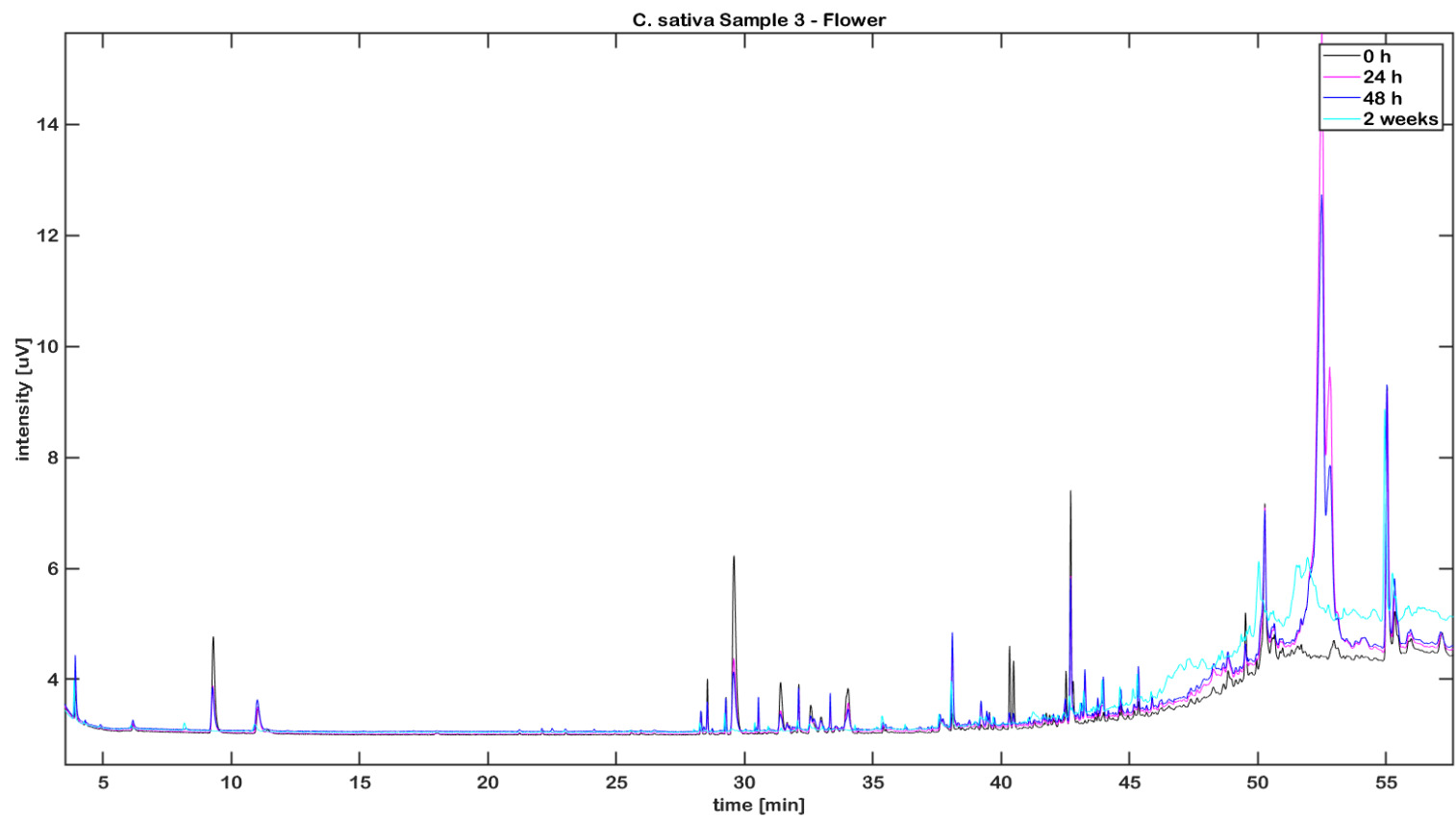


Figure A52: UV-stressed *C. sativa* L. sample 3 as a flower. The overlay shows the chromatogram at time point 0, 24 h, 48 h and 2 weeks of treatment. Figure taken from Raeber et al.¹⁸⁹

Chromatograms using GC-FID equipped with a BGB-178 30% CD capillary column.

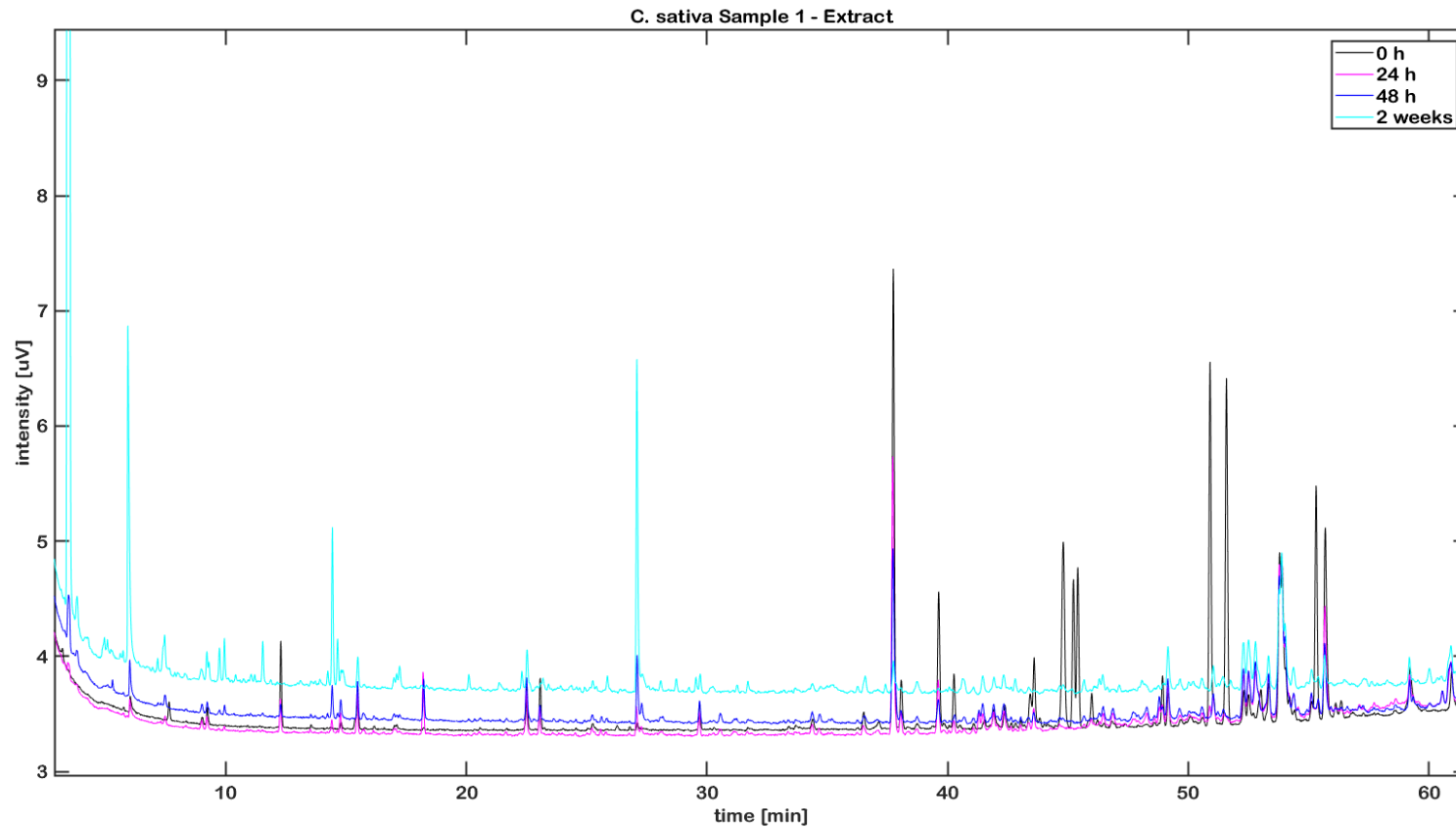


Figure A53: UV-stressed *C. sativa* L. sample 1 as an extract. The overlay shows the chromatogram at time point 0, 24 h, 48 h and 2 weeks of treatment. Figure taken from Raeber et al.¹⁸⁹

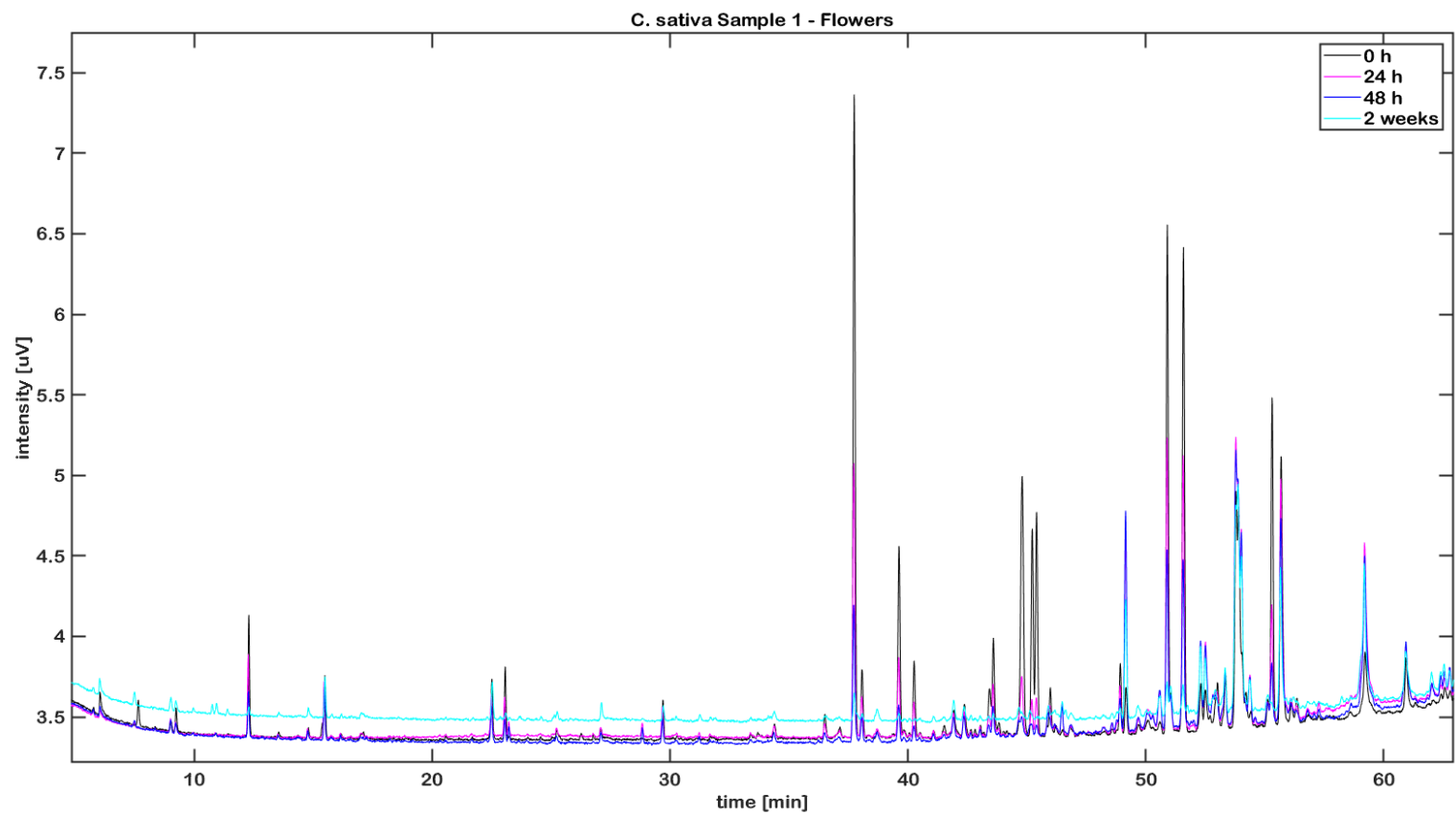


Figure A54: UV-stressed *C. sativa* L. sample 1 as a flower. The overlay shows the chromatogram at time point 0, 24 h, 48 h and 2 weeks of treatment. Figure taken from Raeber et al.¹⁸⁹

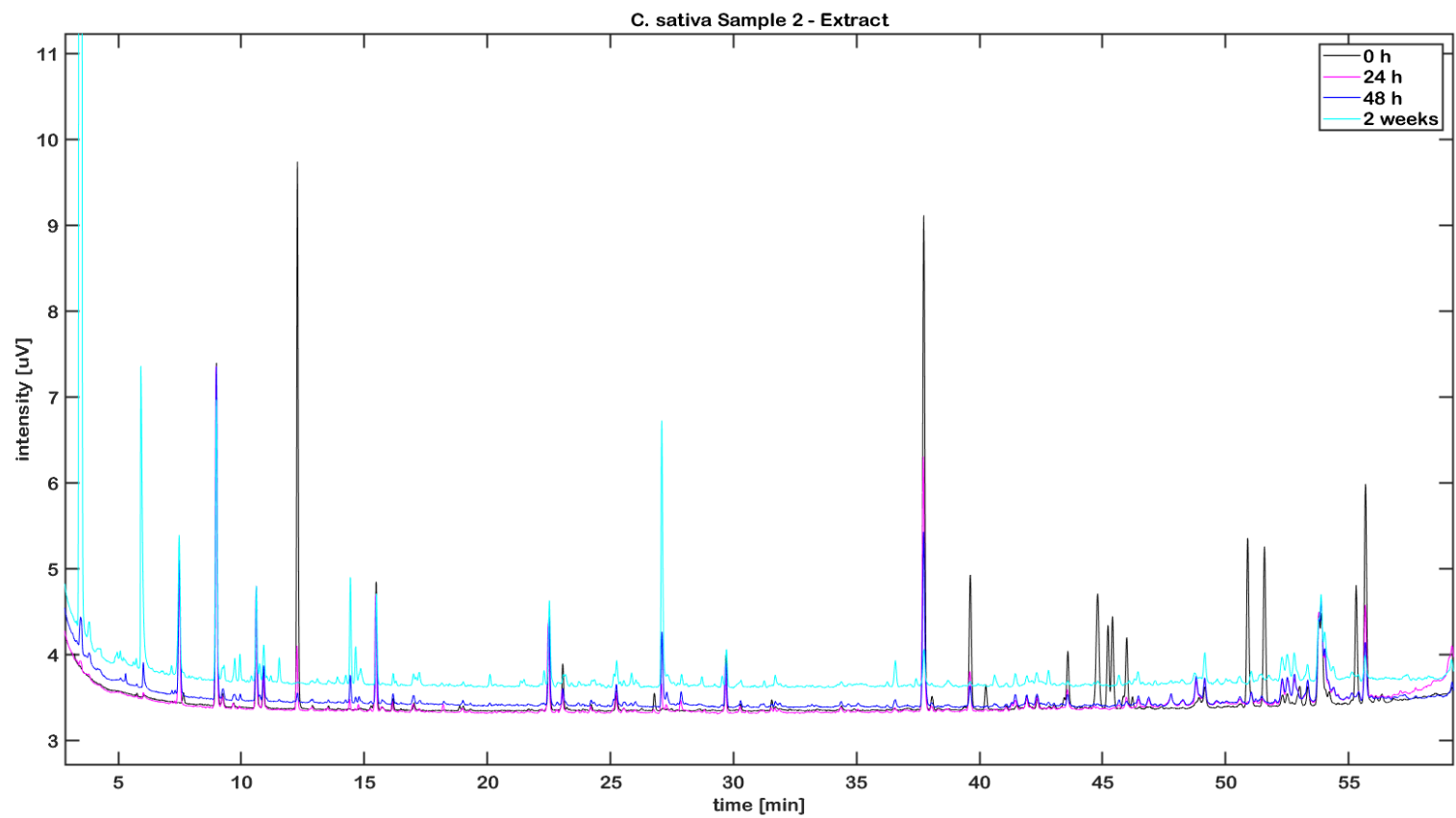


Figure A55: UV-stressed *C. sativa* L. sample 2 as an extract. The overlay shows the chromatogram at time point 0, 24 h, 48 h and 2 weeks of treatment. Figure taken from Raeber et al.¹⁸⁹

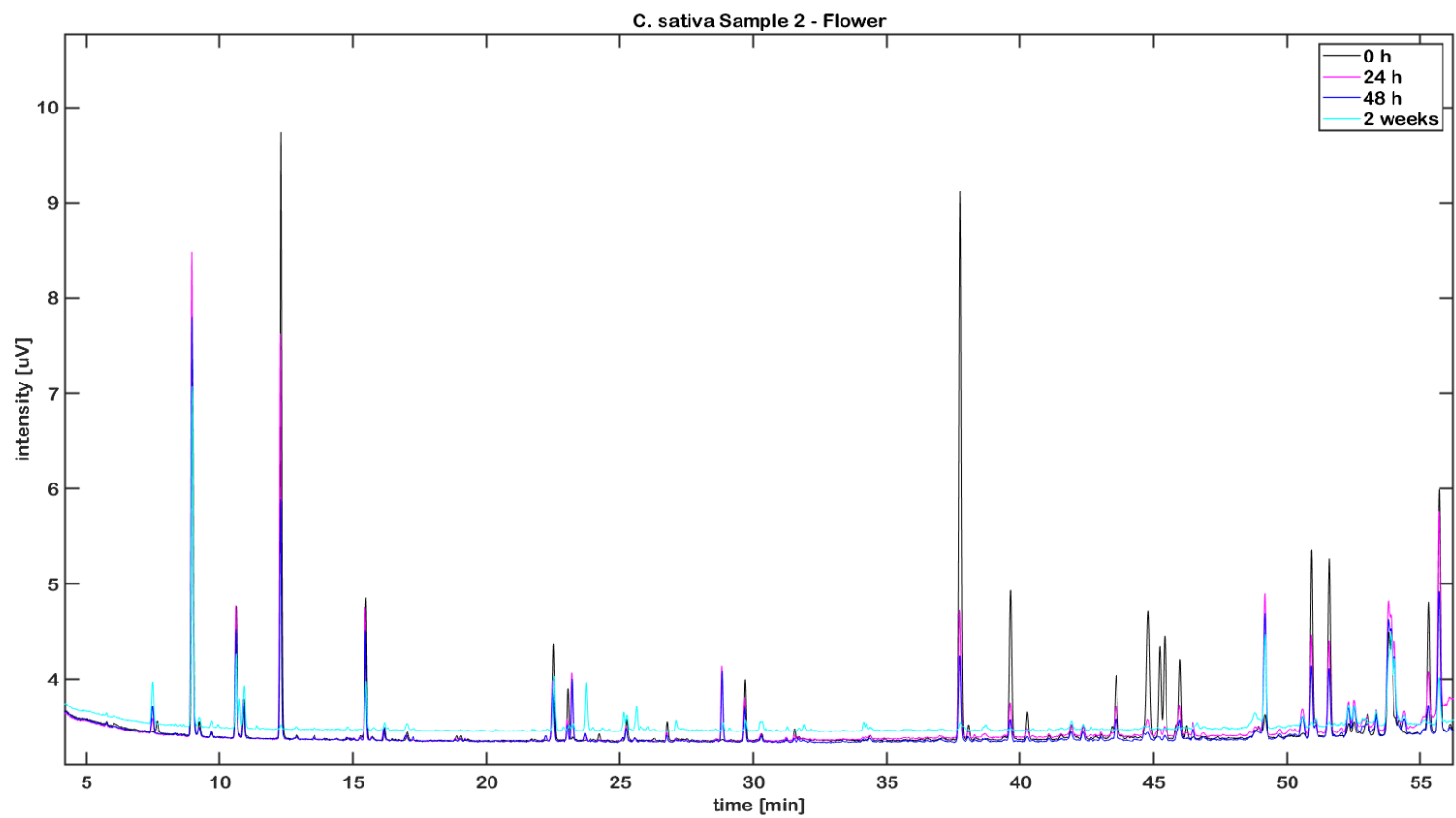


Figure A56: UV-stressed *C. sativa* L. sample 2 as a flower. The overlay shows the chromatogram at time point 0, 24 h, 48 h and 2 weeks of treatment. Figure taken from Raeber et al.¹⁸⁹

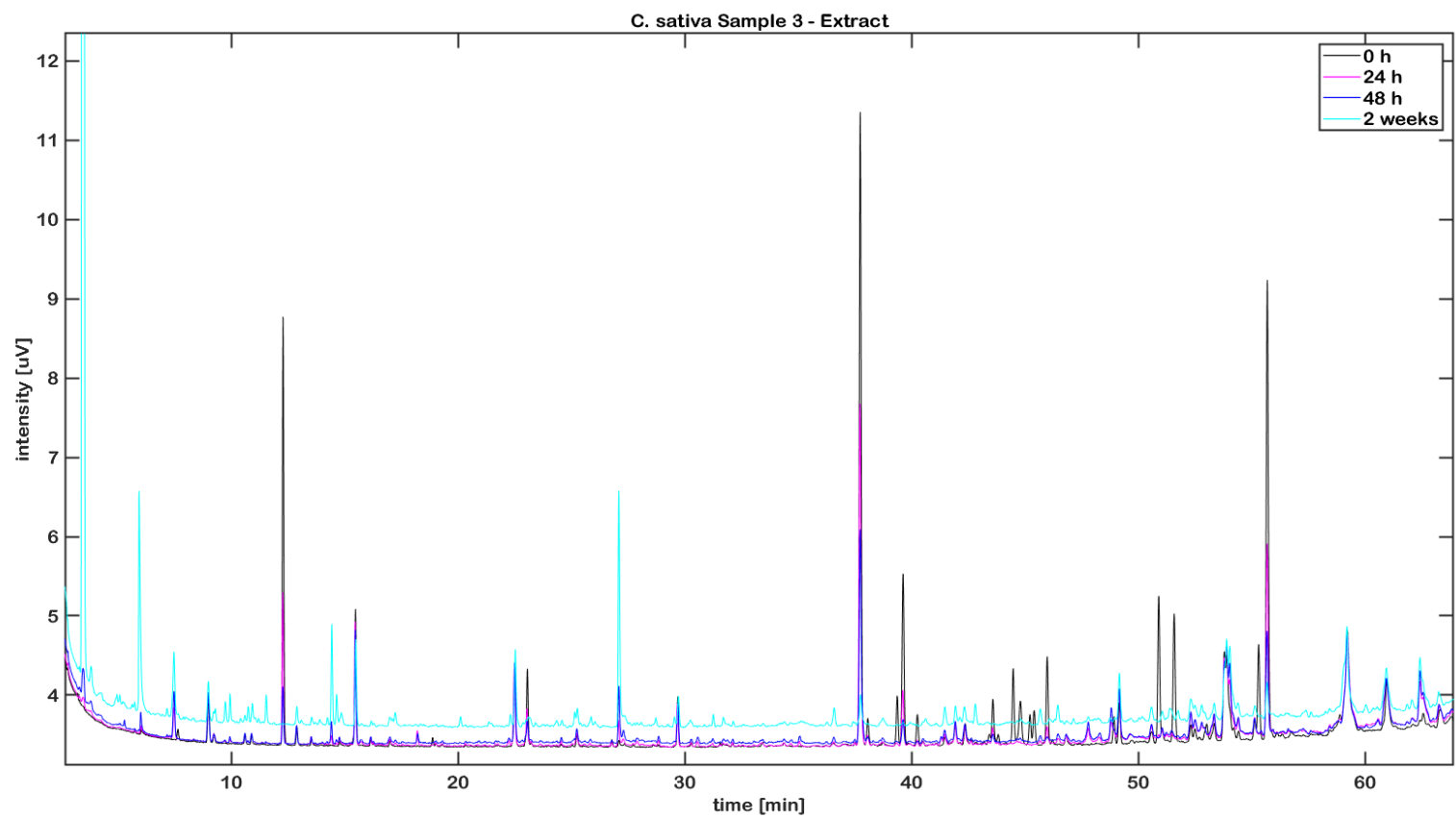


Figure A57: UV-stressed *C. sativa* L. sample 3 as an extract. The overlay shows the chromatogram at time point 0, 24 h, 48 h and 2 weeks of treatment. Figure taken from Raeber et al.¹⁸⁹

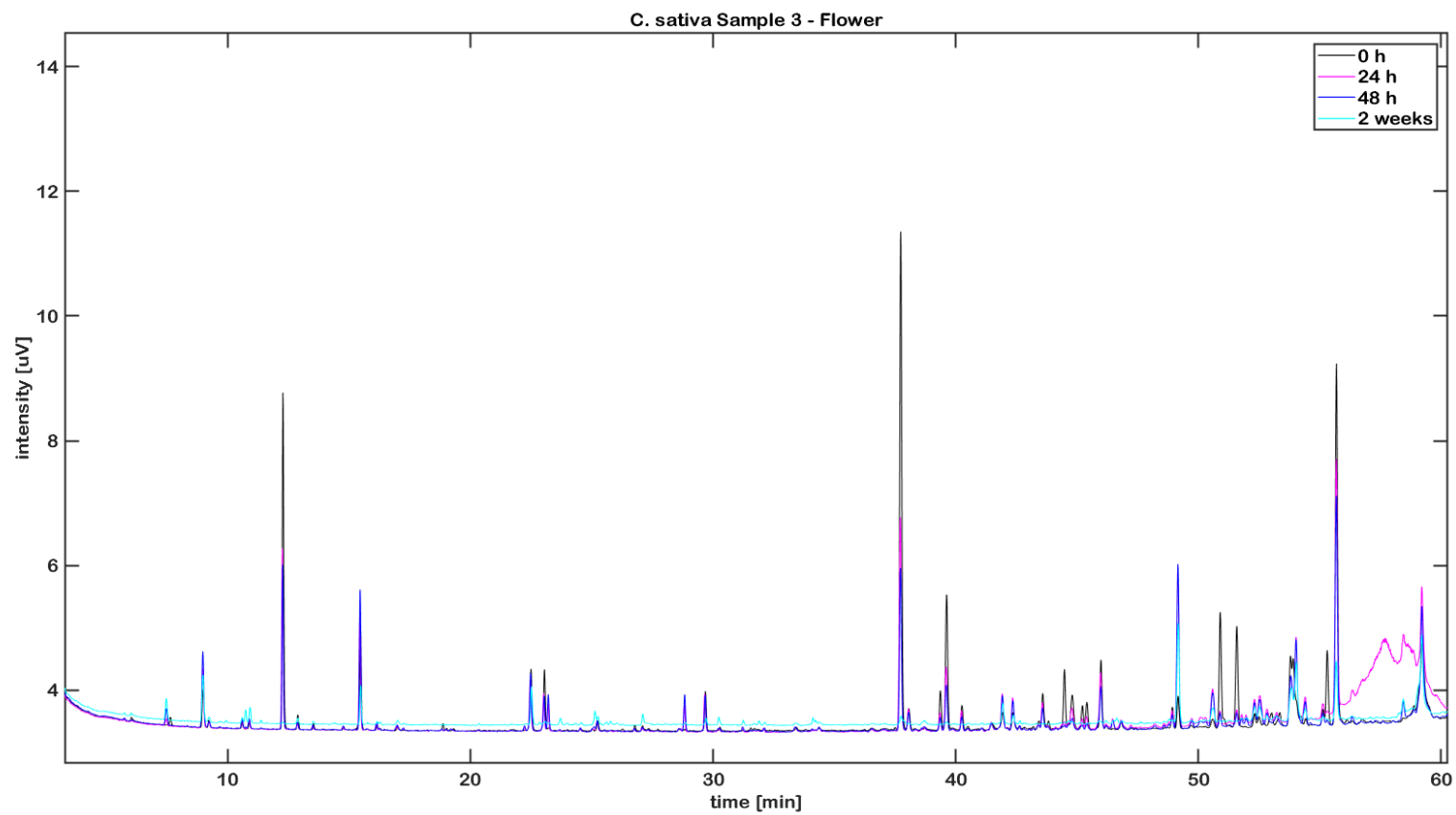


Figure A58: UV-stressed *C. sativa* L. sample 3 as a flower. The overlay shows the chromatogram at time point 0, 24 h, 48 h and 2 weeks of treatment. Figure taken from Raeber et al.¹⁸⁹

Chromatograms using GC-FID equipped with a BGB-176 SE capillary column

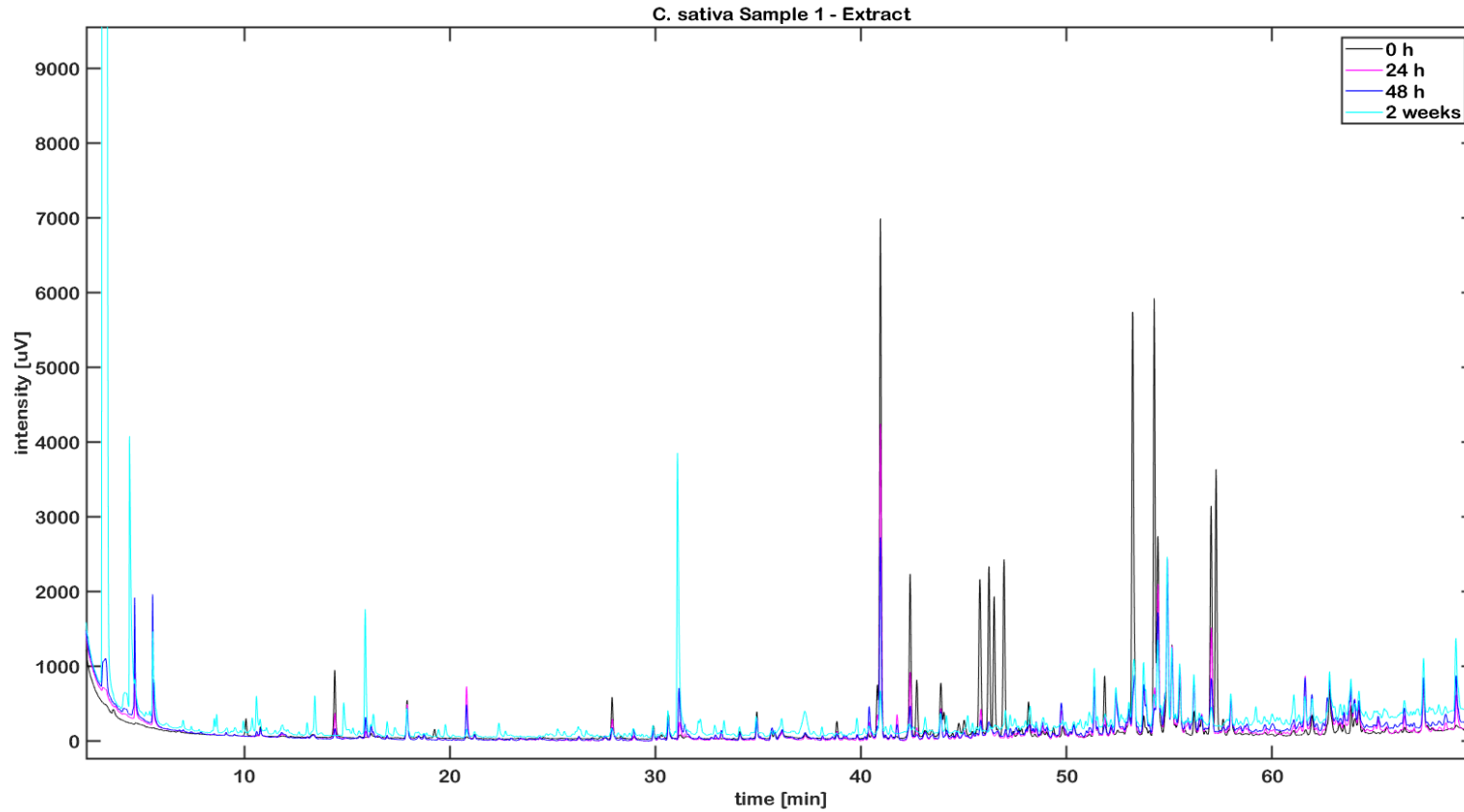


Figure A59: UV-stressed *C. sativa* L. sample 1 as an extract. The overlay shows the chromatogram at time point 0, 24 h, 48 h and 2 weeks of treatment. Figure taken from Raeber et al.¹⁸⁹

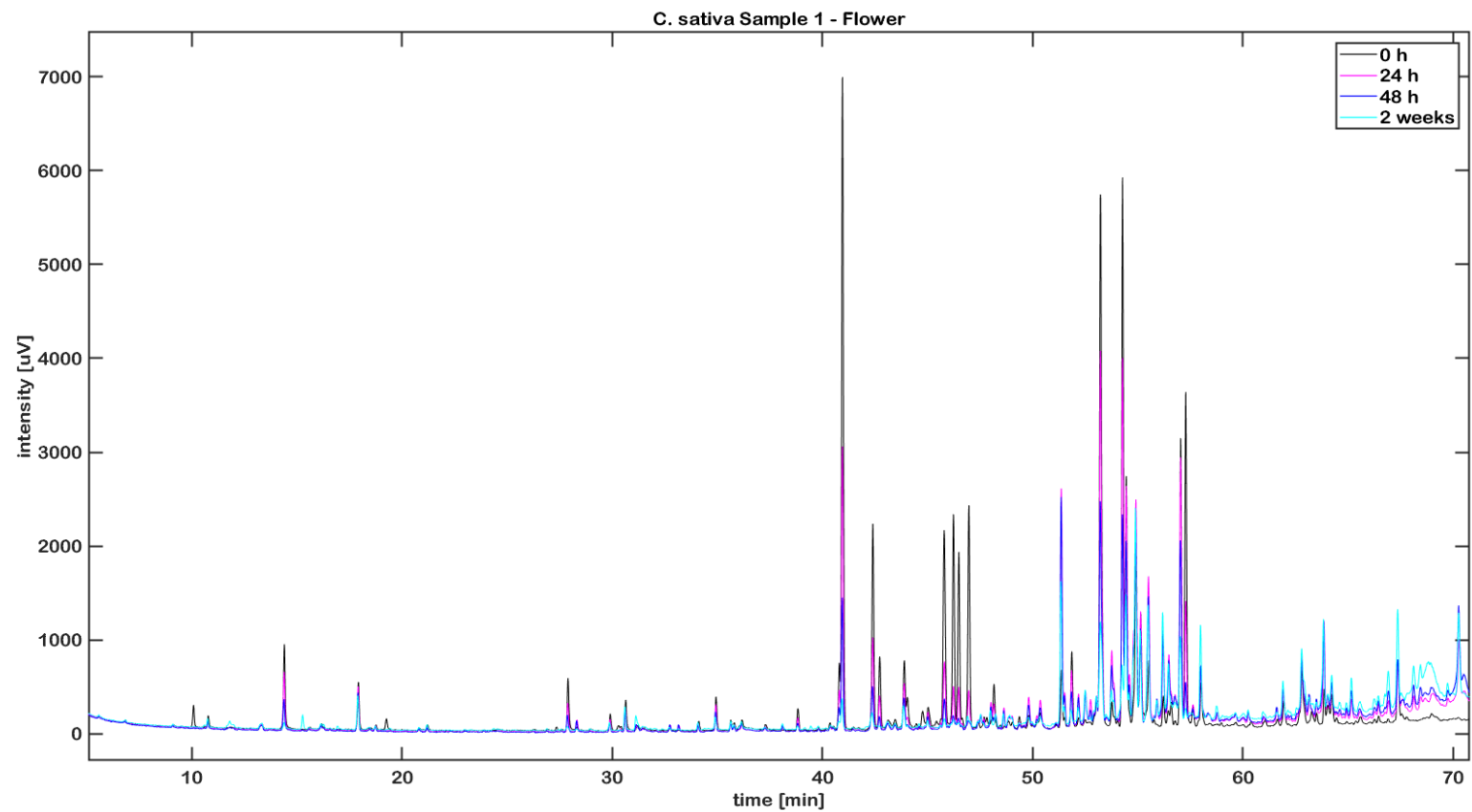


Figure A60: UV-stressed *C. sativa* L. sample 1 as a flower. The overlay shows the chromatogram at time point 0, 24 h, 48 h and 2 weeks of treatment. Figure taken from Raeber et al.¹⁸⁹

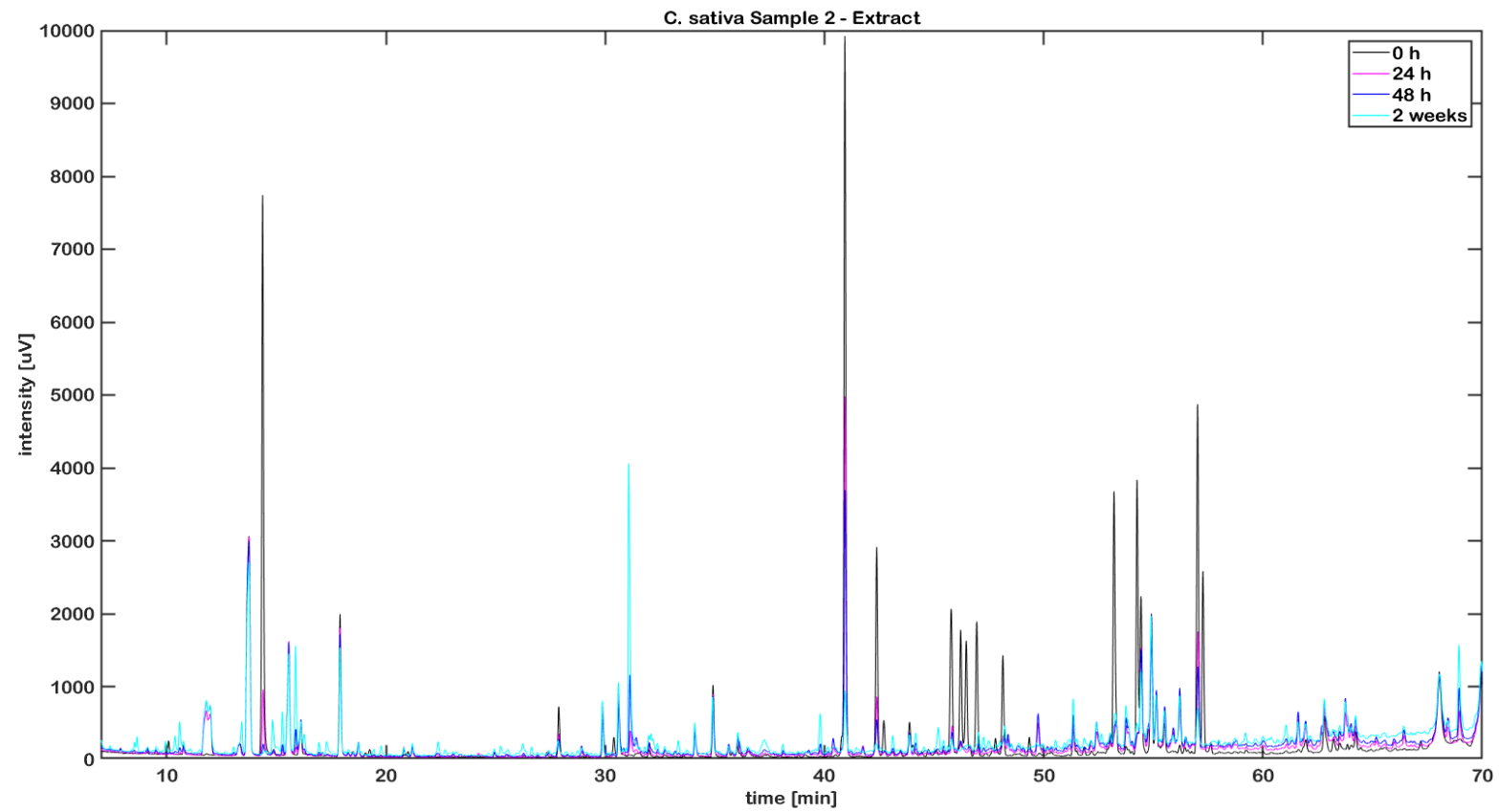


Figure A61: UV-stressed *C. sativa* L. sample 2 as an extract. The overlay shows the chromatogram at time point 0, 24 h, 48 h and 2 weeks of treatment. Figure taken from Raeber et al.¹⁸⁹

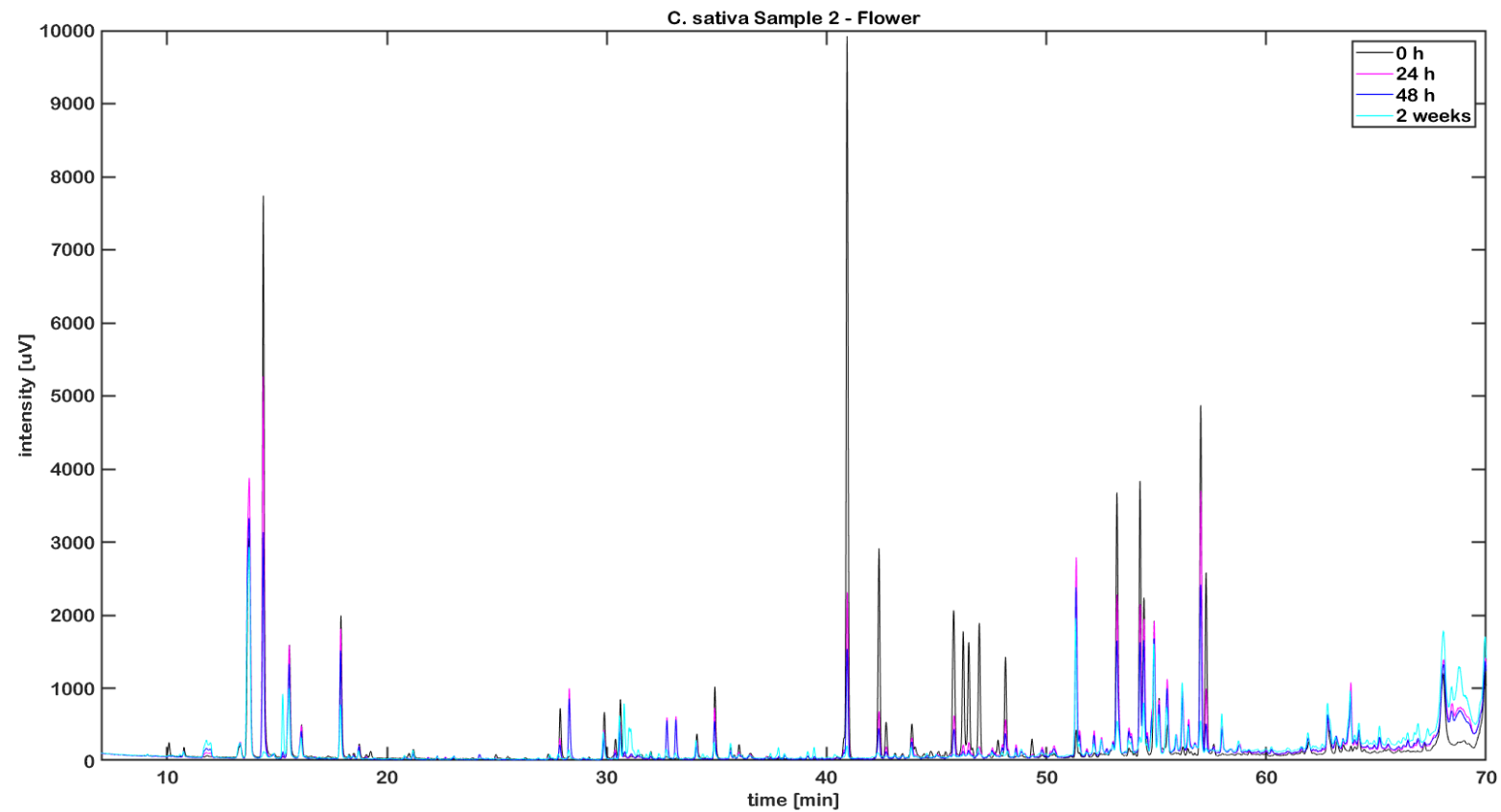


Figure A62: UV-stressed *C. sativa* L. sample 2 as a flower. The overlay shows the chromatogram at time point 0, 24 h, 48 h and 2 weeks of treatment. Figure taken from Raeber et al.¹⁸⁹

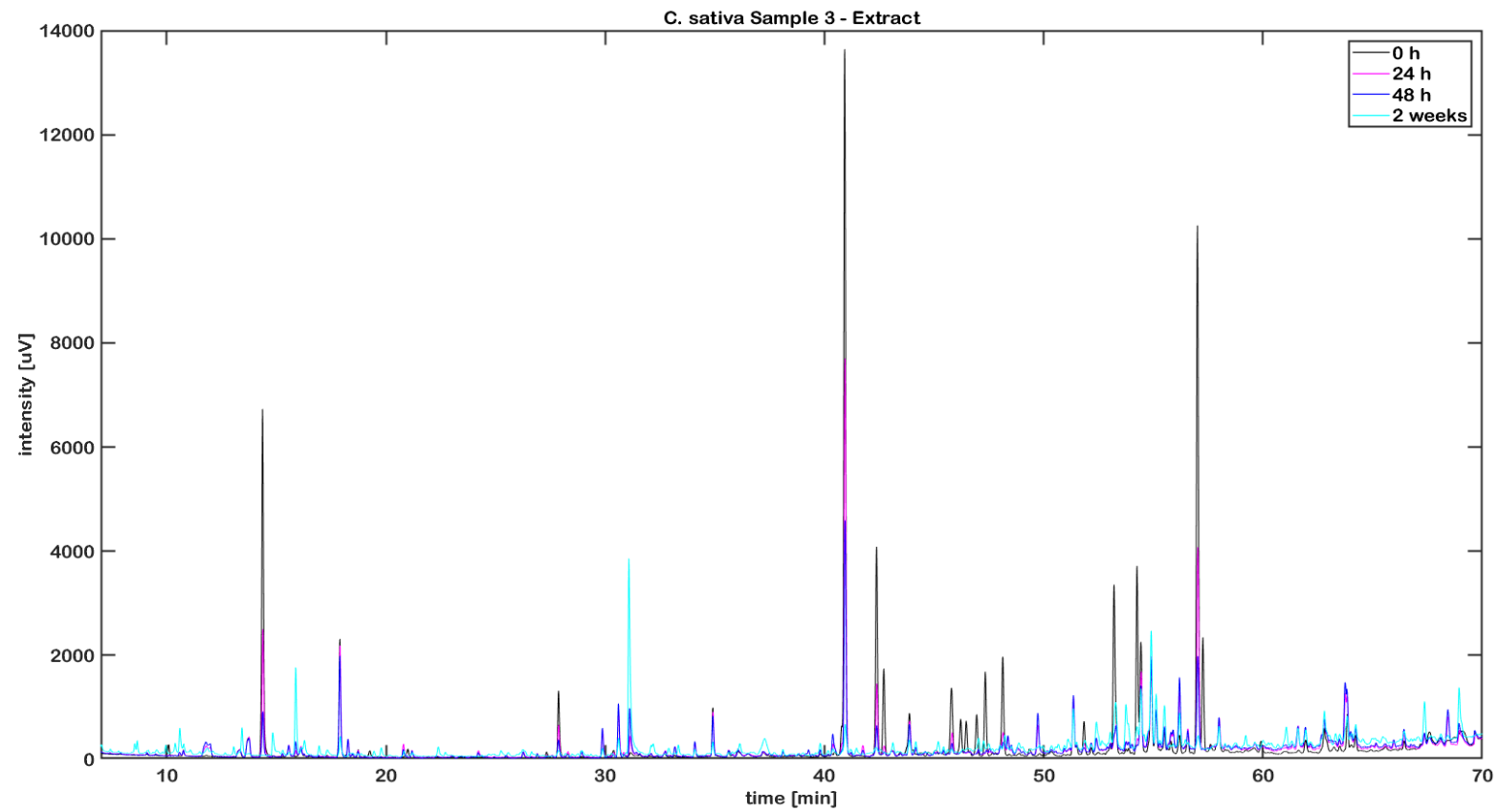


Figure A63: UV-stressed *C. sativa* L. sample 3 as an extract. The overlay shows the chromatogram at time point 0, 24 h, 48 h and 2 weeks of treatment. Figure taken from Raeber et al.¹⁸⁹

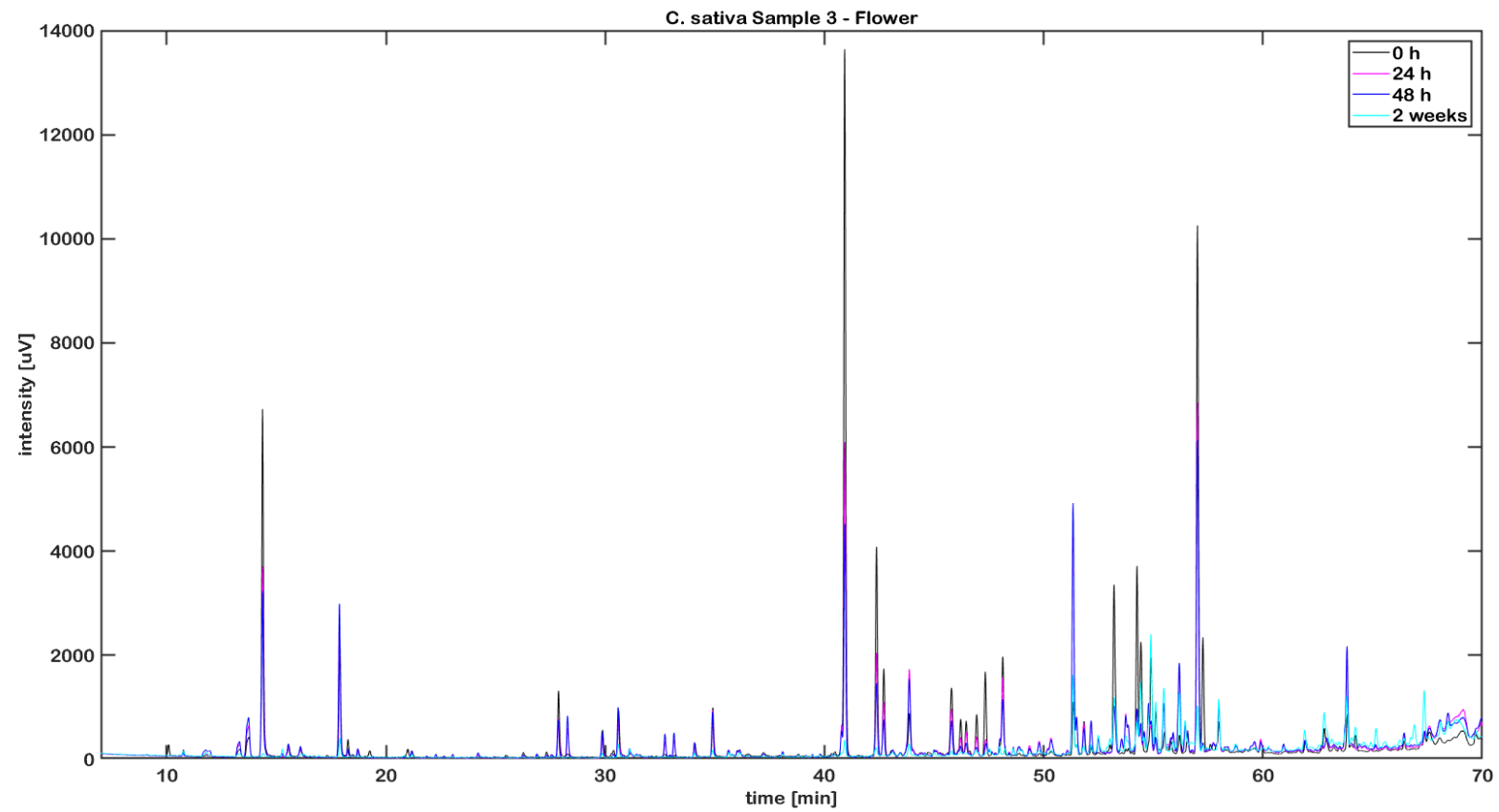


Figure A64: UV-stressed *C. sativa* L. sample 3 as a flower. The overlay shows the chromatogram at time point 0, 24 h, 48 h and 2 weeks of treatment. Figure taken from Raeber et al.¹⁸⁹

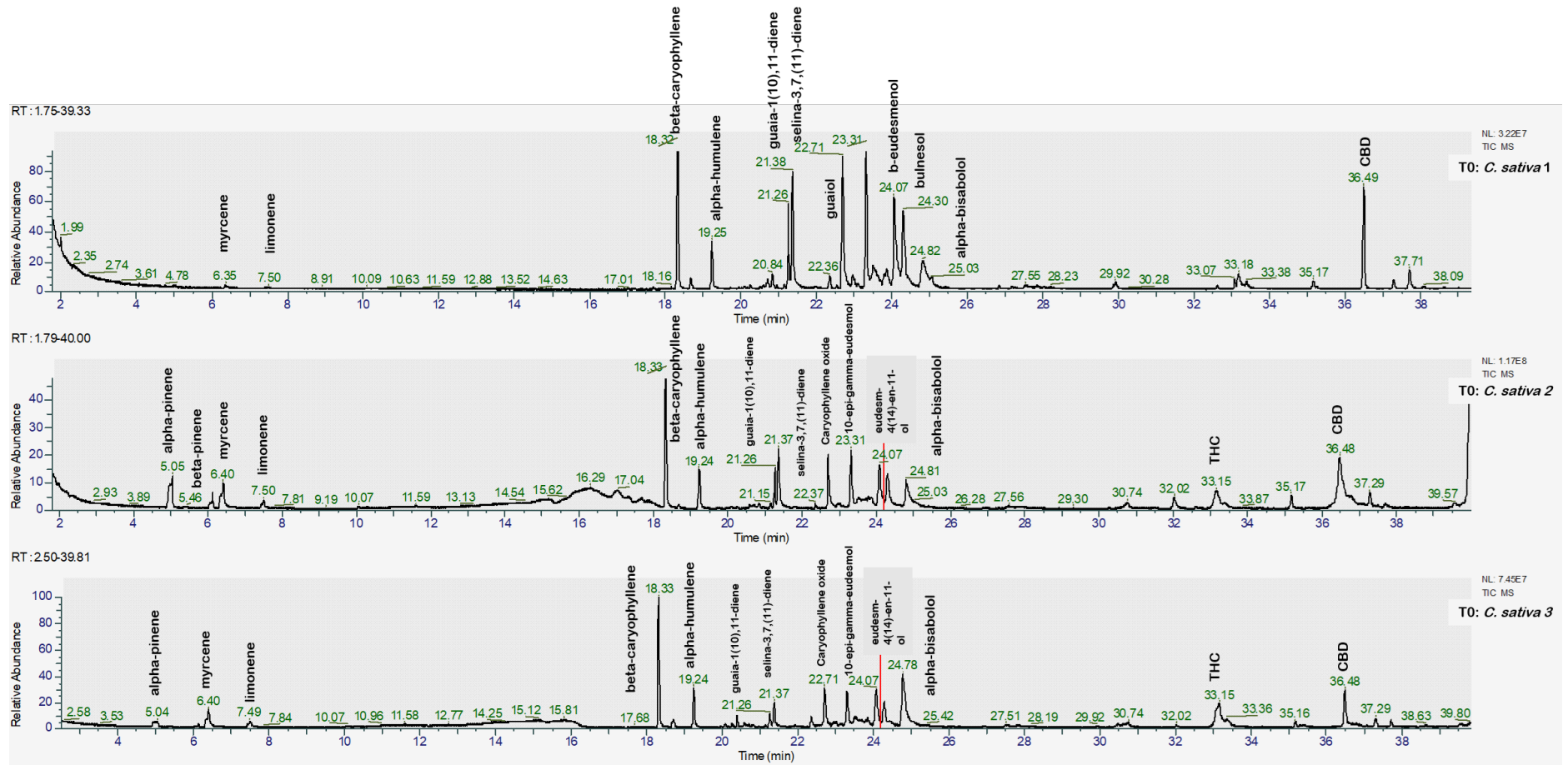


Figure A65: GC-MS chromatogram of authentic *C. sativa* L. samples before UV treatment. Figure taken from Raeber et al.¹⁸⁹

2 weeks UV treatment of *C. sativa* flowers

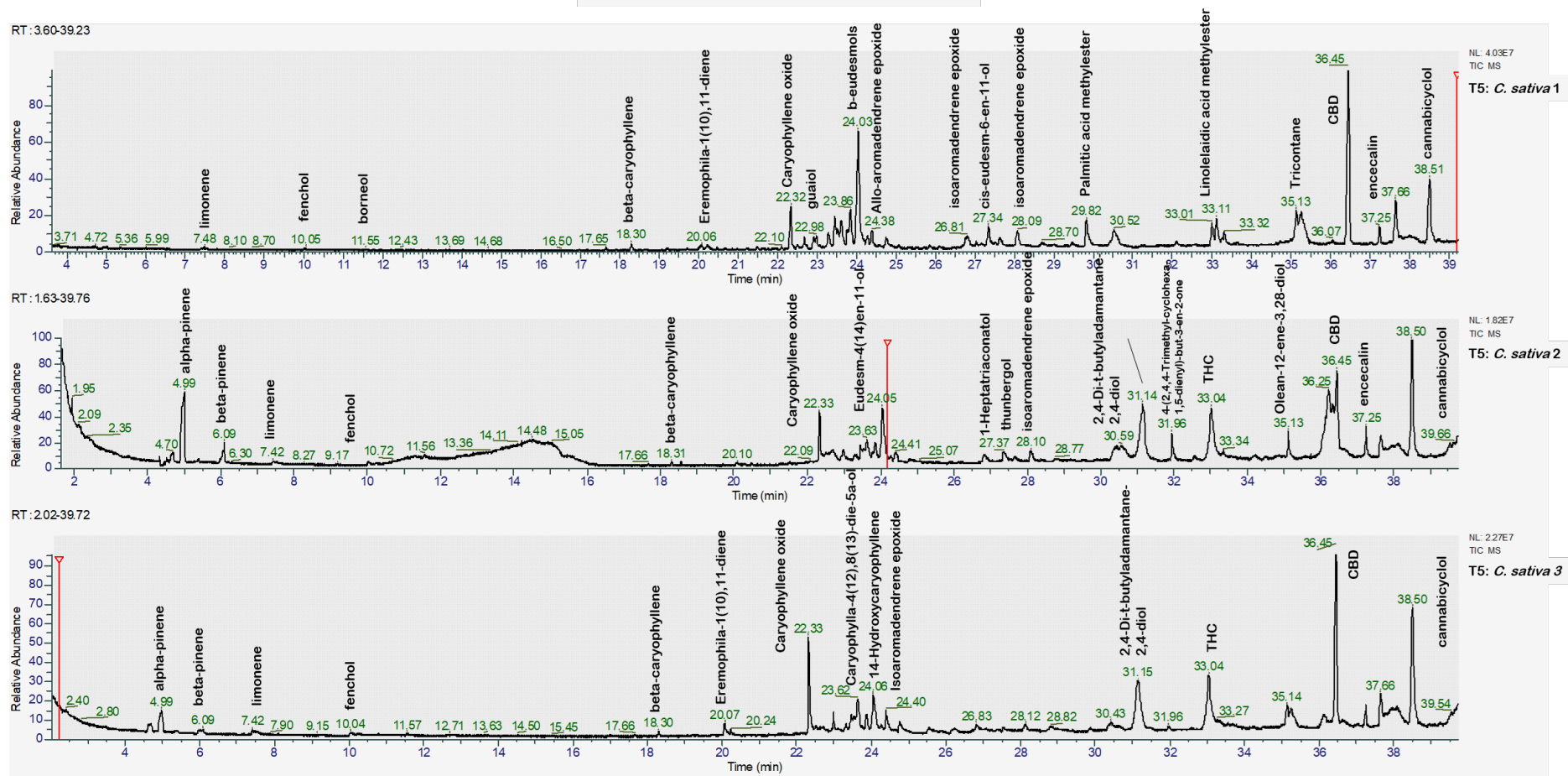


Figure A66: GC-MS chromatogram of authentic *C. sativa* L. flower samples after two weeks of UV treatment. Figure taken from Raeber et al.¹⁸⁹

2 weeks UV treatment of *C. sativa* extracts

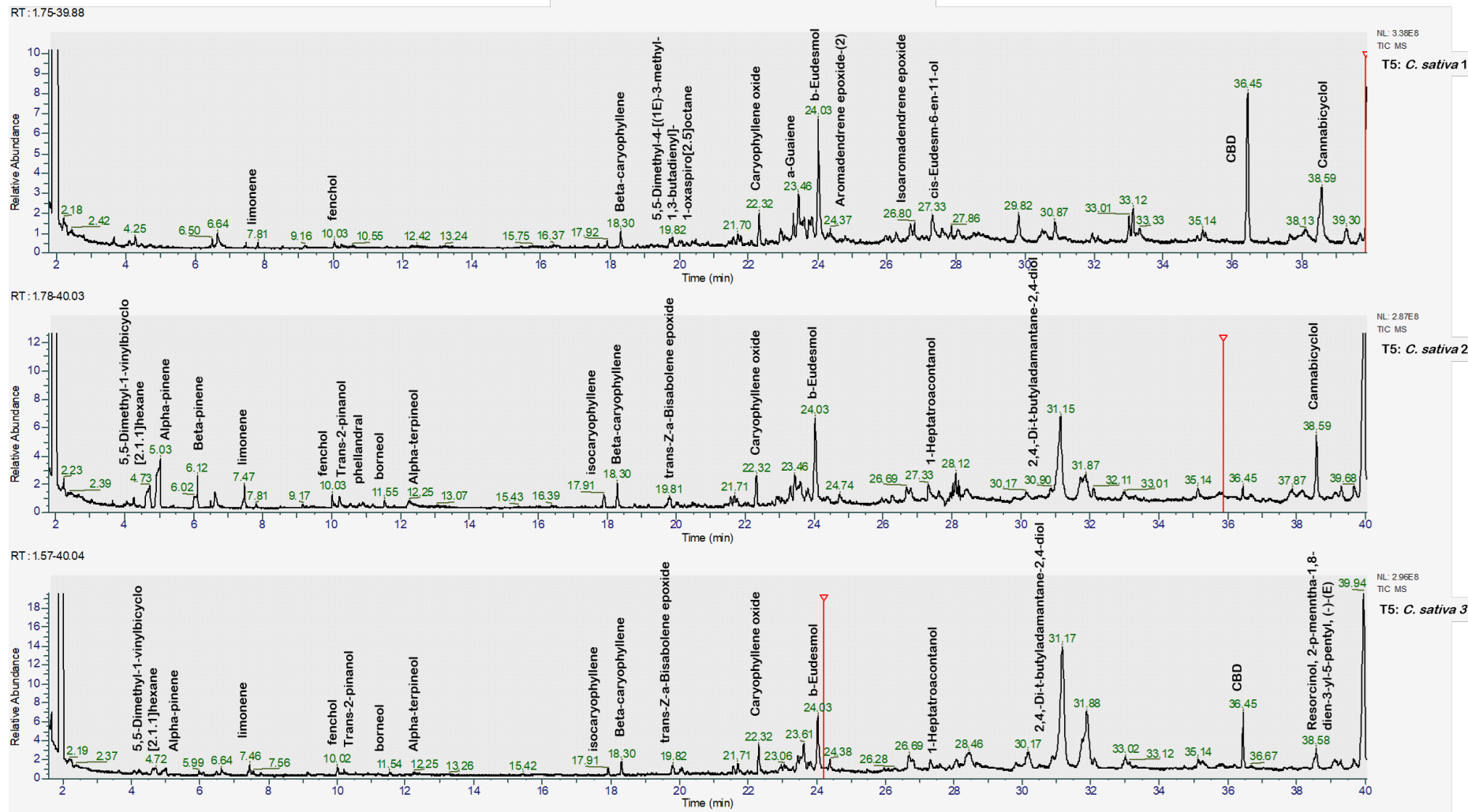


Figure A67: GC-MS chromatogram of authentic *C. sativa* L. extract samples after two weeks of UV treatment. Figure taken from Raeber et al.¹⁸⁹

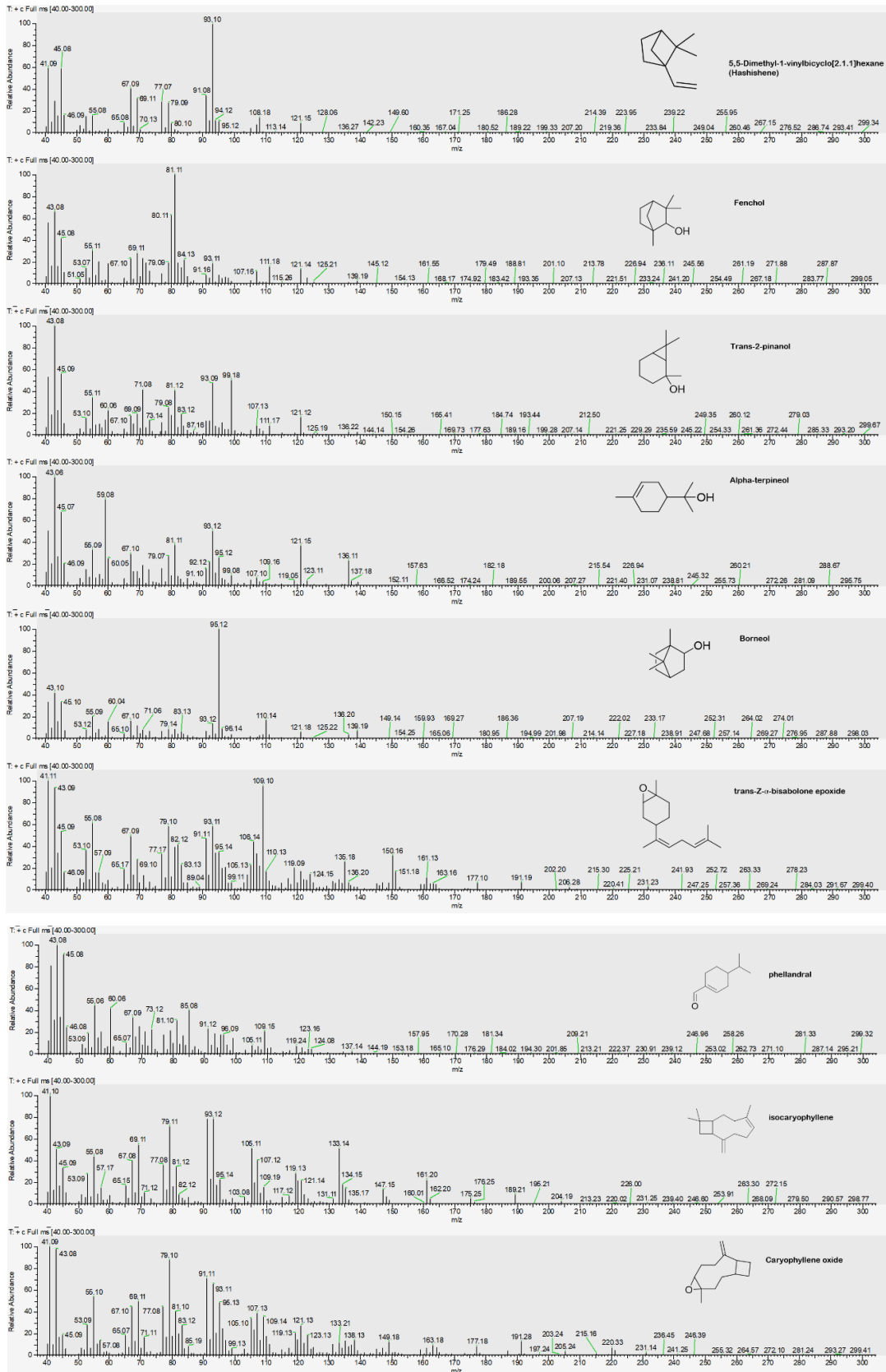


Figure A68: MS spectra of reoccurring oxidation products of authentic *C. sativa* L. samples. Spectra were acquired at 70 eV. Figure taken from Raeber et al.¹⁸⁹

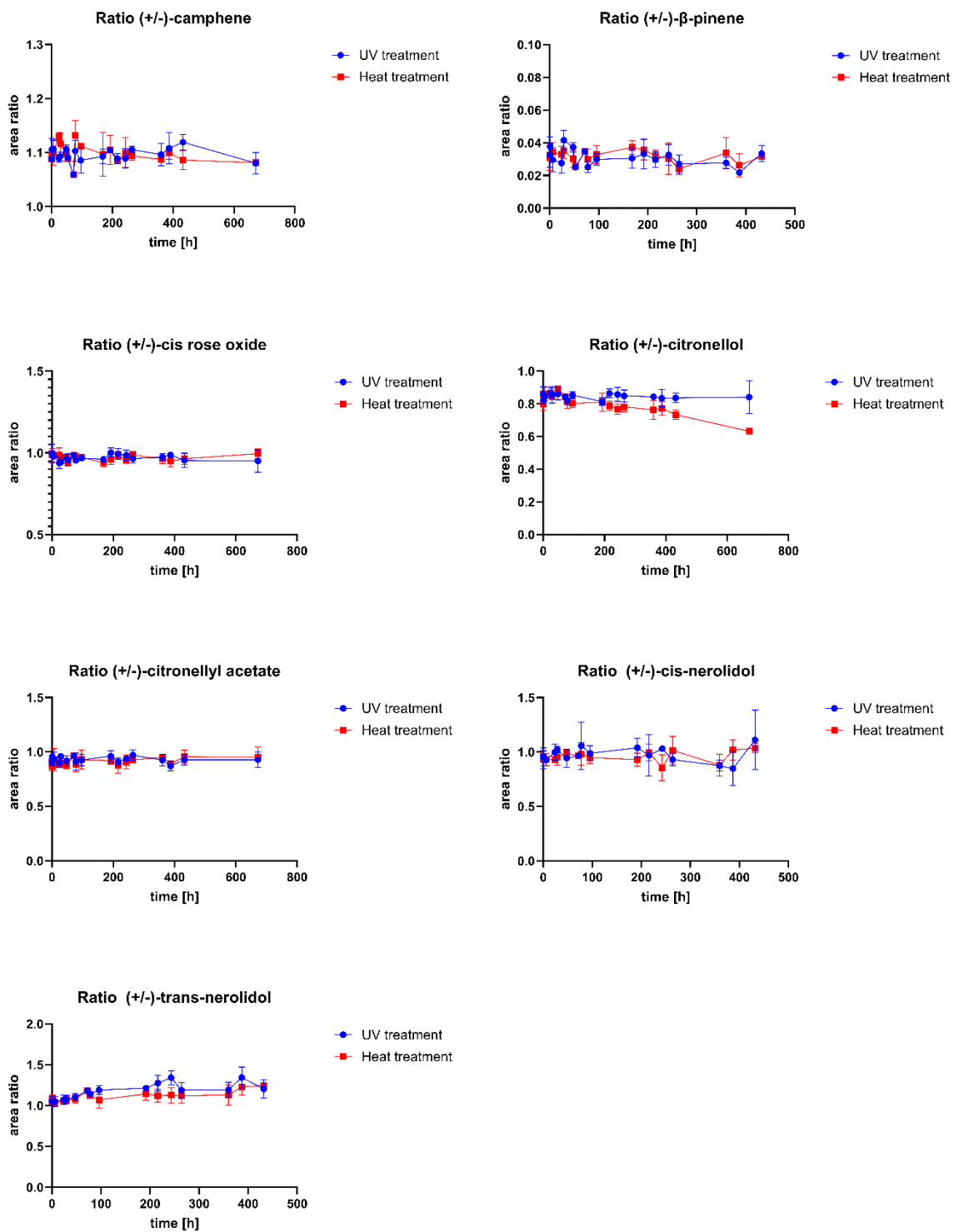


Figure A69: Area ratios of selected enantiomers analysed on a BGB 178 30% CD column. Figure taken from Ræber et al.¹⁸⁹

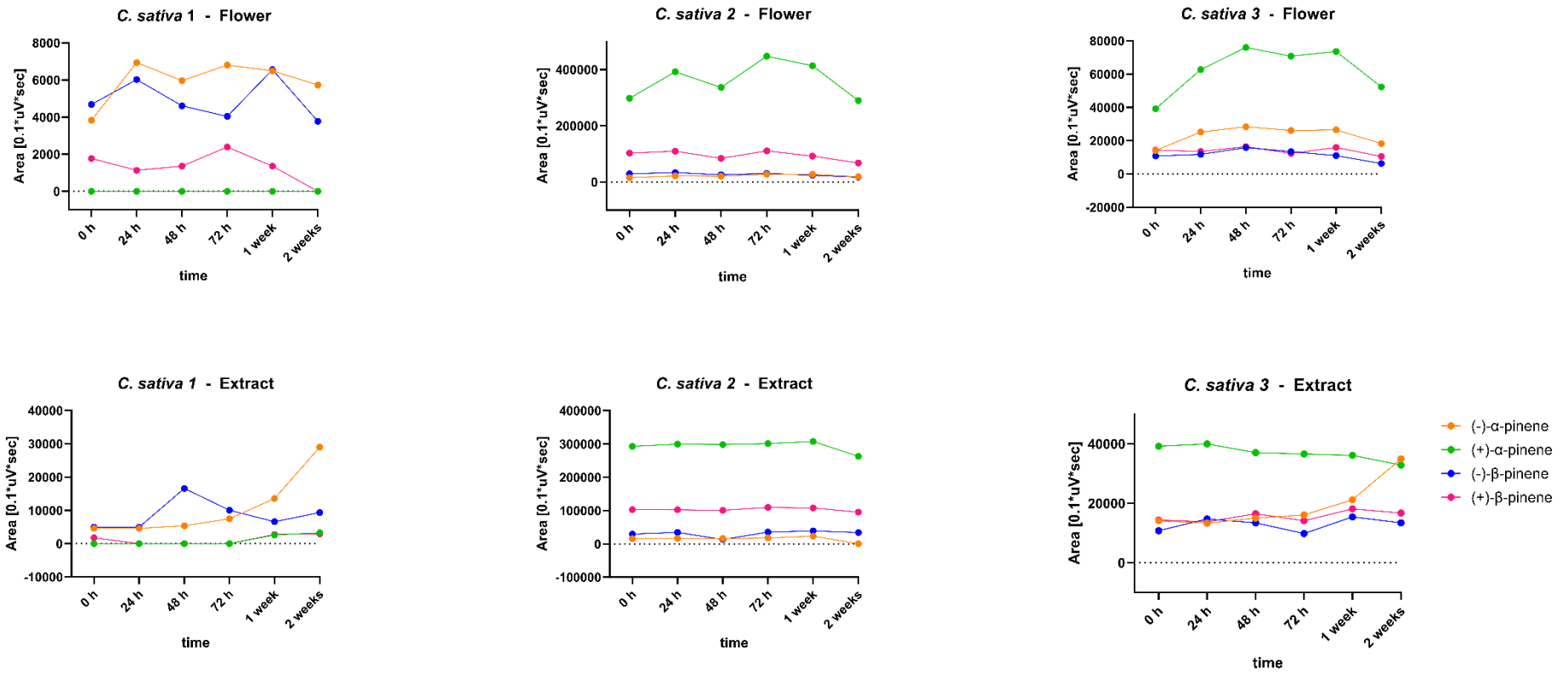


Figure A70: Evolution of pinene areas under prolonged UV exposure. Different intensities were detected in respective *C. sativa* L. samples. Figure taken from Raeber et al.¹⁸⁹

Table A18: EE [%] for 20 authentic *C. sativa* L. samples acquired through chiral GC-FID. Table adapted from Raeber et al.¹⁸⁹

	(+)- α -pinene	(+)- β -pinene	(S)-limonene	(+)-linalool	(-)-citronellol	(-)-camphene	cis-nerolidol 2	(+)-trans-nerolidol	(-)-cis-menthone	Cultivation
<i>C. sativa</i> L. 1	82	31	100	100	n.d.	n.d.	n.d.	n.d.	n.d.	Outdoor
<i>C. sativa</i> L. 2	-42	-59	93	93	n.d.	100	100	100	100	Outdoor
<i>C. sativa</i> L. 3	88	49	89	90	100	100	n.d.	100	100	Outdoor
<i>C. sativa</i> L. 4	100	100	88	89	100	100	n.d.	100	100	Outdoor
<i>C. sativa</i> L. 5	87	42	89	83	100	100	n.d.	100	100	Outdoor
<i>C. sativa</i> L. 6	64	40	84	61	100	100	n.d.	100	n.d.	Outdoor
<i>C. sativa</i> L. 7	80	6	88	93	n.d.	n.d.	n.d.	100	n.d.	Indoor
<i>C. sativa</i> L. 8	-100	-100	93	95	n.d.	100	n.d.	100	100	Indoor
<i>C. sativa</i> L. 9	86	42	89	100	100	44	n.d.	100	100	Indoor
<i>C. sativa</i> L. 10	83	28	87	90	100	100	n.d.	100	n.d.	Indoor
<i>C. sativa</i> L. 11	-100	-100	93	93	n.d.	100	n.d.	100	n.d.	Indoor
<i>C. sativa</i> L. 12	64	-16	96	100	100	n.d.	n.d.	100	n.d.	Indoor
<i>C. sativa</i> L. 13	-62	-53	97	100	n.d.	100	n.d.	100	n.d.	Indoor
<i>C. sativa</i> L. 14	-100	-100	95	98	n.d.	100	n.d.	100	n.d.	Indoor
<i>C. sativa</i> L. 15	-100	-70	92	100	n.d.	100	n.d.	100	n.d.	Indoor
<i>C. sativa</i> L. 16	68	6	92	82	100	100	n.d.	n.d.	n.d.	Indoor
<i>C. sativa</i> L. 17	83	27	93	88	100	100	n.d.	100	100	Indoor
<i>C. sativa</i> L. 18	91	50	88	88	100	100	n.d.	100	100	Greenhouse
<i>C. sativa</i> L. 19	85	36	90	87	100	100	n.d.	100	100	Greenhouse
<i>C. sativa</i> L. 20	93	60	85	81	100	100	n.d.	100	n.d.	Greenhouse

Chapter 2: Ionisation techniques for terpenes

3.1. DBDI coupled to GC for structure elucidation of terpenes

Some of the data presented here was acquired in collaboration with Dr. Alina Begley and Prof. Dr. Renato Zenobi (ETH, Analytical Chemistry).

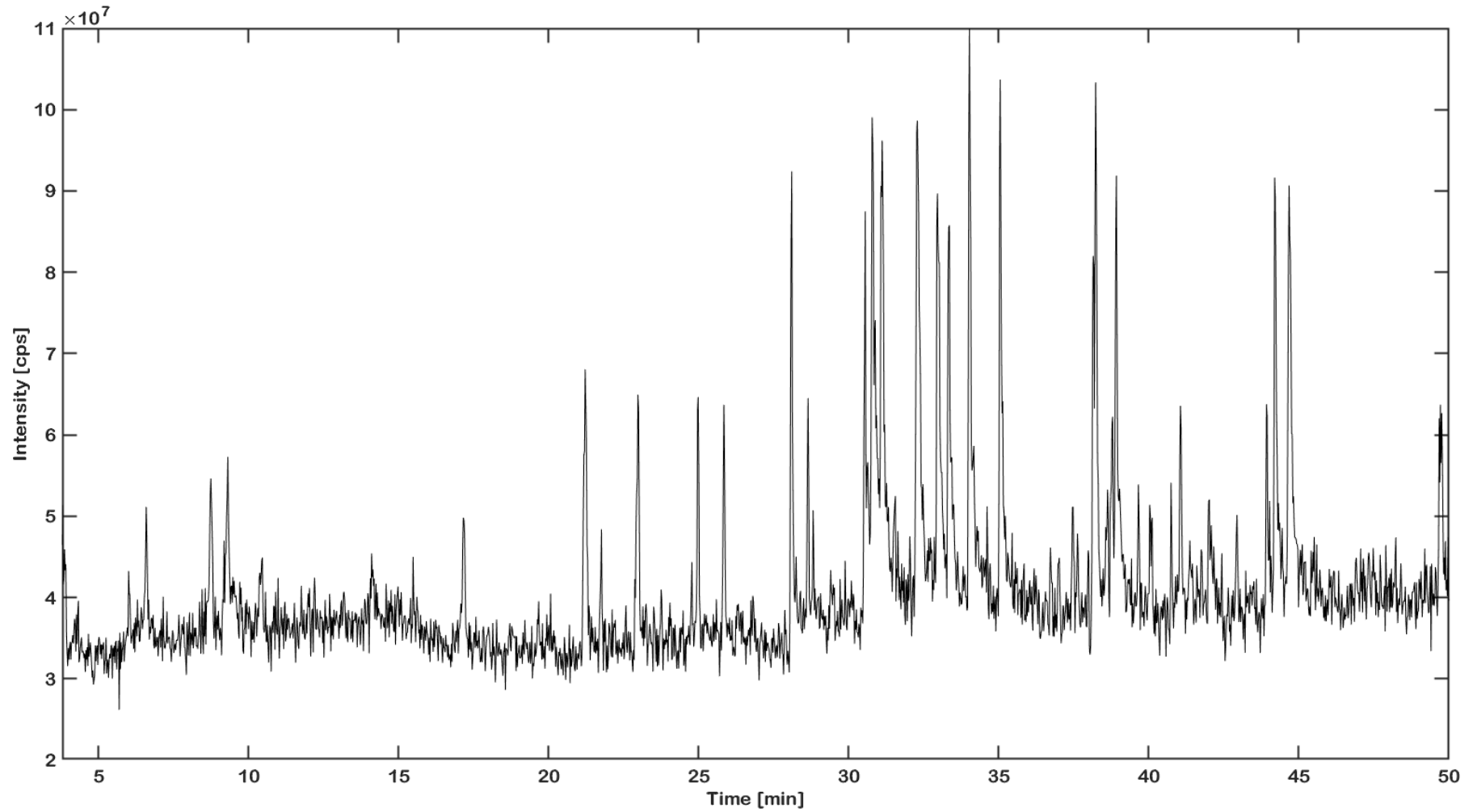


Figure A71: GC-DBDI-MS spectrum acquired at an amplitude of 1500 V and 15,000 Hz.

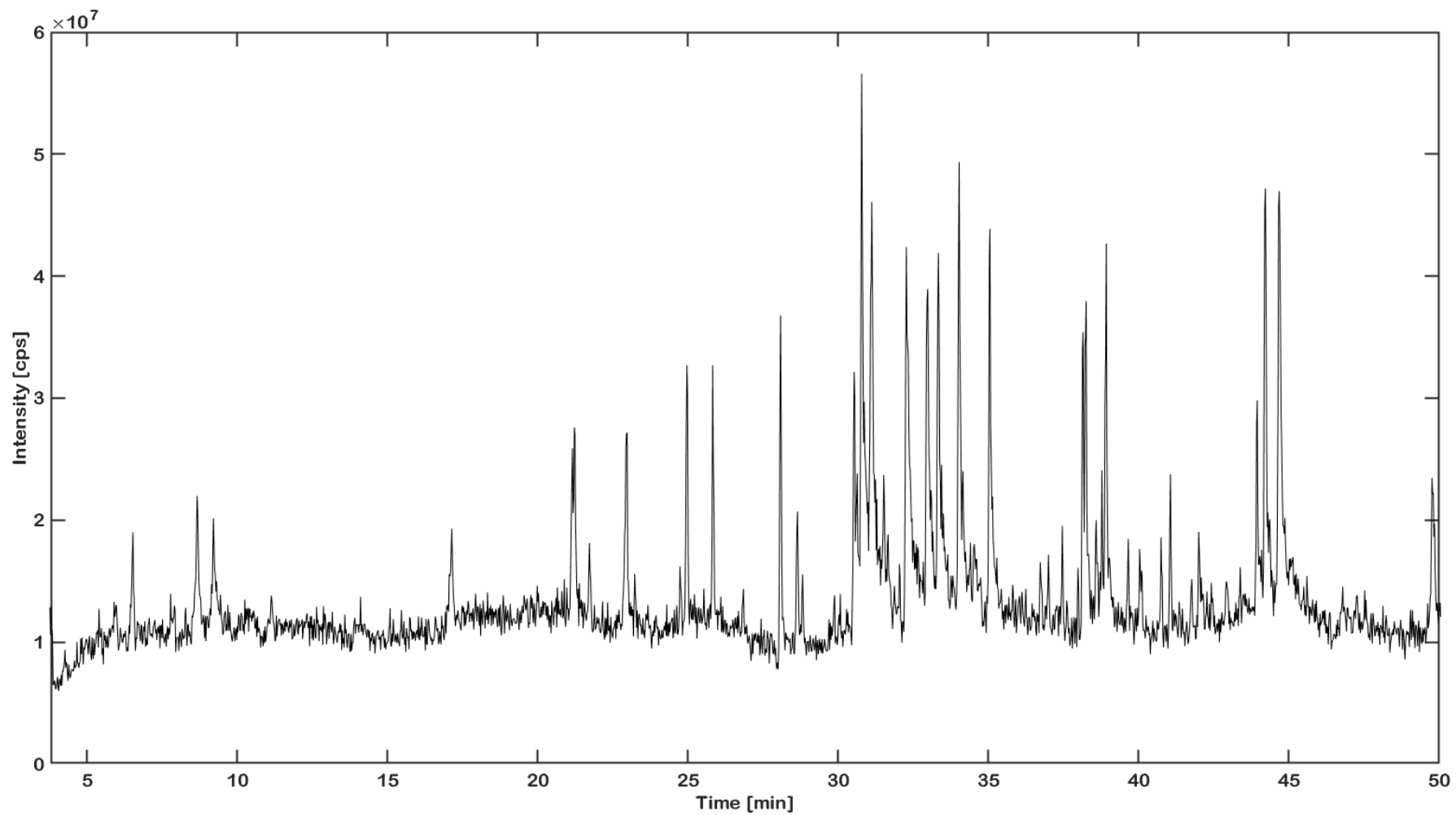


Figure A72: GC-DBDI-MS spectrum acquired at an amplitude of 1500 V and 15,500 Hz.

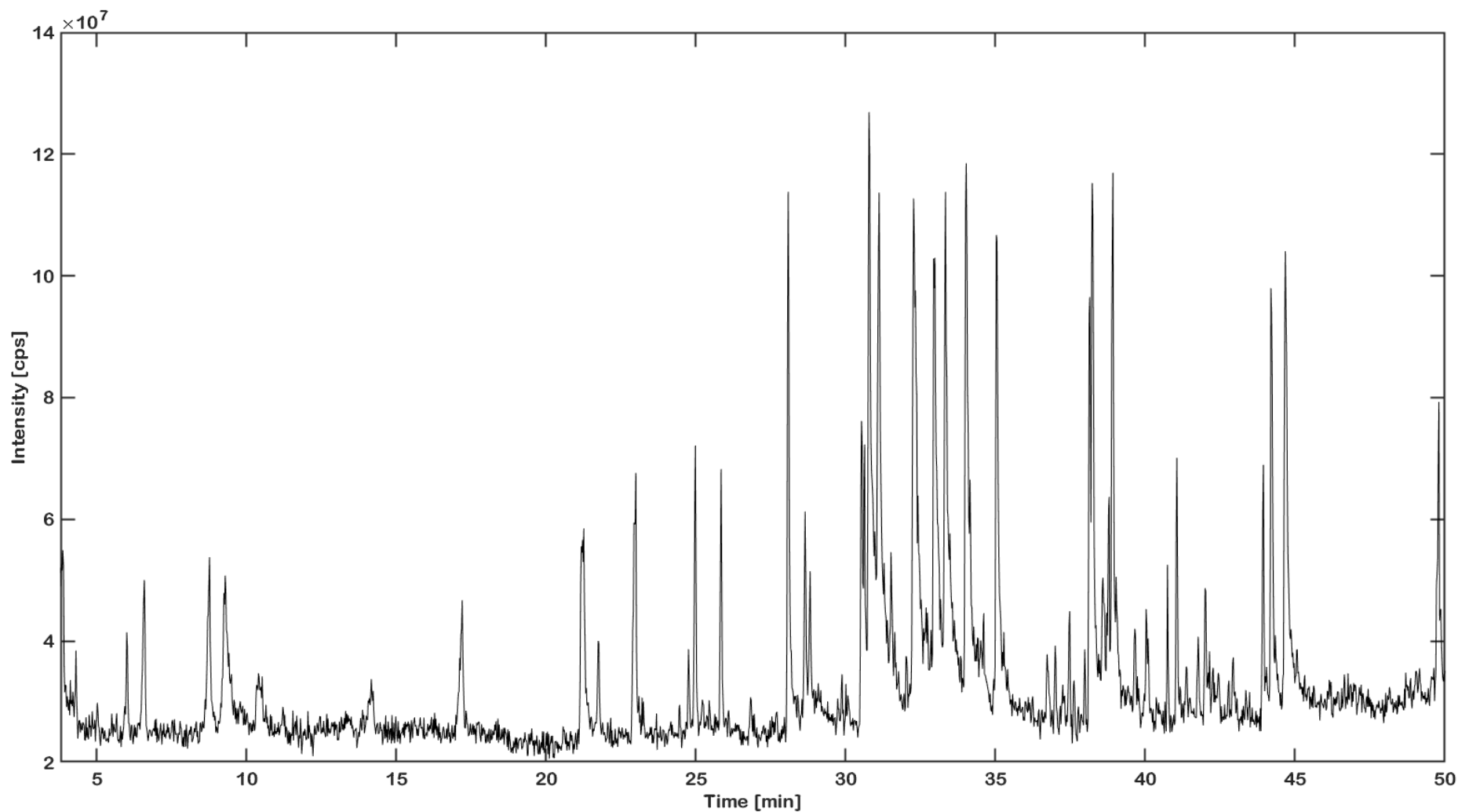


Figure A73: GC-DBDI-MS spectrum acquired at an amplitude of 1600 V and 15,000 Hz.

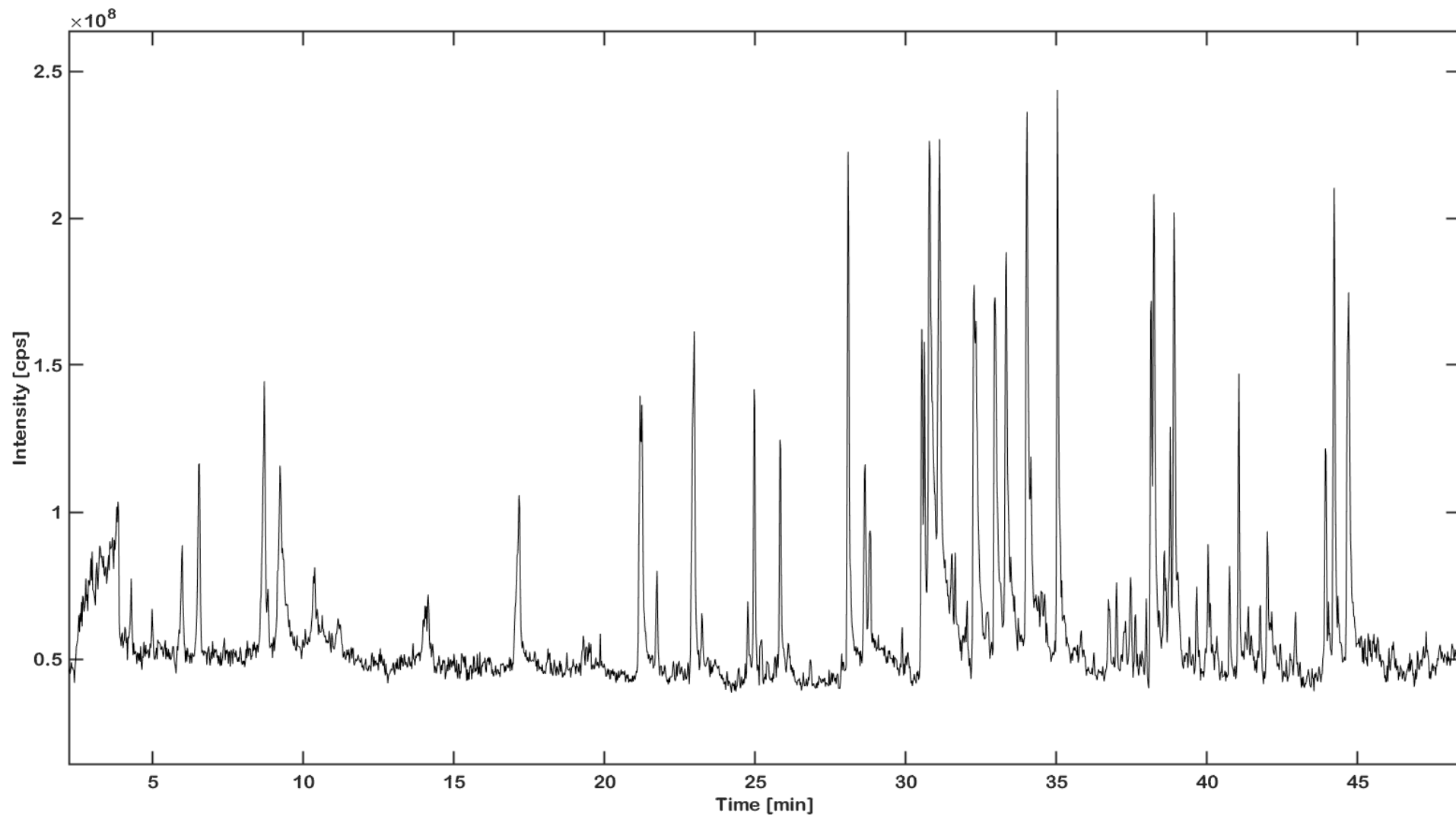


Figure A74: GC-DBDI-MS spectrum acquired at an amplitude of 1700 V and 15,000 Hz.

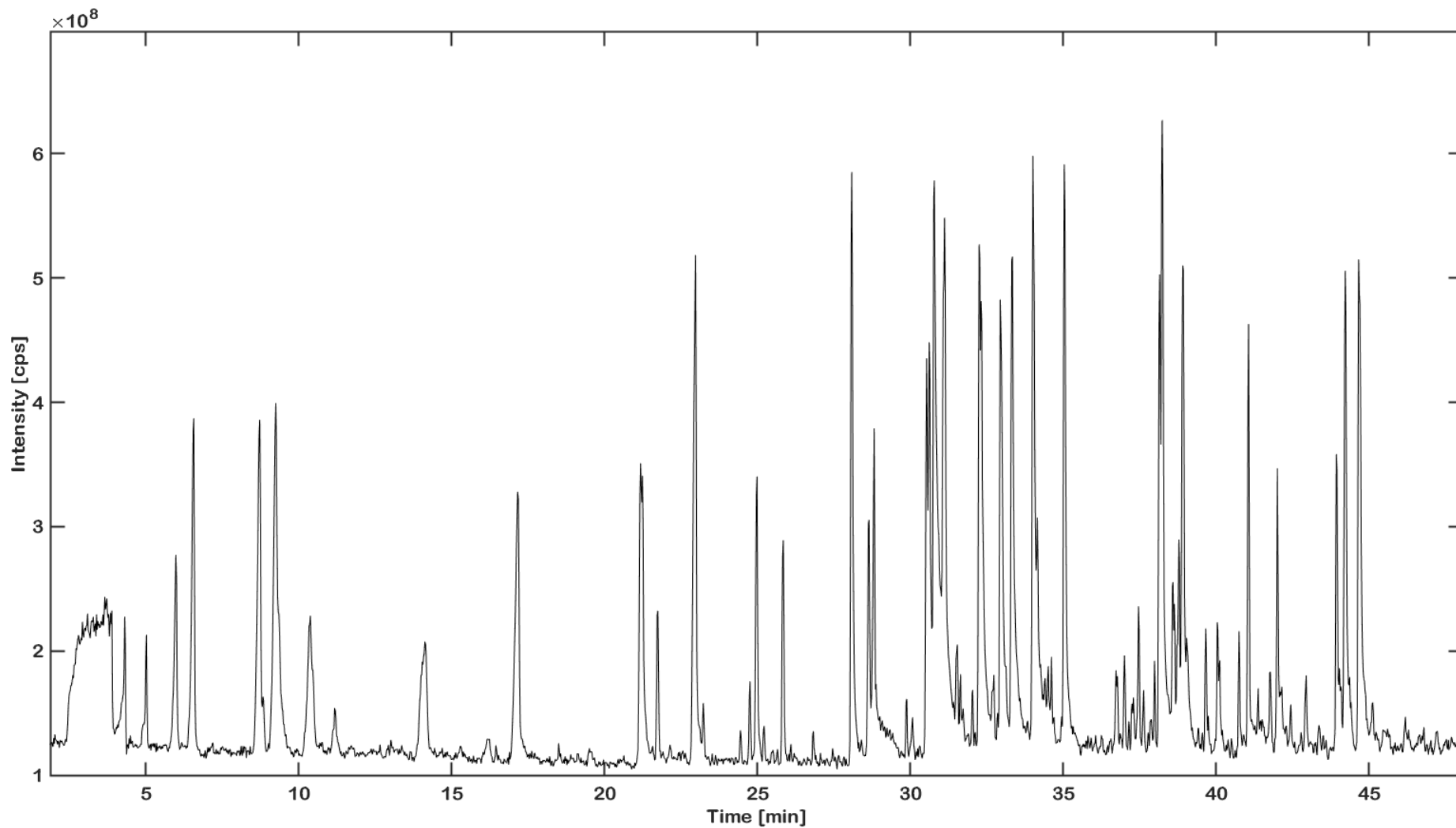


Figure A75: GC-DBDI-MS spectrum acquired at an amplitude of 1800 V and 15,000 Hz.

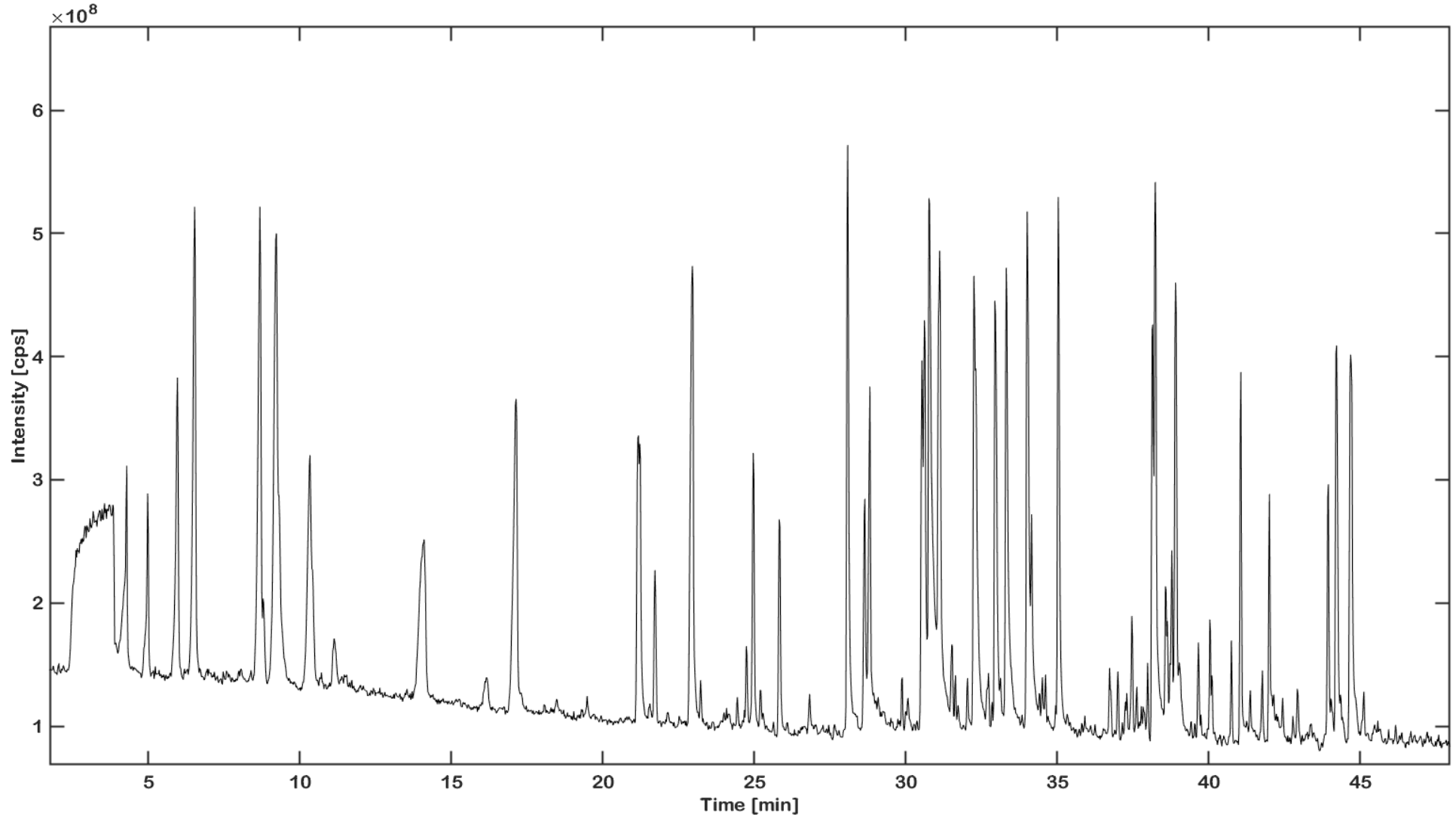


Figure A76: GC-DBDI-MS spectrum acquired at an amplitude of 1900 V and 15,000 Hz.

Table A19: Classification of terpenes included in the analysis.

Analyte name	MW [Da]	Cyclization	Terpene class	Oxygenated	Functional group
α -bisabolol	222.37	monocyclic	sesquiterpene	yes	alcohol
α -cedrene	204.35	tricyclic	sesquiterpene	no	ketone
α -humulene	204.35	monocyclic	sesquiterpene	no	NaN
α -pinene	136.23	bicyclic	monoterpene	no	NaN
α -pinene	136.23	bicyclic	monoterpene	no	NaN
α -terpinene	136.23	monocyclic	monoterpene	no	NaN
α -terpineol	154.25	monocyclic	monoterpene	yes	alcohol
α -terpinolene	136.23	monocyclic	monoterpene	no	NaN
α -thujone	152.23	bicyclic	monoterpene	yes	ketone
α -thujone	152.23	bicyclic	monoterpene	yes	ketone
β -caryophyllene	204.35	bicyclic	sesquiterpene	no	NaN
β -ionone	192.30	monocyclic	monoterpene	yes	ketone
β -pinene	136.23	bicyclic	monoterpene	no	NaN
β -pinene	136.23	bicyclic	monoterpene	no	NaN
borneol	154.25	bicyclic	monoterpene	yes	alcohol
camphene	136.23	bicyclic	monoterpene	no	NaN
camphor	152.23	bicyclic	monoterpene	yes	ketone
carene	136.23	monocyclic	monoterpene	no	NaN
carvacrol	150.22	monocyclic	monoterpene	yes	alcohol
carveol	152.23	monocyclic	monoterpene	yes	alcohol
carvone	150.22	monocyclic	monoterpene	yes	ketone
carvone	150.22	monocyclic	monoterpene	yes	ketone
cedrol	222.37	tricyclic	sesquiterpene	yes	alcohol
cis-abienol	152.23	bicyclic	monoterpene	yes	alcohol
cis-sabinol	152.23	bicyclic	monoterpene	yes	alcohol
citral	152.23	linear	monoterpene	yes	aldehyde
citronellal	154.25	linear	monoterpene	yes	aldehyde
citronellol	156.27	linear	monoterpene	yes	alcohol
citronellyl acetate	198.30	linear	monoterpene	yes	ester
cuminaldehyde	148.20	monocyclic	monoterpene	yes	aldehyde
dihydrolinalool	156.27	linear	monoterpene	yes	alcohol
elemol	222.37	monocyclic	sesquiterpene	yes	alcohol
eucalyptol	154.25	bicyclic	monoterpene	yes	ketone
eugenol	164.20	monocyclic	phenylpropanoid	yes	alcohol, ether
farnesol	222.37	linear	sesquiterpene	yes	alcohol
fenchol	154.25	bicyclic	monoterpene	yes	alcohol
fenchone	152.23	bicyclic	monoterpene	yes	ketone
fenchone	152.23	bicyclic	monoterpene	yes	ketone
γ -terpinene	136.23	monocyclic	monoterpene	no	NaN
geraniol	154.25	linear	monoterpene	yes	alcohol
geranyl acetate	196.29	linear	monoterpene	yes	ester
guaiazulene	198.30	bicyclic	sesquiterpene	no	NaN
isoborneol	154.25	bicyclic	monoterpene	yes	alcohol

isobornyl acetate	196.29	bicyclic	monoterpene	yes	ester
isomenthone	154.25	monocyclic	monoterpene	yes	ketone
isopulegol	154.25	monocyclic	monoterpene	yes	alcohol
limonene	136.23	monocyclic	monoterpene	no	NaN
linalool	154.25	linear	monoterpene	yes	alcohol
menthol	156.27	monocyclic	monoterpene	yes	alcohol
menthone	154.25	monocyclic	monoterpene	yes	ketone
methyleugenol	178.23	monocyclic	phenylpropanoid	yes	ether
myrcene	136.23	linear	monoterpene	no	NaN
myrtenol	152.23	bicyclic	monoterpene	yes	alcohol
nerol	154.25	linear	monoterpene	yes	alcohol
nerolidol	222.37	linear	sesquiterpene	yes	alcohol
neryl acetate	196.29	linear	monoterpene	yes	ester
norcamphor	110.15	bicyclic	monoterpene	yes	ketone
p-cymene	134.22	monocyclic	monoterpene	no	NaN
patchenol	166.26	bicyclic	monoterpene	yes	alcohol
pulegone	152.23	monocyclic	monoterpene	yes	ketone
rose oxide	154.25	monocyclic	monoterpene	yes	ether
sabinene	136.23	bicyclic	monoterpene	no	NaN
safranal	150.22	monocyclic	monoterpene	yes	aldehyde
terpinen-4-ol	154.25	monocyclic	monoterpene	yes	alcohol
terpinolene	136.23	monocyclic	monoterpene	no	NaN
thujone	152.23	bicyclic	monoterpene	yes	ketone
thymol	150.22	monocyclic	monoterpene	yes	alcohol
trans-pinocarveol	152.23	bicyclic	monoterpene	yes	alcohol
trans-verbenol	152.23	bicyclic	monoterpene	yes	alcohol

Table A20: Intensity in [cps] of the ten most intense adducts identified for various terpenes ionised using DBDI.

Analyte name	Dopant	Measurement	[2M+H]	[M + H2O2]	[M + NO2]	[M]	[M+2H]	[M+3H]	[M+CN+NH]	[M+H]	[M+H+2O]	[M+H+3O]	[M+H+H2O]	[M+H-2H2O]	[M+H-H2O]	[M+N]	[M+NH4]	[M+NO]	[M+NOH2]	[M+O]
(-)-alpha thujone	air	Single				4525				23445			325				5193			
(-)-alpha thujone2	air	Single				472	48			3549778			4338889				7721333			
(-)-alpha-cedrene	air	Single		29884							68524									
(-)-alpha-pinene	air	Single	759	74225							4139									
(-)-beta-pinene	air	Single	1648					1417556				113333								
(-)-borneol	air	Single											81583		194417		2277583	79917	159583	488283
(-)-borneol2	air	Single		77333		568667														
(-)-borneol3	air	Single		53667							257								7762667	97667
(-)-carveol1	air	Single				134333									474		514			4149
(-)-carveol2	air	Single		1533692		174977				2366615					5652		1731231			
(-)-carvone1	air	Single					5892											648		
(-)-carvone2	air	Single		19175			882			362825			156175				542833			
(-)-isopulegol	air	Single		1745917				15483		1117417			3931167				45583			1793417
(-)-isopulegol2	air	Single		6354857													52857		722	662286
(-)-limonene	air	Single		886							3935		993							
(-)-menthol	air	Single										18445	2388		2115		23775		2475	1124
(-)-rose oxide 1	air	Single								17455			1365				526			
(-)-rose oxide 2	air	Single								2628154			962				353977			
(-)-terpinen-4-ol1	air	Single		1426333							4528667				1463333		159667			5993333
(-)-terpinen-4-ol2	air	Single				5416					5516								5832	25756
(-)-terpinen-4-ol3	air	Single		1426333							4528667				1463333		159667			5993333
(-)-terpinen-4-ol4	air	Single		1785							539975	97665								3815625

(-)-trans pinocarveol	air	Single		1678					1591			22815		239375		
(-)-trans pinocarveol2	air	Single		1345714						6653143				1235429		1438857
(+)-2-carene	air	Single	125222	2536222					6437778							
(+)-3-carene	air	Single		1136					4216							
(+)-alpha-pinene	air	Single	11572	1252					5976	9836						
(+)-beta-pinene	air	Single	8656							1912						
(+)-carvone1	air	Single		637667		797333	1197667	2781333						2171667		
(+)-carvone2	air	Single		1629188			13525	3848438			222463			5455375		
(+)-cis abienol1	air	Single		31667		586667			597333							1916
(+)-cis abienol2	air	Single				535										
(+)-fenchol1	air	Single									4488	5116		954		2358
(+)-fenchone1	air	Single				374	831333	4333333			2141333			461667		
(+)-fenchone2	air	Single				522526	633895	4934			224632			6273895		847263
(+)-limonene	air	Single		1525					6358	13535	22765					
(+)-pulegone1	air	Single				1165	1228	6797			1533			7262		1667
(+)-pulegone2	air	Single					2125	2155	5755					7299		1369
(+)-pulegone3	air	Single					2939	1613	239		143			48965		
(+)-pulegone4	air	Single							2141467							
(+)-rose oxide 1	air	Single							2779733					34776		
(+)-rose oxide 2	air	Single		2383333					883333		622			2479778		
a_b_thujone	air	Single				64975		4495625			496875	65625		911		627375
alpha-humulene	air	Single							1252231		5789846	123538				
alpha-humulene	air	Mix						1638	364	1684					2276	
alpha-pinene	air	Mix							14381							524381
alpha-terpinene	air	Single		16664					74368	22216						
alpha-terpinene	air	Mix		2972					176133	2768						485333
alpha-terpinene2	air	Single						151417	421417	1874833	18483					
alpha-terpinene4	air	Single	3929143								254571					
alpha-terpineol	air	Single		2142516					99516							1447484
beta caryophyllene 1	air	Single				1291333		4836	186667	1392667						

beta caryophyllene 2	air	Single	672667					222667	2859333										
beta caryophyllene 3	air	Single	1581667						7587	3232	1834333								
beta-caryophyllene	air	Mix	5555						265625	61275									
beta-ionone1	air	Single			789667	228667		85667										931667	
beta-ionone2	air	Single	4296			5912		36168			63136							373	
beta-pinene	air	Mix																	521273
camphene	air	Mix			72182													8364	49791
camphor_rac1	air	Single			544	5552		32732			2416							35248	
camphor_rac2	air	Single			448	4272		2464			161							32864	
camphor_rac3	air	Single			522	72588		5649412			4318							8411176	692588
carvacrol	air	Mix	1876		132875	715		5325	5875									4775	
carvacrol1	air	Single					1419333	859											
carvacrol2	air	Single						8674											
carvacrol3	air	Single																	
carvacrol4	air	Single						1246667											
cedrol1	air	Single				233348		8958348			5699913							1998522	
cedrol2	air	Single						2144593			383444								
cis hexenol	air	Mix	125818															1391	
cis nerolidol	air	Mix				35836		111364			615							165	
cis rose oxide	air	Mix						2441333			91111		792222					2811556	
cis sabinol	air	Single					524167	2713333			1226133		484933					39984	
cis-citral	air	Mix						3928222				5241333						222222	
cis-menthone	air	Mix	225			729		5592667		338667	133333							3858667	
citral 1	air	Single	744667		59667			1278667			1615333							1138	
citral 2	air	Single						1465				348						5615	
citral 3	air	Single			579			3283667			621		95333						
citral 4	air	Single										3292						9256	
citronella1	air	Single	1468					2762667			68667								
citronella2	air	Single						1296933			4448								
citronellol	air	Mix	116425					45675											

citronellol1	air	Single		318												84			
citronellol2	air	Single																	248833
citronellyl acetate	air	Mix				857455		4493818		2864727									
cuminaldehyde1	air	Single				12156		68716		45712						95196			
cuminaldehyde2	air	Single	85835			29775		11338		8895					51995	1633			
dihydrolinalool1	air	Single		7441429												685714			
dihydrolinalool2	air	Single		172347															
dl-patchenol1	air	Single												737					
dl-patchenol2	air	Single			519	259													423
dl-patchenol3	air	Single				55265		1557					8498						
elemol	air	Single																	
eucalyptol1	air	Single				2779929		1526571		37286						4323786			
eucalyptol2	air	Single		82195												71			
eugenol	air	Mix		877556		2236222	961556			561778									
farnesol	air	Single																	
farnesol1	air	Mix					965	41555		517		27333			2174333				
farnesol2	air	Mix			127575	141875		6297		169225		75775			648975				
farnesol3	air	Mix				1674182		7242364		1479455		5762545			5368182				
gamma-terpinene	air	Single		226857					5989714	2786									
gamma-terpinene	air	Mix							427846										545846
gamma-terpinene2	air	Single		1469					9225										52625
gamma-terpinene3	air	Single								5286									6216
gamma-terpinene4	air	Single		12382					79678										5738
geraniol	air	Mix				17348							36652		146				
geraniol1	air	Single				11825				95									
geraniol2	air	Single											137167						
geranyl acetate	air	Mix														1421556			
guajazulene	air	Single										48333							
guajazulene2	air	Single					795667												
isoborenenol	air	Single				784286							244286		86				384

isobornyl acetate	air	Mix							394286					1944286		
isomenthone1	air	Single			95556		6249556		769111	2249778				8249111		
isomenthone2	air	Single	47		835429		5966571		495143	2945571				8714143		
L-fenchone1	air	Single			37667	591333		4348		245333				4646667		
L-fenchone2	air	Single			53857	685		517		2548714				6418286	853143	
L-fenchone3	air	Single					1275333					1538933			4797467	
limonene	air	Mix						3715								55125
linalool	air	Single	174133													
linalool	air	Mix			1157818			158364				254				
maybe_citral	air	Mix				768		35228				51488		7992		
menthone1	air	Single														
menthone2	air	Single					294667									
methyleugenol	air	Mix			176	8332		5768	1364	42776				79156		
myrcene	air	Single								342						
myrcene	air	Mix								49425						492875
myrtenol1	air	Single			964											
myrtenol2	air	Single			594667	4948	2188									
myrtenol3	air	Single			1717333									852667		8578
myrtenol4	air	Single	3826						139267			2767		1866667		
nerol	air	Single														
nerol	air	Mix			275143							3192571				
nerolidol 3	air	Single	8786		14985	6566	33955					26625		2865		
nerolidol 4	air	Single	3518				4492	532571	3998286			2494286				
neryl acetate 1	air	Mix												1539667		
norcamphor	air	Single	439					22975		5494				59265		
p-cymene	air	Single						129333	28667	1384				867333		
p-cymene	air	Mix		24				465765						532588		
sabinene	air	Single	6372				1578							9464		
sabinene	air	Mix													21571	479714
safranal2	air	Single			594										772667	

safranal3	air	Single			1236333											664333		812
terpinolene	air	Single							2382333	4429								
terpinolene1	air	Single							1524364	2981455								
terpinolene2	air	Single	1574333		822						1451667				662333			84333
terpinolene3	air	Single	2227								989				871			847
terpinolene4	air	Single							669714									878286
thymol1	air	Single				591										82		
thymol2	air	Single	254			588667										747333		
trans nerolidol	air	Mix				266444		7471556					3518		1641111			
trans rose oxide	air	Mix				3488		26184			518		758		984			
trans verbenol	air	Single			2469714								3996					4362714
trans verbenol2	air	Single			618	274							2755	284				
trans verbenol3	air	Single		822	1211								4575					
trans-menthone	air	Mix				1148		7433		651	1642				43333		241667	
(-)-alpha pinene	H2 O	Single							11244	2348								
(-)-alpha-cedrene	H2 O	Single	9584						36996		596							
(-)-alpha-thujone1	H2 O	Single						145333			488333				5815333			
(-)-alpha-thujone2	H2 O	Single			193	3175		24425			722				2749			
(-)-beta pinene	H2 O	Single					227667			386333								
(-)-borneol	H2 O	Single									124667		1417		2851		553	964333
(-)-carveol1	H2 O	Single			434857										216286		12	1119429
(-)-carveol2	H2 O	Single	43625					92825					68575		78825			
(-)-carveol3	H2 O	Single					6252	6732					4148		814			
(-)-carvone1	H2 O	Single				699333	245333	3762667			1358667				2523333			
(-)-carvone2	H2 O	Single	788667				115667	358556			119556				3381889			
(-)-isopulegol	H2 O	Single	74438				116769				165615				188615			
(-)-limonene	H2 O	Single							968									184
(-)-menthol	H2 O	Single									891333		614667		1363333		1627333	
(-)-rose oxide	H2 O	Single	22			348		297667			575333		841333		1568			
(-)-rose oxide2	H2 O	Single				2475		15985			385		4685		12155			

(-)-terpinen-4-ol	H2 O	Single		147857					51525	2365214									3879429
(-)-trans-pinocarveol1	H2 O	Single							165						1758				
(-)-trans-pinocarveol2	H2 O	Single							43	155667					681		361667		
(-)-trans-pinocarveol3	H2 O	Single								1239714			755714		281429	374571			
(+)-2-carene	H2 O	Single		5892						28656									
(+)-3-carene	H2 O	Single		324667						2474667									212667
(+)-alpha pinene	H2 O	Single								828857									185714
(+)-beta pinene	H2 O	Single									241								1715
(+)-carvone1	H2 O	Single		888545			2591636	377291						1795273				336455	
(+)-carvone2	H2 O	Single					4172	1328	2148					5976				13776	
(+)-fenchol	H2 O	Single												248667	182			524667	241333
(+)-fenchone1	H2 O	Single							53	37495				1698				4339	
(+)-fenchone2	H2 O	Single			225		4345	31945						16985				5872	659
(+)-limonene	H2 O	Single		2728						2256				4248					
(+)-pulegone1	H2 O	Single		93925					683	4971								1543625	
(+)-pulegone2	H2 O	Single		464						5265				1112				481	2949
(+)-pulegone3	H2 O	Single		553667														1326	
(+)-rose oxide	H2 O	Single		38667						264889				2251111				598889	661111
(+)-rose oxide2	H2 O	Single		735778										28667				88667	
a_b_thujone1	H2 O	Single								3584				28636				15672	4178
a_b_thujone2	H2 O	Single												14548				34788	54568
a_b_thujone3	H2 O	Single									222333			1434667				1584667	311333
alpha-humulene	H2 O	Single																	
alpha-humulene	H2 O	Mix		2164						525375	32525		3692125		678375				
alpha-pinene	H2 O	Mix								9968	2652								
alpha-pinene	H2 O	Mix								7287									18934
alpha-terpinene	H2 O	Mix		216571						1681429	26571								15857
alpha-terpinene1	H2 O	Single		42818						278691	418636			779455					
alpha-terpinene2	H2 O	Single												995667					
alpha-terpineol	H2 O	Single		1124333														572167	59167
beta caryophyllene	H2 O	Single		557143						3196714	616714								5585

beta-caryophyllene	H2 O	Mix							638571	21429								
beta-ionone1	H2 O	Single			246667	621			3778333									
beta-ionone2	H2 O	Single				328667			1993667			4293667			858			
beta-ionone3	H2 O	Single			437333	86667			4578	337333		327333		1228	342667			
beta-pinene	H2 O	Mix																177167
camphene	H2 O	Mix																18325
camphor_rac1	H2 O	Single				463333			3126			3924667			5939333			
camphor_rac2	H2 O	Single				298			2436333			2629333			5334333		471333	
carvacrol	H2 O	Mix	397		851	285				239							2125	196
carvacrol1	H2 O	Single					466462	836154										
carvacrol2	H2 O	Single						515333										
carvacrol3	H2 O	Single						963										
cedrol1	H2 O	Single	3791368								26815				678211			
cedrol2	H2 O	Single							14915	1437833			2563667		1163333			
cedrol3	H2 O	Single											1454571					
cis-abienol	H2 O	Single			133333													
cis-hexen-1-ol	H2 O	Mix	317143									377429			774			
cis-menthone	H2 O	Mix				15225			17375			256			6975			
cis-nerolidol	H2 O	Mix	43			6792			3418				21616					
cis-rose oxide	H2 O	Mix				333833			2599			585	738833		778167			
cis-sabinol	H2 O	Single													134225		8555	
citral	H2 O	Mix				543			427			597	3673		972667			
citral1	H2 O	Single			162				17				1868					
citral2	H2 O	Single				238	1685		1843			384	32			182		
citral3	H2 O	Single								27525			158425		5175			
citronellal 1	H2 O	Single	963789									273737						
citronellal2	H2 O	Single	36445												32575			
citronellol	H2 O	Single	77775														26275	
citronellol	H2 O	Mix	624						5128									
citronellyl acetate	H2 O	Mix	419143						91286			441429						

cuminaldehyde1	H2 O	Single	57388					38684			331			72428			
cuminaldehyde2	H2 O	Single	16152			74		458			31716			2348	594		
dihydrolinalool1	H2 O	Single		5156667										758			
dihydrolinalool2	H2 O	Single		4732										4724			
dihydrolinalool3	H2 O	Single		883818													
dl-patchenol	H2 O	Single				2116								468			2148
dl-patchenol2	H2 O	Single				432286											347714
dl-patchenol3	H2 O	Single				3136											
elemol	H2 O	Single															
eucalyptol	H2 O	Single				1994167	192833	1722			4195	681		3822333			
eucalyptol2	H2 O	Single		837714										552857			
eugenol	H2 O	Mix		3544	14156	6288	2336	2612									
farnesol	H2 O	Single									442667						
farnesol1	H2 O	Mix				23571		125571				1439714		312			
farnesol2	H2 O	Mix			419	436		2494				27315		1135			
farnesol3	H2 O	Mix				367333		23			36333	1343833		437333			
gamma-terpinene	H2 O	Single		12816						848	14148						
gamma-terpinene	H2 O	Mix							356133								179867
geraniol	H2 O	Mix										713					
geranyl acetate	H2 O	Mix												286222			
guajazulene	H2 O	Single										185					
isoborneol	H2 O	Mix										1745		297			1845
isobornyl acetate	H2 O	Mix												54			
isomenthone1	H2 O	Single				67		4971		348	276			5672			
isomenthone2	H2 O	Single				323667		252667			154			36425			
L-fenchone1	H2 O	Single			1515	4515		33685			1635			4413			
L-fenchone2	H2 O	Single			182833	269833		2975			1531			4481333		466833	
L-fenchone3	H2 O	Single										918667		1377		1716667	
limonene	H2 O	Mix							258133								162533
linalool	H2 O	Single		8575													

linalool	H2 O	Mix												393					
maybe_citral	H2 O	Mix				235		1736						2575					
menthone1	H2 O	Single				774667		596667		296	1176667				382				
menthone2	H2 O	Single				451571		3436571			113286				371714		174714		
methyleugenol	H2 O	Mix			33595			1525	333		1575				2638				
myrcene	H2 O	Single									2558								
myrcene	H2 O	Mix									326267								159333
myrtenol1	H2 O	Single	868667						121333					943667	1824667				
myrtenol2	H2 O	Single			395333														
nerol	H2 O	Single	613263																
nerol	H2 O	Mix												643					
norcamphor	H2 O	Single						213			141				13855				
p-cymene	H2 O	Mix						234222							163333				
p-cymene1	H2 O	Single			198			144667	662667	222667					22				
p-cymene2	H2 O	Single			199143			18857							182857				
p-cymene3	H2 O	Single			195111			98889							188				
sabinene	H2 O	Mix															149	17325	
sabinene1	H2 O	Single					3796	5468									544		
sabinene2	H2 O	Single																	149714
sabinene3	H2 O	Single																	154923
safranal1	H2 O	Single																28	
safranal2	H2 O	Single				127		4862333			11667				1297				1174
safranal3	H2 O	Single			4965										283	319			262
terpinolene	H2 O	Single							17215	32275									
terpinolene2	H2 O	Single							2665	23855									
terpinolene3	H2 O	Single	374857						2963143										
thymol	H2 O	Single				226											33333		
trans-menthone	H2 O	Mix				178		14388		1668	2576				12616				
trans-nerolidol	H2 O	Mix				88667		4471333			241667		1945		313333				
trans-rose oxide	H2 O	Mix				13225		979					2815		17625				

trans-verbenol	H2 O	Single			1539667													2315333
(-)-alpha cedrene	N2	Single		957556					237111									
(-)-alpha pinene	N2	Single	7627					264225	596325									
(-)-alpha thujone	N2	Single			42875			14295			271975			7525				
(-)-beta-pinene	N2	Single	3887125					1256375										
(-)-borneol	N2	Single								898	81667		3438	874933	231767		484667	
(-)-carvone	N2	Single		89177		534		153538		76615			352677	685231				
(-)-isopulegol	N2	Single		18796			1728						14876		37611		11516	14734
(-)-limonene	N2	Single	374					1243333	4372667	781	196							
(-)-menthol	N2	Single								798857	634857				1298857		143286	532857
(-)-rose oxide	N2	Single							343363									
(-)-terpinen-4-ol	N2	Single		3233526					352579	3531263								2886842
(+)-2-carene	N2	Single		22					483									
(+)-3-carene	N2	Single		7416					2664									
(+)-alpha pinene	N2	Single	5626					2378	4386									
(+)-beta pinene	N2	Single	48895					3125					23365					
(+)-carvone	N2	Single		1369563			617125	1792563					112313			3843813	639125	
(+)-cis abienol	N2	Single			416143								234714		218857			
(+)-fenchol	N2	Single																1295
(+)-fenchone1	N2	Single			48667	587333		3966					2252			5536		
(+)-fenchone2	N2	Single			53571			2197571					1325286	298571		5156857		18571
(+)-pulegone	N2	Single			6955	771167		113833								3186667		
(+)-rose oxide	N2	Single							5926211									
alpha humulene	N2	Single						292857				418286						
alpha pinene	N2	Mix						1236143	193571									
alpha terpinene	N2	Single						1792577	2925115	36	1594192							
alpha terpinene	N2	Mix		142857		1812286		2698	544286	1319286								
alpha-humulene	N2	Mix						6622	2445	11796	18422							
alpha-terpineol	N2	Single		2414485													9833	7293
beta ionone 1	N2	Single				5792		65224	2796						5484			

beta ionone2	N2	Single		537					235		4155	69895				33475		
beta ionone3	N2	Single				6716	1764		36272			4612		15716		8768		
beta pinene	N2	Mix	28848						45		675	27666						
beta-caryophyllene	N2	Single							336838	3444846	18155	1431692	25655					
beta-caryophyllene	N2	Mix		919					73255	4481	88225	328325						
camphene	N2	Mix							397177									
camphor1	N2	Single			52667	286667			1631333			1486				3651333		
camphor2	N2	Single			389				21615			2362				53745		
camphor3	N2	Single			46	396857			3356857			3492857				9378		148571
carvacrol	N2	Single						9889									667333	
carvacrol	N2	Mix			1195636				6792727	1365273								
cedrol	N2	Single							847867					191567				
cis citral	N2	Mix											1878				1182	
cis hexenol	N2	Mix	4967556															
cis nerolidol	N2	Mix							12876									
cis rose oxide	N2	Mix							996667	81111								
cis rose oxide2	N2	Mix							3653143			612857				677143		858
cis-sabinol	N2	Single		72331				1279172				744138		83469		431621		
citronellal	N2	Single		1118522								195287						
citronellol	N2	Single		146														33412
citronellol	N2	Mix							297923									
citronellyl acetate 1	N2	Mix							518			26676						
citronellyl acetate 2	N2	Mix							1711556			982667						
cuminaldehyde1	N2	Single	5265						341275			2678				855		7145
cuminaldehyde2	N2	Single	24428				16544		67536			4516				3412	8556	
dihydrolinalool	N2	Single		6788857												471143		
dihydrolinalool2	N2	Single		112855														
eucalyptol1	N2	Single					12875		74983			2229				3293333		39833
eucalyptol2	N2	Single		65342												2428		
eugenol	N2	Mix				1218			63852	13868	18176	2376				13736		

farnesol	N2	Single																	
farnesol1	N2	Mix						1276											
farnesol2	N2	Mix						5175455											
farnesol3	N2	Mix						7267231											
fenchone	N2	Single			18875									81775		1153625		3423125	
fenchone2	N2	Single				435	42143	317857				1842429				713571		1299571	
gamma-terpinene	N2	Single		151667					4224	253									
gamma-terpinene	N2	Mix		555				825	226875	1519								56225	
geraniol	N2	Single		752125															
geraniol	N2	Mix																	
geranyl acetate	N2	Mix						1139778											
Guajazulene	N2	Single																	
isoborneol	N2	Single														876		456	17576
isobornyl acetate	N2	Mix														372333			
isomenthone1	N2	Single					522	385222		769333	1734667					7247778			
isomenthone2	N2	Single		319867				21432								5132133			
limonene	N2	Single	1764118						2142353							1176353			
limonene	N2	Mix		1188889				1812889	6498444	728	2386								
linalool	N2	Single		1443412															
linalool	N2	Mix																	
menthone1	N2	Mix						6585								7195			
menthone2	N2	Mix						443667			39667					571333			
menthone3	N2	Mix				36175		1522											
methyleugenol	N2	Mix				8586		651	19415	6755	998								
myrcene	N2	Single									2321429								
myrcene	N2	Mix	1786					14458			4682								
myrtenol	N2	Single				675333													1894
nerol	N2	Single		99933															
nerol	N2	Mix																	
neryl acetate	N2	Mix							826667										

norcamphor	N2	Single	1968333					377333			1554			3389			
patchenol1	N2	Single			21445								52	416			3331
patchenol2	N2	Single			4149			6885		783			1713	5495			
p-cymene	N2	Single	12775						42985	2615			3558		3342		
p-cymene	N2	Mix				186775		223125			346825						
pinocarveol1	N2	Single		1328286					129714					1745429			
pinocarveol2	N2	Single		821						4136				876333		758333	
sabinene	N2	Single	1568														
sabinene	N2	Mix	749167					8961167									
safranal	N2	Single				4315									685		
terpinolene	N2	Single							8382	18314							
terpinolene2	N2	Single							85225	249925							
thujone	N2	Single			44341	321756		1347659			1613512			451927		324537	
thymol	N2	Single				5324									128		3148
trans nerolidol	N2	Mix						7763778									
trans-citral	N2	Mix						1248333				382					
trans-rose oxide	N2	Mix						5561714			125429			937714		1447429	
verbenol1	N2	Single			421333	171							257333				
verbenol2	N2	Single			133832							186464					239416

Table A21: Intensity in [cps] of the ten most intense adducts identified for various terpenes ionised using DBDI.

Analyte name	Dopant	Measurement	[M+OH]	[M-2H]	[M-3H]	[M-3H+2O]	[M-3H+3O]	[M-3H+O]	[M-5H+2O]	[M-5H+O]	[M-7H+2O]	[M-7H+3O]	[M-C+N]	[M-C4H9]	[M-C4H9O]	[M-C5H11]	[M-C5H11O]	[M-CH3]	[M-CH3COO]	[M-CH3O]	[M-H]	[M-H+2O]	[M-H+O]
(-)-alpha thujone	air	Single																					
(-)-alpha thujone2	air	Single																					
(-)-alpha-cedrene	air	Single	29788																	5192	274	1874	
(-)-alpha-pinene	air	Single	85425																				
(-)-beta-pinene	air	Single																					
(-)-borneol	air	Single	282917																	266483 3			
(-)-borneol2	air	Single	835																	455	895333		
(-)-borneol3	air	Single		59333																		6185	
(-)-carveol1	air	Single	958333																	361633 3			
(-)-carveol2	air	Single															228524						
(-)-carvone1	air	Single																					
(-)-carvone2	air	Single																					
(-)-isopulegol	air	Single																		1451			
(-)-isopulegol2	air	Single	926286	544571																316114 3			
(-)-limonene	air	Single																					
(-)-menthol	air	Single																		862		9245	
(-)-rose oxide 1	air	Single	1695																				
(-)-rose oxide 2	air	Single	163538																				
(-)-terpinen-4-ol1	air	Single																		1528	232266 7	986	
(-)-terpinen-4-ol2	air	Single	18636	7216																3484	1888		
(-)-terpinen-4-ol3	air	Single																		1528	232266 7	986	
(-)-terpinen-4-ol4	air	Single																			511775	121447 5	

(-)-trans pinocarveol	air	Single																	1513			
(-)-trans pinocarveol2	air	Single	894857																1226857	6394571		
(+)-2-carene	air	Single	1811556																2363778	1329556		
(+)-3-carene	air	Single																	8996	1524		
(+)-alpha-pinene	air	Single	1196																			
(+)-beta-pinene	air	Single																				
(+)-carvone1	air	Single																				
(+)-carvone2	air	Single																				
(+)-cis abienol1	air	Single																				1398667
(+)-cis abienol2	air	Single																				4
(+)-fenchol1	air	Single	8464	5612																		21464
(+)-fenchone1	air	Single																				
(+)-fenchone2	air	Single																				366526
(+)-limonene	air	Single	154																			
(+)-pulegone1	air	Single																				4739
(+)-pulegone2	air	Single																				1984
(+)-pulegone3	air	Single																				4471
(+)-pulegone4	air	Single																				
(+)-rose oxide 1	air	Single	1678267																			
(+)-rose oxide 2	air	Single	9791778																			1726444
a_b_thujone	air	Single																				
alpha-humulene	air	Single	9724																			
alpha-humulene	air	Mix																				8348
alpha-pinene	air	Mix																				117239
alpha-terpinene	air	Single	9692																			19195
alpha-terpinene	air	Mix																				2512
alpha-terpinene2	air	Single																				3156
alpha-terpinene4	air	Single	2138																			1627714
alpha-terpineol	air	Single	2116452																			1584452
beta caryophyllene 1	air	Single	56																			585333
																						61

beta caryophyllene 2	air	Single																62	96
beta caryophyllene 3	air	Single	234																
beta-caryophyllene	air	Mix																	
beta-ionone1	air	Single	741333																
beta-ionone2	air	Single																	
beta-pinene	air	Mix						135818										222364	
camphene	air	Mix						122182										18182	
camphor_rac1	air	Single							4292										
camphor_rac2	air	Single							3816										
camphor_rac3	air	Single							47176										
carvacrol	air	Mix	21745																
carvacrol1	air	Single																	
carvacrol2	air	Single																	
carvacrol3	air	Single								754182									
carvacrol4	air	Single																	
cedrol1	air	Single	183234 8																138174
cedrol2	air	Single																	
cis hexenol	air	Mix																	
cis nerolidol	air	Mix	18692																
cis rose oxide	air	Mix	876	439111															
cis sabinol	air	Single																	
cis-citral	air	Mix																	
cis-menthone	air	Mix		443333															
citral 1	air	Single	748																
citral 2	air	Single																	
citral 3	air	Single																	
citral 4	air	Single																	
citronellal1	air	Single																	
citronellal2	air	Single																	
citronellol	air	Mix	1215																

citronellol1	air	Single	35585													674			
citronellol2	air	Single																	
citronellyl acetate	air	Mix	854727																
cuminaldehyde1	air	Single																	
cuminaldehyde2	air	Single			59725														
dihydrolinalool1	air	Single	393857 1														136514 3		992571
dihydrolinalool2	air	Single																	
dl-patchenol1	air	Single		49															
dl-patchenol2	air	Single	33667			239366 7	2985										5933		
dl-patchenol3	air	Single	7125														113		
elemol	air	Single													5254				
eucalyptol1	air	Single																	987857
eucalyptol2	air	Single	48265	4635															
eugenol	air	Mix	115177 8													951556			
farnesol	air	Single											135466 7				429333		
farnesol1	air	Mix																	
farnesol2	air	Mix																	851
farnesol3	air	Mix																	72300
gamma-terpinene	air	Single	118571																
gamma-terpinene	air	Mix					164												254462
gamma-terpinene2	air	Single																	
gamma-terpinene3	air	Single	6474																11886
gamma-terpinene4	air	Single																	23
geraniol	air	Mix																	
geraniol1	air	Single	955			2761	255												57775
geraniol2	air	Single																	
geranyl acetate	air	Mix																	337577 8
guajazulene	air	Single																	
guajazulene2	air	Single																	
isoborenol	air	Single	211914 3	529143															263457 1

isobornyl acetate	air	Mix													678571					
isomenthone1	air	Single	421111																	
isomenthone2	air	Single	514143																	
L-fenchone1	air	Single																		
L-fenchone2	air	Single							379786											
L-fenchone3	air	Single	244533 3															142853 3	127967	477426 7
limonene	air	Mix						14775										23975		
linalool	air	Single																65900		
linalool	air	Mix																		
maybe_citral	air	Mix				22664					17268				18336					
menthone1	air	Single	548667																	
menthone2	air	Single	675333																	
methyleugenol	air	Mix				1276		866												
myrcene	air	Single																		
myrcene	air	Mix																	219625	
myrtenol1	air	Single	18965			29995		17995											2651	
myrtenol2	air	Single													2364					
myrtenol3	air	Single	596666 7			39667													837333	
myrtenol4	air	Single	194133																131133 3	
nerol	air	Single																	14824	
nerol	air	Mix																		1392
nerolidol 3	air	Single	94985																	2386
nerolidol 4	air	Single	413429																	163628 6
neryl acetate 1	air	Mix													213667					
norcamphor	air	Single																		
p-cymene	air	Single																		125333
p-cymene	air	Mix																		
sabinene	air	Single																		
sabinene	air	Mix																		218286
safranal2	air	Single						53333												

safranal3	air	Single	183			185166 7		377933 3								582333 3			
terpinolene	air	Single														2848			
terpinolene1	air	Single	14380													419300			
terpinolene2	air	Single	3357													271667			
terpinolene3	air	Single	35475													27365			
terpinolene4	air	Single																285542 9	
thymol1	air	Single					487												
thymol2	air	Single	1138				584												
trans nerolidol	air	Mix	133666 7																
trans rose oxide	air	Mix		5658															
trans verbenol	air	Single														352657 1			
trans verbenol2	air	Single						475											
trans verbenol3	air	Single						384		1555									
trans-menthone	air	Mix		484333															
(-)-alpha pinene	H2O	Single	392																
(-)-alpha-cedrene	H2O	Single			514											17884	846	436	
(-)-alpha-thujone1	H2O	Single																	
(-)-alpha-thujone2	H2O	Single						1745											
(-)-beta pinene	H2O	Single																	
(-)-borneol	H2O	Single	348333													46		281333	
(-)-carveol1	H2O	Single	288857					149714								215657 1			
(-)-carveol2	H2O	Single																5415	
(-)-carveol3	H2O	Single											12118					6222	
(-)-carvone1	H2O	Single																	
(-)-carvone2	H2O	Single																	
(-)-isopulegol	H2O	Single														485692			
(-)-limonene	H2O	Single																	
(-)-menthol	H2O	Single																	7
(-)-rose oxide	H2O	Single	677																
(-)-rose oxide2	H2O	Single	2711													472			

(-)-terpinen-4-ol	H2O	Single																2958429	1224429	
(-)-trans-pinocarveol1	H2O	Single																567		143
(-)-trans-pinocarveol2	H2O	Single																	1456667	
(-)-trans-pinocarveol3	H2O	Single					4559714												713714	
(+)-2-carene	H2O	Single	992																9296	736
(+)-3-carene	H2O	Single						22											321333	219333
(+)-alpha pinene	H2O	Single	198286																	
(+)-beta pinene	H2O	Single																		
(+)-carvone1	H2O	Single																		
(+)-carvone2	H2O	Single																		
(+)-fenchol	H2O	Single		248																
(+)-fenchone1	H2O	Single																		
(+)-fenchone2	H2O	Single																		
(+)-limonene	H2O	Single																		2936
(+)-pulegone1	H2O	Single																		
(+)-pulegone2	H2O	Single																	16965	
(+)-pulegone3	H2O	Single	6578667																421333	
(+)-rose oxide	H2O	Single	869778																	
(+)-rose oxide2	H2O	Single	6244	154															475556	
a_b_thujone1	H2O	Single																		
a_b_thujone2	H2O	Single																		
a_b_thujone3	H2O	Single																		
alpha-humulene	H2O	Single																		
alpha-humulene	H2O	Mix																		4436
alpha-pinene	H2O	Mix						133217											14870	
alpha-terpinene	H2O	Mix																	234	
alpha-terpinene1	H2O	Single																		
alpha-terpinene2	H2O	Single																		366333
alpha-terpineol	H2O	Single	1148333																488833	3932167
beta caryophyllene	H2O	Single																		

beta-caryophyllene	H2O	Mix																	
beta-ionone1	H2O	Single	233																
beta-ionone2	H2O	Single																	
beta-ionone3	H2O	Single																	
beta-pinene	H2O	Mix					137833											12667	
camphene	H2O	Mix					12325												12775
camphor_rac1	H2O	Single						183333											
camphor_rac2	H2O	Single																	
carvacrol	H2O	Mix	735																
carvacrol1	H2O	Single																	
carvacrol2	H2O	Single							778333										
carvacrol3	H2O	Single																	
cedrol1	H2O	Single	351178 9																355368
cedrol2	H2O	Single	224616 7																13167
cedrol3	H2O	Single																	221416 7
cis-abienol	H2O	Single																	729619
cis-hexen-1-ol	H2O	Mix																	
cis-menthone	H2O	Mix		1655															
cis-nerolidol	H2O	Mix	4852																2932
cis-rose oxide	H2O	Mix	455	162833															
cis-sabinol	H2O	Single																	13
citral	H2O	Mix								729333									175633 3
citral1	H2O	Single									4335								7615
citral2	H2O	Single										1362							3475
citral3	H2O	Single																	64425
citronellal 1	H2O	Single																	
citronellal2	H2O	Single	2116																
citronellol	H2O	Single	78825																85975
citronellol	H2O	Mix	872																
citronellyl acetate	H2O	Mix	585714																

cuminaldehyde1	H2O	Single																	
cuminaldehyde2	H2O	Single				3748	6752												
dihydrolinalool1	H2O	Single	451333														247466	7	778667
dihydrolinalool2	H2O	Single	27564														1368		572
dihydrolinalool3	H2O	Single																	
dl-patchenol	H2O	Single	3362					1983										76625	
dl-patchenol2	H2O	Single	597429					516										194771	4
dl-patchenol3	H2O	Single																292	
elemol	H2O	Single												1988					
eucalyptol	H2O	Single																	71333
eucalyptol2	H2O	Single	416857																
eugenol	H2O	Mix	5496										5368						
farnesol	H2O	Single																185333	
farnesol1	H2O	Mix																138571	
farnesol2	H2O	Mix																	
farnesol3	H2O	Mix																	
gamma-terpinene	H2O	Single																	
gamma-terpinene	H2O	Mix						131867											84133
geraniol	H2O	Mix																	
geranyl acetate	H2O	Mix																967333	
guajazulene	H2O	Single																	
isoborneol	H2O	Mix		1865															1115
isobornyl acetate	H2O	Mix																546	
isomenthone1	H2O	Single		213															
isomenthone2	H2O	Single		218833															
L-fenchone1	H2O	Single																	
L-fenchone2	H2O	Single																	
L-fenchone3	H2O	Single		224															96667
limonene	H2O	Mix						13933											119733
linalool	H2O	Single																	71525

linalool	H2O	Mix																		2332
maybe_citral	H2O	Mix			555						1189				455					25333
menthone1	H2O	Single																		18571
menthone2	H2O	Single																		
methyleugenol	H2O	Mix				3														
myrcene	H2O	Single																		
myrcene	H2O	Mix									144									1116
myrtenol1	H2O	Single	724																	
myrtenol2	H2O	Single	528667								66	154667								1674667
nerol	H2O	Single																		
nerol	H2O	Mix																		652
norcamphor	H2O	Single																		
p-cymene	H2O	Mix			129778															
p-cymene1	H2O	Single			212667															
p-cymene2	H2O	Single			184286															
p-cymene3	H2O	Single			171778															
sabinene	H2O	Mix									13675									135
sabinene1	H2O	Single																		
sabinene2	H2O	Single																		
sabinene3	H2O	Single									165385									
safranal1	H2O	Single								25333										
safranal2	H2O	Single	1162333	93333																2244
safranal3	H2O	Single	15885								415									38925
terpinolene	H2O	Single	74375																	1343
terpinolene2	H2O	Single																		743
terpinolene3	H2O	Single																		568857
thymol	H2O	Single								213333										862
trans-menthone	H2O	Mix			1916															
trans-nerolidol	H2O	Mix	343667																	
trans-rose oxide	H2O	Mix	14575	16975																

beta ionone2	N2	Single																		
beta ionone3	N2	Single																		
beta pinene	N2	Mix	13998												866			7112		
beta-caryophyllene	N2	Single	363477										148842 4					168726 9		
beta-caryophyllene	N2	Mix	3482						15415									21475		
camphene	N2	Mix	165646 2						61924						848154	646769				
camphor1	N2	Single						372667												
camphor2	N2	Single						3365												
camphor3	N2	Single						33143												
carvacrol	N2	Single																		
carvacrol	N2	Mix	213981 8						218181 8		112182									
cedrol	N2	Single																		
cis citral	N2	Mix	17398			35878						1153								595
cis hexenol	N2	Mix	241777 8																	
cis nerolidol	N2	Mix	42332						4548									4192	1136	83944
cis rose oxide	N2	Mix	884889																	
cis rose oxide2	N2	Mix							51									173714		124742 9
cis-sabinol	N2	Single																		
citronellal	N2	Single																		
citronellol	N2	Single																		
citronellol	N2	Mix	127846																	
citronellyl acetate 1	N2	Mix	18268						11428											
citronellyl acetate 2	N2	Mix	112244 4																	
cuminaldehyde1	N2	Single																		
cuminaldehyde2	N2	Single				43344														
dihydrolinalool	N2	Single	213															785714	74	
dihydrolinalool2	N2	Single																		
eucalyptol1	N2	Single																		734667
eucalyptol2	N2	Single	18776	3918																
eugenol	N2	Mix	45884											14232				3816		

farnesol	N2	Single										3344		4448					
farnesol1	N2	Mix	1299						254							193266 7			839566 7
farnesol2	N2	Mix	114						159636							197981 8			866618 2
farnesol3	N2	Mix	169538						168124							178615			844924
fenchone	N2	Single		1289													781	259187 5	
fenchone2	N2	Single						316714											
gamma-terpinene	N2	Single	56667																
gamma-terpinene	N2	Mix	321375												123125				
geraniol	N2	Single		81725															
geraniol	N2	Mix	1152													118285 7			373728 6
geranyl acetate	N2	Mix	181111 1												496866 7				
Guajuzulene	N2	Single							724										
isoborneol	N2	Single	6968	5928															
isobornyl acetate	N2	Mix								318					123673 33				
isomenthone1	N2	Single		373111															
isomenthone2	N2	Single		468667															
limonene	N2	Single	172959									872235							138658 8
limonene	N2	Mix	466266 7													155444		882	
linalool	N2	Single																	
linalool	N2	Mix														166785 7			34429
menthone1	N2	Mix	59						1386										
menthone2	N2	Mix							435										
menthone3	N2	Mix	34												7655				27455
methyleugenol	N2	Mix	16315						835										7485
myrcene	N2	Single																	
myrcene	N2	Mix	25548												153				16694
myrtenol	N2	Single	158626 7					454667											214767
nerol	N2	Single		122966 7															
nerol	N2	Mix																	152857 1
neryl acetate	N2	Mix	276												374				353143

norcamphor	N2	Single																		
patchenol1	N2	Single	25275			138		396												6115
patchenol2	N2	Single																		
p-cymene	N2	Single	17485																	3645
p-cymene	N2	Mix																		125625
pinocarveol1	N2	Single																		
pinocarveol2	N2	Single																		374
sabinene	N2	Single																		
sabinene	N2	Mix	124667																	
safranal	N2	Single																		
terpinolene	N2	Single																		1472
terpinolene2	N2	Single																		9615
thujone	N2	Single																		
thymol	N2	Single																		3472
trans nerolidol	N2	Mix	268488 9																	238
trans-citral	N2	Mix																		486667
trans-rose oxide	N2	Mix																		148633 3
verbenol1	N2	Single																		193771 4
verbenol2	N2	Single																		118344

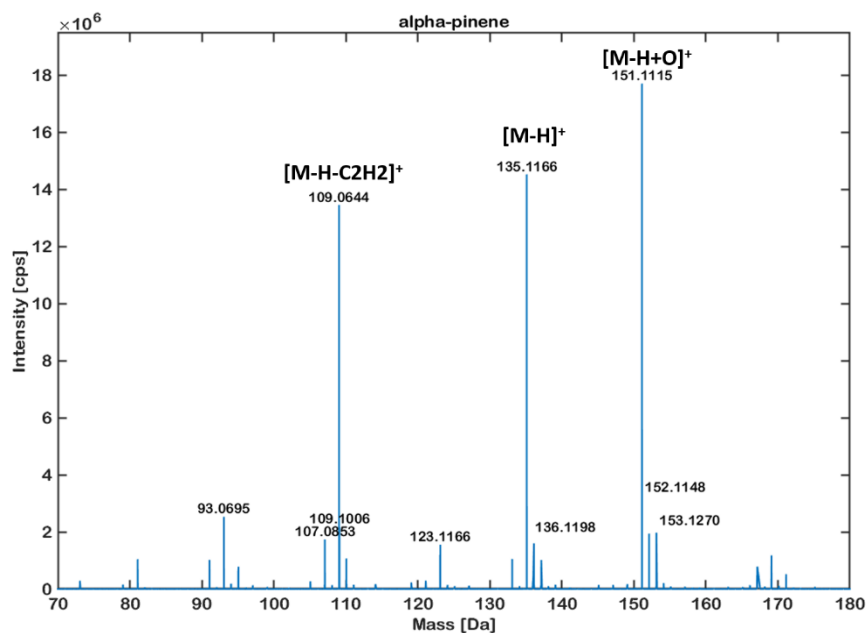


Figure A77: HRMS-spectrum of α -pinene. MS spectra acquired using a custom-made DBDI source at 2700 V and 20,000 Hz. Room air was used for the ionisation process. Spectrum was acquired by Dr. Alina Begley.

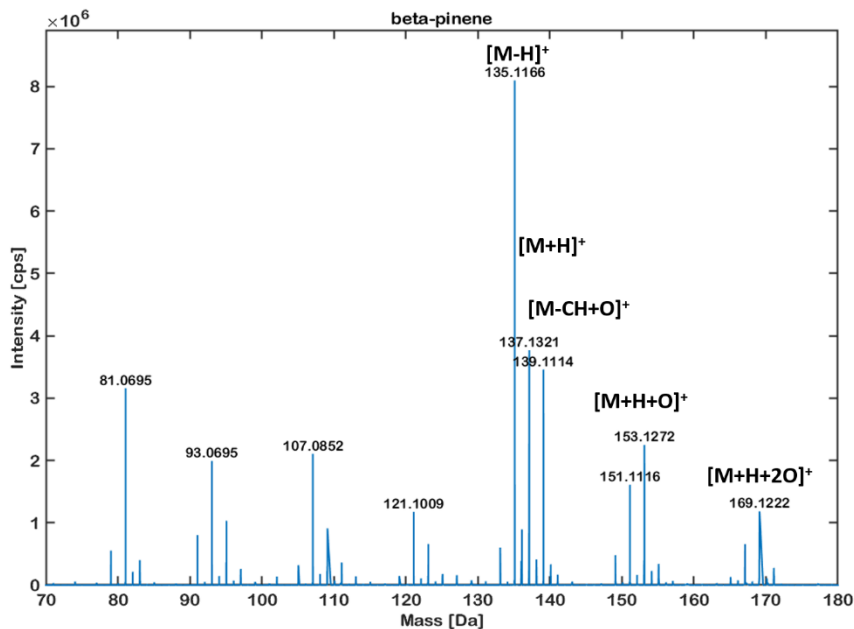


Figure A78: HRMS-spectrum of β -pinene. MS spectra acquired using a custom-made DBDI source at 2700 V and 20,000 Hz. Room air was used for the ionisation process. Spectrum was acquired by Dr. Alina Begley.

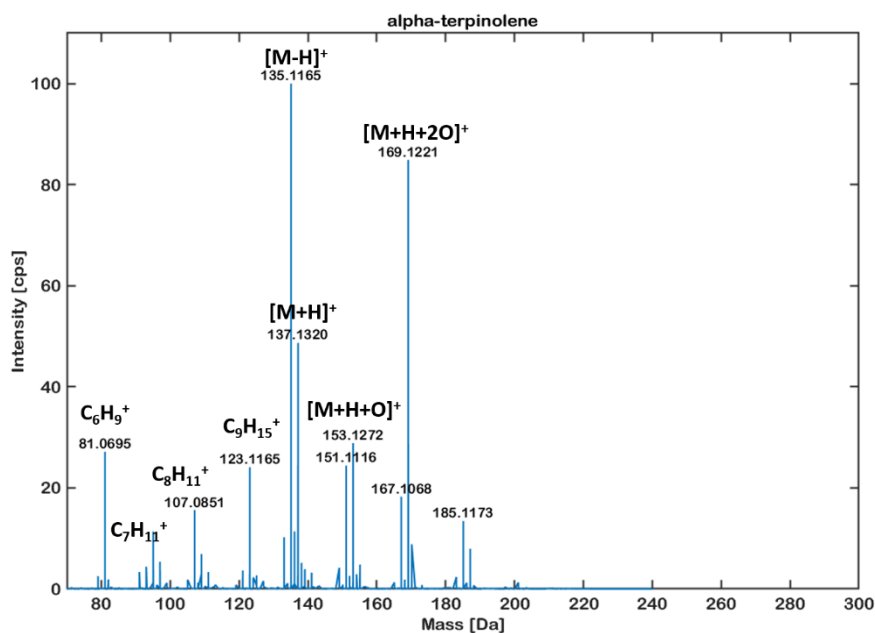


Figure A79: HRMS-spectrum of α -terpinolene. MS spectra acquired using a custom-made DBDI source at 2700 V and 20,000 Hz. Room air was used for the ionisation process. Spectrum was acquired by Dr. Alina Begley.

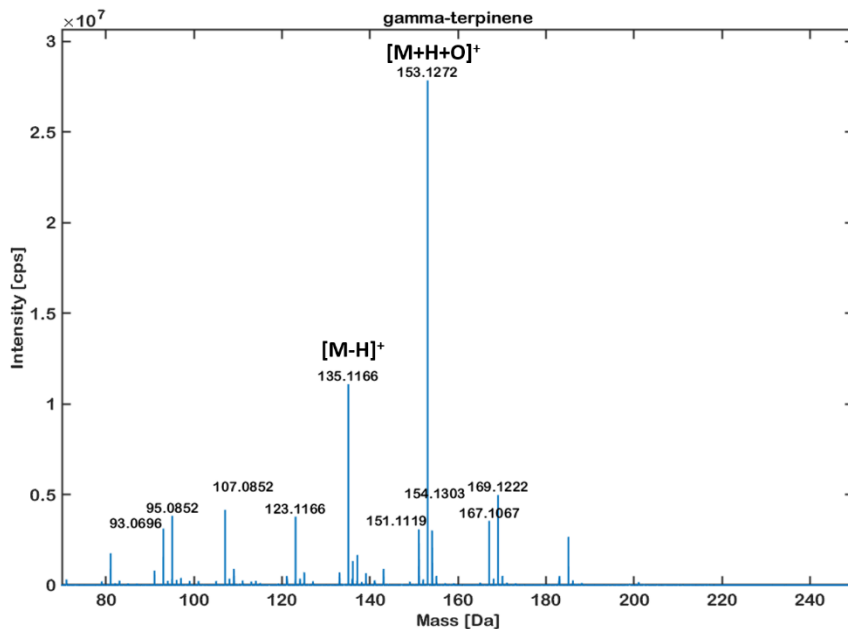


Figure A80: HRMS-spectrum of γ -terpinene. MS spectra acquired using a custom-made DBDI source at 2700 V and 20,000 Hz. Room air was used for the ionisation process. Spectrum was acquired by Dr. Alina Begley.

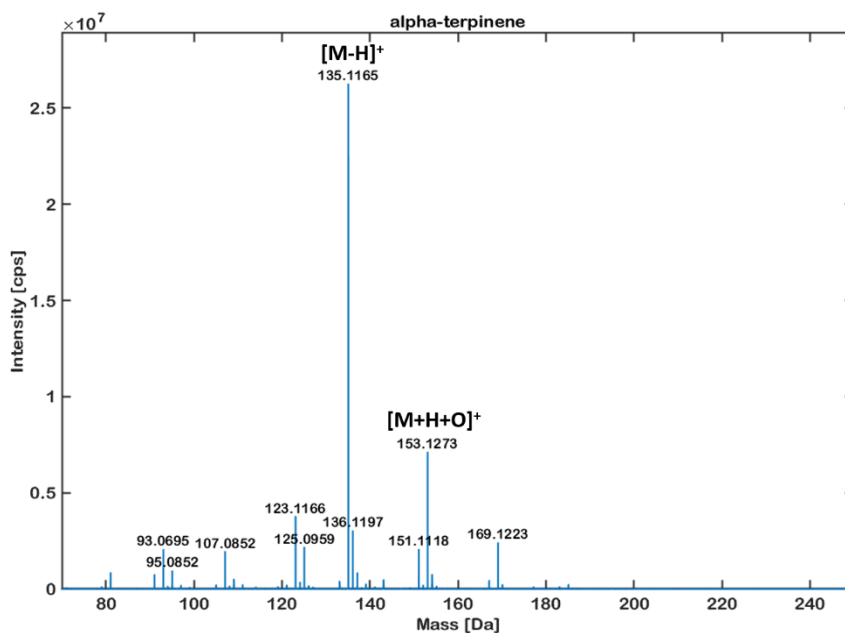


Figure A81: HRMS-spectrum of α -terpinene. MS spectra acquired using a custom-made DBDI source at 2700 V and 20,000 Hz. Room air was used for the ionisation process. Spectrum was acquired by Dr. Alina Begley.

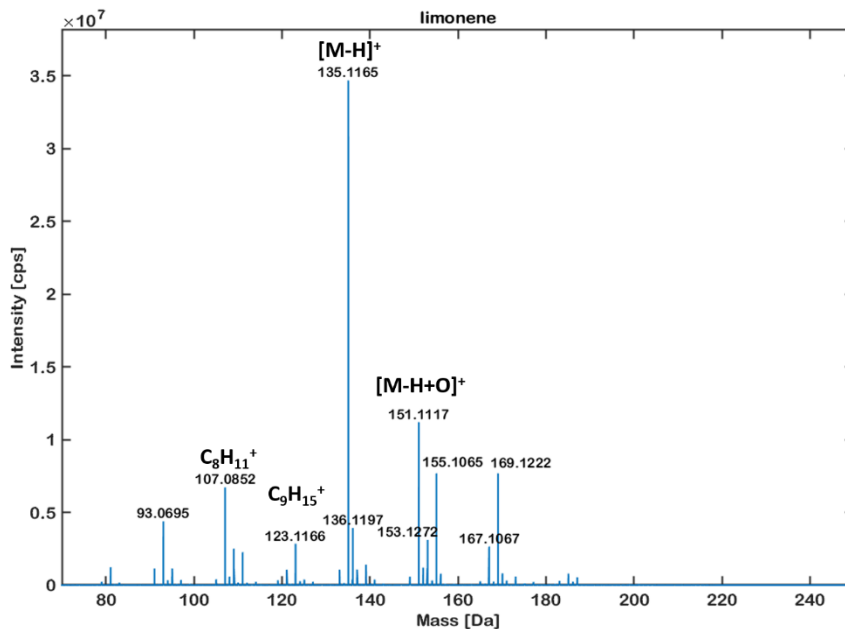


Figure A82: HRMS-spectrum of limonene. MS spectra acquired using a custom-made DBDI source at 2700 V and 20,000 Hz. Room air was used for the ionisation process. Spectrum was acquired by Dr. Alina Begley.

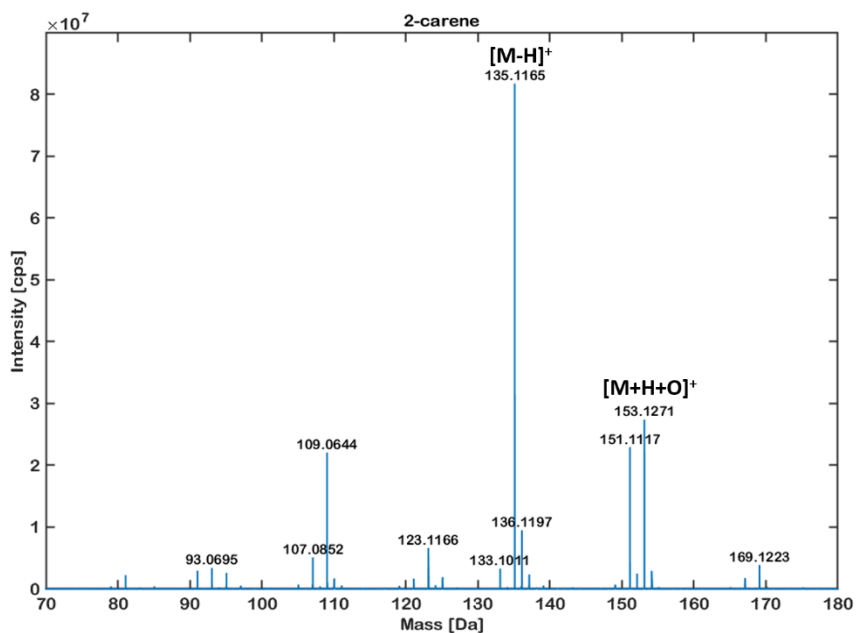


Figure A83: HRMS-spectrum of 2-carene. MS spectra acquired using a custom-made DBDI source at 2700 V and 20,000 Hz. Room air was used for the ionisation process. Spectrum was acquired by Dr. Alina Begley.

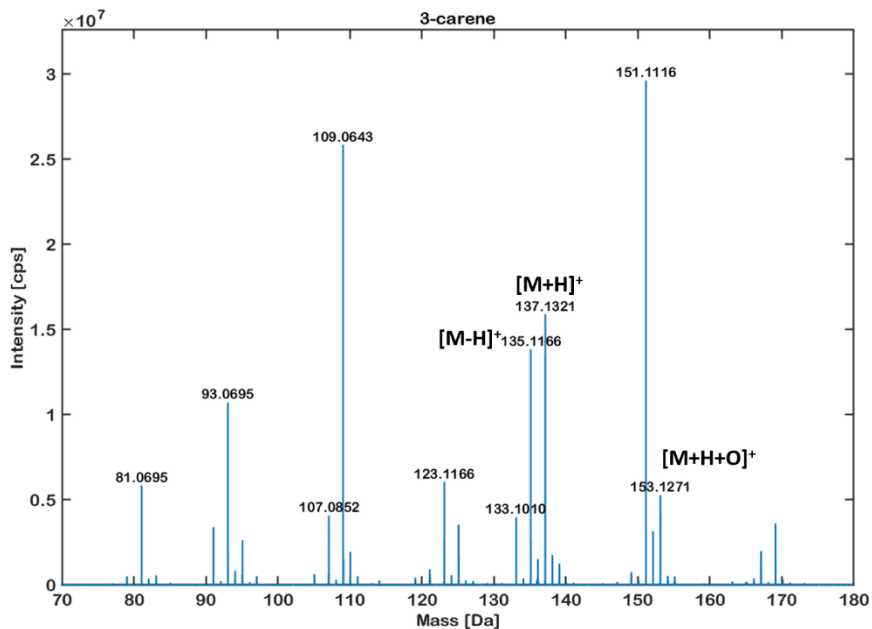


Figure A84: HRMS-spectrum of 3-carene. MS spectra acquired using a custom-made DBDI source at 2700 V and 20,000 Hz. Room air was used for the ionisation process. Spectrum was acquired by Dr. Alina Begley.

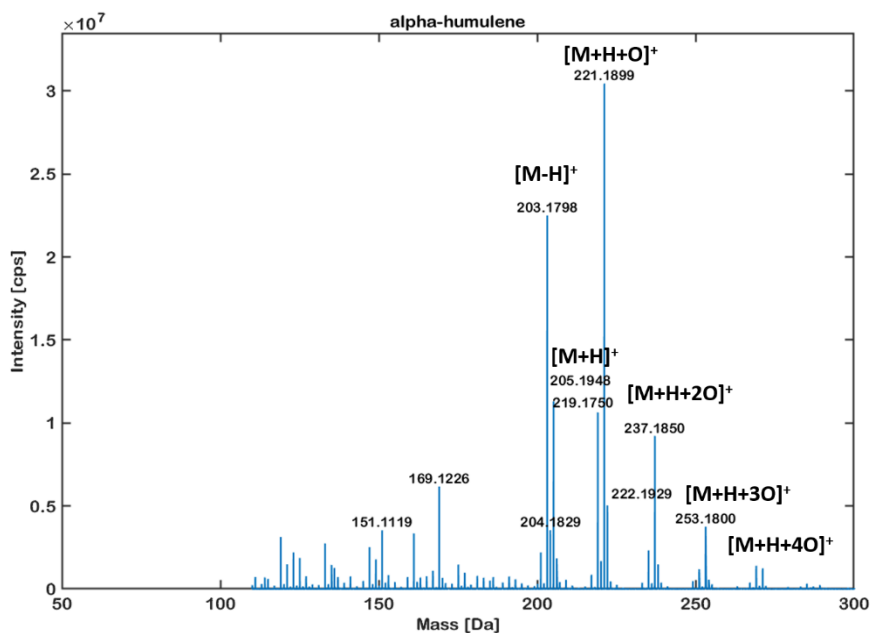


Figure A85: HRMS-spectrum of α -humulene. MS spectra acquired using a custom-made DBDI source at 2700 V and 20,000 Hz. Room air was used for the ionisation process. Spectrum was acquired by Dr. Alina Begley.

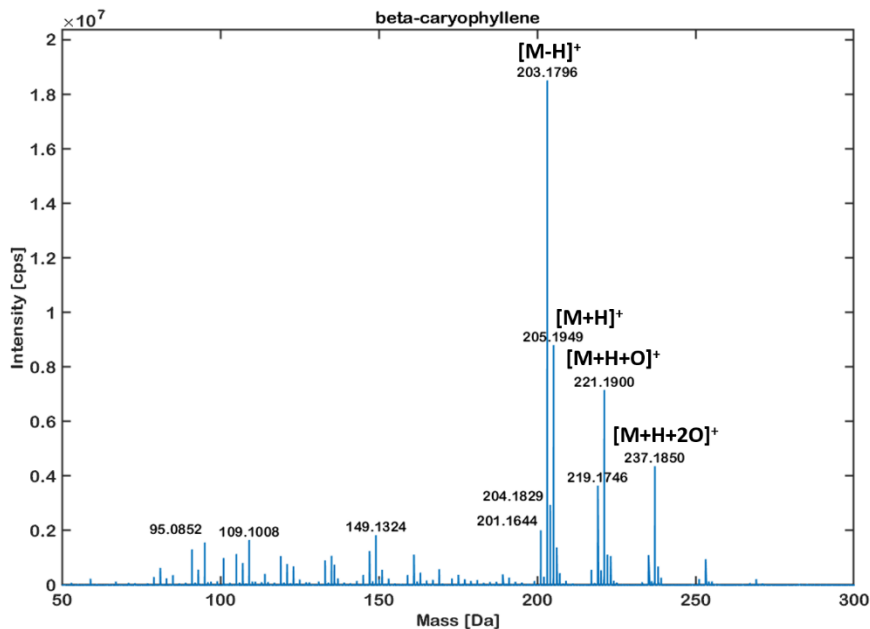


Figure A86: HRMS-spectrum of β -caryophyllene. MS spectra acquired using a custom-made DBDI source at 2700 V and 20,000 Hz. Room air was used for the ionisation process. Spectrum was acquired by Dr. Alina Begley.

Table A22: Chemicals and reagents.

Analyte	Quality	Manufacturer	Origin
(+/-)-sabinene	98%	abcr	Karlsruhe, Germany
geraniol	99%	Acros Organics™, Thermo Fisher Scientific	Reinach, Switzerland
nerol	97%	Acros Organics™, Thermo Fisher Scientific	Reinach, Switzerland
citronellol	99%	Acros Organics™, Thermo Fisher Scientific	Reinach, Switzerland
norcamphor	99%	Acros Organics™, Thermo Fisher Scientific	Reinach, Switzerland
deuterium oxide	> 99.9 Atom %D	Apollo	Stockport, UK
trans-verbenol	NA	in house	in house
cis-sabinol	NA	Dragoco	Holzminden, Germany
cuminaldehyde	NA	Dragoco	Holzminden, Germany
elemol	NA	Dragoco	Holzminden, Germany
water	Purified, 18.2 MΩ	ELGA Labwater, PURELAB flex 3	in house
nerolidol	NA	Essencia	Winterthur, Switzerland
camphor rac.	Ph. Eur.	Essencia	Winterthur, Switzerland
methanol	Optima™, LC-MS grade	Fisher Chemicals	Loughborough, United Kingdom
menthone	purum	Fluka	Buchs, Switzerland
(-)-rose oxide	analytical standard	Fluka	Buchs, Switzerland
(+)-rose oxide	analytical standard	Fluka	Buchs, Switzerland
(S)-(-)-limonene	analytical standard	Fluka	Buchs, Switzerland
α-terpinene	85-90%	Fluka	Buchs, Switzerland
(+)-limonene	> 99%	Fluka	Buchs, Switzerland
γ-terpinene	95%	Fluka	Buchs, Switzerland
(+)-2-carene	>97%	Fluka	Buchs, Switzerland
(+)-carvone	(cis/trans), prouss p. analysis, >98,5%	Fluka	Buchs, Switzerland
(-)-borneol	puriss p. analysis	Fluka	Buchs, Switzerland
(+)-fenchone	>98%	Fluka	Buchs, Switzerland
(+)-fenchol	analytical standard	Fluka	Buchs, Switzerland

(-)-menthol	analytical standard	Fluka	Buchs, Switzerland
guajazulene	puriss, > 99%	Fluka	Buchs, Switzerland
thymol	purum	Fluka	Buchs, Switzerland
(-)-carvone	>99%	Fluka	Buchs, Switzerland
(-)-terpinen-4-ol	>95%	Fluka	Buchs, Switzerland
(+)-pulegone	NA	Fluorochem	Hadfield, UK
β -caryophyllene	NA	Frey & Lau	Henstedt-Ulzburg, Germany
myrtenol	NA	Frey & Lau	Henstedt-Ulzburg, Germany
cedrol	NA	Frey & Lau	Henstedt-Ulzburg, Germany
citronellal	NA	Frey & Lau	Henstedt-Ulzburg, Germany
α -bisabolol	NA	Frey & Lau	Henstedt-Ulzburg, Germany
dihydrolinalool	NA	Haya Schweiz AG	Gossau, Switzerland
(+/-)-isomenthone	NA	in house	in house
safranal	NA	in house	in house
	Emsure®, ISO, Reag.		
ethanol	Ph. Eur., absolute for analysis	Merck	Darmstadt, Germany
nitrogen	5.0	PanGas	Dagmersellen, Switzerland
l-fenchone	>98%	SAFC, Merck	Darmstadt, Germany
isoborneol	>95%	SAFC, Merck	Darmstadt, Germany
(-)-isopulegol	>99%	SAFC, Merck	Darmstadt, Germany
(+)-cis-abienol	NA	Santa Cruz	Heidelberg, Germany
(-)- α -cedrene	98%, sum of enantiomers	Sigma Aldrich	St. Louis, MO, USA
1,8-cineol	99%	Sigma Aldrich	St. Louis, MO, USA
dl-patchenol	techn., 90%	Sigma Aldrich	St. Louis, MO, USA
α -thujone	purum > 96%	Sigma Aldrich	St. Louis, MO, USA
(-)-trans-pinocarveol	>96%, sum of enantiomers	Sigma Aldrich	St. Louis, MO, USA
β -jonone	96%	Sigma Aldrich	St. Louis, MO, USA
α - & β -thujone	10% β -thujone, techn.	Sigma Aldrich	St. Louis, MO, USA
(+)- α -pinene	> 99%	Sigma Aldrich	St. Louis, MO, USA
(-)- α -pinene	> 99%	Sigma Aldrich	St. Louis, MO, USA
(+)- β -pinene	analytical standard	Sigma Aldrich	St. Louis, MO, USA
(-)- β -pinene	99%	Sigma Aldrich	St. Louis, MO, USA
(-)-carveol	97%	Sigma Aldrich	St. Louis, MO, USA
p-cymene	99%	Sigma Aldrich	St. Louis, MO, USA
linalool	97%	Sigma Aldrich	St. Louis, MO, USA
farnesol	95%	Sigma Aldrich	St. Louis, MO, USA
carvacrol	>98%	Sigma Aldrich	St. Louis, MO, USA

α -terpinolene	>90%	Sigma Aldrich	St. Louis, MO, USA
myrcene	analytical standard	Sigma Aldrich	St. Louis, MO, USA
(+)-3-carene	analytical standard	Sigma Aldrich	St. Louis, MO, USA
terpinolene	>90%	Sigma Aldrich	St. Louis, MO, USA
citral	> 98%	TCI	Eschborn, Germany
α -humulene	>93%	TCI	Eschborn, Germany
α -terpineol	>95%	TCI	Eschborn, Germany

Table A23: List of adducts.

Adduct	mass difference Δ
[M+NO ₂] ⁺	46
[M+H ₂ O ₂] ⁺	34
[M] ⁺	0
[M+2H] ⁺	2
[M+3H] ⁺	3
[M+CN+NH] ⁺	41
[M+H] ⁺	1
[M+H+2O] ⁺	33
[M+H+3O] ⁺	49
[M+H+H ₂ O] ⁺	19
[M+H-2H ₂ O] ⁺	-35
[M+H-H ₂ O] ⁺	-17
[M+N] ⁺	14
[M+NH ₄] ⁺	18
[M+NO] ⁺	30
[M+NOH ₂] ⁺	32
[M+O] ⁺	16
[M+OH] ⁺	17
[M-2H] ⁺	-2
[M-3H] ⁺	-3
[M-3H+2O] ⁺	29
[M-3H+3O] ⁺	45
[M-3H+O] ⁺	13
[M-5H+2O] ⁺	27
[M-5H+O] ⁺	11
[M-7H+2O] ⁺	25
[M-7H+3O] ⁺	41
[M-C+N] ⁺	2
[M-C ₄ H ₉] ⁺	-57
[M-C ₄ H ₉ O] ⁺	-73
[M-C ₅ H ₁₁] ⁺	-71
[M-C ₅ H ₁₁ O] ⁺	-87
[M-CH ₃] ⁺	-15
[M-CH ₃ COO] ⁺	-59
[M-CH ₃ O] ⁺	-31
[M-H] ⁺	-1
[M-H+2O] ⁺	31
[M-H+O] ⁺	15
[M-OH] ⁺	-17

Script A5: MATLAB code for MS-spectra visualisation and generation of excel files for the 10 most intense peaks.

```
%% Plot MS Spectra in centroid view. Export from SciexOS as txt
%% Centroid should be based on height

% Specify the directory containing the .txt files
inputDir = 'InputDirectory'; % Replace with your directory path
outputDir = 'OutputDirectory'; % Replace with your output directory path

% Get a list of all .txt files in the directory
txtFiles = dir(fullfile(inputDir, '*.txt'));

% Loop over each file
for i = 1:length(txtFiles)
    % Get the full path to the .txt file
    txtFilePath = fullfile(inputDir, txtFiles(i).name);

    % Read the data from the .txt file
    df = readmatrix(txtFilePath);

    % Extract the mass and intensity data
    mass = df(:, 1);
    intensity = df(:, 2);

    % Identify the 10 highest intensities
    k = 10;
    k_largest_intensities = maxk(intensity, k); % Creates Array with highest
intensities

    idx_largest_intensities = zeros(k, 1); % Create zero matrix

    for j = 1:k
        idx_largest_intensities(j) = find(intensity == k_largest_intensities(j),
1);
    end

    % Plot the data
    figure('Position', [100, 100, 1200, 800]); % Set figure size to 1200x800
pixels
    bar(mass, intensity);
    hold on;

    % Adjust text position to avoid overlap
    textYOffset = max(intensity) * 0.02; % Small offset for better visualization
    for j = 1:k
        text(mass(idx_largest_intensities(j)),
intensity(idx_largest_intensities(j)) + textYOffset, ...
        sprintf('%.2f', mass(idx_largest_intensities(j))), ... % Format the
mass with two digits after the decimal point
        'HorizontalAlignment', 'center', 'VerticalAlignment', 'bottom',
'FontName', 'Arial Rounded MT Bold');
    end
    hold off;

    % Customize the plot appearance
```

```

box on;
ax = gca;
ax.LineWidth = 1.5;
ax.FontSize = 14;
ax.FontWeight = 'bold';
ax.FontName = 'Arial Rounded MT Bold';

ylim([0 max(intensity)*1.2]); % Set y-axis limit slightly above the max
intensity for better visualization
ylabel('Intensity [cps]', 'FontSize', 14, 'FontName', 'Arial Rounded MT
Bold');
xlabel('Mass [Da]', 'FontSize', 14, 'FontName', 'Arial Rounded MT Bold');
title(strrep(txtFiles(i).name, '_', ' '), 'FontSize', 14, 'FontName', 'Arial
Rounded MT Bold'); % Title based on file name

% Save the plot as a .png file
[~, name, ~] = fileparts(txtFiles(i).name); % Get the file name without
extension
saveas(gcf, fullfile(outputDir, [name '.png']));

% Create an array with the 10 highest intensities and the corresponding masses
k_number_highest_intensities = df(idx_largest_intensities, 1:2);

% Save the data to an Excel file
%writematrix(k_number_highest_intensities, fullfile(outputDir, [name
'.xlsx']));

% Close the figure
close(gcf);
end

```

Script A6: Python code used to merge Excel files generated with Script A5.

```
import os
import pandas as pd

# Directory containing the Excel files
directory = 'DIRECTORY' # replace with your directory path

# List to hold all the data to be concatenated later
all_data = []

# Define the columns to be used in the final DataFrame
columns = ['mass [Da]', 'intensity [cps]', 'rel intensity [%]', 'Delta',
'Int', 'Adduct', 'MW [Da]', 'Analyte name']

# Loop through all Excel files in the directory
for filename in os.listdir(directory):
    if filename.endswith(".xlsx") or filename.endswith(".xls"):
        file_path = os.path.join(directory, filename)

        # Read the current Excel file
        df = pd.read_excel(file_path, header=None)

        # Get the name of the analyte
        analyte_name = os.path.splitext(filename)[0]

        # Calculate relative intensity - have rounded values
        df['rel intensity [%]'] = (df[1] / df[1].max() *
100).round().astype(int)

        # Create a new DataFrame for this file's data with the required
structure
        file_data = pd.DataFrame({
            'mass [Da]': df[0],
            'intensity [cps]': df[1],
            'rel intensity [%]': df['rel intensity [%]'],
            'Delta': '',
            'Int': '',
            'Adduct': '',
            'MW [Da]': '',
            'Analyte name': analyte_name
        })

        # Append the file data to the list
        all_data.append(file_data)

        # Add two empty rows (with analyte name for consistency)
        empty_rows = pd.DataFrame(['']*8)*2, columns=columns)
        all_data.append(empty_rows)
```

```
# Concatenate all dataframes in the list
consolidated_data = pd.concat(all_data, ignore_index=True)

# Write the consolidated data to a new Excel file
output_file_path = 'DIRCOTRY/merged_excel_files.xlsx' # Replace
'desired/path/' with your desired directory
consolidated_data.to_excel(output_file_path, index=False)
```

Script A7: Python code to allocate differences m/z to certain adducts (Table A23).

```
import pandas as pd
import re

# Import three Excel files, which contain an adduct list, list of terpenes
with MW and merged file generated from Script A7
# df1 requires analyte names which are free from special signs (+/_/-) and
numbers
df1 = pd.read_excel("DIRECTORY/merged_file.xlsx")
df2 = pd.read_excel("DIRECTORY/List_Terpenes.xlsx")
df3 = pd.read_excel("DIRECTORY/Adduct_List.xlsx")

# Initialize new columns
df1["Cyclization"] = ""
df1["Terpene class"] = ""
df1["Oxygenations"] = ""
df1["Functional group"] = ""
df1["MW [Da]"] = ""

# Function to find the best partial match
def find_best_partial_match(name, names_list):
    best_match = None
    max_consecutive = 0
    for n in names_list:
        if isinstance(n, str): # Check if the value is a string
            match = re.findall(r'(?i)\b{}\b'.format(re.escape(str(name))),
n.replace('-', ''))
            if match:
                consecutive = len(match[0])
                if consecutive >= 4 and consecutive > max_consecutive:
                    best_match = n
                    max_consecutive = consecutive
    return best_match

# Iterate through each row in the first Excel file
for index, row1 in df1.iterrows():
    analyte_name = row1["Analyte name"]
    if isinstance(analyte_name, float):
        continue # Skip rows with float values in the "Analyte name" column
    # Search for partial match in the second Excel file
    matched_name = find_best_partial_match(analyte_name, df2["Analyte
name"].astype(str).tolist())
    if matched_name is not None:
        matched_row = df2[df2["Analyte name"] == matched_name]
        # Fill in corresponding columns from the matched row
        df1.at[index, "Cyclization"] = matched_row.iloc[0]["Cyclization"]
        df1.at[index, "Terpene class"] = matched_row.iloc[0]["terpene class"]
        df1.at[index, "Oxygenations"] = matched_row.iloc[0]["oxygenations"]
```

```

df1.at[index, "Functional group"] = matched_row.iloc[0]["function
group"]
df1.at[index, "MW [Da]"] = matched_row.iloc[0]["MW [Da]"]
# Calculate Delta
mass_da = str(row1["mass [Da]"]).replace(',', '.')
mw_da = str(matched_row.iloc[0]["MW [Da]"]).replace(',', '.')
delta = float(mass_da) - float(mw_da)
df1.at[index, "Delta"] = delta
# Fill in Int column
df1.at[index, "Int"] = round(delta)

# Find matching adducts
# Iterate through each row in df1
for index, row in df1.iterrows():
    # Get the Int value
    int_value = row["Int"]

    # Check if the Int value matches any number in the second column of df3
    adduct = df3[df3.iloc[:, 1] == int_value].iloc[:, 0].values

    # If adduct is not empty, assign the adduct to the "adducts" column
    if len(adduct) > 0:
        df1.at[index, "adducts"] = adduct[0]
    else:
        df1.at[index, "adducts"] = ""

# Generate the new Excel sheet
output_file = 'DIRECTORY/output_excel_MW_deuterated.xlsx'
df1.to_excel(output_file, index=False)

```

Script A8: Python code to extract the adducts with maximum intensity.

```
import pandas as pd
import numpy as np

# Read the main Excel sheet and the list of adducts
main_df = pd.read_excel("DIRECTORY/Adducts_Evaluated.xlsx")
adducts_df = pd.read_excel("Adduct_List.xlsx")

# Get the list of adducts from the adducts DataFrame
adduct_list = adducts_df["Adduct"].tolist()

# Initialize a list to store the data for the new DataFrame
new_data = []

# Function to process a block and extract the required data
def process_block(block):
    # Check if there are any non-NaN values in the "adducts" column
    if not block["adducts"].notna().any():
        return # Skip processing if there are no non-NaN values

    # Extract the first row with a non-empty 'adducts' value
    first_adduct_row = block[block["adducts"].notna()].iloc[0]

    # Extract relevant information for the analyte
    analyte_name = first_adduct_row["Analyte name"]
    cyclization = first_adduct_row["Cyclization"]
    terpene_class = first_adduct_row["Terpene class"]
    oxygenation = first_adduct_row["Oxygenations"]
    functional_group = first_adduct_row["Functional group"]
    mw_da = first_adduct_row["MW [Da]"] # Extract MW [Da] from the first row

    # Initialize a dictionary to store the intensity for each adduct
    adduct_intensities = {adduct: np.nan for adduct in adduct_list}

    # Iterate over each row in the block to find the highest intensities
    for _, row in block.iterrows():
        adduct = row["adducts"]
        intensity = row["intensity [cps]"]

        # Check if the adduct is in the list of adducts
        if adduct in adduct_list:
            # Update the intensity if the current intensity is higher or if
            # it's the first valid entry
            if np.isnan(adduct_intensities[adduct]) or intensity >
            adduct_intensities[adduct]:
                adduct_intensities[adduct] = intensity

    # Append the data for the analyte to the new_data list
```



```

new_data.append({
    "Analyte name": analyte_name,
    "Cyclization": cyclization,
    "Terpene class": terpene_class,
    "Oxygenation": oxygenation,
    "Functional group": functional_group,
    "MW [Da]": mw_da, # Include MW [Da] in the final dictionary
    **adduct_intensities # Unpack the dictionary
})

# Iterate over the DataFrame by blocks of 10 rows with 2 empty rows between
blocks
block_size = 10
start_idx = 0
while start_idx < len(main_df):
    end_idx = start_idx + block_size
    block = main_df.iloc[start_idx:end_idx]

    # Process the block
    process_block(block)

    # Move to the next block, skipping 2 empty rows
    start_idx = end_idx + 2

# Create a new DataFrame from the new_data list
new_df = pd.DataFrame(new_data)

# Reorder columns to have the desired structure
desired_columns = ["Analyte name", "Cyclization", "Terpene class",
"Oxygenation", "Functional group", "MW [Da]"] + adduct_list
new_df = new_df[desired_columns]

# Write the new DataFrame to a new Excel sheet
new_df.to_excel("DIRECTORY/Extracted_Adducts.xlsx", index=False)

```

Script A9: Python code to extract the most intense adduct and create a new Excel file.

```
import pandas as pd
import numpy as np

# Read the existing DataFrame from the Excel sheet
new_df = pd.read_excel("DIRECTORY/Extracted_Adducts.xlsx")

# Identify the columns that contain the adduct intensities (from column 8 onwards)
adduct_columns = new_df.columns[6:]

# Create a copy of the DataFrame to keep the original structure
max_intensity_df = new_df.copy()

# Iterate over each row in the new DataFrame
for index, row in max_intensity_df.iterrows():
    # Find the maximum intensity in the adduct columns
    max_intensity = row[adduct_columns].max()

    # Iterate over each adduct column and replace values with NaN if not the maximum
    for col in adduct_columns:
        if row[col] != max_intensity:
            max_intensity_df.at[index, col] = np.nan

# Write the new DataFrame to a new Excel sheet
max_intensity_df.to_excel("DIRECTORY/Max_Intensity_Adducts.xlsx", index=False)
```

Script A10: Python code to generate bubble plot.

```
import pandas as pd
import matplotlib.pyplot as plt
import numpy as np

# Step 1: Read Data
data = pd.read_excel("DIRECTORY/Max_Intensity_Adducts.xlsx ")

# Step 2: Data Preparation
unique_analytes = data['Analyte name'].unique()
dopants = data['Dopant'].unique()

# Define colors for adducts
adduct_colors = {
    '[2M+H]': 'blue',
    '[2M+N]': 'green',
    '[2M-H+2N]': 'red',
    '[M + H2O2]': 'purple',
    '[M + NO2]': 'orange',
    '[M]': 'cyan',
    '[M+2H]': 'magenta',
    '[M+3H]': 'yellow',
    '[M+CN+NH]': 'black',
    '[M+H]': 'powderblue',
    '[M+H+2O]': 'pink',
    '[M+H+3O]': 'brown',
    '[M+H+H2O]': 'gray',
    '[M+H-2H2O]': 'olive',
    '[M+H-H2O]': 'navy',
    '[M+N]': 'salmon',
    '[M+NH4]': 'teal',
    '[M+NO]': 'lime',
    '[M+NOH2]': 'gold',
    '[M+O]': 'violet',
    '[M+OH]': 'skyblue',
    '[M-2H]': 'orchid',
    '[M-3H]': 'indigo',
    '[M-3H+2O]': 'hotpink',
    '[M-3H+3O]': 'yellowgreen',
    '[M-3H+O]': 'crimson',
    '[M-5H+2O]': 'deepskyblue',
    '[M-5H+O]': 'peru',
    '[M-7H+2O]': 'saddlebrown',
    '[M-7H+3O]': 'lavender',
    '[M-C+N]': 'darkgreen',
    '[M-C4H9]': 'darkred',
    '[M-C4H9O]': 'darkorange',
    '[M-C5H11]': 'darkcyan',
```

```

[M-C5H11O]': 'darkmagenta',
[M-CH3]': 'darkblue',
[M-CH3COO]': 'darkviolet',
[M-CH3O]': 'darkturquoise',
[M-H]': 'darkolivegreen',
[M-H+2O]': 'darksalmon',
[M-H+O]': 'darkslateblue',
[M-OH]': 'darkgoldenrod'
}

# Step 3: Plotting
fig, ax = plt.subplots(figsize=(14, 10))

# Intensity range definitions
intensity_ranges = [(100000, 500000), (500000, 1000000), (1000000, 1500000),
(1500000, 2000000), (2000000, 2500000), (2500000, 3000000), (3000000,
4000000), (4000000, 5000000), (5000000, float('inf'))]
bubble_sizes = [10, 15, 30, 50, 75, 100, 125, 130, 150] # Adjust bubble sizes

# Adjust y-ticks with more spacing
y_positions = np.arange(0, len(unique_analytes) * 5, 5)

# Iterate over each analyte
for i, analyte in enumerate(unique_analytes):
    analyte_data = data[data['Analyte name'] == analyte]
    for _, row in analyte_data.iterrows():
        dopant_index = np.where(dopants == row['Dopant'])[0][0]
        intensity = pd.to_numeric(row.dropna().values[-1], errors='coerce') #
Get the last non-null value in the row
        if np.isnan(intensity): # Skip plotting if intensity is NaN
            continue
        for intensity_range, size in zip(intensity_ranges, bubble_sizes):
            if intensity_range[0] <= intensity < intensity_range[1]:
                break
        color = adduct_colors.get(row.dropna().index[-1], 'gray') # Get the
last non-null column name as adduct
        ax.scatter(dopant_index, y_positions[i], s=size, c=color, alpha=1.0)

# Create Legends for adducts
legend_elements = []
for adduct, color in adduct_colors.items():
    legend_elements.append(plt.Line2D([0], [0], marker='o', color='w',
markerfacecolor=color, markersize=10, label=adduct))

# Place legend for adducts on the far right
adduct_legend = ax.legend(handles=legend_elements, loc='center left',
bbox_to_anchor=(1, 0.5), fontsize=10, frameon=False, title='Adducts',
title_fontsize=14)

```

```

ax.add_artist(adduct_legend)

# Create a second legend for bubble sizes
size_labels = ['100000-500000', '500000-1000000', '1000000-1500000', '1500000-2000000', '2000000-2500000', '2500000-3000000', '3000000-4000000', '4000000-5000000', '>5000000']
size_legend_elements = [plt.Line2D([0], [0], marker='o', color='w', markerfacecolor='gray', markersize=np.sqrt(size), label=label) for size, label in zip(bubble_sizes, size_labels)]

# Place legend for bubble sizes
size_legend = ax.legend(handles=size_legend_elements, loc='center left', bbox_to_anchor=(1.2, 0.5), fontsize=10, frameon=False, title='Intensity (cps)', title_fontsize=14)

# Reduce spacing on the x-axis by setting a smaller limit on xticks
ax.set_xticks(np.arange(len(dopants)))
ax.set_xticklabels(dopants, rotation=45, ha='right', fontsize=10, fontname='Arial Rounded MT Bold')
ax.tick_params(axis='x', which='major', pad=6)

# Set y-axis labels with font settings
ax.set_yticks(y_positions)
ax.set_yticklabels(unique_analytes, fontsize=10, fontname='Arial Rounded MT Bold')

# Set labels and title with font settings
plt.xlabel('Dopant', fontsize=10, fontname='Arial Rounded MT Bold')
plt.ylabel('Analyte', fontsize=10, fontname='Arial Rounded MT Bold')
plt.title('Bubble Plot of Analytes with Dopants', fontsize=10, fontname='Arial Rounded MT Bold')
plt.grid(False) # Remove grid
plt.tight_layout()

# Adjust the aspect ratio to decrease spacing on the x-axis and increase spacing on the y-axis
plt.gca().set_aspect('auto', adjustable='datalim')

plt.show()

```

Chapter 3: Computational methods and data fusion for enhanced classification of natural products

4.1. Exploring new dimensions: Single and multi-block analysis of essential oils using DBDI-MS and FT-IR for enhanced authenticity control.

Some of the data presented here was published in the following publication:

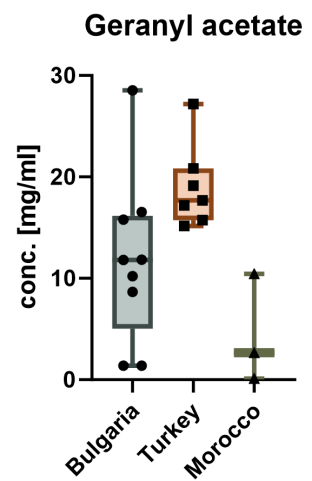
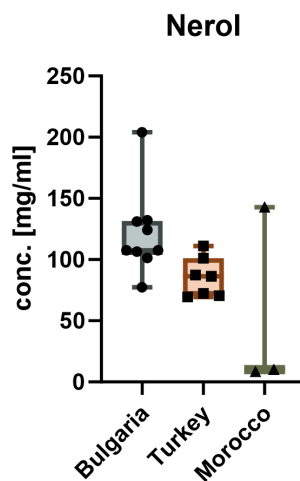
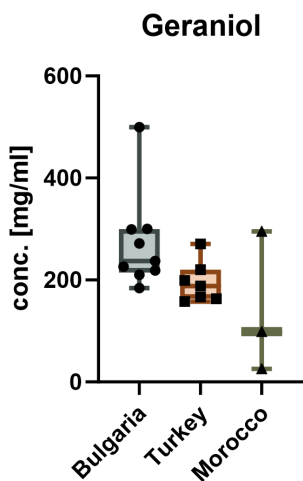
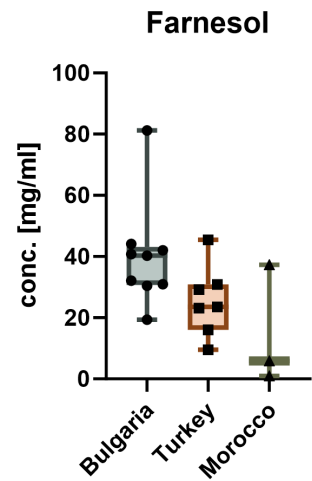
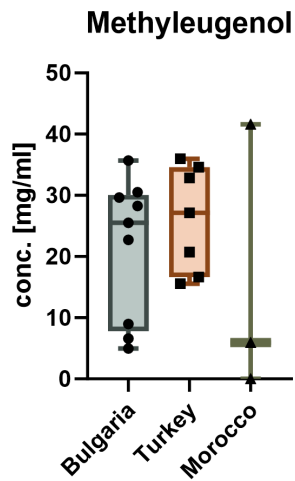
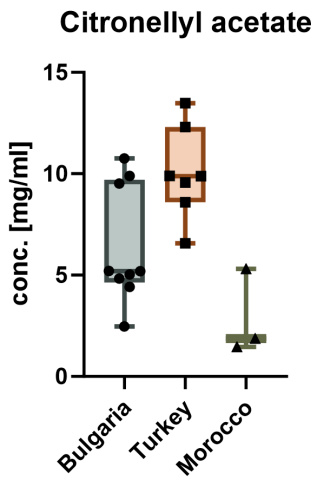
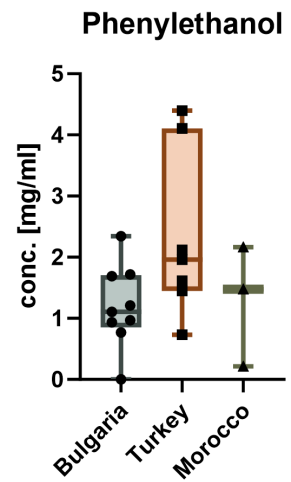
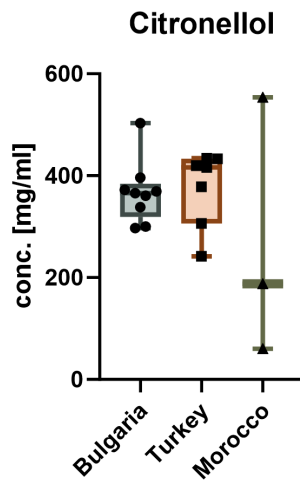
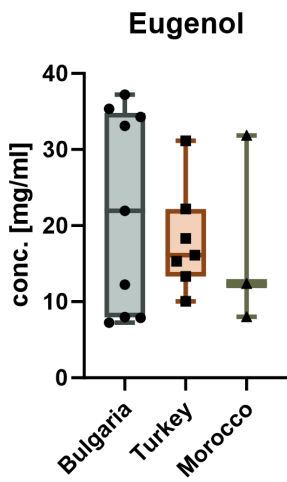
Raeber J, Steuer C. Exploring new dimensions: Single and multi-block analysis of essential oils using DBDI-MS and FT-IR for enhanced authenticity control. *Analytica Chimica Acta* 2023; 1277: 341657. DOI: <https://doi.org/10.1016/j.aca.2023.341657>

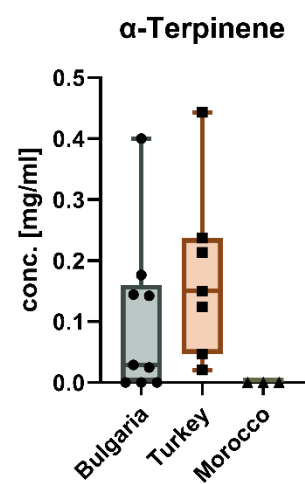
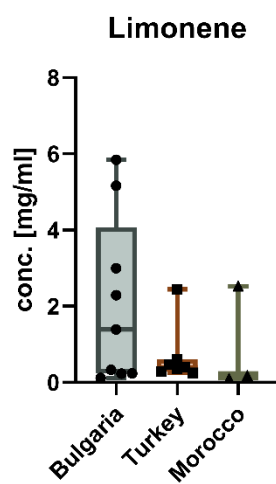
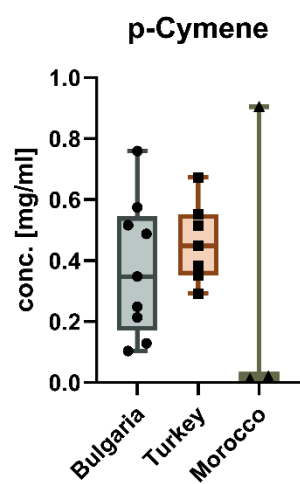
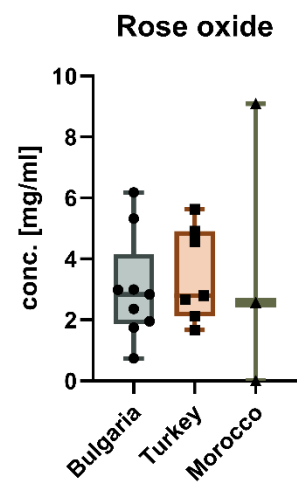
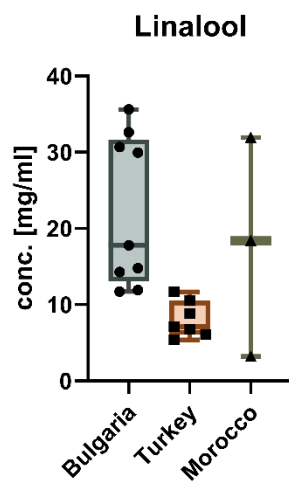
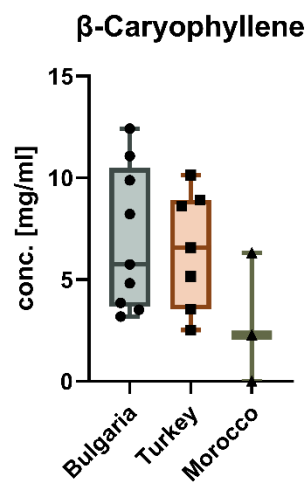
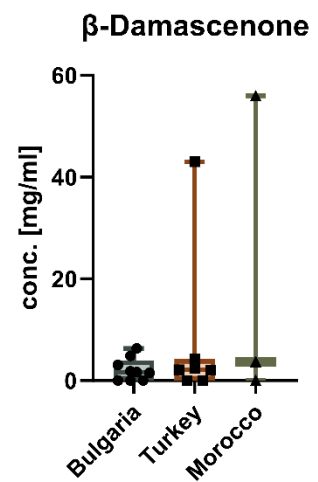
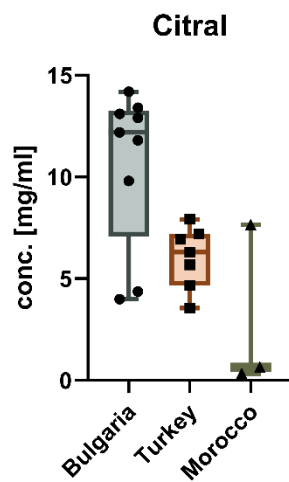
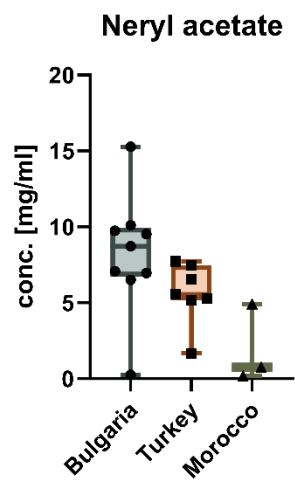
Table A24: 26 authentic EO samples, which were included in the chemometric study. Numbering corresponds to the numbering seen in the main manuscript. Classifier corresponds to the classification into five groups (Bulgaria, Turkey, Morocco, Iran, other). Table taken from Raeber et al.²¹

Number	Origin	Species	EO percentage	Classifier
1	Bulgaria	<i>R. damascena</i>	10%	1
2	unkown	<i>R. damascena</i>	3%	4
3	Turkey	<i>R. damascena</i>	100%	2
4	Turkey	<i>R. damascena</i>	10%	2
5	Turkey	<i>R. damascena</i>	absolute	2
6	Bulgaria	<i>R. damascena</i>	10%	1
7	Bulgaria	<i>R. damascena</i>	100%	1
8	Turkey	<i>R. damascena</i>	100%	2
9	Morocco	<i>R. damascena</i>	absolute	3
10	Bulgaria	<i>R. damascena</i>	100%	1
11	Turkey	<i>R. damascena</i>	100%	2
12	Iran	<i>R. damascena</i>	100%	5
13	Morocco	<i>R. damascena</i>	100%	3
14	Morocco	<i>R. damascena</i>	10%	3
15	Bulgaria	<i>R. damascena</i>	10%	1
16	Egypt	<i>P. graveolens</i>	100%	4
17	Egypt	<i>P. graveolens</i>	100%	4
18	France	<i>C. bergamia</i> / <i>R. damascena</i>	100% (unkown ratio)	4
19	Bulgaria	<i>R. damascena</i>	10%	1
20	Bulgaria	<i>R. damascena</i>	10%	1
21	Bulgaria	<i>R. damascena</i>	100%	1
22	Bulgaria	<i>R. damascena</i>	100%	1
23	Turkey	<i>R. damascena</i>	100%	2
24	Turkey	<i>R. damascena</i>	100%	2
25	synthetic	synthetic	100%	4
26	France	<i>R. centifolia</i>	100%	4

Table A25: Results for different pre-processing methods of FT-IR and DBDI-MS data.
Taken from Raeber et al.²¹

Acquisition Type	Normalization	SNV correction	Smoothing	Scaling
FT-IR	Maximum value	Yes	Savitzky Golay smoothing (order: 3 rd , frame window 11)	Auto-scaling
FT-IR	Maximum value	Yes	Savitzky Golay smoothing (order: 3 rd , frame window 11)	Mean-centering
FT-IR	No	Yes	Savitzky Golay smoothing (order: 3 rd , frame window 11)	Mean-centering
FT-IR	Maximum value	Yes	No	Mean-centering
FT-IR	Maximum value	Yes	No	Auto-scaling
FT-IR	No	Yes	No	Auto-scaling
DBDI-MS	No	No	No	Auto-scaling
DBDI-MS	No	No	No	Mean-centering
DBDI-MS	No	No	Savitzky Golay smoothing (order: 3 rd , frame window 11)	No
DBDI-MS	Maximum value	No	No	No
DBDI-MS	By sum	No	No	No
DBDI-MS	Maximum value	No	No	Mean-centering
DBDI-MS	Maximum value	No	No	Auto-scaling
DBDI-MS	By sum	No	No	Mean-centering
DBDI-MS	By sum	No	No	Auto-scaling
DBDI-MS	By sum	No	Savitzky Golay smoothing (order: 3 rd , frame window 11)	Mean-centering
DBDI-MS	By sum	No	Savitzky Golay smoothing (order: 3 rd , frame window 15)	Mean-centering
DBDI-MS	By sum	No	Savitzky Golay smoothing (order: 3 rd , frame window 21)	Mean-centering
DBDI-MS	By sum	No	Savitzky Golay smoothing (order: 5 th , frame window 11)	Mean-centering
DBDI-MS	By sum	No	Savitzky Golay smoothing (order: 3 rd , frame window 21)	Mean-centering
DBDI-MS	By sum	No	Savitzky Golay smoothing (order: 3 rd , frame window 21)	Auto-scaling
DBDI-MS	No	No	No	Auto-scaling





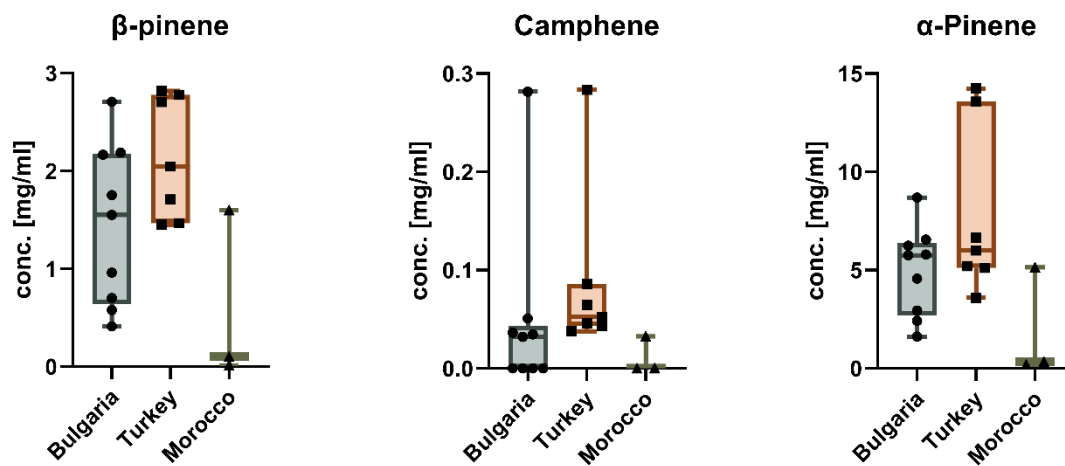


Figure A87: Box and Whisker Plots for the concentrations of various terpenes identified in *R. damascena* EO derived from different countries (Bulgaria, Turkey and Morocco). Figure was adapted from Raeber et al.²¹

Table A26: Validation results for PLS-DA model for five different acquisition methods. Classes correspond to Bulgaria (1), Turkey (2) and Morocco (3). Table taken from Raeber et al.²¹

Type of acquisition	Accuracy [%]			Precision [%]			Sensitivity [%]			Specificity [%]		
	1	2	3	1	2	3	1	2	3	1	2	3
Q1	33.3	85.7	85.7	75.0	66.7	50.0	33.3	85.7	100	83.1	61.5	81.5
Q3	66.7	100.0	100.0	100.0	100.0	50.0	66.7	100	100	100	100	80.8
FT-IR	66.7	71.4	66.7	85.7	83.3	33.3	66.7	71.4	66.7	82.0	85.4	79.7
Wax	88.9	100.0	100.0	100.0	87.5	100	88.9	100.0	100.0	100.0	86.6	84.0
Chiral	88.9	100.0	66.7	100.0	77.8	100	88.9	100.0	66.7	100.0	75.9	84.0

Script A11: Programming Code used in MATLAB ((Release R2022b, version: 9.13.0; The Mathworks Inc.). The code further requires the “Statistics and Machine Learning Toolbox” (Version: 12.3) and the “Signal Processing Toolbox” (Version: 9.1).

Pre-processing: Auto-scaling as well as different PCA plots

```
%% Auto-scaling function used for pre-processing

origin = readtable('Table with the Origin of the oils as Excel file');
df = readmatrix('Dataframe matrix as Excel file');

wavenumbers = df(1,:);           % Extraction of x-axis, for FT-IR e.g. wavenumber
transmission = df(2:end,:);     % Extraction of y-axis, for FT-IR e.g.
                                % transmission

% Calculate each mean per column

means_columns = zeros(1, length(wavenumbers));

for k = 1 : length(wavenumbers);
    average = mean(transmission(:,k));
    means_columns(k) = average;
end

% subtract each column by the means value

mean_centered = transmission - means_columns;

% calculate the standard deviation per column

std_dev_columns = zeros(1, length(wavenumbers));

for k = 1 : length(wavenumbers);
    std_dev = std(transmission(:,k));
    std_dev_columns(k) = std_dev;
end

% autoscale {x - average(x)}/{std dev} describes function

autoscaled_data = mean_centered ./ std_dev_columns;

%% Optional: plot auto-scaled data - generates FT-IR spectrum
% plot(wavenumbers, autoscaled_data);
% xlim([600 4000])
% set(gca, 'xdir','reverse');

data_variables = [wavenumbers; autoscaled_data];

T = table(data_variables);
auto_scaled_data = [origin T];

% Export auto-scaled data
```

```

filename = 'FileName.xlsx';
writetable(auto_scaled_data, filename);

%% %% Optional: Generate PCA plot

labels = readtable("labels.xlsx");
class_num = table2array(labels(1:25,4)); % select desired range
percentage = table2cell(labels(:,2));

% Generate coefficient and scores from PCA

[coeff,score,latent,tsquared,explained,mu] = pca(autoscaled_data);

%% %% Optional: Create 2D PCA plot
pca_plot = gscatter(score(:,1), score(:,2), class_num);
xlabel('PC 1');
ylabel('PC 2');
set(pca_plot,'markersize', 50);
legend('Bulgaria', 'Turkey', 'Morocco', 'other', 'Iran');
x = 1:25;
x = transpose(x);
text(score(:,1)+1, score(:,2)+1, num2str(x));

%% %% Optional: Create 3D PCA plot
% classifier = class_num;
% colour_plot = zeros(length(classifier),3);
%
% for k = 1:length(classifier)
%     if classifier(k) == 1;
%         colour_plot(k,:) = [0 0.4470 0.7410];
%     elseif classifier(k) == 2;
%         colour_plot(k,:) = [0.8500 0.3250 0.0980];
%     elseif classifier(k) == 3;
%         colour_plot(k,:) = [0.9290 0.6940 0.1250];
%     elseif classifier(k) == 4;
%         colour_plot(k,:) = [0.4940 0.1840 0.556];
%     else
%         colour_plot(k,:) = [0.4660 0.6740 0.1880];
%     end
% end
%
% pca_plot_2 = scatter3(score(:,1), score(:,2), score(:,3), [],
colour_plot,'filled');
% xlabel('PC 1');
% ylabel('PC 2');
% zlabel('PC 3');
%
%% %% Optional: Create loading plot
%
% plot(wavenumbers, coeff(:,1));
% hold on
% plot(wavenumbers, coeff(:,2));
% set(gca, 'XDir', 'reverse');
% xlabel('wavenumber [cm-1]');
% ylabel('loading');
% legend('PC 1', 'PC 2');
% xlim([650 4000]);

```

```

% plot(wavenumbers, autoscaled_data);
% set(gca, 'xdir', 'reverse');
% xlim([650 4000]);
% xlabel('wavenumber [cm-1]');
% ylabel('transmission');

```

Pre-processing: Standard Normal Variate (SNV)

```

%% Standard normal variate

% Import dataframes

origin = readtable('Table with the Origin of the oils as Excel file');
df = readmatrix('Dataframe matrix as Excel file');

wavenumbers = df(1,:); % Extract x-axis
df_reduced = df(2:end,:); % Optional, can be used if df includes strings

% Calculate mean of each row

av_row = mean(df_reduced,2);

% denominator of equation

delta_value_mean = df_reduced - av_row;
delta_value_mean_square = delta_value_mean.^2;
sum_delta_value_mean_square = sum(delta_value_mean_square,2);
wavelength_points = length(wavenumbers)-1;

denominator = sqrt(sum_delta_value_mean_square ./ wavelength_points);

SNV = delta_value_mean ./ denominator;

%% Export data

variables_data = [wavenumbers; SNV];
T = table(variables_data);
normalized_data_variables = [origin T];

filename = 'FileName.xlsx';
writetable(normalized_data_variables, filename);
clear all

```

Pre-processing: Mean centering

```
%% Mean centering data

origin = readtable('Table with the Origin of the oils as Excel file');
df = readmatrix('Dataframe matrix as Excel file');

wavenumbers = df(1,:);
transmission = df(2:end,:);

% calculate each mean per column

means_columns = zeros(1, length(wavenumbers));

for k = 1 : length(wavenumbers);
    average = mean(transmission(:,k));
    means_columns(k) = average;
end

% subtract each column by the means value

mean_centered = transmission - means_columns;
```

Pre-processing: Normalize by maximum value

```
%% Normalize by maximum value

origin = readtable('Table with the Origin of the oils as Excel file');
df = readmatrix('Dataframe matrix as Excel file');

wavenumbers = df(1,:);
df_reduced = df(2:end,:);

%% find maximum value in each dataset

max_val = zeros(length(df_reduced(:,1)),1);

for k = 1:length(max_val);
    x = max(df_reduced(k,:));
    max_val(k) = x;
end

max_normalized_data = df_reduced ./ max_val;

%% export data

variables_data = [wavenumbers; max_normalized_data];
T = table(variables_data);
normalized_data_variables = [origin T];

filename = 'normalized_by_max_data.xlsx';
writetable(normalized_data_variables, filename);
```

Pre-processing: Normalize by Sum

```
%% Normalize data by sum

origin = readtable('Table with the Origin of the oils as Excel file');
df = readmatrix('Dataframe matrix as Excel file');

wavenumbers = df(1,:);
df_reduced = df(2:end,:);

%% calculate sum of each observation

sum_obs = zeros(length(df_reduced(:,1)),1);

for k = 1:length(sum_obs);
    x = sum(df_reduced(k, :));
    sum_obs(k) = x;
end

df_normalized = df_reduced ./ sum_obs;

%% export data to excel file

variables_data = [wavenumbers; df_normalized];
T = table(variables_data);
normalized_data_variables = [origin T];

filename = 'FileName.xlsx';
writetable(normalized_data_variables, filename);
```

Pre-processing: Savitzky-Golay Smoothing

```
%% Savitzky Golay Smoothing
% import data set, columns are wavenumbers and rows observations (for e.g. FT-IR)
% requires Signal Processing Toolbox version 9.1

origin = readtable('Table with the Origin of the oils as Excel file');
df = readmatrix('Dataframe matrix as Excel file');

wavenumbers = df(1,:);
transmission = df(2:end,:);

%% Smoothing function
sgf_smoothed = zeros(length(transmission(:,1)), length(transmission(1,:)));
order = 3;
framelen = 11;

for k = 1:length(transmission(:,1));
    sgf = sgolayfilt(transmission(k,:), order, framelen);
    sgf_smoothed(k,:) = sgf;
end

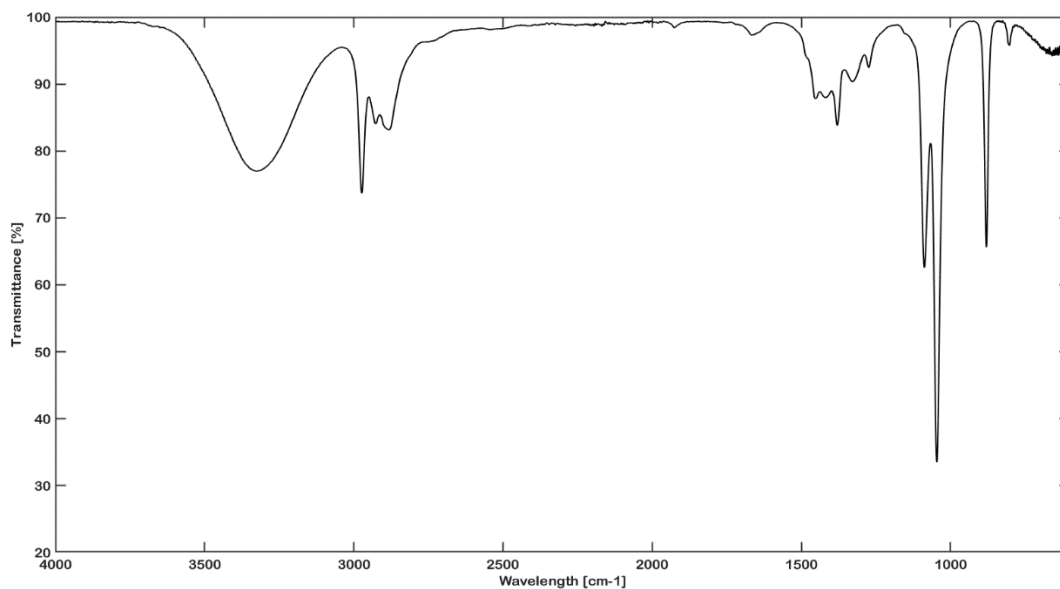
%% Export smoothed data

variables_data = [wavenumbers; sgf_smoothed];
T = table(variables_data);
```

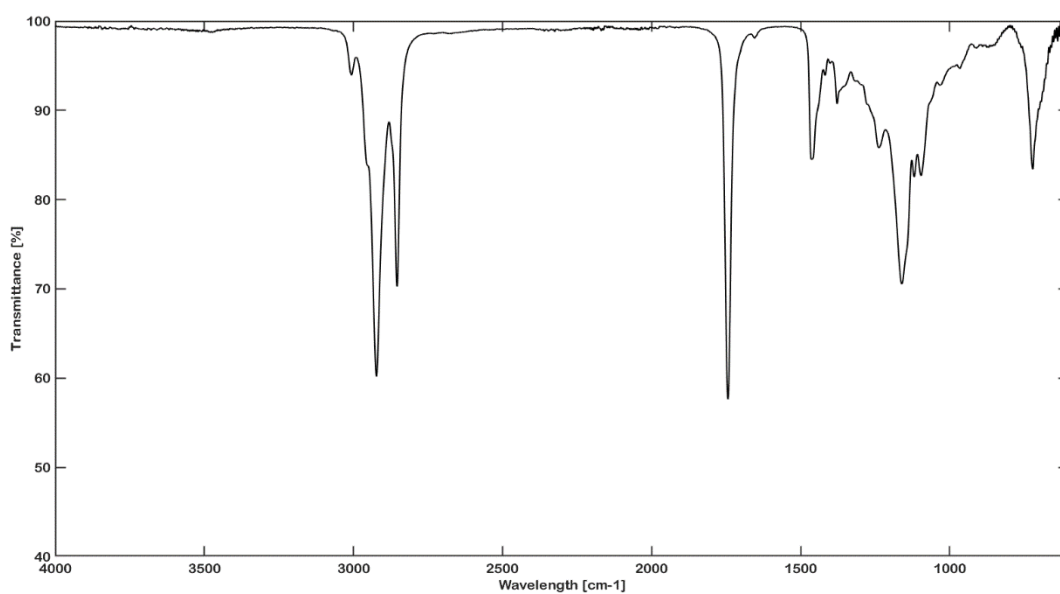
```
golay_smoothed_data = [origin T];  
filename = 'smoothed_data.xlsx';  
writetable(golay_smoothed_data, filename);
```

Figure A88: FT-IR spectra for predominantly *R. damascena* EOs used in chemometric study.

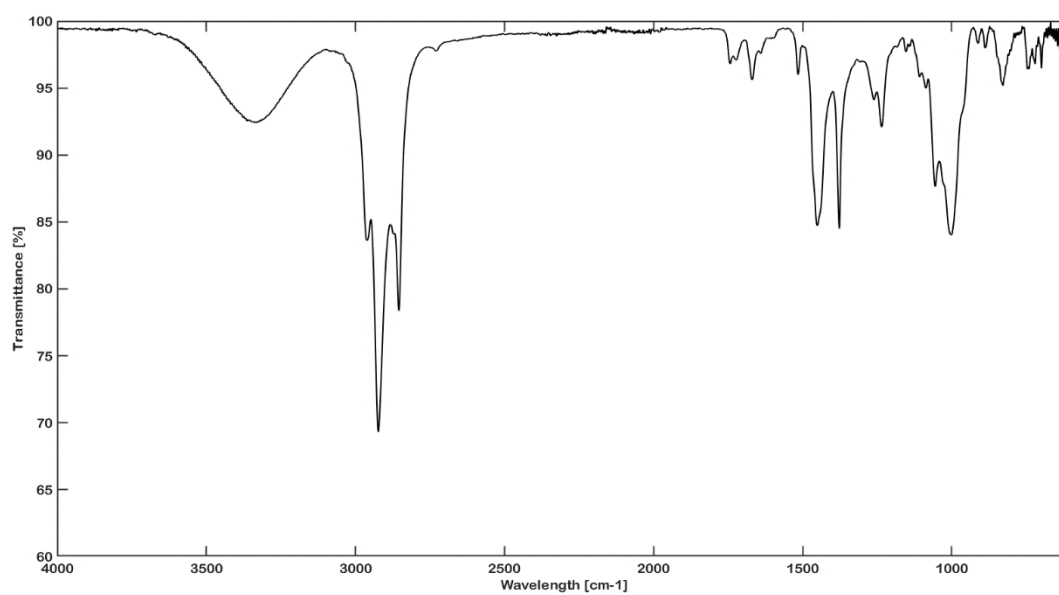
R. damascena Sample 1



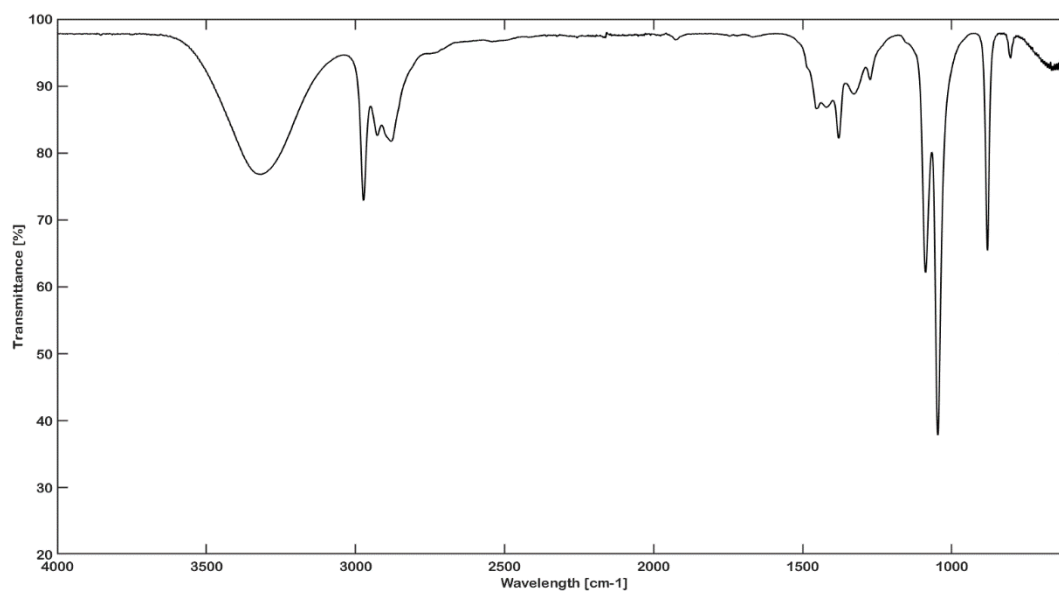
R. damascena Sample 2



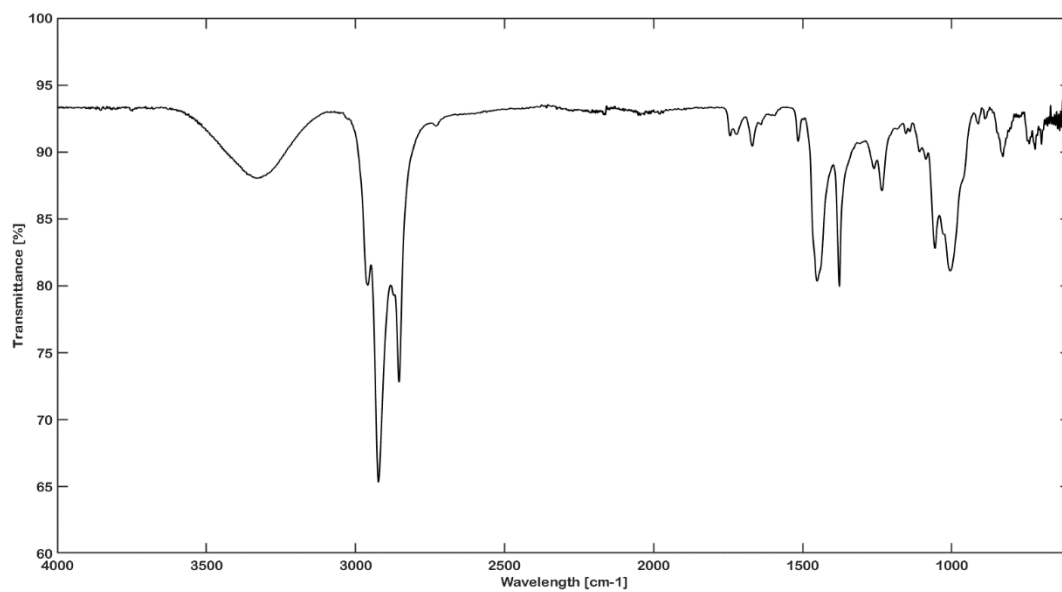
R. damascena Sample 3



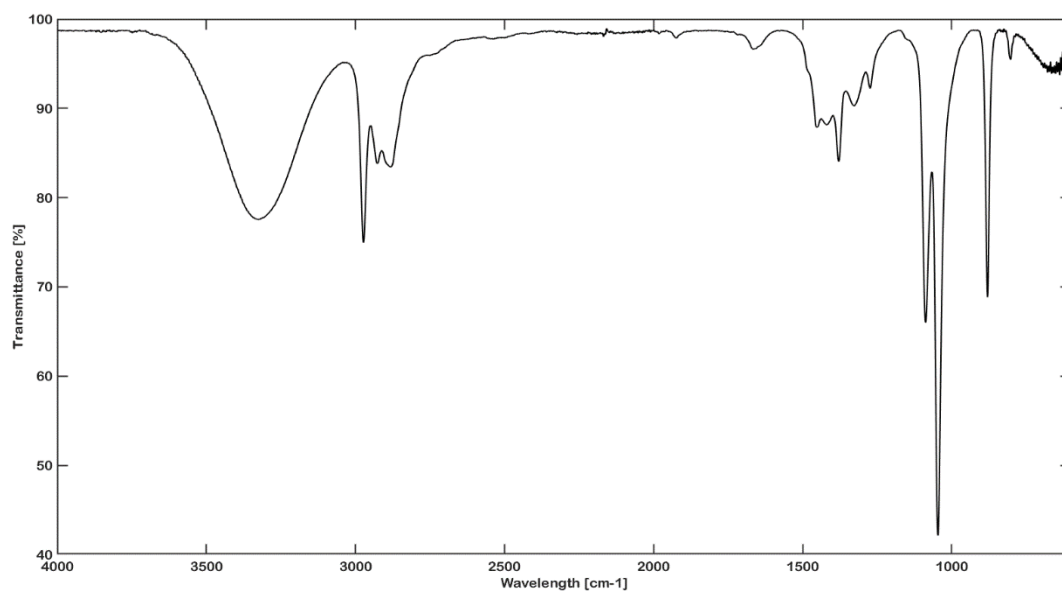
R. damascena Sample 4



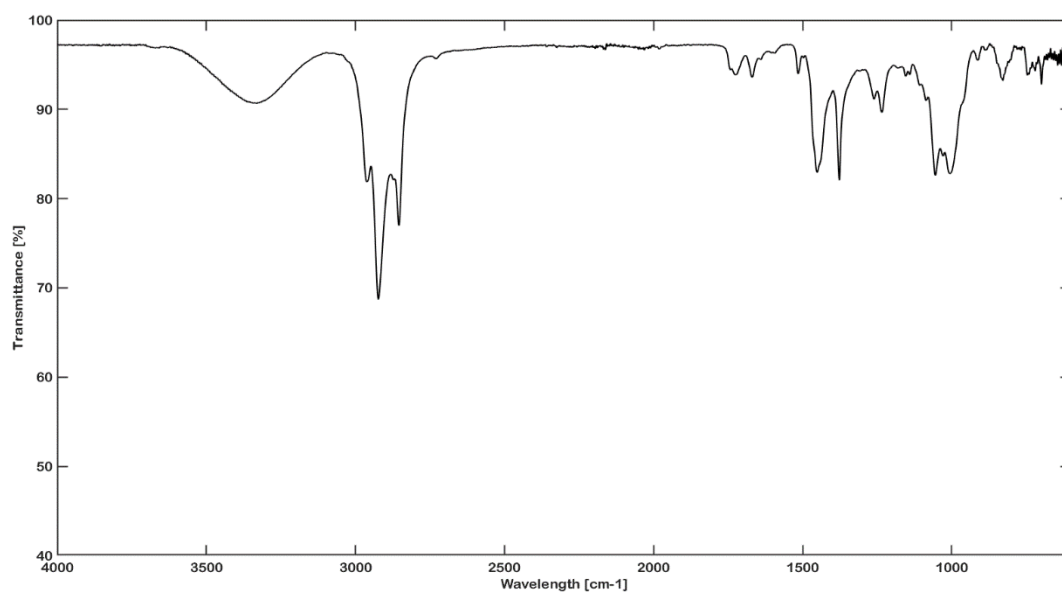
R. damascena Sample 5



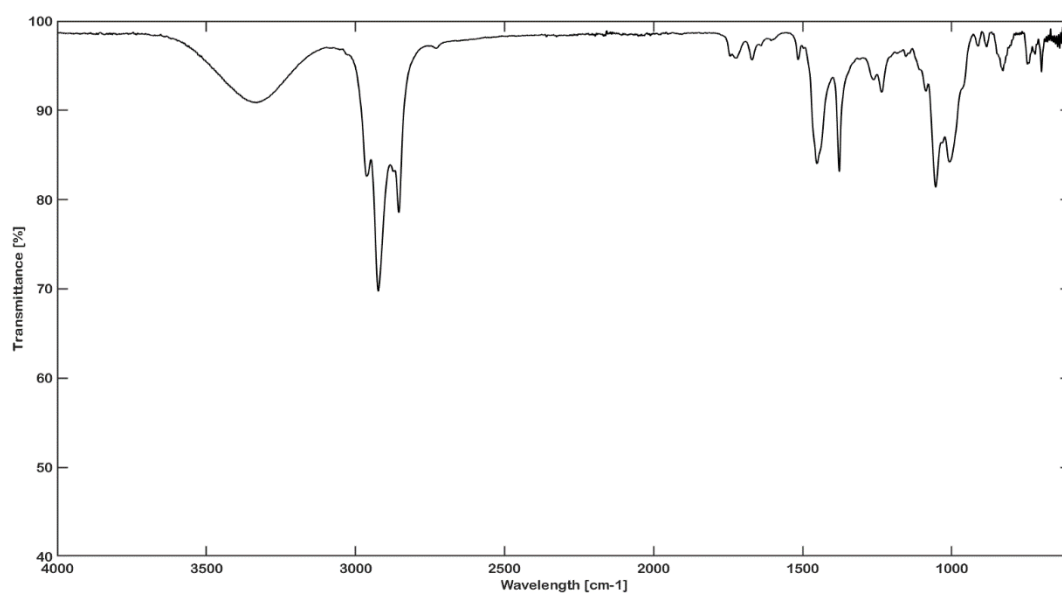
R. damascena Sample 6



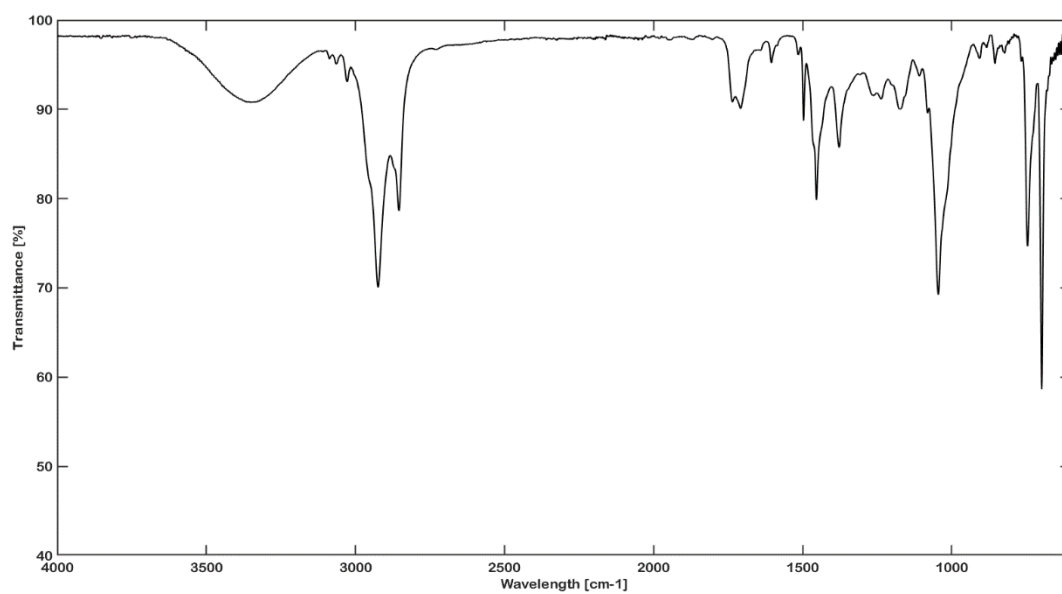
R. damascena Sample 7



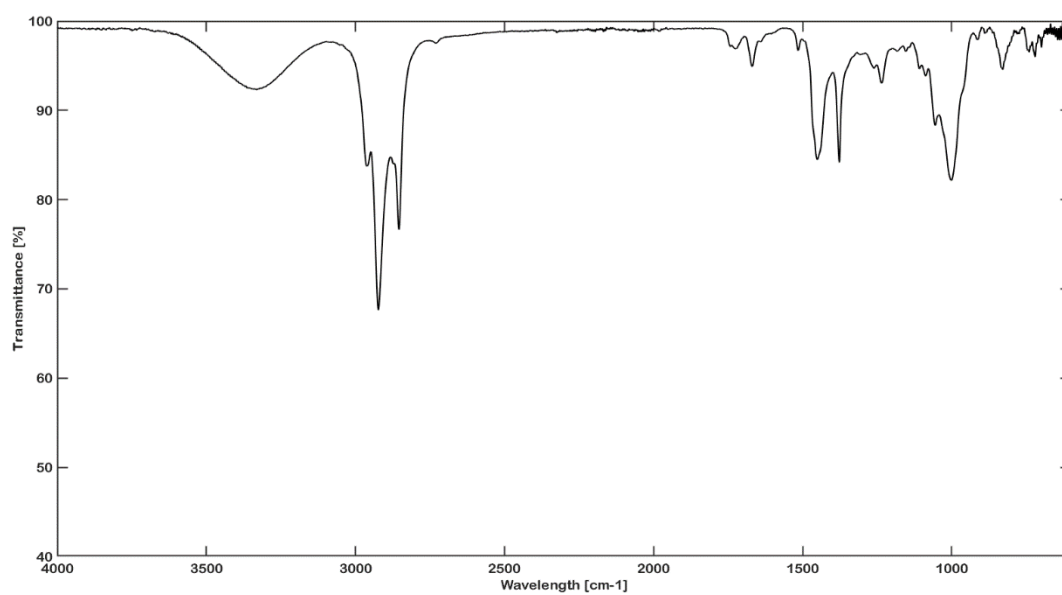
R. damascena Sample 8



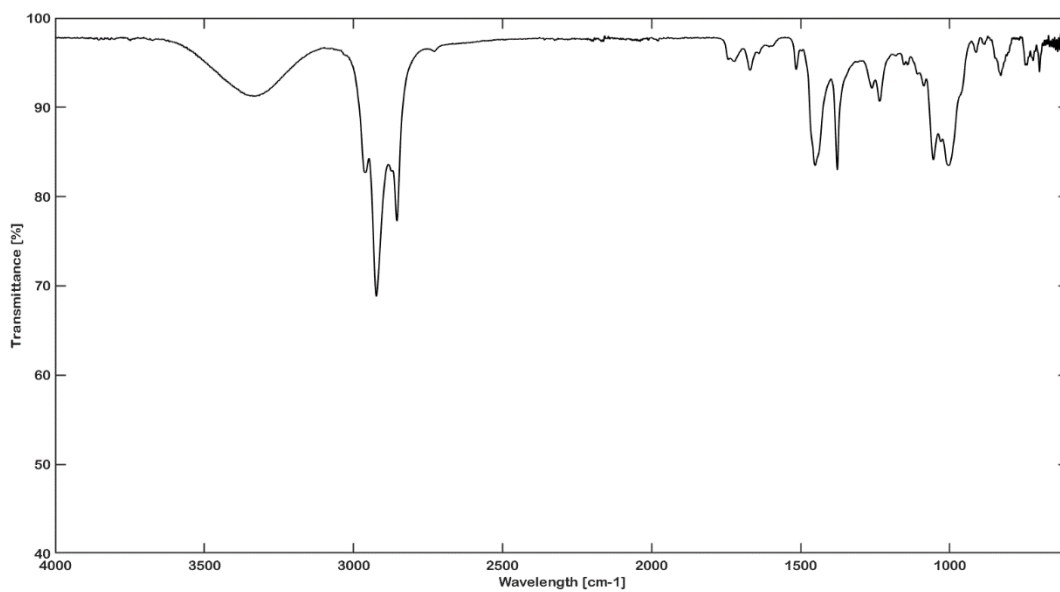
R. damascena Sample 9



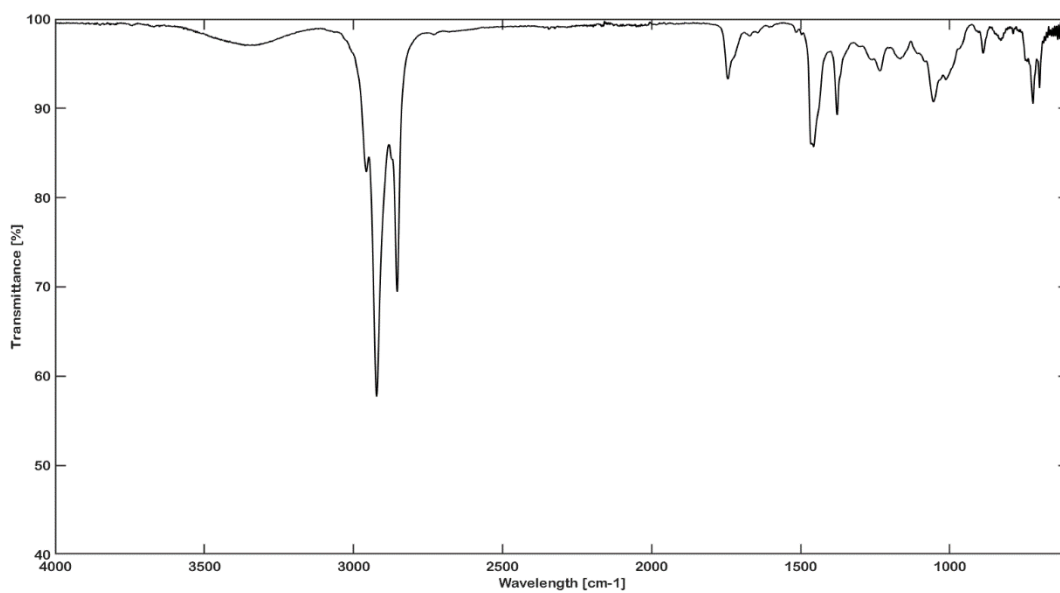
R. damascena Sample 10



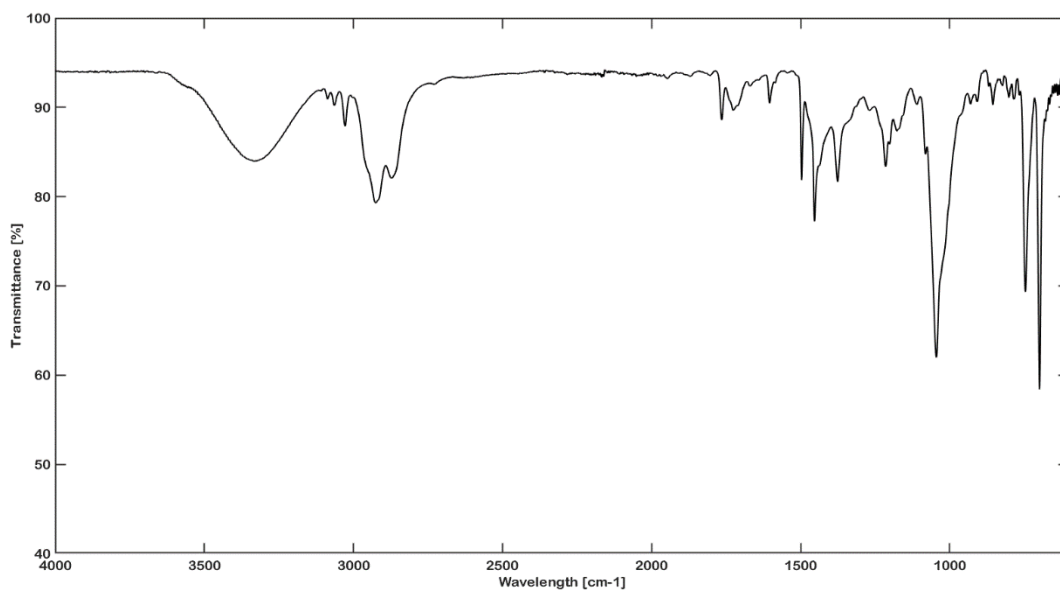
R. damascena Sample 11



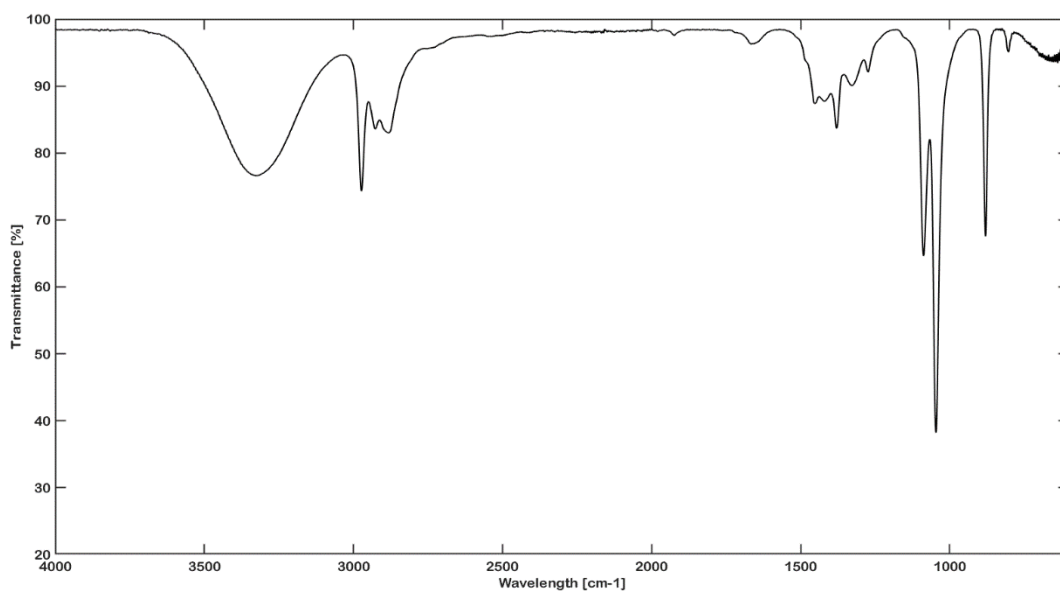
R. damascena Sample 12



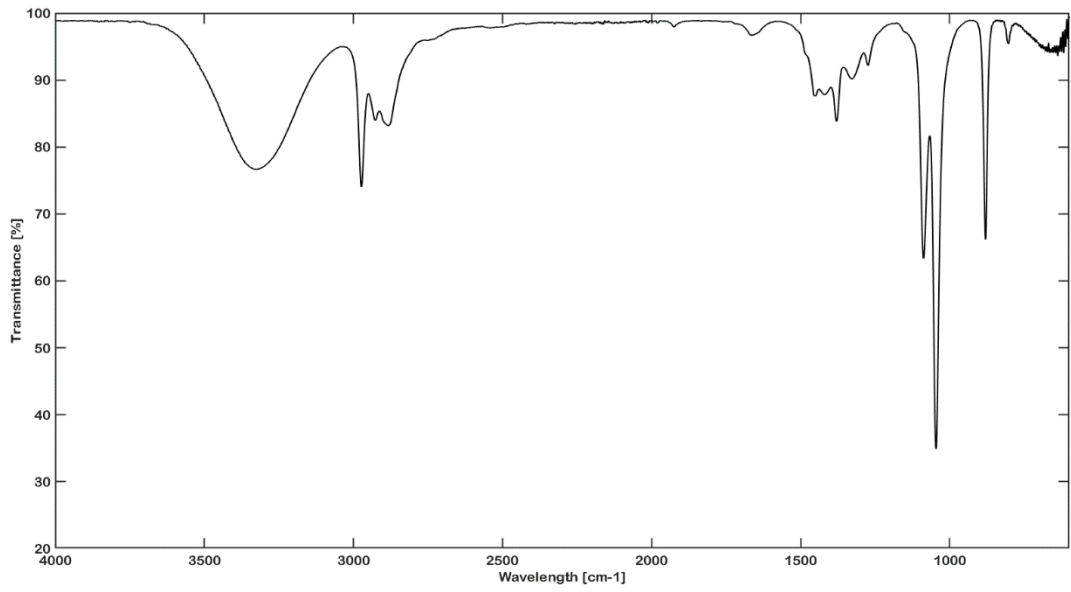
R. damascena Sample 13



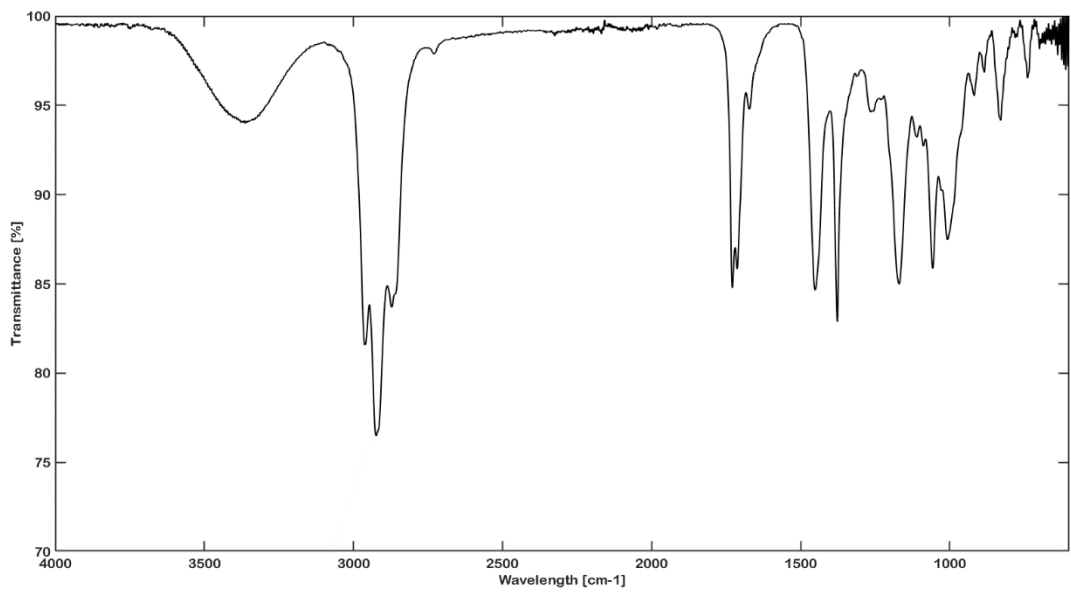
R. damascena Sample 14



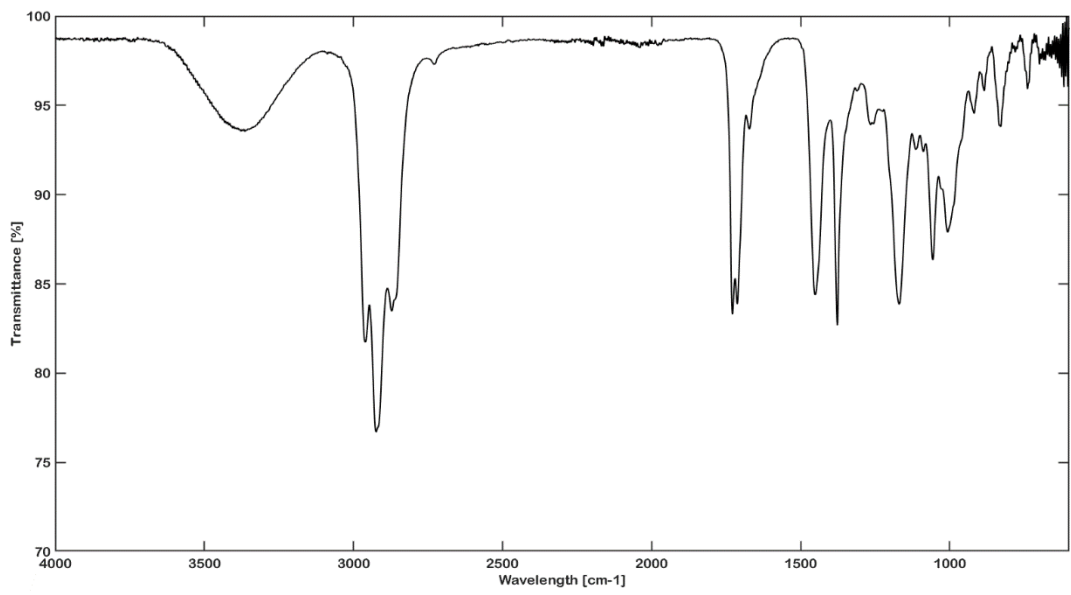
R. damascena Sample 15



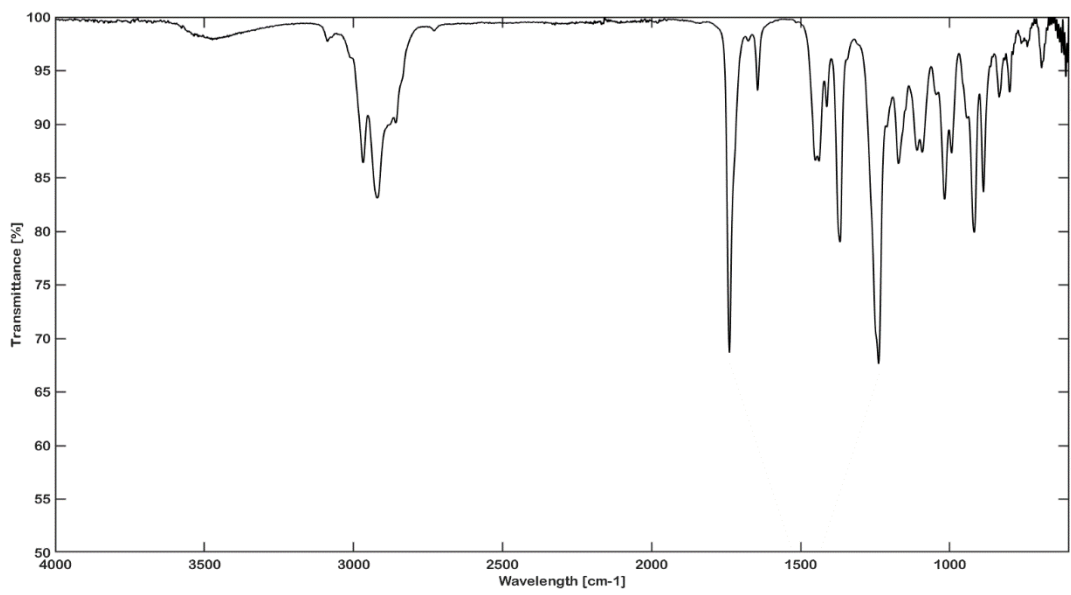
P. graveolens Sample 16



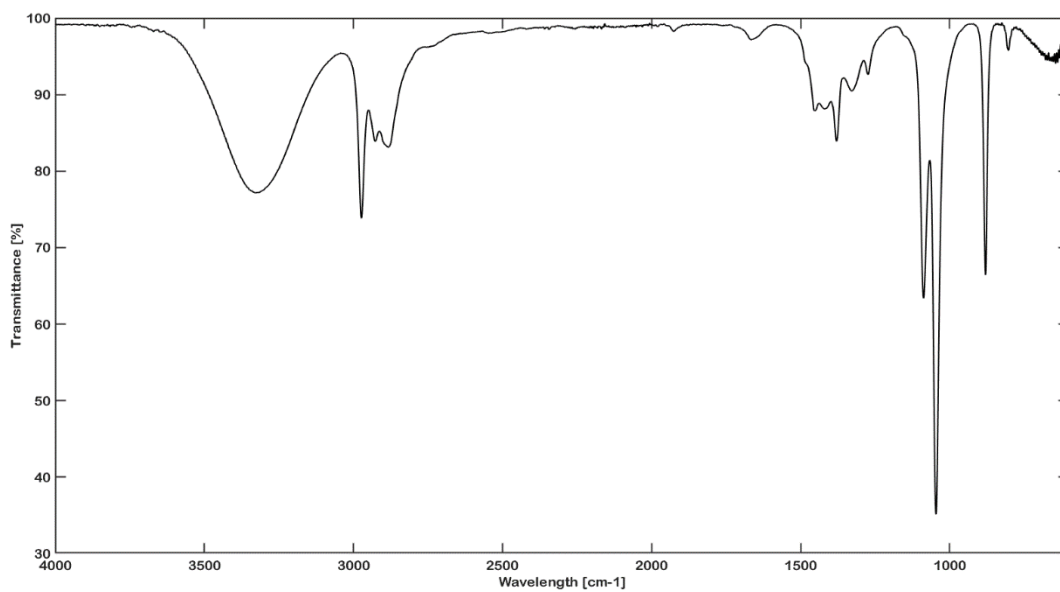
P. graveolens Sample 17



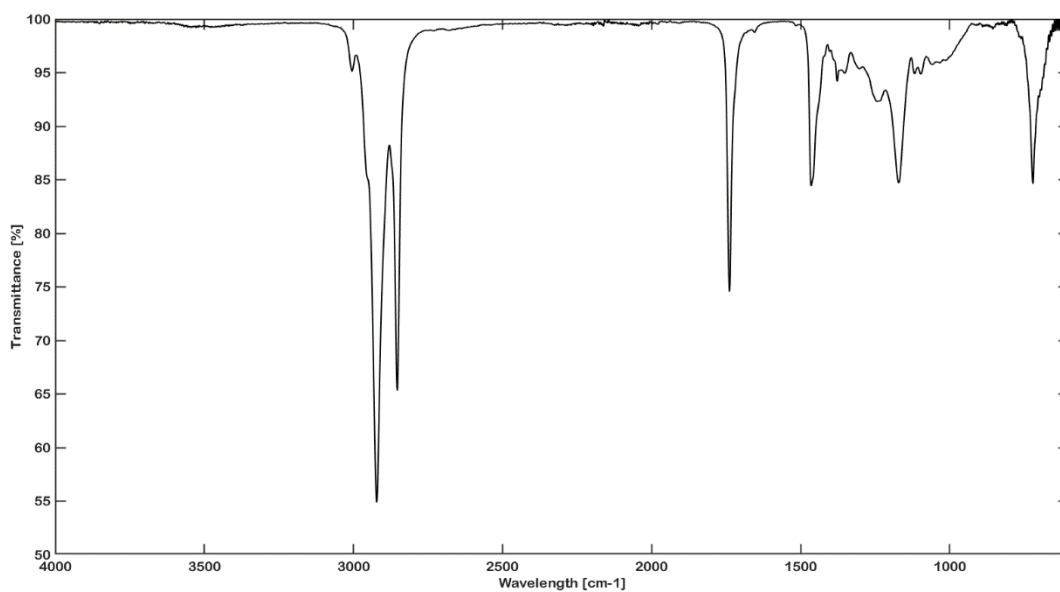
C. bergamia / *R. damascena* Sample 18



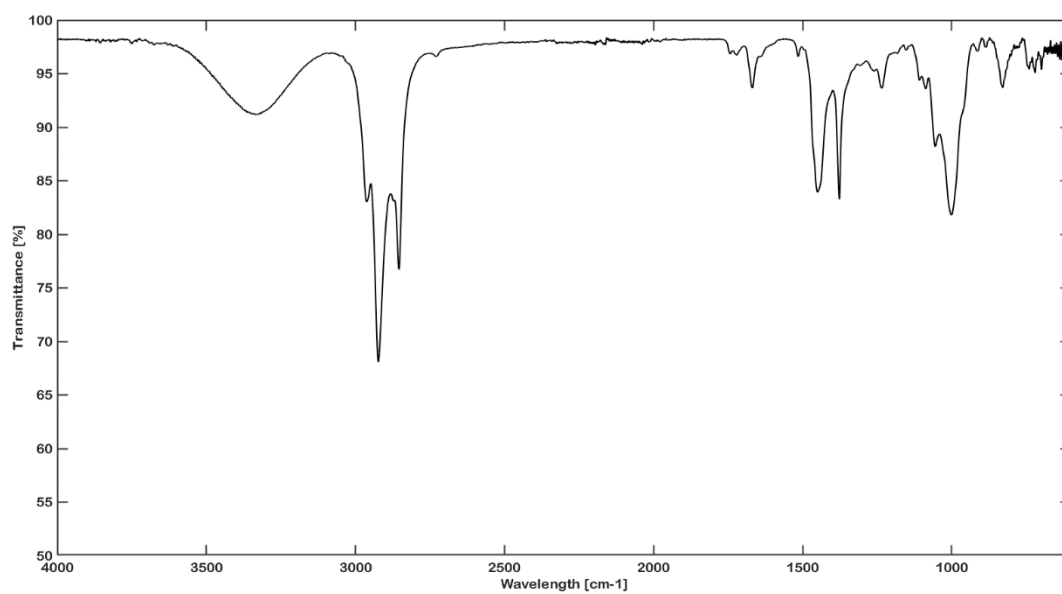
R. damascena Sample 19



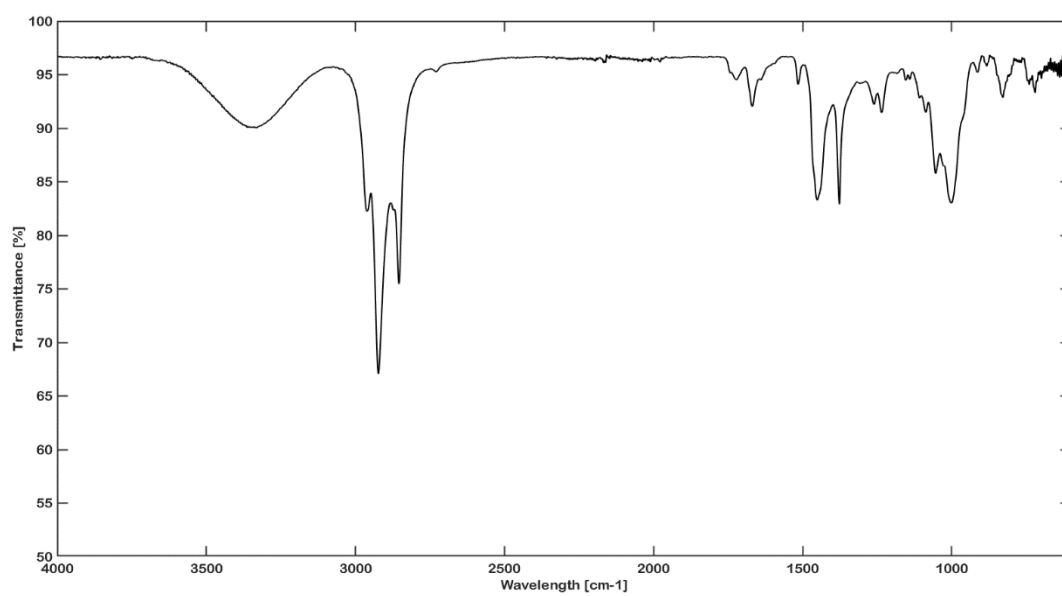
R. damascena Sample 20



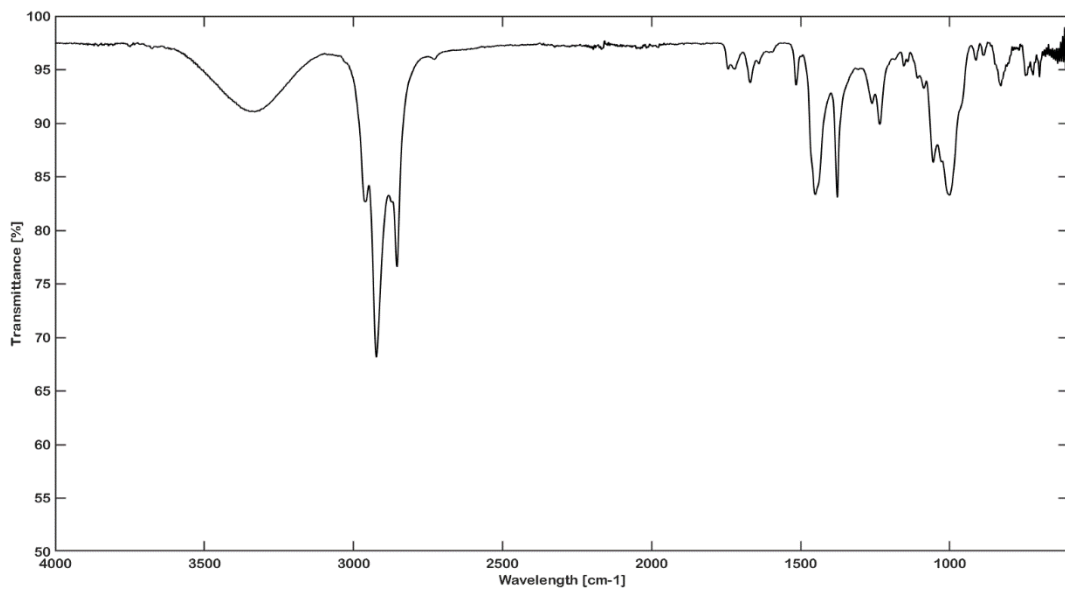
R. damascena Sample 21



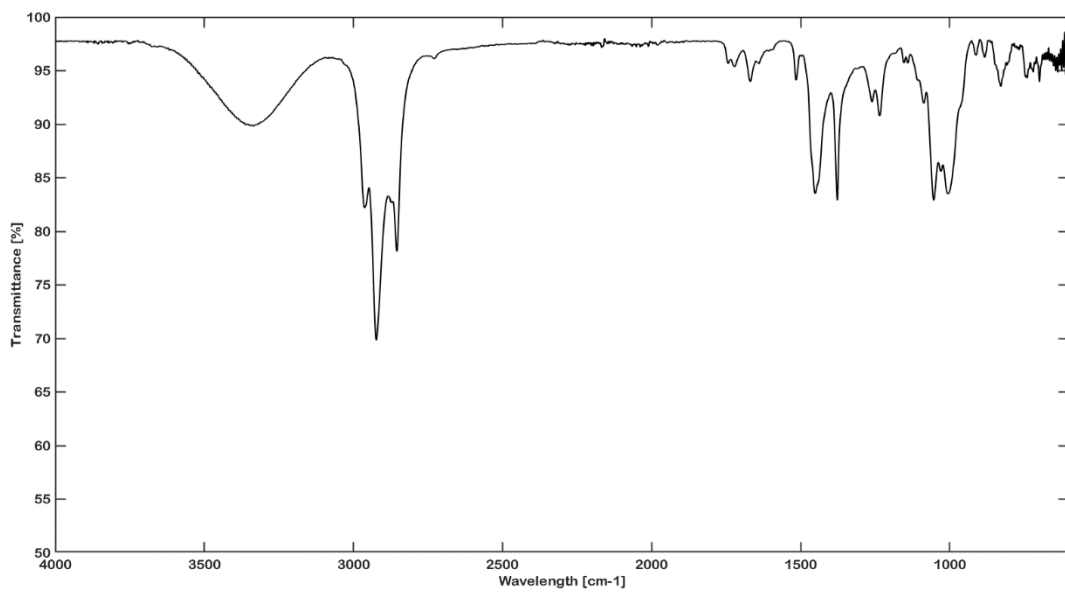
R. damascena Sample 22



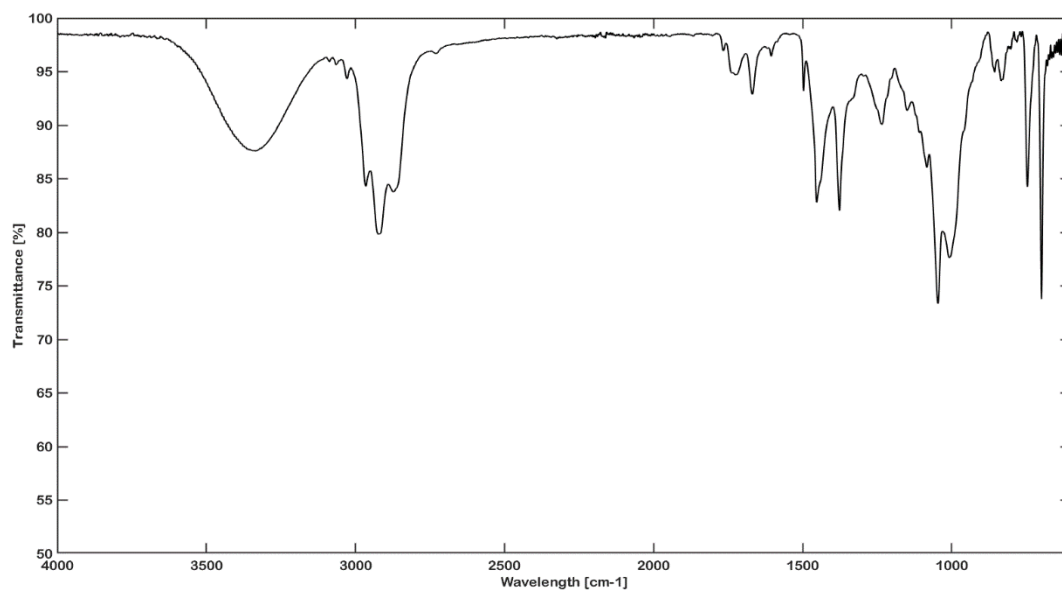
R. damascena Sample 23



R. damascena Sample 24



Synthetic Rose oil Sample 25



R. centifolia Sample 26

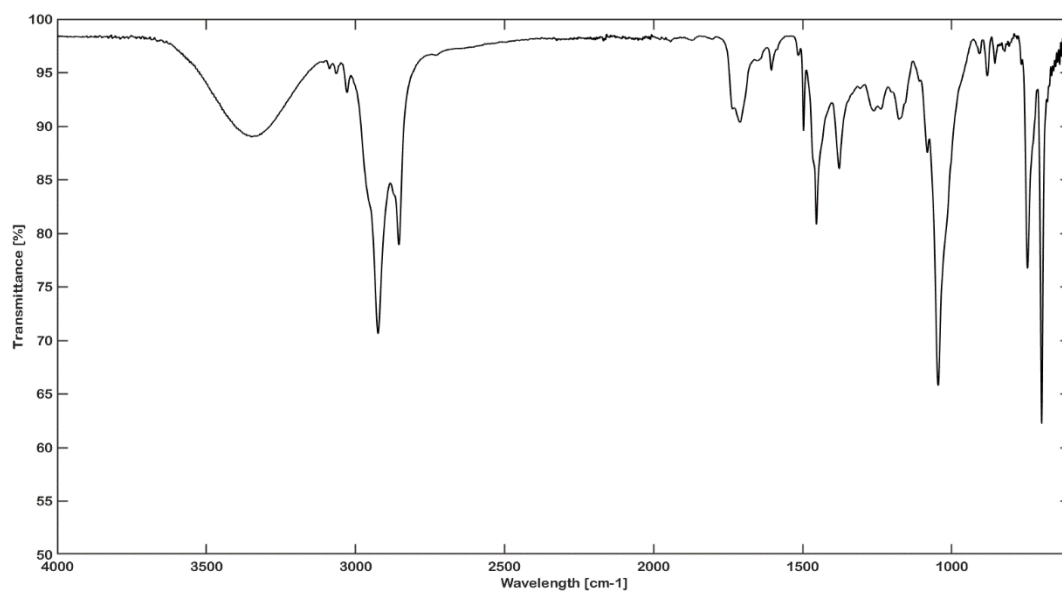
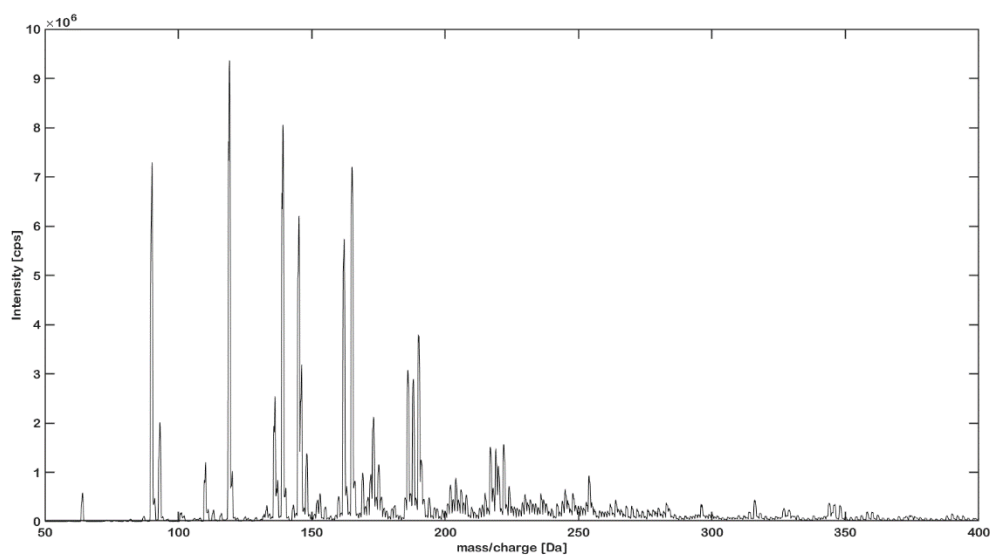
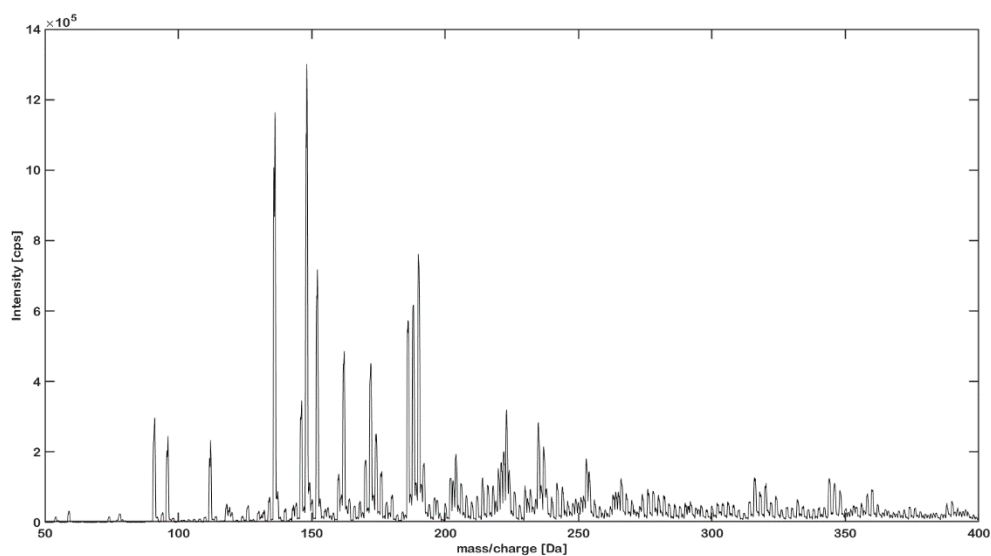


Figure A89: DBDI-Q1 spectra for predominantly *R. damascena* EOs used in chemometric study.

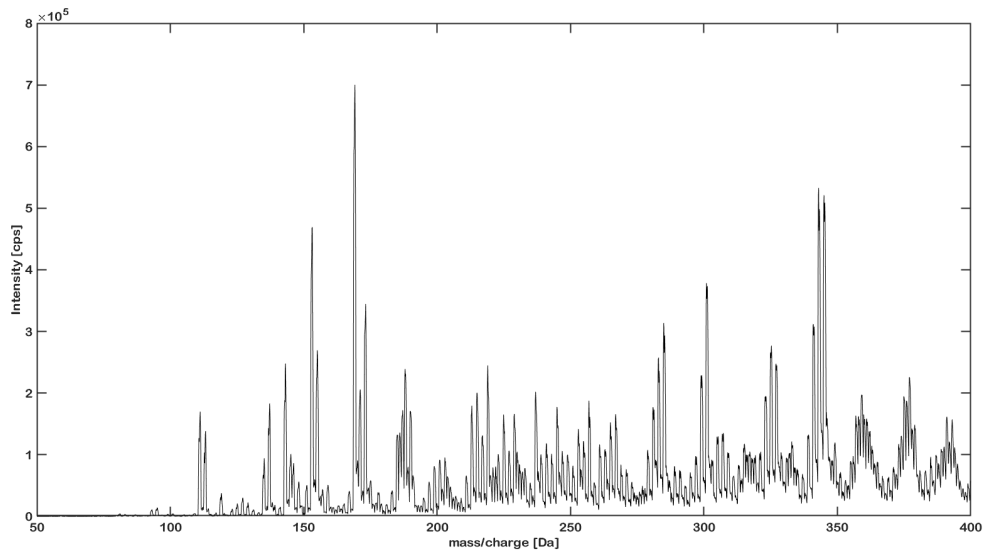
R. damascena Sample 1



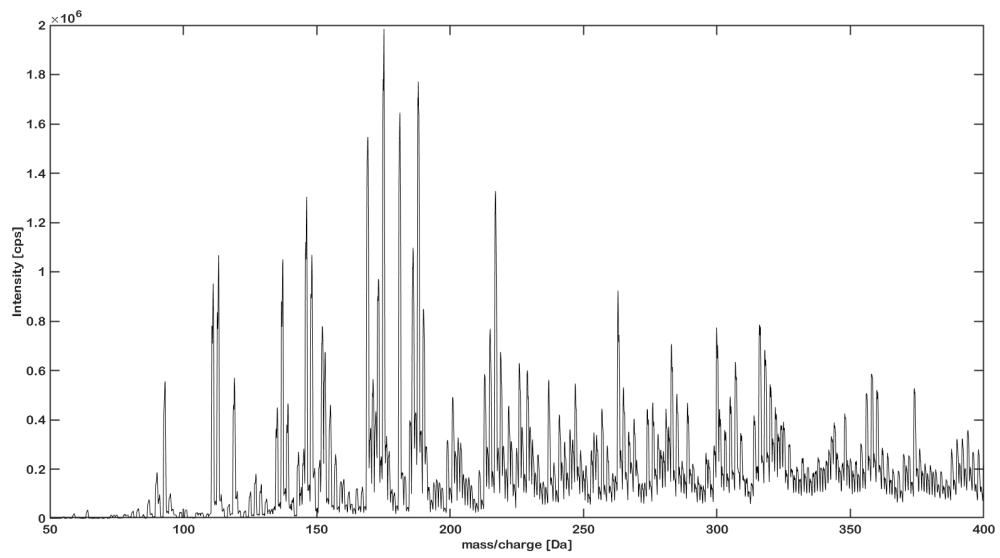
R. damascena Sample 2



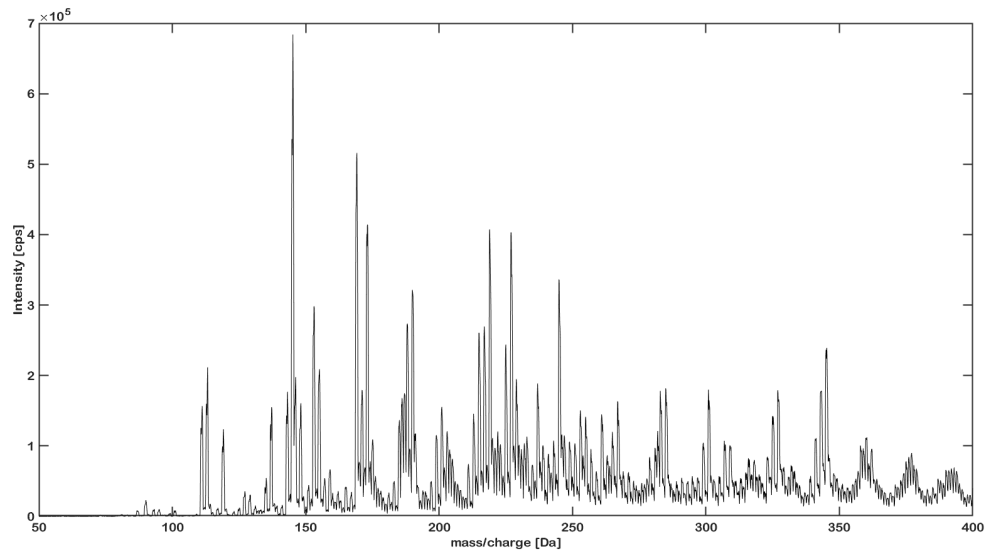
R. damascena Sample 3



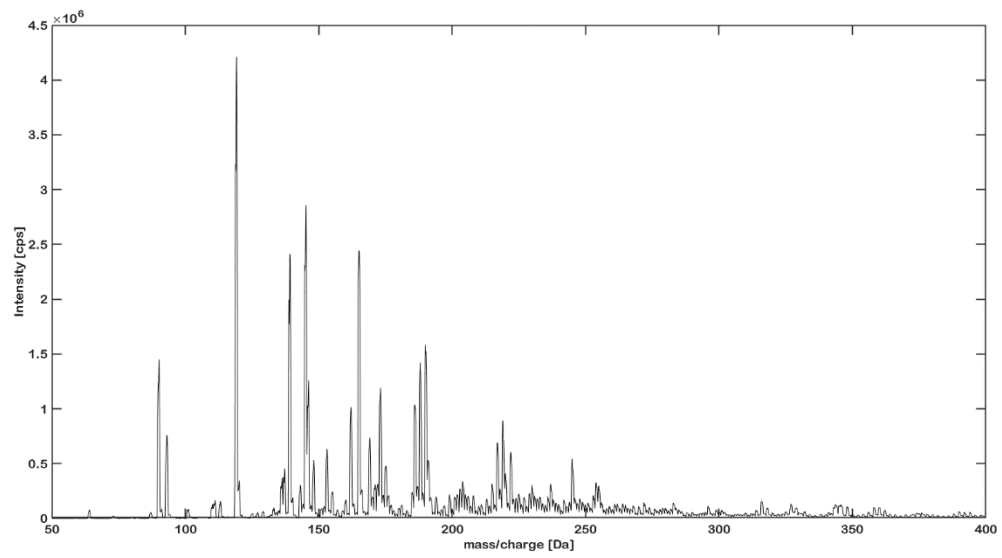
R. damascena Sample 4



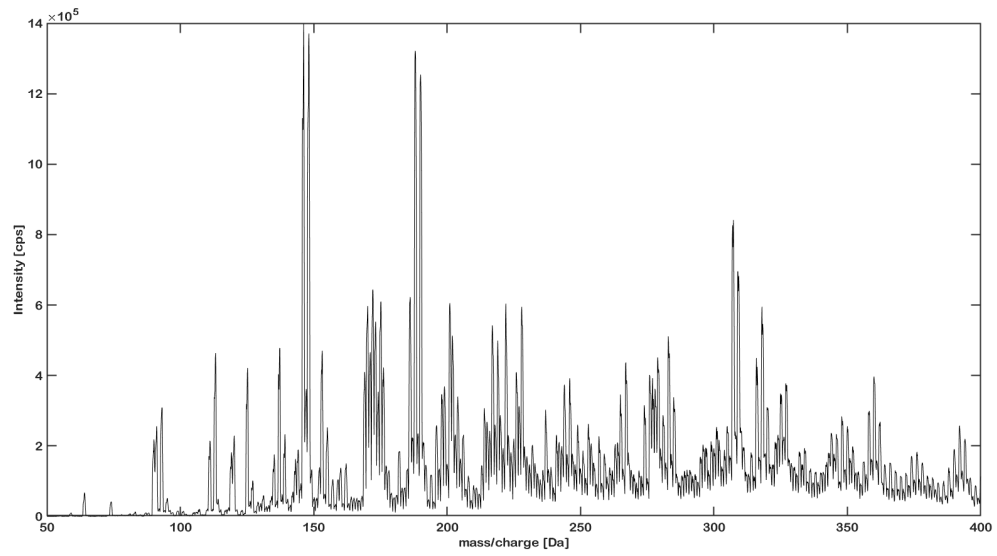
R. damascena Sample 5



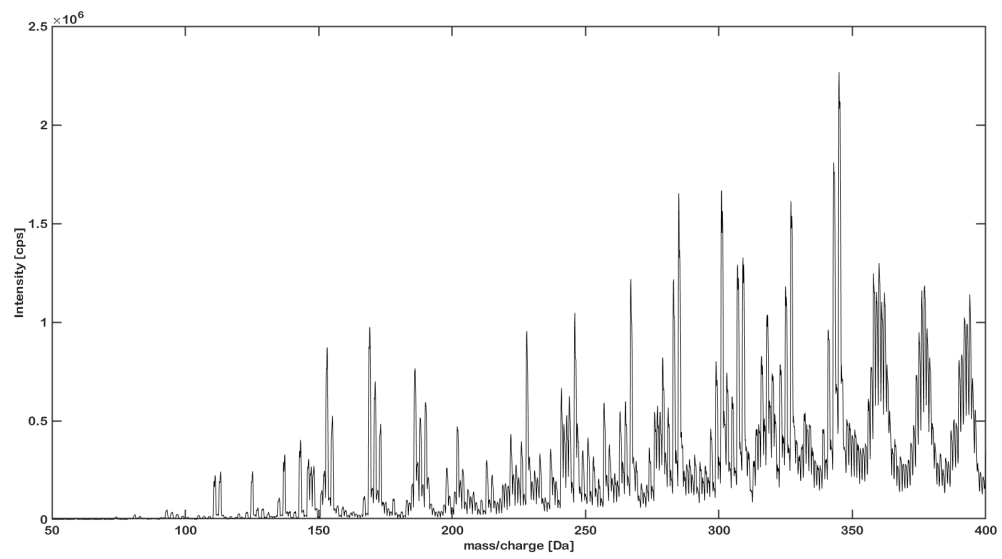
R. damascena Sample 6



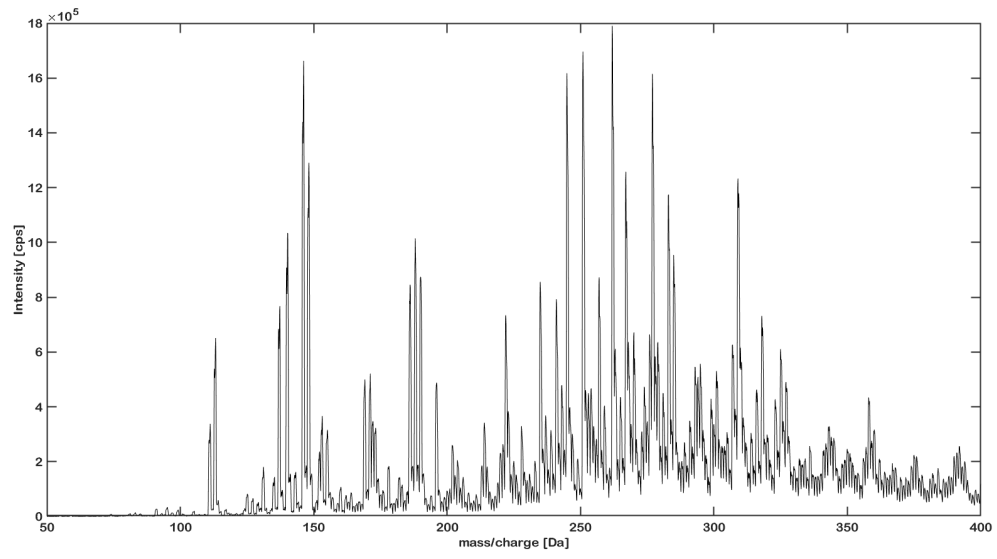
R. damascena Sample 7



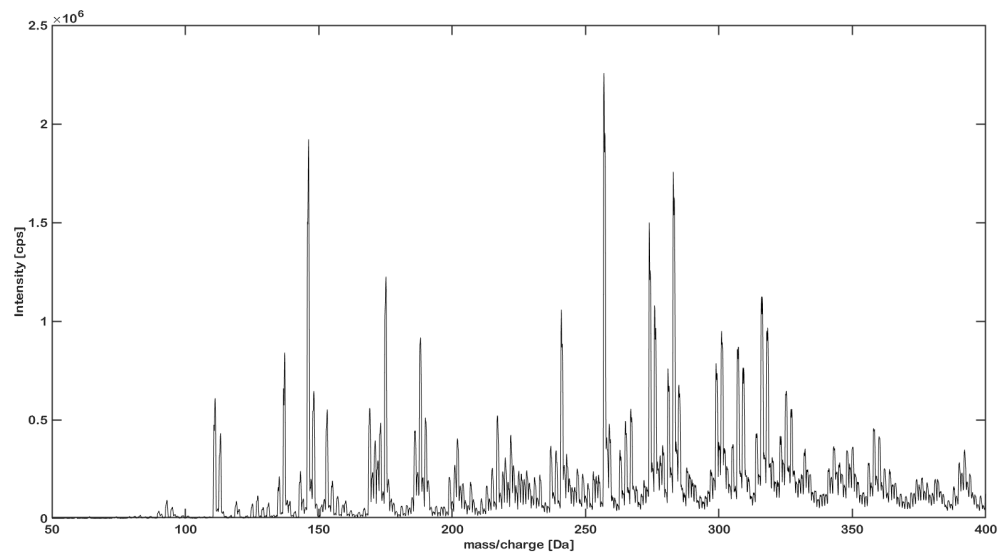
R. damascena Sample 8



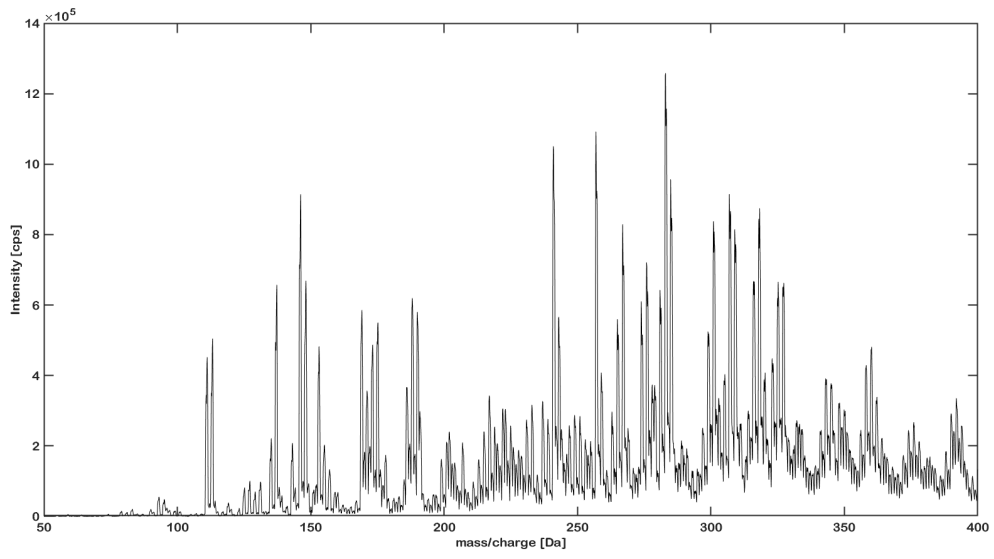
R. damascena Sample 9



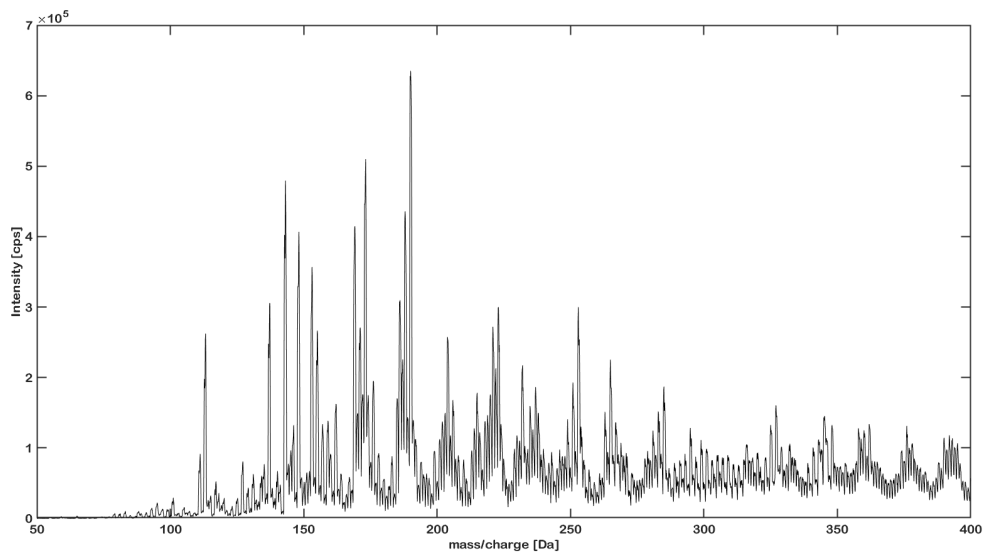
R. damascena Sample 10



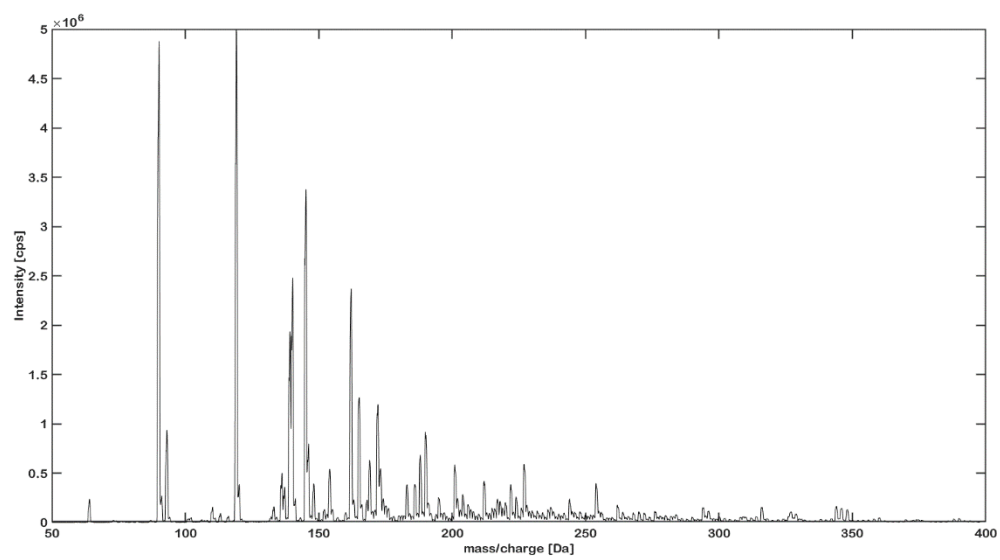
R. damascena Sample 11



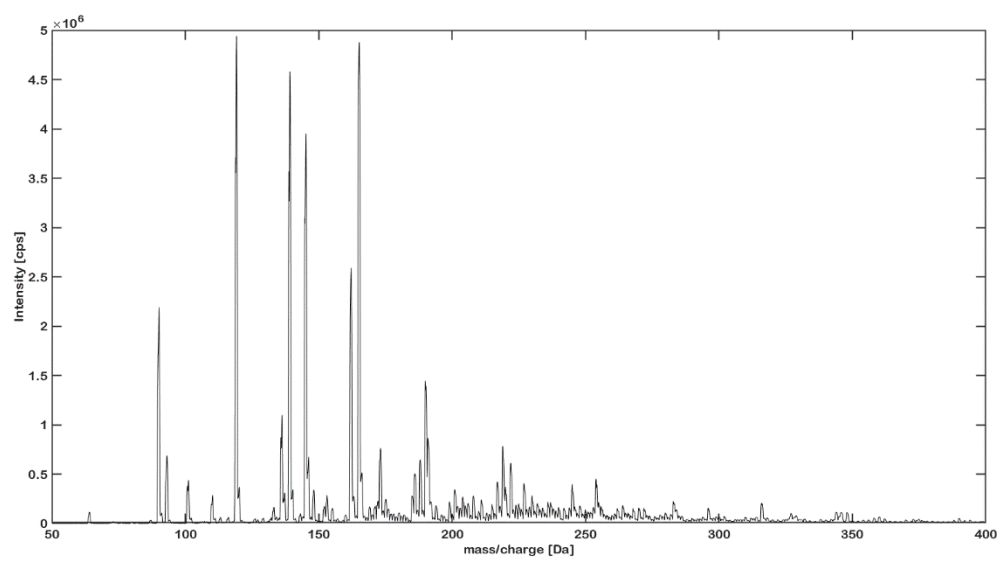
R. damascena Sample 12



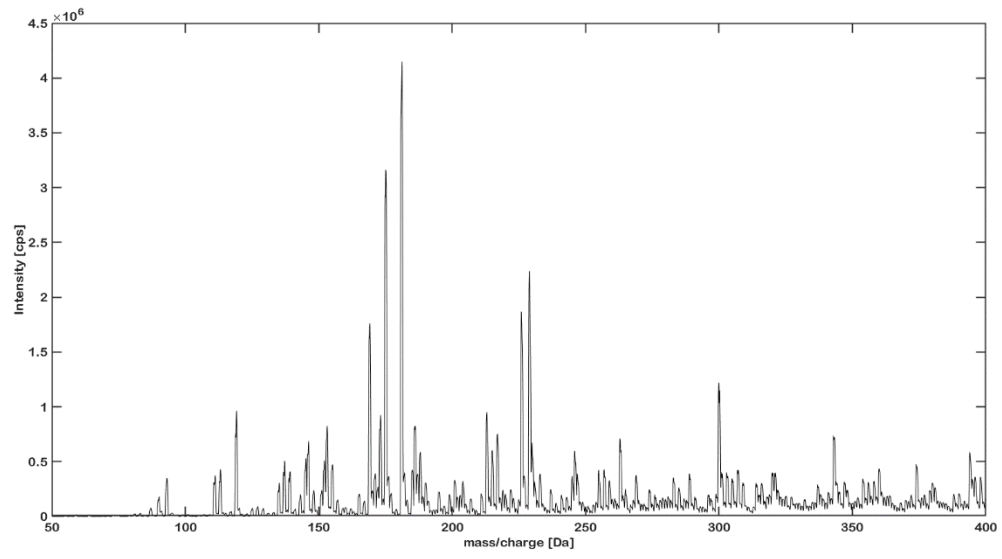
R. damascena Sample 13



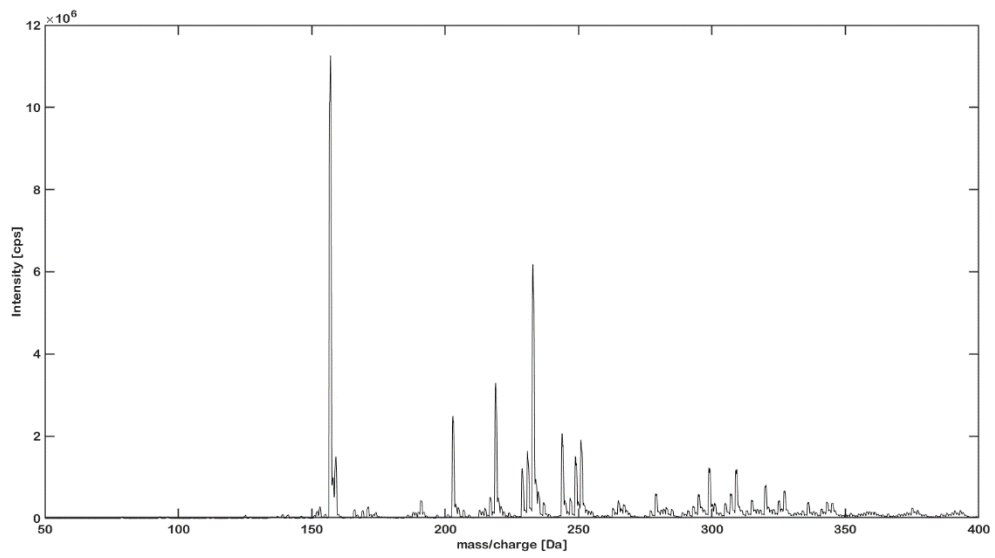
R. damascena Sample 14



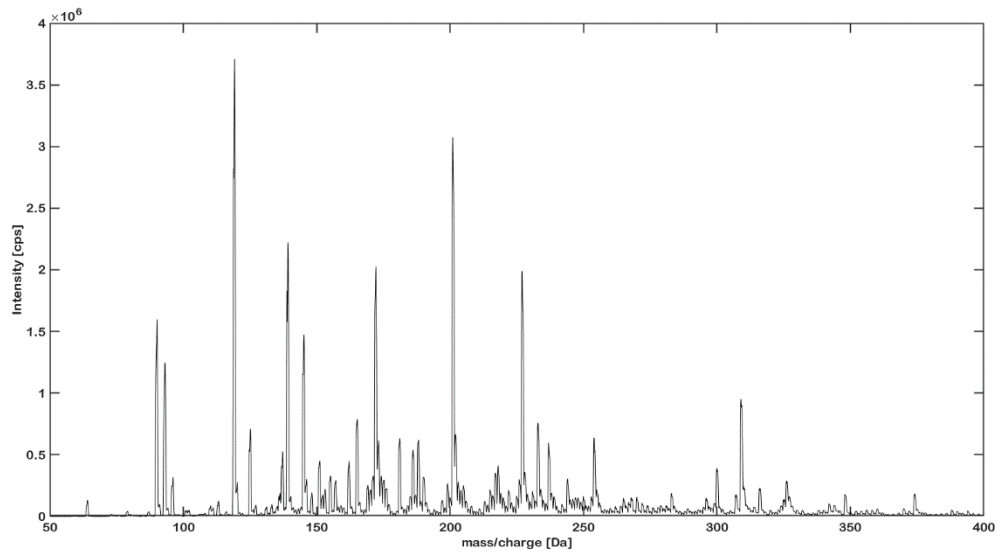
R. damascena Sample 15



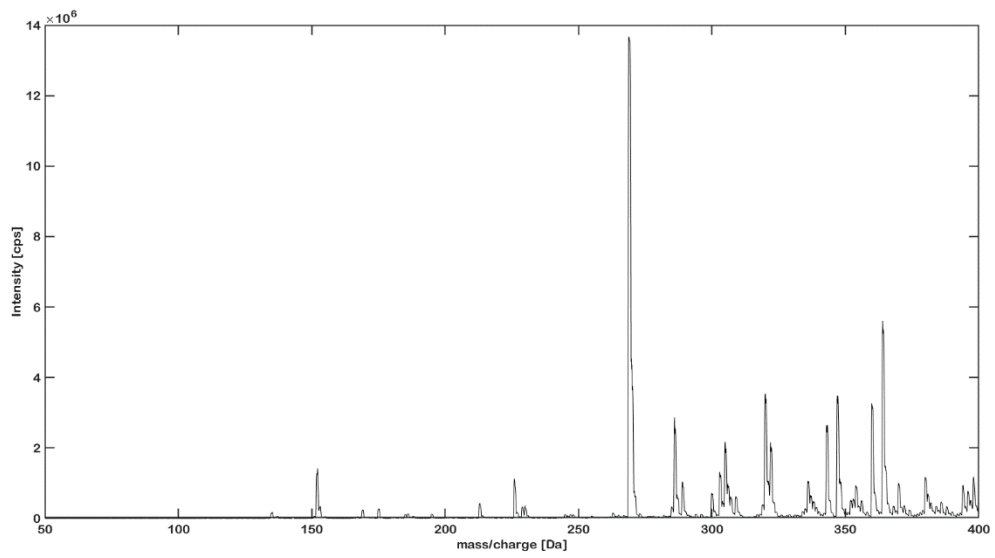
P. graveolens Sample 16



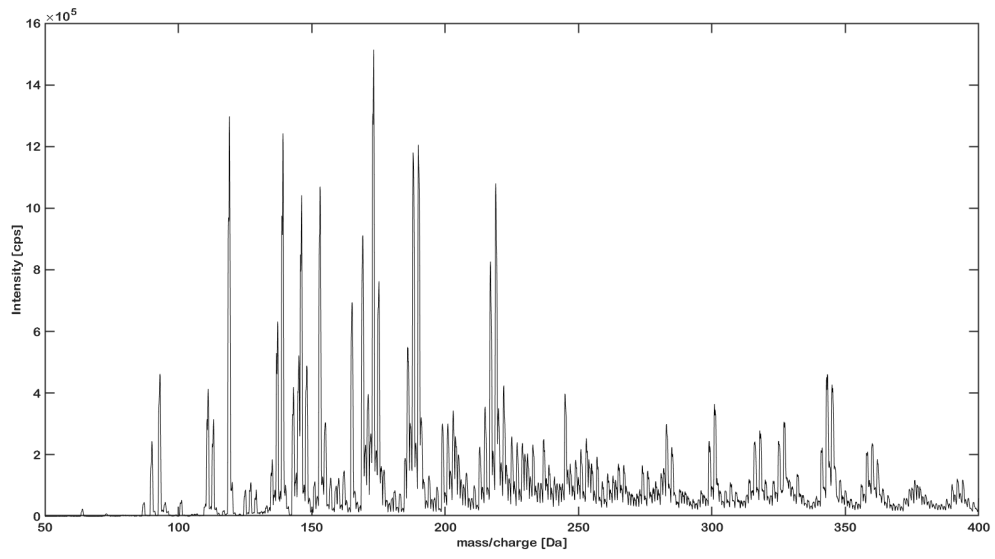
P. graveolens Sample 17



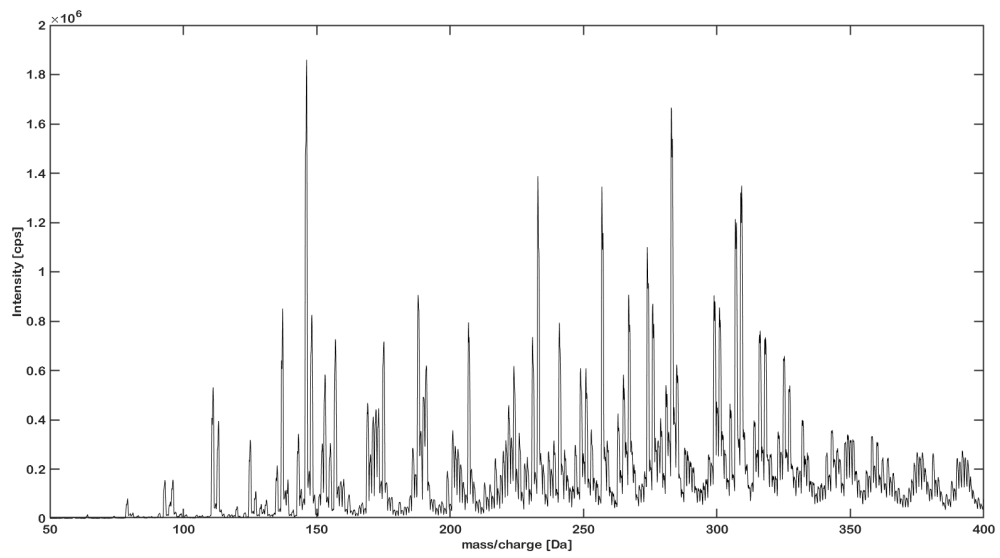
C. bergamia / *R. damascena* Sample 18



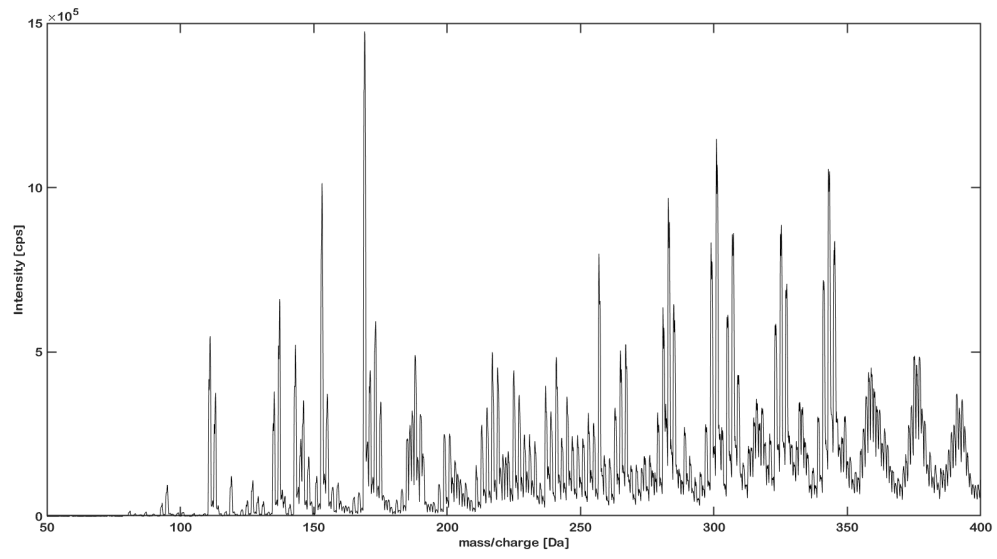
R. damascena Sample 19



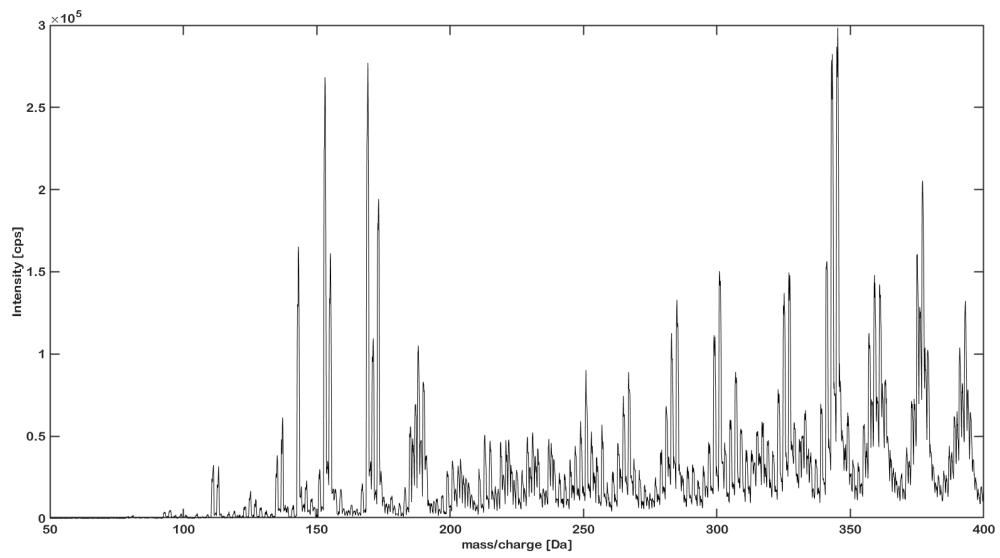
R. damascena Sample 20



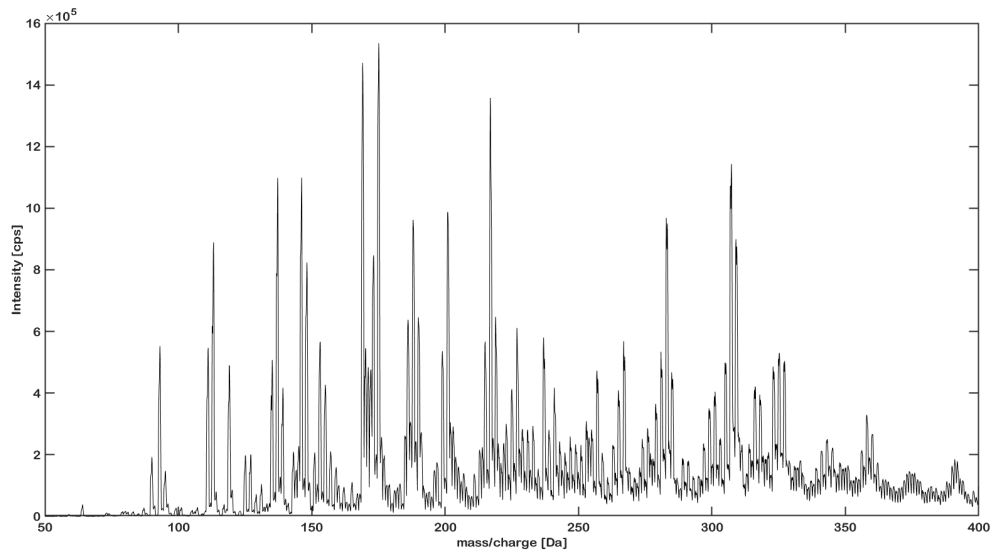
R. damascena Sample 21



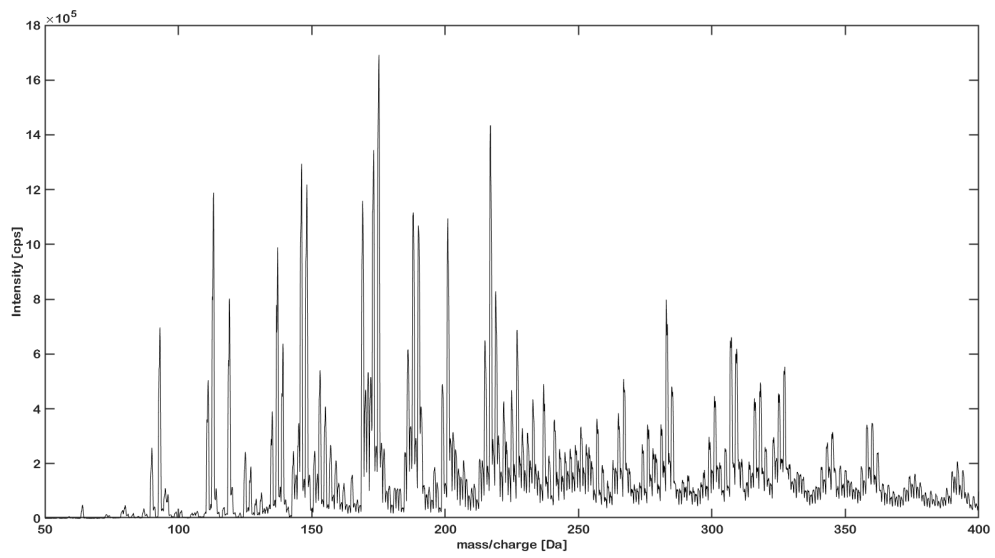
R. damascena Sample 22



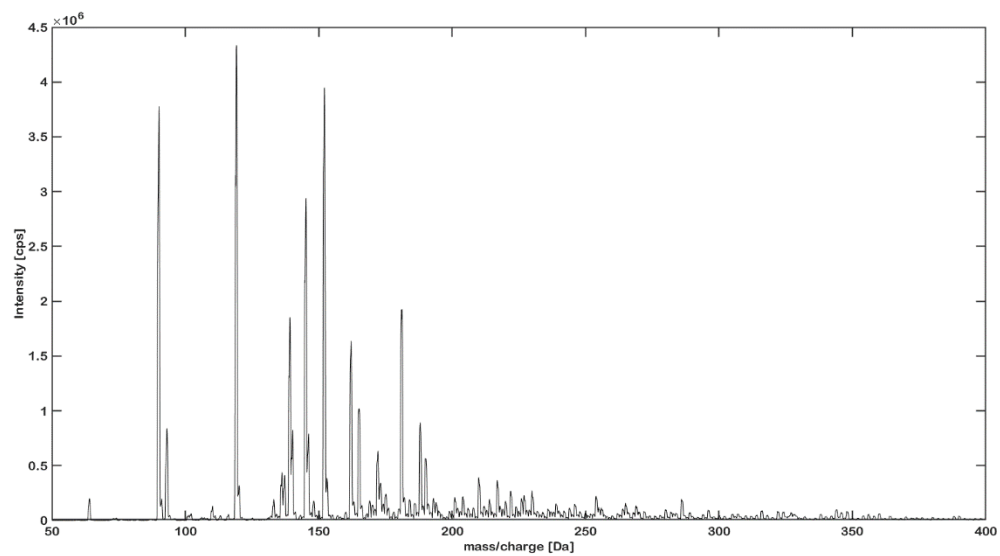
R. damascena Sample 23



R. damascena Sample 24



Synthetic Rose oil Sample 25



R. centifolia Sample 26

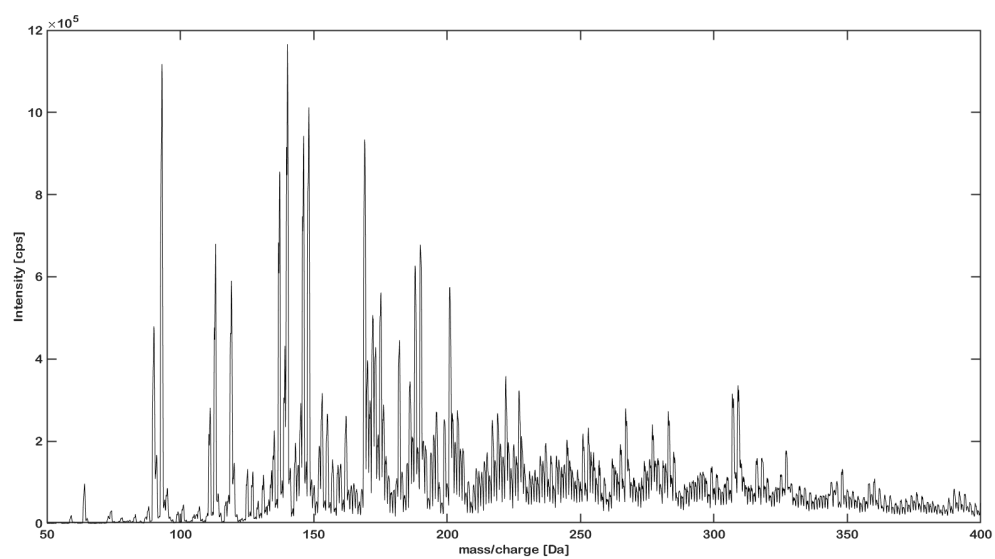
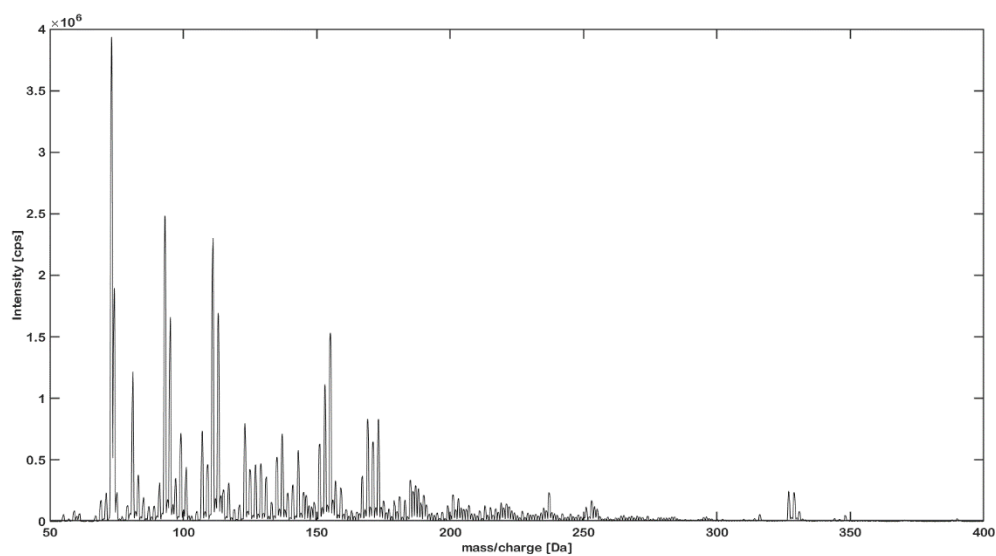
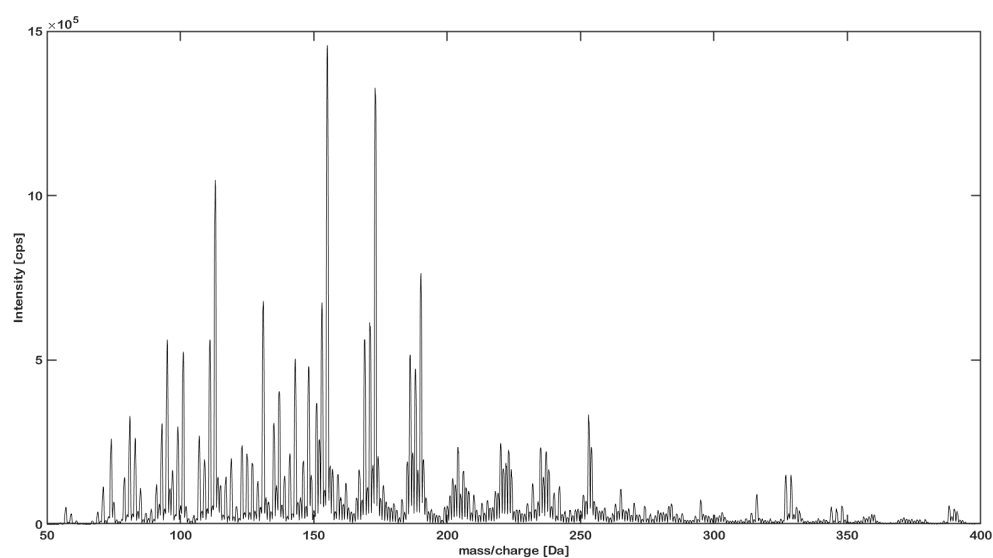


Figure A90: DBDI-Q3 spectra for predominantly *R. damascena* EOs used in chemometric study.

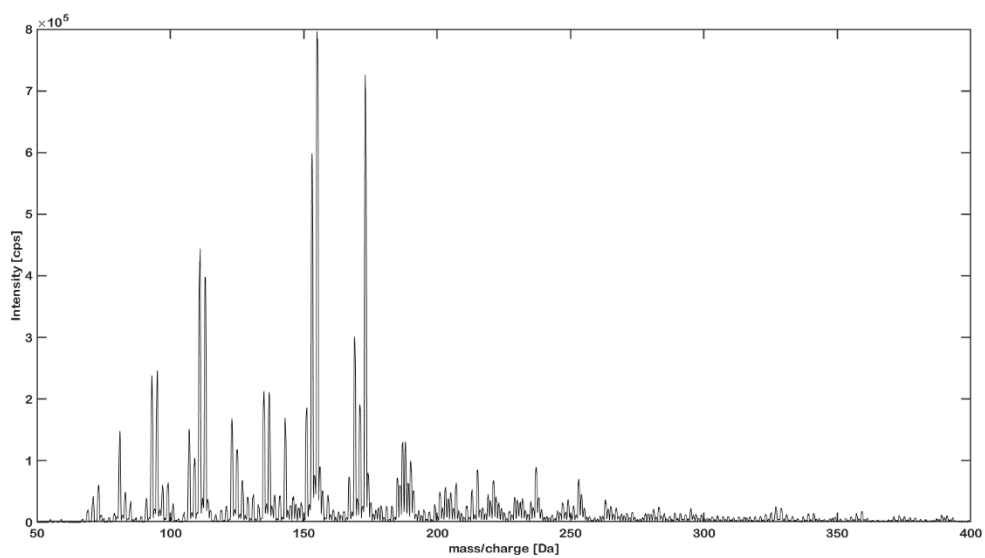
R. damascena Sample 1



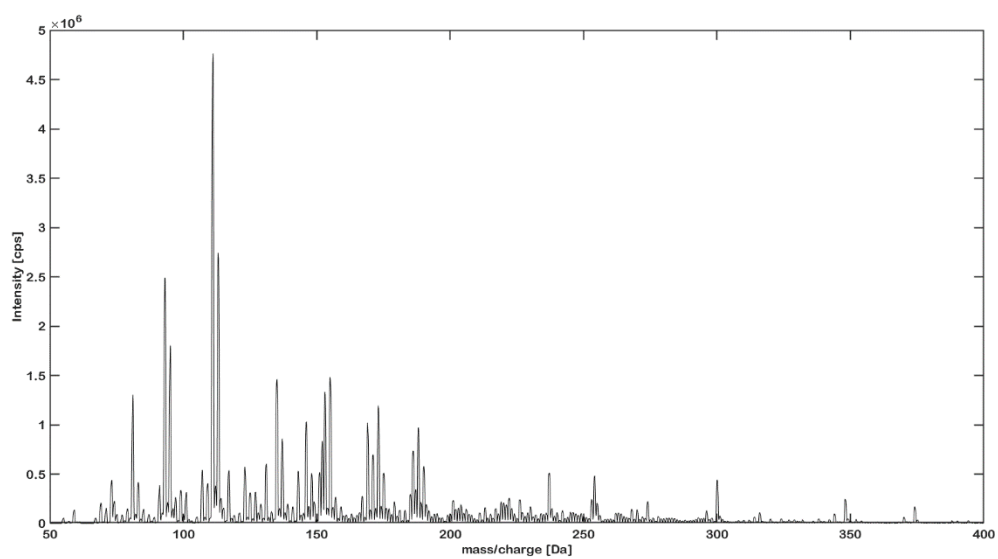
R. damascena Sample 2



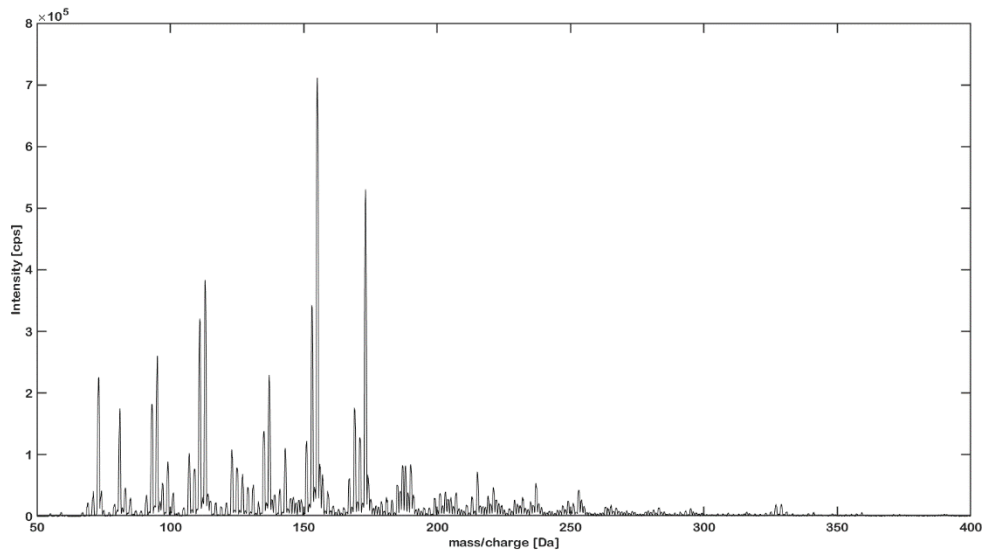
R. damascena Sample 3



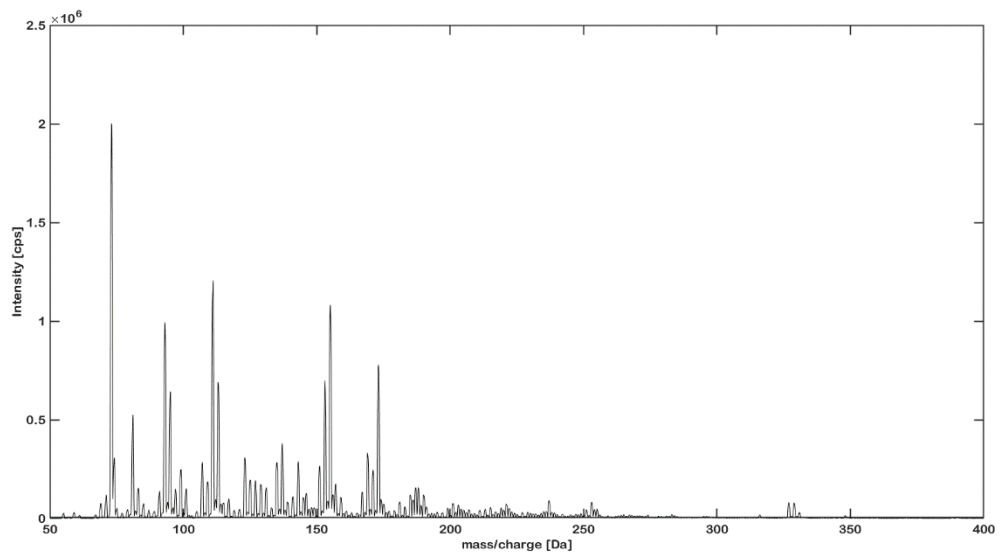
R. damascena Sample 4



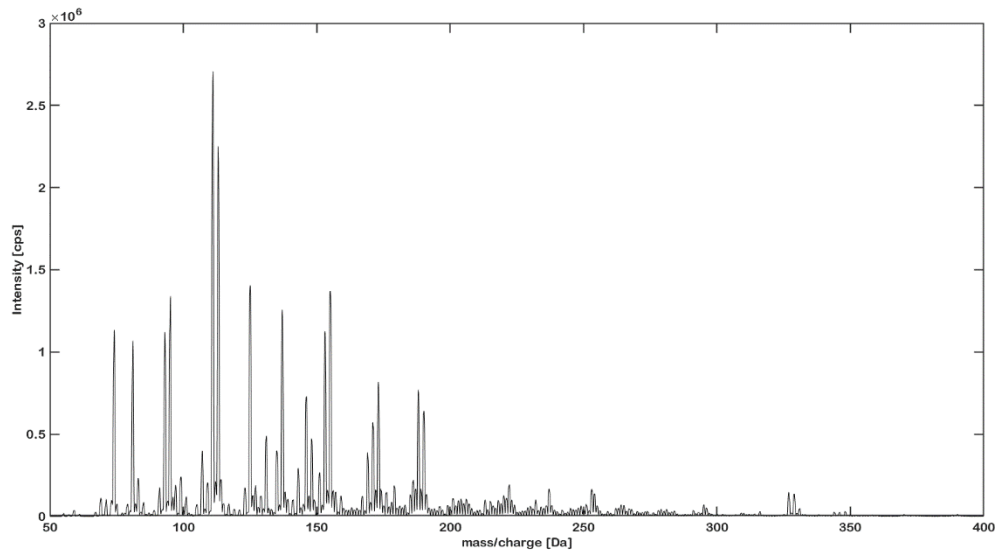
R. damascena Sample 5



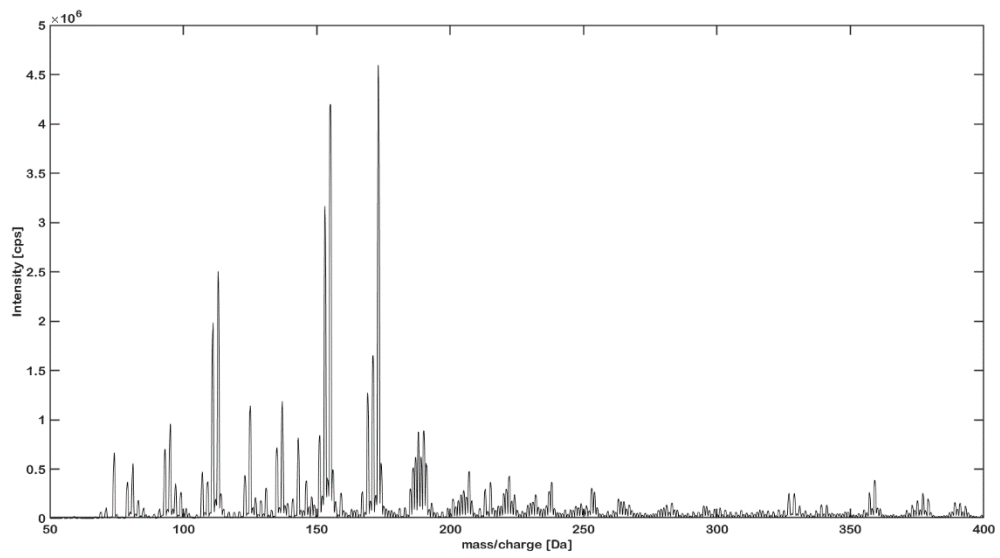
R. damascena Sample 6



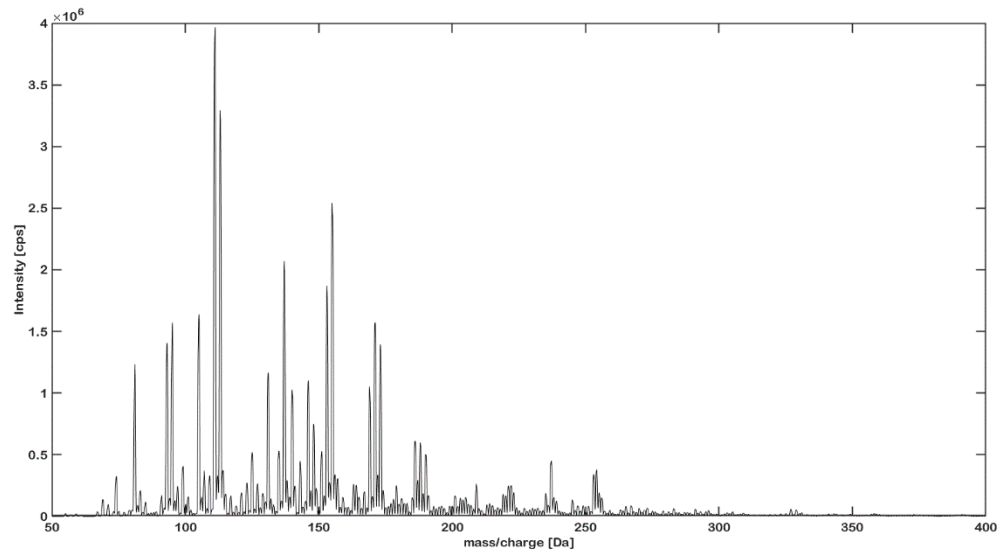
R. damascena Sample 7



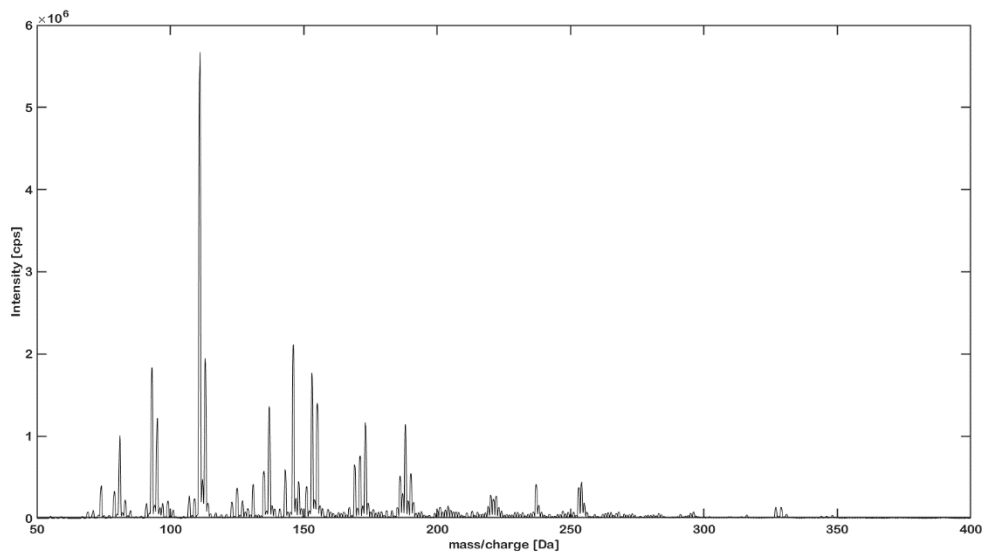
R. damascena Sample 8



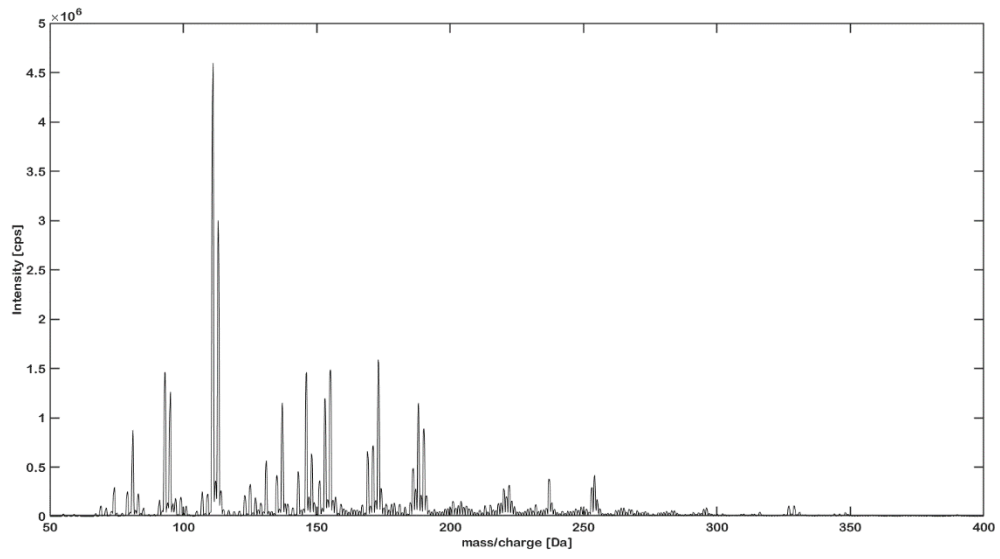
R. damascena Sample 9



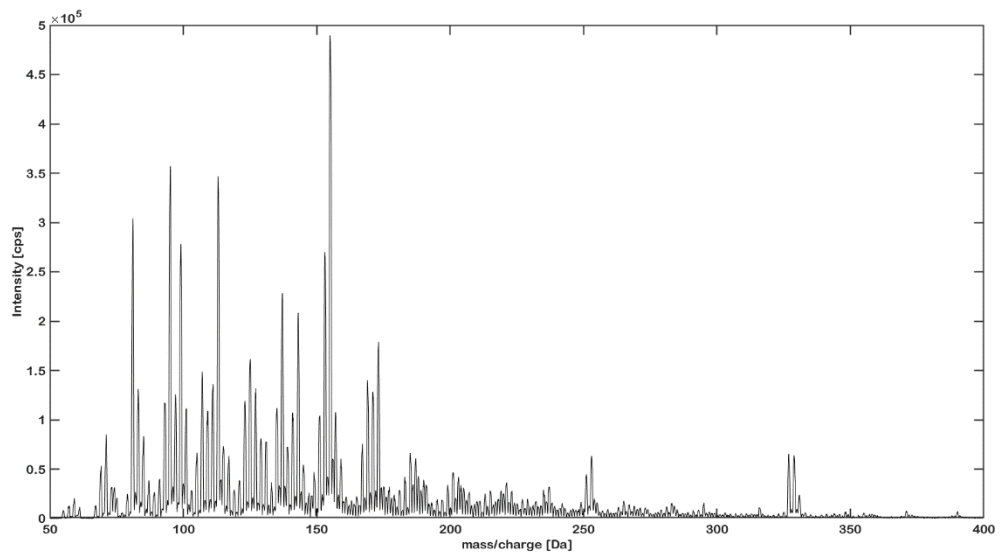
R. damascena Sample 10



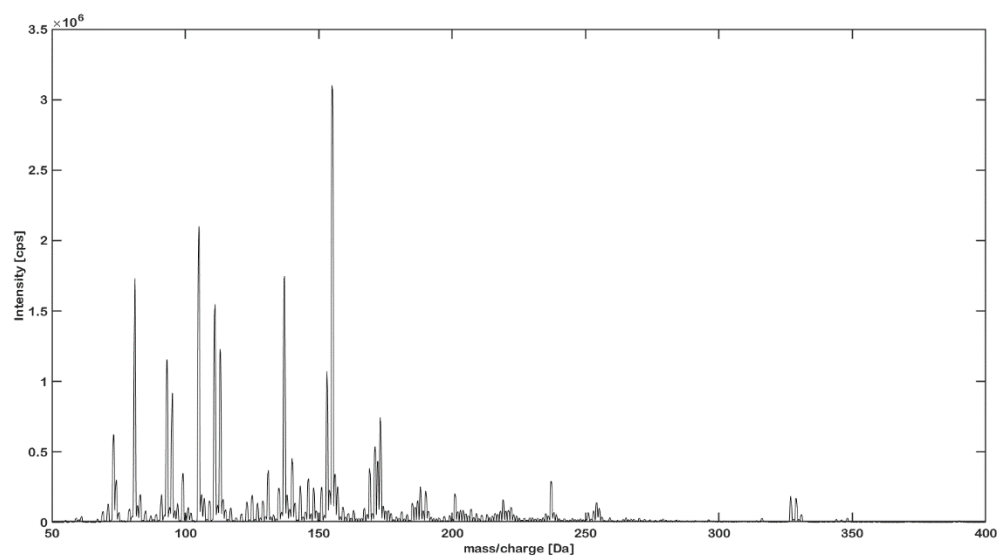
R. damascena Sample 11



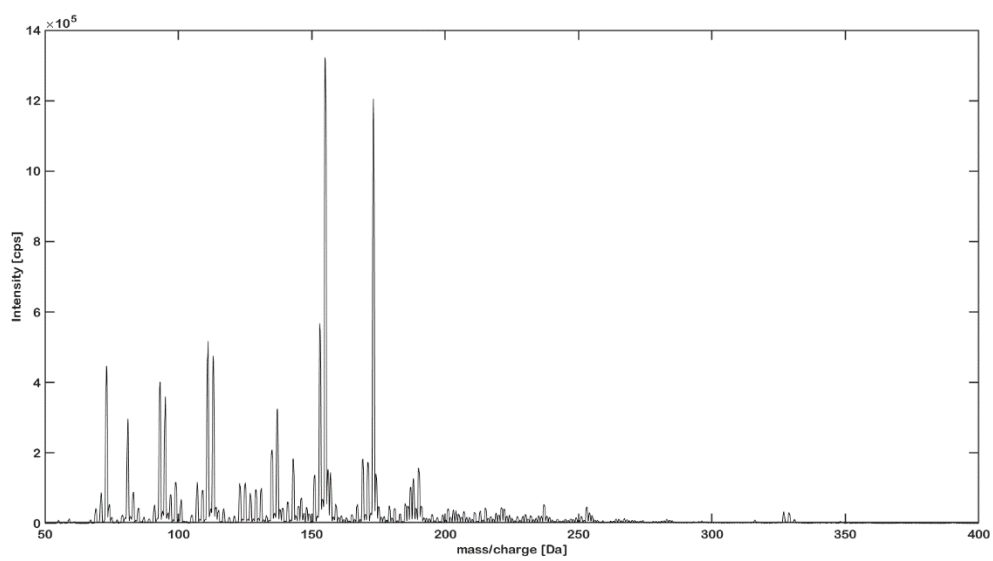
R. damascena Sample 12



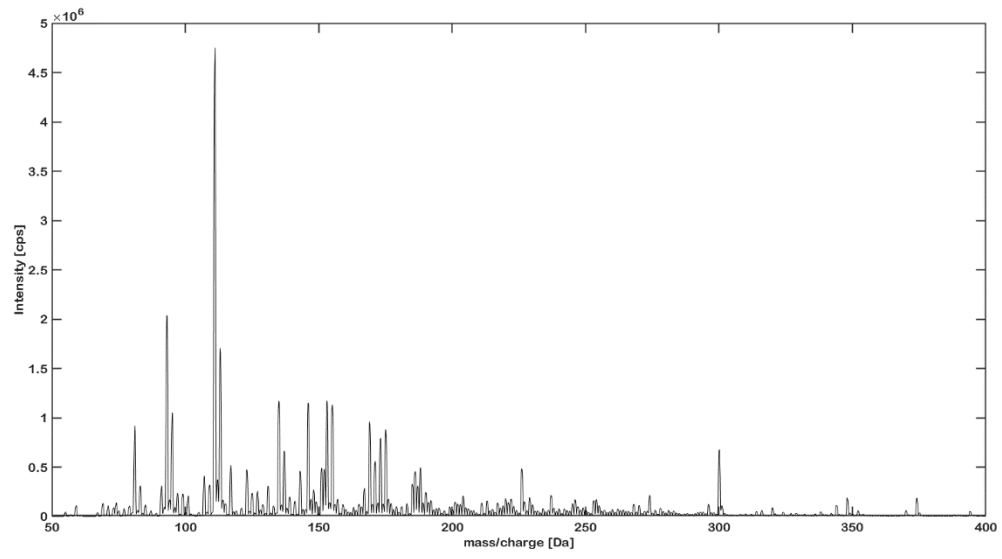
R. damascena Sample 13



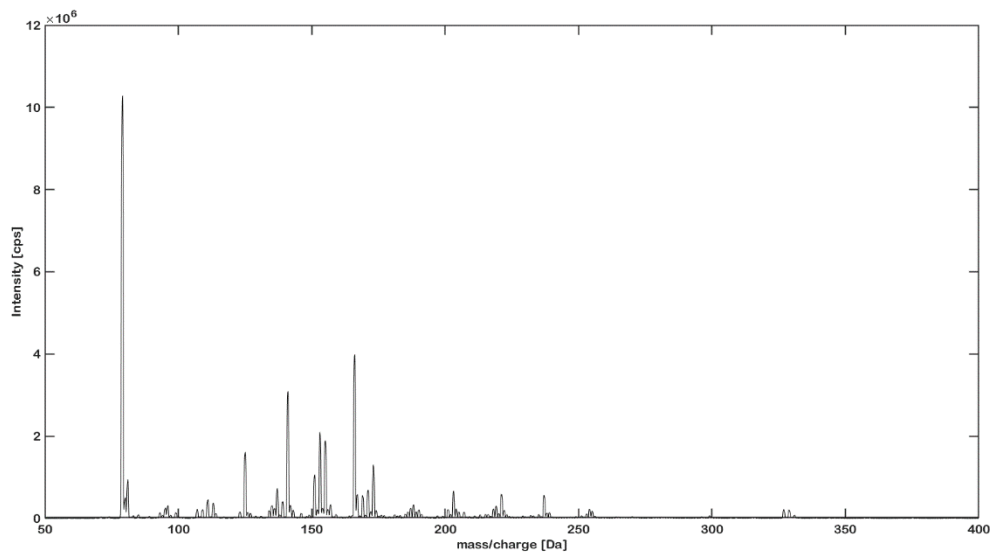
R. damascena Sample 14



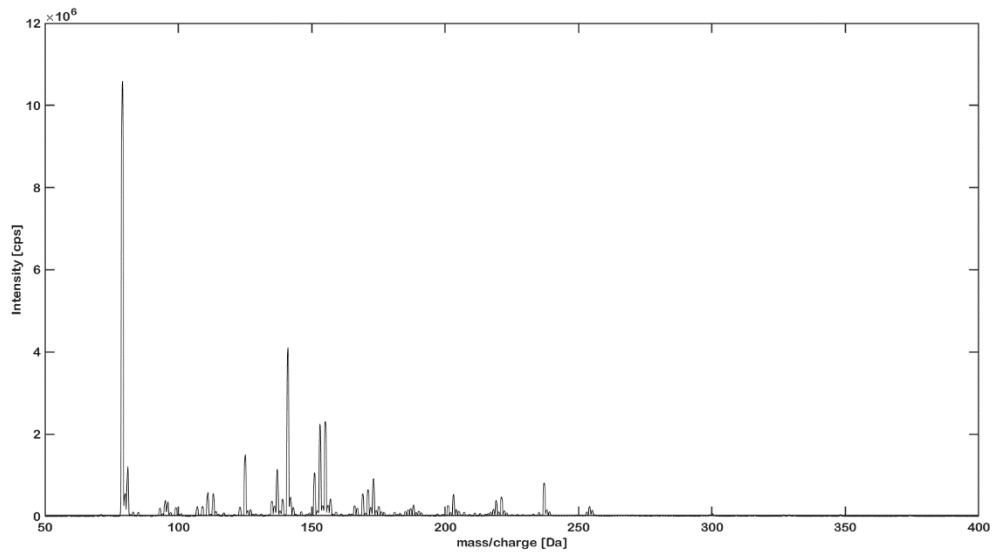
R. damascena Sample 15



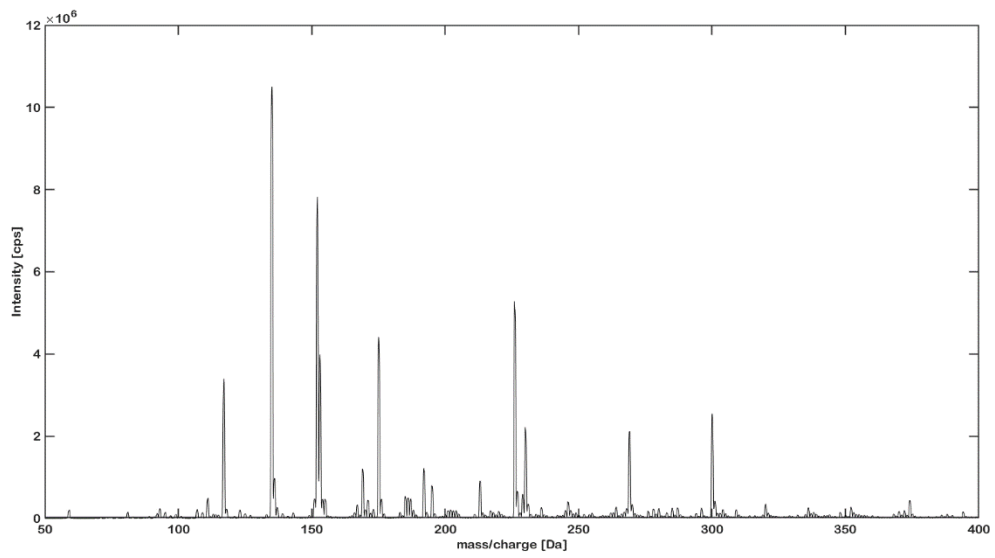
P. graveolens Sample 16



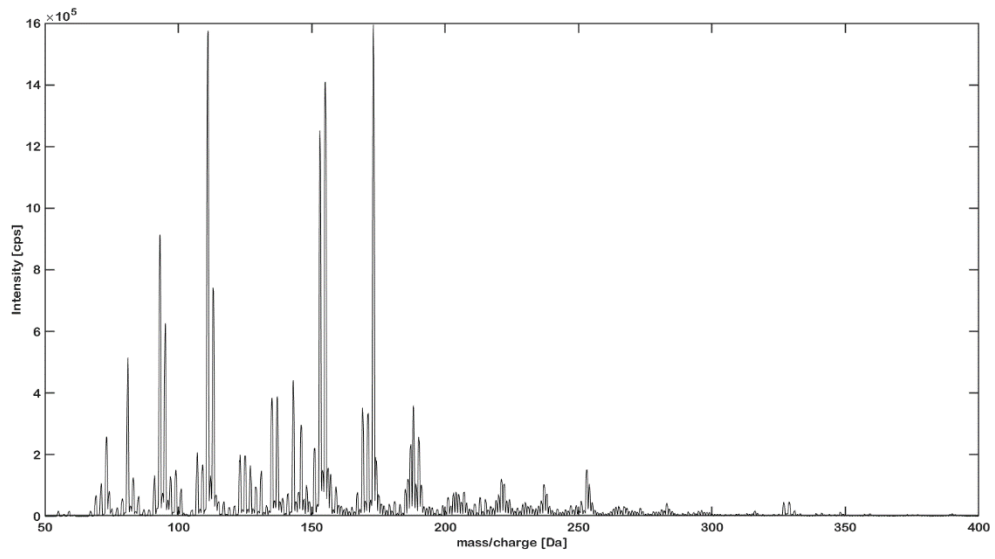
P. graveolens Sample 17



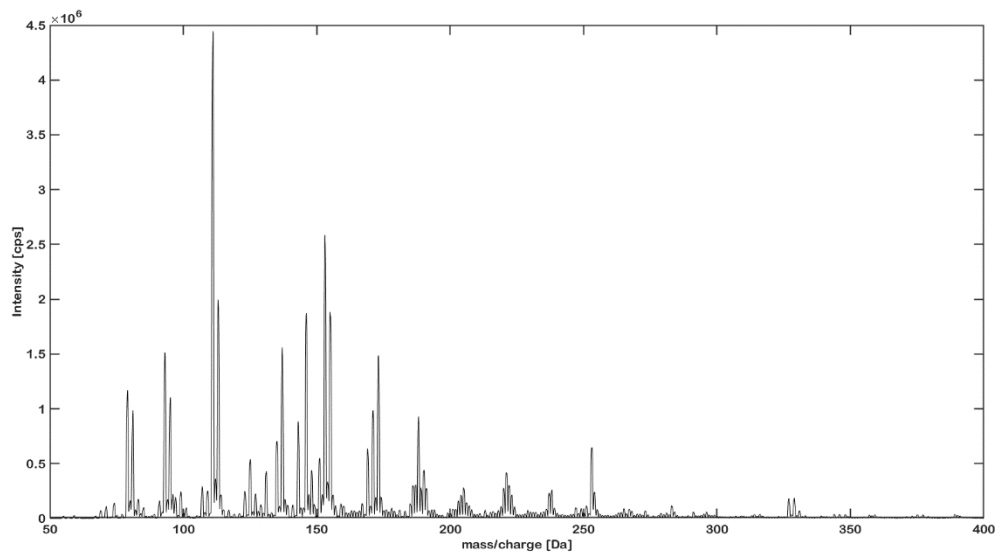
C. bergamia / *R. damascena* Sample 18



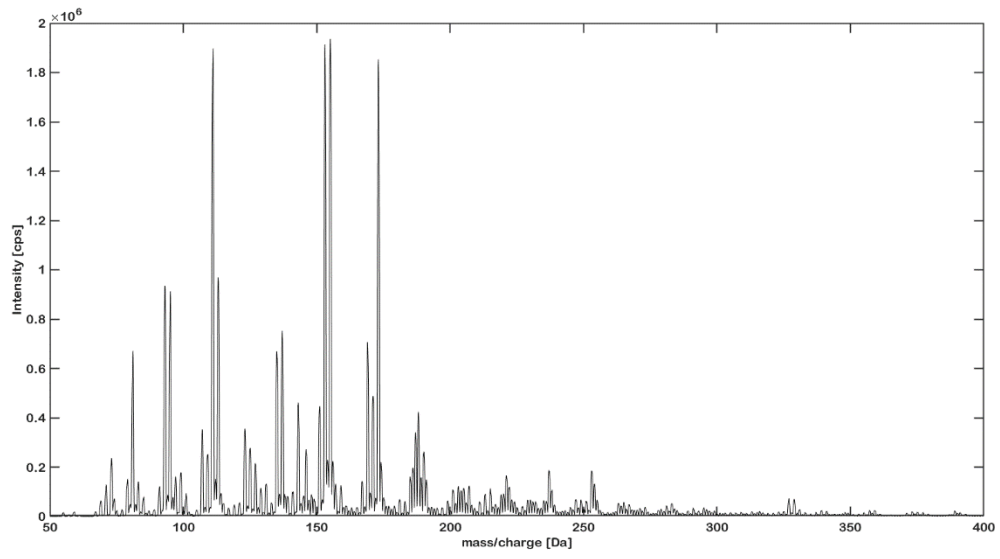
R. damascena Sample 19



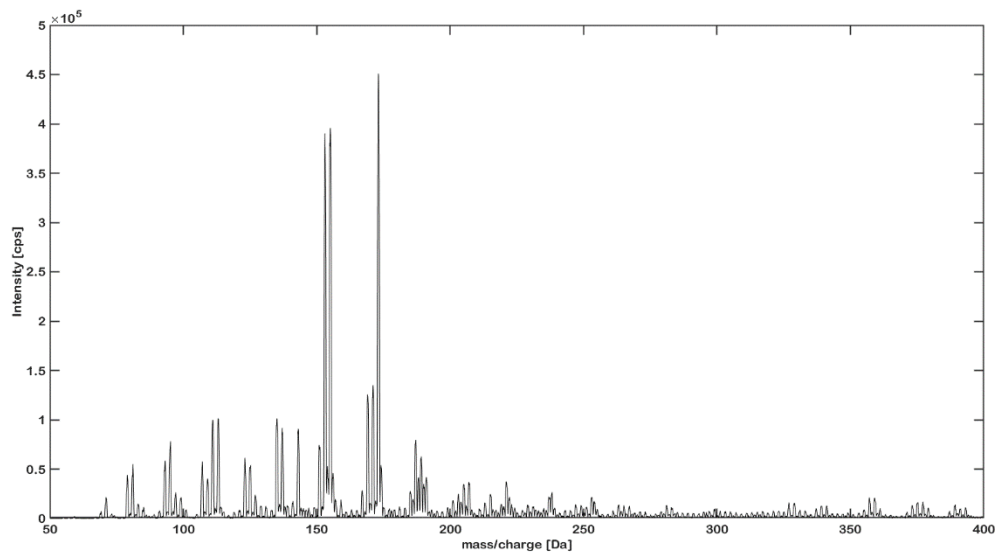
R. damascena Sample 20



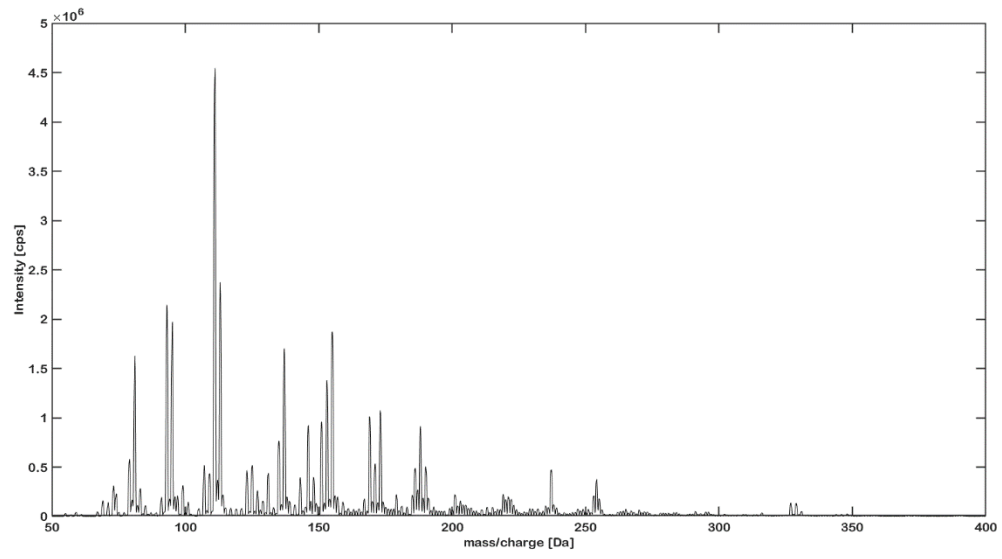
R. damascena Sample 21



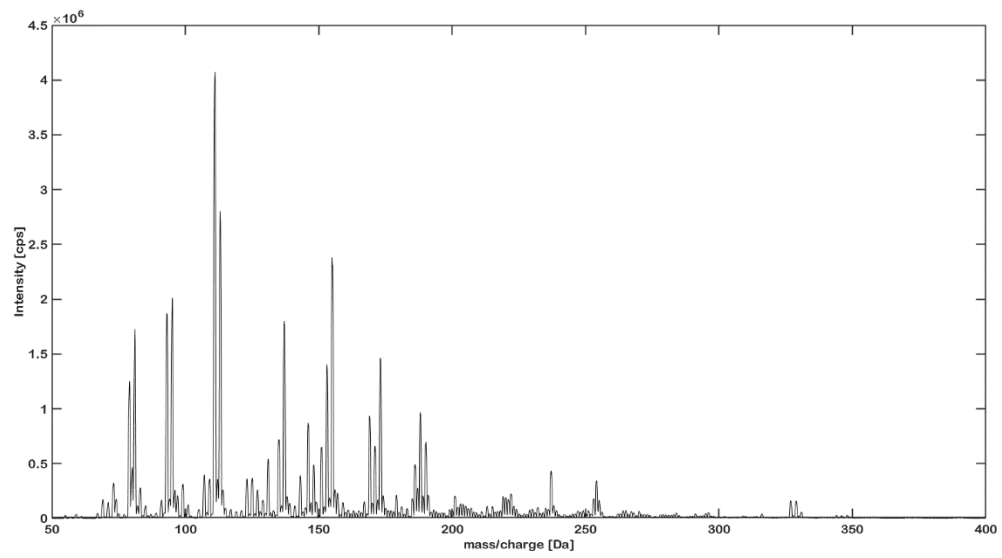
R. damascena Sample 22



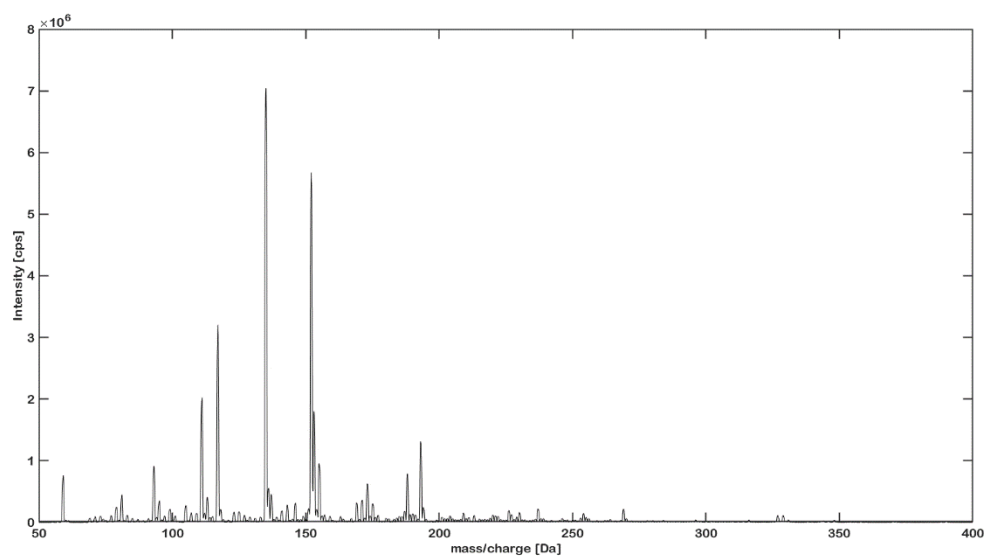
R. damascena Sample 23



R. damascena Sample 24



R. damascena Sample 25



R. damascena Sample 26

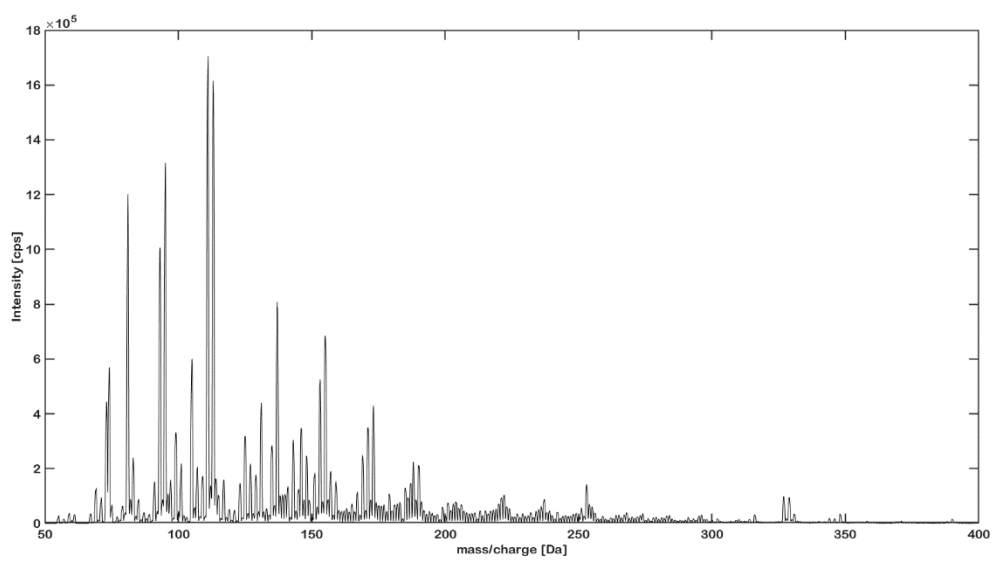
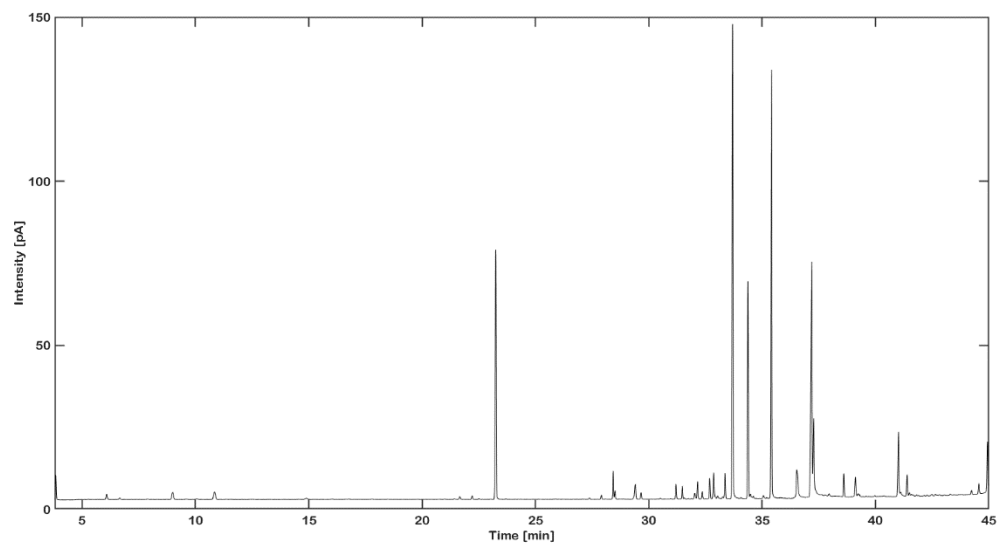
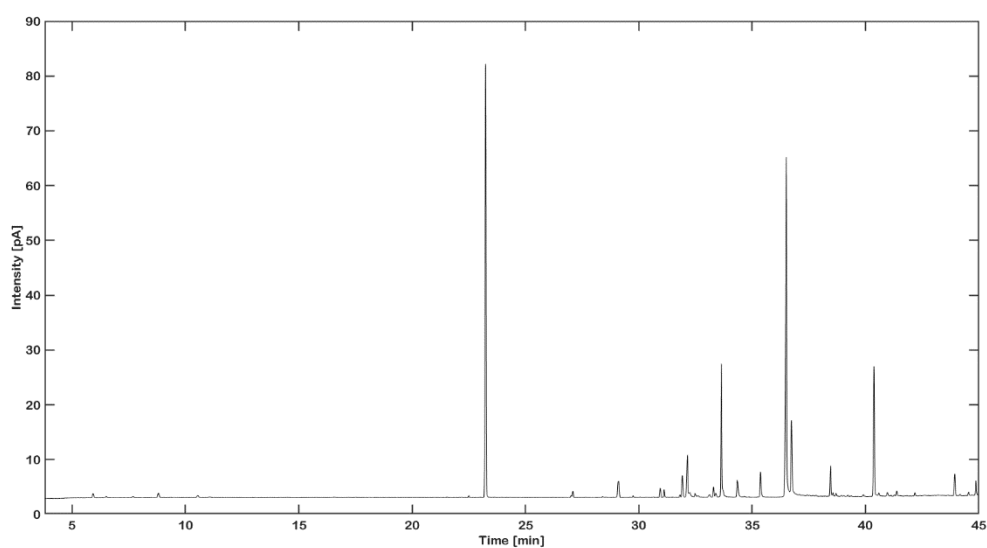


Figure A91: GC-FID chromatograms acquired on a DB-wax column for predominantly *R. damascena* EOs used in chemometric study

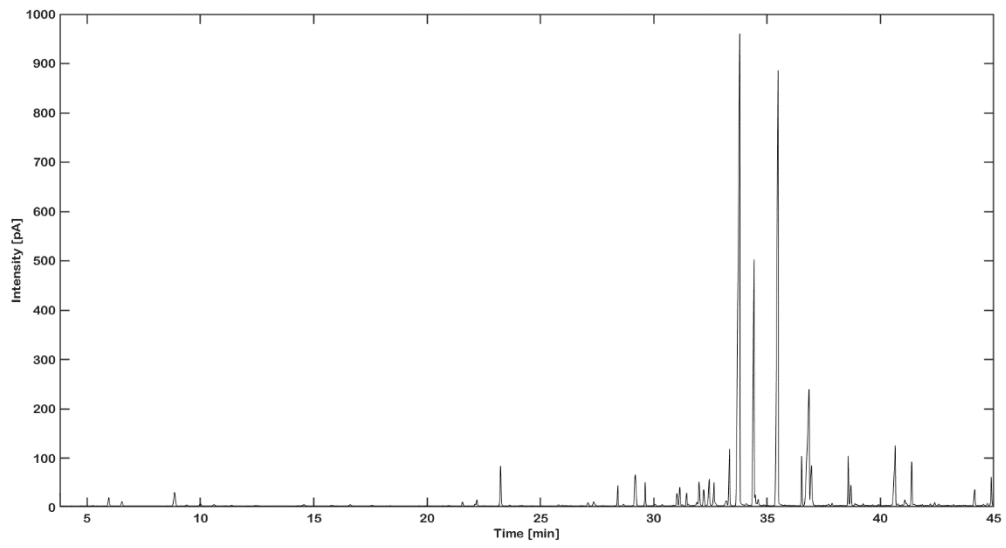
R. damascena Sample 1



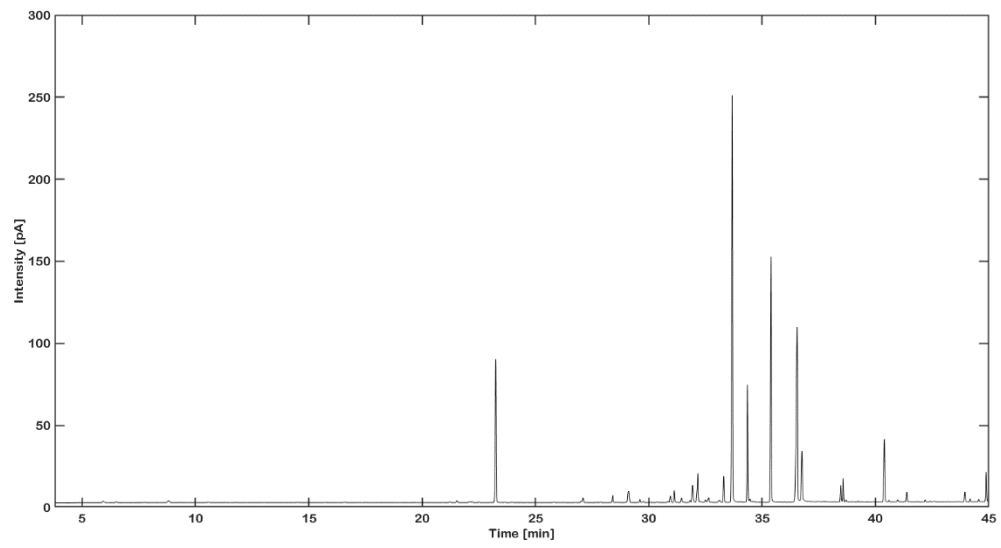
R. damascena Sample 2



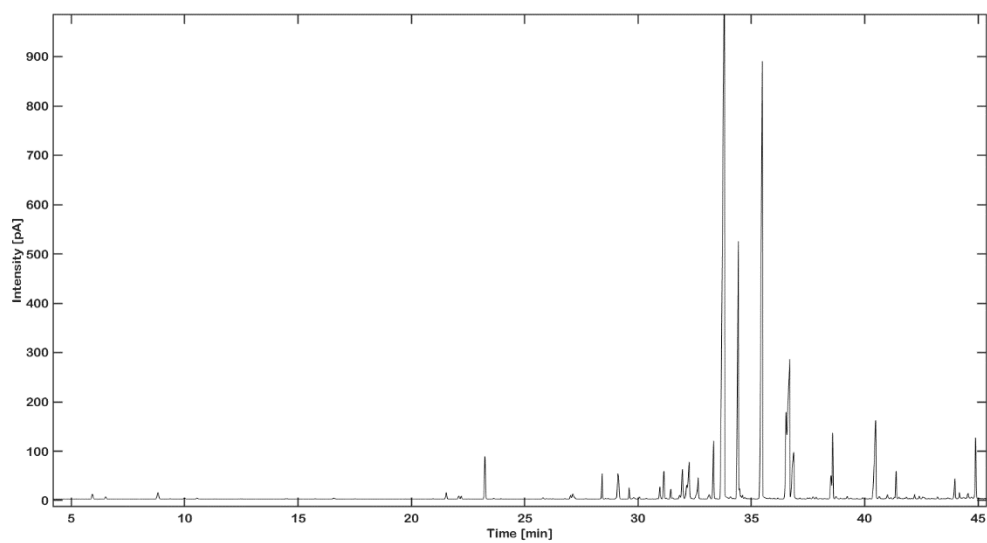
R. damascena Sample 3



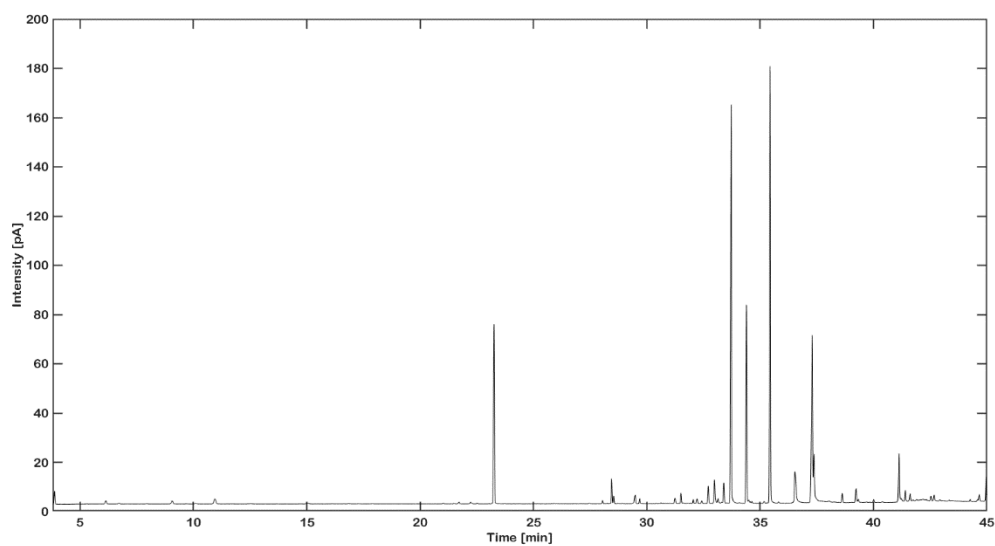
R. damascena Sample 4



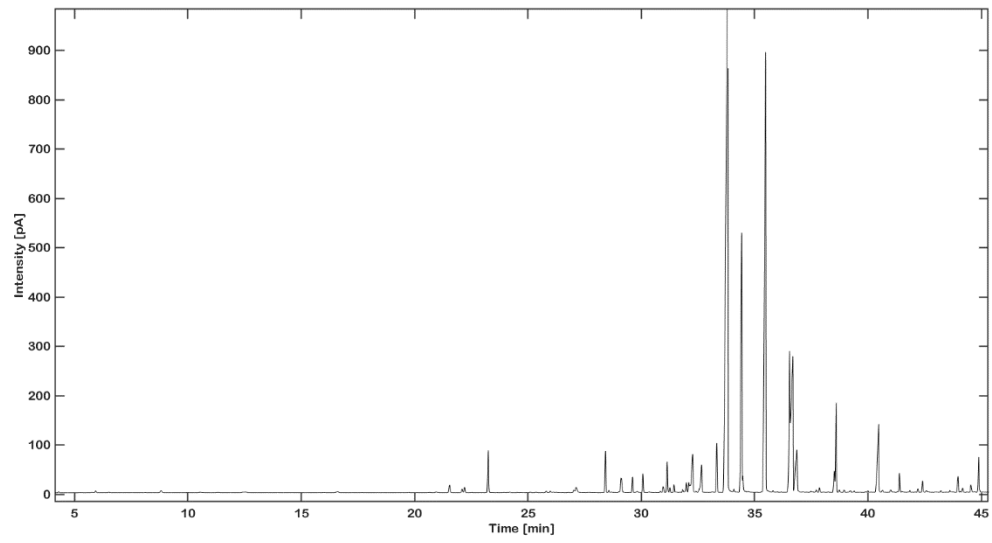
R. damascena Sample 5



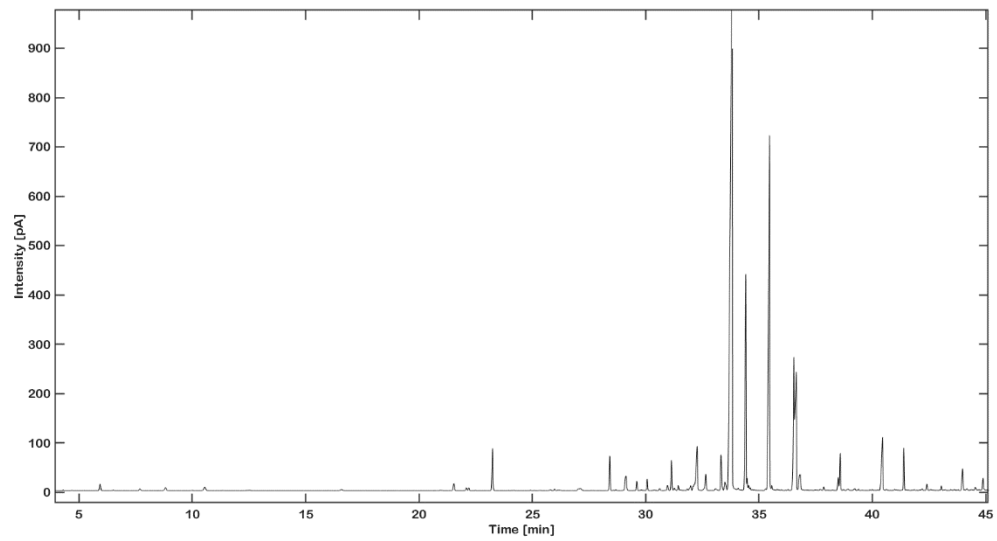
R. damascena Sample 6



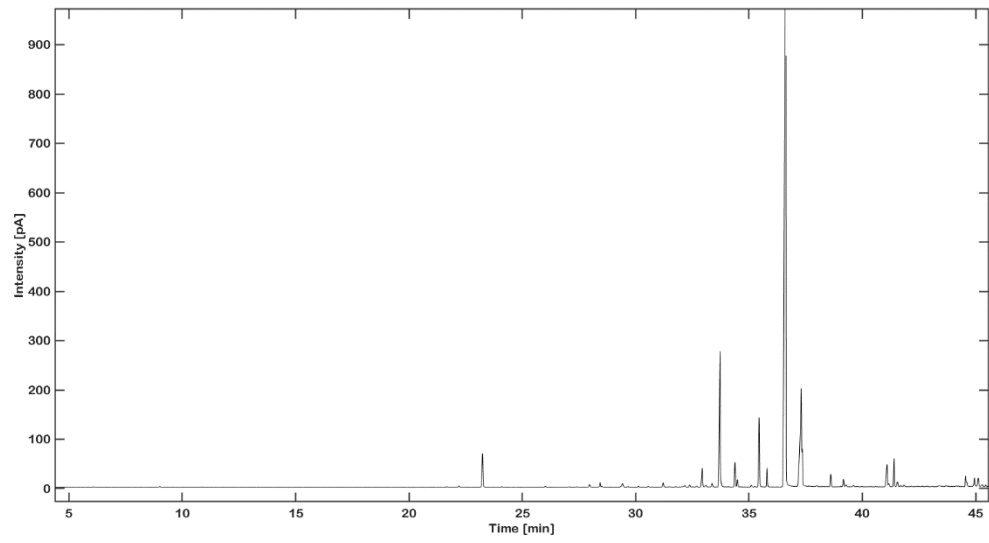
R. damascena Sample 7



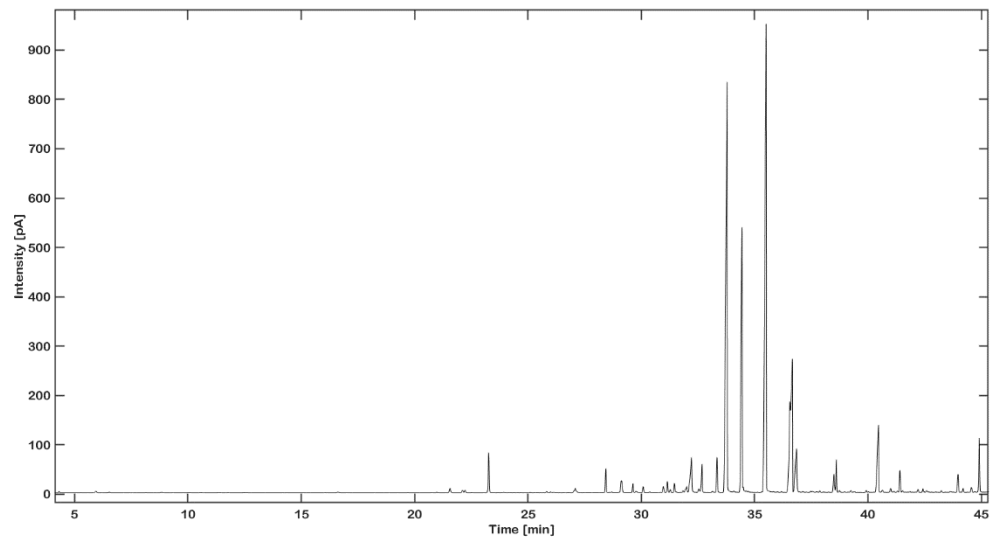
R. damascena Sample 8



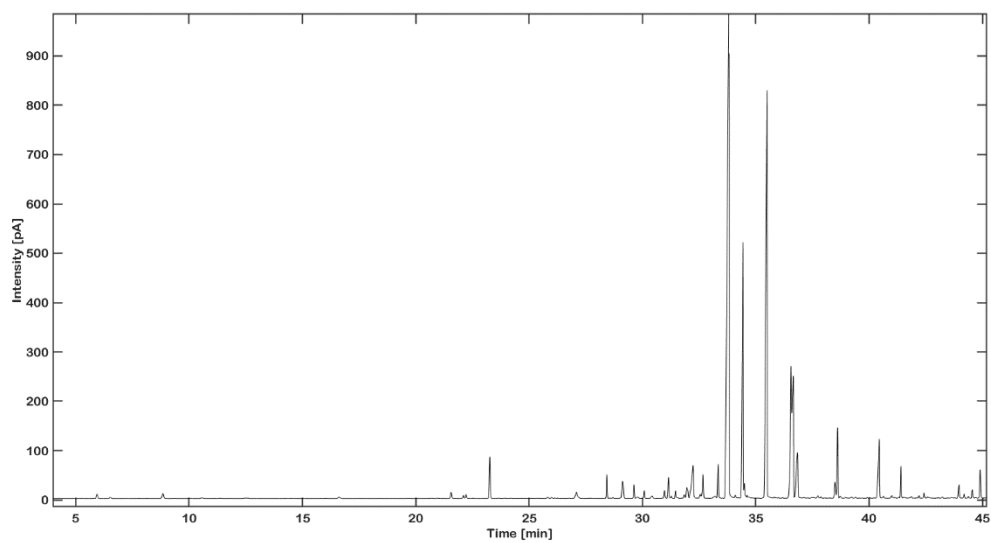
R. damascena Sample 9



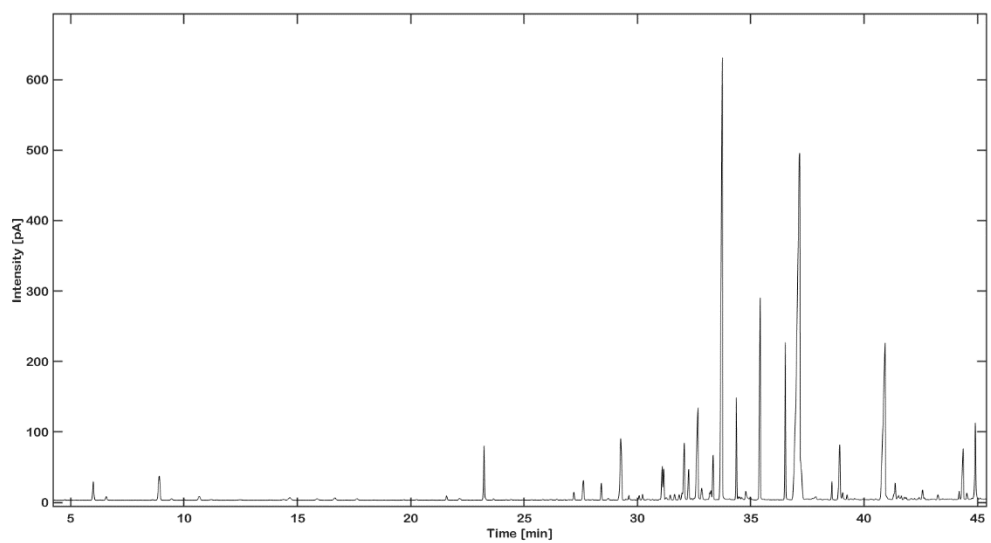
R. damascena Sample 10



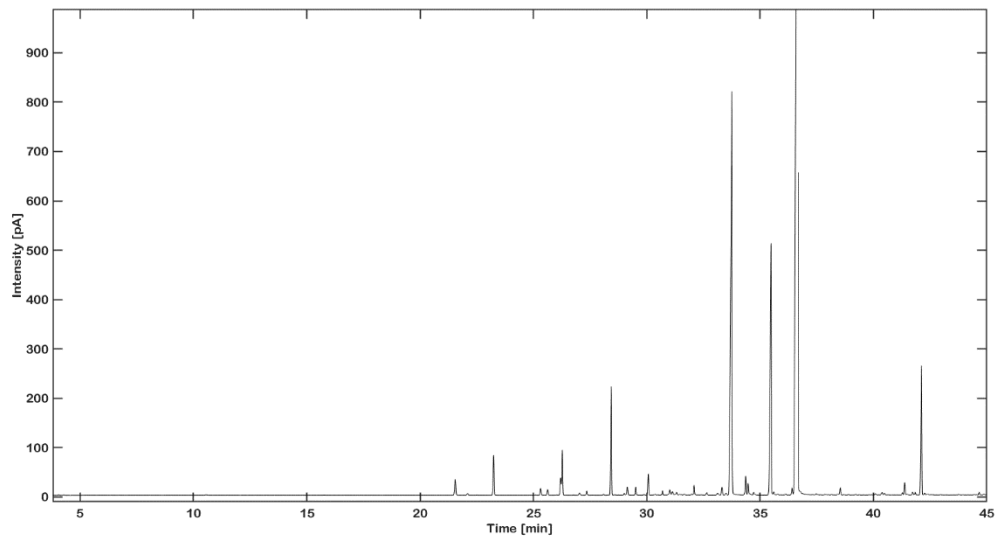
R. damascena Sample 11



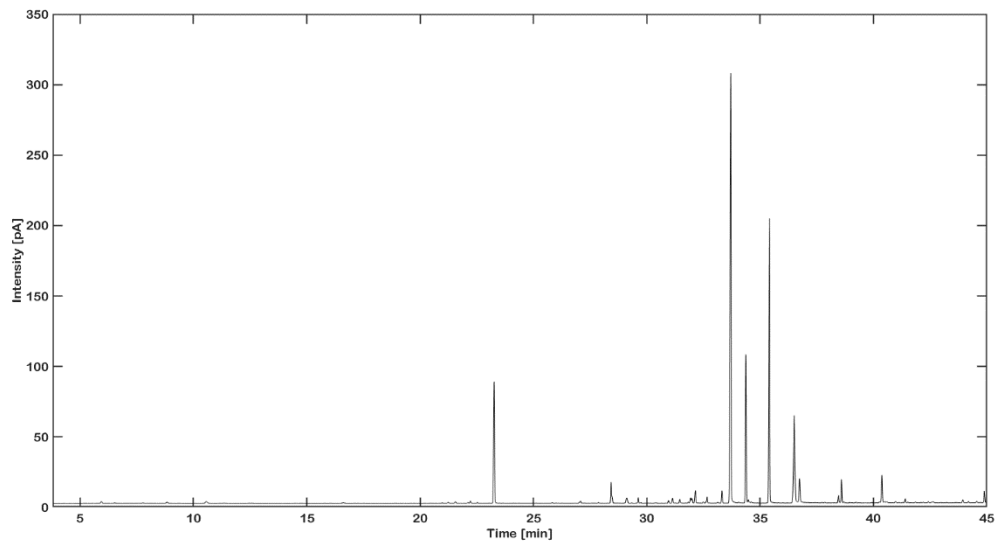
R. damascena Sample 12



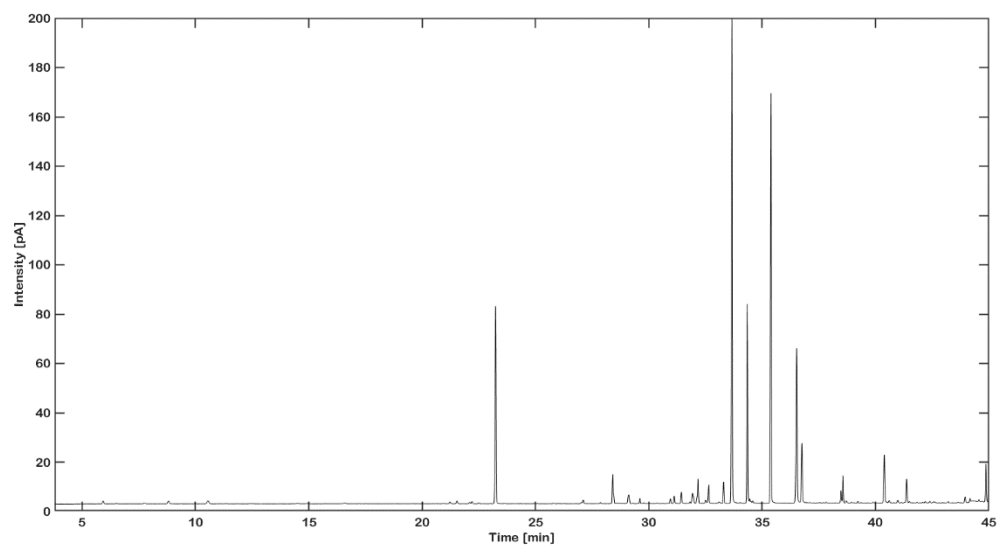
R. damascena Sample 13



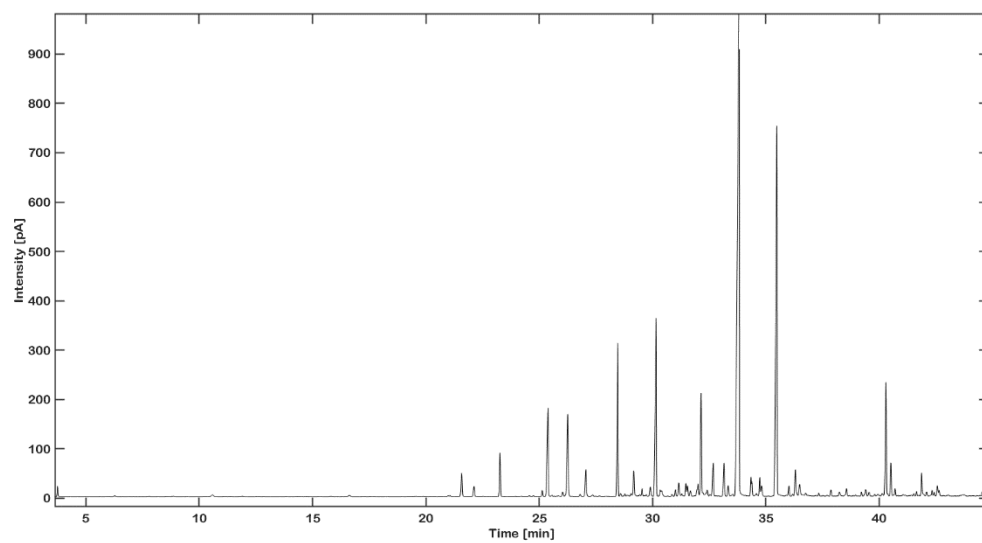
R. damascena Sample 14



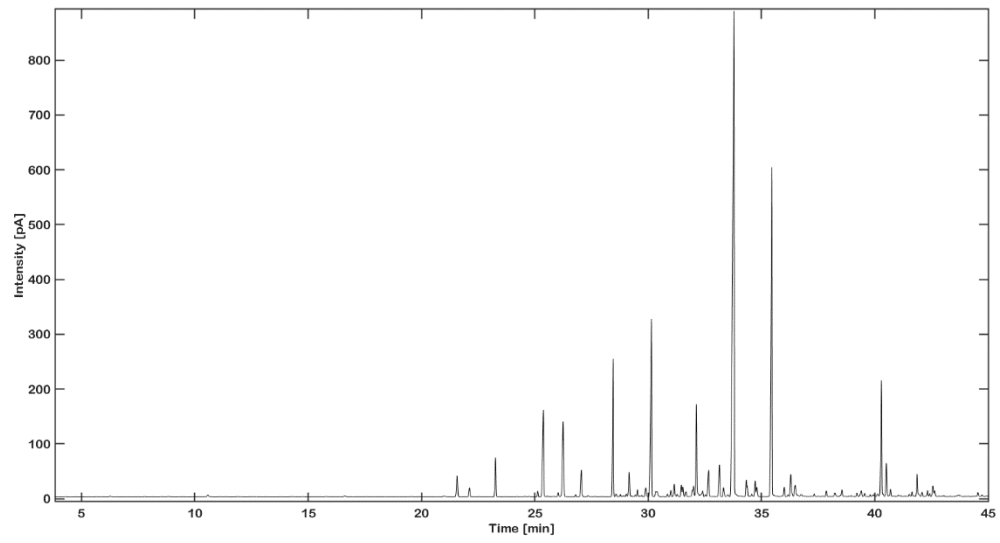
R. damascena Sample 15



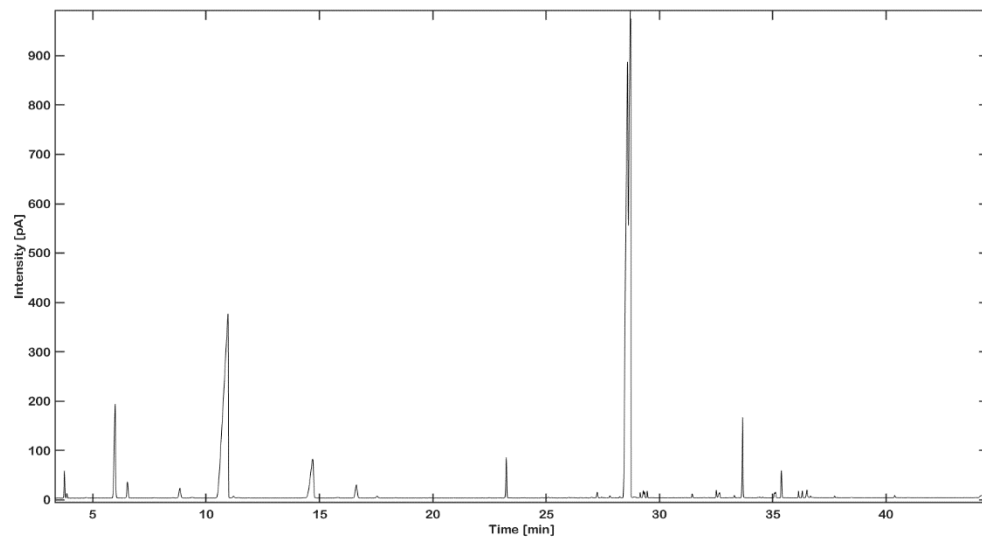
P. graveolens Sample 16



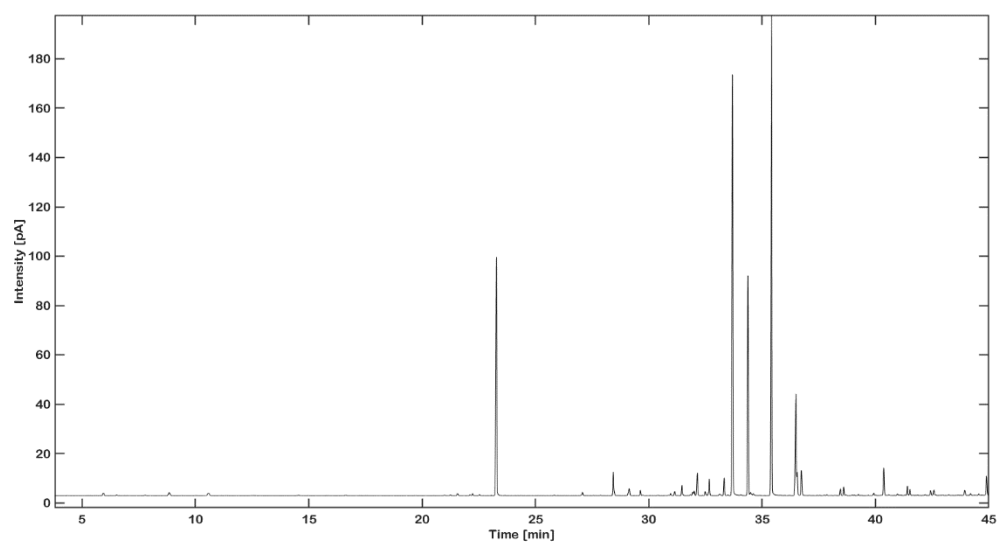
P. graveolens Sample 17



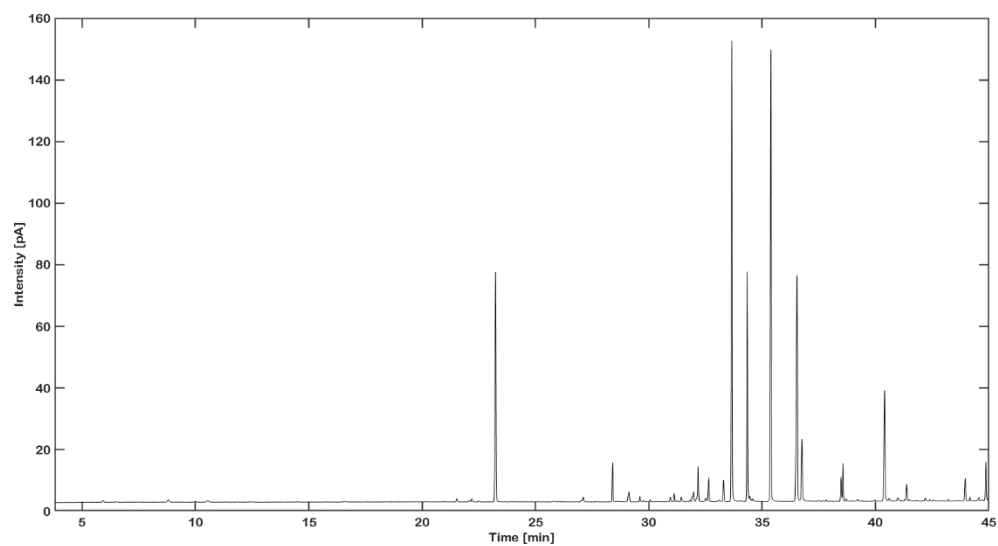
C. bergamia / *R. damascena* Sample 18



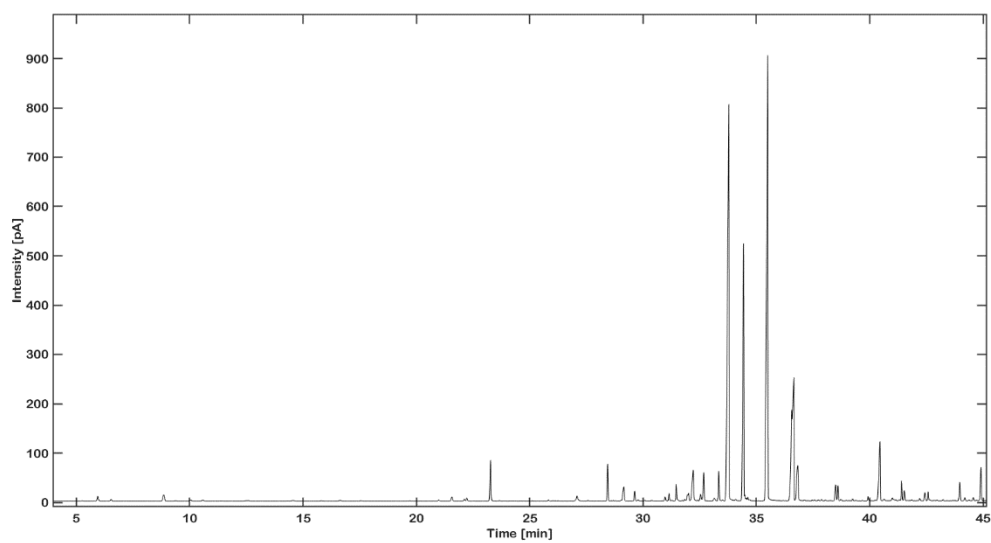
R. damascena Sample 19



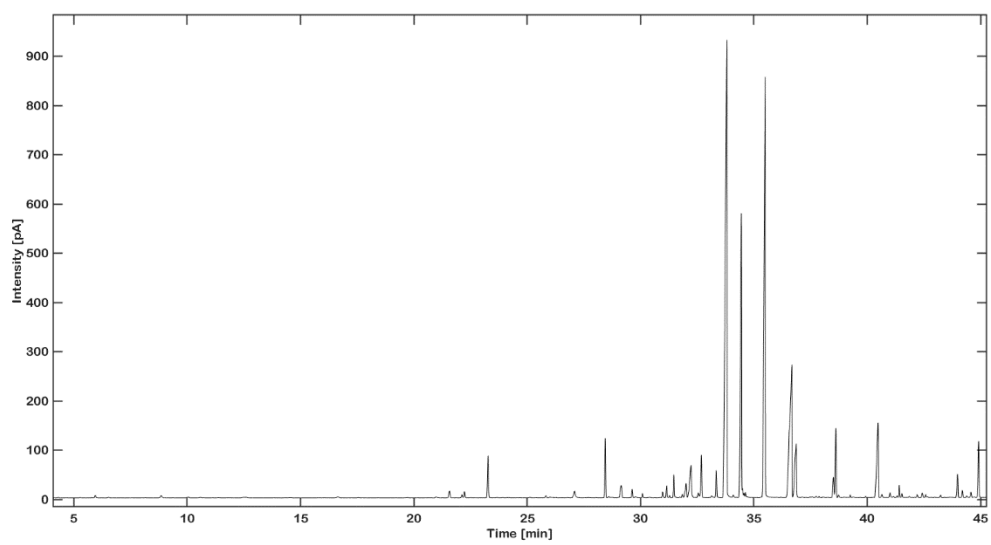
R. damascena Sample 20



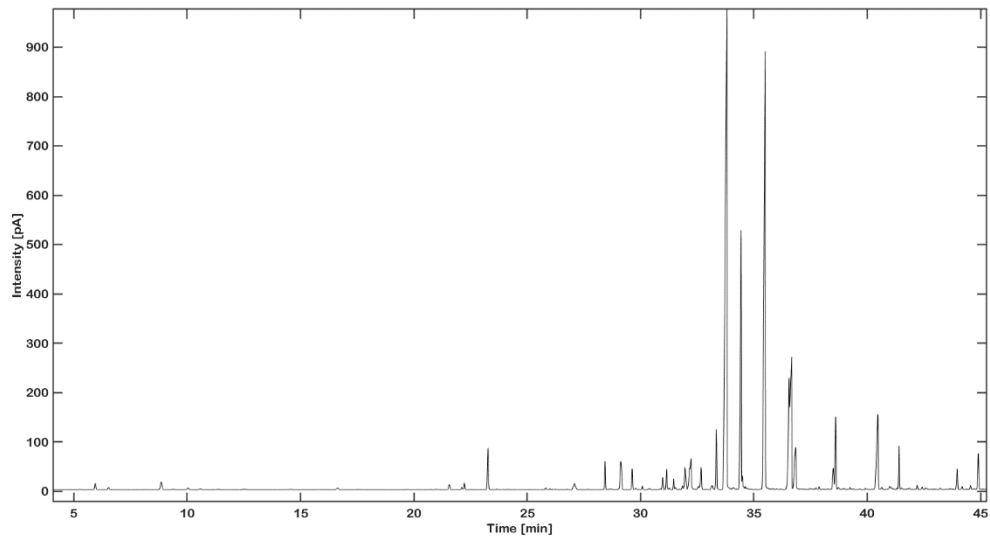
R. damascena Sample 21



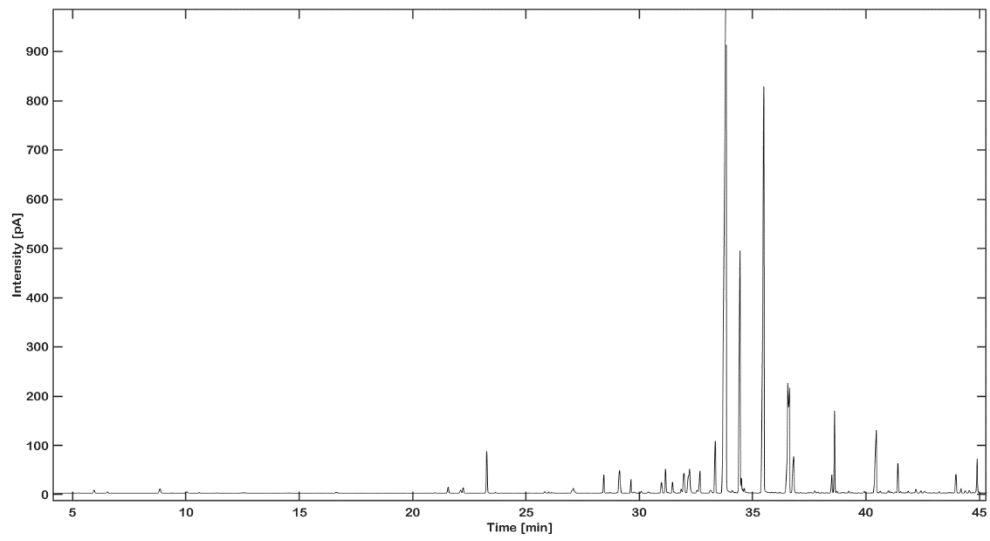
R. damascena Sample 22



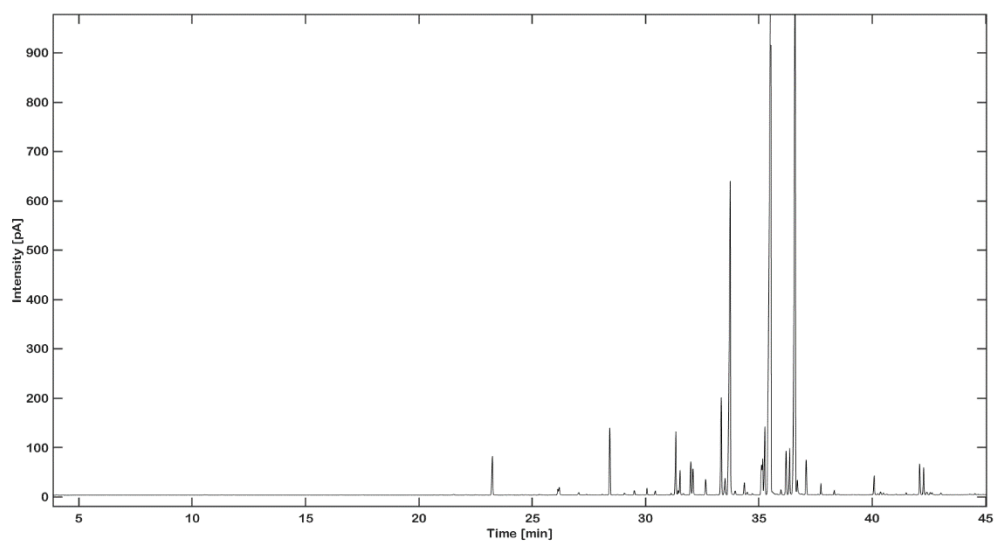
R. damascena Sample 23



R. damascena Sample 24



Synthetic Rose oil Sample 25



R. centifolia Sample 26

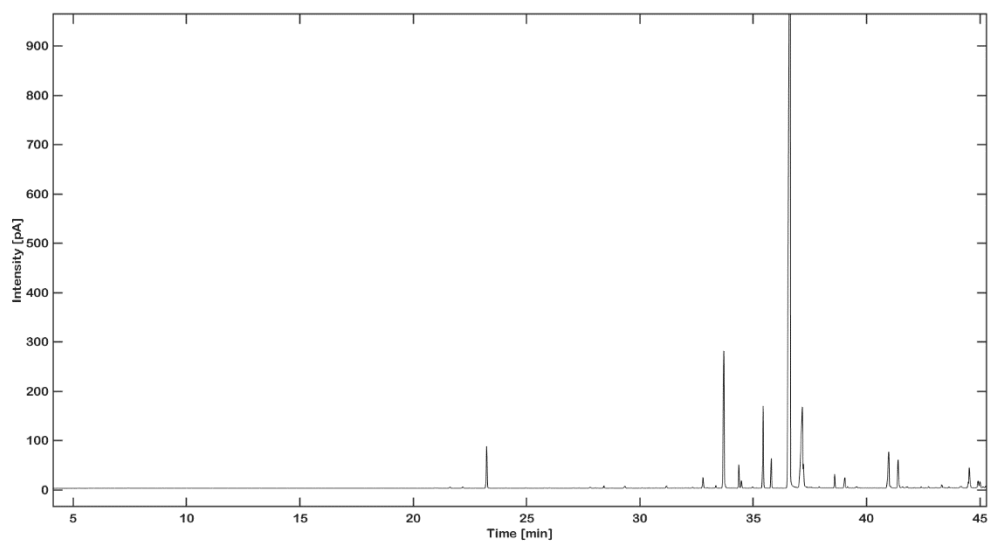
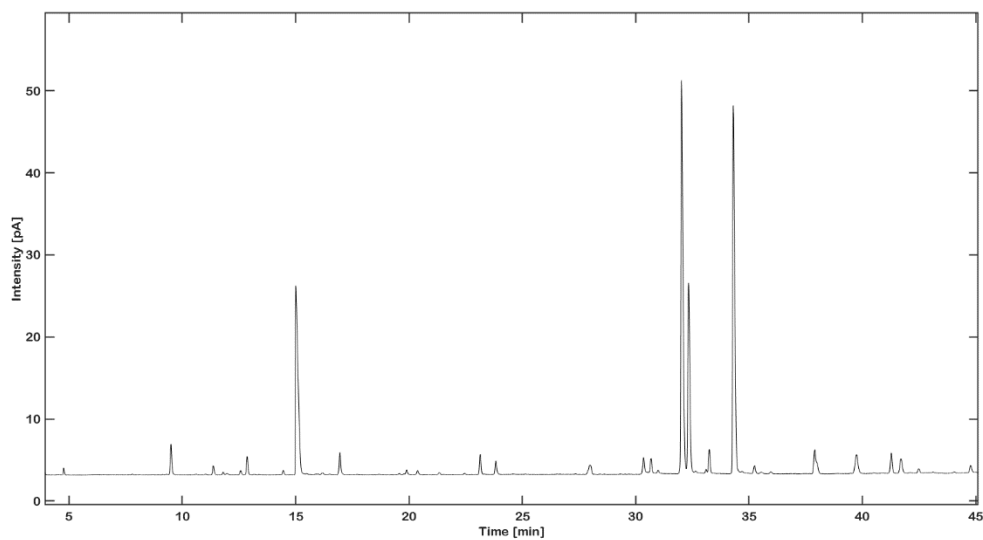
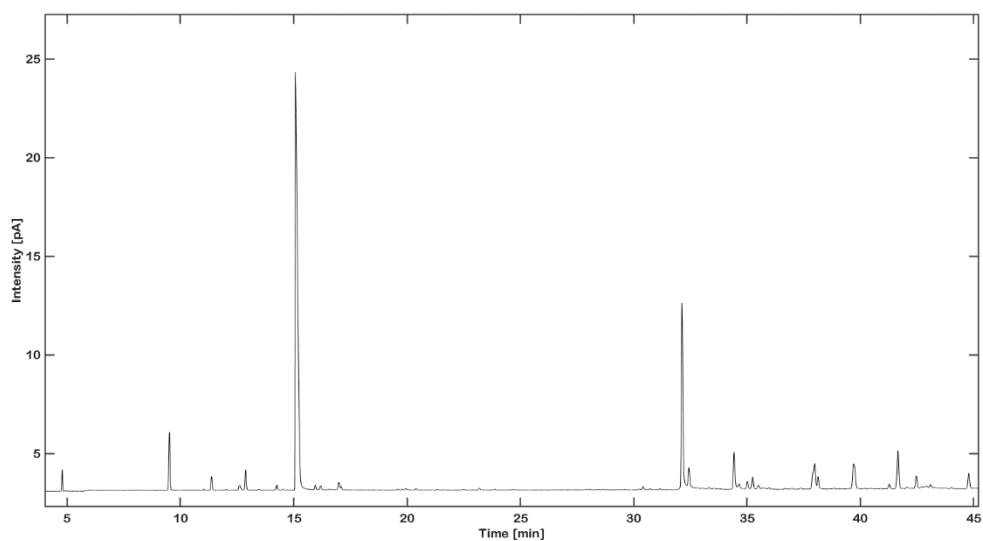


Figure A92: GC-FID chromatograms acquired on a chiral column for predominantly *R. damascena* EOs used in chemometric study

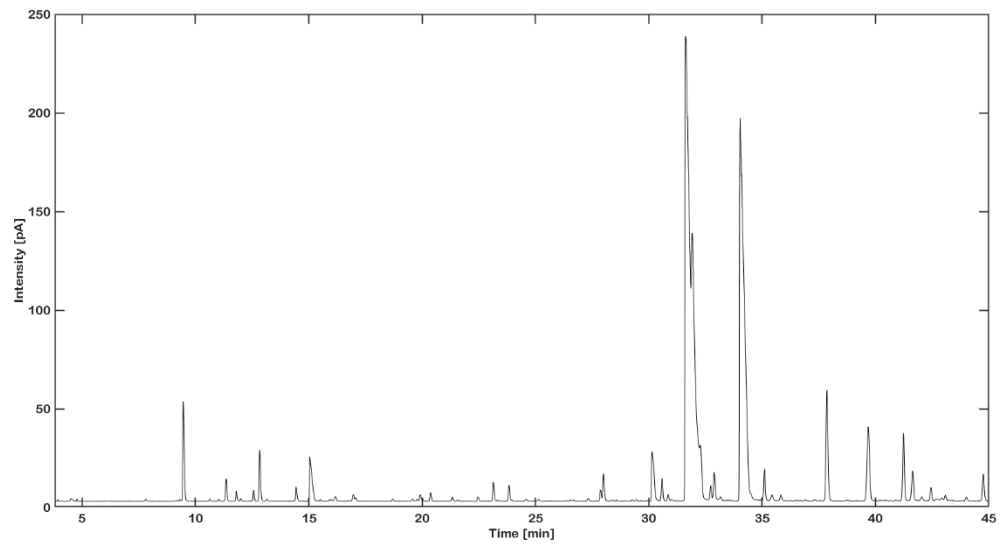
R. damascena Sample 1



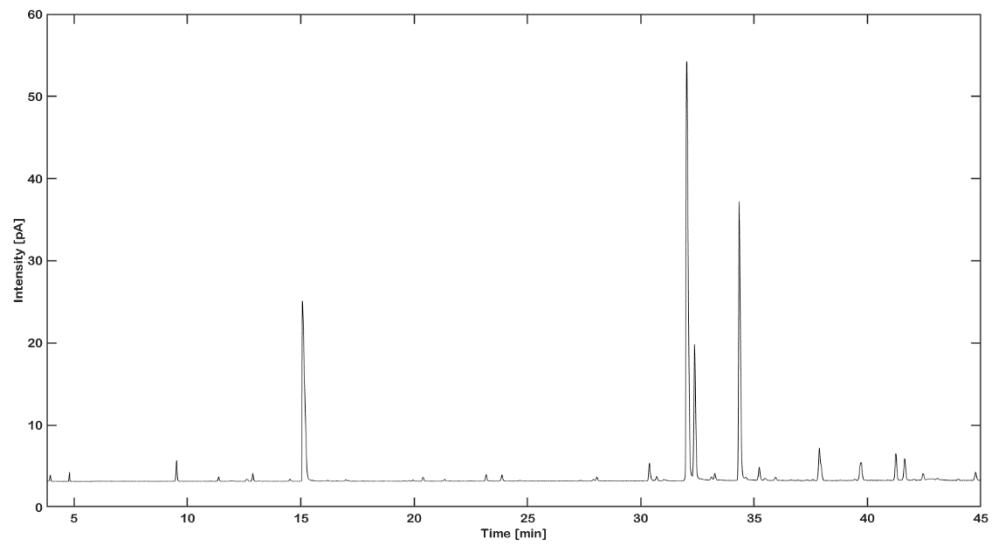
R. damascena Sample 2



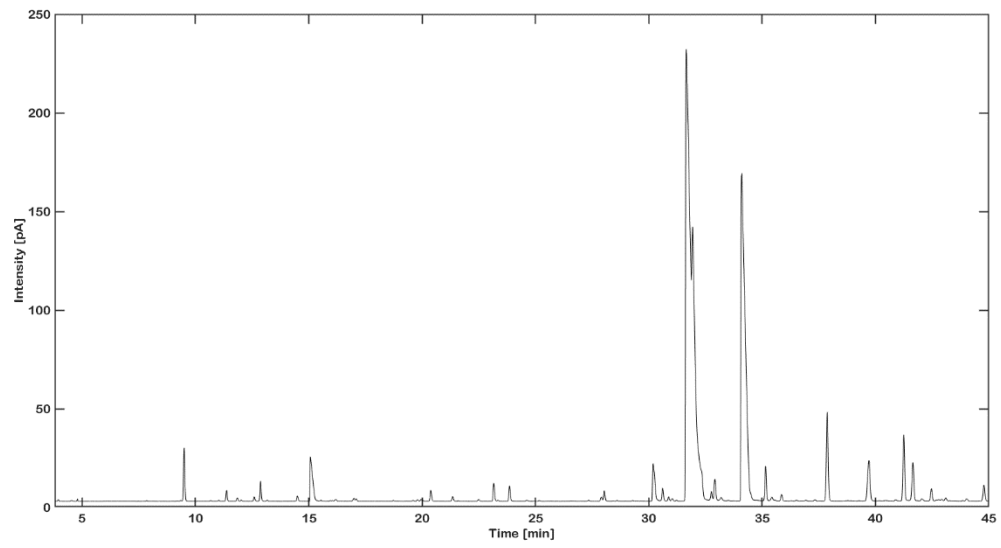
R. damascena Sample 3



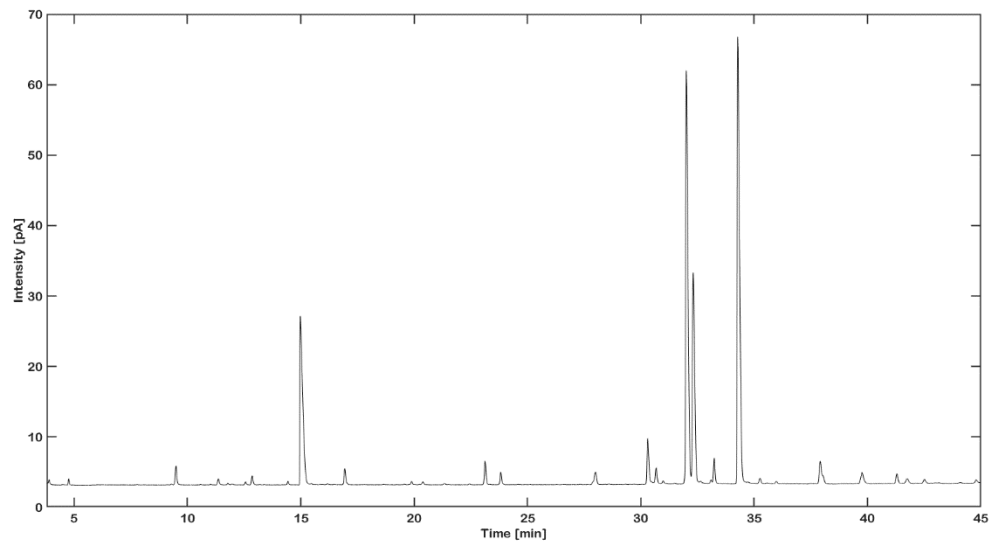
R. damascena Sample 4



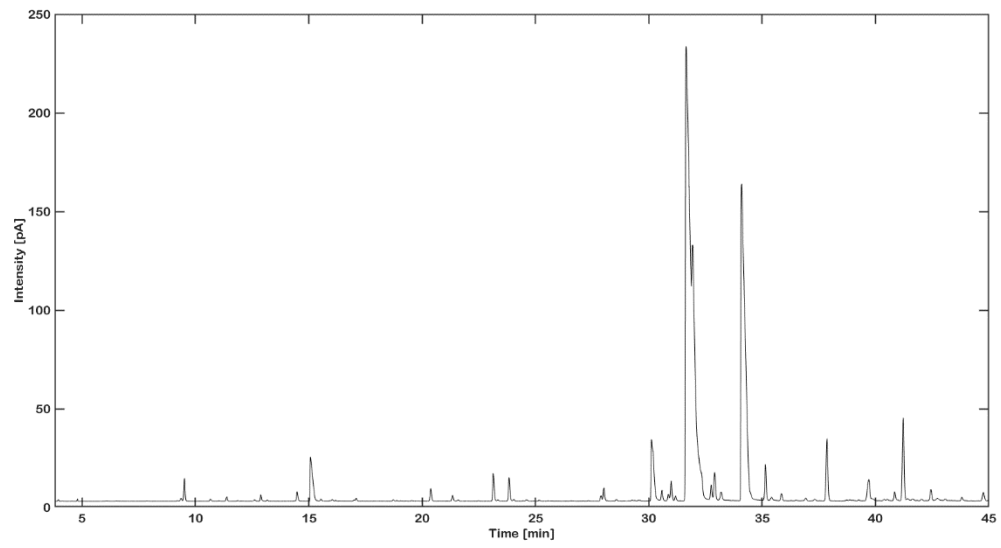
R. damascena Sample 5



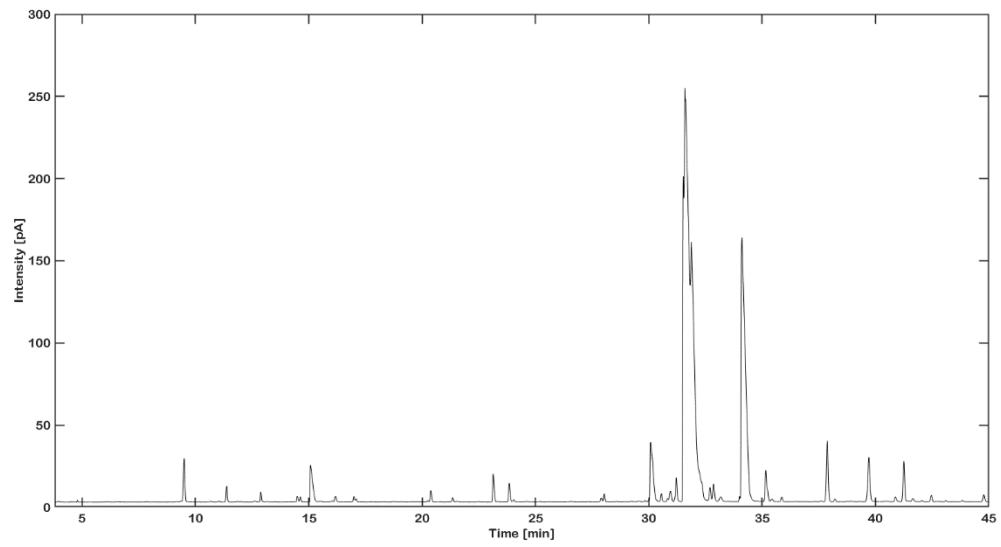
R. damascena Sample 6



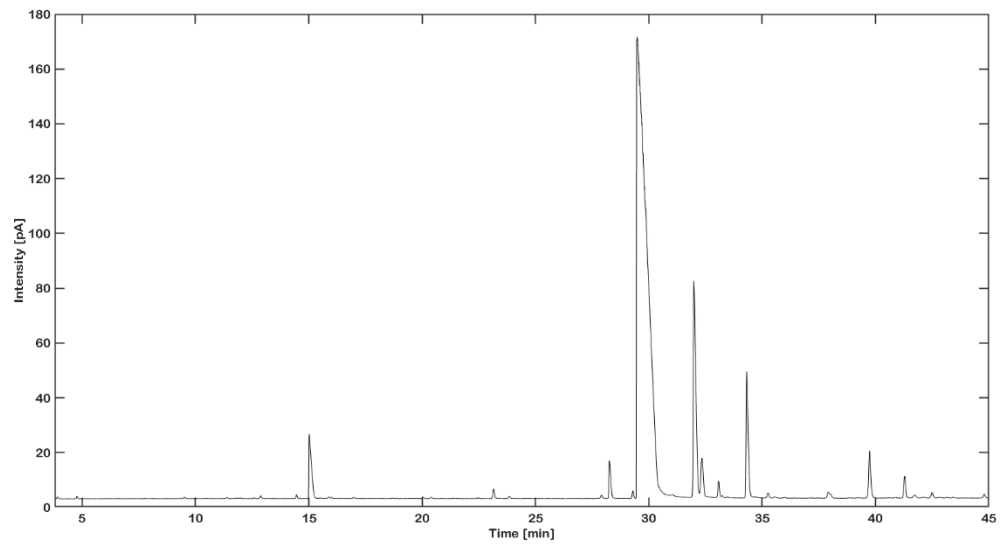
R. damascena Sample 7



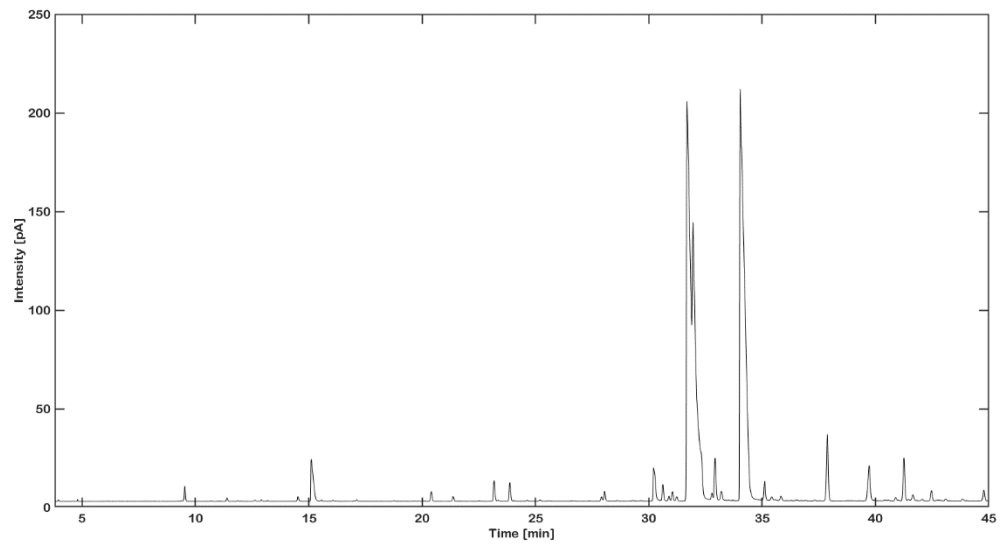
R. damascena Sample 8



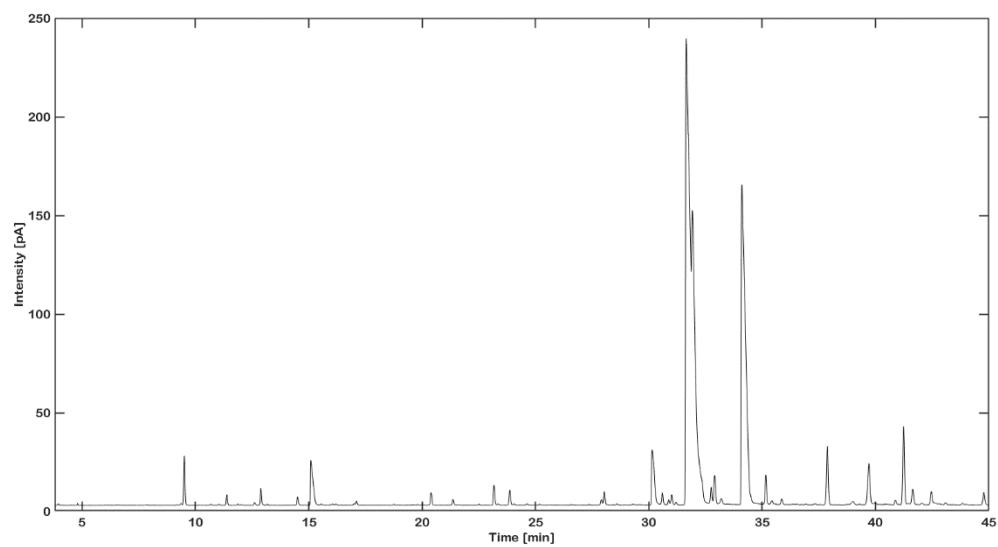
R. damascena Sample 9



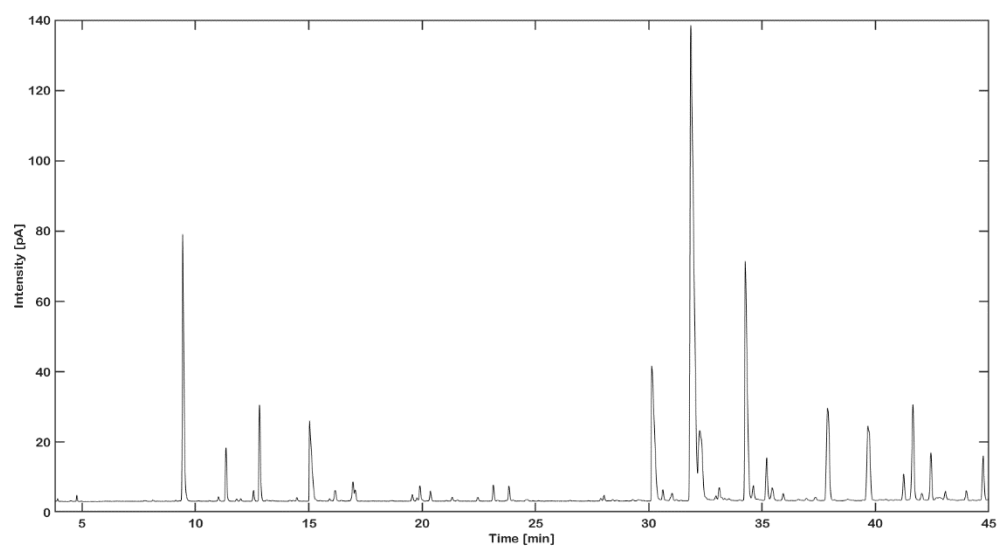
R. damascena Sample 10



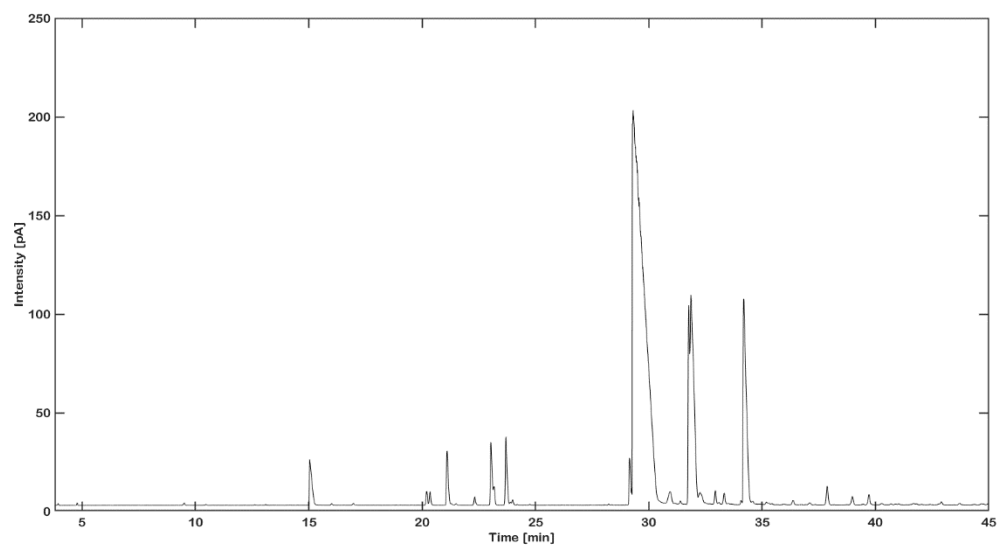
R. damascena Sample 11



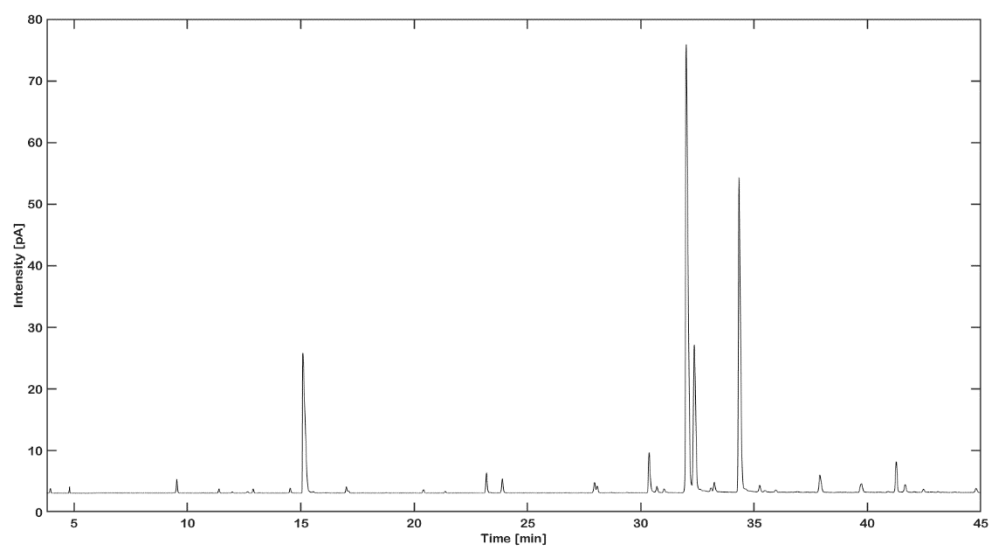
R. damascena Sample 12



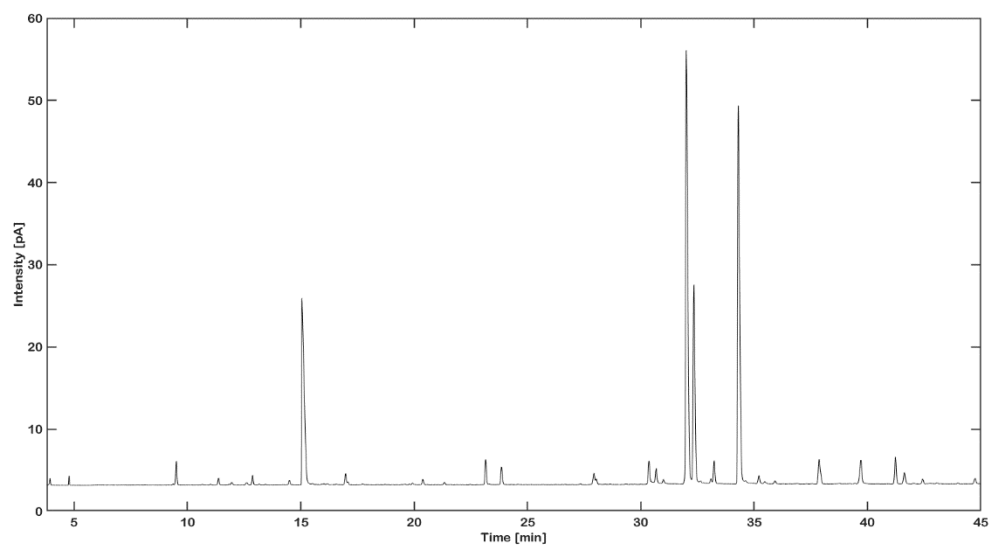
R. damascena Sample 13



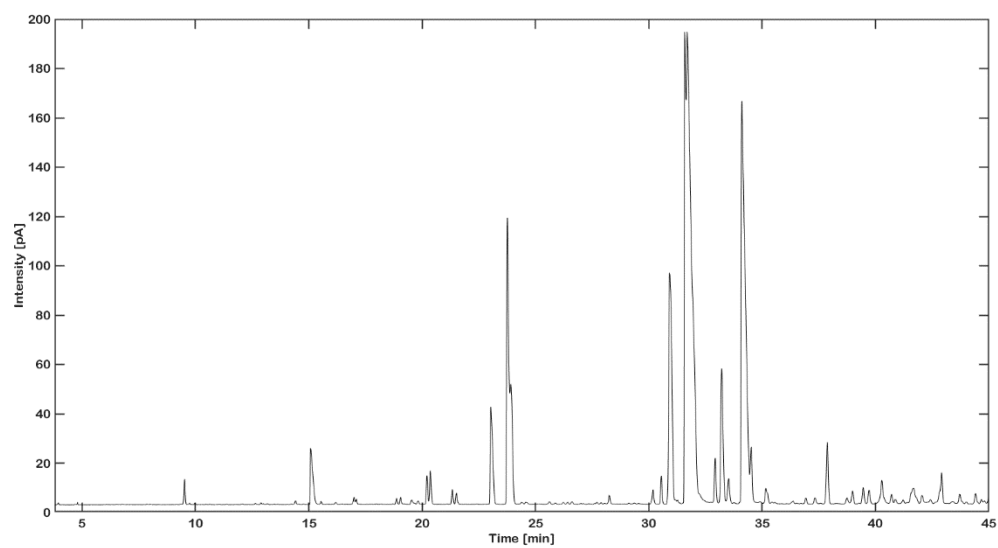
R. damascena Sample 14



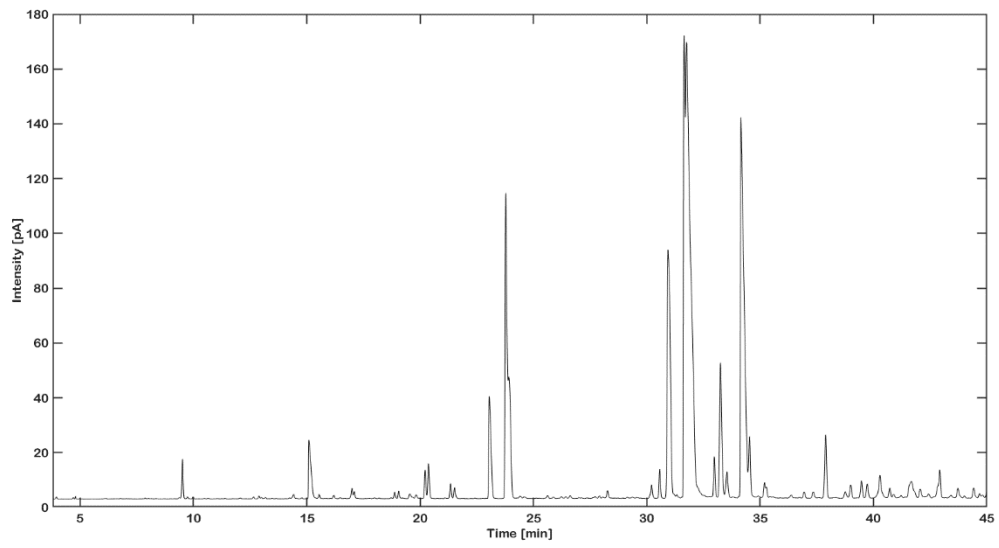
R. damascena Sample 15



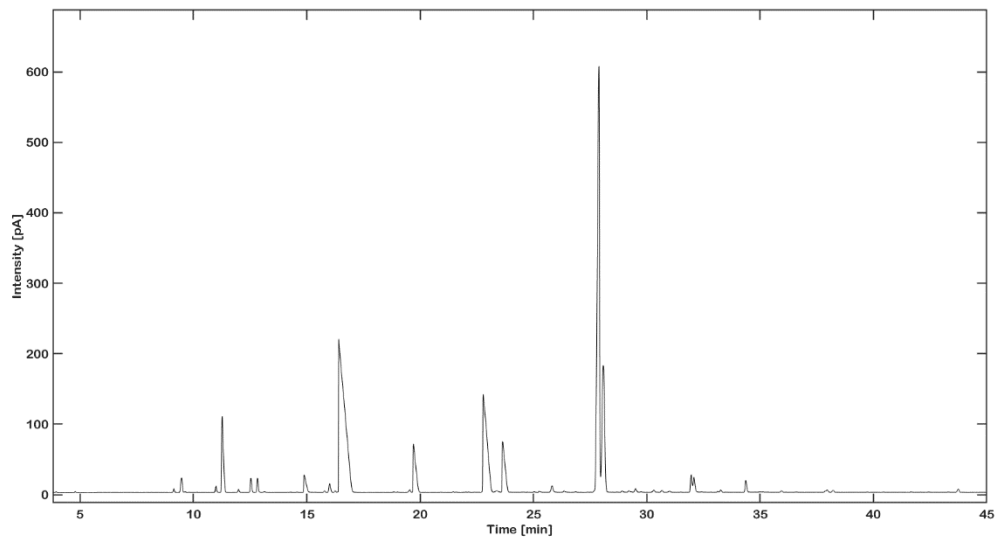
P. graveolens Sample 16



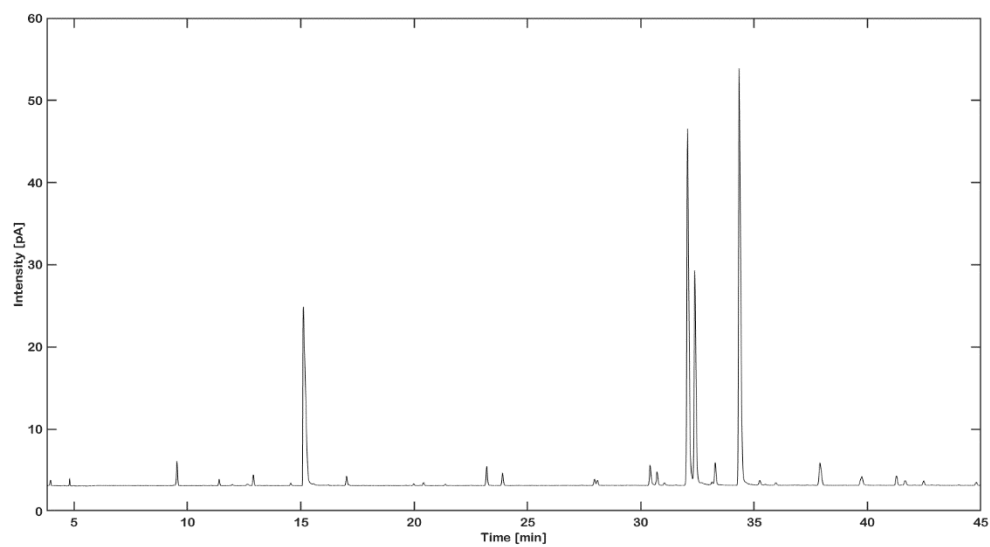
P. graveolens Sample 17



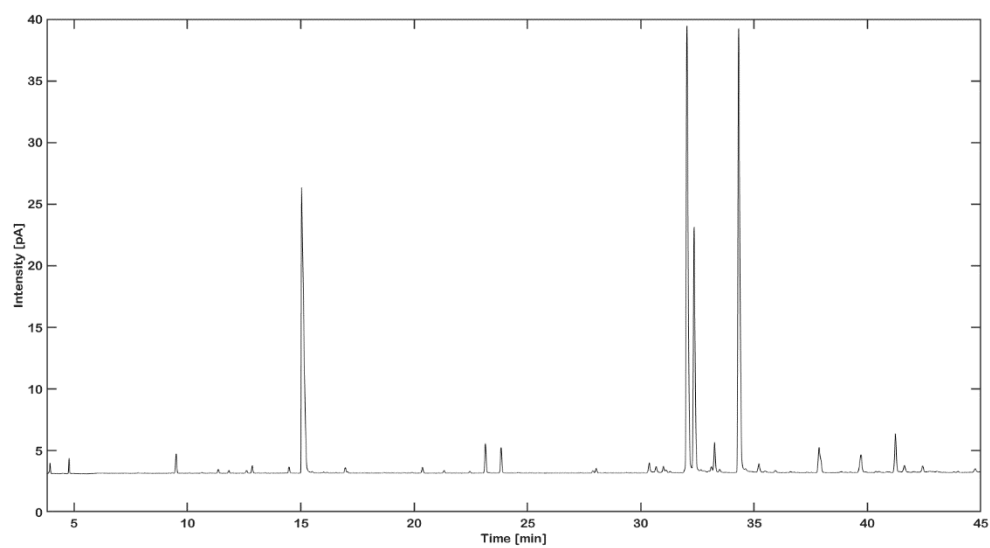
C. bergamia / *R. damascena* Sample 18



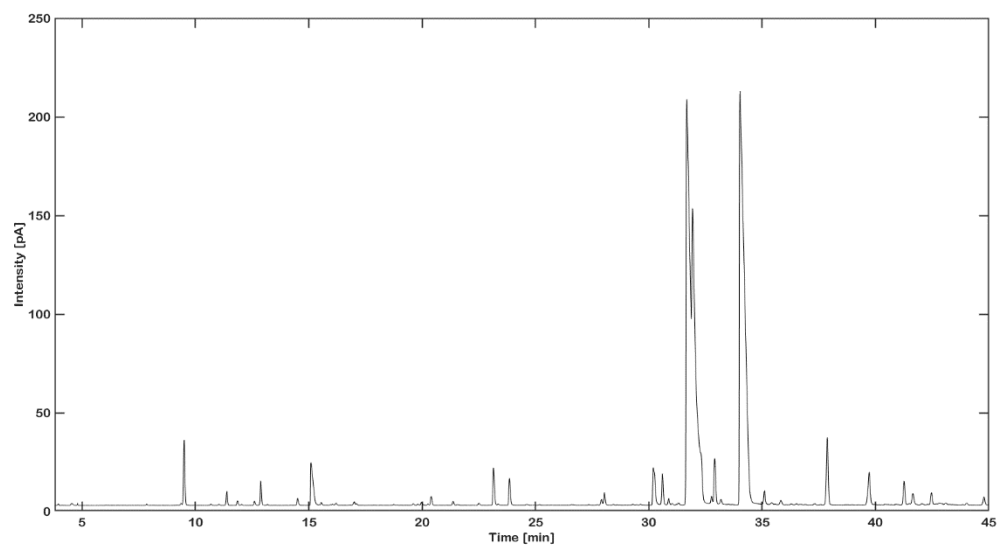
R. damascena Sample 19



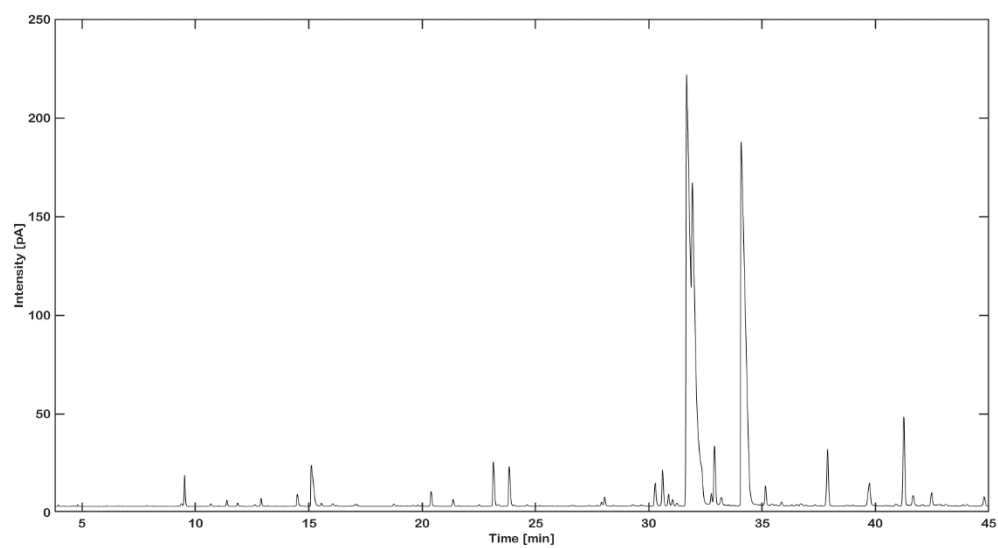
R. damascena Sample 20



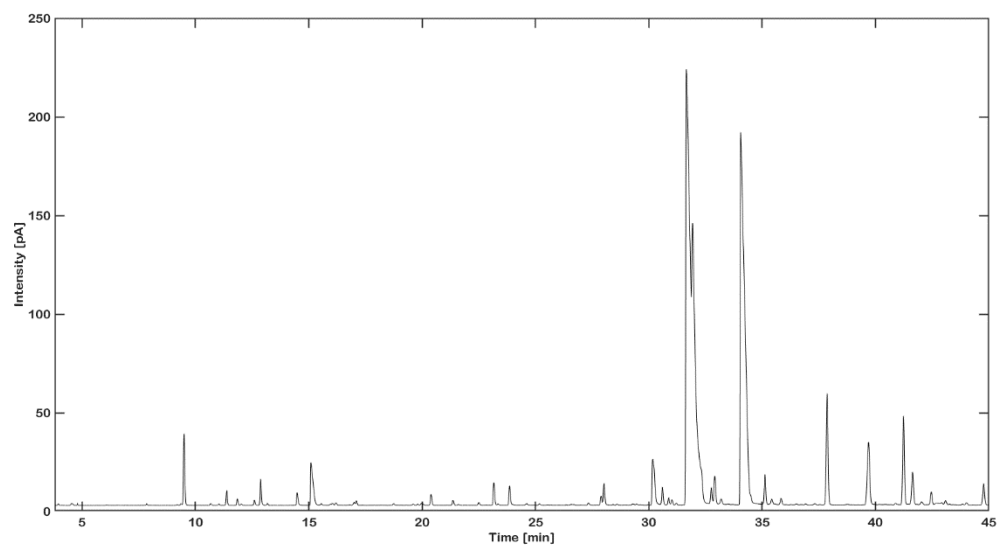
R. damascena Sample 21



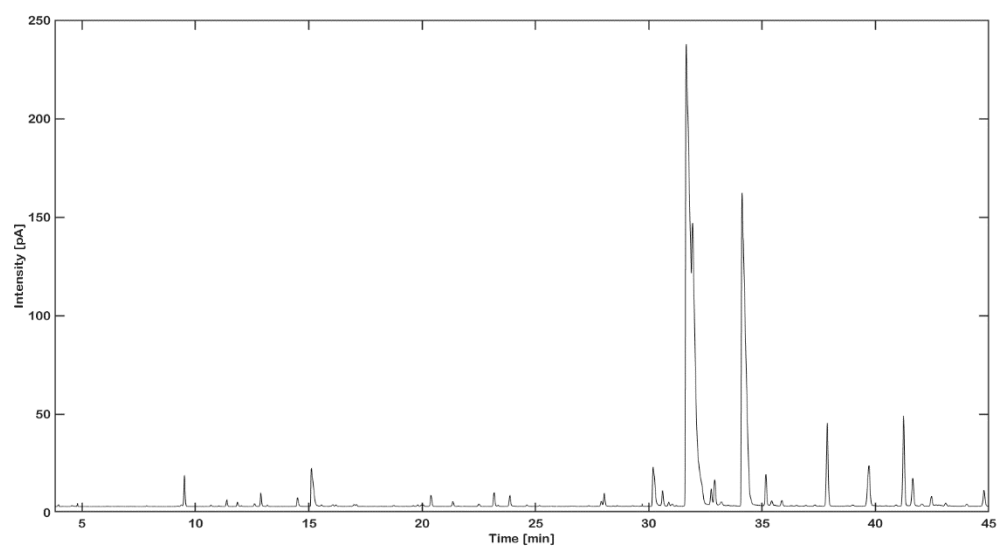
R. damascena Sample 22



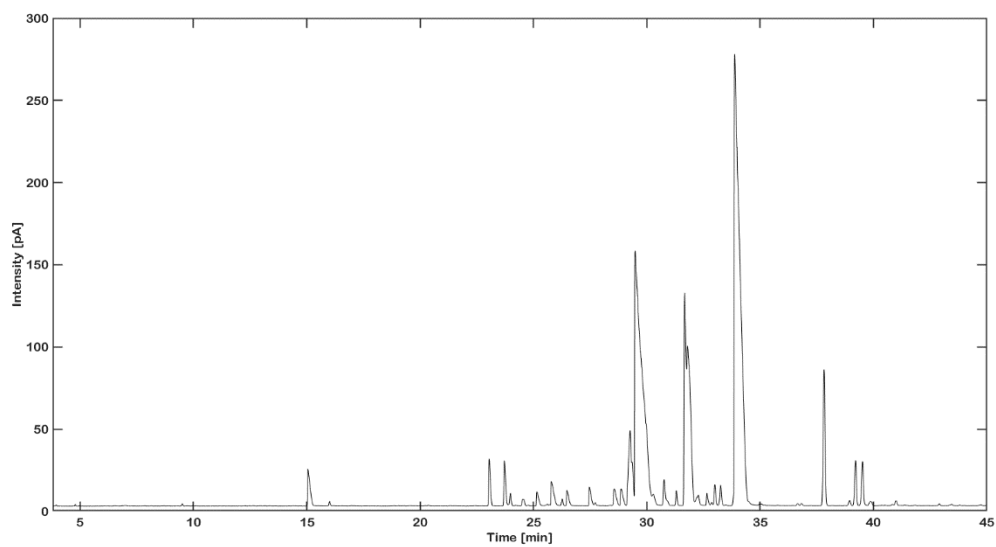
R. damascena Sample 23



R. damascena Sample 24



Synthetic Rose oil Sample 25



R. centifolia Sample 26

